MANOEUVRING BEHAVIOUR OF SHIPS IN EXTREME ASTERN SEAS

by
ZAFER AYAZ

A thesis submitted in accordance with the regulation of University of Strathclyde in part fulfilment of the requirements for the degree of Doctor of Philosophy

Department of Naval Architecture and Marine Engineering,
Universities of Glasgow and Strathclyde
GLASGOW

August 2003

'The copyright of this thesis belongs to the author under the terms of the United Kingdom Copyright Acts as qualified by University of Strathclyde Regulation 3.49. Due acknowledgement must always be made of the use of any material contained in, or derived from, this thesis.'

To my parents, Ayla and Hüseyin AYAZ, and my brother Mehmet AYAZ

ABSTRACT

In an attempt to contribute the efforts for the robust and effective numerical tools concerning ship motions in astern seas, this thesis presents the development of a coupled non-linear 6-DOF model with frequency dependent coefficients, incorporating memory effects in random waves with a new axis system that allows straightforward combination between seakeeping and manoeuvring model whilst accounting for extreme motions.

A combination of seakeeping and manoeuvring is achieved through the adoption of relatively new "horizontal body axis system" which accounts for large vertical motions as well. Furthermore, the frequency dependent terms are incorporated in order to improve the accuracy of the numerical model for non-zero encounter frequencies which are experienced especially when the ship has large heading angle. The effect of encounter frequency and so called "memory effects" are calculated in terms of radiation forces using convolution integrals. Equations of motions and external forces are described in terms of a new axis system. The wave forces are calculated through incident and diffraction wave forces. The incident wave forces are calculated using the instantaneous wave surface while low encounter frequency model is adopted for the calculation of diffraction forces. Finally, the whole numerical model is expressed in random sea environment including the convolution terms to carry out the simulations in more realistic sea environments.

The validation of the numerical model with the results of benchmark tests commissioned by ITTC Specialist Group on Stability, showed reasonably satisfactory agreement while the inclusion of frequency dependent terms affected the accuracy of the numerical model. Parametrical studies were carried out to investigate the effect of different environmental and operational parameters to ship motions in extreme astern seas along with the effects of degrees of freedom and encounter frequency.

In order to enhance the accuracy of the numerical model and to obtain further information about the coupling of the motions and the adequacy of the numerical model to carry out further simulations regarding dangerous situations during ship motions in random following and quartering seas, extensive captive and free running model tests were carried out. The numerical model provided good agreement with the experiments. The terms resulting from the coupling of vertical motions and large heeling angle to wave forces are obtained.

It is believed that the numerical model has a good potential for providing a more rational basis for predicting the dangerous conditions which a ship could face in extreme astern seas, and for offering insights about the link of behaviour with the design parameters of a ship in the light of the validation with the experiment results and parametrical studies.

ACKNOWLEDGMENTS

There are so many people of whom I would like to acknowledge gratefully for helping me to complete this thesis and hence to achieve one of my most important lifetime goals.

My supervisor, Prof. Dracos Vassalos for his support, encouragement, especially in "compulsory" turbulent times of PhD study, friendship, useful discussions, and above all providing me with the opportunity to study at SSRC. His contribution to my professional life has an immeasurable value to me.

Dr. Kostas Spyrou and Dr. Naoya Umeda for helping me in understanding the many aspects of manoeuvring in waves and guidance in theoretical and experimental parts of my studies. I am appreciated for their contribution to my study and my professional life.

Dr. Osman Turan and other colleagues at SSRC for their friendship and assistance.

University of Strathclyde for the John Anderson studentship award.

Mr. Akihiko Matsuda and members of National Research Institute of Fisheries Engineering of Japan (NRIFE) for providing me the opportunity to carry out the experiments at their institution, their wonderful technical support, help, friendship and hospitality throughout my stay in Japan. Also, I would like to express my sincere gratitude to Ministry of Education of Japan for their collaboration in funding of my experimental studies at NRIFE.

Mr. David Clelland for his invaluable technical help, assistance and friendship throughout the experiments in Japan.

I would like to express my appreciation for my parents Ayla and Hüseyin, my brother Mehmet and cousin or "big sister" Nigar for their love and support. Also, I would like to thank Prof. Mehmet Atlar for his support, assistance and "occasional" criticism but most importantly for inspiring his nephew throughout his life. Finally, I would like to thank Jane Wilkinson or my "rescuer" for sharing the pain in final parts of my study and for her wonderful smile.

MANOEUVRING BEHAVIOUR OF SHIPS IN EXTREME ASTERN SEAS

CONTENTS

1. INTRODUCTION

1.1 General Remarks

The motion of a ship in following and quartering seas, whether caused by waves or by her own manoeuvres, can strongly affect her stability and more generally her safety. Over many years, different types of ships and, notably small types such as trawler since they are more vulnerable to the sea impact, faced dangerous situations in these seas, often resulted with tragic consequences. Marine community have been aware of these dangerous situations for a long time. Especially in late 50's and early 60's with the support and encouragement of organizations and marine safety branches around world led by the International Maritime Organisation (IMO), both theoretical and experimental research studies have been carried out. Based on the experimental studies, stability criteria have been implied by the IMO. However, since these motions involve highly dynamic effects and due to well-known restrictions of the experimental efforts, those recommendations by the governing bodies and developed numerical models could be inadequate to a certain extent.

When a vessel encounters waves from the astern, usually three different modes, which lead to dangerous situations, are observed. The first is the so-called pure loss of stability on a wave crest where there is not enough buoyancy under the free surface to keep the vessel upright. This is an essentially static mode but capsize happens suddenly and abruptly. However, the majority of the research work has been focused on the other two modes which involve the dynamic stability of the vessel. One of these modes is the low cycle resonance which is caused by the parametric built-up of large roll motion, whilst the other is a combined mode that involves strongly the manoeuvring motion of the ship and is known as broaching. The latter mode is often realised in relatively high Froude numbers and increased wave-steepness leading where the ship experiences the so-called "surf-riding" condition. When the frequency of encounter is low, the vessel restoring force provided by rudder could be inadequate to impede the increasing oscillatory yawing motion. In other terms, when a periodic motion becomes less stable a ship can be attracted by an unstable "surf riding" point as a saddle and then repelled with a violent yaw motion despite maximum opposite rudder. This dangerous situation termed as "broaching–to" could lead a vessel to capsize. In astern seas, coupling

between surge and lateral motions cannot be avoided therefore it is essential to take both surf riding and broaching into account.

Until recently, many developed numerical tools were based on the linear theory as it is performed for simulations of ships motion in other sea conditions. Recent model experiments demonstrated that an intact ship complying with the International Maritime Organisation (IMO) stability criteria could capsize owing to broaching. However, it has been difficult to prevent these phenomena by understanding their dynamics even in regular waves because in principle a linear theory, as a basic tool for engineering, could not deal with non-harmonic motions. Surf riding and broaching are, as it is mentioned before, strongly non-linear, so it is essential to use a non-linear approach. Nevertheless, methodology based on non-linear dynamics has not yet been fully established for this application.

In the numerical tools, there are other problems apart from the non-linear approach. Firstly, ship motion leading to capsizing is very slow because the natural roll frequency of a ship with poor stability running in following and quartering seas with relatively high speed is very low. As a result, hydrodynamic forces acting on a ship consist mainly of lift components and wave-making components are negligibly small. These two points, inevitably, pave the way for using manoeuvring models rather than traditional sea keeping models, which are used to simulate the ship motions in wave. However, in case of highly dynamical motions such as broaching-to with extreme vertical motions at relatively high speeds, this approach fails to simulate ship motions adequately. This is due to fact that when the ship advances at high speed, the encounter frequency becomes much smaller than the natural frequency in heave and pitch. Therefore, these motions can be calculated by simply tracing their static equilibrium and equations of motion, for which the mathematical models can be reduced to 4 degrees-of-freedom. However, extreme pitch and heave motions can drastically change the instantaneous wave surface and, in turn, wave forces. These effects will increase when ship the yaws off during to surf-riding associated with broaching-to. In order to solve this problem, seakeeping models were combined with manoeuvring ones. However, due to complexity of the equations of motion, the large pitch angles were ignored. Therefore, those problems in simulation of aforementioned ship motion remain unsolved.

The second problem is to investigate how the behaviour of the ship is influenced by the consideration of the frequency-dependence of the hydrodynamic coefficients: Since the frequency of encounter in following seas is quite low, it is currently quite common to use "zero-frequency" constant hydrodynamic coefficients, as it is done in calm-water manoeuvring calculations. However, wave effects associated with the unsteady motion of the hull at the free surface and vortices which are shed from the oscillating hull, especially when a ship has very large heading angle, indicates that the convolution terms (representing the so-called "memory effects") cannot be negligible.

These restrictions and assumptions are applied to the experimental studies. In order to reduce to large number of completely captive model tests, covering a matrix of sinkage and trim, the ship model is allowed the freedoms to sink and trim in the vertical plane during these tests. As a result, it brought the aforementioned problem of not having reliable data for verifying 6 DOF fully non-linear numerical tools.

These problems are reflected by the International Towing Tank Conference in 1999 (22nd ITTC). Both the Manoeuvring Committee [1] and the Specialist Committee on Stability [2] emphasised on the need for more experimental investigations to study these motions. Furthermore improved numerical models have been urged for accurate prediction of broaching-to and capsizing of ships in extreme astern seas.

1.2 A Fresh Start

Deriving from this background, a research study has been carried out at the University of Strathclyde. The main intention of this research study is to develop a coupled non-linear 6-DOF model with frequency dependent coefficients, incorporating memory effects in random waves with a new axis system that allows straightforward combination between seakeeping and manoeuvring model whilst accounting for extreme motions.

The approach of the research reflects the above intention, so the main emphases were adopting a mathematical model which would allow a meaningful combination of manoeuvring and seakeeping motions in the prediction of extreme ship motions. Furthermore, convolution terms (so called "memory effects") are being incorporated

that would improve the prediction of the behaviour of the vessel in non-zero encounter frequencies.

The research was diverted into two phases. First one was the verification of the numerical model with existing experimental data and carrying out extensive parametric studies to explore different aspects of the adopted approach in terms of its capability to simulate ship motions in extreme astern seas adequately. The second one was the strong experimental tool to provide feedback to the numerical model. In the light of the stated requirements in experimental studies, extensive captive model tests in 6 DOF and free running model tests in irregular waves have been carried out at model basin of National Research Institute of Fisheries Engineering of Japan. However, there were obviously restrictions in extremity of the ship motions due to the limitations of the model for the captive model tests. Therefore, the results were also used to forecast the more dangerous situations.

Although it is open for more conclusive arguments, it is seen that the improved numerical model has a good potential for providing a more rational basis for predicting the dangerous conditions which a ship could face in extreme following and quartering seas, and for offering insights about the link of behaviour with the design parameters of a ship.

1.3 Contents of the Thesis

The thesis can be divided into four parts as the concerns expressed within the framework of Section 1.2. A brief outline of the structure of thesis is as follows:

In the first part, an introduction was given in Chapter 1. The statement of objectives is presented in Chapter 2. In Chapter 3, a critical review is presented where the previous research in understanding the ship motions in extreme astern seas and the numerical and experimental studies carried out for these purpose are discussed. It paves the way for introducing the key elements of the adopted approach in Chapter 4. These elements are outlined before the detailed presentations are given in the next chapters.

The second part gives details of the developed axis system and other components of the developed numerical tools. In Chapter 5, the mathematical model is given in the detail. A new axis system, equations of motion and the integration of the external forces are described. The second important emphasis on the effect of the frequency (or so-called "memory effects") and its incorporation to the mathematical

model are presented in Chapter 6. The verification of this numerical tool with existing model experiments is performed in Chapter 7. The numerical model is verified against results of experiments which were carried out in Japan for a fishing vessel and a container.

The third part introduces the efforts to explore the phenomena and establishing the reliability of the numerical model. In Chapter 8, extensive numerical studies were carried out to investigate the contribution of the numerical model with respect to the different parameters. In an attempt to carry the numerical tool into a more realistic environment the mathematical model and its components are expressed in the random waves in Chapter 9. The experimental studies as an important tool to achieve the goal of the research are presented in Chapter 10. The fully captive model tests for different speed, trim angle and sinkage and free running model tests in ITTC and JONSWAP wave spectrums for different heading, speed and wave conditions are carried out in manoeuvring and seakeeping basin of National Research Institute of Fisheries Engineering in Japan (NRIFE). Those experiment results along with the comparisons to the numerical results are displayed.

The final part draws conclusions into these efforts in the understanding the behaviour of ship motions in extreme astern seas. The achievement of the research work is discussed in Chapter 11 and the conclusions are given in Chapter 12. The details about the numerical model and experimental studies are given in appendixes along with the references used in the literature review and other chapters.

2. AIMS OF THE THESIS

The main aim of this work is to develop a coupled non-linear 6-DOF model with frequency dependent coefficients, incorporating memory effects in random waves with a new axis system that allows straightforward combination between seakeeping and manoeuvring model whilst accounting for extreme motions. A specific objectives can be outlined as follows;

- To undertake a critical review the numerical and experimental studies concerning the manoeuvring behaviour of ships in extreme astern seas and effect of frequency in understanding of this phenomena.
- To develop and validate a numerical code which will include a coupled non-linear 6-DOF model with frequency dependent coefficients with no restrictions on the motion amplitudes.
- To undertake extensive parametrical studies concerning the ability of the numerical model focusing on two main aspects of a new axis system and incorporation of frequency dependent coefficients along with the other important parameters and the improvement of the current model in comparison with the existing tools.
- To carry out extensive experimental studies focusing on the obtaining the wave forces data for fully captive model tests and the ship motions for free running model tests in irregular waves to provide feedback to enhance the numerical model in the effort of understanding the ships motions in extreme astern seas for realistic sea conditions.

3. LITERATURE REVIEW

3.1. General Remarks

The main objective of this chapter is to review the theoretical and experimental research on ship motions in extreme astern seas, and efforts to develop numerical tools to provide the basis for simulation of ship motions.

The review begins by investigating the theoretical studies. It can be subdivided into two parts. The first part reviews the efforts on developing mathematical models in terms of combined seakeeping-manoeuvring modules and dynamic stability. The second part undertakes a review of efforts to incorporate the effect of frequencies in those numerical tools. This is followed by the review of ships motions in extreme random waves. This is accompanied by the review of literature on experimental research, to which this research study also intends to contribute.

Finally, the key findings on these investigations are presented. This chapter is concluded with discussion based on those key findings which underline the problems observed in the previous research.

3.2. Theoretical Studies

Motions of ships in extreme seas, and in particular, dangerous situations that they are likely to face have been major research subjects from late 40's. As mentioned in previous chapters, dynamic characteristics of phenomena and complex mathematical notions concerning the simulation of such motions attracted researchers and a great amount of experience and knowledge has been gained through experimental and theoretical studies.

The attempts to establish numerical models and other theoretical studies have generally followed the experimental studies. The first real attempt is attributed to Davidson [3]. He studied directional stability and steering behaviour in following seas using manoeuvring model. The wave force terms were calculated by carrying out captive model tests, therefore the special attention was given to lateral forces. However, the surge force is neglected assuming the ship is travelling at wave speed.

Following his work, the manoeuvring models were preferred for the mathematical models. Grim [4] has included surge motion and formulated non-linear equations for surging motions in irregular seas identifying conditions for surf-riding. He

used the experimental method to obtain the wave induced surge force. He noted that by the effect of Froude-Krylov forces, for ship motions in following seas, the speed of vessel travelling slower than the predominant wave speed, could be increased significantly for a certain amount of time. This speed increase may have an important effect on the possibility of broaching.

As the milestone in this research study, Du Cane and Goodrich [5] extensively investigated phenomenon of broaching and related aspects in quantitative way. An overview of the problem was presented. They gave criteria and indices as related to directional stability and manoeuvrability. They also illustrated examples of broaching from the first hand accounts. Although the work remained on the discussion level, it paved the way for further research.

Wahab and Swaan [6] investigated theoretically the problem of coursekeeping and broaching in following seas by concentrating on the limiting condition of ship's speed equal to wave velocity (zero frequency of encounter). They concluded that "all unsteered ships appear to be unstable somewhere on the downward slope of a wave." They also assumed that the wave forces could be calculated only with the Froude-Krylov forces. The justification was given that encounter frequency is very low when broaching occurs.

From a different perspective, but related to the theoretical efforts on this subject, Paulling and Rosenberg [7] contributed to these studies. They investigated the non-linear equations of motion of a ship having the three degrees of freedom of heave, pitch and roll. Paulling and Rosenberg stated that " For coupled case, unstable motion may occur in any degrees of freedom through excitation by one of the other two." That was an important aspect and has laid the foundations of dynamic stability research.

Eda [8] modelled the coupled surge-yaw and sway motions of ship in waves and studied the directional stability in following seas. He also examined the effect of Froude-Krylov surge motion in such motions.

In order to highlight the efforts on manoeuvring in waves, in particular the danger of broaching, Conolly [9] assessed the conditions which broaching-to may occur, illustrated by documented cases. The distinction was made between the broaching-to that occurs when a ship proceeds at high speed and broaching-to at lower speed. He concluded that "The steering control should be maintained " and " The existing mathematical models are not adequate to provide a satisfactory representation of very complex physical phenomena that occur in severe following seas."

In the light of early findings, research attempts have focused for more extensive theoretical studies to develop robust mathematical models in understanding the phenomena and eventually the numerical models for simulation of such ship motions. Time-domain simulations gained importance in these efforts thanks to development in computer technology. The developments in computer technology realized time domain simulations of non-linear motions with some sets of initial conditions. Even though this dependence on initial conditions may seem to be a restriction, those initial conditions have great influences on the modelling of transient phenomena like broaching-to and inevitably capsize. So, in the context of research works of manoeuvring behaviour of ships in extreme seas, time-domain simulations take place along with the developing mathematical models.

In improving mathematical models, the one of major concerns was whether to approach the problem in the context of manoeuvring or seakeeping. Abkowitz [10] stated the facts that display differences between manoeuvring and seakeeping. Manoeuvring dealt with steady state and transient (or zero and low frequency) motions in calm water surface, while seakeeping dealt only with higher frequency wave-induced motions.

Although the fundamental difference between traditional manoeuvring and seakeeping was in fact a consequence of the waves rather than the free surface, it may be noted that seakeeping (or frequency dependent) hydrodynamics has always been sharply divided into two separate parts. One dealing with wave excited forces on a restrained ship and the other with forces due to ship oscillations in calm water while the later being more closely related to manoeuvring than the former.

Due to the traditionally steady state nature of manoeuvring motions and cyclic nature of seakeeping motions, two correspondingly different mathematical methodologies were developed. Manoeuvring was treated as a deterministic phenomenon in the time domain and seakeeping as a spectral and statistical phenomenon in the frequency domain.

However, in both disciplines, and for similar reasons of convenience, hydrodynamic and inertial forces are formulated in terms of body-axes that rotate and translate with regards to signs and location of the origin, the space orientation of a ship is expressed in terms of the same three Euler angles, in both disciplines.

On the other hand as mentioned in the previous chapter, hydrodynamic forces acting on ship which travels in stern seas consist mainly of lift components and wave-

making components are negligibly small, therefore manoeuvring models are used to simulate the ship motions in wave. However, those manoeuvring models, which are based on calm water conditions, cannot describe dynamics encountered in a wave environment. As a result, the time domain models used to describe motions in stern seas and capsizing usually simulate both manoeuvring forces and wave forces based on modular approach. Having assessed those outcomes, the research focused on obtaining meaningful combination of manoeuvring and seakeeping models.

Eda [11] and Son et al. [12] also realised the effect of roll motion and combined the roll to surge-sway-yaw manoeuvring model and their works became references for efforts to creating 6 DOF models.

Motora et al. [13] carried out numerical simulations of surge, sway, yaw and roll motions of a ship travelling in following waves by making use of the results of captive model tests. They also carried out free running model test and full-scale measurements in order to identify the casual factors resulting in the occurance of broaching-to phenomena. Based on the their investigations, they concluded that " wave exciting yaw moment which exceeds the course-keeping ability of the rudder results in broaching-to phenomena". This finding was in contrast to previous opinions that the extreme yaw motion comes from hydrodynamic moments as a result of the unsymmetrical underwater volume following large heeling.

In a similar pattern but using 3 DOF (surge, sway, yaw), Renilson [14] developed a mathematical model for use on an analogue/digital hybrid simulation to predict the conditions which could lead to broaching. He also developed a theoretical method for calculating the coefficients in the mathematical model and discussed the effect of varying rudder based on experiments. However, since linear theory was used the correct prediction of large amplitude yaw during broaching was not feasible.

Hirano et al. [15] calculated the trajectory of a merchant ship in regular waves, neglecting oscillatory forces and obtained reasonably good prediction results with experiments.

Ohkusu [16] proposed a strip theory method for the prediction of diffraction wave forces acting on a vessel running with low encounter frequency in oblique following seas and presented results for sway, heave, roll pitch and yaw motions. The comparison with experimental results proved that their effect was small. However, in the case of yaw motion, which is very important for broaching, the inclusion of a diffraction term improved the theoretical prediction. He also pointed out that the strip

theory, despite the efforts, is in the strict sense not sufficient for predicting correctly the wave exciting forces and wave loads in such motions. Although, it should be noted that his theory was validated using semi-displacement craft, therefore validation for displacement type, which could be important, especially in large heading angles, was not investigated.

Elsimillawy and Miller [17] used a time domain-simulation of the ships motions in regular sinusoidal waves in six degrees of freedom to find dangerous situations which may lead a ship to capsize. They calculated the coefficients of the equations of motions at steps in time, according to the exact wave and vessel position, using strip theory. The verification of their model with results of real sea disaster illustrated that ship's oscillatory motions, which are usually neglected, have the most influence on the righting moment. However the model, using the linear uncoupled strip theory equations of motion, fails in the calculation of coupled non-linear phenomena.

Hamamoto et al. [18], [19], [20] presented analytical and experimental studies of ships motions and capsizing in three reports. They highlighted the dangerous situations that occur in such motions and used a time domain numerical simulation program for motions and capsizing. A six degrees of freedom mathematical model was developed and the calculation of incident wave forces was based on analytical approximations and diffractions forces were not included. A quasi-steady theory under the assumption of low encounter frequency was incorporated and hydrodynamic forces were evaluated using practical formulae. The influence of wave height and length, relative position of ship to wave, heading angle and KG on the GZ curve was examined. Capsizing due to parametric excitation and pure loss of stability was simulated. Broaching was not investigated but the amplitude of yaw angle was examined for certain wave encounter frequencies.

Meanwhile, Chislett [21] introduced the Horizontal Body Axis system to the studies. The Horizontal Body Axes, which are closely related to, but not a special case of General Body Axes, can hardly be claimed to be original, since they have effectively been used in many other studies of ship manoeuvring. It was a serious attempt with inclusion of roll to create combined seakeeping-manoeuvring model. Following the path, Hamamoto has modified the equations of motion and the model for Froude-Krylov forces in his third report [20]. However, it made many simplifications and assumptions, such as ignoring the pitch angle and reducing the non-linear coupling terms, which raised the questions over the advantage and reliability of the modification.

Ottoson and Bystrom [22] presented an extension of the previous model of six-degree-freedom [23] including interaction effects such as influence of wave generated water particle velocities on the manoeuvring hydrodynamic forces or influence of rudder-induced forces on the ship motions in waves. Hydrodynamic forces on manoeuvring motion were calculated in calm water. However, the details of the mathematical model were not given, and it intended to combine manoeuvring and seakeeping models in an effort to investigate course-keeping problems rather than dynamic stability problems such as broaching-to. Therefore, it failed to show validation for extreme sea state such as varying heading angles and excessive roll angles. Also, the wave forces and frequency dependent radiation coefficients were calculated using strip theory despite its shortcomings.

De Kat and Paulling [24] presented a numerical model for simulating large amplitude motions in severe waves and capsizing. They used linear potential theory for determining the wave induced pressures and the body radiation and diffraction forces. Froude-Krylov forces were calculated up to instantaneous free surface. Manoeuvring derivatives associated with the viscous flow affecting the sway force and yaw moments were incorporated. Low cycle resonance, loss of static stability, broaching phenomenon was realised not by one wave action but when subsequent steep quartering waves were striking the vessel. In further work, parametric investigation using numerical simulations is proposed as a tool for development of criteria against wave induced capsize of intact ships.

Hamomoto and Kim [25], later on, gave more detailed description of the new equations of motion based on the new axis system. They carried out the time domain simulations for turning and zig-zag trial of a ship in waves. Although theoretical comparisons were given between the new axis system and the existing systems, it did not present the effect of the new axis system in the numerical simulations.

In the light of this approach, Hamamoto et al. [26], [27], [28] implemented the same model for analyses on low cycle resonance. They discussed the analytical expression on varying GZ curves with respect to relative position of ship to waves and non-linear equations of motion, describing phenomena and the effects of righting arm, stability range and encounter period on low cycle resonance.

Hamomoto et al. [29] also used this mathematical model to study combined motions of sway, roll and a yaw in following seas. They linearized the mathematical

model and numerical simulations were carried out to show unstable behaviour in limiting situations at zero frequency of encounter and in overtaking waves of low frequency of encounter.

In a similar way, Umeda and Renilson [30], [31], introduced a practical method for calculating the wave forces on a ship running in quartering seas. It was claimed to be a limiting case of a strip method where the effect of encounter frequency was ignored since it is very low for this case. The experimental and numerical studies revealed that Froude-Krylov forces alone can not predict wave forces with sufficient accuracy and by utilizing the Ohkusu[16]'s study, it was found that the method could be useful if the broaching only is investigated for a transient period.

Vassalos and Maimun [32], giving a brief review of individual mechanism likely to contribute to broaching, confirmed, using numerical and experimental investigations, that coupling between longitudinal and lateral motion are of paramount importance for broaching as well as the ensuing extreme vessel behaviour. They have shown that a six degrees of freedom model including an autopilot is necessary to realistically simulate a broaching-to situation.

Time domain simulations are limited in their ability to identify the critical conditions for broaching because, like any other non-linear phenomena, broaching depends very much on the initial conditions. To overcome this difficulty, it is desirable to analyse behaviour of solution sets instead of a solution itself. This practise is known as the non-linear dynamical system approach. Repeating time domain simulations, Spyrou [35], [36], [37] discussed the topology of boundaries between capsizing, surf riding and broaching and he found chaotic surf riding and a jump of periodic orbit to be extreme cases. Umeda [38] presented a method for predicting the approximate critical condition for broaching with stability analyses on fixed points and periodic orbits but without time domain simulations; they validated their method with model experiments.

Tsangaris [40] considered a mathematical model in order to simulate the ship behaviour during the broaching up the point of a potential capsize. The coupling of vertical and planar motion, which is expected to contribute both to the vessel directional stability and capsize behaviour, is taken into account. Modelling is restricted to low encounter frequencies where broaching is encountered and hydrodynamic phenomena are dominant. He also described the potential use of dynamical systems theory by the use of geometrical methods.

Tsangaris and Vassalos [41] presented a time domain simulation model for the behaviour of a vessel in severe stern seas of low encounter frequency. Wave forces were validated with experimental results. They classified the behaviour of the ship for a range of operational and environmental parameters. Vassalos et al. [42] continued the similar studies using the same time domain simulation model to identify conditions leading to extreme motions by examining both transient and long term behaviour. They concluded that period doubling phenomena can be regarded as precursor of "imminent danger of capsize" and bifurcation analysis could be used to identify possible danger and provide safety criteria.

Bailey et al. [43] developed a unified mathematical model to study dynamical behaviour and manoeuvring of a ship travelling in seaway, encapsulating the theories of seakeeping and manoeuvring. They presented relations between the fluid actions defined in manoeuvring analyses using a body fixed frame of reference and those for a seakeeping analysis using an equilibrium frame of reference. They transformed those different data sets allowing a hybrid approach integrating experimentally and theoretically derived data. However, as they conceded in the study, all the mathematical models were linearised for simplicity.

Hamamoto and Munif [45], in an attempt to develop their previous mathematical model, used a method which takes the variation of metacentric height, into account. They conducted simulations to predict stability against capsizing and computed stable and unstable areas. Major drawbacks were the linearised equations of motions and using strip theory in calculation of hydrodynamic coefficients.

However, they completed the modification of model by the work of Munif et al. [46]. They developed a fully non-linear six degrees of freedom numerical model in which large angles were taken into account even though hydrodynamic forces were estimated from strip theory. They concluded after the extensive numerical simulations that capsizing due to parametric resonance occurs only for lower metacentric height and lower speed and ship running with encounter angle of 30-45 degrees is more dangerous for capsizing than when the encounter angle is 0-15 degrees.

3.3. The Effect of Frequency

In the calculation of ship motions in astern seas since the frequency of encounter in those seas is quite low, it is currently quite common to use "zero-frequency" constant hydrodynamic coefficients, as it is done in calm-water manoeuvring calculations. However, as mentioned in Chapter 1, wave effects associated with the unsteady motion of the hull at the free surface and vortices which are shed from the oscillating hull indicates that the convolution terms ("memory effects") do have considerable effects. Within the context of ship manoeuvring, these effects have been investigated both theoretically and experimentally. Those research efforts have laid foundations for the investigations to the effect of frequency on ship motions in stern seas.

In a monumental theoretical, Cummins [48] introduced memory effects in linearized equations of motion by assuming that the velocity potential relating to ship motions includes two parts, one depending upon the history of the motion, the other depending upon the instantaneous motion. The principles introduced by the author have led to important developments, both theoretically and experimentally. Lin [49] used perturbation theory and classical hydrodynamics in a similar model to solve the problem of a ship moving about a straight-line path with constant velocity.

Perez y Perez [50] developed a model for steering in waves which takes the effect of frequency dependent coefficients into account by convolution integrals. Frequency dependent non-linearities are considered to be part of the arbitrary forces. The non-linearities caused by the rudder were also included. It was restricted to 3-D motion, though the author claimed it could be used in all 6 DOF motions.

In a series of theoretical and experimental investigations, Bishop et al. [51], [52] challenged the use of linear theory and the Taylor-series representation of the hydrodynamic forces based on the assumption of "quasi-steady" flow, i.e. the fluid forces are determined exclusively by the prevailing motions of the ship. They noted that this assumption renders history of the motion unimportant. Several objections have been made, however, against this statement, arising from the role of the free surface and from the vortex shedding taking place around the hull. Following those remarks, they introduced the use of functional analysis and the adoption of a Volterra, rather than a Taylor-series type of representation, with the memory "stored" in convolution integrals over the time history of the motion variables in manoeuvring equations. This approach was later to be modified for motions in waves.

In similar research effort, Frank et al. [53] brought both experimental and analytical approaches to the problem of manoeuvring in calm water. They described the equations of motion in linearized Taylor series while the coefficients depended upon the Froude number but not upon the velocity components associated with a manoeuvre. The constants and functions associated with the proposed analytical approach were calculated from model experiments.

Following this work, Scragg [54] showed that the impulse response techniques, using a set of linearized equations, are superior to the traditional regular-motion tests in determination of stability derivatives. Also, using the same method, memory effects in shallow and deep water were discussed. Loeser [55] showed in his study of the memory effects in shallow water that for the large ships the effect of frequency are not important in prediction of manoeuvre in either deep water or shallow water. However, classes of ships which are more manoeuvrable may require analysis with the equation including memory effects. Scragg [56] also discussed the error introduced into manoeuvring predictions by the use of a set of linearized equations of motion which ignore memory effects. After incorporating certain improvements into the impulse-response technique, experiments were conducted to measure a complete set of the coefficients. Manoeuvring predictions were then made using two different sets of linearized equations of motion, one which included memory effects and one which excluded memory effects. It was determined that the significant errors occurred only during the initial phase of the manoeuvring, and that memory effects could be safely ignored for most deepwater manoeuvring problems.

Emphasizing similar problems, Newman [57], [59] discussed the effect of memory in different manoeuvring conditions for slender ships. Effects of free-surface waves and viscous separation are not considered, but the attention focused on the low-aspect-ratio geometries, including vortices shed from the sharp trailing edges on the ship hull. He asserted that there is reason to assume much longer life expectancy for the fluid memory in shallow water. Evidence for this statement is the mariner's experience that ships manoeuvre more slowly in shallow water. He stated also that the convolution integral in time is appropriate for all cases where the present state of the flow is affected by previous motion of the ship. He noted also that other factors were wave motions on free surface, and vorticity shed along the hull.

Fujino [60] discussed the effect of frequency and using impulse response functions instead of the making use of constant hydrodynamic coefficients in very

extensive theoretical work. Through the knowledge of hydrodynamic coefficients as functions of frequency, which he called "stability derivatives"; equations of manoeuvring motions were derived with the "causality" being taken into consideration. He stated that "it is not always true to say that if allowance is made for the memory effect, the linear prediction can be remarkably accurate". However, he also noted that experimental studies should be concentrated on different hull forms to reach certain conclusions.

Guo [61] developed a non-linear theory of ship manoeuvring, based upon the hydrodynamics of arbitrary small motions superimposed upon constant forward speed. He extended the previous work by Lin [49]. The results then have been applied to equations of manoeuvring allowing only surging, swaying and yawing motion. The aim of the analysis was to establish the form of second-order terms in the equations. The various potentials were found as solutions of integral equations constructed using time-dependent Green functions and they exhibit, therefore, memory effects. Then the complete rigid body equations of motion were adjoined, resulting in a set of integro-differential equations. Numerical calculations for the determination of the kernel functions were carried out. Results of the numerical model against the experimental data for Series 60 ship showed generally satisfactory agreement. However, viscous and lifting surface effects caused by the manoeuvring motions were not considered.

Much of these works were focused on ship manoeuvrability in calm water. However, the theoretical foundations were being used in studies of the manoeuvring motions of ship in waves from the 80's.

Aukudinov [62] presented a simplified non-linear manoeuvring in waves model, taking account of frequency dependence of the coefficients. He mentioned that all previous models were restricted to linearized theory. Therefore, the possible non-linearity caused by non-linear boundary conditions (both at free surface and body boundary), by separation drag, and by vortex shedding have not been taken into consideration. Hence as far as higher accuracy is concerned, it is desirable to incorporate these types of effects into formulation of the ship manoeuvring in waves equations. In his 6 DOF model, heave and pitch were decoupled from surge as well as from the lateral plane motions. The mathematical model was applied to deterministic calculation of seakeeping and manoeuvring prediction in irregular seas.

In addition, although time domain simulations of ship motions can actually be carried out with memory effects being updated at each time step, by recalculating all

convolution integrals, Holappa et al. [63] show that it is numerically far more efficient to use a finite state space approximation. Moreover, this was found to be the only practical way to perform a dynamic stability analysis including memory effect.

McCreight [64] used the same approach in his study of manoeuvring in waves. He developed a six degrees of freedom time domain model for predicting the motions of ship manoeuvring in waves and wind, including wave induced motions. He combined the full non-linear calm water manoeuvring equations of motions with wave effects derived from the linear ship motion theory. Through the use of system identification techniques, added mass and damping data are approximated by the use of extended state space. Similar techniques have been employed in wave power devices by Jeffreys [65]. Jiang et al. [66], Schellin et al. [67] and Chung et al. [68] followed the method also in simulation of mooring.

Rhee et al. [70] developed a mathematical model in which external forces due to wind and current were included. The hydrodynamic forces and moments in calm water are empirically represented according the experimental results and memory effects caused by the wave forces were taken into account. They discussed the effect of past motion on the steady turning motion and found that those memory effects have no applicable influence for such motion. However, the kernel function was applied only for the external wave force and the model was tested only for basic steady manoeuvring motions. Almost in similar manner, Hamamoto and Saito [71] presented a practical method for the time-domain description of ship motions in following waves. They simplified the aforementioned Horizontal Body Axis system. In calculation of heave and pitch motions they compared hydrodynamic forces described at the fixed frequency with convolution methods. They claimed that it could be useful in terms of computing time if the representative frequency to evaluate the hydrodynamic forces can be found. However, the model is not exact even for small amplitude motion problem since the frequency of motion cannot be determined when the non-linear equations are involved in the equation.

Price and Tan [72], meanwhile, developed a viscous boundary element method involving a convolution-integral formulation to determine directly the fluid actions and velocity flow field associated with a body manoeuvring in a viscous fluid. They highlighted the development in seakeaping using potential theory and their inability to describe manoeuvring motions where viscous effects dominate. Therefore, they stated

"there is need to develop fundamental viscous solution which contains the description of the viscous nature of the fluid".

Lee et al [73] compared the traditional ordinary set of differential equations with constant coefficients and integro-differential equations with impulse response functions for surge-sway-yaw manoeuvring motion in waves. They derived linear integro-differential surge-sway-yaw motion equations with rudder deflection in regular waves. The difference between the integro-differential equations and ordinary differential equations were discussed by comparing the response of typical manoeuvre like zig-zag test. They concluded that " Confined to the linear manoeuvring motion in waves, the usual constant coefficients equation gives good agreement with the exact integro-differential equation. However, for the sake of simplification, effect of varying encounter frequency was neglected, and the numerical coefficients were carried out for a fixed heading angle.

Bailey et al. [43] discussed the phenomena through and representation of fluid actions. They incorporated the impulse response functions into mathematical model. They conceded that "the use of linear theory may be open to criticism and more general non-linear theory required. However, it is important that fluid-structure mechanism should be fully understood before such a non-linear approach is developed." Slow motion derivatives, oscillatory derivatives and hydrodynamic coefficients calculated using the traditional formulations adopted manoeuvring and seakeeping theories. Comparisons between measured PMM (Plane Motion Mechanism) data and predicted hydrodynamic data based on potential theory showed differences at low frequencies of oscillation. These differences were reflected in their calculated impulse response functions.

Lee [74] modified his previous work on manoeuvring in waves, by including the convolution of the radiation forces. However, he reached the same conclusion as his previous work. This time integro-differential equations are compared with ordinary differential equations in calculation of a 10°-10° zig-zag manoeuvre in wave. However, the effect of varying encounter angle was again neglected.

3.4. Motion In Random Waves

Since the introduction of the principle of linear superposition into ship motion theory by St.Denis and Pierson [82], the responses of a ship and/or a marine structure to

the sea are usually described in terms of the frequency response functions. In the linear dynamic system, the responses of a ship to irregular waves can be represented by a linear summation of its responses to the components of the irregular waves.

Since the development of numerical tools in the astern seas focused on the motions in regular waves, irregular seas studies mostly consisted of experimental results. Although, the studies on uncoupled ship motions for parametric excitation especially for roll motion gained importance since Grim's [4] study. On this aspect, Price [83] used the stochastic process theory with taking expectations of an integral solution of equation of motion, while Roberts [84] used approximate Markov method based on stochastic average method. However difficulties due to relationships between restoring moments and wave profile of ship in 6 DOF have meant that a relatively small number of researches have focused on the full 6 DOF motions in random stern seas.

Amongst the first significant studies of ship motions in random astern seas, Chou et al. [75] conducted a series of experiments in San Francisco Bay to study of ship motions and capsizing in extreme seas. They used a time domain simulation program for motions and capsizing to investigate motions in a variety of wave group configurations. Experimental results have been compared a linear strip theory calculations. They concluded that the characteristics of wave groups encountered by the ship have considerable influence on the tendency to capsize. Having admitting lack of study, they urged for more investigations of such ship motions in random seaways.

However, comparing to other studies in regular wave motions, studies in random waves have been remained limited to experimental studies. In the late eighties in an effort to revive previous findings by the Berkeley team, De Kat and Paulling [24] investigated the behaviour of ship in random following and quartering seaway focusing on the time dependent, spatial wave characteristics along the length of the vessel, their influence on ship motions and the usage of an equivalent wave system to replace a random sea. They found that in the following and quartering sea conditions, the wave elevation observed amidships appears to be regular over certain periods of time in spite of the randomness of the sea. Therefore, they suggested characterizing the random wave process by superposition of only two regular wave system which would yield an equivalent wave system. Although, discrepancies existed when comparing with experimental results, it is thought to be fairly reasonable way to characterize a random seaway. It also lacked enough comparisons for different environmental conditions in order assess the method in more detail.

Meanwhile, Takaishi [85] carried out the similar study deriving data from statistical analysis of casualty records about flooding and capsizing accidents. He showed an example of encountered waves measured in following seas and stated that the ship travelling in irregular wave could be accompanied with the highest waves in the irregular waves in certain probability and be attacked successively by largest waves for a long time which would be sufficient to result a large amplitude of rolling motion or to catch a large amount of water shipped on deck. He also verified previous findings which showed certain wave and navigation condition encountered wave characteristics in following and quartering seas that act like regular waves. Transforming the encounter wave spectrum from the wave spectrum but without taking into account the fluctuation of metacentric height, he defined a diagram that displays aforementioned wave conditions in following and quartering seas.

De Kat [86] investigated random waves in relation to capsizing and broaching of a steered, intact ship while particular attention is paid to validity of the random Gaussian wave model when simulating motion in severe, long-crested seas. Model experiments were carried out to determine joint distributions of individual wave parameters and group speed effects in astern seas. It was found that joint distributions of overall wave properties are reasonably well predicted by the Gaussian wave model even for steepest sea state. Furthermore, for a ship sailing in astern seas at speed close to the mean group speed, wave group length increases and it is shown that during the movement of an overtaking wave group the same, spatially irregular, wave will repeat itself every wave encounter and this can lead to large amplitude excitation of a regular nature.

As part of their long running research, Hamomoto et al. [28] investigated low cycle resonance using the similar approach to Takaishi while taking the fluctuation of metacentric height into account. They derived the equations of motions for random waves which was previously developed for regular waves. They concluded that the power spectrum band of GM fluctuation has a narrow frequency band for the ship running at high speed. However, the numerical results have not been verified against the experimental findings.

3.5. Experimental Studies

Experimental studies were pioneers in these research efforts. In theoretical studies many models have been developed based on the experimental results. Model experiments have been used extensively in order to simulate the dangerous situations in stern seas and obtain an insight into ship capsize. Model experiments have also formed the foundations for the IMO recommendations for operational guidance in stern seas.

Eda [8] examined the stability and oscillatory motions of ship in the horizontal plane for the case of regular following seas. Analysis of directional stability is made for the case of zero encounter frequency. It was found that at relatively high frequency the rudder and control can give the ship directional stability when it ship located on the wave trough but not when it is located on the wave crest.

As a milestone for the experimental efforts, the detailed theoretical and experimental studies of these phenomena have been conducted by Chou, Oakley, Paulling and Wood [75]. An extensive series of experiments were carried out in San Francisco Bay using large radio-controlled ship models to investigate the large motion behaviour and the occurrence of capsizing of ships in severe following to beam sea conditions. Several modes of capsizing were observed, characterized as loss of static stability, parametric excitation or low cycle resonance and broaching, and a first generation numerical model was developed in an attempt to simulate the observed behaviour. This time domain model was developed specifically for slender ships in severe, following sea conditions, where all six degrees of freedom of motion were considered. As in other large amplitude motion models applied to slender ships, this procedure was based on an extension of linear theory.

Bishop et al, [77] presented the stability calculations of a Series 60 hull. They examined the stability of ship as problem of dynamics. The phenomena of directional instability, broaching –to and capsizing were shown to be related, and this relation was found to be caused by anti-symmetric motions.

Motora et al. [13] carried out measurement of the wave forces in a seakeeping and manoeuvring basin with an X-Y towing carriage. The model of a semi-displacement fishing craft was towed in quartering waves with low encounter frequencies. As a result, measured wave forces in sway and yaw were far from the Froude-Krylov forces. The wave-induced yaw moment calculated with the Froude-Krylov assumption has the maximum value when the centre of ship gravity situates on wave trough. Nevertheless,

the measured yaw moment has the maximum value on the down slope of wave. Although a significant amount of knowledge has been gathered through these experiments, the phenomenon of broaching was not linked to capsize.

Renilson [14], meanwhile, developed his mathematical model on what was described as "true broach" condition. Two sets of constrained model experiments were carried out in order to verify the numerical simulation. In the first one, the model was oscillated using a planar motion mechanism (PMM) whilst remaining in the same longitudinal position in the wave. From the author's aforementioned linearized mathematical model, most derivatives agreed poorly, although most important derivatives of rudder and surge agreed well. The experiment was only carried out for one wave condition. Furthermore, constrained model experiments were carried out in calm water in order to determine the approximate value of the roll coupling terms and it was found that, since they were small, the roll equation could be ignored as a first approximation. However, the tests were only carried out in one heel angle. Therefore, the effect of changing heel angle was not shown experimentally.

Kan [78] also takes into account non-linear effects on phase speed, which leads to higher speeds for the steeper waves with a given period. The interesting results of the model tests displayed that the ship can reach speeds well beyond the (steady) wave phase speed for an extended period.

Umeda et al. [79] and Hamomoto et al. [80] performed a series of free running model experiments to investigate potential capsizing behaviour in stern seas. The experiments were conducted at the seakeeping basin of the National Research Institute of Fisheries Engineering [79] and the square basin of Ship Research Institute [80]. Two models were tested, a purse seiner fishing vessel and a containership. The tests were performed in both regular and irregular seas in various environmental conditions and for a several model heel angles and the speeds. Modes of behaviour that were identified include harmonic and parametric resonance, pure loss of stability, surf riding and broaching-to. In the first report, long crested and short crested waves were investigated and short crestness was proved to reduce capsizing. The experimental results were found to comply with the IMO draft of operational guidance to the master. In the second report, an analytical approach is also adopted in an attempt to compare with the experiments. Regions of behaviour were drawn for surf riding and broaching using a surge, sway and yaw model capable of describing ship motion but not capsize. Numerical results were in agreement with the experimental results.

Umeda et al. [81] carried out model experiments and validated theoretical formulae for the prediction of wave forces in surge, sway, yaw and roll. The model uses a semi-displacement fishing vessel. The experimental results showed good agreement indicating that diffraction components are significant. The theoretical formulation was based on the strip method including some terms for hydrodynamic lift due to free vortices at the aft. Analyses of the results indicated that wave forces remain unchanged if encounter frequency is kept low. Furthermore, up to wave steepness of 0.1 the wave forces were regarded as linear.

Umeda et al [39] proposed a systematic method for assessing intact ship stability with a free running model in a seakeeping and manoeuvring basin. The model experiments were carried out for a model drifting, running in head seas and quartering seas. This method was applied to two purse seiner fishing vessels, and efficiently identified thresholds in metacentric heights for capsizing of these ships. They stated that, model experiments in the steepest regular waves may generally overestimate the danger of capsizing in irregular waves or may represent worst scenario among actual situations. Thus, the use of regular waves is not simply conservative, and the more attention should be paid to experiments in regular waves for more efficient and rational assessment of stability. They found that no capsizing was observed for a model complying with the IMO IS Code if its operation was based on the recommendation of the IMO guidance in following and quartering seas. Their work has been used as a guideline in ITTC studies of intact ship stability.

Meanwhile, as part of joint research effort amongst the navies, De Kat and Thomas III [89] carried out experimental and numerical studies for a steered frigate-type hull in astern waves of moderate to extreme steepness for different loading conditions. They presented the experiments for motions covered surf-riding, broaching, extreme rolling and capsizing. For the surf-riding conditions experiments demonstrated that in contrast to typical conjecture, the ship attains a steady speed once a captured by a wave, the model ship reached speeds well beyond the wave phase speed for an extended period. In cases of broaching, broaching associated with surf-riding with steadily increasing heading deviations and large amplitude, low-frequency yaw oscillations were observed. While, the extreme rolling occurred at high speeds ($Fn \geq 0.3$) in stern quartering waves. They also found that a ship in astern quartering waves of moderate to extreme steepness is subjected to large variations in transverse drift velocities. They compared the experimental results with their numerical model based on linear strip

theory. Although, it showed similar characteristics, its predictions of surf-riding speeds were lesser than experiments for steep wave conditions.

3.6. Key Findings

Recent progress in research towards the ships motions in extreme astern seas and identifying the dangerous situations occur in such motions and capsize is remarkable, as mentioned above.

It was found that a meaningful combination of seakeeping and manoeuvring models would have positive contribution in modelling of complex characteristics of the phenomena. In the context of mathematical models, manoeuvring models with inclusion of hydrodynamic forces on a modular approach are preferred since, although in most studies empirically, it takes the effect of viscous shedding on motions of ship in astern seas into account.

Since early studies began, dangerous situations such as broaching-to have been treated in connection with the loss of directional stability rather than capsize. A direct method for predicting the critical condition has not yet been established for broaching-to, whereas it was established for surf riding of uncoupled system. It was found that this is mainly because stable surf riding is an attractor of the system, and broaching is not. Broaching in regular waves results in capsizing or periodic orbits.

Surf-riding and lateral instability are linked to each other in broaching-to. Consistent with earlier ship operation experience, it is observed that broaching is triggered for all liable vessel at zero encounter frequency, vessel heading relative to the wave between 20°-30°, and wave length to ship length ratio about 2.0. However, the exact mechanism has not been clarified yet. Motora's experimental studies and Munif et al. 's [46] numerical models reinforced those findings. Renilson [14] proposed $\lambda/L \approx 1.0$ and wave height twice the draught. Umeda [93] briefed the studies on dangerous situations in following and quartering seas. As for surf-riding and broaching-to phenomenon, it was claimed that critical velocity for such vessels are not dependent upon hull form and Fn=0.3 was given after analytic and experimental analysis of several type of conventional type of ships. An example is given in Figure 3.1.

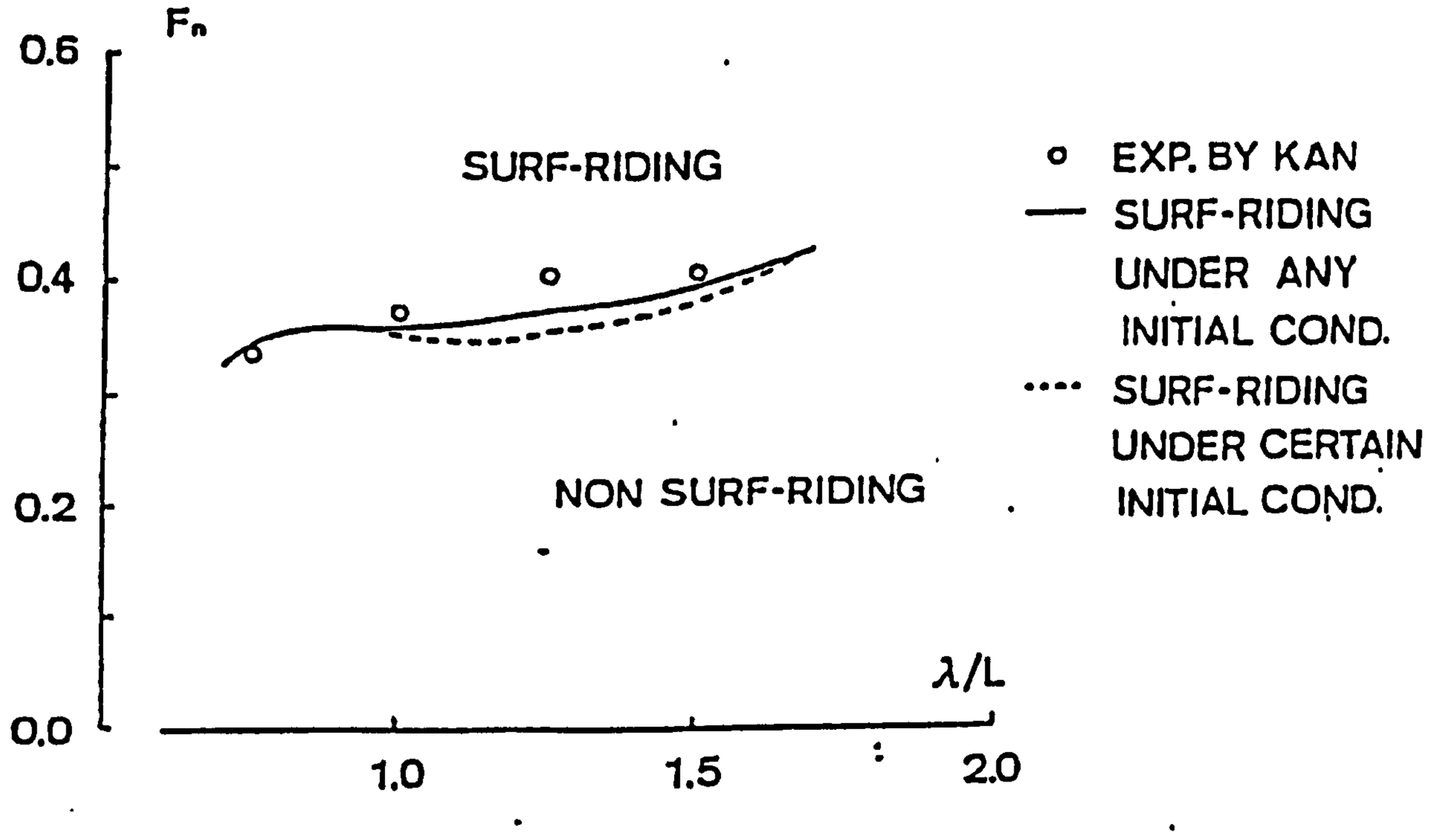

Figure 3.1 Critical Fn number for surf-riding of a stern trawler in a following waves, with respect to wave length to ship length ratio, wave steepness 0.05 ([93])

For the surf riding condition the guidance is given as follows:

$$V(\text{knot}) > 1.8\sqrt{L(\text{metre})}$$

Equation 3.1

Furthermore, in terms of capsizing due to pure loss of stability it is confirmed that GZ curve and roll motion play dominant roles. Umeda [93] gave guidance for the occurrence of pure lost of stability in the context of reducing stability condition and severe rolling condition. Using Beaufort scale B, the reducing stability condition is described as follows:

$$B > B_c$$

Equation 3.2

Here the value of B_c corresponds to the Beaufort scale from the IMO weather criteria where heeling energy "a" equals to dynamic stability "b"(Figure 3 2).

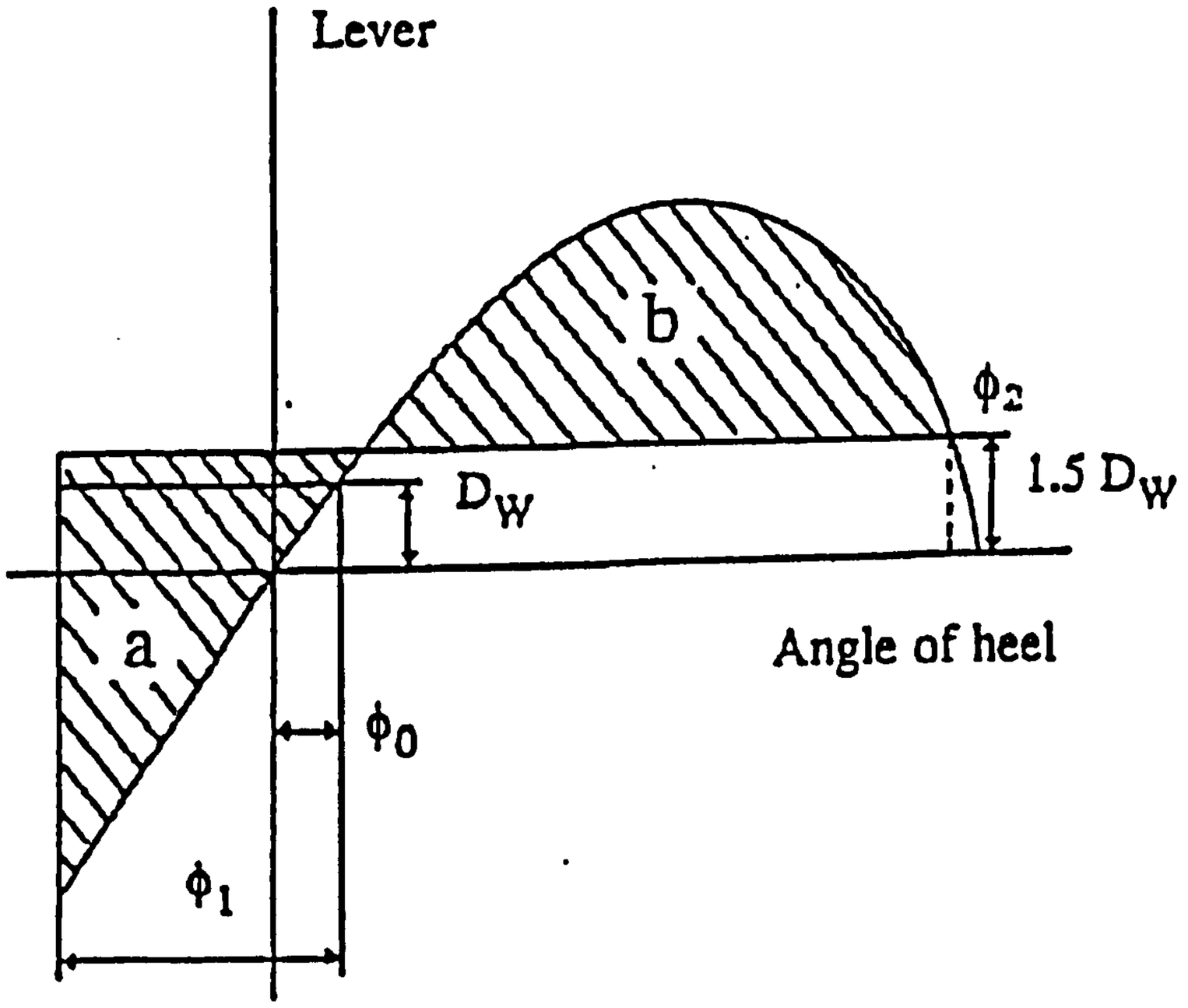

Figure 3.2 Energy balance in IMO Weather criteria

For severe rolling, the condition is obtained as follows:

$$3.03\{1-(T_w/T_\varphi)/0.875\} < V\cos\chi < 3.03\{1-(T_w/T_\varphi)/1.63\}$$

Equation 3.3

where T_w, χ, T_ϕ indicate mean wave period, wave direction from stern and natural roll period with small amplitude. The dangerous zone determined by this formula also illustrated graphically (Figure 3.3).

As result of the series of studies from early eighties to date, a high number of proposals from Europe, USA and Japan were submitted to IMO to establish guidelines for ship's master to avoid dangerous situations in following and quartering seas. Finally, in 1994, IMO Marine Safety Committee issued the guidelines [94] to avoid dangerous situations in following and quartering seas. Stability issues are not directly addressed, however safety in terms of wave parameters and speed are primary objectives and it is practically easy to use (Figures 3.4-3.5).

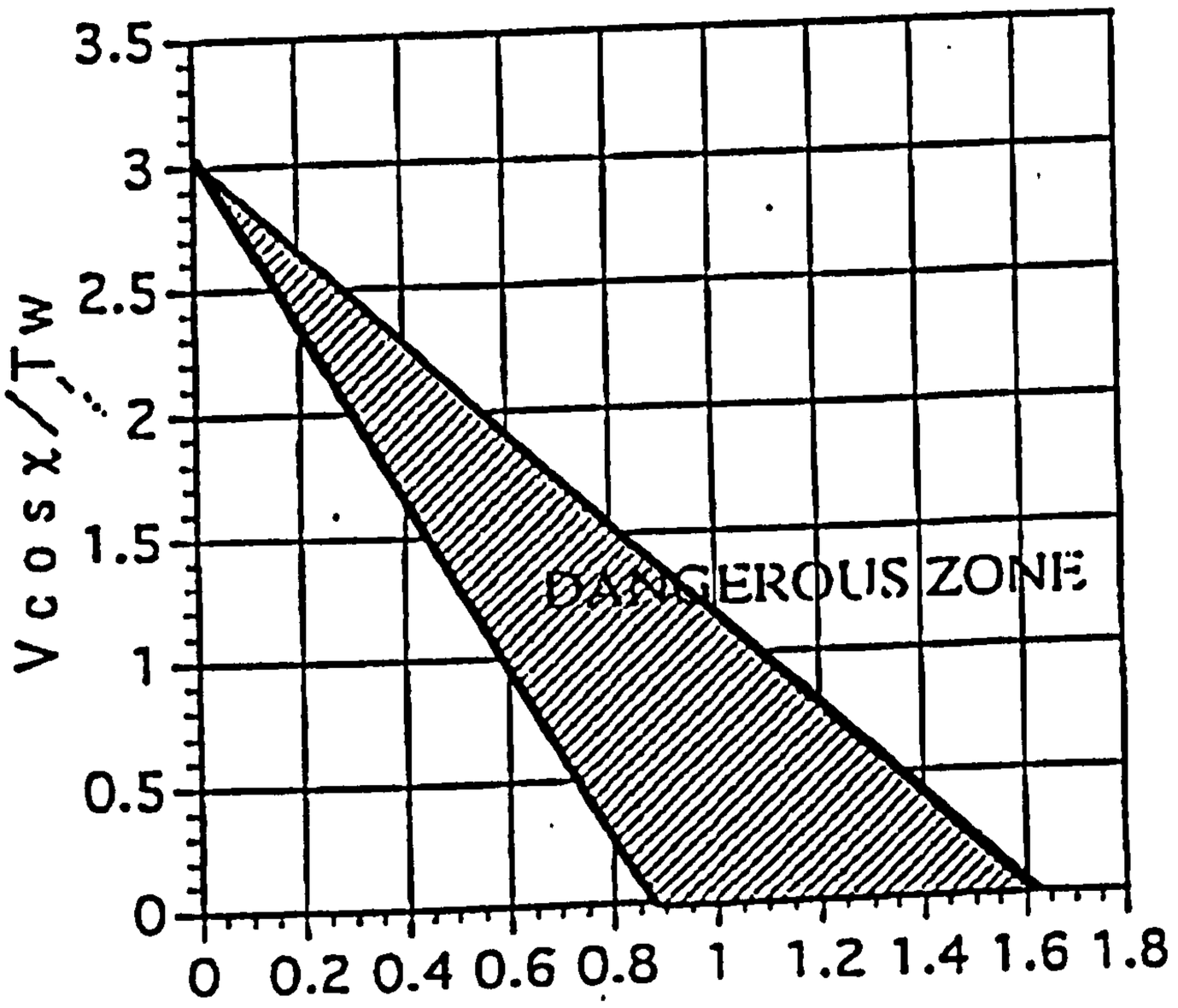

Figure 3.3 Dangerous zone (severe rolling condition) (Umeda [93])

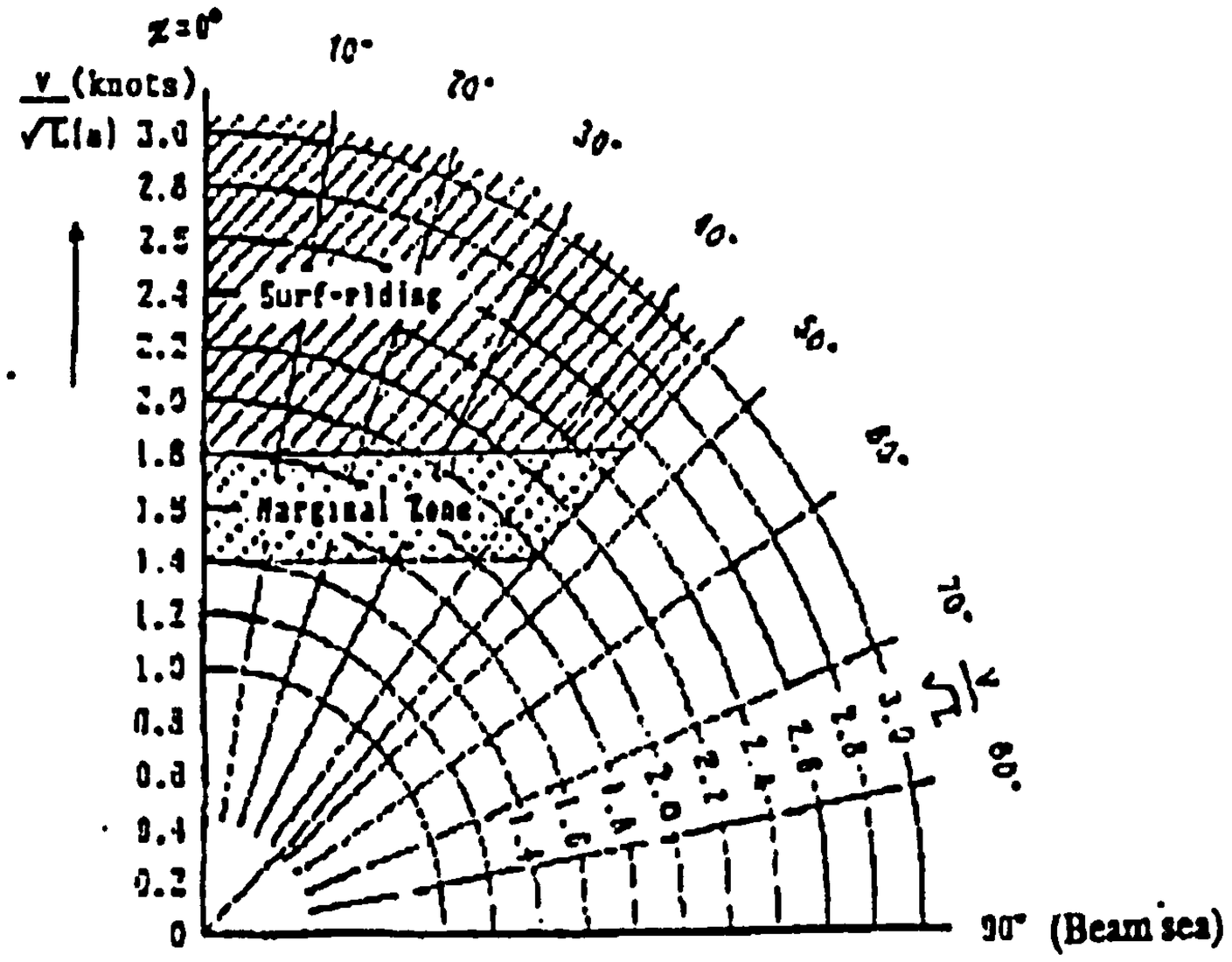

Figure 3.4 Diagram indicating dangerous zone due to surf-riding [94]

Since the above requirements do not include head seas conditions, Germany presented its national guidelines for masters in all sea conditions for determination of coincidence rolling periods and encounter periods at different speeds. The example for a ship (M/V Nautilus, L_{pp}= 117.6 m and maximum speed 16.5 knots) is given in Figure 3.6.

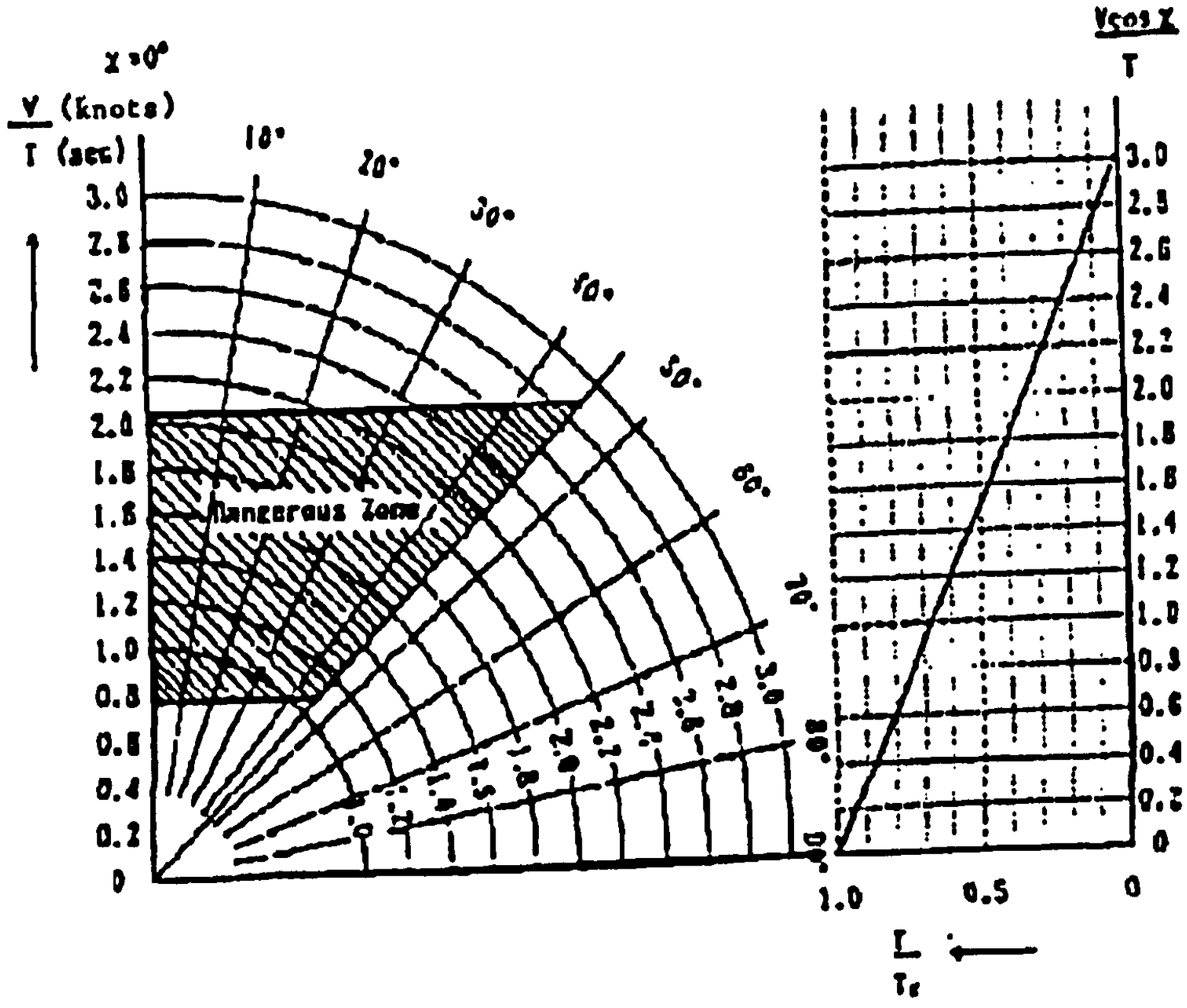

Figure 3.5 Diagram indicating dangerous zone of encountering high wave group and relation between mean wave period and encountering wave period in following and quartering seas [94]

The six degree of freedom non-linear mathematical models are proving to be most robust tools in order to simulate manoeuvring behaviour of vessels in waves. However, in order to overcome complex non-linear problems and to simplify equations of motion, a series of assumptions has been made. These were based on the fact that if the ship advances at high speed, the encounter frequency becomes much smaller than the natural frequency in heave and pitch. Therefore, these motions can be calculated by simply tracing their static equilibrium and equations of motion from which the mathematical models can be reduced to 4 degrees-of-freedom.

The strong coupling caused by the roll motion to sway-roll in horizontal plane was recognized. Experimental studies were carried to investigate these effects in more detail. The one of other interdisciplinary examples is the case of rudder induced rolling, which can be a real problem for fast ships with low transverse stability and high centre of gravity. Although, some cases were reported for big conventional vessels, small vessels such as trawlers were considered more vulnerable to the dangers in such situations.

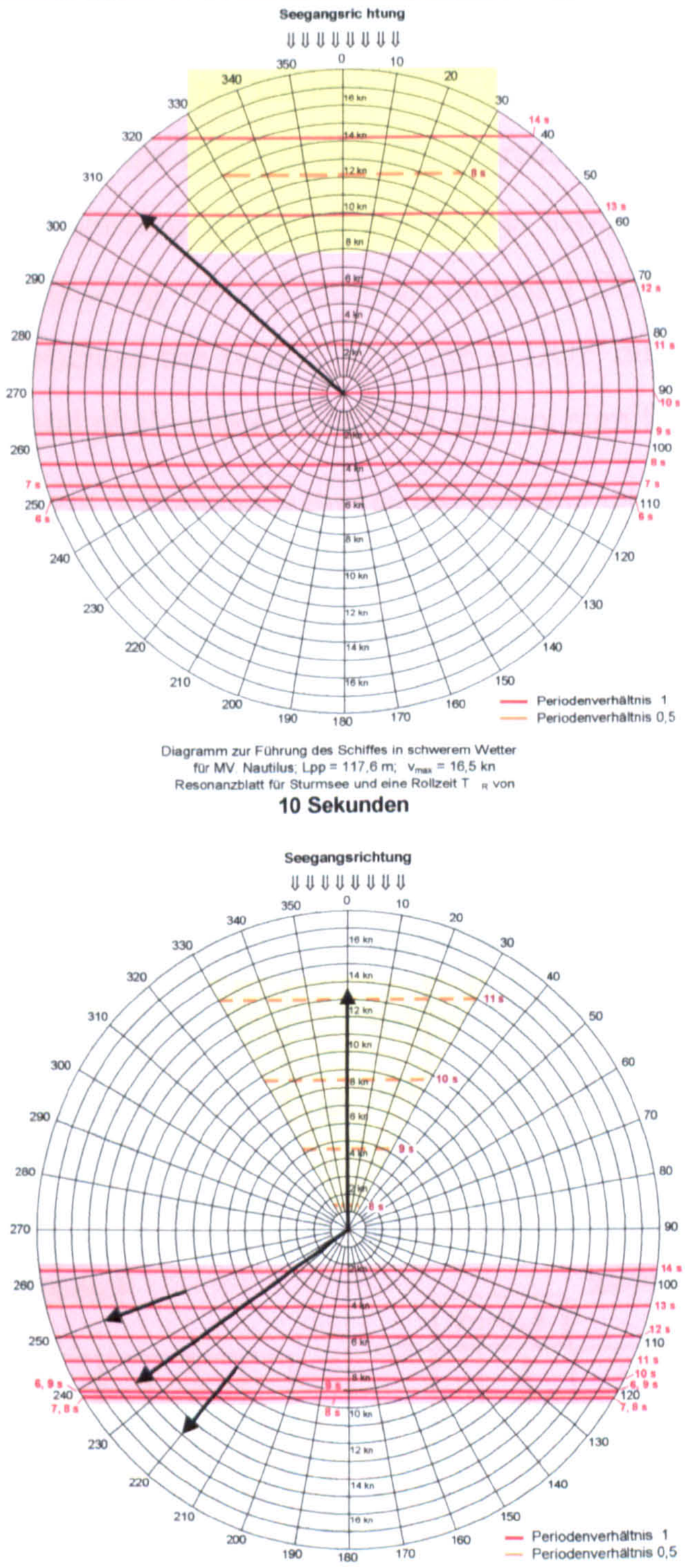

Figure 3.6 Coincidence rolling periods(ratio 1:1) and encounter periods (ratio 1:0.5) in different speed.

As members of the ITTC Specialist Committee on Prediction of Extreme Ship Motions and Capsizing, Umeda and Renilson [95] gave a detailed account of the benchmark study and presented the results. Based on the results of the benchmark study, they investigated the elements affecting the accuracy of the numerical models. Amongst

these, degrees of freedom and frequency effect or so called "memory effect" were seen to be the most important for the container vessel.

From the comparisons of the effect of degrees of freedom, it is concluded that 1 DOF model overestimates capsizing danger whilst it was ascertained that difference between the 4 DOF model ignoring vertical motions, named 4 DOF A, and the 6 DOF model can be significant whereas the results from the 4 DOF numerical model with static equilibrium in heave and pitch, named 4 DOF B, are not significant.

The reason for the small difference is due to the fact that when the ship advances in following and quartering seas the wave excitation frequency becomes much smaller than the natural frequency in heave and pitch. The comparisons along with capsizing boundaries for different wave steepness with respect to autopilot course in different Froude numbers are given in Figure 3.7 from aforementioned study [95].

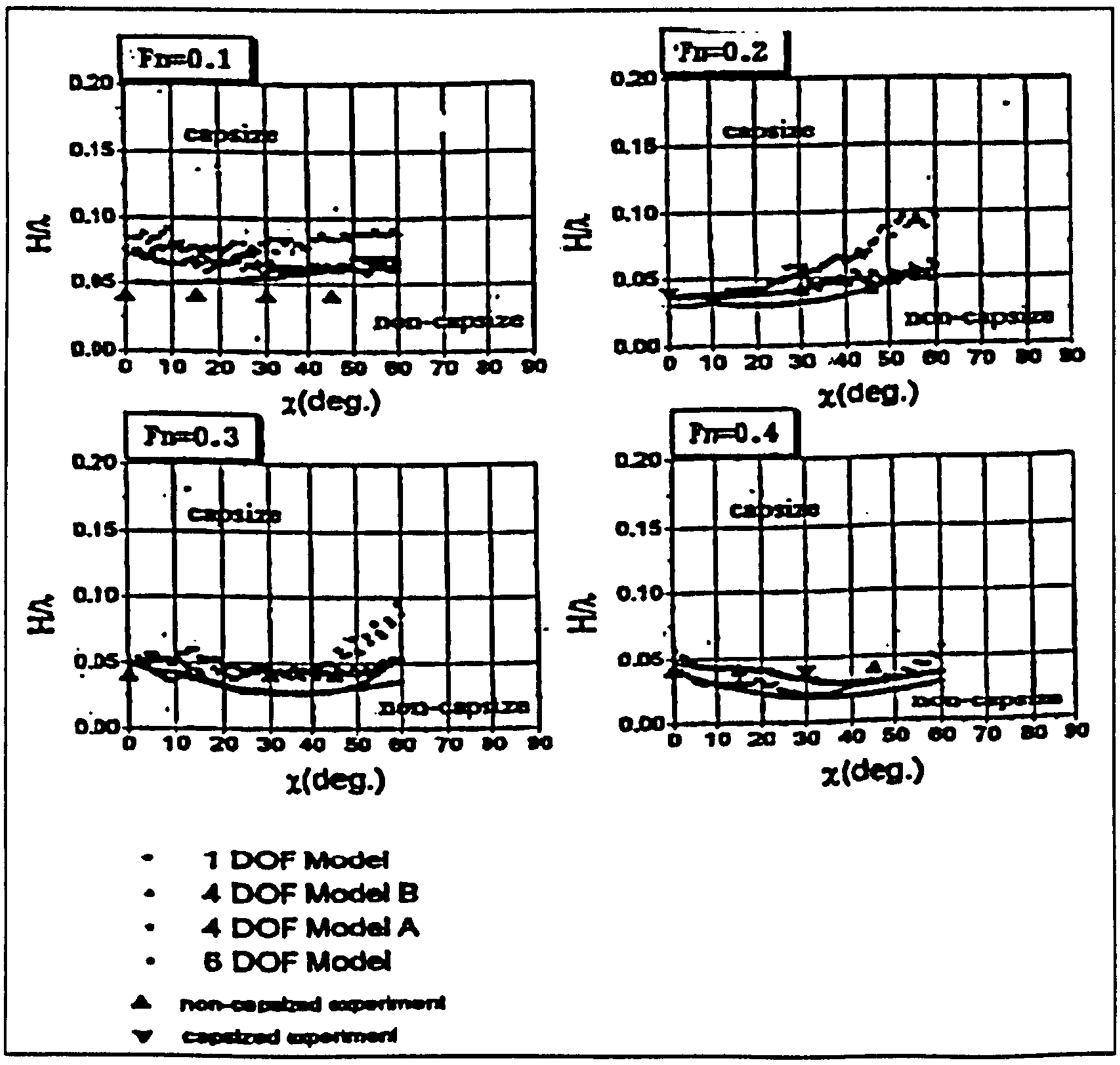

Figure 3.7 Capsizing boundaries of the container vessel with $\lambda/L=1.5$ for different wave steepness (H/λ) with respect to the autopilot course (χ_c) ([95])

The importance of the second aspect concerning hydrodynamic memory effects on capsizing prediction is rather debatable considering that an extreme motion leading to capsizing is non linear and the hydrodynamic forces acting on a ship running in following and quartering seas do not significantly depend on the encounter frequency. However, Matusiak [96] carried out a further study with the container vessel and concluded that the inclusion of memory effects can improve agreement with experiments. The ITTC benchmark review committee urged, meanwhile that the exact calculation of memory effects to be carried out from the start of the waves. Therefore, the ITTC benchmark testing which does not specify initial conditions of fluid motions, is not appropriate for this purpose.

For the wave irregularity, they mentioned that the applicability of numerical models to realistic seaways, that is, short-crested seaways, should be examined. They referred to experimental results indicating that capsizing danger is least in short-crested irregular waves, followed by long-crested and finally regular waves. From a qualitative conclusion wave short-crestedness reduces capsizing danger. However, it was stated that numerical simulations in time domain for capsizing in short-crested irregular waves are very limited.

Notwithstanding the above other important elements to be examined for the vessels in such condition are as follows: Coupling effects from heave and pitch motions, wave effect on roll restoring moment, hydrodynamic lift due to the wave fluid velocity and trapped water on deck.

De Kat et al. [89], meanwhile clarified that wave height to ship length ratio, wave steepness, heading angle, speed, trim, sinkage, varying of metacentric height and the modelling of autopilot were found to be important parameters in dynamic stability of ships in extreme motions.

For this purpose, they carried out test at high speeds in beam seas through following seas of wave steepness between 1/20 to 1/10 and wave length to ship length ratios between 0.75 to 2.50. They have tested the model vessel in three different loading conditions, while two of them satisfied U.S Navy criterion for stability, the one condition failed. The only the model with failed GM capsized in conditions of ship speed at Froude numbers higher than 0.3 in following to quartering seas (heading angle between 0 and 45 degrees).

As part of same study De Kat [86] investigated the effect of irregular waves on capsizing and broaching of a steered, intact ship. In this study, referring to previous

studies in this field, it is emphasized that the characteristic steepness of a seaway tends to be bounded as follows:

$$0.02 < \frac{H_s}{\lambda_p} < 0.05$$

Equation 3.4

Therefore, the maximum steepness is typically less than 0.05, and the steepest sea state occurs when the significant wave height in deep water is typically:

$$H_{s,max} = 0.05\frac{gT_p^{\,2}}{2\pi}$$

Equation 3.5

where T_p is modal period.

The impulse response function presented the fundamental building block describing the fluid-structure interaction mechanisms and contains the inherent dynamic characteristics of the interacting systems. Through impulse response functions any type of motion may be examined. This is believed to become necessary in a general stability analysis. It does not require, a priori, the determination of the values of hydrodynamic data since the value of the fluid actions depend on the type of motion (i.e. sinusoidal, transient) and the form of the excitation resulting from the analysis.

Experimental and theoretical evidence confirmed that a vessel having sinusoidal oscillations with frequency ω_e in calm water experiences forces and moments at this frequency of oscillation. The magnitude and variation of the fluid actions with frequency depends on whether the vessel is surface piercing or submerged. The deeper the vessel below the free surface, the less variation is observed.

Hooft et al. [118] summarised that when the ship is excited at higher frequency motions in waves, by wind gusts, etc. it is observed that damping forces are excited originating mainly from free surface effects which can be described by potential flow theories. Due to these potential theories added mass coefficients as well as the damping coefficients depend on the frequency of oscillation of motion. These potential forces were determined by means of various existing strip theories. However, it was shown later that a major failing of strip theory approaches is their inability to treat adequately

three-dimensional effects. The removal of geometric limitations of slender body theory by an adequate three-dimensional description of the hull enables the interaction effects between various parts of the hull and end effects, which are important for manoeuvring, to be suitably treated. However, Chang [120] showed that agreement of three-dimensional methods in forward speed is not as good as for the zero forward speed.

Although real ocean waves are obviously irregular, experiments with irregular waves should be repeated with many different realizations to obtain statically meaningful results. The number of realizations increases significantly when the probability of capsizing is reasonably small, as it is for most actual ships. Thus, this kind of experiment is not appropriate for the practical purposes. To avoid this difficulty, Takashi [85] proposed the use of encounter group waves, which is nearly, equal to group velocity to principal wave components, for capsizing experiments in irregular waves as the worst scenario. On the other hand, the experimental results up to now have not yet shown clear evidence of a unique mode of capsizing in irregular waves. In most cases, if the maximum amplitude of the wave-maker is limited to a certain value, capsizing in long-crested waves occurs much more easily than in short-crested waves and capsizing in regular waves occurs much more easily than in irregular waves. Takaishi's proposal is also based on the fact that capsizing due to regular excitation is more dangerous than that due to random excitation. In other words, model experiments in the steepest regular waves may generally overestimate the danger of capsizing in irregular waves or may represent worst scenario among actual situations.

More recently, ITTC Specialist Committee on Waves [97] reviewed the studies in this field and stated that although the stability problems in following and quartering seas are often investigated in regular waves, irregular wave conditions should be investigated in detail because the probability of capsize is directly related to the probability of encountering dangerous wave situations. From this point of view, studies on capsizing using steep breaking waves are often carried out in concentric transient waves as one realization of freak waves.

3.7. Concluding Remarks

Based on the cited background and key findings, it is quite obvious that there has been extensively theoretical and experimental research in the field.

Current, state-of-the-art time simulation numerical codes now employ non-linear 6 DOF numerical models while either incorporating the memory effects in regular and irregular waves or hydrodynamic coefficients provided by the experiments. The coupling effects, despite not yet completely understood, are taken into account. Especially, the effect of vertical motions is not yet full investigated. Therefore, in the light of all these drawbacks, it is not surprising that numerical models are still not fully reliable tools for drawing stability and safety guidelines. They usually accompany the experimental studies. Experimental studies, due to the practical limitations, have been used less for irregular waves.

Deriving from this background, it is now required to have a coupled non-linear 6-DOF model with frequency dependent coefficients, incorporating memory effects in random waves. It would also be enhanced by providing straightforward combination between seakeeping and manoeuvring models accounting for extreme motions. This research is led by these required outcomes. An outline of the approach will be presented in the next Chapter.

4. APPROACH ADOPTED

4.1. General Remarks

In the light of previous findings, it was emphasized in Chapter 3 that a coupled non-linear 6-DOF model, in which frequency dependent coefficients are incorporated, is required to simulate manoeuvring behaviour of ships in extreme astern seas and to identify the dangerous conditions that may trigger catastrophic results such as capsizing.

It is also believed that experimental studies along with this mathematical model could play a crucial role offering insights to the design aspects and tackling stability problems that ship may have in terms of safety. Previous efforts showed that there is work to be done in both theoretical and experimental studies to improve design and operational aspects of ships. Since they are more vulnerable small vessels like trawlers should be particularly considered, in order to bring safety guidelines and resolutions to more satisfactory level.

Following these outcomes, this chapter presents the approach of work which is undertaken in this thesis towards the achieving the above goals. Within the context of the following sections, each of these aspects of the approach is outlined. First, a framework of the approach is given. Then, key aspects of the approach are presented. The chapter is concluded with remarks on the adopted approach.

4.2. Framework of Approach

As it can be seen from aforementioned remarks, the framework of approach can be represented in 3 phases.

- Developing the mathematical model for the simulation of ship motions
- Validation and Parametric investigation of the developed numerical model
- Experimental studies

In the first phase, an improved coupled non-linear 6 DOF mathematical model is developed that can be used for identifying the dangerous situations encountered by ships that travel in following and quartering seas. A relatively newly proposed Horizontal Body Axis system is used in the effort to have an axis system, which is suitable for extreme motions, and in general to provide the eagerly anticipated combination of manoeuvring and seakeeping models in the simulations of those motions and capsize. As a step forward to extracting the true natures of mathematical models,

the simplifications on the equations of the motion were minimized while the certain aspects such as symmetry were taken into account. Furthermore, first-order convolution terms (so called "memory effects") were incorporated to improve the prediction of the behaviour of the vessel in non-zero frequencies of encounter. The effect of frequency on the mathematical model was exploited whilst testing was based on different variables such as changing of heading angle, speed and wave parameters.

As the second phase of the approach, following the adjustments to the mathematical model, the numerical results of time simulation model were compared against the experimental results obtained in Japan. However, in order to test the model's reliability in a wider spectrum, effect of parameters such as position of ship on the wave, heading, wave steepness and vessel speed are investigated along with comparison of the mathematical model including impulse-response functions with those which use ordinary differential equations including the constant coefficients.

Yet another significant outcome of the review of previous research studies: is the lack of focus on the fully captive model tests, with a view of investigating effect of extreme vertical motions for the fully coupled 6 DOF mathematical models. Also, due to the well-documented facts, the model experiments concerning the effect of frequency concentrated on regular waves. The possibility of dangerous situations such as broaching-to and ultimately capsize were not extensively investigated in irregular waves. Boundaries for the probability of these dangerous situations both in narrow-band and broad-band wave spectrum were limited to cases defined in regular waves. It is necessary that the developed non-linear coupled 6 DOF time simulation models that incorporate impulse response functions should be verified against aforementioned conditions in random waves for a more useful assessment of the accuracy of numerical modelling.

Those revelations are reflected in the approach. Therefore, the third phase is involved with the fully captive model tests and the free running model tests in irregular waves carried out in Japan. A Japanese purse seiner fishing vessel was tested. In captive model tests, the priority was to obtain results in possible extreme conditions within the limitations of the model basin and the model for different trim angle and sinkage and roll angles whilst the model runs were performed in different speed and heading angles. From the free running tests point of view, the priority was to have a realistic wave spectrum to lay foundations to the numerical models in the effort of determining the accuracy of the numerical model which could be used for the detailed research of

boundaries of dangerous situations and capsizing in random waves. The model was run for different speeds and heading angles in both ITTC and JONSWAP wave spectrums.

The detail descriptions regarding those phases of approach are given as follows.

4.3. Mathematical Model

One of the aims of this research study is to obtain an improved numerical model for capsizing involving all degrees of freedom. For this reason the numerical model incorporates non-linear six-degrees-of-freedom coupling of heave/pitch with transverse motions in time-domain and, with no restrictions on the motion amplitudes. Therefore, equations of motion are written with respect to a "horizontal body axes" system which allows more easily the handling of large angles in pitch (measured between the ship's longitudinal axis and the horizontal plane) which may be realised during operation in steep waves. The reasonable combination here is to find such a coordinate system by using the formulae with respect to hydrodynamic forces, which have been developed in the field of manoeuvrability. Especially to describe large amplitude motions in extreme astern seas.

Having agreed on these conclusions, a relatively new coordinate system, Horizontal Body Axis system, is presented for describing the equations of motion of a ship in waves. External forces on a ship are evaluated with respect to the new axis system. During the calculations of incident wave forces, in contrast with the linear Froude-Krylov theory the pressure is integrated up to instantaneous water surface on the hull. This method is strongly suggested and used by many researchers (De Kat and Paulling [24], Hamamoto et. al. [20], Ankudinov [62] and Chapman [88]) since it enables the calculation of large amplitude ship motions. In essence the most important wave excitation component (Froude-Krylov) is calculated following this approach. Other main components of external forces manoeuvring (hull) forces, rudder forces, propeller and resistance forces, and occasionally wind forces are incorporated in the numerical model. In order to keep the vessel on course, autopilot is used in the real environment. That fact was not ruled out in numerical model and it also includes a proportional-differential (PD) autopilot model. Effect of autopilot and, in particular the effect of autopilot parameters will be discussed.

As it is given previously, one of the important emphasises of this thesis is to present impulse response functions and their implementation in the equation of motions

to investigate how the behaviour of the ship is influenced by the consideration of the frequency-dependence of the hydrodynamic coefficients. Also, wave effects associated with the unsteady motion of the hull at the free surface and vortices which are shed from the oscillating hull, especially when a ship has very large heading angle, indicates that the convolution terms ("memory effects") should be taken into account. Those convolution terms will be incorporated in order to improve the prediction of the behaviour of the vessel at encounter frequencies which are not very near to zero in terms of radiation forces. Effect of convolution terms in the simulation of these motions against to the commonly used "zero-frequency" coefficients will be shown. Impulse-response tests are required for this, while for a purely theoretical prediction, at this stage, the frequency-dependent coefficients are derived within the limits of potential theory. The numerical code will be used to present the results from the developed numerical model. Following the validation and parametrical investigation of the numerical model, as the final step, the numerical model is expressed in irregular waves using the model developed in The Ship Stability Research Centre [138] for seakeeping studies. In this context, the focus is to give the details of the numerical model and its components.

4.4. Numerical Studies

After having obtained a non-linear 6 DOF numerical model and the computer tool to simulate the numerical model, a two-part investigation will be carried out. First, the validation of the numerical model against the experiments carried out in Japan with a fishing vessel and a container ship, for which the details are given, will be attempted in order to have objective assessment of the developed numerical tool. While using the environmental conditions of experiments, first account of the investigation concerning the accuracy and reliability of the numerical model within the boundaries of experimental conditions will be given. Continuing from this stage, the numerical model via the code developed, will be extensively investigated using the parameters that effect ship motions in astern seas conditions such as wave steepness, wave length to ship length ratio, speed, heading angle and position of ship in waves for the same vessels. Throughout those parametric studies, the focus will be on: 1) the effect of the equations of motions based on the new axis system and 2) the frequency dependent coefficients. The comparisons will be made for the incorporation of those aspects in the tool against

the existing numerical models in regular waves. Those investigations will draw the boundaries for the accuracy and reliability of the numerical code in wider scale for the simulation of ship motions in extreme astern seas. Also, the feedback from the experimental studies will be provided to modify the numerical code, if it is found to be necessary, in terms of contributing the accuracy and the robustness of the numerical tool.

4.5. Experimental Studies

First, the results of the captive and free running model experiments carried out in Japan in order to validate the numerical model in all 6 DOF and extreme random seas will be presented. Extensive captive and free running model experiments were carried out at National Research Institute of Fisheries Engineering, Japan for 712 tonnes Japanese fishing vessel which operates in Pacific Ocean. The captive model experiments were carried out while model was fixed in 6 DOF. Hence, it was aimed to observe effect of large vertical motions to the manoeuvring and course-keeping behaviour of the vessel in extreme astern seas. Following the same purpose, the free running model experiments were carried out in random seas using both ITTC and JONSWAP spectrum. The captive model experiments carried out for different speed, heading angle, sinkage, trim angles and, in some cases, different wave steepness. Extremity of the conditions of model runs will be defined within limits and strength of model that was used for these experiments. The free running model experiments were carried out in different frequencies, speed and heading angle in ITTC and JONSWAP spectrums.

Having completed those experiments, the further validation will be made between the experiments and the numerical model to have full understanding in terms of reliability of the numerical tool in 6 DOF for extreme regular and random seas conditions. The links will be exploited between the design parameters and their effects on the dangerous motions and capsizing of the vessel in the light of the comparisons performed. Additional terms will be integrated to the numerical model in the aforementioned attempt to enhance its ability to simulate extreme ship motions in astern seas.

4.6. Discussion and Further Development

In the light of the outcomes of those phases, the discussion on the developed numerical tool will be given. The highlights of the important findings in parametric and experimental investigations will be presented. The conditions that could lead the dangerous situations and the improvement on the modelling those situations will be identified with courtesy of the results. In addition, the areas in which further research could lead to enhanced reliability of the numerical tool will be assessed.

The following Chapters will be devoted to the presentation of the progress achieved along the above lines.

5. MATHEMATICAL MODEL

5.1. General Remarks

One of the aims of this research study is to obtain an improved numerical model for capsizing involving all degrees of freedom. For this reason the numerical model incorporates non-linear six-degrees-of-freedom coupled motion equations in the time-domain, with no restrictions on the motion amplitudes. Therefore, the objective of this chapter is to write the equations of motion with respect to a new "horizontal body axes" system which handles more easily large angles in pitch (measured between the ship's longitudinal axis and the horizontal plane) which may be realised during operation in steep waves. The aim is to find such a coordinate system by using the formulae with respect to hydrodynamic forces, which have been developed in the field of manoeuvrability. Especially to describe large amplitude motions in extreme astern seas. Furthermore, the chapter aims to demonstrate a formulation for the calculation of the major excitation forces concerning the ship travelling in extreme astern sea environment.

A new coordinate system, Horizontal Body Axis system, is presented for describing the equations of motion of a ship in waves. External forces on a ship are evaluated with respect to the new axis system.

Within the above framework the following sections of the chapter present the formulation of the proposed new set of motion equations and the associated terms in the equations. This is followed by presentation of the external forces which are placed on the right hand side of the equations of motion. They include wave forces, through incident and diffraction components, manoeuvring (hull) forces, rudder, resistance, propulsive, wind forces and the autopilot which is used in control of the rudder. Since, the numerical solution of wave forces is validated with model experiments previously, the numerical simulations in various sea conditions for wave forces are presented under Chapter 10.

5.2. Equations of Motion

The aim, here, is to obtain the equations of motion using a reasonable combination describing the manoeuvring motions in a new axes system in which the origin is located at the centre of gravity.

As it is stated in previous chapters, seakeeping and manoeuvrability are both specialised hydrodynamic branches dealing with ship motion in the sea, but the methods used to predict these motions are quite different. Theoretical seakeeping studies which treat wave excitation from seaway are usually based on rather sophisticated mathematical techniques, although most practical results are obtained using linearized methods. Although such analyses have led to remarkable results, there are basic difficulties in using linearized methods. Commonly such methods ignore significant viscous effects, and the influence of rudders, propellers, stabilization and autopilot devices.

Based on above background, in order to provide a meaningful combination of seakeeping and manoeuvring, the equations of motions are expressed in terms of a Horizontal Body Axes system. The Horizontal Body Axes, which are closely related to, but not a special case of General Body Axes, is quite a common system which has been used in many other studies of ship manoeuvring that include roll [21], in studies of manoeuvring motion of ships in waves especially for the study of capsizing motion, [20], [25]. [26], and for studies of the dynamic stability of ships in following and quartering seas, [28].

Horizontal body axes are obtained by the rotation of the earth fixed axes about the vertical axis. In general, the equations of motion of a ship are described with respect to the inertial coordinate system. In deriving the basic equations of motion, we make use of three different coordinate systems as shown in Fig. 5.1. The first is an Earth fixed system, defined by 0-ξηζ. The second is a general body axes which is fixed in the ship with the origin G being located at the centre of gravity of the ship defined by G-xyz. The third is the Horizontal body axes fixed in the ship with the origin at G and defined by G-x'y'z'.

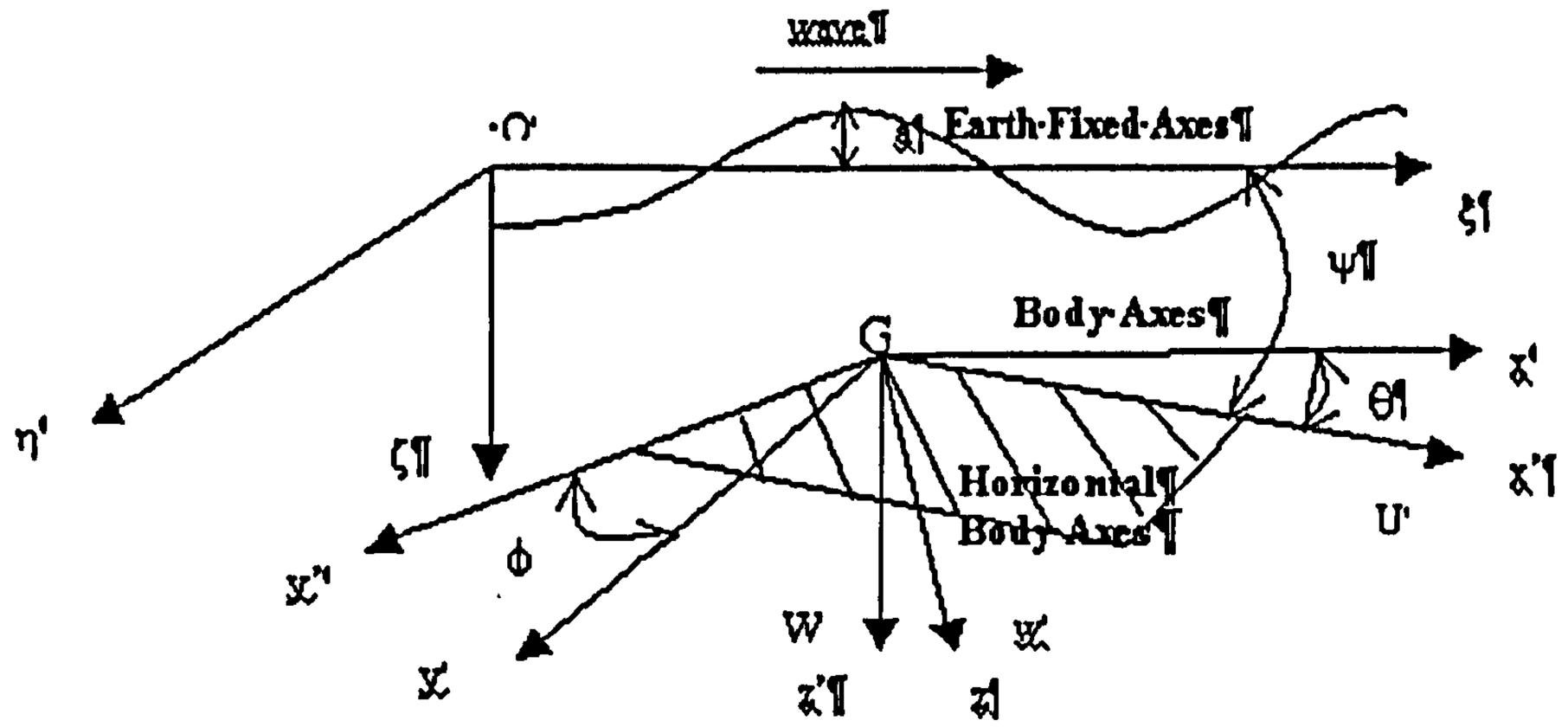

Figure 5.1- Existing coordinate systems

Notice that in contrast with conventional methods, no assumptions made of a small pitch angle and the motions will be solved for large amplitudes. Thus results will be obtained from the non-linear equations.

In the light of above facts, from Newton's second law of motions, equations of motion were obtained. The details are given in Appendix A. Here, considering force and moment components, the force and moment will individually be divided into components:

$$\begin{aligned} m(\dot{U} - V\dot{\Psi}) &= X' \\ m(\dot{V} + U\dot{\Psi}) &= Y' \\ m\dot{W} &= Z' + mg \end{aligned}$$

Equation 5.1

and moment:

$$\begin{aligned} &\frac{d}{dt}\left(I_{x'x'}\dot{\Phi} - I_{x'y'}\dot{\Theta} - I_{x'z'}\dot{\Psi}\right) - \dot{\Psi}(I_{y'y'}\dot{\Theta} - I_{y'z'}\dot{\Psi} - I_{y'x'}\dot{\Phi}) = K' \\ &\frac{d}{dt}(I_{y'y'}\dot{\Theta} - I_{y'z'}\dot{\Psi} - I_{y'x'}\dot{\Phi}) + \dot{\Psi}(I_{x'x'}\dot{\Phi} - I_{x'y'}\dot{\Theta} - I_{x'z'}\dot{\Psi}) = M' \\ &\frac{d}{dt}(I_{z'z'}\dot{\Psi} - I_{z'z'}\dot{\Phi} - I_{z'y'}\dot{\Theta}) = N' \end{aligned}$$

Equation 5.2

or putting Equation 5.2 in matrix form :

$$\begin{bmatrix} H_{x'} \\ H_{y'} \\ H_{z'} \end{bmatrix} = \begin{bmatrix} I_{x'x'} & -I_{x'y'} & -I_{x'z'} \\ -I_{y'x'} & I_{y'y'} & -I_{y'z'} \\ -I_{z'x'} & -I_{z'y'} & I_{z'z'} \end{bmatrix} \begin{bmatrix} \ddot{\Phi} \\ \ddot{\Theta} \\ \ddot{\Psi} \end{bmatrix} + \begin{bmatrix} \dot{I}_{x'x'} & -\dot{I}_{x'y'} & -\dot{I}_{x'z'} \\ -\dot{I}_{y'x'} & \dot{I}_{y'y'} & -\dot{I}_{y'z'} \\ -\dot{I}_{z'x'} & -\dot{I}_{z'y'} & \dot{I}_{z'z'} \end{bmatrix} \begin{bmatrix} \dot{\Phi} \\ \dot{\Theta} \\ \dot{\Psi} \end{bmatrix}$$

Equation 5.3

Expanding the above matrix equation, equations of moment can be derived. In order to simplify these equations the following expressions are used. Substituting P for $\dot{\Phi}$, Q for $\dot{\Theta}$ and R for $\dot{\Psi}$, representing the angular accelerations, the moment equations will be

$$\begin{aligned} m(\dot{U} - VR) &= X' \\ m(\dot{V} + UR) &= Y' \\ m\dot{W} &= Z' + mg \end{aligned}$$

Equation 5.4

$$K' = (I_{yy} - I_{xx})\left[\sin 2\theta\left(QP + \frac{1}{2}\dot{R}\right) + \cos 2\theta\, QR\right] + (I_{xx}\cos^2\theta + I_{yy}\sin^2\theta)\dot{P} - I_{yy}RQ$$

$$M' = (I_{yy} - I_{xx})\left[\sin 2\theta\left(\frac{1}{2}R^2\right)\right] + (I_{xx}\cos^2\theta + I_{yy}\sin^2\theta)RP + I_{yy}\dot{Q}$$

$$N' = (I_{xx} - I_{zz})\left[\sin 2\theta\left(Q.R - \frac{1}{2}\dot{P}\right) - \cos 2\theta\, QP\right] + (I_{xx}\sin^2\theta + I_{zz}\cos^2\theta)\dot{R}$$

Equation 5.5

where X′, Y′, Z′, K′, M′, N′ are surge, sway, heave, roll, pitch, yaw external forces and moments. U, V, R are surge, sway, heave linear velocities, Q, P, R are roll, pitch, yaw angular velocities in horizontal body axes system and I_{xx}, I_{yy}, I_{zz} are roll, pitch, yaw moments of inertias, respectively. The above equations contain 12 variables. However, because of the non-linearity of moment equations, those equations need to be solved by using some computer numerical methods. The aforementioned variables are defined as follows:

$$
\begin{aligned}
&1)\ x' \\
&2)\ y' \\
&3)\ z' \\
&4)\ \dot{U} = g_1(U,V,W,P,Q,R,x',y',z',\varphi,\theta,\psi,X',t) \\
&5)\ \dot{V} = g_2(U,V,W,P,Q,R,x',y',z',\varphi,\theta,\psi,Y',t) \\
&6)\ \dot{W} = g_3(U,V,W,P,Q,R,x',y',z',\varphi,\theta,\psi,Z',t) \\
&7)\ \dot{P} = g_1(U,V,W,P,Q,R,x',y',z',\varphi,\theta,\psi,K',t) \\
&8)\ \dot{Q} = g_2(U,V,W,P,Q,R,x',y',z',\varphi,\theta,\psi,M',t) \\
&9)\ \dot{R} = g_3(U,V,W,P,Q,R,x',y',z',\varphi,\theta,\psi,N',t) \\
&10)\ \dot{\varphi} = \frac{P}{\cos\theta} \\
&11)\ \dot{\theta} = \dot{\Theta} \\
&12)\ \dot{\psi} = R + P\tan\theta
\end{aligned}
$$

Equation 5.6

or in a matrix form along with rudder angle and position on waves, that will be discussed in next sections,

$$X:(\zeta_a,\xi_G,x',y',z',U,V,W,P,Q,R,\varphi,\theta,\psi,\delta)^T$$

Equation 5.7

where x', y', z' are kinematics, U, V, W are linear and P, Q, R are angular velocities, φ, θ, ψ are Euler angles of rotations, δ denotes rudder angle, ξ_g and ζ_a represent horizontal and vertical component of wave amplitude respectively. In a more common way, from general seakeeping models, equations of motions in Equations 5.4 and 5.5 can be written as:

X: State Vector $x \in |R''$

$$(M+A)\ddot{X} + B(X)\dot{X} + C(X)X = F(\zeta_w, X, \dot{X}, \ddot{X})$$

Equation 5.8

where, **M** is inertia Matrix, **A** is added inertia matrix, **B** is damping coefficient matrix, **C** is restoring coefficient matrix, **F** is external force vector and ζ_w is wave amplitude.

In Equation 5.8, added inertia and mass, which is proportional to acceleration of the vessel motion, and damping forces, which is proportional to the velocity of ship motion, are dependent on encounter frequency of vessel and restoring forces greatly

influenced by the change of restoring due to waves for the motions in astern seas. Here, issues concerning the frequency dependent hydrodynamic coefficients and effect of wave forces to equations of motions for fully 6 DOF model will be tackled in Chapters 6, 7 and 10. In this Chapter, it is intended to demonstrate mathematical model in terms of fundamental equations of motions and excitation components.

As it is mentioned previously, due to unique nature of ship motions in astern seas, sometimes numerical model can be reduced to 4 DOF with static equilibrium of heave and pitch motions. It could be achieved in Equations 5.4 and 5.5 by simply ignoring the coupling with pitch angle term θ in the equations. Furthermore, in the uncoupled heave force Z' and pitch moment M' the external force and moment only consist of Froude-Krylov force and moments.

Comparisons of traditional and new equations of motion are shown at Table A.1 in Appendix A. Here, external forces, mainly, the wave forces and other hydrodynamic forces on a ship will be evaluated with respect to the new axis system.

Having stated that, we'll now focus on the external forces which are taken place at right hand side of the equations.

5.3. External Forces

When the ship travels in following and quartering seas, several external factors have an influence on the dynamic behaviour. However in this study, wave forces, manoeuvring (hull) forces, rudder and propeller and wind forces will be taken into account in the estimation of the external forces, since they represent the most important components of the excitation. Although, this cannot be considered as an absolute remark since effects such as hydrodynamic drift forces could be included to investigate effects of excitation in a wider range, however it is not covered within the scope of this study. The remarks for the importance of other excitation forces will be given in next Chapters and Appendix B. External forces are estimated using modular approach. The concept of modularity means separate considerations of the forces acting on ship. Each element can be considered as a separate module in mathematical model, with the added requirements that each module is not purely independent in its action but can include the effects of interactions with the other modules representing the total system model for a ship.

The aforementioned external forces in modular form can be given as follows;

$$X' = X_W + X_H + X_{RS} + X_{RD} + X_P$$
$$Y' = Y_W + Y_H + Y_{RD} + Y_P$$
$$Z' = Z_W + Z_H$$
$$K' = K_W + K_H + K_{RD} + K_P$$
$$M' = M_W + M_H$$
$$N' = N_W + N_H + N_{RD} + N_P$$

Equation 5.9

Here, W indicates wave forces and moments, H indicates hull (manoeuvring) forces and moments and radiation forces and moments for vertical motions, RS indicates resistance forces, RD indicates rudder forces and moments and P indicates propeller forces and moments, respectively.

5.3.1. Wave Forces

As well as being an important factor in identifying the safety of vessel and sometimes a major cause in dangerous situations and capsizing, waves can have a significant effect on coursekeeping and manoeuvring of a ship in following and quartering seas. A ship, attempting a steady course in rough seas, experiences wave-induces oscillatory motions in all six degrees of freedom.

According to classical linear theory fluid is assumed to be inviscid and incompressible and the flow is irrotational. Surface tension is neglected and infinite water depth is assumed.

From the relationship of velocity, length and period of waves, the equation for the sinusoidal waves can be expressed as

$$\varsigma = \varsigma_a \cos k(x - V_w t)$$

Equation 5.10

or

$$\varsigma = \varsigma_a \cos(kx - \frac{2\pi}{\lambda}\sqrt{\frac{g\lambda}{2\pi}}t)$$
$$= \varsigma = \varsigma_a \cos(kx - \omega_w t)$$

Equation 5.11

where ζ_a is wave amplitude, ω_w is circular frequency of sinusoidal waves, λ is the wave length, V_w is the wave celerity. The wave number k is:

$$k = \frac{\omega_w}{V_w} = \frac{2\pi}{\lambda}$$

Equation 5.12

From the classical seakeeping theory, wave forces will be considered in two parts; forces induced by incident waves or so-called "Froude-Krylov" forces and forces induced by diffracted waves. Furthermore, the effect of forces concerning motion in random waves is given in Chapter 9. Here, the former part will be presented in following sections.

Froude-Krylov Forces Including Hydrostatic Forces on A Ship

It is emphasised in Chapter 3 that earlier studies in ship motions in extreme astern seas have focused on effect of Froude-Krylov forces assuming they are the major excitation for such motions. Indeed, both experimental and numerical studies confirmed that Froude-Krylov forces acting on surge direction in following and quartering seas can be significant, especially, for investigating dangerous phenomenon such as surf-riding. Furthermore the introduction of the wave profile in to the simulation of such motion was found to be crucial. It is known very well that when motions in extreme following and quartering seas are concerned, there is significant change in restoring moment of vessel due to the wave, also the occurrence of large trim and sinkage during the extreme seas condition would require certain coupling of vertical and horizontal motions and this is done in the form of instantaneous wave surface modelling. For instance, De Kat and Paulling [24] pointed out that linear wave theory applied to large amplitude waves in deep water has been found to yield very adequate results as regards wave profile, water particle kinematics and pressure and in case of the aforementioned important surge forces obtained from integration of pressure gradient over the wetted volume. In steep waves however, pressure gradient may be reduced below the one predicted by Froude-Krylov and this generally leads to lower stability in real motions. Hence, the integration of pressure over instantaneous wave surface is a very common method in the investigation of ship motions in extreme astern seas conditions. Therefore, this is

followed in the present study as well. By applying this method, in contrast to the traditional linear theory, the restoring component given in Equation 5.8 will be calculated under static wave pressure of Froude-Krylov pressure.

The generalized Froude-Krylov force vector is given by integration of pressure in the undisturbed wave system up to the instantaneous wetted surface:

$$\iint pndS = \iint p(H.S.)ndS + \iint p(H.D.)ndS$$

Equation 5.13

The former is static the latter is dynamic wave pressure, they are written as;

$$p_s = -\rho g \varsigma$$
$$p_d = -\rho \frac{\partial \Phi_I}{\partial t}$$

Equation 5.14

where ρ is density and Φ_I is the potential associated with the incoming wave potential. Froude-Krylov forces and moment are written as:

$$F_{F.K} = -\iint pndS$$
$$M_{F.K} = -\iint p(r \times n)dS$$

Equation 5.15

where n is normal vector and r×n is vector fixed with respect to centre of gravity.

In order to evaluate the Froude-Krylov forces two different methods are used. First, pressure is integrated using 3-D panel method and the second is Gauss theorem, [20], [25], while hull is modelled in 2-d. The idea behind the first method is to form the ship hull by panels and calculate the pressure on those panels. The method first introduced to marine studies by Hess & Smith [98], has gained great importance in recent years thanks to high-speed computers. The hull is modelled by plane quadrilateral surface elements. Using quadrilateral or triangular elements can not make a significant differences however Hess et al. [98] pointed out that the use of triangular elements eliminates the so-called "edge-effects" and the choice of point where velocity

and pressure are to be evaluated is not obvious for triangular element. The panel method used in the current study has been based on a modified method as used by Tsangaris [41], Hughes et al. [99].

Here, the point where pressure is to be evaluated is chosen as the mid-point of the quadrilateral element (P). For each panel the intersection points of the wave are calculated and the points defining the hull are interpolated from the points intersecting between wave and hull as illustrated in Figure 5.2.

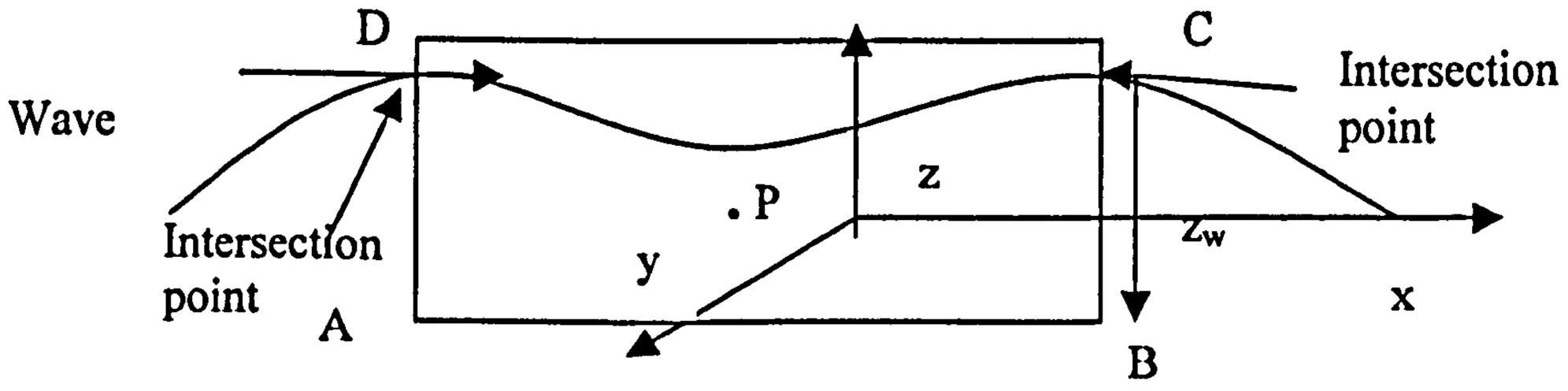

Figure 5.2-Hull panel and intersection with wave

The details of the panel method and its incorporation to the numerical model are given in Appendix F. However, as it is mentioned earlier, one important requirement of the panel method is to use geometrically equally distributed panels. Sometimes it can be difficult to obtain such a hull mesh and for very curved forms, like fishing vessels, inaccuracy of the results obtained from panels may rise due unequal or sometimes overlapping panels of the hull mesh. Therefore, Froude-Krylov forces calculations are carried out using 2-d Gauss theorem. The method is given in Appendix B.

Diffraction Forces

From the previous research given in Chapter 3 and especially experimental studies such as Motora et al [13] indicated wave forces other than Froude-Krylov forces are important during ship motions in astern seaway. In cases, such as broaching-to, when wave yaw moment exceeds rudder moment, there are forces caused by disturbance of the incident waves. Furthermore, when a ship is running in the following waves, she encounters the wave crests with very long period. Traditionally, the strip theory with forward speed [101], [102], has been used for calculation of wave forces

and loads in these waves. However, due to now well-established fact of low encounter frequency in this situation, strip theory could be inadequate to calculate those motions.

Based on the above background, this study follows the method proposed by Ohkusu [16]. In this method effort is focussed on taking into account the effect of waves resulting from the disturbance of the incident waves by the ship. Those waves are supposed to be of higher order than the incident waves and their effect is naturally of higher order than the Froude-Krylov forces. The terms include the effect between the disturbed incident waves and the stationary waves generated when the ship runs on otherwise calm water.

Calculation method and all other details concerning the diffraction forces are presented in Appendix B. Using dynamical pressure on the hull we obtained general wave force equations. For our purpose, we only write disturbance equation as follows,

$$F_{DIF} = \rho U \int_{\Gamma_x} \Phi_D N_j ds$$

Equation 5.16

Here, j=1,2,3 denotes sway, heave, roll respectively, Φ_D indicates the disturbance of waves, and N_j is the normal vector. For the pitch and yaw, values of the heave and sway at each cross section are multiplied by the distance between the cross section and centre of gravity of the ship.

5.3.2. Manoeuvring (Hull) Forces

As it is given in Chapter 3, manoeuvring and seakeeping usually deal with differently motivated situations in terms of steadiness and frequency, however when ship motions in astern seas are concerned, the hydrodynamic matters arise in this unique phenomena and directional stability or more generally course-keeping problems require combined approach of manoeuvring and seakeeping. Directional stability problems are discussed in previous chapters, in order to remind us that, in the hydrodynamic terms, since the encounter frequency is very low, hydrodynamic forces acting on a ship, including wave- induced forces mainly consist of hydrodynamic lift and buoyancy. Wave making effects that depend on the encounter frequencies are negligibly small. Therefore a manoeuvring mathematical model focusing on lift components can be used

in this situation. While the wave steepness is much smaller than 1, the drift angle due to waves is ignored. Having stated those facts, the main question here what type of manoeuvring mathematical model that employs hydrodynamic reaction forces can be used in our numerical model? In the context of manoeuvring hydrodynamic reaction forces consist of ideal fluid forces associated with potential flow theory, first order viscous forces in the presence of hydrodynamic lift forces and second order or higher viscous flow forces associated with cross-flow and separation effects. In terms of the accuracy of a manoeuvring mathematical model, the most crucial element is the accuracy of the hydrodynamic reaction forces. Therefore, a large amount of work in manoeuvring area has been focused on accurate prediction of those forces. These studies could be divided into three types: Theoretical models using potential flow theories, semi-empirical methods and CFD techniques. Background of the evolution of these methods is given in Appendix C.

In our study, we follow the semi-empirical methodology where it is assumed that the fluid forces are uniquely determined at any instant and independent of any other details of the motion except for the geometrical properties of the ship and physical properties of the fluid. Therefore the fluid forces can be expanded as Taylor series in powers of displacements, velocity and accelerations and this leads directly to a set of linear and non-linear terms in the equation of motion. Indeed, it provides a simple mathematical descriptions of the fluid forces, but the force coefficients themselves remain to be determined either through analytical or experimental technique. Therefore, for the calculation of the hull or manoeuvring forces, equations based on the MMG model [112], [113] and [114] and Tasai [115] formulations were used. Surge, sway, roll and yaw, manoeuvring coefficients were obtained from the model experiments in Japan for the vessels used in numerical tests in next Chapters 7,8, 9 and 10. The heave and pitch radiation coefficients were found using Tasai's [115] empirical formulae.

$$X_H = X_{\dot{u}}\dot{u} - Y_{\dot{v}}vr - \frac{u}{|u|}Y_{\dot{r}}r^2 + X_{vr}vr - Res(u)$$

$$Y_H = Y_{\dot{v}}\dot{v} + Y_{\dot{r}}\dot{r} + Y_v vU + \frac{u}{|u|}Y_r rU + Y_{v|v|}v|v| + Y_{v|r|}v|r| + \frac{u}{|u|}Y_{r|r|}r|r|$$

$$N_H = N_{\dot{r}}\dot{r} + N_{\dot{v}}\dot{v} + N_r rU + \frac{u}{|u|}N_v vU + N_{r|r|}r|r| + \frac{u}{|u|}N_{rrv}\frac{1}{U} + N_{vvr}vvr\frac{1}{U}$$

$$K_H = K_{\dot{p}}\ddot{\varphi} + C(\dot{\varphi}) - z_y Y_H$$

$$Z_H = m_z\dot{w}_G + Z_w w_G + Z_{\dot{q}}\dot{q} + Z_q q$$

$$M_H = J_y q + M_q q + M_{\dot{w}}\dot{w}_G + M_w w$$

Equation 5.17

where, X_H, Y_H, Z_H, K_H, N_H, M_H, surge, sway, heave, roll, pitch, yaw hull forces, respectively, Res (u), resistance force, $C(\dot{\varphi})$, damping moment, z_y, vertical coordinate of the centre of action of lateral force. Others represent the acceleration and velocity coefficients and they are described in the Nomenclature section. Detailed description of these formulations can be found in Spyrou [109].

As it can be seen above formulations include acceleration terms, first, second and third order linear and non-linear velocity terms. The added mass and moment terms are taken into left hand side of the equation in Equations 5.4 and 5.5 for the solution matrix described in Chapter 7 and Appendix F. Here, acceleration and velocity terms are estimated independent of frequency, however when frequency dependent added mass and damping terms are incorporated to the motions with convolution integrals, the left hand side of the Equations 5.4 and 5.5 will be linearised. This will be explained in Chapter 6. Furthermore, Equation 5.17 does not include coupling between vertical and horizontal motions. However hydrodynamic terms which result from combined sinkage and rotation occur during heeling and are added to sway force and yaw moment in Equation 5.17 if experimental values are available (They were available for the fishing vessel model but not for the container ship in the numerical simulations). These terms are represented in the first order on the basis of linear sway and yaw velocity coefficients and they are given in Equation C.3 in Appendix C.

5.3.3. Rudder Forces

As an important element of the excitation for ship motions in following and quartering seas, the forces on a rudder, when considered as a separate individual element, can be obtained with the derivation of the lift and drag generated from the rudder, which is essentially vertically oriented lift surface, considered as a wing and oriented at some effective angle of attack to the oncoming, extremely non-uniform flow behind the ship hull and propeller. Therefore, performance of rudder is greatly influenced by the interactions between rudder to hull and rudder to propeller, due to the change of the lift.

Based on the above background, for calculation of rudder forces, Japanese MMG' s (Japanese Manoeuvring Group) model [113] was adopted, including the aforementioned interactions. The rudder forces and moments including rudder-to-hull interaction as follows;

$$
\begin{aligned}
X_R &= -F_N \sin\delta \\
Y_R &= -(1+a_H)F_N \cos\delta \\
N_R &= -(1+a_H(x_H/x_R))x_R F_N \cos\delta \\
K_R &= (1+a_H)z_R F_N \cos\delta
\end{aligned}
$$

Equation 5.18

where, X_R, Y_R, N_R, K_R, surge, sway, yaw, roll rudder forces respectively, F_N, rudder normal force, a_H, rudder–to-hull interaction coefficient, x_H, longitudinal coordinate of the point of action of the rudder to hull interaction force, x_R, z_R, longitudinal and vertical coordinates of the rudder's centre of pressure. The background of the method and some important aspects are given in Appendix C. Furthermore, detailed explanation of those expressions and some useful information of the rudder can also be found in Spyrou [109].

5.3.4. Propulsive Forces

Calculation of propulsive forces is modelled with respect to the thrust system used in the ship whether it is propeller, water jet or the brand new azimuthing pod system. The calculation of propulsive forces therefore is dependent upon accurate

representation of wake, lifting and drag or more generally in the context of propeller-hull-rudder interaction as it is mentioned in the previous section. In the current model, propulsive forces are calculated using formulations in MMG model [113] and Spyrou [109] for the propeller system. All the dependents were obtained from model tests results.

$$X_P = (1-t_p)\rho n^2 D^4 K_T.$$
$$Y_P = \rho n^2 D^4 Y_{p^*}$$
$$N_P = \rho n^2 D^5 N_{p^*}$$

Equation 5.19

where, X_P, Y_P, N_P, surge, sway, yaw propulsive forces, respectively, t_P, thrust deduction at the propeller in forward motion, K_T, thrust coefficient, D, propeller diameter, n, propeller rate of rotation. Y_{p^*} and N_{p^*} are generally dependent upon u/(nP) where P is propeller pitch. Further details and the evolution of the formulations are given in Appendix C.

5.3.5. Resistance Forces

Resistance force is calculated from the model tests results. However, if the model experiments are not available, it could be calculated with the methods such as Holtrop and Mennen [128] or if the certain regression coefficients exist from the model data it could be calculated with below formulation

$$Res(u) = a_0 u + a_1 u|u| + a_2 u^3$$

Equation 5.20

where a_0, a_1, a_2 regression coefficients

5.3.6. Wind Forces

In the present study, effects of wind forces are not investigated in detail due to experimental data for the vessels tested were not available for the validation. However, for the vessels like cruise liners and high speed vessels, wind force effects should be

effectively investigated. Furthermore, due to nature of motions in random waves, those forces could be play significant effects as wind effects are already taken into account in the modelling of wave spectrum. As Spyrou [109] pointed out, wind forces can be modelled by prescribing the forces for any relative to the ship wind direction in the range of 0-360 degrees or by making use of approximate formulae. In our numerical model, following expressions from Aage [116] are used.

$$X_W = -U_{rw}^2 \rho A_X C_X \sin[(9/7)(|\psi_{rw}| - \pi/2)]$$
$$Y_W = U_{rw}^2 \rho A_Y C_Y \sin\psi_{rw}$$
$$N_W = -U_{rw}^2 \rho A_Y X_S C_N \sin(2\psi_{rw})$$
$$K_W = U_{rw}^2 \rho A_Y Y_S C_K \sin\psi_{rw} \cos^2\varphi$$

Equation 5.21

$$U_{rw} = \left[(U_w \cos(\psi_w - \psi) - u)^2 + (U_w \sin(\psi_w - \psi) - v)^2\right]^{1/2}$$
$$\psi_{rw} = \arctan\left[U_w \sin(\psi_w - \psi) - v)/(U_w \cos(\psi_w - \psi) - u\right]$$

Equation 5.22

where, X_W, Y_W, N_W, K_W, surge, sway, yaw, roll wind forces, respectively, C_X, C_Y, C_N, C_K are coefficients depending on ship type, U_{rw} and ψ_{rw} are effective wind speed and angle to the ship, A_x, A_y are maximum longitudinal and transverse projections, X_S and Y_S are longitudinal and transverse coordinates of the centre of wind force, respectively. The details of the formulations and effects of wind forces can be found in Spyrou [109] and Tsangaris [41].

5.4. Autopilot Control

Although, automatic control systems can be regarded as parameter of ship steering and control, as it is well known, the steering mechanism of the ships also provides another external force. In general, the complete steering may be thought as a close-loop servomechanism involving either an autopilot or human in its feedback. This system produces a response in the form of rudder deflection to an input stimulus in the form of heading and the rate of change of heading. Such control system modifies the dynamic response to the waves and under certain conditions may actually result in unfavourable conditions such as broaching-to. In using automatic controls, the tendency

is for the system is to call for high frequency rudder movements that produce increased resistant but have little effect on ship heading. Hence, it is desirable to select appropriate control settings or to minimize unnecessary rudder motions, as done in adaptive autopilots. Following the previous research and experimental set-up use in this study, the standard proportional-differential (PD) autopilot, [41], [117], is employed in order to keep the vessel on course:

$$\delta_R + t_r\dot{\delta}_R = K_R(\psi - \psi_R) + K_P\dot{\psi}$$

Equation 5.23

δ_R is the actual rudder angle, ψ_R is the desired heading angle, K_R is yaw gain constant, K_P is a yaw rate gain constant and t_r is the time constant in rudder activation. Effect of autopilot is discussed in detail in Appendix D.

5.5. Concluding Remarks

In the context of this chapter, aforementioned mathematical model is presented. A new axis system and derivation of new equations of motion are illustrated. Here, it can be seen that new equation of motions are highly non-linear. The solution method and the results will be presented in the Chapter 7.

The modified state of the new equations of motion which includes the effect of frequency and large vertical motions will be described in Chapter 6 and Chapter 9 respectively.

In the calculation of wave forces, a model which has already been verified in previous research, is employed. The Froude-Krylov forces are calculated using instantaneous wave surface since this is non-linear and it also accounts for large motions. Both 3-D and 2-D methodologies are used and brief descriptions have been given. Diffraction forces are calculated using the method developed by Ohkusu [16], which is based on the slender body theory and only applied to low encounter frequency motions such as motions of ships in astern seas.

As is stated in previous chapters, the manoeuvring model is employed to account for low frequency motions in astern seas. Therefore, hydrodynamic reaction forces which are calculated using the empirical method by MMG are used. The hydrodynamic coefficients are obtained from experiments since they are still more reliable than the

theoretical models. The coupling between and vertical and horizontal motions were not taken into account in the modelling but heeling effect on sway and yaw motions are added as the linear sway and yaw accelerations to sway and yaw force and moment equations in the manoeuvring model if the data from model experiments are available. The attempt to include frequency effects and its effect on the manoeuvring models will be mentioned in Chapter 6.

Other external forces (resistance, propulsive, wind) are calculated using empirical models while coefficients are obtained through model experiments. The PD autopilot model is employed. The details on the effect of autopilot will be discussed in Chapter 7 and 8 while the validation of numerical model is presented.

The first main points on the research, herein, are presented. As the next step, the equations of motions and external forces will be incorporated to the Kernel functions to include the effect of frequency. Also, using the feedback from the model experiments the modification to model to improve its accuracy on the large vertical motions will be presented in the next Chapters. However, the model, in the current form, can be used to simulate the motions of ships in astern seas with reasonable accuracy, as it will be shown in Chapter 7.

6. IMPULSE RESPONSE FUNCTIONS (MEMORY EFFECTS)

6.1. General Remarks

The objective of this chapter is to present impulse response functions and their implementation in the equation of motions to investigate how the behaviour of the ship is influenced by the consideration of the frequency-dependence of the hydrodynamic coefficients. Since the frequency of encounter in following seas is quite low, it is currently quite common to use "zero-frequency" constant hydrodynamic coefficients, as it is done in calm-water manoeuvring calculations. However, wave effects associated with the unsteady motion of the hull at the free surface and vortices which are shed from the oscillating hull, especially when a ship has very large heading angle, indicates that the convolution terms (representing the so-called "memory effects") cannot be negligible. Such convolution terms are incorporated in order to improve the prediction of the behaviour of the vessel at encounter frequencies which are not approximately zero. Impulse-response tests are required for this, while for a purely theoretical prediction, at this stage, the frequency-dependent coefficients are derived within the limits of potential theory.

Within the above framework the following sections of the chapter present the concept of convolution terms or so called "memory effects" and the hydrodynamic expression of these terms. This is followed by the numerical solution of Kernel functions. The simple numerical module for this solution is developed and the results are presented for a Wigley model hull, a fishing vessel model and a container model. This is followed by the description of implementation methods of so called "memory effects" in terms of convolution integrals. The calculation method for the frequency dependent hydrodynamic coefficients is briefly described. Some critical aspects concerning the implementation of memory effects are discussed.

6.2. Memory Effects

As discussed in the literature review in Chapter 3, studies on the effect of frequency in ship manoeuvring motions began focusing on manoeuvring in calm water and later were taken into manoeuvring in waves. The manoeuvring motions of a ship in the horizontal plane are governed significantly by the viscosity of the flow, and it is not

surprising that most of the work in this field is semi-empirical. In the standard ship manoeuvring approach it is assumed that the fluid forces are uniquely determined at any instant and independent of any other details of the motion except for the geometrical properties of the ship and physical properties of the fluid. Therefore the fluid forces can be expanded as Taylor series in powers of displacements, velocity and accelerations and this leads directly to a set of linear and non-linear terms in the equation of motion. It does provide a simple mathematical descriptions of the fluid forces, but the force coefficients themselves remain to be determined either through analytical or experimental technique.

However, as Ankudinov [62] and Spyrou [109] indicated, there are fundamental objections to the assumption that the forces are analytical functions of ship geometry and its simple elements of motion. This weakness of ship manoeuvring techniques is well established. It has been shown that at any instant a fluid force is determined in part by previous motion. So-called "memory effects" associated with the effects of the free surface and vortices, respectively, result in the representation of the hydrodynamic forces arising from transient ship motions in terms of a convolution integral over the entire time history of the motion. This situation has been recognised for many years in the field of unsteady aerodynamics and control theory and more recently became of interest to the marine community. Also it has been established that, for standard manoeuvres of a conventional ship in calm water, a frequency dependence of the hydrodynamic forces is not very important, and simplified mathematical model based on Taylor series expansion is justified. When the manoeuvring motion of a ship in a sea is of interest, the influence of the frequency on forces is significant. The "memory effects" have an origin from two sources: 1) Wave effects associated with the unsteady motion of the hull at the free surface, 2) Vortices which are shed from the oscillating hull. Ankudinov [62] indicated that wave frequency dependence should not be confused with Froude number dependency frequency, which is not oscillatory. However, the unsteady wave motions depend on forward ship speed. Both sources of the "memory effects" are definitely functions of the frequencies. Newman [137] defined the characteristics non-dimensional frequency parameter associated with the vortex wake as a reduced frequency $\omega L/g$ while for surface unsteady effects the corresponding parameter is $\omega u/g$. Here, ω is the radian frequency of oscillations, g is gravitational acceleration. For sufficiently small frequencies these two parameters tend to zero and

pseudo-steady-state analysis is valid. Newman's tentative conclusion is that unsteady viscous effects will become significant before those associated with the free surface, especially for slower vessels. This conclusion is important for analysing the experimental results from the captive model tests where both "memory effects" are present. Wave frequency effects could be important not only for ship motions in regular and especially irregular waves, where, theoretically speaking, all frequencies are present, but also, for instance, for a ship with automatic control sensitive to heading and lateral disturbances in calm water.

Based on the theory of a linear physical system, the hydrodynamic force due to an arbitrary motion can be described with the convolution integral of the motion and the impulse response function for hydrodynamic force, as far as linearity of hydrodynamic force is assured. The linearity is manifest with respect to the hydrodynamic force which stems from the velocity potential, as far as the ship's motion is small.

The hydrodynamic force acting on a manoeuvring ship in astern seas includes another kind of hydrodynamic force: hydrodynamic force due to vorticity and circulation, as it is in the manoeuvring in calm water.

Since the effectiveness of linear assumption in the two dimensional and three dimensional theory of wing theory of oscillation is proved [135], it can be anticipated that the hydrodynamic force acting on manoeuvring ship in astern seas satisfies the assumption of linearity, as far as the ship's motion is small. Here, it could be the subject of argument because the motions this study is dealing with have mostly significantly high amplitudes. However, it will be exploited in this study, whether the above point is case for extreme motions as well.

When a body performs an irregular motion around its mean position, it is appropriate to express the hydrodynamic force acting on the body in the time domain. Following the work by Cummins [48] and others, the radiation force in the time domain is written as:

$$F_{ij} = -a_{ij}(\infty)\dot{V}_j - \int_0^\infty K_{ij}(t)V_j(t-\tau)d\tau$$

$$i, j = 1,2,3,4,5,6$$

Equation 6.1

It should be noted that this formulation is based on the linear theory. The retardation (Kernel) function of Eq.6.1 (K_{ij}) is the real part of Fourier transform of the frequency domain damping function. In addition, the retardation can be described in terms of damping as

$$K_{ij}(t) = \frac{2}{\pi}\int_0^{\infty} B_{ij}(\omega)\cos(\omega t)\,d\omega$$

Equation 6.2

where B_{ij} is damping. The equations are standard relations in linear system theory. Cummins showed how they could be derived for ship motions from hydrodynamic considerations. The impulse response function (K_{ij}) will be solved from damping data and the convolution integral (Equation 6.1) then evaluated for each term in the equations of motion at each time step during the simulation.

6.3. Numerical Solution of Kernel Functions

To solve Kernel functions, use is made of the Discrete Fourier transforms (DFT). The DFT is particularly suitable for describing phenomena related to a discrete time series. It can be developed from the Fourier transform of the continuing waveform samples of which are taken to form the time series. Hence, the retardation (Kernel) function for any number of sample values is shown as

$$K_{ij}(t) = \sum_{n}^{N-1} B(\omega)\cos(\omega\, t)\,d\omega$$
$$0 \le n \le N-1$$

Equation 6.3

where $B(\omega)$ is damping coefficient, $d\omega$ is frequency range. Note that the ωt expression can be written by means of general physical description as

$$\omega\, t = \frac{2}{N}\pi\, n\, t(N)$$

Equation 6.4

where t(N) indicates the each time step.

The above methodology model was tested for the Wigley model hull, particulars of which given below. Added mass and damping values in frequency domain were obtained by 3-D potential theory [124].

Main dimensions of Wigley Model	
Fn	0.2
Lentgh (L)	3.0(m)
Breadth (B)	0.3(m)
Draught (d)	0.1875(m)
Trim (t)	0.000
Displacement (∇)	0.0946(m^3)

Table 6.1-Dimensions of Wigley Model Hull

Some results of the computed kernel function in 6 DOF can be seen the graphs given next:

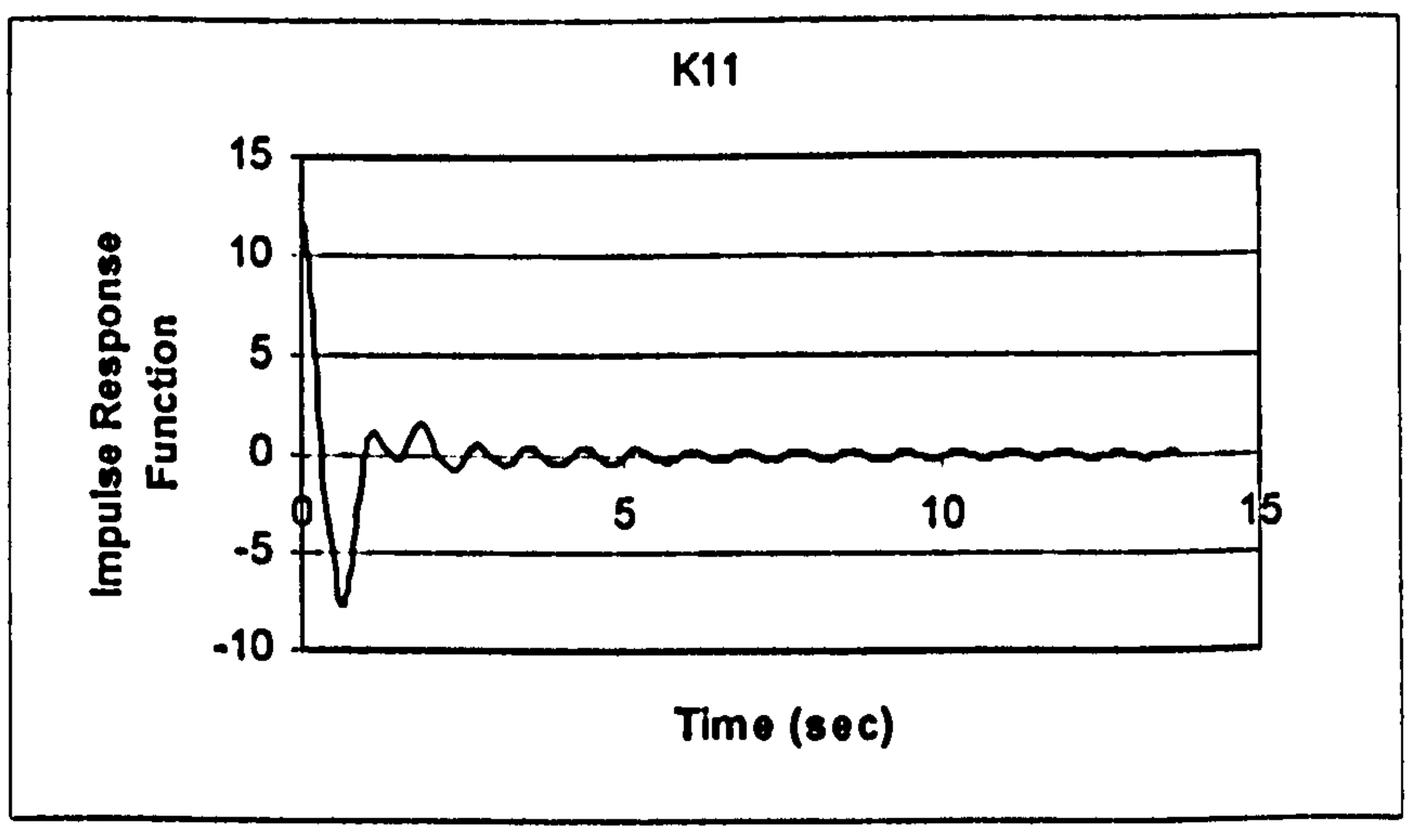

Figure 6.1 Impulse response function of surge motion for Wigley hull (non-dimensional)

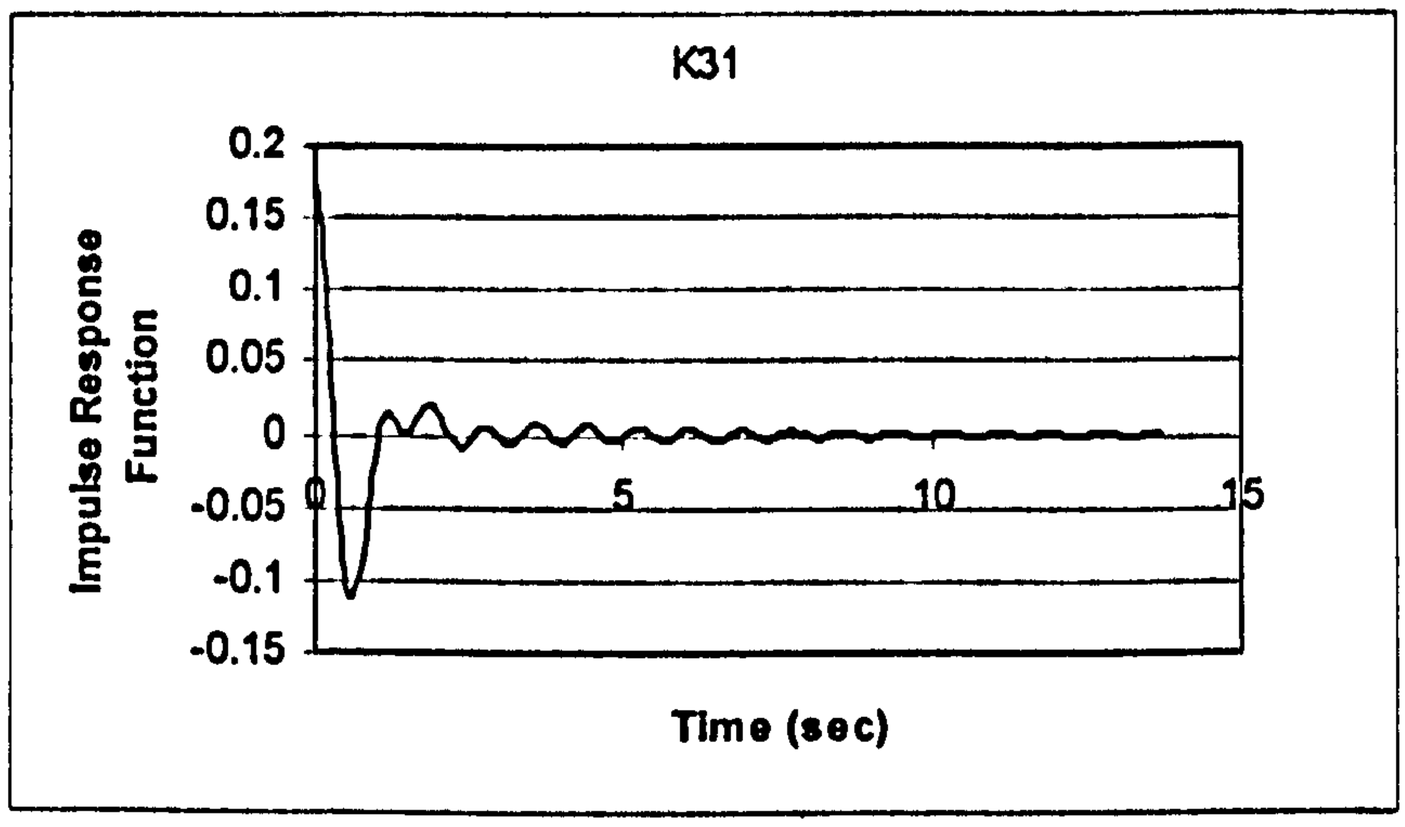

Figure 6.2 Impulse response function of coupled heave-surge motion for Wigley hull (non-dimensional)

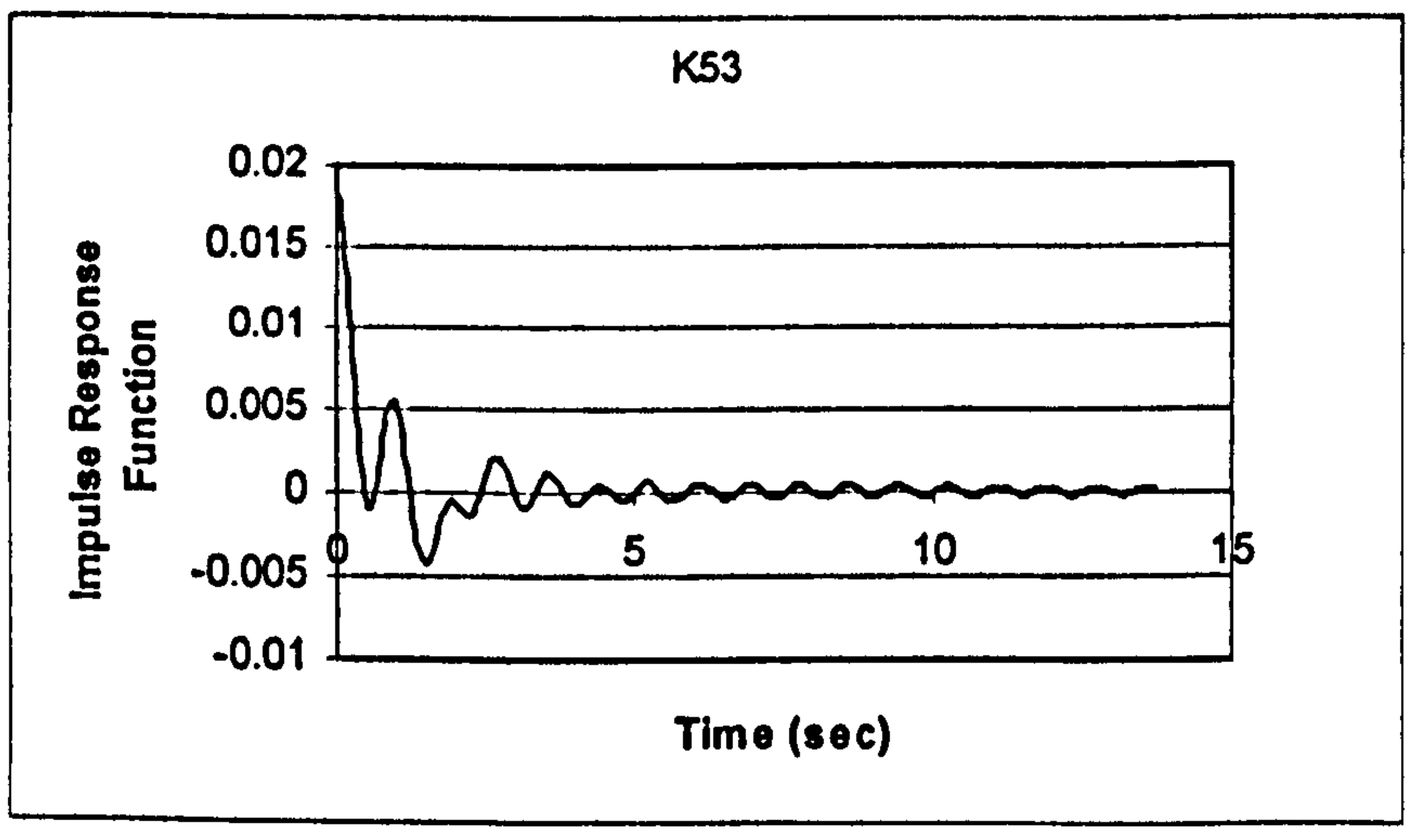

Figure 6.3 Impulse response function of coupled pitch-heave motion for Wigley hull (non-dimensional)

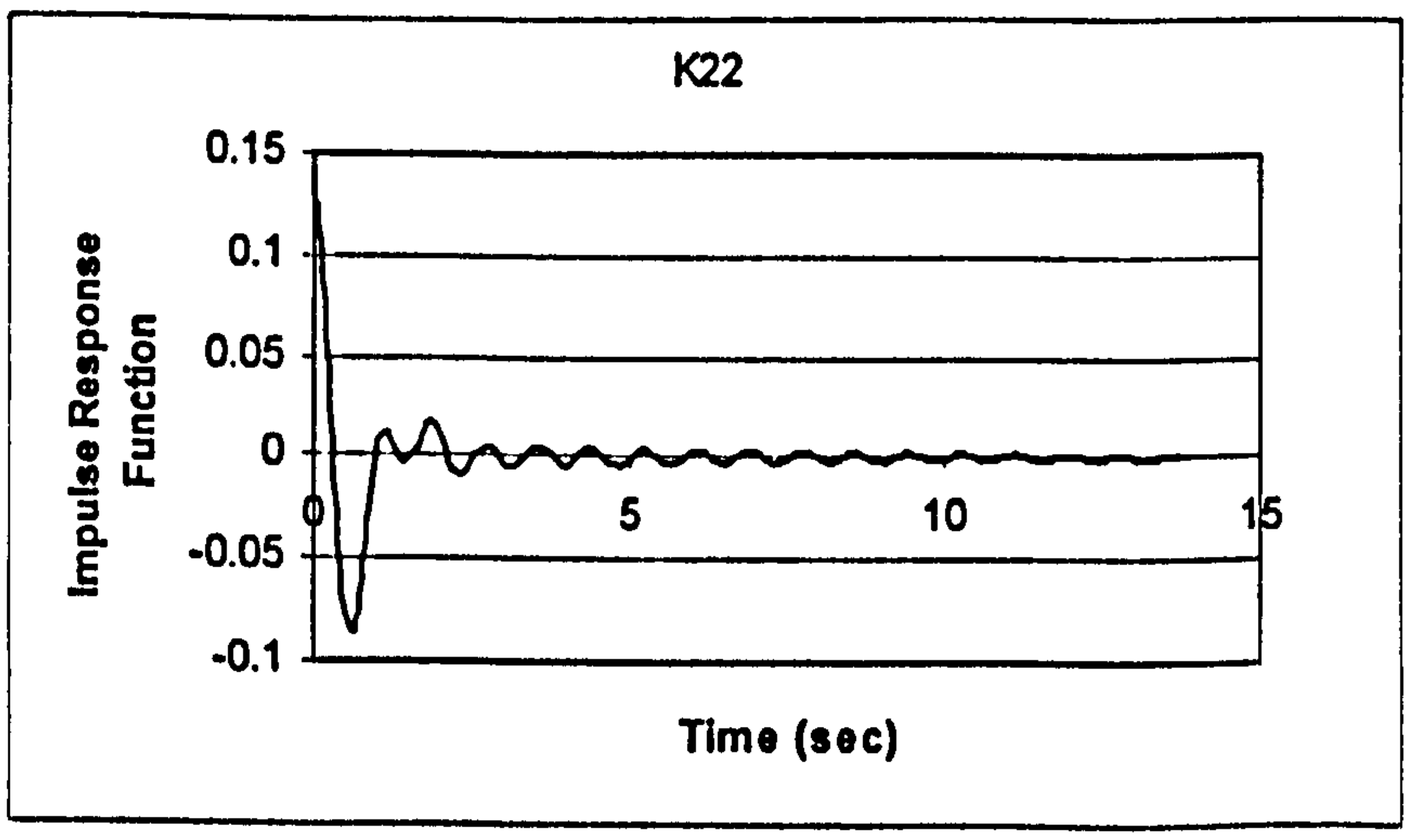

Figure 6.4 Impulse response function of sway motion for Wigley hull (non-dimensional)

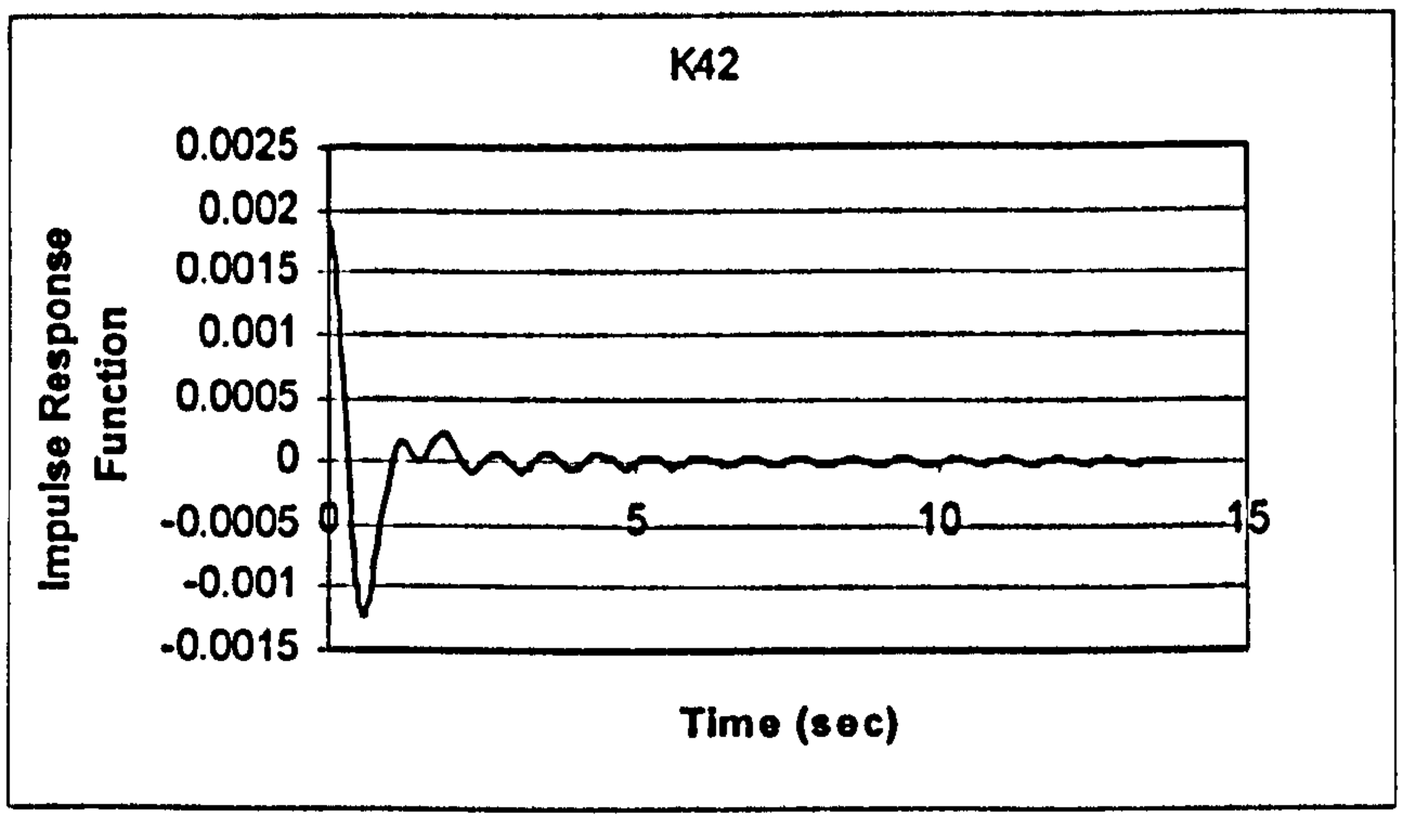

Figure 6.5 Impulse response function of coupled roll-sway motion for Wigley hull (non-dimensional)

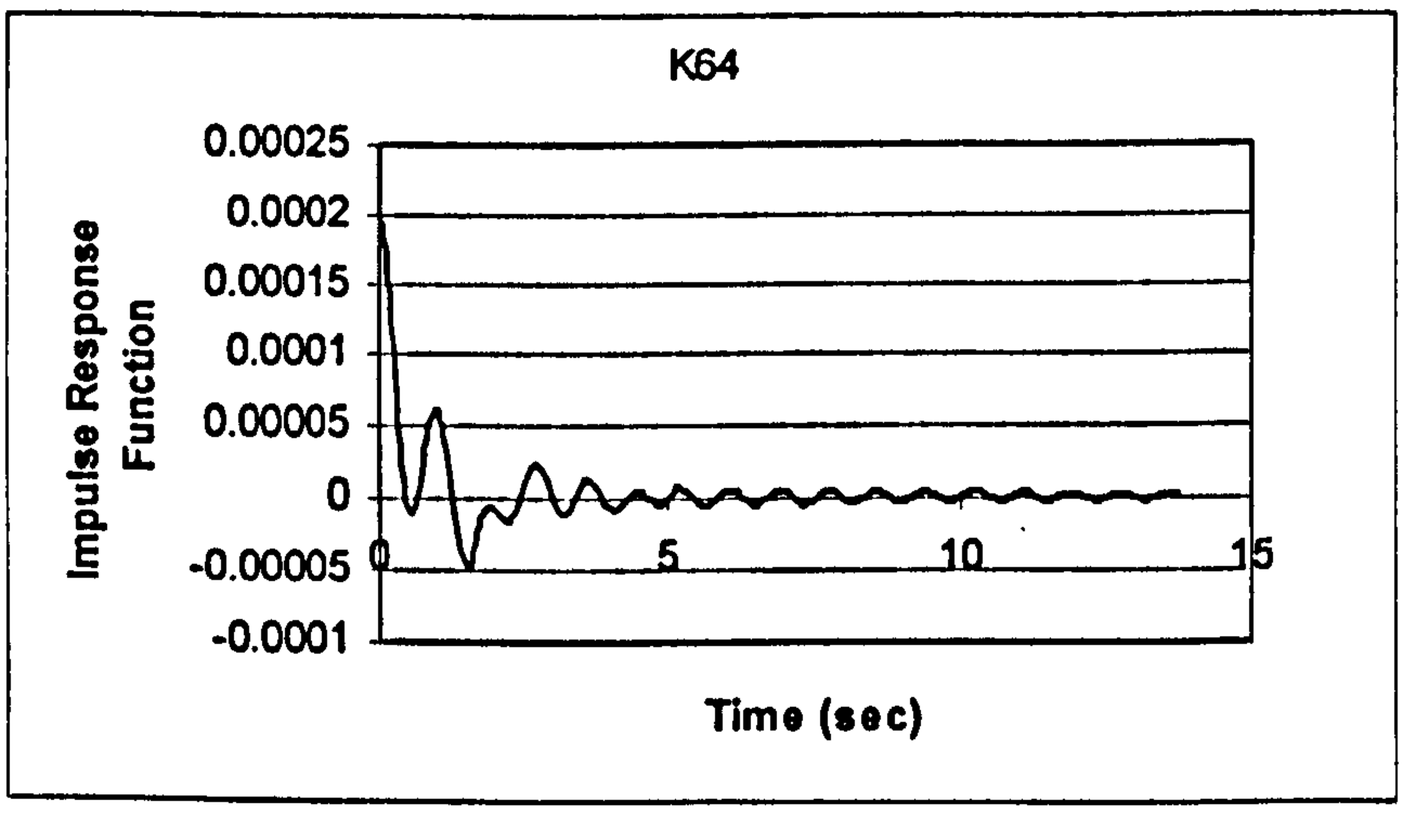

Figure 6.6 Impulse response function of coupled yaw-roll motion for Wigley hull (non-dimensional)

It could be seen from the above graphs that for an impulse, Kernel function produces a response which linearly reaches to maximum about 2 seconds and eventually dies off.

6.4. A Simple Independent Module for Kernel Functions

As mentioned above, first-order convolution terms (so called "memory effects") are being incorporated that would improve the prediction of the behaviour of the vessel in non-zero frequencies of encounter. For this purpose, a simple independent module is developed to compute the retardation (Kernel) function (Equation 6.2) for the ship. These computations are later be incorporated in the equations of motions to investigate the behaviour of the ship in non-zero frequencies. Some of the results of the module are presented in the figures below (See Figure 6.7-6.24) for Purse Seiner fishing trawler and container vessel which will presented in detail in the next Chapter and Appendix E.

Damping values of the ships were by 2-D strip theory [138] in 52 different frequencies with 0.07 range of frequency. In these figures, all the results are non dimensional, for zero heading angle and zero speed. The detail of the 2-D strip theory program and calculation methods will be given in next section. Further and comprehensive details of the calculation method can be found in [138].

Frequency dependent 3D added mass and damping values have been made non-dimensional as follows,

sway, heave

$$A_{22}, A_{33} = \frac{A_{22}, A_{33}(kg)}{\rho[kg/m^3] \cdot \nabla[m^3]}$$

yaw – roll, roll

$$A_{64}, A_{44} = \frac{A_{64}, A_{44}[kg/m^2]}{\rho[kg/m^3] \cdot \nabla[m^3] \cdot (B[m])^2}$$

pitch, yaw

$$A_{55}, A_{66} = \frac{A_{55}, A_{66}[kg.m^2]}{\rho[kg/m^3] \cdot \nabla[m^3] \cdot (L_{pp}[m])^2}$$

heave – pitch

$$A_{35} = \frac{A_{35}[kg.m]}{\rho[kg/m^3] \cdot \nabla[m^3] \cdot L_{pp}[m]}$$

Equation 6.5

sway, heave

$$B_{22}, B_{33} = \frac{B_{22}, B_{33}[kg/s]}{\rho[kg/m^3] \cdot \nabla[m^3] \cdot \sqrt{\frac{g[m/s^2]}{L_{pp}[m]}}}$$

yaw – roll, roll

$$B_{64}, B_{44} = \frac{B_{64}, B_{44}[kg.m^2/s]}{\rho[kg/m^3] \cdot \nabla[m^3] \cdot (B[m])^2 \cdot \sqrt{\frac{2 \cdot g[m/s^2]}{L_{pp}[m]}}}$$

pitch, yaw

$$B_{55}, B_{66} = \frac{B_{55}, B_{66}[kg.m^2/s]}{\rho[kg/m^3] \cdot \nabla[m^3] \cdot (L_{pp}[m])^2 \cdot \sqrt{\frac{g[m/s^2]}{L_{pp}[m]}}}$$

heave – pitch

$$B_{35} = \frac{B_{35}[kg.m/s]}{\rho[kg/m^3] \cdot \nabla[m^3] \cdot L_{pp}[m] \cdot \sqrt{\frac{g[m/s^2]}{L_{pp}[m]}}}$$

Equation 6.6

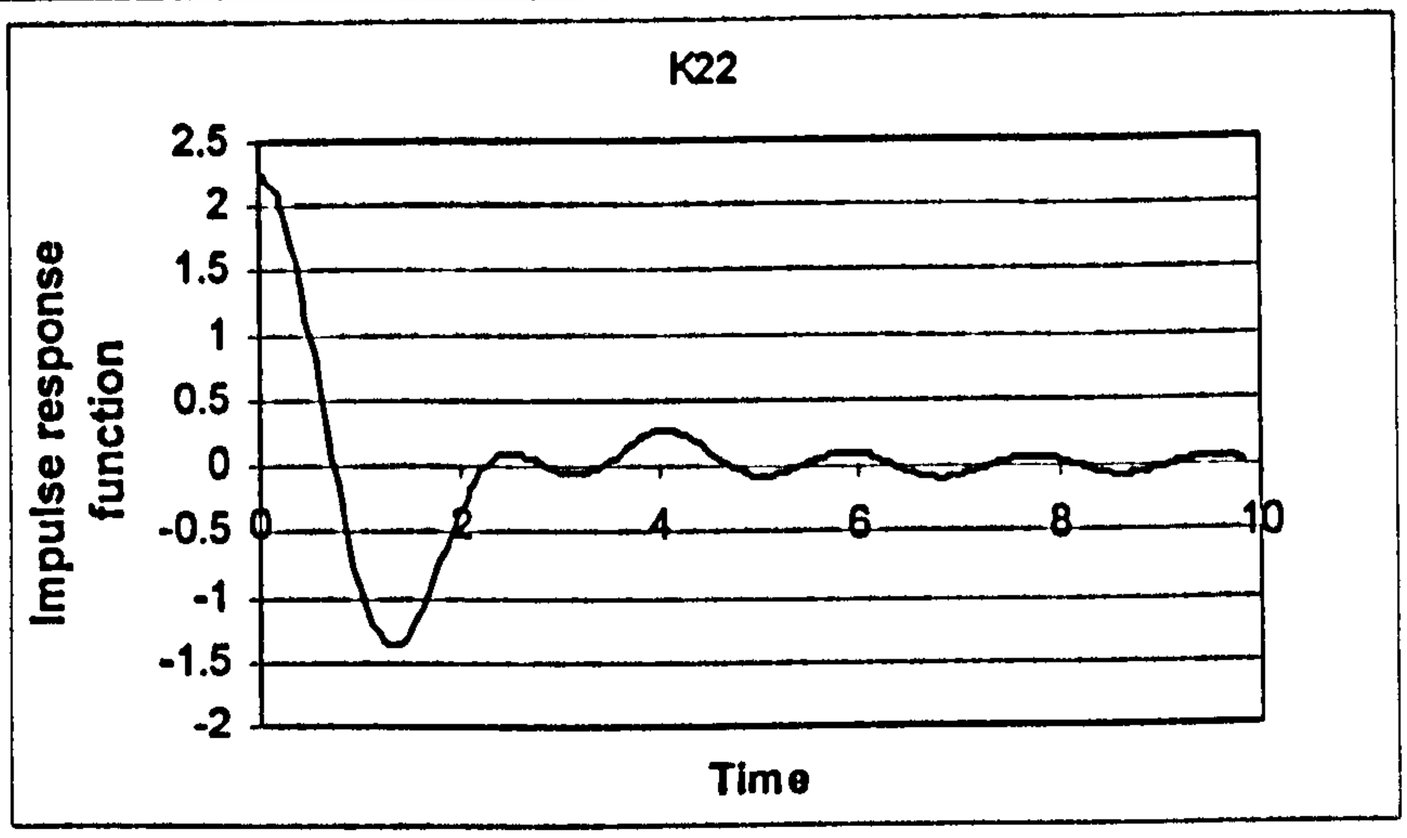

Figure 6.7 Impulse response function of sway motion for Purse Seiner

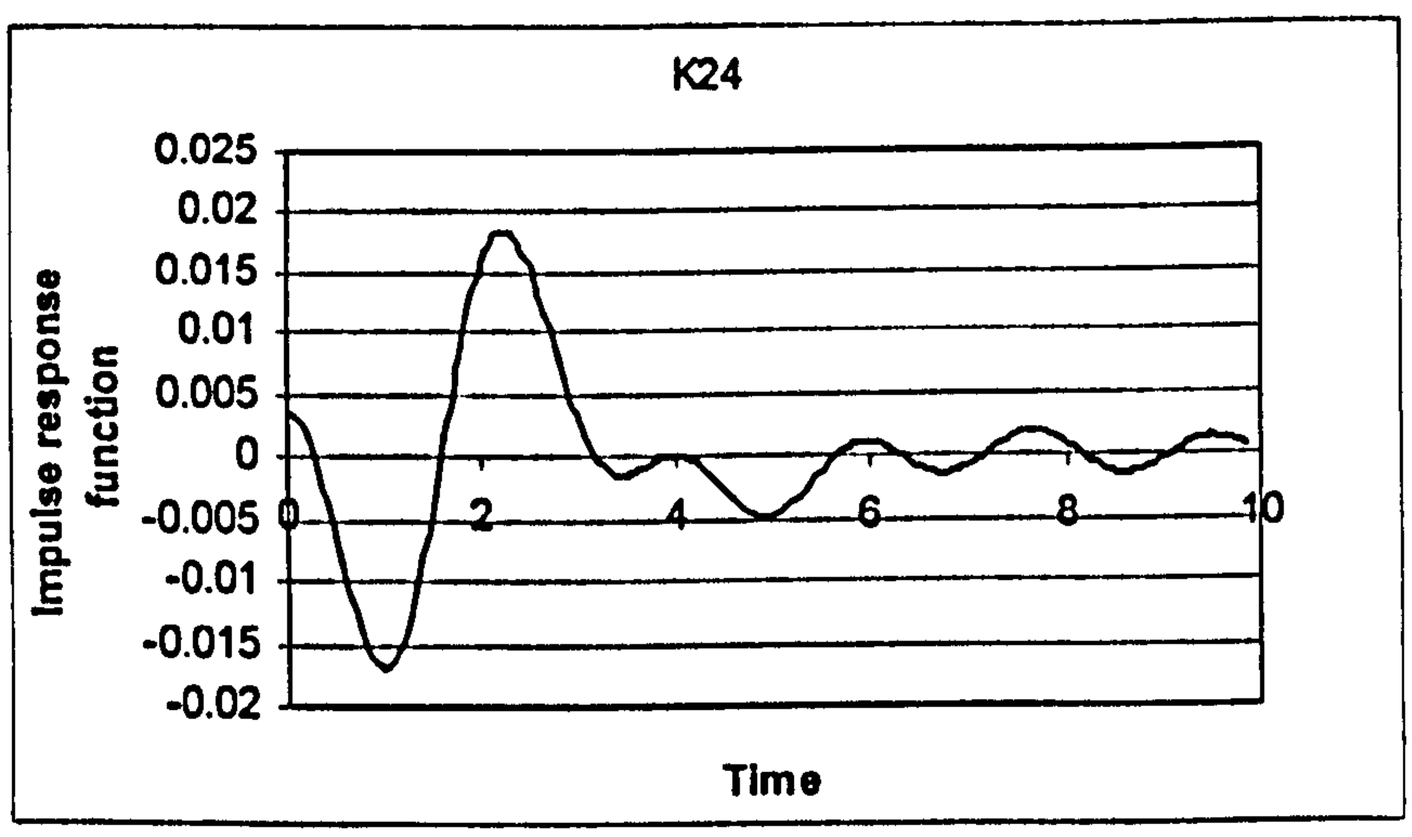

Figure 6.8 Impulse response function of sway-roll coupled motion for Purse Seiner

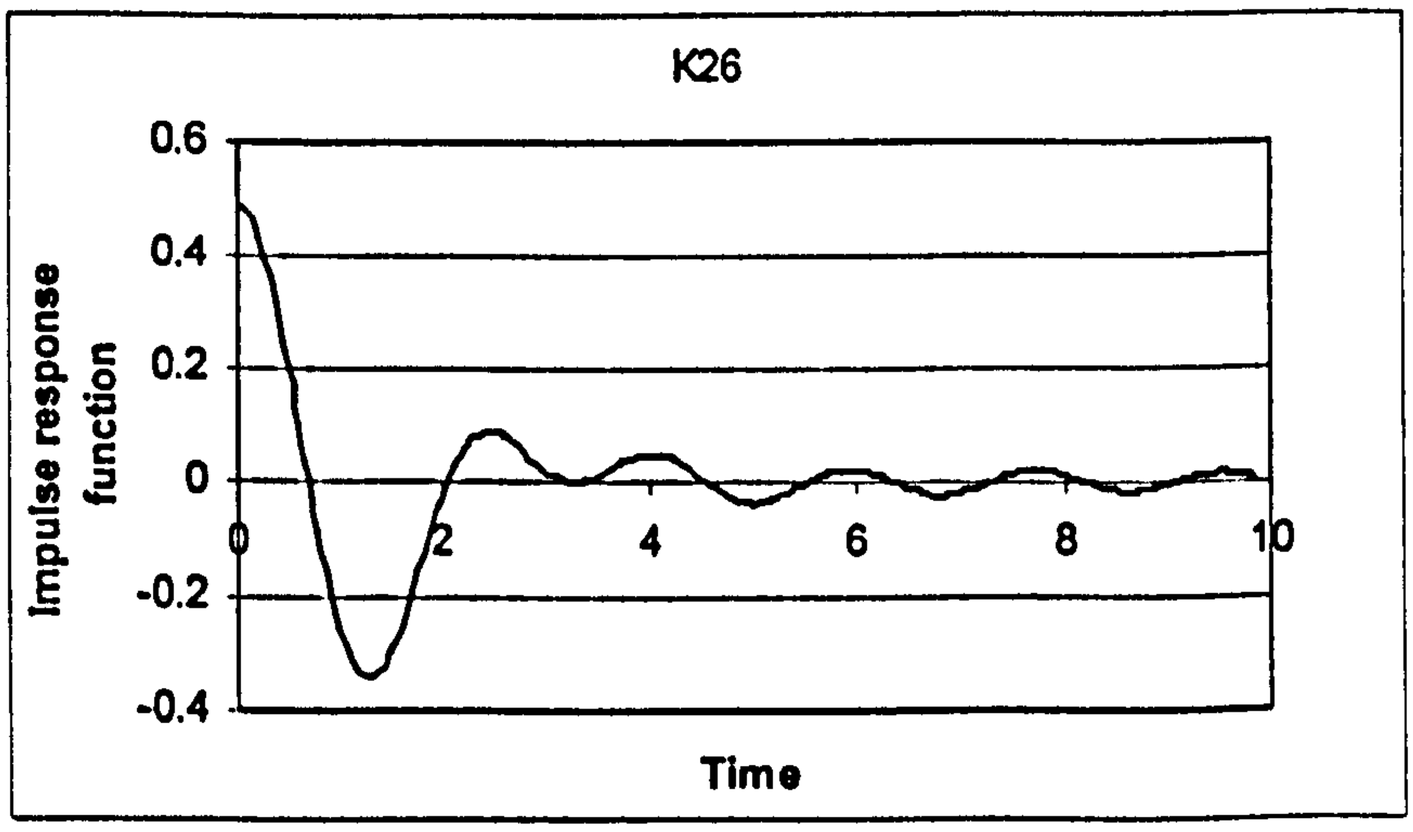

Figure 6.9 Impulse response function of sway-yaw coupled motion for Purse Seiner

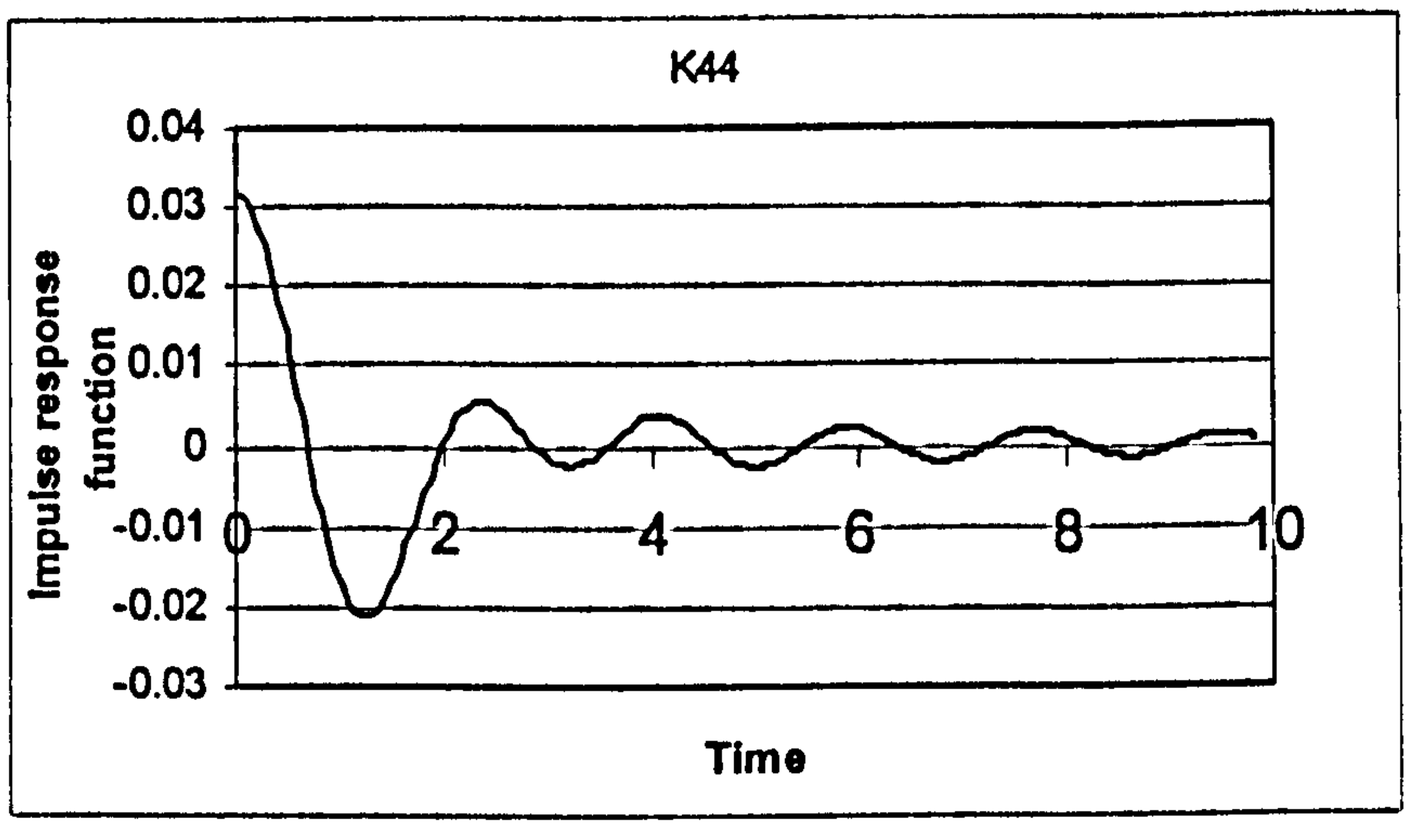

Figure 6.10 Impulse response function of roll motion for Purse Seiner

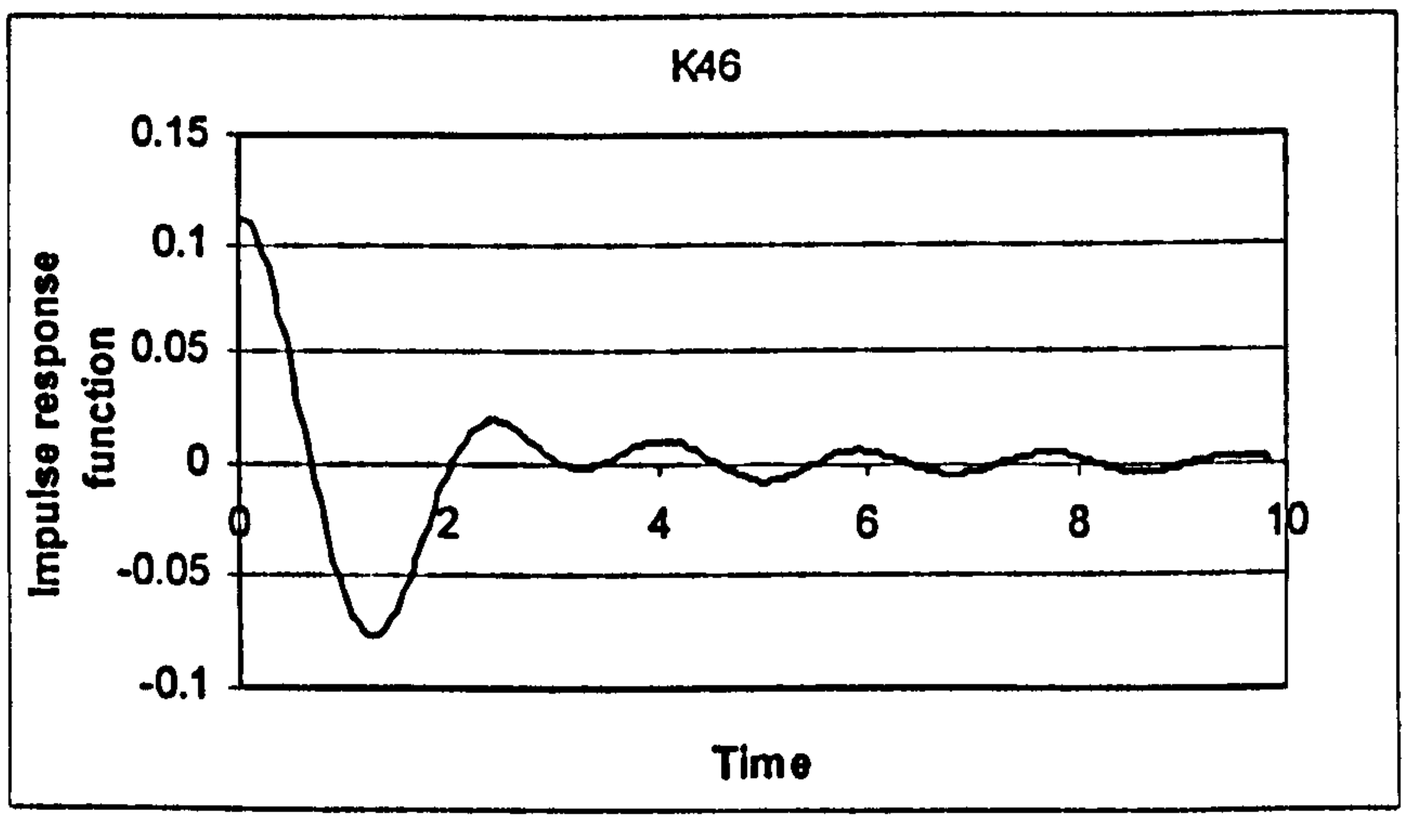

Figure 6.11 Impulse response function of roll-yaw coupled motion for Purse Seiner

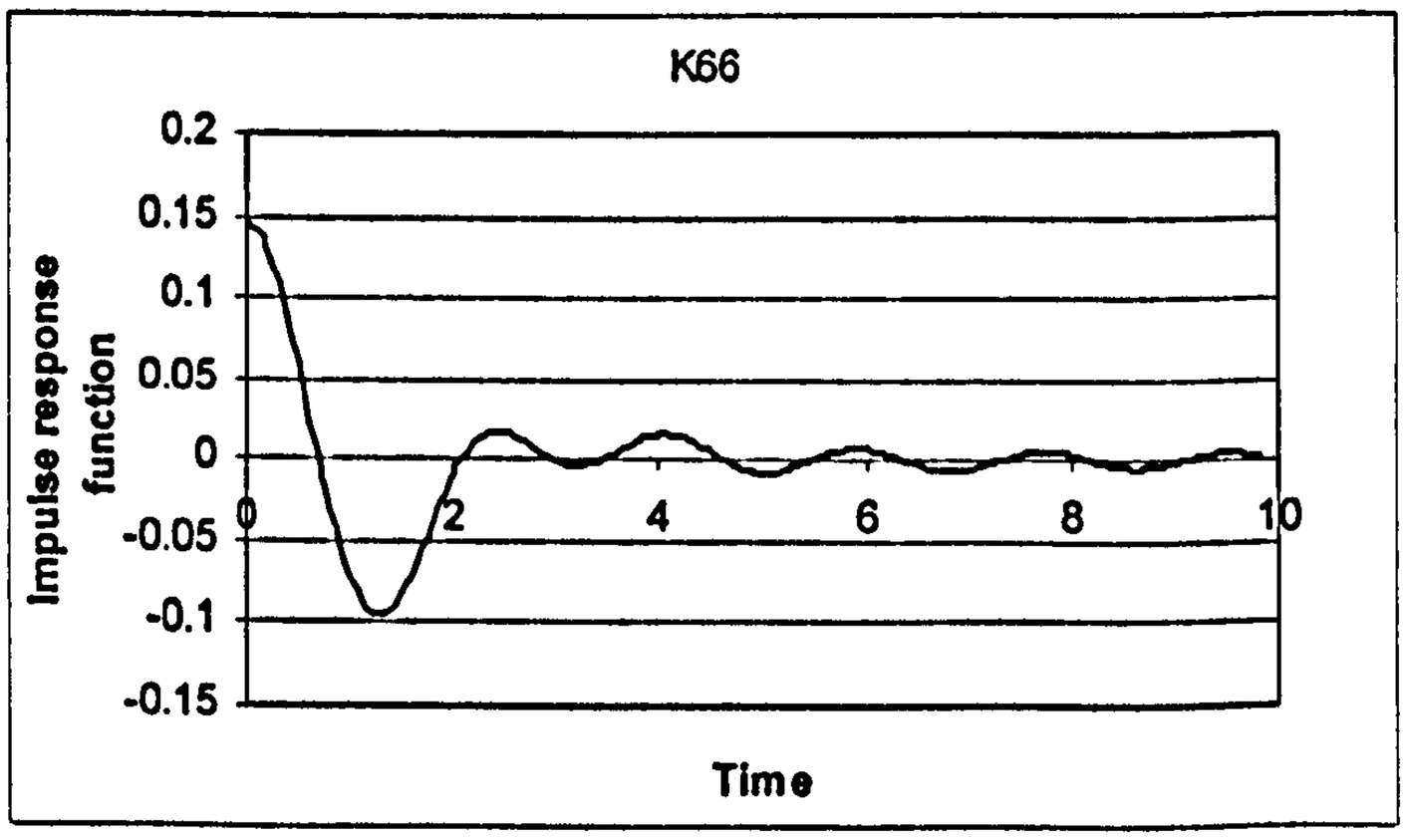

Figure 6.12 Impulse response function of yaw motion for Purse Seiner

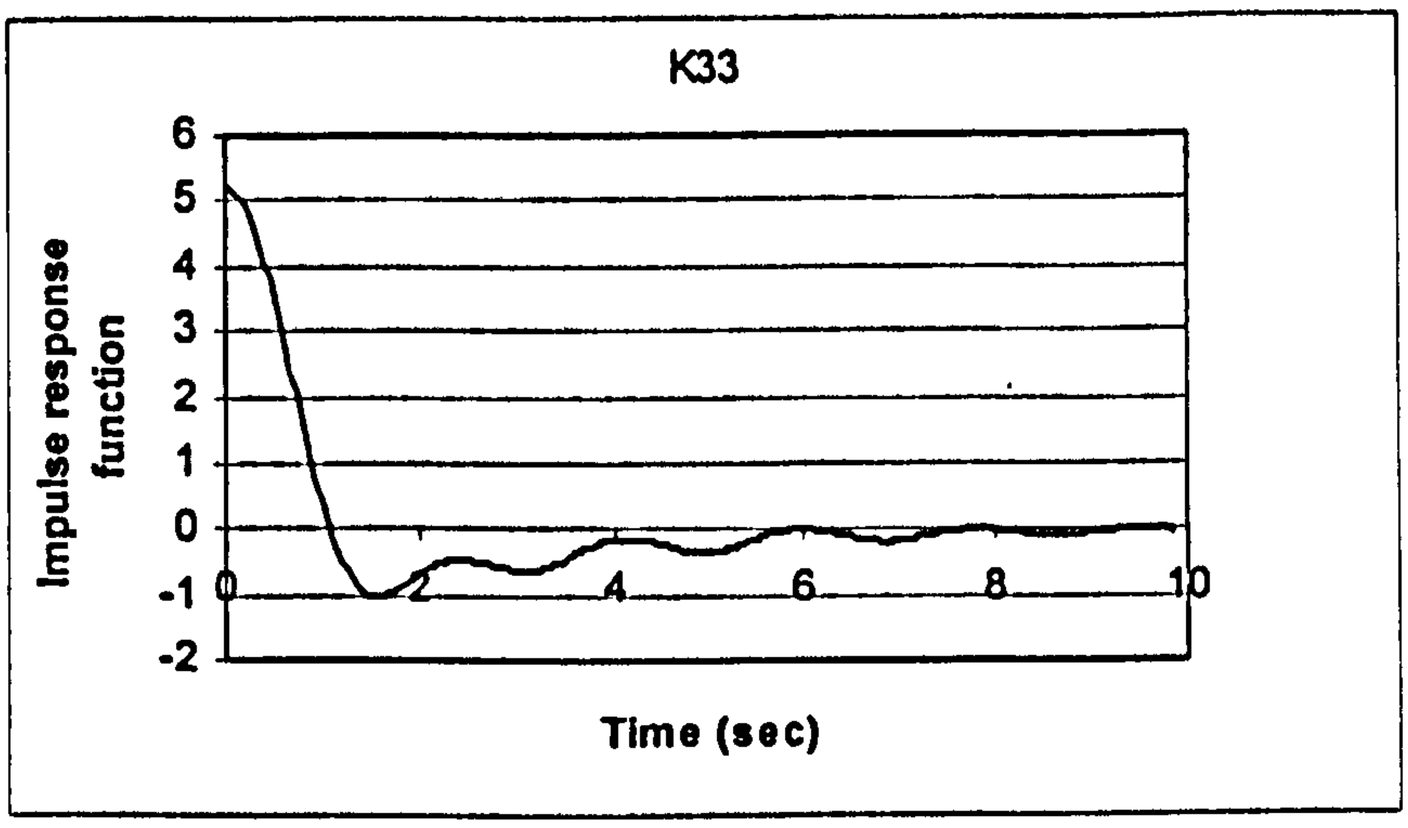

Figure 6.13 Impulse response function of heave motion for Purse Seiner

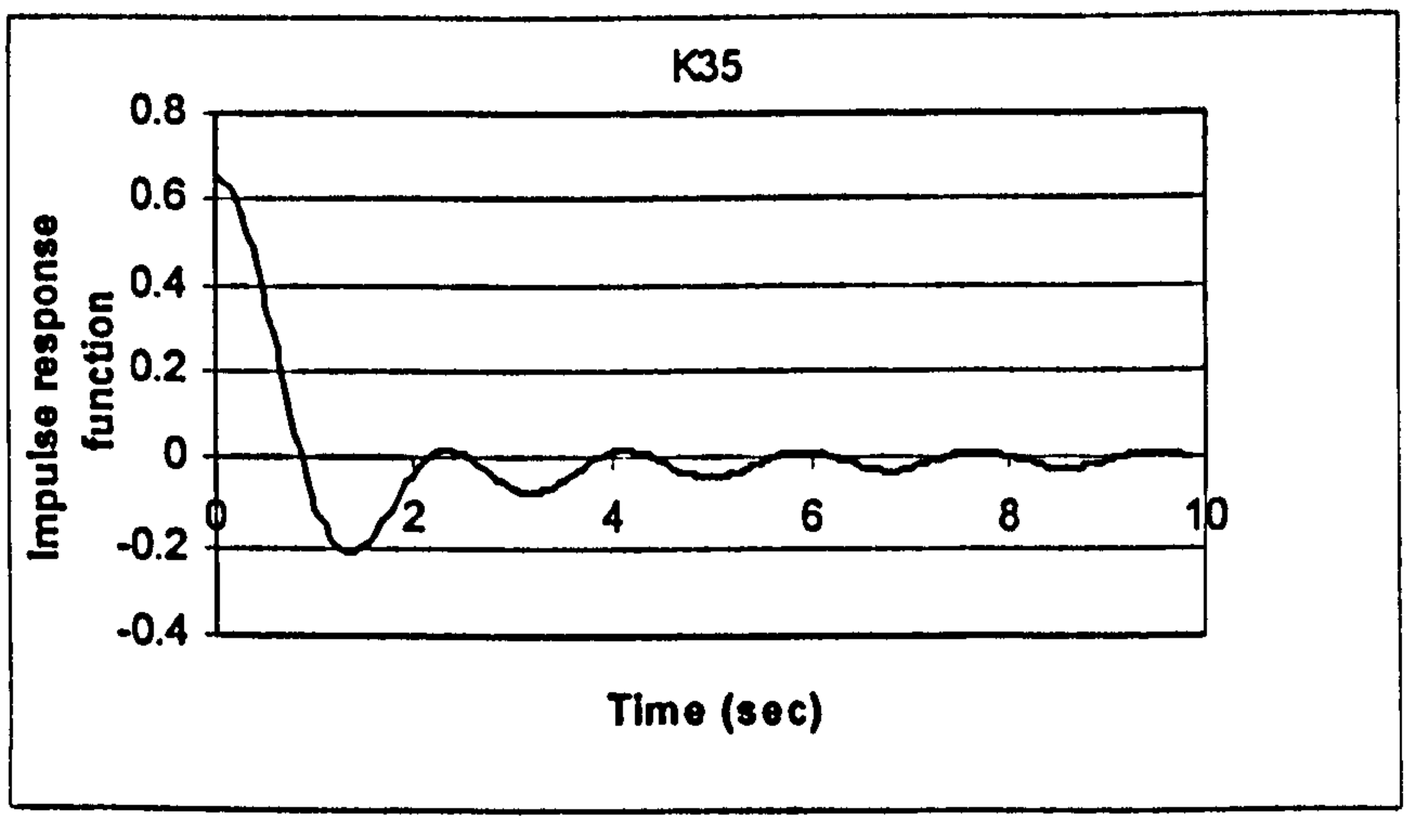

Figure 6.14 Impulse response function of heave-pitch coupled motion for Purse Seiner

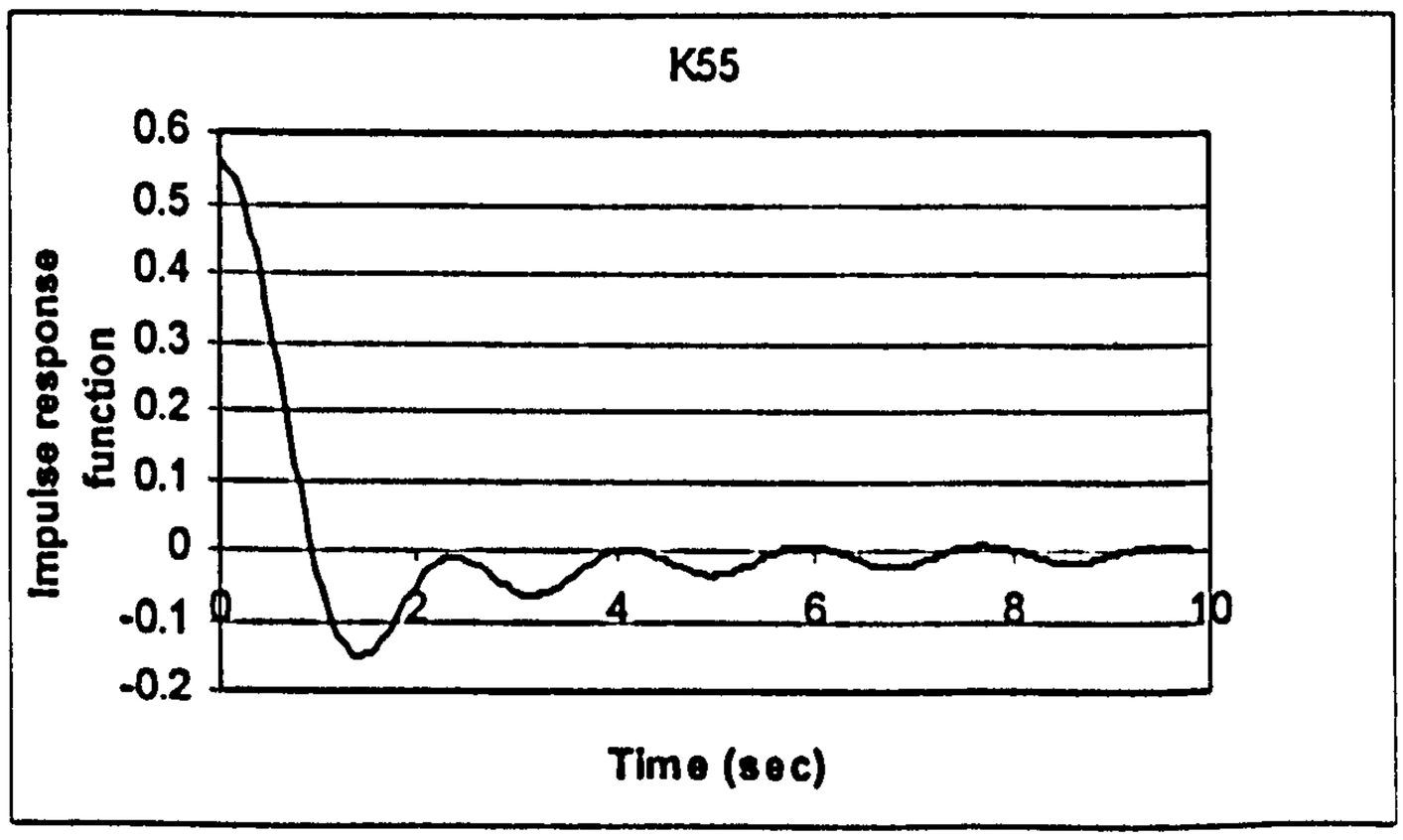

Figure 6.15 Impulse response function of pitch motion for Purse Seiner

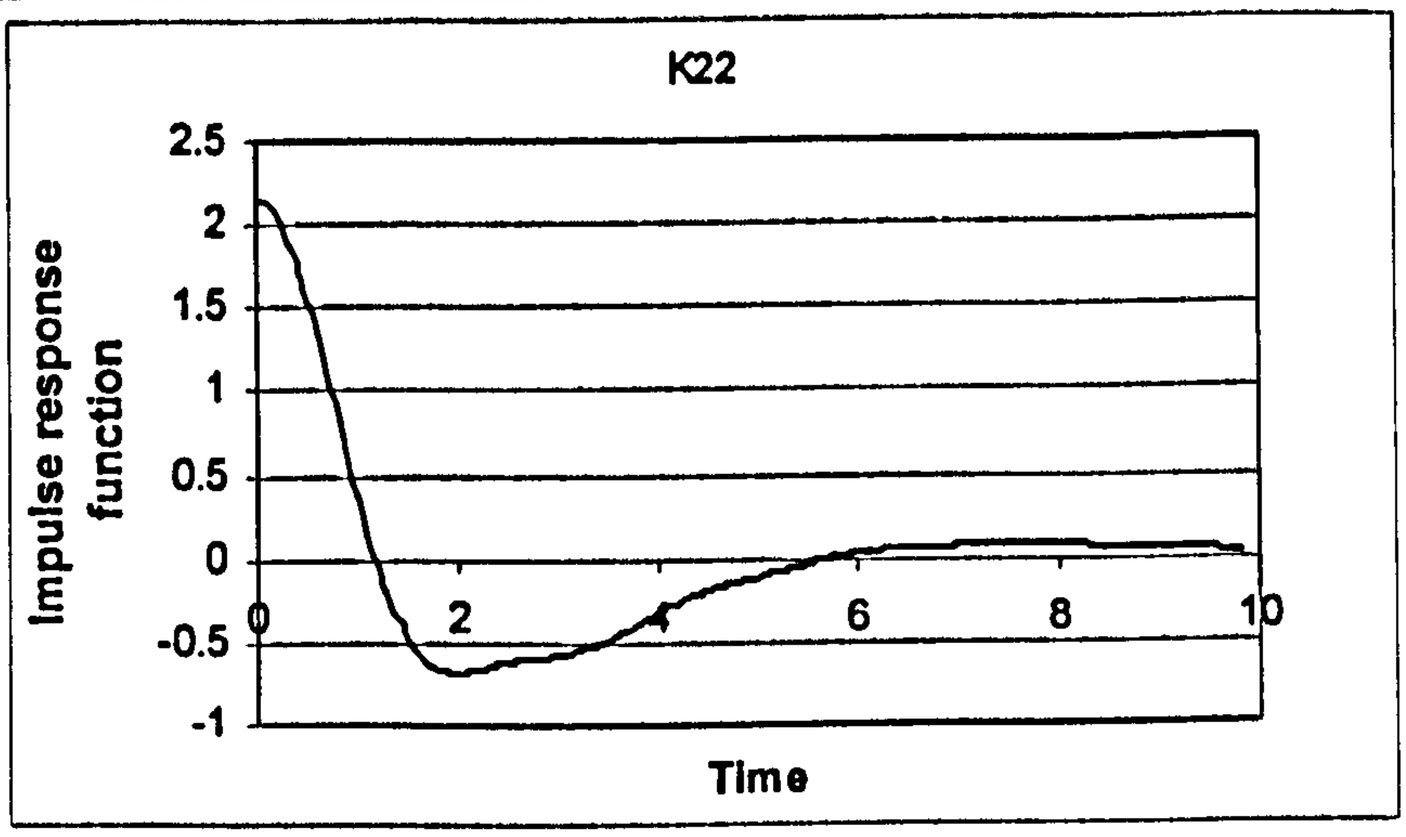

Figure 6.16 Impulse response function of sway motion for Container

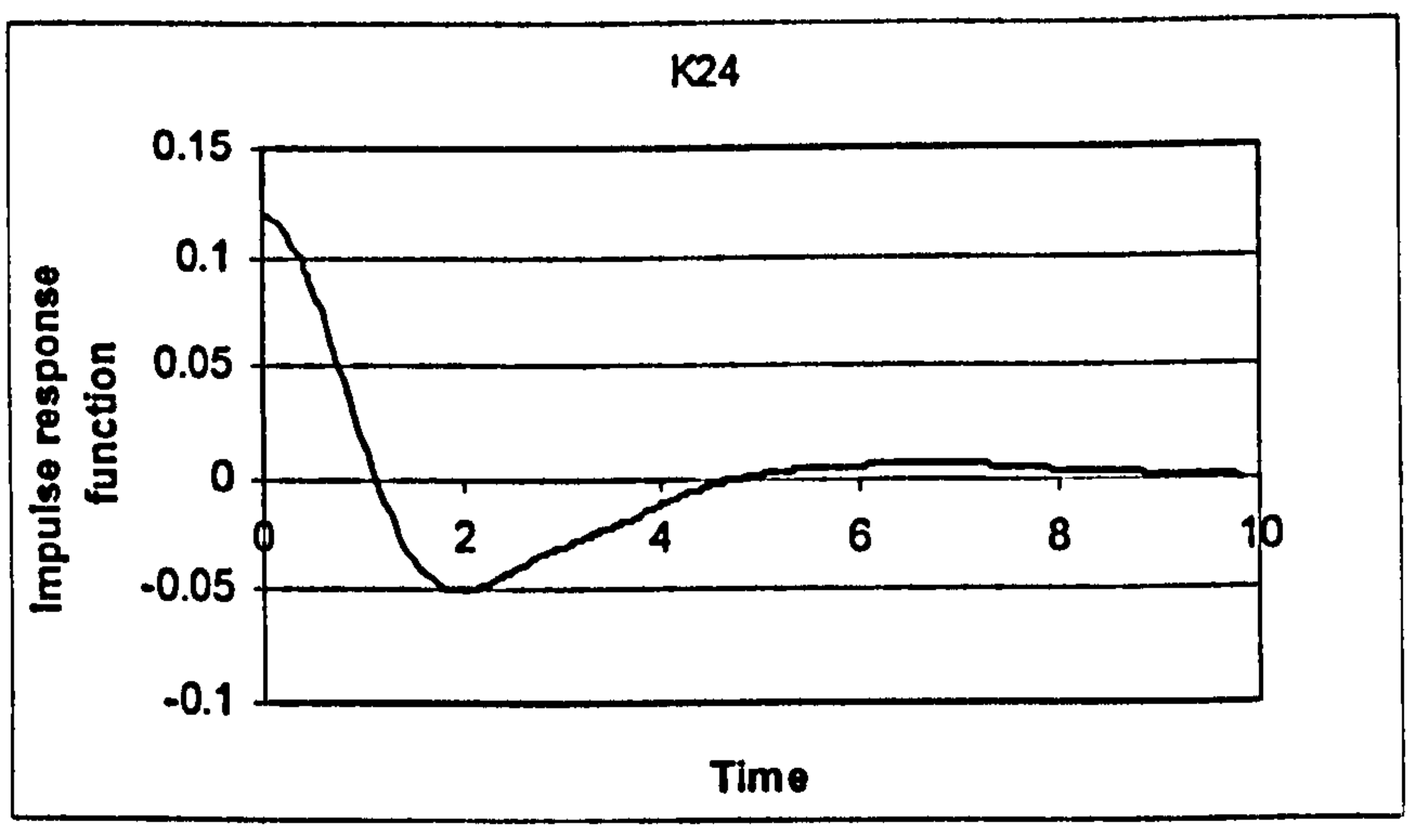

Figure 6.17 Impulse response function of sway-roll coupled motion for Container

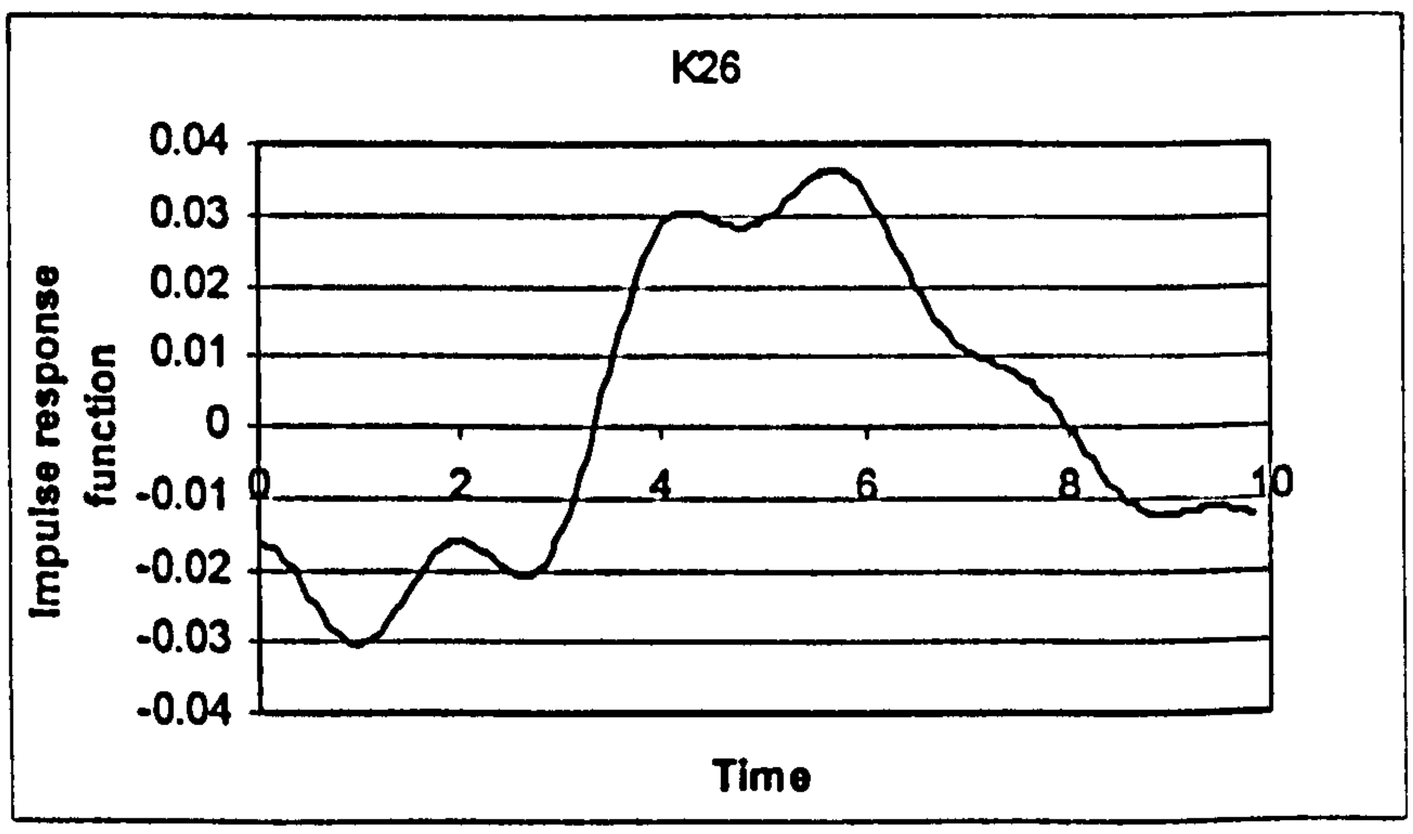

Figure 6.18 Impulse response function of sway-roll coupled motion for Container

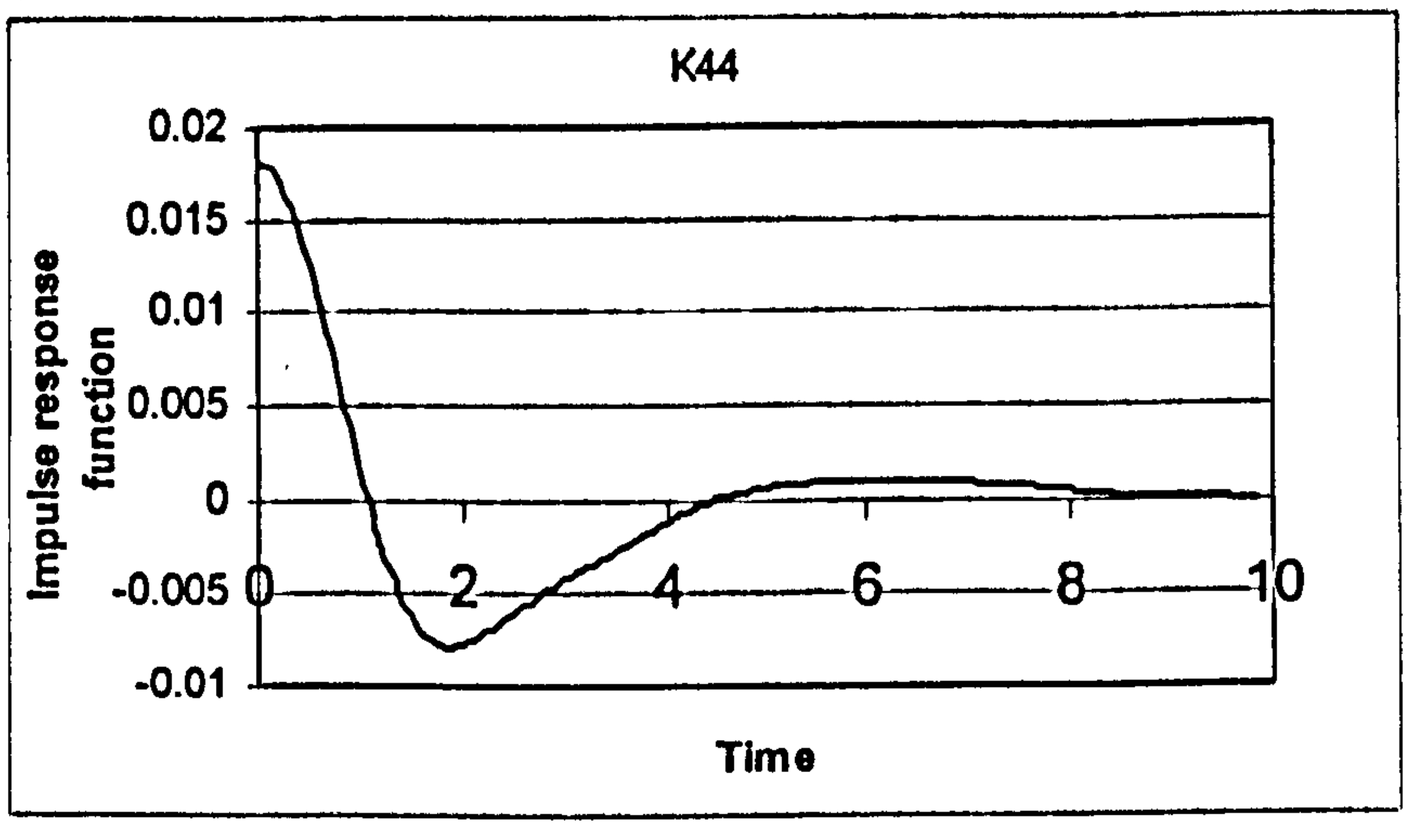

Figure 6.19 Impulse response function of roll motion for Container

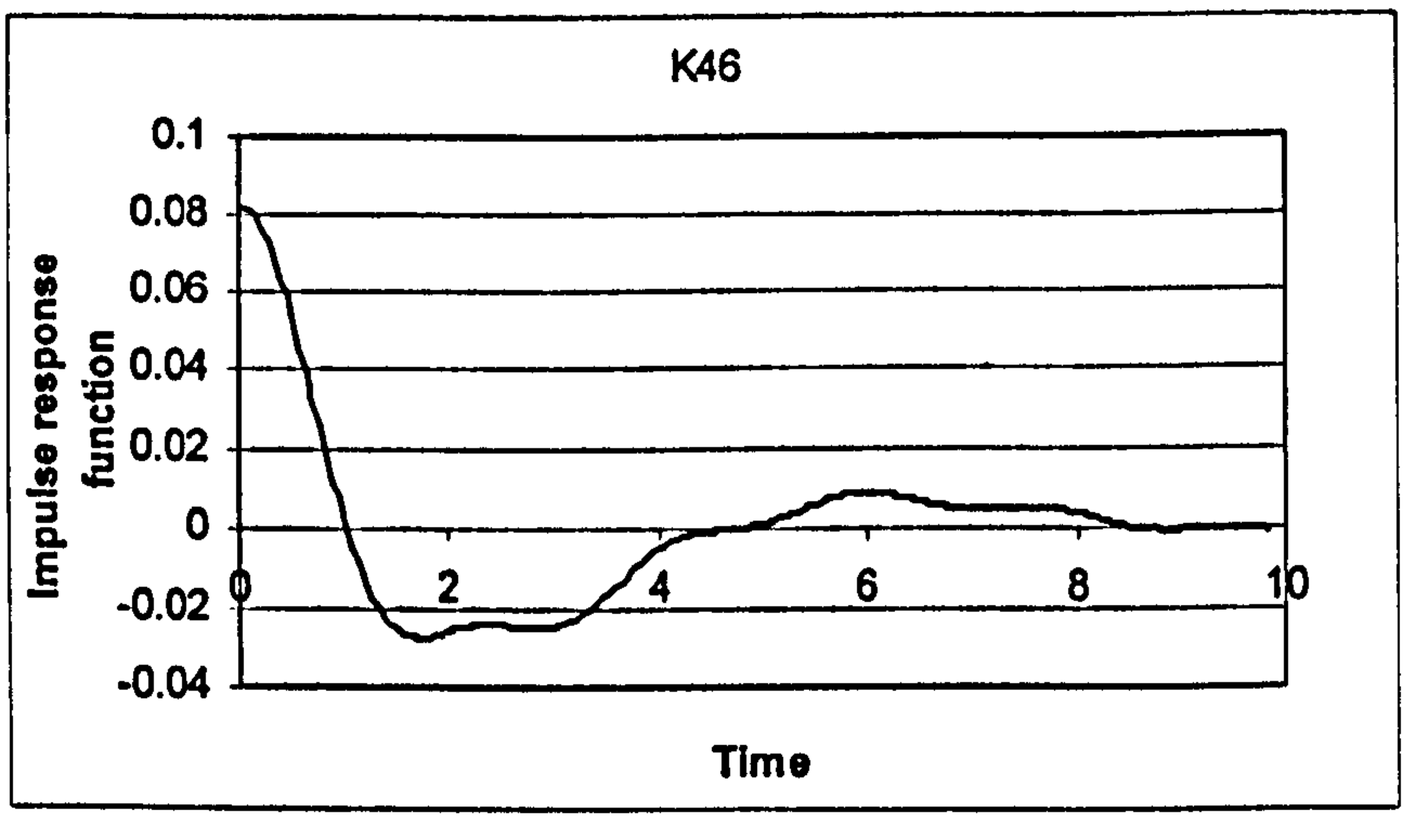

Figure 6.20 Impulse response function of roll-yaw coupled motion for Container

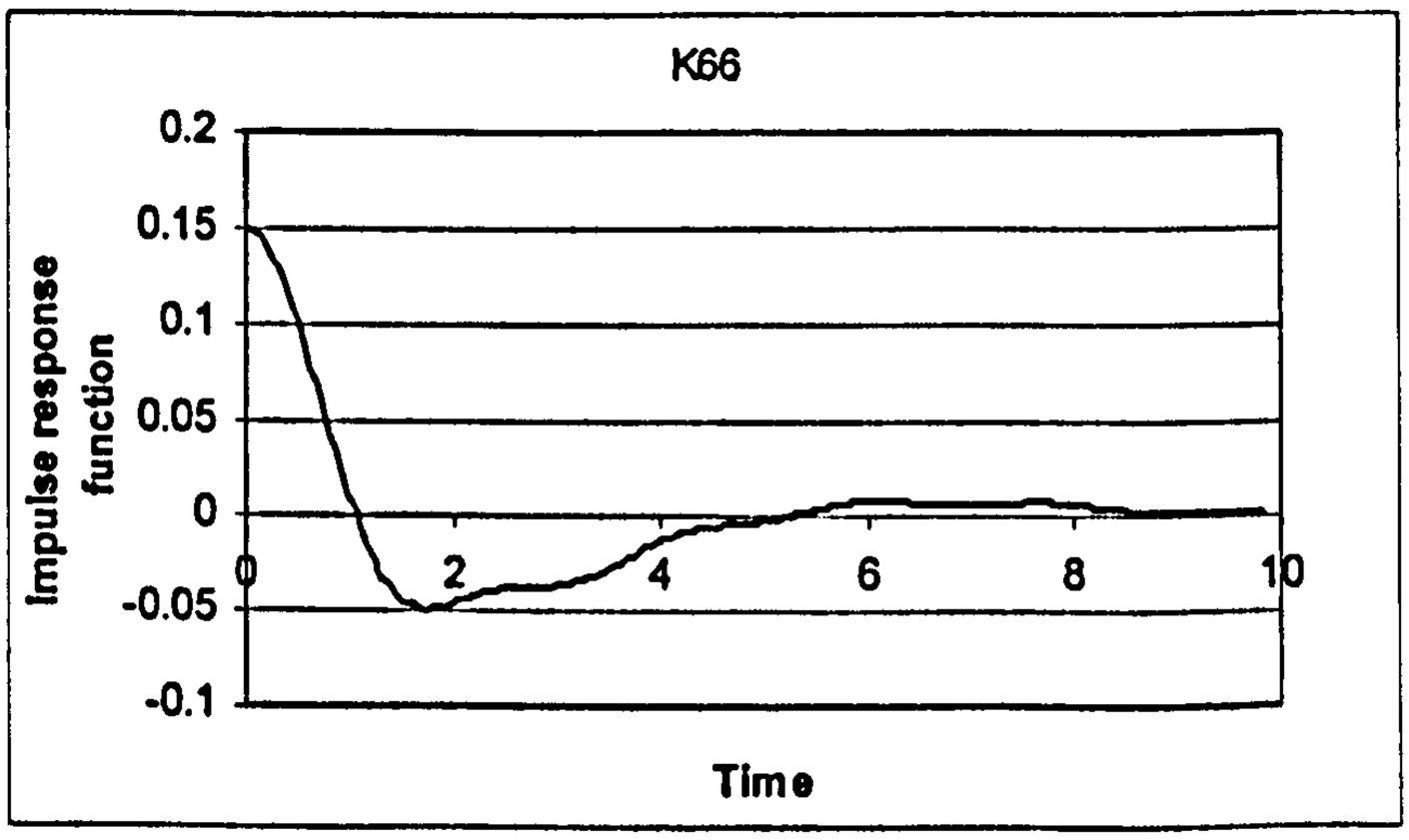

Figure 6.21 Impulse response function of yaw motion for Container

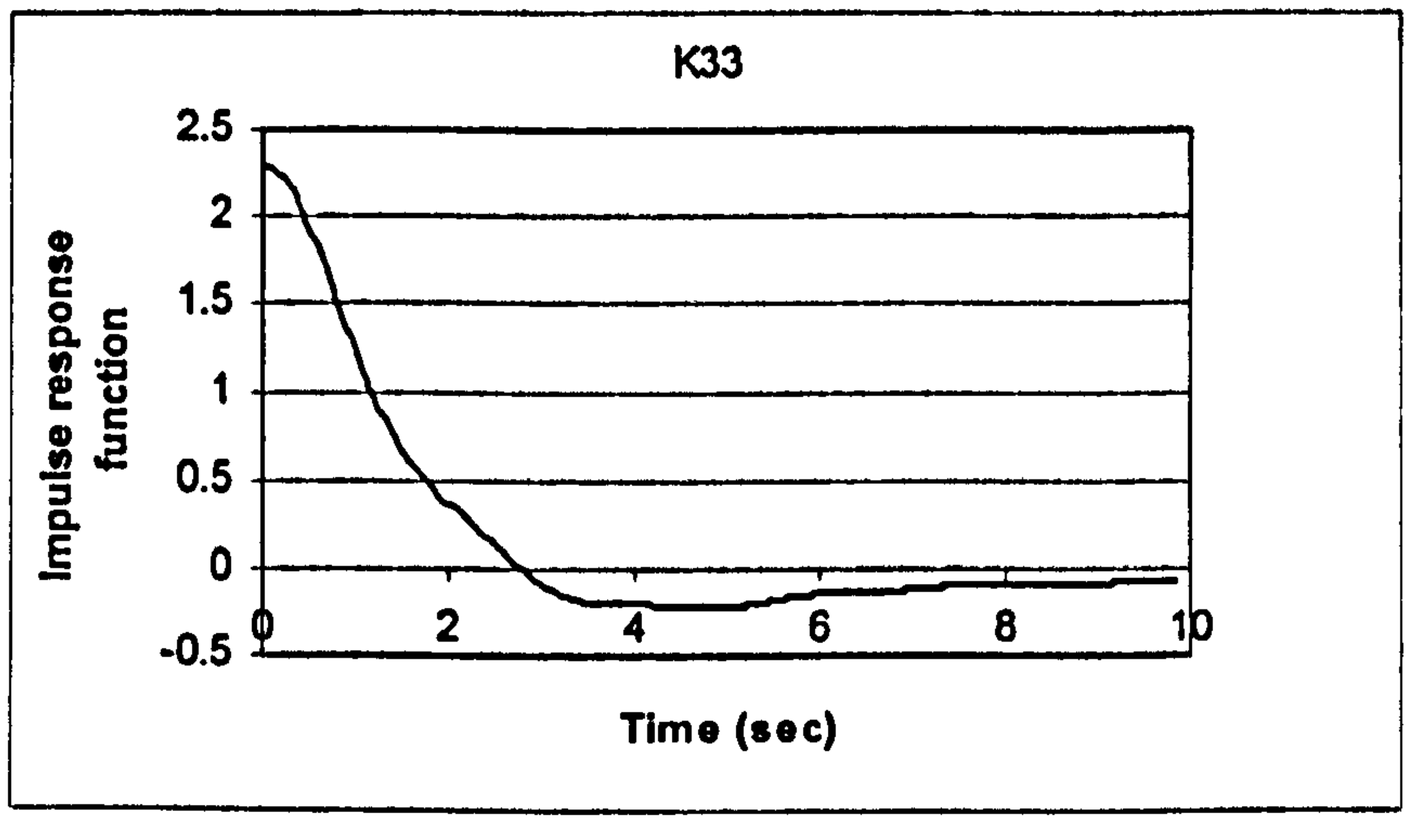

Figure 6.22 Impulse response function of heave motion for Container

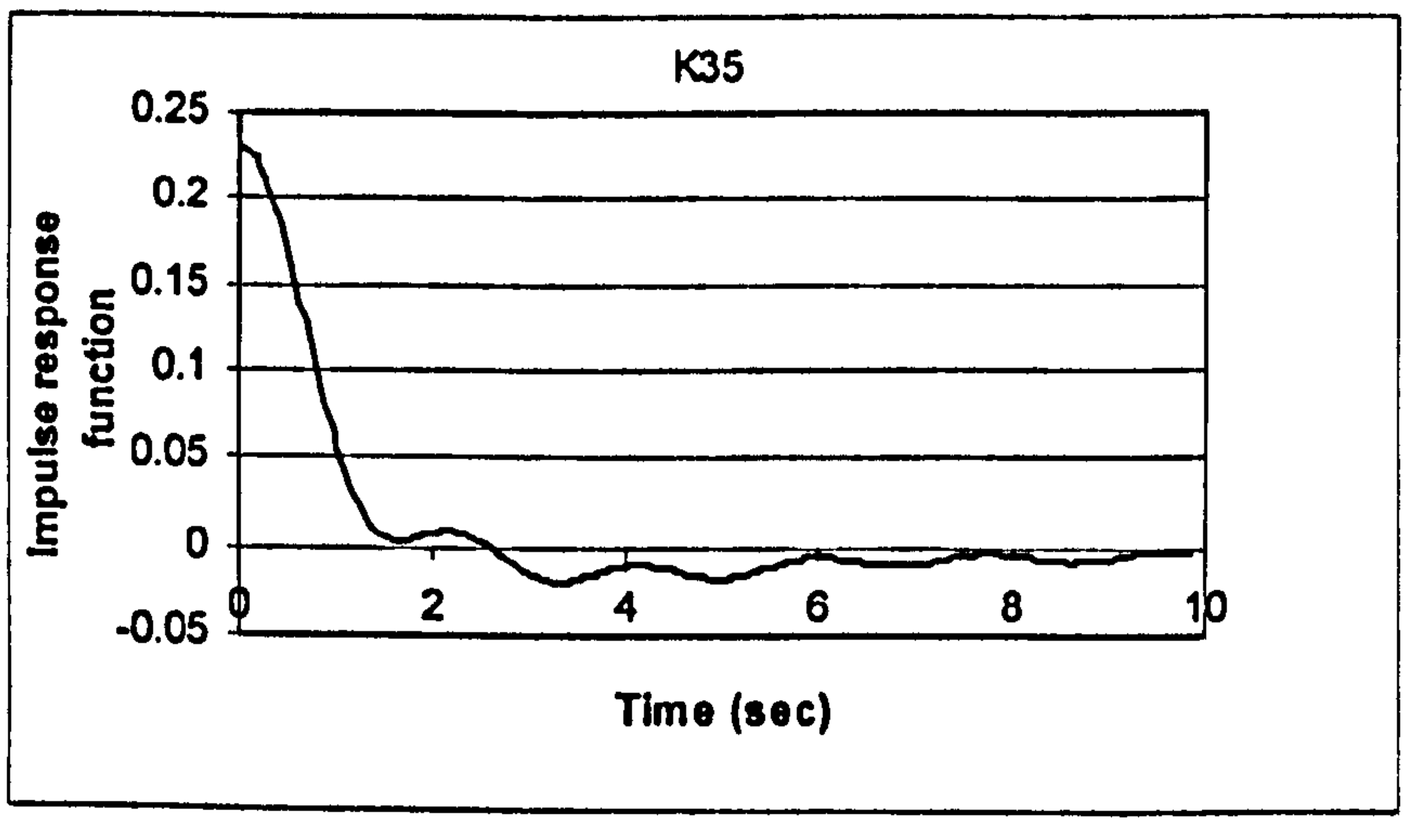

Figure 6.23 Impulse response function of heave-pitch coupled motion for Container

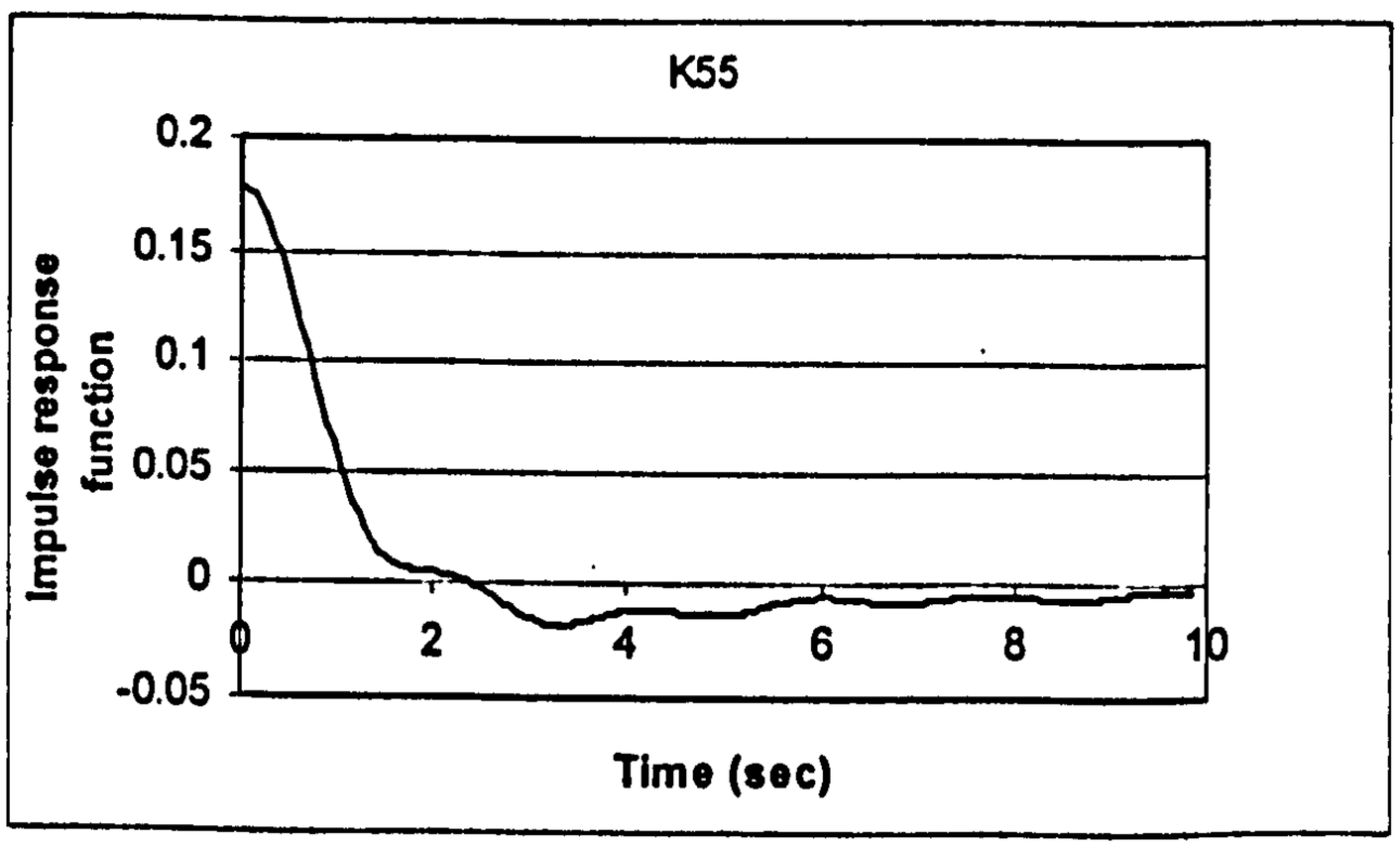

Figure 6.24 Impulse response function of pitch motion for Container

6.5. Implementation of Convolution Terms

As was shown in previous chapter, in the conventional numerical calculation of ship manoeuvring motion the effect of frequency is not usually taken into account. In

the implementation of those terms, frequency dependent excitation forces (radiation) are calculated by using convolution terms. The impulse response terms were calculated for radiation forces in terms of excitation as it is given in Equation 6.1 and its effect to numerical calculation is shown in the next Chapter.

For the calculation of radiation forces as aforementioned above, 2-D strip theory is used. Although, strip theory has certain disadvantages (mentioned in Chapter 3), its practicality and availability during the course of the study have made usage of this numerical tool inevitable. Furthermore, as it is stated in previous section impulse response functions given in Equation 6.1 are calculated based on the linear theory. Therefore, the radiation forces are calculated using the linear approach.

The radiation forces and moments are obtained from integration of the fluid pressure over the wetted surface of the ship, S:

$$F_{Radiation} = -\iint_S p_R n_j dS$$

Equation 6.7

In the numerical tool [138] the radiation forces are evaluated by a strip theory formulation. That is the 2D pressure distribution due to harmonic body oscillation is first evaluated from linearised momentum equation by only considering dynamic terms and neglecting the convective terms, ignoring therefore any influence of the radiation velocity potential in the longitudinal direction:

$$p_R = -\rho i\omega_E \int_S \varphi_k n_j dS$$

$$\Phi_R = \varphi e^{i\omega_E t} \quad \rightarrow \quad \frac{d\Phi}{dt} = i\omega_E \varphi e^{i\omega_E t}$$

Equation 6.8

The force amplitude in j direction due to motion in k mode can be derived:

$$T_{jk} = \rho i\omega_E \int_S \varphi_k n_j dS$$

Equation 6.9

Velocity potential ϕ_k in Equation 6.9 is the solution to the boundary element method with boundary conditions as is described in [101].

Sectional added mass and damping coefficients are found according to the following:

$$a_{jk} = \frac{\mathrm{Re}(T_{jk})}{\omega_E^{\,2}} \qquad b_{jk} = \frac{\mathrm{Im}(T_{jk})}{-\omega_E}$$

Equation 6.10

The sectional coefficients are integrated along the length of the ship. To account for speed and "end" effects according to strip theory formulation the corrections have been applied as derived in [101] and [102]. The further details of the numerical tool and its validation with experimental results can be found in [138].

Radiation forces therefore can be calculated using Equation 6.1 and 6.2 in time domain as follows:

$$F_{Rad,ij} = -a_{ij}(\infty)\dot{V}_j - \int_0^\infty K_{ij}(t)V_j(t-\tau)d\tau$$
$$i,j = 1,2,3,4,5,6$$

Equation 6.11

where the first term is the infinite frequency added mass, and the second term is the so-called memory effect in which representing Kernel function is calculated using Equation 6.2 as it is shown in the previous sections.

The radiation force terms calculated in Equation 6.11 are given in a body fixed axis system and hydrodynamic coefficients are evaluated for stationary ship attitude which follows the assumption that ship motions are small amplitude. However, as it is stated in the previous sections, the ship amplitude can be very high for the motions in extreme astern seas therefore those radiation forces are transformed into the horizontal body axis system as shown in Appendix A.

With the inclusion of frequency dependent coefficients, Equation 5.8 can be written as follows:

$$(M+A)\ddot{X} + B(X)\dot{X} + C(X)X + \int_0^\infty K_{ij}(t)V_j(t-\tau)d\tau = F(\zeta_w, X, \dot{X}, \ddot{X})$$

Equation 6.12

Here the three-dimensional added mass coefficients from Equation 5.4, 5.5 and 5.17 are evaluated for the infinite frequency case using strip theory [138]. The potential

damping terms are calculated using the same tool [138]. The kernel functions are based on these coefficients for each stations so that the radiation forces in the time domain are subject to same limitations of the strip theory. As it is well known surge is not considered with the slender body theory as surge forces are of higher order. However radiation effects associated with surge could be of importance when considering motions in following seas. In this study considering the Froude-Krylov forces are most likely to be dominant forces in this case, the radiation forces are omitted. However, surge added mass and damping coefficients could be obtained for slender type of ships by means of a full three-dimensional method. These coefficients were then used to generate kernel functions related to surge.

In Equation 6.12 in contrast to Equations 5.6 and 5.7, frequency dependent added mass (at infinite frequency) and potential damping terms are calculated, again using the numerical tool [138] which includes the "end" terms as it is stated before. Therefore, the damping coefficients in Equation 6.2 might include the linear manoeuvring components given in Equation 5.17 and inevitably resulting the overlapping of those terms in calculation with memory effects. Due to nature of using linear radiation forces by memory effects or "linear filter" the left hand side of the Equation 6.12 is linearized. The added mass term calculated at infinite frequency and damping terms calculated for each encounter frequency are taken into the solution matrix. However this results in the removal of non-linear coupled terms described in Equations 5.5 and 5.6. Furthermore, those added mass and damping terms are stored for every 10 degree heading angles between 0 and 360 degrees and they were interpolated for the wave heading concerned during the motions. Then, the response (Kernel) functions are sent to motions continuously during the specific encounter frequency therefore assuming unsteady characteristics of motion even though the ship might have steady motion when reaching the certain ship speed in following and quartering seas.

Although wave excitation can be calculated using similar impulse response functions, certain conditions of ship motions in extreme following and quartering seas require to follow methods shown in Chapter 5 for Froude-Krylov and diffraction.

As the major component of wave forces in extreme astern seas, Froude-Krylov forces, including restoring forces, are evaluated as it is shown in Chapter5. It is found from previous research [62] that hydrostatic and hydrodynamic forces should be calculated using the instantaneous positions, not the mean of the hull and water surface. Similarly, the instantaneous hull wetted surface should be determined and used as the

surface of integration for all hydrostatic and hydrodynamic forces. This is not a significant problem for calculation of hydrostatic forces but for calculating hydrodynamic forces as a function of ship surface is a very difficult task, as it requires the change of the boundary conditions. Therefore, in order to avoid restraining the Froude-Krylov forces in linearised surface due to linear filter of convolution, the current method which takes into account instantaneous wave surface will be prevailed.

The calculation of diffraction can be carried out similarly the radiation forces however the unique nature of Ohkusu's methodology which is based on low encounter frequency can be used for the calculations. The assumptions of low encounter frequency allow calculation of diffraction forces to be similar to Ohkusu's method, as it is described by Bailey et al. [43]. Therefore, they were obtained as it is given in Chapter 5 and Appendix B.

Other force components which were shown in Equation 5.9, also are included as they are already calculated in time domain. However, rudder motions could be described similar to wave forces calculations in terms of convolution integrals. The current accuracy of the rudder numerical model described in Chapter 5 does not require such an approach.

6.6. Concluding Remarks

One of aims of the current study was to introduce the so-called "memory effects" (impulse response functions) and their implementation in the equation of motions to investigate how the behaviour of the ship is influenced by the consideration of the frequency-dependence of the hydrodynamic coefficients. As it is stated in this chapter, although this methodology is firmly established for seakeeping calculations, the unique nature of ship motions in astern seas in which since the frequency of encounter in following seas is quite low, "zero-frequency" constant hydrodynamic coefficients are employed, as it is done in calm-water manoeuvring calculations. However, the arguments for this methodology are presented. Broadly, they indicate that due to wave effects associated with the unsteady motion of the hull at the free surface and vortices which are shed from the oscillating hull, especially when a ship has very large heading angle, the convolution terms (representing the so-called "memory effects") cannot be negligible.

Therefore, the convolution terms representing radiation forces are incorporated in order to improve the prediction of the behaviour of the vessel at encounter frequencies which are not very near to zero.

It is also accepted that the experimental data for different ship forms and covering the practical range of frequencies and ship speeds are very limited. Furthermore, the full impulse response matrix can be found by solution of initial value hydrodynamic problem or combining both experiment and numerical solution. However, this will be very difficult and expensive task therefore the frequency-dependent coefficients are derived within the limits of potential theory.

In order to solve the impulse response functions, the numerical solution of Kernel functions and numerical module for this solution is developed and the results are presented for a Wigley model hull, a fishing vessel model and a container model. The description of implementation methods of so called "memory effects" in terms of convolution integrals is presented. The calculation method for the frequency dependent hydrodynamic coefficients is also described. Some concessions were being made, however, in order to achieve the above solution.

First of all, despite its well-known drawbacks for ship motions in astern seas, the strip theory is employed for the two main vessels used in numerical simulations and it will be employed for the numerical simulations shown in Chapter 7, 8 and 10. This is due to fact of problems with the homogenous panelling of hull form described in Chapter 5 for wave force calculations. Therefore, the current 3-D tool which is used for Wigley hull form cannot be used for other two vessels. Introducing the memory effects or "linear filter" was resulted the left hand side of the equations of motion including added mass and potential damping terms are described linearly. Since the strip theory method employed in the numerical model calculates end terms, the damping terms might include linear manoeuvring components, which are also taken into account in the manoeuvring (hull) forces, therefore the overlapping could occur during these calculations. Furthermore, owing to the importance of non-linear hydrostatic and Froude-Krylov forces prevented the use of the convolution terms for these exciting forces/responses. Similarly, the diffraction modelling which is based on the low encounter frequency approach was kept in the numerical model including memory effects.

Based on above background, the numerical simulations were carried out to investigate the effect of frequency and the results will be shown in Chapter 8 and

Appendix G. Furthermore, it is investigated in verification of the numerical tool against the model experiments taken for ITTC Benchmark study and for fully captive ship motions they will be presented in Chapters 7 and 10. Also, the numerical method is being modified for random waves in order to investigate the effect of frequency in a realistic ship environment. The modified numerical method and the numerical simulations carried out against the model experiments will be presented in Chapters 9 and 10, respectively.

7. VALIDATION OF NUMERICAL MODEL

7.1. General Remarks

The objective of this chapter is to present the validation of the improved numerical model with the model experiments. In order to validate the numerical code, a time simulation numerical analysis program "Simurg" has been developed in C++ code. For the validation of numerical program two different model ships were tested. A 23,720 tonnes displacement containership, investigated using systematic model experiments at Osaka University in Japan and a 712 tonnes displacement fishing vessel, investigated using systematic model experiments at National Institute of Fisheries Engineering in Japan. The models are tested in different speeds, wave steepness, wave height to ship length ratio and heading angles.

Within the above framework the following sections of the chapter present the solution of the equations of motions for the numerical code. It is followed by the brief description of test methods, instrumentation and all other details in the experiments. The full results of experiments are presented. This is followed by the comparison of numerical test with the model tests according to the guidance given by the ITTC. The results are discussed and the significant points in the comparison are mentioned.

7.2. Solutions of Equations of Motions

In order to validate the numerical code, a time simulation numerical analysis program "Simurg" has been developed in C++ code. There are two different approaches adopted in the program which are already covered in Chapters 5 and 6. The first one is the classical approach of using zero frequency added mass and damping coefficients for time-domain non-linear equations of motion given in Equations 5.3-5.4-5.5. The second approach is to incorporate the frequency dependent coefficients or so called "memory effects" represented in Equation 6.1 by the help of convolution integrals into the Equations 5.8. The details of program and solution of numerical equations can be found in Appendix G.

The solution of the equations of motion in the first approach can be roughly represented as follows. The system of motion equations in six degree of freedom is expressed in the form

$$\dot{X}(t) = A^{-1}F(t)$$

Equation 7.1

or with detailed expressions given in Equation 5.6,

1) x'
2) y'
3) z'
4) $\dot{U} = g_1(U, V, W,, P, Q, R, x', y', z', \varphi, \theta, \psi, X', t)$
5) $\dot{V} = g_2(U, V, W,, P, Q, R, x', y', z', \varphi, \theta, \psi, Y', t)$
6) $\dot{W} = g_3(U, V, W,, P, Q, R, x', y', z', \varphi, \theta, \psi, Z', t)$
7) $\dot{P} = g_1(U, V, W,, P, Q, R, x', y', z', \varphi, \theta, \psi, K', t)$
8) $\dot{Q} = g_2(U, V, W,, P, Q, R, x', y', z', \varphi, \theta, \psi, M', t)$
9) $\dot{R} = g_3(U, V, W,, P, Q, R, x', y', z', \varphi, \theta, \psi, N', t)$
10) $\dot{\varphi} = \dfrac{P}{\cos\theta}$
11) $\dot{\theta} = \dot{\Theta}$
12) $\dot{\psi} = R + P\tan\theta$

Equation 7.2

where the vector X contains the linear velocities and angular rates. Matrix A contains the added mass manoeuvring forces and F contains damping, restoring and the external forces which were mentioned above. Vector F is function of linear velocities and angular rates as shown in Equation 7.2. The system of equations is formed from the above six equations, six kinematics relations furthermore the autopilot model described in Equation 5.23 and position on the wave which will be exploited in detail in Chapter 8 and 10. Calculation of the second approach has already been presented in Chapter 6. The calculations are performed using the Runge-Kutta method.

7.3. Instrumentation

For the validation of numerical program two different model ships were tested, a 23,720 tonnes displacement containership denoted Ship A-1, investigated using systematic model experiments at Osaka University in Japan. A 712 tonnes displacement fishing vessel, investigated using systematic model experiments at National Institute of Fisheries Engineering in Japan denoted Ship A-2. Notions Ship A-1 and Ship A-2 will be used in the rest of this chapter and following chapters for the simplicity.

As for the instrumentation in the model tests, for instance, Ship A-2 model was tested in seakeeping and manoeuvring basin of the National Research Institute of Fisheries Engineering (NRIFE) in Japan. It is 60m long, 25m wide, and 3.2 m deep. The wave maker of this basin consists of 80 plungers driven by digitally controlled electric motors. The model was propelled with electric motors, whose power was supplied by batteries on board with feedback controls of propeller revolution. The maximum Froude number for the model was set to be 0.43, defined by length between perpendiculars. The model was steered by autopilots whose rudder gain was 1. The maximum rudder angle was 35 degrees. Roll, pitch, and yaw angles were detected by fiberoptical gyroscopes. These measured signals as well as the rudder angle and propeller revolutions were recorded by on-board computers in a digital form. The measured yaw angle was also used for the autopilot control. The propeller revolution is indicated by the nominal Froude number (Fn), which is the Froude number when the ship runs in calm water with specified propeller revolution. The procedure for the container model tests at Osaka University is also very similar. The maximum Froude number was set to be 0,4 while the maximum rudder angle was 10 degrees. The power of the motor has been increased from the model experiments of Ship A-2 to achieve higher speed to investigate surf-riding and broaching-to phenomenon. The similar control system is used for the free running experiments in Chapter 10 and details of radio control system are given in that Chapter. Test methods, instrumentation and all other details can be found in Hamamoto et al. [80] and Umeda et al. [79]. Particulars of ships and models are given in Tables 7.1 and 7.2. All other details concerning test ships are given in Appendix F.

7.4. Guidelines For Benchmark Tests

Here, the overview of the benchmark testing is presented focusing on the specification of the environmental data and the specification of benchmark model runs.

The specification of environmental data: The specification of environmental data refers to the definition of the benchmark incident wave conditions. Benchmark tests were performed within the boundaries of the following conditions:

Parameter	Vessel	Model
Model scale		1/60
L_{BP}	150.0 m	2.5 m
B	27.2 m	0.453 m
D	13.5 m	0.225 m
d_f	8.5 m	0.142 m
d_a	8.5 m	0.142 m
C_b	0.667	0.667 m
Δ	23,720 tonne	109.815 kg
LCG	-1.01 m	-0.0168 m
KG	11.48 m	0.1913 m
GM	0.15 m	0.0025 m
T_φ	43.3 sec	5.59 sec

Table 7.1 Principal particulars of Ship A-1 in full scale and model scale

Parameter	Vessel	Model
Model scale		1/15
L_{BP}	34.50 m	2.3 m
B	7.60 m	0.507 m
D	3.07 m	0.205 m
d_f	2.50 m	0.166 m
d_a	2.80 m	0.186 m
C_b	0.597	0.597 m
Δ	425 tonne	125.588 kg
LCG	-1.31 m	-0.087 m
KG	3.36 m	0.224 m
GM	1.0 m	0.0667 m
T_φ	7.4 sec	1.9 sec

Table 7.2 Principal particulars of Ship A-2 in full scale and model scale

Regular Wave Conditions (Ships A-1)

- Wavelength to ship length ratio: 0.25 to 3.00 in steps of (0.25)
- Wavelength to ship length ratio: 0.25 to 3.00 in steps of (0.25)
- Wave height to wavelength ratio: 1 to 25 (constant), alternatively, in addition, 1:20 and 1:30 for specific tests (see 7.1).

Regular Wave Conditions (Ship A-2)

- Wave length to ship length ratio: 1.637 and wave height to wave length ratio: 1/10
- Wave length to ship length ratio: 1.127 and wave height to wave length ratio: 1/8.7

The specification of the benchmark test:

Initial Motion Studies on Ship A1,2:

- *Initial Calm Water Studies (optional)*: Numerical Simulation of the time histories for -35° Turning Manoeuvre for Ship A-2 at $F_n = 0.3$
- *Seakeeping - Zero Forward Speed Case:* 6DOF Response Amplitude Operators (frequency domain techniques) or Time Histories (time domain techniques) of intact Ships A-1 (optional) for varying wavelength, as specified in previous section, and wave headings as follows: 0^0 (following seas), 15^0, 30^0, 45^0
- *Seakeeping - Non-Zero Forward Speed Case:* At service speed, 6 DOF Response Amplitude Operators (frequency domain techniques) or Time Histories (time domain techniques) of intact Ship A-1, for $\lambda/L = 1.5$, wave headings as specified above and varying speed, namely $F_n = 0.20$, 0.30 and 0.40.

Intact Stability Studies on Ship A-1:

- *Non-Zero Forward Speed – Regular Waves Excitation:* Capsize simulation of intact Ship A-1 for the following environmental and ship conditions:

- Wave length to ship length ratio, $\lambda/L = 1.5$,
- Wave height to length ratio $H/\lambda = 1/25$ (standard), study on the effect of change of wave height between 1/20 and 1/30,
- GM=0.15m (constant),
- Case A: Autopilot course: 0^0 (following seas), Fn = 0.20 (capsize).
- Case B: Autopilot course: 30^0 (stern quartering seas), Fn = 0.40 (capsize),
- Case C: Autopilot course: 30^0 (stern quartering seas), but for Fn = 0.30 (non-capsize),
- Case D: Autopilot course: 45^0 (stern quartering seas), Fn = 0.20 (non-capsize)
  - Non-Zero Forward Speed – Regular Waves Excitation: Capsize simulation of intact Ship A-2 for the following environmental and ship conditions:
- GM=1.0 (constant)
- Wave length to ship length ratio, $\lambda/L=1.637$ (for Cases A & B)
- Wave height to length ratio $H/\lambda=1/10$ (for Cases A& B),

- Case A: Auto pilot course: -30° (stern quartering seas), Fn=0.30 (non-capsize).
- Case B: Autopilot course: -10° (stern quartering seas), Fn=0.43 (capsize).

- Wave length to ship length ratio, $\lambda/L=1.127$ (for capsize C &D),
- Wave height to length ratio, $H/\lambda=1/8.7$ (for capsize C & D),
- Case C: Autopilot course: -30° (stern quartering seas), Fn=0.30 (non-capsize).

Case D: Autopilot course: -30° (stern quartering seas), Fn=0.43 (capsize).

Initial conditions of above four cases are specified in the Tables 7.10 and 7.11. An overview of the test cases described above is given in Tables 7.3-7.7.

[$H/\lambda = 1/25$]

$\lambda/L\Rightarrow$ Heading $\Downarrow$	0.25	0.50	0.75	1.00	1.25	1.50	1.75	2.00	2.25	2.50
45^0	√	√	√	√	√	√	√	√	√	√
30^0	√	√	√	√	√	√	√	√	√	√
15^0	√	√	√	√	√	√	√	√	√	√
0^0	√	√	√	√	√	√	√	√	√	√

Table 7.3 Zero Speed Seakeeping Cases for Ships A-1 (Intact Ship, Regular Waves)

[$H/\lambda = 1/25$, $\lambda/L = 1.50$]

Fn⇒ Heading ⇓	0.20	0.30	0.40
45^0	√	√	√
30^0	√	√	√
15^0	√	√	√
0^0	√	√	√

Table 7.4 Non-Zero Speed Seakeeping Test Cases for Ship A-1 (Intact Ship, Regular Waves)

[$H/\lambda = 1/25$ (1/20 – 1/30), $\lambda/L = 1.50$, GM = 0.15m]

Nominal Fn⇒ Autopilot course ⇓	0.20	0.30	0.40
45^0	√ non-capsize		
30^0		√ non-capsize	√ capsize
0^0	√ capsize		

Table 7.5 Intact Stability Test Cases for Ship A-1) (Nonzero speed, Regular Waves)

[H/λ=1/10, λ/L=1.637, GM=1.0m]

Fn⇒ Autopilot course ⇓	0.20	0.30	0.43
-30°		√non-capsize	
-10°			√capsize

Table 7.6 Intact Stability Test Cases for Ship A-2 (Nonzero speed, Regular Waves)

[H/λ = 1/8.7, λ/L=1.1127, GM = 1.0m]

Fn⇒ Autopilot course ⇓	0.20	0.30	0.43
-30°		√non-capsize	√capsize

Table 7.7 Intact Stability Test Cases for Ship A-2 (Nonzero speed, Regular Waves)

In our validation study, the focus of the simulation will be the model runs described in Table 7.3-7.7. Therefore, those parameters along with the control parameters provided in benchmark tests are given in Tables 7.8-7.9.

Nominal Froude number	Fn	0.2	0.2	0.3	0.4
Autopilot course from the wave direction	χ_c (degree)	0.0	45.0	30.0	30.0
Wave steepness	H/λ	1/25	1/25	1/25	1/25
Wave length to ship length ratio	λ/L_{pp}	1.5	1.5	1.5	1.5
Proportional gain	K_P (sec)	1.2	1.2	0.8	0.5
Differential gain	K_R (sec)	6.84	6.84	4.56	2.85

Table 7.8 Control parameters of capsizing model runs of Ship A-1

For Ship A-1, the righting arm curves in calm water, as well as in longitudinal wave are calculated for the ship metacentric height of 0,15m shown in Figure 7.1. The GM selected is not the design GM value, but one that only just satisfies the IMO

regulations. Deckhouses were not included in the model because stability criteria ignore them as non-watertight structures.

During the experiments, the ship model was self-propelled and was completely free. The formulation below, instead of open water test results, was provided for the propeller thrust coefficient;

$$K_T = \frac{T}{\rho n^2 D_p^4} = -0.0844J^2 - 0.4882J + 0.4539$$

Equation 7.3

where J is the propeller advance coefficient, ρ is the water density, n is the propeller revolution number.

For Ship A-2, the similar techniques were used. The righting arm curves in calm water with the ship metacentric height of 1.00 m are shown in Figure 7.2. Once again, this ship critically complies with the IMO intact stability code.

The details of other experiments take place under benchmark tests are displayed in Appendix F.

Nominal Froude number	Fn	0.3	0.43	0.3	0.43
Autopilot course from the wave direction	χ_c (degree)	-30.0	-10.0	-30.0	-30.0
Wave steepness	H/λ	1/10	1/10	1/8.7	1/8.7
Wave length to ship length ratio	λ/L_{pp}	1.637	1.637	1.127	1.127
Proportional gain	K_P (sec)	1.0	1.0	1.0	1.0
Differential gain	K_R (sec)	0.0	0.0	0.0	70.0

Table 7.9 Control parameters of capsizing model runs of Ship A-2

Nominal Froude Number	Fn	0.2	0.2	0.3	0.4
Autopilot course	χ_c(degree)	0	45	30	30
Non-dimensional longitudinal position from a wave trough	ξ_G/λ	0.22	0.79	0.51	0.26
Ship velocity in x direction	u(m/sec)	0.99	0.90	1.49	1.98
Ship velocity in y direction	v(m/sec)	0.0	0.0	0.0	0.0
Non-dimensional vertical position from the still water level	ζ_G/a	0.28	0.13	-0.20	0.07
Ship velocity in z direction	w(m/sec)	0.053	-0.087	0.015	0.034
Roll angle	ϕ(degree)	-10.01	-5.77	-0.71	-0.71
Roll angular velocity	p(degree/sec)	30.3	1.30	-6.29	-1.70
Pitch angle	θ(degree)	-4.17	4.48	0.30	-2.50
Pitch angular velocity	q(degree/sec)	-3.00	-7.8	12.73	6.99
Yaw angle from the wave direction	χ(degree)	0.65	44.74	41.56	39.32
Yaw angular velocity	χ(degree)	-0.88	-11.00	2.40	8.60
Rudder angle	δ(degree)	10.0	10.0	-10.0	-10.0

Table 7.10 Initial conditions of capsizing model runs of Ship A-1 in model scale

Nominal Froude Number	Fn	0.3	0.43	0.3	0.43
Autopilot course	χ_c(degree)	-30.0	-10.0	-30.0	-30.0
Non-dimensional longitudinal position from a wave trough	ξ_G/λ	0.863	0.033	0.875	0.130
Ship velocity in x direction	u(m/sec)	0.254	0.254	0.428	0.214
Ship velocity in y direction	v(m/sec)	0.0	0.0	0.0	0.0
Non-dimensional vertical position from the still water level	ζ_G/a	0.301	0.502	0.160	0.099
Ship velocity in z direction	w(m/sec)	-0.236	-0.012	-0.094	0.089
Roll angle	ϕ(degree)	6.22	-5.49	-0.115	-1.41
Roll angular velocity	p(degree/sec)	1.15	11.56	21.36	-6.95
Pitch angle	θ(degree)	-8.17	-0.52	-5.99	1.95
Pitch angular velocity	q(degree/sec)	-15.00	-38.	-20.6	-21.0
Yaw angle from the wave direction	χ(degree)	7.08	-29.8	-21.6	-19.1
Yaw angular velocity	χ(degree)	-5.15	4.61	-18.31	9.02
Rudder angle	δ(degree)	10.5	12.1	-10.1	-6.0

Table 7.11 Initial conditions of capsizing model runs of Ship A-2 in model scale

Based on above background, now the validation study and the matters arise during it will be presented in the next section.

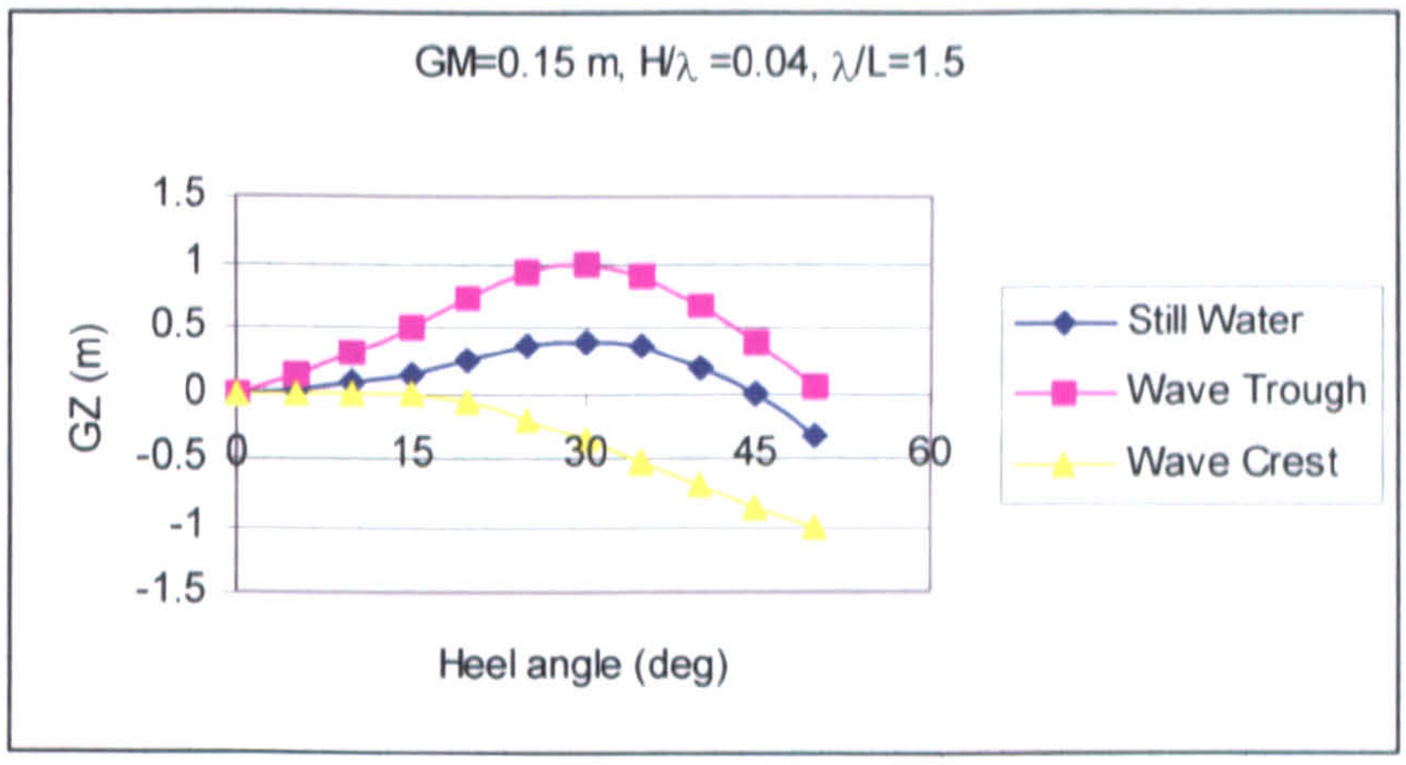

Figure 7.1. Calculated righting arms curves of Ship A-1 in still water, wave trough and crest in full scale

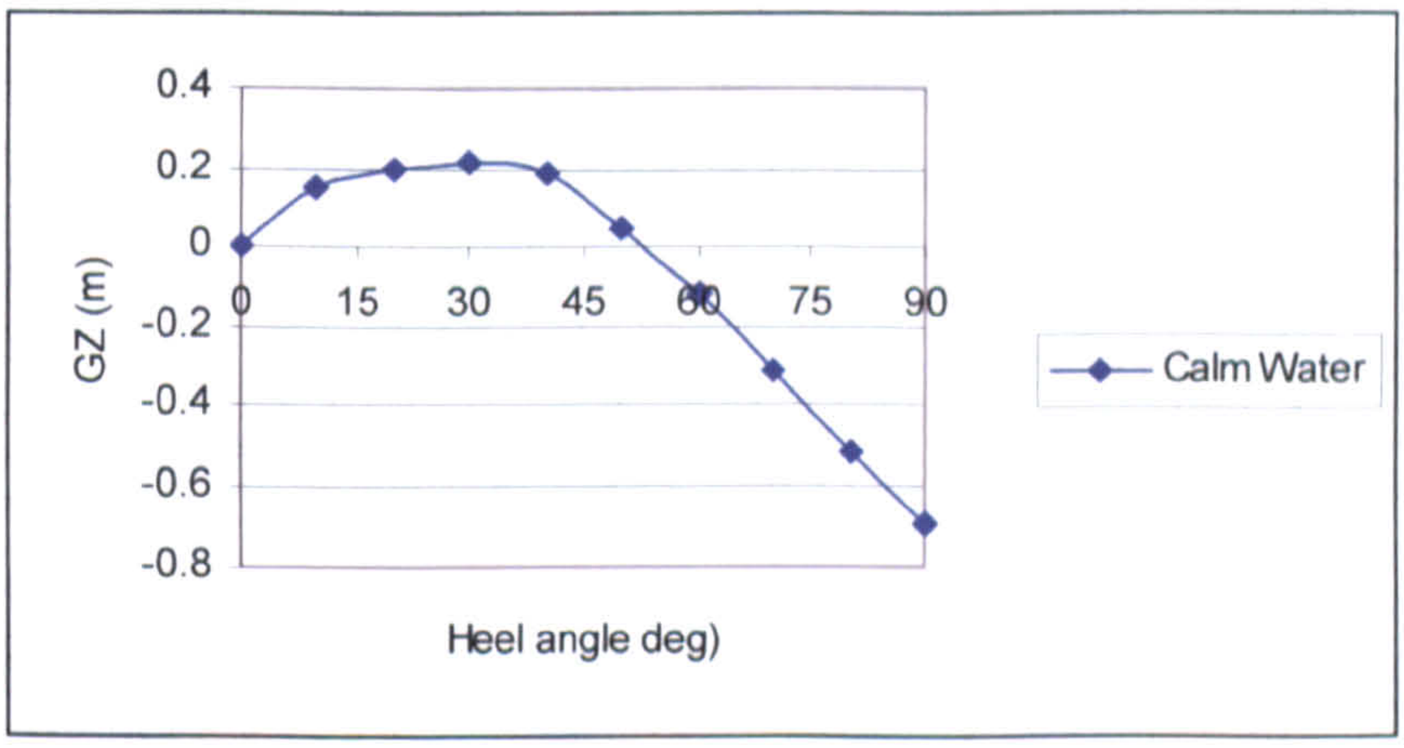

Figure 7.2. Calculated righting arm curve of Ship A-2 in calm water in full scale

7.5. Comparisons of Numerical Model With Experiments

In the case of Ship A-1, two aforementioned approaches in the numerical model have been tested against the experiment results. The first approach represented in Equations 7.1 and 7.2 was used in the numerical model for 6 DOF and the results presented in Figures 7.3-7.6. The second approach represented in Equation 5.23 and with the methods explained in Chapter 6 was employed in the numerical model for 6 DOF and the results presented in Figures 7.7-7.10. Environmental and control parameters are same for each case and the results for the runs are given in same order.

In the experiments, based on the parameters given in Table 7.8, capsizing due sub-harmonic roll, sub-harmonic roll without capsizing, harmonic roll, capsizing due harmonic roll, respectively, were observed. Experiments were conducted from relatively low speed to relatively very high speed for the vessel, therefore increased the chance of occurrence of different types of dangerous situations. The dangerous situations observed were low cycle resonance in low speed case and capsizing due to harmonic roll with

rapid parametric build-up of roll motion for high speed case, which eventually resulted in capsizing.

For Ship A-2, the first approach was used in the numerical model. The results in 6 DOF were almost identical to ones which are calculated for 4 DOF with static equilibrium in heave and pitch by Ayaz et al. [130]. The only difference to calculation for Ship A-1 was to use of mean water surface for wave forces and restoring which were thought to be convenient when very high speed and the environmental conditions and the situations like surf-riding are concerned. Therefore it is opted to present the same results.

As it can be seen, these experiments were conducted in high speeds in which broaching-to associated with surf-riding are likely to occur. Indeed, non-capsizing, broaching-to associated with surf-riding, non-capsizing and capsizing due to rapid build-up of roll motion, respectively, were observed in the experiments.

7.6. Discussion on Results

Herein, the models are tested in different speeds, wave steepness, wave height to ship length ratio and heading angles (See Table 7.8 and Table 7.9). The graphs presented (See Figure 7.3-7.14), show the comparison of the results of experiment and numerical method for the roll, yaw and rudder angles. For Ship A-1, comparisons of model runs are presented in Figures 7.3-7.10. In Figure 7.3 and 7.7, the model was run in 0.2 Froude number and 0 degrees autopilot course from the wave direction. The second test (Figures 7.4-7.8) was carried out in 0.2 Froude number and 45 degrees autopilot course from the wave direction. The third and fourth tests (Figures 7.5-7.6,7.9-7.10) were conducted for 30 degrees autopilot course and 0.3 and 0.4 Froude numbers, respectively.

For Ship A-2, comparisons for benchmark tests are presented in Figure 7.11-14. In Figure 7.11, the model was run in 0.3 Froude number and –30 degrees autopilot course from the wave direction. The second test (Figures 7.12) was carried out for similar wave steepness and wave height while Fn was set to be 0.43, which is the maximum speed defined by the length between perpendiculars, and autopilot course was taken –10 degrees. For the next two runs (Figures 7.13, 7.14), the wave steepness was increased, the wave length was decreased and autopilot course was set to –30 degrees. The model was run in Froude number 0.3 and 0.43, respectively. Model was tested for

given time intervals in benchmark tests. All external forces were added. Principal particulars and initial conditions capsizing model runs of Ship A-1 and Ship A-2 are given in Table 7.1 and Table 7.2, Table 7.10 and Table 7.11 respectively.

For Ship A-1, 6 DOF model in aforementioned two approaches is used for model runs. For the first approach, in the first run (Figure 7.3) model experiences wave crest at amidships for a while and this leads to significantly large roll angle. After 15 seconds, the model cannot find the enough buoyancy the keep herself upright and it eventually capsizes. In the numerical model, the model reaches capsizing limit after a huge jump in roll angle, instead of parametric build up as it happened in the experiment. On the other hand, the very large rudder deflection, first to the port and then to the starboard, is seen before the capsizing. The numerical model seems to be causing problems in simulating rudder and inevitably yaw motions. The model proves to be too stiff. Here the "stiffness" means that deviations in the yaw or rudder amplitudes are small or the motion attitude is very rigid contrast to large deviations in the experiments. This leads to smaller roll angles in numerical model despite the large angles are fully taken into account in the numerical model. The numerical model catches up satisfactorily the pitch angle, which is important in calculating the instantaneous wave surface.

When the second approach was used in the same case (Figure. 7.7), the roll motion simulates sub-harmonic roll case with better accuracy in terms of amplitude. Problems are encountered again, however, in simulating rudder motion and yaw motions. The model proves to be too stiff again. However, this time yaw and rudder characteristics are highly affected by frequency dependent terms and coupling between yaw and roll motion leads to large roll periods and amplitude in the numerical model. The pitch angle is almost identical to the first approach.

In the second run (Figure 7.4) the model yet again experiences wave crest at amidships and large roll angle after the autopilot course is set to 45 degrees, however this time model finds the enough buoyancy the keep herself upright eventually. The numerical model displays rudder and yaw motions rather well, despite the same "stiffness" problem in the first run still existing. Also, the roll motion has similarities to sub-harmonic roll motion observed in the experiment.

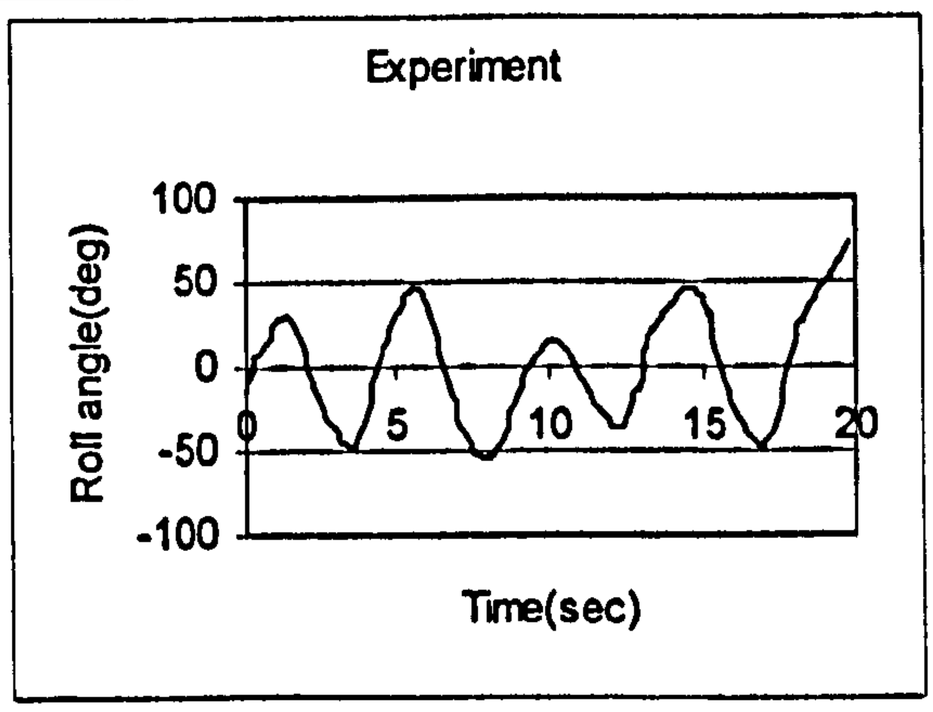

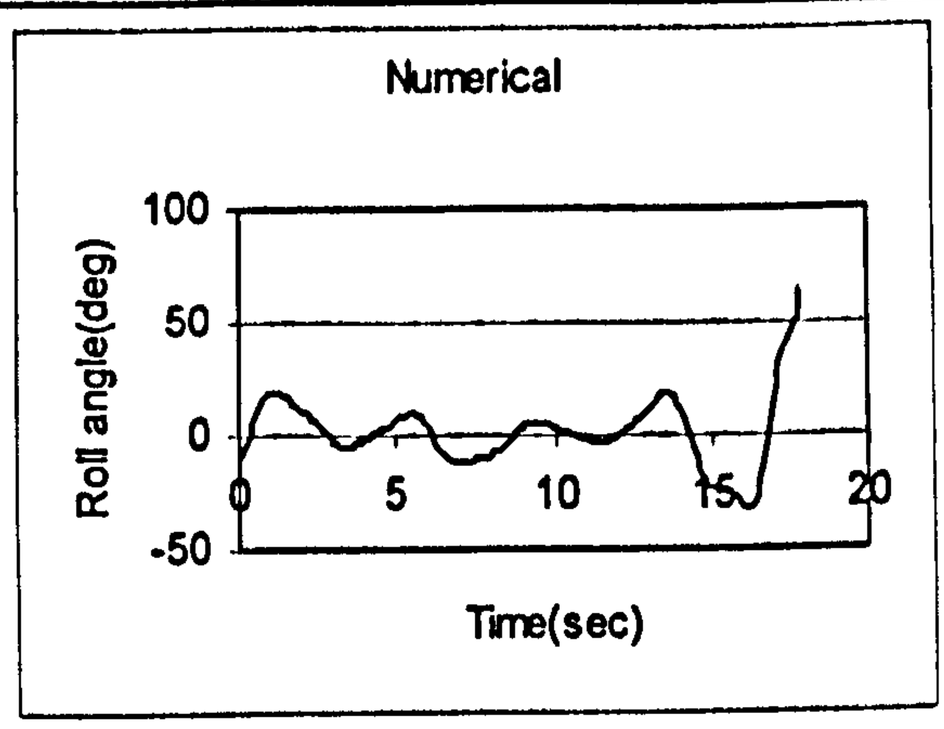

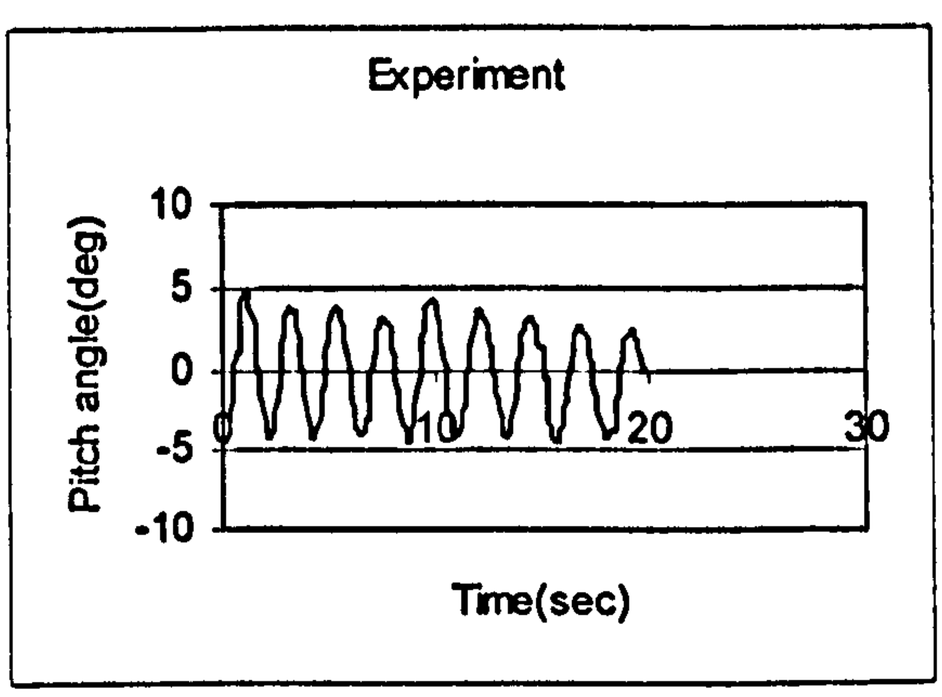

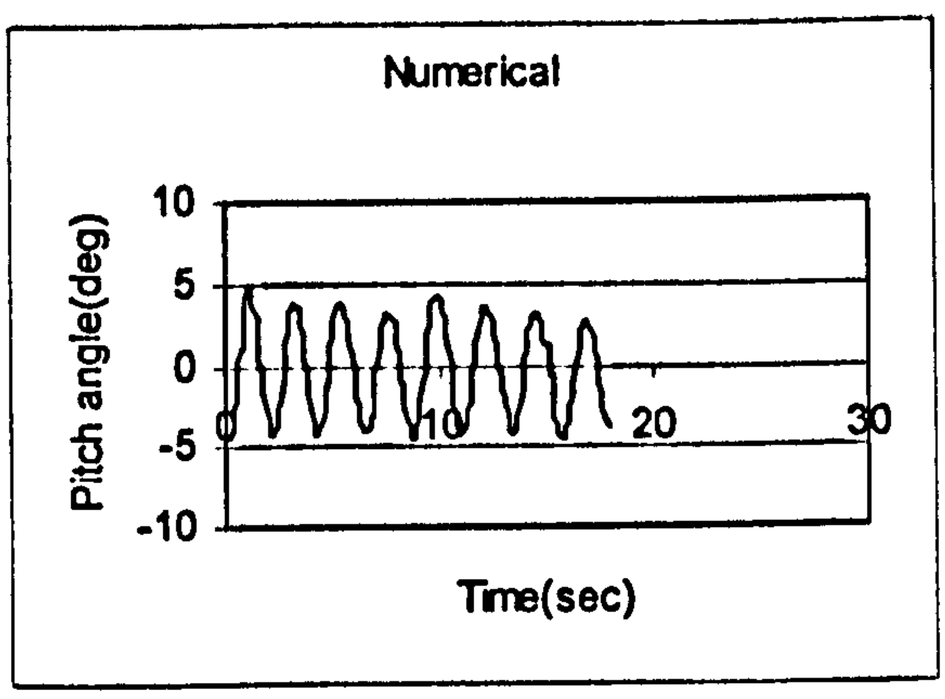

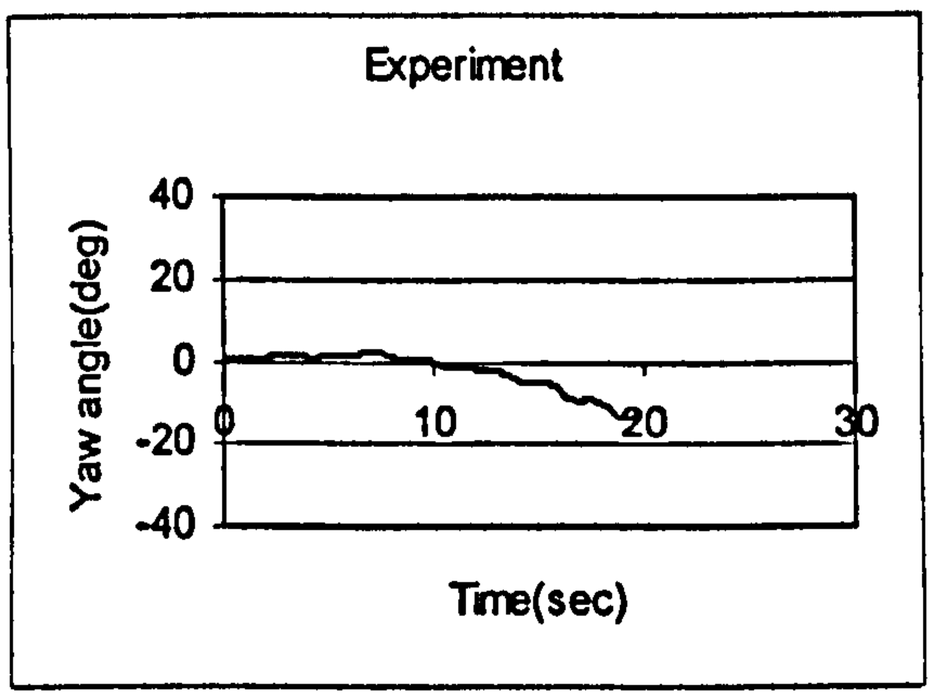

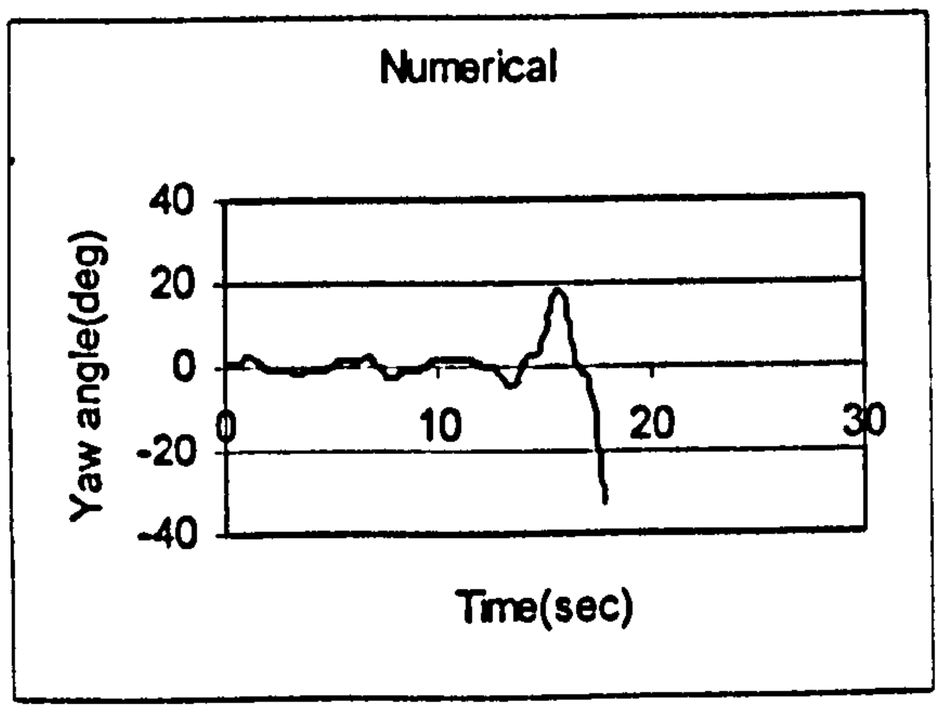

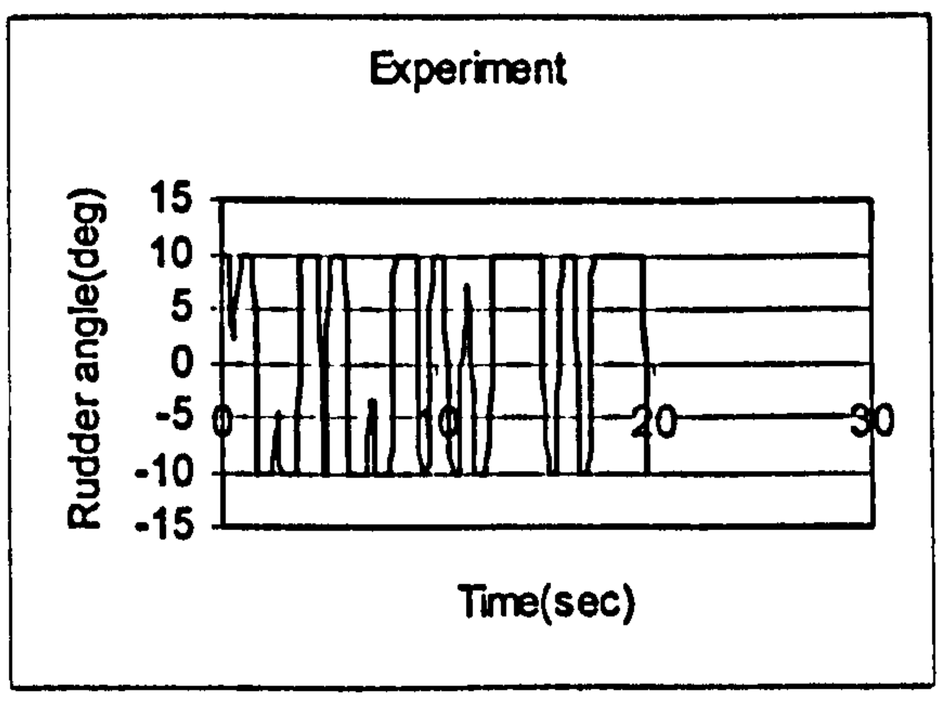

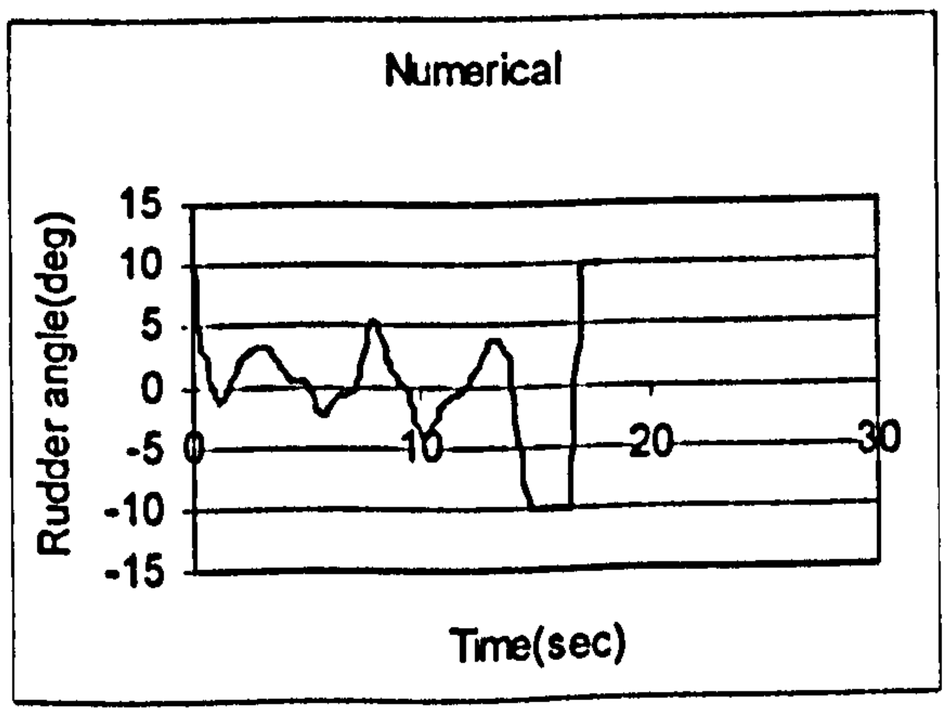

Figure 7.3 Comparison of model experiment and numerical method for the model of Ship A-1 in $H/\lambda=1/25$, $\lambda/L_{pp}=1.5$, $Fn=0.2$, $\chi_c=0$ degrees

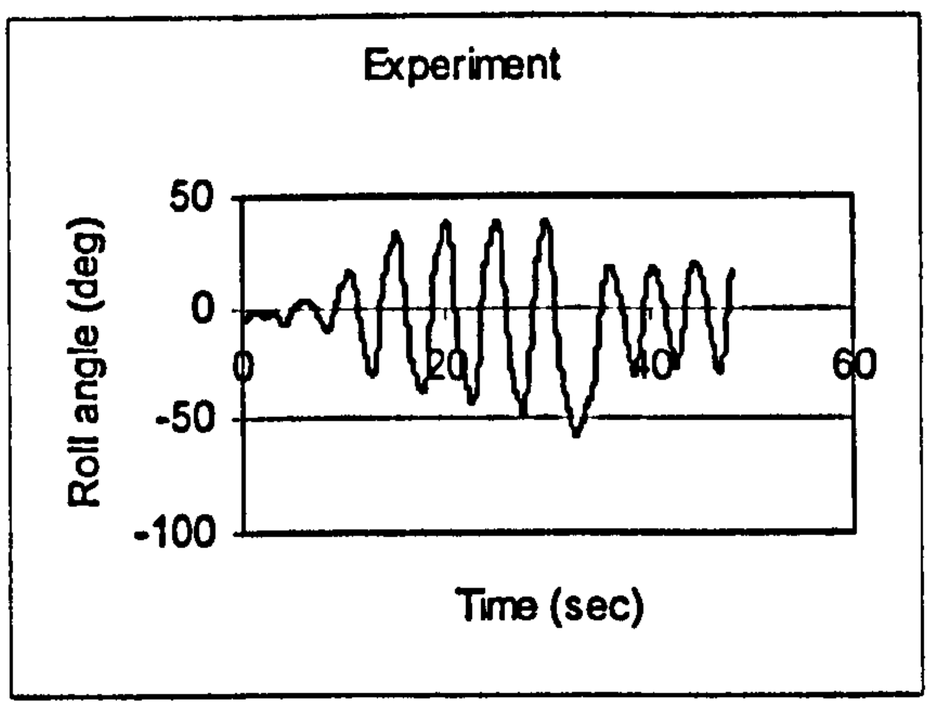

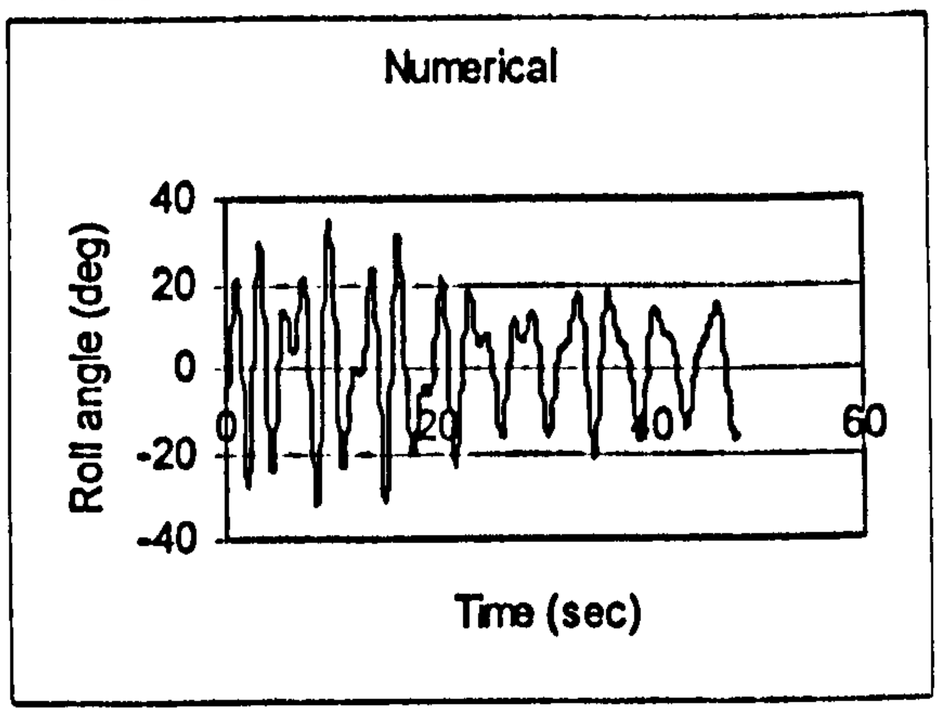

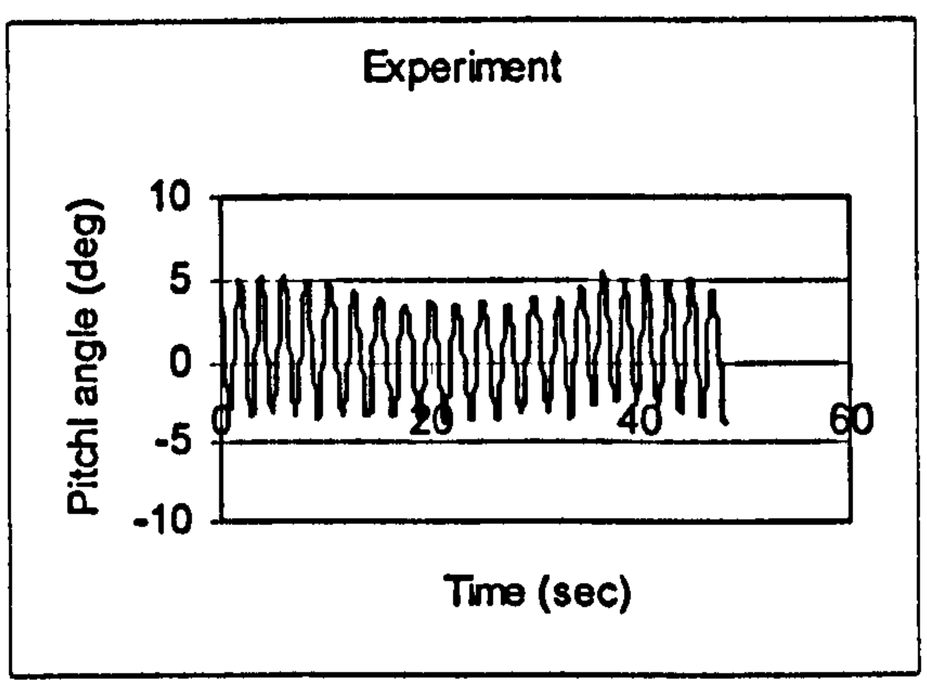

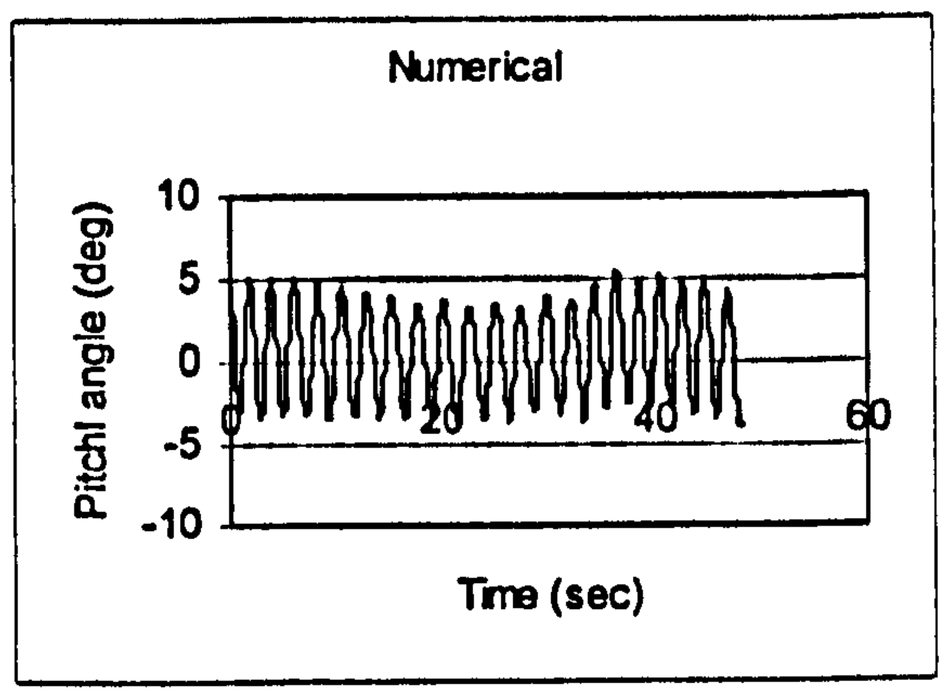

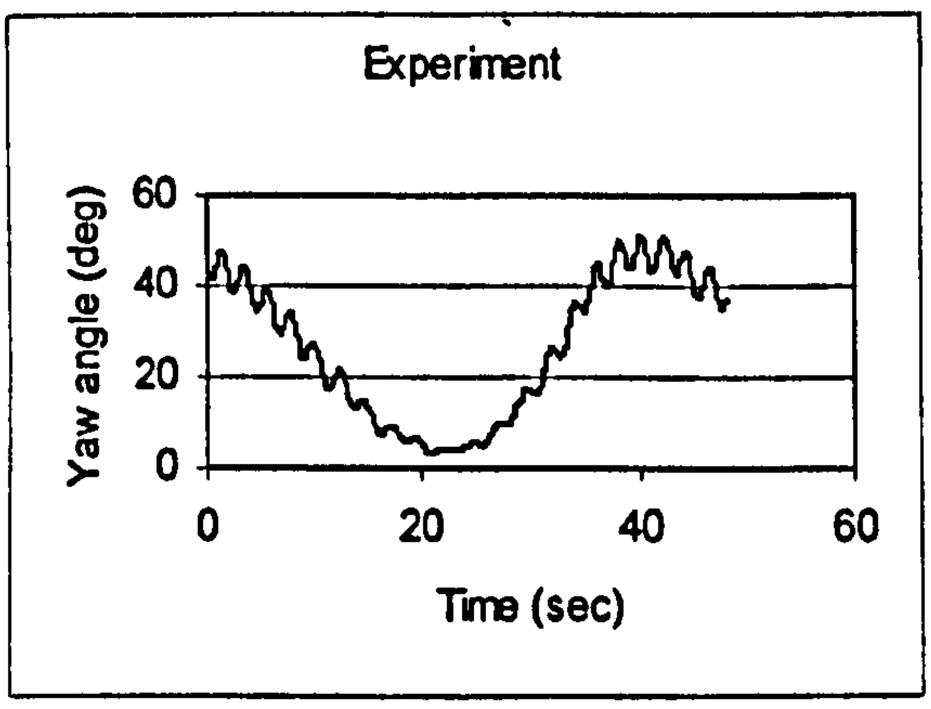

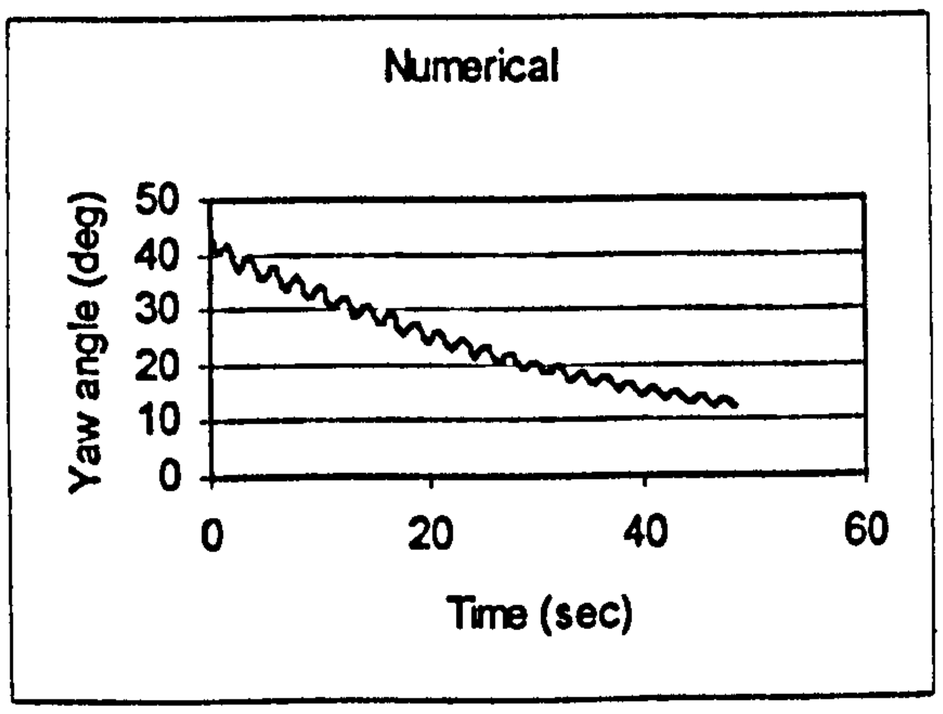

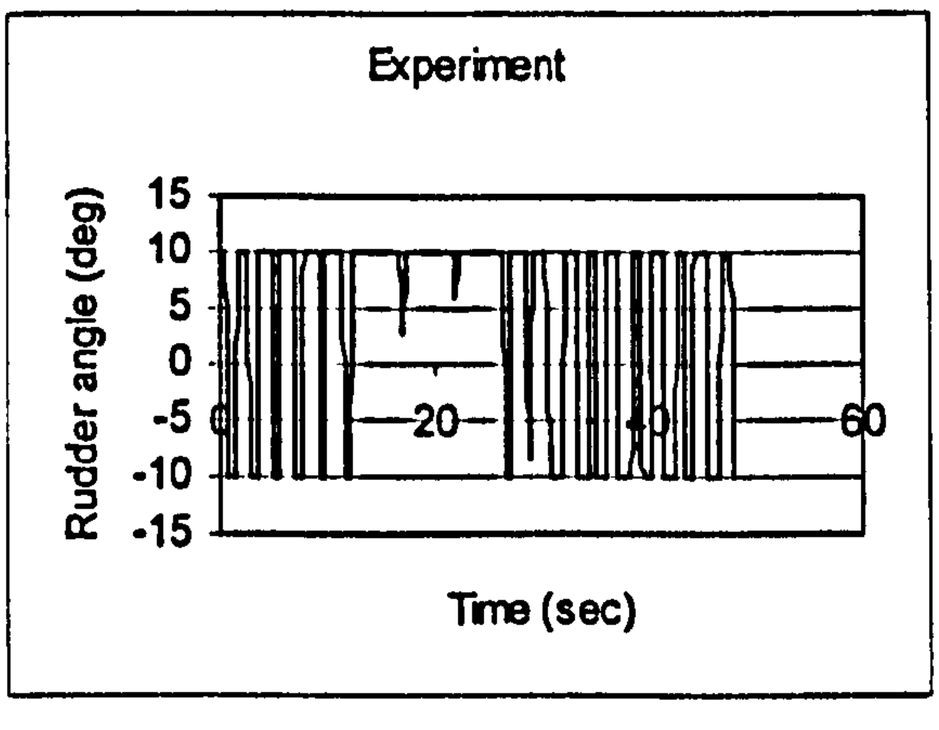

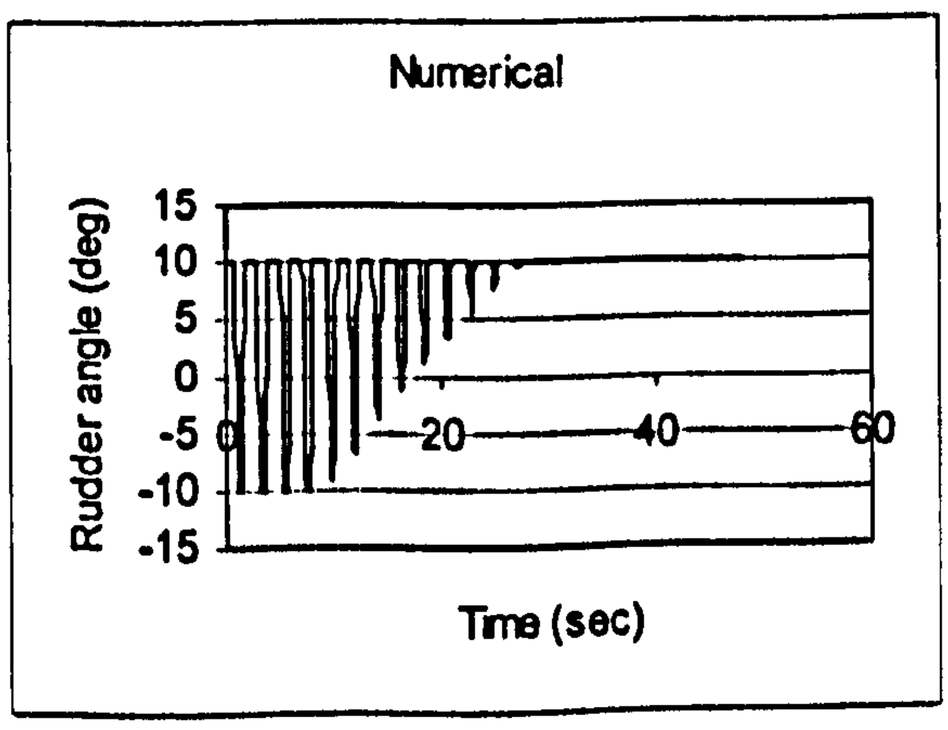

Figure 7.4 Comparison of model experiment and numerical method for the model of Ship A-1 in $H/\lambda=1/25$, $\lambda/L_{pp}=1.5$, $Fn=0.2$, $\chi_c=45$ degrees

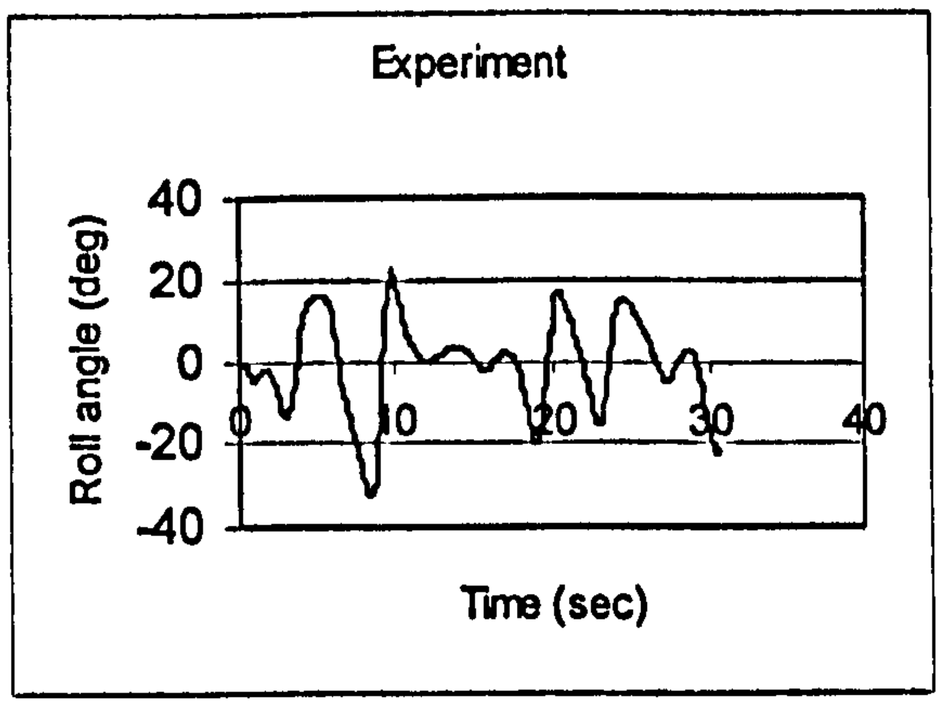

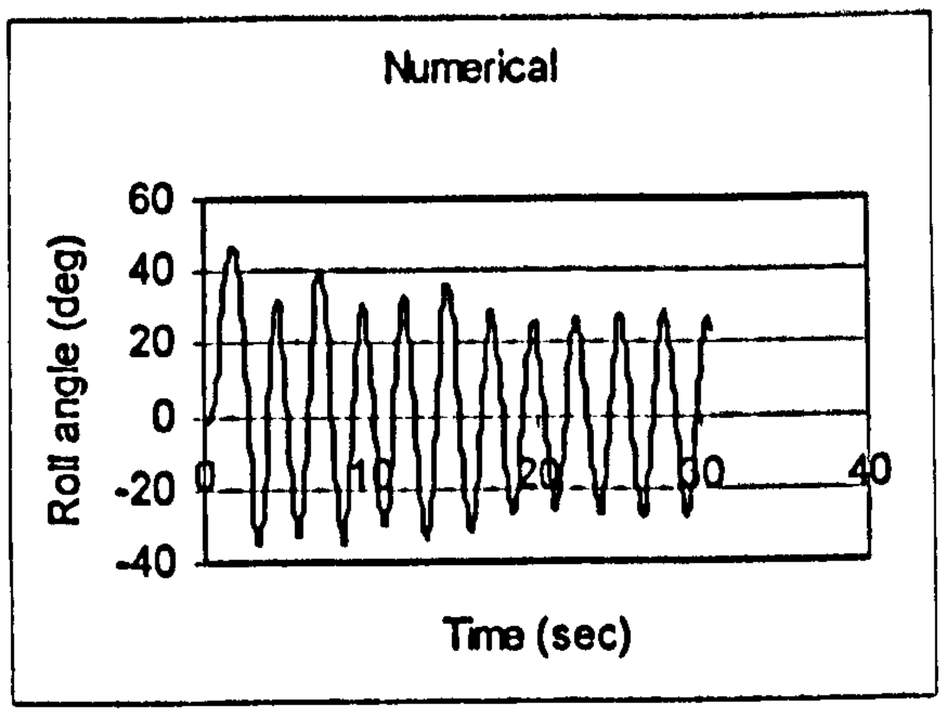

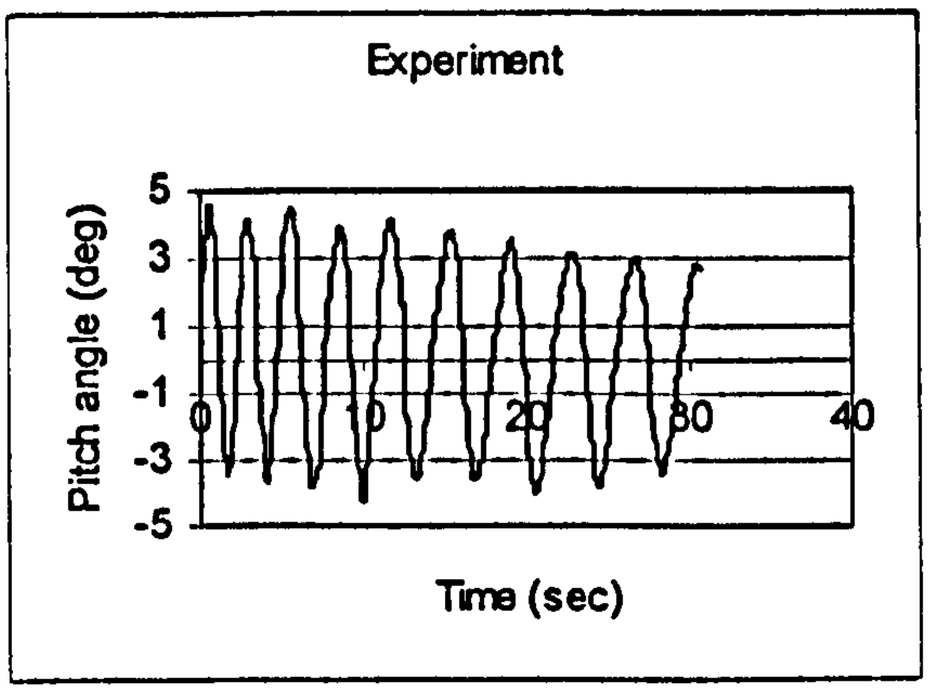

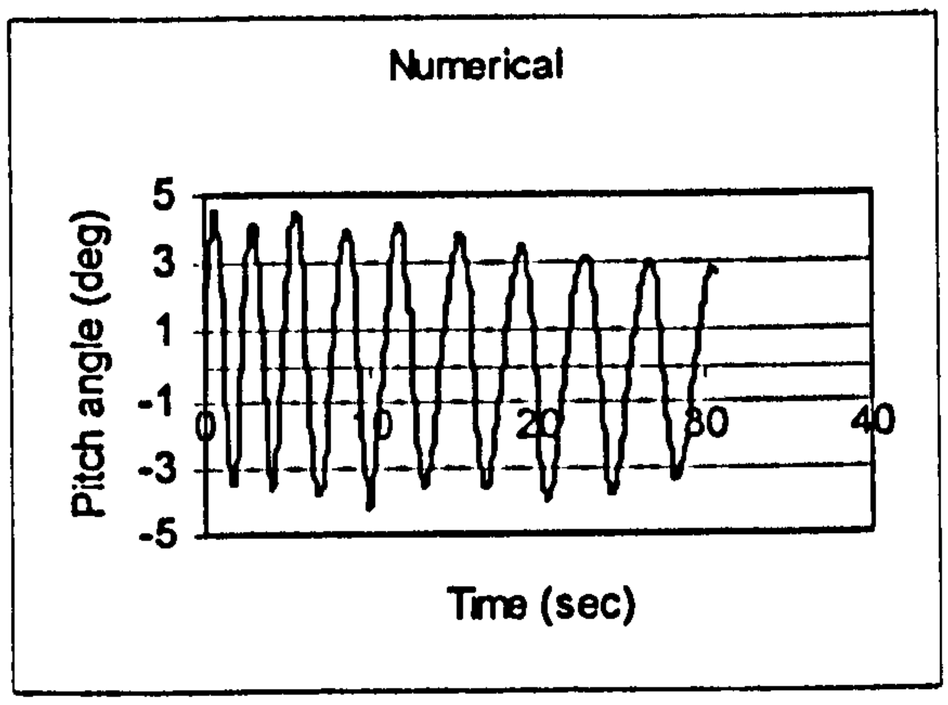

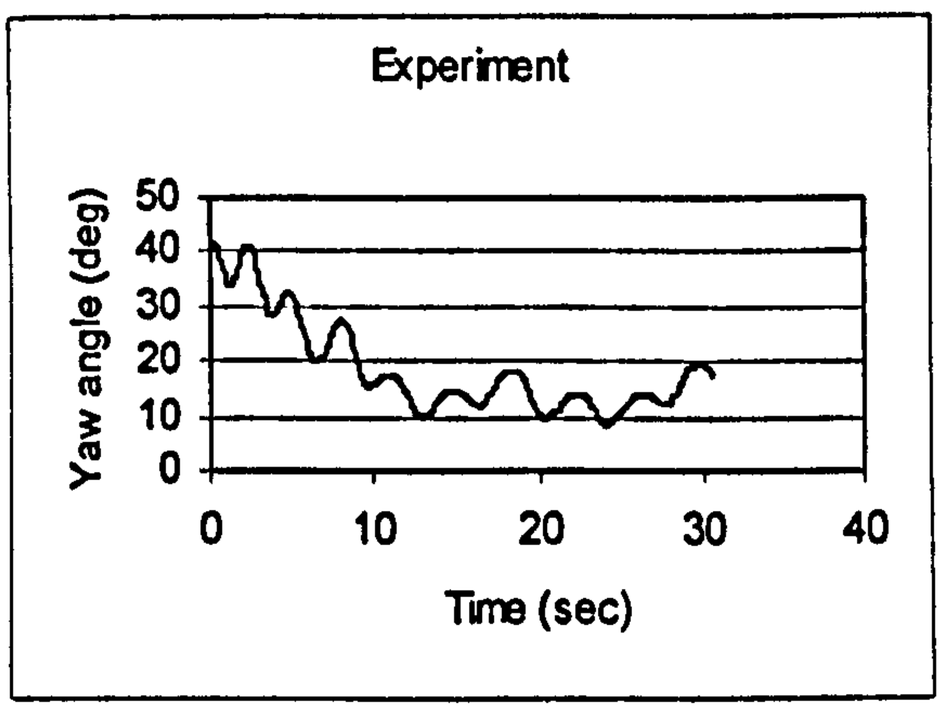

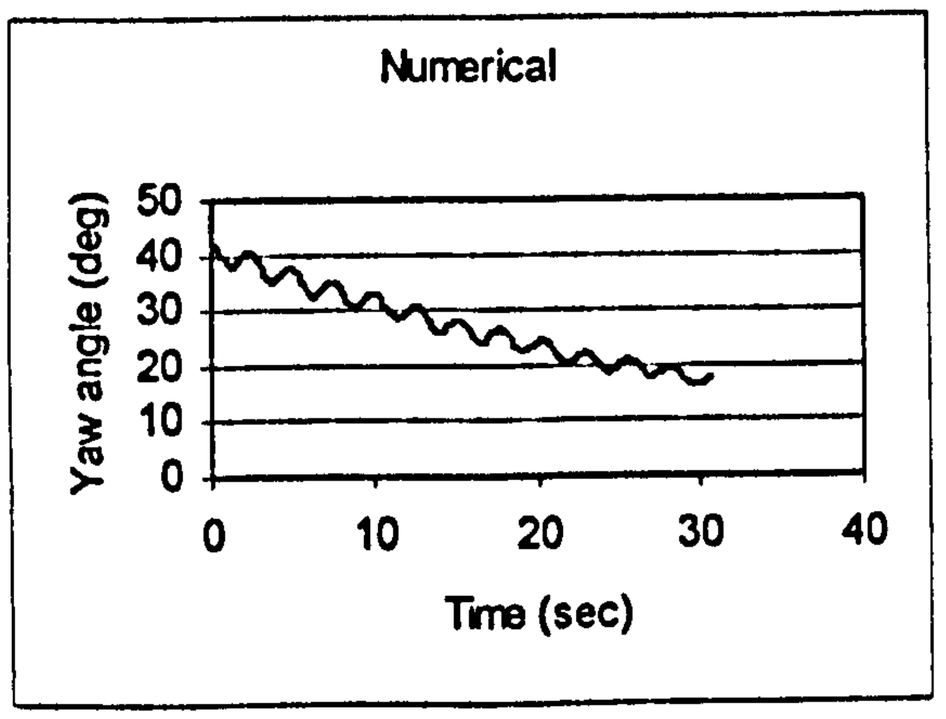

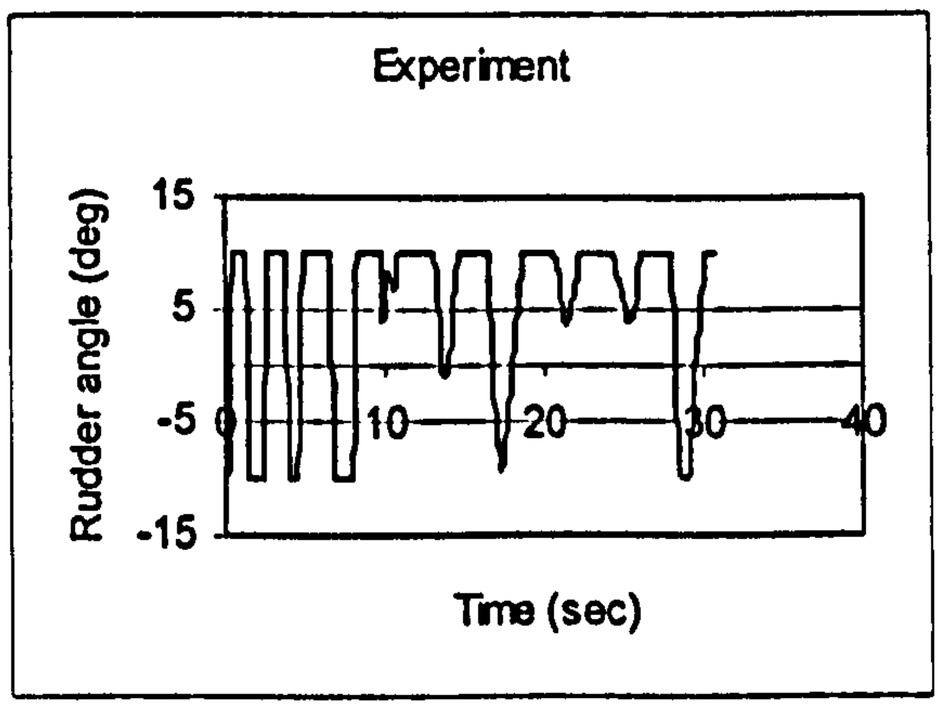

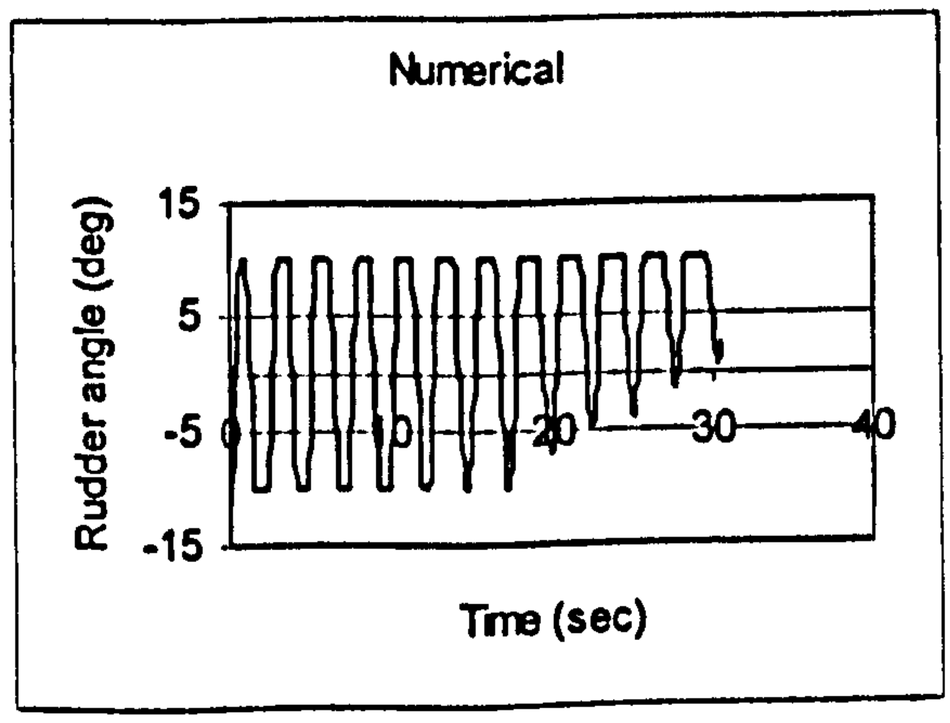

Figure 7.5 Comparison of model experiment and numerical method for the model of Ship A-1 in $H/\lambda=1/25$, $\lambda/L_{pp}=1.5$, $Fn=0.3$, $\chi_c=30$ degrees

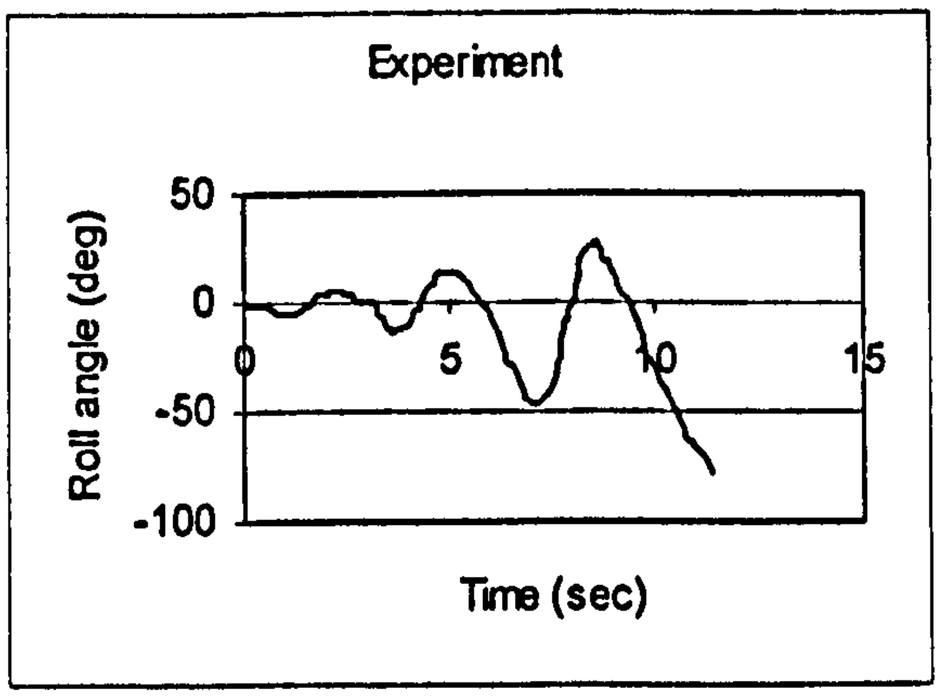

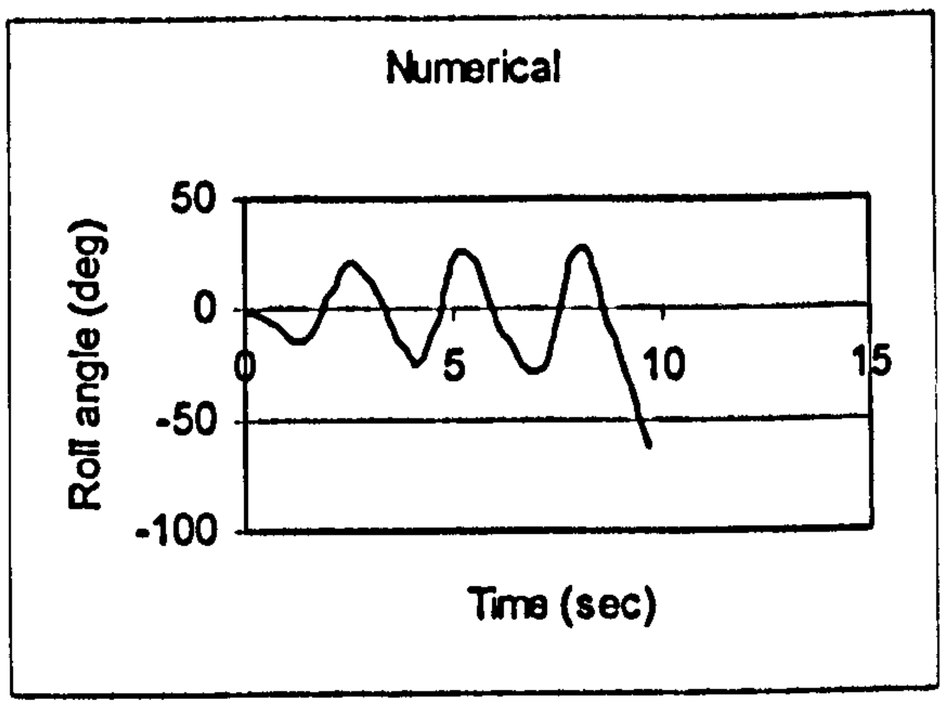

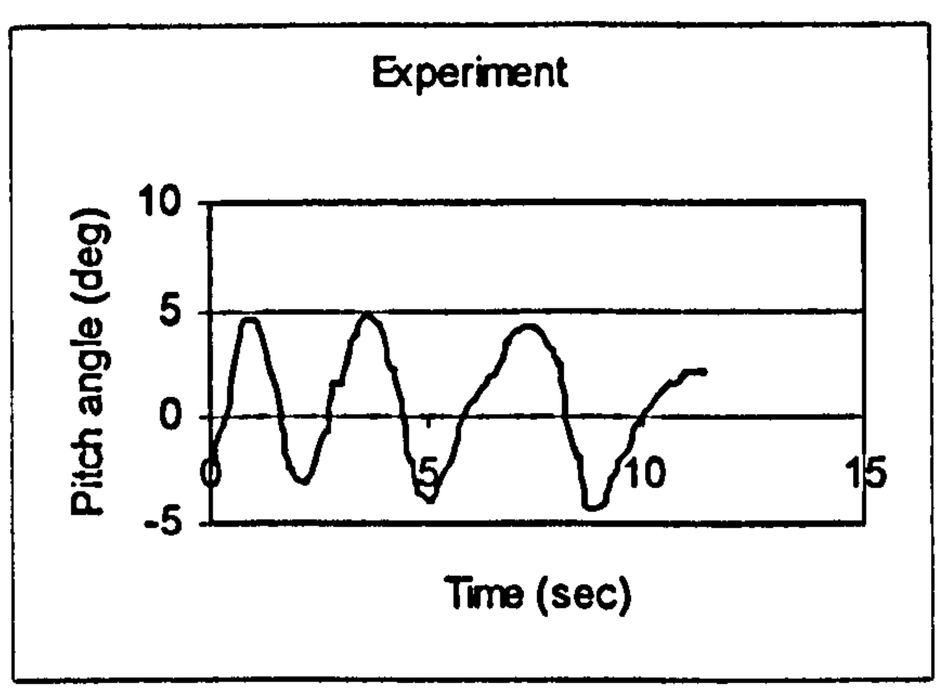

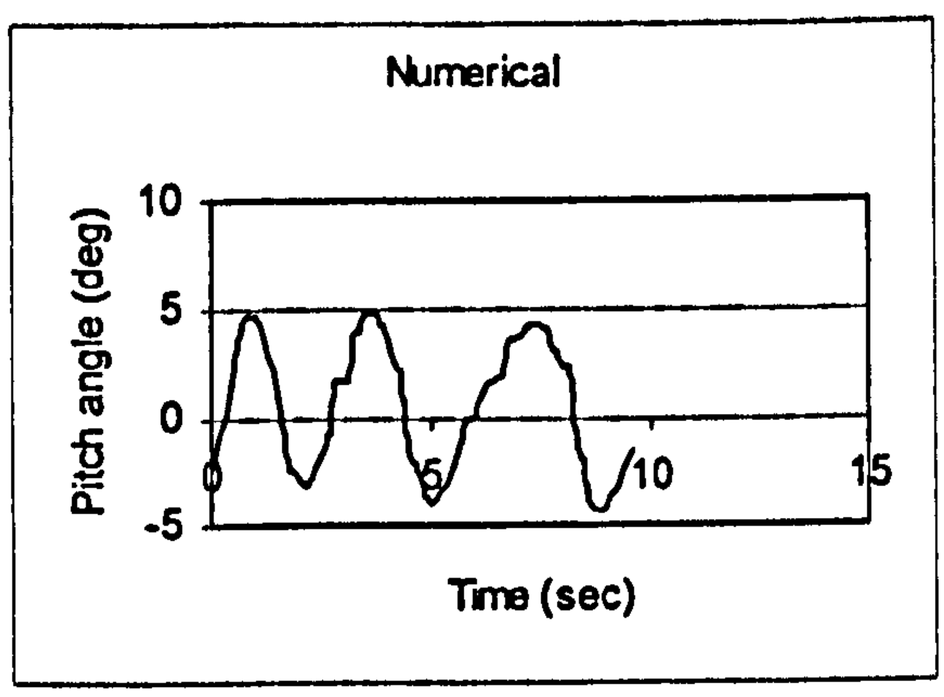

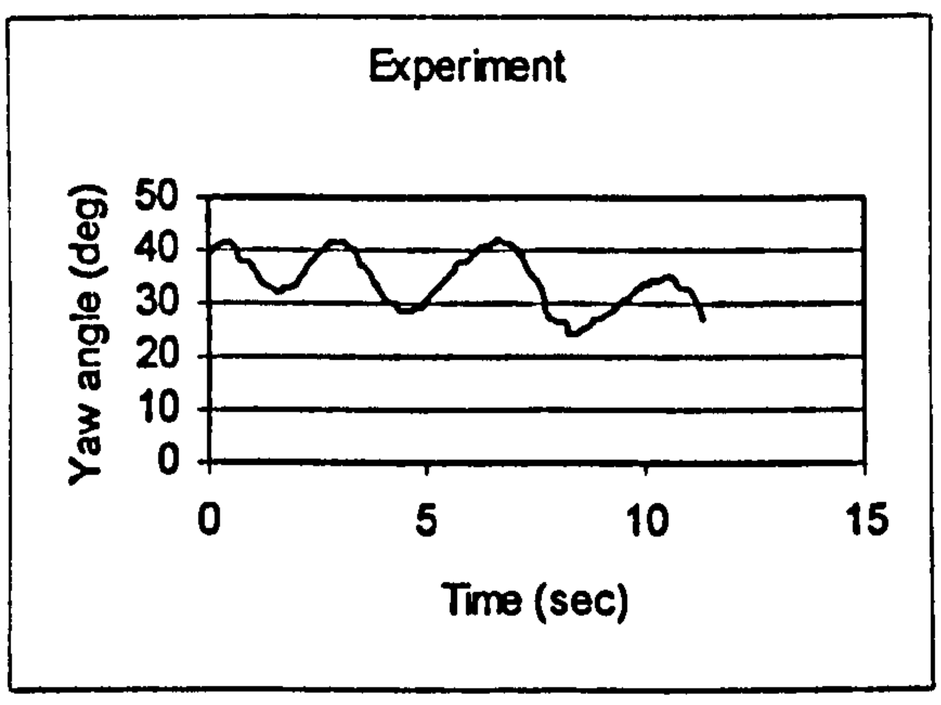

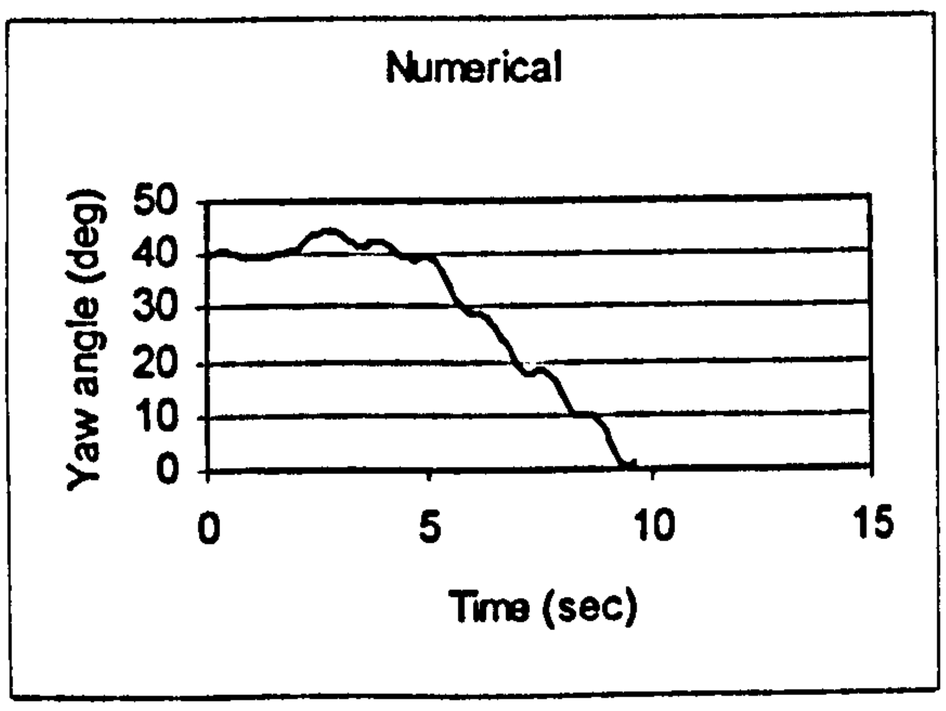

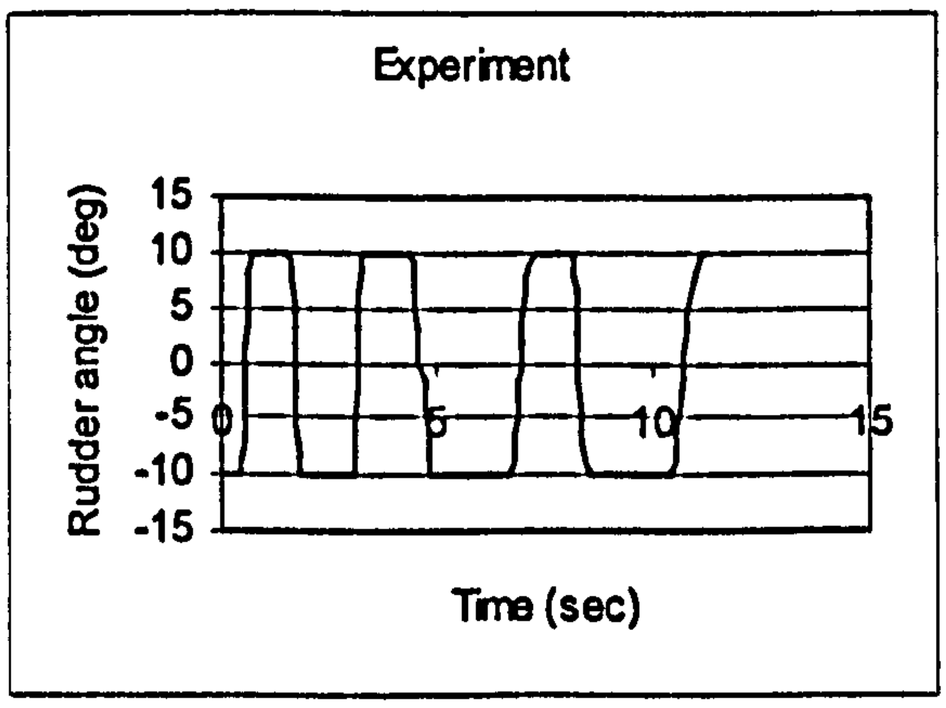

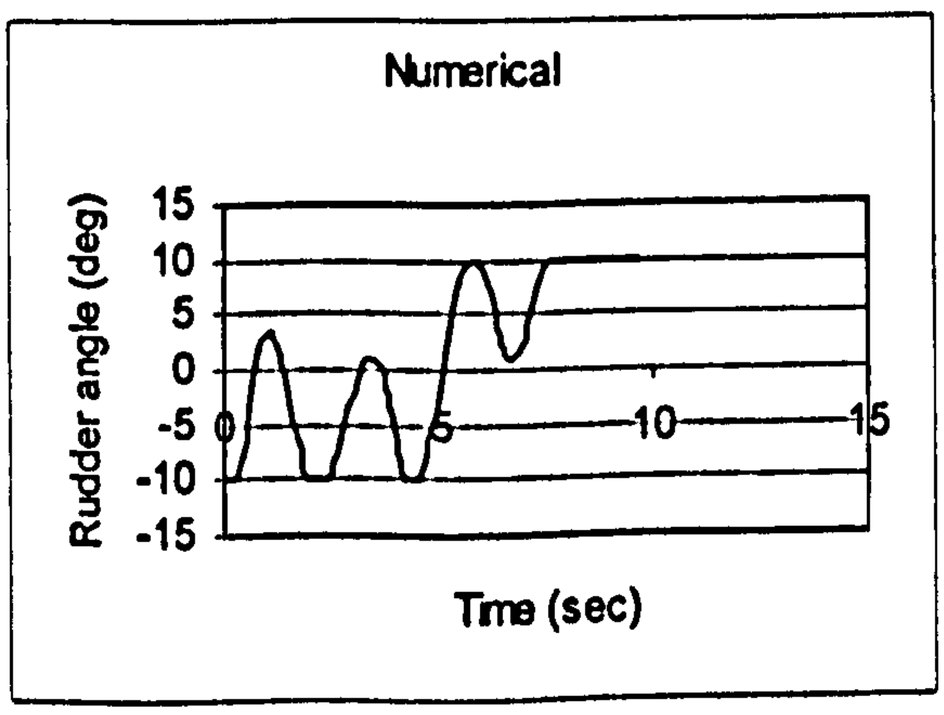

Figure 7.6 Comparison of model experiment and numerical method for the model of Ship A-1 in $H/\lambda=1/25$, $\lambda/L_{pp}=1.5$, $Fn=0.4$, $\chi_c=30$ degrees (Capsizing)

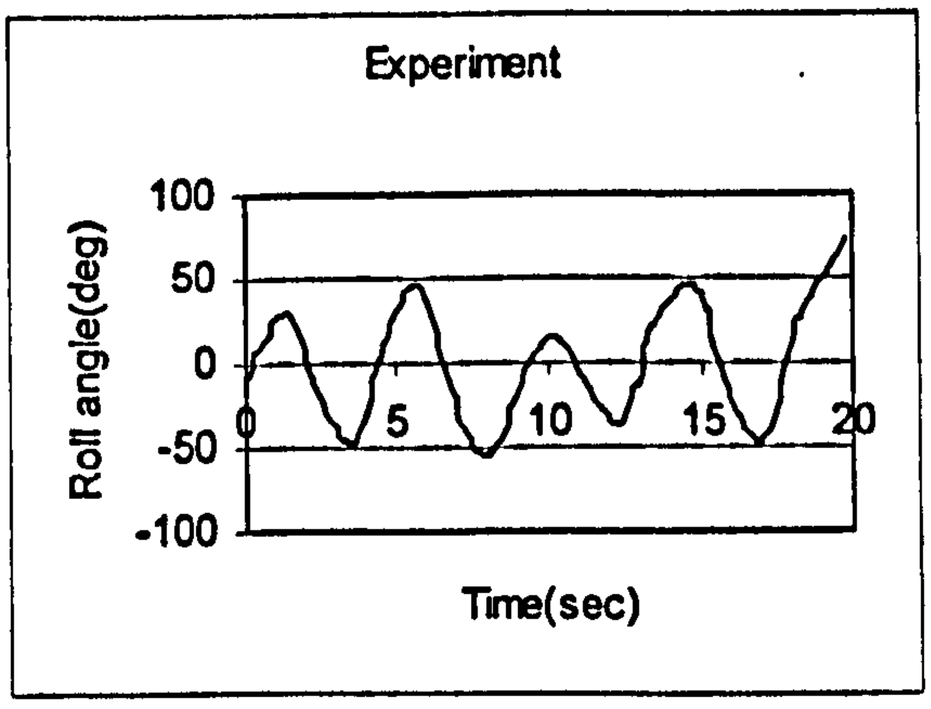

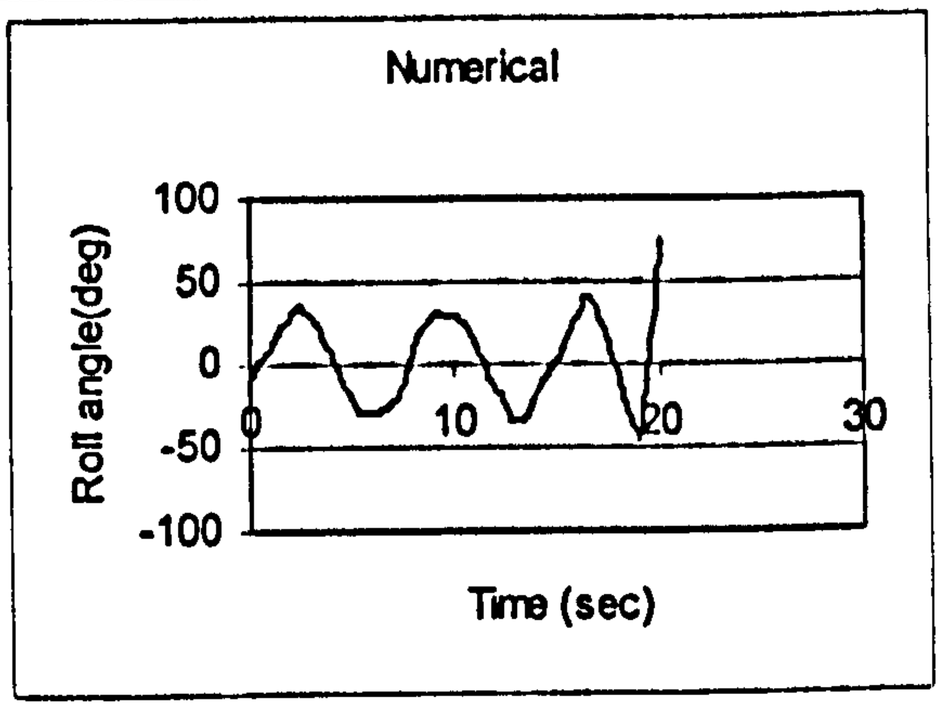

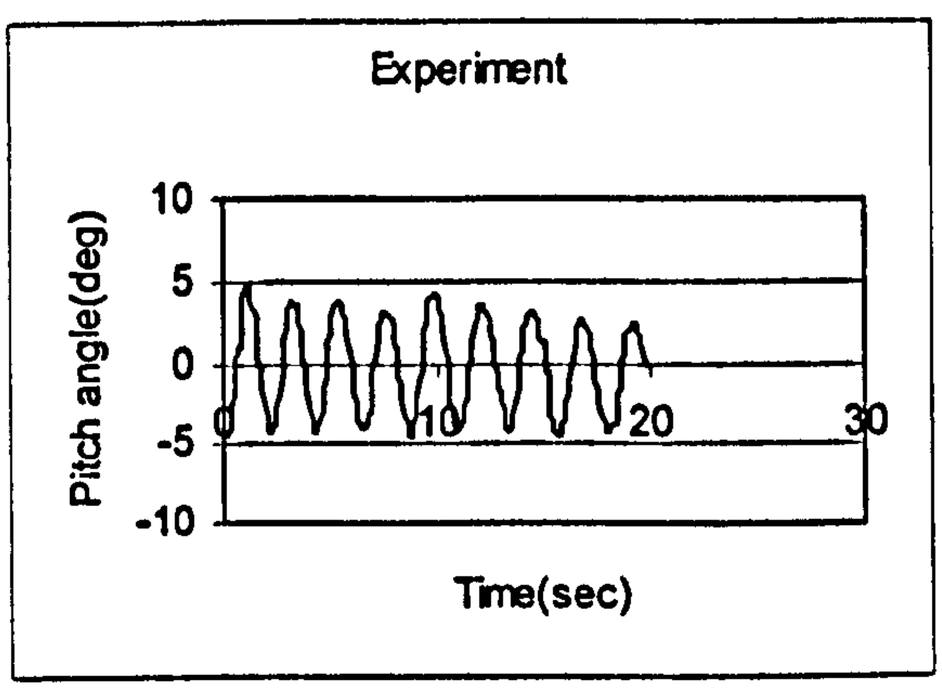

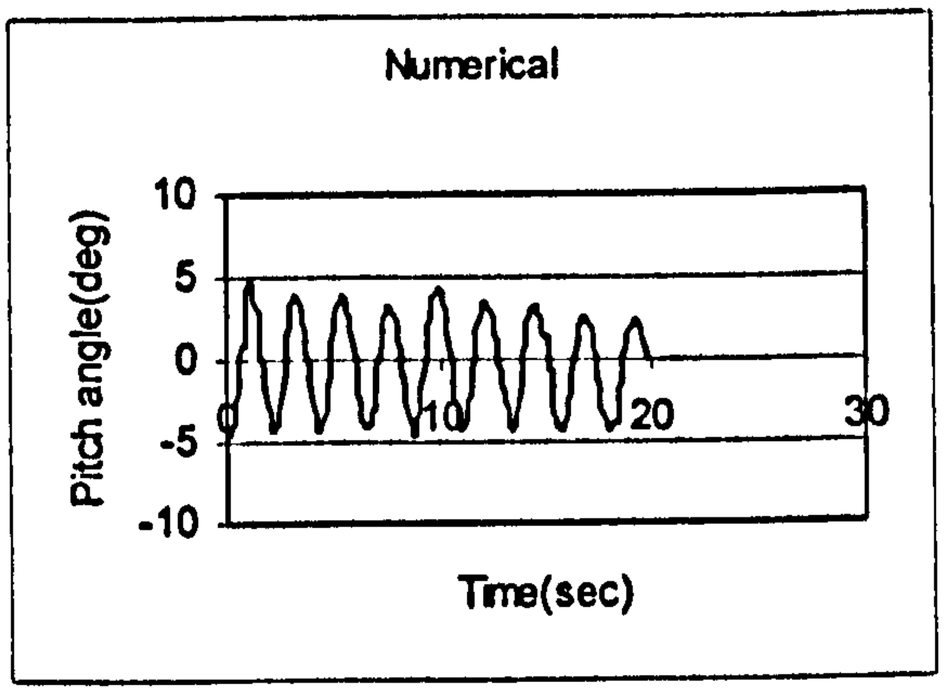

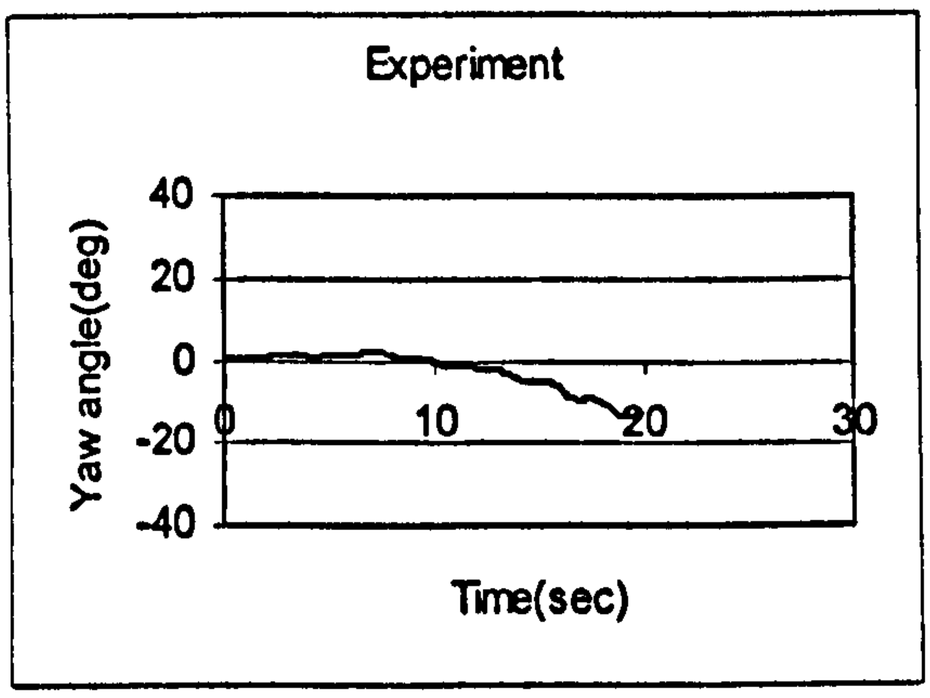

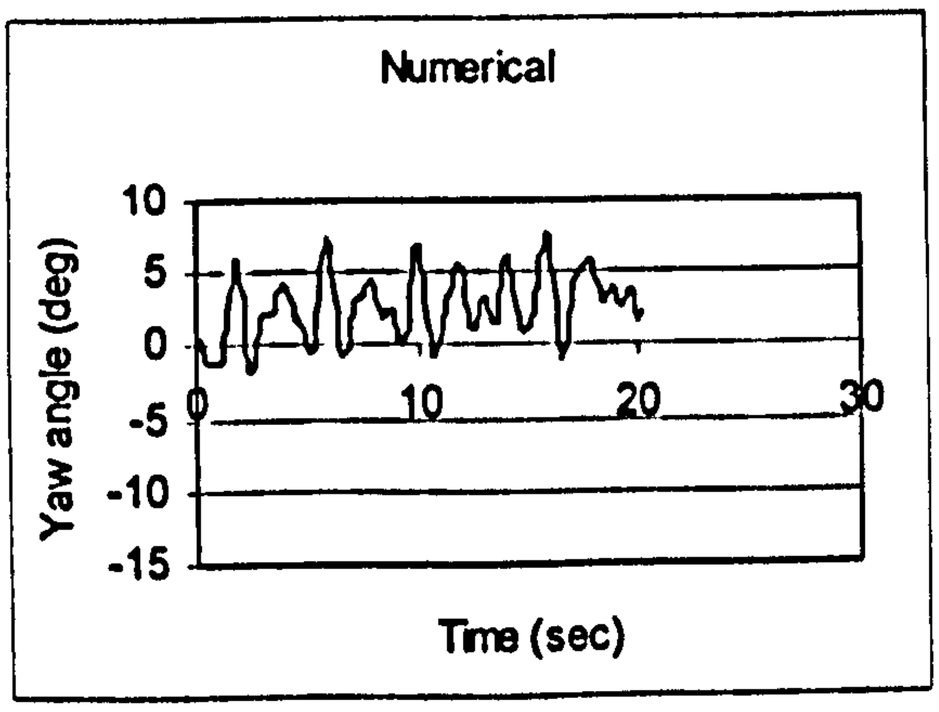

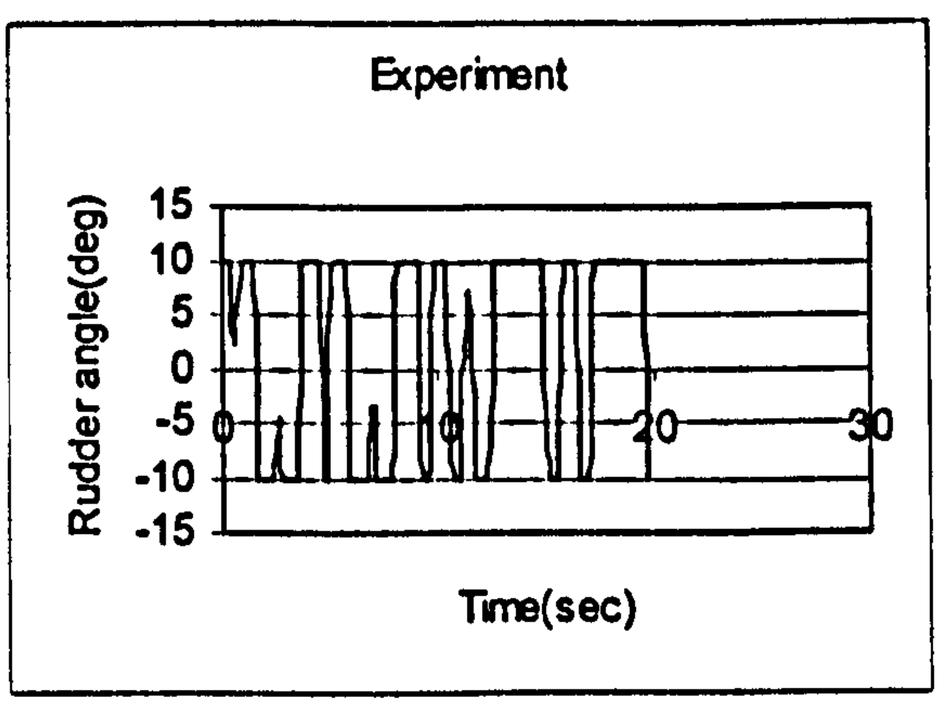

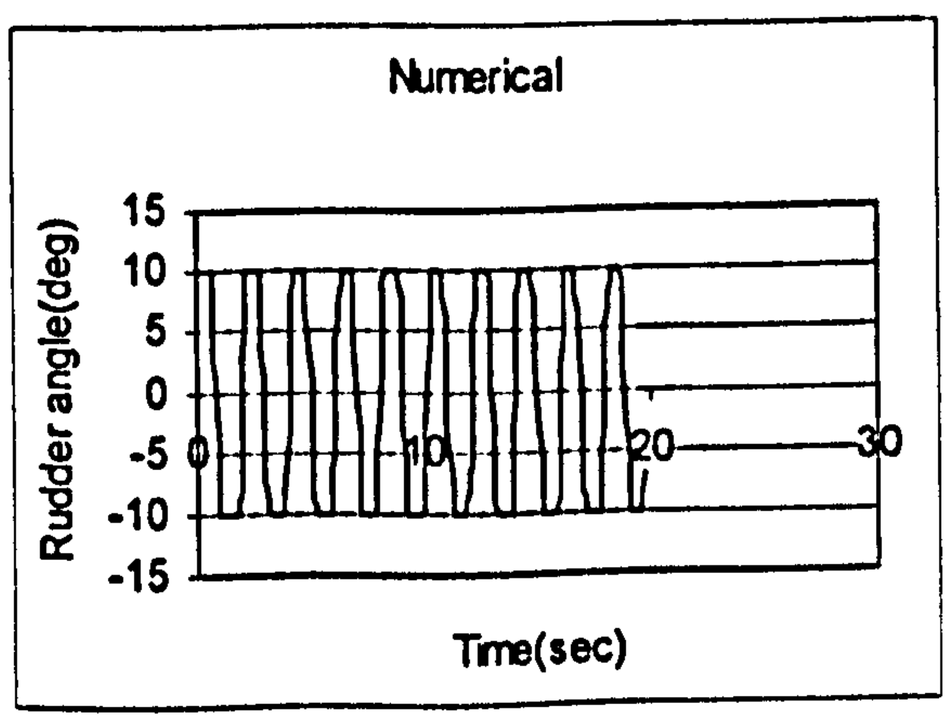

Figure 7.7 Comparison of model experiment and numerical method for the model of Ship A-1 in $H/\lambda=1/25$, $\lambda/L_{pp}=1.5$, $Fn=0.2$, $\chi_c=0$ degrees (Including the memory effect)

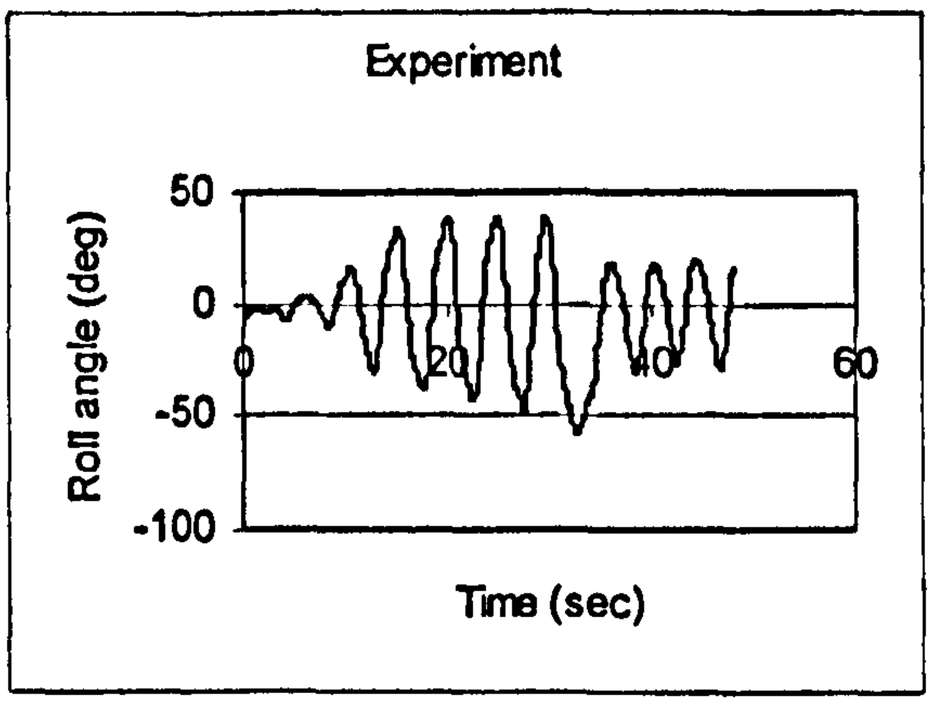

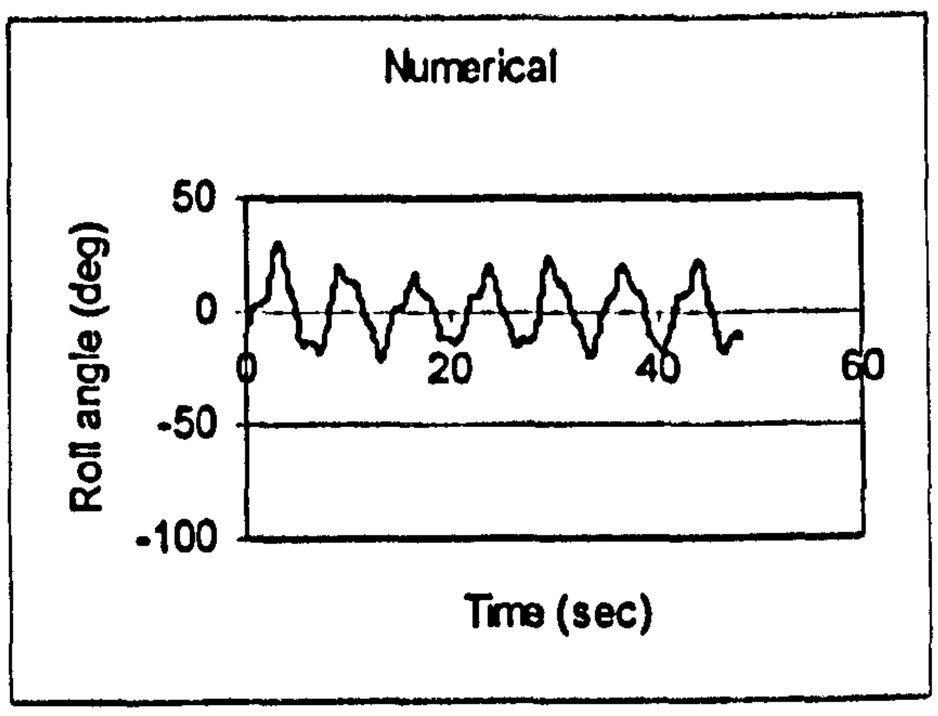

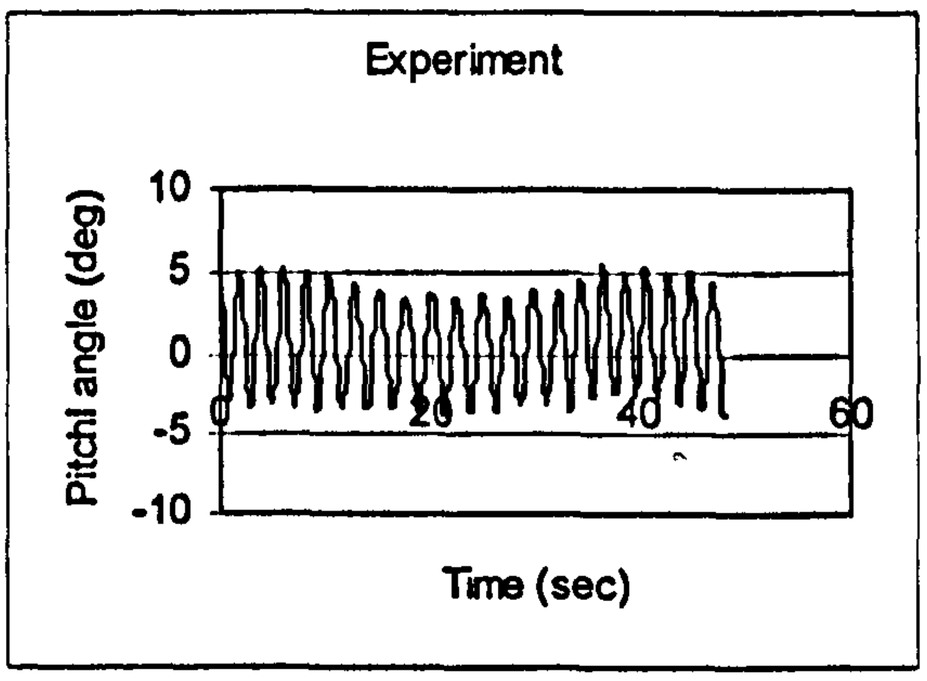

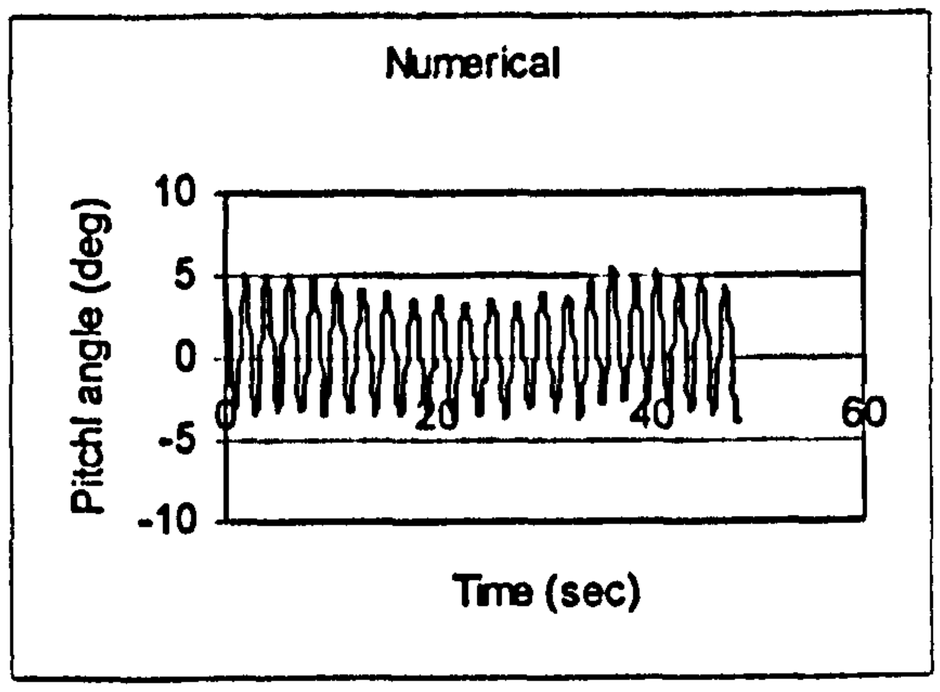

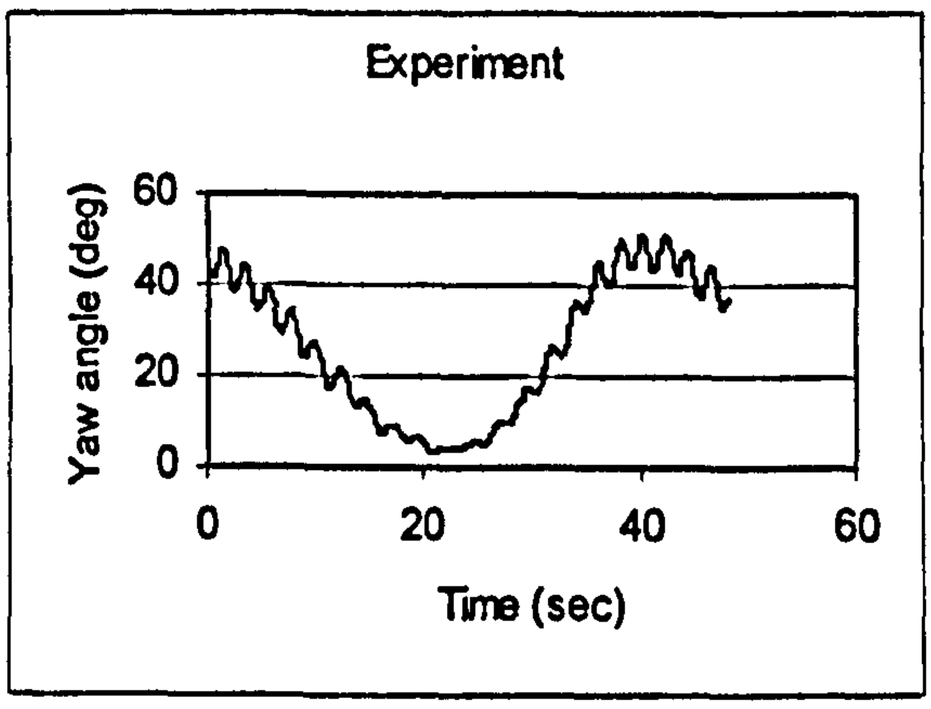

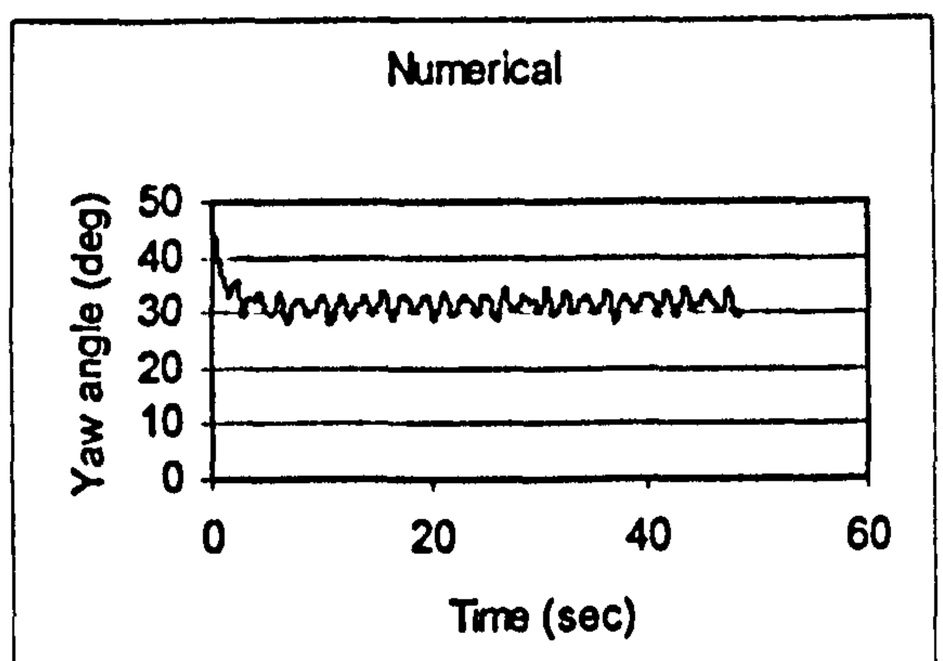

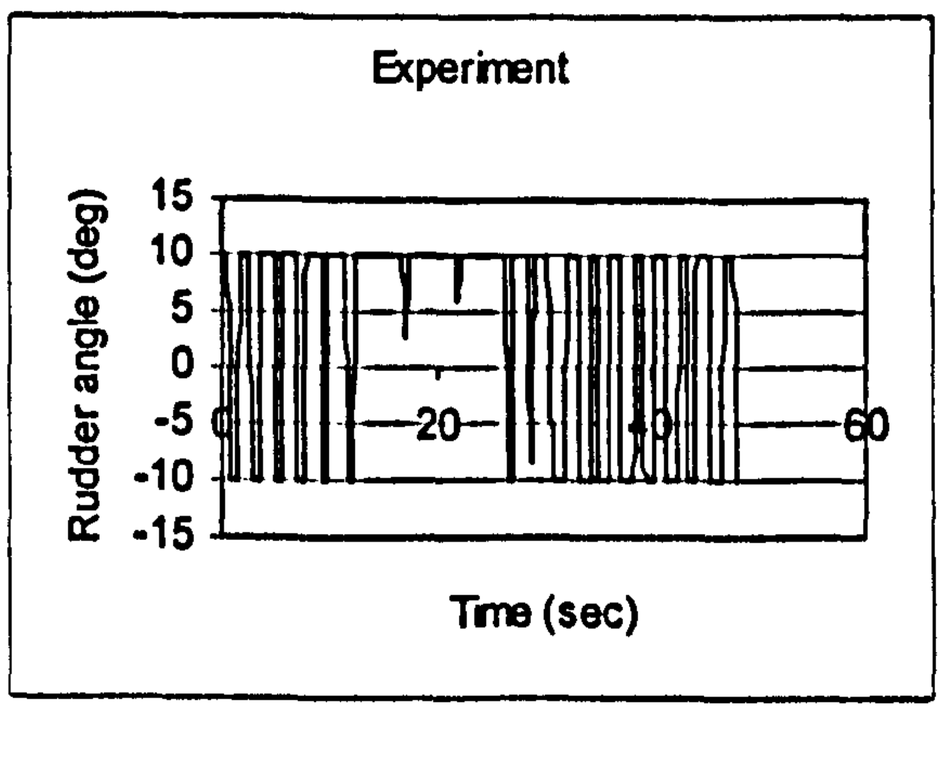

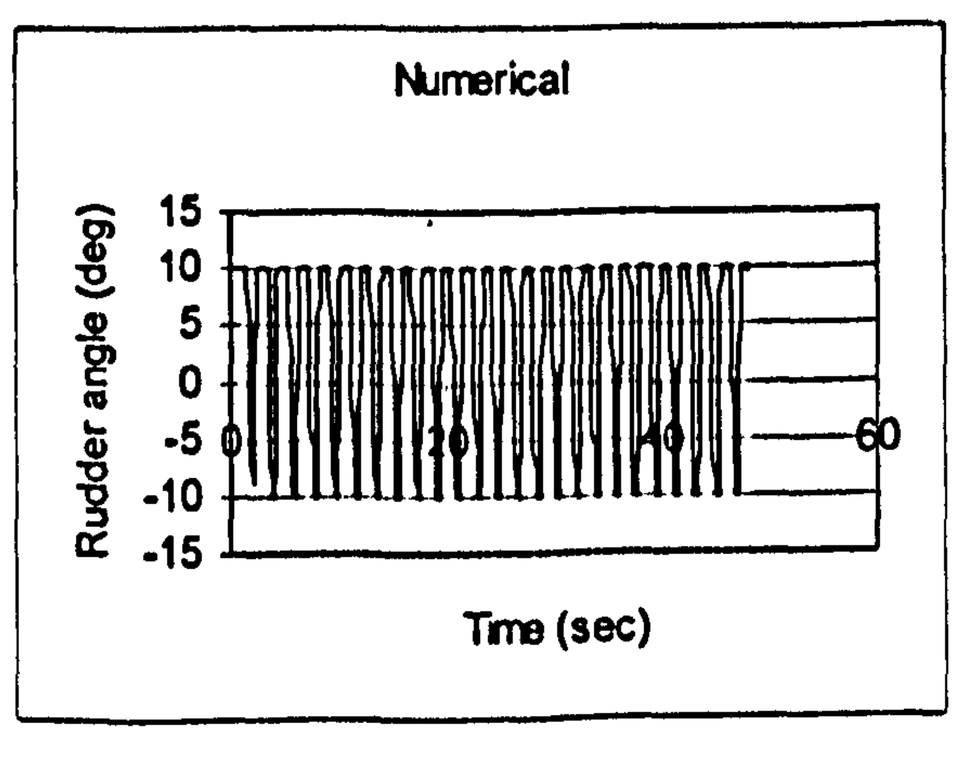

Figure 7.8 Comparison of model experiment and numerical method for the model of Ship A-1 in $H/\lambda=1/25$, $\lambda/L_{pp}=1.5$, $Fn=0.2$, $\chi_c=45$ degrees (Including the memory effect)

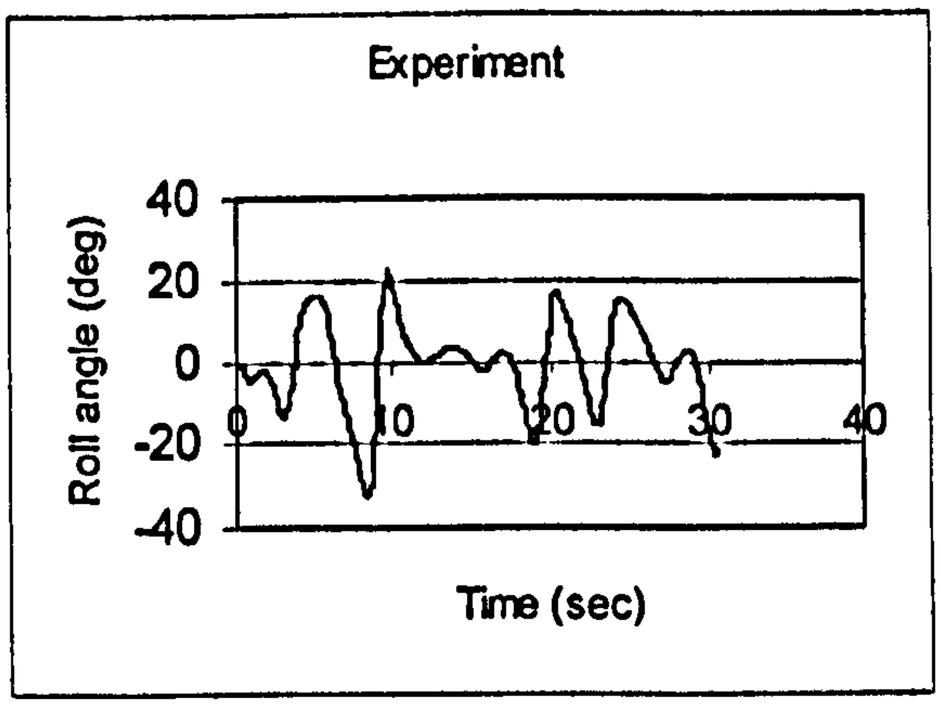

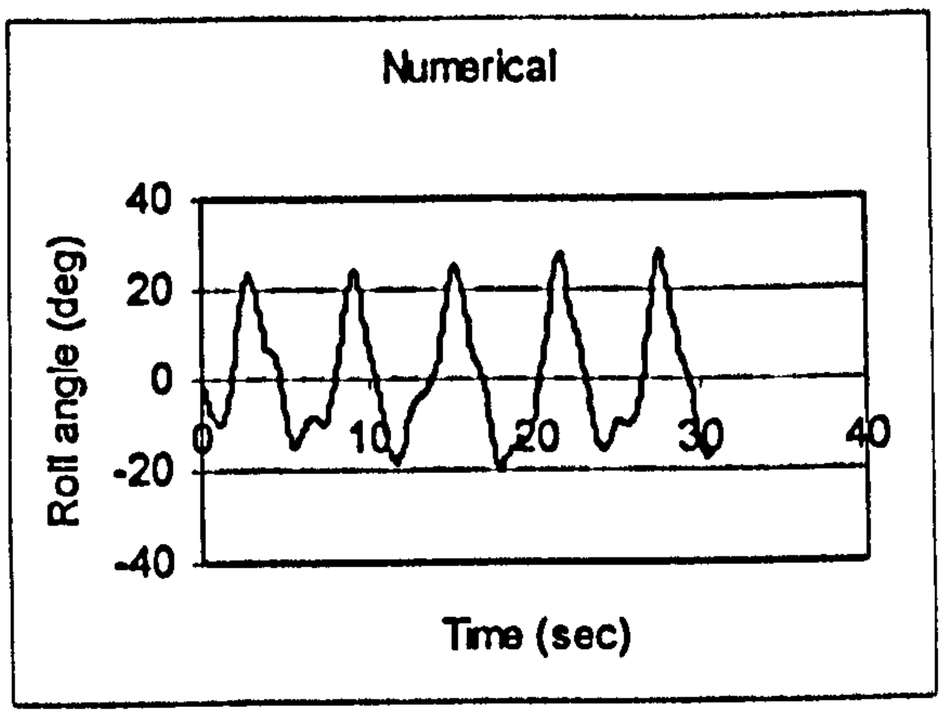

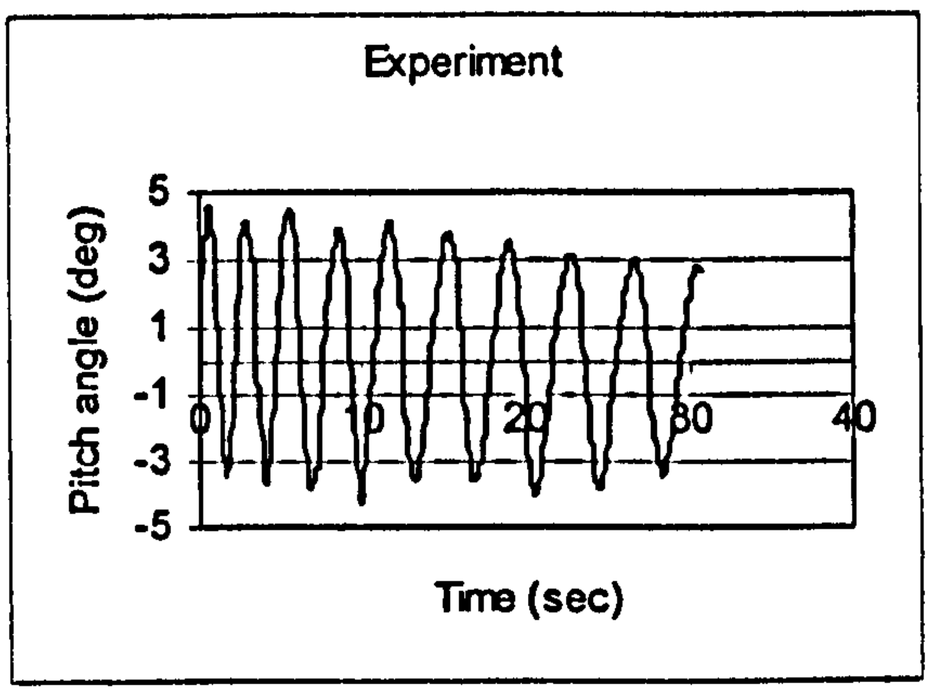

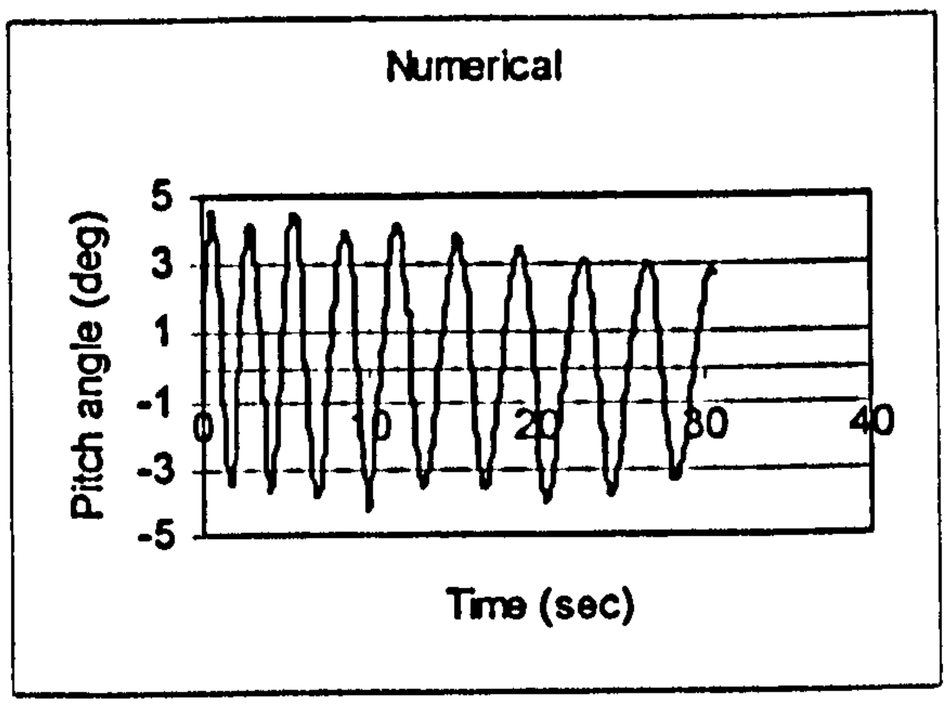

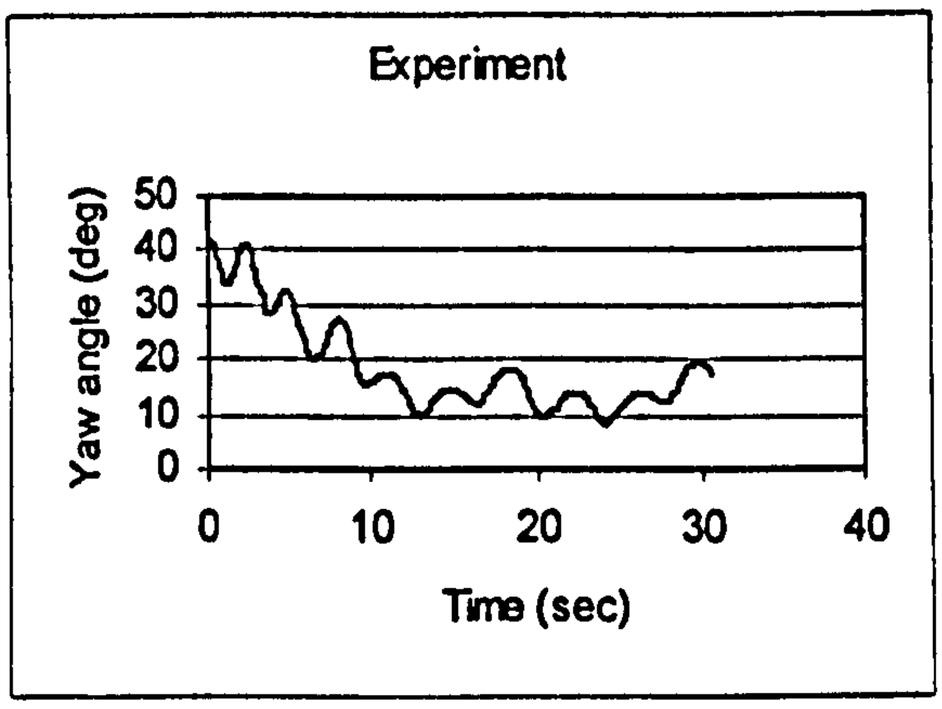

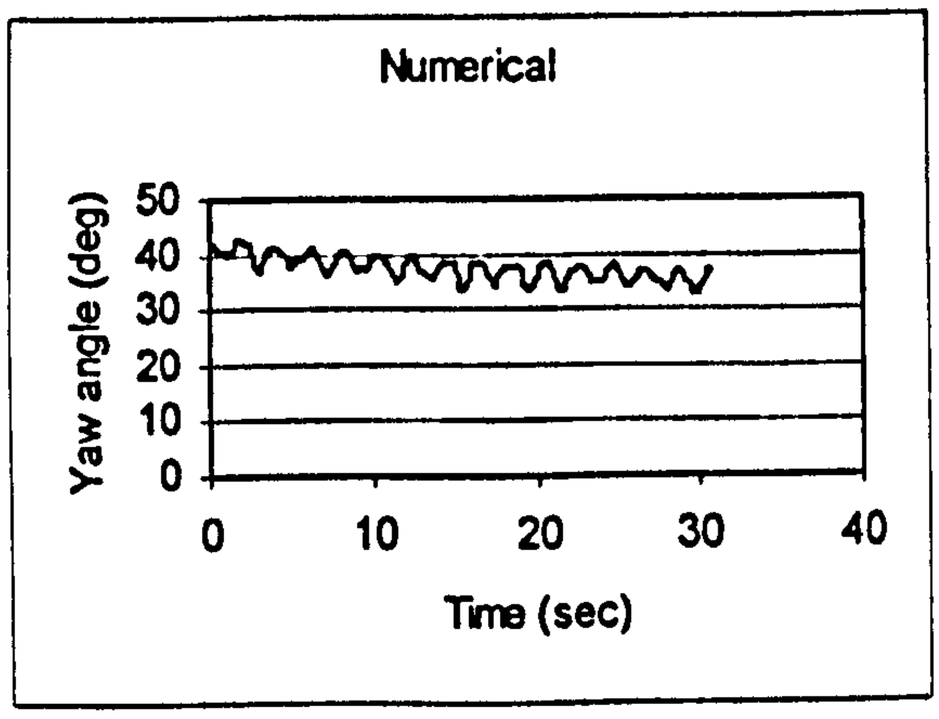

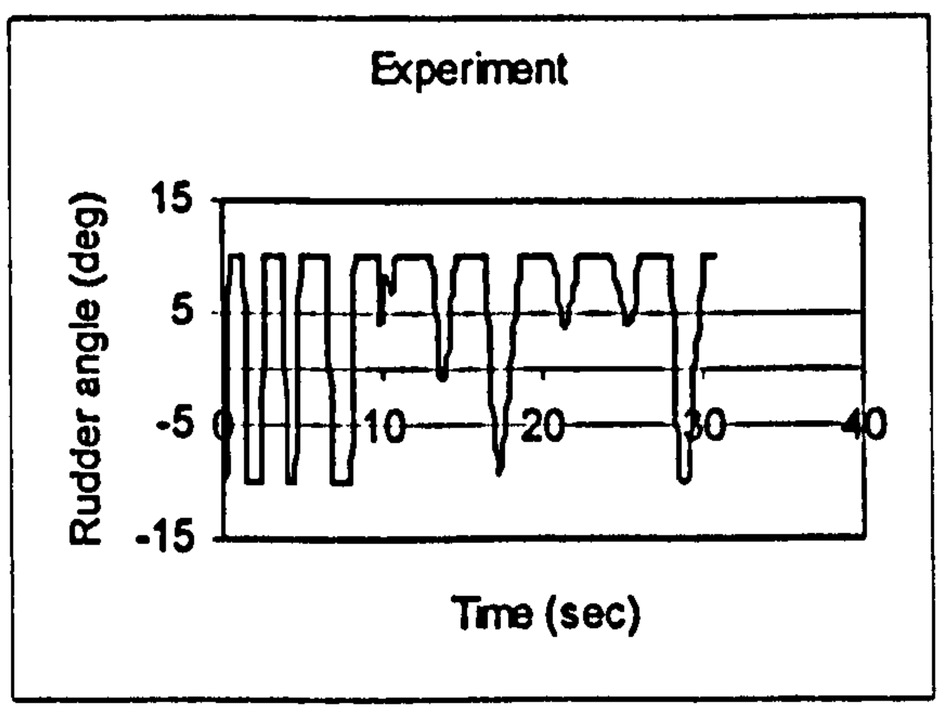

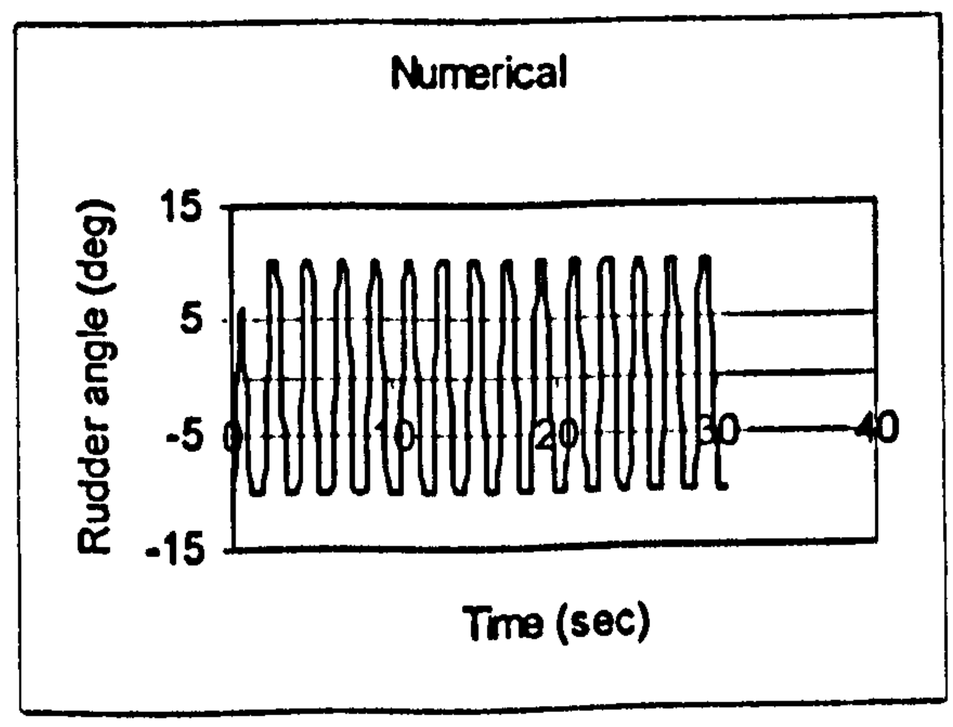

Figure 7.9 Comparison of model experiment and numerical method for the model of Ship A-1 in $H/\lambda=1/25$, $\lambda/L_{pp}=1.5$, $Fn=0.3$, $\chi_c=30$ degrees (Including the memory effect)

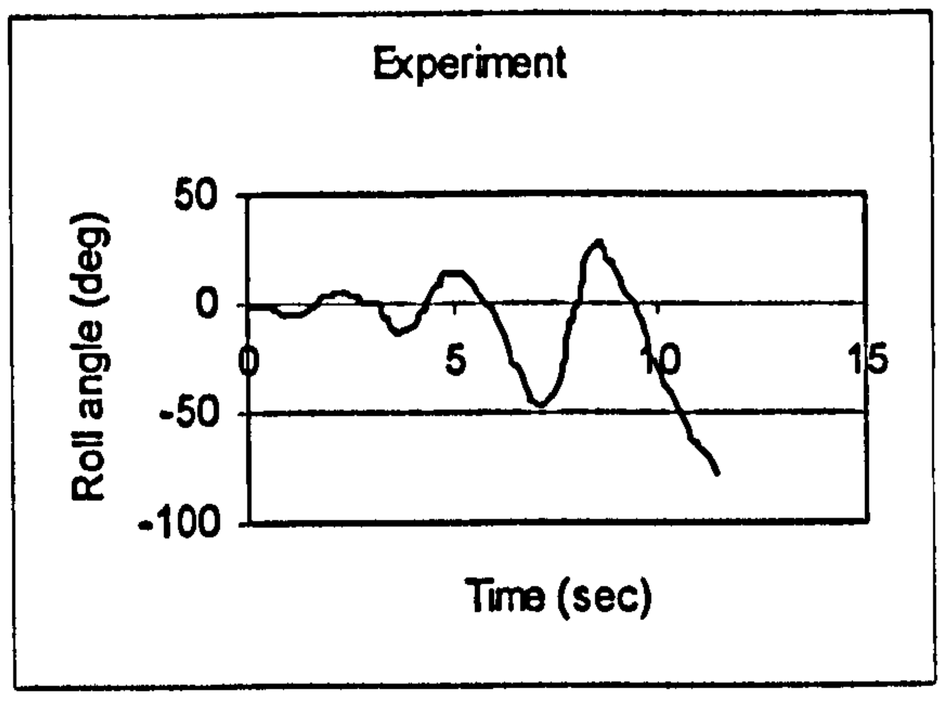

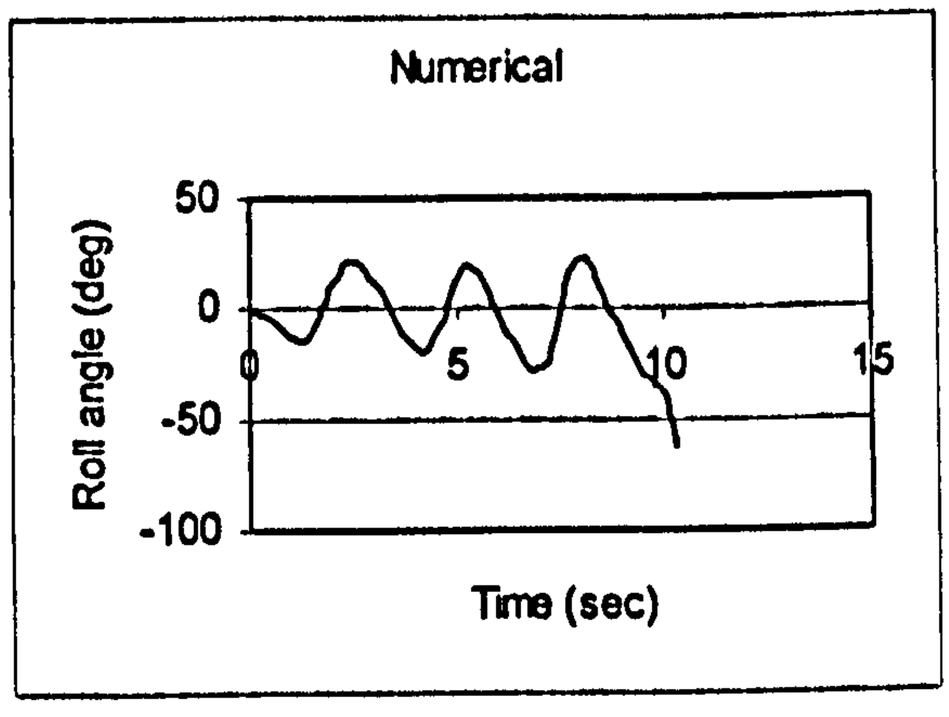

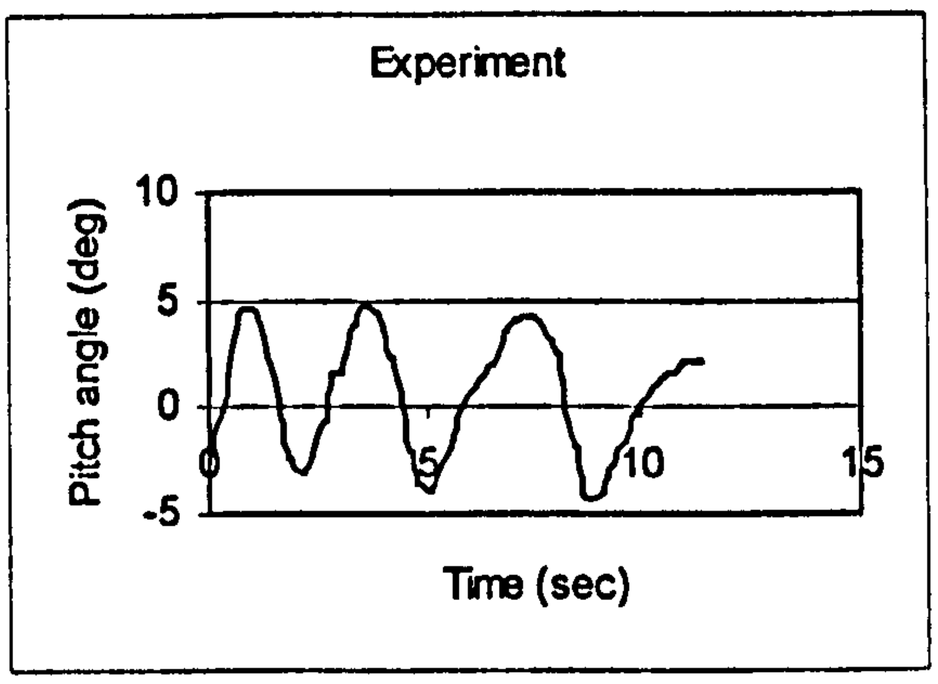

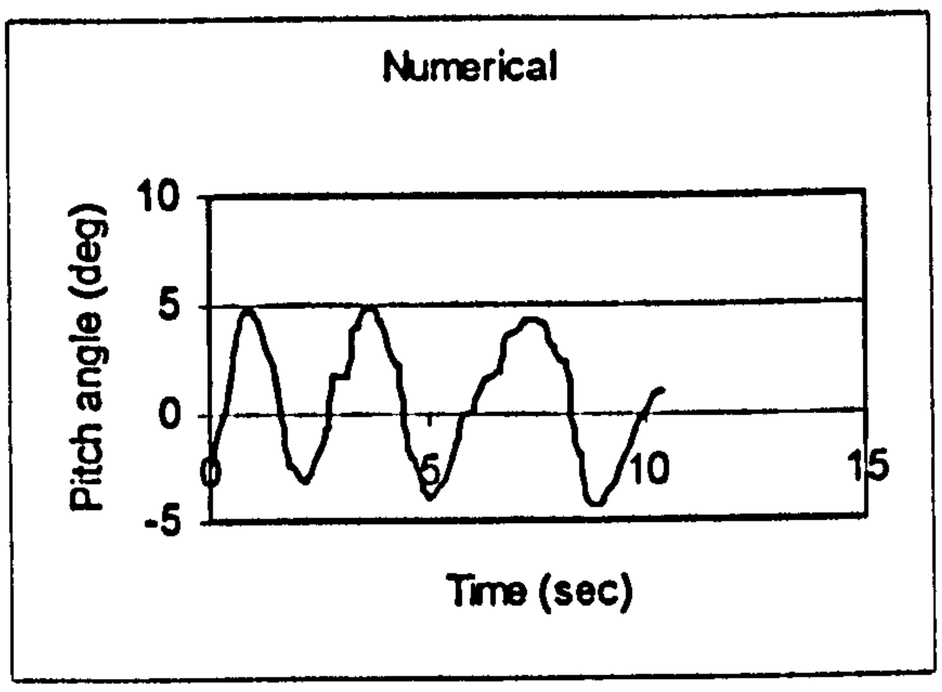

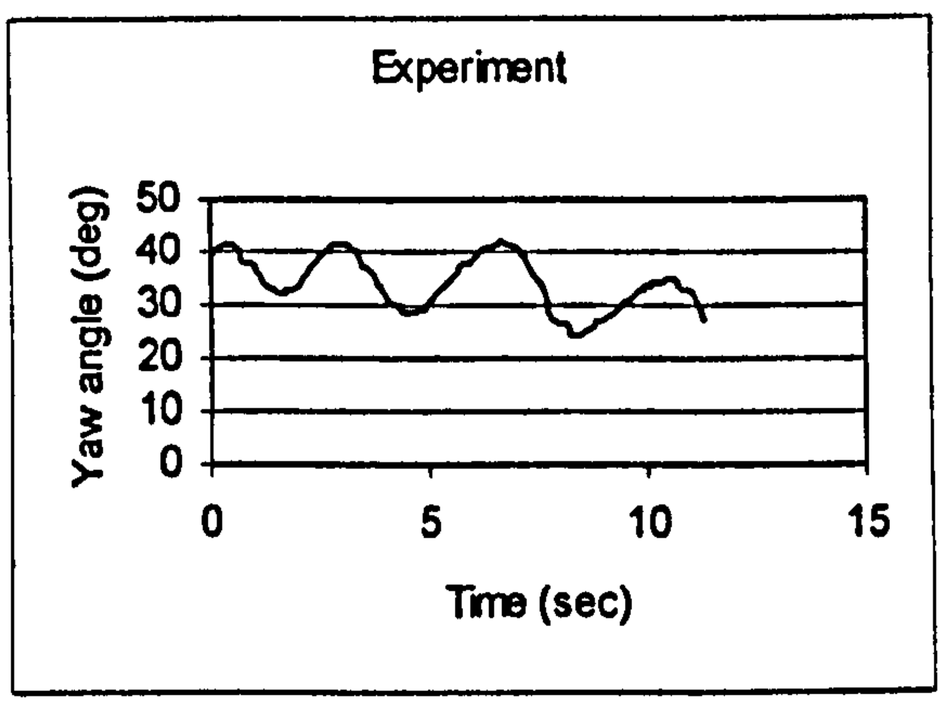

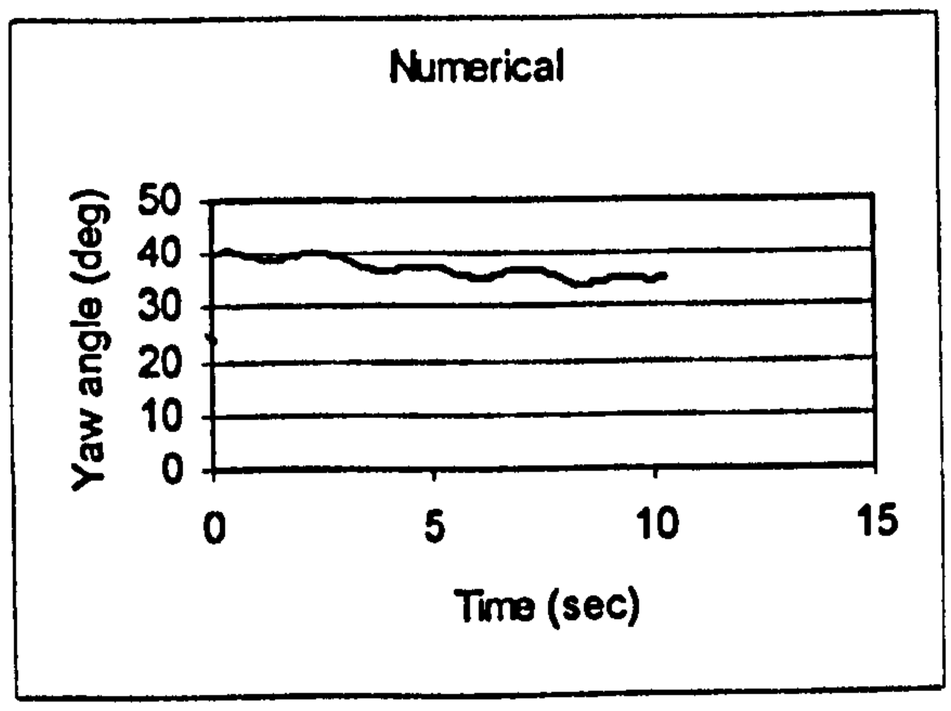

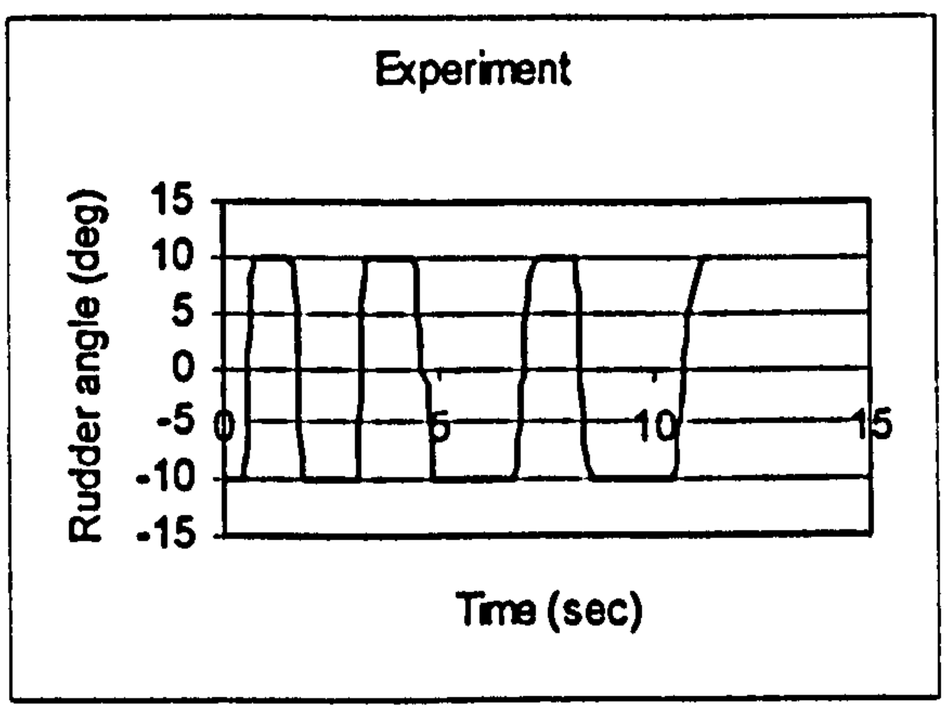

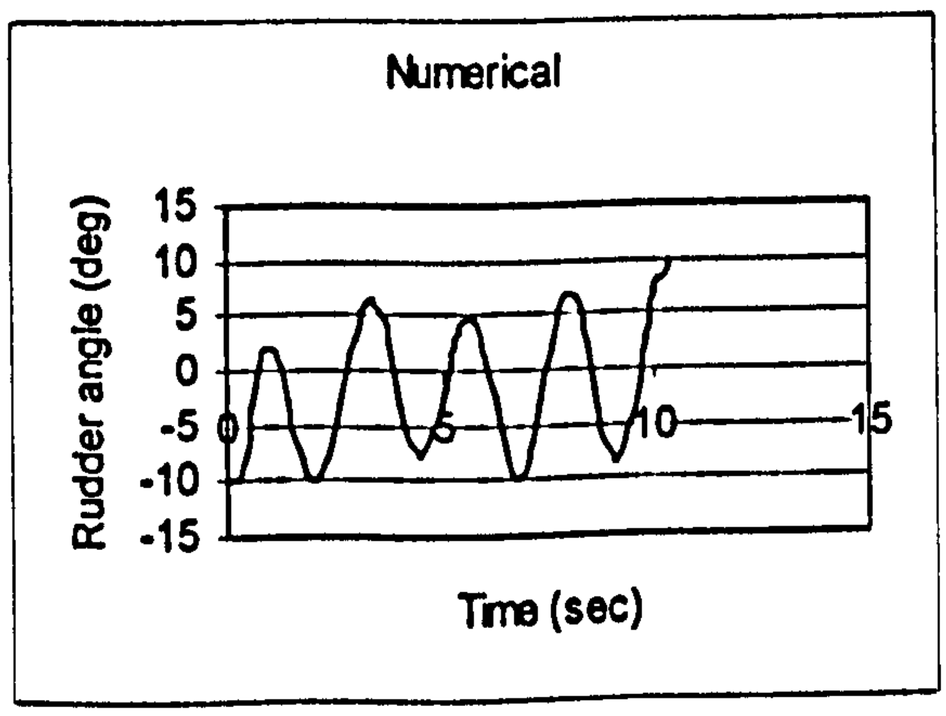

Figure 7.10 Comparison of model experiment and numerical method for the model of Ship A-1 in $H/\lambda=1/25$, $\lambda/L_{pp}=1.5$, $Fn=0.4$, $\chi_c=30$ degrees (Capsizing) (Including the memory effect)

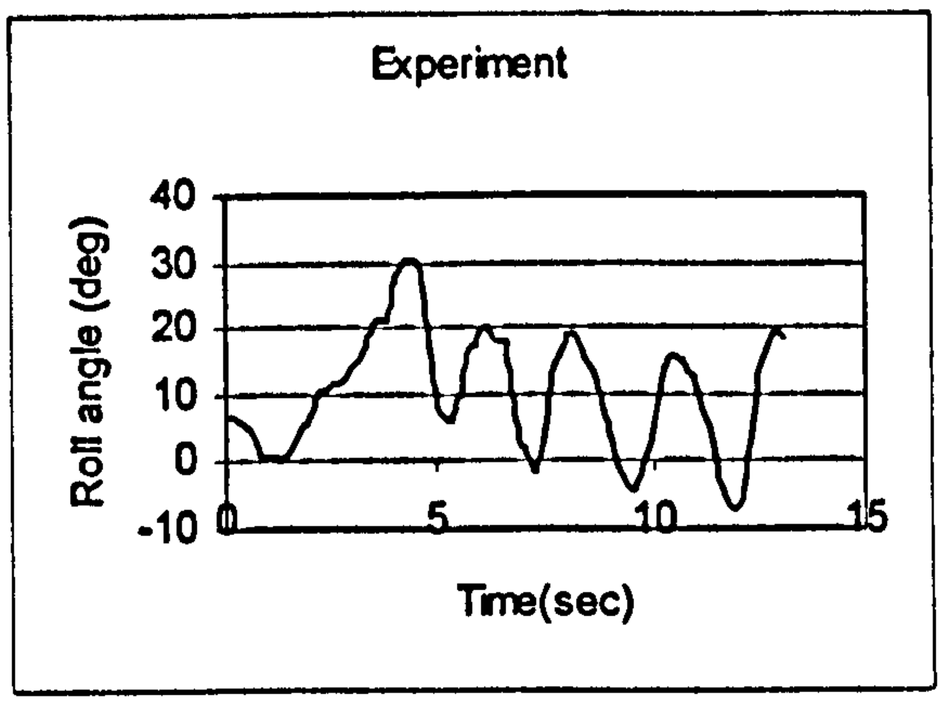

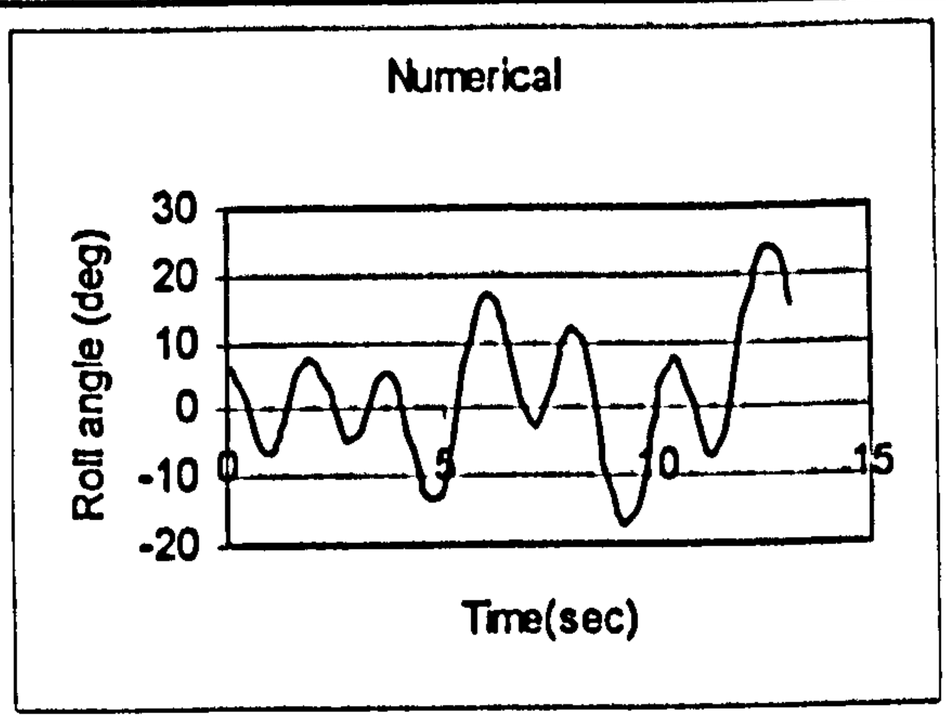

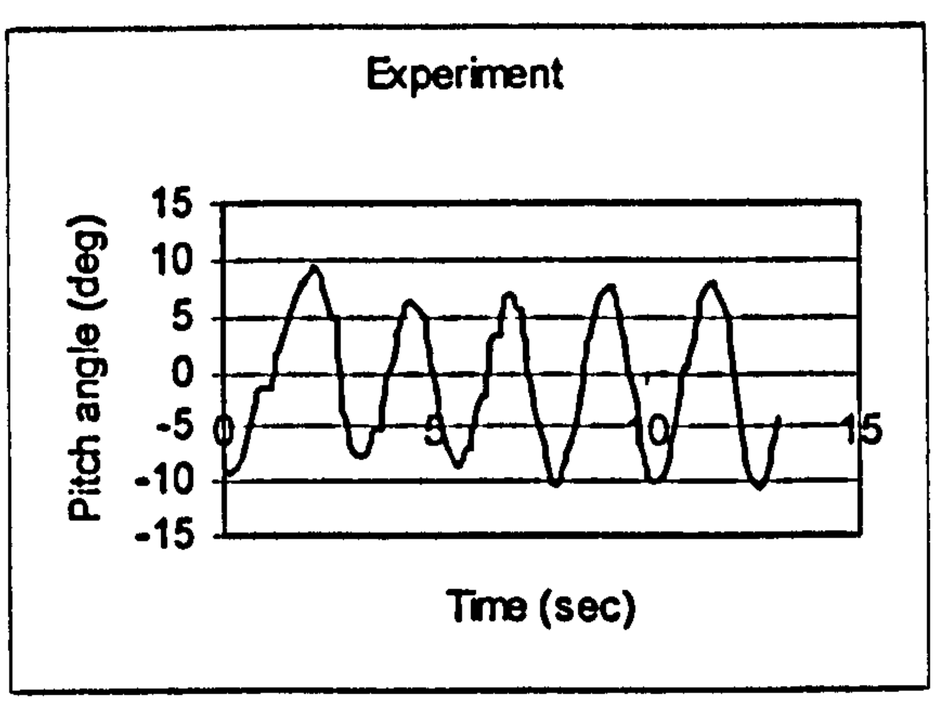

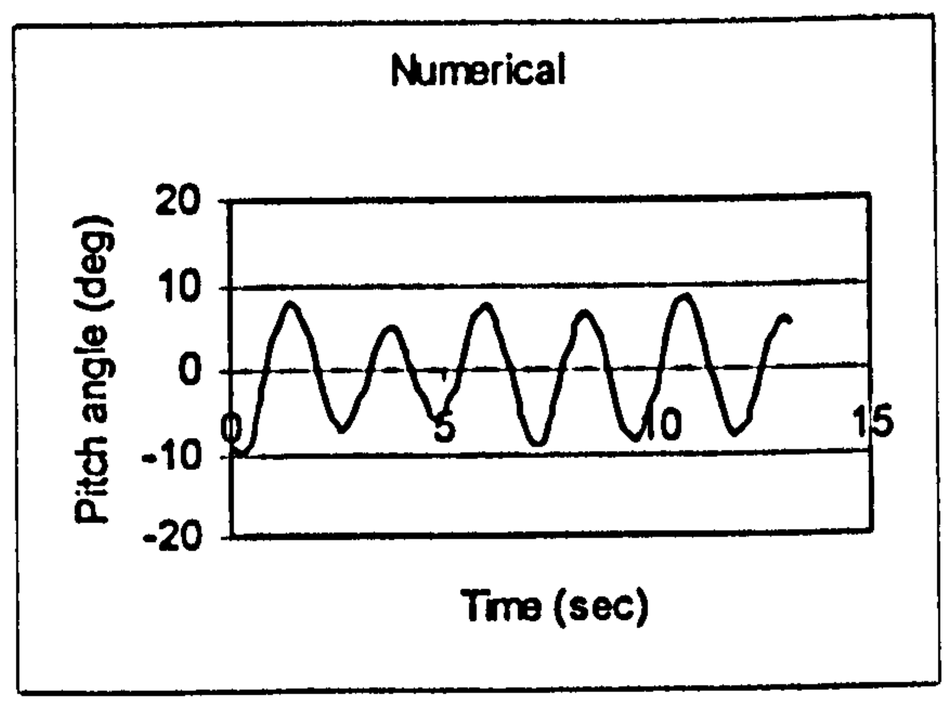

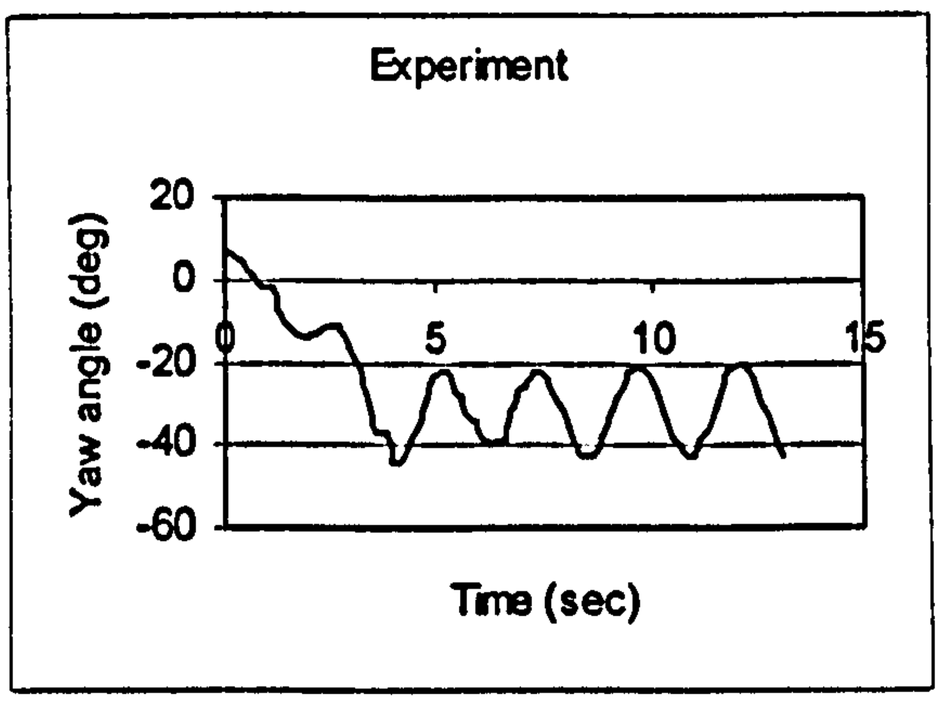

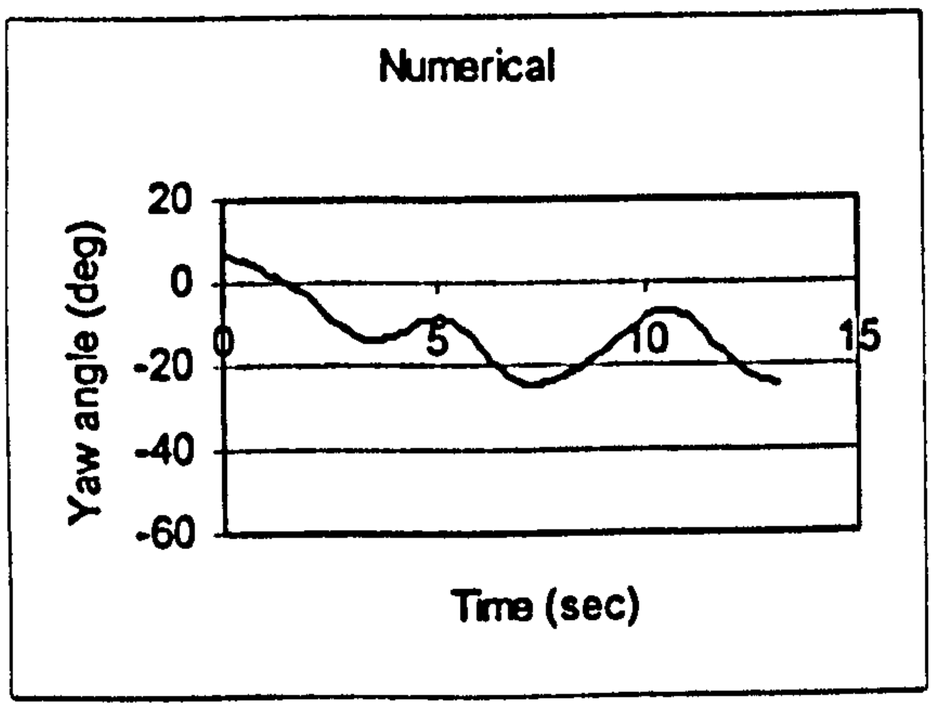

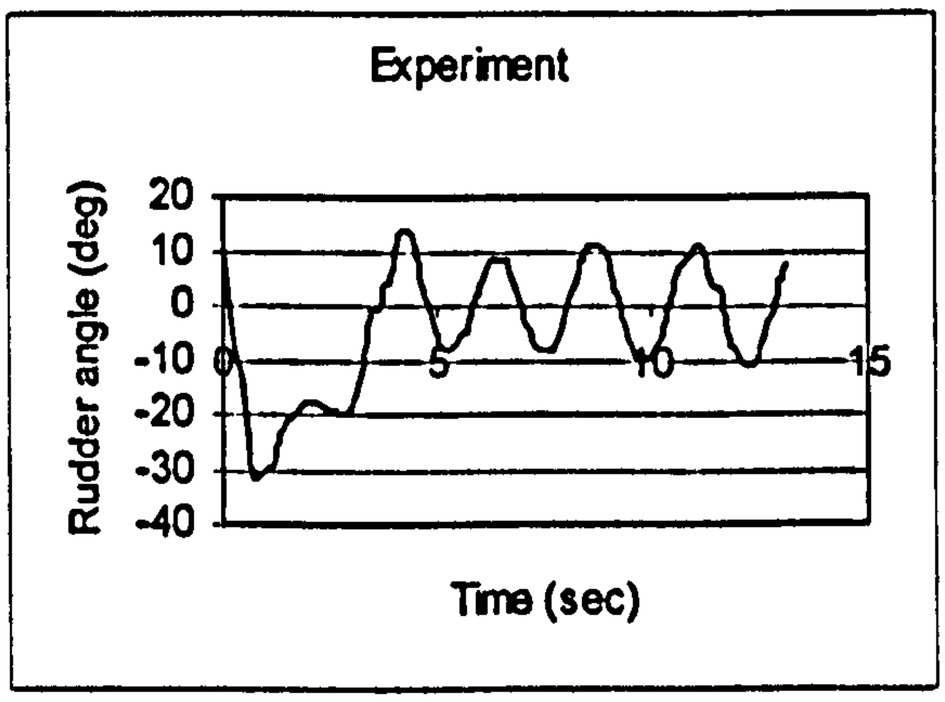

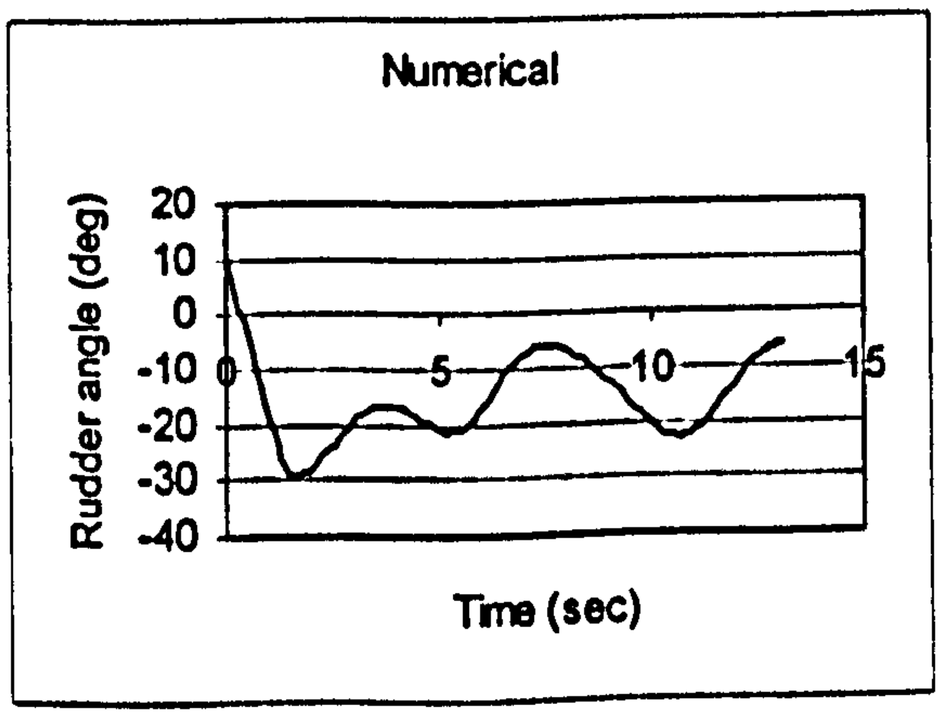

Figure 7.11 Comparison of model experiment and numerical method for the model of Ship A-2 in $H/\lambda=1/10$, $\lambda/L_{pp}=1.637$, $Fn=0.3$, $\chi_c=-30$ degrees

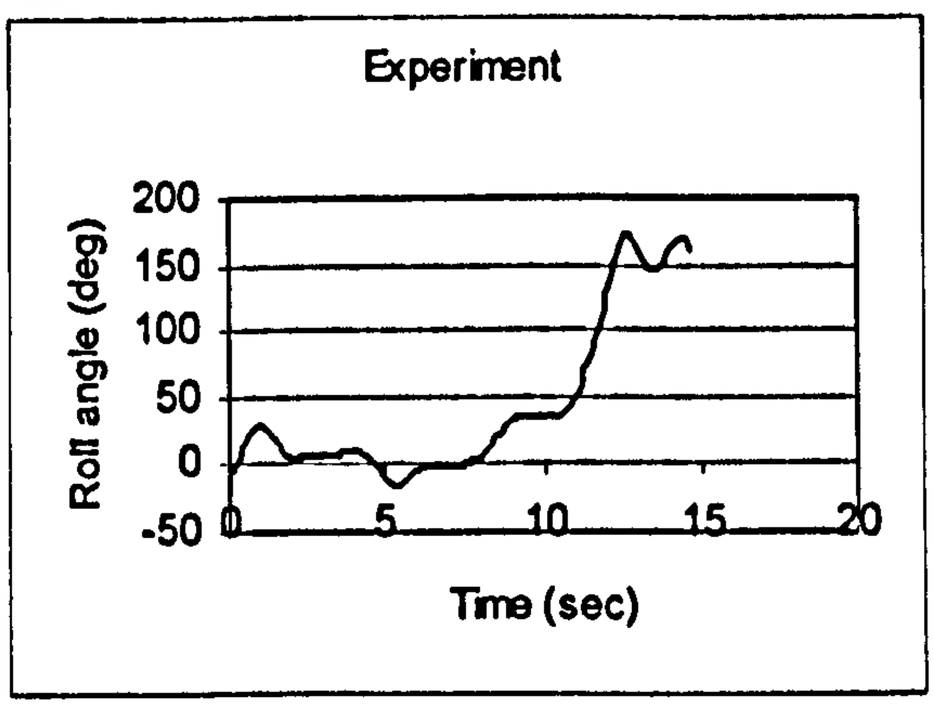

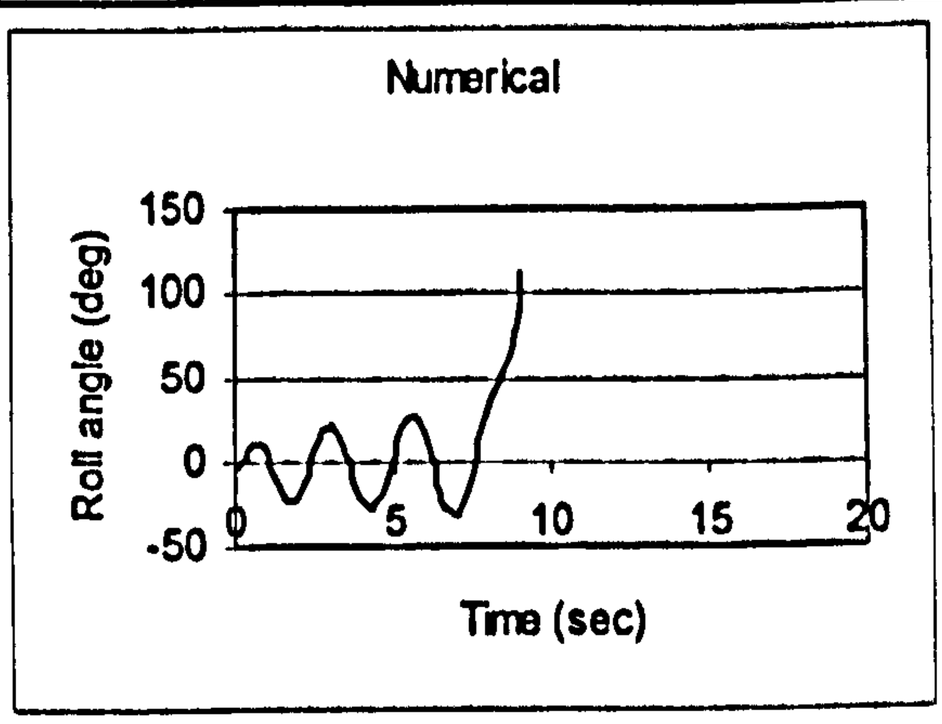

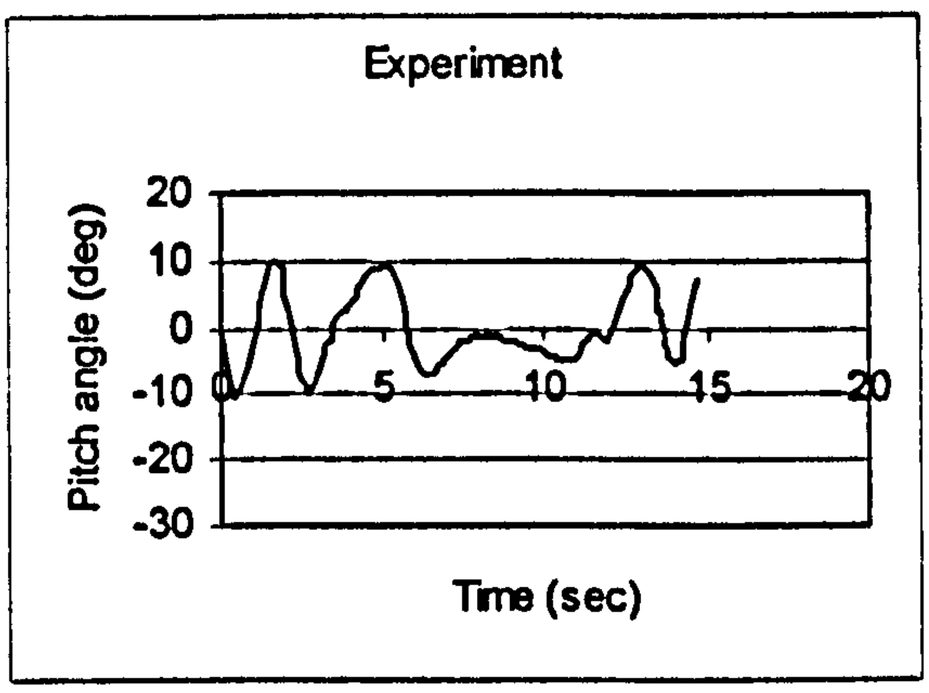

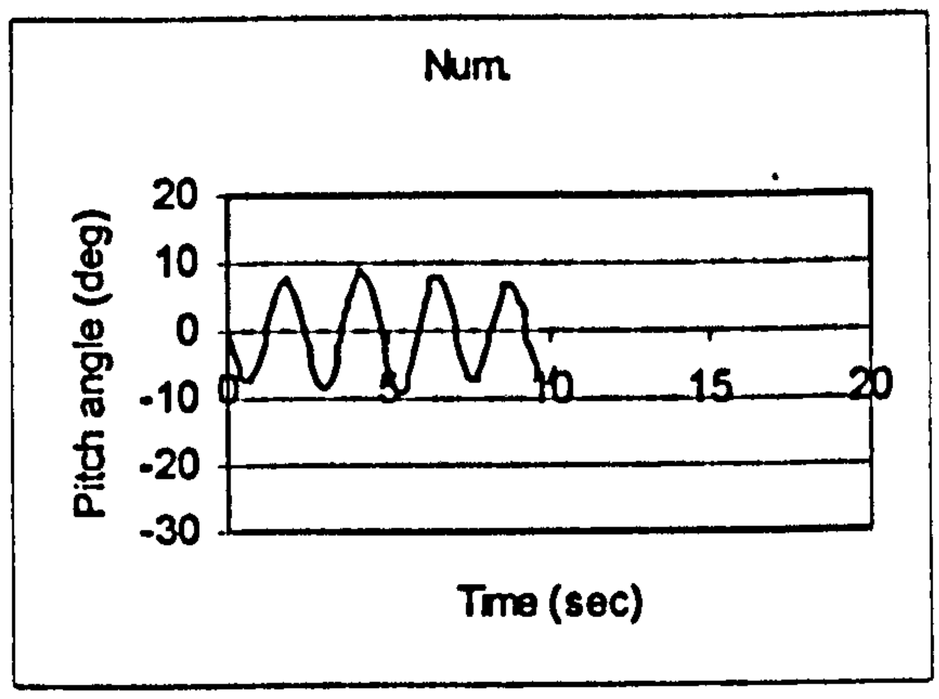

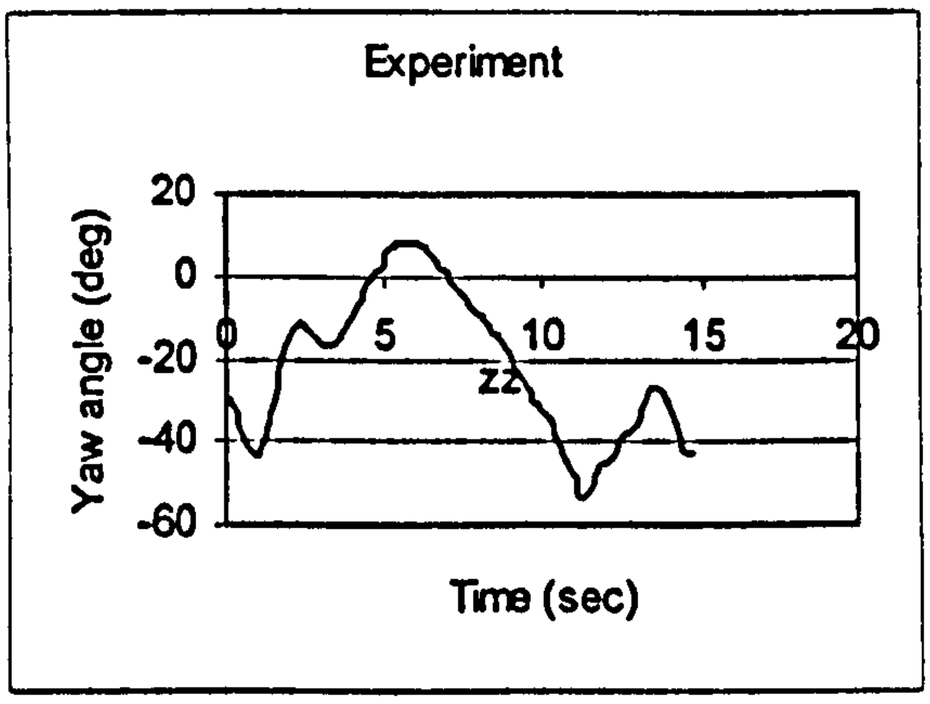

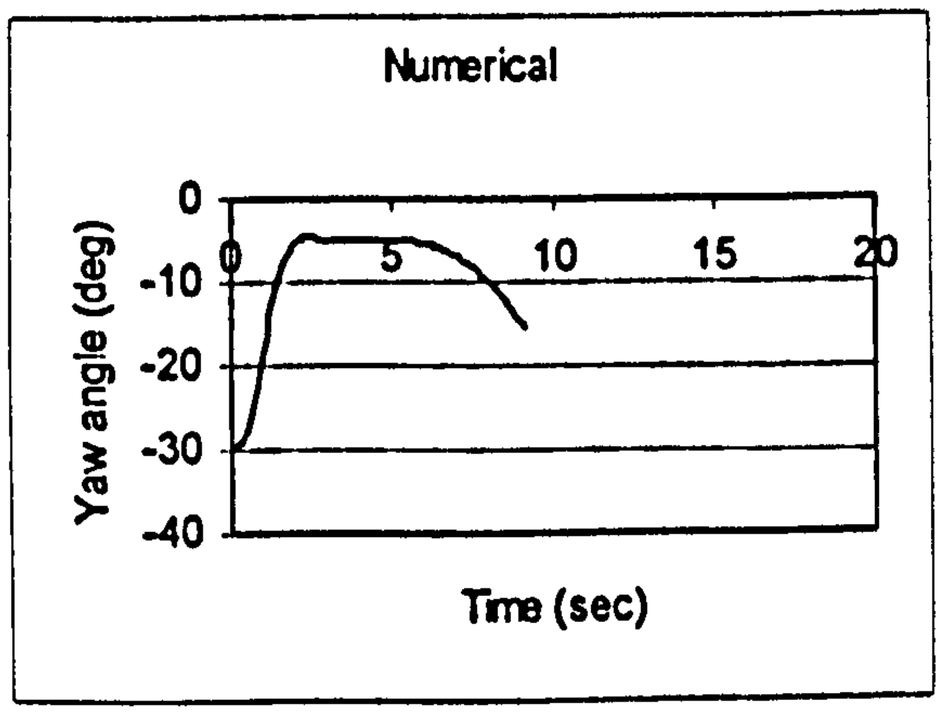

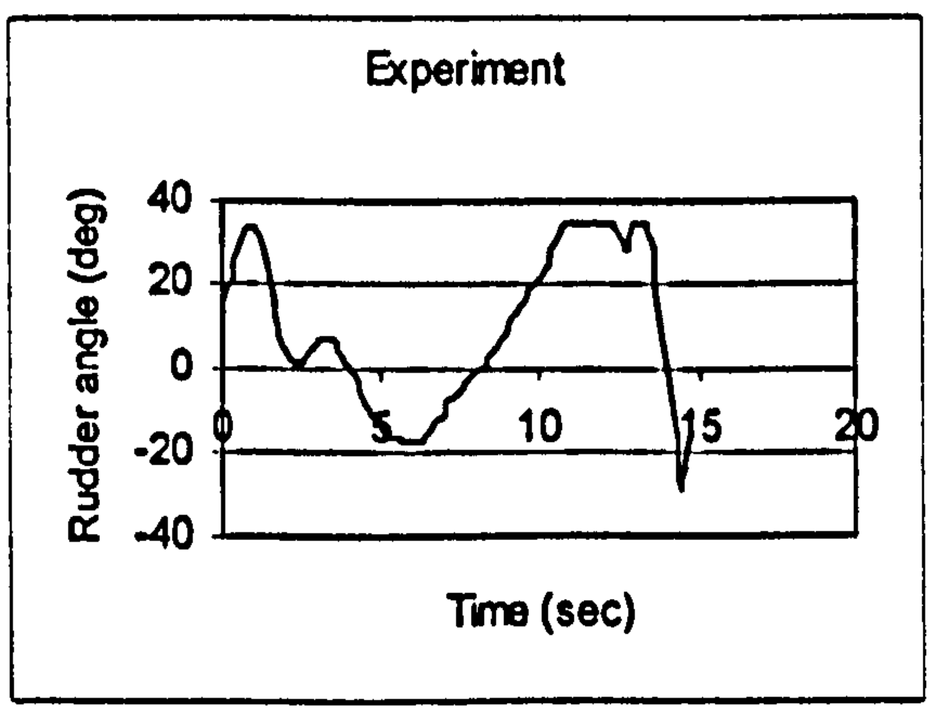

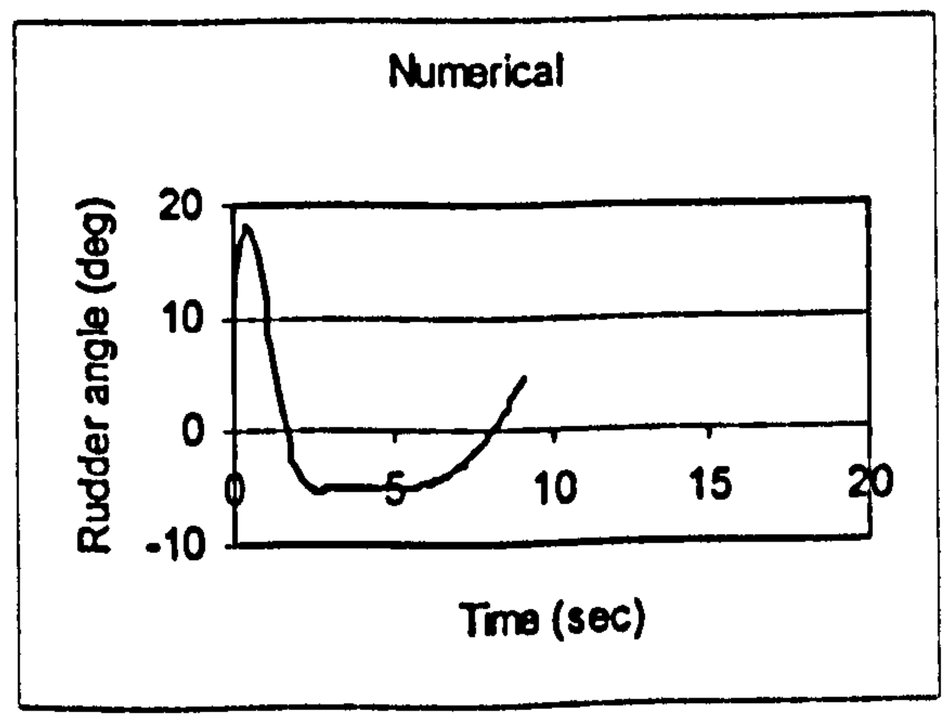

Figure 7.12 Comparison of model experiment and numerical method for the model of Ship A-2 in $H/\lambda=1/10$, $\lambda/L_{pp}=1.637$, $Fn=0.43$, $\chi_c=-10$ degrees (Capsizing)

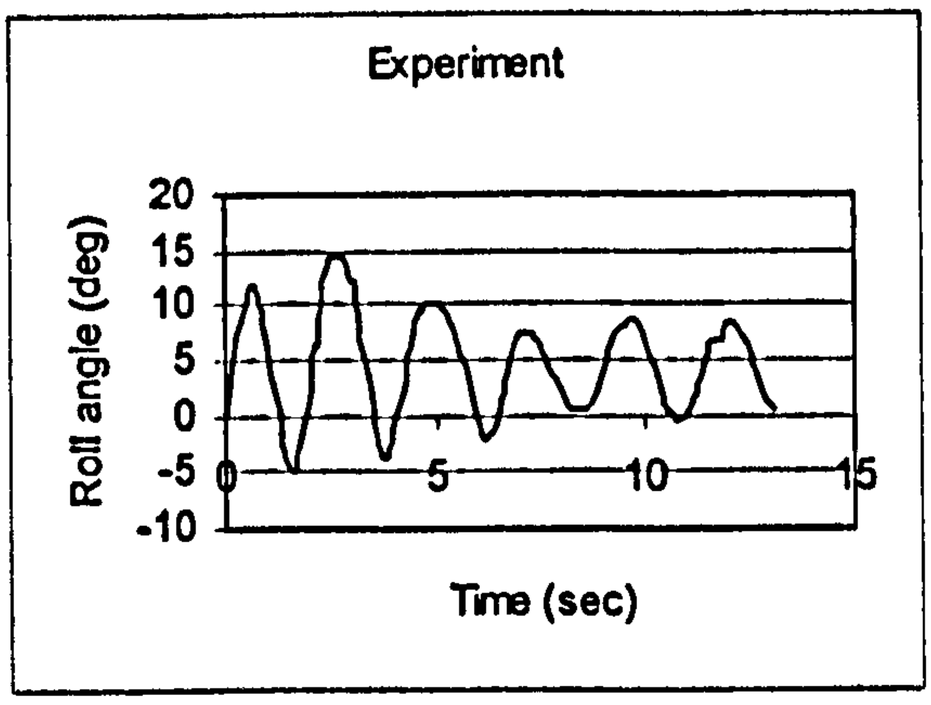

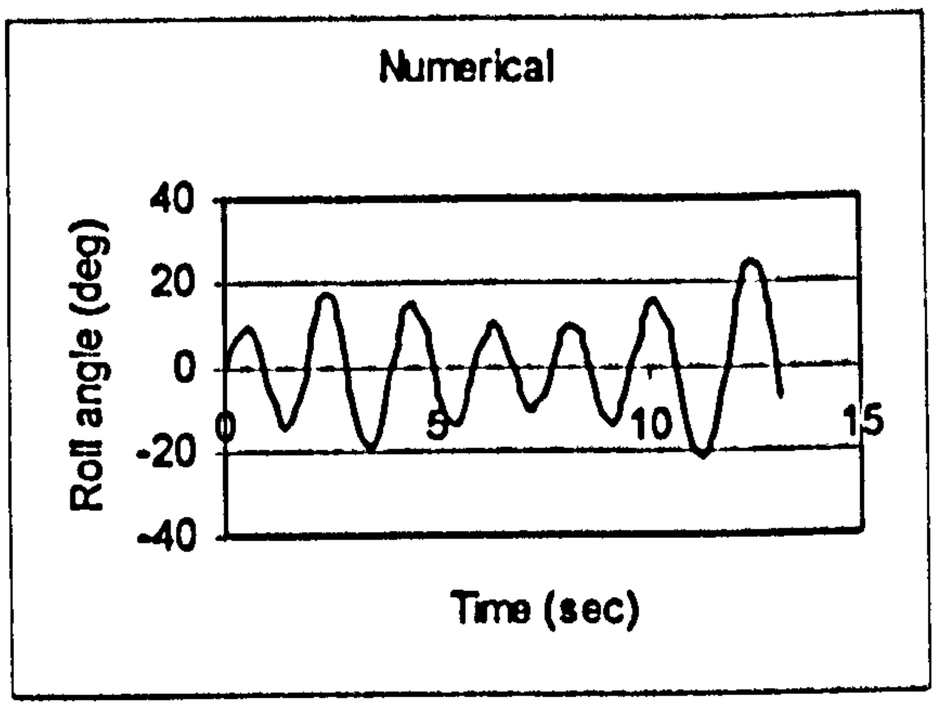

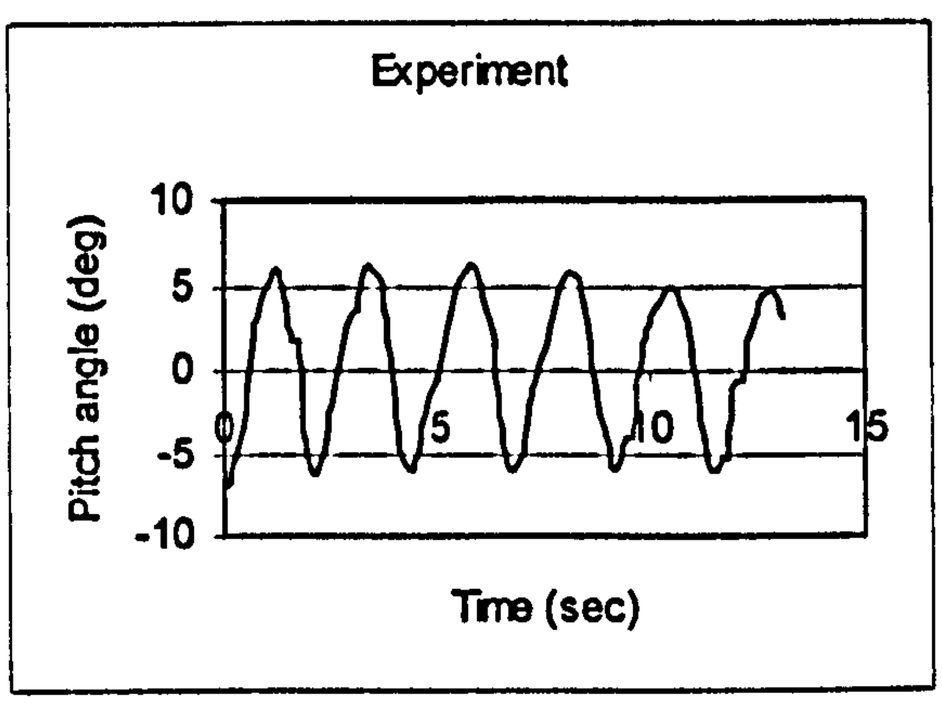

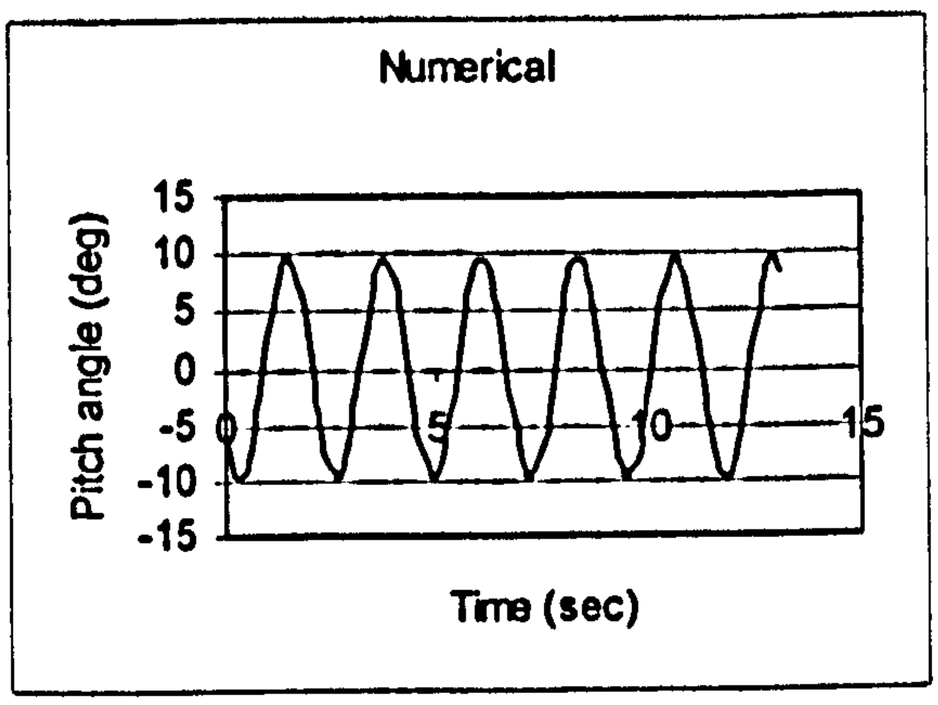

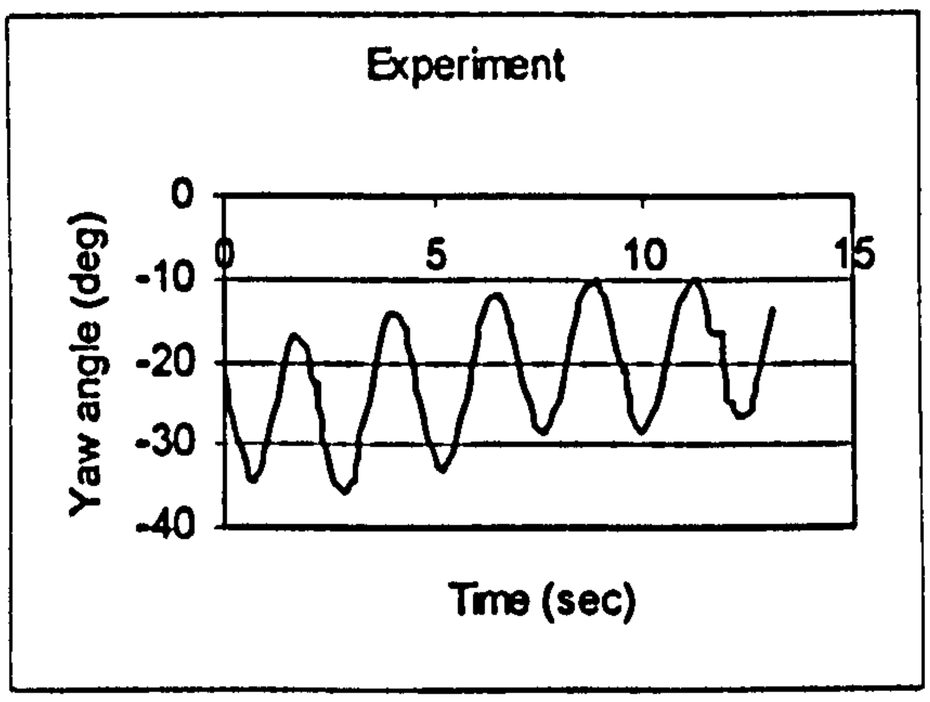

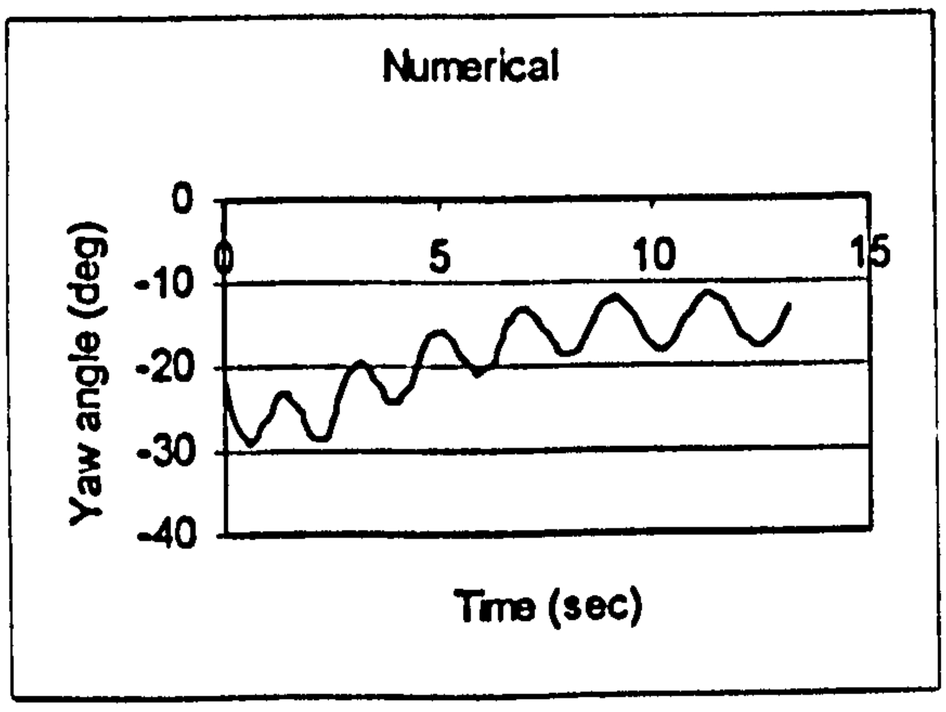

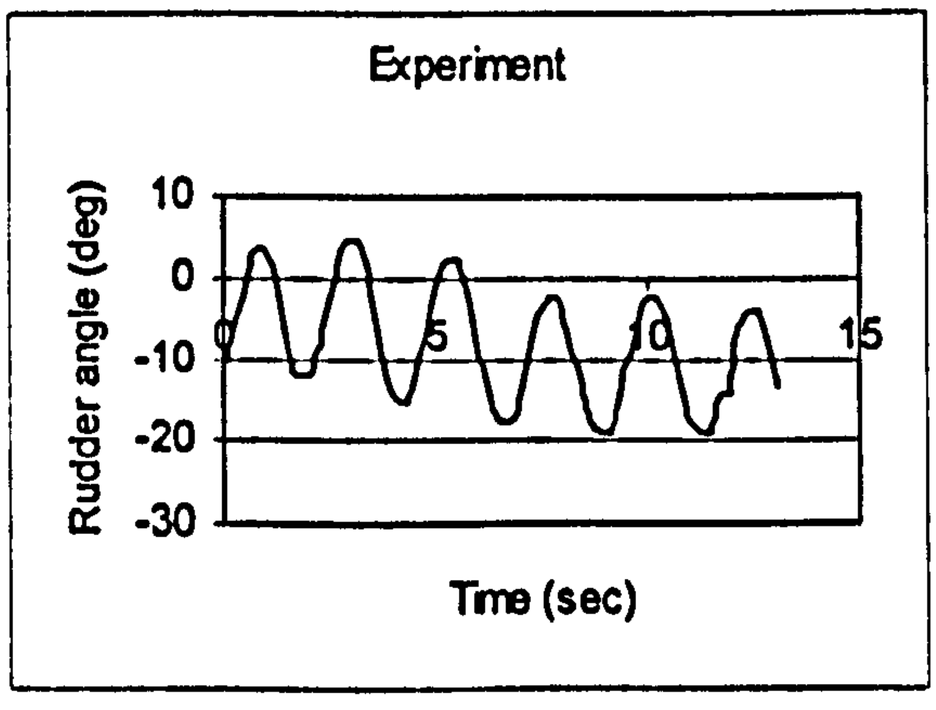

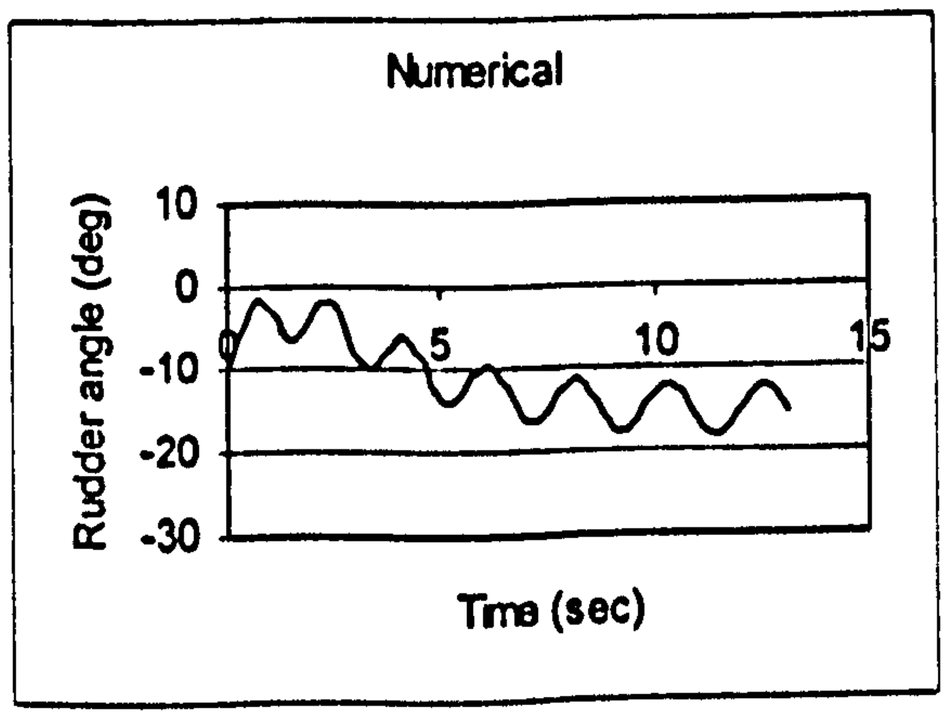

Figure 7.13 Comparison of model experiment and numerical method for the model of Ship A-2 in $H/\lambda=1/8.7$, $\lambda/L_{pp}=1.127$, $Fn=0.3$, $\chi_c=-30$ degrees

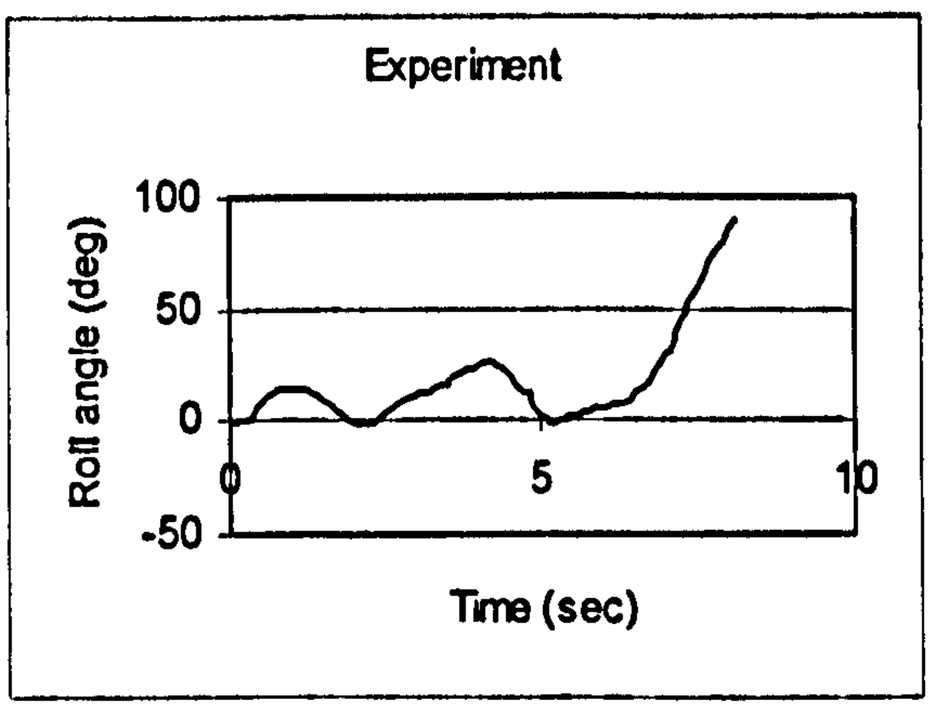

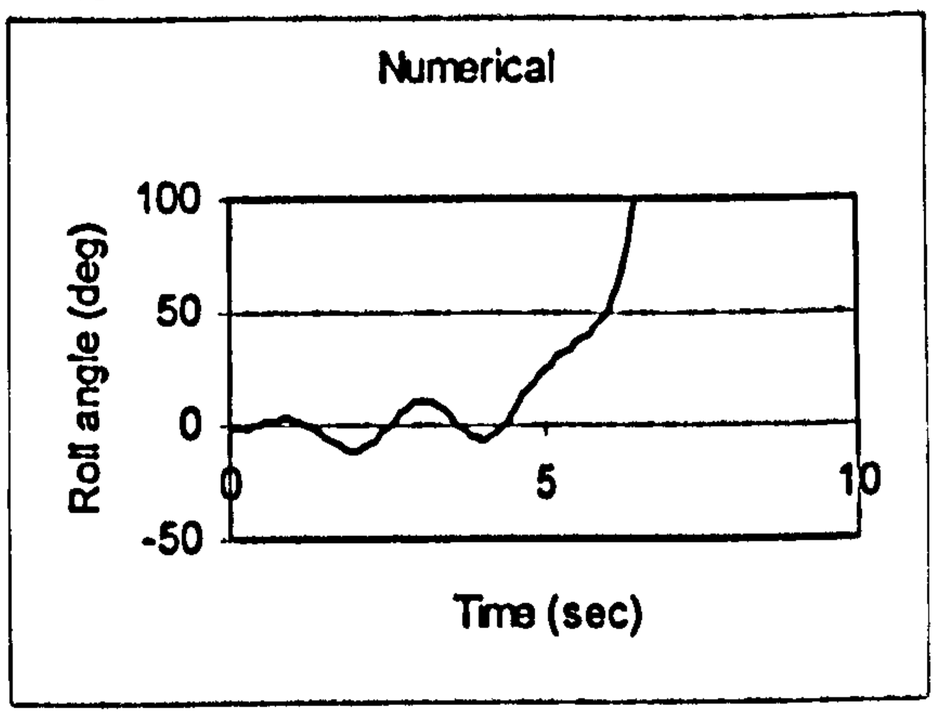

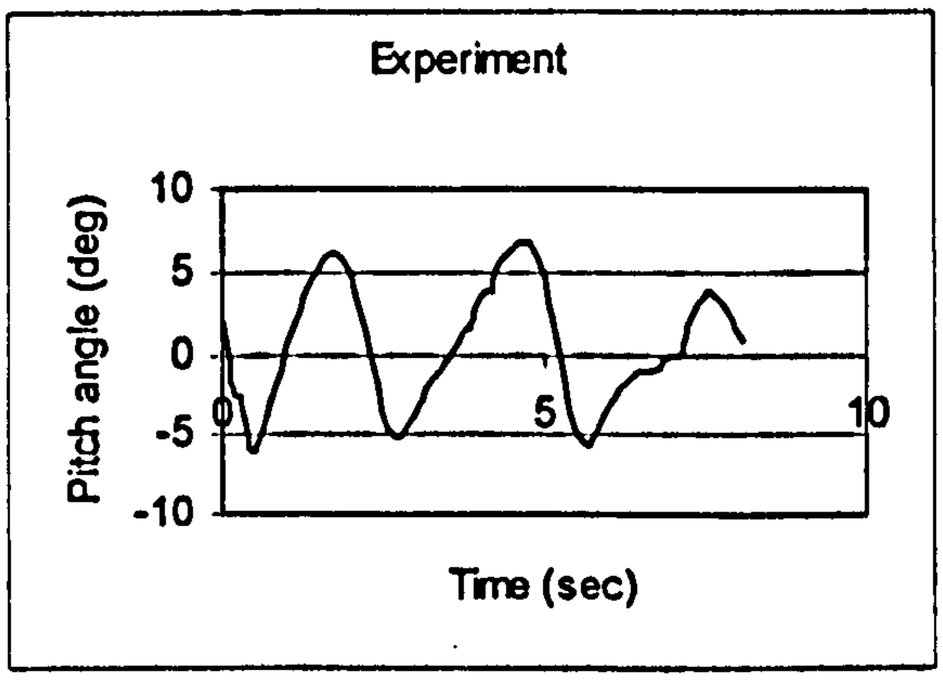

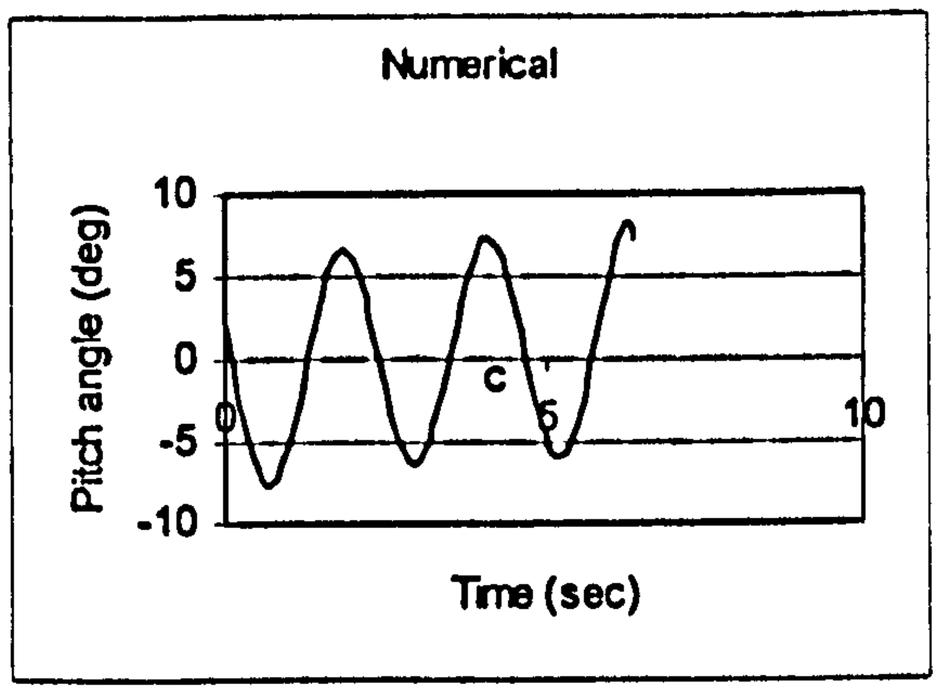

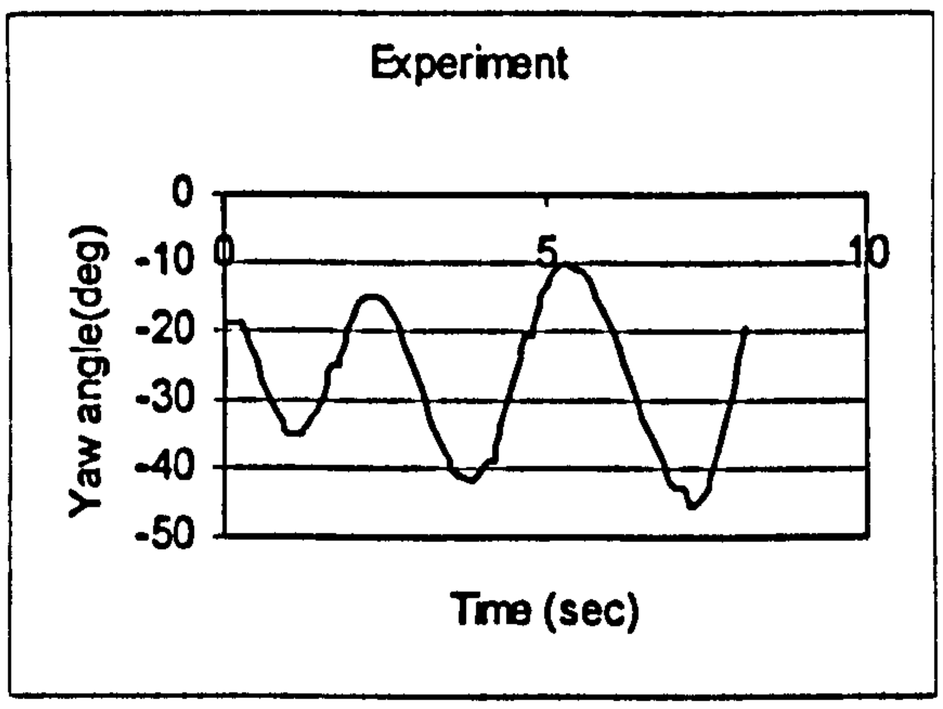

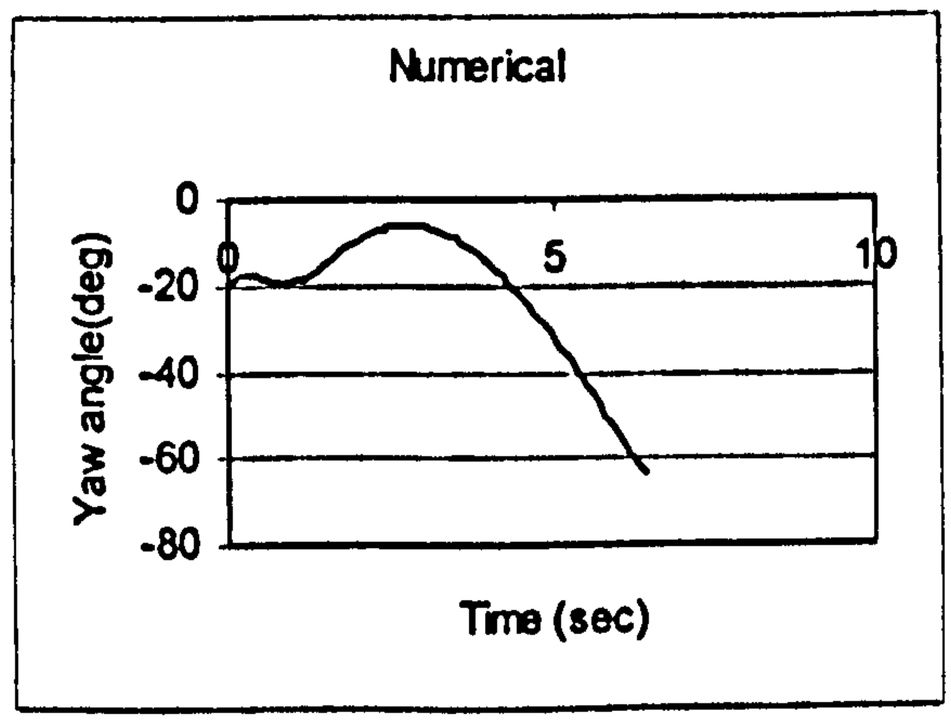

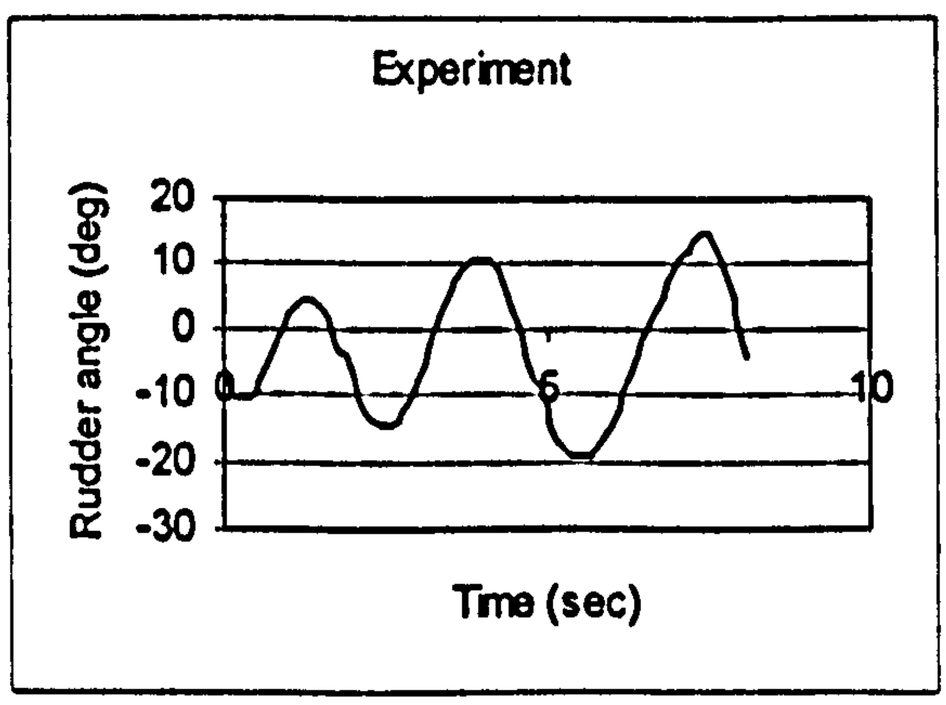

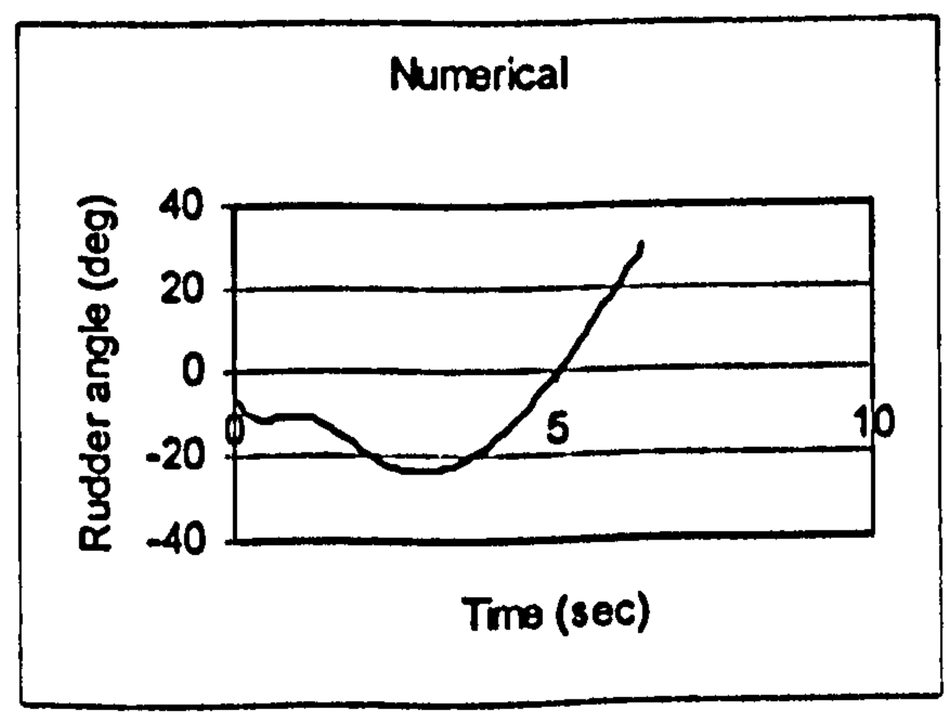

Figure 7.14 Comparison of experiment and numerical method for the model of Ship A-2 in $H/\lambda=1/8.7$, $\lambda/L_{pp}=1.127$, $Fn=0.43$, $\chi_c=-30$ degrees (Capsizing)

With the second approach, (Figure 7.8) the experiment displays sub-harmonic roll the numerical model agrees rather well the exception of yaw angle which appears to be larger than the experiment result. This might explain the larger roll angles that occur in this simulation. The pitch angle yet again has not changed for the numerical model.

When speed increased and autopilot course is getting closer to astern waves (Figure 7.5), the model experiences smaller roll angle and eventually keeps herself in straight course. This time, the yaw and rudder characteristics are displayed more satisfactorily. However, the roll angle is estimated larger than experiment for first 10-15 seconds. This might be caused by not having enough damping force initially.

For the numerical run with the second approach (Fig. 7.9), although the improvement is visible in the roll motion, the stiffness in yaw and rudder still persists with the estimated roll angle larger than experiment for some periods. Therefore, it could be seen that the numerical model without memory effect has better simulated the yaw and rudder motions compared to the numerical model including memory effect. However, the harmonic roll motion is better simulated comparing to the first approach (Fig. 7-5). Pitch motion is yet again unaffected from the change in the numerical model.

After the speed is further increased (Figure 7.6), the model experiences very large roll angle and ultimately reaches capsize. The numerical model satisfactorily displays the roll and pitch motions and estimates the rudder and yaw angles with reasonable accuracy.

When the second numerical approach is adopted (Figure 7.10), this time though, similar roll and pitch characteristics to the first approach are found. However this numerical model predicts the rudder and yaw behaviour with more reasonable accuracy.

For Ship A-2, the first approach model was performed in numerical simulation. In the first run (Figure 7.11), the method approximated the roll motion rather well apart from the initial disturbance. This might be caused by the initial values or by not having enough damping force during this short period. For the yaw and rudder, the autopilot model seems to be too stiff. However, it catches up the overall characteristics of the motion.

With the increasing speed and when the heading angle is getting closer to astern, the model is suffering from surf-riding. After about 8 s, the yaw angle violently increased to port while the rudder controlled by the autopilot responded to prevent this yaw motion. However, despite hard starboard, the increase continued for a while and here the centrifugal force due to large wave-induced force and rudder force the model

rolled uncontrollably to starboard. As a result, the model *capsized due to broaching* (Figure 7.12).

On the other hand, in the numerical model the behaviour of the motion does not display the same characteristics. When the model experienced a wave crest near amidships for a while, the roll increased when the wave crest passed amidships the model capsized at the wave crest. It displayed almost identical characteristics for fully 6 DOF numerical model. Here, in contrast to highly oscillating yaw motion in the experiments, numerical model displays continuously negative yaw reaching to desired heading angle after about 7 seconds yet this leads to rapid parametric build up of the roll motion. The characteristic of the numerical simulation resembles *capsizing due to loss of stability on a wave crest*. This is usually due to the reduced restoring moment at the wave crest amidships, which cannot counteract the heeling moment. However in this numerical model calm water restoring is used therefore such conclusion cannot be made. The stiff autopilot model might cause these differences between experimental and numerical results here. Also, in the numerical model capsizing occurred before the actual capsizing in model tests.

With increased wave steepness and reduced wave length to ship length ratio, the model undergoes sinusoidal motions in the experiment while the numerical model approximate well this behaviour apart from some disturbances in roll motion (Figure 7.13).

When the speed increased, similar characteristics with the second run are displayed in the model tests (Figure 7.14). However, the model reaches the capsizing limit earlier than in the previous case due to increased wave steepness. The numerical model, this time, estimates the motions rather well. The difference caused by the stiff autopilot model continues. The period of the numerical model is also slightly shorter than the actual model runs.

For the pitch motions, all cases except the third run (Figure 7.13), numerical simulation display reasonable agreement with harmonic pitch motions. In Figure 7.13, the overestimation of pitch angle is due to the poor prediction of yaw angle which has very small deviations and therefore amplitude comparing to the experiments. However, it displays the same periodic motion characteristics as the experiment.

In all the experimental and numerical runs assessed here, the pitch angle is less than 10 degrees, therefore the assumption of large pitch angles does not display any difference comparing to the previous numerical models.

When surf-riding occurs, the relationship between propeller revolution and the ship forward speed can be changed. However, the propeller revolution is assumed constant due to simplicity in the numerical model. Note also that, wave forces are modelled using mean water level instead of the instantaneous wave surface for Ship A-2 using 3-D panel method or 2-D strip method explained in Chapter 5 and Appendix B. This is important point in calculating the restoring moment because it is thought that for the environmental and operational conditions concerned here if the GZ curve in calm water is obtained, the use of instantaneous water surface is not required. The instantaneous water surface should be taken into account in simulating 6 DOF motions and in identifying dangerous situations in lower speed regions as it is carried out for Ship A-1.

An overview for the simulations of Ship A-1 indicates that there is a better agreement with experiments for the second approach result, than for to the first approach in terms of roll amplitude. The second approach estimates larger roll amplitude and more harmonic motions which are closer to experiments. It could be a result of better damping forces when the effect of encounter frequency is included. However, this difference could be more realistically explained in terms of changes in the yaw and rudder motions. The coupling between roll and yaw-rudder motions seems to create aforementioned larger roll amplitudes. The change in yaw and rudder characteristics indicates the effect of frequency to the control systems.

As for Ship A-2, when the given environmental and control parameters are concerned, the model could give reasonable agreement, the effect of wave surface is thought to be not as significant, as it is in the surf-riding case. However, in contrast this time vessel is unstable and motions are likely to result in capsizing as it was in Figure 7.11.

7.7. Concluding Remarks

As mentioned earlier, the numerical model was designed to estimate dangerous motions in following and quartering seas. Therefore the results from the numerical method can be assumed as reasonably satisfactory.

For the two vessels tested here, numerical models with and without memory effect were employed for the container vessel, while the mean water level surface was taken into account for the numerical simulation of Ship A-2. Therefore, it was aimed to

demonstrate a wide range of approaches in order to have to clear view of the accuracy of the new mathematical model.

For the first approach in Ship A-1, a number of factors were identified as affecting the accuracy of the numerical model. The numerical model seems to have less amplitude in roll motion that could be affected by estimated damping value or the initial damping assumed in the calculation. Furthermore, the calculation of the wave forces should be under scrutiny for the detailed examination and this will be done in Chapter 10. Although, the pitch motions which are dependent upon the instantaneous wave surface modelling for this case are displayed with satisfactory agreement.

When the effect of frequency was taken into account, there were clear improvement in the amplitude of roll motion and the results were more in line with the experiments as well. Yaw and rudder motions however were seen to be the result of this improvement. They were highly affected and displayed more "stiffer" characteristics due to frequency effects. However they were better simulated in the numerical model when the speed was increased. Therefore, an important observation will be the sensitivity of the yaw and rudder motions to the frequency effects. This could inevitably be concluded as the effect of frequency to the control systems. Further information on that matter is given in Appendix D. However, recalling from Chapter 3.6, which concerns the aforementioned experiments, the ITTC benchmark review committee [92] urged that the exact calculation of memory effects be carried out from the start of the waves. Therefore, the ITTC benchmark testing, which does not specify initial conditions of fluid motions, is not appropriate for this purpose. Based on this finding, the effect of frequency or so called "memory effects" will be looked in the detail in Chapters 8 and 10.

While the first approach with different wave modelling was used, for the simulations of Ship A-2, 6 DOF and 4 DOF model with static equilibrium with heave and pitch were identical as it was mentioned in Section 7.5. This conclusion might not be clarified perhaps because the mean water level is assumed for both cases. However, this kind of approach seems to be practical and can give reasonable accuracy in terms of motions of ship in extreme astern seas at relatively high speed although not quantitatively. In this approach there were problems in yaw and rudder motions like in the case of Ship A-1. Pitch motions were again reasonably predicted except for one model run which overestimated the pitch motion due to the very small yaw deviation on the numerical simulation.

For the effect of the environmental and performance parameters, factors that would appear to govern behaviour include wave steepness and speed.

However, the above conclusions cannot be completely verified until wider parametric studies are carried out and the accuracy of wave force calculations is exploited. The former will be attempted in the next chapter while Chapter 10 will look into the effect of wave force with the fully captive model tests for Ship A-2 which include the combination of vertical motions in terms of large sinkage and trim and large roll motions from pure following seas through beam seas. Therefore, it will also help us to investigate the effect of frequency and the improvement in the numerical model after the incorporation of the "memory effect". Furthermore, the similar kind of comparisons in this Chapter will be carried out for random waves where the modified numerical model in random waves, which are presented in Chapter 9, will be verified against the free running model tests and the results will be given in Chapter 10.

8. PARAMETRICAL STUDIES

8.1. General Remarks

The objective of this chapter is to present the numerical simulations carried out to investigate the contribution of the new numerical model to the simulation of the capsizing behaviour of ships in following and quartering seas in a wider scale. As it is well known, the experimental studies are limited to certain conditions and number of model runs. However, in the real environment, a number of parameters, which are not effectively included at model experiments, affect the ship's motion while she travels in extreme following and quartering seas. Deriving from this background and in the light of the validation of numerical model with model experiments, it is required to extend the tests for varying parameters in terms of numerical simulations.

Within the above framework the following sections of the chapter present the numerical simulations in the extreme following and quartering seas for various conditions. The mathematical model is applied for simulating the dynamic behaviour of Purse seiner fishing vessel and of a containership, for which very extensive input and seakeeping test data for a following-sea environment is available. The two ships are numerically tested for various speeds, wave steepness, wave lengths and loading conditions. Comparisons have been made between the new axis system and the traditional axis systems in order to determine the differences in the simulated behaviour for the two cases. This is followed by the parametrical studies to investigate the accuracy of the improved numerical model to determine the aforementioned dangerous conditions which often result in capsizing, such as broaching associated with surf-riding and low cycle resonance. The numerical simulations in different heading angles have been carried out in various conditions to investigate the effect of frequency for ship motions in extreme astern seas. Finally, deriving from all these numerical studies, the insights about the link of behaviour with operation and design parameters of a ship which numerical code exploited are discussed. The further simulations for the container vessel using numerical model are presented in Appendix G.

8.2. Parametric Studies

In order to carry out parametrical study using the developed code, a container ship and a purse seiner fishing vessel for which very extensive input and seakeeping test data for a following-sea environment is available, are used. The developed numerical

model already has been validated using this test data in Chapter 7. Those validation results and all details regarding the model tests can be found in Chapter 7. Lines plans and particulars of the ships are given in Chapter 7 and Appendix F.

As it is mentioned in Chapter 7, the GM selected is not the design GM value, but one that only just satisfies the IMO regulations. In the numerical simulations parameters and conditions were chosen to be similar to the previous ITTC Benchmark tests presented in Chapter 7.

Here, the numerical calculations were carried out in order to compare the simulation of ship motions in different degrees of freedom and with and without the memory effects. The difference between coupled 6 DOF numerical model and 4 DOF with static equilibrium of heave and pitch motions is investigated in the context of effect of wave steepness, otherwise coupled 6 DOF numerical model was employed throughout the numerical simulations. The details regarding every case are presented in the following sections.

8.2.1. Effect of Wave Steepness

It was shown in the literature that difference between 6 DOF and 4 DOF numerical model with static equilibrium in heave and pitch that has traditionally been used in the simulation of ship motions in astern seas, is not so significant. Based on this conclusion both ships have been tested in different wave steepness for the parameters and conditions given in Table 8.1 and 8.2. Maximum rudder angle is also set 10 and 35 degrees, respectively. Results for the numerical simulations are given in Figures 8.1-8.6. Here, A indicates the 6 DOF numerical model and B indicates the 4 D0F numerical model with static equilibrium in heave and pitch.

For the container ship, as it was defined in ITTC Benchmark tests, the conditions were chosen for the ship to be marginally stable. Therefore, the ship experiences very large roll angles (Figures 8.1-8.3). As wave steepness becomes more linear or smaller, the difference between two numerical models decreases. However, 4 DOF numerical model with static equilibrium in heave and pitch slightly overestimates the amplitude of the roll motion. 6 DOF numerical model also displays larger yaw deviations and slightly more stiff rudder turnings The difference between two numerical models in terms of maximum roll angle and with respect to wave steepness is shown in Fig. 8.7.

Nominal Froude number	Fn	0.2	0.2	0.2
Autopilot course from the wave direction	χ_c (degree)	45	45	45
Wave steepness	H/λ	1/25	1/30	1/35
Wave length to ship length ratio	λ/L_{pp}	1.5	1.5	1.5
Proportional gain	K_P (sec)	1.2	1.2	1.2
Differential gain	K_R (sec)	53.0	53.0	53.0

Table 8.1 Control parameters of numerical runs for Ship A-1.

Nominal Froude number	Fn	0.43	0.43	0.43
Autopilot course from the wave direction	χ_c (degree)	-10	-10	-10
Wave steepness	H/λ	1/10	1/12.5	1/15
Wave length to ship length ratio	λ/L_{pp}	1.637	1.637	1.637
Proportional gain	K_P (sec)	1.0	1.0	1.0
Differential gain	K_R (sec)	0.0	0.0	0.0

Table 8.2 Control parameters of numerical runs for Ship A-2.

For purse seiner fishing vessel, as for container ship, the conditions chosen provide marginal stability. Here, the vessel capsizes in all numerical simulations. Both numerical models (6 DOF and 4 DOF with static equilibrium of heave and pitch motions) show identical characteristics and are resulted in capsize around the same time (Figures 8.4-8.6). As wave steepness becomes smaller, the difference between two numerical models again decreases, although in this case even this decrease is not large enough to consider as difference. 4 DOF numerical model with static equilibrium in heave and pitch very slightly almost unnoticeably overestimates the amplitude of the roll motion and 6 DOF numerical model also displays slightly larger yaw deviations and stiff rudder turnings.

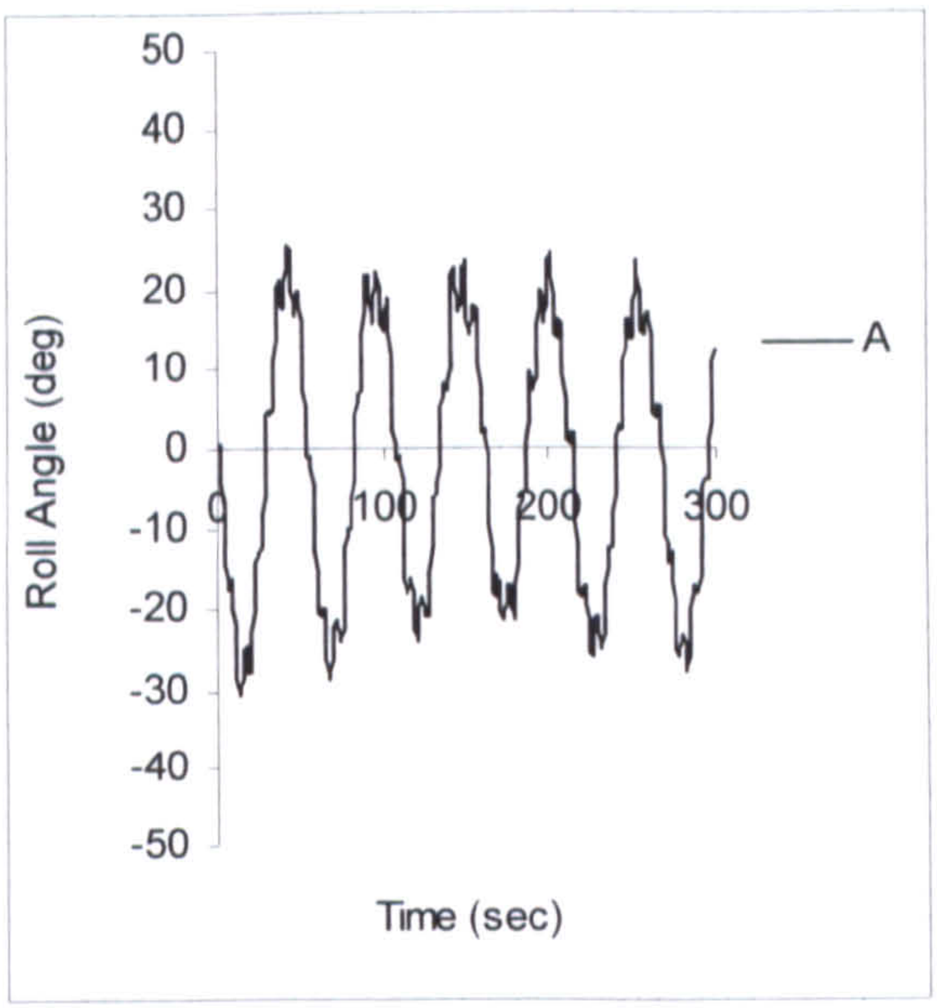

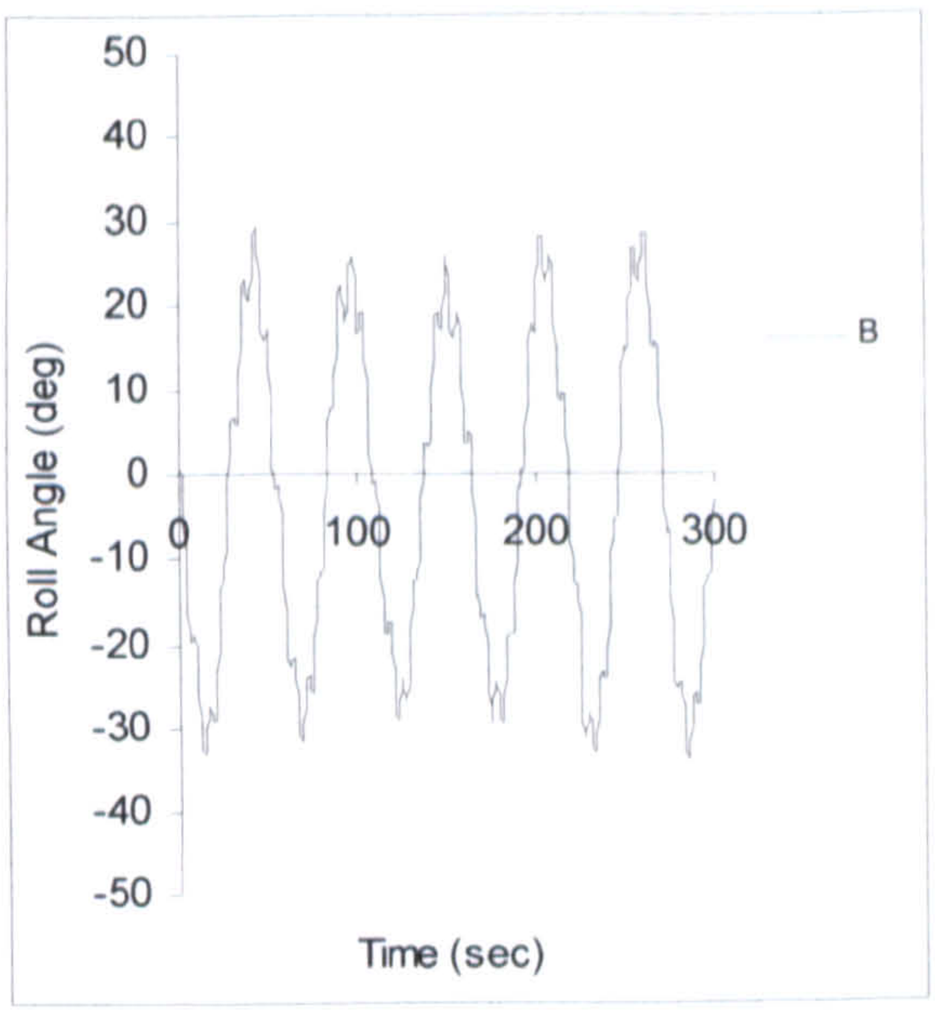

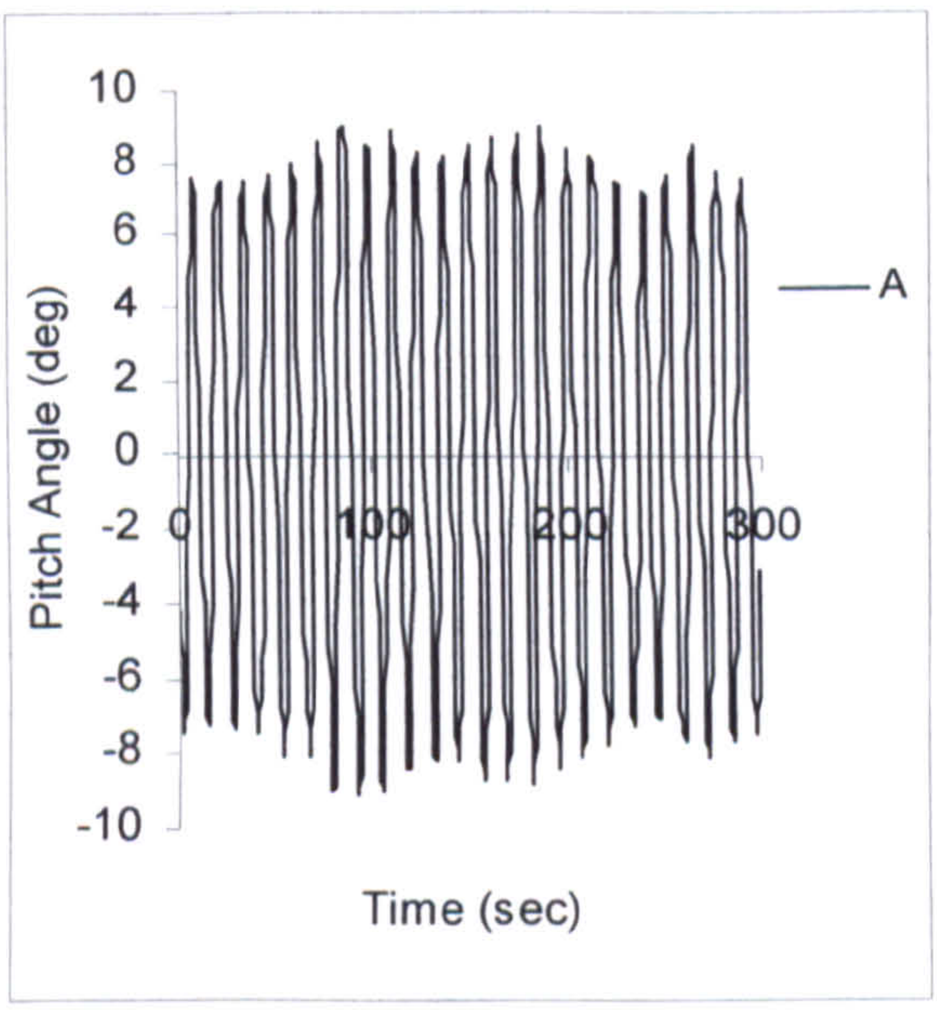

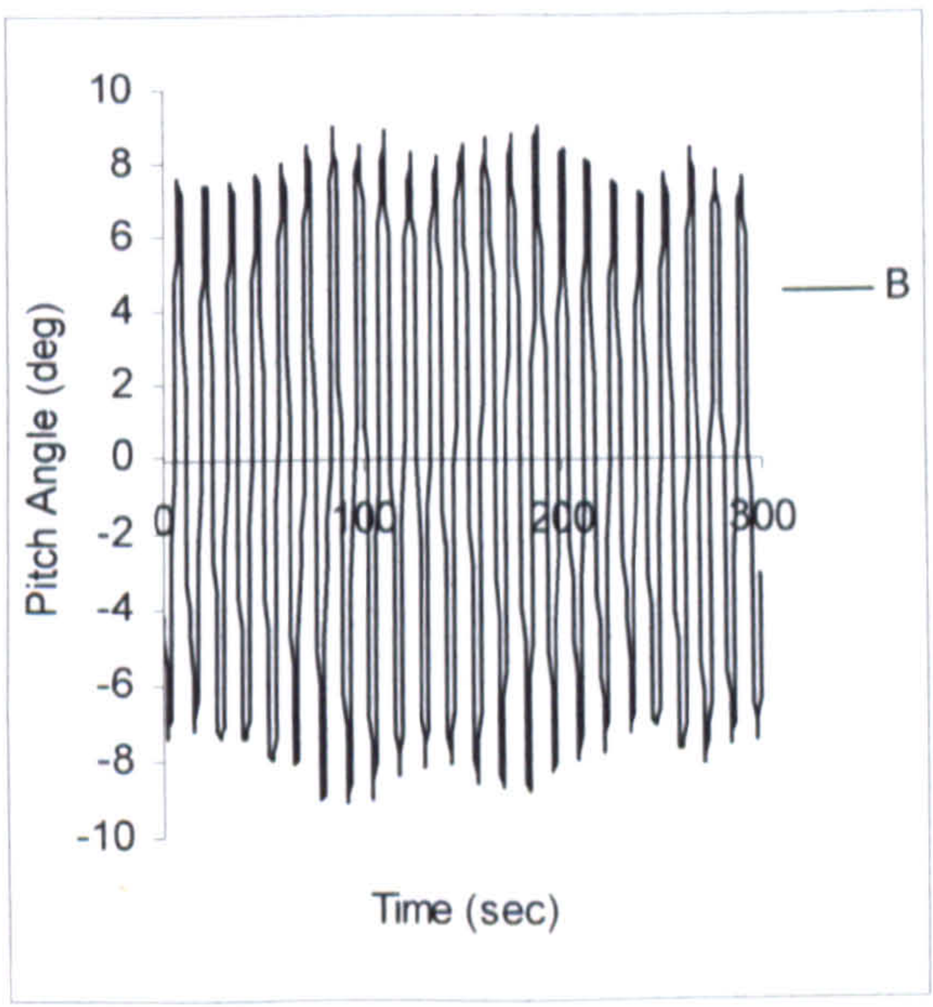

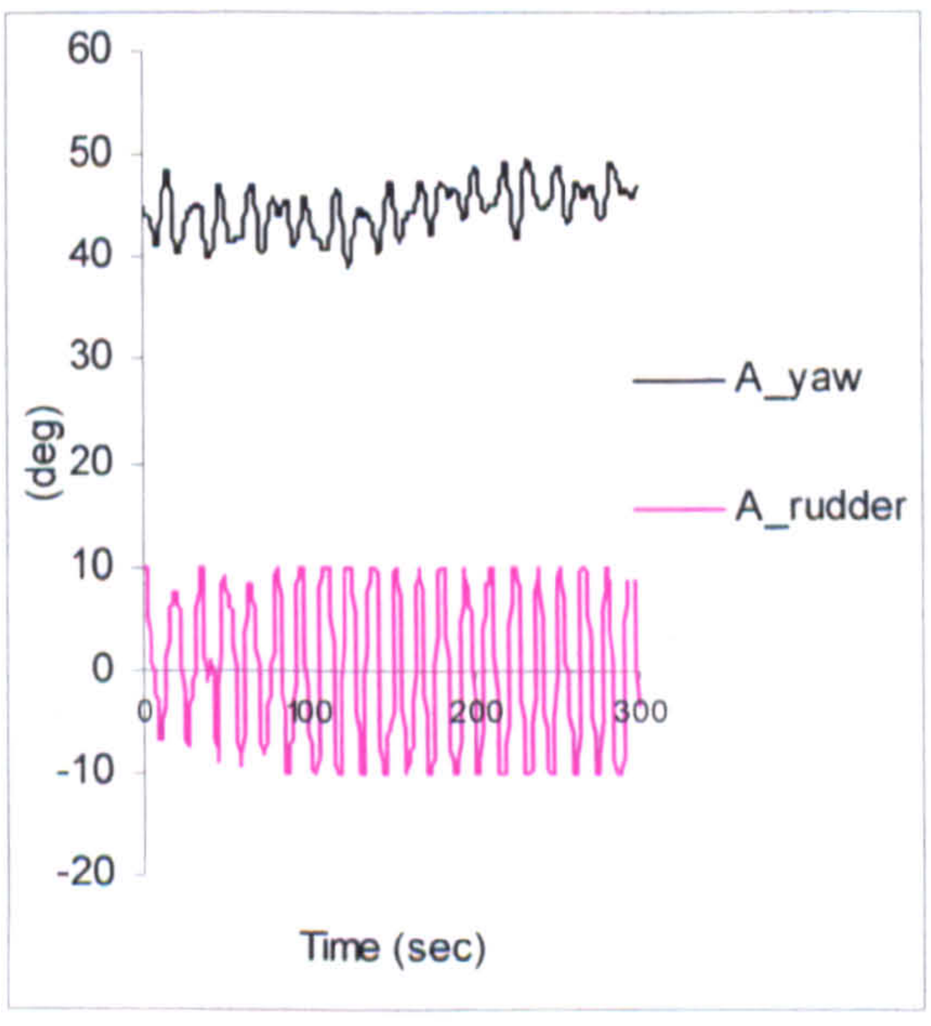

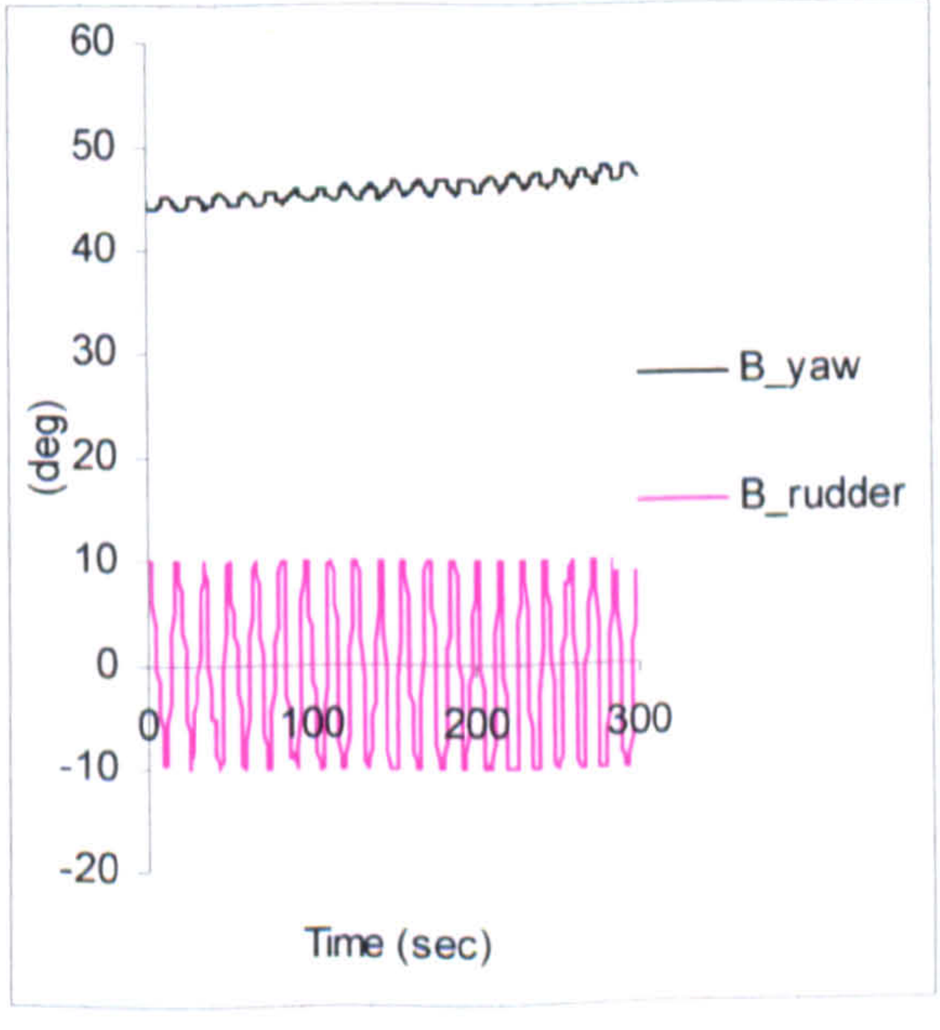

Figure 8.1 Comparison of 4 DOF and 6 DOF for Ship A-1 in $H/\lambda=1/25$, $\lambda/L_{pp}=1.5$, $Fn=0.2$, $\chi_c=45$ degrees

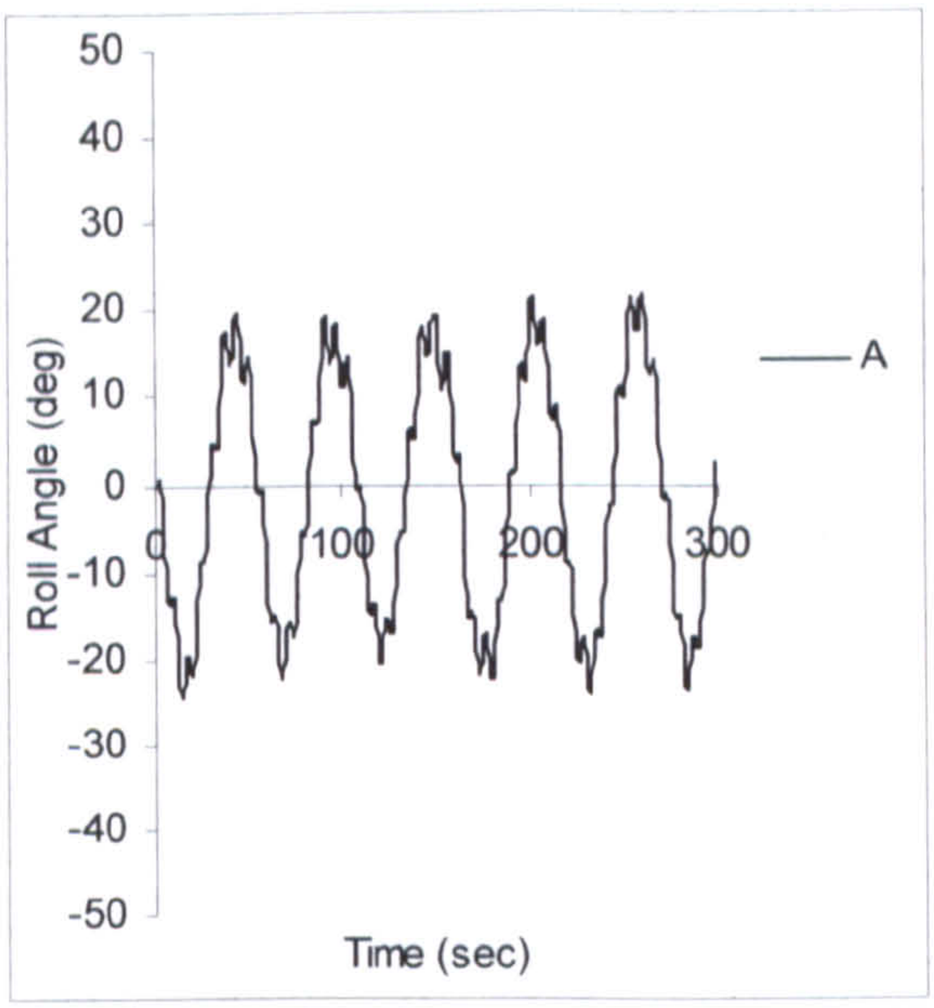

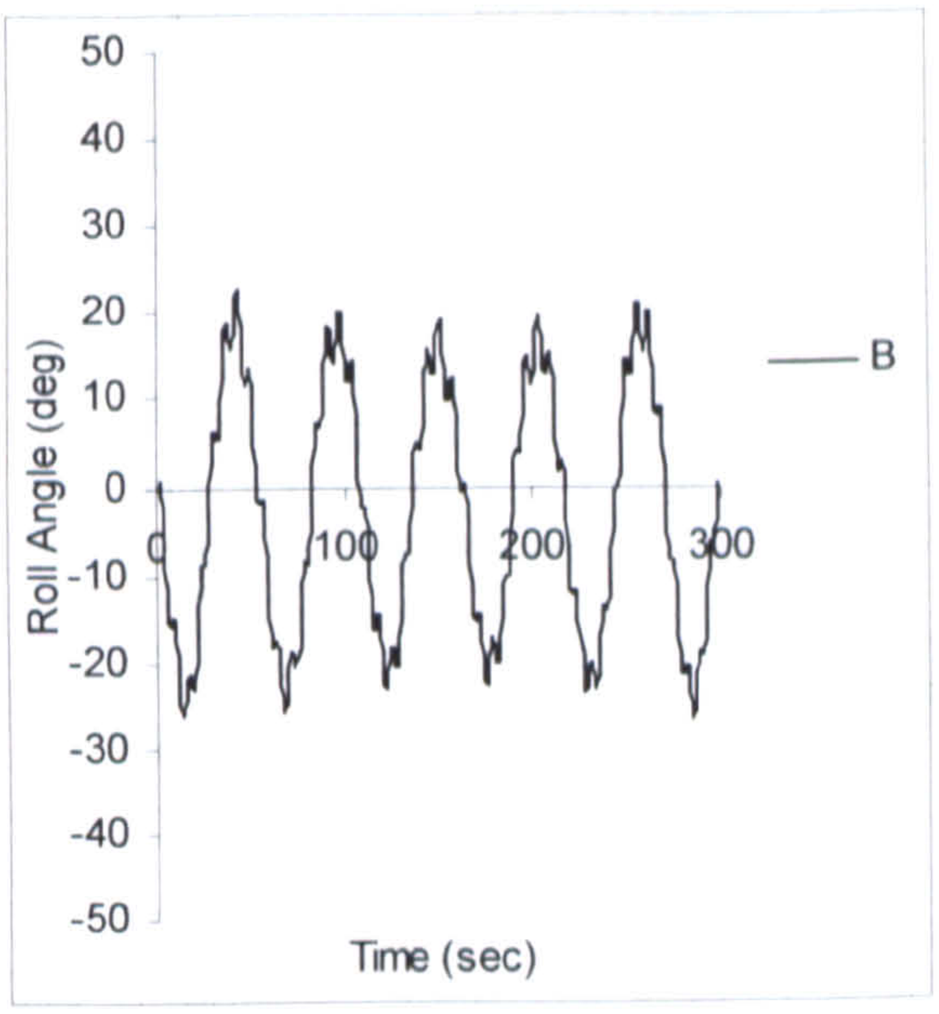

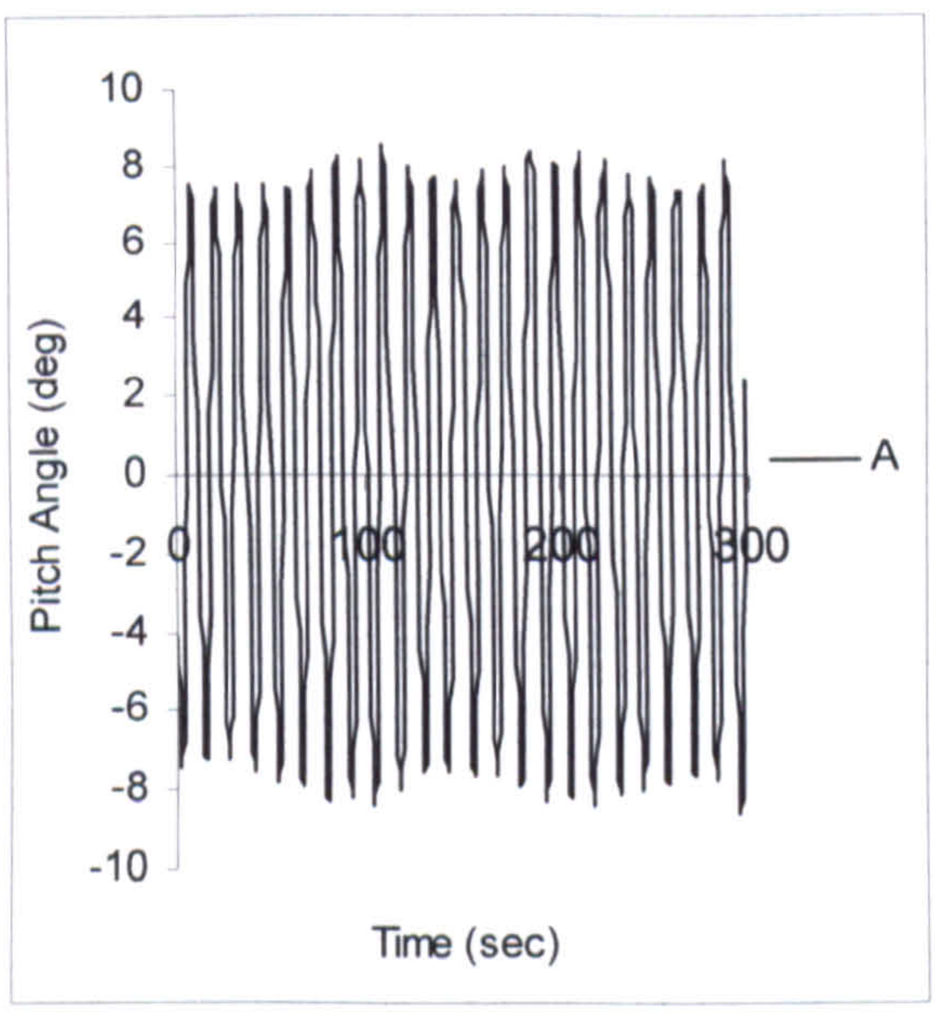

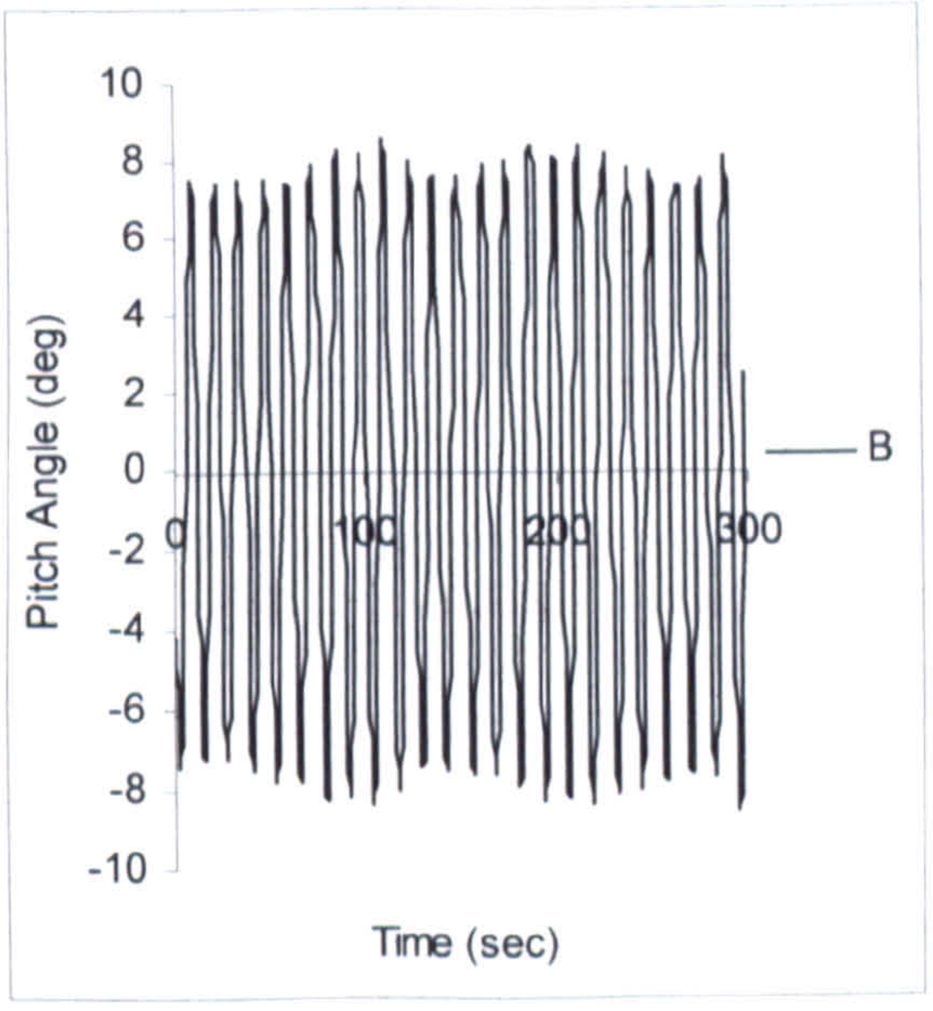

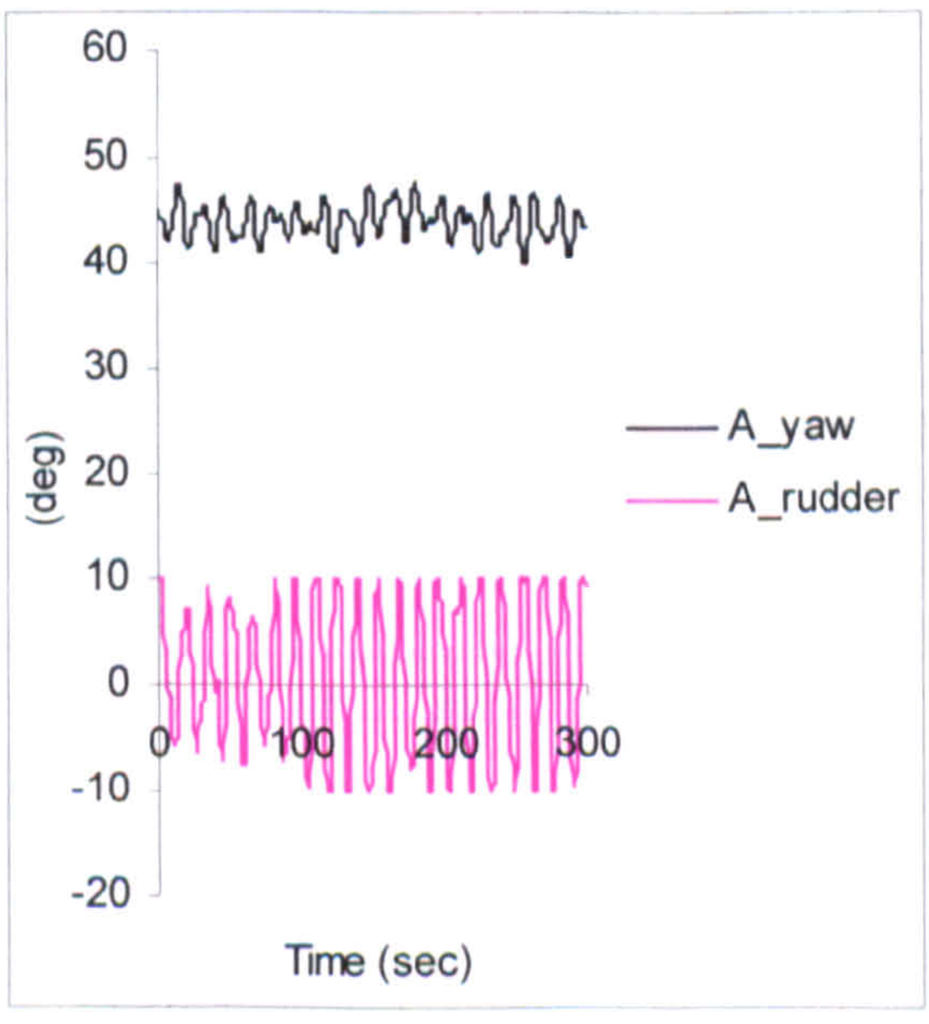

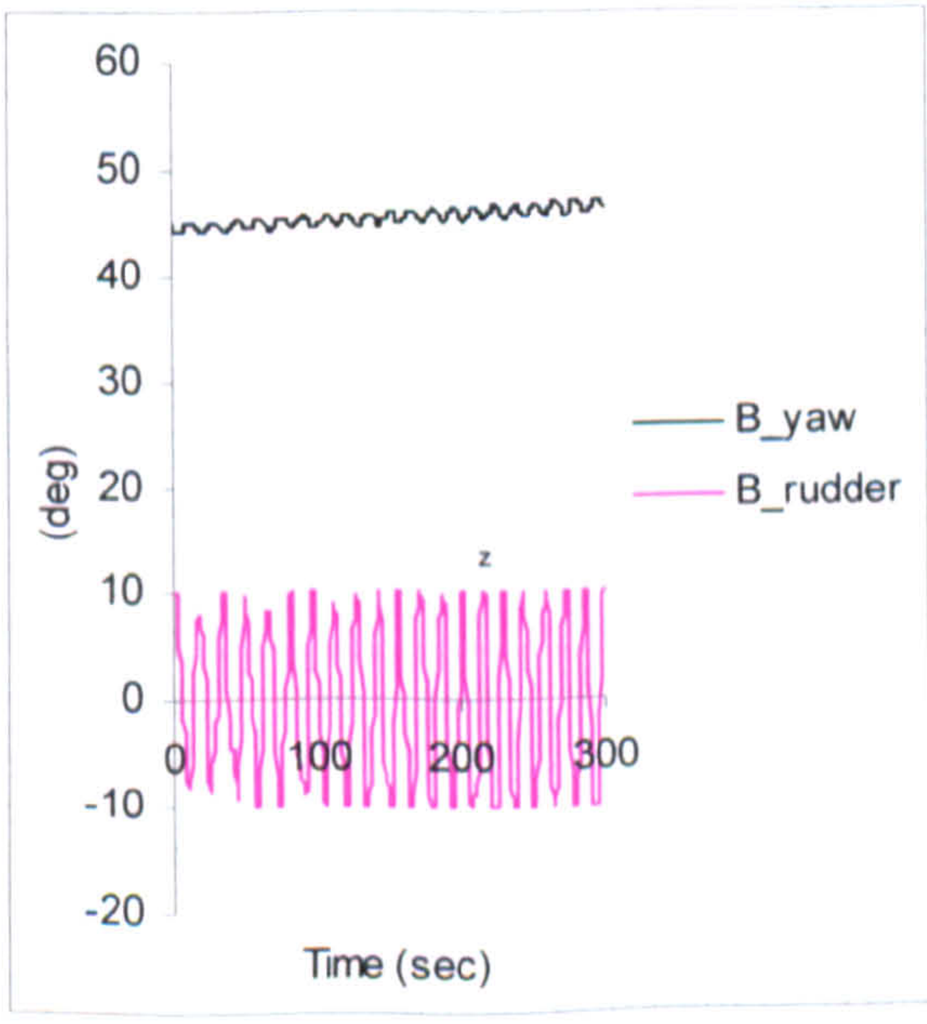

Figure 8.2 Comparison of 4 DOF and 6 DOF for Ship A-1 in $H/\lambda=1/30$, $\lambda/L_{pp}=1.5$, $Fn=0.2$, $\chi_c=45$ degrees

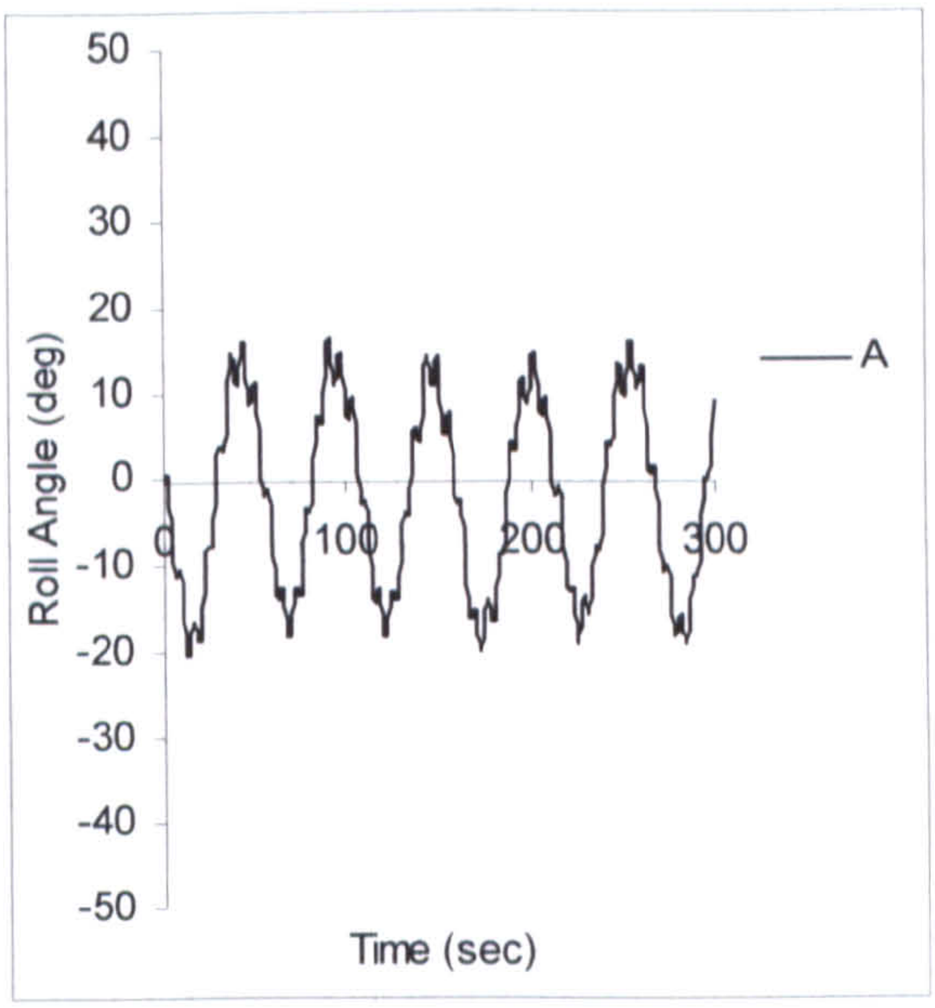

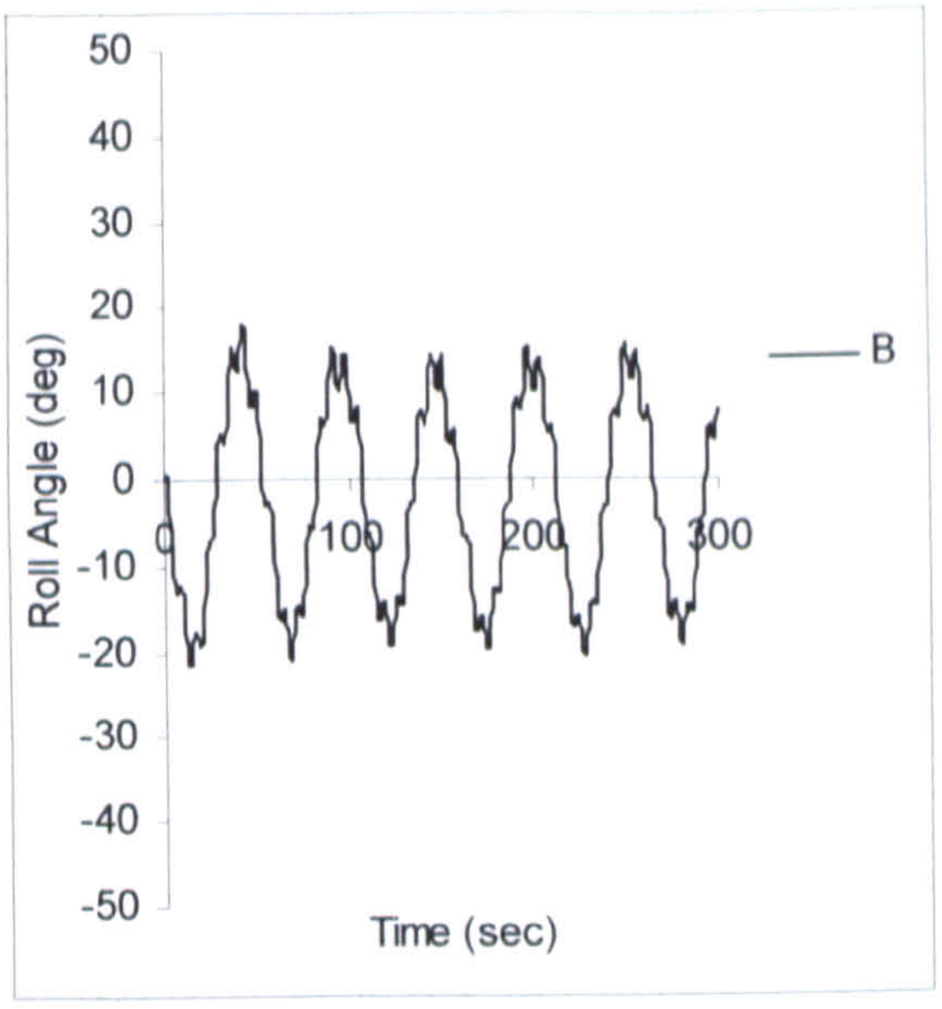

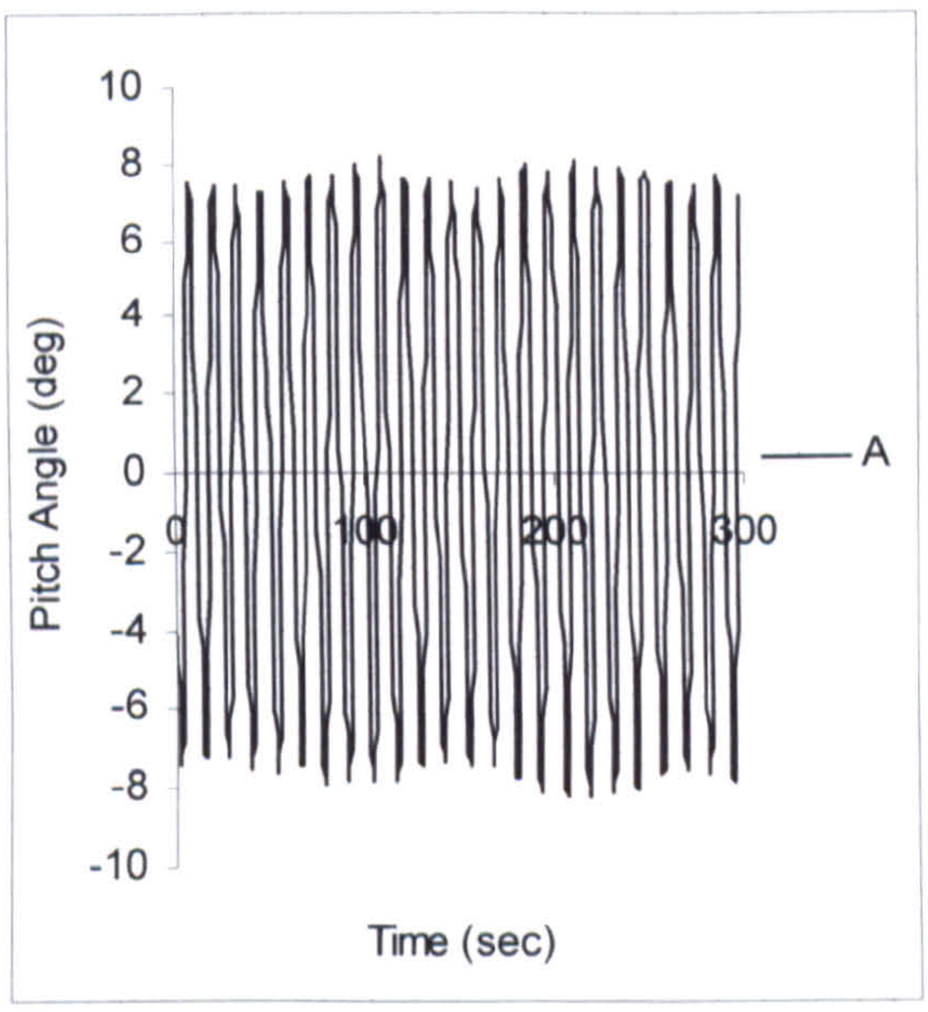

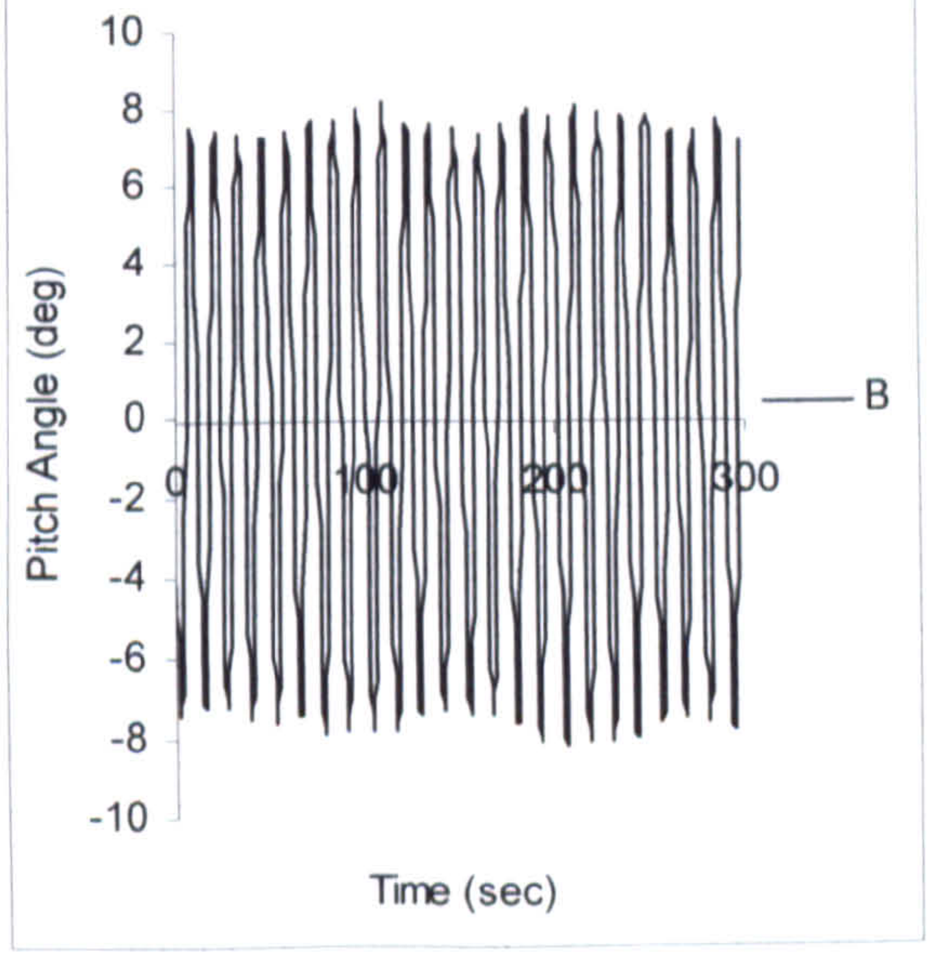

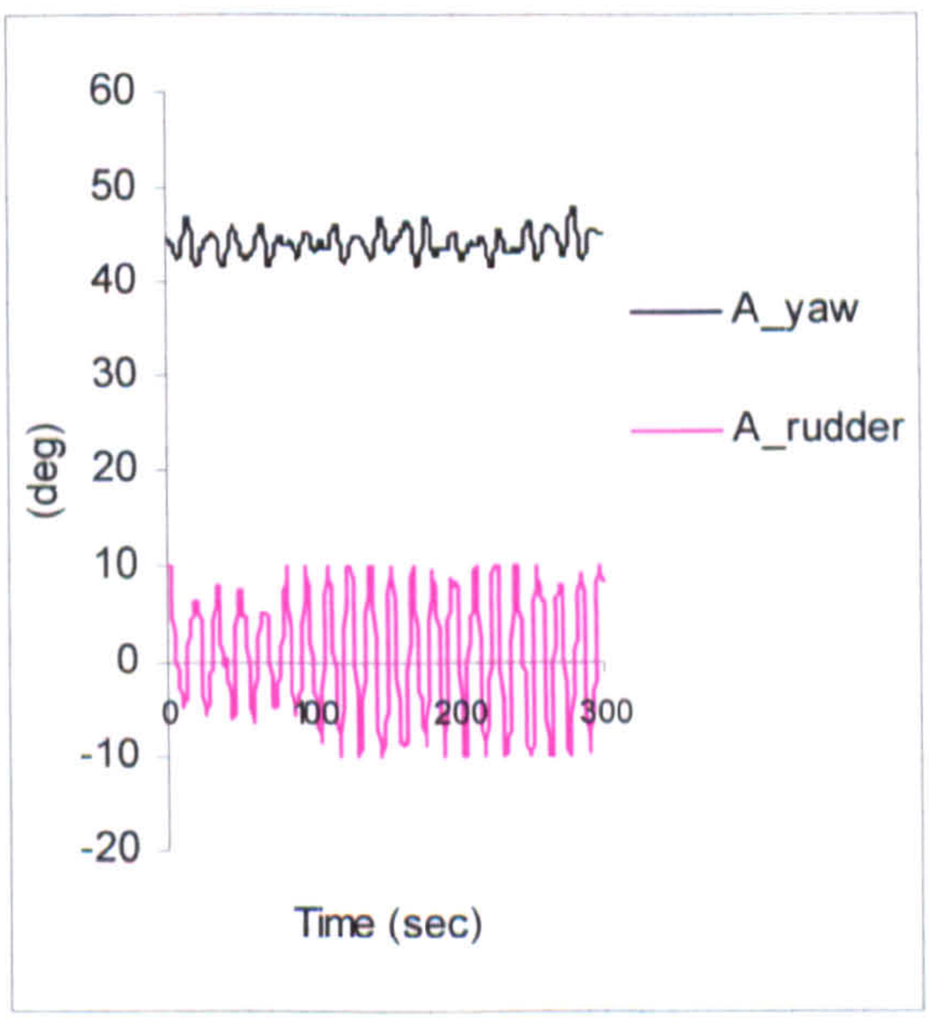

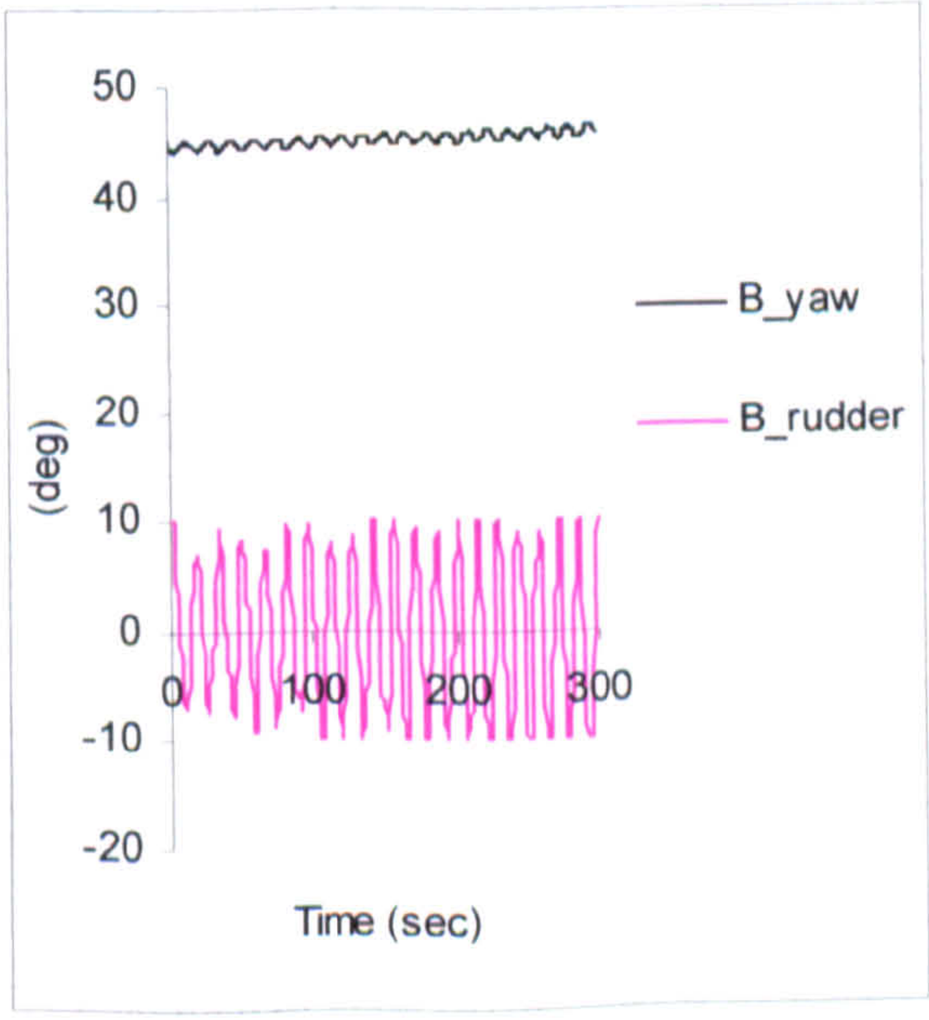

Figure 8.3 Comparison of 4 DOF and 6 DOF for the container Ship A-1 in $H/\lambda=1/35$, $\lambda/L_{pp}=1.5$, Fn=0.2,χ_c =45 degrees

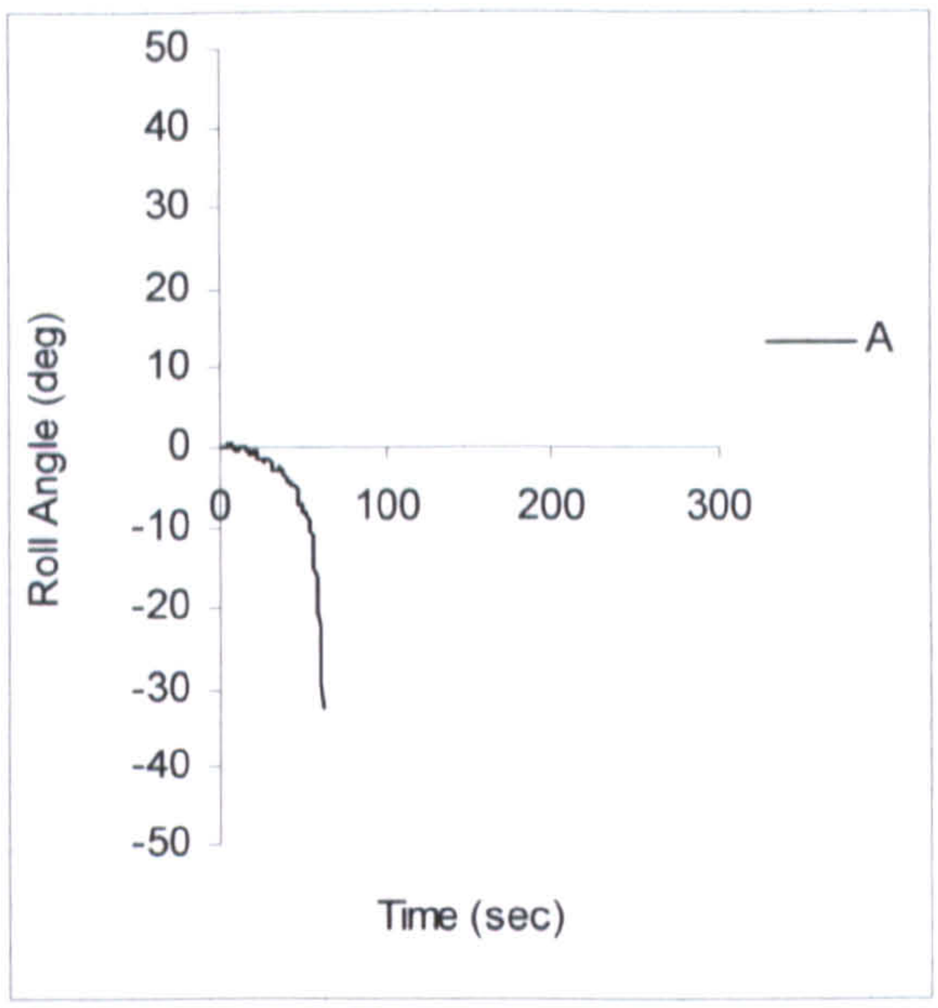

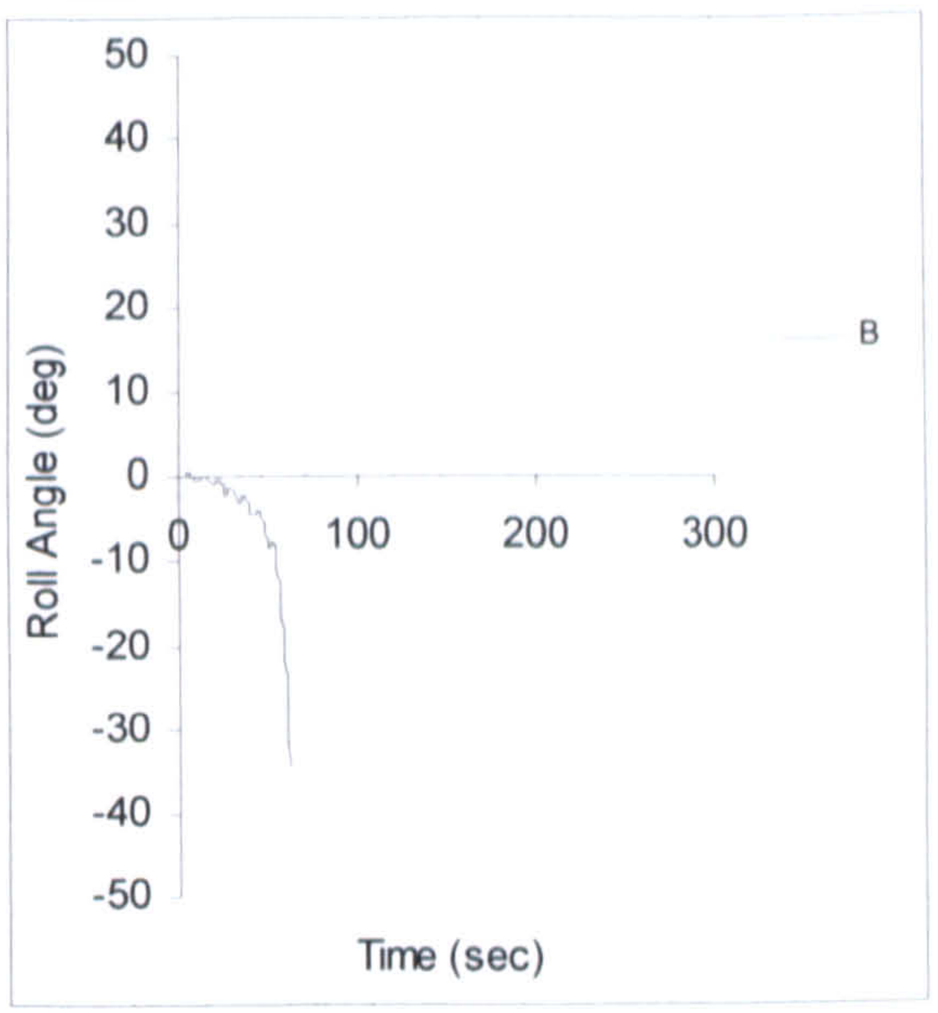

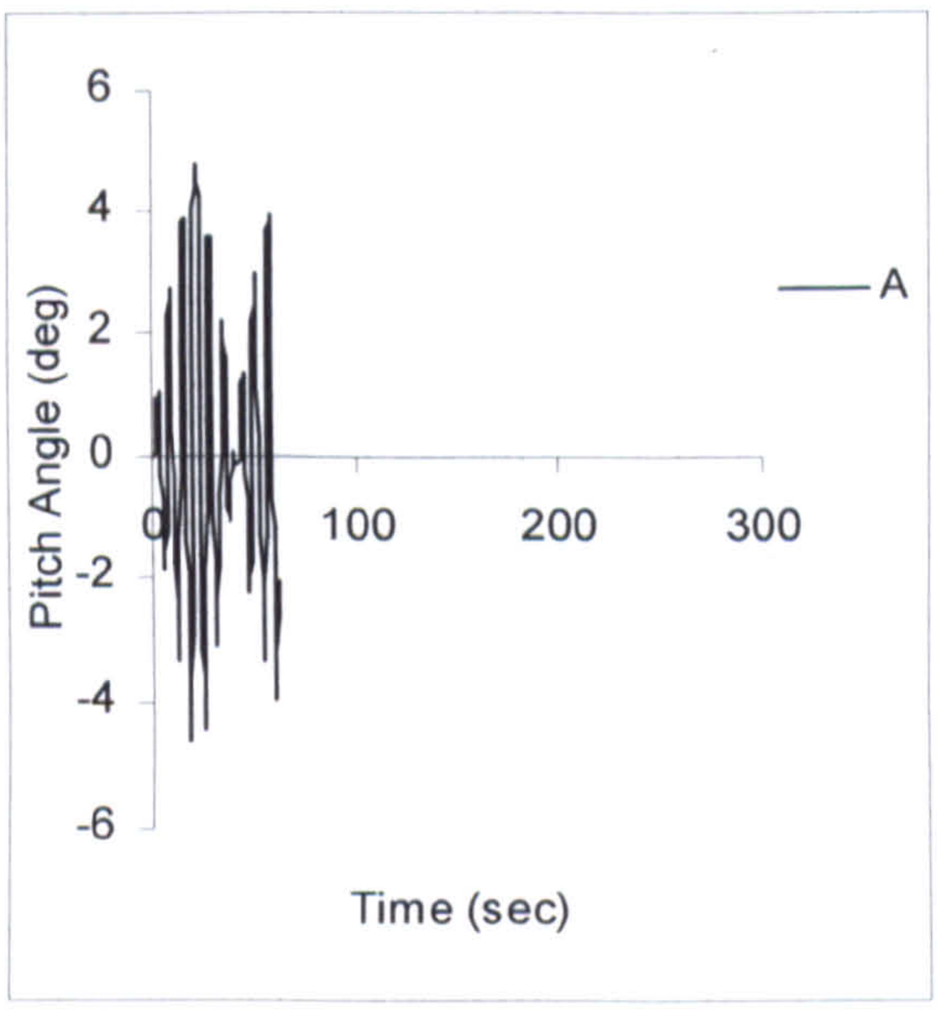

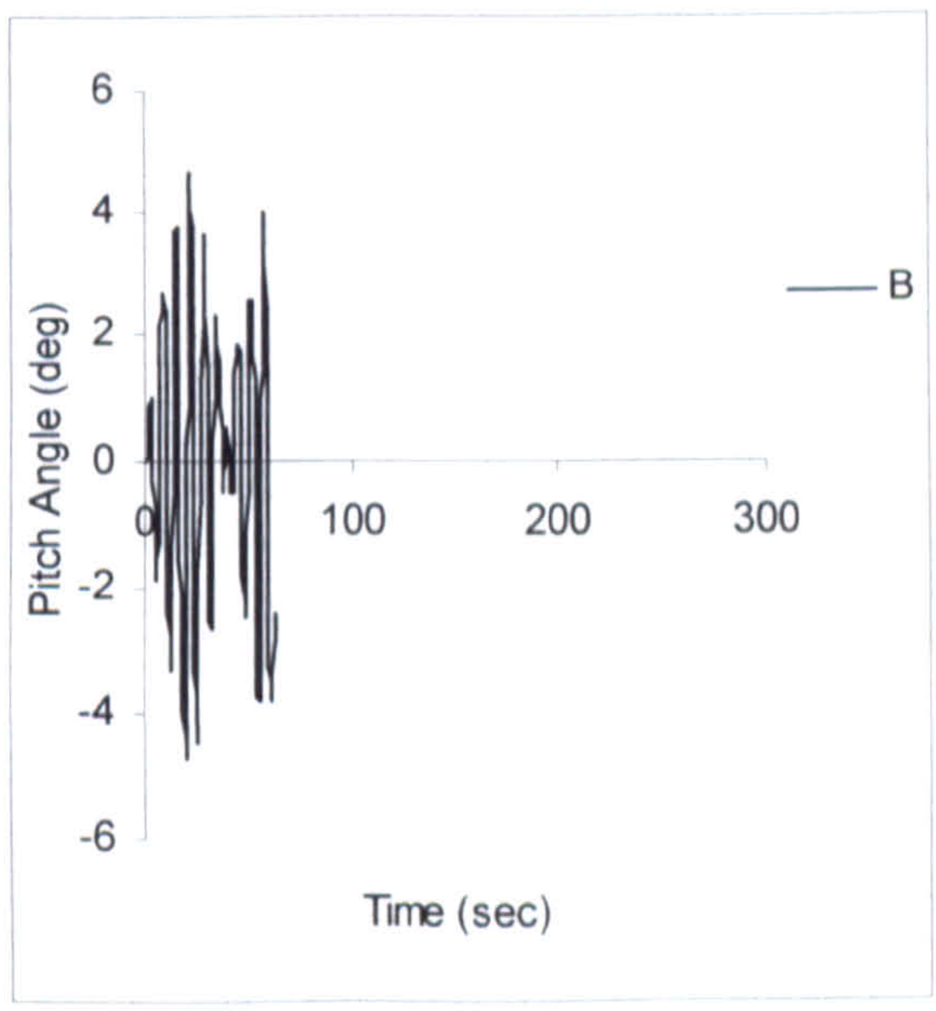

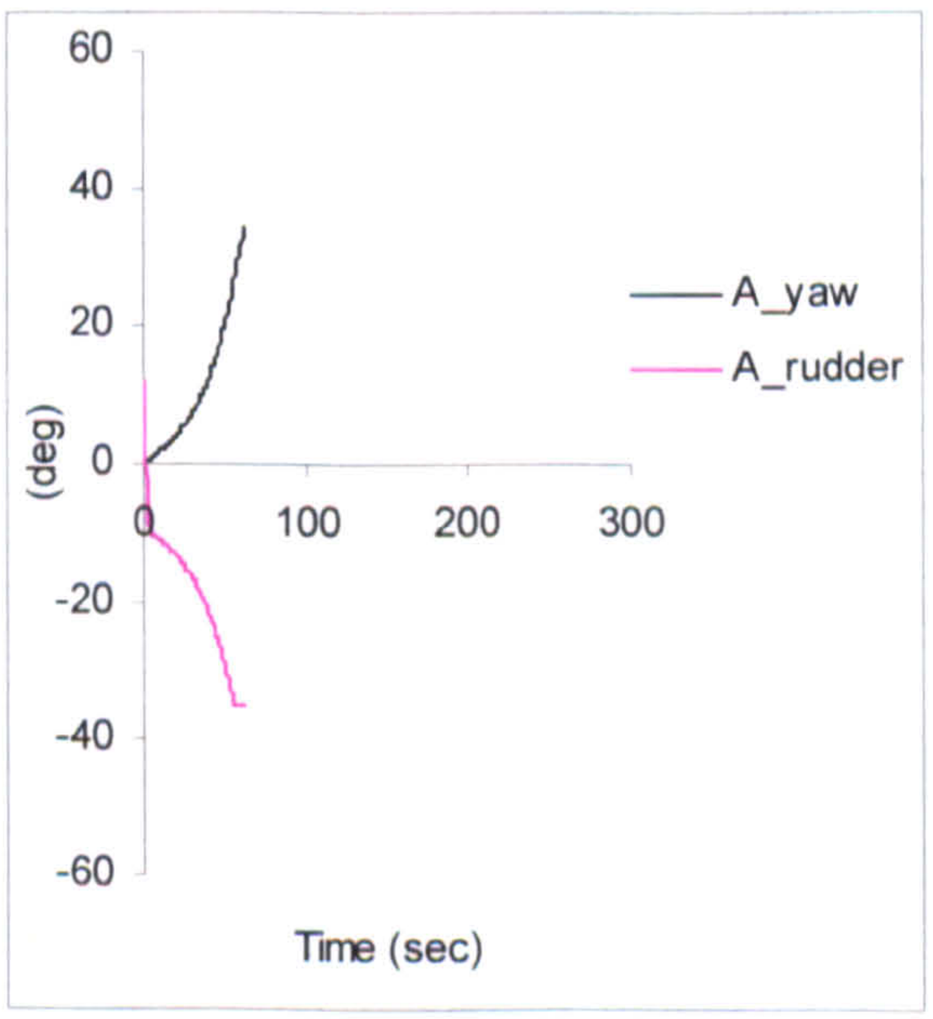

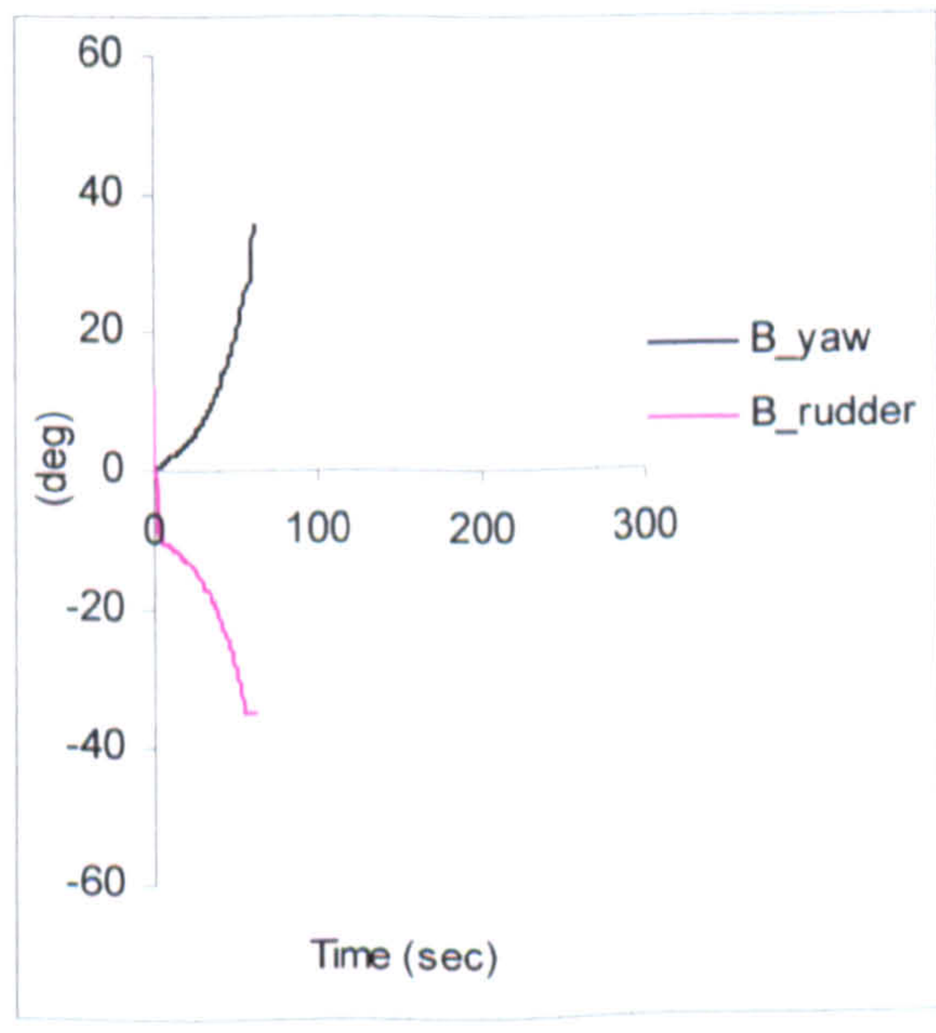

Figure 8.4 Comparison of 4 DOF and 6 DOF for Ship A-2 in $H/\lambda=1/10$, $\lambda/L_{pp}=1.637$, $Fn=0.43$, $\chi_c=-10$ degrees

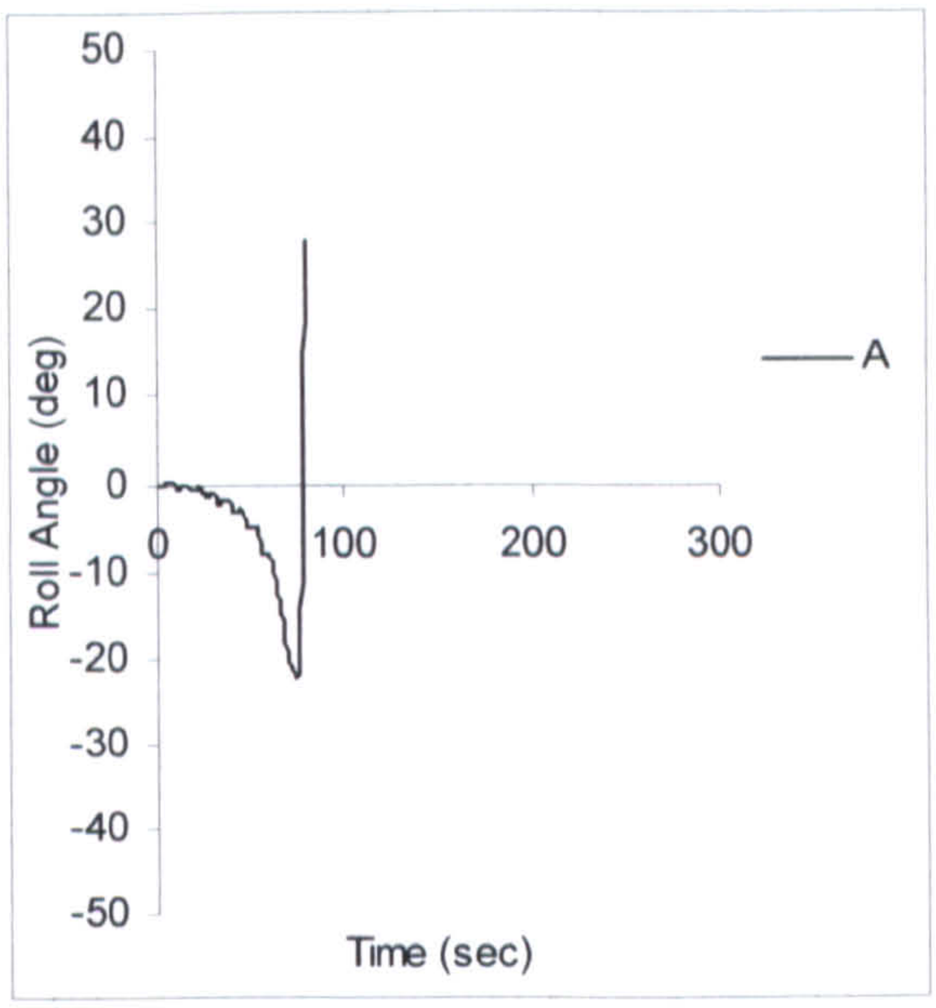

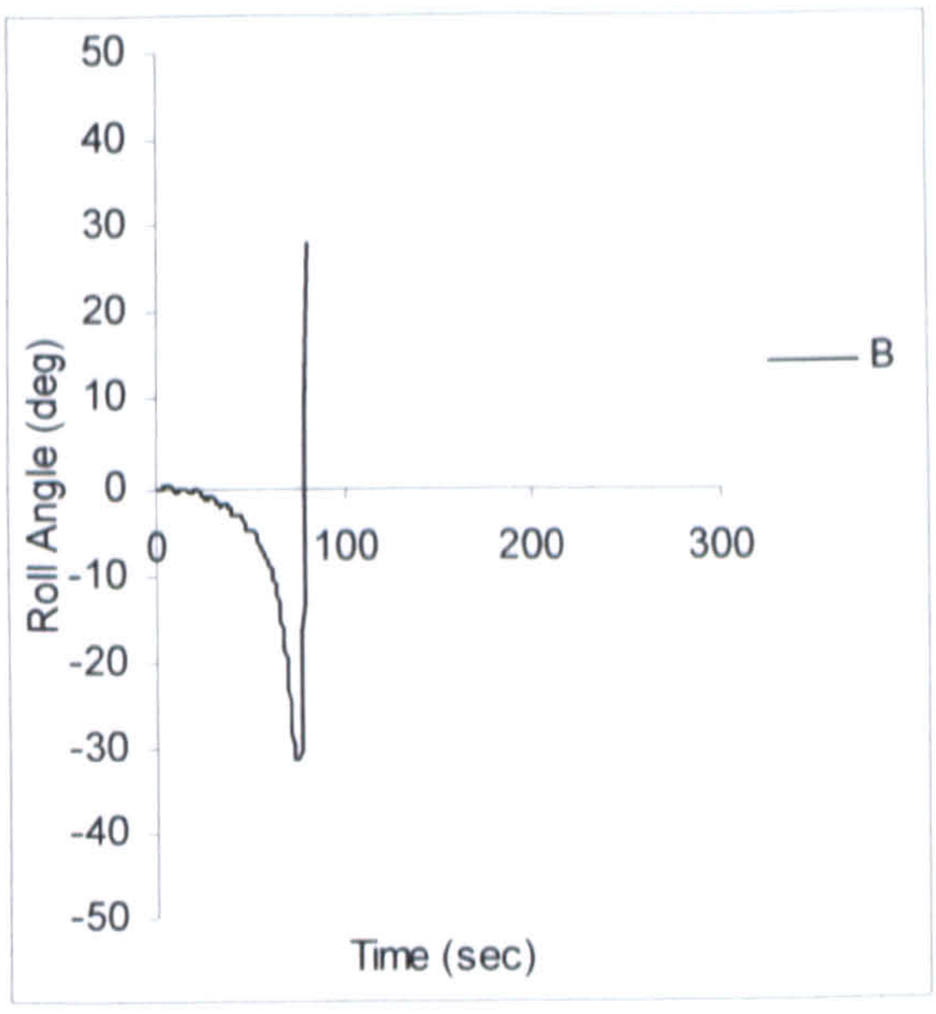

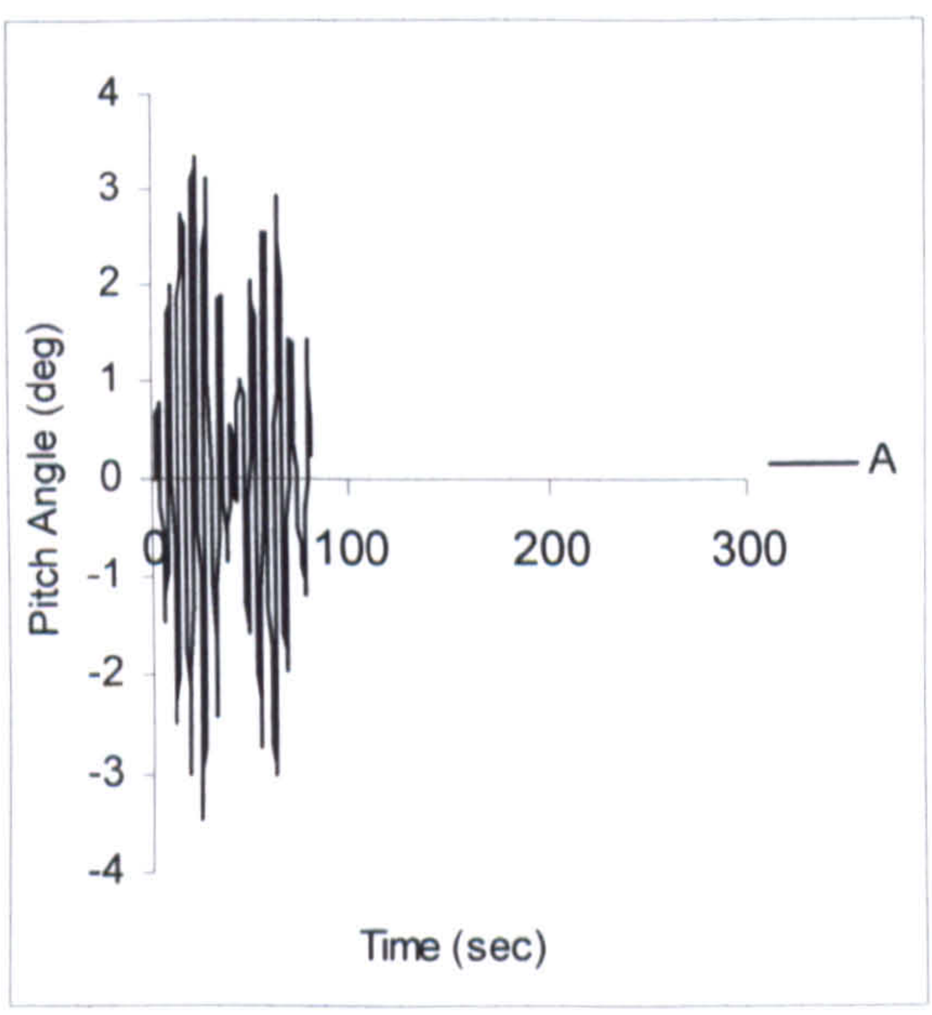

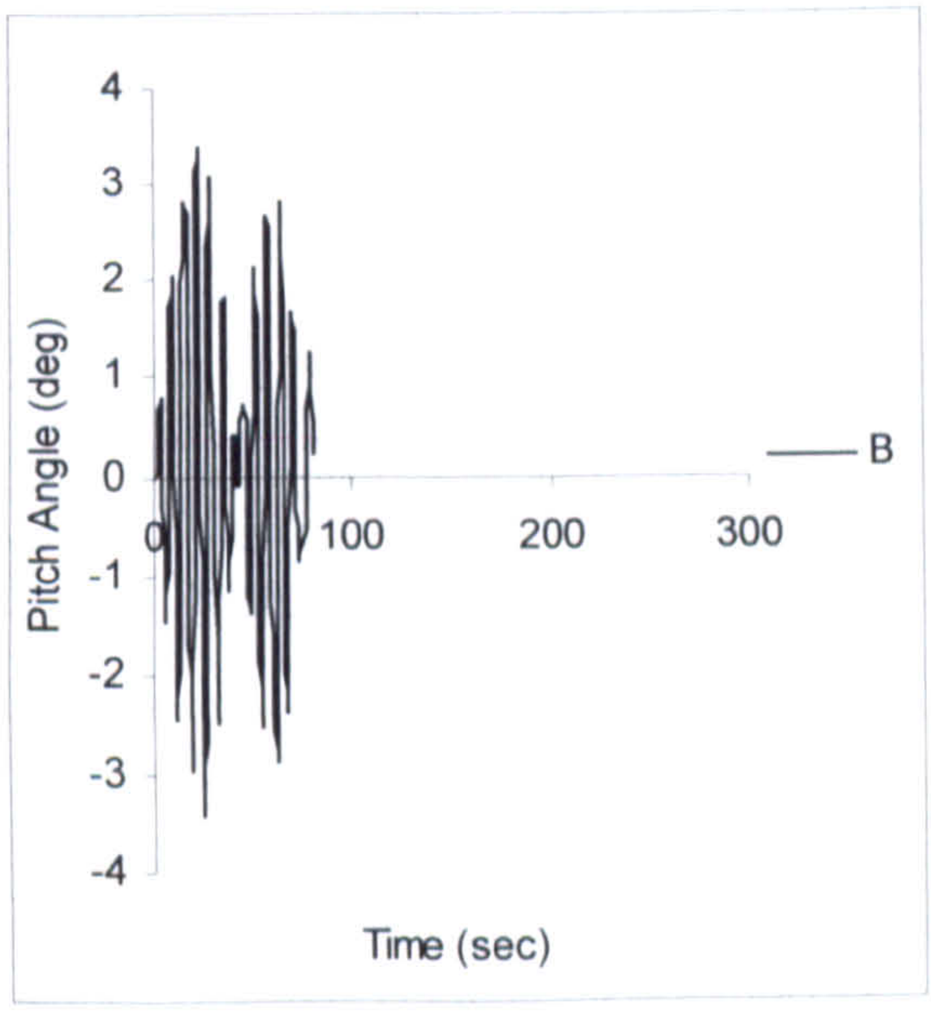

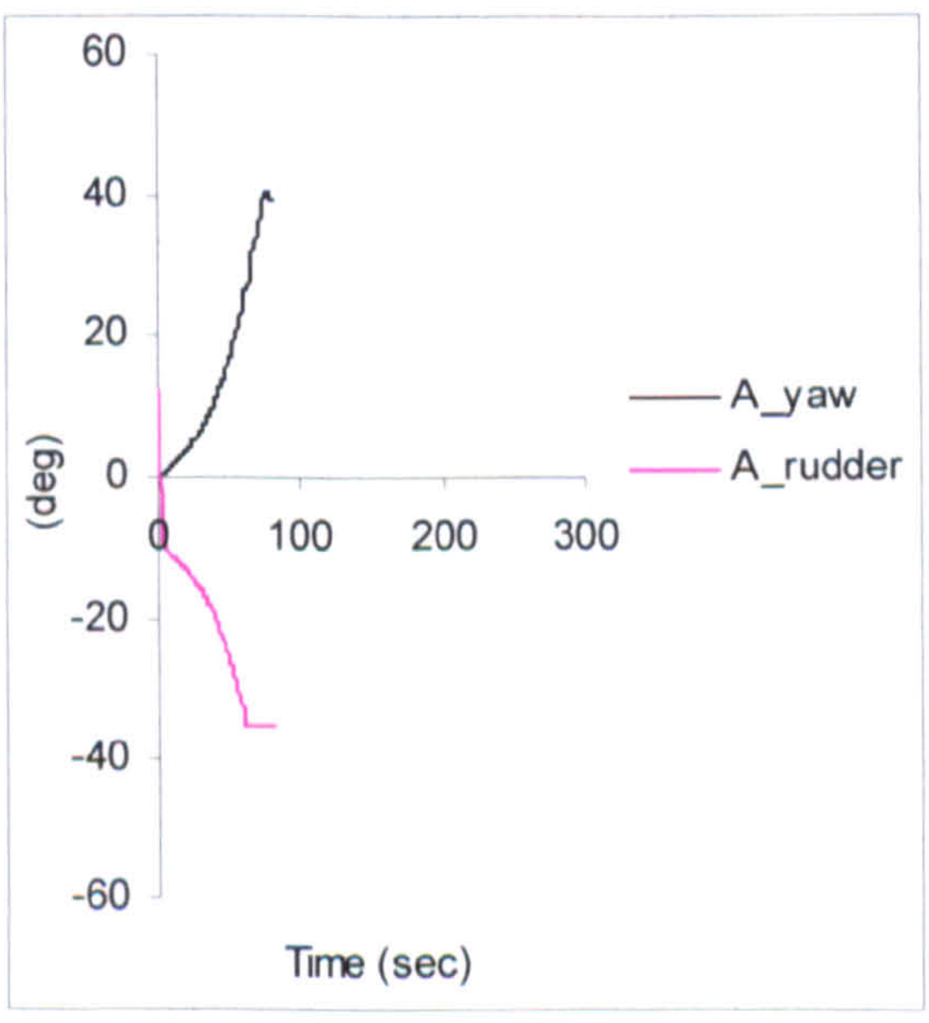

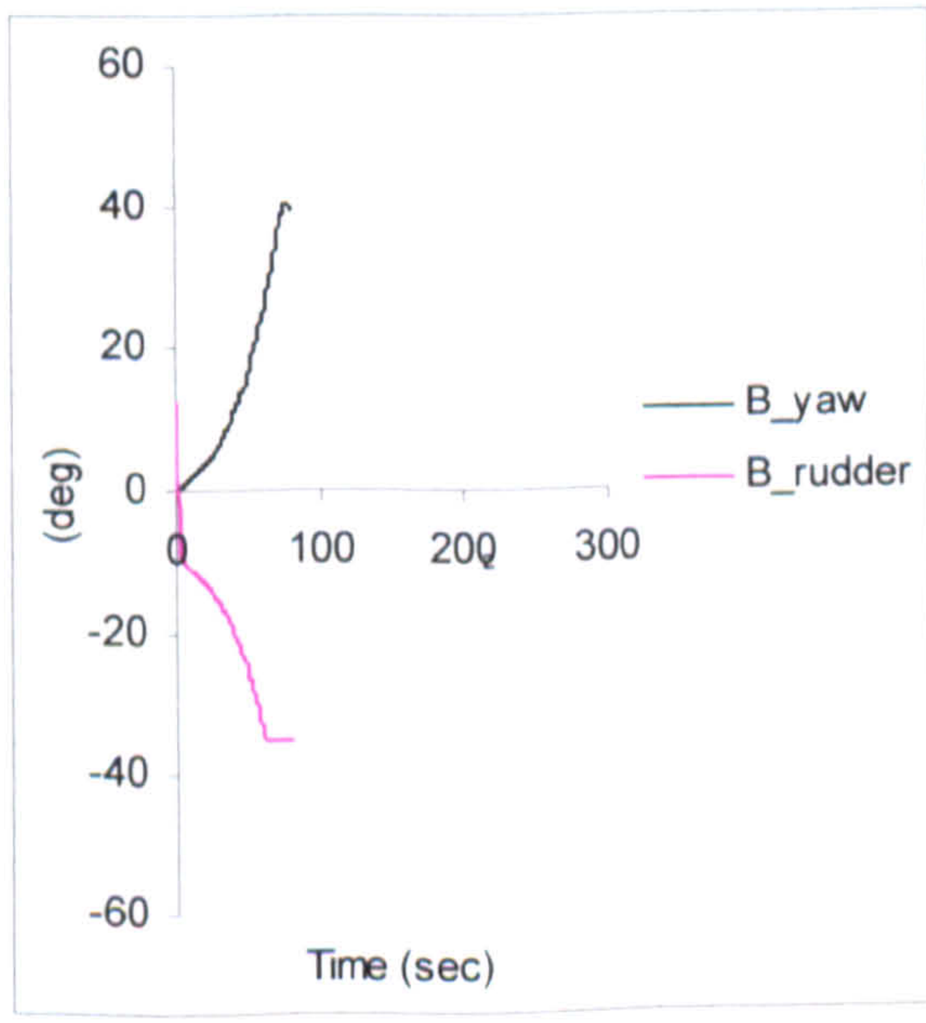

Figure 8.5 Comparison of 4 DOF and 6 DOF for Ship A-2 in $H/\lambda=1/12.5$, $\lambda/L_{pp}=1.637$, $Fn=0.43$, $\chi_c=-10$ degrees

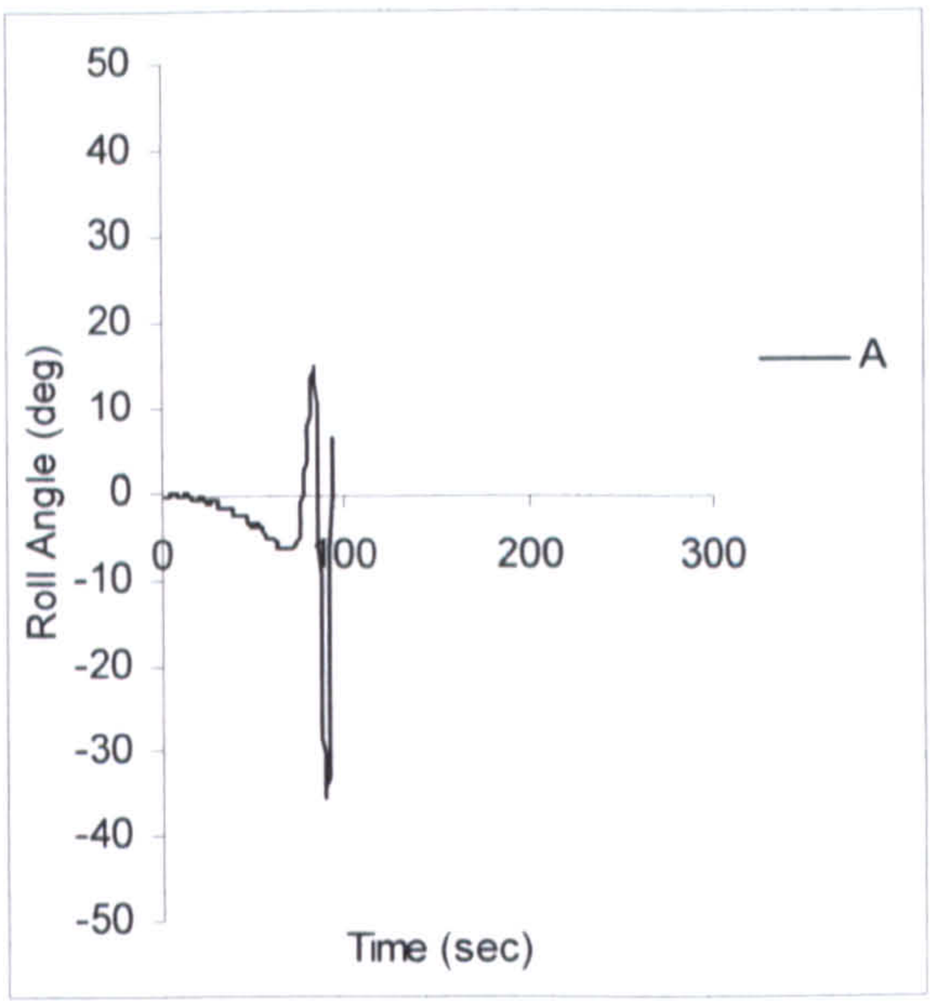

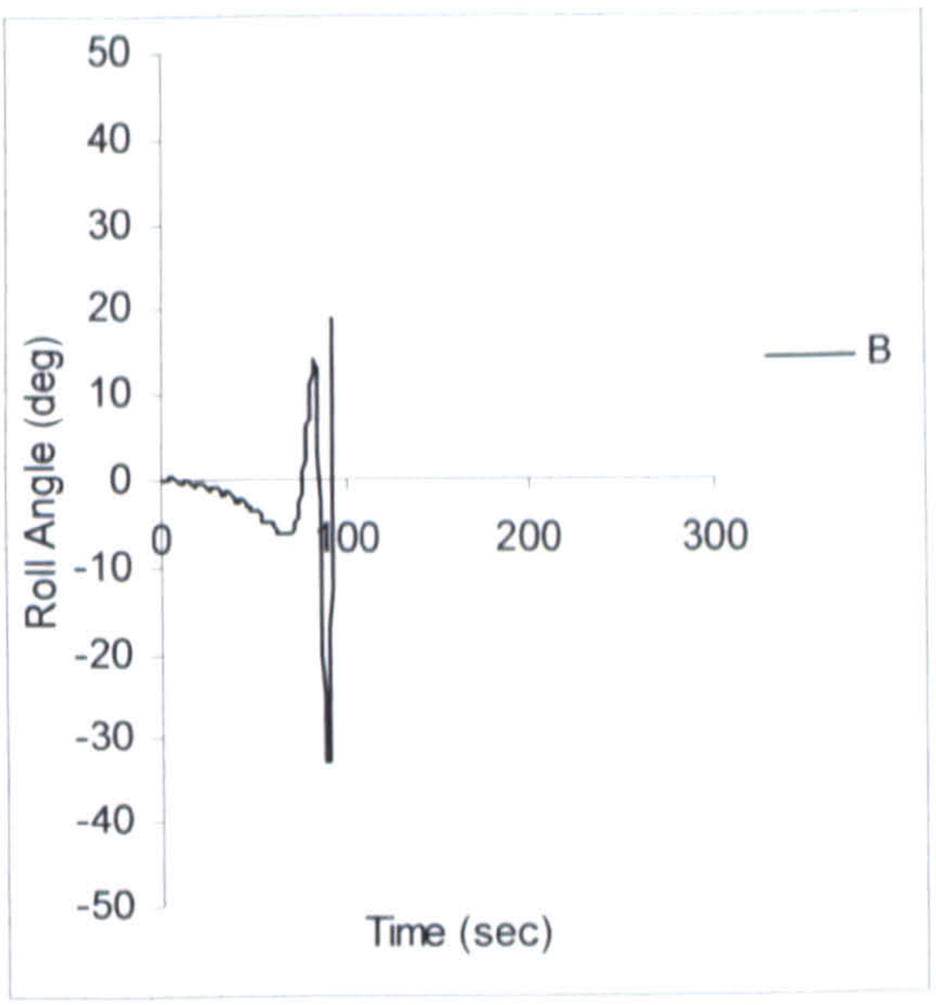

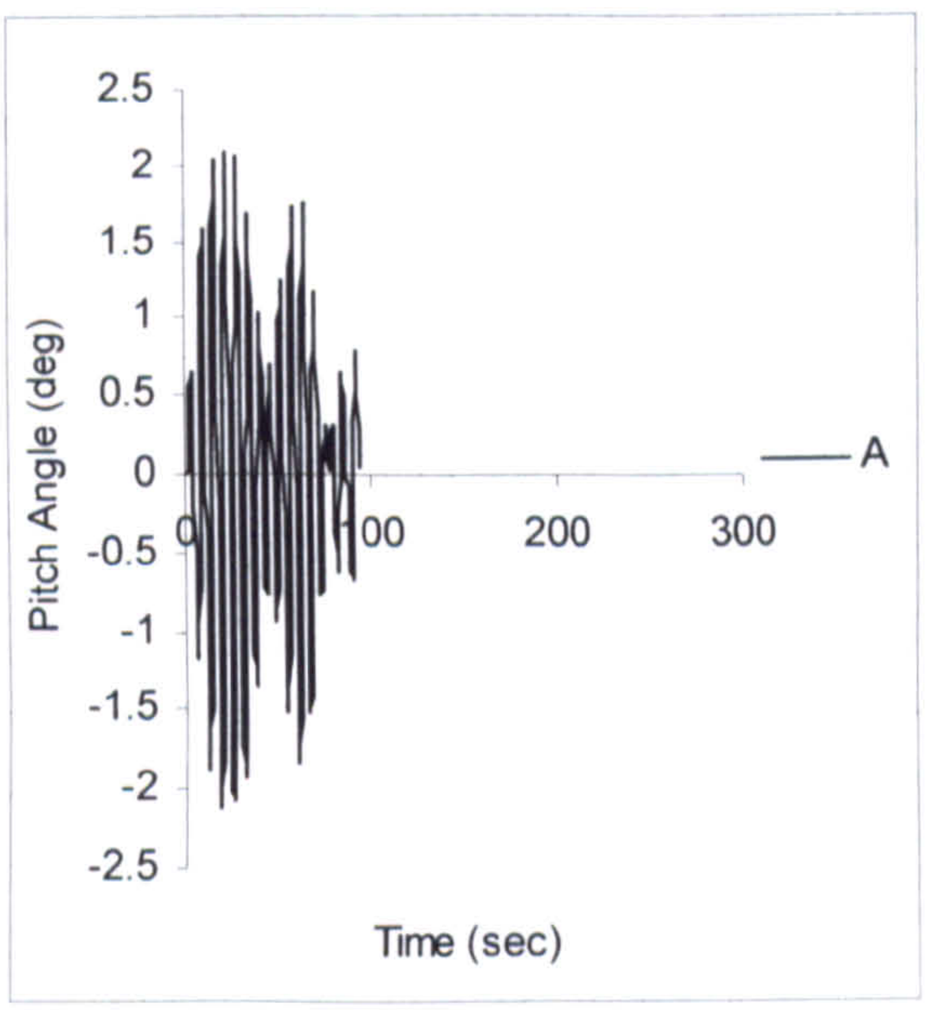

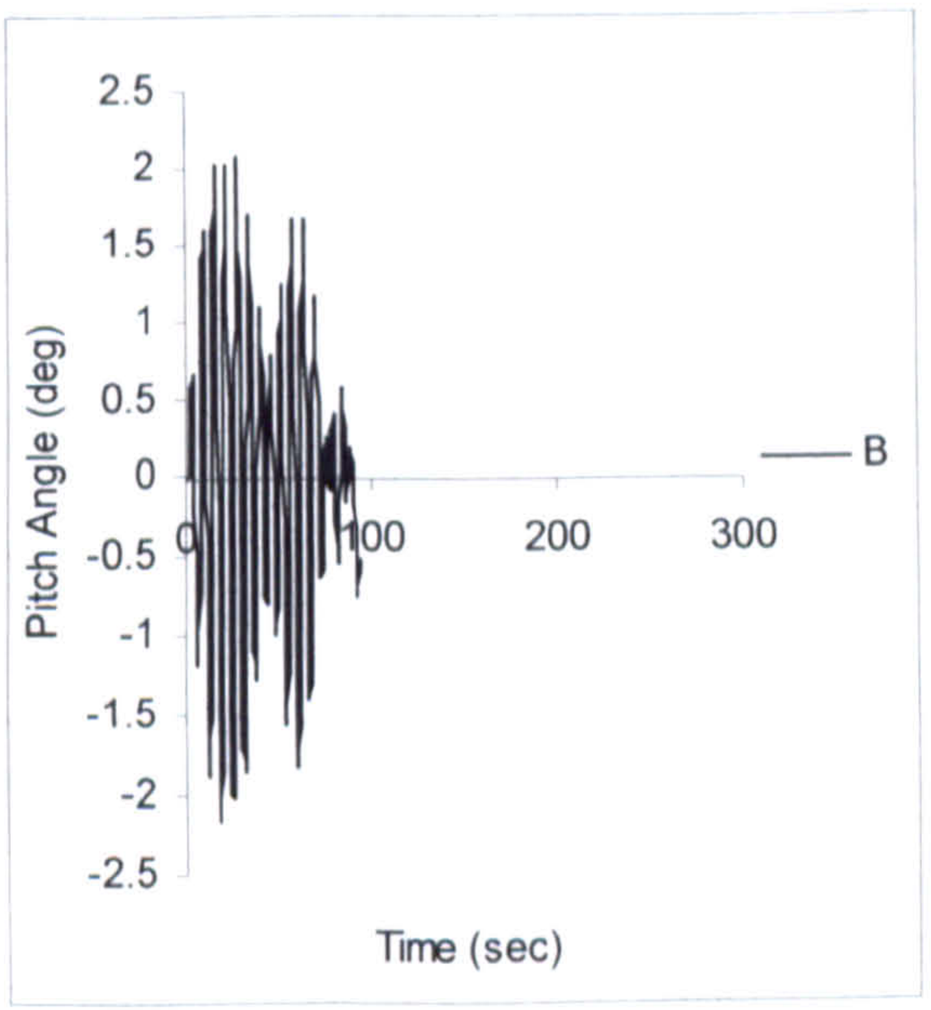

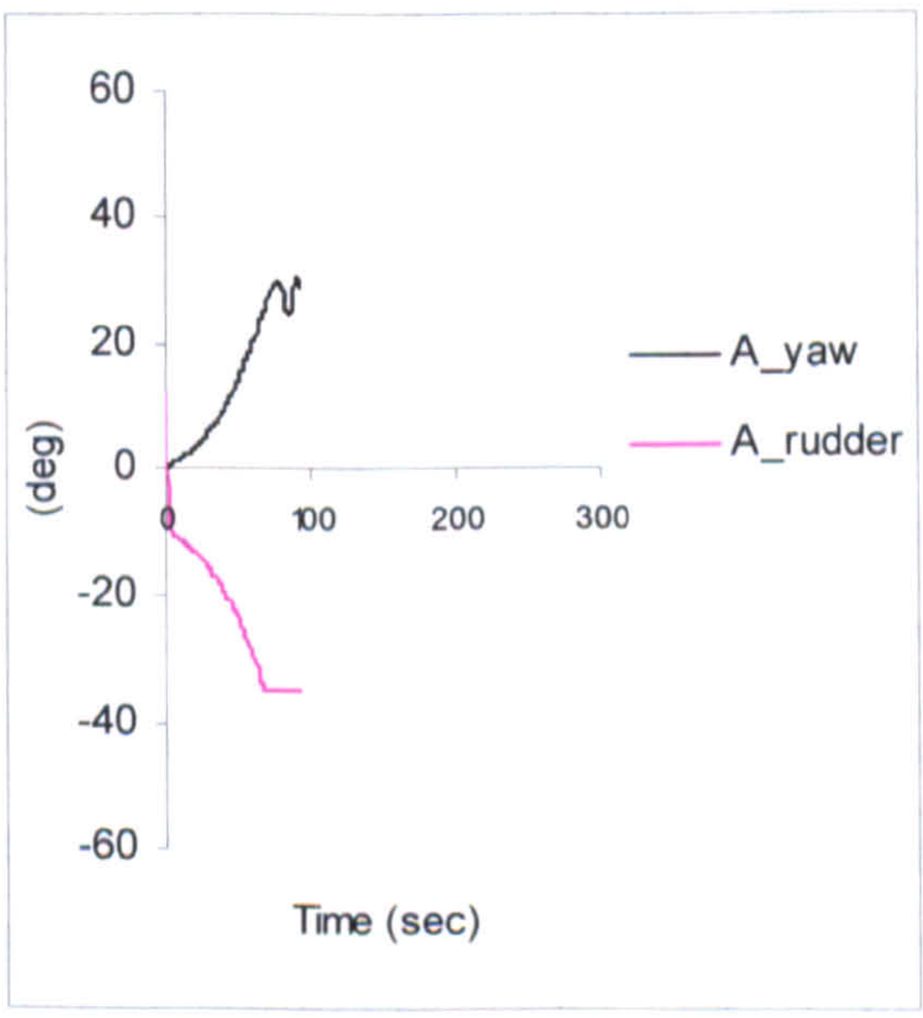

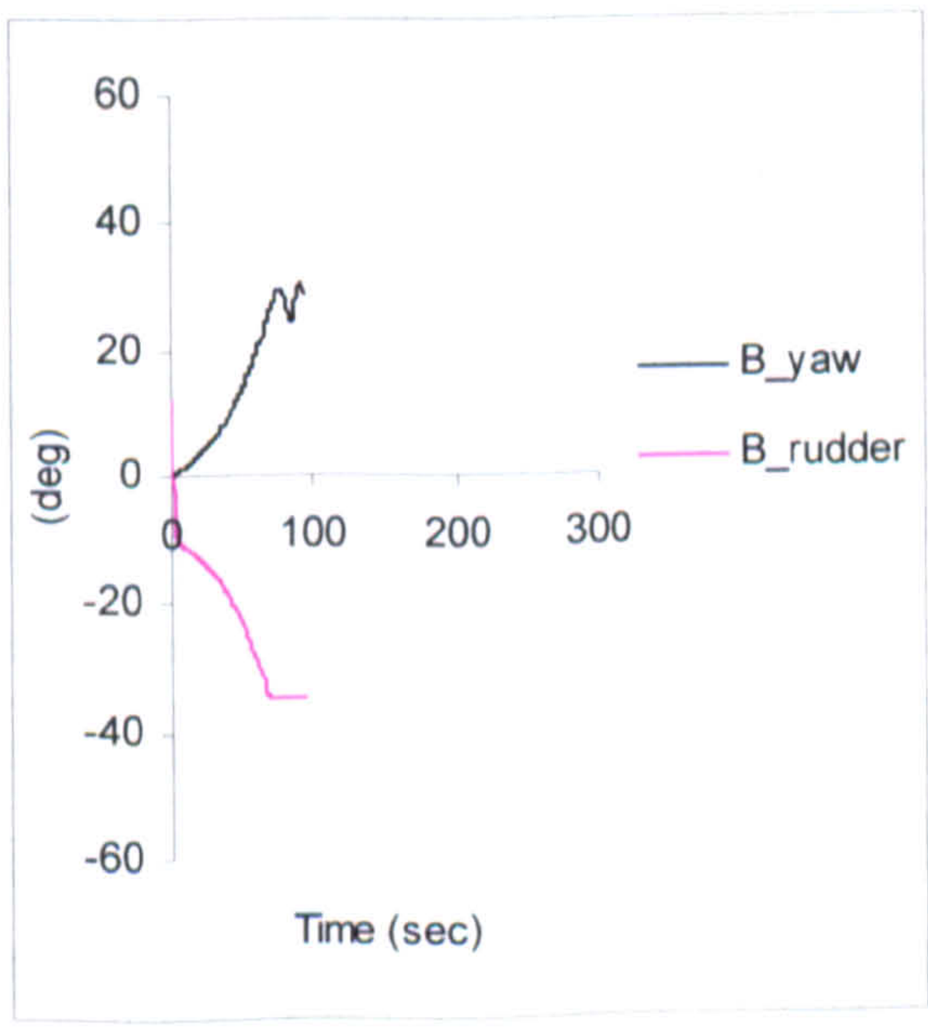

Figure 8.6 Comparison of 4 DOF and 6 DOF for Ship A-2 in $H/\lambda=1/15$, $\lambda/L_{pp}=1.637$, $Fn=0.43$, $\chi_c=-10$ degrees

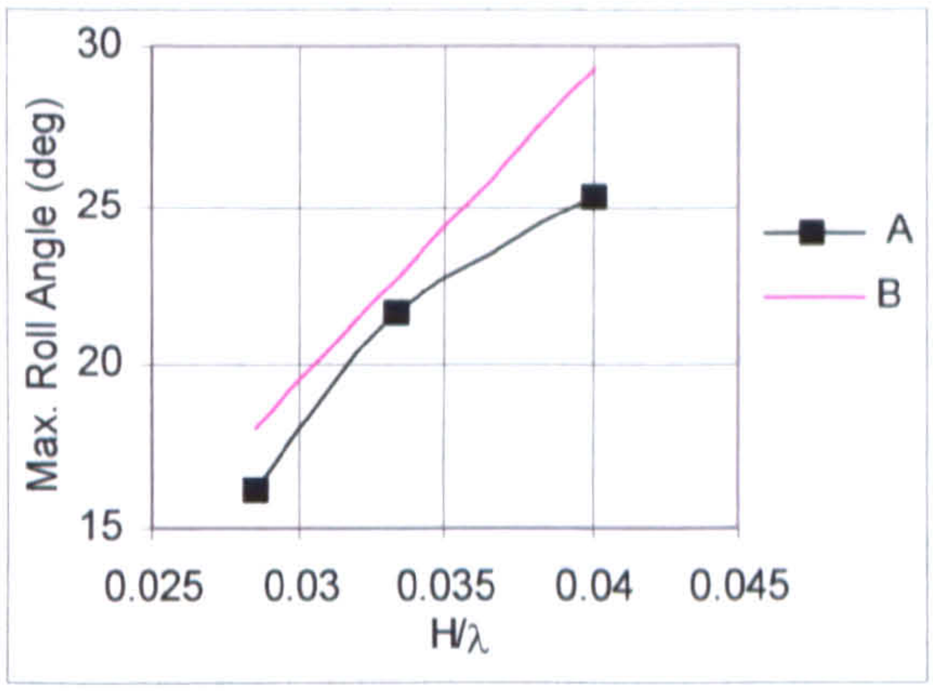

Figure 8.7 Comparison of 4 DOF and 6 DOF for Ship A-1 and with respect to maximum roll angle and wave steepness

The difference between two numerical models in terms of mean roll angle and with respect to wave steepness is also shown in Fig. 8.8. Pitch angles are almost identical for both vessels Further comparisons for the container vessel are presented in Appendix G.

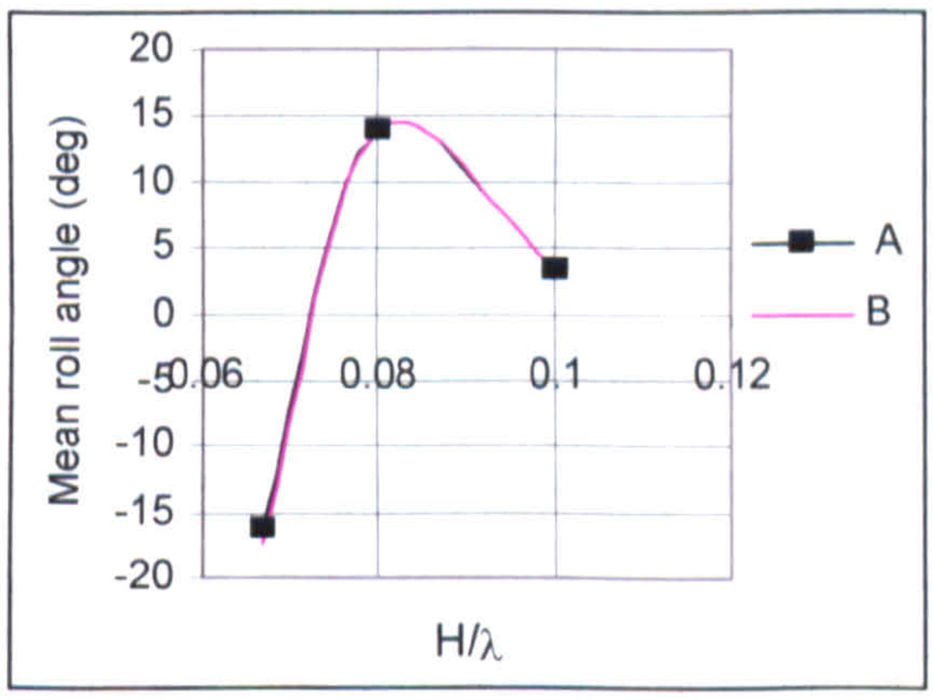

Figure 8.8 Comparison of 4 DOF and 6 DOF for Ship A-2 and with respect to maximum roll angle and wave steepness.

8.2.2. Effect of Wave Length to Ship Length Ratio

It has been known from the research that when wave length to ship length ratio is equal to 1.0 or higher in astern seas, encounter frequency becomes so small and ship could almost travel in the wave speed and she could be overtaken by the waves. Many dangerous conditions can be observed in such cases. As it can be seen from numerical and experimental simulations so far, wave length to ship length ratio has been higher than 1.0 for the test vessels.

Here, an interesting example of the effect of wave length to ship length ratio is given in Figure 8.9 and Figure 8.10 in terms of surge velocity, roll and yaw and rudder

motions for Ship A-2 (Purse Seiner). The vessel is simulated in conditions of H/λ=0.1, Fn=0.3 and χ_c=-30 degrees for wave length to ship length ratio, λ/L, is 1.637 and 1.0, respectively.

In the first run (Figure 8.9) with the similar conditions to previous sections with the different autopilot course and reduced speed, the vessel yet again capsizes due to extreme waves. However, when the wave length to ship length ratio is reduced to 1.0 (Figure 8.10), the ship is overtaken by wave and encounters the what is called a "surf-riding" condition. It might be caused by the initial conditions given and also, because of the ship speed is very near to wave celerity of which the overtaking is very likely. Further numerical simulations for the effect of wave length to ship length ratio are presented in Appendix G.

8.2.3. Effect of Loading Conditions (GM)

It is well known from the current knowledge that when a ship experiences waves from astern, the ship's restoring moment significantly changes and that could cause the serious conditions like static loss of stability or very dynamic mode of low cycle resonance. Therefore, the loading condition or GM (metecentric height) is the important parameter to assess the ship's ability to find enough restoring for such conditions. In this study, the both vessels chosen have GM values which are critically complies with IMO requirements. By using the instantaneous wave surface, change of GM can be taken into account.

In Figures 8.11-8.12, the effect of loading condition is simulated for Ship A-1, for H/λ=1/25, Fn=0.2 and χ_c=0 degrees, λ/L=1.5 and GM values 0.15 and 0.30, respectively.

Here for the first run (Figure 8.11) the model experiences the wave crest at amidship and she encounters the parametric build-up of the roll motion and the vessel eventually capsize due to low cycle resonance. For, the second run (Figure 8.12) when GM value is increased, despite the high roll amplitude which increased until 20 seconds, the vessel finds the enough restoring to stay upright and capsizing is avoided. However, this could be rather explained that vessel phases out of the parametric resonance boundary for this condition and dangerous situations could still be observed in the new GM condition.

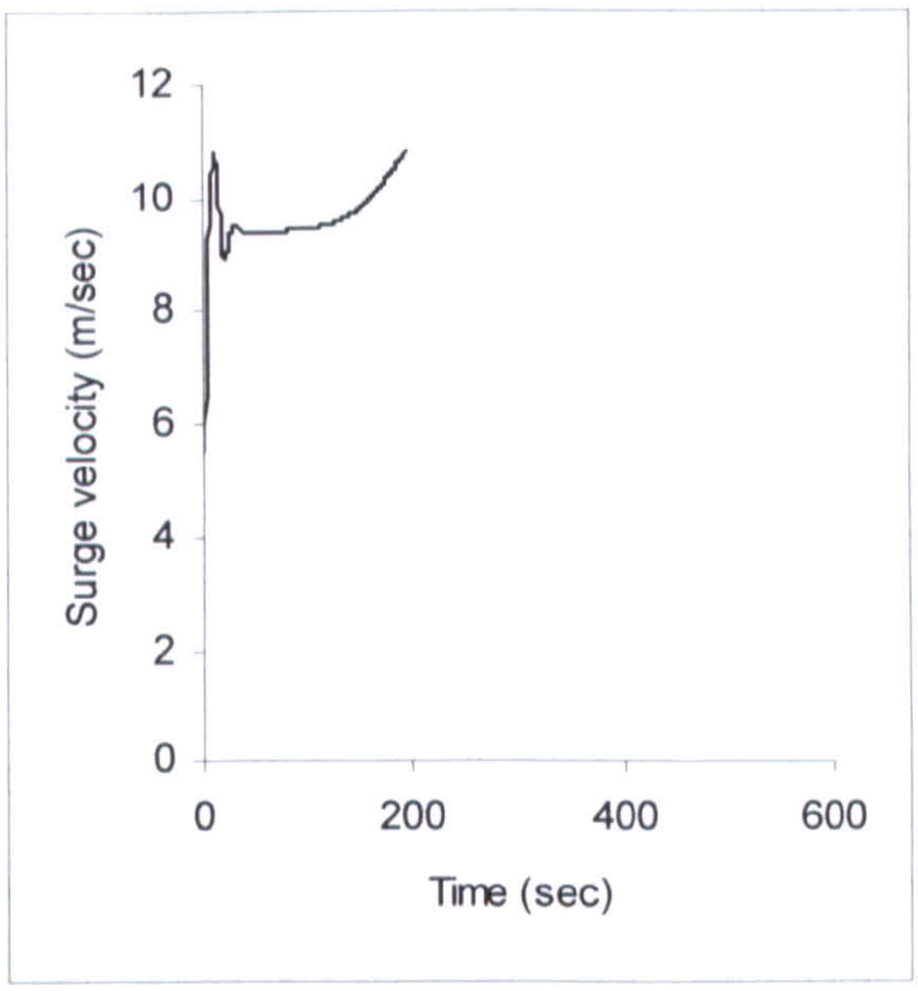

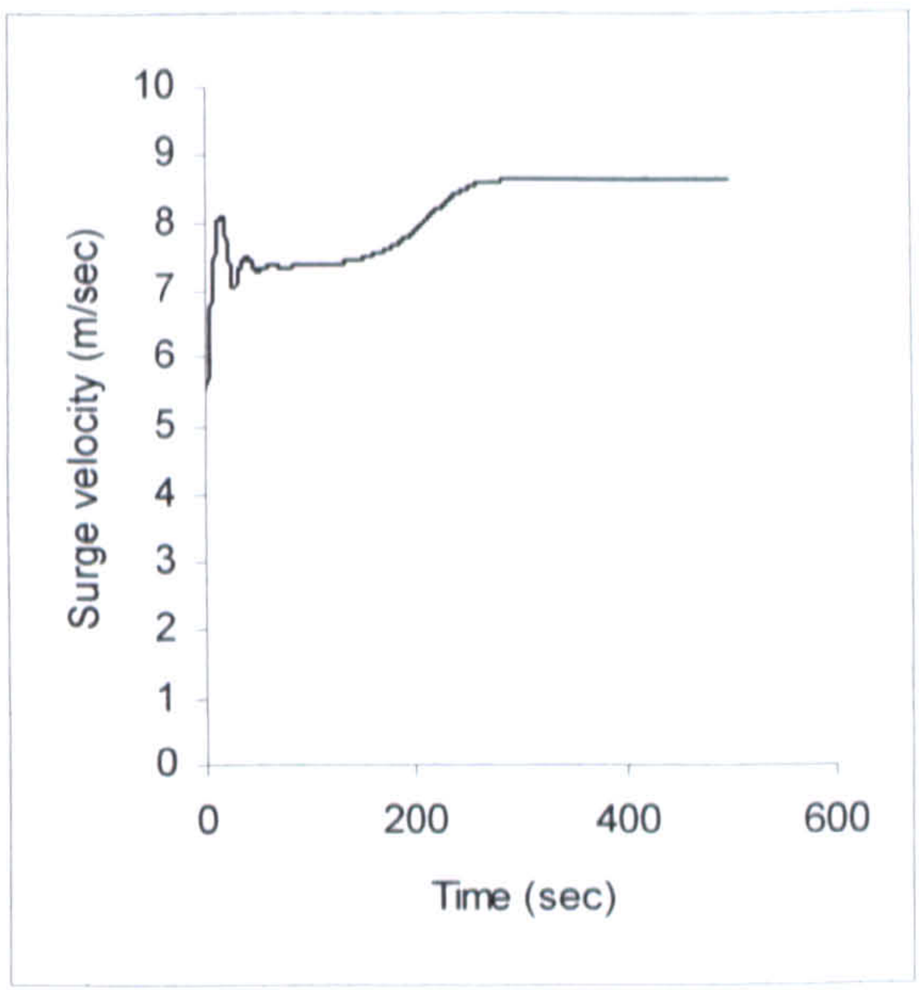

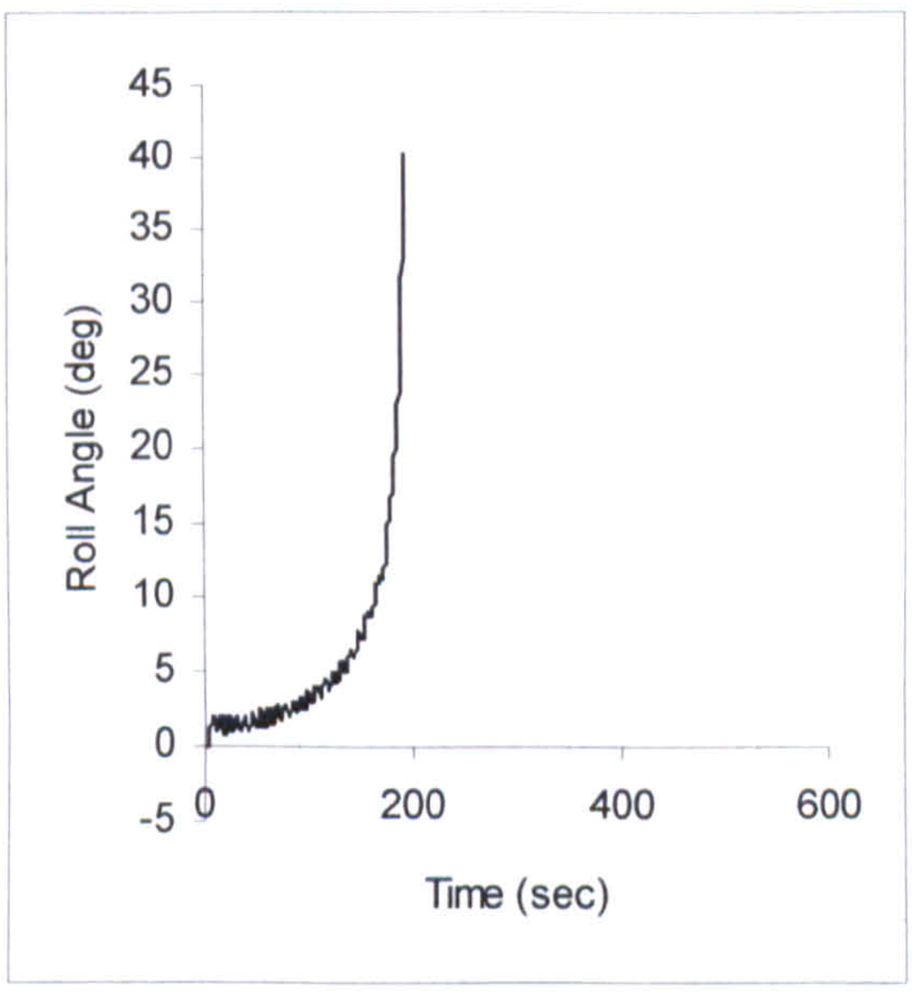

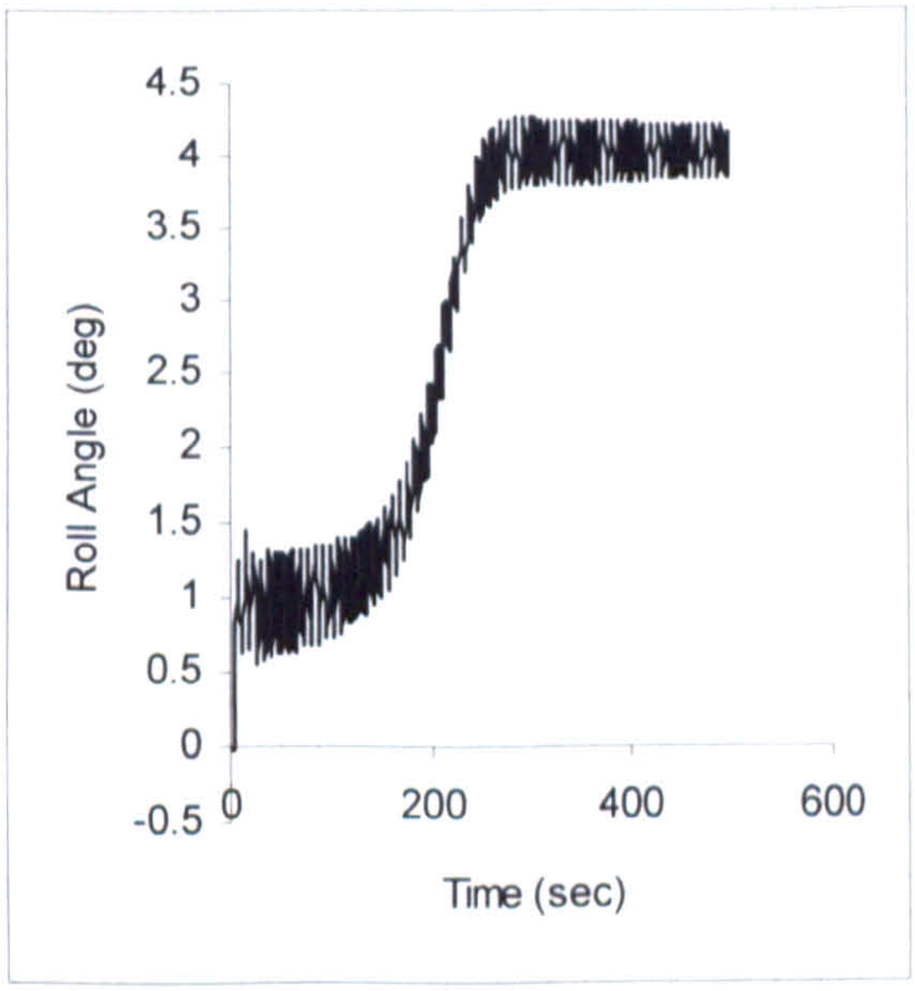

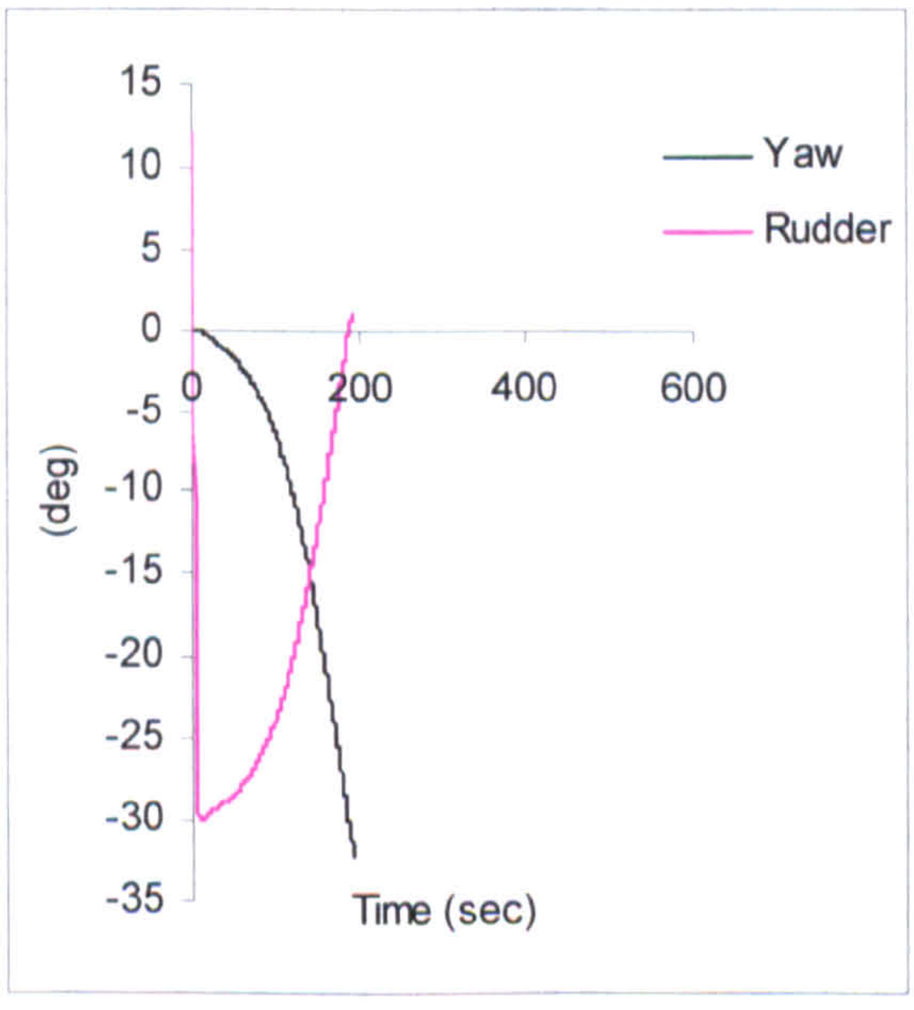

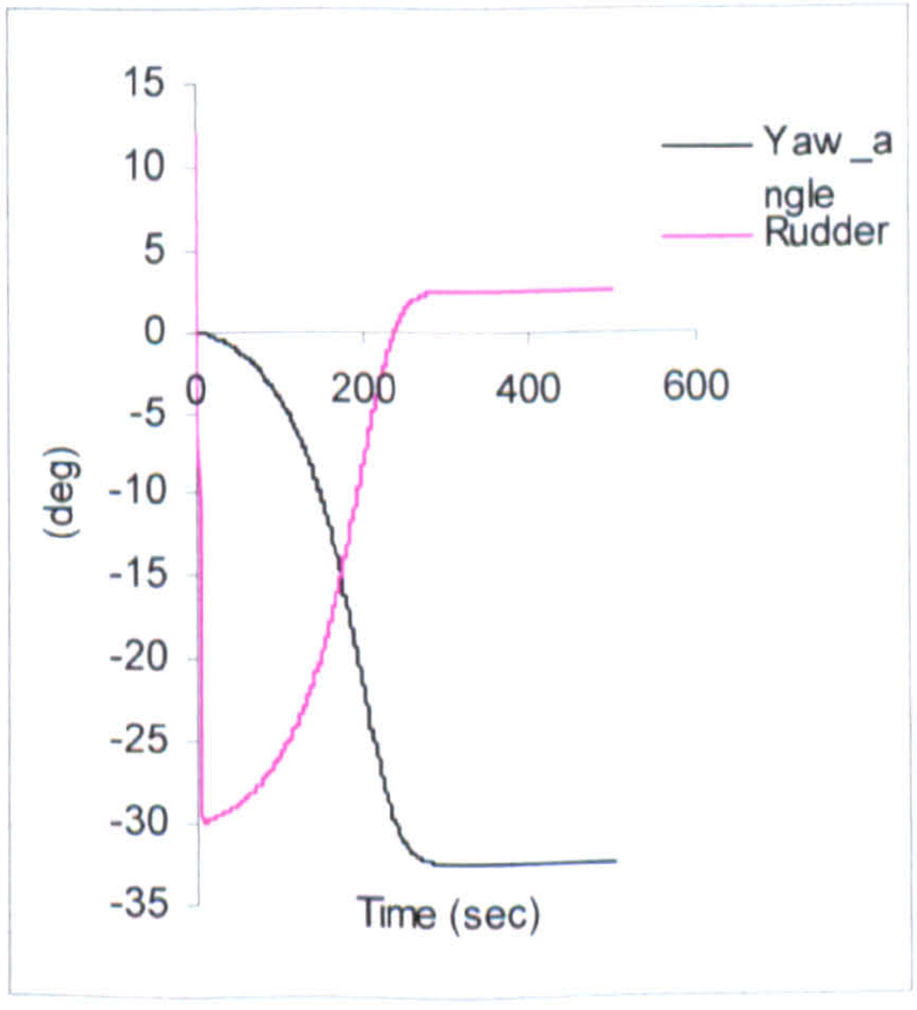

Figure 8.9 Numerical simulation of the Ship A-2 in $H/\lambda=1/10$, $\lambda/L_{pp}=1.637$, Fn=0.3, χ_c =-30 degrees

Figure 8.10 Numerical simulation of the Ship A-2 in $H/\lambda=1/10$, $\lambda/L_{pp}=1.0$, Fn=0.3, χ_c =-30 degrees

In order to broaden the knowledge for the effect of GM to the ship motions in following and quartering seas, the further simulations were carried out in Appendix G.

8.2.4. Effect of Speed and Heading Angle

According the IMO Regulations and guidance, the change of speed and or the autopilot course might help to avoid dangerous situations in following and quartering seas. In an attempt to investigate these recommendations in terms of numerical model's reliability, Ship A-1 and Ship A-2 were numerically simulated for different speed and the autopilot course in Figures 8.13-8.18. The control parameters and environmental conditions are given in Table 8.3 and 8.4.

Nominal Froude number	Fn	0.2	0.3	0.4	0.3
Autopilot course from the wave direction	χ_c (degree)	0	30	30	30
Wave steepness	H/λ	1/25	1/25	1/25	1/255
Wave length to ship length ratio	λ/L_{pp}	1.5	1.5	1.5	1.5
Proportional gain	K_P (sec)	1.2	1.2	1.2	1.2
Differential gain	K_R (sec)	53.0	53.0	53.0	53.0

Table 8.3 Control parameters of numerical runs for Ship A-1.

Nominal Froude number	Fn	0.43	0.3
Autopilot course from the wave direction	χ_c (degree)	-10	-30
Wave steepness	H/λ	1/10	1/10
Wave length to ship length ratio	λ/L_{pp}	1.637	1.637
Proportional gain	K_P (sec)	1.0	1.0
Differential gain	K_R (sec)	0.0	0.0

Table 8.4 Control parameters of numerical runs for Ship A-2

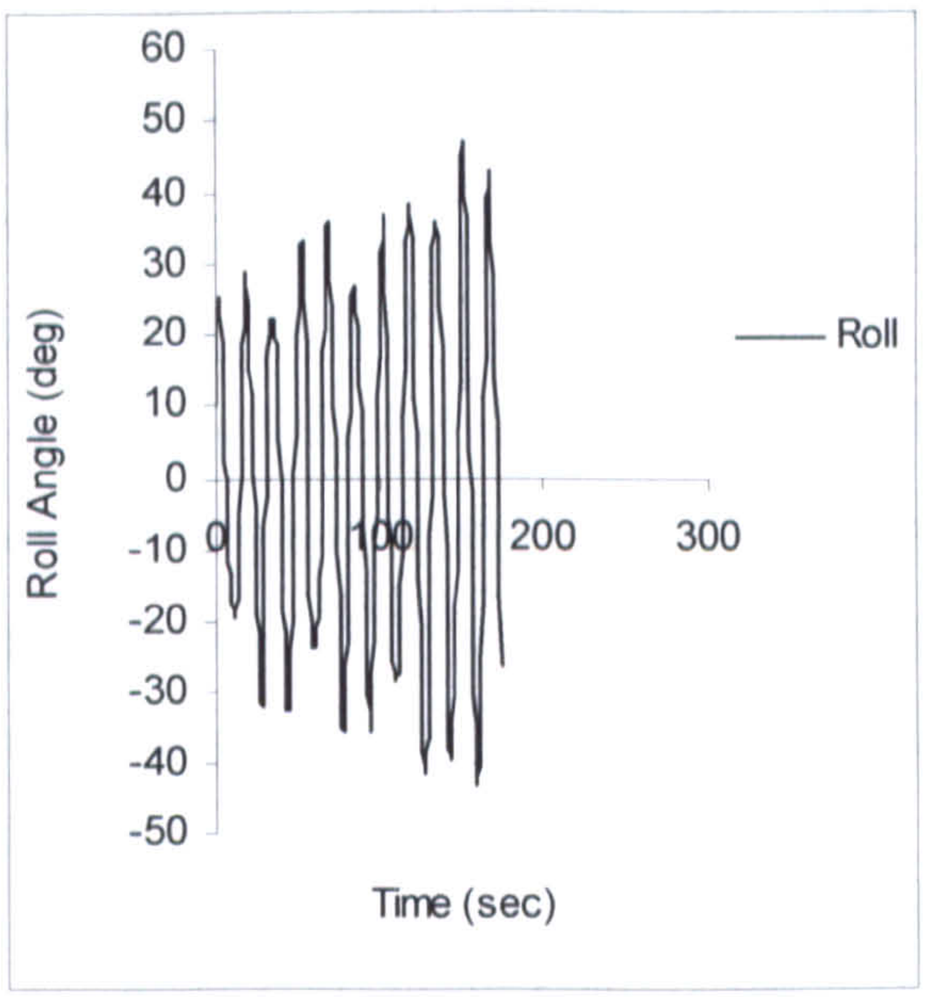

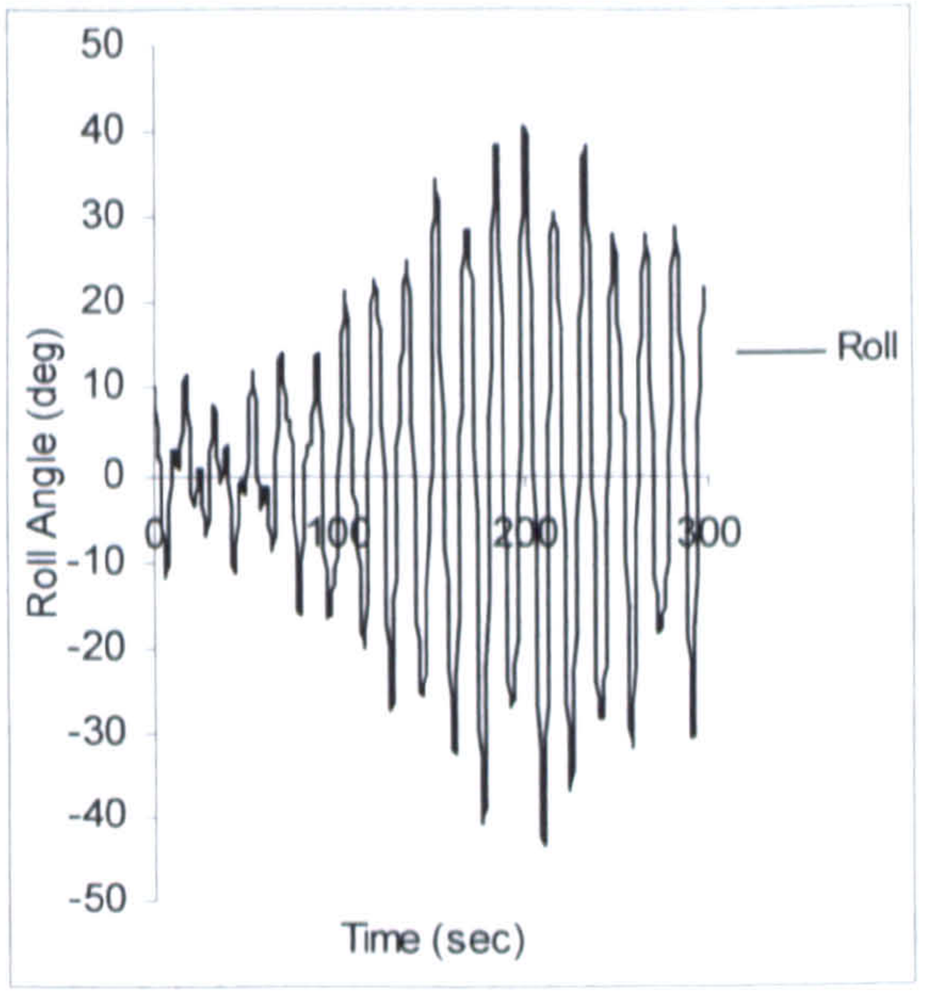

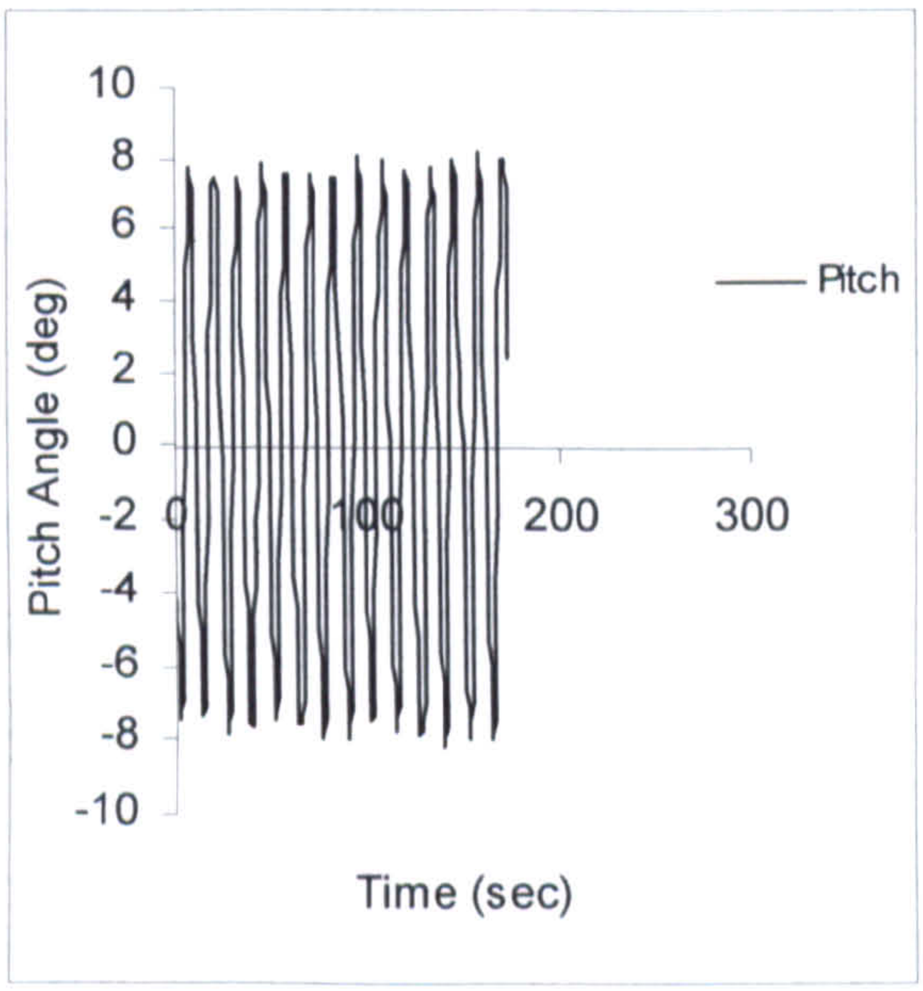

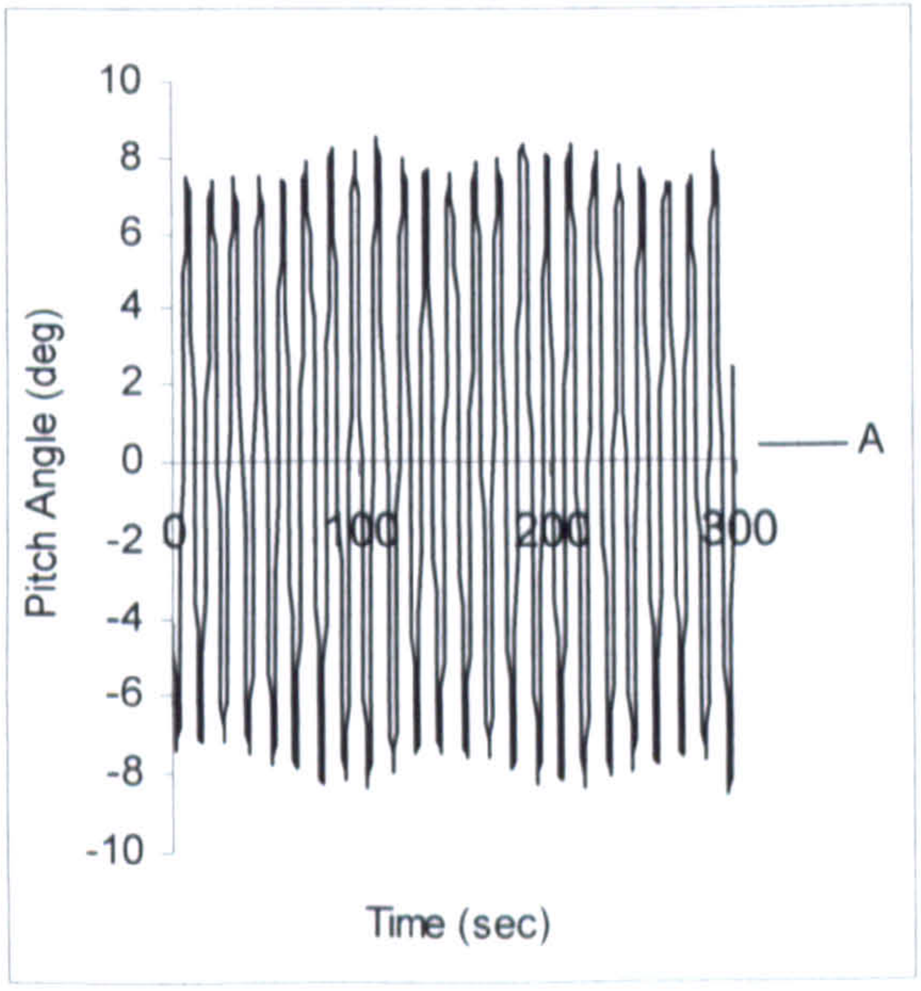

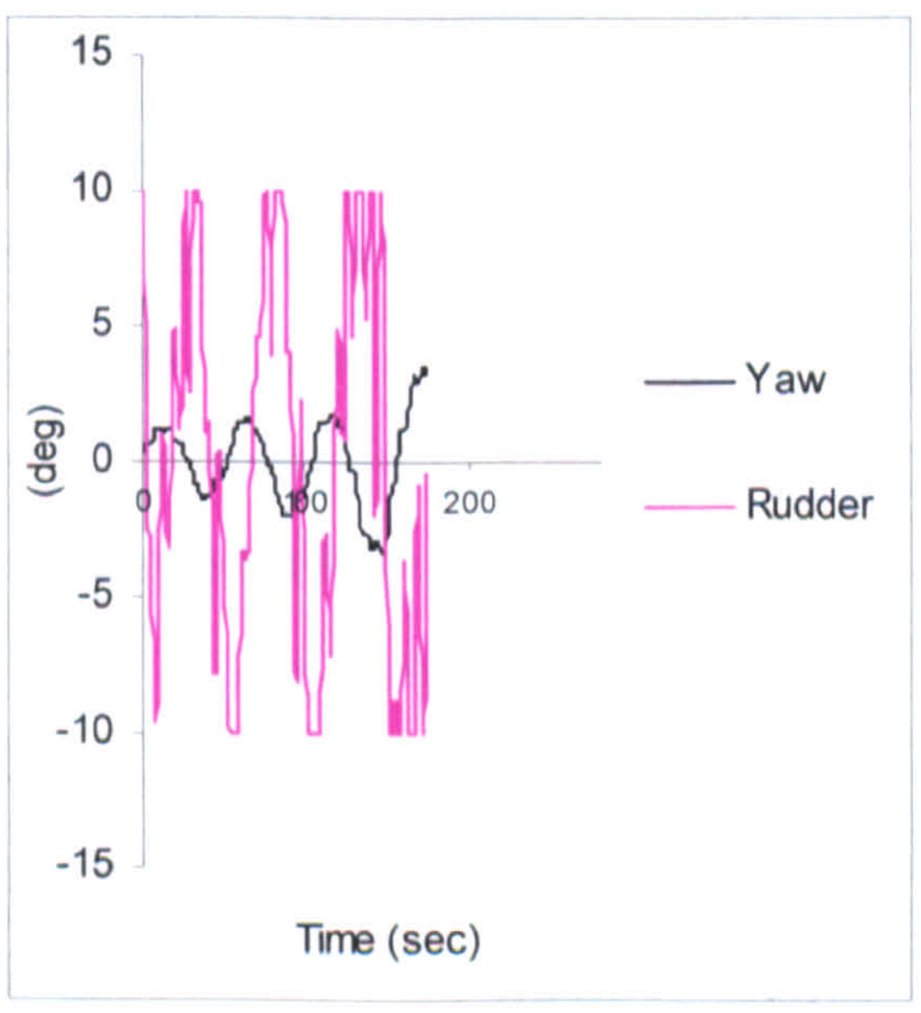

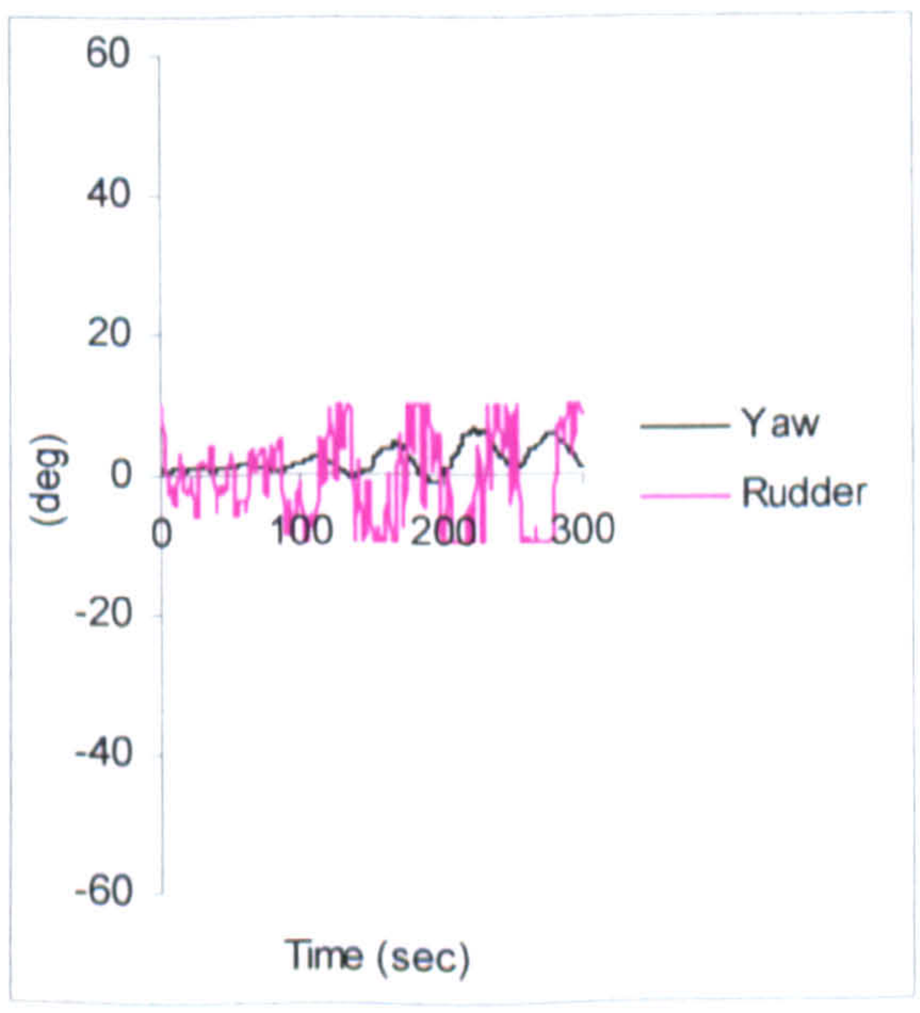

Figure 8.11 Numerical simulation of the Ship A-1 in $H/\lambda=1/25$, $\lambda/L_{pp}=1.5$, Fn=0.2, $\chi_c=0$ degrees, GM=0.15m

Figure 8.12 Numerical simulation of the Ship A-1 in $H/\lambda=1/10$, $\lambda/L_{pp}=1.637$, Fn=0.3, $\chi_c=-30$ degrees, GM=0.30m

Herein, the vessels were tested for different heading angle and speed for constant wave conditions. The purpose of these simulations, therefore, is to determine whether to change in the speed and the autopilot course would be efficient to avoid dangerous situations.

For Ship A-1, the starting point is the conditions given in the previous section of which the vessel suffered the parametric rolling (Figure 8.11-8.13). Due to low speed and ship's travel in pure following seas where the parametric rolling is very likely, the vessel's speed increased and the autopilot course was taken to quartering seas (Figure 8.14).

In the second part of numerical simulation of the container vessel, the starting conditions was chosen for very high speed (Figure 8.15) and this time the only speed is reduced to determine the effect of the reduced speed to the motions in extreme astern seas (Figure 8.16).

For Ship A-2, the very high speed and extreme conditions were considered (Table 8.4). As was in simulations of Ship A-1, the previous condition in 8.4.1 where the vessel suddenly capsized was re-simulated (Figure 8.4-8.17) and the effect of the reduced speed and the different autopilot course to avoid capsizing is investigated in Figure 8.18.

In the analysing of results, for the Ship A-1, as it was shown in the previous section, the vessel suffers the parametric rolling (Figure 8.13), where there is a parametric build-up of roll motion and therefore the decrease in the speed could be observed. In the second simulation, the attempt has been made to increase speed and the change the course (Figure 8.14). The result was large roll angles, and interestingly constant rudder turn to the port to keep the vessel on course and this provides the restoring to avoid the capsizing. The speed decreases again, although it tends to reach to constant amplitude.

In the second part, when Ship A-1 travels with relatively very high speed, the vessel yet against suffers from the capsizing with the harmonic and rapidly accelerating roll motion, the speed decreases due to very transient motion the autopilot is unable to effect motion. When the speed was decreased and the autopilot course to waves are getting closer quartering seas, however, the vessel is able to survive despite the very large angle, the surge velocity indicates eventually constant speed. The rudder yet again shows very stiff characteristics in the numerical simulations.

PAGINATION AS IN ORIGINAL

It was chosen to run with a very high speed and extreme wave heights for the Ship A-2, this results with the sudden capsize in Figure 8.17, as it was also shown in Section 8.2.1 (Figure 8.10). Here the attempt was to reduce speed and change the autopilot course toward quartering seas (Figure 8.18) and this proves to be efficient for capsizing point of view however as similarly to the numerical simulation to 8.2.2, the vessel encounters surf-riding condition. If it is recalled from Section 3.5, the experiments had shown that for over 0.3 Fn speed, for certain conditions, there is increasing chance to encounter surf-riding condition. Therefore, since the similar initial conditions have been assumed for both cases, this conclusion can be confirmed for this numerical simulation is concerned.

The numerical simulations verify the recommendations from the IMO guidelines that change of speed and heading angle could be effective to avoid the dangerous situation which often results in capsizing. In order to demonstrate the clearer picture of those effects, the further numerical simulations were carried out in Appendix G.

8.2.5. Effect of Frequency

In the previous Chapters, the importance of effect of frequency has already been emphasized and in Chapter 7, the comparison between the numerical simulation including frequency dependent terms, and the one including the classical approach of using zero frequency hydrodynamic reaction force terms are presented. However, referring the ITTC Committee report [92], the exact calculation of memory effects to be carried out from the start of the waves and therefore, the findings of this numerical simulation could open to argument.

In this part of the parametrical study, the Ship A-1 is numerically tested for different heading angles, hence different encounter frequencies. Here, the motions of ship were compared with and without the radiation terms, described in Chapter 6.

Figure 8.19(a) shows the Ship A-1 for the condition and parameters given in Table 8.1 with the memory effects included, for Froude number is 0.3 and heading angles are 0, 30, 45, 60 degrees, respectively. The initial yaw angle was set to be the autopilot course from the wave direction. The ship was tested for same conditions and without the memory effects (Figures 8.19 (b)).

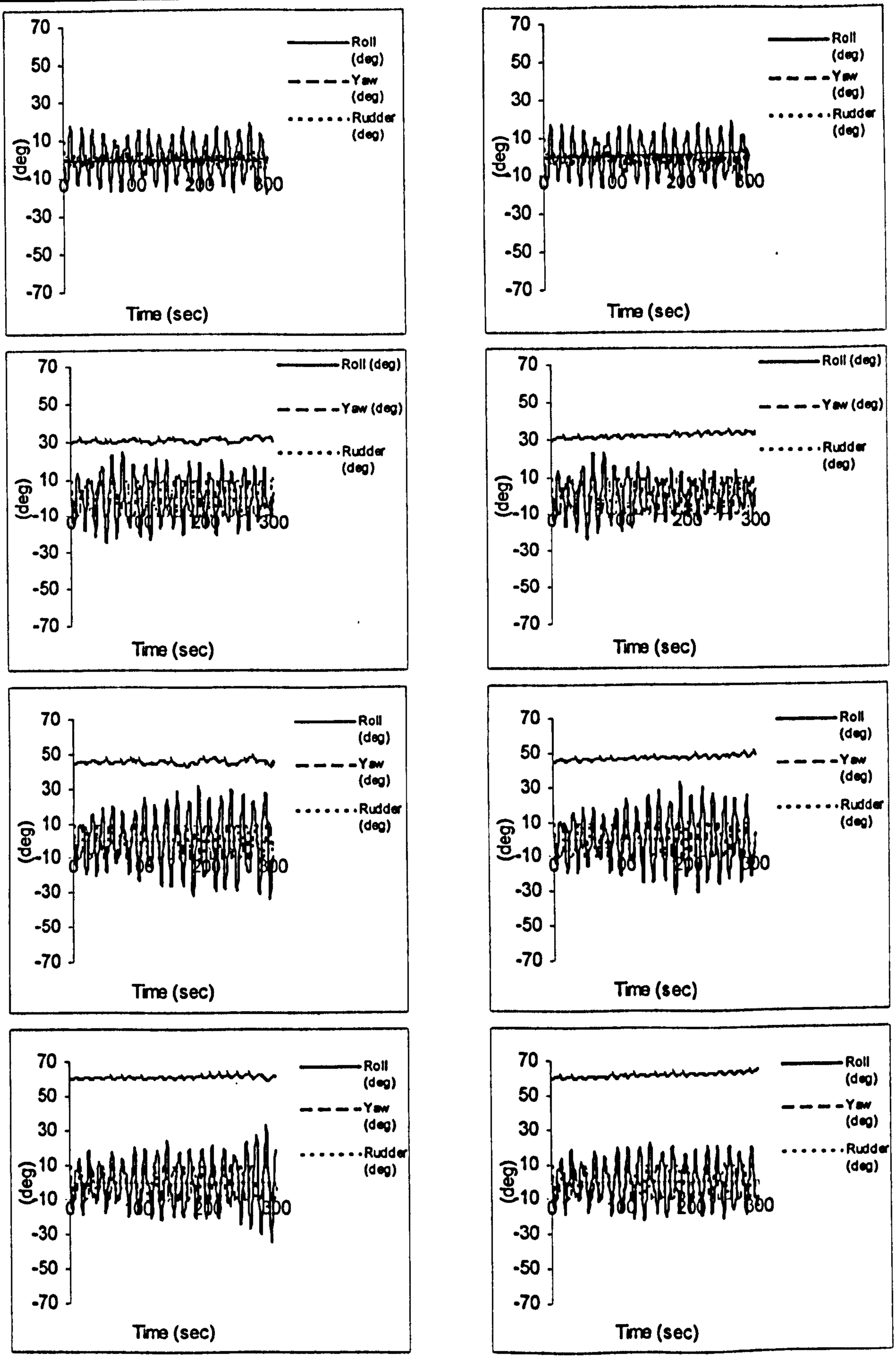

(a) (b)

Figure 8.19 Numerical simulation of Ship A-1 motion in following and quartering seas with (a) without (b) the memory effects

Here, the difference between the numerical model with and without the memory effects is not significant. However, for controlled ship motions, the yaw and rudder angles are sensitive to the wave frequency effects as was mentioned for the simulation in Chapter 7 and there is slight deviation for yaw motions without the memory effects (Figure 8.19 (b)).

This result obviously cannot be limited with the findings of one simulation, therefore further simulations with taking change of heading angles from following seas through beam seas into account are presented in Appendix G. Furthermore, the effect of frequency in terms of random wave modelling and wave excitation will be emphasized in Chapters 9 and 10.

8.3. Concluding Remarks

As it is stated in Chapter 1, the main intention of this research study is to develop a coupled non-linear 6-DOF model with frequency dependent coefficients, incorporating memory effects in regular and random waves with a new axis system that allows straightforward combination between seakeeping and manoeuvring model whilst accounting for extreme motions. Therefore, the objective of this chapter to present the numerical simulations carried out to investigate the contribution of the improved numerical model to the simulating the capsizing behaviour of ship in following and quartering seas in a wider scale.

The verification of the numerical model against the experiment has already been presented in the previous Chapter. Here, based on those results and choosing the conditions similar to the experiments, the numerical simulations were carried out for different environmental and control parameters. Effect of wave steepness, wave length to ship length ratio, loading condition, speed and wave heading and finally effect of frequency were investigated.

In the first section (8.2.1) the effect of wave steepness is investigated in terms of the degrees of freedom employed in the numerical model. It is stated that 4 DOF numerical model with static equilibrium of heave and pitch motions is usually common approach to study the ship motions in astern seas. Therefore, the one of new features of the current mathematical model was compared against the traditional method. Comparisons between the 6 DOF and 4 DOF numerical models considered in this numerical study displayed that the difference between them is not very significant. For

the numerical simulations of Ship A-1 of which covers relatively low speed range, the difference increases with increasing wave steepness. However, it is difficult to call this a significant difference. The 6 DOF model displays slightly stiffer control characteristics and the 4 DOF slightly overestimates the motion amplitudes.

When the numerical simulations of Ship A-2, which covers, relatively, a very high speed range and highly extreme wave conditions, were analysed, the comparisons have been made for the capsizing prediction of both models. Here, the difference was even less and almost unnoticeable for the both numerical models. Therefore, it could be concluded that for very high speed range, it may not be necessary to employ full 6 DOF numerical models.

In the numerical simulations, similar problems regarding the simulation of rudder and yaw motions were observed. In terms of pitch motions, as it is stated in the previous Chapter, since the amplitude of pitch motion is less than 10 degrees for all numerical simulation, the assumption of large pitch angles does not make any difference.

Additional parametric studies with more environmental and control parameters are carried out for more definitive conclusions and those results are presented in Appendix G.

The numerical investigations focusing on identifying the effect of frequency, showed no significant difference either, although small differences exist for yaw and rudder, and, control characteristics are sensitive to the effect of frequency for the controlled ship motions in astern seas. One of the reasons for these results could be the well-known difficulty of using 2-D strip theory approach where frequency dependent damping terms could be near zero in the calculation as it was stated in Chapter 6. Furthermore, the full incorporation of hydrodynamic memory effects using 3-D numerical model thus including the aft effect can improve the numerical accuracy. Further numerical simulations for the effect of frequency are presented in Appendix G.

Also, the parametric study has looked into other important environmental, design and operational parameters. The recommendations by IMO guidelines have been investigated as the reliability of the numerical model is permitted.

The effect of wave length to ship ratio, which could identify the occurrence of dangerous conditions such as surf-riding, was investigated in Section 8.2.2. It was seen that as the current knowledge emphasizes that when wave length to ship ratio is equal 1.0 or higher there is serious possibility of being overtaken by waves. It was shown in

Figures 8.9 and 8.10 that while the ship motion was resulted with capsizing in the former and the numerical model identified the surf-riding in the latter. Further numerical simulations for this effect are also given in Appendix G.

Another important factor, especially for design, is loading condition or in another representation choosing of GM parameter. This could determine ship's stability which is highly affected in extreme astern seas. The vessels used in this study have GM values which are not design values but the ones critically complies with IMO regulations. Therefore, GM values were changed for Ship A-1 to identify the effect of loading condition and it was shown that with increasing GM the vessel could be phased out of one dangerous situation boundary. However ships could still be exposed to new dangerous situations in extreme astern seas. It should also be noted especially concerning the container vessel in the light of new findings that the parametric rolling could be very likely in the extreme head seas conditions as well. Therefore, effect of GM should be investigated for all wave heading conditions. Further numerical simulations regarding the effect of GM in extreme astern seas are presented in Appendix G.

In order to assess the operational factors, and the numerical model's capability to demonstrate the effects which could be crucial in avoiding dangerous situations in extreme astern seas environment according to IMO requirements, the effect of speed and heading angle combined was investigated. It was seen that indeed reducing or increasing speed when the special condition is concerned, such as the parametric rolling or broaching-to, and the change of autopilot course could be effective methods to avoid those dangerous situations. The numerical model identified parametrical rolling and surf riding for relatively low speed ship A-1 and relatively high speed ship A-2, respectively. The detailed numerical simulations for this case are also presented in Appendix G.

So far, the numerical and experimental simulations presented were for the steep regular wave conditions. Based on the findings of this chapter and the previous chapter, investigations to assess the motion of the vessel in long crested irregular waves will be carried out with the frequency dependent terms are included in random waves. Furthermore, in a final attempt to clearly identify the effect of coupling between vertical and horizontal motions, the results of the fully captive model tests and the verification of the numerical simulation against wave force calculations in the captive model test, will be presented in Chapter 10.

9. MOTIONS IN RANDOM WAVES

9.1. General Remarks

The objective of this chapter is to present the modified numerical model in random waves in order to assess the importance of the sea state in identifying the dangerous situations in extreme astern seas. More broadly, it could be summarized that in an attempt to carry the numerical tool into more realistic environment the mathematical model and its components are expressed in the random waves.

As it is emphasized in Chapter 3, it has been known that possibility of dangerous situations such as broaching-to or parametric rolling and the situation leading to the capsizing were not extensively investigated in irregular astern waves. Boundaries for probability of these dangerous situations both in narrow-band and broad- band wave spectrum limited to defined cases in regular waves. Furthermore, those developed non-linear coupled 6 DOF time simulation models that incorporate impulse response functions were not verified against aforementioned conditions in random waves. Recalling from Chapter 3, ITTC Specialist Committee on Waves [97] stated that although the stability problems in following and quartering seas are often investigated in regular waves from aforementioned facts, irregular wave conditions should be investigated in detail because the probability of capsize is directly related to the probability of encountering dangerous wave situations.

Deriving from this background, within the above framework the following sections of the chapter present the descriptions of modified numerical model and equations of motions in random waves. They are followed by the presentation of numerical method to calculate the equations of motions in random waves. The process was discussed and critical aspects were given in concluding remarks. The validation study for the numerical model in random astern seas is taken under Chapter 10 where the experimental studies to accomplish this work will also be presented.

9.2. Random Waves and Spectral Techniques

Although many numerical models have been built up with assumption of regular waves and the research involves the current study emphasized many times regarding the danger of steep regular waves for the ship motions in astern seas, the realistic sea environment is the irregular, mostly short-crested, seas. However, due to effect of

weather, the dangerous conditions, especially combined with long crested wave motions, such as freak waves, can occur for ships in a certain time frame during sea motions.

It is known the open ocean can be irregular even under relatively calm conditions. The wide spread literature on the ocean waves revealed that ocean waves are irregular both in time and space. However, same statistics also indicate that over a certain period these waves are very nearly steady [82]. Therefore, it is very common to rely on the assumption that irregular waves can be described with superimposition of large number of regular waves having different lengths, directions and amplitudes.

Analyses also indicate that aforementioned short time steady sea motions are Gaussian character for instance in terms of probability density functions. This significantly simplifies the application of Fourier analysis or statistical methods into numerical model. We will not look into the details of theory of random waves as they were well established and commonly used in marine studies. Here, the details of random wave spectrum models used in this study will be given.

In order to comply with the experimental studies, which are described in Chapter 10, ITTC and JONSWAP wave spectrums used in this study for the calculation of ship motions in random astern seas. The details of standard terms wave modelling and ITTC and JONSWAP spectrums are given in Tables 9.2 and 9.3.

Although the choice of two different spectrum might seem to be unnecessary, one of the vessels used, Purse Seiner vessel, operates around Japan where ITTC Spectrum is usually used for Pacific Ocean wave spectrum and JONSWAP is the preferred wave spectrum for seas around UK since it is based on the statistical data from North Atlantic. These spectrums also regarded as a good representation of open sea (unlimited fetch conditions) and short crested seas (limited fetch conditions).

Further details of evolution and application of these spectrums are widely available in the literature.

Spectral Form	$S(\omega) = \frac{A}{\omega^5}\exp(-B/\omega^4)$
A and B	$A = \frac{0.0081}{K^4}g^2, B = \frac{0.0081}{K^4}\frac{4g^2}{H_s^2}$ $K = \frac{T_p}{2.492}\sqrt{\frac{g}{H_s}}$
Input parameters	H_s, significant wave height (m) T_z, modal period (s)

Table 9.1 ITTC Spectrum

Spectral Form	$S(\omega) = \alpha g^2 \omega^{-5}\exp\left[-\frac{5}{4}\left(\frac{\omega}{\omega_p}\right)^{-4}\right]\gamma^{\exp\left[-\omega-\omega_p/2\sigma^2\omega_p^2\right]}$
Parameters	γ 3.3 σ 0.07 for $\omega<\omega p$ 0.09 for $\omega>\omega p$ α 0.0081 or $0.076\hat{F}$ ($\hat{F} = gx/V^2_{w10}$) x fetch V_{w10} wind speed at 10 m. above sea level ω_p $2\pi/T_p$
Input parameters	H_s, significant wave height (m) T_p, modal period (s)

Table 9.2 JONSWAP Spectrum

The random wave elevation in the earth fixed system can be written as a series of harmonic components and it is given as:

$$\zeta(t) = \sum_i^N a_i \cos(\omega_{wi} t - k_i x + \sigma_i)$$

Equation 9.1

where $\zeta(t)$ is the irregular wave elevation, a_i, ω_{wi} and k_i are the component wave amplitudes, circular frequencies and wave numbers, respectively, and σ_i are normally

uniformly distributed random phase angles. N is the total number of component waves, taken as large as possible.

If an infinite number of waves are utilized to not repeat itself:

$$\zeta(t) = \int_0^{\infty} \cos(\omega_{wi} t - k_i(\omega)x + \sigma_i(\omega) \cdot \sqrt{2S(\omega)}$$

Equation 9.2

The number of harmonics are used to avoid repetition of the simulated wave record. The repetition time can be found from:

$$t_{signal\_repetition} = \frac{1}{\Delta\omega_w}$$

Equation 9.3

where $\Delta\omega_w$ is the circular frequency interval used to derive component waves characteristics from the given spectrum in between maximum and minimum frequency range taken into consideration

However, as in the case of regular motions, equations of motions should be evaluated in ship-orientated system and this system can be described in terms of the wave pressure with respect to horizontal body-axis system in the similar method shown in Chapter 5 and Appendices A and B as follows;

$$p = \rho g(\zeta_G - x'\theta + z') - \rho g \sum_i^N a_i e^{-k_i z'} \cos(\omega_{wi} t - k_i(\xi_G + x'\cos\psi - y'\sin\psi i + \sigma_i)$$

Equation 9.4

Further points regarding the numerical model and the evaluation and calculation of forces will be discussed in the next section.

9.3. Numerical Method

In the numerical calculation of motions in random seas, the model developed in [138] and [139] was used. Based on Equation 9.1 and 9.4 the total incident wave excitation and diffraction forces due to the action of confused sea can be written as:

$$F_{wave\_exc}(t) = \sum_{i}^{N} a_i (F^{A}{}_{FK+DIF})_i \cos(\omega_{wi} t - k_i(\xi_G + x'\cos\psi - y'\sin\psi i + \sigma_i) + (F^{\delta}{}_{FK+DIF})_i)$$

Equation 9. 5

where $F^{A}{}_{FK+DIF}$ is the amplitude of the force in random seas and $F^{\delta}{}_{FK+DIF}$ is the phase lag angle of the force. However, it should be noted that since the Froude-Krylov forces are not linear, Equation 9.5 is approximate solution. This is the approach followed in this study in accordance with the numerical tool employed for random wave calculations [138], [139].

Similar to regular waves, speed as well as heading of the vessel can change and this inevitably affects the forces. Therefore, once the ship changes its mean speed and heading, Froude-Krylov and diffraction forces will be updated.

The amplitude, a_i, and phase angles, σ_i, of each harmonic component is usually found from a given wave energy spectrum and through digital random number generators which procedure is widely discussed in literature.

As it was emphasized in [139] that the same random phase angles used to simulate the wave history, have been retained in the calculations of the force time record. This requires some explanation. When dealing with regular waves, a phase lag between the wave occurrence and the force associated to that is generally readily accepted. For irregular waves, the use of random phase angles to evaluate wave and force realisations, relaxes the perception of the importance of time relation between these two events.

As for the effect of encounter frequency in random waves, the same method [138], [139] have been employed for random waves applying the same procedure given in Chapter 6. Here following Cummins [48] work, discrete form of the Kernel function can be written as it is given Equation 6.3 as follows:

$$K_{ij}(t) = \frac{2}{\pi} \sum_{n=0}^{100} B_{ij}(n\frac{\omega_{max}}{100}) \cos(n\frac{\omega_{max}}{100} t)\frac{\omega_{max}}{100}$$

Equation 9.6

where the range of frequencies determined by the vanishing value of ω_{max} is generally a function of characteristics of $B_{jk}(\omega)$ (this implies that energy dissipated by the radiating wave at frequencies higher than ω_{max} is negligible) and the number of frequency

components has been assumed equal to 100 after examining the inverse transformation of Kernel functions and having made sure that the integral of these over convolution time range would be reasonably close to zero.

In the method adopted [138] here, finding the mean response of the ship in the time domain solution relies on processing of a continuous data stream instantaneously so that the filtered output is obtained in parallel. There are a number of techniques available, as it is explained in the literature, from Fourier transform-based filters to moving averages, but following the adopted method Finite Impulse filter has been used and applied as follows.

$$y(t) = \frac{1}{K} \cdot \int_{-T/2}^{T/2} x(t-\tau)h(\tau)d\tau$$

Equation 9.7

where:

$x(t)$	time domain signal to be analysed
$h(t) = W(t) \cdot \frac{1}{2 \cdot \pi} \int_{-\omega_{cut}}^{\omega_{cut}} H(\omega)e^{-i\omega t}d\omega$	time domain impulse response function
$H(\omega)= 1$ if $\omega<\omega_{cut}$	parameters of the filter
$H(\omega)= 0$ if $\omega>=\omega_{cut}$	
$W(t) = \cos^2\left(t \cdot \frac{\pi}{2T}\right)$	windowing function
$K = \int_{-T/2}^{T/2} h(\tau(\tau)$	correction coefficient
ω_{cut}=0.1 [rad/sec]	low-pass band of the filter
T=30[sec]	span of the signal x(t) to be filtered

However it is noted in [138] that the signal in Equation 9.7 has some time lag behind the original signal.

The detailed applications of the aforementioned numerical model can be found in [138] and [139]. The numerical simulations carried out using aforementioned mathematical method have been verified against the experiments and the results have been presented in Chapter 10.

9.4. Concluding Remarks

As it is stated in first section, the aim of this chapter was to present the modified numerical model in random waves in order to assess the importance of the sea state in identifying the dangerous situations in extreme astern seas.

First, the important points mentioned in the application of random waves and it is once again emphasized based on the previous research that the solution could rely on the assumption that irregular waves can be described with superimposition of large number of regular waves having different lengths, directions and amplitudes.

Furthermore it is known that short term steady sea motions are Gaussian in character for instance in terms of probability density functions and this significantly simplifies the application of Fourier analysis or statistical methods into numerical model.

Based on the aforementioned findings a model which has been developed during seakeeping studies in University of Strathclyde [139], [138] has been combined with the numerical model described in Chapter 5 and 6. The equations of motions for random wave models and critical aspects regarding wave spectrums and its applications were given.

After presenting the mathematical model the final challenge is to verify the model against experimental studies and that work is taken in the next Chapter.

10. BENCHMARK STUDY OF ITTC VESSEL

10.1. General Remarks

The objective of this chapter is to present the results of the captive and free running model experiments carried out in Japan in order to validate the numerical model in all 6 DOF and extreme random seas. Extensive captive and free running model experiments were carried out at National Research Institute of Fisheries Engineering, Japan for 712 tonnes Japanese fishing vessel which operates in Pacific Ocean. The captive model experiments were carried out while model was fixed for all 6 DOF. Hence, it was aimed to observe the manoeuvring and course-keeping behaviour of the vessel in large vertical motions. Following the same purpose, the free running model experiments were carried out in random seas using both ITTC and JONSWAP spectrum. The captive model experiments carried out for different speed, heading angle, sinkage, trim angles and for some cases with different wave steepness, while the free running model experiments were carried out in different significant wave heights, modal frequencies, speed and wave directions. Extremity of the conditions of captive model runs were defined within limits and strength of model that was used for these experiments.

Within the above framework the following sections of the chapter present the descriptions model experiments, particulars of the model, test matrix, instrumentation and all other details regarding model runs. They are followed by the presentation of model run simulations and comparisons of the numerical model with those experimental results. The results were discussed and critical aspects were given in concluding remarks.

10.2. Experiment Method

The experiments was carried out in the seakeeping and manoeuvring basin named "Marin Dynamics Basin" of the National Research Institutes of Fisheries Engineering, Japan. The basin is 60 m long, 25 m wide and 3.2m deep (Figure 10.1). It has an X-Y towing carriage consisting of main sub carriages: the main carriage runs in longitudinal direction of the basin and the sub carriage on the main carriage runs in the transverse direction of the basin. The maximum velocities of the main and sub carriages are 3m/s and 1.5 m/s respectively. The basin equips an 80-segmented wave maker.

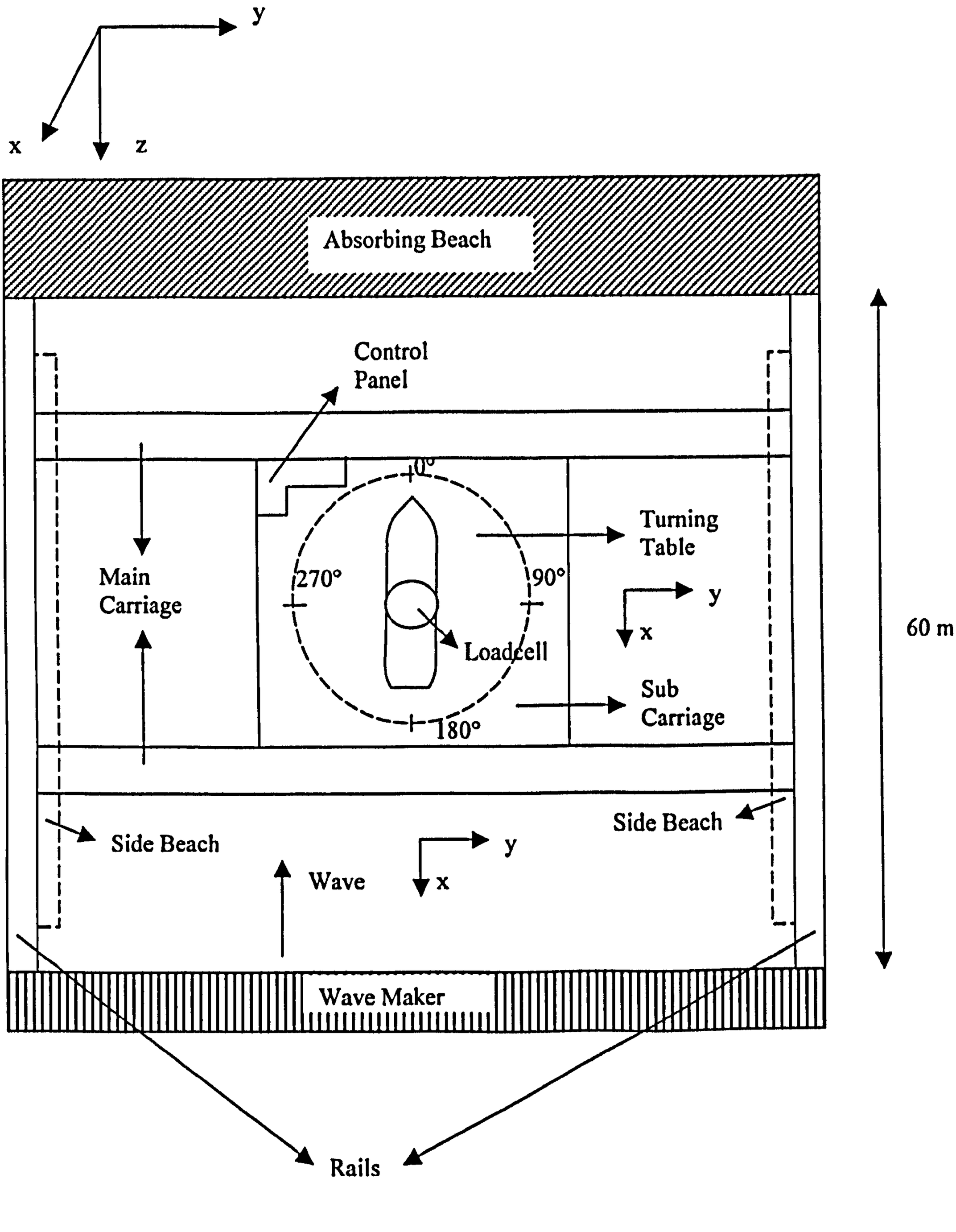

Figure 10.1 General layout of the model basin

The carriages and wave maker were controlled by the digital feedback system. Captive and free- running model tests, instrumentation and all other details as follows;

10.2.1. Captive Model Tests

For these tests 2 m length (1/17.25 scale) model is used (Figure 10.2). This vessel has been tested as part of series of the benchmark tests commissioned by the ITTC Specialist Group on Stability. Its principal particulars are given in Table 10.1. The model was equipped with rudder but without propeller and bilge keels.

Parameter	Vessel	Model
Model scale		1/17.25
L_{BP}	34.50 m	2 m
B	7.60 m	0.441 m
D	3.07 m	0.178 m
d_f	2.50 m	0.145 m
d_a	2.80 m	0.162 m
d	2.65	0.154
C_b	0.597	0.597 m
Δ	425 tonne	81.08 kg
LCG	-1.31 m	-0.076 m
KG	3.36 m	0.195 m
GM	1.0 m	0.058 m
T_φ	7.4 sec	1.6 sec

Table 10.1 Principal Particulars

The model, which is fixed in all 6DOF, was fitted with a turning table on the sub carriage (Figure 10.3-10.4). Previously, the model is weighted and balanced with 6 components loadcell on displacement. The 6 DOF forces and moments (surge, sway, heave forces, roll, pitch and yaw moments) detected by a dynamometer, which is placed on loadcell (Figure 10.5). The centre of yaw moment is longitudinal centre of buoyancy, L.C.B., and that of the roll moment above still water surface, OG. The centres of heave and pitch are defined from the centre of X-Y axes on loadcell. A servo-needle wave probe was also fitted with the sub carriage. Based on the coordinate systems shown in Figure 10.6, the sign convention as follows. The positive surge force acts towards bow, the positive sway force acts starboard, the positive yaw moment induces the starboard turn, the positive roll moment results in downward movement of the starboard side and positive wave elevation indicates downwards. The positive heave force indicates towards up and the positive pitch moment aft downwards.

positive wave elevation indicates downwards. The positive heave force indicates towards up and the positive pitch moment aft downwards.

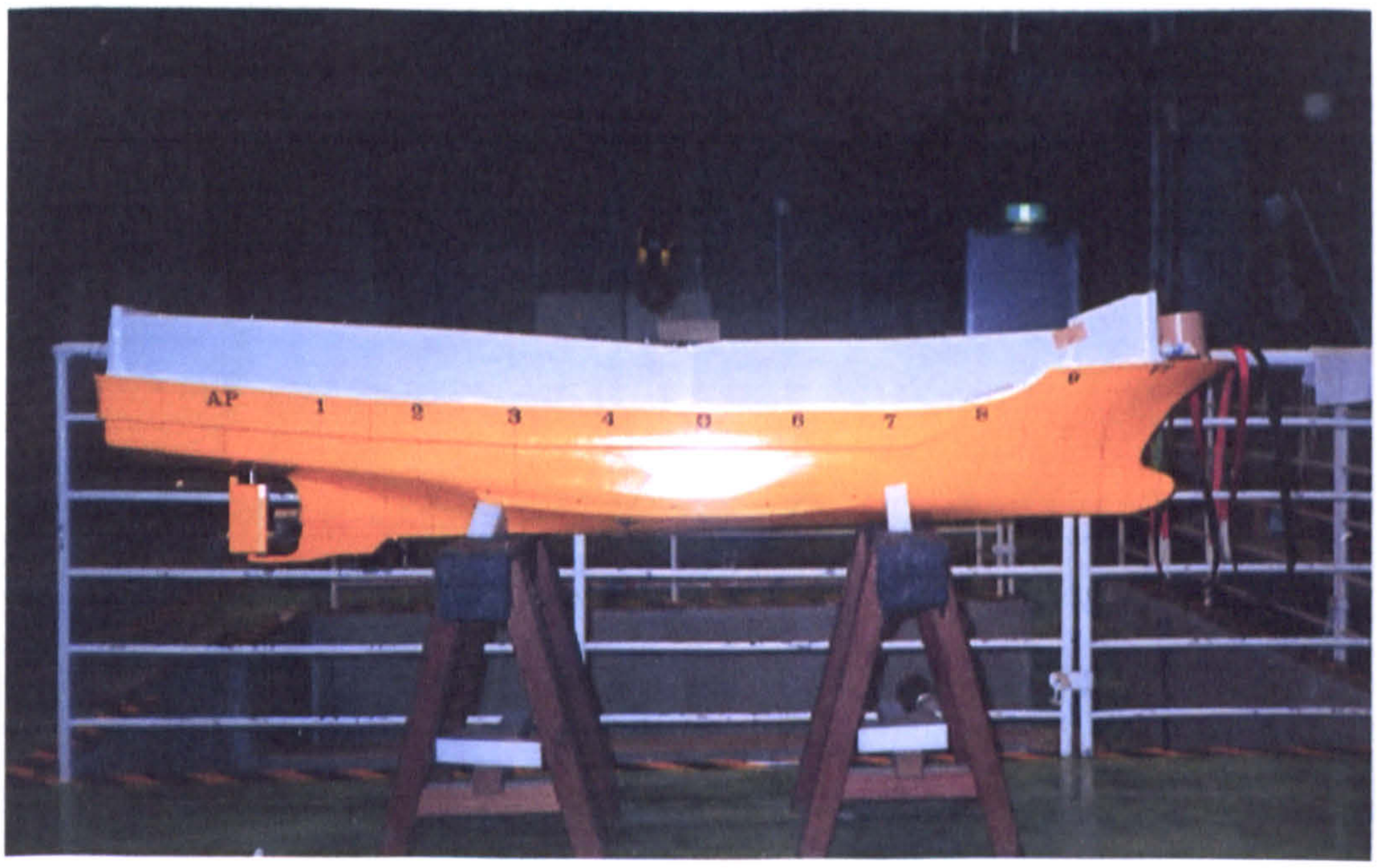

Figure 10.2 The model used in the captive tests

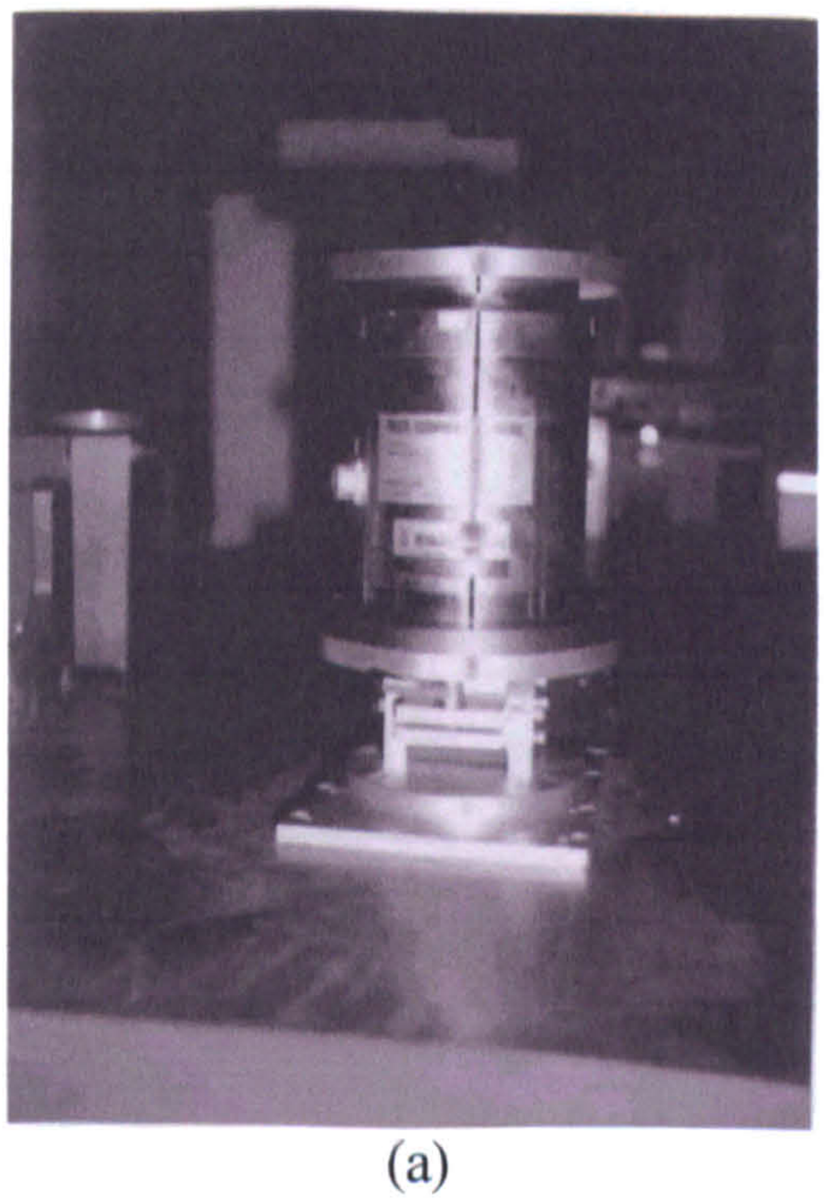

(a)

(b)

Figure 10.3 Loadcell (a) for zero heel angle (b) for 10 degrees to starboard

Figure 10.4 Loadcell on the balanced model

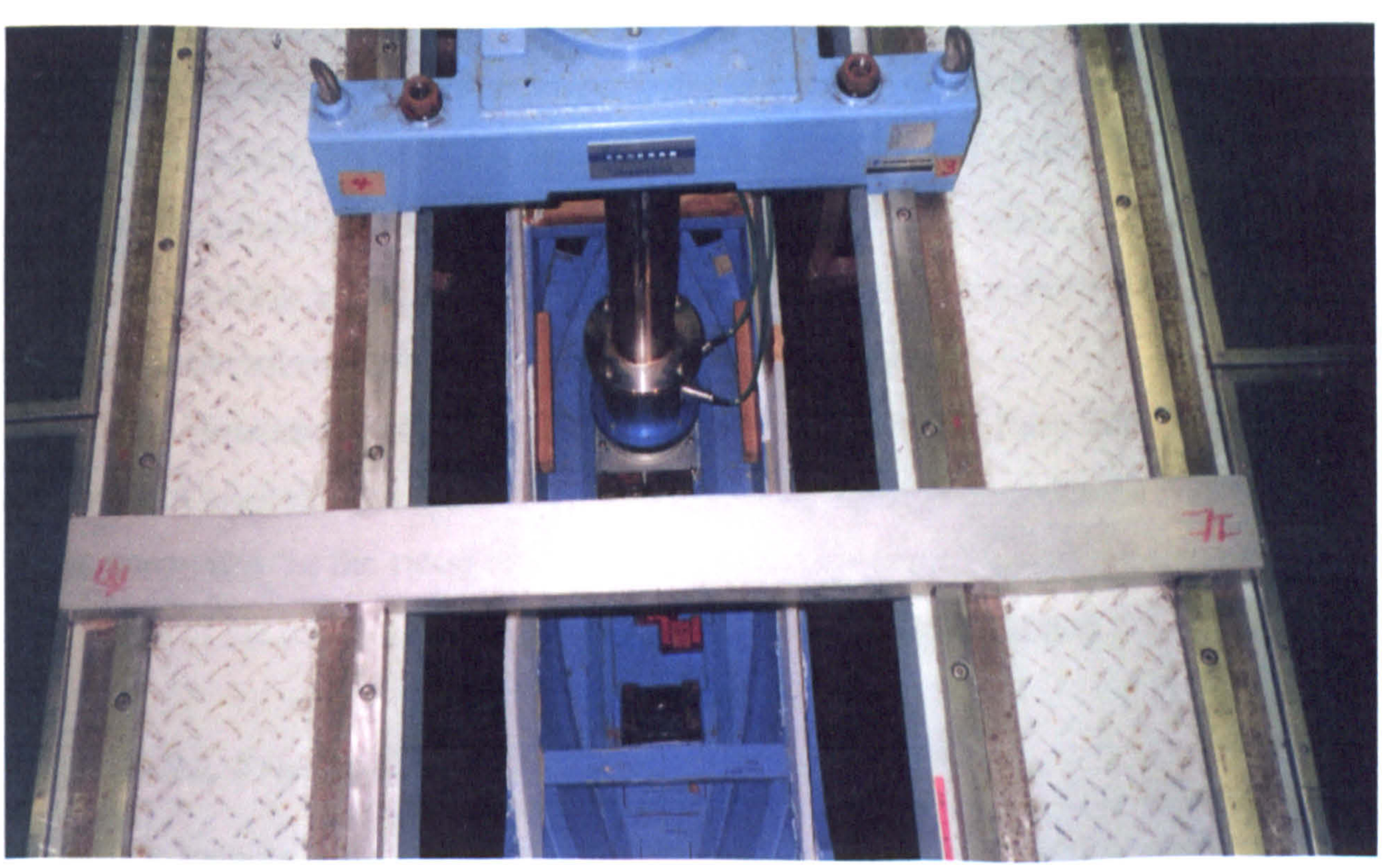

Figure 10.5 Dynamometer on the loadcell

The relative position of centre of ship gravity to a wave trough behind the ship is non-dimensionalized with wavelength. This non-dimensional value, ξ_G/λ, of 0.0

indicates that the ship situates on wave trough; that of 0.5 indicates that the ship centre situates on the wave crest. The value between 0.5 and 1.0 indicates that the ship centre situates on the down slope of the wave. Hydrodynamic forces and moments are non-dimensionalised as follows:

$$X' = X_w/(\rho g \zeta_w BL)$$
$$Y' = Y_w/(\rho g \zeta_w BL)$$
$$Z' = Z_w/(\rho g \zeta_w BL)$$
$$K' = K_w/(\rho g \zeta_w B^2 L)$$
$$M' = M_w/(\rho g \zeta_w BL^2)$$
$$N' = N_w/(\rho g \zeta_w BL^2)$$

Equation 10.1

where prime superscript, "'", refers to non-dimensionalised quantities and ζ_w is the wave amplitude.

The experimental procedure is as follows. First, the wave maker generated a regular wave train propagating in the longitudinal direction of the basin. Next, combining movements of two carriages, the model was towed with a certain angle from the wave direction. Since the centre line of model had been adjusted to this towing direction, the model runs with a specified heading angle from waves but no drift angle. Test matrix for the aforementioned conditions is given in Table 10.2. Here the vessels tested for different combination of sinkage, trim and heel angle.

The resistance force is subtracted from the surge wave force and the additional roll moment created from the vertical distance of the dynamometer to the water surface is also accounted for the calculation of the wave roll moment. Results are also presented as function of the relative position on the wave as it is explained above.

10.2.2. Free Running Model Tests

In the free running tests, 2.3 m model (1/15 scale) (Figure 10.7), which was previously mentioned in Chapter 7 in validation of numerical method for capsizing model experiments, was used. The principal particular of the model is given in Table 10.3. The model was equipped with bilge keels, rudder and propeller. The details of the experiment procedure and the data measurements are similar to the ones in Chapter 7.

H/λ	Fn	χ (deg)			Sinkage (m)			0 (deg)			ϕ (deg)		
		0	45	60	-0.2	0	0.2	-1.43	0	1.43	-10	0	10
1/25	0.2	√				√			√			√	
	0.3	√		√		√			√		√	√	√
	0.4	√				√			√			√	
1/20	0.3	√	√	√	√	√	√	√	√	√	√	√	√
	0.4	√	√		√	√	√	√	√	√	√	√	√
1/15	0.3	√	√		√	√	√		√			√	
	0.4	√	√		√	√	√		√			√	

Table 10.2 Test matrix for λ/L=1.5, nominal GM

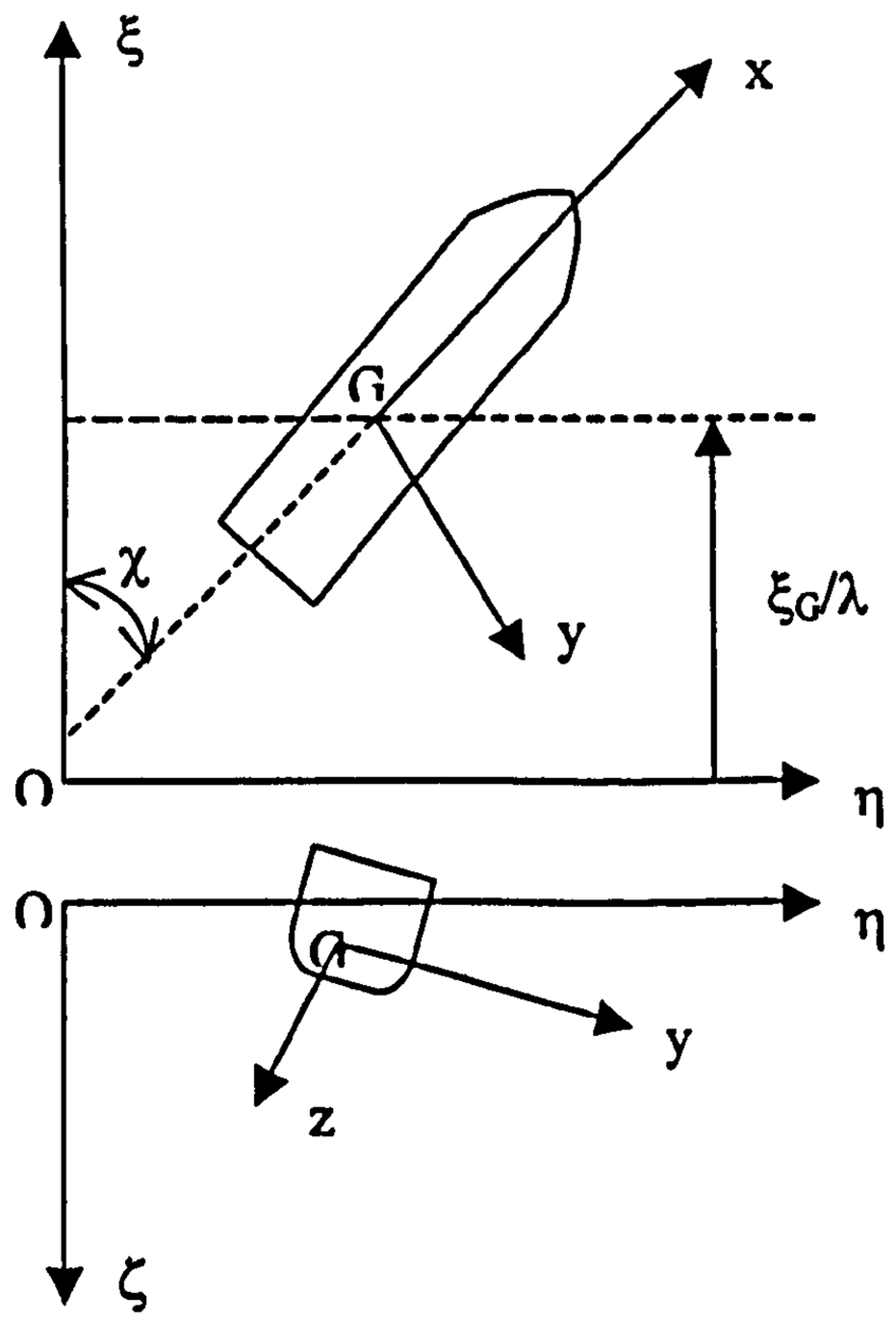

Figure 10.6 Coordinate systems

The details of those procedure and measurement methods are also explained in [80] [79]. The revolution-speed diagram and the test system have been given in Figures 10.8 and 10.9.

Figure 10.7 The model used in free running tests

From the free running tests point of view, the priority was to have a healthy wave spectrum to lay foundations to the numerical models in the effort of determining the boundaries of capsize. The model was run for different speeds and heading angles in both ITTC and JONSWAP wave spectrums.

The model was run for three different heading angles (-5, 45 and 60 degrees) for in 3 different modal period, T_p (4.7 sec., 5.76 sec., 6.48 sec. at full scale) for three different significant wave heights H_s (1.725 m., 2.5875 m., 3.45 m. at full scale) at two different speeds (Fn=0.3 and Fn=0.4) in both ITTC and JONSWAP spectrums.

In order to simulate the motions of ships in random following and quartering seas numerically, the numerical tool developed by The Ship Stability Research Centre [138] was employed. The wave history of motions is taken as the inertial co-ordinate system of the ship. Although the ship travels along the model tank therefore the encounter wave history will be different with time, the numerical model calculates the ship motions for the point wave history measured in the experiments. In other words, the ship is always fixed to the one point in which the wave history is measured.

Parameter	Vessel	Model
Model scale		1/15
L_{BP}	34.50 m	2.3 m
B	7.60 m	0.507 m
D	3.07 m	0.205 m
d_f	2.50 m	0.166 m
d_a	2.80 m	0.186 m
C_b	0.597	0.597 m
Δ	425 tonne	125.588 kg
LCG	-1.31 m	-0.087 m
KG	3.36 m	0.224 m
GM	1.0 m	0.0667 m
T_φ	7.4 sec	1.9 sec

Table 10.3 Principal Particulars

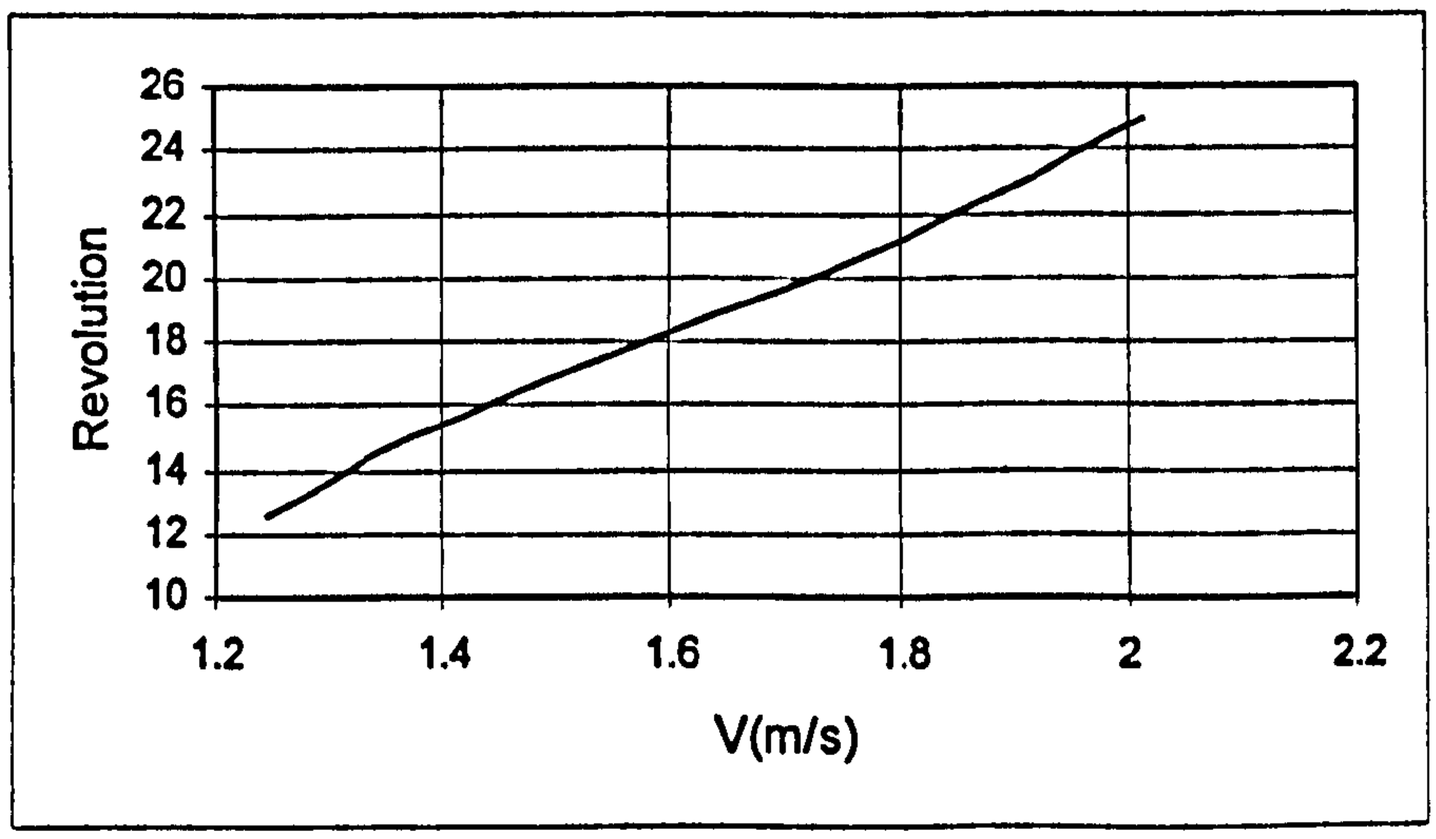

Figure 10.8 Revolution-speed for instrumentation

10.3. Test Results and Comparisons

The mathematical model in the light of captive model tests can be written as follows;

Mathematical Modelling of 6 DOF Motions

Recalling from Equation 5.8,

X: State Vector $x \in |R''$

$$X:(\zeta_a, u, v, \xi_G, w.\varphi.p, \theta, q, \psi, r)^T$$

M: Inertia Matrix
B: Damping Coefficient matrix
F: External Force Vector
A: Added Inertia Matrix
C: Restoring Coefficient Matrix
ζ_w: Wave amplitude

Full expression

$$(M+A)\ddot{X}+B(X)\dot{X}+C(X)X=F(\zeta_w,X,\dot{X},\ddot{X})$$

Equation 10.2

If waves are ignored

$$(M+A)\ddot{X}+B(\dot{X})X+C(X)X=0$$

Equation 10. 3

If all non-linear terms are ignored

$$(M+A)\ddot{X}+B_0\dot{X}+C_0X=F_0(\zeta_w)$$

Equation10. 4

where B_0 and C_0 are constant

If the model from the captive model tests is formulated as follows;

$$(M+A)\ddot{X}+B(\dot{X})+C(X)=F_{00}(\zeta_w)+F_{01}(\zeta_w,X)+F_{02}(\zeta_w,\dot{X})+F_{03}(\zeta_w,\ddot{X})$$

Equation 10 5

F_{00}, F_{01} ↔ captive model experiments

F_{02}, F_{03} ↔ non-linear terms

$B(\dot{X})$,$C(X)$ ↔ from forced tests in calm water or hydrodynamics

Based on the above equation of outcome, the challenge will be identifying the first two terms on right hand side of Equation 10.5 with respect to number of parameters such as wave steepness, heading angle and encounter frequency and as it is explained in the previous section, relative position of the ship on the wave.

Therefore, the following figures were plotted (Figs.10.10-10.57) for this purpose, Experiment results were computed against numerical model explained in Chapter 5-6 and Appendixes A and B. The presentation method of the results are similar to [81] and [40], except, this time it was carried out for fully captive model with different heel angle, sinkage and trim angles.

Following the above statement, the presentation of the results were divided into two points, first the case for zero heel angle, sinkage and trim angle were plotted with respect two wave steepness, heading angle and encounter frequency [Figs 10.10-10.34) and in the second part the cases for whole heading angle, sinkage and trim angle changes were taken into account (Figs 10.35-10.57).

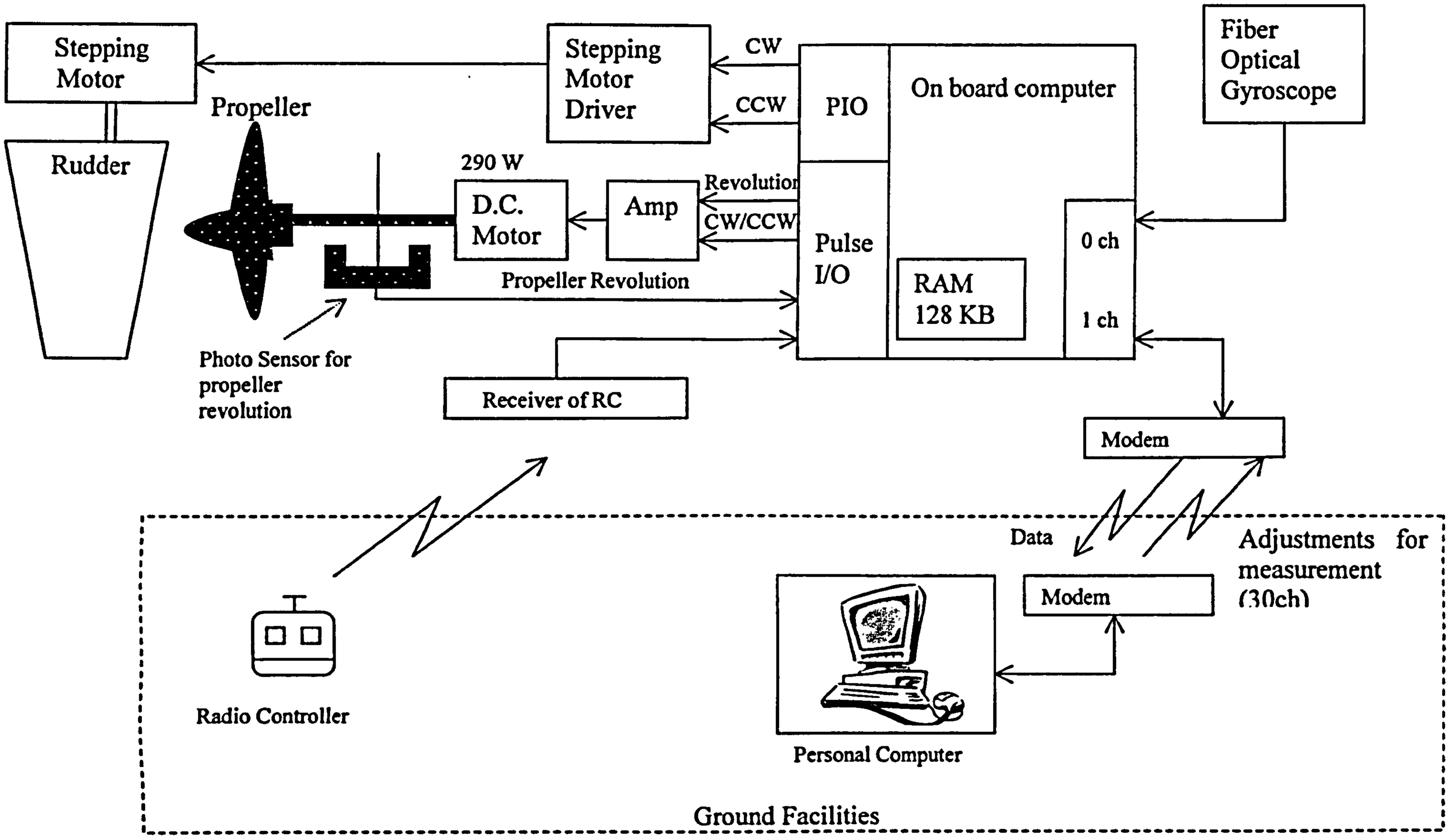

Figure 10.9 Experiment system for the free running model tests

PAGINATION AS IN ORIGINAL

Here the effect of encounter frequency were shown both in respect to heading angle and also, τ, Hanaoka parameter, as described in [81]. The Hanaoka parameter, τ, is defined by

$$\tau = \frac{U\omega_e}{g}$$

Equation 10.6

This parameter governs wave patterns from an oscillating obstacle with forward velocity.

The captive model results based on test matrix given in Table 10.2 and aforementioned formulations and parameters are presented below and the results are discussed in the following section.

For the free running model tests as it is given previously, the model was run for three different heading angles (-5, 45 and 60 degrees) for in 3 different modal period, T_p (4.7 sec., 5.76 sec., 6.48 sec. at full scale) for three different significant wave heights H_s (1.725 m., 2.588 m., 3.45 m. at full scale) at two different speeds (Fn=0.3 and Fn=0.4) in both ITTC and JONSWAP spectrums.

Here, the numerical model described in Chapter 9 was also used to carry out the simulations for the above conditions and they are verified against the some of the experimental results. In order to test the accuracy of the numerical model two different environmental conditions of two spectrums were chosen and the numerical simulations were verified against the experimental results in those conditions for roll, pitch, yaw and rudder angles.

In Figures 10.58-10.81, the simulations were carried out for the T_p = 5.76 sec. (1.487 sec at model scale), and H_s = 2.588 meter (0.1725 meter at model scale) at two different speeds Fn=0.3 and Fn=0.4 in ITTC spectrum and in Figures 10.82-10.105 the model was simulated and compared against experiments T_p = 6.48 seconds (1.717 seconds at model scale), and H_s = 3.45 meter (0.23 meter at model scale) at two different speeds Fn=0.3 and Fn=0.4 in JONSWAP spectrum. Both simulations were carried out for heading angle, χ, 0, 45, 60 degrees, respectively. For the simulations, the initial conditions, propeller revolution and autopilot parameters were modelled according to the experiment results.

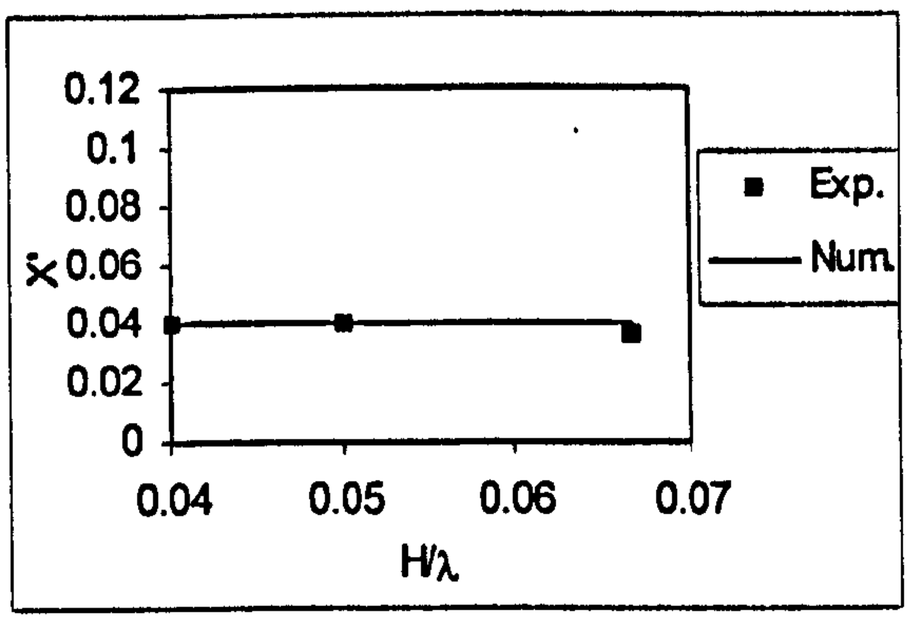

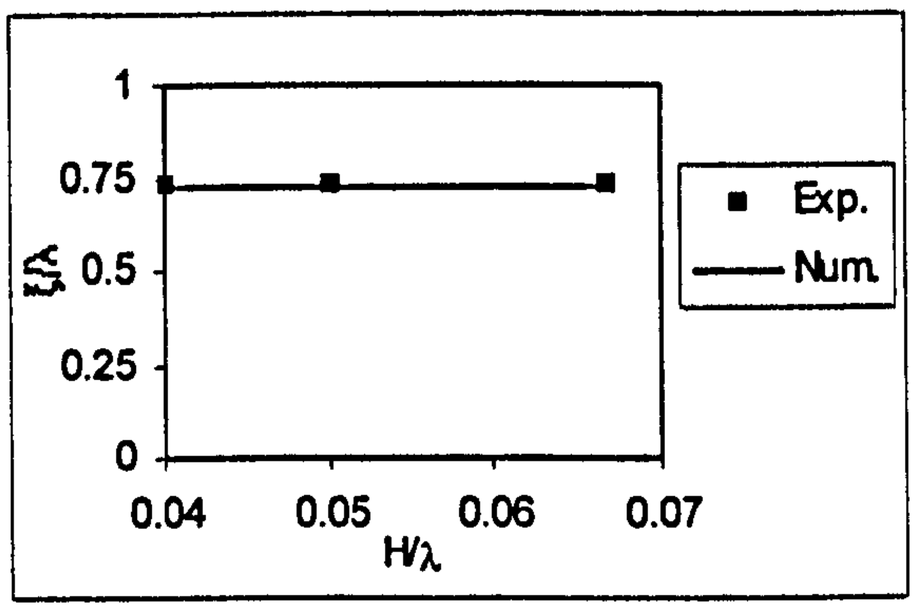

Figure 10.10 Wave induced surge force (Fn=0.3, λ/L=1.5, χ=0°, ϕ=0°, θ=0°, sinkage=0 m)

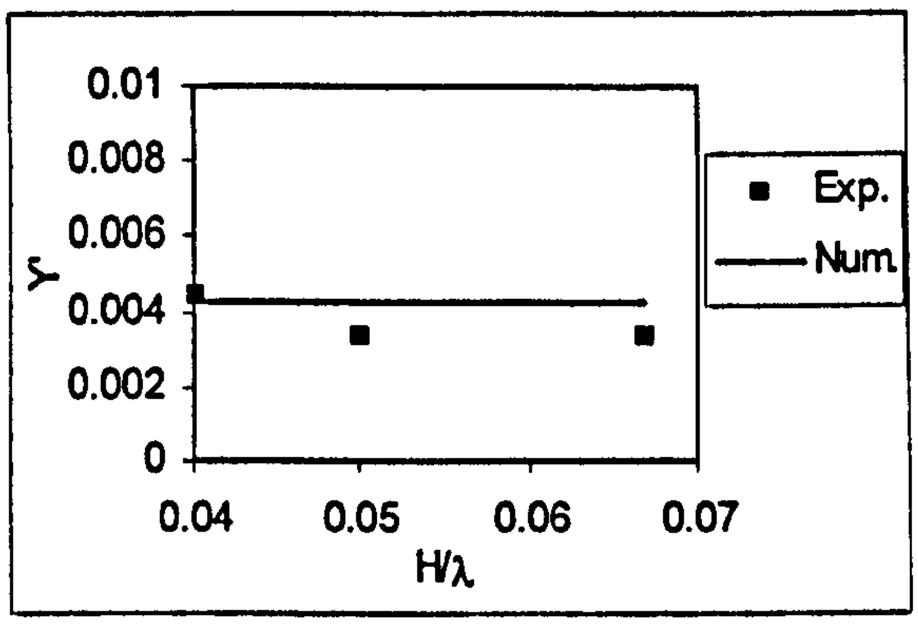

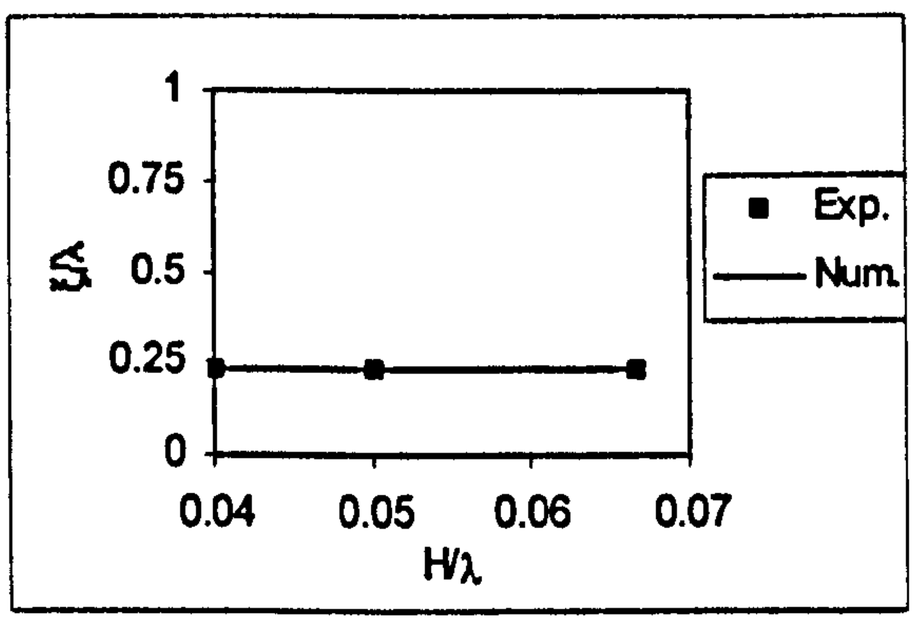

Figure 10.11 Wave induced sway force (Fn=0.3, λ/L=1.5, χ=0°, ϕ=0°, θ=0°, sinkage=0 m)

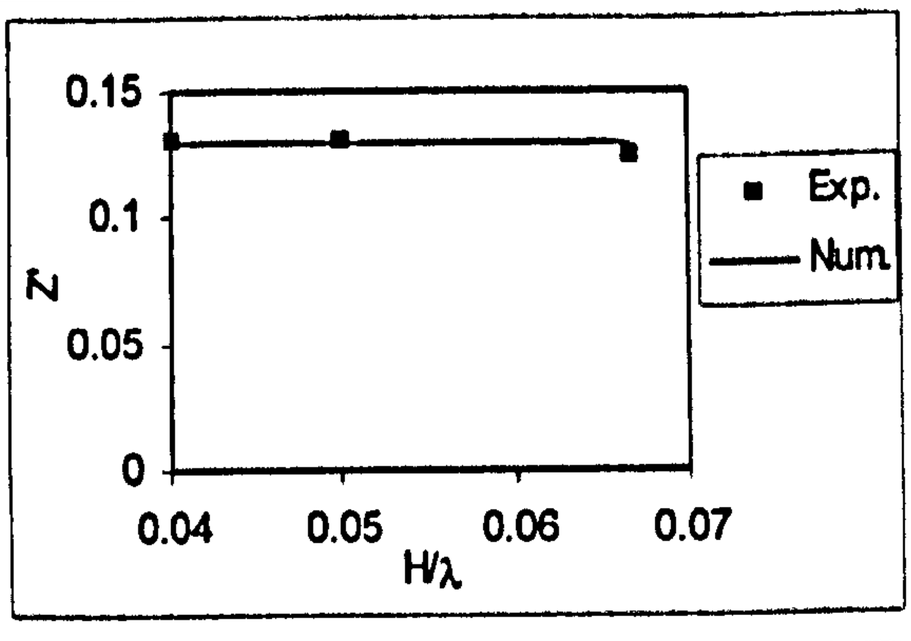

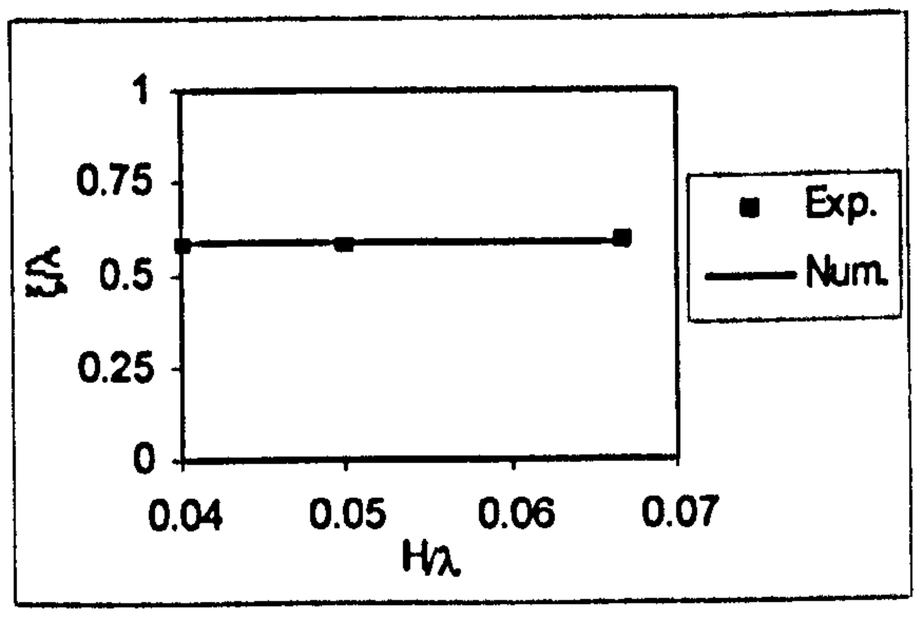

Figure 10.12 Wave induced heave force (Fn=0.3, λ/L=1.5, χ=0°, ϕ=0°, θ=0°, sinkage=0 m)

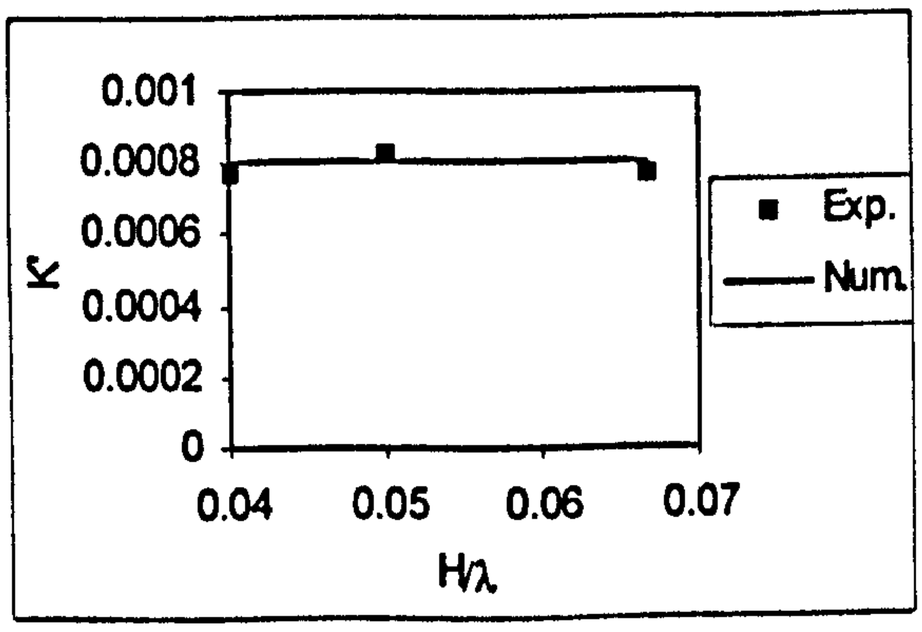

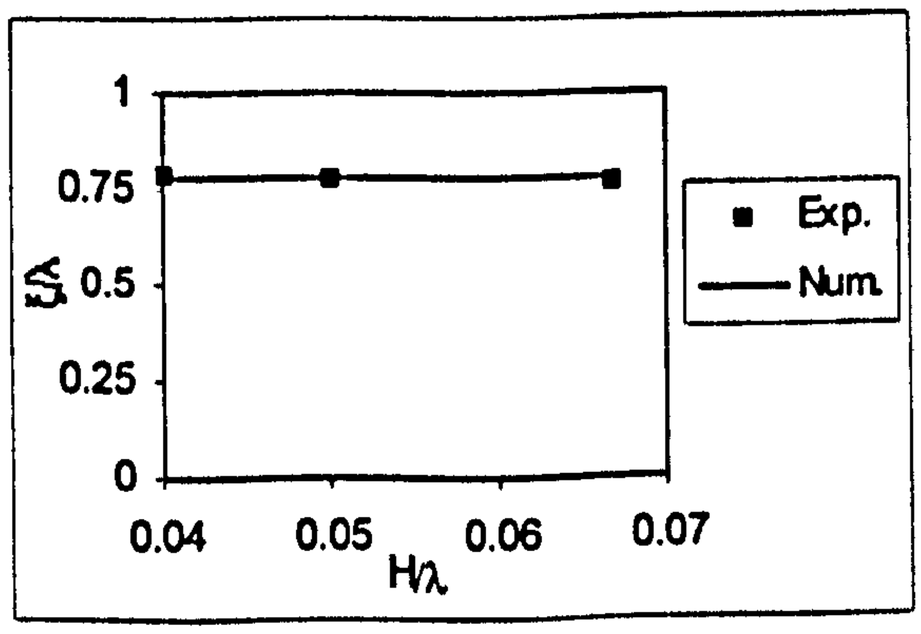

Figure 10.13 Wave induced roll moment ((Fn=0.3, λ/L=1.5, χ=0°, ϕ=0°, θ=0°, sinkage=0 m)

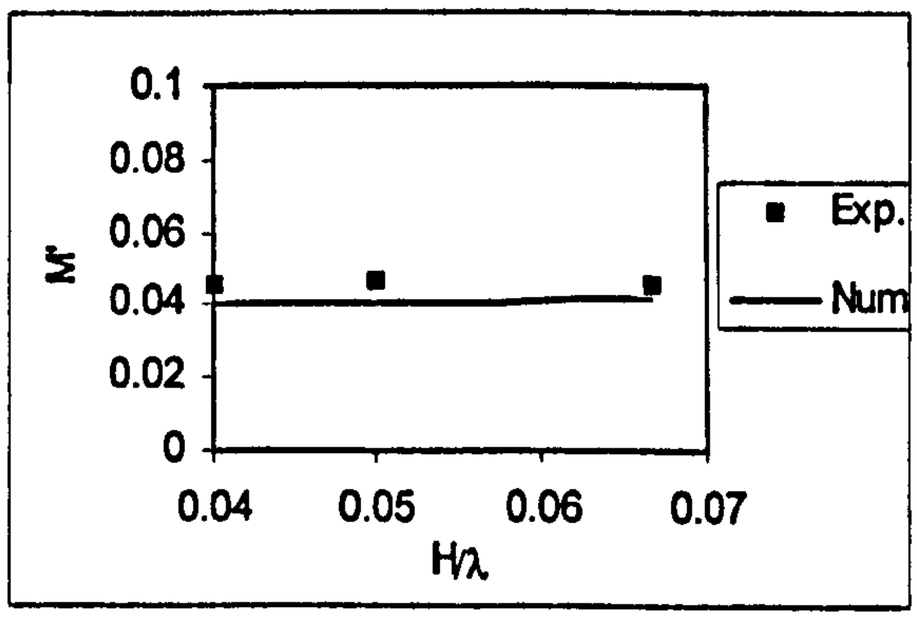

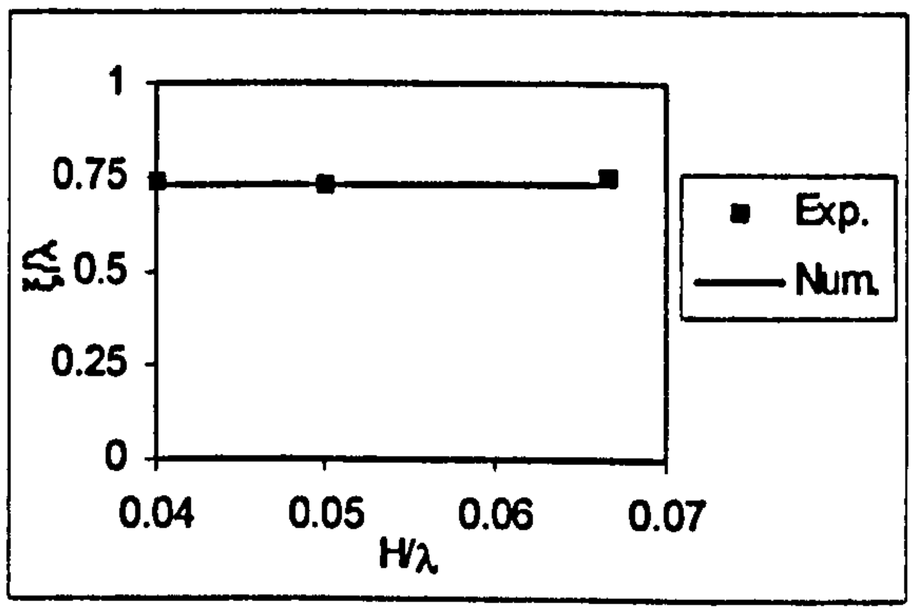

Figure 10.14 Wave induced pitch moment (Fn=0.3, λ/L=1.5, χ=0°, ϕ=0°, θ=0°, sinkage=0 m)

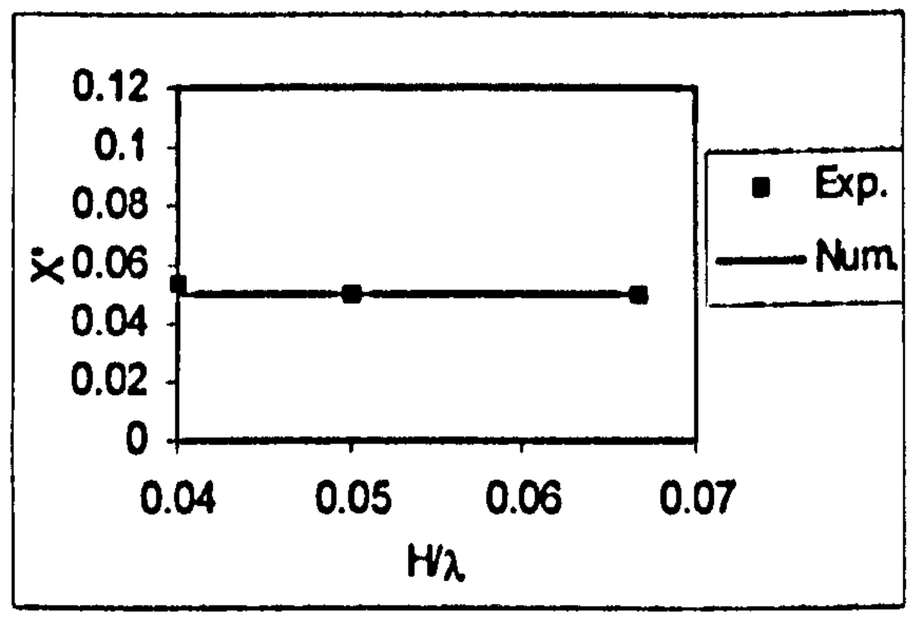

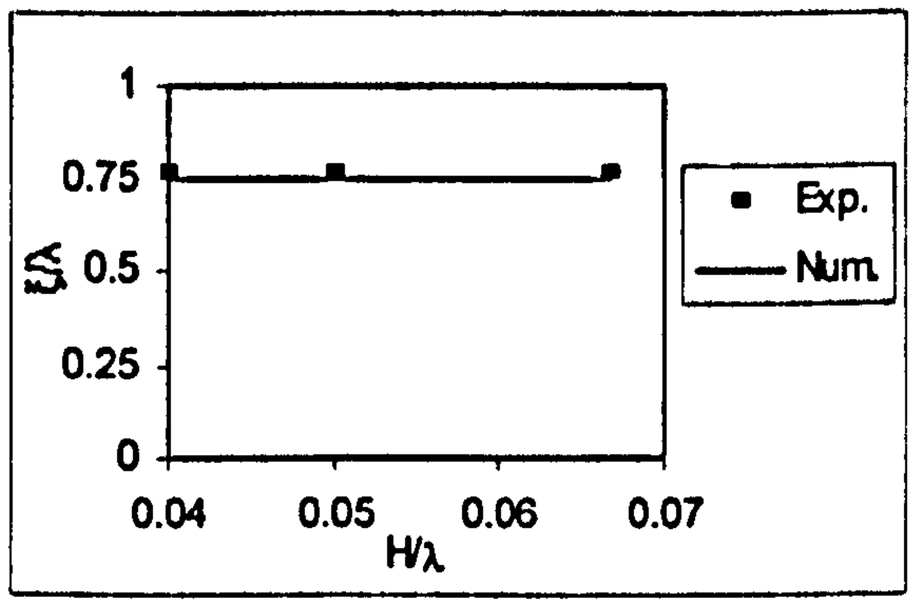

Figure 10.16 Wave induced surge force (Fn=0.4, λ/L=1.5, χ=0°, ϕ=0°, θ=0°, sinkage=0 m)

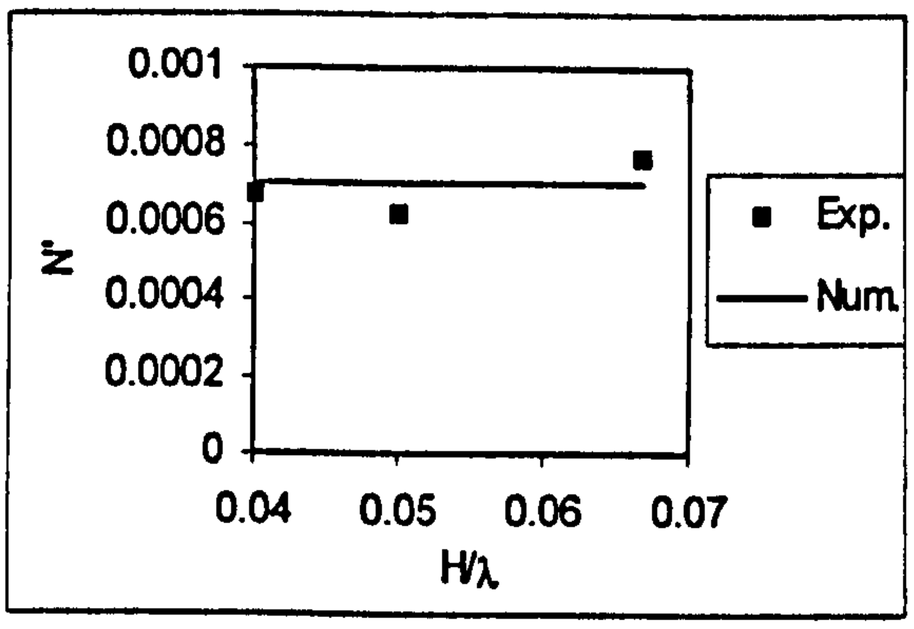

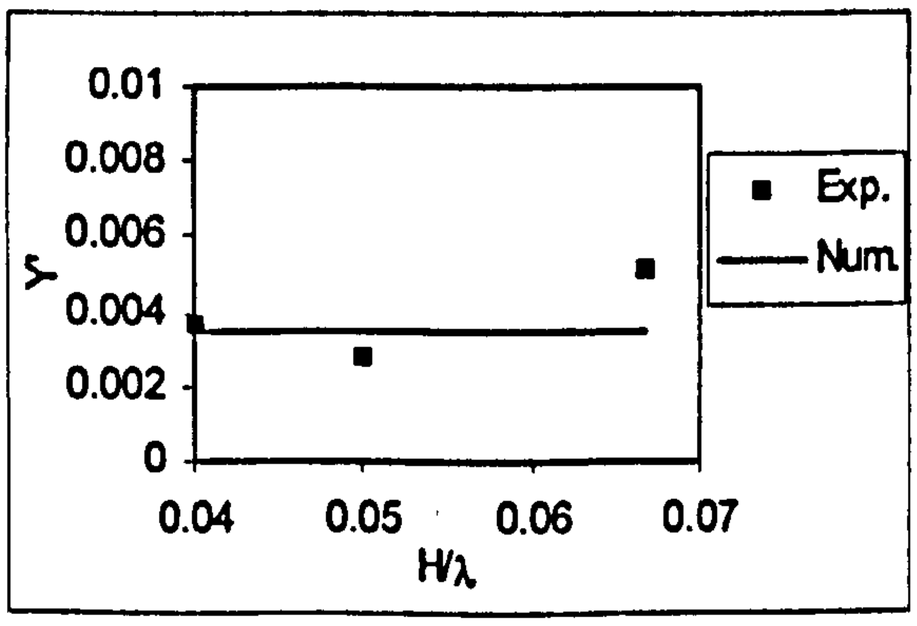

Figure 10.15 Wave induced yaw force (Fn=0.3, λ/L=1.5, χ=0°, ϕ=0°, θ=0°, sinkage=0 m)

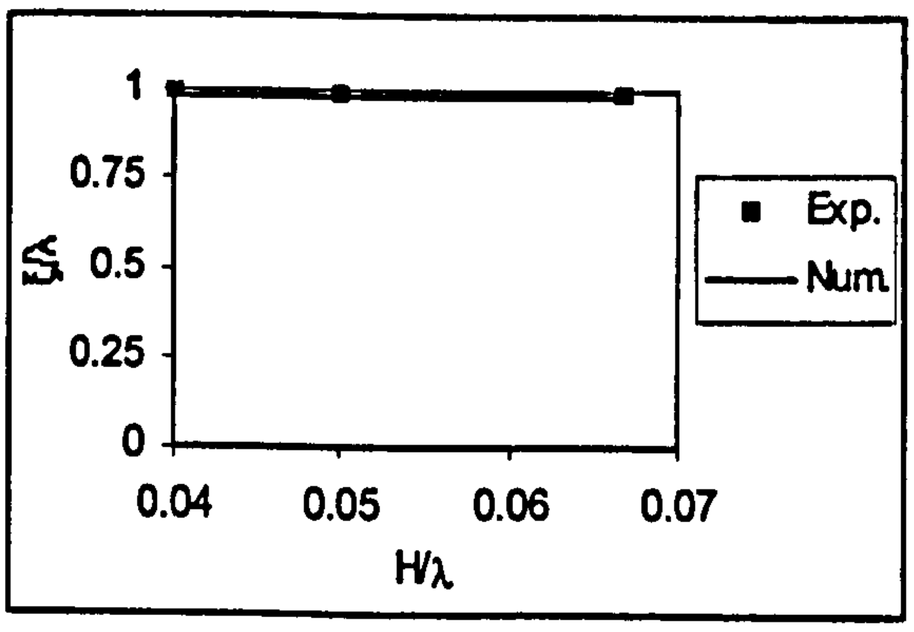

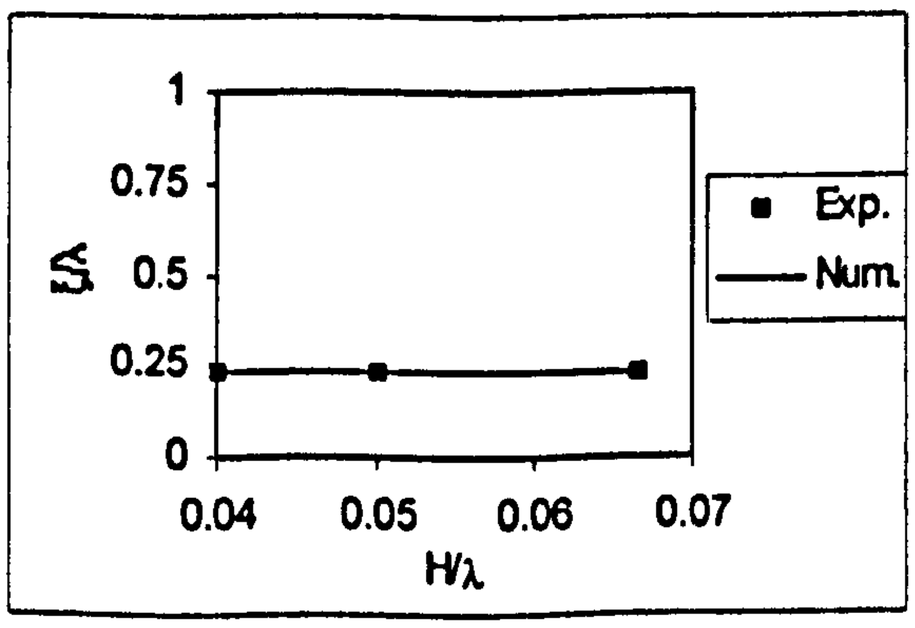

Figure 10.17 Wave induced sway force ((Fn=0.4, λ/L=1.5, χ=0°, ϕ=0°, θ=0°, sinkage=0 m)

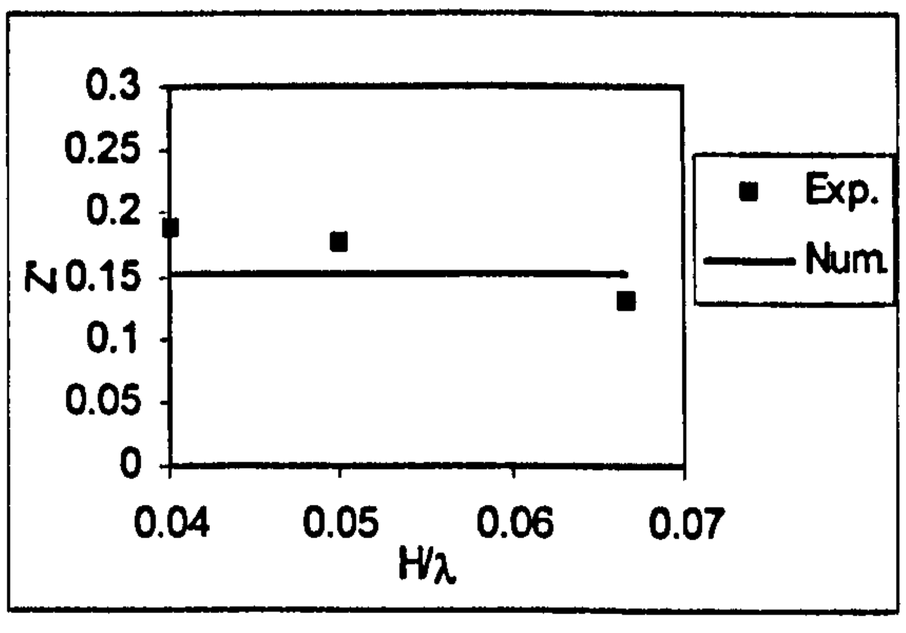

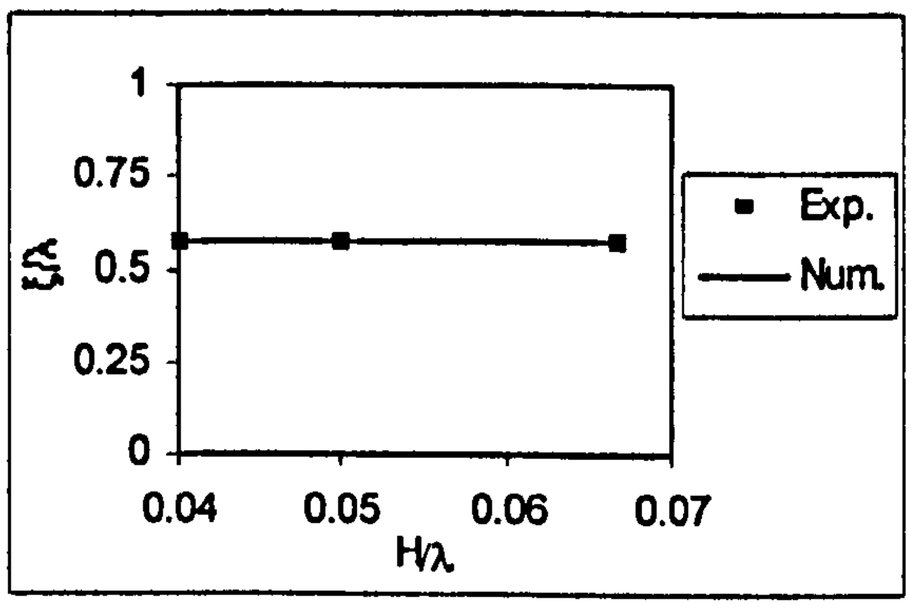

Figure 10.18 Wave induced heave force (Fn=0.4, λ/L=1.5, χ=0°, ϕ=0°, θ=0°, sinkage=0 m)

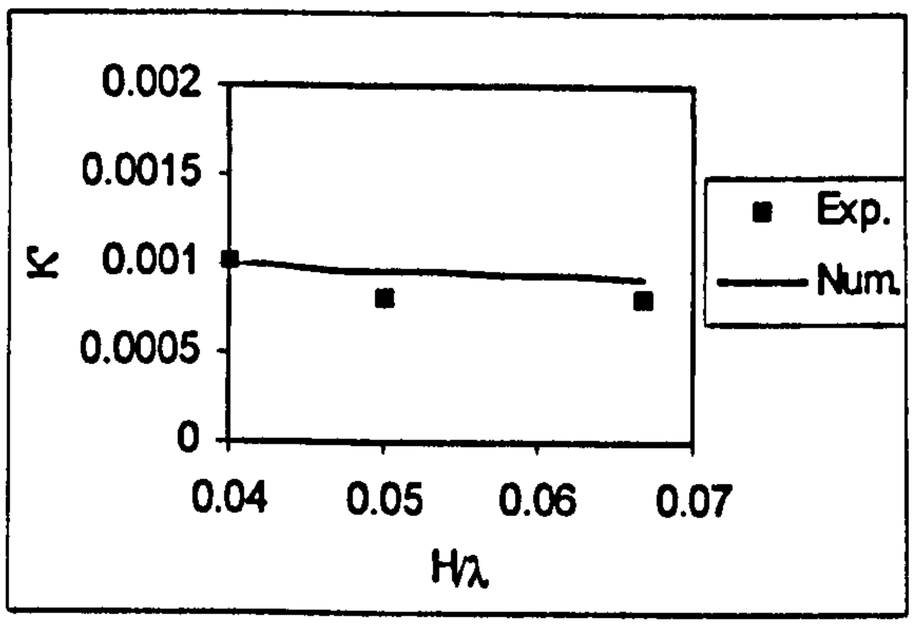

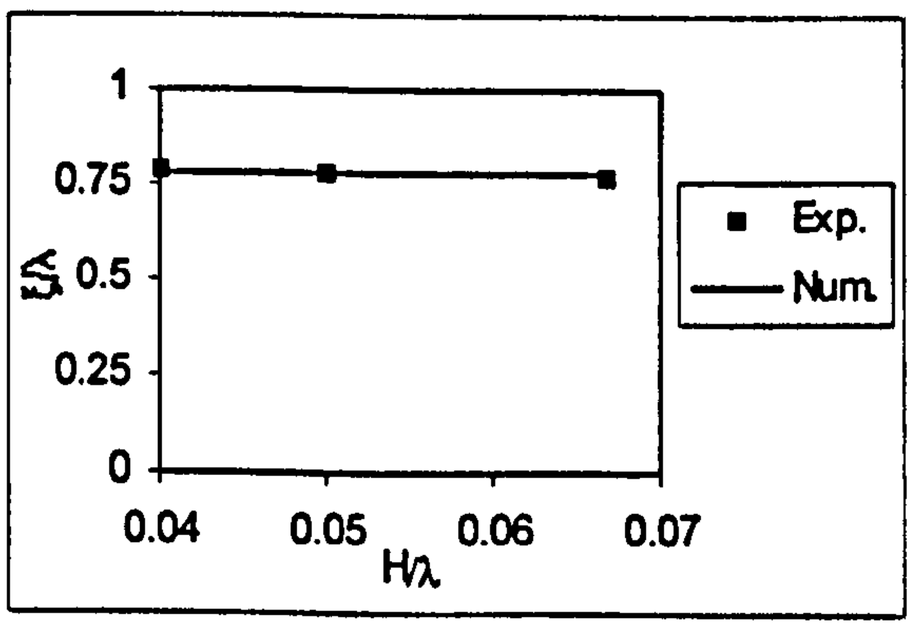

Figure 10.19 Wave induced roll moment (Fn=0.4, λ/L=1.5, χ=0°, ϕ=0°, θ=0°, sinkage=0 m)

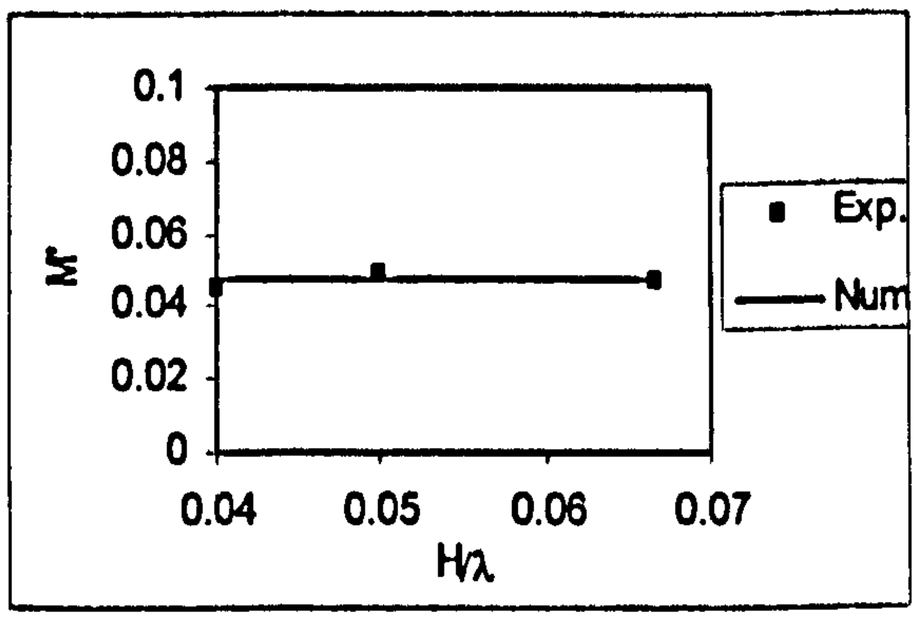

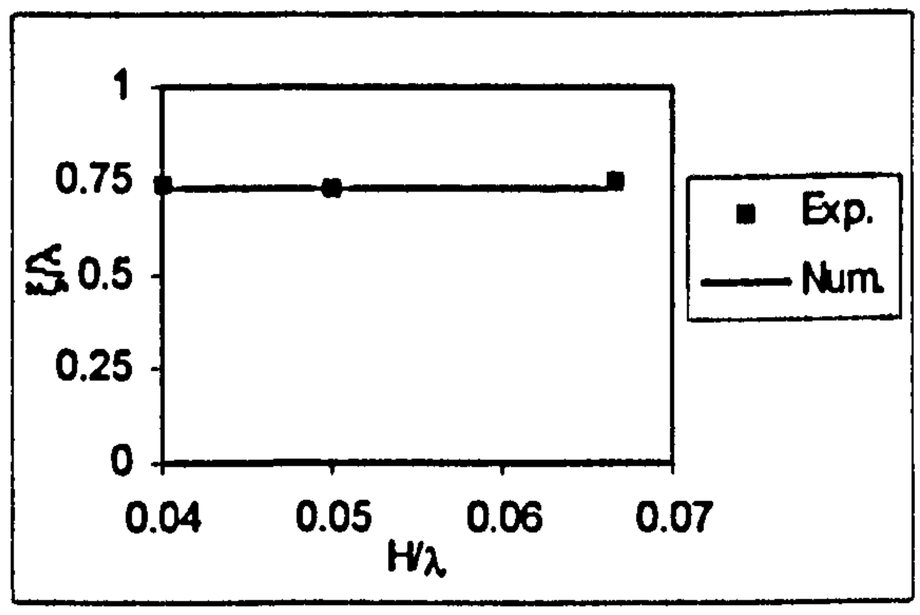

Figure 10.20 Wave induced pitch moment (Fn=0.4, λ/L=1.5, χ=0°, ϕ=0°, θ=0°, sinkage=0 m)

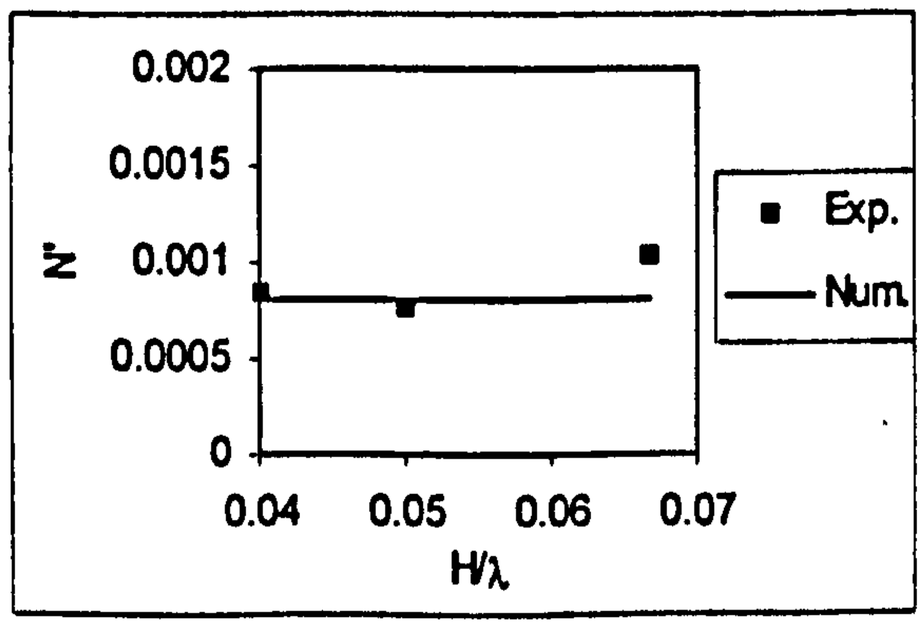

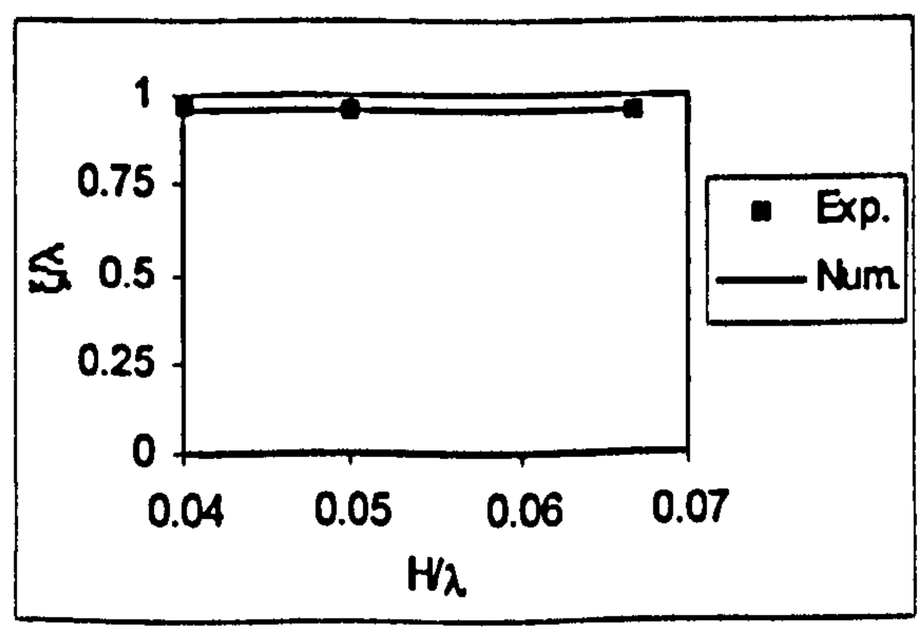

Figure 10.21 Wave induced yaw moment ((Fn=0.4, λ/L=1.5, χ=0°, ϕ=0°, θ=0°, sinkage=0 m)

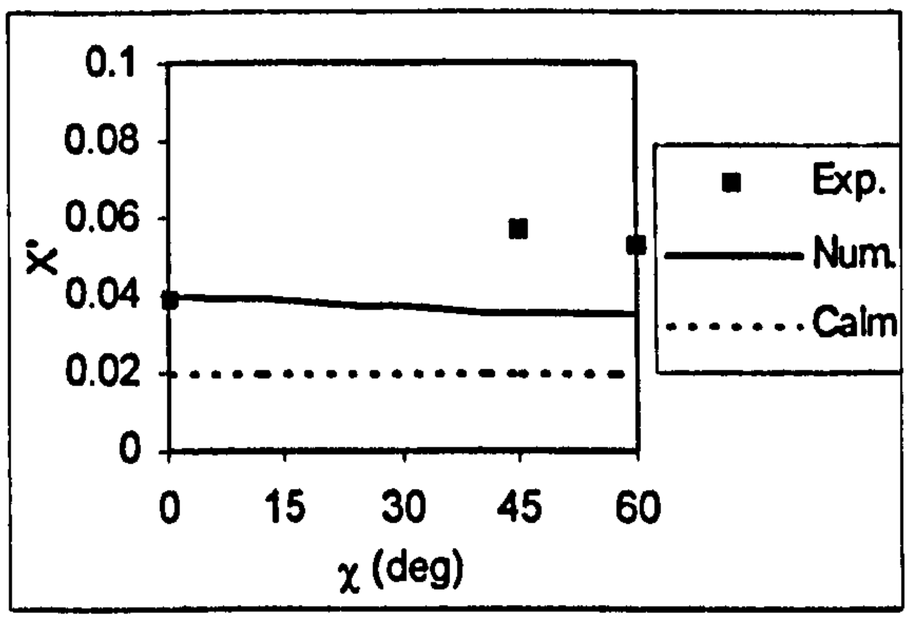

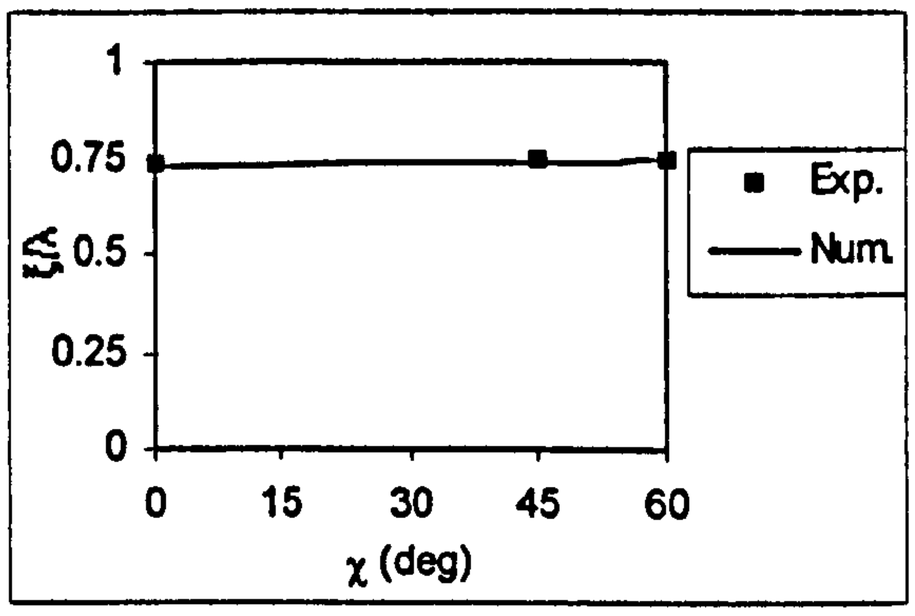

Figure 10.22 Wave induced surge force (Fn=0.3, λ/L=1.5, H/λ=1/20, ϕ=0°, θ=0°, sinkage=0 m)

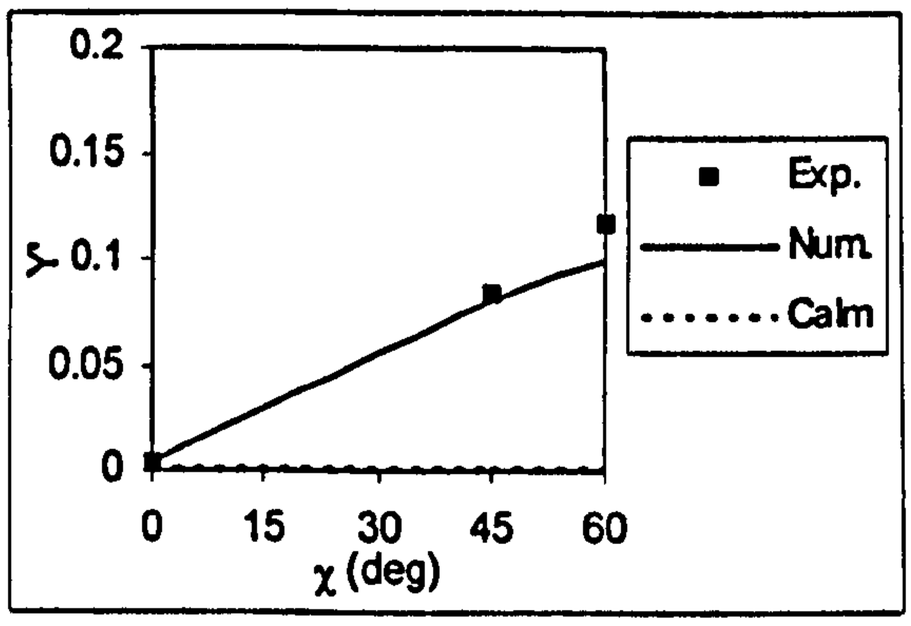

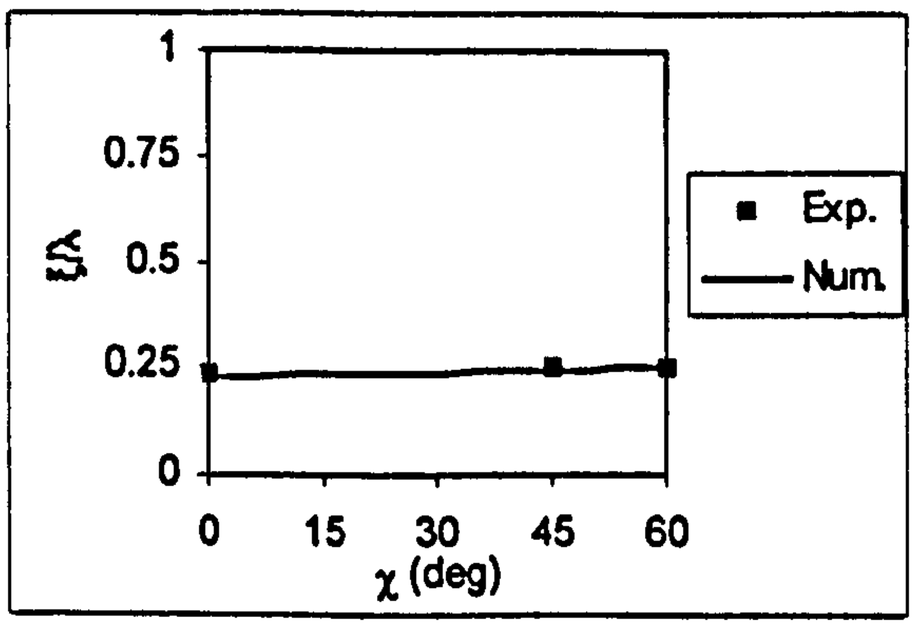

Figure 10.23 Wave induced sway force (Fn=0.3, λ/L=1.5, H/λ=1/20, ϕ=0°, θ=0°, sinkage=0 m)

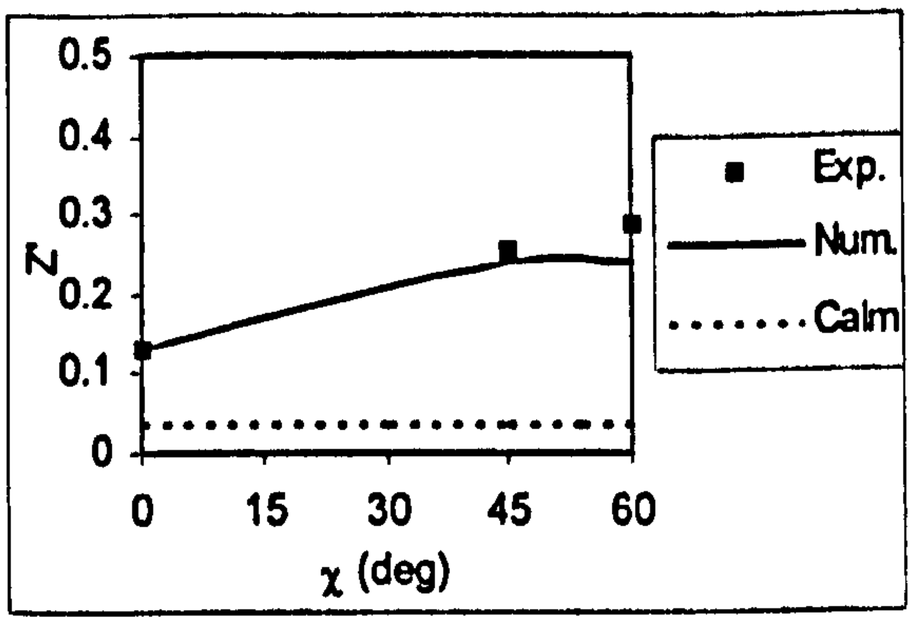

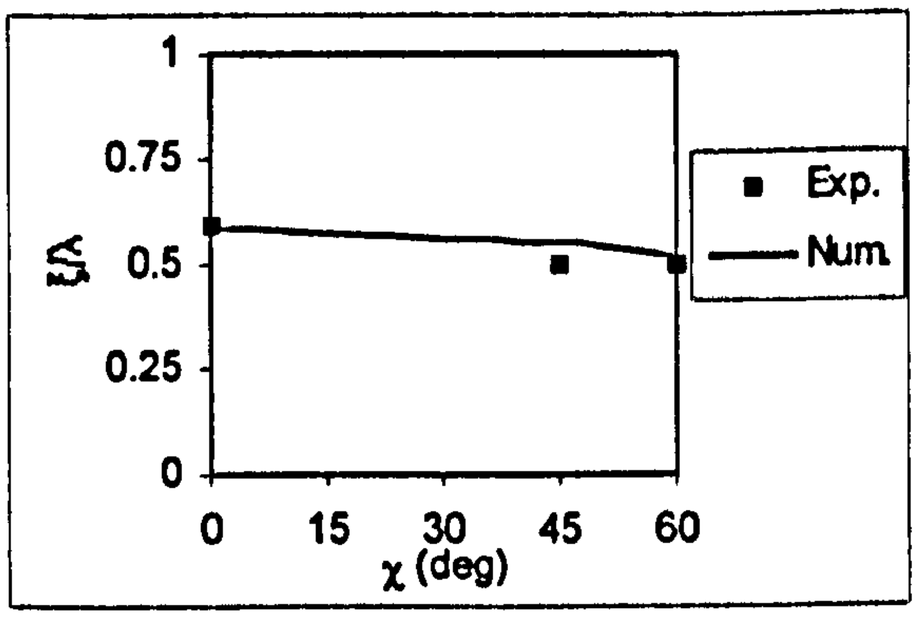

Figure 10.24 Wave induced heave force (Fn=0.3, λ/L=1.5, H/λ=1/20, ϕ=0°, θ=0°, sinkage=0 m)

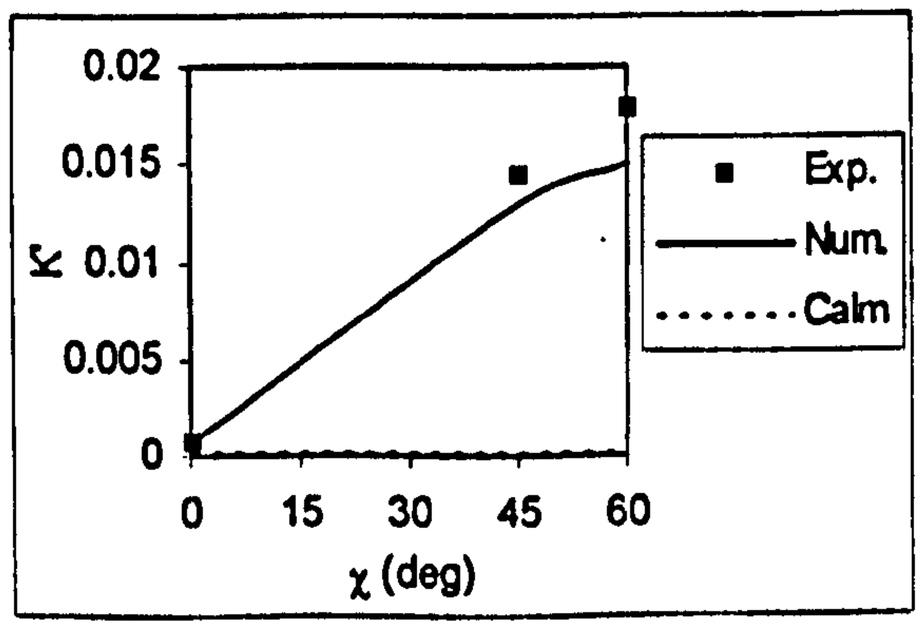

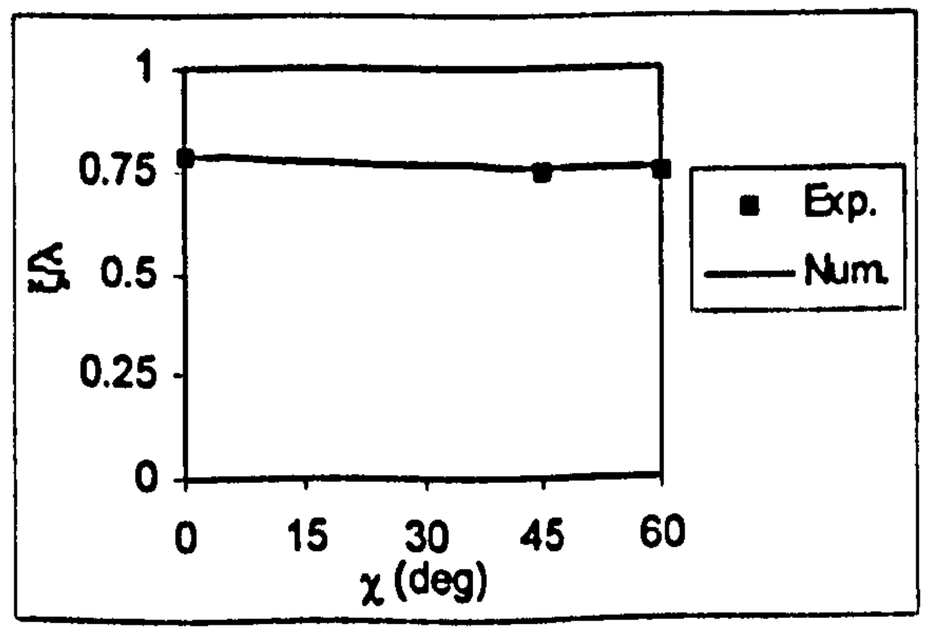

Figure 10.25 Wave induced roll moment (Fn=0.3, λ/L=1.5, H/λ=1/20, ϕ=0°, θ=0°, sinkage=0 m)

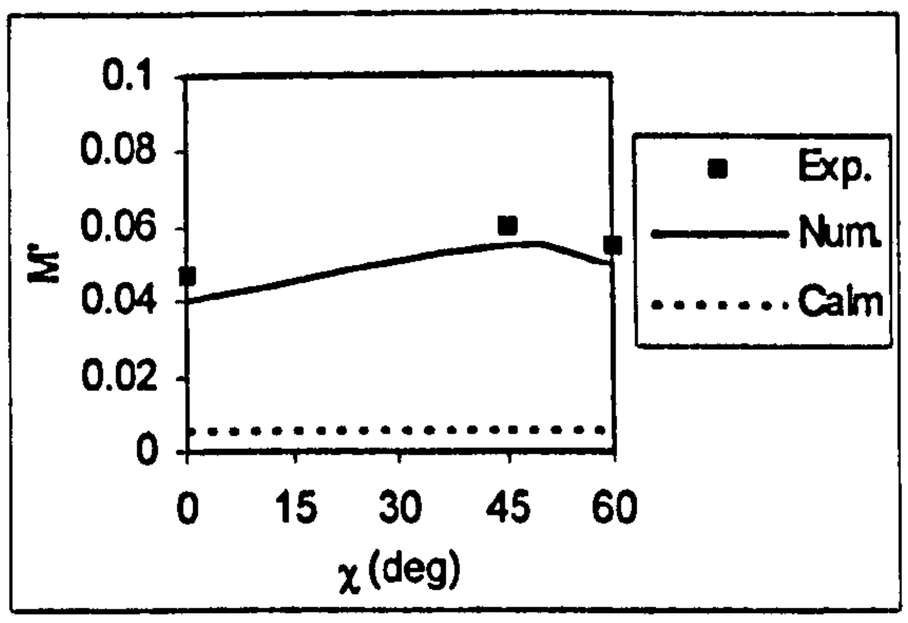

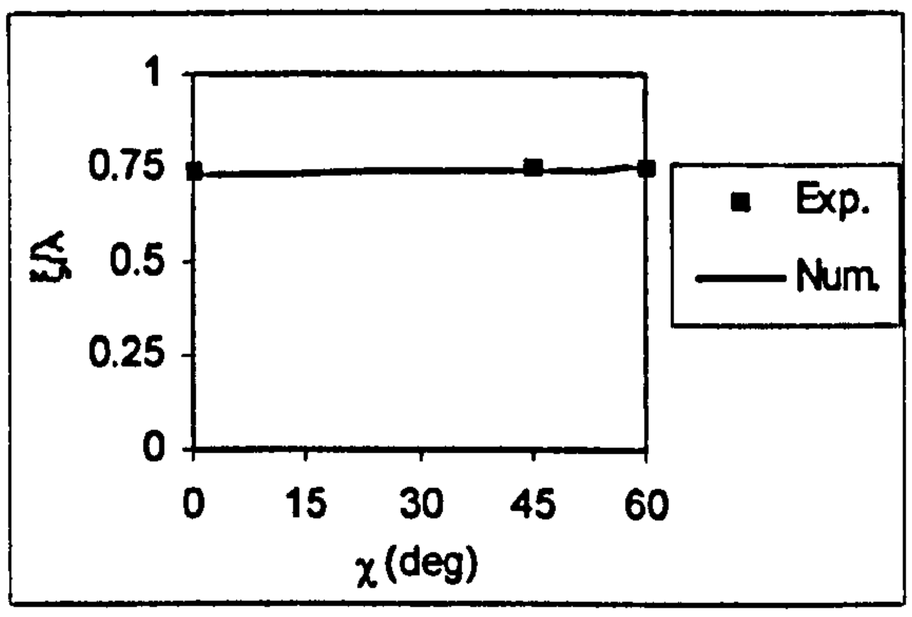

Figure 10.26 Wave induced pitch moment (Fn=0.3, λ/L=1.5, H/λ=1/20, ϕ=0°, θ=0°, sinkage=0 m)

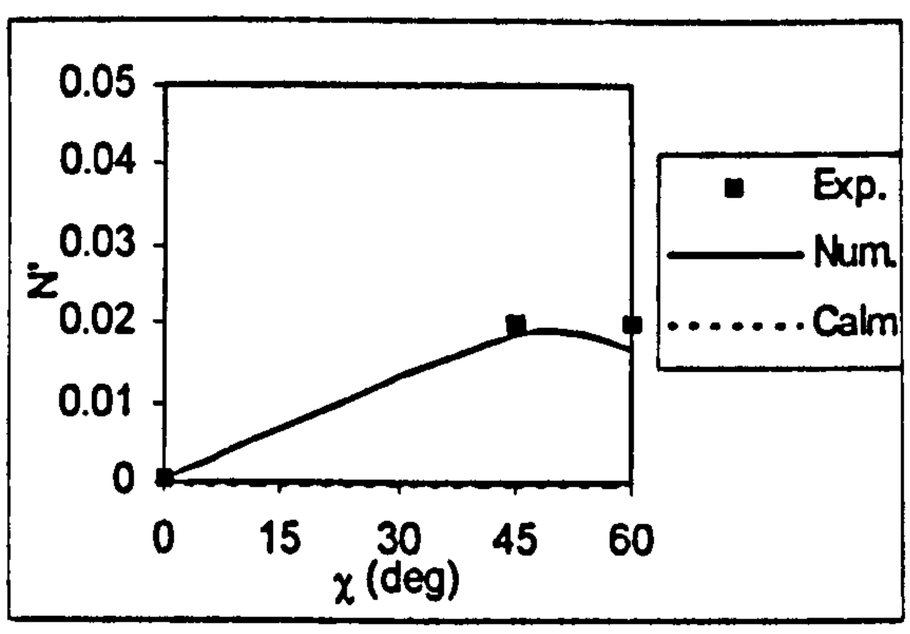

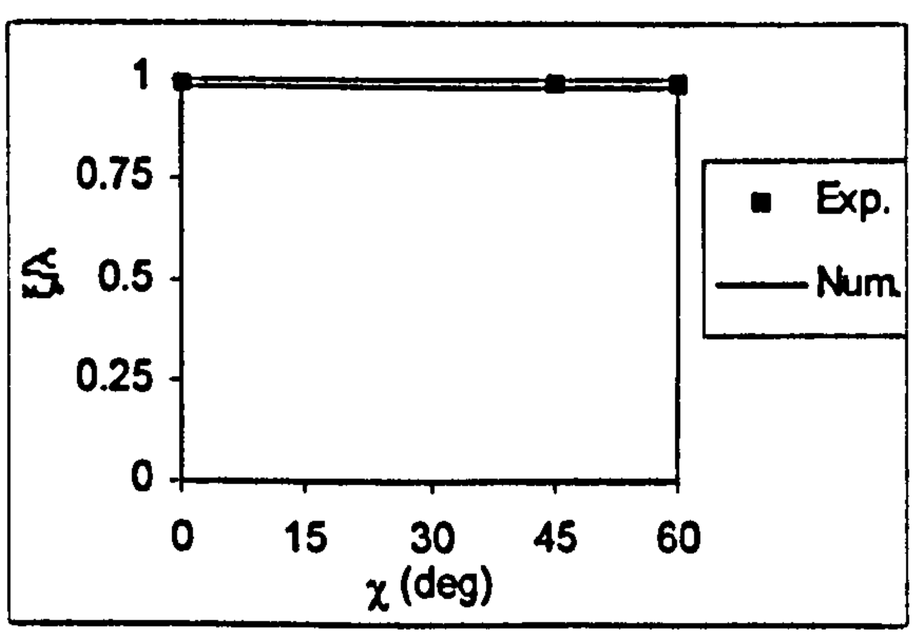

Figure 10.27 Wave induced yaw moment (Fn=0.3, λ/L=1.5, H/λ=1/20, ϕ=0°, θ=0°, sinkage=0 m)

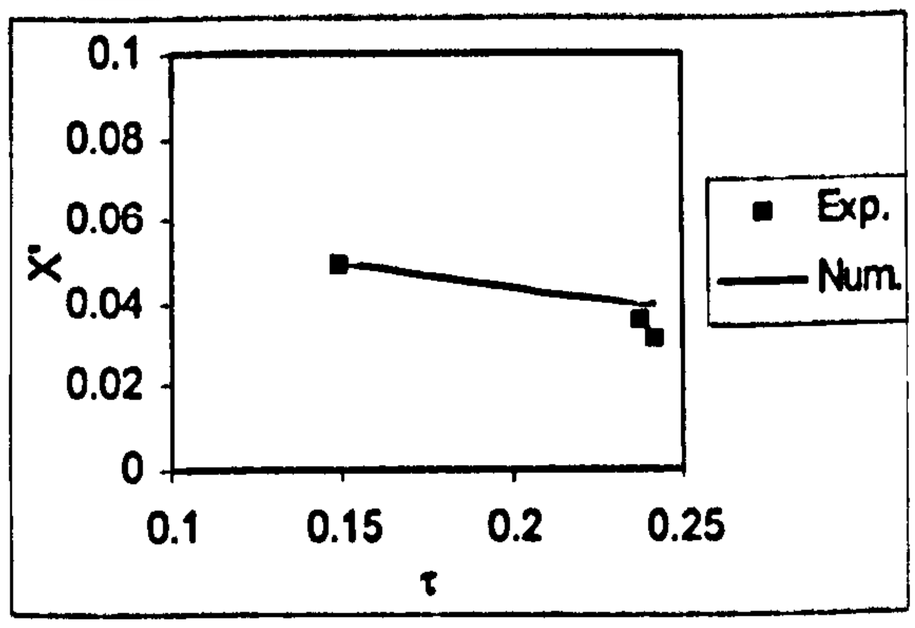

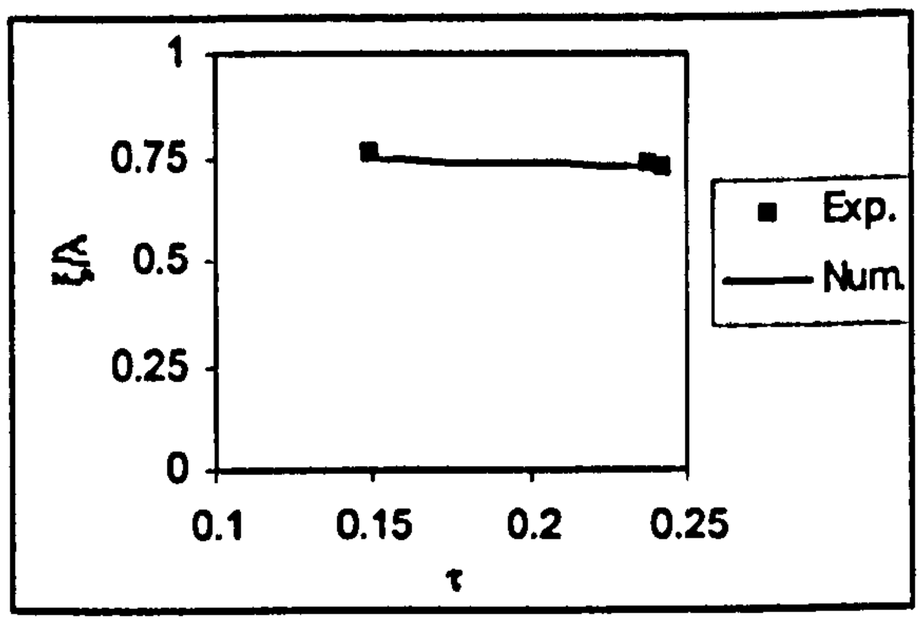

Figure 10.28 Wave induced surge force (λ/L=1.5, H/λ=1/15, χ=0°, ϕ=0°, θ=0°, sinkage=0 m)

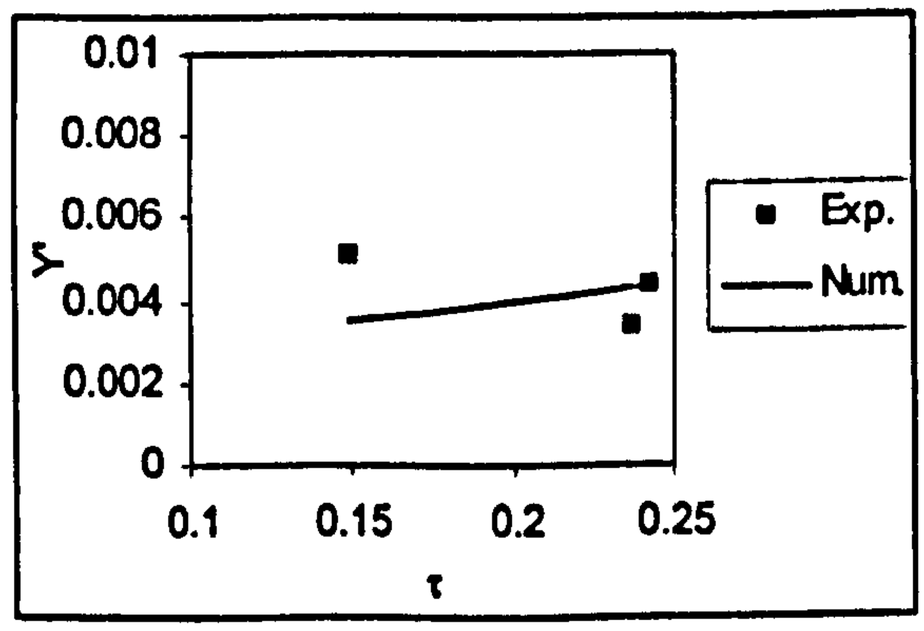

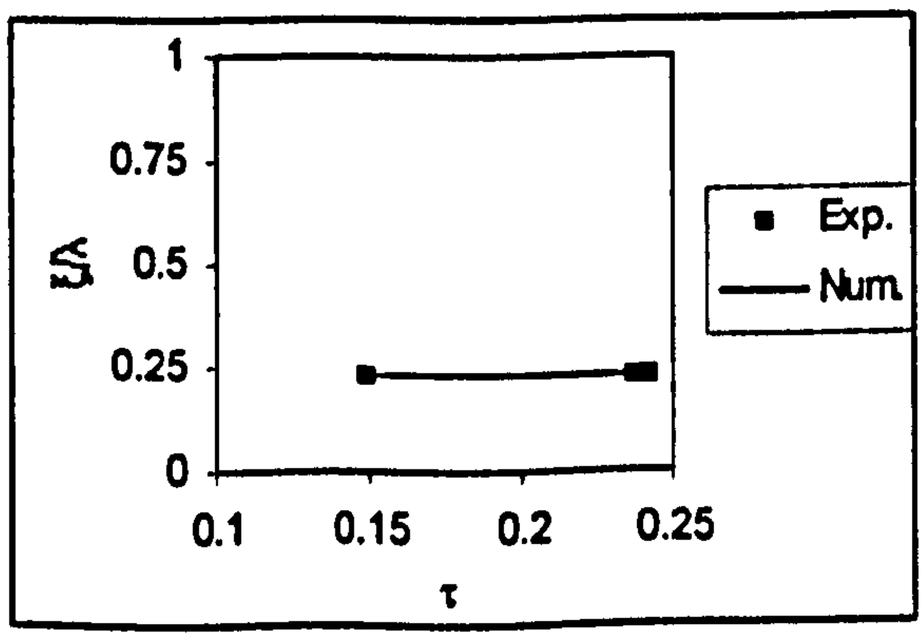

Figure 10.29 Wave induced sway moment (λ/L=1.5, H/λ=1/15, χ=0°, ϕ=0°, θ=0°, sinkage=0 m)

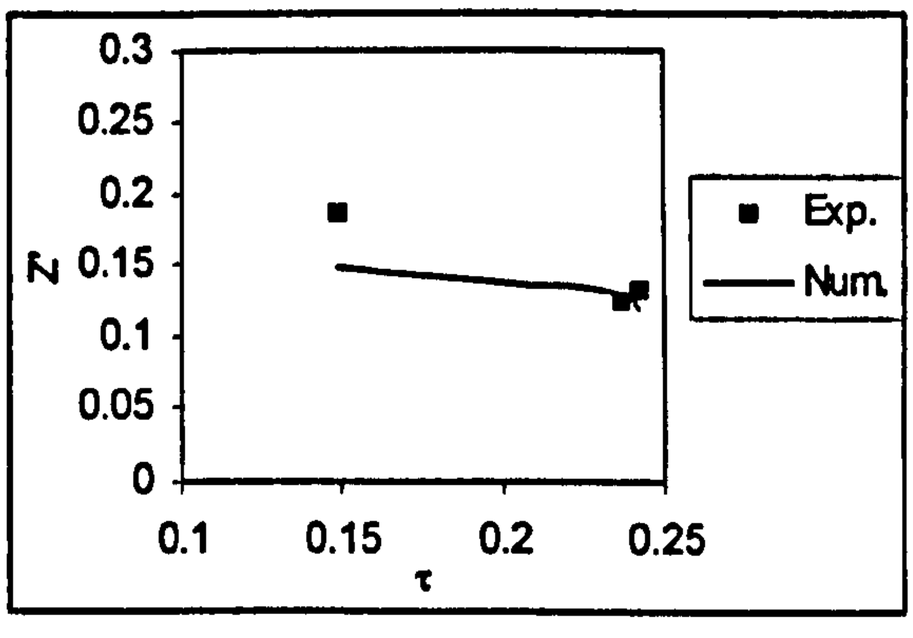

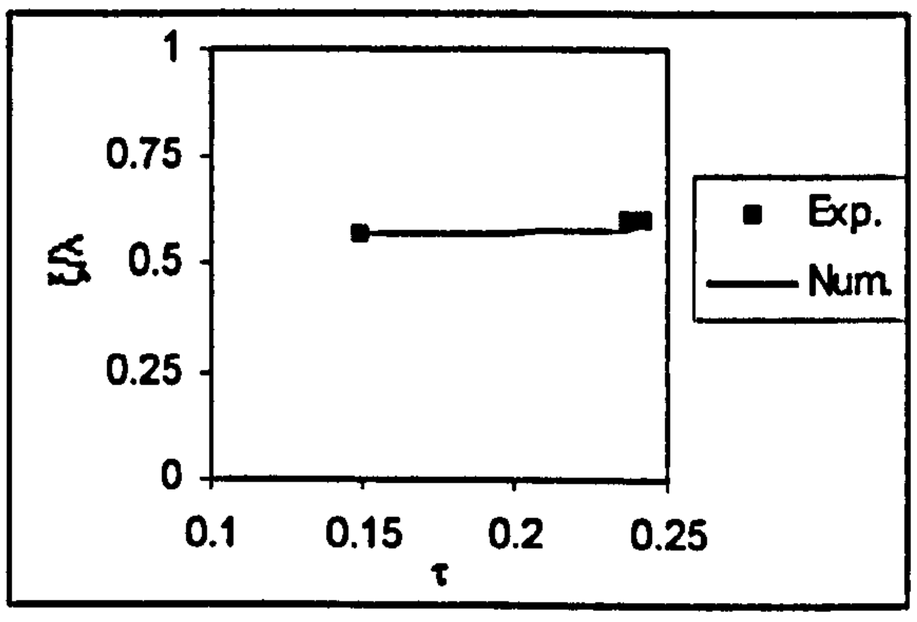

Figure 10.30 Wave induced heave force ($\lambda/L=1.5$, $H/\lambda=1/15$, $\chi=0°$, $\phi=0°$, $\theta=0°$, sinkage=0 m)

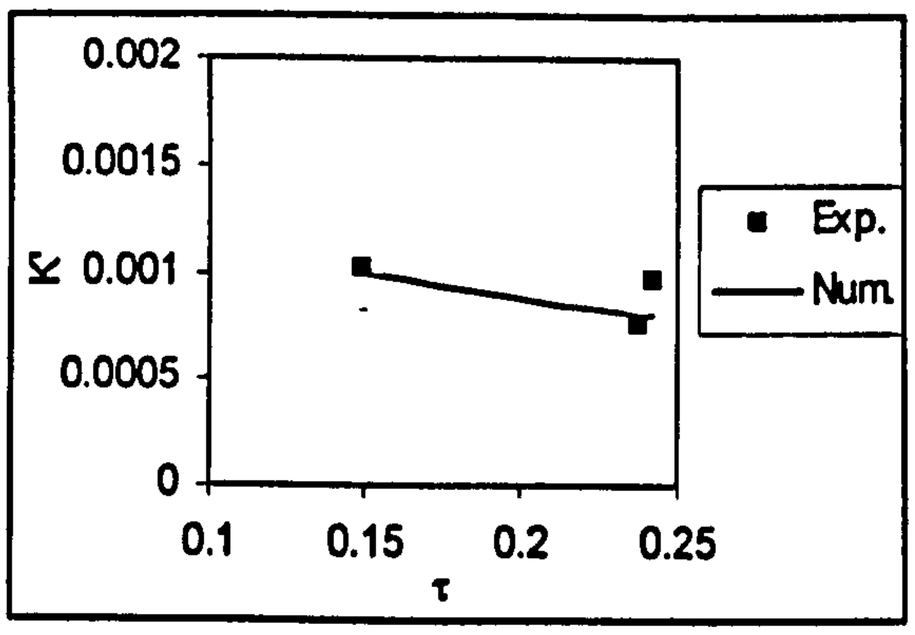

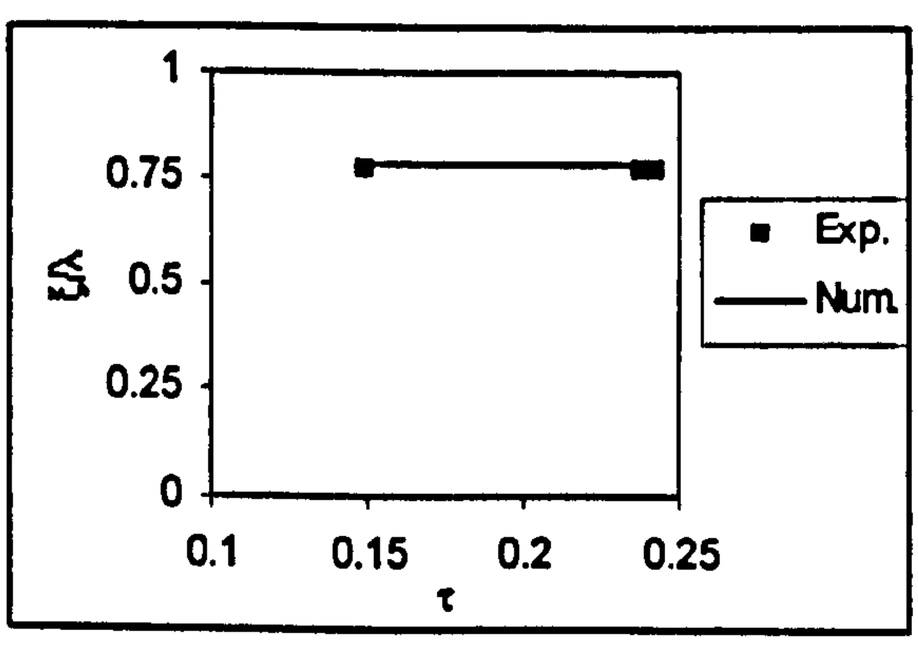

Figure 10.31 Wave induced roll moment ($\lambda/L=1.5$, $H/\lambda=1/15$, $\chi=0°$, $\phi=0°$, $\theta=0°$, sinkage=0.m)

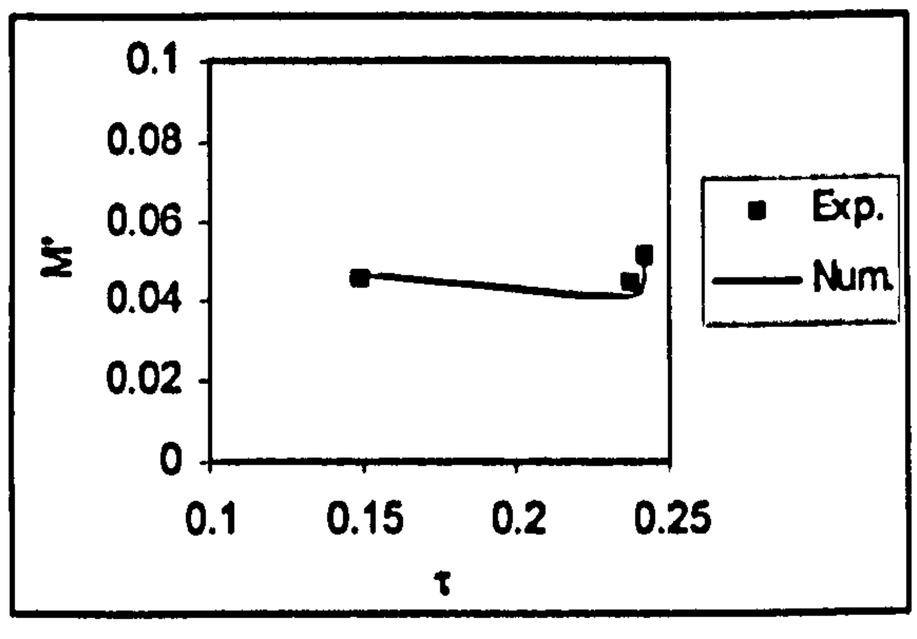

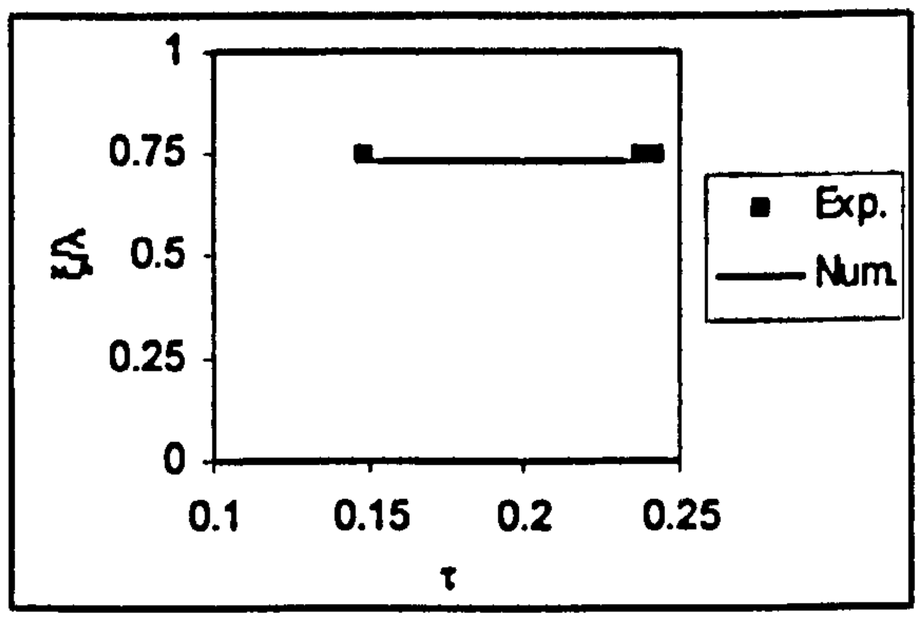

Figure 10.32 Wave induced pitch moment ($\lambda/L=1.5$, $H/\lambda=1/15$, $\chi=0°$, $\phi=0°$, $\theta=0°$, sinkage=0 m)

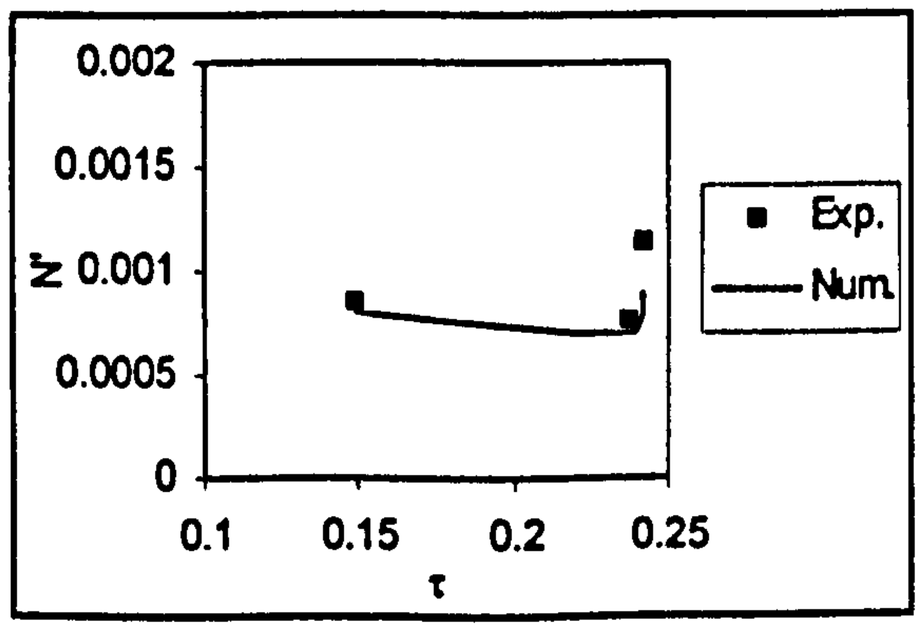

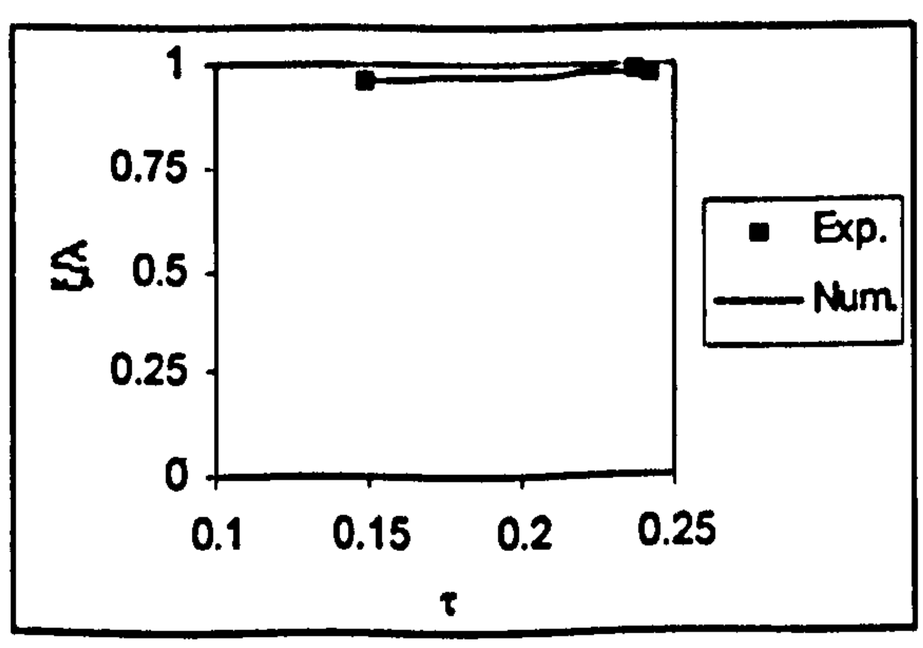

Figure 10.33 Wave induced yaw moment ($\lambda/L=1.5$, $H/\lambda=1/15$, $\chi=0°$, $\phi=0°$, $\theta=0°$, sinkage=0m)

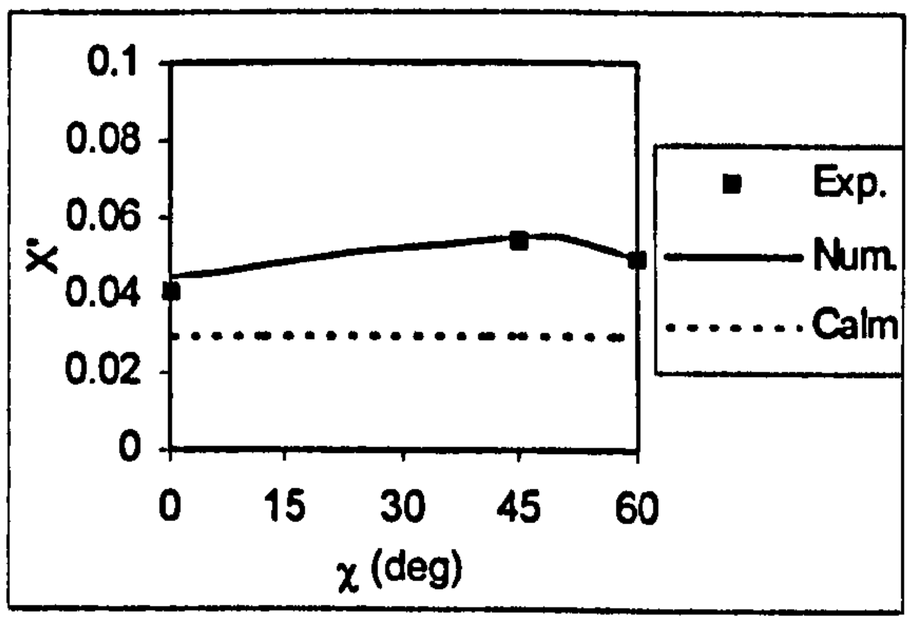

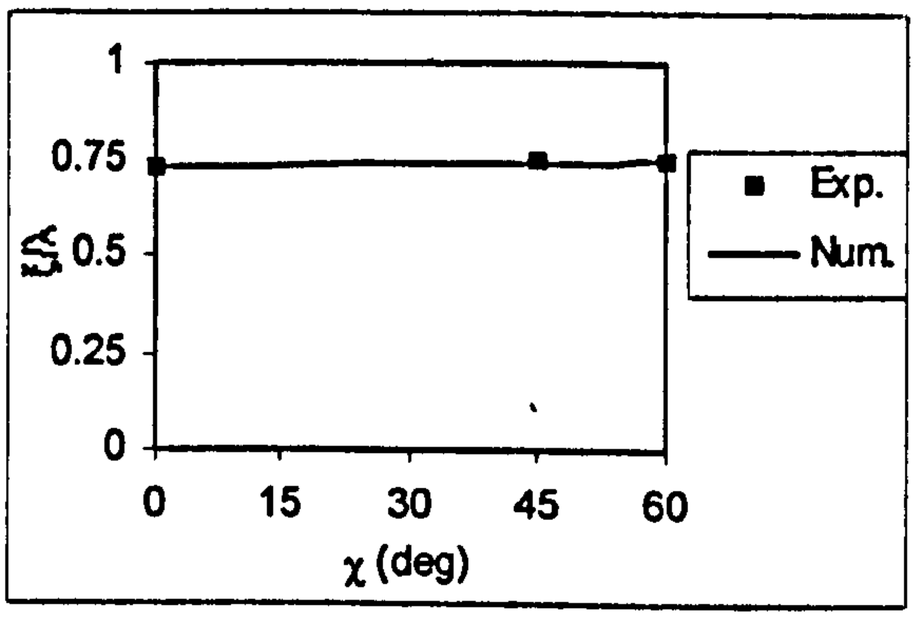

Figure 10.34 Wave induced surge force (Fn=0.3, λ/L=1.5, H/λ=1/20, ϕ=10°, θ=-1.43°, sinkage=-0.2m)

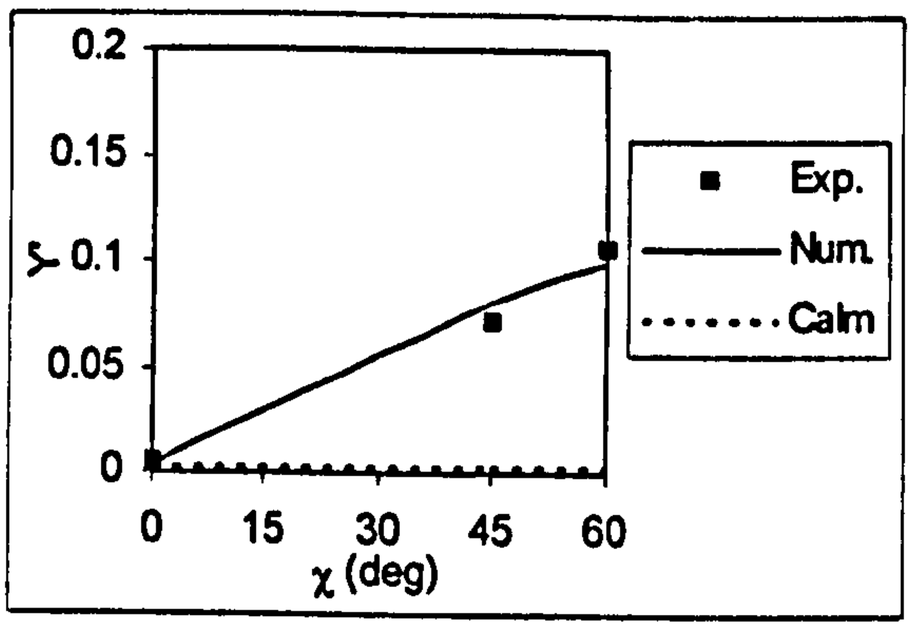

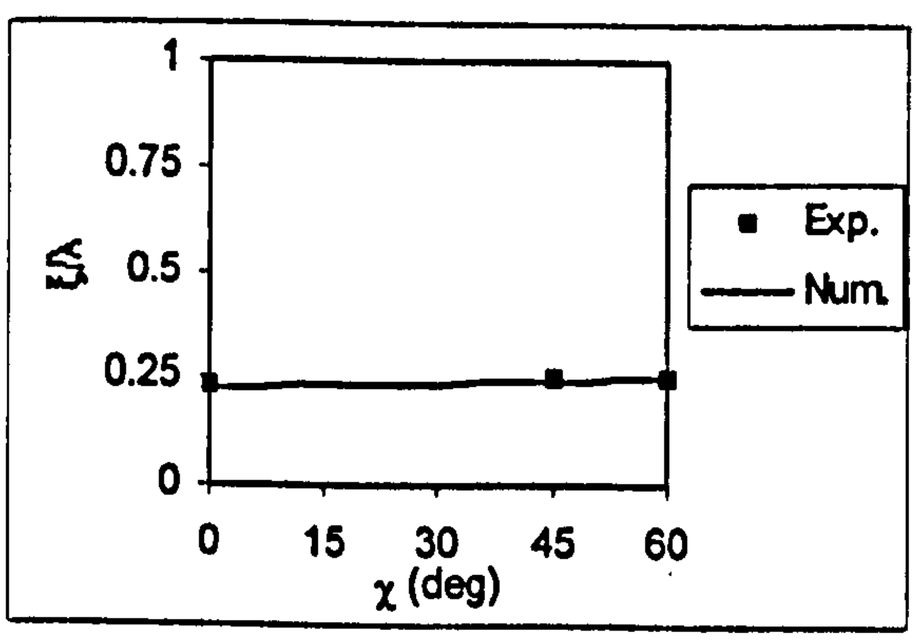

Figure 10.35 Wave induced sway force (Fn=0.3, λ/L=1.5, H/λ=1/20, ϕ=10°, θ=-1.43°, sinkage=-0.2m)

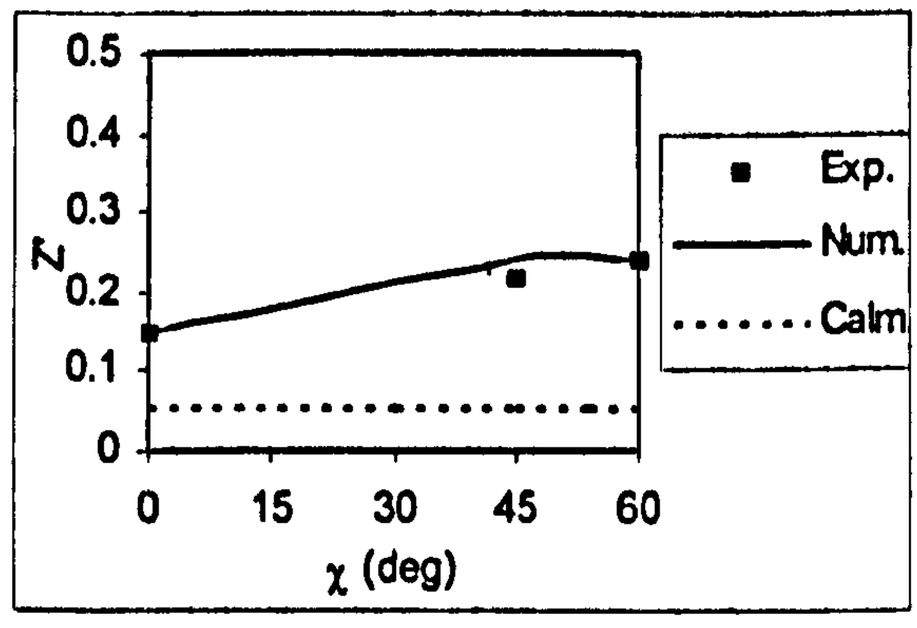

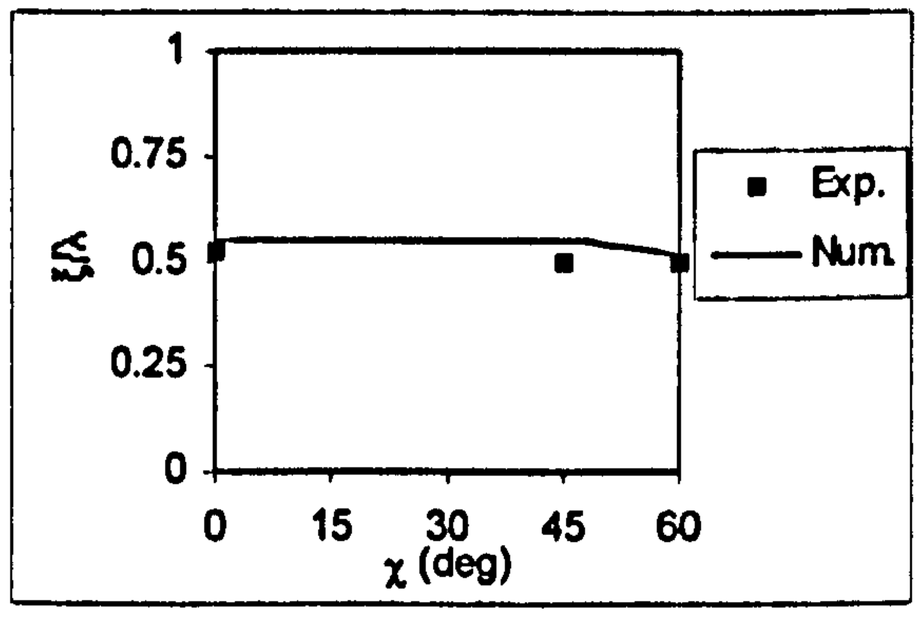

Figure 10.36 Wave induced heave force (Fn=0.3, λ/L=1.5, H/λ=1/20, ϕ=10°, θ=-1.43°, sinkage=-0.2m)

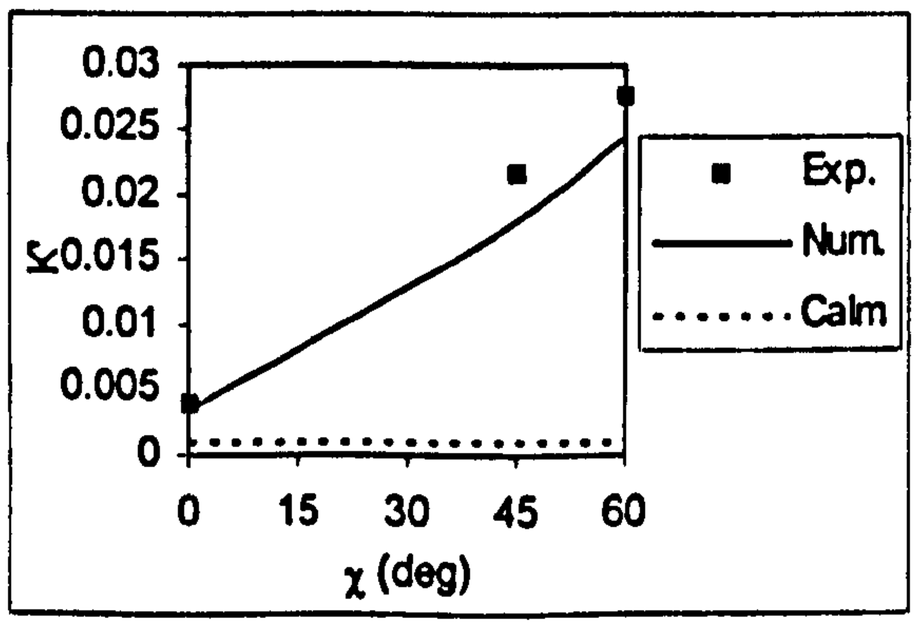

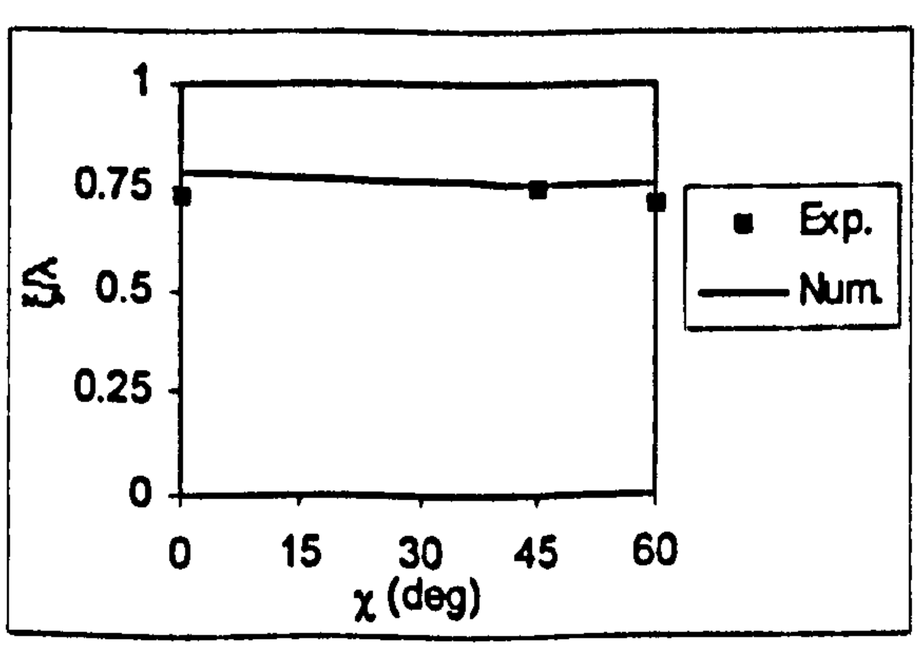

Figure 10.37 Wave induced roll moment (Fn=0.3, λ/L=1.5, H/λ=1/20, ϕ=10°, θ=-1.43°, sinkage=-0.2m)

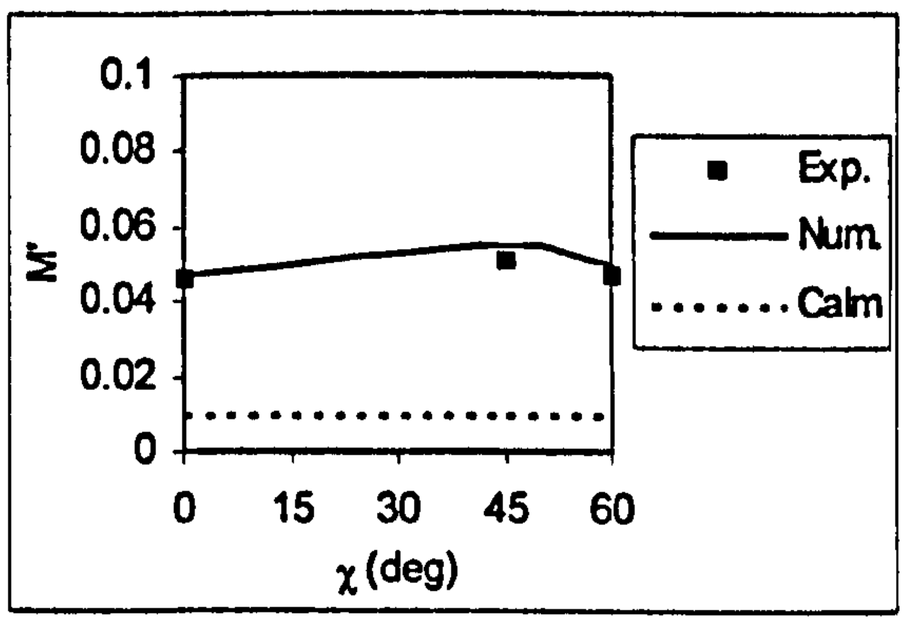

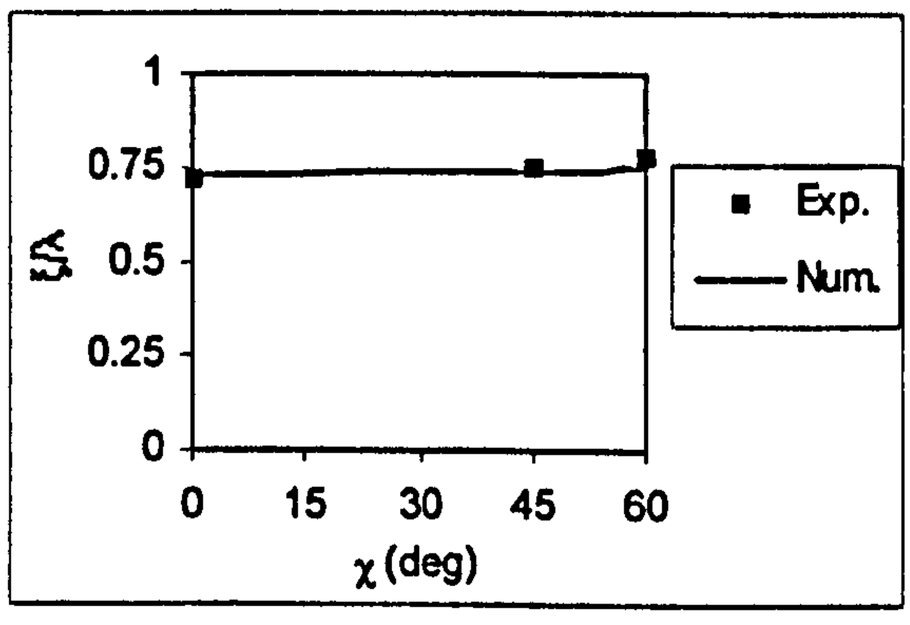

Figure 10.38 Wave induced pitch moment (Fn=0.3, λ/L=1.5, H/λ=1/20, ϕ=10°, θ=-1.43°, sinkage=-0.2m)

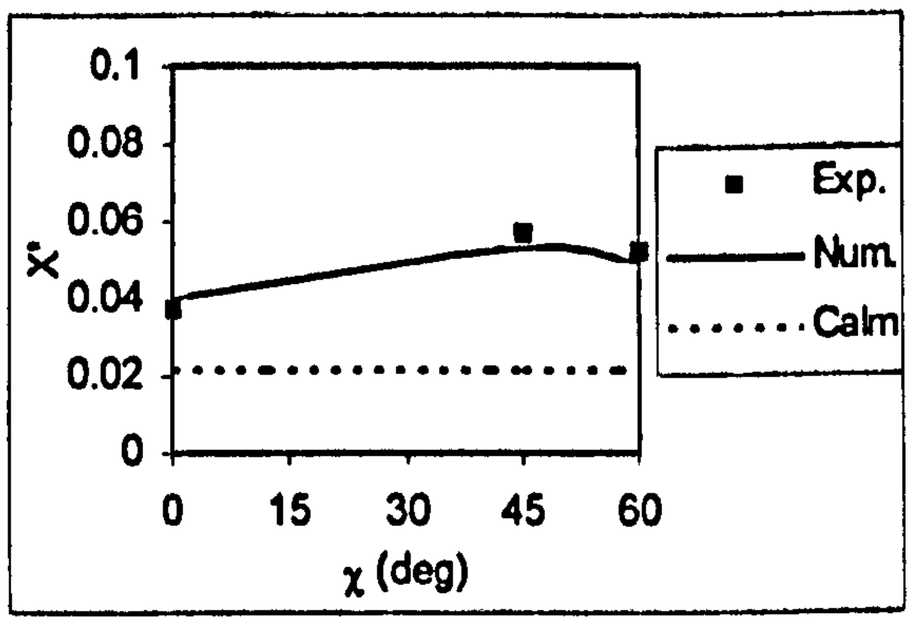

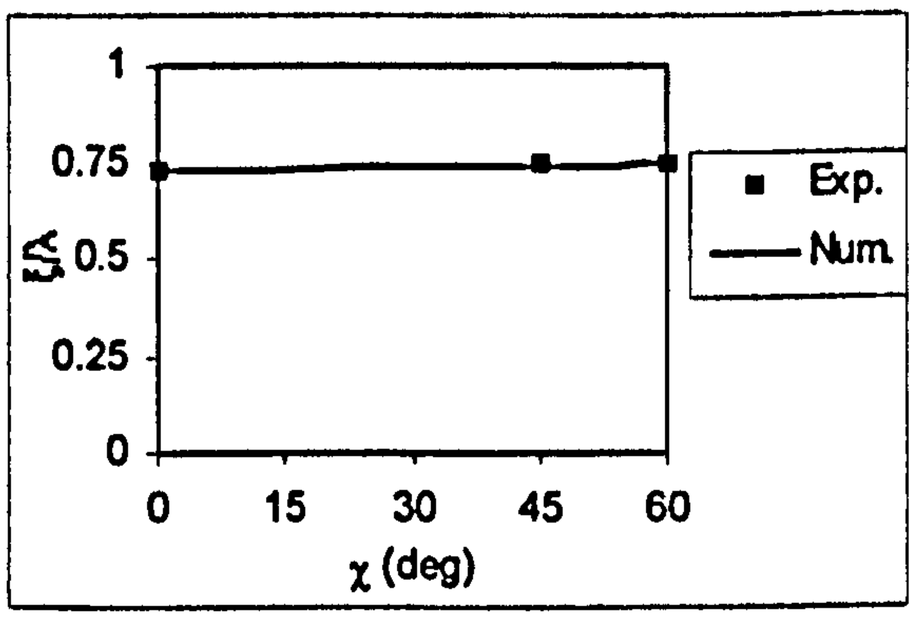

Figure 10.40 Wave induced surge force (Fn=0.3, λ/L=1.5, H/λ=1/20, ϕ=10°, θ=-1.43°, sinkage=0.2m)

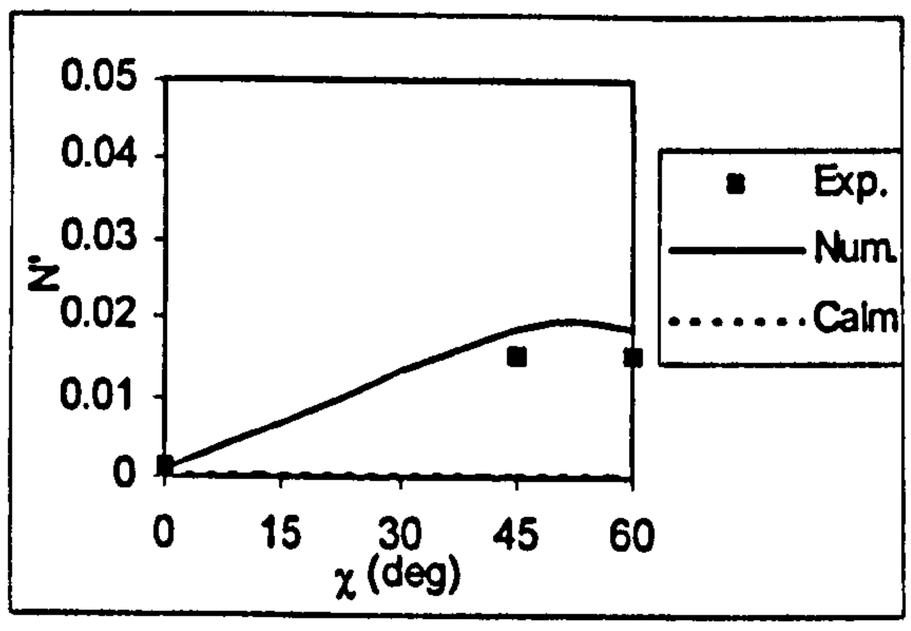

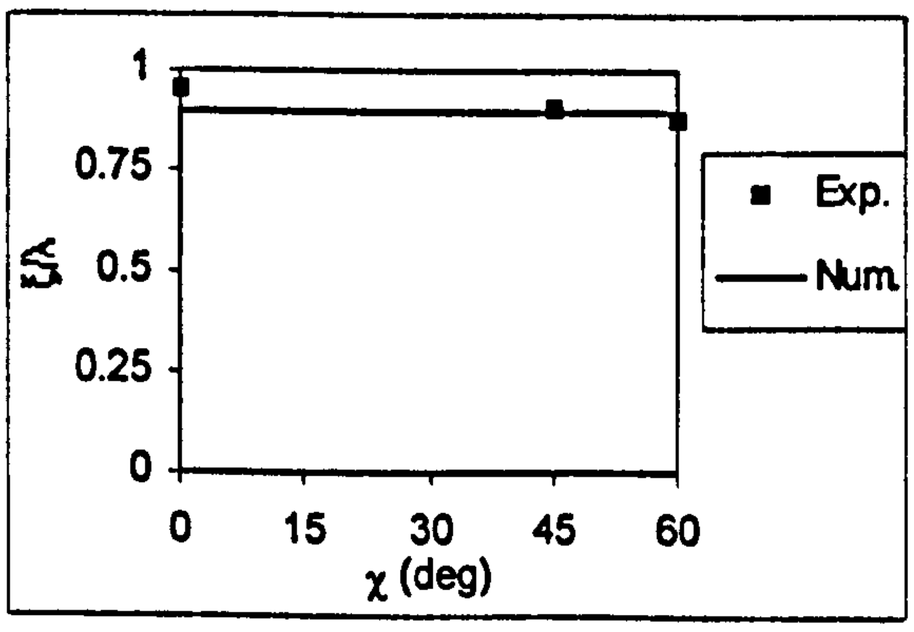

Figure 10.39 Wave induced yaw moment (Fn=0.3, λ/L=1.5, H/λ=1/20, ϕ=10°, θ=-1.43°, sinkage=-0.2m)

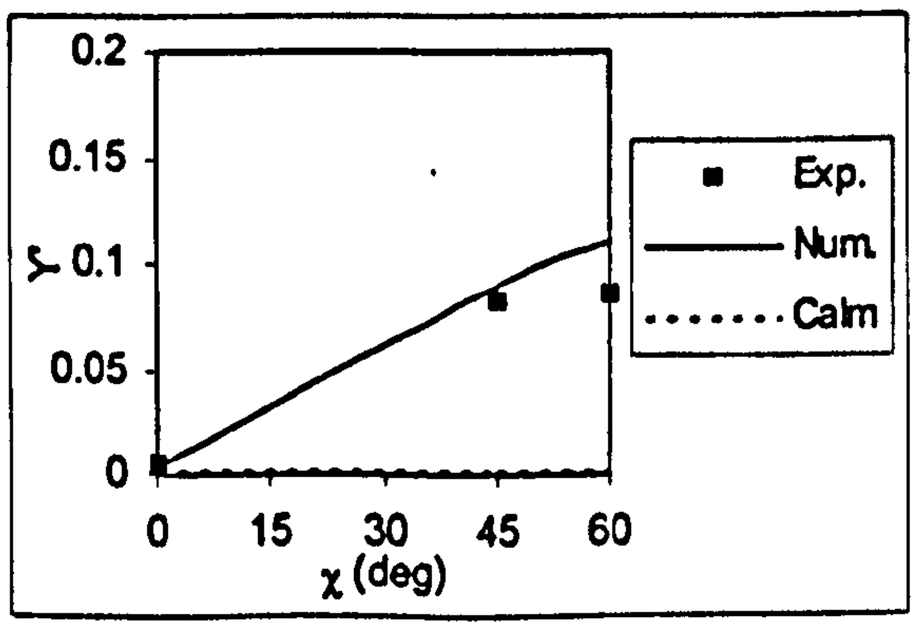

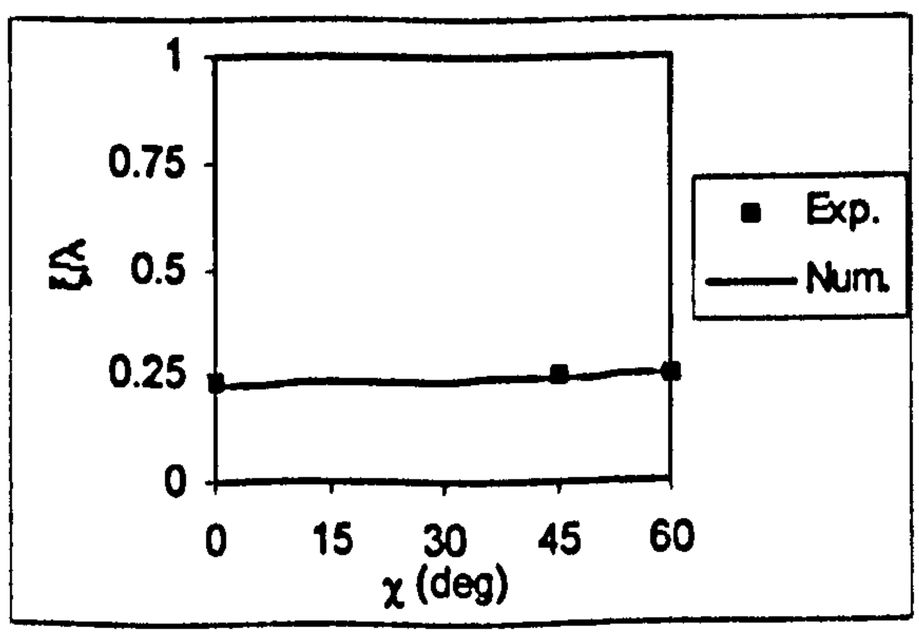

Figure 10.41 Wave induced sway force (Fn=0.3, λ/L=1.5, H/λ=1/20, ϕ=10°, θ=-1.43°, sinkage=0.2m)

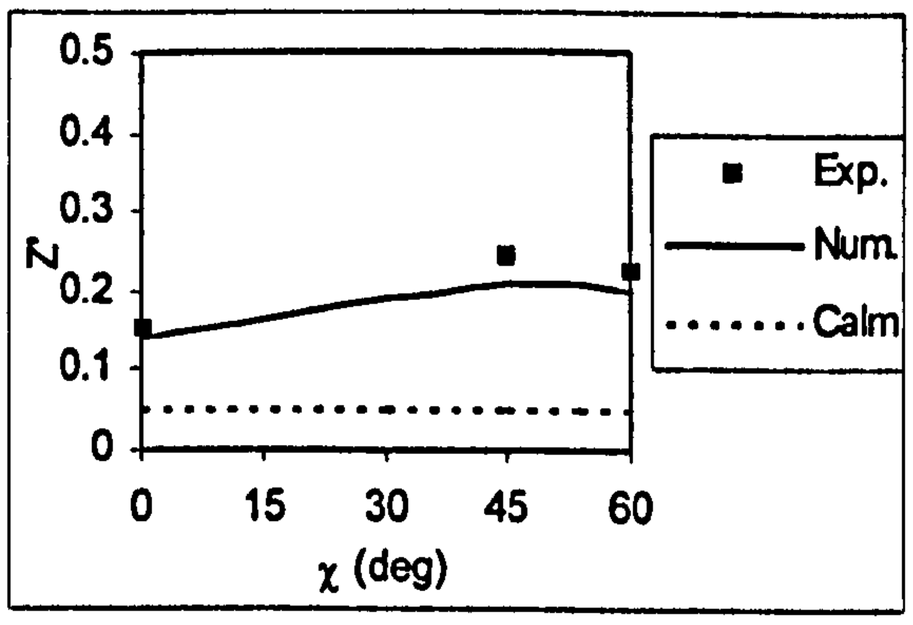

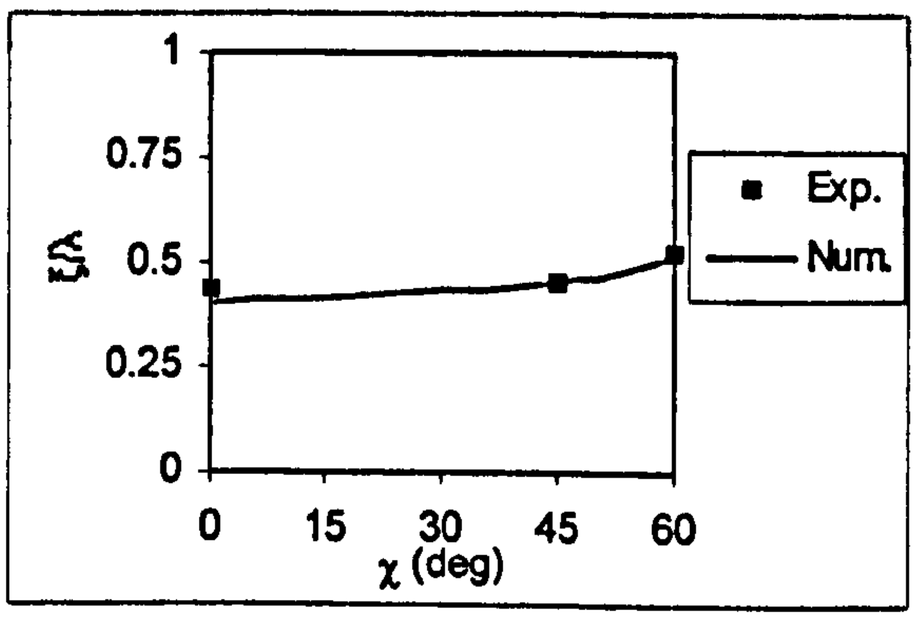

Figure 10.42 Wave induced heave force (Fn=0.3, λ/L=1.5, H/λ=1/20, ϕ=10°, θ=-1.43°, sinkage=0.2m)

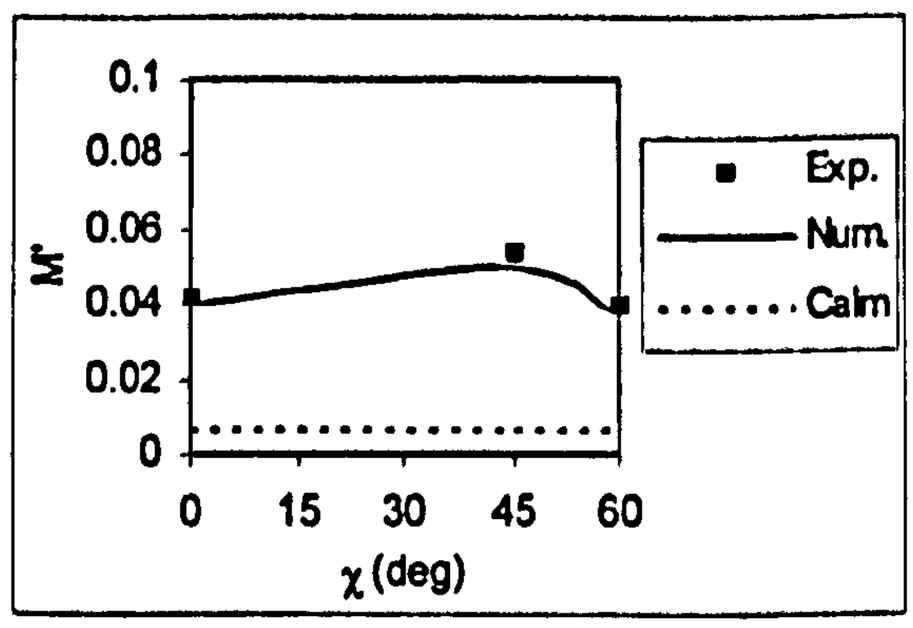

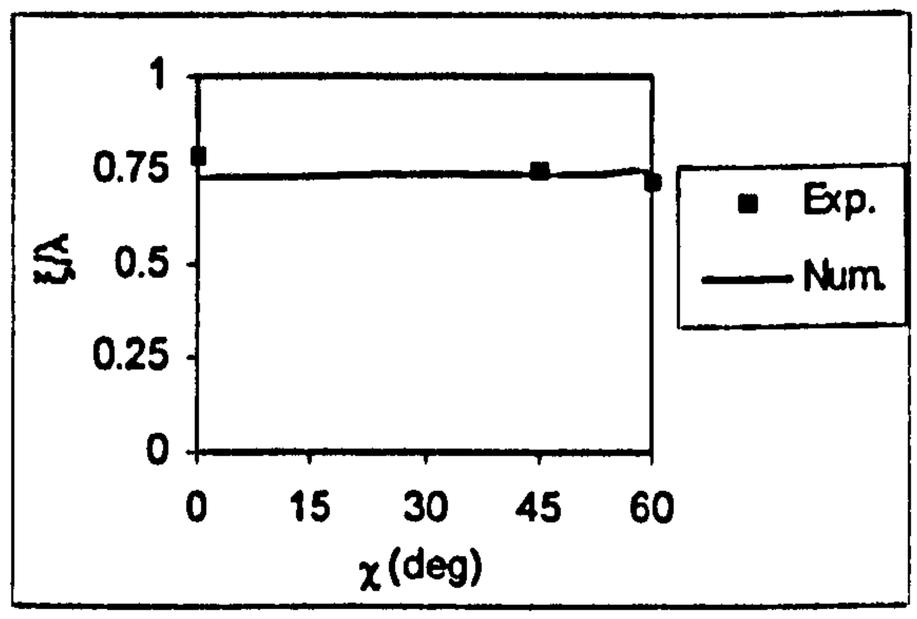

Figure 10.44 Wave induced pitch moment (Fn=0.3, λ/L=1.5, H/λ=1/20, ϕ=10°, θ=-1.43°, sinkage=0.2m)

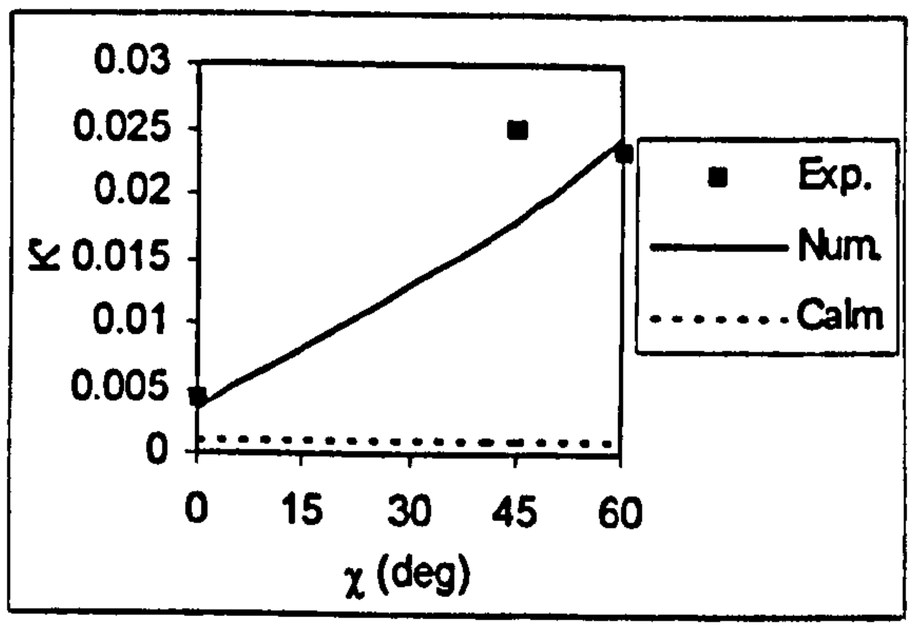

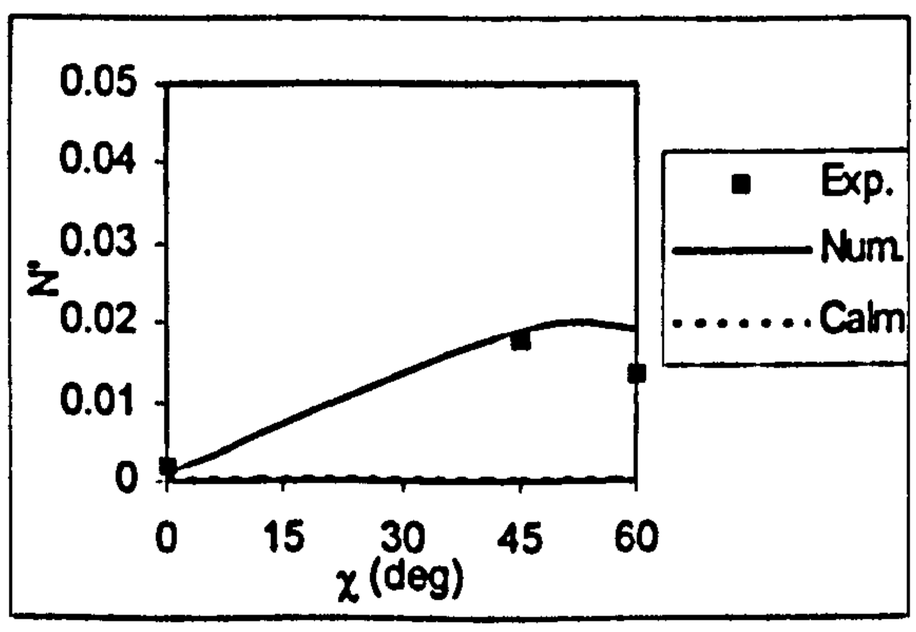

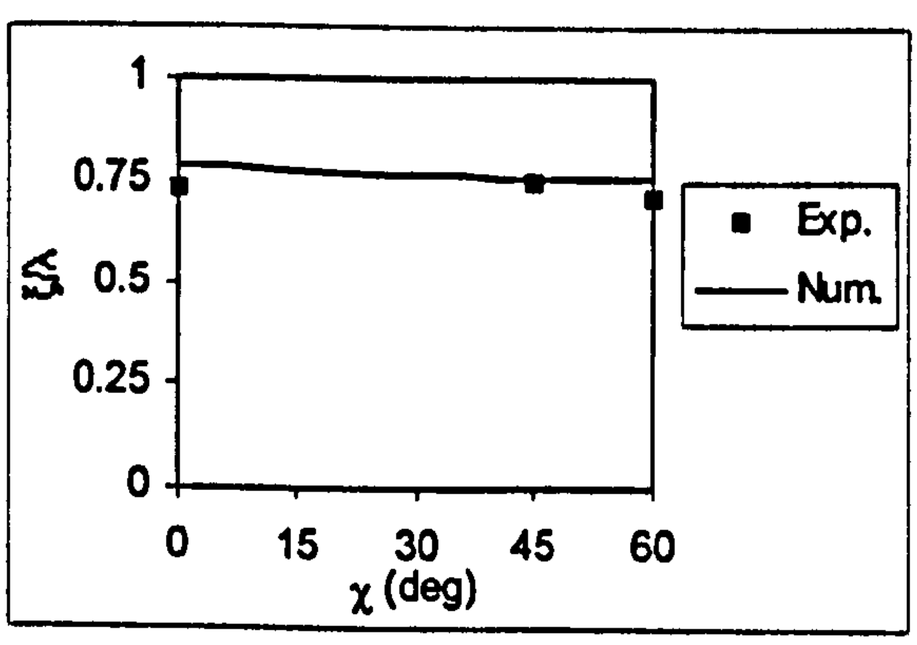

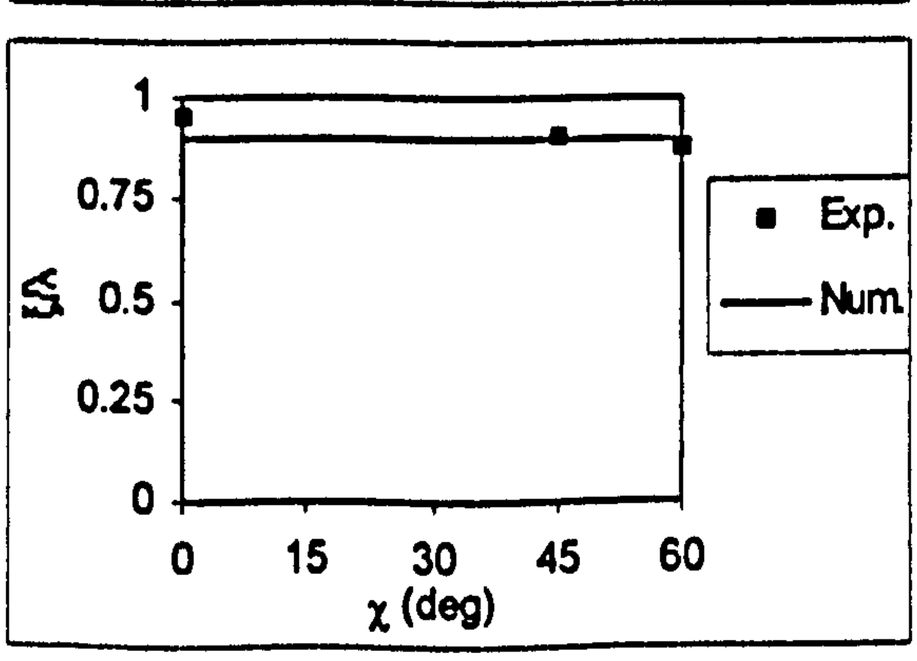

Figure 10.43 Wave induced roll moment (Fn=0.3, λ/L=1.5, H/λ=1/20, ϕ=10°, θ=-1.43°, sinkage=0.2m)

Figure 10.45 Wave induced yaw moment (Fn=0.3, λ/L=1.5, H/λ=1/20, ϕ=10°, θ=-1.43°, sinkage=0.2m)

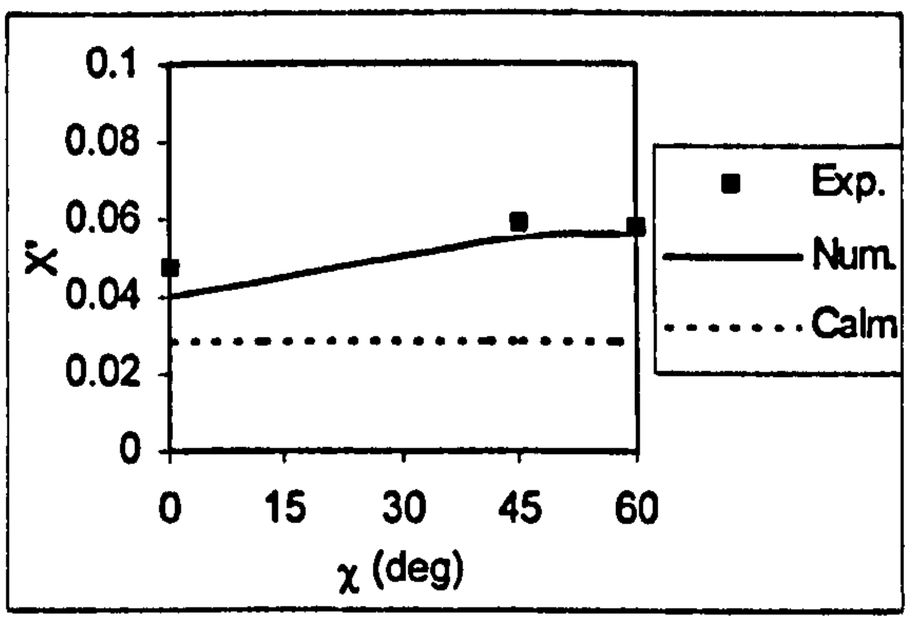

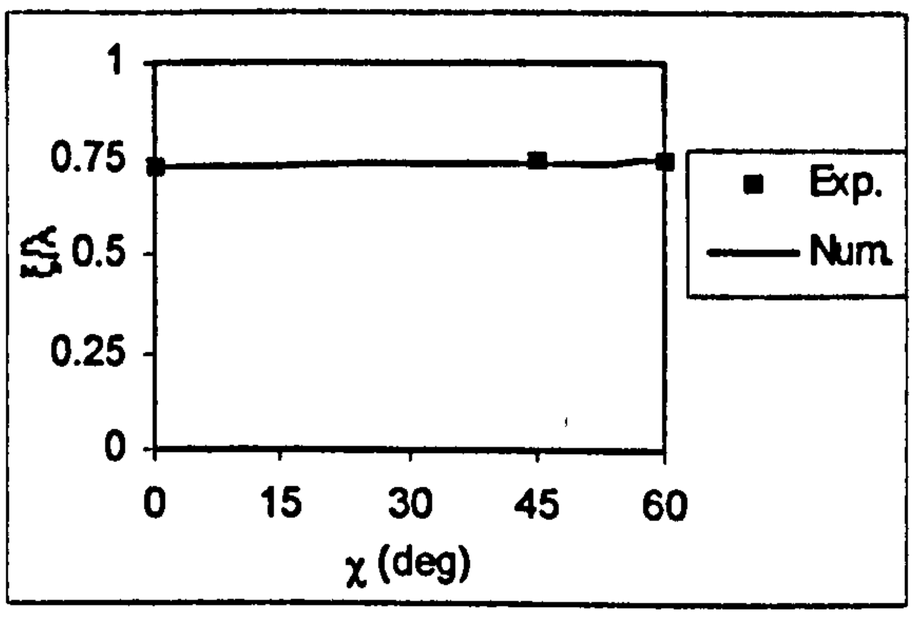

Figure 10.46 Wave induced surge force (Fn=0.3, λ/L=1.5, H/λ=1/20, ϕ=10°, θ=1.43°, sinkage=-0.2m)

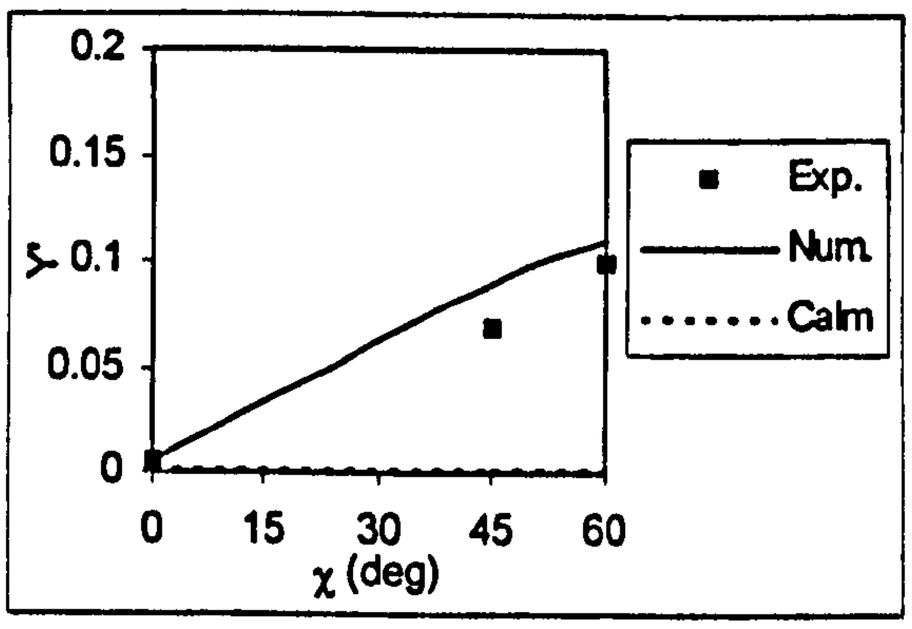

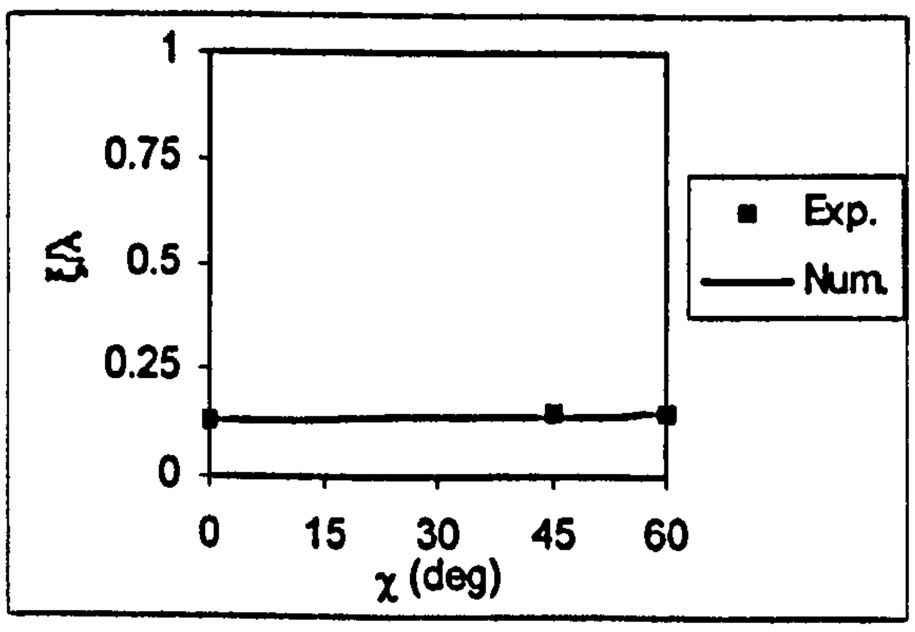

Figure 10.47 Wave induced sway force (Fn=0.3, λ/L=1.5, H/λ=1/20, ϕ=10°, θ=1.43°, sinkage=-0.2m)

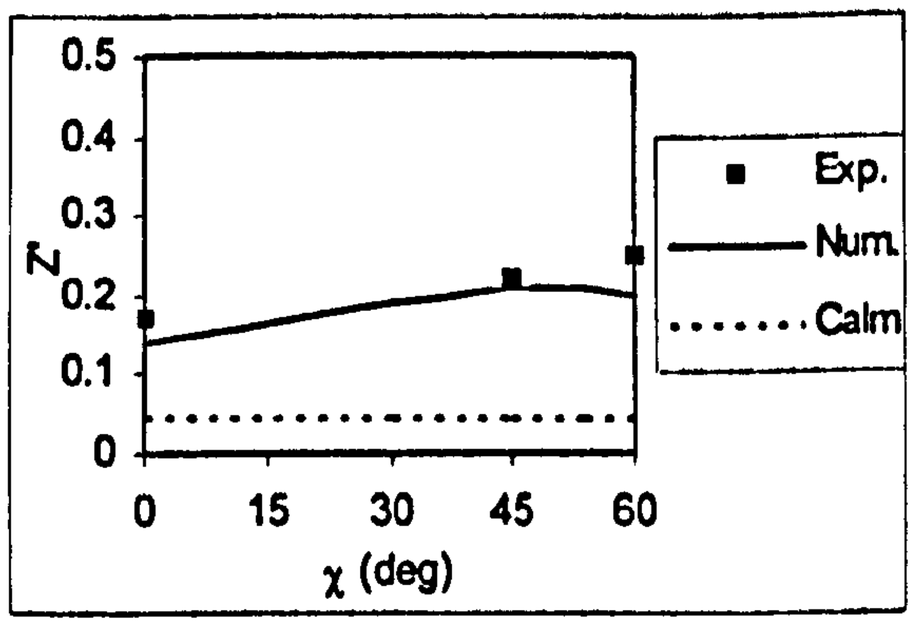

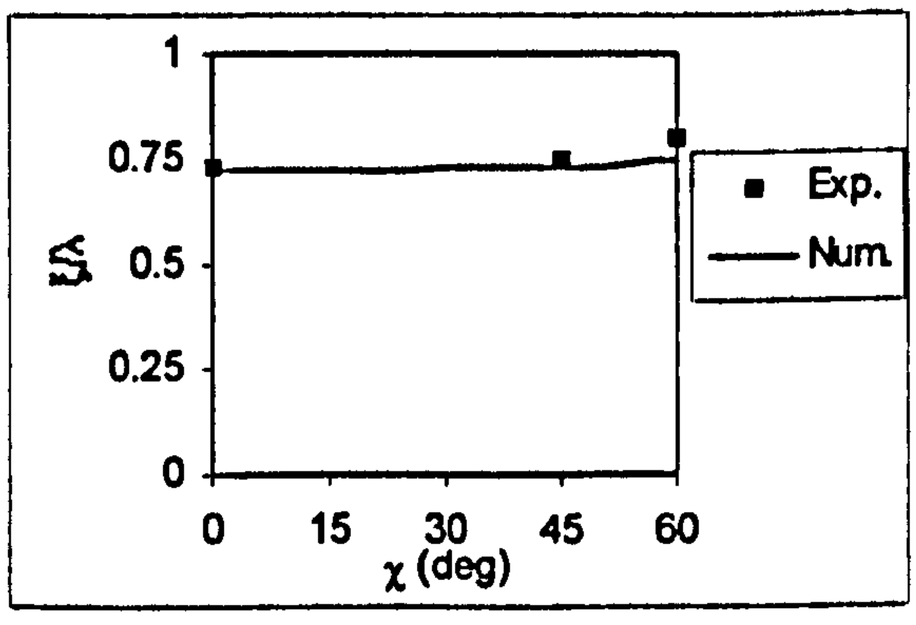

Figure 10.48 Wave induced heave force (Fn=0.3, λ/L=1.5, H/λ=1/20, ϕ=10°, θ=1.43°, sinkage=-0.2m)

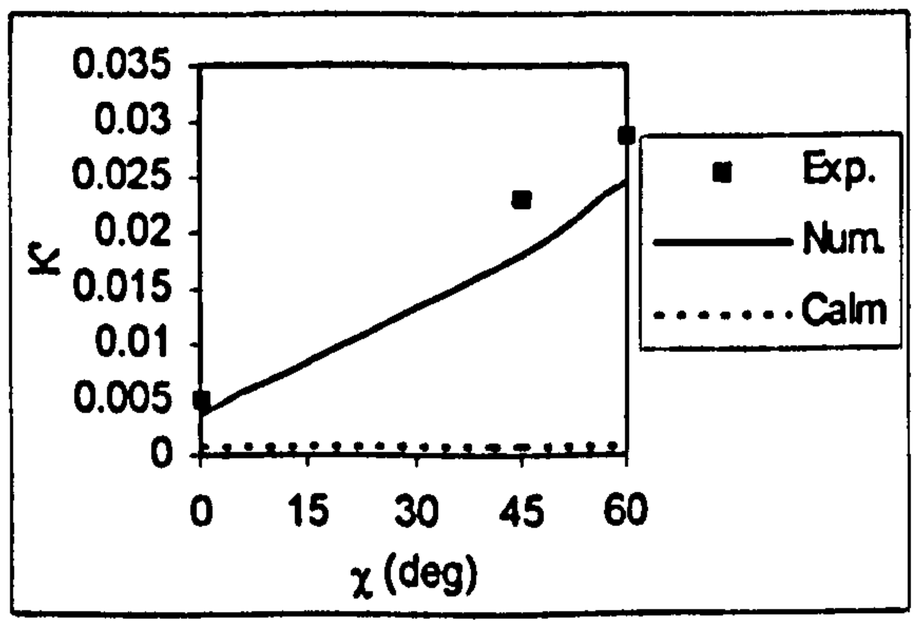

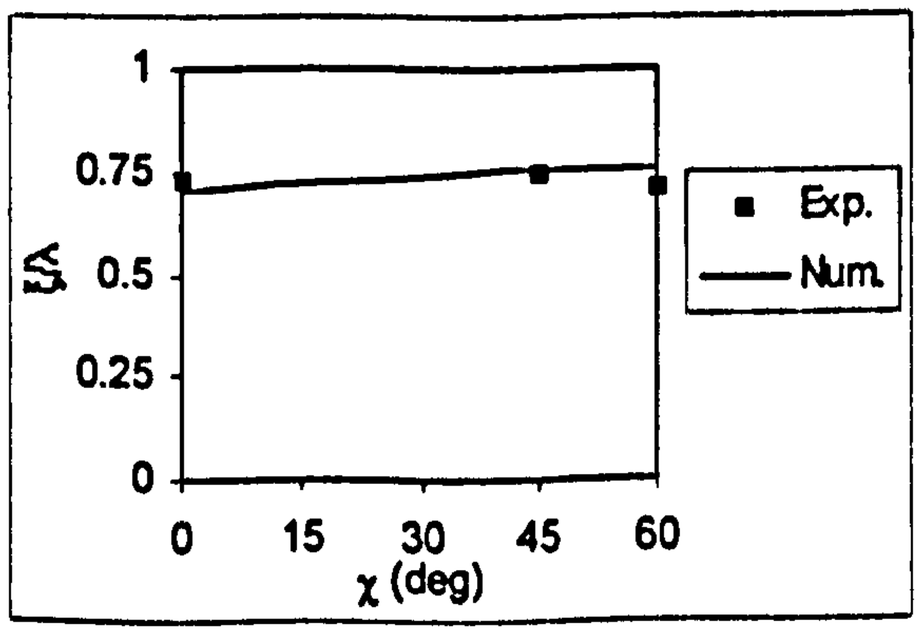

Figure 10.49 Wave induced roll moment (Fn=0.3, λ/L=1.5, H/λ=1/20, ϕ=10°, θ=1.43°, sinkage=-0.2m)

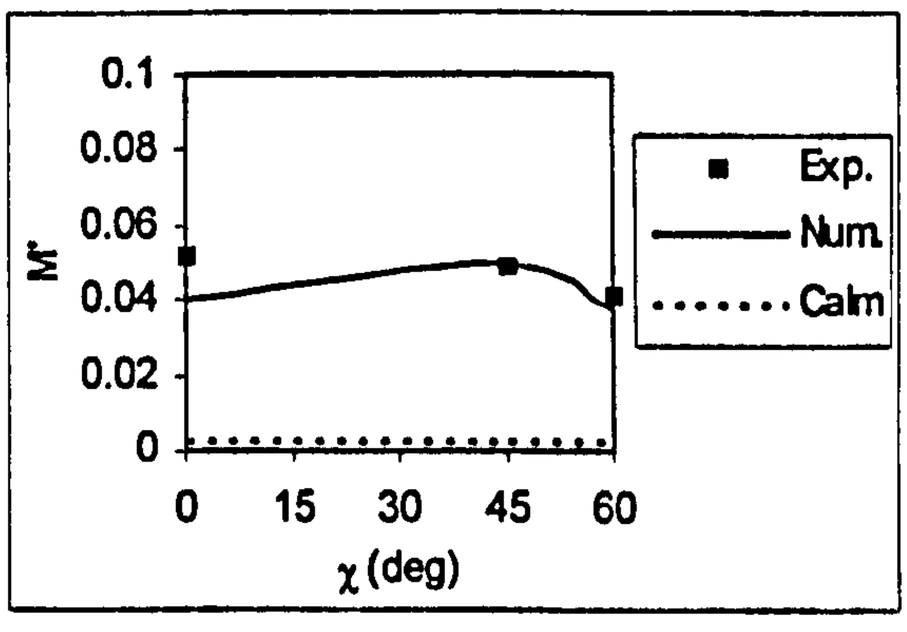

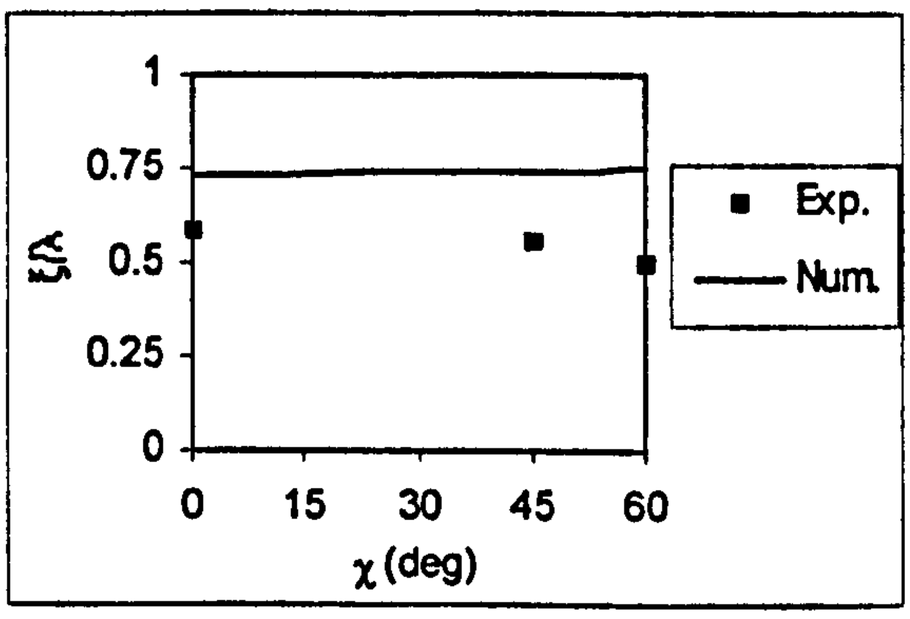

Figure 10.50 Wave induced pitch moment (Fn=0.3, λ/L=1.5, H/λ=1/20, ϕ=10°, θ=1.43°, sinkage=-0.2m)

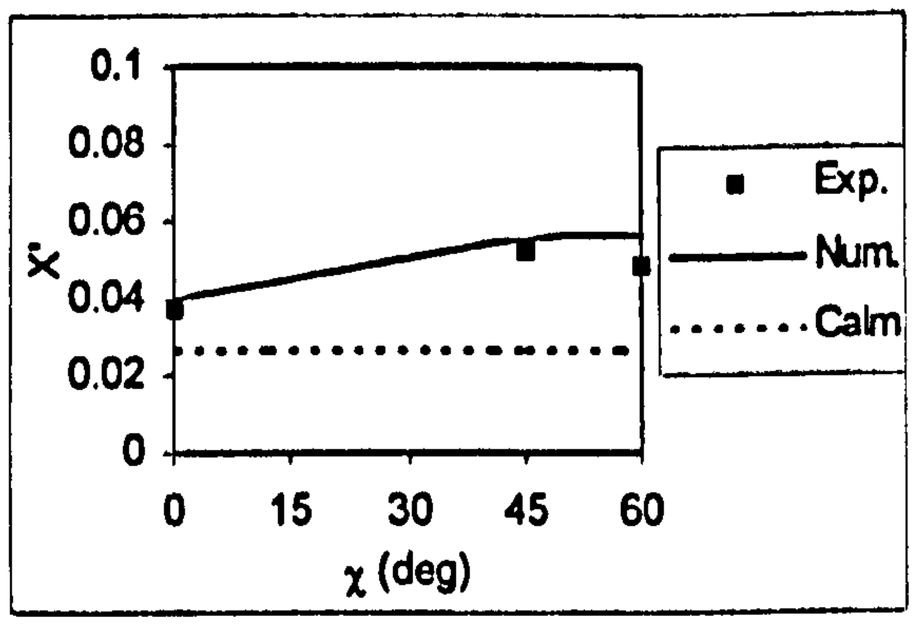

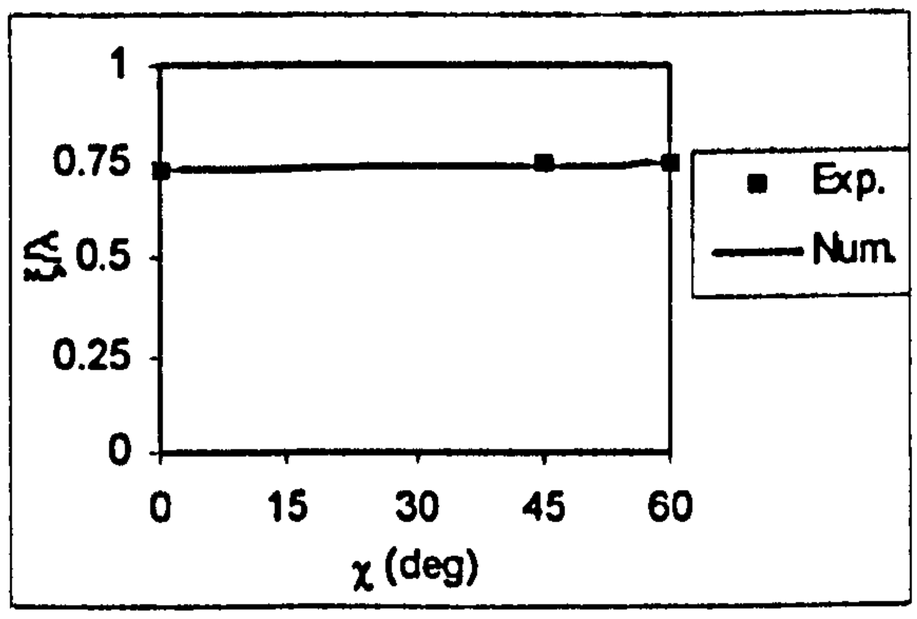

Figure 10.52 Wave induced surge force (Fn=0.3, λ/L=1.5, H/λ=1/20, ϕ=10°, θ=1.43°, sinkage=0.2m)

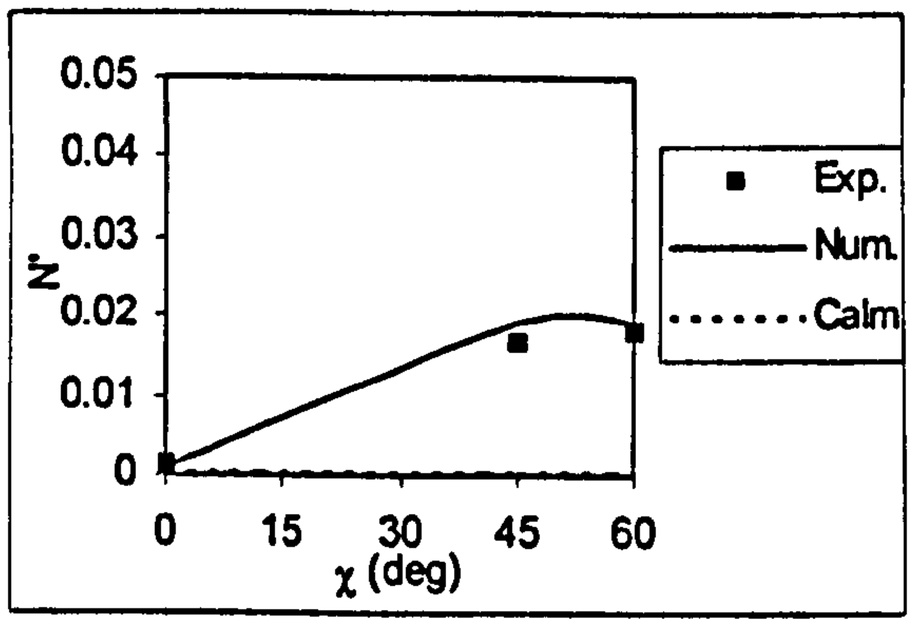

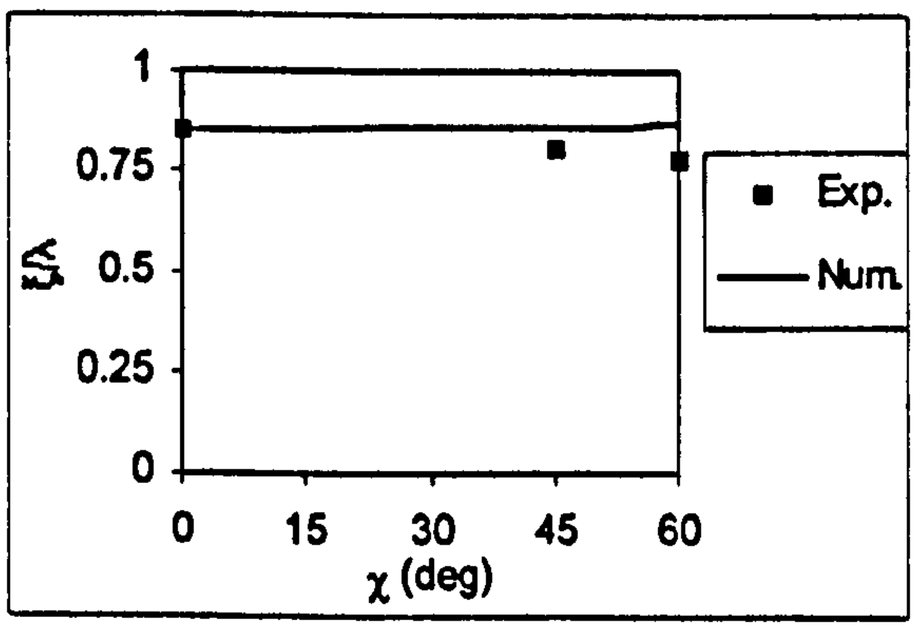

Figure 10.51 Wave induced yaw moment (Fn=0.3, λ/L=1.5, H/λ=1/20, ϕ=10°, θ=1.43°, sinkage=-0.2m)

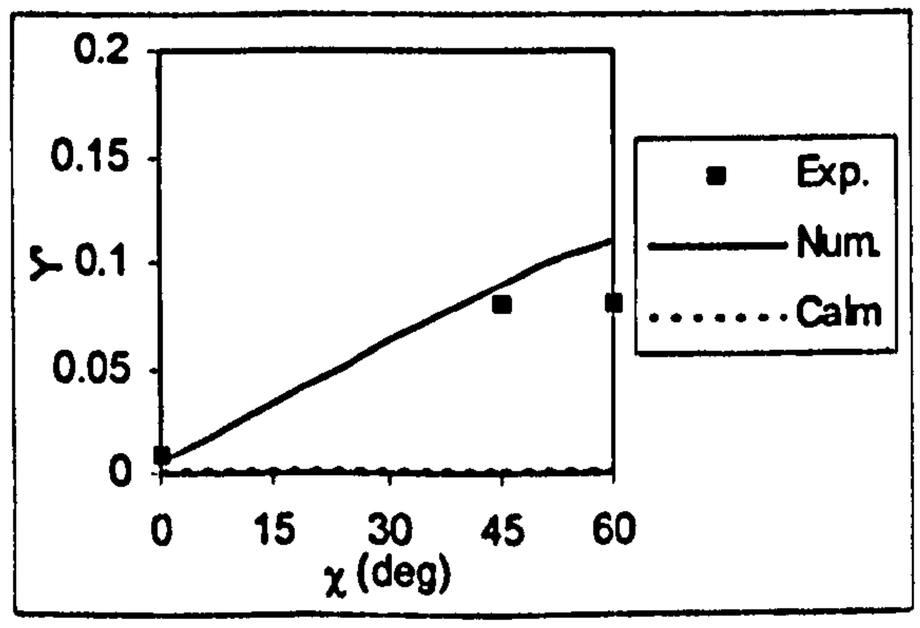

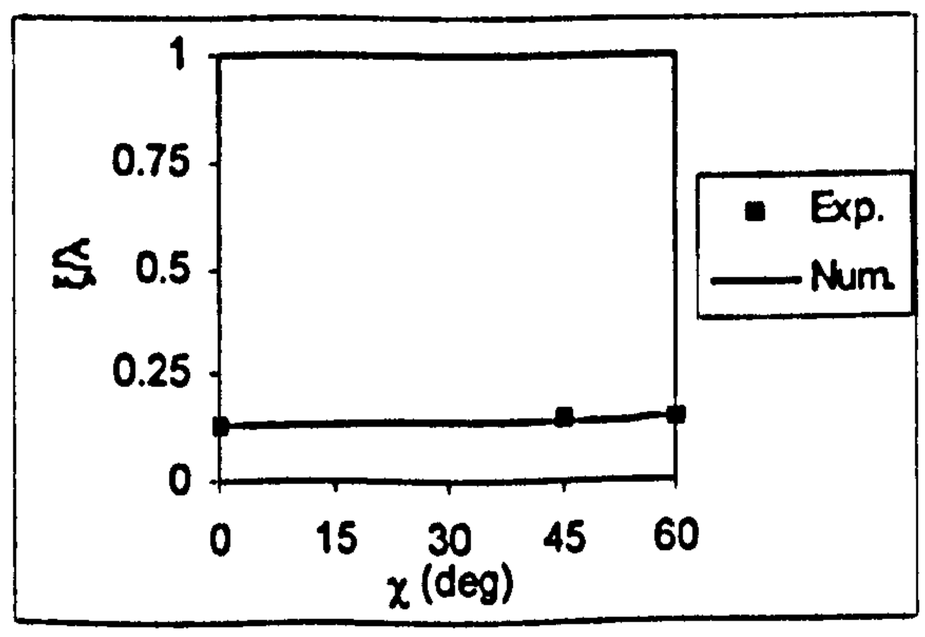

Figure 10.53 Wave induced sway force (Fn=0.3, λ/L=1.5, H/λ=1/20, ϕ=10°, θ=1.43°, sinkage=0.2m)

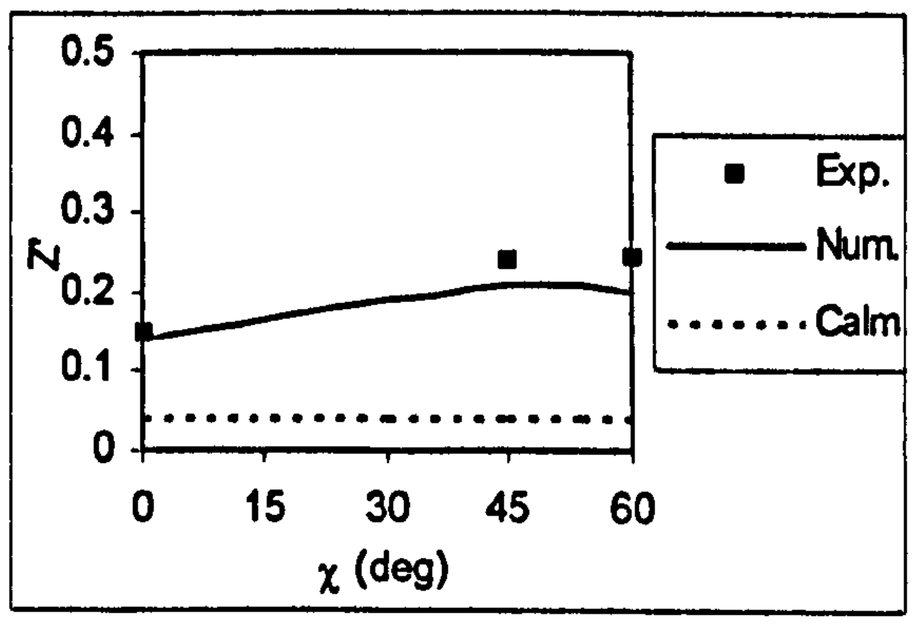

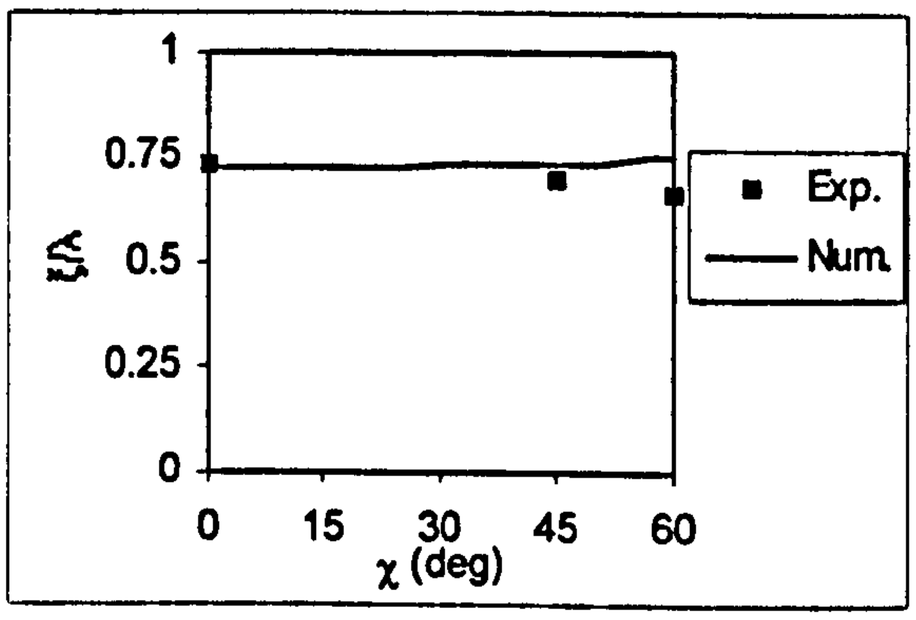

Figure 10.54 Wave induced heave force (Fn=0.3, λ/L=1.5, H/λ=1/20, ϕ=10°, θ=1.43°, sinkage=0.2m)

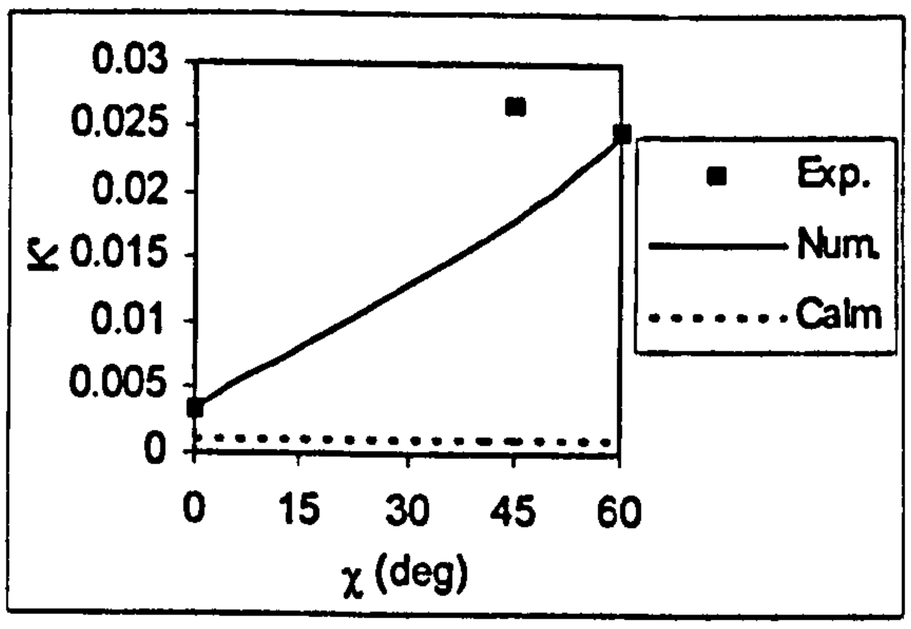

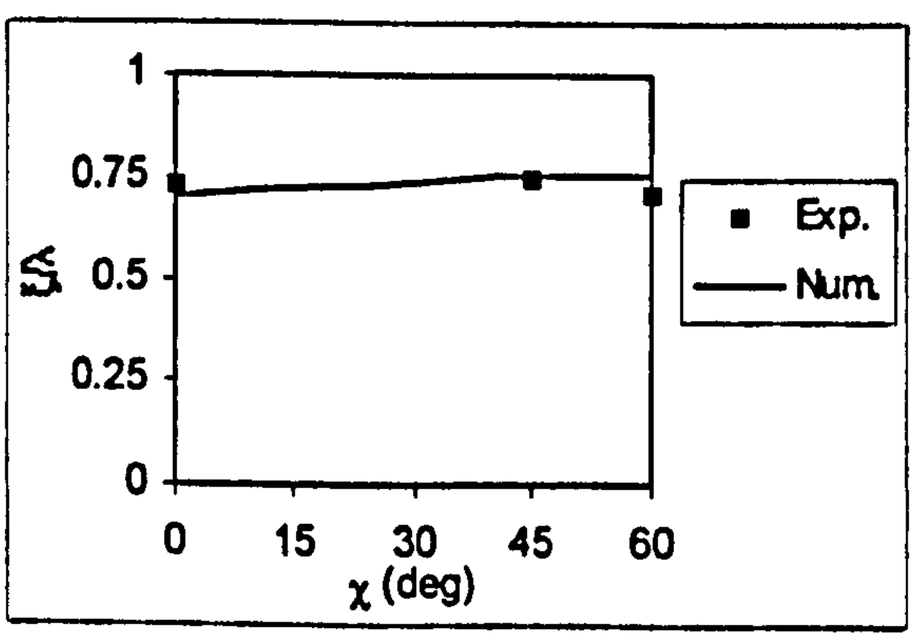

Figure 10.55 Wave induced roll moment (Fn=0.3, λ/L=1.5, H/λ=1/20, ϕ=10°, θ=1.43°, sinkage=0.2m)

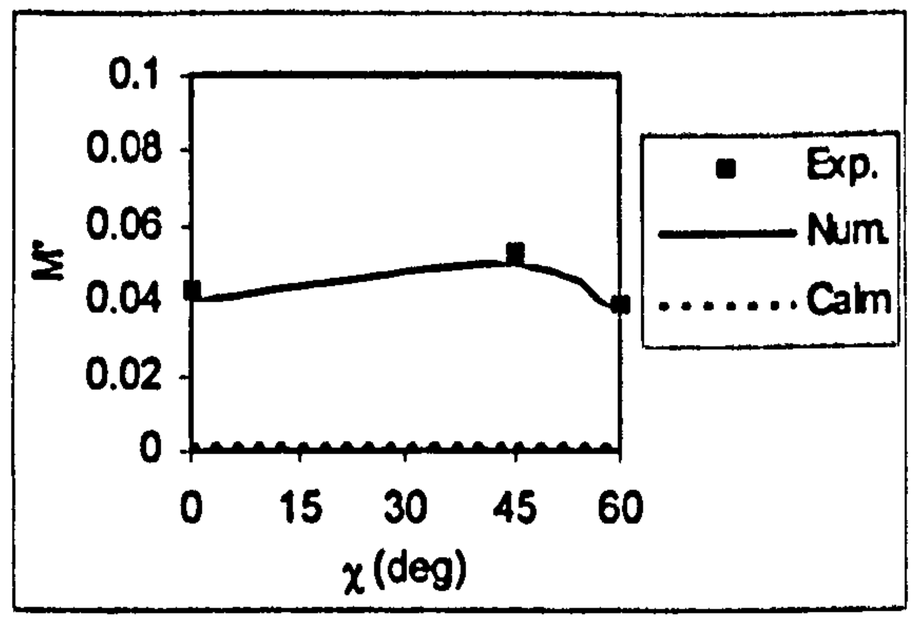

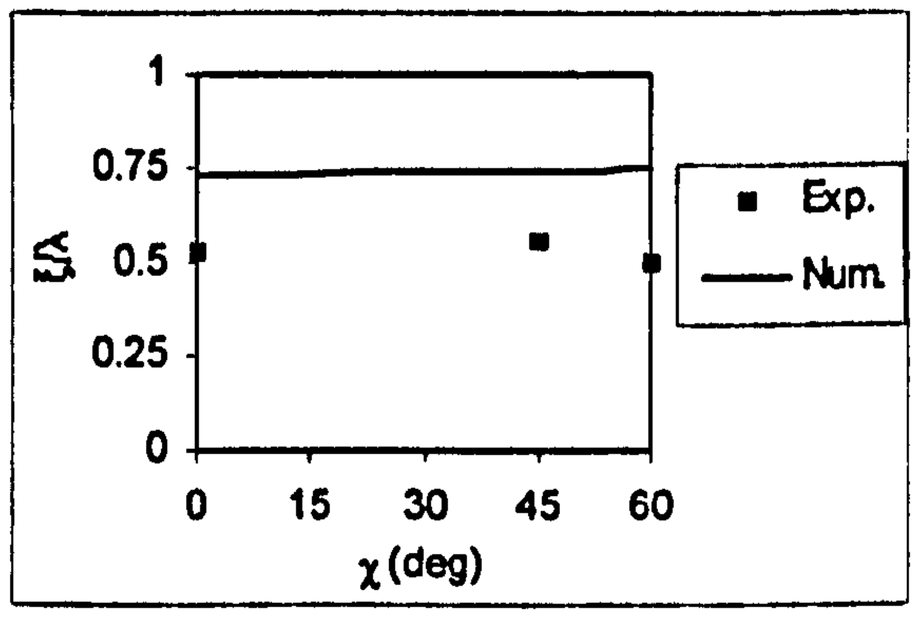

Figure 10.56 Wave induced pitch moment (Fn=0.3, λ/L=1.5, H/λ=1/20, ϕ=10°, θ=1.43°, sinkage=0.2m)

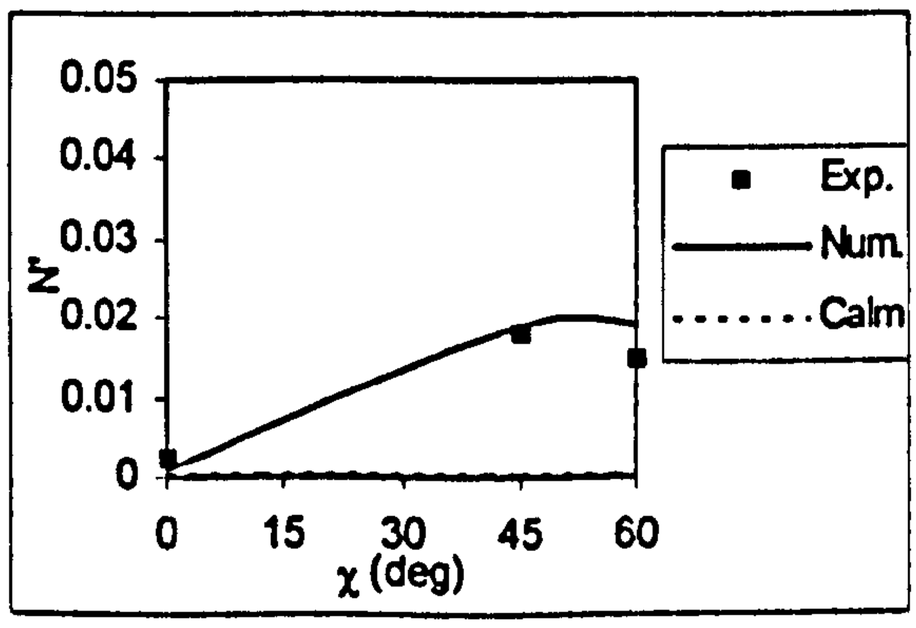

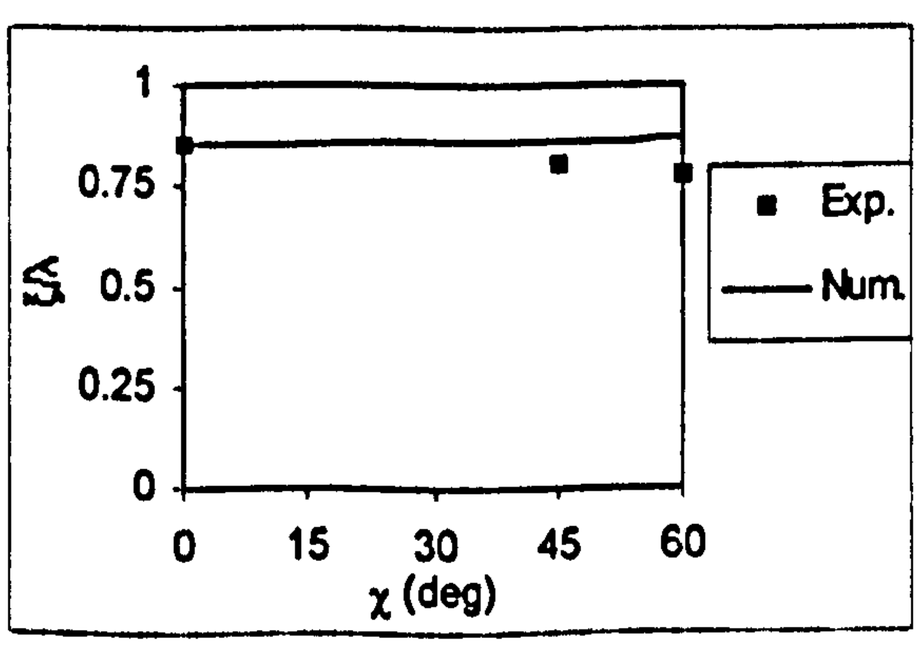

Figure 10.57 Wave induced yaw moment (Fn=0.3, λ/L=1.5, H/λ=1/20, ϕ=10°, θ=1.43°, sinkage=0.2m)

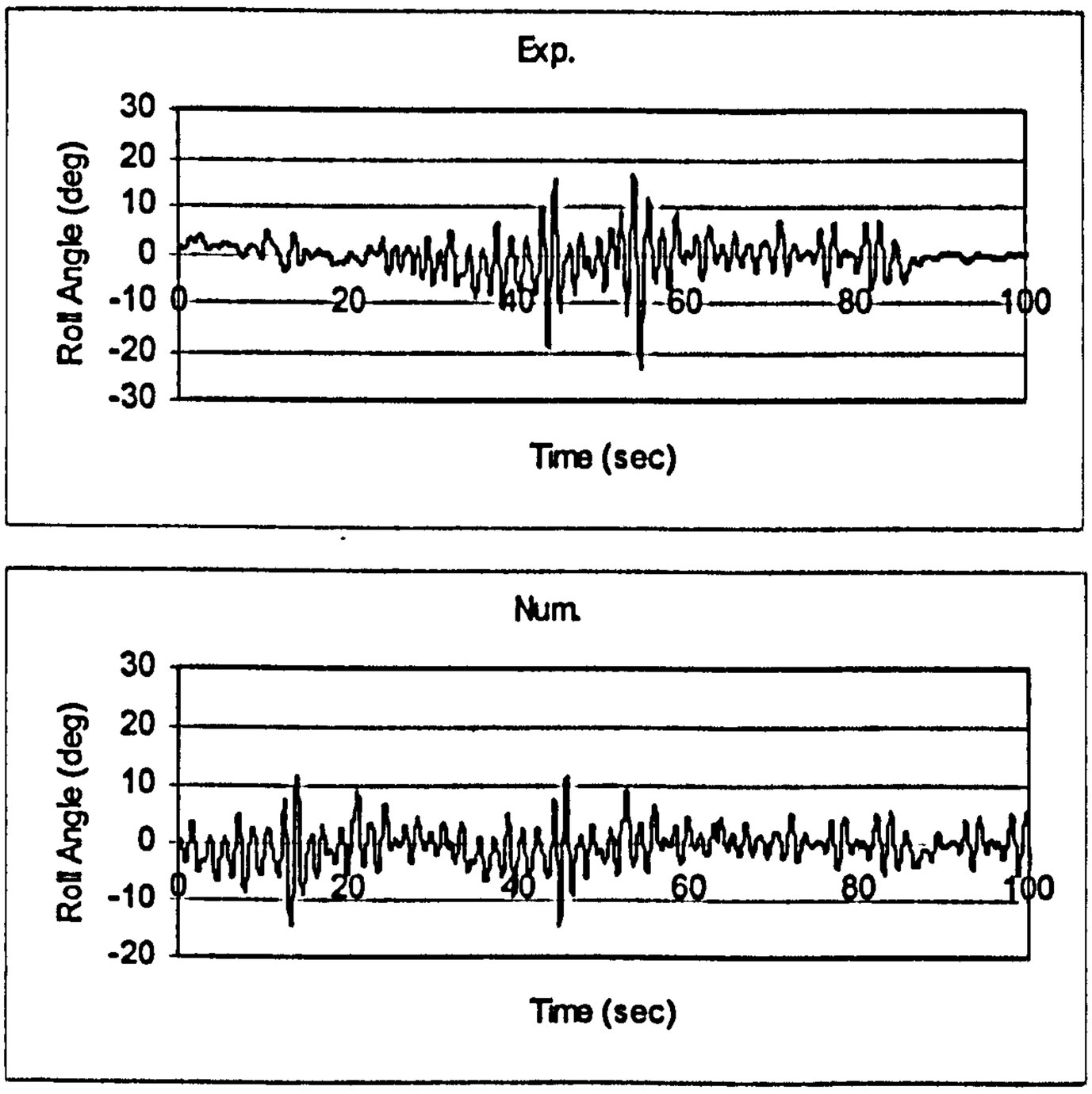

Figure 10.58 Roll, ITTC, Fn=0.3, χ= -5°, H_s=0.1725m, T_p=1.487 sec.

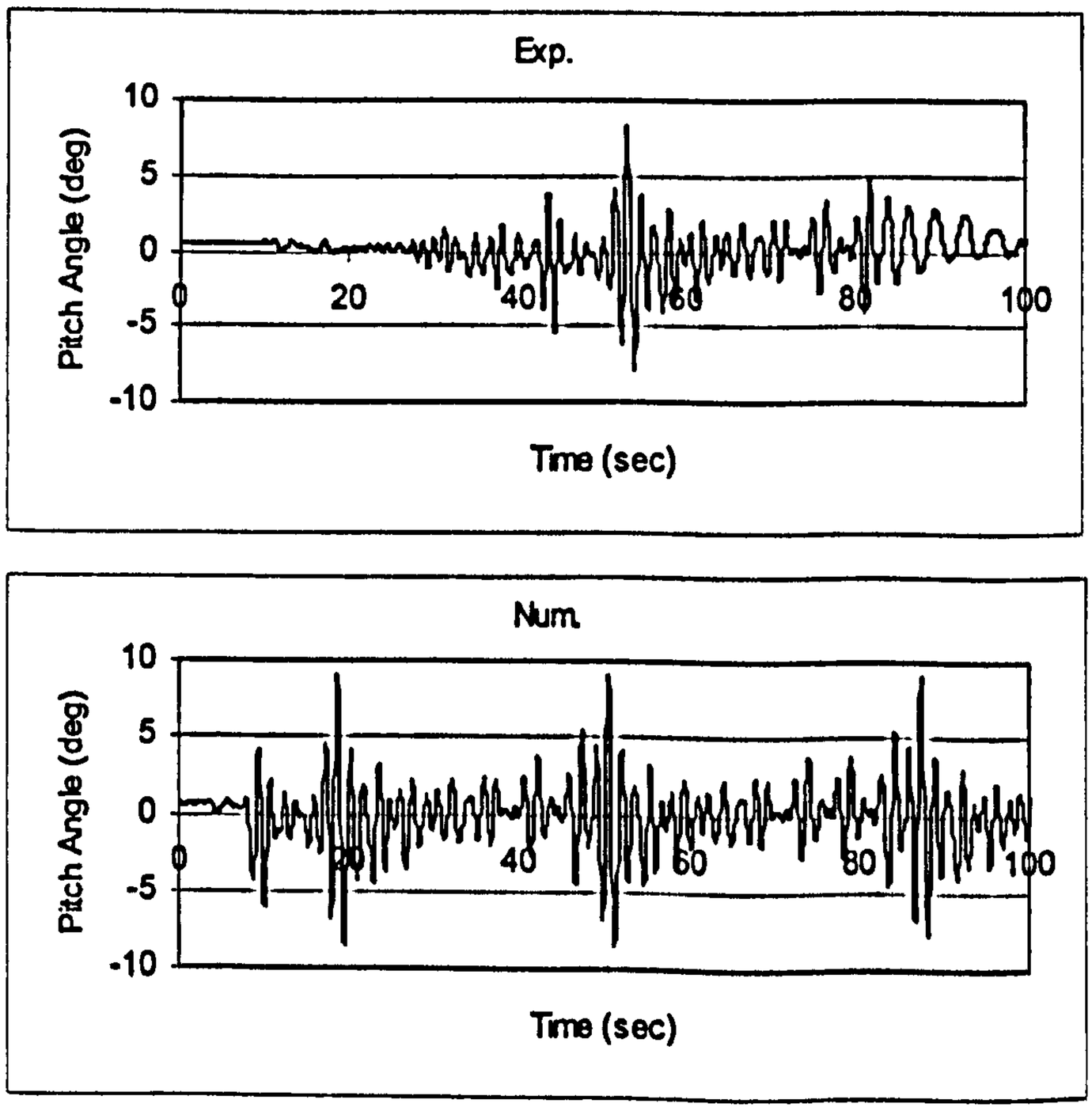

Figure 10.59 Pitch, ITTC, Fn=0.3, χ= -5°, H_s=0.1725m, T_p=1.487 sec.

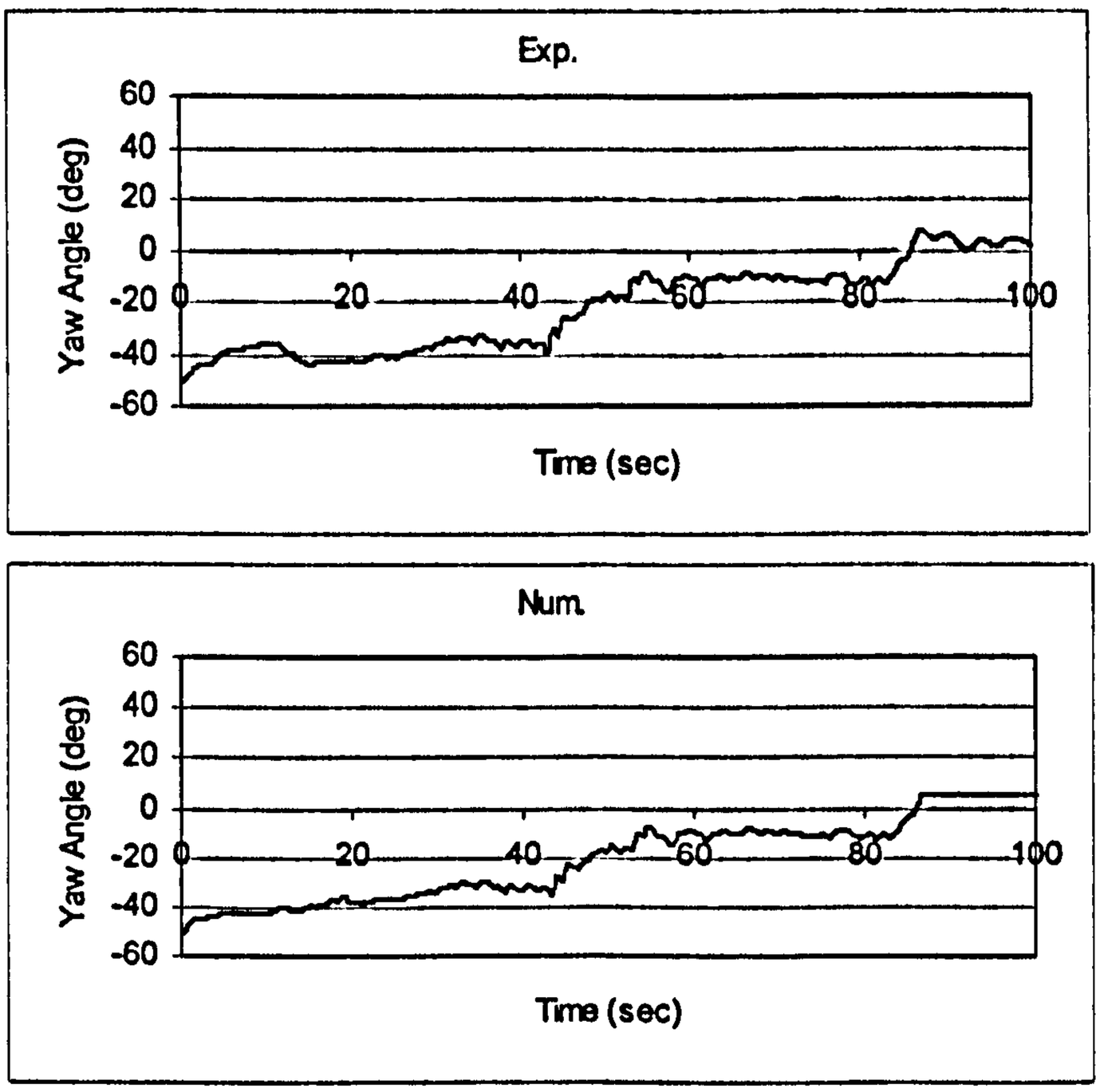

Figure 10.60 Yaw, ITTC, Fn=0.3, χ= -5°, H_s=0.1725m, T_p=1.487 sec.

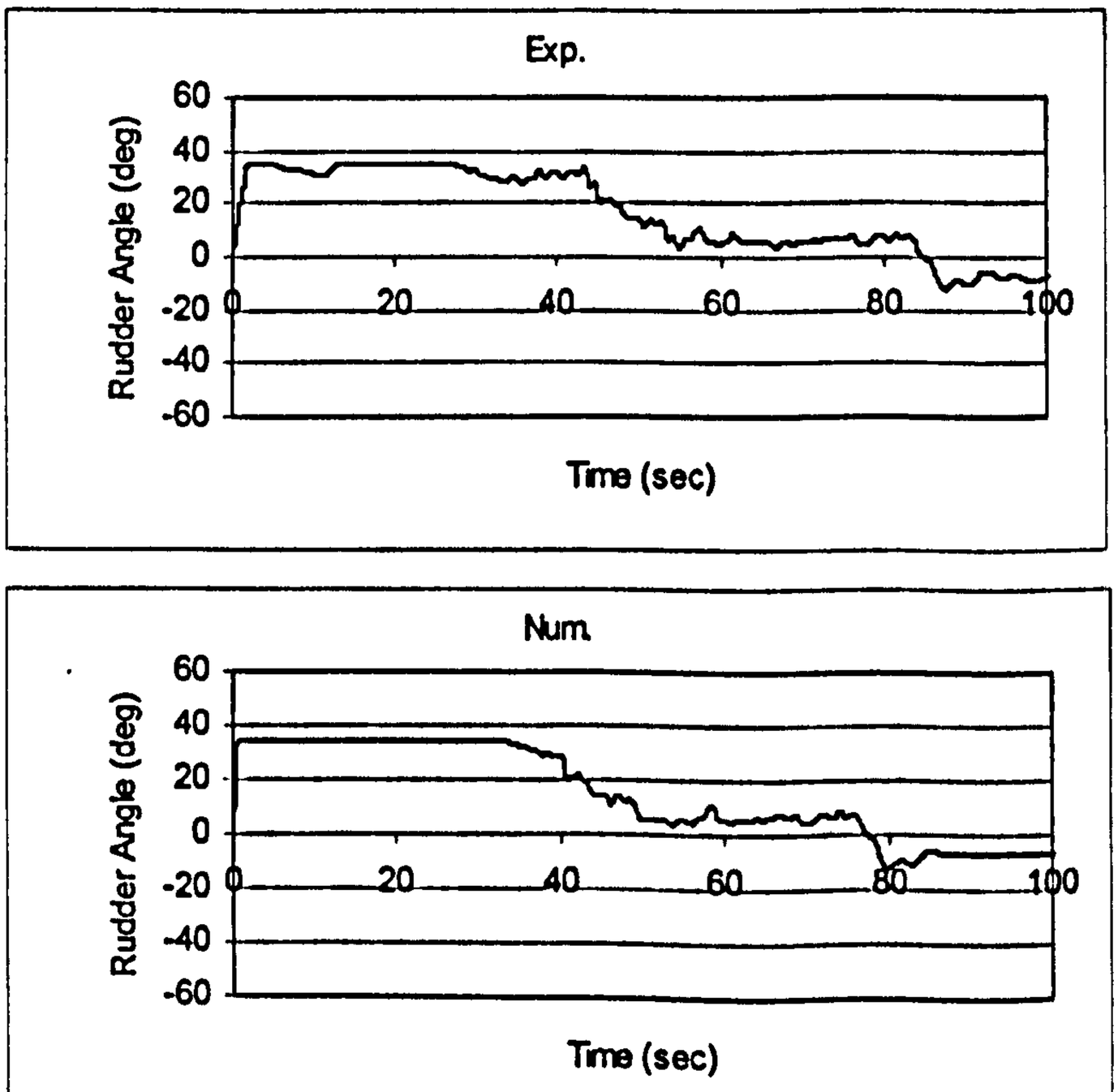

Figure 10.61 Rudder, ITTC, Fn=0.3, χ= -5°, H_s=0.1725m, T_p=1.487 sec.

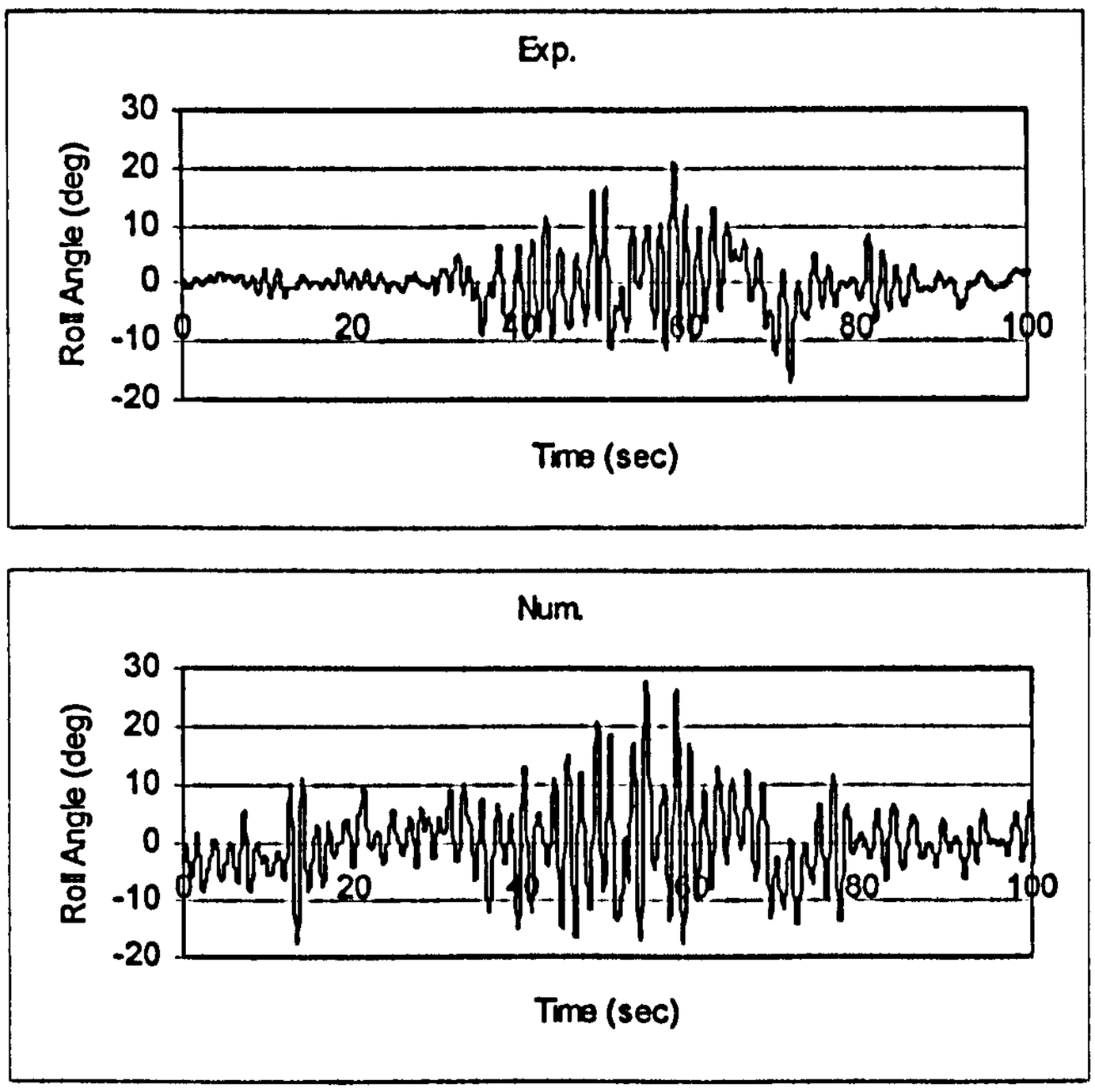

Figure 10.62 Roll, ITTC, Fn=0.4, χ= -5°, H_s=0.1725m, T_p=1.487 sec.

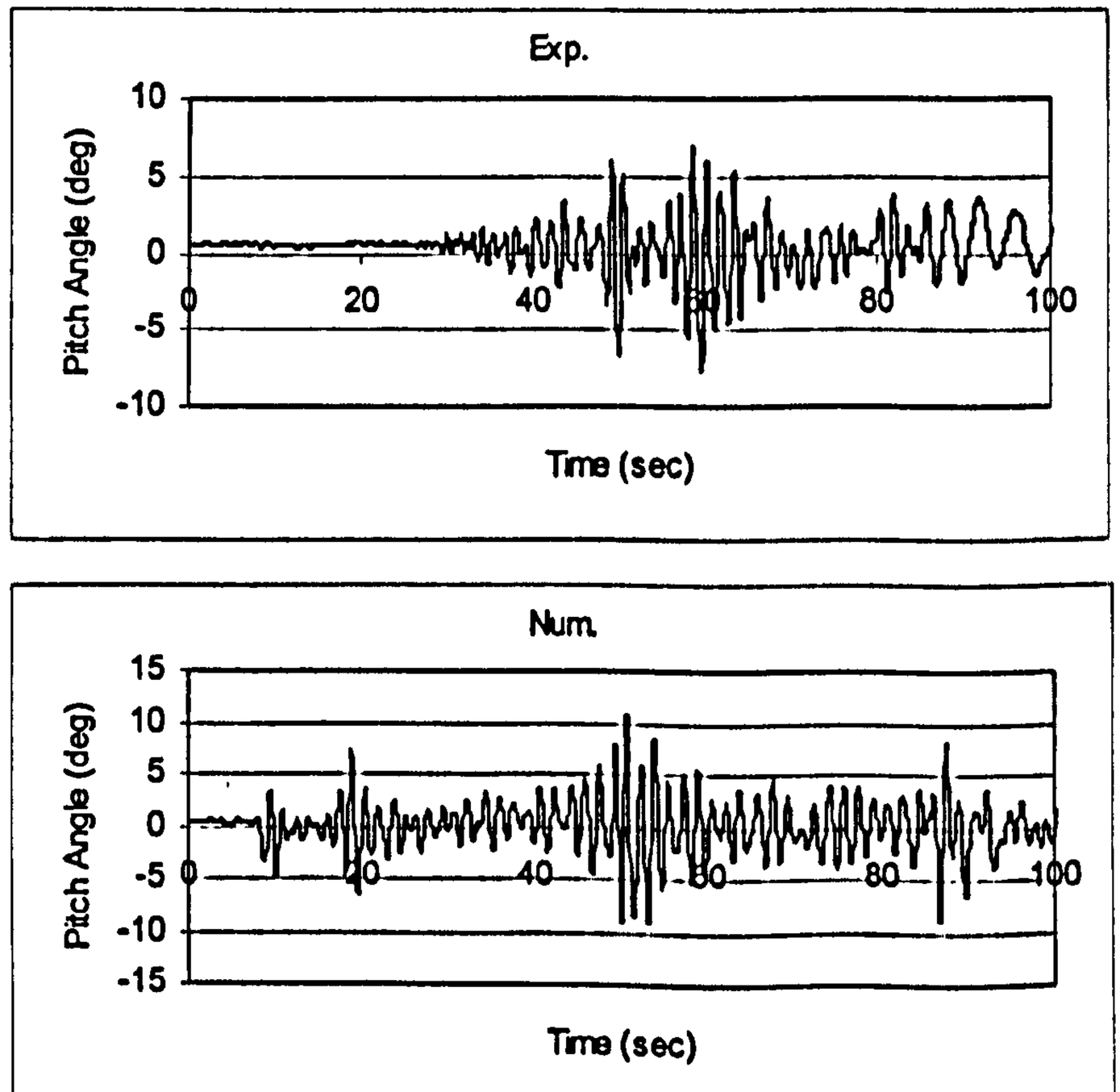

Figure 10.63 Pitch, ITTC, Fn=0.4, χ= -5°, H_s=0.1725m, T_p=1.487 sec.

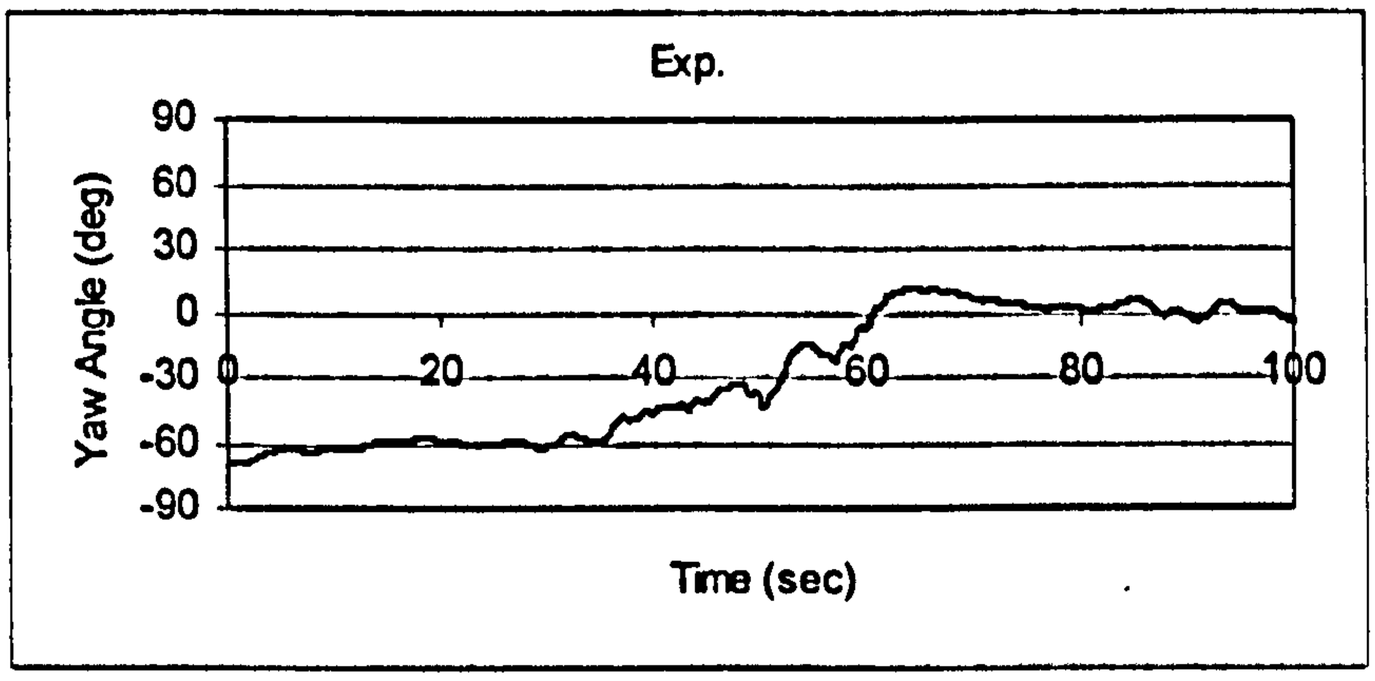

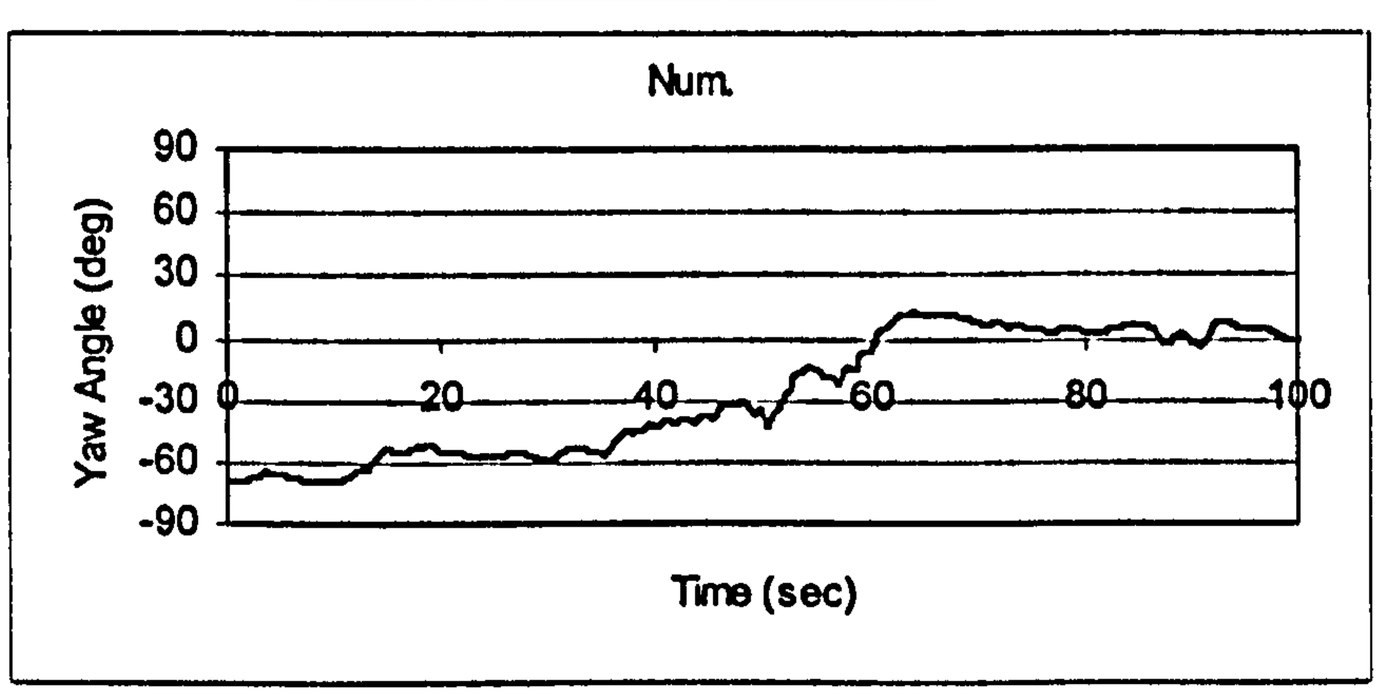

Figure 10.64 Yaw, ITTC, Fn=0.4, χ= -5°, H_s=0.1725m, T_p=1.487 sec.

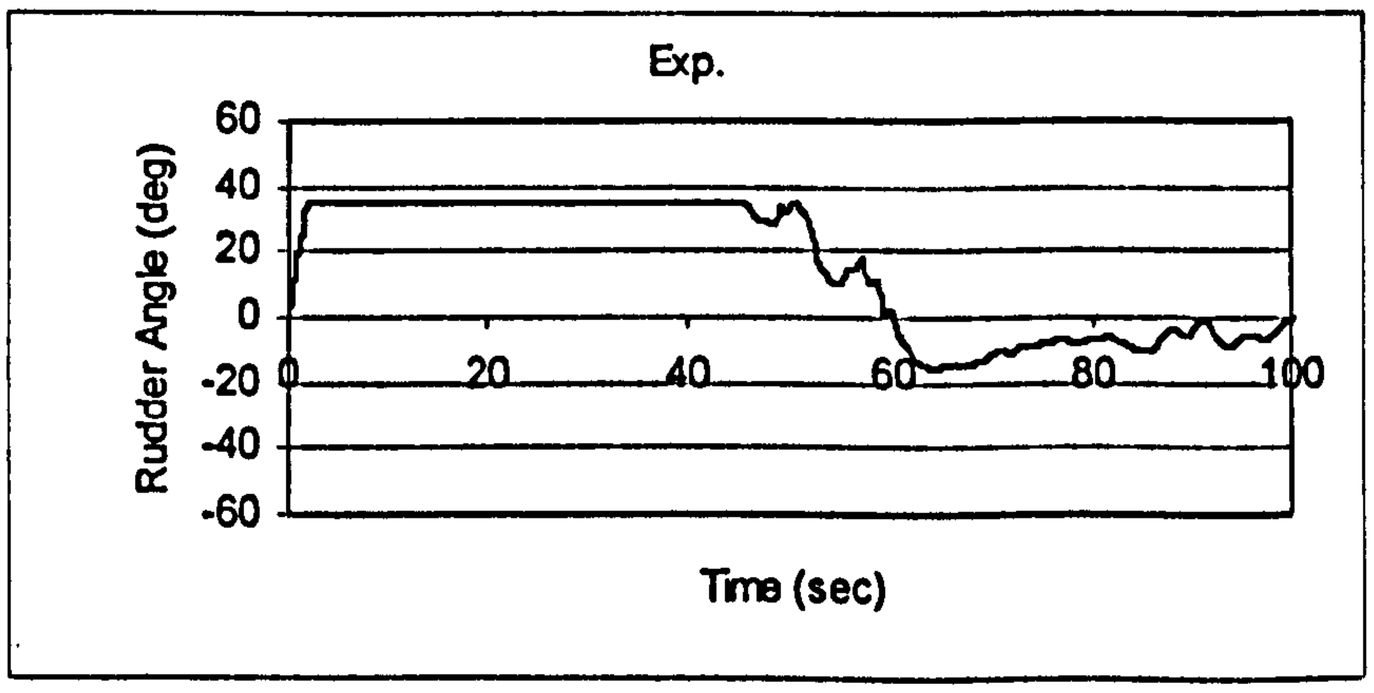

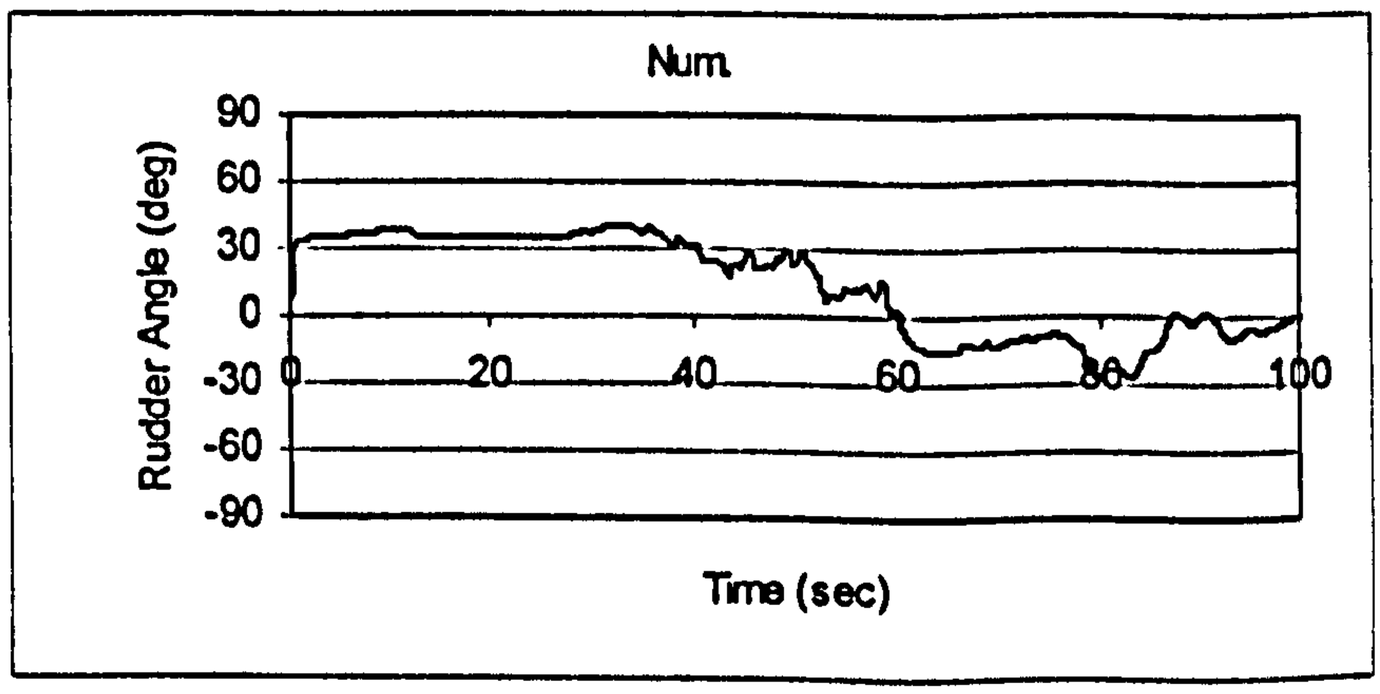

Figure 10.65 Rudder, ITTC, Fn=0.4, χ= -5°, H_s=0.1725m, T_p=1.487 sec.

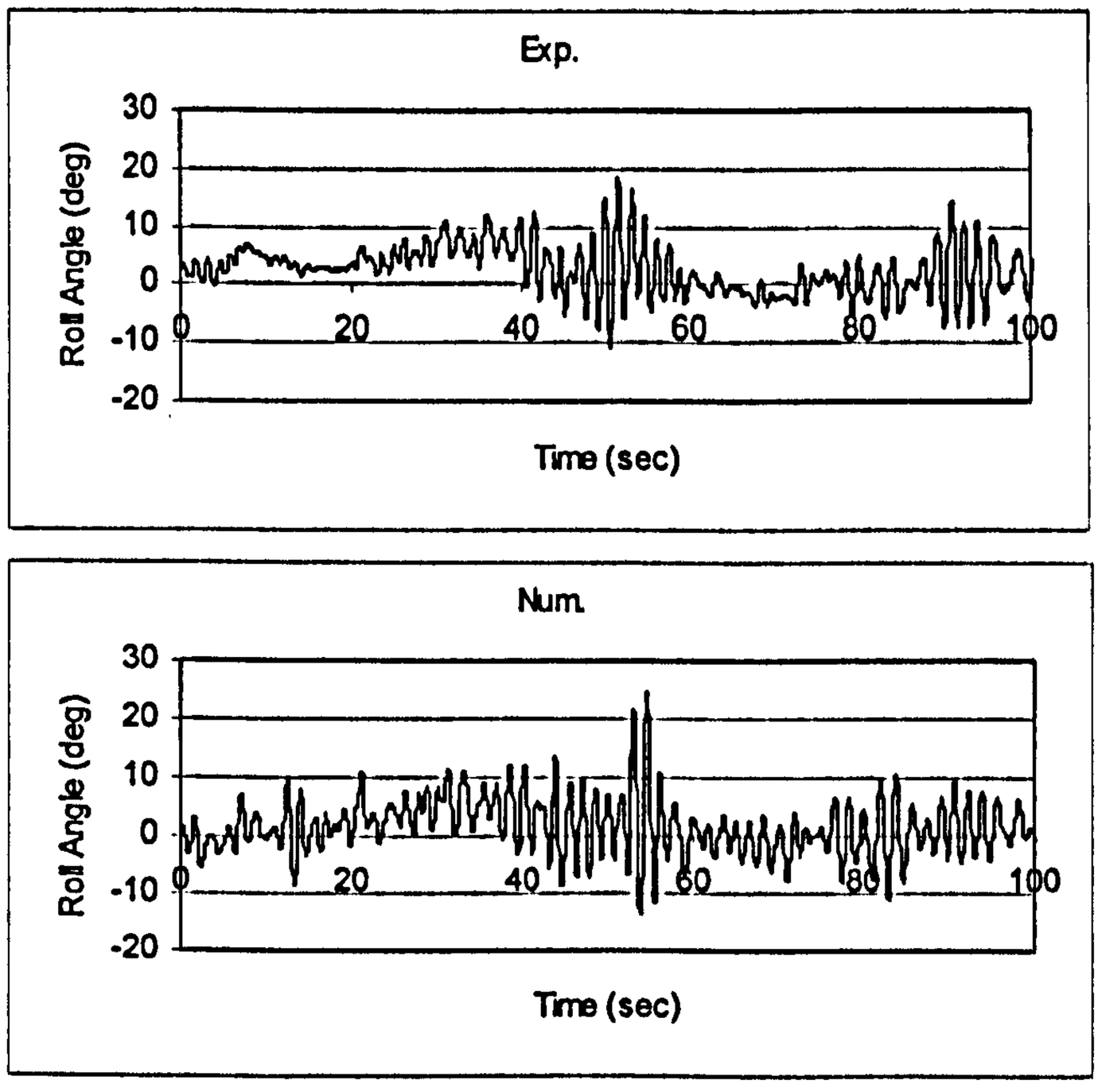

Figure 10.66 Roll, ITTC, Fn=0.3, χ= -45°, H_s=0.1725m, T_p=1.487 sec.

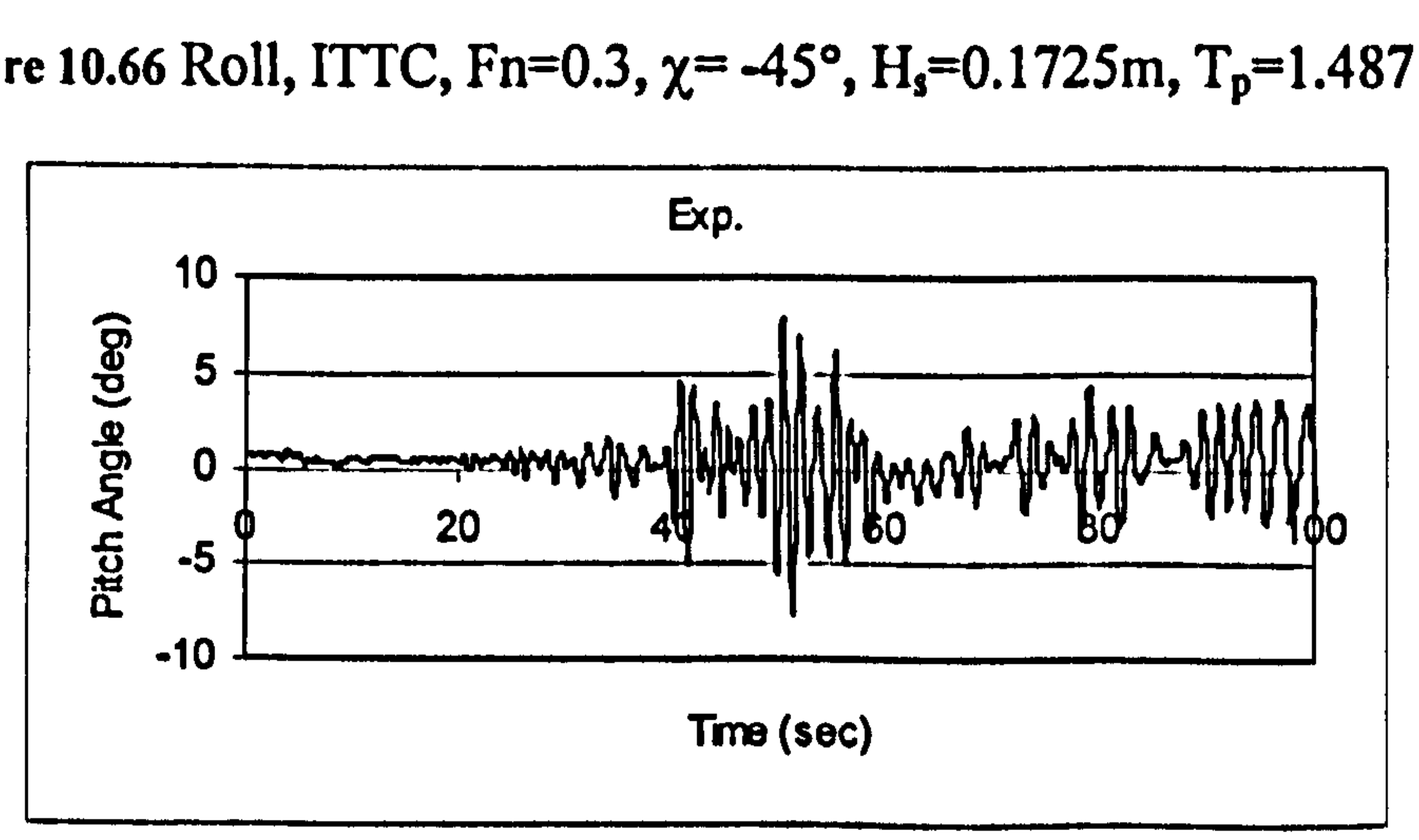

Figure 10.67 Pitch, ITTC, Fn=0.3, χ= -45°, H_s=0.1725m, T_p=1.487 sec.

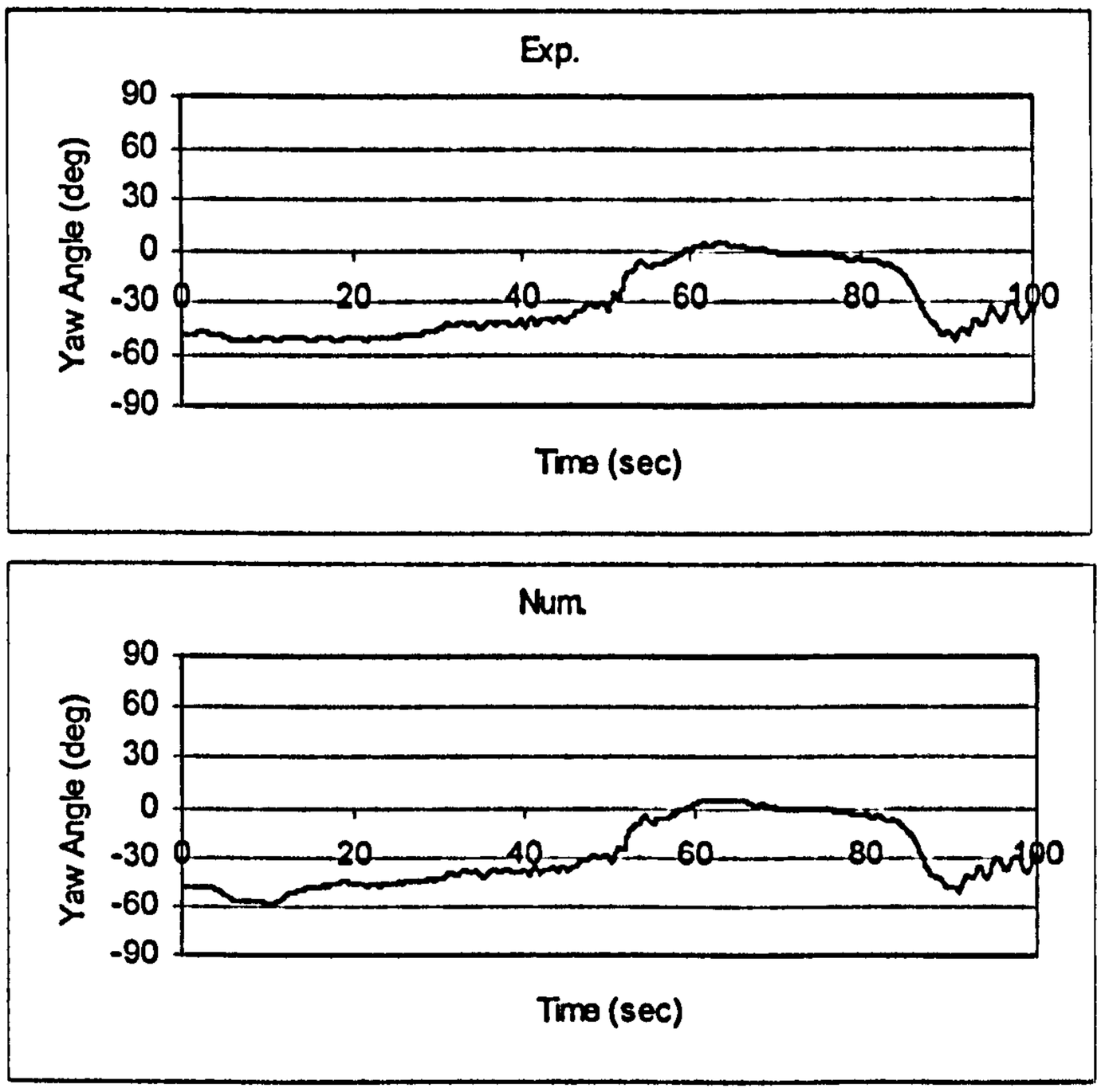

Figure 10.68 Yaw, ITTC, Fn=0.3, χ= -45°, H_s=0.1725m, T_p=1.487 sec.

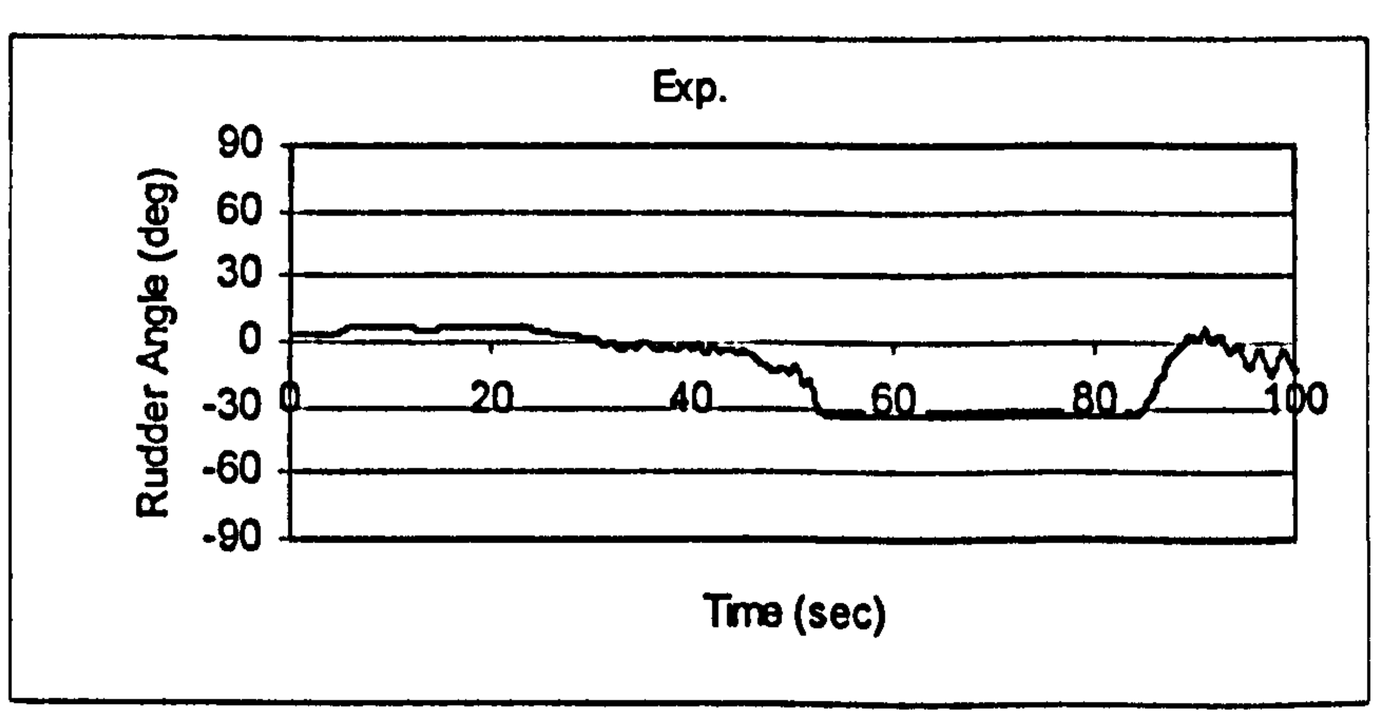

Figure 10.69 Rudder, ITTC, Fn=0.3, χ= -45°, H_s=0.1725m, T_p=1.487 sec.

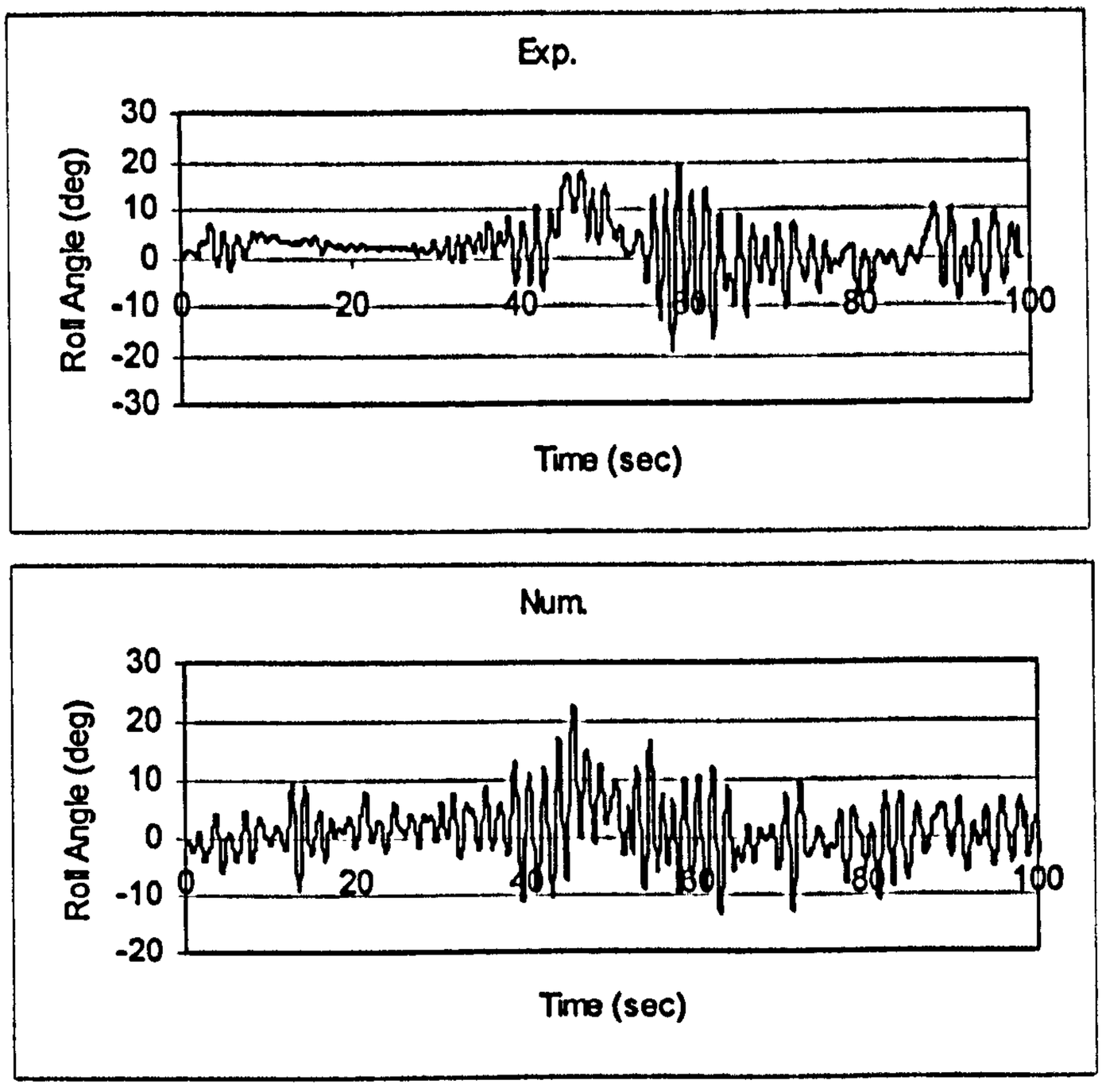

Figure 10.70 Roll, ITTC, Fn=0.4, χ= -45°, H_s=0.1725m, T_p=1.487 sec.

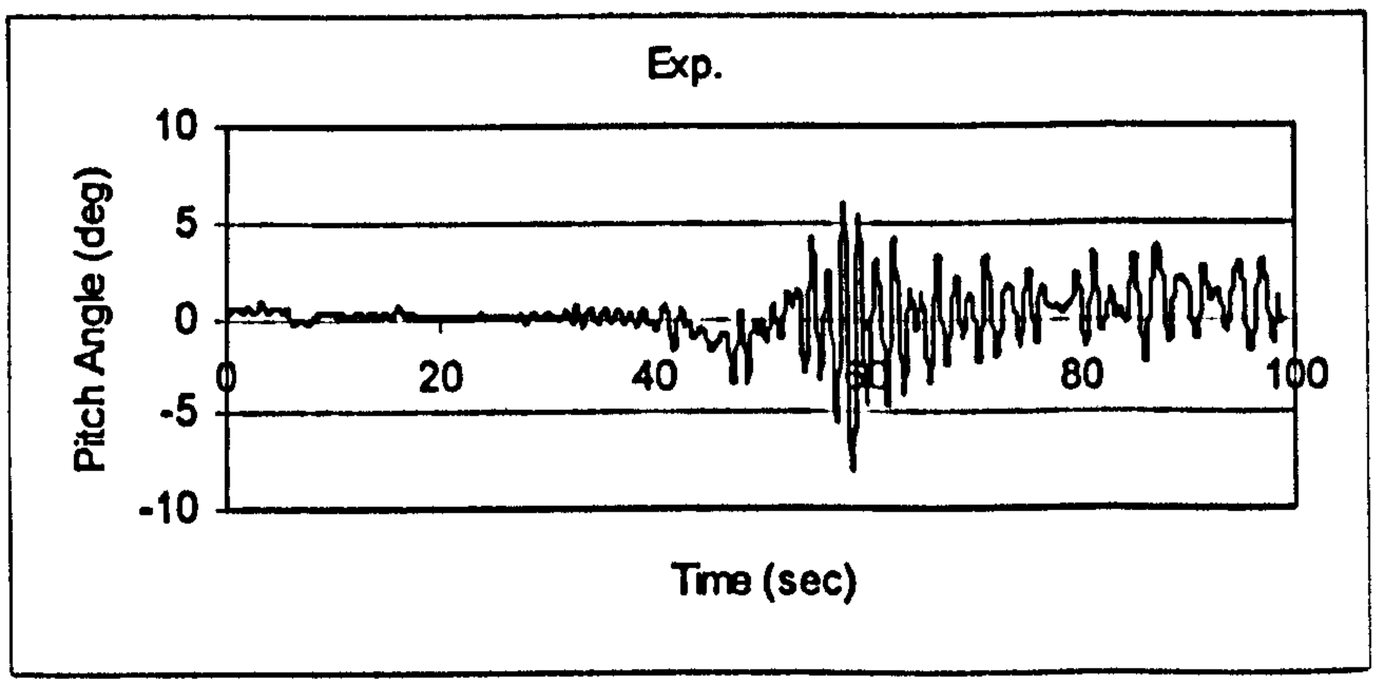

Figure 10.71 Pitch, ITTC, Fn=0.4, χ= -45°, H_s=0.1725m, T_p=1.487 sec.

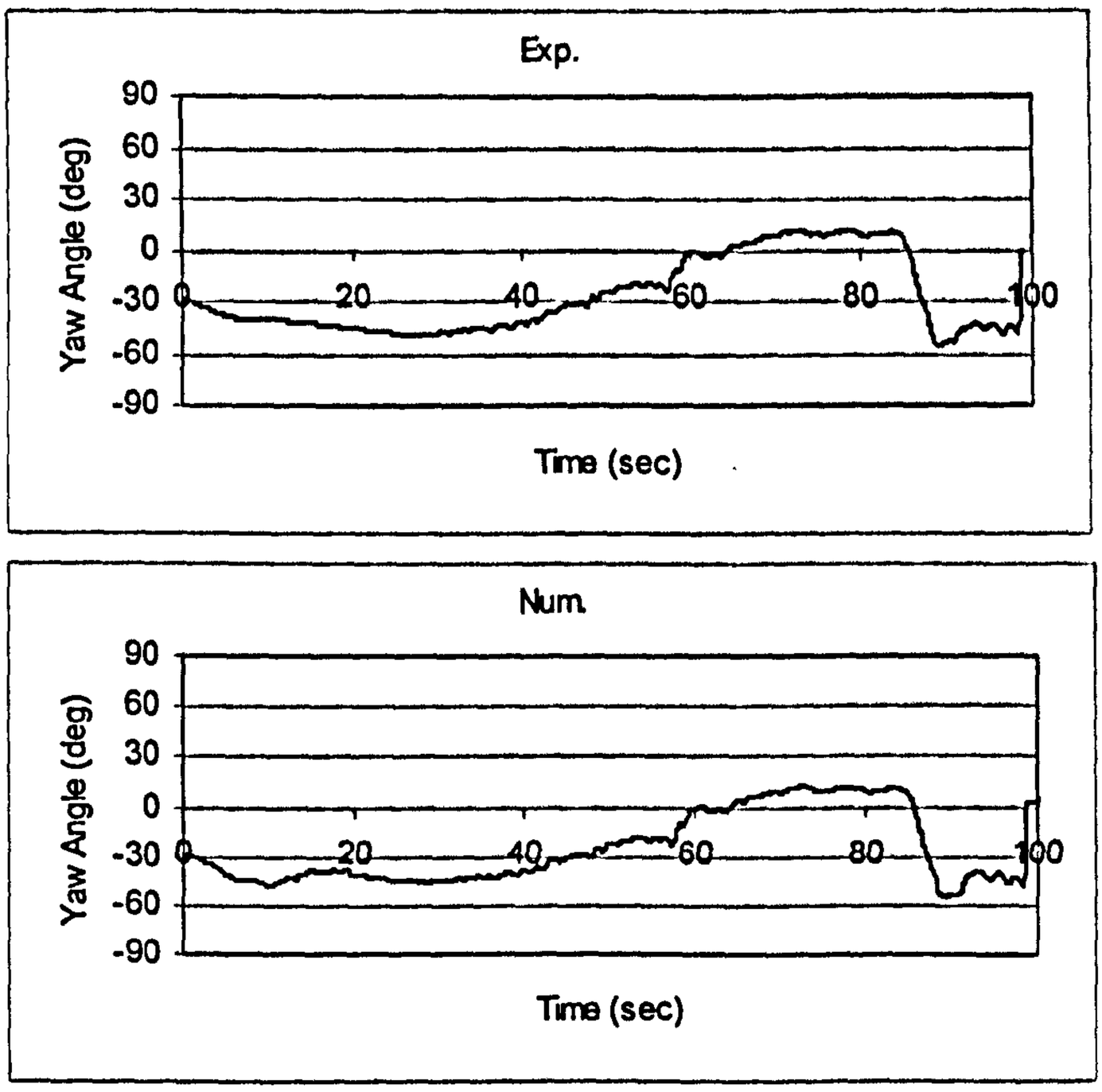

Figure 10.72 Yaw, ITTC, Fn=0.4, χ= -45°, H_s=0.1725m, T_p=1.487 sec.

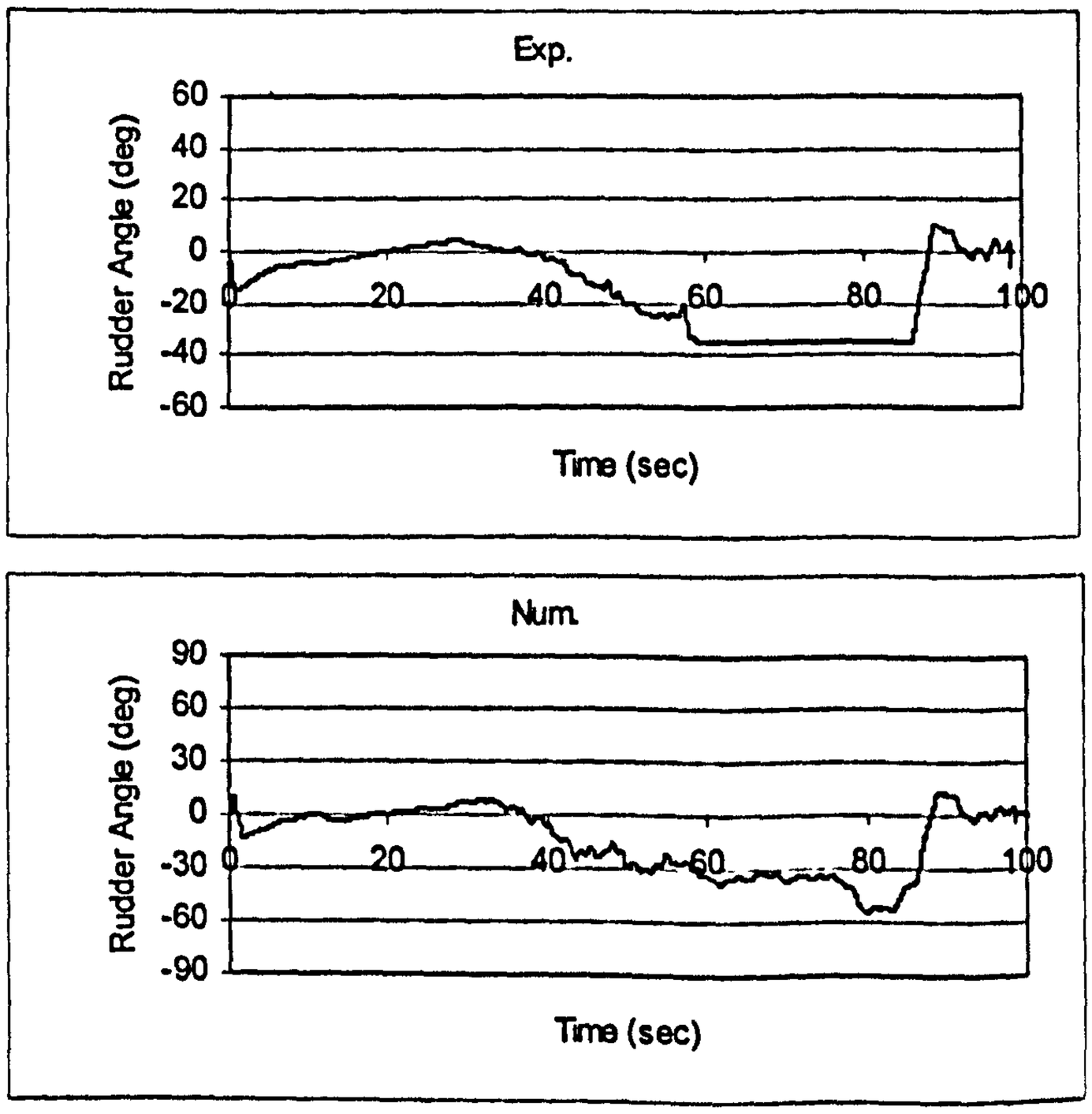

Figure 10.73 Rudder, ITTC, Fn=0.4, χ= -45°, H_s=0.1725m, T_p=1.487 sec.

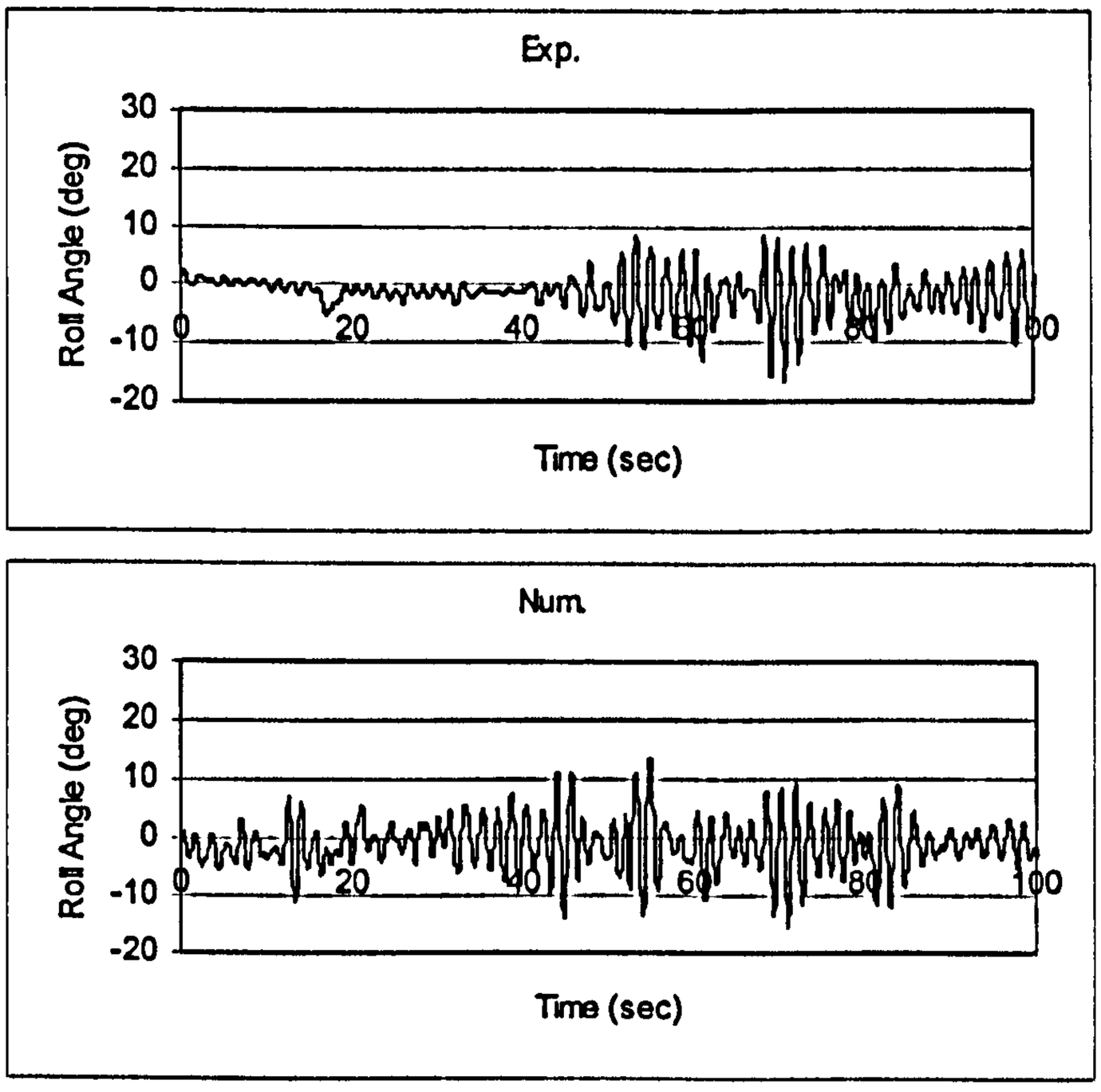

Figure 10.74 Roll, ITTC, Fn=0.3, χ= -60°, H_s=0.1725m, T_p=1.487 sec.

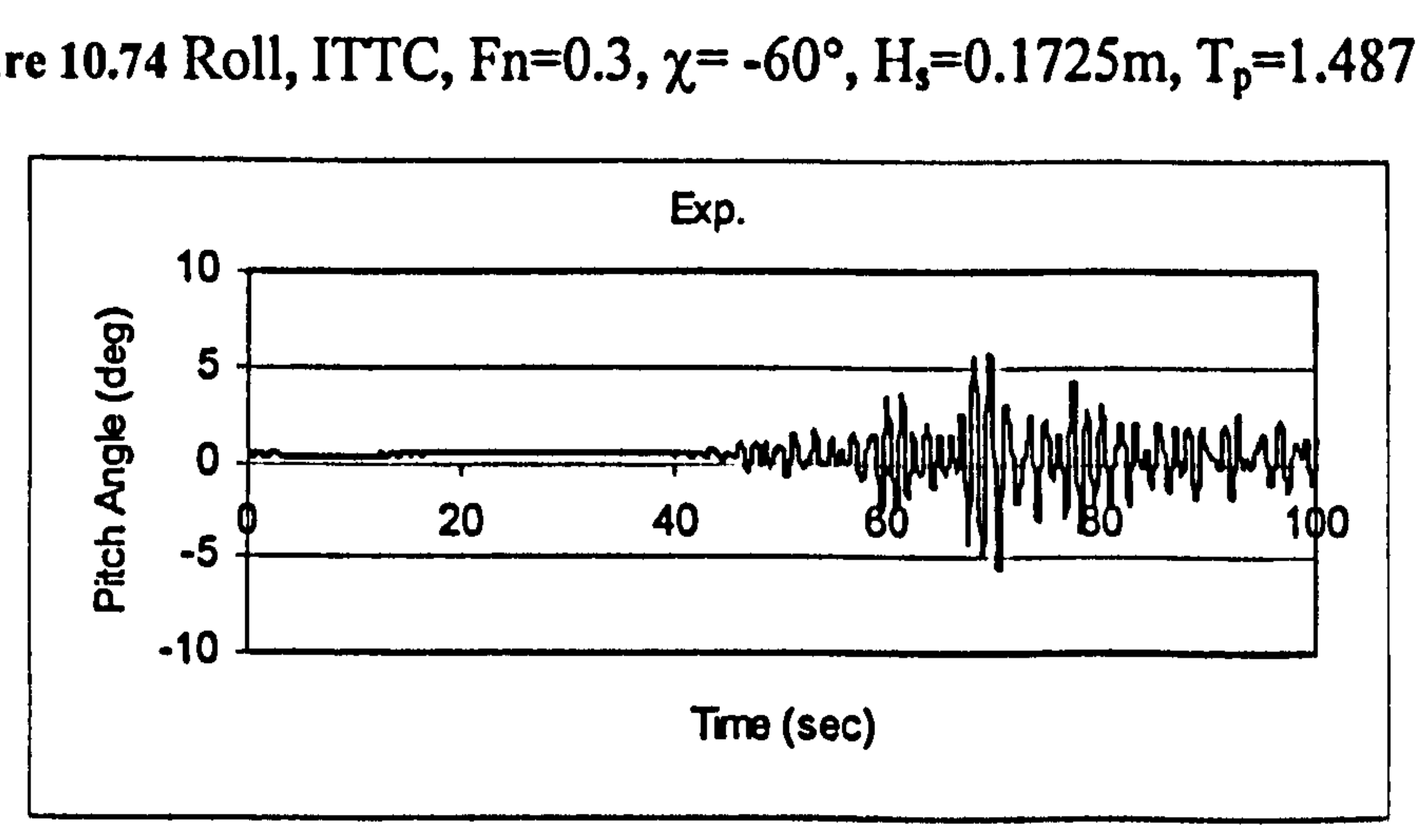

Figure 10.75 Pitch, ITTC, Fn=0.3, χ= -60°, H_s=0.1725m, T_p=1.487 sec.

Figure 10.76 Yaw, ITTC, Fn=0.3, χ= -60°, H_s=0.1725m, T_p=1.487 sec.

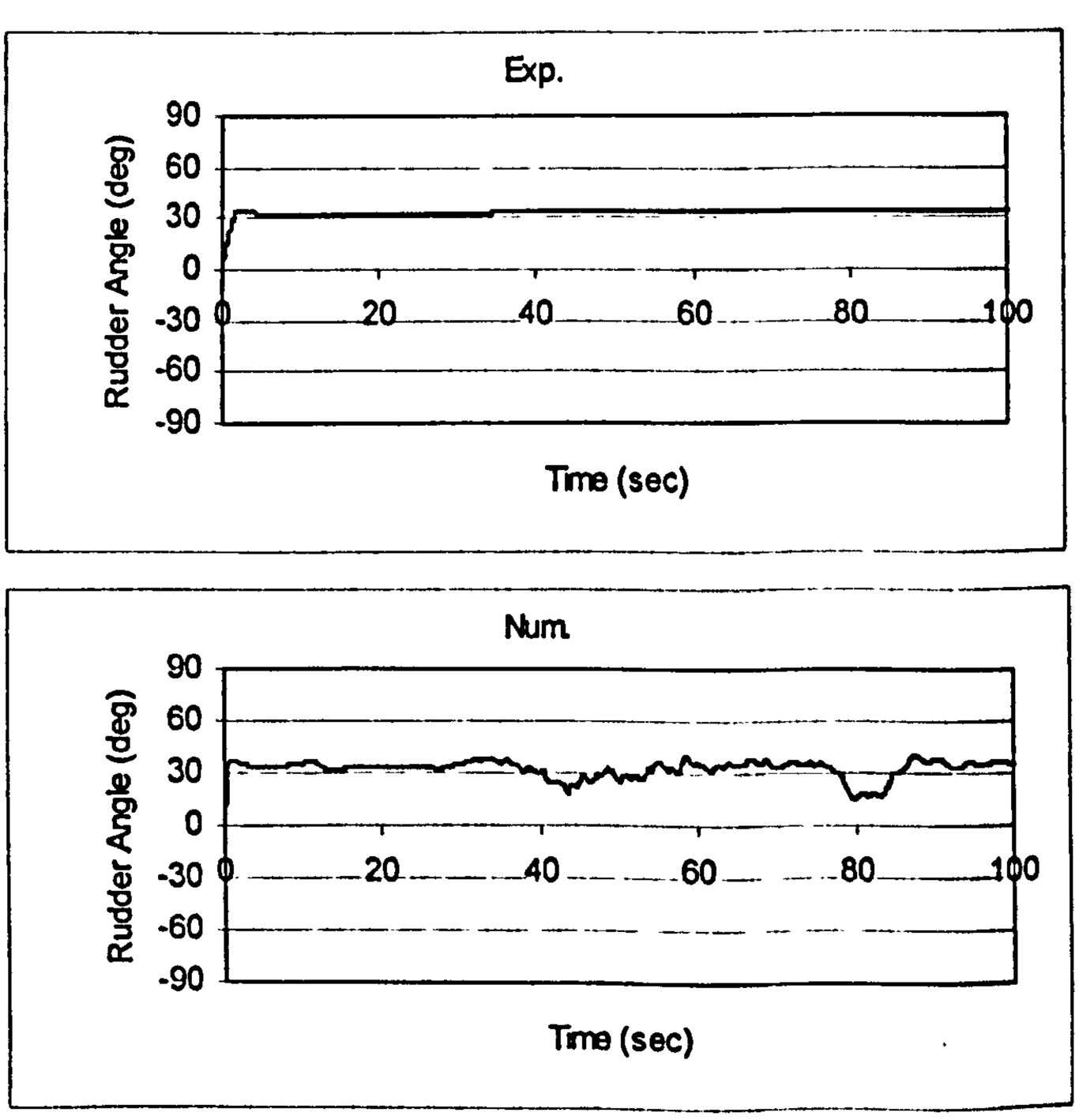

Figure 10.77 Rudder, ITTC, Fn=0.3, χ= -60°, H_s=0.1725m, T_p=1.487 sec.

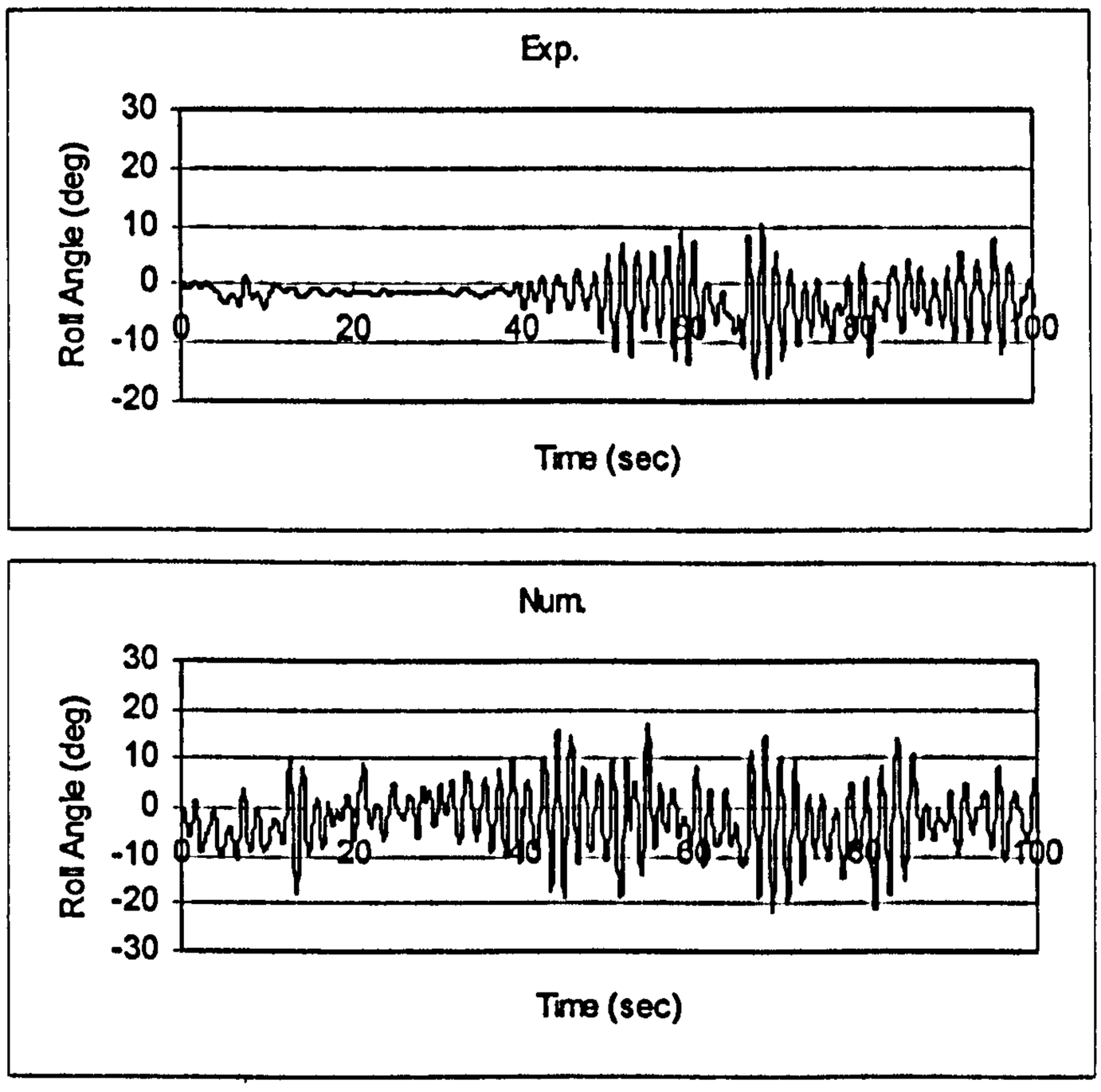

Figure 10.78 Roll, ITTC, Fn=0.4, χ= -60°, H_s=0.1725m, T_p=1.487 sec.

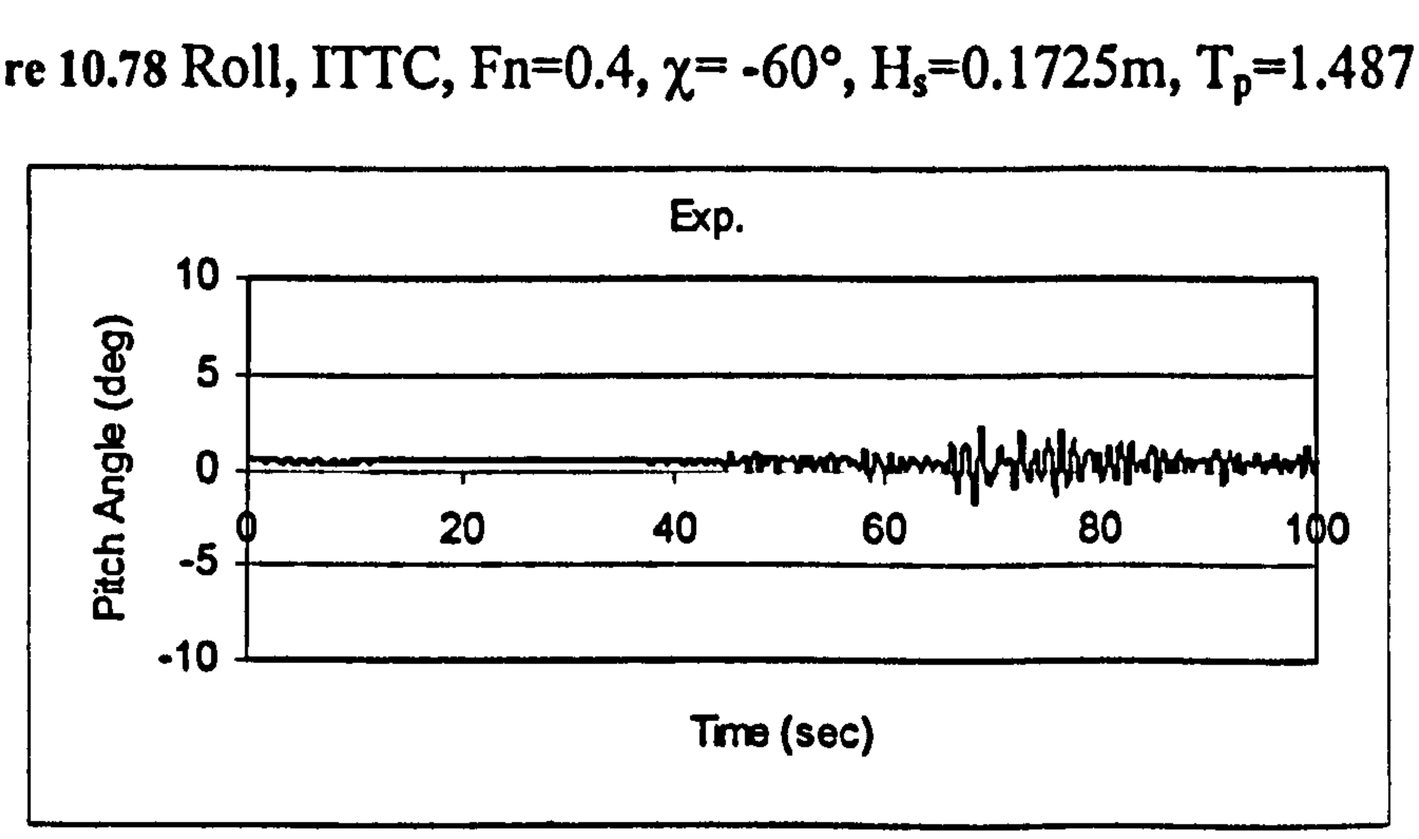

Figure 10.79 Pitch, ITTC, Fn=0.4, χ= -60°, H_s=0.1725m, T_p=1.487 sec.

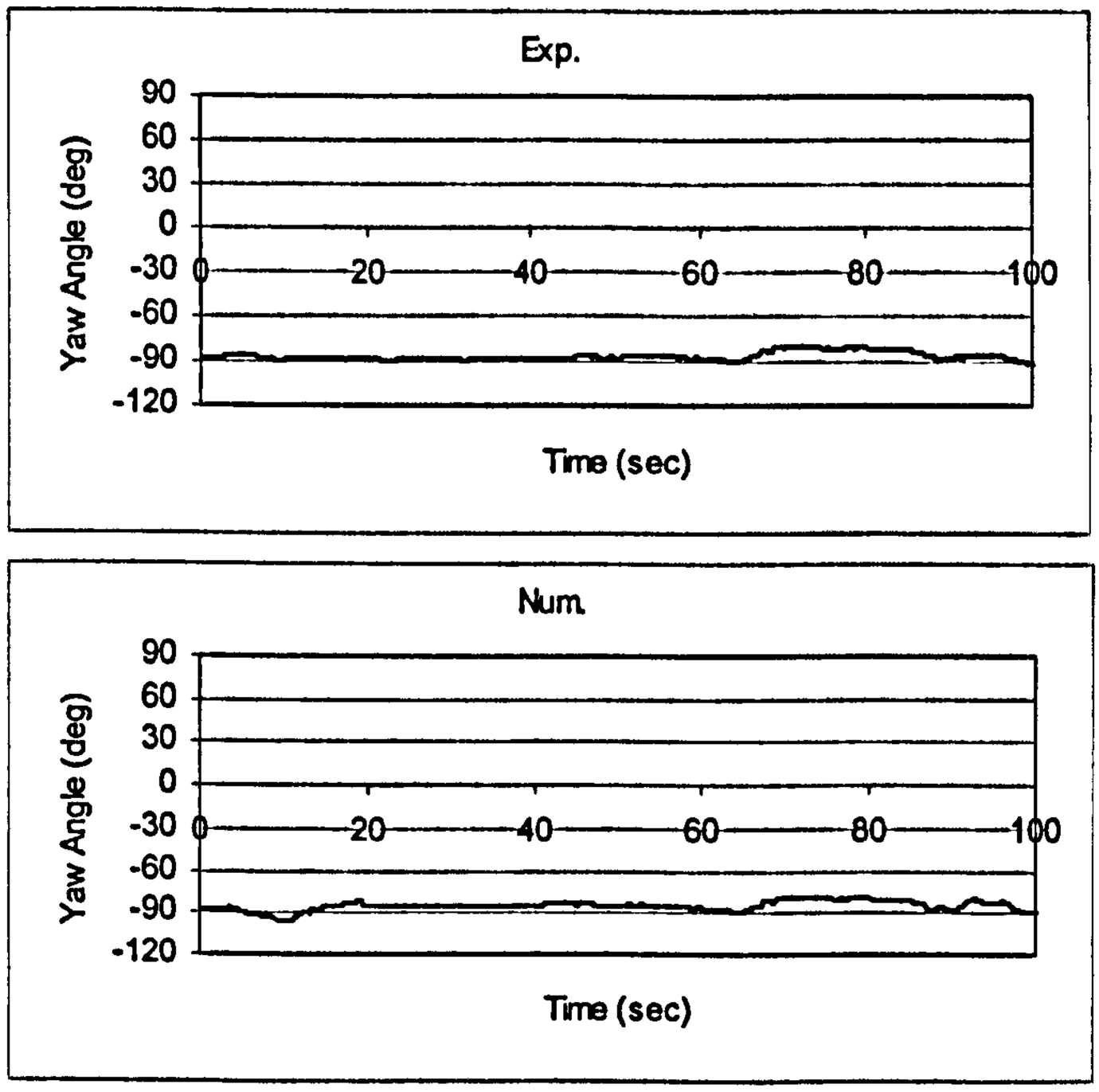

Figure 10.80 Yaw, ITTC, Fn=0.4, χ= -60°, H_s=0.1725m, T_p=1.487 sec.

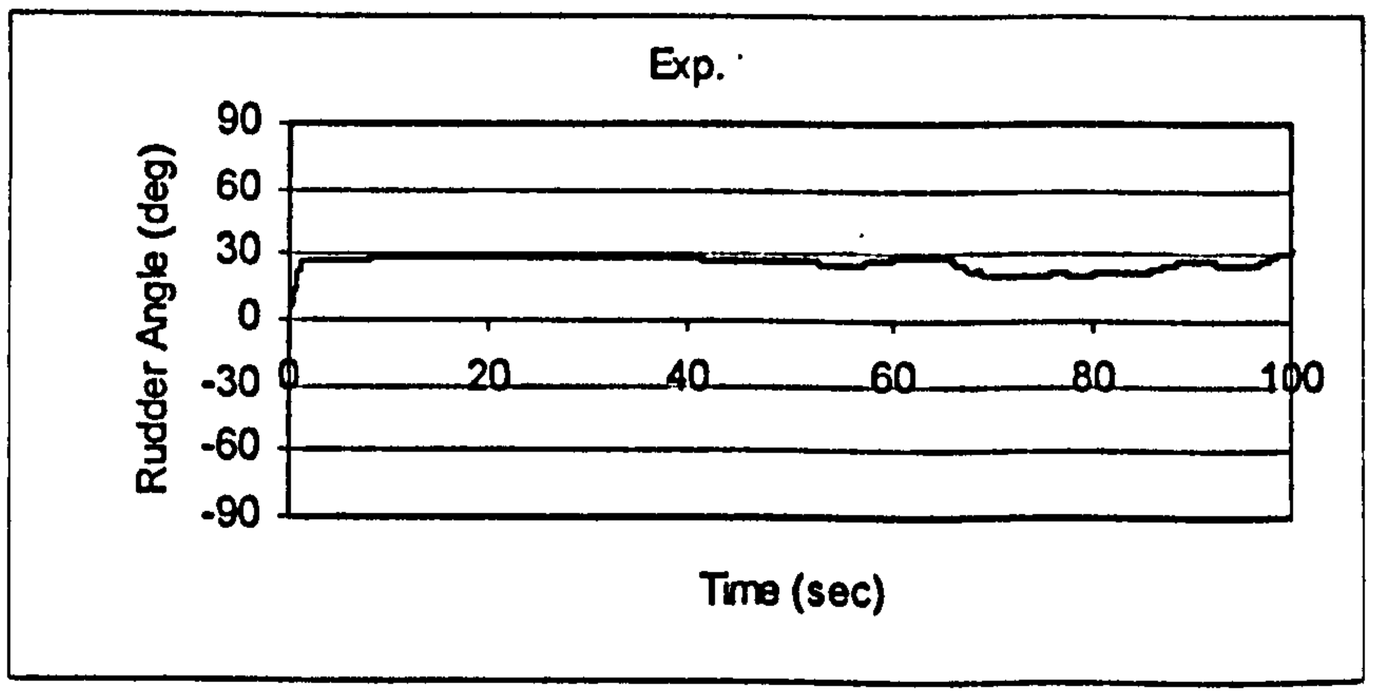

Figure 10.81 Rudder, ITTC, Fn=0.4, χ= -60°, H_s=0.1725m, T_p=1.487 sec.

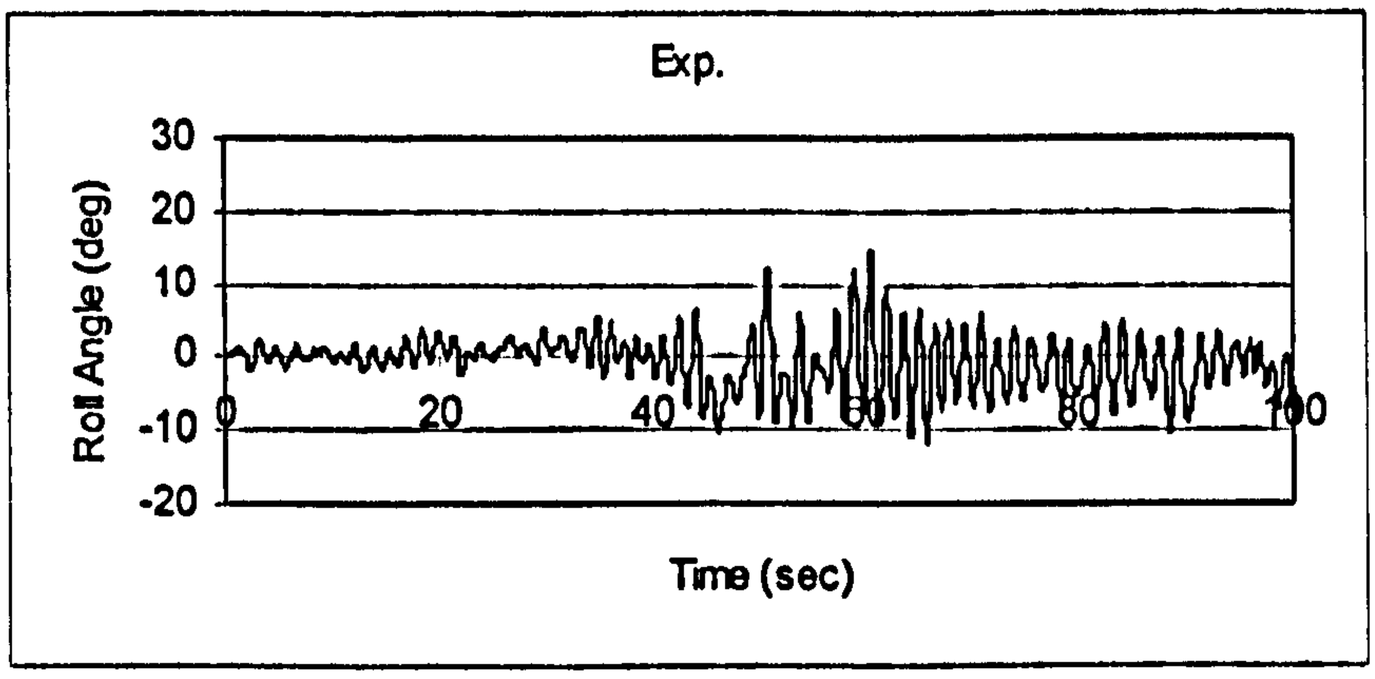

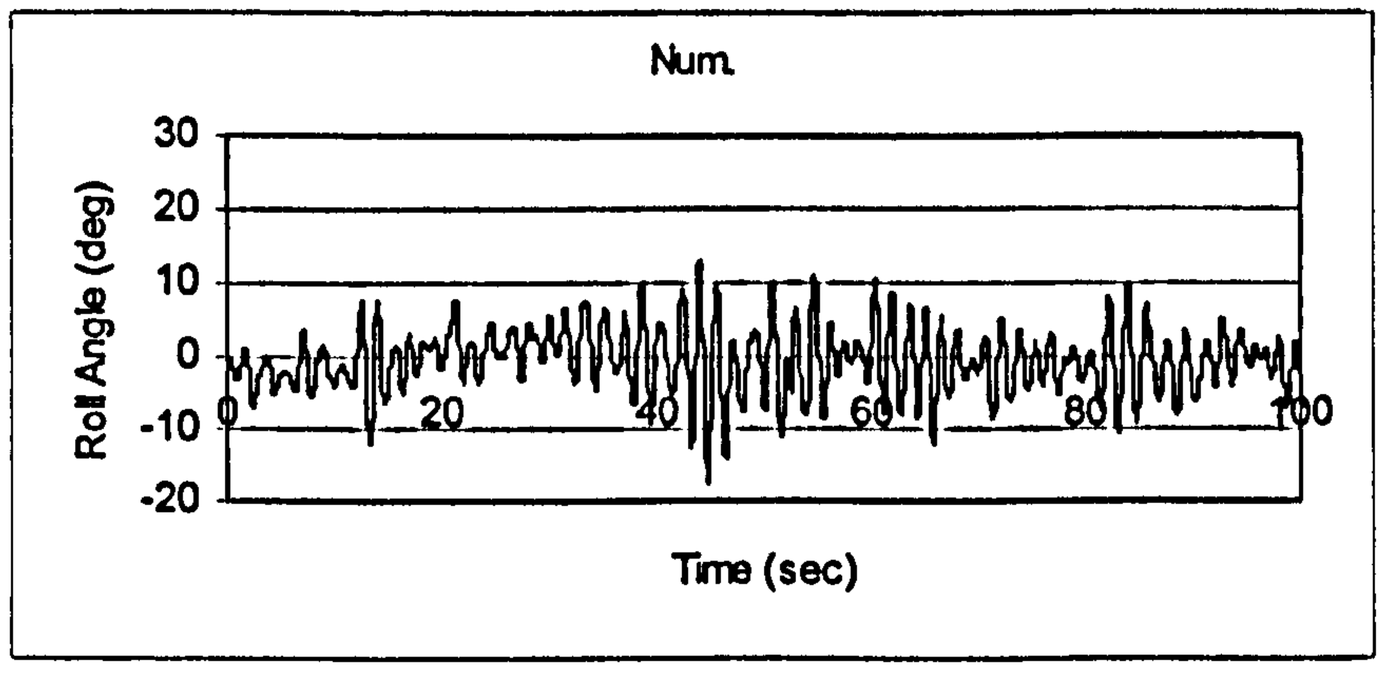

Figure 10.82 Roll, JONSWAP, Fn=0.3, χ= -5°, H_s=0.23m, T_p=1.717 sec.

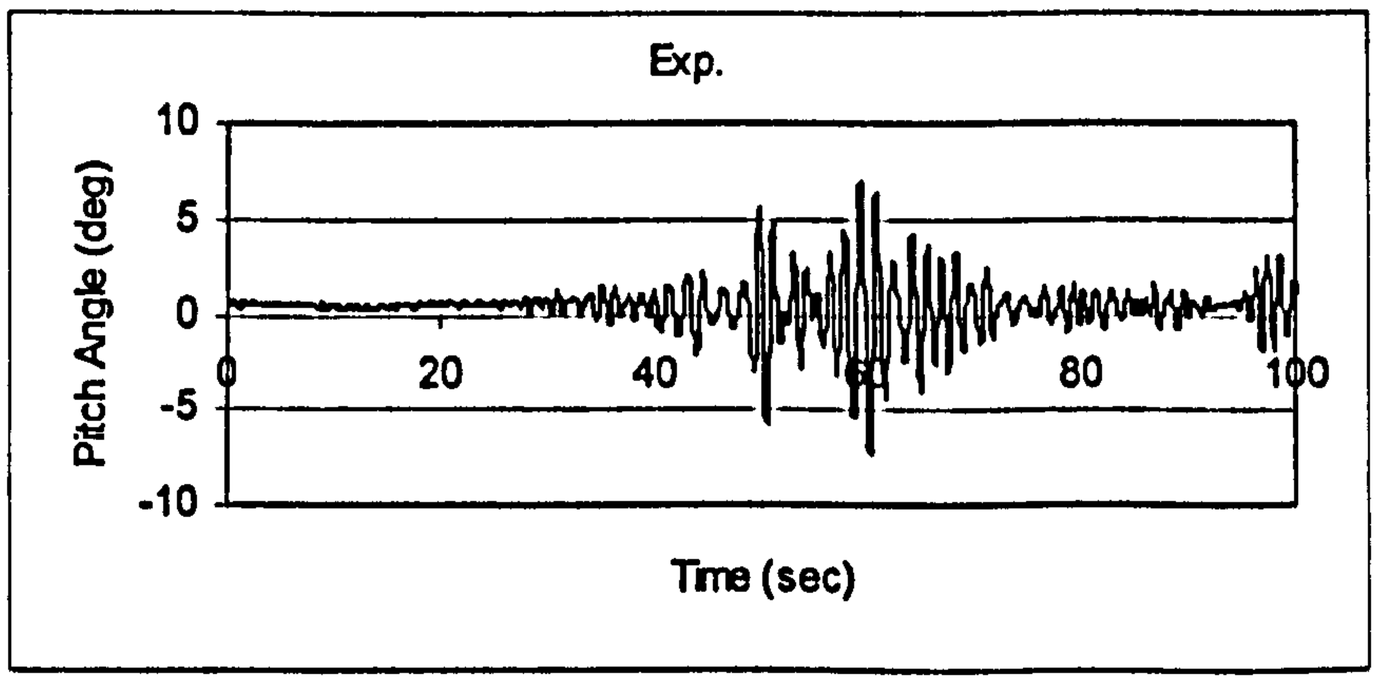

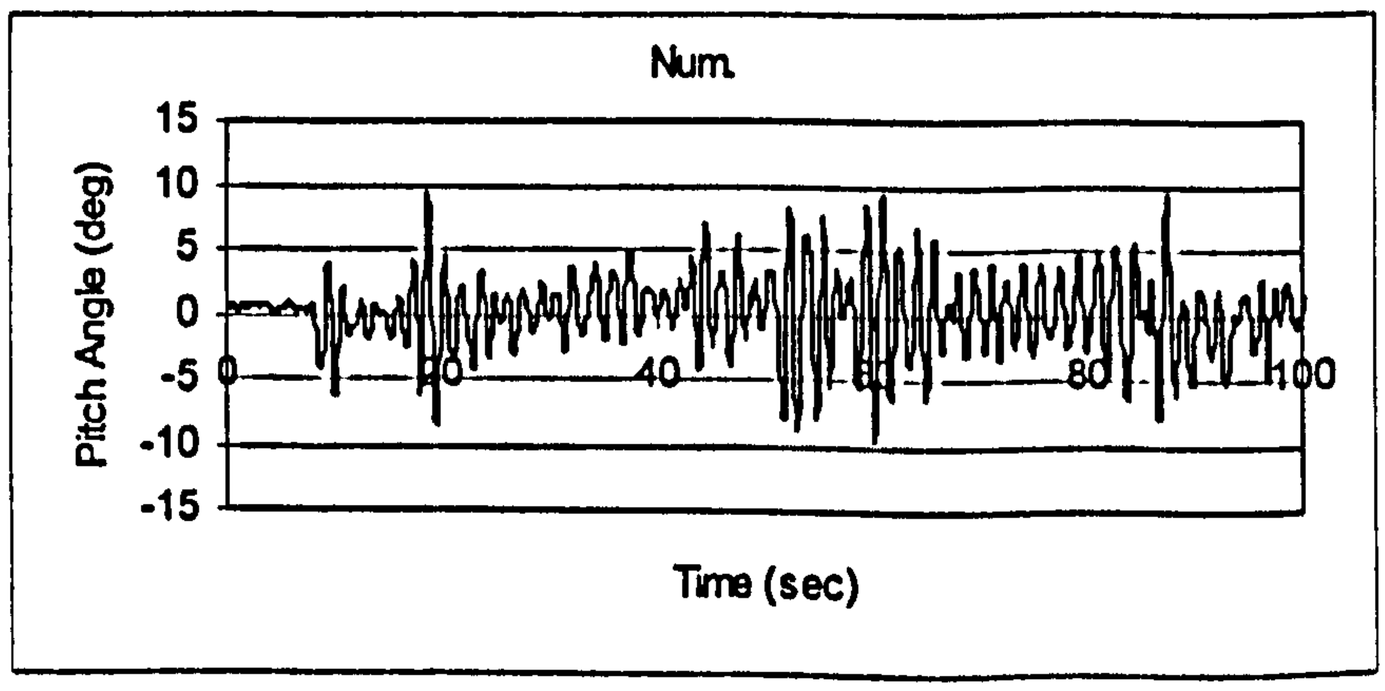

Figure 10.83 Pitch, JONSWAP, Fn=0.3, χ= -5°, H_s=0.23m, T_p=1.717 sec.

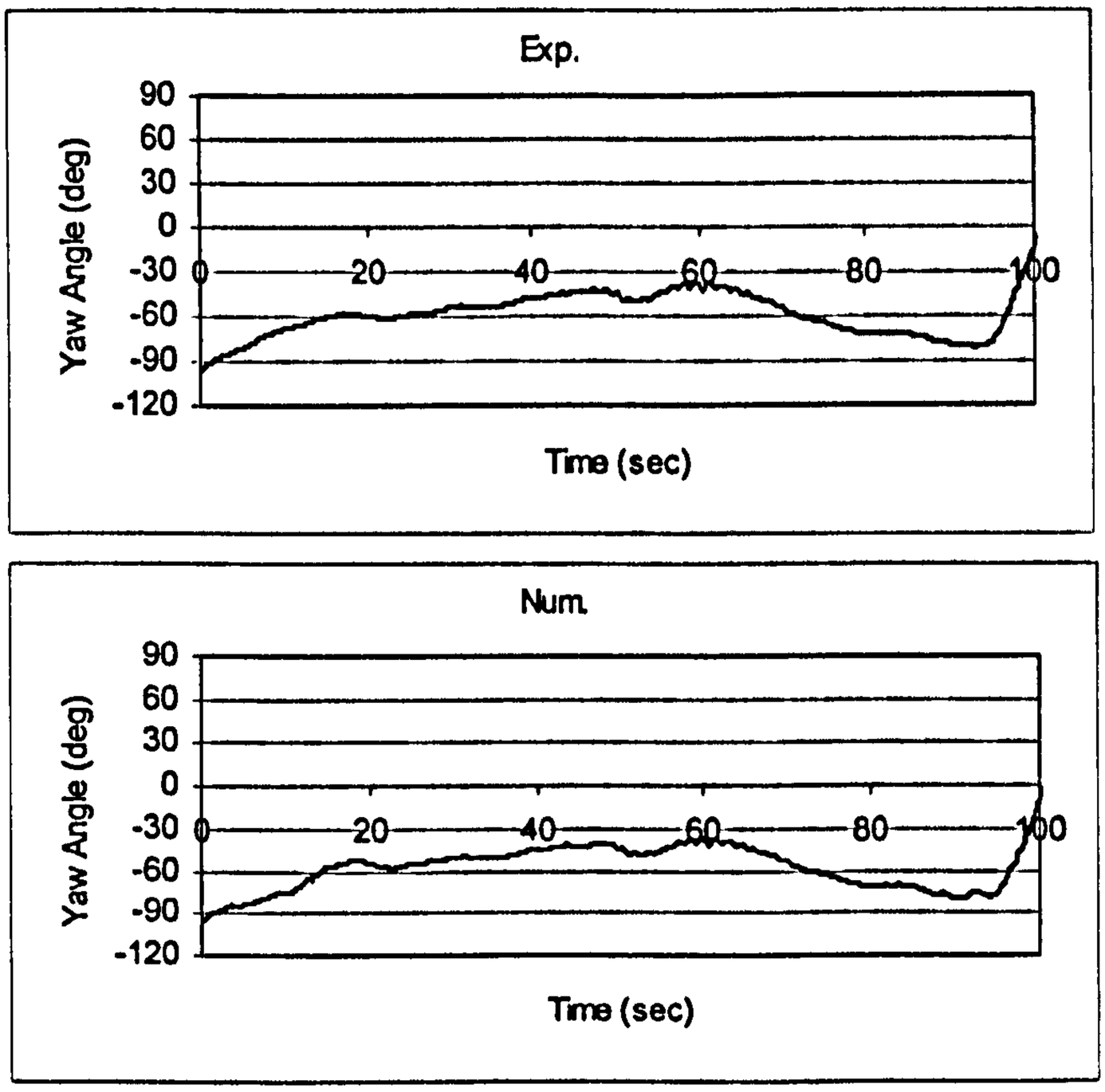

Figure 10.84 Yaw, JONSWAP, Fn=0.3, χ= -5°, H_s=0.23m, T_p=1.717 sec.

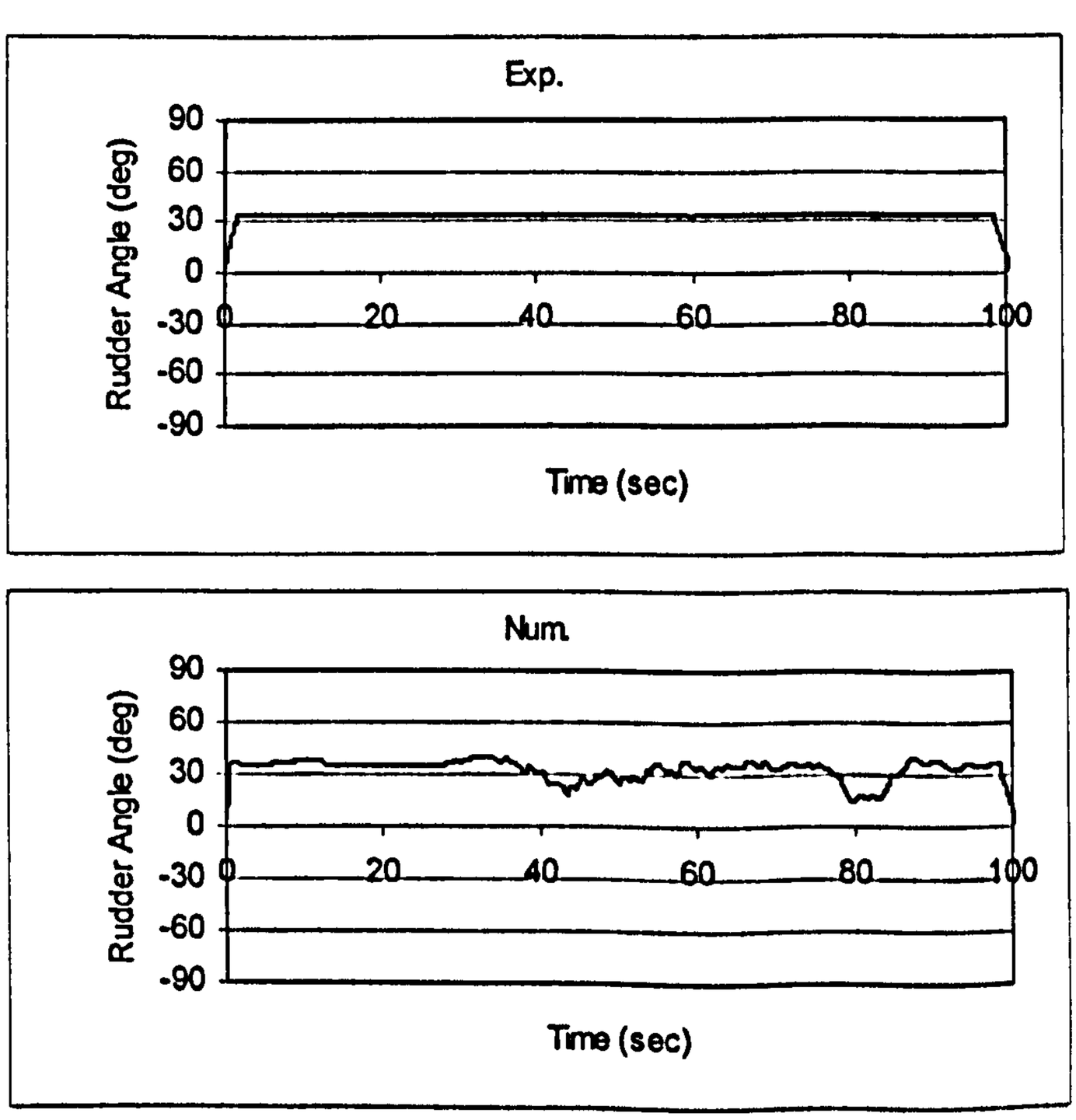

Figure 10.85 Rudder, JONSWAP, Fn=0.3, χ= -5°, H_s=0.23m, T_p=1.717 sec.

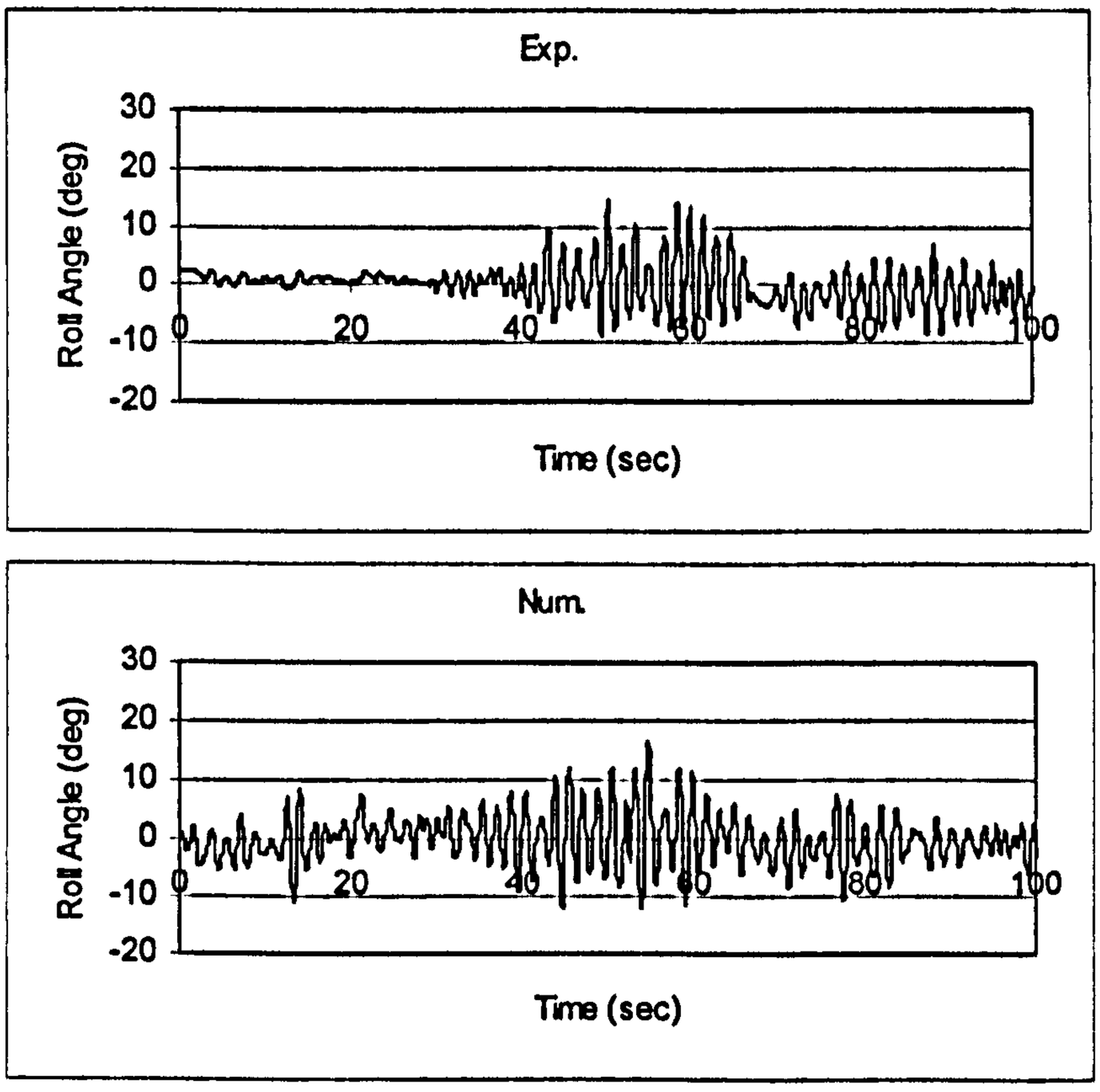

Figure 10.86 Roll, JONSWAP, Fn=0.4, χ= -5°, H_s=0.23m, T_p=1.717 sec.

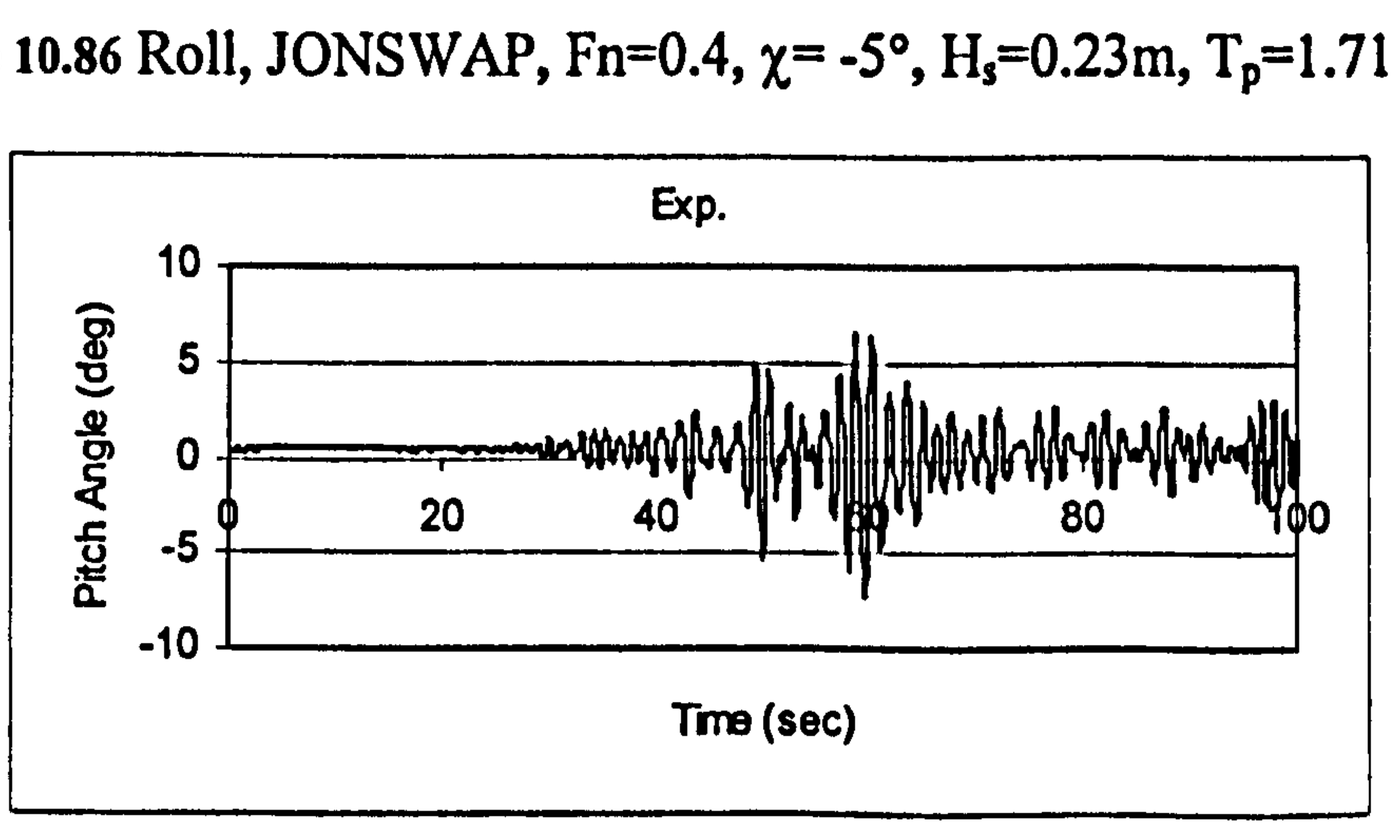

Figure 10.87 Pitch, JONSWAP, Fn=0.4, χ= -5°, H_s=0.23m, T_p=1.717 sec.

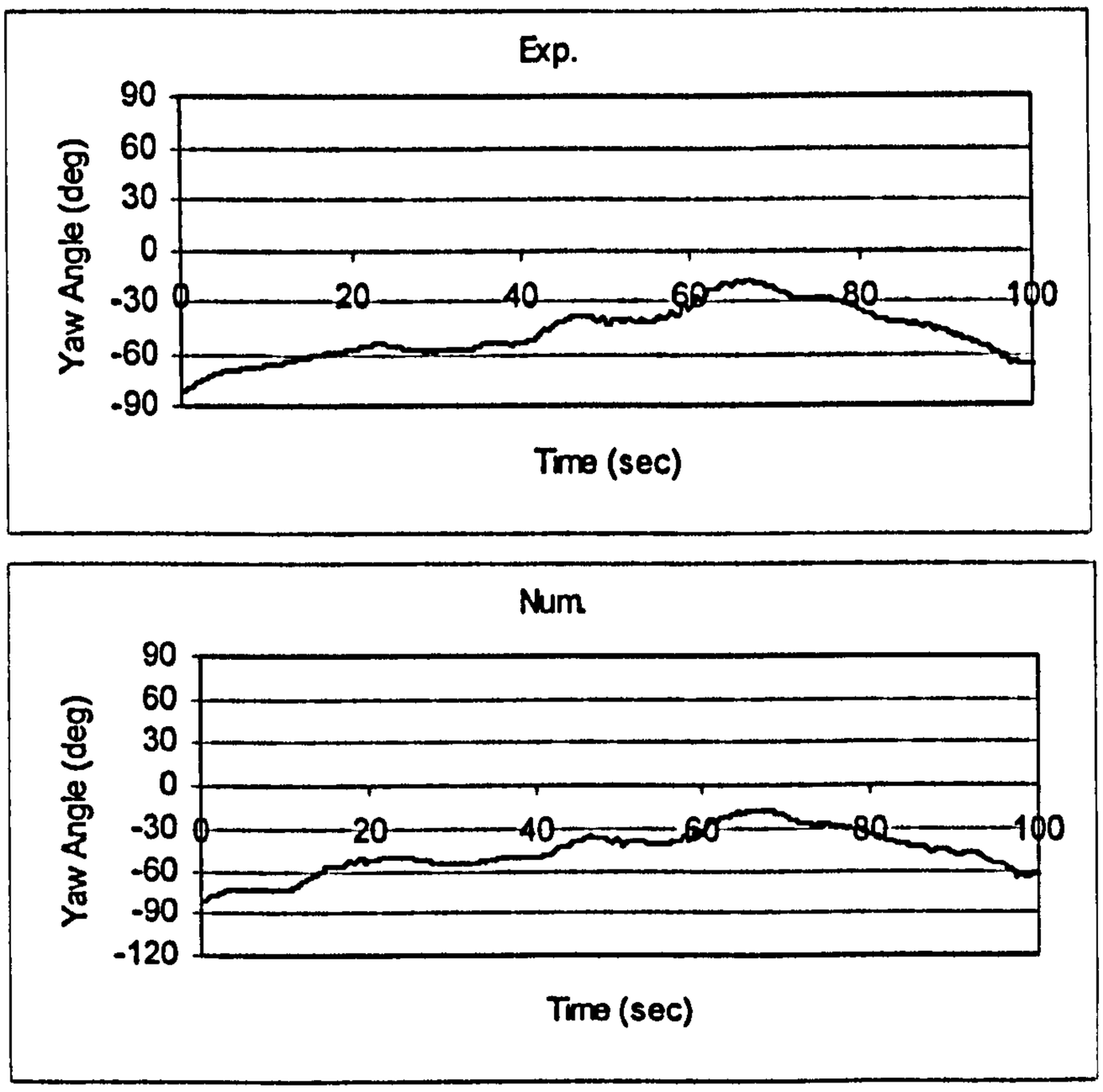

Figure 10.88 Yaw, JONSWAP, Fn=0.4, χ= -5°, H_s=0.23m, T_p=1.717 sec.

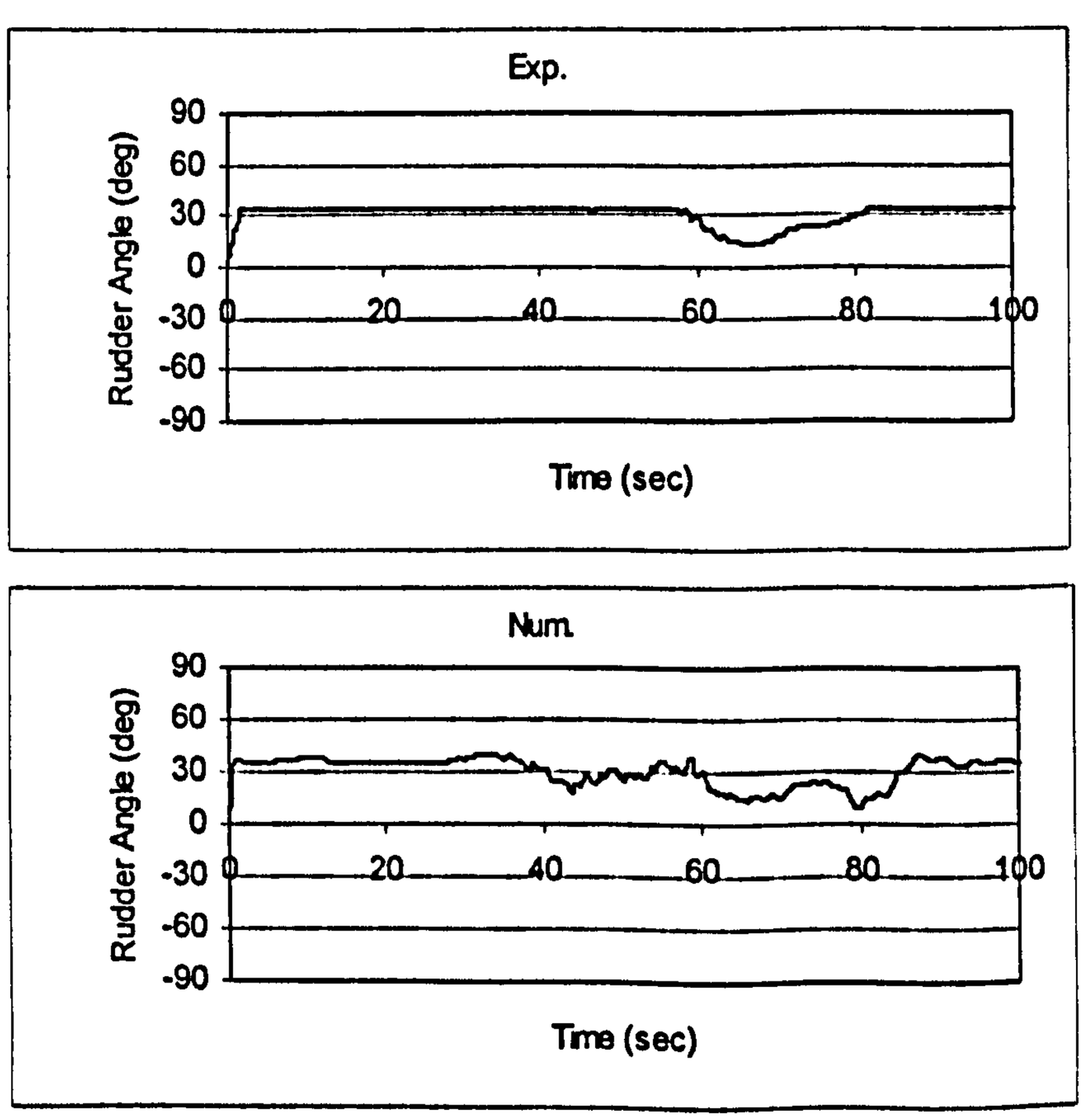

Figure 10.89 Rudder, JONSWAP, Fn=0.4, χ= -5°, H_s=0.23m, T_p=1.717 sec.

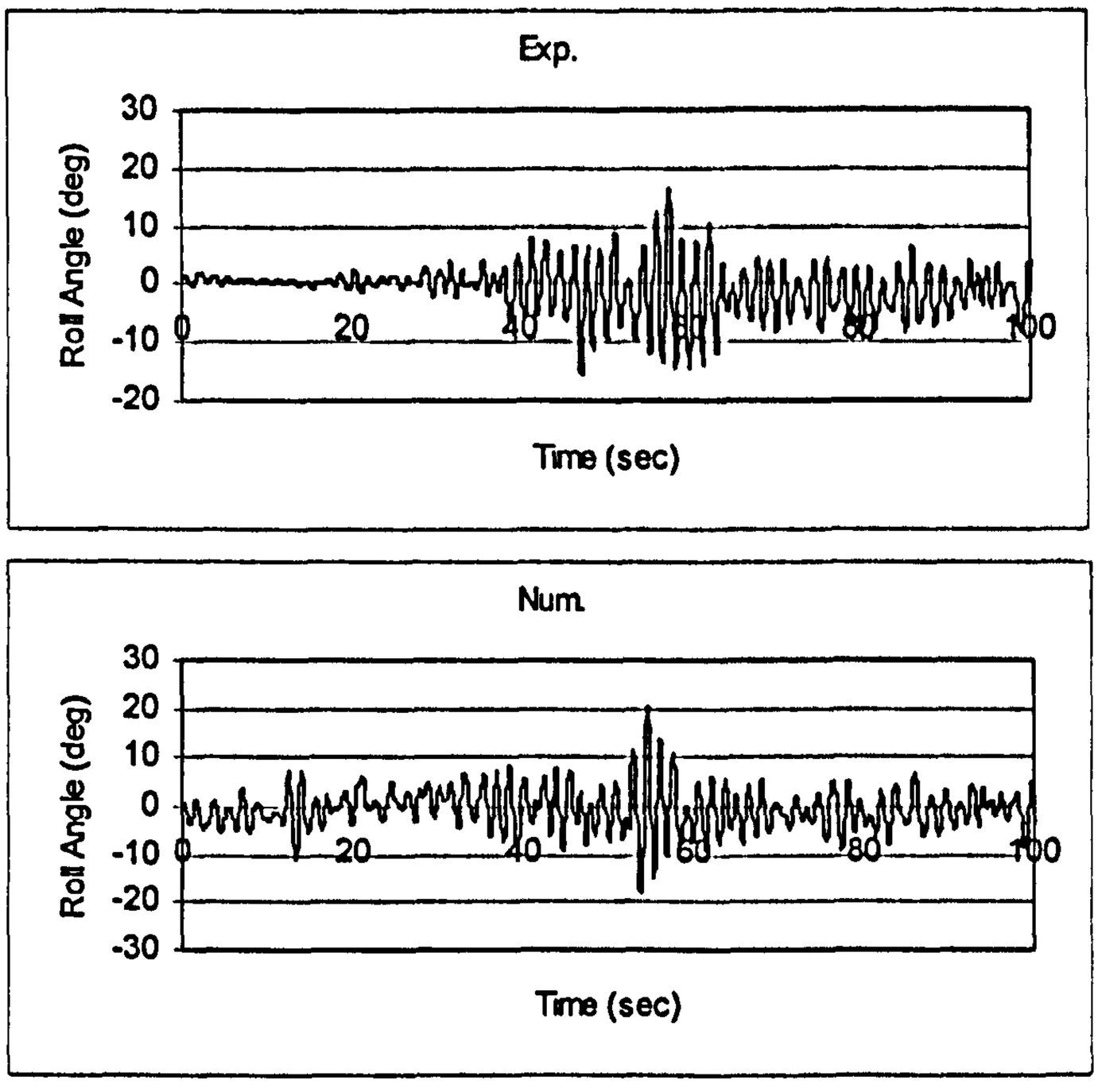

Figure 10.90 Roll, JONSWAP, Fn=0.3, χ= -45°, H_s=0.23m, T_p=1.717 sec.

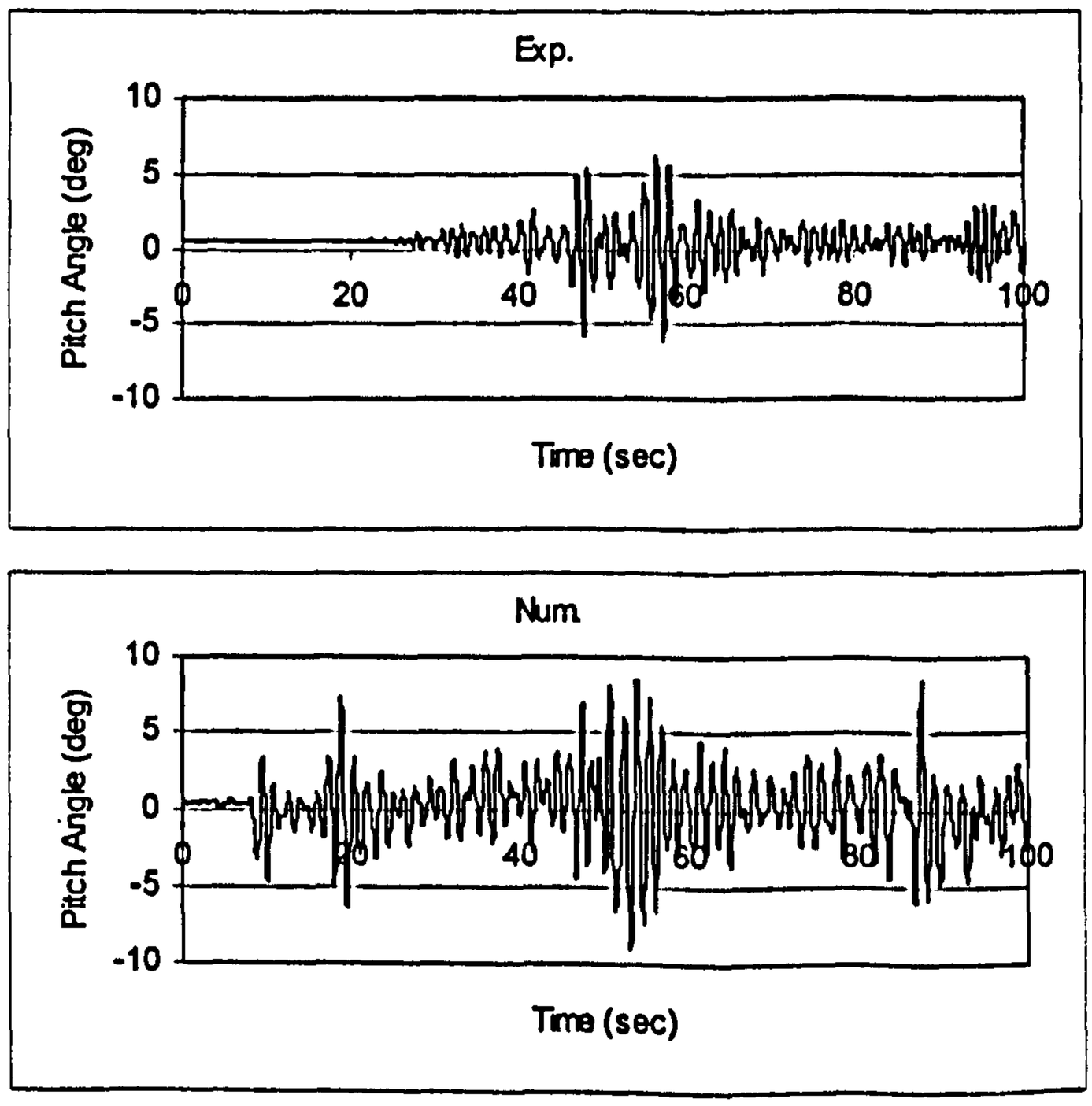

Figure 10.91 Pitch, JONSWAP, Fn=0.3, χ= -45°, H_s=0.23m, T_p=1.717 sec.

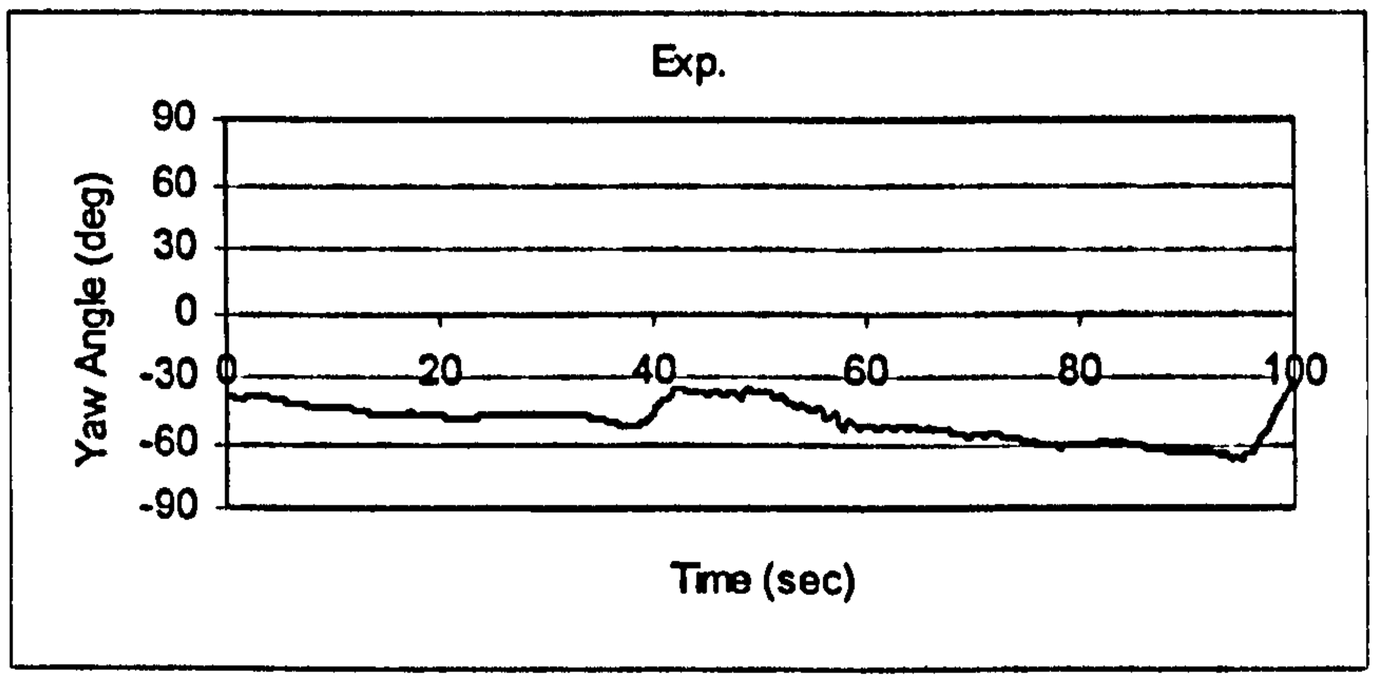

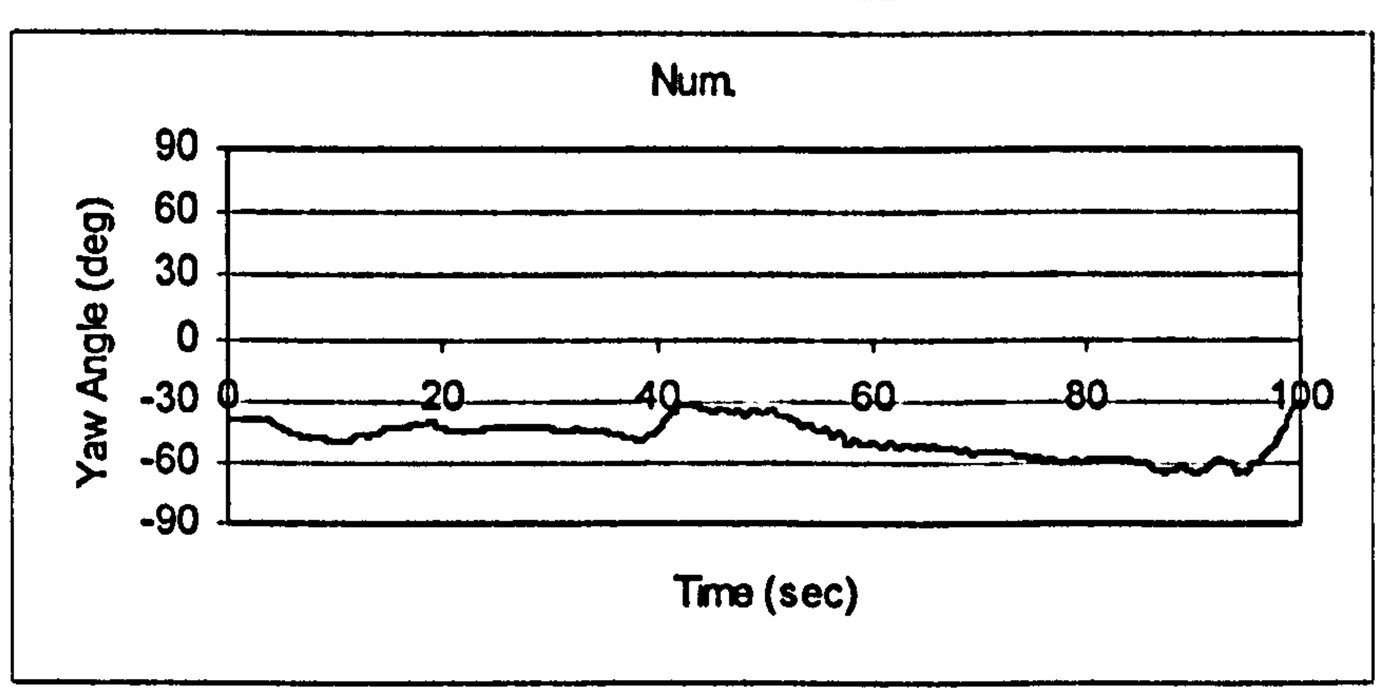

Figure 10.92 Yaw, JONSWAP, Fn=0.3, χ= -45°, H_s=0.23m, T_p=1.717 sec.

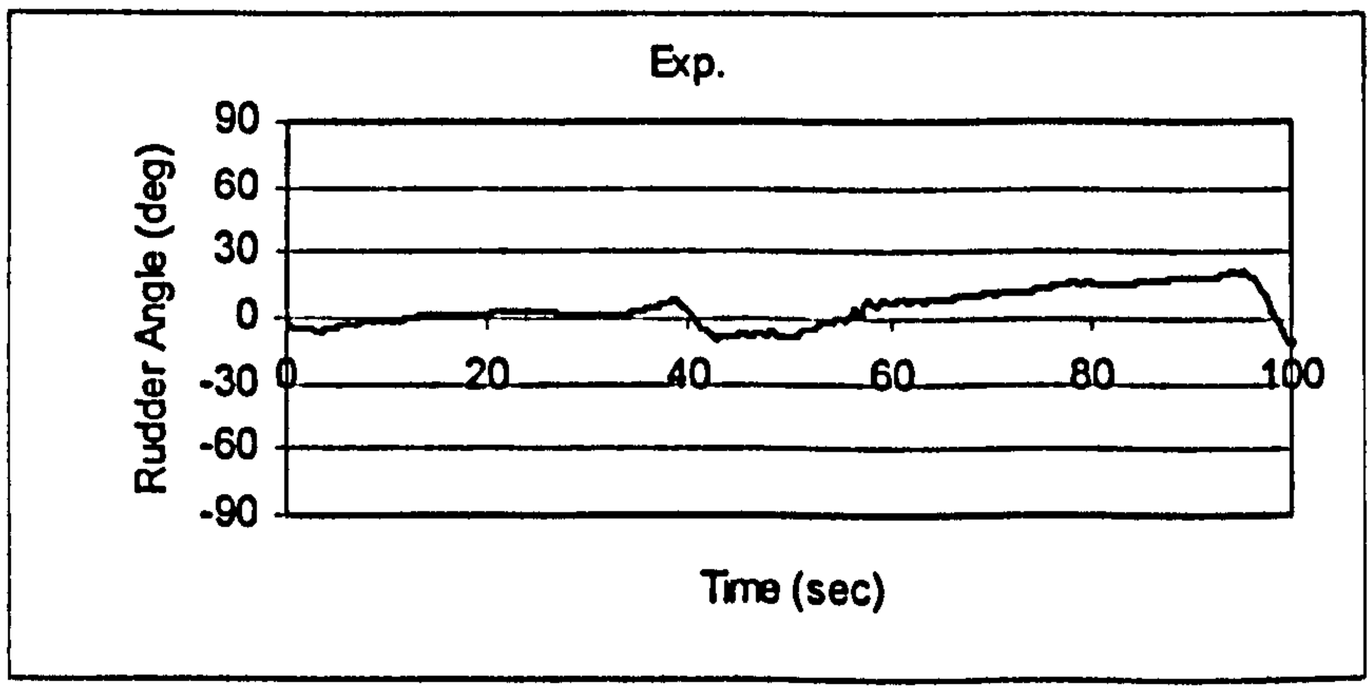

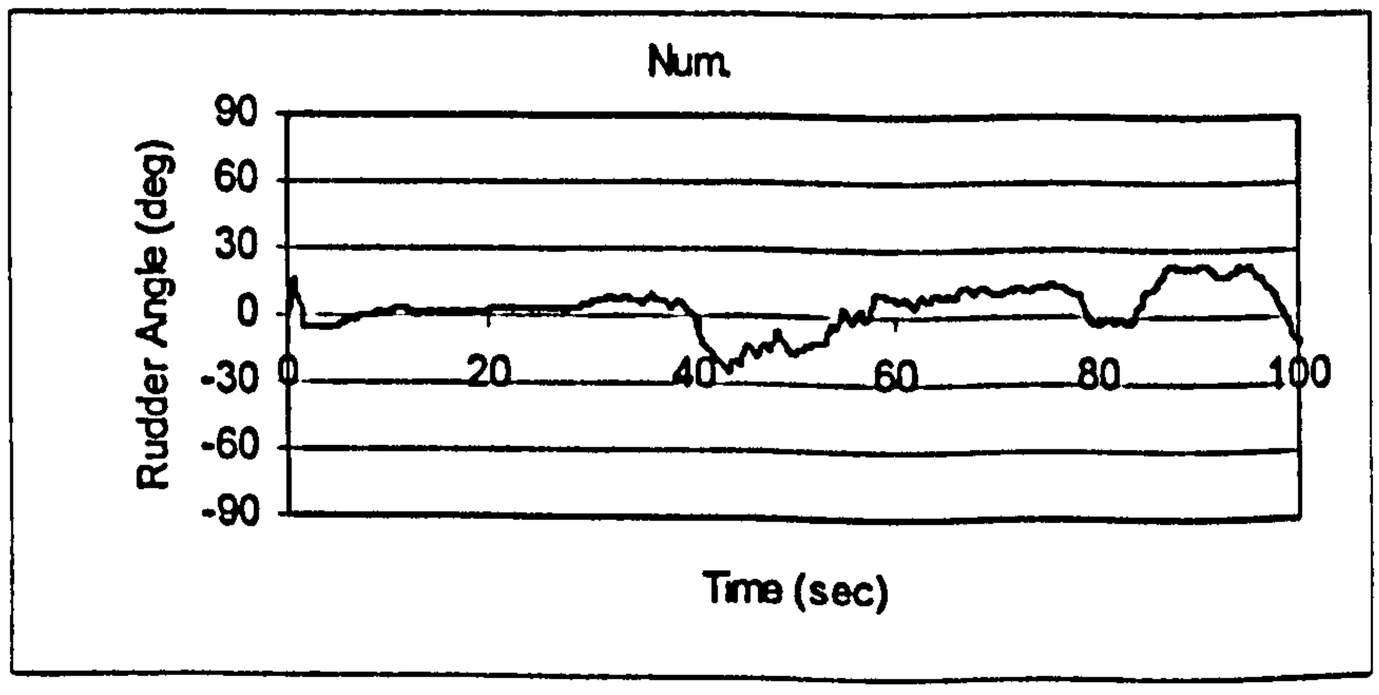

Figure 10.93 Rudder, JONSWAP, Fn=0.3, χ= -45°, H_s=0.23m, T_p=1.717 sec.

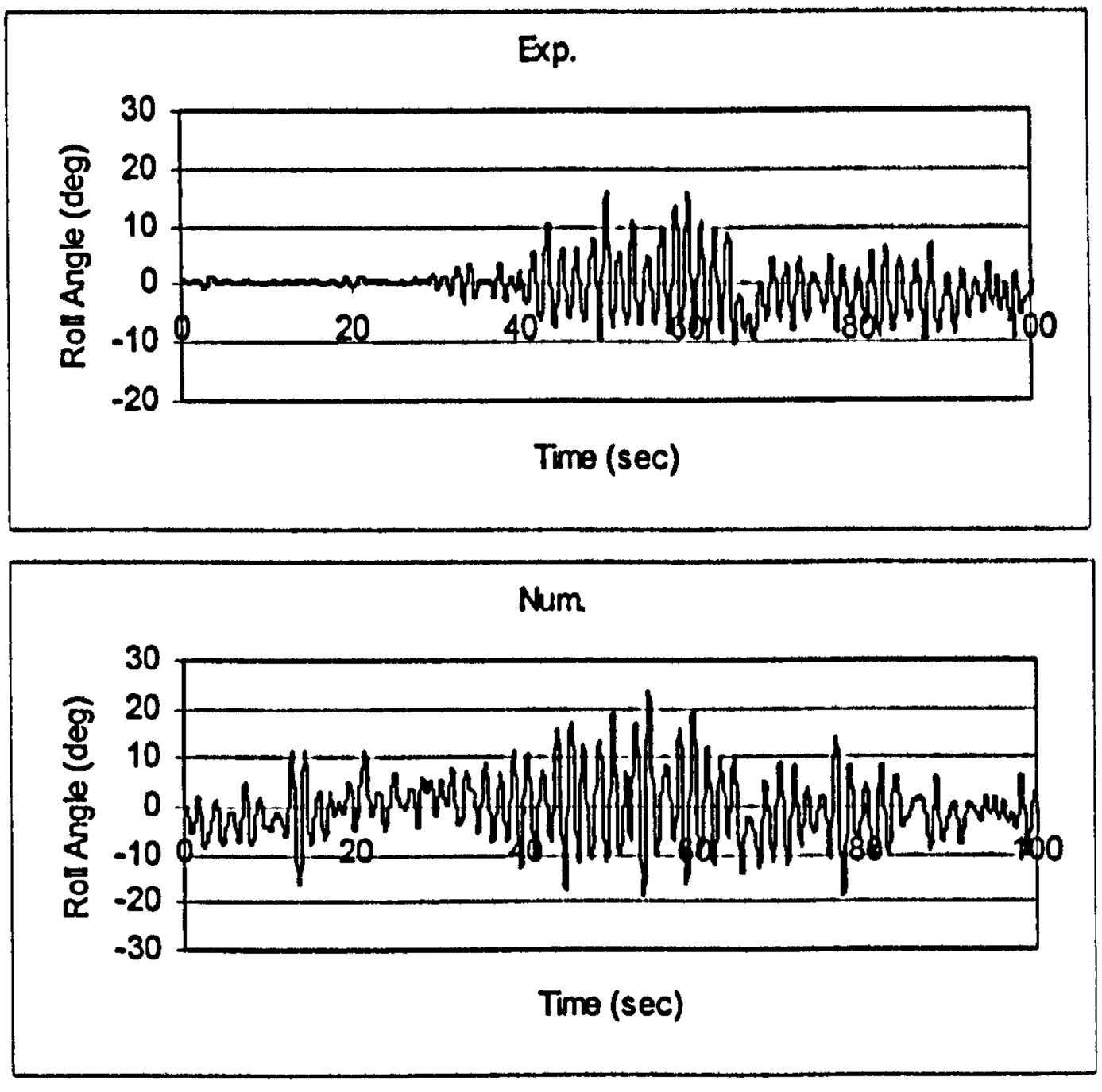

Figure 10.94 Roll, JONSWAP, Fn=0.4, χ= -45°, H_s=0.23m, T_p=1.717 sec.

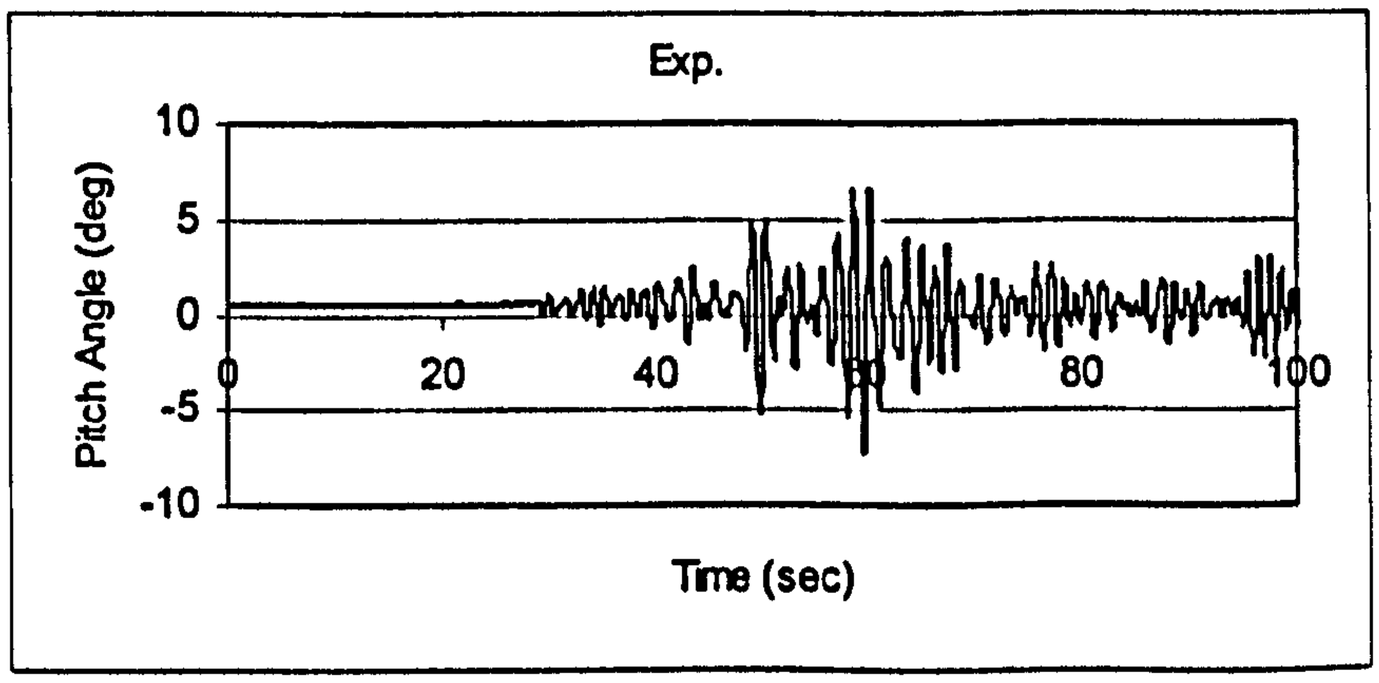

Figure 10.95 Pitch, JONSWAP, Fn=0.4, χ= -45°, H_s=0.23m, T_p=1.717 sec.

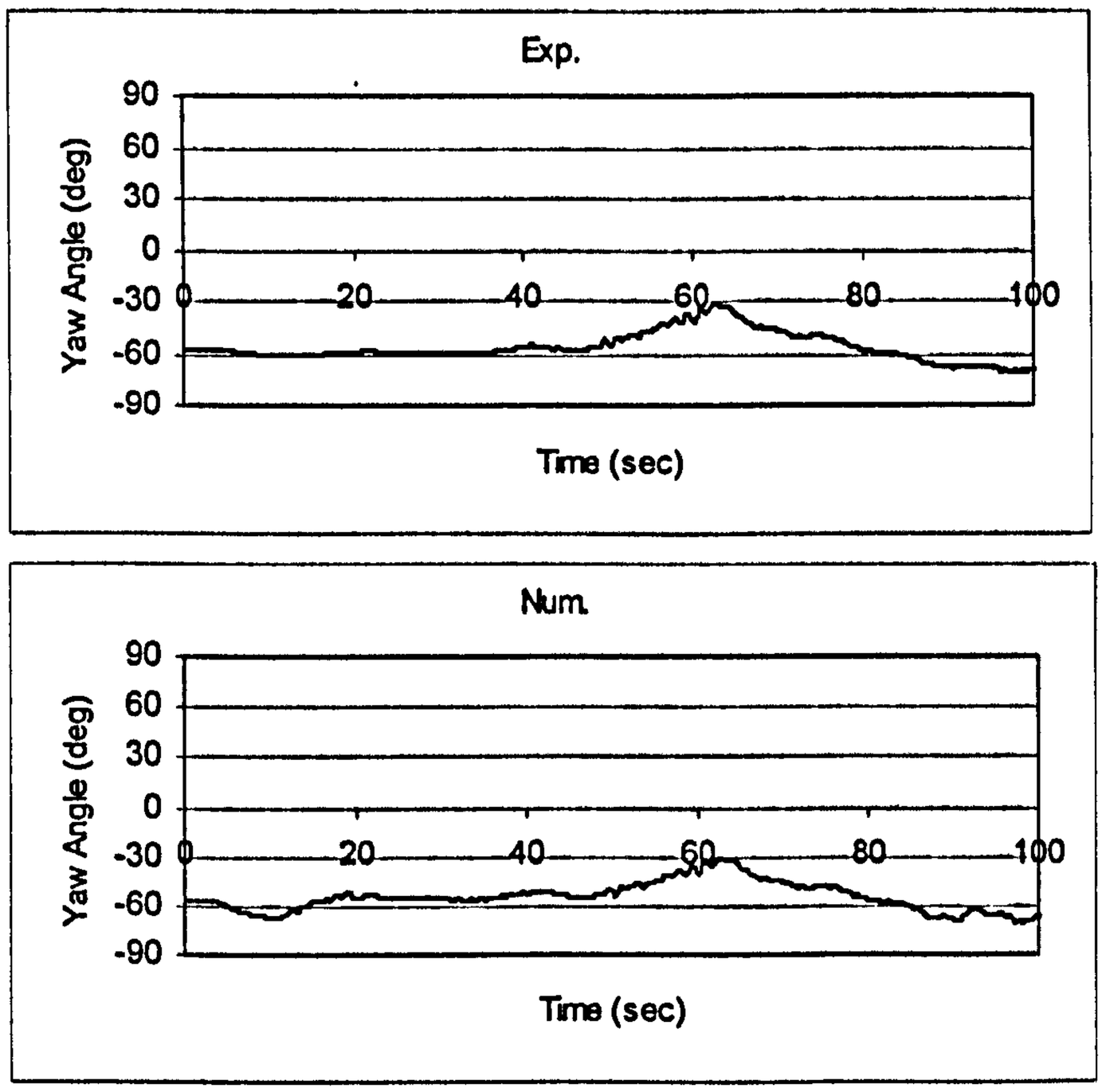

Figure 10.96 Yaw, JONSWAP, Fn=0.4, χ= -45°, H_s=0.23m, T_p=1.717 sec.

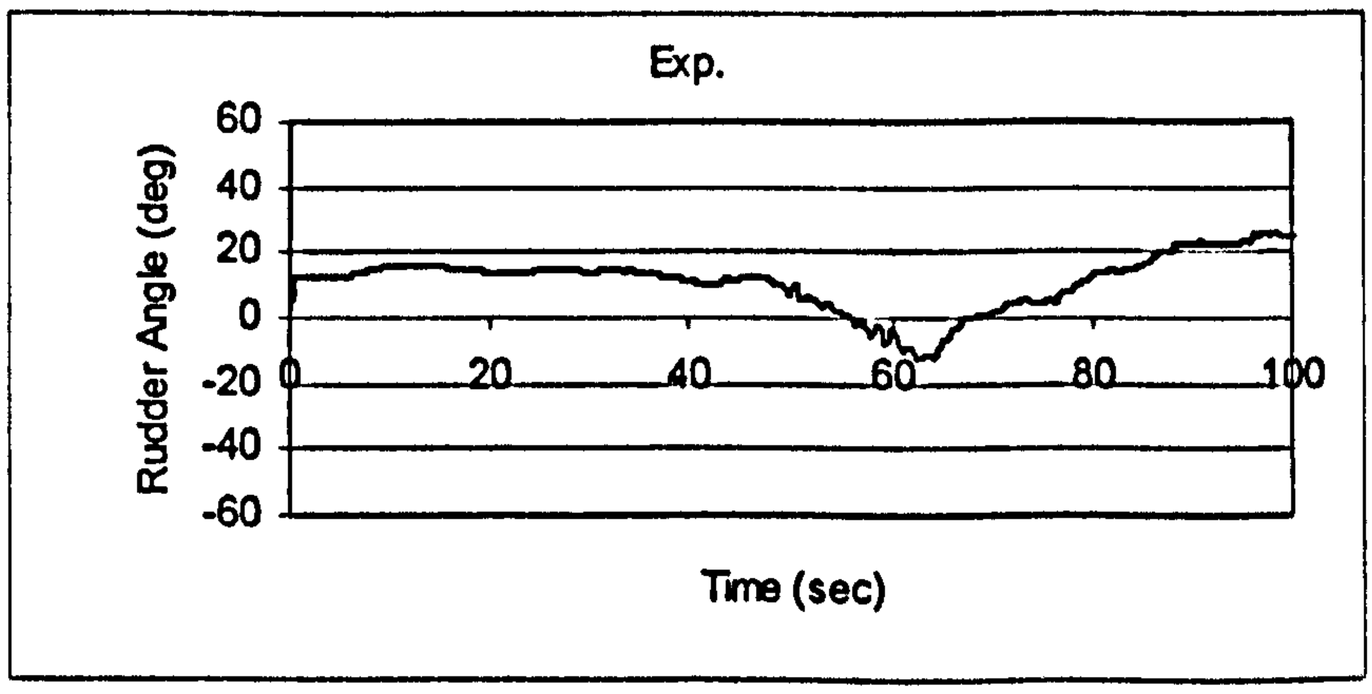

Figure 10.97 Rudder, JONSWAP, Fn=0.4, χ=45°, H_s=0.23m, T_p=1.717 sec.

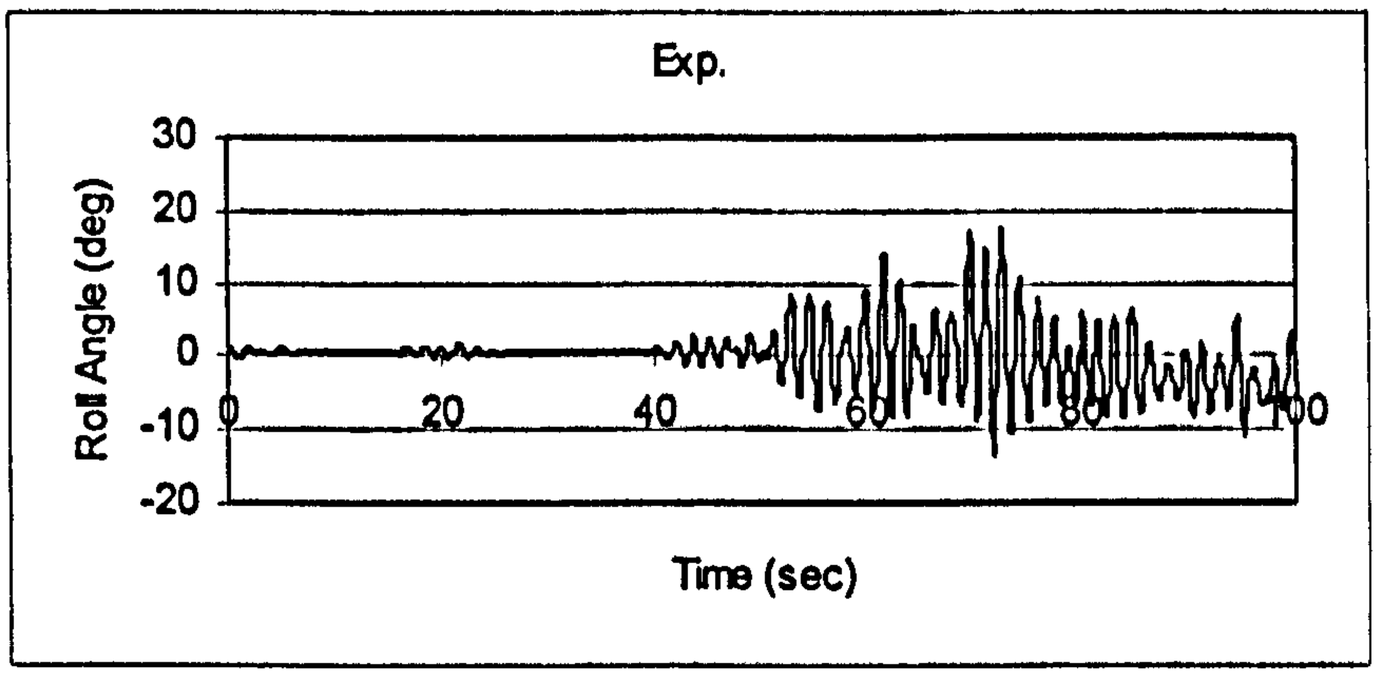

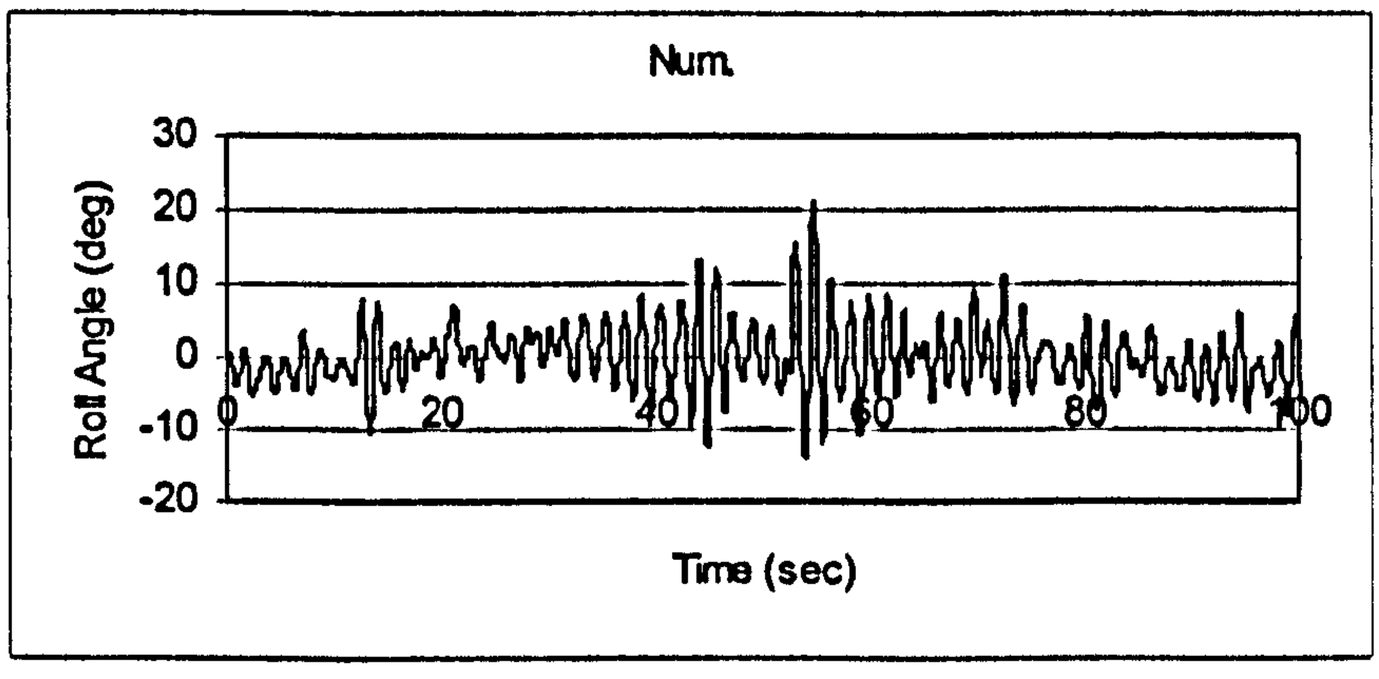

Figure 10.98 Roll, JONSWAP, Fn=0.3, χ=60°, H_s=0.23m, T_p=1.717 sec.

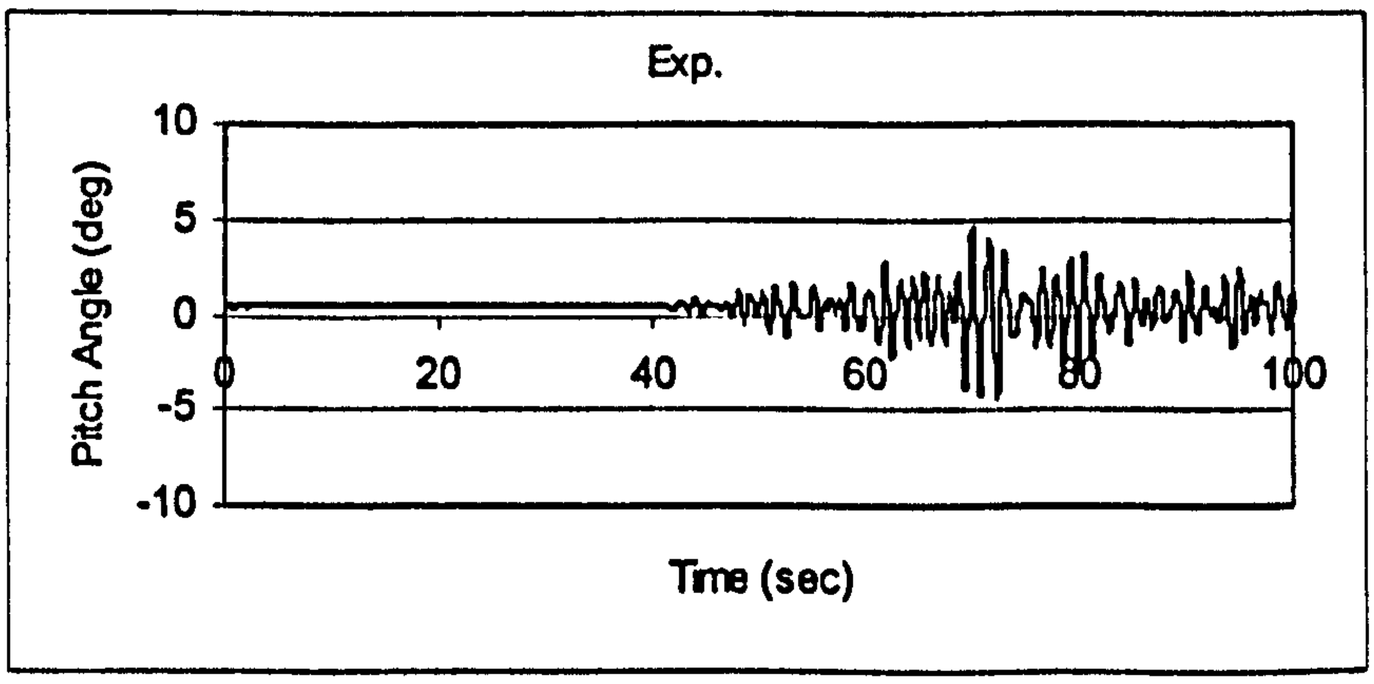

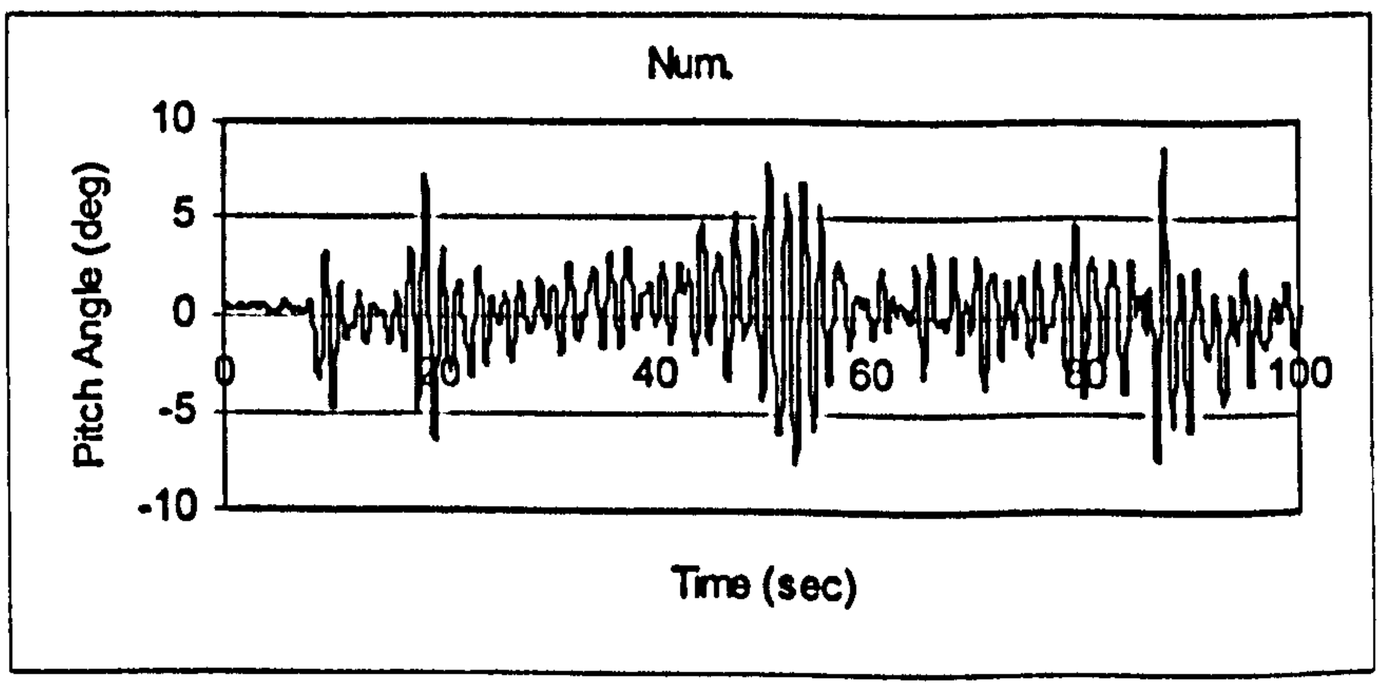

Figure 10.99 Pitch, JONSWAP, Fn=0.3, χ= -60°, H_s=0.23m, T_p=1.717 sec.

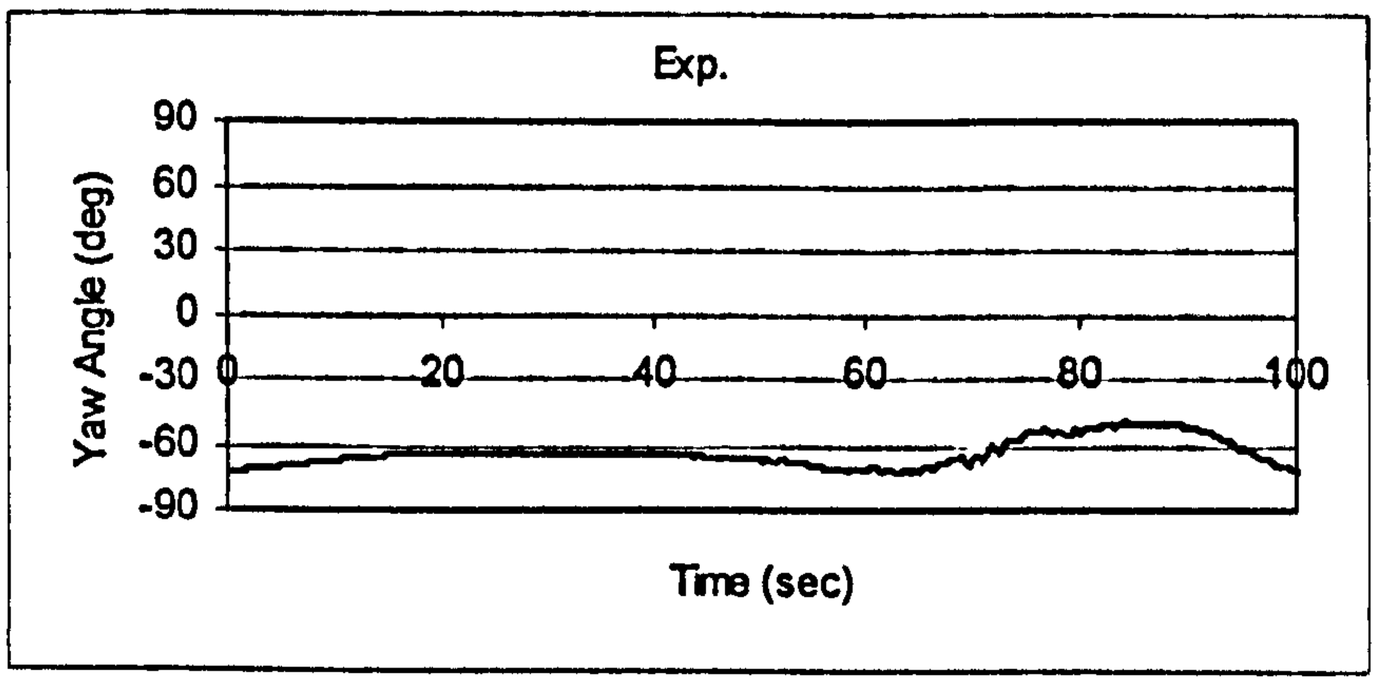

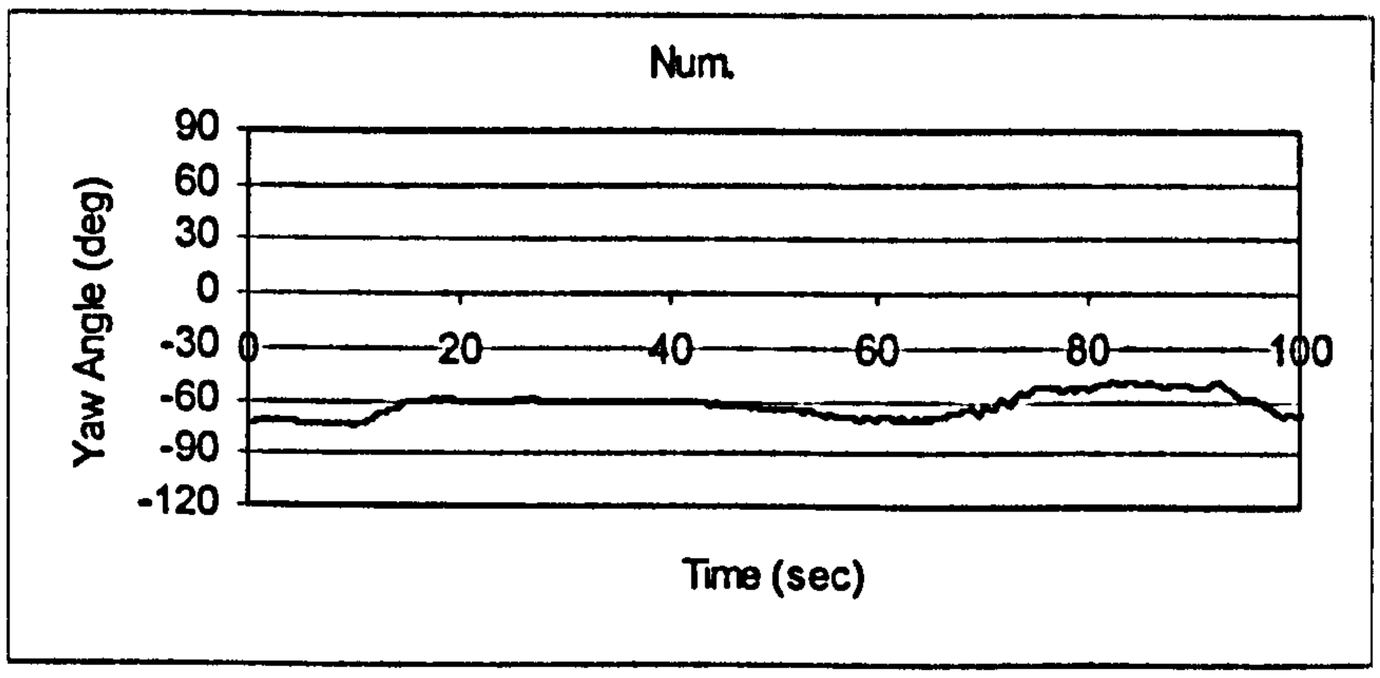

Figure 10.100 Yaw, JONSWAP, Fn=0.3, χ= -60°, H_s=0.23m, T_p=1.717 sec.

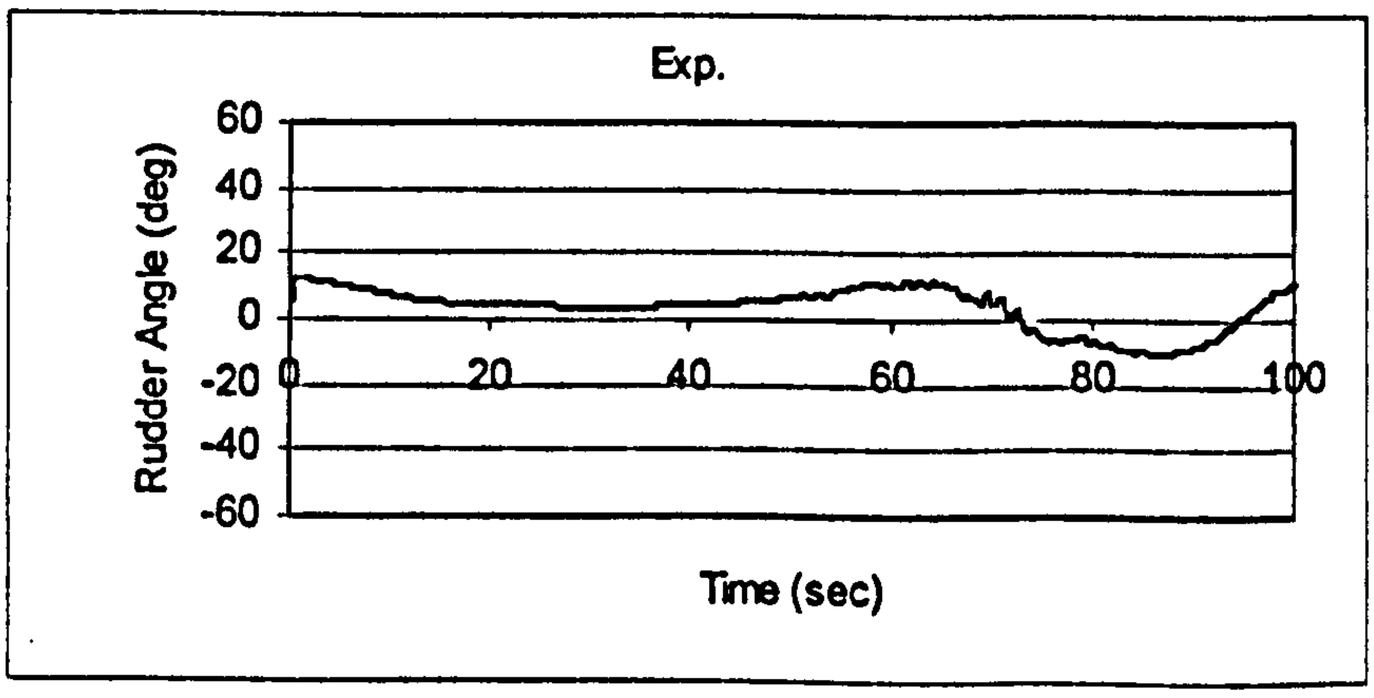

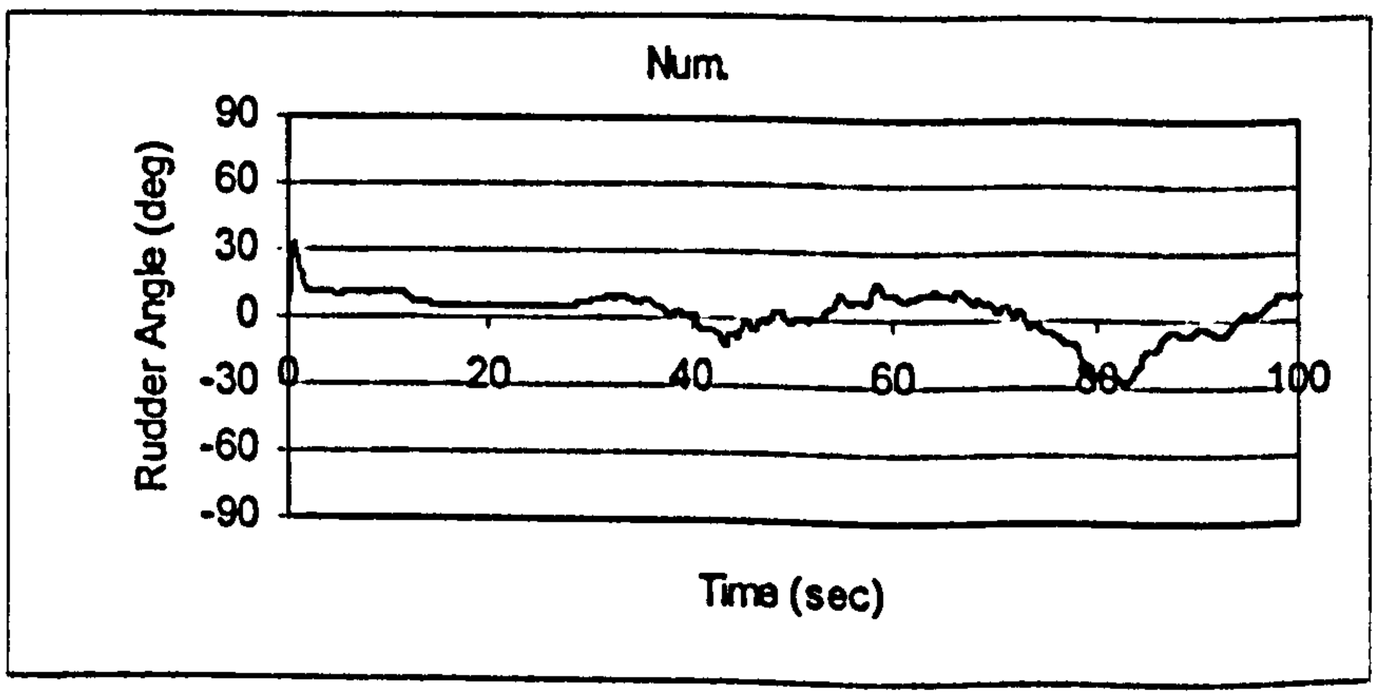

Figure 10.101 Rudder, JONSWAP, Fn=0.3, χ= -60°, H_s=0.23m, T_p=1.717 sec.

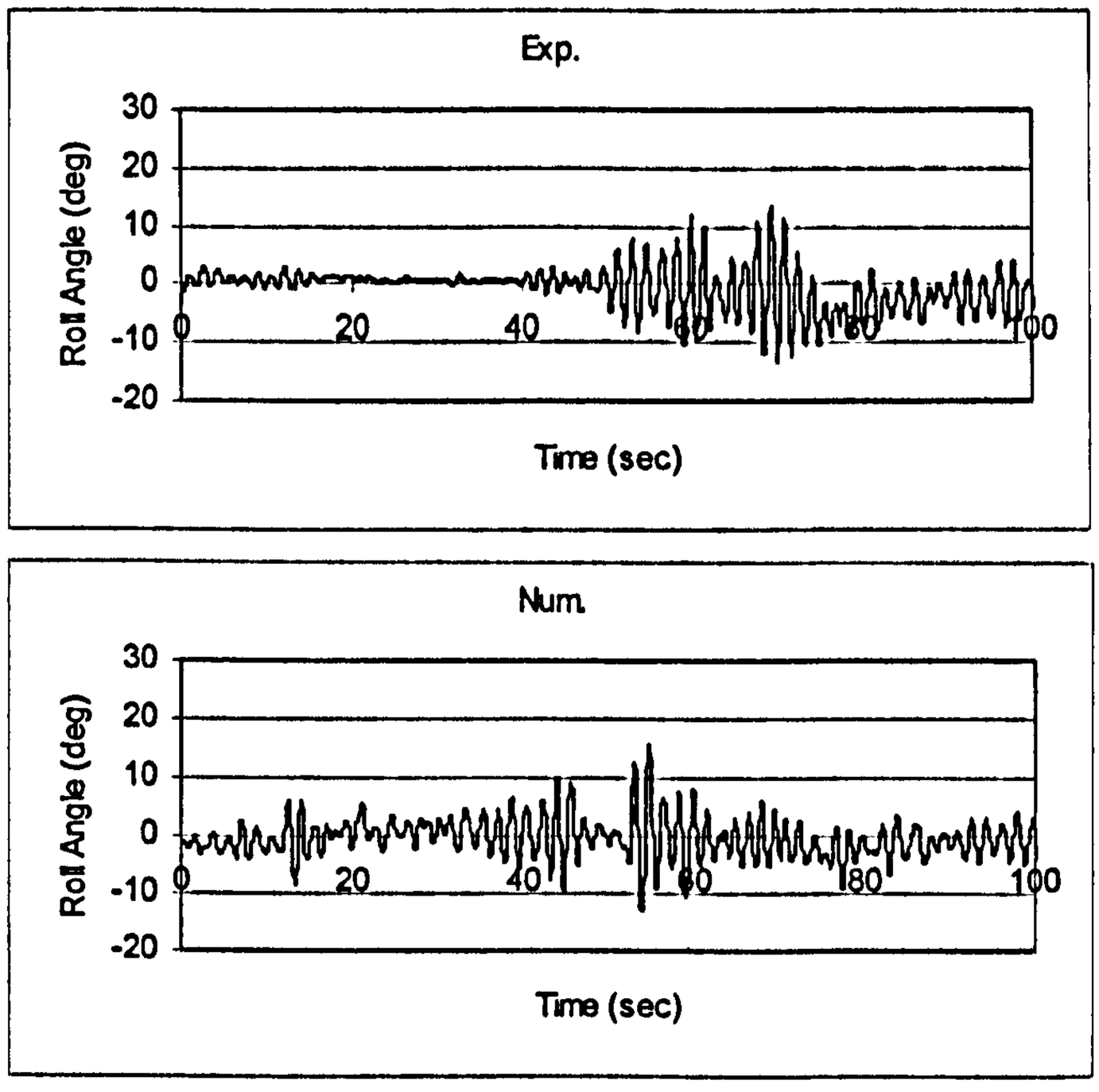

Figure 10.102 Roll, JONSWAP, Fn=0.4, χ= -60°, H_s=0.23m, T_p=1.717 sec.

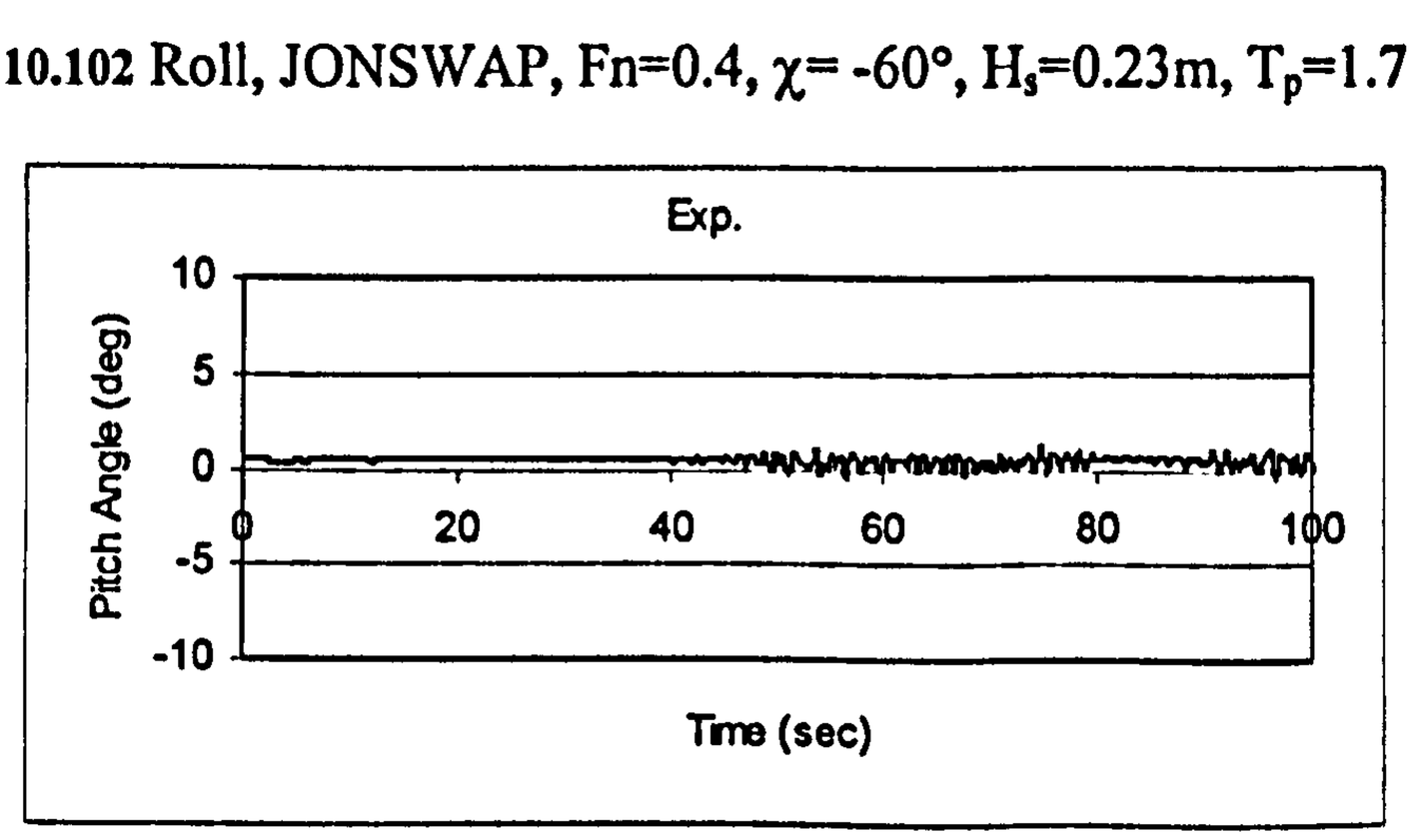

Figure 10.103 Pitch, JONSWAP, Fn=0.4, χ= -60°, H_s=0.23m, T_p=1.717 sec.

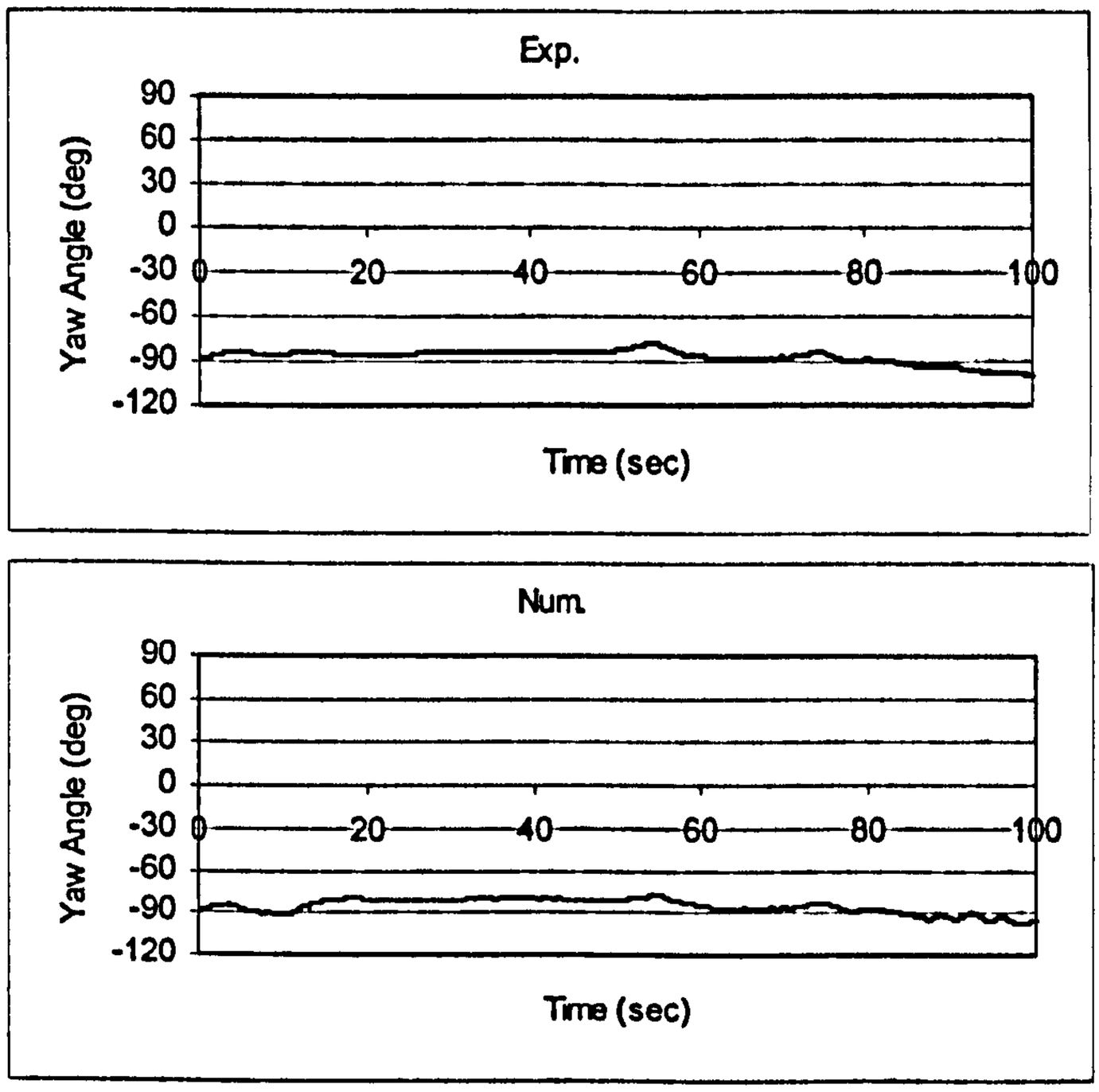

Figure 10.104 Yaw, JONSWAP, Fn=0.4, χ= -60°, H_s=0.23m, T_p=1.717 sec.

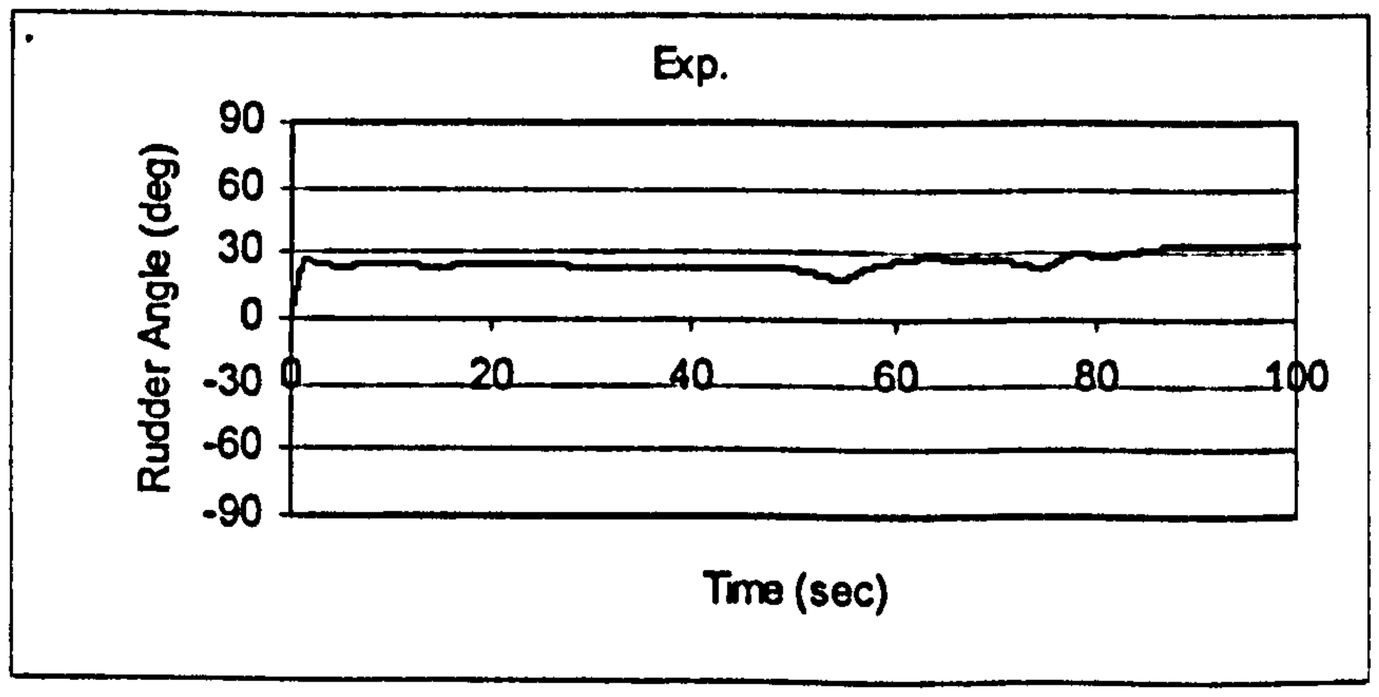

Figure 10.105 Rudder, JONSWAP, Fn=0.4, χ= -60°, H_s=0.23m, T_p=1.717 sec.

In order to assess the overall results, in Figures 10.106-10.109, single amplitude significant roll and pitch angles for the both spectrum with respect to heading angle in Fn=0.3 and Fn=0.4 were plotted for experiments and numerical model.

The outcome of these results and critical aspects will be discussed in the next sections. Full model experiment results are presented in Appendix H.

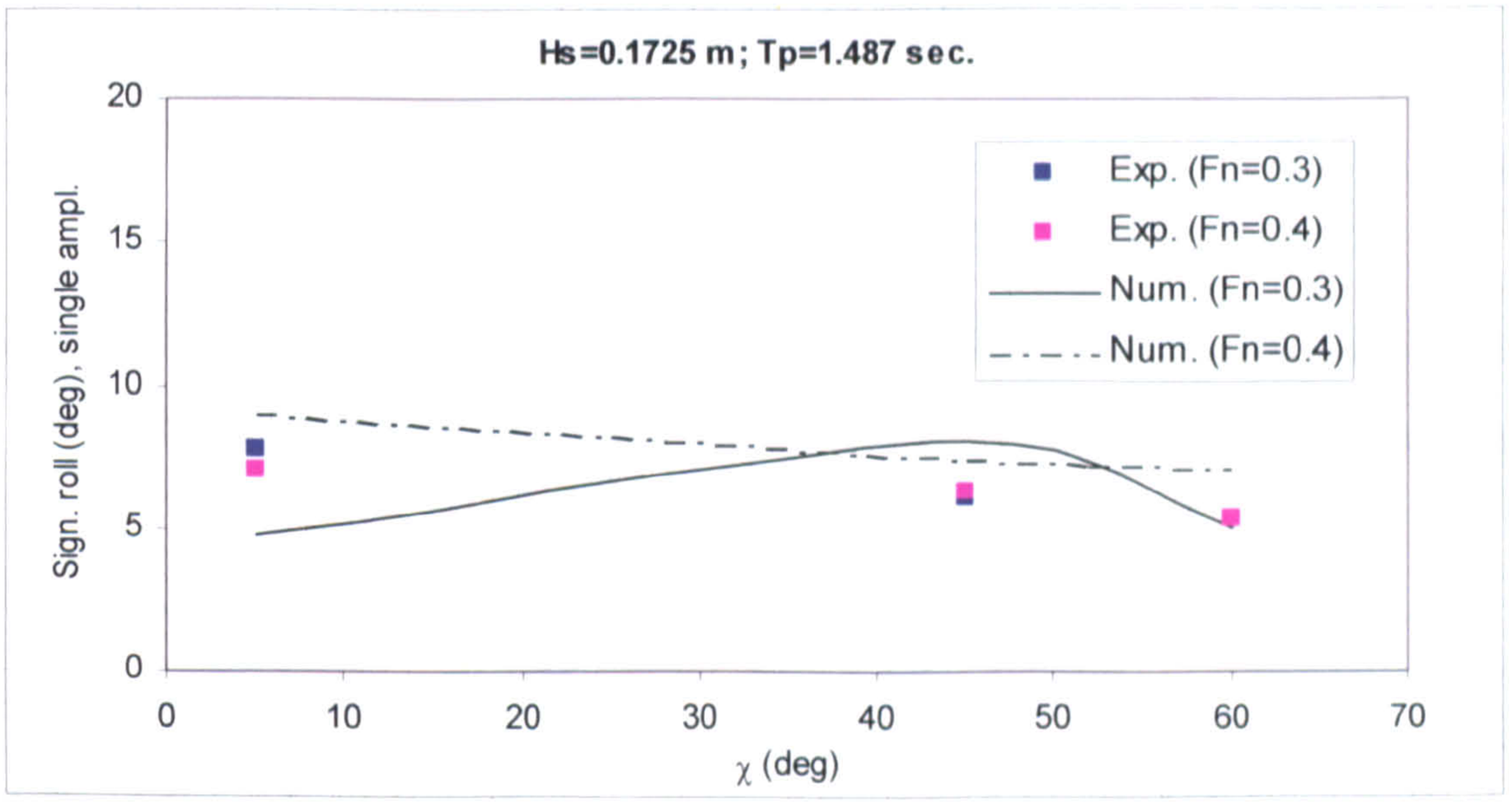

Figure 10.106 Single amplitude significant roll angle with respect to wave direction for Fn=0.3 and Fn=0.4 in ITTC spectrum

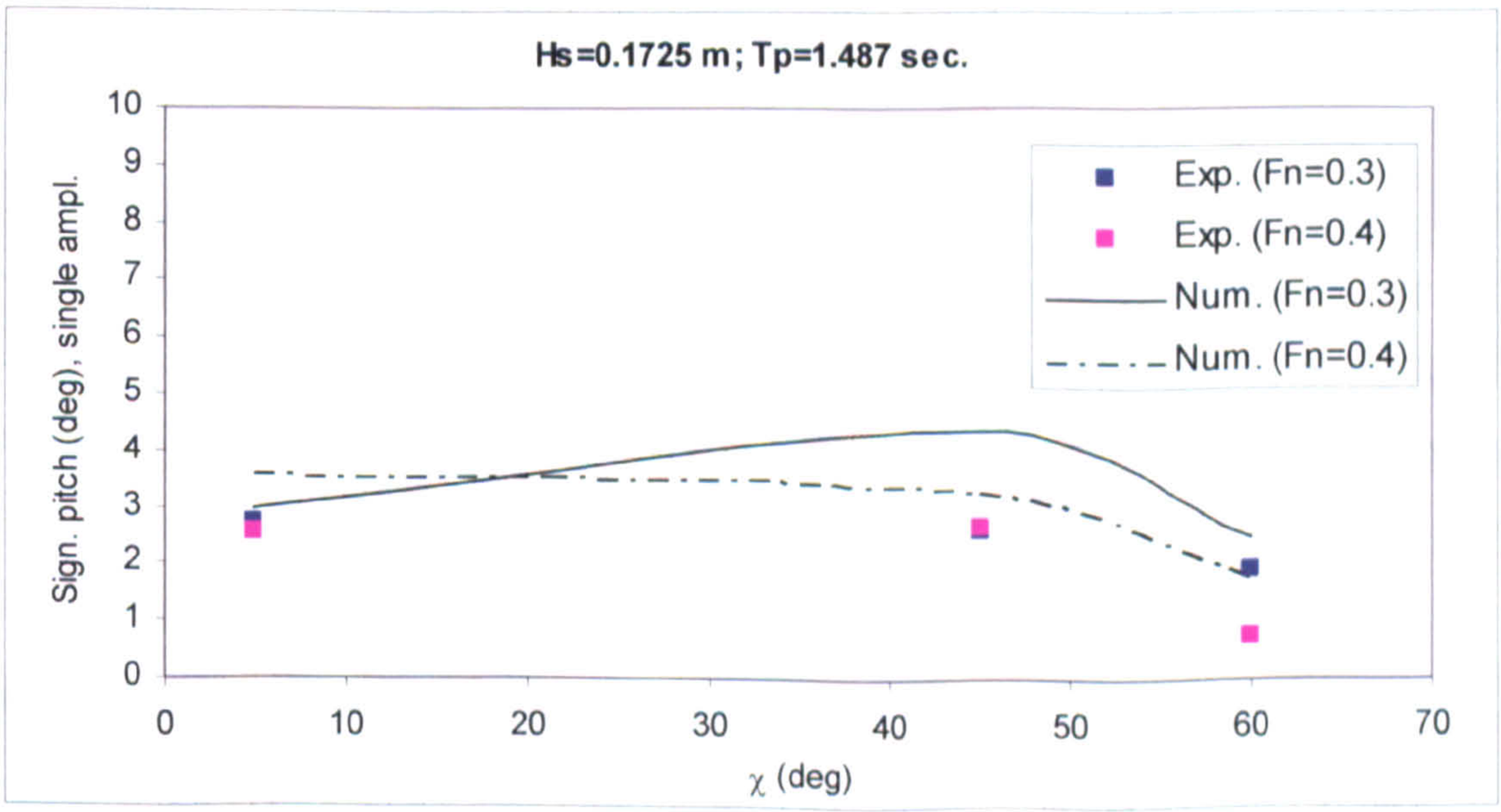

Figure 10.107 Single amplitude significant pitch angle with respect to wave direction for Fn=0.3 and Fn=0.4 in ITTC spectrum

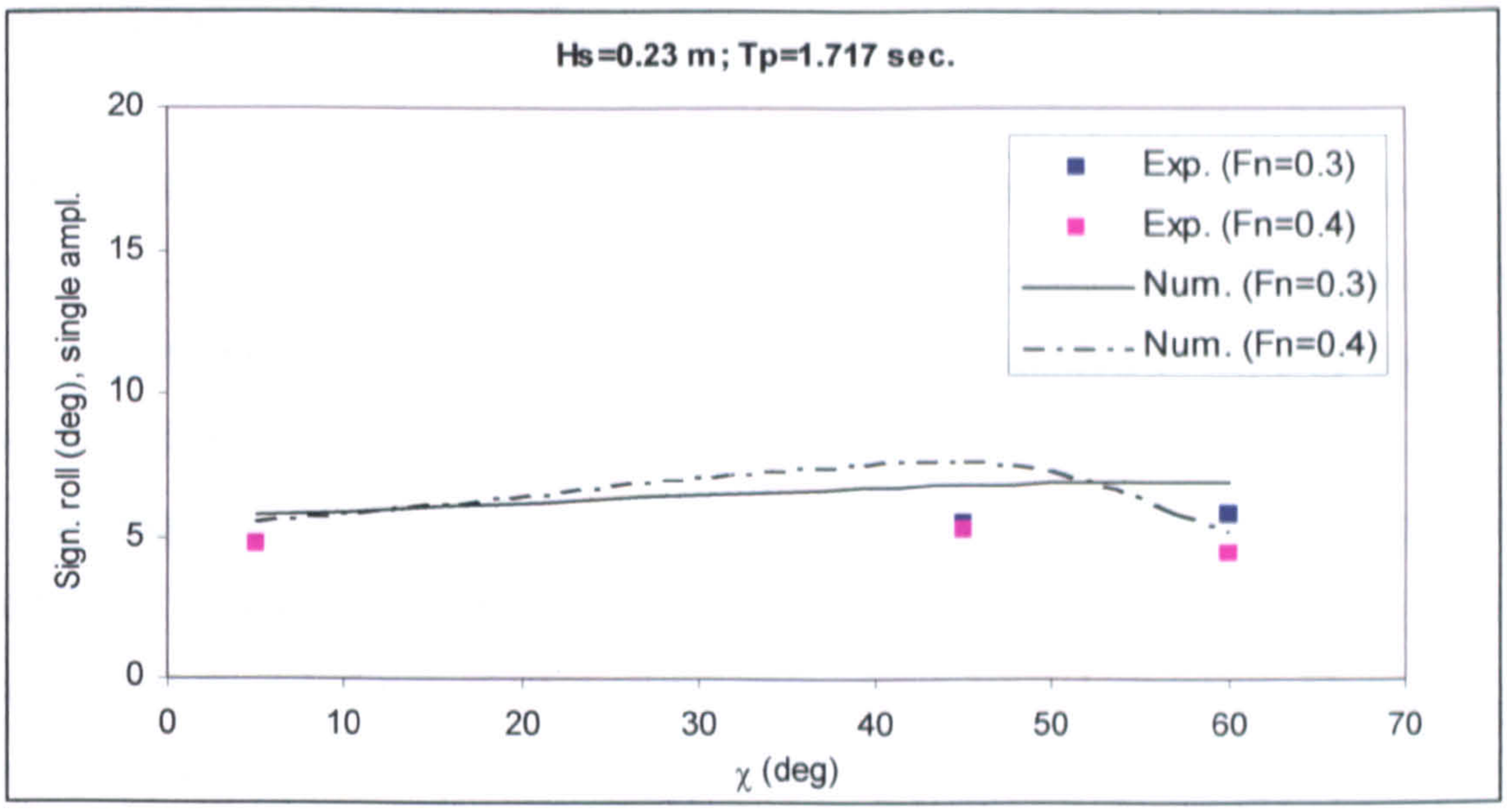

Figure 10.108 Single amplitude significant roll angle with respect to wave direction for Fn=0.3 and Fn=0.4 in JONSWAP spectrum

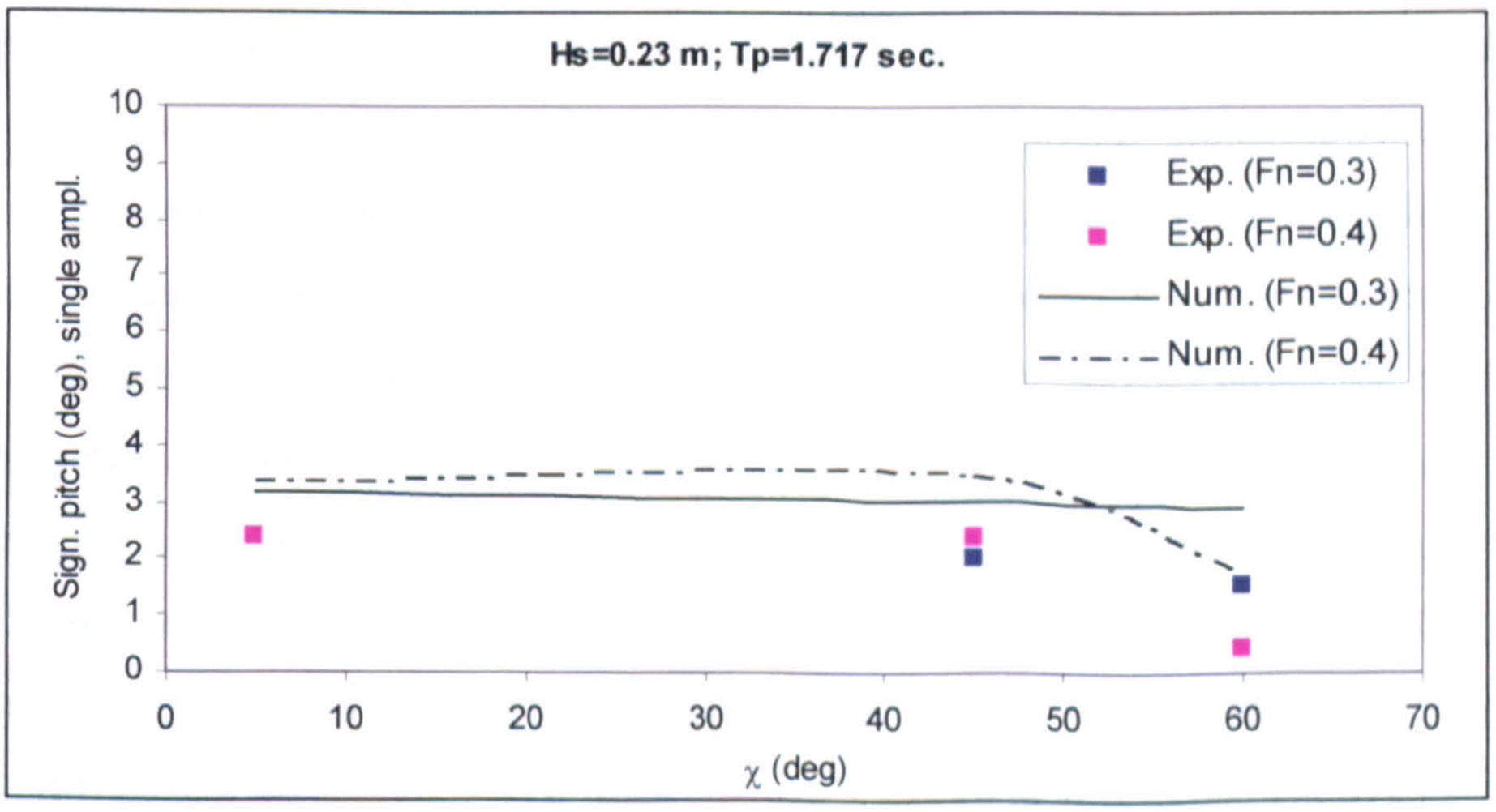

Figure 10.109 Single amplitude significant roll angle with respect to wave direction for Fn=0.3 and Fn=0.4 in JONSWAP spectrum

10.4. Discussion on Results

As it is described in the previous sections, two types of experiments: captive and free running, were conducted to provide feedback to the mathematical model and to modify it for the realistic ship motions. The results of the numerical simulations and experiment are given and they are illustrated as it is described in the previous sections.

Captive model experiments:

Here, the results obtained will be of interest for the first two terms in the Equation 10.5. It is stated previously that one of the aims of this study is to obtain fully coupled (6 DOF) numerical model for the accurate representation of the ship motions in the extreme astern seas.

The requirement of obtaining those terms was accomplished through the wave force values in the captive model tests. Since the aim was to carry out this study in full 6 DOF numerical model, the vertical motions were given special attention. Therefore, the above results were demonstrated in two different conditions. The first group is the zero heel, sinkage and trim (10.10-10.34) and the second group with the maximum roll, sinkage and trim values (10.34-10.57) the model allowed. Here, the results are represented in terms of amplitude and phase. The results are given in terms of wave steepness, effect of encounter frequency and heading angle in order to assess the fully captive motions and the accuracy of numerical model to simulate those motions. The effect of the heading angle could also be considered as indicator to the effect of encounter frequency. In the first group, the effect of wave steepness, encounter frequency and heading angle were investigated. While, in the second group the results were represented in terms of wave forces and moments with respect to heading angle. The aforementioned Hanaoka parameter represents the effect of encounter frequency.

There are other major points that will need to be mentioned here. In the calculation of wave force, while surge force includes Froude-Krylov forces, others are included diffraction forces calculated from Ohkusu's theory as it is explained in Chapter 5 and Appendix B. It is also emphasized in [81] that Ohkusu's theory deal with hydrodynamic lift components due to trailing free vortices by so-called end terms. In other words, the trailing vortices are approximated as a doublet layer trailing from the end section to downstream. However, as Umeda et al. [81] indicate again, this approximation is straightforward for a ship with transom stern while it is not for a ship with other stern type. It is due to the fact that if the aft end has no breath and draught, the strength of trailing vortices will be zero in the Ohkusu's theory even though in reality they exist. The strength of trailing vortices could be calculated easily for a ship with transom stern because the aft end term will too small and therefore, Ohkusu's assumption will be almost adequate. However, if a substantial area exists behind the aft perpendicular, Ohkusu's theory will ignore the trailing vortices occurring in that part. In

this work, the aft end was also geometrically modelled and the in the Ohkusu theory model. However it is not a proper solution to the real problem of shedding of trailing vortices from a hull surface.

Figures 10.10-10.21 show the effect of wave steepness on the wave forces and moments for both Fn=0.3 and Fn=0.4. For the experimental and numerical simulations in Fn=0.3 (10.10-10.15) it could be seen that non-dimensionalized surge and heave forces and horizontal force and moments are almost constant up to wave steepness, 1/15 which is highest wave steepness in the calculations. In the numerical simulations, there is reasonably satisfactory agreement for both in terms amplitude and phase despite some deviances in sway and yaw values for higher wave steepness (Figs.10.11 and 10.15).

When the speed is increased (Figs 10.16-10.21) there is a substantial increase in vertical forces and moments. The numerical simulations displays more discrepancy in sway and yaw values although it could not be regarded as significant. The heave force amplitude reduces for increasing wave steepness however the numerical model remains constant yet the agreement can be seen satisfactory (Figure 10.18).

As the second criteria, the wave forces and moment were plotted with respect to the wave heading (Figs. 10.22-10.27) for Fn=0.3 and H/λ=1/20. Here, the calm water values for wave forces and moments are also added to show the difference between wave motions and calm values especially in terms of vertical motions. As it can be seen for figures there is linear increase for wave force and moment values. The agreement is again reasonably satisfactory. For the surge forces although the experiments show increase in the amplitude when wave heading is getting closer to 60 degrees, in accordance with Froude-Krylov assumption the numerical model shows linear decrease (Figure 10.22). For other motions the biggest deviation is seen in 60 degrees. Therefore, this could be attributed to the diffraction modelling. Yet, the Hanaoka parameter which will be investigated later, indicates that the encounter frequency does not significantly differ, therefore the other factors could be considered. Especially, the increasing gap in the roll motion (Figure 10.25) indicate that this could be the calculation of the wave forces which considers change in wetted surface due to the position on thee wave and the additional roll moment created from the vertical distance of the dynamometer to the water surface where the model believed to be more accurate for pure following or head se conditions however there seems to some inadequacies exist for quartering seas cases where all rotations are highly important. Due to these problems the amplitudes seem to be slightly lesser when wave heading is getting closer to the beam seas. The phase of

motions show satisfactory agreement in this comparison as well. Comparisons between the amplitude of vertical forces and moment and dynamic forces and moments calculated in calm water indicate that there is a significant wave effect which might justify the relying on 6 DOF mathematical models (Figures 10.34-10.57).

Although, the wave heading could be regarded as another indicator, here, wave forces and moments with respect to the Hanaoka parameters were plotted in $H/\lambda=1/15$, $\chi=0°$ to display the effect of encounter frequency (Figures 10.28-10.33). It is emphasized in [81] based on the experiments in the previous literature that the effect of frequency is very small and wave-induced sway forces, roll and yaw moments are almost constant for $\tau< 0.25$. This conclusion can be confirmed in a certain extent for these experiments as well. The deviations in the sway and yaw (Figures 10.29 and10.33) might change this conclusion because there are certain differences. Then, the same conclusion could be extended for the vertical motions (Figures 10.29 and 10.32). The numerical simulation compared reasonably well in terms of amplitude and phase. However, one interesting point was seen in the numerical simulation of pitch and yaw moments (Figs. 10.32-10.33) for the values very near 0.25 of the Hanaoka parameter. Here, the singular behaviours exist that could be explained by a 3D wave making theory. Such theory is not employed in this study, however the effect of 3D correction terms given in Equation B.18 of Appendix B from Ohkusu's theory is believed to be likely source of this behaviour in the numerical simulation.

In the second part of the experiments, results for the model runs with maximum heel angle, trim angle and sinkage are shown. In the first part (Figures 10.34-10.51) the results for wave forces and moments with respect to wave heading in $H/\lambda=1/20$, $Fn=0.3$ $\theta= -1.43°$ and sinkage = ±0.2 metres are presented.

For the model runs with sinkage = -0.2 metre (Figs. 10.34-10.39) there is no significant difference with the results in zero values in vertical force and moment amplitudes. Yet, this time numerical model overestimates the amplitudes for vertical motions and roll for heading angles 45 and 60 degrees. However, it cannot be seen as significant difference. The similar problems with previous case persist in the calculation of wave forces and moments in these motions as well. Furthermore, in the case of negative trim angle, the model underestimates the amplitudes of vertical motions (Figures 10.42 and 10.44) for positive sinkage while it overestimates them in negative sinkage values (Figures 10.36 and 10.38). In case of the positive trim angle they seem to

be similar (Figures 10.48 and 10.50- Figures 10.54 and 10.56) although the phases of force and moment amplitudes change. The similar discrepancies with zero sinkage and trim cases exist in sway and yaw motion amplitudes as well.

Overall, the numerical model gives reasonably satisfactory agreement with experimental results. Although, the effect of each individual wave force components has not been shown, the differences occurring between numerical and mathematical model can be attributed to calculation of incident wave forces due to position on the wave. The conclusions for those results will be given in the next section.

Free running model experiments:

The accurate representation of the ship motion is required in the real physical environment. Therefore, as a part of model experiments, the free running tests were carried out and those results were compared with the numerical model which is modified to random wave motions as was described in Chapter 9. Those results were compared for the model runs at two spectrums in terms of roll, pitch, yaw and rudder angles.

In Figures 10.58-10.81, the simulations were carried out for the T_p = 1.487 sec. (5.76 sec. at full scale), and H_s = 0.1725 meter (2.588 m. at full scale) at two different speeds Fn=0.3 and Fn=0.4 in ITTC spectrum and in Figures 10.82-10.105 the model was simulated and compared against experiments T_p = 1.717seconds (6.48 seconds at full scale), and H_s = 0.23 meter (3.45 meter at full scale) at two different speeds Fn=0.3 and Fn=0.4 in JONSWAP spectrum. Both simulations were carried out for heading angle, χ, 0, 45, 60 degrees, respectively. For the simulations, the initial conditions, propeller revolution and autopilot parameters were modelled according to the experiment results.

As it can be seen from the graphs time simulation is filtered for 100 seconds by applying the methods described in Chapter 9. Incident and diffraction wave excitation terms and radiation terms are also expressed following the same methodology. The ship motions for the actual time frame are given in Appendix H.

When assessing the ship motions, there are universally recognised wave spectrums that used the describe realistic sea environments. Although, as it stated they each useful to describe the different areas across world, here two of those wave spectrums were assessed in terms of significant wave height and wave periods.

In general, these experiments have not been carried out to find boundaries of capsizing for dangerous situations that occur in the extreme astern seas, it is intended to verify the accuracy of the numerical model which could be used for such purpose as it is stated in Chapter 1 and Chapter 3. Therefore, the amplitude of the experimental results and the accuracy of numerical model to predict those values will be regarded as an indicator for the further studies.

In Figures 10.58-10.81, the simulations were carried out for the T_p = 1.487 sec. (5.76 sec. at full scale), and H_s = 0.1725 meter (2.588 m. at full scale) at two different speeds Fn=0.3 and Fn=0.4 in ITTC spectrum. In figures it could be seen that best agreement are provided in simulation and yaw and rudder motions in contrast to previous regular wave motions. During the numerical models, initial conditions and values are taken from experiments using the actual rudder and autopilot parameters. Since the motions do not have the same extreme amplitudes and transient behaviour in the regular wave motions, the accuracy of the simulations for rudder and inevitably yaw motions can be expected. Therefore, it can be assumed that coupling effects of those motions are predicted with reasonably satisfactory agreement.

For the roll and pitch motions, the best indictor can be seen as the graphs illustrated in Figures 10.106 and 10.107. Here, the single amplitude significant roll and pitch angles are plotted versus the wave heading.

As for the roll motion, it is usually considered that, since viscous effects play the major part, the amplitude is usually less than for the numerical simulations ignoring viscous effects. However, when the ship motions in astern seas are concerned, the rapid change in the restoring and its modelling in the numerical model could be major factor in the results as it was seen in Chapter 7 and 8. Here, too, the roll amplitude was found larger than the actual experiment value because of, presumably, the same reason. In Figure 10.106, it is seen that the roll amplitude is better predicted for the high-speed range, as the change of restoring is less than at the slower speed. The accuracy of the numerical model for the high-speed range has been seen throughout the simulations in this study. The difference, however, in the experimental results are almost insignificant.

As for the pitch motions, however, the accuracy is not as good as the roll motion. The similar problem in the amplitude for Purse Seiner trawler has been seen for the regular wave tests in Chapter 7 as well. Therefore, it could be attributed to geometrical form of this particular vessel in the numerical model. The pitch motions for the container vessel in Chapter 7, for instance, had shown a good agreement. The

agreement between the numerical model and experiments are similar to the roll motion, although there is significant difference in the amplitude for 45 degrees wave heading in Fn=0.3 (Fig. 10-107).

In Figures 10.82-10.105 the model was simulated and compared against experiments T_p = 1.717 seconds (6.48 seconds at full scale), and H_s = 0.23 meter (3.45 meter at full scale) at two different speeds Fn=0.3 and Fn=0.4 in JONSWAP spectrum. When significant wave height increases with longer modal period, the overall characteristics of the motions do not show significant difference. The yaw and rudder motions yet again were predicted with good agreement. Similar to the first case, single amplitude significant roll and pitch angles were plotted with respect to wave heading in Figures 10.108 and 10.109. Here, there is a better agreement for both motions especially in Fn=0.4. However, the same difference in significant pitch angle amplitude for Fn=0.3 and 45 degree wave direction exists for this motion as well The amplitude of the motions is slightly less than the previous case despite the higher significant wave height. That shows the important effect of the frequency in the motions.

Overall, the results indicate that motions with higher amplitudes occur closer to pure following seas. This verifies the common knowledge in the motions of ships in extreme astern seas.

When the effect of frequency is concerned, the numerical model shows similarly good agreement for motions in 60 degree as in the following and quartering seas. However, the difference between the motion attitudes is not significantly different. The diffraction model based on the low encounter frequency may contribute the difference in wave headings near to beam quartering seas.

Phase angle and other parameters are obtained from the wave spectrums and the simulations display the good agreement for the phase of motion.

10.5. Concluding Remarks

As it is stated, the objective of this chapter was to present the results of the captive and free running model experiments carried out in Japan in order to validate the numerical model in all 6 DOF and extreme random seas and verification of the simulation results of the developed numerical model described in the previous Chapters with those experimental results.

The details regarding instrumentation, set up and models of the extensive captive and free running model experiments at National Research Institute of Fisheries Engineering were presented. The ultimate aim of this study is to develop the coupled non-linear 6-DOF model with frequency dependent coefficients, incorporating memory effects in random waves with a new axis system that allows straightforward combination between seakeeping and manoeuvring model whilst accounting for extreme motions. Therefore, these experiments are believed to provide feedback for two major points in this numerical model. For the combination seakeeping and manoeuvring motions in 6 DOF whilst accounting for extreme motions at large attitudes, the captive model experiments were carried out while model was fixed for 6 DOF. Hence, it was aimed to observe the manoeuvring and course-keeping behaviour of the vessel in large vertical motions. For simulation of the motions in random waves including memory effects, the free running model experiments were carried out in random seas using both ITTC and JONSWAP spectrum. The experiments carried out for different speed, heading angle, sinkage, trim angles and for same cases different wave steepness. However it should be noted again that "extremity" of the conditions of captive model runs were defined within limits and strength of model that was used for these experiments.

In Section 10.3, the equations of the numerical model, in which the wave forces and moment obtained contributes, were presented. Following that, experimental results with a respect to number of environmental and performance criteria were shown for both zero heeling, sinkage and trim and maximum heeling, sinkage and trim. Those parameters were wave steepness, heading angle and effect of frequency which represented in terms of Hanaoka parameter, τ.

The resistance force is subtracted from the surge wave force and the additional roll moment created from the vertical distance of the dynamometer to the water surface is also accounted for the calculation of the wave roll moment. In the calculation of wave force, while surge force includes Froude-Krylov forces, others are included diffraction forces calculated from Ohkusu's theory as it is explained in Chapter 5 and Appendix B. Although the effects of each individual wave force components were not investigated in the study, due to the aforementioned fact that if the aft end has no breath and draught, strength of trailing vortices will be zero in the Ohkusu's theory even though in reality they exist, aft end behind the aft perpendicular was also geometrically modelled in the Ohkusu's method. However, it should be noted again, this is not actual solution to the

real problem of shedding of trailing vortices from hull surface. It could be regarded that this calculation method can be applicable to different hull forms.

Overall comparisons show good agreement with the measured values in the experiments. In case zero heel angle, trim angle and sinkage, effect of wave steepness to wave forces and moments are found to be not significant except some small deviations in pitch moment and in higher speeds for heave force up to wave steepness of 1/15. In case of effect of encounter frequency, the results in experiments and numerical simulations verified the fact that effect of frequency is very small and wave-induced sway forces, roll and yaw moments do not significantly change for $\tau < 0.25$. Based on the experiments, this conclusion could be extended for the vertical motions. The one interesting point was the singular behaviours exist near 0.25 of the Hanoka parameter, although this kind of behaviour could be explained by a 3D wave making theory, the 3D correction terms used in Ohkusu's theory is seen to be the source of this behaviour in the numerical model. In the effect of wave heading, it can be seen for figures there is linear increase for wave force and moment values with respect wave heading from pure following seas through beam seas. The agreement is yet again satisfactory. The biggest deviation is seen in 60 degrees for motions except surge forces. Therefore, it could be thought that this is due to the diffraction modelling which based on the low encounter frequency. However, Hanaoka parameter indicated that the encounter frequency does not significantly differs, therefore the incident wave force modelling was considered to be major factor.

In the second part of the experiments results for the model runs with maximum heel angle, trim angle and sinkage, which were allowed by the model, are shown.

It is found that apart from the roll amplitude there is no significant difference with the results in zero values in vertical force and moment amplitudes. The similar discrepancies with zero sinkage and trim cases exist for the vertical forces and moments and sway and yaw forces and moments. The only differences were shown in the phases. The numerical model displayed the similar good agreement as in the first case and the similar problems with the roll motion. The effect of heading angle for near the beam sea conditions were not found to be significant.

However, comparisons between the amplitude of vertical forces and moment and calm water results indicate that there is a significant wave effect which might justify the relying on 6 DOF mathematical models. Yet, this could also confirm the findings at

Chapter 8 that 4 DOF numerical model with static equilibrium of vertical motions could be efficient tool to simulate the ship motions in astern seas.

For the free running model tests, experiment results (ITTC, JONSWAP) were compared for the model runs at two spectrums in terms of roll, pitch, yaw and rudder angles.

There is good agreement between the numerical model and experiments for yaw and rudder motions in two different sea conditions.

For the roll motion, the amplitude is found to be higher than experiments which is in contrast to general problem of numerical methods which does not adequately models viscous effects during the roll motion. However, since the restoring is highly significant for the ship motion in following and quartering seas, this is attributed to instantaneous wave modelling as it is happened for regular wave tests in Chapter 7. The difference of amplitude is slightly less for increasing speed.

As for the pitch motions the numerical model displayed rather large differences with the numerical model especially for quartering sea condition in Fn=0.3.

Despite the tests in beam quartering seas, the effect of frequency was not seem to be significant however the model including memory effects gives reasonably good agreement.

The overall agreement for the ship motions are thought to be reasonably satisfactory and it is believed that this model could be useful tool to identify dangerous situations that the ship might face in extreme random seas conditions. The pure following seas conditions was seen to be most dangerous situation based on the motion amplitudes and in same assessment quartering beam seas are safer comparing to aft quartering seas. However, since it covered the long crested wave conditions, it needs to be tested for the short crested waves to investigate the ship motions in more realistic conditions.

The final discussion and conclusions including the findings of this chapter will be given in next two chapters. Further details and the results of free running model tests are presented in Appendix H.

11. DISCUSSION

11.1. General Remarks

Ship motions in extreme astern seas have been of great interest in experimental and theoretical studies in last 40 years or so. The highly non-linear and unpredictable nature of the phenomena has attracted many studies which employed different approaches to investigate the problems that arise in that condition. Yet, the studies for ship motions could still be seen as limited comparing to the other two important field of hydrodynamics which these motions are assumed to be related to: seakeeping and manoeuvring. However, due to the unique nature of phenomenon that involves two fields of hydrodynamics, the study of these motions could be considered as a catalyst to achieve the long overdue marriage of seakeping and manoeuvring studies which were evaluated separately over the years as it is explained in Chapter 3. Another important factor was the strong requirement from the marine community and academia to establish adequate and robust stability and safety rules covering the ship motions in extreme astern seas. The dangerous situations which may lead to capsizing are relatively higher for ship motions in astern seas than other wave directions. Many of the aforementioned non-linear and dynamic modes occur due to significant change of ship restoring in such motions. Yet, traditional stability criteria issued by IMO does not take these effects into account.

Based on this background, there has been an upsurge in efforts to establish strong numerical and theoretical models to simulate manoeuvring of ships in extreme astern seas and to identify the dangerous situations or other interesting phenomenon occur during those motions. The phenomena like broaching-to or parametric rolling have been extensively investigated.

The achievements of the numerical and experimental studies have been presented. Furthermore, the certain disadvantages or inadequacies of these studies have been observed. Therefore, the aim of this study was to contribute to aforementioned efforts focusing on the some specific issues which are believed to be influential to obtain an successful tool for the studies of ship motions in astern seas.

11.2. Present Approach

In order to achieve the successful assessment of the characteristics of ship motions in extreme astern seas, and to identify the dangerous conditions that may occur during these motions, a numerical model representing the approach is required. Therefore, as it stated, a coupled non-linear 6-DOF model with frequency dependent coefficients, incorporating memory effects in random waves with a new axis system that allows straightforward combination of seakeeping and manoeuvring models whilst accounting for extreme motions was developed.

In an effort to combine the seakeeping and manoeuvring model whilst taking the large amplitudes motions into account, especially in vertical direction, a relatively new horizontal body axis system has been employed. Secondly, the convolution terms were incorporated, in order to include to effect of encounter frequencies in the solution.

In the second phase, the numerical model has been compared with results of the experiments carried out in Japan for the benchmark tests of the numerical models developed for ship motions in astern seas by ITTC Specialist Committee on Stability. These experiments have been conducted for steep regular waves. The result show reasonably good agreement for parametric rolling, sub-harmonic roll motions and capsizing due to rapid build-up of roll motion at very high speed but suggest room for furher improvement for harmonic roll motion and broaching-to associated with surf-riding. Following the verification of the numerical model, the further parametrical study has been carried out to assess the effect of number parameters which are believed to provide important link to design problems and the numerical model has also been employed to investigate adequacy of certain guidelines for the operation of ship motions in following and quartering seas.

Furthermore, in an effort to assess the ship motions in more realistic physical conditions, the numerical model was expressed in terms of irregular waves including the convolution terms.

Following this modification in the numerical model, in order to enhance the current knowledge in this field and to provide feedback into the numerical modelling, the captive and free running model experiments were carried out using the same model ship in ITTC benchmark tests. The tests have been conducted in different environmental and performance conditions. In the captive model tests the special attention was given to the effect of vertical motions and their contribution to the wave forces and moments.

The free running models tests aimed to assess the accuracy of a numerical model in random waves to be used for further numerical simulations in ship motions in random astern seas.

The following sections describe the approaches and the outcome of those phases of the research.

11.3. Mathematical Model

In order achieve the improved numerical model for capsizing involving all degrees of freedom, the numerical model incorporates non-linear six-degrees-of-freedom coupled motion equations in time-domain and, with no restrictions on the motion amplitudes. Therefore, equations of motion are described with respect to a "horizontal body axes" system which handles more easily large angles in pitch (measured between the ship's longitudinal axis and the horizontal plane) which may be realised during operation in steep waves. External forces on a ship are evaluated with respect to the new axis system. External forces include wave forces, through incident and diffraction components, manoeuvring (hull) forces, rudder, resistance, propulsive, wind forces and the autopilot which is used in control of the rudder. Those forces are calculated using the highly efficient modular method in which each individual forces are calculated and superimposed for each separate motion.

The Froude-Krylov forces are calculated using the instantaneous wave surface which is non-linear and it also accounts for large motions. Both 3-D and 2-D methodologies are used. The 3-D method consists of integrating the pressure over quadrilateral panels. However, since it is observed that if the hull form is not formed by homogenously distributed panels it could cause the accuracy problems, therefore as the second approach the pressure is calculated in each section then integrated along the ship length including the aft and bow. Diffraction forces are calculated using the numerical method developed by Ohkusu [16], which is based on the slender body theory and low encounter frequency which is observed for ship motions in astern seas. The one exception of the Ohkusu's model was the modelling of the aft end since if the aft end has no breath and draught, the strength of trailing vortices will be zero in the Ohkusu's theory even though in reality they exist. The manoeuvring model is employed to account for low frequency motions in astern seas. Therefore, hydrodynamic reaction forces which are calculated using the empirical method by MMG is used. The

hydrodynamic coefficients are obtained from experiments since they're still more reliable than the theoretical models. The coupling between and vertical and horizontal motions were not taken into account in the modelling but heeling effect on sway and yaw motions are added as the linear sway and yaw accelerations to sway and yaw force and moment equations in the manoeuvring model if the data from model experiments are available. Therefore, the overall numerical cannot be considered as "fully" coupled and exact non-linear. Other external forces (resistance, propulsive, wind) are calculated using empirical models while coefficients are obtained through model experiments. The PD autopilot model is employed because of its simplicity and practicality. The effect of autopilot was found to be highly important during the numerical simulations.

The second part of the mathematical model study was to incorporate the so-called "memory effects" (impulse response functions) to take the effect of encounter frequency into consideration in such motions. Therefore, the convolution terms in the radiation forces are incorporated in order to improve the prediction of the behaviour of the vessel at encounter frequencies which are not very near to zero. It should be noted that the experimental data for different ship forms and covering the practical range of frequencies and ship speeds are very limited. Although, the full impulse response matrix can be found by solution of initial value hydrodynamic problem or combining both experiment and numerical solution, this will very difficult and expensive task therefore the frequency-dependent coefficients were derived within the limits of potential theory in this research. In order to solve the impulse response functions, the numerical solution of Kernel functions and numerical module for this solution was developed and the results show that the impulse response functions die off within 10 seconds which could be assumed satisfactory. Some concessions were being made for incorporation of frequency dependent terms. Despite its well-known drawbacks for ship motions in astern seas when encounter frequencies is very low, the strip theory is employed for the vessels used in numerical simulations. The main reason for this situation, since 3-D methods available during the course of the research did not provide the satisfactory results due to aforementioned problems of panelling of hull form, the solution relied on the strip theory calculations. Introducing the linear radiation terms into equation resulted the non-linearity was removed caused by coupling in the left hand side of the equations of motion. Furthermore, due to requirements of ship motions in extreme astern seas, led by importance of calculation of restoring and Froude-Krylov forces for instantaneous wave surface and since certain assumptions shown in the literature indicate the

diffraction model, similar to Ohkusu's model at low encounter frequency led to abandoning the transformation of these forces in terms convolution terms.

Finally, in order to carry out the research in a more realistic sea environment, the numerical model is expressed in the random waves including convolution terms. Since it proved its accuracy, the solution relied on the assumption that irregular waves can be described by the superimposition of a large number of regular waves having different lengths, directions and amplitudes. Here, the numerical model incorporated into the model developed for seakeeping studies in University of Strathclyde [139], [138]. The equations of motions and wave forces have been transformed into the horizontal body axis system. The convolution terms in random waves were calculated following this model. Yet, the transfer function of Froude-Krylov forces is utilized even though the calculation of Froude-Krylov forces is non-linear. This method therefore is an approximate solution.

11.4. Numerical Studies

Numerical studies can be discussed under the two parts. The first one is validation of the numerical model against the benchmark tests carried out in Japan. The second one is the parametric studies carried out to investigate the effect of parameters such as wave steepness, loading condition (GM), speed and wave direction. Furthermore, the parametric studies compared the developed numerical tool against the traditional methods in terms of some important issues such as degrees of freedom in mathematical model and effect of encounter frequency.

11.4.1. Validation of Numerical Model

For the validation of the numerical program two different model ships were tested. A 23,720 tonnes displacement containership, investigated using systematic model experiments at Osaka University in Japan and a 712 tonnes displacement fishing vessel, investigated using systematic model experiments at National Institute of Fisheries Engineering in Japan. The models were tested in different speeds, wave steepness, wave height to ship length ratio and heading angles.

The results from the numerical method are reasonably good when capsizing due t rapid build-up of roll motion, parametric rolling and sub-harmonic motions occur and

poor when broaching-to associated with surf-riding and harmonic motions are observed. The series of assumption and approaches have been used in the simulations of these vessels in order to investigate some important issues.

The numerical model seems to have less amplitude in roll motion that could be affected by estimated damping value or the initial damping assumed in the calculation. Although, the pitch motions which are dependent upon the instantaneous wave surface modelling for this case are displayed with satisfactory agreement. When the effect of frequency was taken into account, there were clear improvement in the amplitude of roll motion and the results were more in line with the experiments as well. However, this is probably due to significant change in the attitude of yaw and rudder motions. They were displayed more "stiffer" yet there is improvement in modelling when the speed was increased. This could be concluded as the effect of frequency to the control systems. However, since the ITTC benchmark review committee [92] urged that the exact calculation of memory effects to be carried out from the start of the waves, therefore, the ITTC benchmark testing, which does not specify initial conditions of fluid motions, is not appropriate for this purpose.

In terms of the effect of degrees of freedom in the numerical model the results of the simulations of fishing vessel, 6 DOF and 4 DOF model with static equilibrium with heave and pitch were identical. This conclusion might not be clarified perhaps because the mean water level is assumed for both cases instead of using instantaneous wave surface. However, this kind approach seems to be practical and can give reasonable accuracy for the motions of ship in extreme astern seas at relatively very high speed although not quantitatively. The deviation problems existed in yaw and rudder motions for both approaches. Pitch motions were again reasonably predicted except for one model run which resulted with poor agreement of yaw motion in terms of amplitude. For the effect of the environmental and performance parameters, factors that would appear to govern behaviour include wave steepness and speed.

Overall, the numerical model provided the reasonable qualitative agreement for the simulations of ship motions in astern seas.

11.4.2. Parametrical Studies

Following the validation study of the numerical model, relying on the accuracy it provides, the numerical simulations carried out to investigate the contribution of the

improved numerical model to the simulating the capsizing behaviour of ship in following and quartering seas in a wider scale. The two vessels used in the ITTC Benchmark study were numerically tested for various speeds, wave steepness, wave lengths and loading conditions. Comparisons have been made between the new axis system and the traditional axis systems in order to determine the differences in the simulated behaviour for the two cases. Accuracy of the improved numerical model to determine the dangerous conditions which often result in capsizing, such as broaching associated with surf-riding and low cycle resonance are exploited.

Comparisons between the 6 DOF and 4 DOF numerical models considered in this numerical study displayed that the difference between them is not very significant. For the numerical simulations with relatively low speed range, the difference increases with increasing wave steepness. However, it is difficult to call this a significant difference. In the relatively very high speed range (Fn>0.3) and highly extreme wave conditions, comparisons have been made for the capsizing prediction of both models in terms of the amplitude of motions with respect to wave steepness. Here, the difference was even less and almost unnoticeable for the both numerical models. Therefore, it could be concluded that for very high speed range, it is not necessary to employ full 6 DOF numerical models. In the numerical simulations, similar problems regarding the simulation of rudder and yaw motions were observed in both models. Throughout the verification of the numerical model and parametric studies, the amplitude of pitch angle was less than 10 degrees therefore the assumption of large pitch angles in the numerical model does not display any significant difference.

The numerical investigations focusing on identifying the effect of frequency showed no significant difference either, although small differences exist for yaw and rudder. Also control characteristics are sensitive to the effect of frequency for the controlled ship motions in astern seas. One of the reasons for these results could be the well-known difficulty of using 2-D strip theory approach where frequency dependent damping terms could be near zero in the calculation.

The effect of wave length to ship ratio, which could identify the occurrence of dangerous conditions such as surf-riding, was investigated. It was seen that as the when wave length to ship ratio is equal 1.0 or higher there is serious possibility of being overtaken by waves which may lead to surf-riding.

Another important factor is GM parameter since it could determine ship's stability which is highly affected in extreme astern seas. The vessels used in this study

have GM values which are not design values but values that critically comply with IMO regulations. Higher GM value resulted the vessel phases out one dangerous condition yet it could still be subject to new dangerous conditions in extreme astern seas. However, this result cannot be justified as a general conclusion and the effect of GM should be investigated in detail with more numerical simulations. Furthermore, current IMO limits for GM could be seen as adequate for ship's stability. In terms of operational factors, the combined effect of speed and heading angle was investigated. Reducing or increasing speed when the special condition is concerned, such as the parametric rolling or broaching-to, and the change of autopilot course could be effective methods of avoiding those dangerous situations. The ship could suffer due to low cycle resonance in relatively low speed and near pure following sea conditions. While, for following and quartering seas conditions surf-riding associated with broaching-to or capsizing due to sudden increase in the roll motion could be important at relatively very high speed (Fn>0.4). Reducing the speed and changing of heading angles when aforementioned situations are experienced could be effective way to avoid those situations as it is recommended by IMO studies. Furthermore, the position of the ship on the wave could be a highly important factor, with the ship's centre of gravity on the wave crest, in line with current experience, is seen to be most dangerous situation.

11.5. Experimental Studies

In order to enhance the knowledge in the field and to validate the numerical model for the full 6 DOF in terms of wave forces and realistic sea environment, captive and free running model experiments were carried out, at National Research Institute of Fisheries Engineering, Japan, for a 712 tonnes Japanese fishing vessel. The captive model experiments were carried out while the model was fixed for all 6 DOF. The free running model experiments were carried out in random seas using both ITTC and JONSWAP spectrum. The captive model experiments were carried out for different speed, heading angle, sinkage, trim angles and for some cases with different wave steepness, while the free running model experiments were carried out in different significant wave heights, modal frequencies, speed and wave directions. Extremity of the conditions of captive model runs were defined within limits and strength of model that was used for these experiments.

For the captive model tests, the comparisons show good agreement with the measured values in the experiments. In the case of zero heel angle, trim angle and sinkage, the effect of wave steepness on wave forces and moments are found to be not significant except for some small deviations in pitch moment and in higher speeds for heave force up to wave steepness of 1/15. For the effect of encounter frequency, the results in experiments and numerical simulations verified the fact that the effect of frequency is very small and wave-induced sway forces, roll and yaw moments do not significantly change for τ (Hanaoka parameter)< 0.25. Based on the experiments, this conclusion could be extended for the vertical motions. For the effect of wave heading, there is linear increase in wave force and moment values with respect wave heading from pure following seas through beam seas. The agreement is reasonably satisfactory. The biggest deviation is seen in 60 degrees for motions while the Froude-Krylov assumption is resulted bigger differences in quartering and beam quartering seas for surge motion compared to the experiments. Therefore the incident wave force modelling was considered to be important due to the fact that in case of aft of beam quartering seas, combined heel and vertical motions are important. For the effect of large heel angle, trim angle and sinkage, it is found that apart from the roll amplitude there is no significant difference with the results for zero values, in vertical force and moment amplitudes. The similar discrepancies with zero sinkage and trim cases exist for the vertical forces and moments and sway and yaw forces and moments. The only differences were shown in the phases. The reason for this could be the chosen values for "extremity" in the experiments. Those values might not actually reflect the large amplitudes the comparison requires. The numerical model displayed similar good agreement as in the first case. The effect of heading angle for near the beam sea conditions was not found to be significant. However, comparisons between the amplitude of vertical forces and moment and calm water results indicate that there is a significant wave effect which might justify relying on 6 DOF mathematical models.

For the free running model tests, there is good agreement between the numerical model and experiments for yaw and rudder motions in different sea conditions. As for the roll motion, the amplitude is found to be higher than experiments which is in contrast to general problem of numerical methods which does not adequately models viscous effects during the roll motion. However, since the restoring is highly significant for the ship motion in following and quartering seas, this is attributed to instantaneous wave modelling for regular wave tests. The difference of amplitude is slightly less for

increasing speed. As for the pitch motions the numerical model displayed rather large differences with the numerical model especially for quartering sea condition in Fn=0.3.

Despite the tests in beam quartering seas, the effect of frequency was not seem to be significant however the model including memory effects gives reasonably good agreement.

The overall agreement for the ship motions are thought to be reasonably satisfactory and it is believed that this model could be useful tool to identify dangerous situations that the ship might face in extreme random seas conditions. The pure following seas conditions was seen to be most dangerous situation based on the motion amplitudes. Quartering to beam seas are safer comparing with aft to quartering seas.

11.6. Main Contributions of Present Research

It has been described in the beginning of the thesis and reiterated in the chapters that the main aim of this research is to develop a coupled non-linear 6-DOF model with frequency dependent coefficients, incorporating memory effects in random waves with a new axis system that allows straightforward combination between seakeeping and manoeuvring model whilst accounting for extreme motions. The experimental and theoretical research activities in the literature, the lack of information and the requirement for the new approaches led to this work.

In order to achieve this goal a new mathematical model was developed which allowed meaningful combination of manoeuvring and seakeeping motions in the prediction of extreme ship motions. It is enhanced by the convolution terms (so called "memory effects") that improve the prediction of the behaviour of the vessel in non-zero encounter frequencies. Furthermore, the numerical model is expressed for random waves to simulate behaviour of ship motions in realistic physical environment.

Validation of the numerical model indicates that the numerical model could provide reasonably adequate behaviour of ship motions in extreme astern seas, especially qualitatively, and it could identify the dangerous situations that may lead to capsizing. The numerical calculations showed that a fully non-linear coupled 6 DOF mathematical model could be the most robust way to simulate behaviour of ships in extreme seas. The coupling between vertical motions and other motions should be taken into account in an attempt to improve the accuracy of numerical calculations. For certain initial conditions and wave conditions the frequency dependent terms could

improve the accuracy of the numerical model and there is a considerable effect of the encounter frequency on the ship control.

Parametrical investigation was undertaken concerning operational and environmental parameters. It justified the general knowledge on the effect of environmental parameters and the recommendations provided for the operations in following and quartering seas. In terms of loading condition, it is seen that the ship phases out of the dangerous condition boundary with higher GM while current IMO criteria provides just enough GM value to avoid capsizing. It also shown that 4 DOF numerical model with static equilibrium of vertical motions are reliable and effect of encounter frequency up to 60 degrees or aft beam seas conditions is not significant for random initial conditions.

In an attempt to enhance the knowledge regarding the effect of vertical motions and to assess the reliability of the numerical model in random waves environment, the captive and free running model experiments were conducted. The numerical model provides good agreement for fully captive model and difference between wave and calm water values indicate the importance of vertical forces and moments, yet differences in terms of wave steepness, heading angle and encounter frequency are not so significant when the maximum heeling, sinkage and trim values used in these experiments are concerned.

The agreement of the numerical model in random astern waves is reasonably satisfactory and it is believed that this model could be a useful tool to identify dangerous situations that the ship might face in extreme random seas conditions. The pure following seas conditions was seen to be most dangerous situation based on the motion amplitudes and quartering to beam seas are safer comparing to aft to quartering seas.

In overall, the numerical model has a good potential for providing a more rational basis for predicting the dangerous conditions which a ship could face in extreme following and quartering seas, and for offering insights about the link of behaviour with the design parameters of a ship.

11.7. Recommendations for Future Work

The present work has demonstrated the viability of the numerical model employed in the simulation of ship motions in extreme astern seas. Furthermore, the

experimental studies exploited the effect of coupling between the motions and the ship motions in random astern waves. However, further improvements could be made.

Further recommendations to this work will be concerned with both theoretical and experimental studies.

Further development of the numerical model would improve the accuracy of its predictions. A good starting point would be to study broaching-to associated with surf-riding where the predictions were found to be less good. For the calculation of the frequency dependent coefficients, due to the inadequacy of the strip theory approaches, a 3-D methodology including the aft effect could improve the accuracy of the numerical model. Also, shedding of trailing vortices from hull sources should be taken into account and this could be achieved by CFD methodologies. Following the importance of hydrodynamic lift and viscous effects in ship motions in astern seas, CFD tools can also be employed using boundary layer theory and Navier-Stokes equations. Furthermore, the coupling between vertical and horizontal motions in the manoeuvring models could be fully taken into account.

As a result of the current developments into new hull forms and propulsion systems, effect of design parameters in different hull forms and very high speed range and directional stability of these vessels can be investigated. The effect of control parameters on the vessel motions is also important. Use of more sophisticated autopilot models, therefore, could be attempted. As an important design parameter, the effect of GM should be investigated in detail with experimental and numerical studies.

Furthermore, the extensive parametrical studies should be carried out to identify the thresholds for the dangerous situations in short and long crested random wave systems.

For the experimental research, the focus should be on the test effect of the vertical motions in more extreme conditions with more extensive environmental and operations parameters. The same approach could be applied to random wave tests to provide a healthy data for the behaviour of ship motions in extreme astern seas.

12. CONCLUSIONS

- A coupled non-linear 6-DOF model with frequency dependent coefficients, incorporating memory effects in random waves with a new axis system that allows straightforward combination between seakeeping and manoeuvring model whilst accounting for extreme motions was developed. The coupling between vertical and horizontal motions was not taken into account in the manoeuvring (hull) force modelling.
- The numerical model has been validated using benchmark test results. The reasonably satisfactory agreement was obtained except for broaching situation while frequency dependent terms have affected the characteristics of the numerical calculations especially in terms of yaw and rudder motions.
- Parametrical studies with a range of important environmental and operational parameters were undertaken. The 6 DOF model successfully showed the characteristics observed in the similar experimental conditions and it underlined the importance of effect of number of factors such as wave steepness, speed, GM and heading angle. It justified the recommendations of the international guidelines for the ship motions in astern seas.
- Extensive captive and free running experiments were undertaken to enhance knowledge on the effect of fully coupled 6 DOF motions and the to provide data to improve accuracy of the numerical model for random astern sea motions. The comparisons with the captive model tests results showed satisfactory agreement, while it indicated that effects of encounter frequency, wave steepness and heading angle were not significant even in the beam quartering sea conditions at the "extreme" conditions considered in the model tests. The agreement with free running tests was also satisfactory and the numerical model is shown to be a useful tool for further studies regarding the ship motions in astern random seas.

REFERENCES

[1] - Report of The Manoeuvring Committee (1999), 22nd. ITTC.

[2] - Report of The Specialist Committee on Stability (1999), 22nd. ITTC

[3] - Davidson K.S.M (1948) "The Steering of Ships in Following Seas" Proceedings of Sixth International Conference for Applied Mechanics, Vol. 2, pp. 554-568

[4] - Grim O. (1963) " Surging Motion and Broaching Tendencies in A Severe Irregular Sea", D.H.Z, Vol. 16, No.5, pp. 201-231

[5] - Du Cane, P. and Goodrich, G.J (1962) "The Following Sea, Broaching And Surging" RINA Quarterly Transactions, Vol.104, No.2, pp. 109-140

[6] - Wahab R. and Swaan W. A. (1964) " Course-keeping and Broaching of Ships in Following Seas", Journal of Ship Research, April

[7] - Paulling and Rosenberg (1959) "On Unstable Ship Motions Resulting From Non-linear Coupling", Journal of Ship Research, Vol. 3, No.1, pp. 36-46

[8] - Eda H. (1972) "Directional Stability and Control of Ships in Waves", Journal of Ship Research, SNAME,

[9] - Conolly J.E. (1972) "Stability and Control in Waves: A Survey of the Problem" Proceedings of International Symposium On Directional Stability and Control of Bodies Moving In Water", Journal of Mechanical Science, Vol. 14, No. 7, Supplementary Issue, pp. 186-193

[10] - Abkowitz, M.A. (1969) "Stability and Motion Control of Ocean Vehicles" The M.I.T Press, Cambridge, Massachusetts, USA

[11] - Eda, H. "A Digital Simulation Study of Steering Control with Effects of Roll Motions" Proceedings of 5th Ship Control Systems Symposium, Annapolis, 1978

[12] - Son, K.H and Nomoto, K. (1981) "On the Coupled Motion of Steering and Rolling of a High Speed Container Ship" Proceedings of Journal of Naval Architects, Japan, Vol.150, pp. 73-83

[13] - Motora, S., Fujino, M. and Fuwa, T. (1982) "On the Mechanism of Broaching-To Phenomena " Proceedings of STAB'82, Tokyo

[14] - Renilson, M.R. (1981) "The Broaching of Ships in Following Seas" PhD Thesis, University of Glasgow, UK

[15] -Hirano, M and Takashina, J (1980) "A Calculation of Ship Turning Motion Taking Coupling Effect Due to Heel Into Consideration", Transactions of West Japan Society of Naval Architects, Vol. 59

[16] -Ohkusu, M. (1986) "Prediction of Wave Forces on a Ship Running in Following Waves with Very Low Encountered Frequency", Journal of the Society of Naval Architects of Japan, Vol. 159, pp.129-138

[17] -Elsimillawy, N. and Miller, N.S. (1986) "Time Simulation of Ship Motions: A Guide to the Factors Degrading Dynamic Stability", SNAME Transactions, Vol. 94, pp.215-240

[18] -Hamamoto, M. and Akiyoshi, T. (1988) "Study on Ship Motions and Capsizing in Following Seas (1st. Report –Equation of Motion for Numerical Simulation)", Journal of The Society of Naval Architects of Japan, Vol. 163

[19] -Hamamoto, M. and Shirai, T. (1989) "Study on Ship Motions and Capsizing in Following Seas (2nd. Report –Simulation of Capsizing)", Journal of The Society of Naval Architects of Japan, Vol. 165

[20] -Hamamoto, M. and Kim, Y. (1992) "Study on Ship Motions and Capsizing in Following Waves (Final Report)" Proceedings of Journal of Naval Architects, Japan

[21] -Chislett, M.S (1990) "The Addition of A Hell-Roll Servo Mechanism to the DMI Horizontal Planar Motion Mechanism" International Conference on Marine Simulation and Ship Manoeuvrability, Tokyo, Japan, pp. 349-359

[22] -Ottoson, P. and Bystrom, L. (1991) "Simulation of the Dynamics of a Ship Manoeuvring in Waves" SNAME Transactions, Vol. 99, pp. 281-298

[23] -Rutgersson O. and Ottoson, P. (1987) "Model Tests and Computer Simulations-An Effective Combination for Investigation of Broaching Phenomena" Transactions of SNAME, Vol. 95, pp. 263-281

[24] -De Kat, J. and Paulling, J.R. (1989) "The Simulation of Ship Motions and Capsizing in Severe Seas" SNAME Transactions, Vol.97, pp. 139-168

[25] -Hamamoto, M. and Kim, Y (1993) "A New Coordinate System and the Equations Describing Manoeuvring Motion of a Ship in Waves" Journal of the Society of Naval Architectures of Japan, Vol. 173

[26] -Hamamoto, M. et al. (1996) "Analyses on Low Cycle Resonance of Ship in Astern Seas" Journal of the Society of Naval Architects of Japan, Vol. 177

[27] - Hamamoto, M and Panjaitan, J. P., (1997) "A Critical Situation leading to Capsize of Ships in Astern Seas" Journal of the Society of Naval Architects of Japan, Vol. 180

[28] - Hamamoto, M., Sera, W., and Panjaitan, J., P., (1996) "Analyses on Low Cycle Resonance of Ships in Irregular Astern Seas" Journal of the Society of Naval Architects of Japan, Vol. 178

[29] - Hamamoto, M. Fujino, M and Kim, Y.S (1994) "Dynamic Stability of A Ship in Ouartering Seas" Proceedings of Stabitility'94

[30] - Umeda N. and Renilson M. (1992) "Braoching-A Dynamic Analysis of Yaw Behaviour of A Vessel In A Following Sea" Manoeuvrability and Control of Marine Craft (Edited by Wilson, P.A.), Computational Mechanics Publications, Southampton, UK, pp. 533-543.

[31] - Umeda N. and Renilson M. (1992) "Wave Forces on A Ship Running In Quartering Seas-A Simplified Calculation Method", 11th. Australasian Fluid Mechanics Conference, University of Tasmania, Hobart, Australia

[32] - Vassalos, D. and Maimun, A. (1994) "Broaching-To: Thirty Years On" Proceedings of STAB'94

[33] - Spyrou, K. (1995) "Surf-riding and oscillations of a Ship in Quartering Seas" Journal of Marine Science and Technology, Vol:1, pp. 24-36

[34] - Spyrou, K. (1995) "Surf-Riding, Yaw Instability and Large Heeling of Ships in Fallowing/Quartering Waves" Schifftechnik Bd. 42, pp. 103-112

[35] - Spyrou, K. (1996) "Dynamic Instability in Quartering Seas: The Behaviour of a Ship During Broaching" Journal of Ship Research, Vol. 40, No. 1, pp. 46-59

[36] - Spyrou, K. (1996) "Dynamic Instability in Quartering Seas-Part II: Analysis of Ship Roll and Capsize for Broaching" Journal of Ship Research, Vol. 40, No. 4, pp. 326-336

[37] - Spyrou, K. (1997) "Dynamic Instability in Quartering Seas-Part III: Non-linear Effects on Periodic Motions" Journal of Ship Research, Vol. 41, No. 3, pp. 210-233

[38] - Umeda, N. (1994) "Application of Non-linear Dynamical System Approach to Ship Capsize and Broaching-to in Regular Following and Quartering Seas" Report on the Research Supported, University of Strathclyde, United Kingdom

[39] - Umeda, N. Matsuda A. Hamamoto M. and Suzuki, S. (1999) "Stability Assessment for Intact Ships in the Light of Model Experiments" Journal of Marine Science and Technology, Vol. 4, pp. 45-57

[40] - Tsangaris, M. (1998) "Ship Capsize By Broaching-To in Extreme Astern Seas" PhD Thesis, University of Strathclyde, Glasgow, UK

[41] - Tsangaris, M. and Vassalos, D. (1997) "Behaviour of Ships in Severe Astern Seas" Int. Conference on Operation and Design for Abnormal Conditions, October, Glasgow

[42] - Vassalos, D. Umeda, N. Hamamoto, M. and Tsangaris, M. "Modelling Extreme Ship Behaviour in Astern Seas"

[43] - Bailey, P.A Price, W.G and Temarel, P. (1998) "A Unified Mathematical Model Describing the Manoeuvring of A Ship Travelling in A Seaway" Trans. RINA, Volume 140

[44] - Westlake, P.C. Wilson, P.A. and Bailey, P.A. (2000) "Time Domain Simulation of Ship Motions" Transactions of R.I.N.A

[45] - Hamamoto, M., Munif, A., (1999) "A Mathematical Model to Describe Ship Motions Leading to Capsize in Severe Astern Seas" Journal of the Society of Naval Architects of Japan, Vol. 184

[46] - Munif, A. and Umeda, N. (2000) "Modelling Extreme Roll Motions and Capsizing of Moderate-Speed Ship in Astern Waves" Journal of Naval Architects of Japan, Vol. 187

[47] - Umeda, N., Munif, A. and Hashimoto, H. (2000) "Numerical Prediction of Extreme Motions and Capsizing for Intact Ships in Following/Quartering Seas" OC 2000, Seakeeping, Osaka, Japan

[48] - Cummins, W.E. (1962) "The Impulse Response Function and Ship Motions", Schiffstechnik, pp. 101-109

[49] - Lin, W.C., (1966) " An Initial Value Problem for the Motion of A Ship Moving With Constant Mean Velocity In A Arbitrary Seaway" Dissertation, University of California at Berkeley

[50] - Perez y Perez (1974) "A Time Domain Solution to the Motions of A Steered Ship in Waves" Journal of Ship Research, Vol. 18, No.1, pp.32-45

[51] - Bishop, R.E.D, Burcher, R.K., and Price, W.G. (1973) "The Uses of Functional Analysis in Ship Dynamics" Proc. Royal Society of London, Ser. A, Vol. 332, pp. 23-35

[52] -Bishop, R.E.D., Price, W.G., Temarel, P., (1984) "A Functional Representation of Fluid Actions on Ships" International Shipbuilding Progress, Vol. 31, pp. 239-250

[53] -Frank, T., Loeser, D.J, Scragg, C.A., Sibul, O.J., Webster, W.C., Wehausen, J.V. (1976) "Transient-Manoeuvre Testing and The Equations of Manoeuvring" 11th. Symposium on Naval Hydrodynamics, London

[54] -Scragg, C.A. (1979) "Memory Effect in Deepwater Manoeuvring" Journal of Ship Research, Vol. 23, No.3, pp. 175-187

[55] -Loeser, D.J. (1982) "Determination of Manoeuvring Properties in Shallow Water by Impulse Response Techniques" Journal of Ship Research, Vol. 26, No.1, pp. 1-15

[56] -Scragg, C.A. (1977) "Determination of Stability Derivatives By Impulse Response Techniques" Marine Technology, Vol. 14, No. 2, pp. 265-275

[57] -Newman, J.N. (1972) "Some Theories For Ship Manoeuvring" Journal of Mechanical Engineering Science (Supplementary Edition), Vol. 14, No. 7

[58] -Newman, J. (1977) "Marine Hydrodynamics" The M.I.T Press, Cambridge, Massachusetts, USA

[59] -Newman, J.N. (1978) "Theoretical Methods in Ship Manoeuvring" International Symposium on Advance in Marine Technology, pp. 335-359

[60] -Fujino, M. (1975) "The Effect of Frequency Dependence of The Stability Derivatives on Manoeuvring Motion " International Shipbuilding Progress, Vol. 22, No. 256, pp. 416-432

[61] -Guo, C. "Non-linear Theory of Ship Manoeuvring" Journal of Ship Research, Vol.25, No.1, pp. 21-43

[62] -Ankudinov, V. (1983) "Simulation Analysis of Ship Motions" The Proceedings of International Workshop on Ship and Platform Motions, October 26-28, pp. 384-403

[63] -Holappa, K.W. and Falzarano, J.M. (1999) "Application of Extended State Space to Non-linear Ship Rolling" Ocean Engineering, Volume 26, pp. 227-240

[64] -McCreight, W.R (1986) "Ship Manoeuvring in Waves" Sixteenth Symposium on Naval Hydrodynamics, Berkeley, California, USA

[65] -Jefferys, E.R. (1984) "Simulation of Wave Power Devices" Applied Ocean Research No: 6, Volume1, pp. 31-39

[66] -Jiang, J.T. Schellin, T.E. and Sharma, S.D. (1987) "Manocuvring Simulation of A Tanker Moored In A Steady Current Including Hydrodynamic Memory Effects and Stability Analysis" Proceedings of International Conference on Ship Manoeuvrability, RINA, London, Vol.1, paper 25.

[67] -Schellin, T.E., Jiang, T., and Sharma, S.D. (1990) "Motion Simulation and Dynamic Stability of An Anchored Tanker Subject to Current, Wind and Waves" Schiffstechnik Bd., Vol. 37, pp. 64-84

[68] -Chung, J-S. and Bernitsas, M. (1997) "Hydrodynamic Memory Effect on Stability, Bifurcation and Chaos on Two-Point Mooring Systems" Journal of Ship Research, Vol. 1, pp.26-44

[69] -Chen, S. Shaw, S.W and Troesch, A.W (1999) "A Systematic Approach to Modelling Non-linear Multi-DOF Ship Motions in Regular Seas" Journal of Ship Research, Vol. 43, No.1, pp. 25-37

[70] -Rhee, K.P., Kim, C.K. and Lee, C.M. (1990) "The Manoeuvring Motion of The Marad Type Ship in Waves" , MARSIM&ICSM, Tokyo, pp. 413-419

[71] -Hamamoto, M. and Saito, K. (1992), "Time Domain Analysis of Ship Motions in Following Waves", 11th. Australasian Fluid Mechanics Conference, University of Tasmania, Hobart, Australia, pp. 355-358

[72] -Price W.G and Tan, M (1992) "Fundamental viscous solutions or transient oseenlets associated with a body manoeuvring in a viscous fluid", Proceedings pf Royal Society of London, A438, pp. 447-466

[73] -Lee, S., Hasegawa, K., and Kim, S-J. (1993) "The Calculation of Zig-Zag Manoeuvre in Regular Waves With Use of the Impulse Response Functions" Seminar On the Stability of Ships and Offshore Structures, Pusan, Korea

[74] -Lee, S-K. (2000) "The Calculation of Zig-Zag Manoeuvre in Regular Waves With Use of The Impulse Response Functions" Ocean Engineering, Volume 27, pp. 87-96

[75] -Chou, S.J., Oakley, O.H., Paulling, J.R. et al. (1974) " Ship Motions and Capsizing in Astern Seas" Report No. CG-D-103-75, Department of Transportation, United States Coast Guard, Office of Research and Development

[76] -Paulling, J.R. and Wood, P.D. (1973) "Numerical Simulation of Large Amplitude Ship Motions in Astern Seas", Vol. 8-3

[77] -Bishop, R.E.D, Burcher, R.K. and Price, W.G. (1982) "On the role of encounter frequency in capsizing of ships", 2nd. International Conference on Stability of Ships and Ocean Vehicles, Tokyo, Japan, pp. 103-112.

[78] -Kan, M. and Taguchi, H. (1991) "Chaos and Fractals in Asymmetric Capsize Equation" J.S.N.A Japan, Vol.169

[79] -Umeda, N et al. (1994) "Model Experiments of Ships Capsize in Astern Seas" Journal of the Society of Naval Architects of Japan, Vol. 177

[80] -Hamamoto, M et al. (1995) " Model Experiments of Ships Capsize in Astern Seas –Second Report- " Journal of the Society of Naval Architects of Japan, Vol. 179

[81] -Umeda, N. Yamakoshi, Y., and Suzuki, S., (1995) "Experimental Study for Wave Forces on a Ship Running Quartering Seas with Very Low Encountering Frequency" The Sevastianov Symposium, The International Symposium Ship Safety in a Seaway, Kaliningrad, Russia

[82] -St.Denis, M. and Pierson, W.J. (1953) "On The Motions of Ship in Confused Seas" SNAME Transactions, Vol. 61

[83] -Price W.G. (1975) " A Stability Analysis of the Roll Motion of A Ship In An Irregular Seaway" International Shipbuilding Progress, Vol. 22, pp. 103-112

[84] -Roberts, J.B. (1982) "Effect of Parametric Excitation on Ship Rolling Motion In Random Waves" Journal of Ship Research, Vol. 26, No.4, pp. 246-253

[85] -Takaishi, Y. (1982) " Consideration On the Dangerous Situations Leading To Capsize of Ships In Waves" Proceedings of Second International Conference on Stability od Ships in Ocean Vehicles, Tokyo, Japan,

[86] -De Kat, J. (1994) " Irregular Waves and Their Influence on Extreme Ship Motions" Proceeding of 19th. Naval Hydrodynamics Symposium, Santa Barbara, USA

[87] -De Kat, J. (1990) "The Numerical Methods of Ship Motions and Capsizing in Severe Seas" Journal of Ship Research, Vol. 34, No. 4, pp. 289-301

[88] -Chapman, R.B. (1979) "Large Amplitude Transient Motion of Two-Dimensional Floating Bodies" Journal of Ship Research, Vol. 23, No. 14, pp. 20-31

[89] -De Kat, J and Thomas III, W (1998) "Extreme Rolling, Broaching and Capsizing-Model Tests and Simulations of A Steered Ship Waves" 22nd Symposium on Naval Hydrodynamics, Washington, D.C., USA, August, pp. 359-375

[90] - Wehausen, J.V., (1971) "The Motion of Floating Bodies" Annual Review of Fluid Mechanics, Vol. 3, pp. 237-268

[91] - Wehausen, J.V., (1978) "Lecture Notes on Ship Hydrodynamics" University of Berkeley, USA

[92] - "Report of The Specialist Committee on Prediction of Extreme Ship Motions and Capsizing", (2002) Proceedings of 23rd ITTC, Volume 2,

[93] - Umeda, N. (1994) " Operational Stability in Following and Quartering Seas –A Proposed Guidance and Its Validation-" Proceeding of International Conference on Stability on Ships and Offshore Platforms, Florida, USA.

[94] - IMO MSC Circular 707 (1995) "Guidance to the Master For Avoiding Dangerous Situations in Following and Quartering Seas"

[95] - Umeda N., and Renilson, M. (2001) "Benchmark Testing of Numerical Predictions on Capsizing of Intact Ships in Following and Quartering Seas" Proceedings of the 5th. International Workshop on Stability and Operational Safety of Ships, Trieste, Italy

[96] - Matusiak, J. (2001) "Importance of Memory Effect for Capsizing Prediction" Proceedings of the 5th. International Workshop on Stability and Operational Safety of Ships, Trieste, Italy

[97] - "Report of The Specialist Committee on Waves", (2002) Proceedings of 23rd ITTC, Volume 2

[98] - Hess, J.L. and Smith, A.M.O (1964) "Calculation of Nonlifting Potential Flow About Arbitrary Three-Dimensional Bodies" Journal of Ship Research, pp. 22-44

[99] - Hughes, M. and Bertram V. (1995) "A Higher Order Panel Methods for 3-D Free Surface Flows" Report No.558, Institut Fur Schiffbau Der Universitat Hamburg

[100] - "User's Manual Program Suite Swath3 for Swath Motion and Loads" American Bureau of Shipping Research and Development Department Technical Report RD-92001

[101] - Salvesen, N., Tuck, E.O. and Faltinsen, O. (1970) "Ship Motions and Sea Loads", Trans. of SNAME, Vol. 78, pp. 250-287

[102] - Kim, C.H, Chou, F.S. and Tien, D. (1980) "Motions and Hydrodynamics Loads of A Ship Advancing in Oblique Waves" Trans. of SNAME, Vol. 88, pp. 225-256

[103] - Tuck, E.O. (1964) "A Systematic Expansion Procedure for Slender Ships" Journal of Ship Research, Vol.8, No. 1

[104] - Tuck, E.O. (1964) "On Line Distributions of Kelvin Sources" Journal of Ship Research, Vol.8, No. 2

[105] - Landweber, L. and Macagno, M. (1957) "Added Mass of a Three- Parameter Family of Two Dimensional Forces Oscillating in a Free Surface" Journal of Ship Research, pp. 36-48

[106] - Landweber, L. and Macagno, M. (1975) "Accurate Parametric Representation of Ship Sections by Conformal Mapping" Proceedings of 1st. Int. Conference on Numerical Ship Hydrodynamics, Gaithersburg, M.Y

[107] - Westlake, P.C. and Wilson, P.A. (2000) "A New Conformal Mapping Technique For Ship Sections" International Ship Building Progress, Vol. 47, No. 449, pp. 5-22

[108] - Conceicao, C.A. L., Price, W.G., and Temarel, P. (1984) "The influence of heel on the hydrodynamic coefficients of ship like sections and trawler form." International Ship Building Progress, Vol. 31, No. 355, pp. 56-66

[109] - Spyrou, K.J, (1990) "A New Approach for Assessing Ship Manoeuvrability Based On Dynamical Systems Theory" PhD Thesis, University of Strathclyde

[110] - Ogawa, A. and Kasai. H. (1978) "On the Mathematical Model of Manoeuvring Motion of Ships" International Shipbuilding Progress, Vol.25, No.242, pp. 306-319

[111] - Clarke, D. Gentling, P. and Hine, G. (1983) "The Application of Manoeuvring Criteria in Hull Design Using Linear Theory" RINA Transactions, Vol. 125

[112] - Inoue, S., Hirano, M. and Kijima, K. (1981) "Hydrodynamic Derivatives on Ship Manoeuvring" International Shipbuilding Progress, Vol. 28, No. 321

[113] - Inoue, S., Hirano, M., Kijima, K. and Takashina, J. (1981) "A Practical Calculation Method of Ship Manoeuvring" International Shipbuilding Progress, Vol. 28, No. 324

[114] - Kose, K. (1982) "On A New Mathematical Model of Manoeuvring Motions of A Ship and Its Applications" International Shipbuilding Progress, Vol. 29, No. 336

[115] - Tasai, F. (1961) "Damping Force and Added Mass of Ships in Heaving Pitching" Trans. of the West Japan Society of Naval Architects, Vol. 21

[116] - Aage, C. (1971) "Wind Coefficients for Nine Ship Models" Hydro-or Aerodynamisk Laboratorium, Report No. A-3.

[117] - Fossen, T.I. (1994) " Guidance and Control of Ocean Vehicles" John Wiley & Sons

[118] - Hooft, J.P. and Pieffers, J.B.M. (1988) "Manoeuvrability of Frigates in Waves" Marine Technology Vol. 25, No.4. Oct, 1988, pp.262-271

[119] - Frank, W. (1967) "Oscillation of Cylinders In or Below the Free Surface of Deep Fluids" DTNSRDC Report 2375, 1967.

[120] - Chang, M.S. (1977) "Computations of Three-Dimensional Ship Motions with Forward Speed " International Conference on Numerical Ship Hydrodynamics, Berkeley, California, 1977

[121] - Sclavounos, P.D. (1996) "Computation of Wave Ship Interactions" In Advances in Marine Hydrodynamics, M. Okhusu, Ed., Computational Mechanics Publications, Southampton, Chapter 4, pp 233-278

[122] - Inglis, R.B. and Price, W.G. (1981) "Comparison Responses For Arbitrary Shaped Bodies Using Two and Three – Dimensional Theories" International Shipbuilding Progress

[123] - Beck, R. (1989) "Ship Responses to Regular Waves" Principle of Naval Architecture Volume 3, Section 3

[124] - Kara, F. (2000) "Time Domain Hydrodynamic and Hydroelastic Analysis of Floating Bodies" PhD Thesis, University of Strathclyde, Glasgow, UK

[125] - Vassalos, D., Spyrou, K. and Umeda, N. (1994) "Captive Model Tests of A Purse Seiner Model In Regular Seas", National Research Institute of Fisheries Engineering, Japan

[126] - Spyrou, K.J. and Umeda, N. (1995) "From Surf-Riding to Loss of Control and Capsize: A Model of Dynamic Behaviour of Ships in Following/Quartering Seas" The Sixth International Symposium on Practical Design of Ships and Mobile Units, Seoul, Korea, pp. 1.494-1.505

[127] - Papanikolau, A. (1985) "On the calculation of Non-linear Hydrodynamic Effects in Ship Motion", Shiffstechnick, Vol. 31, No. 3, pp. 91-129

[128] - Holtrop, J. and Mennen, G.G.J. (1982) " An Approximate Power Prediction Method" International Shipbuilding Progress, Vol. 29, No. 335,

[129] - Fujino, M. (1996) "Prediction of ship manoeuvrability: State of the art" Marine Simulation and Ship Manoeuvrability Conference, Balkema, Rotterdam, Chislett (ed.)

[130] - Ayaz, Z., Spyrou, K.J. and Vassalos, D (2001) "An Improved Numerical Model for the Study of Controlled Ship Motions in Extreme Following and Quartering Seas" IFAC Ship Control Symposium, July, Glasgow

[131] - Ayaz, Z., Spyrou, K.J. and Vassalos, D (2002) "An Improved Numerical Model for the Study of Controlled Ship Motions in Extreme Following and Quartering Seas" Proceedings of the 6th. International Workshop on Stability and Operational Safety of Ships, Webb Institute, New York, USA

[132] - Soding, H. (1998) "Limits of Potential Theory in Rudder Flow Prediction" 22nd Symposium on Naval Hydrodynamics, Washington, D.C., USA, August, pp. 622-637

[133] - Sato, T., Izumi, K., and Miyata, H. (1998) "Numerical Simulation of Manoeuvring Motion" 22nd Symposium on Naval Hydrodynamics, Washington, D.C., USA, August, pp. 724-737

[134] - Ankudinov, V., Kaplan, P. and Jacobsen, B. (1993) " Assessment and Principal Structure of the Modular Mathematical Model for Ship Manoeuvrability Prediction and Real-Time Manoeuvring Simulations" Proceedings of MARSIM'93, St. Johns, Canada, September

[135] - Kaplan, P., Ankudinov, V. and Jacobsen, B. (1993) "Modular Mathematical Models for Ship Manoeuvring" Technical and Research Report No. 56, SNAME

[136] - Himeno, Y. (1981) "Prediction of Ship Roll Damping-State of the Art" Report No.239, Department of Naval Architecture and Marine Engineering, University of Michigan

[137] - Newman, J.H. (1967) "The Drift Force and Moment of Ships in Waves" Journal of Ship Research, Vol. 11, No.1

[138] - Jasionowski, A. (2001) "An Integrated Approach to Damage Stability Survivability Assessment" Ph D Thesis, University of Strathclyde, Glasgow, UK

[139] - Letizia, L (1996) "Damage Survivability of Passenger Ships In A Seaway", Ph D Thesis, University of Strathclyde, Glasgow, UK

NOMENCLATURE

a	Amplitude of wave (m)
a_{II}	Interaction factor between hull and rudder
a_i,	component wave amplitude (m)
a_R	Rudder inflow angle (deg)
A_x	maximum longitudinal projection (m^2)
A_y	maximum transverse projection (m^2)
B	Beam (m)
c	Phase velocity of wave (m/s)
C_b	Block coefficient
$C(\dot{\varphi})$	Damping force (Nt)
d_f	Draught at fore (m)
d	Mean draught (m)
d_a	draught at aft
D	Depth (m)
D_P	Propeller diameter (m)
$f(\Lambda)$	Open water rudder normal force coefficient
F_N	Rudder normal forces (Nt)
Fn	Nominal Froude number
g	Gravitational acceleration (m/s^2)
GM	Metacentric height (m)
GZ	Righting Arm (m)
$GZ(\phi)$	Restoring moment (kg. m)
H	Wave height (m)
H_0	Struve function
H_s	Significant wave height (m)
I_{xx}	Roll moment of inertia ($kg.m^2$)
I_{yy}	Pitch moment of inertia ($kg.m^2$)
I_{zz}	Yaw moment of inertia ($kg.m^2$)
J_p	Advance coefficient
k	Wave number
k_i	Component wave number

K′	Roll external moment (Nt.m)
KG	Vertical position of centre of gravity from keel line (m)
K_P	Proportional gain (sec.)
K_R	Differential gain (sec.)
K_T	Thrust coefficient
L_{BP}	Length between perpendiculars (m)
LCG	Longitudinal position of centre of gravity from the amidships (m)
m	Ship mass (kg)
M′	Pitch external moment (Nt.m)
n	propeller rate of rotation (rpm)
N′	Yaw external moment (Nt.m)
n_i	Ratio of propeller diameter to the rudder height
N_j	Normal Vector
p	Pressure (N/m^2)
p_s	Static wave pressure (N/m^2)
p_d	Dynamic wave pressure (N/m^2)
P	Angular roll velocity (deg/s)
Q	Angular pitch velocity (deg/s)
R	Angular yaw velocity (deg/s)
Res(u)	Resistance force (Nt)
S	Propeller slip ratio
t_p, t_{p0}	Thrust deduction in forward motion and during a turn at the propeller
t_r, t_{r0}	Thrust deduction in forward motion and during a turn at the rudder position
t_D	Time constant (s)
t(N)	Time step in kernel function (s)
T_φ	Roll period (s)
T_z	modal period (sec)
U	Surge velocity (m/s)
U_{rw}	Effective wind speed (m/s)
U_R	Rudder inflow velocity (m/s), and angle
V	Sway velocity (m/s)
V_R	Mean rudder inflow velocity (m/s)
w_p, w_{p0}	Wake fraction in forward motion and during a turn at the propeller

w_r, w_{r0} Wake fraction in forward motion and during a turn at the rudder position

W Heave velocity (m/s)

X′ surge external force (Nt)

X_S Longitudinal coordinate of the centre of wind force (m)

x_H Longitudinal position of the point of action of the to hull interaction force (m)

x_R Longitudinal position of the rudder's centre of pressure (m)

Y′ Sway external force (Nt)

Y_S Transverse coordinates of the centre of wind force (m)

Y_0 0-th order Bessel function of second kind

Z′ heave external force (Nt)

z_R Vertical position of the rudder's centre of pressure (m)

z_y Vertical coordinate of the centre of action of lateral force (m)

Greek symbols

β_R Equivalent drift angle (deg)

β_p Propeller inflow angle (deg)

χ Heading angle (deg)

χ_c Autopilot course from the wave direction (deg)

δ Rudder Angle (deg)

δ_R Actual rudder angle (deg)

ϕ Heel angle (deg)

γ Flow straightening coefficient due to hull and propeller

λ Wave length (m)

θ Pitch angle (deg)

ρ Density (kg/m^3)

σ_i Random phase angle (deg)

τ Hanaoka parameter (Chapter 10 only)

ω Wave frequency (rad/s)

ω_e Wave encounter frequency (rad/s)

ω_w circular frequency of sinusoidal waves (rad/s)

ω_{wi} Component circular frequency (rad/s)

ω_G Angular velocity (deg/s)

ξ Position of ship on the wave (m)

ψ Autopilot course (deg)

ψ_R The desired heading angle (deg)

ψ_{rw} Effective wind angle to the ship (deg)

ζ Vertical position of ship (m)

$\zeta(t)$ Irregular wave elevation (m)

ζ_a Wave amplitude (m)

Δ Displacement (kg)

Φ_I Potential associated with the incoming wave potential

Φ_D Potential of disturbed wave

Λ Rudder aspect ratio

Hydrodynamic Coefficients

J_y Pitch added inertia

$K_{\dot{p}}$ Roll added inertia

m_z Heave added mass

M_q, M_w Pitch velocity coefficients

$N_{\dot{v}}$, $N_{\dot{r}}$ Yaw acceleration coefficients

N_r, N_v Yaw velocity coefficients

$Y_{\dot{v}}$, $Y_{\dot{r}}$ Sway acceleration coefficients

Y_v, Y_r Sway velocity coefficients

$X_{\dot{u}}$ Surge acceleration coefficient

X_u Surge velocity coefficient

Z_q, Z_w, Heave velocity coefficients

APPENDICES

A. EQUATIONS OF MOTION

Traditionally, the equations of motion of a ship are described with respect to the inertial coordinate system. However, since the ship travels along a path which might deviate from this coordinate system, it was found to be much more sensible to have co-ordinate frame of reference that is fixed in the ship, rather than being earth fixed. Newton's second law of dynamics describes the equations of motion for an object (ship) having six degrees of freedom and under the action of certain external forces for body-fixed axis. It can be formulated for translations and rotations in vector form as follows.

$$m(\dot{V}_G + \omega \times V_G) = X_F$$

$$\dot{H}_G + \omega \times H_G = X_M$$

Equation A.1

where m is the mass of a ship, H_G the angular momentum about the centre of gravity, ω the angular velocity, V_G the linear velocity, X_F the external force vector and X_M the moment vector.

The first term of right hand side of Equation (A.1) is the reactive forces acting on the hull and it will be divided into two parts: hydrostatic and hydrodynamic forces.

In order to describe the situation of the ship in the earth fixed axes, it is normal to use a transformation of Equation (A.1) in terms of Eulerian angles ϕ,θ,ψ which are defined as the rotations about the body fixed axes (Fig.A.1).

We use instead Equation (A.2) instead of Equation (A.1), in which the only one rotation about the absolutely vertical axis is considered and this is called here as the Horizontal body axes, G-x'y'z' in Fig.A.1.

$$m(\dot{V}_G + k\dot{\psi} \times V_G) = -\iint_S pndS$$

$$\dot{H}_G + k\dot{\psi} \times H_G = -\iint_S p(r \times n)dS$$

Equation A.2

and

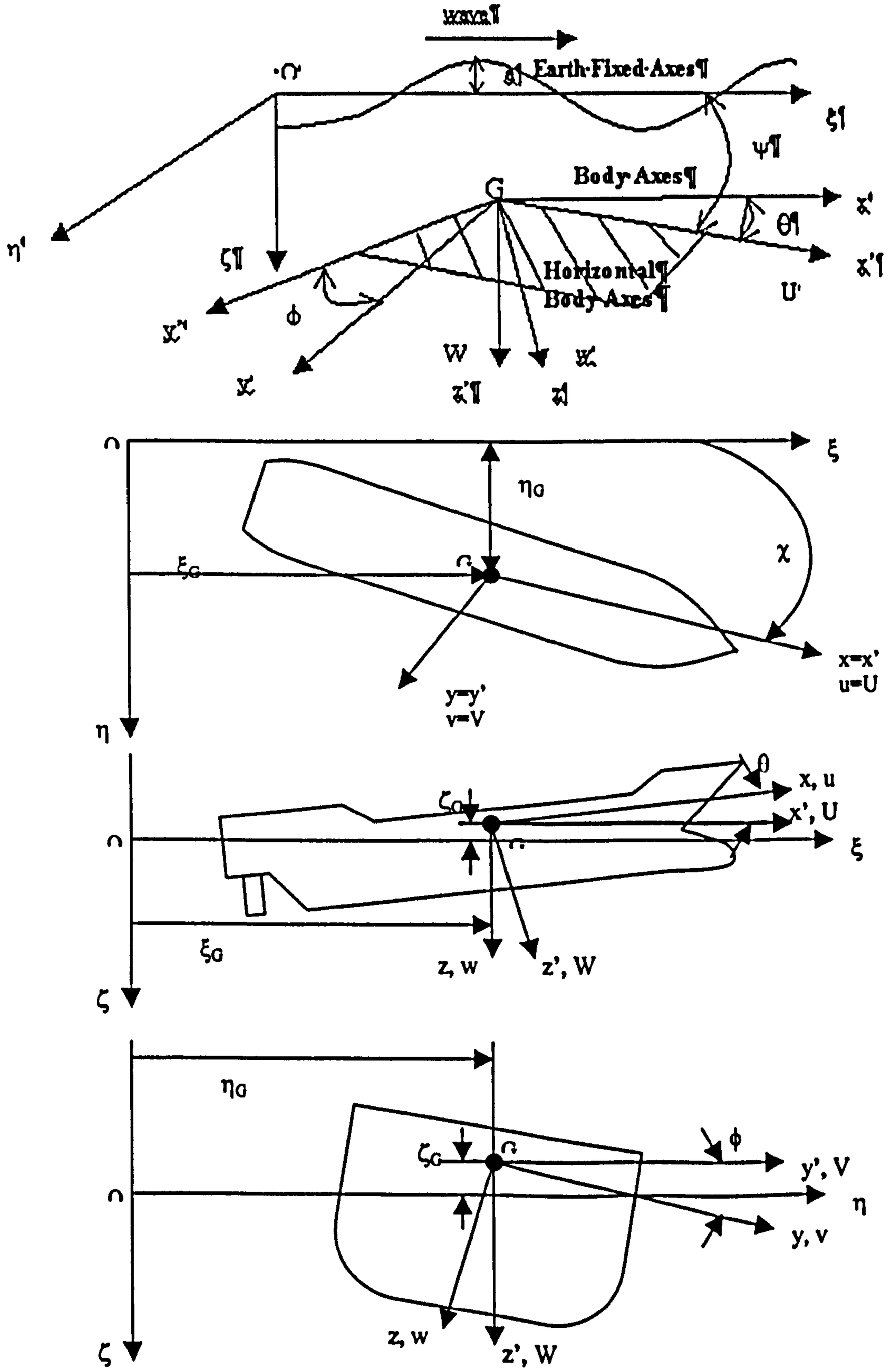

Figure A.1 Horizontal Body Axis System

$$V_G = iU + jV + kW, \quad H_G = iH_x + jH_y + kH_z$$

Equation A.3

where U, V and W are the linear velocities, $H_{x'}$, $H_{y'}$ and $H_{z'}$ the components of moment vector with respect to the Horizontal body axes.

The transformation between body axes and horizontal body axes in terms of the Eulerian angles is as follows

$$\begin{bmatrix} x' \\ y' \\ z' \end{bmatrix} = \begin{bmatrix} \cos\theta & \sin\varphi\sin\theta & \cos\varphi\sin\theta \\ 0 & \cos\varphi & -\sin\varphi \\ -\sin\theta & \sin\varphi\cos\theta & \cos\varphi\cos\theta \end{bmatrix} \begin{bmatrix} x \\ y \\ z \end{bmatrix}$$

Equation A.4

The angular velocity ω is described for the horizontal body axis system as

$$\omega = i\dot{\Phi} + j\dot{\Theta} + k\dot{\Psi}$$

Equation A.5

The transformation between the angular velocity of the horizontal system and the body axis system is shown as

$$\begin{bmatrix} \dot{\Phi} \\ \dot{\Theta} \\ \dot{\Psi} \end{bmatrix} = \begin{bmatrix} \cos\theta & 0 & 0 \\ 0 & 1 & 0 \\ -\sin\theta & 0 & 1 \end{bmatrix} \begin{bmatrix} \dot{\varphi} \\ \dot{\theta} \\ \dot{\psi} \end{bmatrix}$$

Equation A.6

Now we can define the components of the moment vector in terms of the angular velocity and moments of inertia:

$$\begin{bmatrix} H_{x'} \\ H_{y'} \\ H_{z'} \end{bmatrix} = \begin{bmatrix} I_{x'x'} & -I_{x'y'} & -I_{x'z'} \\ -I_{y'x'} & I_{y'y'} & -I_{y'z'} \\ -I_{z'x'} & -I_{z'y'} & I_{z'z'} \end{bmatrix} \begin{bmatrix} \dot{\Phi} \\ \dot{\Theta} \\ \dot{\Psi} \end{bmatrix}$$

Equation A.7

In equation A.8, prime (') indicates moments of inertia for the horizontal body axis system.

$$I_{x'x'} = \int_m (y'^2 + z'^2)dm \qquad I_{x'y'} = \int_m x'y'dm$$
$$I_{y'y'} = \int_m (z'^2 + x'^2)dm \qquad I_{y'z'} = \int_m y'z'dm$$
$$I_{z'z'} = \int_m (x'^2 + y'^2)dm \qquad I_{z'x'} = \int_m z'x'dm$$

Equation A.8

In order to derive the equations of motion some approximations are made. First, because of symmetry and since the origin is located at the centre of gravity, it is assumed that $I_{yz}=0$, $I_{xy}=0$, $I_{xz}=0$ and in the horizontal system $I_{yy} \cong I_{zz}$. Furthermore, using Equation A.4 and A.8, the moments of inertia and product moments of inertia are obtained as:

$$I_{x'x'} = I_{xx}\cos^2\theta + [(I_{zz}\cos^2\varphi + I_{yy}\sin^2\varphi)\sin^2\theta]$$
$$I_{y'y'} = I_{yy}\cos^2\varphi + I_{zz}\sin^2\varphi = I_{yy} = I_{zz}$$
$$I_{z'z'} = I_{xx}\sin^2\theta + [(I_{zz}\cos^2\varphi + I_{yy}\sin^2\varphi)\cos^2\theta]$$

Equation A.9

$$I_{x'y'} = 0$$
$$I_{y'z'} = 0$$
$$I_{z'x'} = (I_{xx} - I_{zz}\cos^2\varphi - I_{yy}\sin^2\varphi)\sin(0).\cos(0)$$

Equation A.10

Newton's law of motion for a rigid body can be written as two equations: a force equation and a moment equation. These equations are:

$$m\frac{dV_G}{dt} = F$$
$$\frac{dH_G}{dt} = G$$

Equation A.11

In the above equation, dV_G/dt is derived in the following form:

$$\frac{dV_G}{dt} = i\dot{U} + j\dot{V} + k\dot{W} + U\frac{di}{dt} + V\frac{dj}{dt} + W\frac{dk}{dt}$$
$$= i(\dot{U} - V\dot{\Psi}) + j(\dot{V} + U\dot{\Psi}) + k\dot{W}$$

Equation A.12

Here, the horizontal body axis coordinate system is derived by a rotation about the z' axis with no rotations about the y' and x' axes. The ship however can rotate about the y' and x' axes, so that the time derivatives of the unit vectors can be manipulated as:

$$\frac{di}{dt} = j\dot{\Psi} \quad \frac{dj}{dt} = -i\Psi \quad \frac{dk}{dt} = 0$$

Equation A.13

In the same manner, the vector component of moment

$$\frac{dH_G}{dt} = i(\dot{H}_{x'} - H_{y'}\dot{\Psi}) + j(\dot{H}_{y'} + H_{x'}\dot{\Psi}) + k\dot{H}_{z'}$$

Equation A.14

Notice that in contrast with conventional methods, no assumption is made of a small pitch angle and the motions will be solved for large amplitudes. Thus results will be obtained from the non-linear equations.

In the light of these results, considering force and moment components, the force and moment will individually be divided into components:

$$m(\dot{U} - V\dot{\Psi}) = X'$$
$$m(\dot{V} + U\dot{\Psi}) = Y'$$
$$m\dot{W} = Z' + mg$$

Equation A.15

and moment:

$$\frac{d}{dt}\left(I_{x'x'}\dot{\Phi} - I_{x'y'}\dot{\Theta} - I_{x'z'}\dot{\Psi}\right) - \dot{\Psi}(I_{y'y'}\dot{\Theta} - I_{y'z'}\dot{\Psi} - I_{y'x'}\dot{\Phi}) = K'$$
$$\frac{d}{dt}(I_{y'y'}\dot{\Theta} - I_{y'z'}\dot{\Psi} - I_{y'x'}\dot{\Phi}) + \dot{\Psi}(I_{x'x'}\dot{\Phi} - I_{x'y'}\dot{\Theta} - I_{x'z'}\dot{\Psi}) = M'$$
$$\frac{d}{dt}(I_{z'z'}\dot{\Psi} - I_{z'x'}\dot{\Phi} - I_{z'y'}\dot{\Theta}) = N'$$

Equation A.16

where m is mass of the ship and g is gravitational acceleration. Putting Equation A.17 in matrix form:

$$\begin{bmatrix} H_{x'} \\ H_{y'} \\ H_{z'} \end{bmatrix} = \begin{bmatrix} I_{x'x'} & -I_{x'y'} & -I_{x'z'} \\ -I_{y'x'} & I_{Y'Y'} & -I_{y'z'} \\ -I_{z'x'} & -I_{z'y'} & I_{z'z'} \end{bmatrix} \begin{bmatrix} \ddot{\Phi} \\ \ddot{\Theta} \\ \ddot{\Psi} \end{bmatrix} + \begin{bmatrix} \dot{I}_{x'x'} & -\dot{I}_{x'y'} & -\dot{I}_{x'z'} \\ -\dot{I}_{y'x'} & \dot{I}_{y'y'} & -\dot{I}_{y'z'} \\ -\dot{I}_{z'x'} & -\dot{I}_{z'y'} & \dot{I}_{z'z'} \end{bmatrix} \begin{bmatrix} \dot{\Phi} \\ \dot{\Theta} \\ \dot{\Psi} \end{bmatrix}$$

Equation A.17

Expanding the above matrix equation, equations of moment can be derived. In order to simplify these equations the following expressions are used. Substituting P for $\dot{\Phi}$, Q for $\dot{\Theta}$ and R for $\dot{\Psi}$ the moment equations will be

$$\begin{aligned} m(\dot{U} - VR) &= X' \\ m(\dot{V} + UR) &= Y' \\ m\dot{W} &= Z' + mg \end{aligned}$$

Equation A.18

$$K' = (I_{yy} - I_{xx})\left[\sin 2\theta\left(QP + \frac{1}{2}\dot{R}\right) + \cos 2\theta\, QR\right] + (I_{xx}\cos^2\theta + I_{yy}\sin^2\theta)\dot{P} - I_{yy}RQ$$

$$M' = (I_{yy} - I_{xx})\left[\sin 2\theta\left(\frac{1}{2}R^2\right)\right] + (I_{xx}\cos^2\theta + I_{yy}\sin^2\theta)RP + I_{yy}\dot{Q}$$

$$N' = (I_{xx} - I_{zz})\left[\sin 2\theta\left(Q.R - \frac{1}{2}\dot{P}\right) - \cos 2\theta\, QP\right] + (I_{xx}\sin^2\theta + I_{zz}\cos^2\theta)\dot{R}$$

Equation A.19

where X′, Y′, Z′, K′, M′, N′ are surge, sway, heave, roll, pitch, yaw external forces and moments. U, V, R are surge, sway, heave linear velocities, Q, P, R are roll, pitch, yaw angular velocities in horizontal body axes system and I_{xx}, I_{yy}, I_{zz} are roll, pitch, yaw moments of inertias, respectively.

The comparison between the new horizontal body axis system and existing systems is given in Table A.1

Earth Fixed Axis System	Body Fixed Axis System	Horizontal Body Axis System (Small Angles Assumption)	Horizontal Body Axis System (Large Angles Assumption)
Translation Motions and Forces $m\dot{V}_G = F$ **Rotational Motions and Forces** $\dot{H}_G = G$ where $V_G = i\dot{\xi}_G + j\dot{\eta}_G + k\dot{\zeta}_G$ $H_G = iH_\xi + jH_\eta + kH_\zeta$ $\omega = i\omega_\xi + j\omega_\eta + k\omega_\zeta$ $\omega_\xi = \dot{\phi}\cos\theta\cos\psi - \dot{\theta}\sin\psi$ $\omega_\eta = \dot{\phi}\cos\theta\sin\psi + \dot{\theta}\cos\psi$ $\omega_\zeta = \dot{\psi} - \dot{\phi}\sin\theta$	**Translation Motions and Forces** $m(\dot{V}_G + \omega \times V_G) = F$ **Rotational Motions and Forces** $\dot{H}_G + \omega \times H_G = G$ where $V_G = iu + jv + kw$ $H_G = iH_x + jH_y + kH_z$ $\omega = ip + jq + kr$ $p = \dot{\phi} - \dot{\psi}\sin\theta$ $q = \dot{\phi}\cos\varphi + \dot{\psi}\sin\varphi\cos\psi$ $r = \dot{\psi}\cos\varphi\cos\theta - \dot{\theta}\sin\varphi$	**Translation Motions and Forces** $m(\dot{V}_G + k\dot{\Psi} \times V_G) = F$ **Rotational Motions and Forces** $\dot{H}_G + k\dot{\Psi} \times H_G = G$ where $V_G = iU + jV + kW$ $H_G = iH_{x'} + jH_{y'} + kH_{z'}$ $\omega = i\dot{\Phi} + j\dot{\Theta} + k\dot{\Psi}$ $\dot{\Phi} = \dot{\varphi}\cos\theta$ $\dot{\Theta} = \dot{\theta}$ $\dot{\Psi} = \dot{\psi} - \dot{\varphi}\sin\theta$	**Translation Motions and Forces** $m(\dot{V}_G + k\dot{\Psi} \times V_G) = F$ **Rotational Motions and Forces** $\dot{H}_G + k\dot{\Psi} \times H_G = G$ where $V_G = iU + jV + kW$ $H_G = iH_{x'} + jH_{y'} + kH_{z'}$ $\omega = i\dot{\Phi} + j\dot{\Theta} + k\dot{\Psi}$ $\dot{\Phi} = P = \dot{\varphi}\cos\theta$ $\dot{\Theta} = Q = \dot{\theta}$ $\dot{\Psi} = R = \dot{\psi} - \dot{\varphi}\sin\theta$
Translation motions and Forces $m\ddot{\xi}_G = F_\xi$ $m\ddot{\eta}_G = F_\eta$ $m\ddot{\zeta}_G = F_\zeta + mg$ **Rotational Motions and Forces** $I_{xx}\ddot{\phi} - I_{xx}\dot{\theta}\dot{\psi} = G_\xi$ $I_{yy}\ddot{\theta} + I_{xx}\dot{\phi}\dot{\psi} = G_\eta$ $I_{zz}\ddot{\psi} - I_{xx}\dot{\theta}\dot{\phi} = G_\zeta$ where $I_{yy} \cong I_{zz}, I_{xz} \cong 0, \theta \cong 0, \psi \cong 0$	**Translation motions and Forces** $m(\dot{u} + wq - vr) = X$ $m(\dot{v} + ur - wp) = Y + mg\sin\phi$ $m(\dot{w} + vp - uq) = Z + mg\cos\phi$ **Rotational Motions and Forces** $I_{xx}\dot{p} = K$ $I_{yy}\dot{q} - (I_{zz} - I_{xx})rp = M$ $I_{zz}\dot{r} - (I_{xx} - I_{yy})pq = N$ where $I_{yy} \cong I_{zz}, I_{xz} \cong 0, \theta \cong 0$	**Translation motions and Forces** $m(\dot{U} - V\dot{\psi}) = X'$ $m(\dot{V} + U\dot{\psi}) = Y'$ $m\dot{W} = Z' + mg$ **Rotational Motions and Forces** $I_{xx}\ddot{\phi} - I_{xx}\dot{\theta}\dot{\psi} = K'$ $I_{yy}\ddot{\theta} + I_{xx}\dot{\psi}\dot{\phi} = M'$ $I_{zz}\ddot{\psi} - I_{xx}\dot{\phi}\dot{\theta} = N'$ where $I_{yy} \cong I_{zz}, I_{xz} \cong 0, \theta \cong 0$	**Translation motions and Forces** $m(\dot{U} - VR) = X'$ $m(\dot{V} + UR) = Y'$ $m\dot{W} = Z' + mg$ **Rotational Motions and Forces** $K' = (I_{yy} - I_{xx})\left[\sin 2\theta\left(QP + \frac{1}{2}\dot{R}\right) + \cos 2\theta\, QR\right] + \left(I_{xx}\cos^2\theta + I_{yy}\sin^2\theta\right)\dot{P} - I_{yy}RQ$ $M' = (I_{yy} - I_{xx})\left[\sin 2\theta\left(\frac{1}{2}R^2\right)\right] + \left(I_{xx}\cos^2\theta + I_{yy}\sin^2\theta\right)RP + I_{yy}\dot{Q}$ $N' = (I_{xx} - I_{zz})\left[\sin 2\theta\left(Q.R - \frac{1}{2}\dot{P}\right) - \cos 2\theta\, QP\right] + \left(I_{xx}\sin^2\theta + I_{zz}\cos^2\theta\right)\dot{R}$ $I_{yy} \cong I_{zz}, I_{xz} \cong 0,$

Table A.1 Comparison of horizontal body system with traditional systems

B. WAVE FORCES

(This Appendix is based on Hamamoto and Kim [20]) and Ohkusu [16]. The equations are given for completeness.)

Froude-Krylov Forces Including Hydrostatic Forces on A Ship (from Hamamoto and Kim [20])[

The hydrostatic forces and moments can be obtained by integrating the pressure (p) over the entire wetted surface of the ship. The hydrostatic pressure p including that of a sinusoidal wave ζ_w at any time and position ξ in the earth fixed axes is given by

$$p = \rho g(\zeta_G - x'\theta + z') - \rho g a e^{-kd}\cos(k(\xi_G + x'\cos(\psi) - y'\sin(\psi) - ct))$$

Equation B.1

with

$$\zeta_w = -\zeta_G + x'\theta + a\cos(k(\xi_G + x'\cos(\psi) - y'\sin(\psi) - ct))$$

Equation B.2

where a the amplitude of wave, c the phase velocity of wave and d the draught of the ship. Using the above expressions in Gauss theorem, the Froude-Krylov forces are described with respect to the horizontal body axes in the form:

$$X'_{F.K}(\zeta_G, \theta, \psi, \varphi) \equiv -\iiint_V \frac{\partial p(F,K)}{\partial x'} dV$$
$$\equiv \rho g \theta \int_L A(x)dx - \rho g \cos(\psi) \int_L F(x)A(x)\sin(k(\xi_G + x\cos(\psi) - ct))dx$$

Equation B.3

$$Y'_{F.K}(\zeta_G, \theta, \psi, \varphi) \equiv -\iiint_V \frac{\partial p(F,K)}{\partial y'} dV$$
$$\equiv \rho g \sin(\psi) \int_L F(x)A(x)\sin(k(\xi_G + x\cos(\psi) - ct))dx$$

Equation B.4

$$Z'_{F.K}(\zeta_G,\theta,\psi,\varphi) \equiv -\iiint_V \frac{\partial p(F,K)}{\partial z'} dV$$
$$\cong -\rho g \int_L A(x)dx - \rho g \int_L F(x)A(x)\cos\left(k(\xi_G + x\cos(\psi) - ct)\right)dx$$

Equation B.5

$$K'_{F.K}(\zeta_G,\theta,\psi,\varphi) \equiv -\iiint_V \left[y' \frac{\partial p(F,K)}{\partial z'} - z' \frac{\partial p(F,K)}{\partial y'} \right] dV$$
$$\cong -\rho g \int y'_B A(x)dx - \rho g \sin(\psi) \int F(x)A(x)z'_B \sin\left(k(\xi_G + x\cos(\psi) - ct)\right)dx$$

Equation B.6

$$M'_{F.K}(\zeta_G,\theta,\psi,\varphi) \equiv -\iiint_V \left[z' \frac{\partial p(F,K)}{\partial x'} - x' \frac{\partial p(F,K)}{\partial z'} \right] dV$$
$$\cong \rho g \int_L xA(x)dx + \rho g \int_L F(x)A(x)x\cos\left(k(\xi_G + x\cos(\psi) - ct)\right)dx$$

Equation B.7

$$N'_S(\zeta_G,\theta,\psi,\varphi) \equiv -\iiint_V \left[x' \frac{\partial p(F,K)}{\partial y'} - y' \frac{\partial p(F,K)}{\partial x'} \right] dV$$
$$\cong \rho g \sin(\psi) \int_L F(x)A(x)x\sin\left(k(\xi_G + x\cos(\psi) - ct)\right)dx$$

Equation B.8

where

$$F(x) = ak \frac{\sin\left(k\frac{B(x)}{2}\sin(\psi)\right)}{k\frac{B(x)}{2}\sin(\psi)} e^{-kd} A(x)$$

Equation B.9

In addition, A(x) the immersed sectional area, B(x) the breadth, V immersed volume of the ship and (y_b', z_b') the centre of buoyancy of the immersed section.

Diffraction Forces (from Ohkusu [16])

It is assumed that the ship is advancing into the positive x direction with a constant forward velocity U. A translating reference frame (x, y, z) is defined to be fixed relative to the ship's mean position, with z-axis positive upward and z=0 is the plane of the undisturbed free surface (Figure B.1).

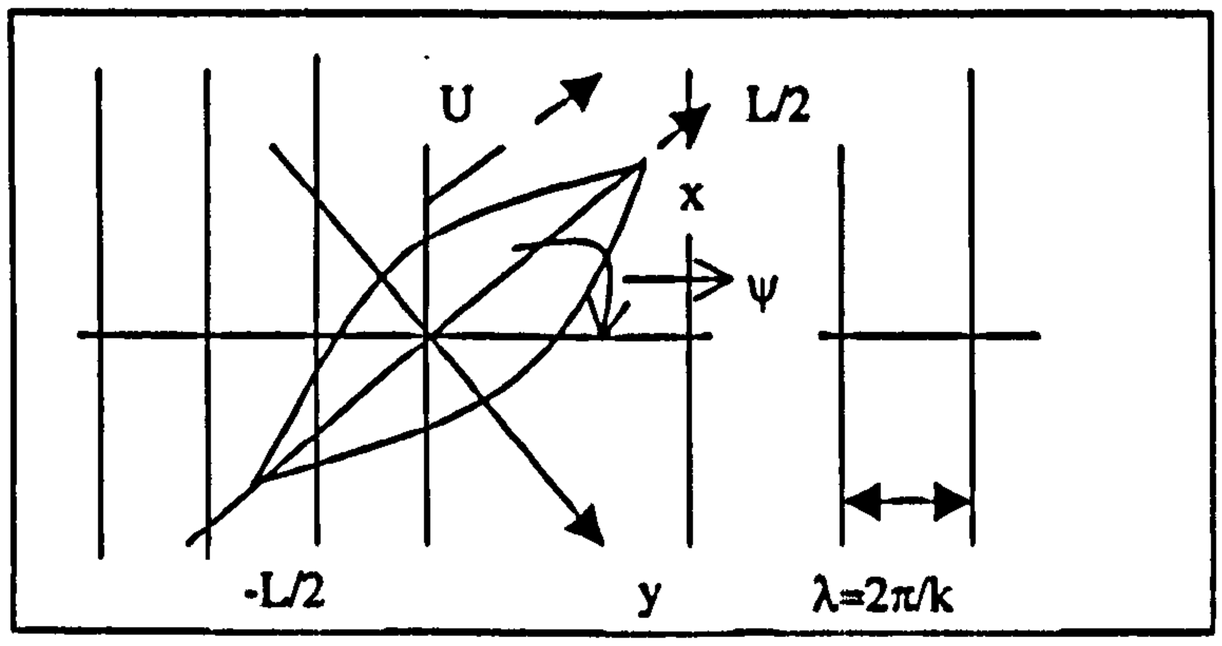

Figure B.1- Coordinate System

Incident waves are progressing into direction making an angle ψ with their x-axis and their velocity potential is given by

$$\Phi_I e^{i\omega_e t} = e^{-kz} e^{i(\omega_e t - kx\cos(\chi) - ky\sin(\chi))}$$

Equation B.10

where ω_e is the encounter circular frequency

The ship is advancing in those waves with very low encounter frequency and its motions suppressed. We define diffraction wave velocity potential by $\Phi e^{i\omega e t}$ satisfies the kinematic boundary and free-surface condition,

$$\nabla^2 \Phi_D = 0$$

$$\left(i\omega_e - U\frac{\partial}{\partial x}\right)^2 \Phi_D - g\frac{\partial \Phi_D}{\partial z} = 0 \text{ on } z = 0$$

$$\frac{\partial \Phi_D}{\partial n} = -\frac{\partial \Phi_I}{\partial n} \qquad \text{on the body}$$

Equation B.11

In the derivation of the condition on z=0 we linearize the problem with respect to parameter δa related to the smallness of the amplitude of the incident waves. Besides those conditions, Φ_D should satisfy the radiation condition.

Assume that ship is very slender and slenderness parameter ε, related to the beam-to-length ratio, is very small. ω_e in the following waves is also assumed to be very low and of the order O(ε).

Considering $\omega_e^2\ \partial\Phi_D/\partial x \sim O(\varepsilon^2\Phi_D)$ and $\omega_e\partial\Phi_D/\partial x \sim O(\varepsilon\Phi_D)$, and taking the lowest order terms with respect to Φ_D under those assumptions the free surface condition is,

$$U^2\frac{\partial^2\Phi_D}{\partial x^2}\Phi_D - g\frac{\partial\Phi_D}{\partial z} = 0 \text{ on } z = 0$$

Equation B.12

When the ship is advancing the waves with very low encounter frequency; the incident waves appear as if they might not move relative to the ship while she advances some distance. Then that will approximate disturbance of the incident waves by the ship when she keeps running quite along time without changing her position relative to the incident waves. Φ_D might not be called the diffraction waves in such situation. So it is simply called the disturbance imply the disturbance of the incident waves.

Assuming the wavelength of the incident waves being of the order O(1) in the near field. Φ_D in the near field;

$$\frac{\partial^2\Phi_D}{\partial y^2} + \frac{\partial^2\Phi_D}{\partial z^2} = 0$$

$$\frac{\partial\Phi_D}{\partial z} = 0 \quad \text{on } z = 0$$

$$\frac{\partial\Phi_D}{\partial N} = -\frac{\partial\Phi_I}{\partial N} \quad \text{on the body}$$

Equation B.13

where N is outward normal to the contour of the 2-D sectional form. Free surface condition in Equation B.13 can also be given according to Ohkusu's theory as follows [81]:

$$\frac{\partial\Phi_D}{\partial z} = -z_I\frac{\partial^2}{\partial z^2}\Phi_s, \quad z = 0$$

Equation B.14

where z_I is incident wave and Φ_S indicates the potential due to the ship running in calm water [103]. However, it is found by Umeda et al. [81] that non-homogenous term of

Equation B.14, which Ohkusu does not include, should be included by the principle of perturbation method. Using the terms from [81], it is written as:

$$\Phi'_D = \Phi_D + z_I \frac{\partial}{\partial z}\Phi_S$$

Equation B.15

Therefore, Equation B.13 can be transformed as follows

$$\frac{\partial^2 \Phi'_D}{\partial y^2} + \frac{\partial^2 \Phi'_D}{\partial z^2} = 0$$

$$\frac{\partial \Phi'_D}{\partial z} = 0 \quad \text{on } z = 0$$

$$\frac{\partial \Phi'_D}{\partial N} = -\frac{\partial \Phi_I}{\partial N} + z_I \frac{\partial}{\partial z}\left(U \frac{\partial}{\partial x} n\right) \quad \text{on the body}$$

Equation B.16

For the sake of simplicity, (') sign will be dropped in the rest of Appendix, however Φ_D will represent the term in Equations B.15 and B.16.

Φ_D will be given in the much same manner as the slender body theory given by Tuck [103], [104]. The velocity potential takes the form as;

$$\Phi_D = \frac{\sigma(x)}{\pi}\log(k_0)R + F(x) \times \sum_{n=1}^{\infty}\left[P_{2n}(x).\cos(2n)\theta/R^{2n} + P_{2n-1}(x).\sin(2n-1)\theta/R^{2n-1}\right]$$

Equation B.17

where $R=\sqrt{y^2+z^2}$ $\theta=$ arctan (y/z) and $k_0=g/U^2$ σ and P_n are to be determined such that body condition is satisfied. The additive function F(x) is determined from the far-field description of $\Phi_D.\Phi_D$ must satisfy the free surface condition [103] and the first condition in [104] in the far field.

Φ_D appears as if it might have been caused by line singularities on the centre line of the ship which in this case we take to be sources and dipoles. F(x) then can be evaluated as

$$F(x)=-\frac{1}{2\pi}\int d\xi\frac{d\sigma}{d\xi}\left[\log(2k_0)|x-\xi|\mathrm{sgn}(x-\xi)-\frac{\pi}{2}\left\{H_0(k_0(x-\xi))-2\mathrm{sgn}(x-\xi)Y_0(k_0|x-\xi|)\right\}\right]$$

Equation B.18

where H_0 is Struve function ([103]) and Y_0 the 0-th order Bessel function of second kind Φ_D in the near field has the form

$$\Phi_D(y,z:x)=\Phi_{2D}{}^S(y,z:x)+F(x)+\Phi_{2D}{}^A(y,z:x)$$

Equation B.19

where $\Phi_{2D}{}^S$ and $\Phi_{2D}{}^A$ are 2-D solutions symmetrical and antisymmetrical with respect to the z-axis. They must satisfy the following the body conditions and must approach to zero when $R\rightarrow\infty$

$$\frac{\partial\Phi_{2D}{}^S}{\partial N}=\left[kN_Z\cos(ky\sin\chi)+kN_y\sin(\chi)\sin(ky\sin(\chi))\right]e^{-kz}e^{-ik\chi\cos(\chi)}$$

$$\frac{\partial\Phi_{2D}{}^S}{\partial N}=(kN_z+O(\varepsilon))e^{-ikx\cos(\chi)}$$

Equation B.20

$$\frac{\partial\Phi_{2D}{}^A}{\partial N}=\left[-ikN_z\sin(ky\sin(\chi))+ikN_y\sin(\chi)\cos(ky\sin(\chi))\right]e^{-kz}e^{-ik\chi\cos(\chi)}$$

$$\frac{\partial\Phi_{2D}{}^A}{\partial N}=(ikN_y\sin(\chi)+O(\varepsilon))e^{-ikx\cos(\chi)}$$

Equation B.21

where N denotes outward normal to the ship's section contour, N_y the y-component of it and N_z the z-component.

In this study the cross section form of the ship is approximated by a Lewis form, [105], of a half circle with unit radius. So we can easily obtain solutions $\Phi_{2D}{}^S$ $\Phi_{2D}{}^A$ and F (x) for the boundary problems above. Lewis forms have been modified for more realistic hull shapes as was used by some researchers on calculation of added mass and influence of heeling [106], [107], [108].

The coordinate of a point (y, z) on a section is expressed in the coordinate (r,θ) with parameters a_1, a_3 and M dependent on the cross section's form.

$$y = M(r\sin(\theta) + a_1\sin(\theta)/r - a_3\sin(3\theta)/r^3)$$
$$z = M(r\cos(\theta) - a_1\cos(\theta)/r + a_3\cos(3\theta)/r^3)$$

Equation B.22

Then $\Phi_{2D}{}^S$ $\Phi_{2D}{}^A$ are given by

$$\Phi_{2D}{}^S = \frac{\sigma}{\pi}\log(k_0)Mr + \sum_{n=1}^{\infty} A_{2n}\cos(2n)\theta/r^{2n}$$
$$\Phi_{2D}{}^A = \sum_{n=1}^{\infty} A_{2n-1}\sin(2n-1)\theta/r^{2n-1}$$

Equation B.23

With boundary conditions on the ship's section given by Equations (B.21), (B.22), σ and A_n (n=1,2...) are determined as follows,

$$\sigma = -\int_{\Gamma_x} \frac{\partial\Phi_I}{\partial N}\partial s$$
$$\sigma = e^{-ikx\cos(\chi)} \int_{-\pi/2}^{\pi/2} ky`d\theta$$
$$\sigma = 2kM(1 + a1 + a3)e^{-ikx\cos(\chi)}$$

Equation B.24

$$A_{2N} = \frac{1}{n\pi}\int_{\Gamma_x} \frac{\partial\Phi_I}{\partial N}\cos(2n)\theta ds$$
$$A_{2N} = -\frac{1}{n\pi}e^{-ikx\cos(\chi)} \int_{-\pi/2}^{\pi/2} ky'\cos(2n)\theta d\theta$$
$$A_{2N} = -\frac{kM}{n\pi}e^{-ikx\cos(\chi)}\left[2(1+a1)\frac{(-1)^n}{4n^2-1} - 18a_3\frac{(-1)^n}{4n^2-9}\right]$$

Equation B.25

$$A_{2n-1} = \frac{2}{(2n-1)\pi}\int_{\Gamma_x}\frac{\partial\Phi_I}{\partial N}\sin(2n-1)\theta d\theta$$

$$A_{2n-1} = \frac{2i}{(2n-1)\pi}e^{-ikx\cos(\chi)} \times \int_{-\pi/2}^{\pi/2} kz'\sin(x)\sin(2n-1)\theta\, d\theta$$

$$A_{2n-1} = ikM\sin(\chi)e^{-ikx\cos(\chi)}(a_1 - 1); \quad n = 1$$
$$-ikM\sin(\chi)e^{-ik\cos(\chi)}a_3; \quad n = 2$$
$$0; \quad n \geq 3$$

Equation B.26

where Γx denotes the contour of the section under the still water surface.

Incident waves $\Phi_I e^{i\omega et}$, disturbance waves $\Phi_D e^{i\omega et}$ and their interaction with stationary waves Φ_S generated by the ship running on otherwise calm water induce fluid pressure proportional to δ, the amplitude of the incident waves.

Dynamic pressure P on a section of the ship is

$$P = -\rho\left(i\omega_e - U\frac{\partial}{\partial x}\right)\varphi_I e^{i\omega_e t} - \rho\left(i\omega_e - U\frac{\partial}{\partial x}\right)(\Phi_I + \Phi_D e^{i\omega_e t})$$
$$+\frac{\rho}{2}\left[\Gamma\left(\Phi_I e^{i\omega_e t} + \Phi_S + \Phi_D e^{i\omega_e t}\right)\right]^2$$

Equation B.27

Taking the linear terms of δ, the equation becomes

$$P = -\rho\left(i\omega\omega_I e^{\omega_e t}\right) + \rho U\frac{\partial\Phi_D}{\partial x}e^{i\omega_e t} - \rho\left(\frac{\partial\Phi_S}{\partial y}\frac{\partial\Phi_I}{\partial y} + \frac{\partial\Phi_S}{\partial z}\frac{\partial\Phi_I}{\partial z}\right)e^{i\omega_e t}$$
$$-\rho\left(\frac{\partial\Phi_S}{\partial y}\frac{\partial\Phi_{2D}{}^S}{\partial y} + \frac{\partial\Phi_S}{\partial z}\frac{\partial\Phi_{2D}{}^S}{\partial z}\right)e^{i\omega_e t} - \rho\left(\frac{\partial\Phi_S}{\partial y}\frac{\partial\Phi_{2D}{}^A}{\partial y} + \frac{\partial\Phi_S}{\partial z}\frac{\partial\Phi_{2D}{}^A}{\partial z}\right)e^{i\omega_e t}$$

Equation B.28

In deriving this equation, the pressure due to Φ_S alone and the terms of higher order with respect to ε or δ than O (δε) are ignored. Φ_S is assumed to be order O (δε) and $\partial\Phi_S/\partial y$, z~ O (δε), $\partial\Phi_S/\partial x$ ~ O (ε^2) in the near field according to result of the slender body theory on calm water [103], [104].

The first term on the right hand side of the equation (B.27) is the pressure due to Φ_I alone namely Froude-Krylov pressure. The second is disturbance wave pressure, the third is interaction between the stationary waves Φ_S and the incident waves Φ_I, and the 4^{th}. and 5^{th}. are interaction between Φ_S and Φ_D.

Wave force of the j- th. direction acting on the ship is given by

$$\omega_j = \rho i\omega_e e^{i\omega_e t}\int_{\Gamma_x}\Phi_I N_j ds - \rho U e^{i\omega_e t}\int_{\Gamma_x}\frac{\partial \Phi_D}{\partial x}N_j ds +$$

$$\rho e^{i\omega_e t}\int_{\Gamma_x}\left(\frac{\partial \Phi_{2D}{}^{S.A}}{\partial y}\frac{\partial \Phi_S}{\partial y}+\frac{\partial \Phi_{2D}{}^{S.A}}{\partial z}\frac{\partial \Phi_S}{\partial z}\right)N_j ds$$

$$\omega_j = +\rho e^{i\omega_e t}\int_{\Gamma_x}\left(\frac{\partial \Phi_{2D}}{\partial y}\frac{\partial \Phi_S}{\partial y}+\frac{\partial \Phi_{2D}}{\partial z}\frac{\partial \Phi_S}{\partial z}\right)N_j ds$$

Equation B.29

Here, j=1,2,3 denotes sway, heave, roll respectively. The superscripts A and S on the third integration term of the right hand side of the first equation in Equation B.29 are adopted for j=odd and j=even respectively.

Using dynamical pressure on the hull general wave force equations is obtained. For the purpose of this study, the disturbance equation can be written as follows,

$$F_{DIF} = \rho U\int_{\Gamma_x}\Phi_D N_j ds$$

Equation B.30

With substituting the equations (B.27), (B.28), (B.29) we have the expressions of those integral convenient for computation.

$$= \rho U\int_{-\pi/2}^{\pi/2}\sum_{n=1}^{2}A_{2n-1}(\dot{X})\sin(2n-1)\theta\, n_j(X)d\theta$$

$$j = 1,3 \quad \text{sway, roll}$$

Equation B.31

$$= \rho U \int_{-\pi/2}^{\pi/2} \left[\frac{\sigma(X)}{\pi} \log(k_0) M(X) + \sum_{n=1}^{\infty} A_{2n}(X) \cos(2n)0 \right] n_2(X) d0$$

$j = 2$ heave

Equation B.32

where $(n_1, n_2, n_3)=(-z', y', yy'+zz')$ and $A_n(X)$, $\sigma(X)$ and so on are specified as the values at a cross section of x=X. For the pitch and yaw, values of the heave and roll at each cross section are multiplied by distance between cross section and C.G of the ship.

C. OTHER EXCITATION TERMS

a. Hydrodynamic Reaction (Hull) Forces

As it is emphasised in Chapter 5, in the subject of calculation of manoeuvring (hull) forces, efforts mostly focused on estimation of hydrodynamic (reaction) coefficients. If we recall from Chapter 1 and 5, since the encounter frequency is very low, hydrodynamic forces acting on a ship, including wave- induced forces mainly consist of hydrodynamic lift and buoyancy. Wave making effects that depend on the encounter frequencies are negligibly small. Therefore a manoeuvring mathematical model focusing on lift components can be used in this situation and it eventually requires the accurate estimation of hydrodynamic hull reaction coefficients in calm water condition.

In the present context of manoeuvring studies, as it is given in Chapter 5, three types of method have mainly been exploiting by researchers; Theoretical models using potential flow theories, semi-empirical methods associated with experimental studies and CFD techniques.

The theoretical methodologies now provide a significant degree of accuracy to the calculation, yet not as reliable as experimental results. Due to the aforementioned phenomenon of viscous forces and cross-flow and separation effects, theoretical methodologies have been divided into different areas to reach considerable accuracy in total calculation. These studies have expanded to a wide spectrum, from the potential flow approach to accounting for wave-making effects along with three dimensional effects, hull lifting, cross flow considerations or calculation of the separation line and of the strength the trailing vortex. However, those models had already included some empirical assumptions. Spyrou [109], Fujino [129] and others have presented detail background of the evolution of these theories with references.

On the other hand, studies commonly faced difficulties because motions of ships on the horizontal plane are governed significantly by the viscosity of the flow, and it is not surprising that most of the work in this field is semi-empirical. With this approach, hull forces are assumed to be analytic functions of the kinematic ship variables and they are written as a Taylor series expansion with regard to kinematic variables while assumptions such as: the terms of higher order are negligible, acceleration terms are uncoupled from velocities and first order and inertial force coefficients do not depend on the direction of the resultant acceleration relative to the vessel's heading, are made.

Hydrodynamic coefficients of these models normally rely on tests like Planar Motion Mechanism tests, oblique flow testing or a rotating arm tests. This is still believed to be most reliable way of deriving coefficients. Inoue et al. [113] and Spyrou [109] gave detailed account of these models as well. However, as we mentioned in Chapter 6, there are fundamental objections to the assumption that the forces are analytical functions of ship geometry and its simple elements of motion. It has been shown that at any instant a fluid force is determined in part by previous motion. So-called "memory effects" associated with the effects of the free surface and vortices, respectively, result in the representation of the hydrodynamic forces arising from transient ship motions in terms of a convolution integral over the entire time history of the motion. The further discussion had already been given in Chapter 6 on that matter.

Recently, thanks to the developments in computer technology, new and very powerful numerical solvers from CFD such as Navier-Stokes Solvers [133] are being used in manoeuvring studies. At the current stage, mathematical motions and hull-rudder-propeller interactions are coupled with Navier-Stokes equations for calculation of hydrodynamic forces [133]. However, further discussion on these studies beyond the scope of current study.

Finally, deriving from the above background, the Japanese MMG model [112], [113] which had been already employed for the manoeuvring motions in astern seas such as Tsangaris [41] and Spyrou [109], has been used for the calculation of the manoeuvring forces. Furthermore, radiation forces for vertical motions are obtained using Tsai's [61] methodology.

$$X_H = X_{\dot{u}}\dot{u} - Y_{\dot{v}}vr - \frac{u}{|u|}Y_{\dot{r}}r^2 + X_{vr}vr - Res(u)$$

$$Y_H = Y_{\dot{v}}\dot{v} + Y_{\dot{r}}\dot{r} + Y_v vU + \frac{u}{|u|}Y_r rU + Y_{v|v|}v|v| + Y_{v|r|}v|r| + \frac{u}{|u|}Y_{r|r|}r|r|$$

$$N_H = N_{\dot{r}}\dot{r} + N_{\dot{v}}\dot{v} + N_r rU + \frac{u}{|u|}N_v vU + N_{r|r|}r|r| + \frac{u}{|u|}N_{mv}\frac{1}{U} + N_{vvr}vvr\frac{1}{U}$$

$$K_H = K_{\dot{p}}\ddot{\varphi} + C(\dot{\varphi}) - z_y Y_H$$

$$Z_H = m_z\dot{w}_G + Z_w w_G + Z_{\dot{q}}\dot{q} + Z_q q$$

$$M_H = J_y q + M_q q + M_{\dot{w}}\dot{w}_G + M_w w$$

Equation C.1

where, X_H, Y_H, Z_H, K_H, N_H, M_H, surge, sway, heave, roll, pitch, yaw hull forces, respectively, Res (u), resistance force, $C(\dot{\varphi})$, damping moment, z_y, vertical coordinate of the centre of action of lateral force. Now we can look at the components in above equations.

Resistance: Calculation of resistance is given in Chapter 5, which is generally based on experiments.

Point of action of lateral force: During a turning operation, point of action of the lateral forces, z_y, is varying. It could be estimated by the practical formula following Spyrou [109]:

$$z_y = g\,GZ(\varphi)/(U^2/R)$$

Equation C.2

where $GZ(\phi)$ is restoring moment, R is the turning radius. It could be given by the experiments or in most practical cases, it is simply assumed as the half of the draught.

Roll motion effect on sway and yaw coefficients: Although it is not represented in Equation C.1 or 5.17, combined sinkage and rotation occasionally occurs during heeling and affects the hydrodynamic coefficients. From [113] and [109] this dependence is expressed up to first order on the basis of linear sway and yaw velocity coefficients and

it can be added to the above sway and yaw force and moment terms in Equations C.1 or 5.17 as follows:

$$Y_H = Y_\varphi \varphi + Y_{v|\varphi|} v|\varphi| + Y_{r|\varphi|} r|\varphi|$$
$$N_H = N_\varphi \varphi + N_{v|\varphi|} v|\varphi| + N_{r|\varphi|} r|\varphi|$$

Equation C.3

It should be noted that this model is only valid for small heeling angles and it does not include the effect on the acceleration and higher order velocity coefficients. These coefficients are employed for the validation of the numerical results with the fishing trawler experiments and numerical simulations in Chapter 7 and 8, where they are obtained from the experiments (Figure F.10).

Roll damping: Calculation of roll damping in theoretical terms is very complex due to strong viscous effect in the motion. Therefore, semi-empirical methods based on certain assumptions or experimental studies were used for the calculation of roll damping. It is generally a non-linear function of the heeling angle and the calculation method of damping forces including all other parameters such as appendages are given in [136]. In the current study, for all the numerical studies, the damping force was obtained using the data from roll decay tests without forward speed (For instance, see Figure E.5). In the roll decay tests, the model (ship) is inclined to a relatively large roll angle and then released impulsively. The time history of motion is then recorded. Because roll is so lightly damped, the model (ship) oscillates at its natural frequency before the motion decays to the roll amplitude too small to measure accurately. The information in the time history can be used to determine the nonlinear coefficients of roll damping at the roll resonance frequency. The forward speed effect is included using Takahashi's empirical formula (See Equation E.1).

b. Rudder Forces

As it is given in Chapter 5, in calculation of rudder forces, JMG' s (Japanese Manoeuvring Group) model [113] is used. The rudder forces and moments including rudder-to-hull interaction as follows;

$$X_R = -F_N \sin\delta$$
$$Y_R = -(1+a_H)F_N \cos\delta$$
$$N_R = -(1+a_H)(x_H/x_R))x_R F_N \cos\delta$$
$$K_R = (1+a_H)z_R F_N \cos\delta$$

Equation C.4

where, X_R, Y_R, N_R, K_R, surge, sway, yaw, roll rudder forces respectively, F_N, rudder normal force, a_H, rudder–to-hull interaction coefficient, x_H, longitudinal coordinate of the point of action of the rudder to hull interaction force, x_R, z_R, longitudinal and vertical coordinates of the rudder's centre of pressure.

A rudder is essentially a vertically oriented lifting surface which, in case of a free stream velocity U_R, with the rudder oriented at some effective incident angle a_R, develops a lateral or normal force given by

$$F_N = \frac{\rho}{2} A_R U_R^2 f(\Lambda) \sin a_R$$

Equation C.5

where $f(\Lambda)$ is the open water rudder normal force coefficient which is a function of the rudder aspect ratio. Based on Fuji's formula as referred in Japanese MMG work [113] it can be written as

$$f(\Lambda) = \frac{6.13\Lambda}{\Lambda + 2.25}$$

Equation C.6

where Λ is rudder aspect ratio. Here, rudder inflow angle a_R and velocity U_R can be determined as follows.

Rudder inflow velocity, U_R and angle, a_R: It is assumed that wake fraction and thrust deduction ratios at the propeller and rudder positions are approximately equal:

$$w_r/w_{ro} = w_p/w_{Po}$$
$$t_r/t_{ro} = t_p/t_{Po}$$

Equation C.7

where w_p, w_{p0}, w_r, w_{r0}, are wake fraction in forward motion and during a turn, at the propeller and at a rudder position, t_p, t_{p0}, t_r, t_{r0} are thrust deduction in forward motion and during a turn, at the propeller and at the rudder position. Here, the mean rudder inflow velocity, V_R, can be expressed as:

$$V_R = (u_R^2 + v_R^2)^{1/2}$$
$$u_R = u(1-w_r)[1.0 + c_2 g(s)]^{1/2}$$
$$v_R = u_R \gamma \beta_R$$

Equation C.8

where γ is flow straightening coefficient due to hull and propeller, β_R is the equivalent drift angle at the rudder position. According to Japanese MMG model, [113], [114] this expression derive from an estimation of the axial momentum generated from the propeller assumed as an actuator disc, supplemented with a number of empirical corrections such as regarding the finite rudder-propeller distance or the wake variation. The term $c_2 g(s)$ represents the effect of propeller slipstream on V_R and it is therefore expressed as function of the propeller slip ratio defined as:

$$s = 1 - u(1-w_p)/(n_i P)$$
then
$$g(s) = n_i k[2-(2-k)s]s/(1-s)^2$$

Equation C.9

where s is the propeller slip ratio, n_i represents the ratio of propeller diameter D to the rudder height H_R and k denotes intensity of the speed increase of the propeller stream at the position of the rudder:

$$k = 0.6(1-w_p)/(1-w_R)$$

Equation C.10

From Spyrou [109] and Inoue et al. [114] the constant c_2 the value of 1.065 for port (positive rotation direction) and 0.935 for starboard (negative rotation direction) have been suggested.

The effective rudder inflow angle, a_R, can be written as:

$$a_R = \delta + \delta_0 - \beta_R$$

Equation C.11

where δ is the actual rudder angle, δ_0 is the rudder inflow angle at straight ahead motion, which depends mainly on the advance ratio of the ship. Geometrical relationship between propeller and rudder is illustrated in Figure C.1 from [135].

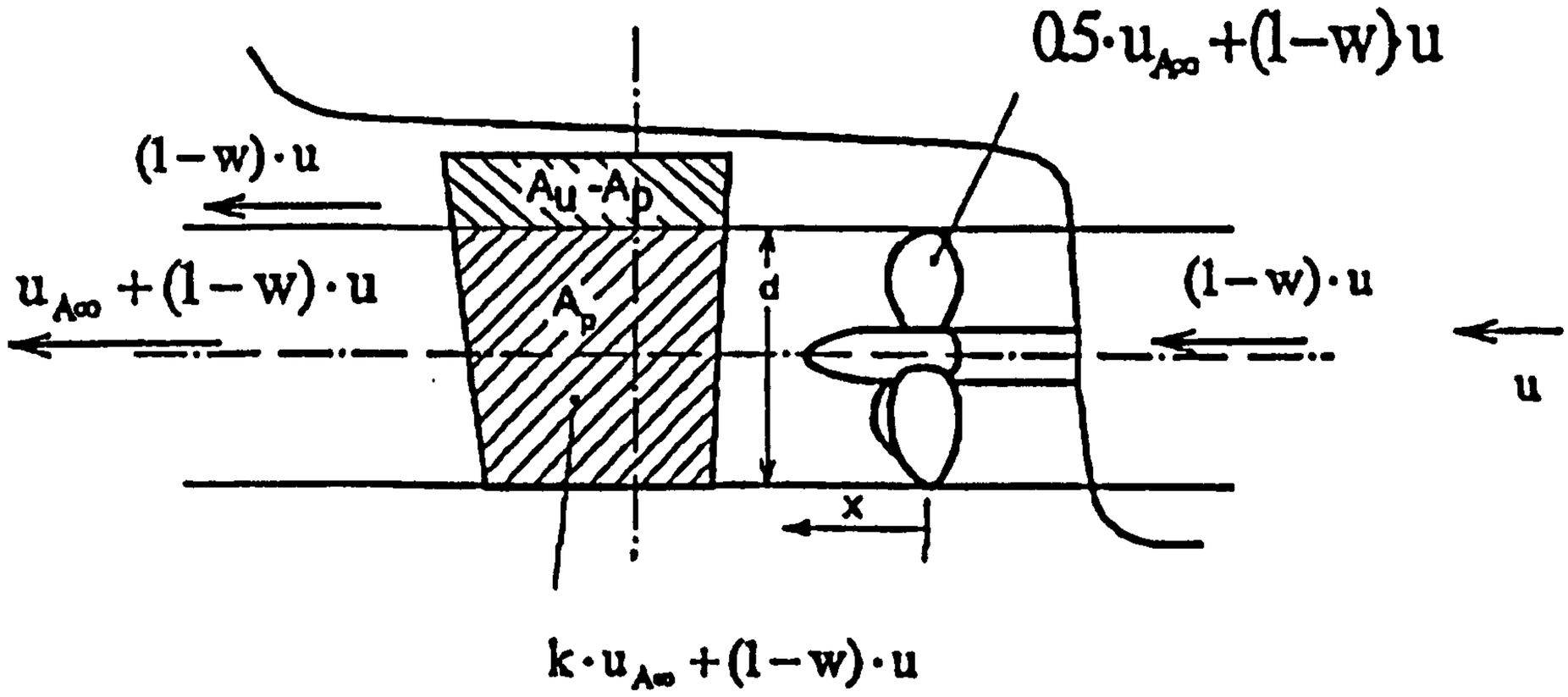

Figure C.1 Geometrical relationship between propeller and rudder. Propeller race according to momentum theory ([135])

Rudder to hull interaction coefficient: Finally, as the rudder to hull interaction concerns, a_H was adopted to represent it. It has been expressed by Japanese Manocuvring group as a function of ship fullness. It has also been related to the distance between the rudder and hull.

Further details of the above equations and useful discussion on the matter arise regarding rudder and rudder forces can be found in Spyrou [109], Inoue et al.[114] and Ankudinov et al. [134]

c. Propulsive Forces

Propeller net thrust force and torque can be represented as follows;

$$X_p = (1-t_p)\rho n^2 D_p{}^4 K_T(J_p)$$
$$K_p = \rho n^2 D_p{}^5 K_Q(J_p)$$

Equation C.12

where t_p is the thrust deduction fraction, n is the propeller rotational rate, D is the propeller diameter, J_p is the advance coefficient and K_T is the thrust coefficient. The thrust and torque coefficients K_T and KQ, as it can bee seen from Equation C.12, are expressed as functions of the advance coefficient as follows;

$$K_T = c_0 + c_1 J_p + c_1 J_p{}^2$$

Equation C.13

where coefficients c_i, i=0,2 can be obtained from propeller tests or propeller series information. The propeller force in sway direction and moment in yaw, can be written as:

$$Y_p = \rho n^2 D^4 Y_{p^*}$$
$$N_p = \rho n^2 D^5 N_{p^*}$$

Equation C.14

where coefficients Y_{p^*} and N_{p^*} are generally dependent upon u/(nP) and being zero at first quadrant (u>0,n>0).

Propeller inflow angle, β_p: The effective propeller wake fraction depends significantly on the vessel's lateral motion while it is less sensitive to propeller loading. The opposite is seen for the thrust deduction. From Japanese MMG model [114] and Spyrou [109]:

$$w_p = w_{p0} e^{-4.0}$$

Equation C.15

It has been assumed for simplicity that t_p is invariant to the operating conditions. Both quantities w_{p0} and t_{p0} are calculated according Holtrop and Mennen method [128]. The inflow velocity at the propeller position, x_p, is:

$$v_p = v - x_p r$$

Equation C.16

It could be written with effect of roll included as follows;

$$v_p = v - x_p r - z_p p$$

Equation C.17

This is leading to the approximate geometrical inflow angle expression:

$$\beta_P = \beta - (x_P/L)(rL/U) = \beta - x_{p'} r'$$

Equation C.18

As it is stated in above section, further details of the above equations and useful discussion on the propeller forces can be found in Spyrou [109].

D. EFFECT OF AUTOPILOT

During numerical testing and validation studies, it was observed that effect of the autopilot should be seriously considered and the choice of autopilot systems or the parameters employed could have significant effect of the motions of the vessel, as it is emphasized in Section 5.4. Therefore, it is appropriate to exploit the autopilot systems. A large number of references exist in the literature on control engineering with links to aerospace, marine, electronic etc.... For instance, Fossen [117] provided a highly comprehensive account of autopilot systems in use for all type of vessels. Here, a discussion will be stimulated on the effect of the autopilot systems.

Automatic control systems design involves the design of systems for forward speed control, motion (vibration) damping, steering, tracking and positioning. The development of modern control theory with faster digital computer systems allows more sophisticated control systems to be designed. The most important features of modern ship control systems are improved performance, robustness and the fuel saving potential. In the last two decades fuel saving autopilots have been designed by applying optimal control theory.

Autopilots for course-keeping are normally based on feedback from a gyrocompass measuring the heading. Heading rate measurements can be obtained by a rate sensor, gyro and numerical differentiation of the heading measurement or a state estimator. This is common practice in most control laws utilizing proportional, derivative and integral action. The control objective for a course-keeping autopilot can be expressed as:

$$\psi_d = \text{constant}$$

Equation D.1

where ψ_d is the desired heading angle. This is illustrated in below Figure D.1. On the contrary, course-changing manoeuvres suggest that the dynamics of the desired heading should be considered in addition.

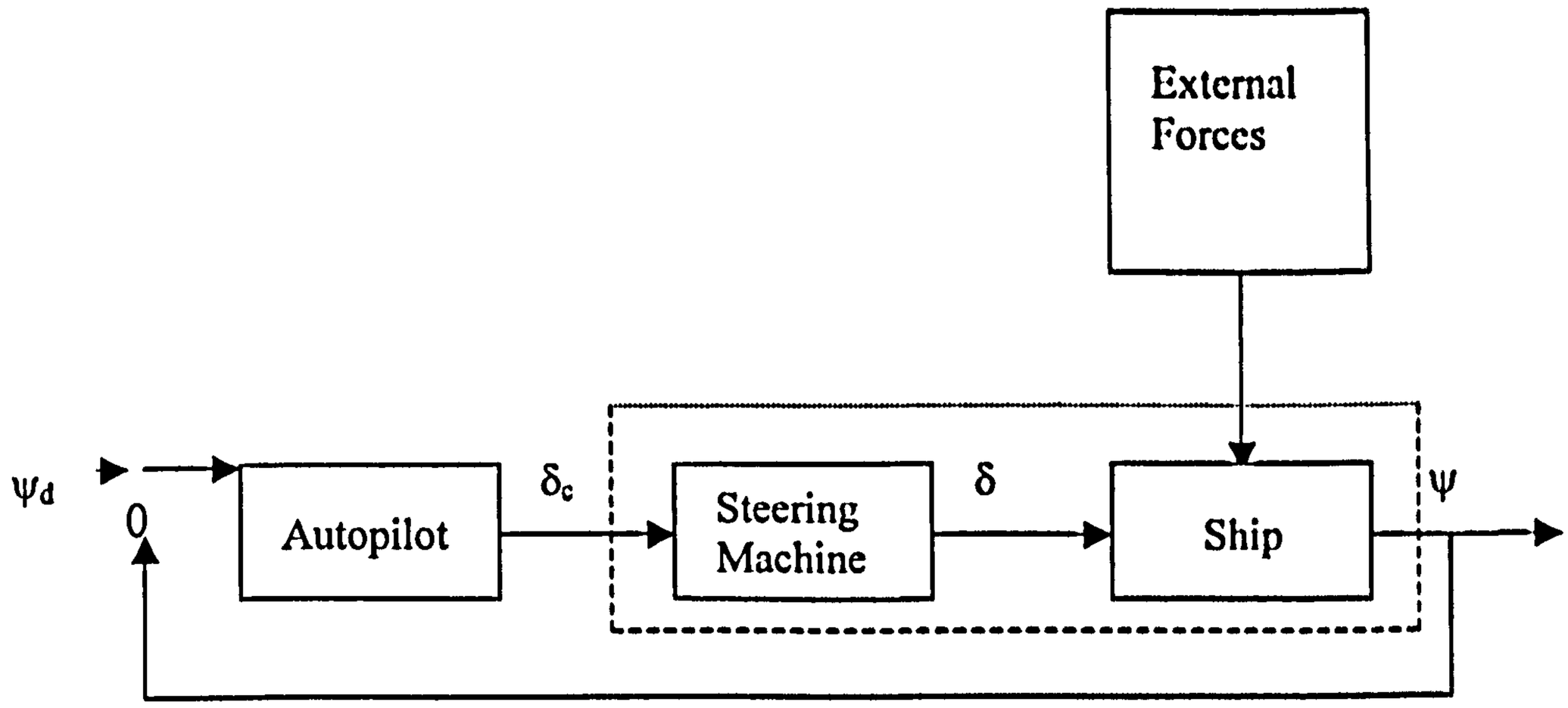

Figure D.1 Course-keeping autopilot feedback system

Most autopilots for ship steering are based on simple PID- control laws with fixed parameters. To prevent that the performance of the autopilot deteriorating in bad weather and when the speed of ship changes, high frequency rudder motions are suppressed by wave filtering, while a gain scheduling technique is applied to remove the influence of the ship speed on the hydrodynamic parameters, as it is described by Fossen [117].

Therefore, current PID control systems laws are utilized with feedback from low frequency state estimates. Since, they have been employed in experiments, in numerical research in this study, we'll discuss the P (Proportional) and PD (Proportional-Differential) control systems.

P- Control: A proportional control law can be written as follows:

$$\delta = K_P(\psi_d - \psi)$$

Equation D.2

where $K_p > 0$ is a regulator design parameter. Typical P-control systems will not stabilize an open-loop unstable ship, for the stable ship the oscillatory motion can be modified adjusting the regulator gain K_p. For instance, K_p for a critically damped system is obtained by choosing;

$$K_p = \frac{1}{4TK}$$

Equation D.3

where K Nomoto gain constant [117] and T is time constant.

PD-Control: Since P-controller restricted to open-loop stable ships with a certain degree of stability, a more sophisticated system should be used for marginally and unstable ship and this is achieved by introducing derivative action in control equation. A proportional and differential control equation can be written as follows;

$$\delta = K_p(\psi_d - \psi) - K_d\dot{\psi}$$

Equation D.4

where $K_p>0$ and $K_d>0$ are the controller design parameters. For a critically damped ship, those parameters are obtained as follows [117]:

$$K_p = \frac{T\omega_n^2}{K} \quad K_d = \frac{2T\zeta T_n - 1}{K}$$

Equation D.5

where ζ is the damping ratio, ω_n is the natural frequency of the closed-loop system.

In an attempt to demonstrate the effect of autopilot system, for a vessel with and without PD autopilot system is shown in Figure D.2. Here, poles of the unstable and the PD controlled vessel are displayed

In the current study, the standard proportional-differential (PD) autopilot is employed, as it is given Equation 5.23, in order to keep the vessel on course. From the above background, the choice of the autopilot system is to provide as robust as possible control with simplicity and this was found in PD type autopilot systems. They are currently the most commonly used type in marine studies for same reason.

In the current model, several no-linearities are included to avoid excessive rudder movement in head seas in which encounter frequency is very high with small yaw that could potentially damage the steering box.

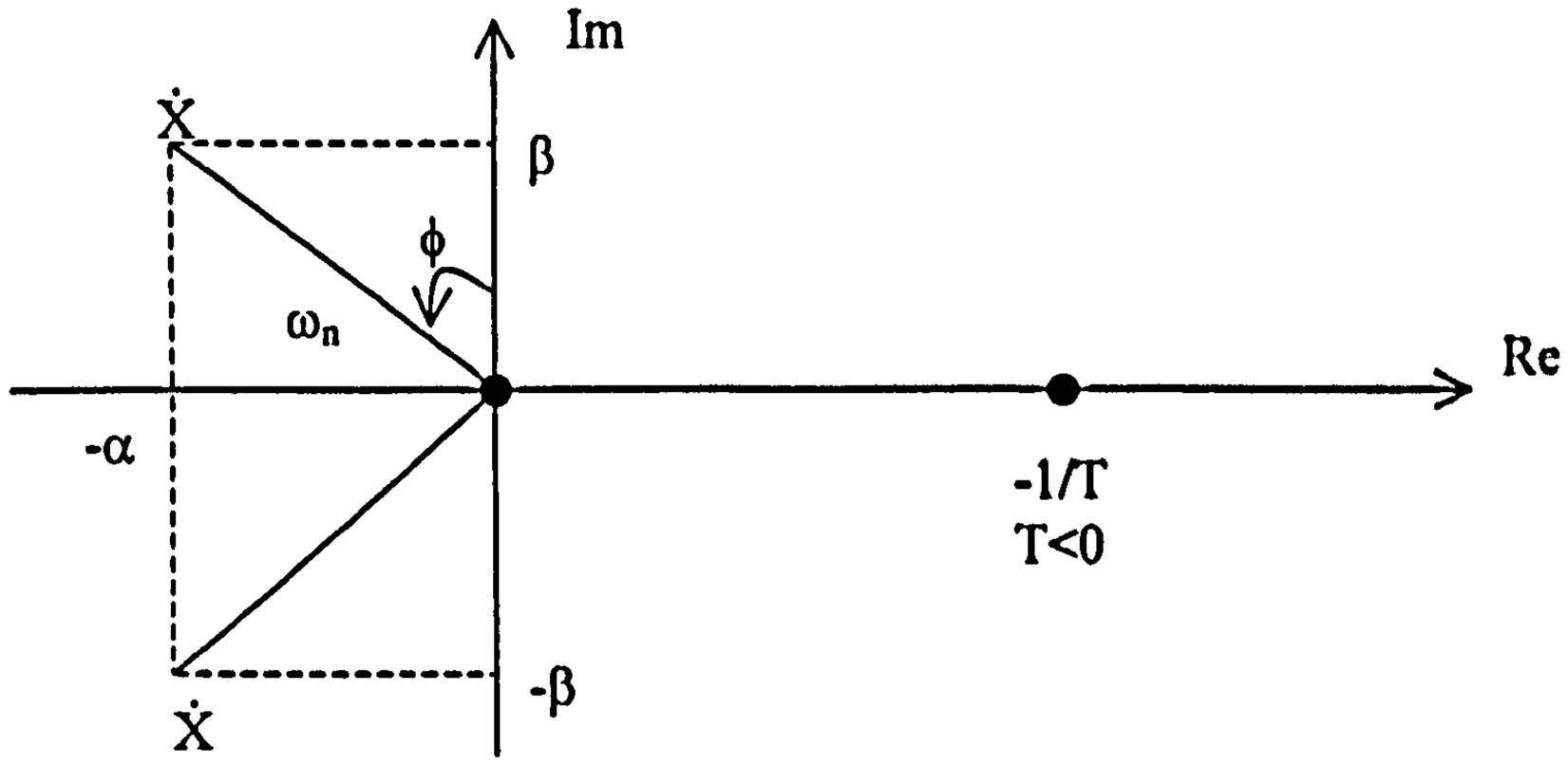

Figure D.2 The poles of the unstable ship (.) and the PD-controlled ship (X). The relative damping ratio and natural frequency of the closed-loop system is $\zeta = \sin\phi$ and $\omega_n = \sqrt{\alpha^2 + \beta^2}$, respectively. (From Fossen [117])

However, this non-linearity seems to be not important in following and quartering seas. It was also concluded in ITTC tests that yaw-rate gain seems to be inappropriate. This could be regarded as another important indicator of the selection of accurate parameters of the control system for the motion of ships in following and quartering seas.

E. BENCHMARK TESTS AND SHIP PARTICULARS

E.1 Benchmark Testing Vessels

As discussed in Chapter 7, in order to validate the mathematical model and to carry out parametric study for motions of ships in extreme astern seas environment, a 23,720 tonnes displacement containership, investigated using systematic model experiments at Osaka University in Japan and a 712 tonnes displacement fishing vessel, investigated using systematic model experiments at National Institute of Fisheries Engineering in Japan, were used. These vessels were chosen by ITTC Specialist Committee on Stability to carry out numerical benchmark testing. Here, the details of ships and the experimental details are given in below figures.

Ship A-1 (Containership)

The GM parameter of ship is just on the limit of compliance with IMO intact stability code. The model is fitted with forecastle, poop and bilge keels. Deckhouses were not included because stability criteria ignore them as non-watertight structures. In order to store experimental equipment, additional watertight hatches and their coamings were fitted on the upper deck. Lines of the vessel and the details of the layout of upper deck are given in Figure E.1 and E.2.

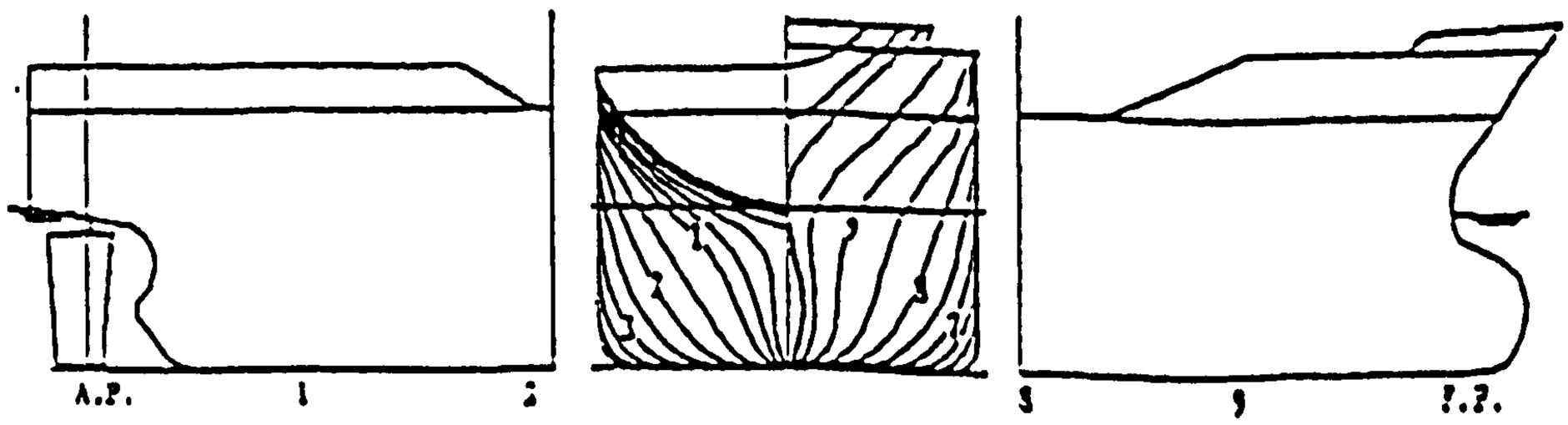

Figure E.1 Lines of Ship A-1

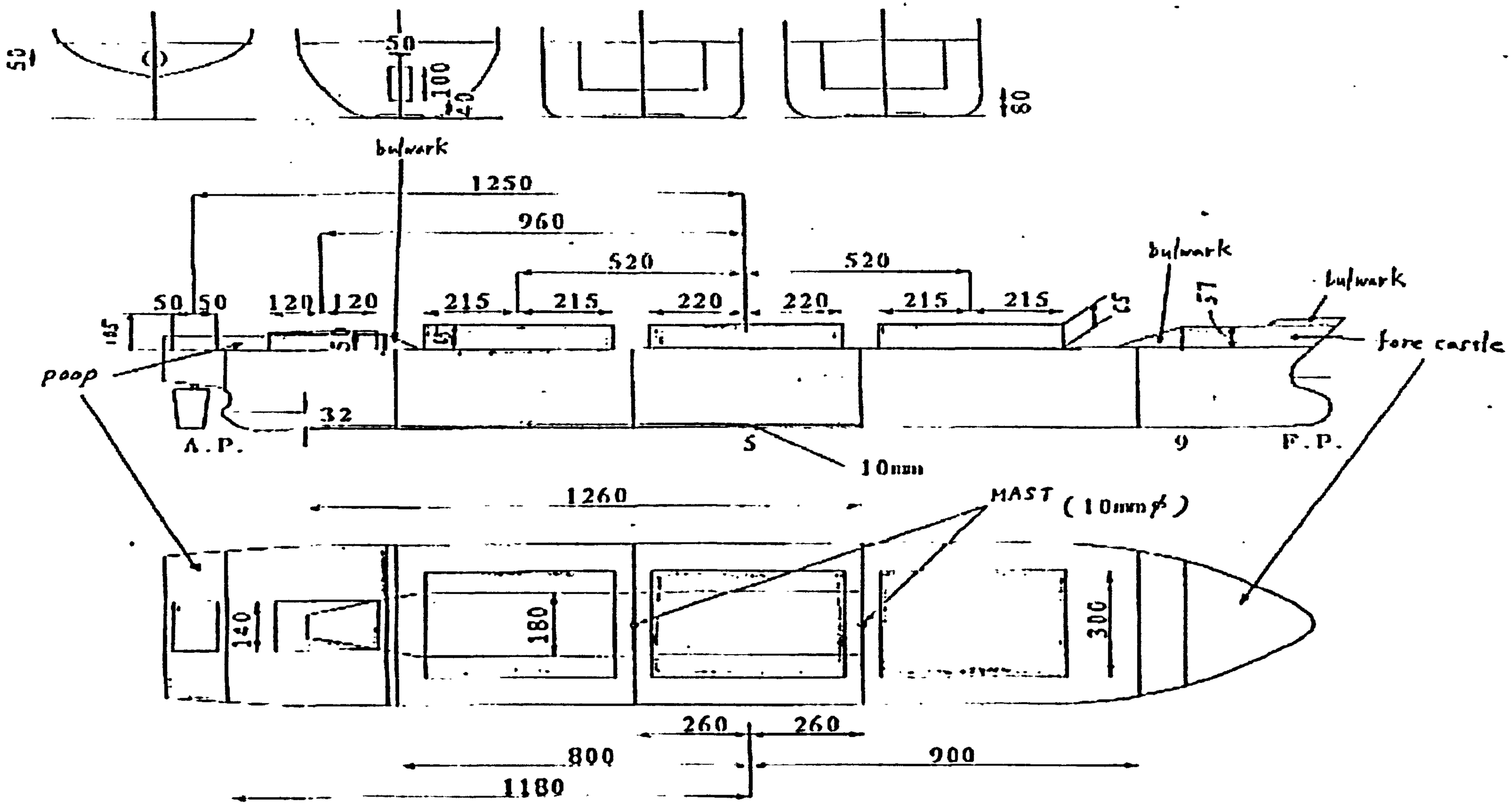

FigureE.2 Layout of the superstructure of the model of ship A-1 in model scale

Data of captive model tests: For estimating hydrodynamic coefficients, several captive model tests were carried out. The results of the resistance test and the rudder tests in model scale at the towing tank of Osaka University are shown Figure E.3 and E.4.

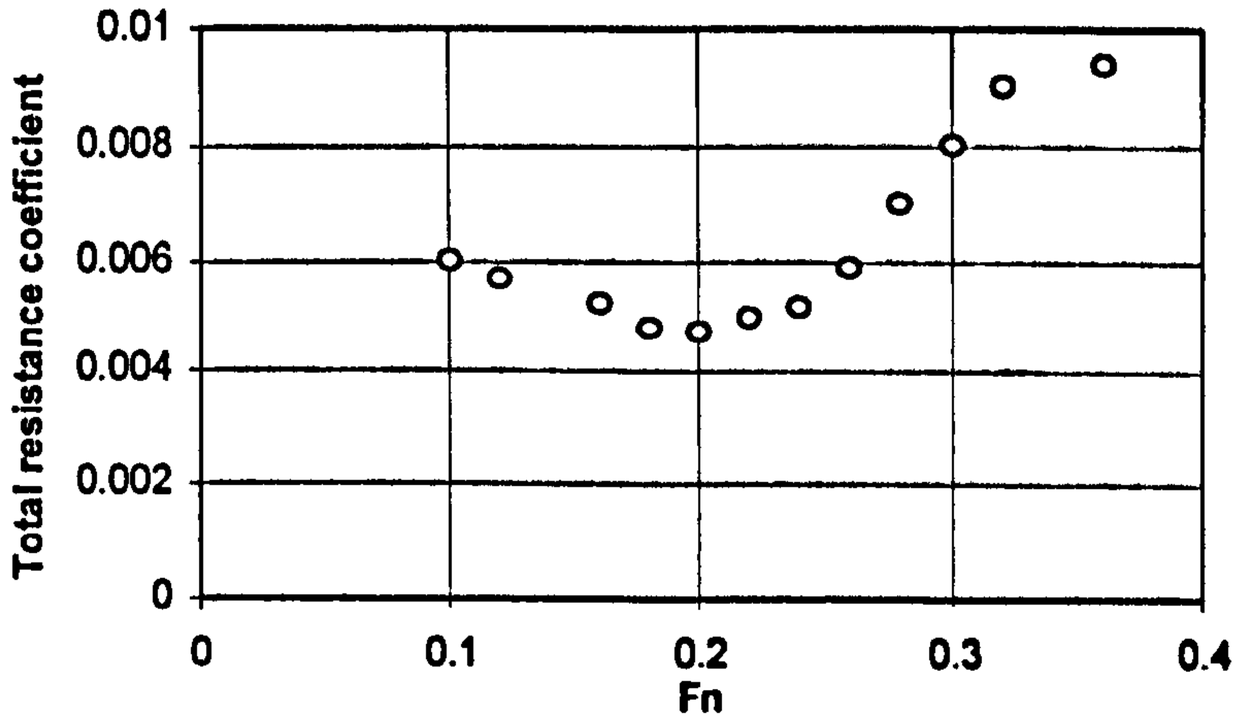

Figure E.3 Measured total resistance coefficient, C_T, as the function of the Froude number, Fn, obtained from the resistance test of the Ship A-1.

The results of the circular motion tests (CMT) at the seakeeping and manoeuvring basin of the National Research Institute of Fisheries Engineering are shown in Figure E.5. In the Figure E.4 and E.5, sway force, Y, the yaw moment, N, the roll moment, K, and the rudder normal force, F_N, are plotted as functions of rudder angle,δ, the drift angle,β, and the non-dimensional yaw rate, r'.

Damping force was obtained using the data from roll decay tests without forward speed (Figure E.5). The forward speed effect is included using Takahashi's empirical formula.

$$\varepsilon^* n = \varepsilon^{(0)} n[1.0 + 0.8[1.0 - e^{(-10Fn)} / \omega_e{}^2] \; n = 0,1...$$

Equation E.1

where ε* is roll damping ratio.

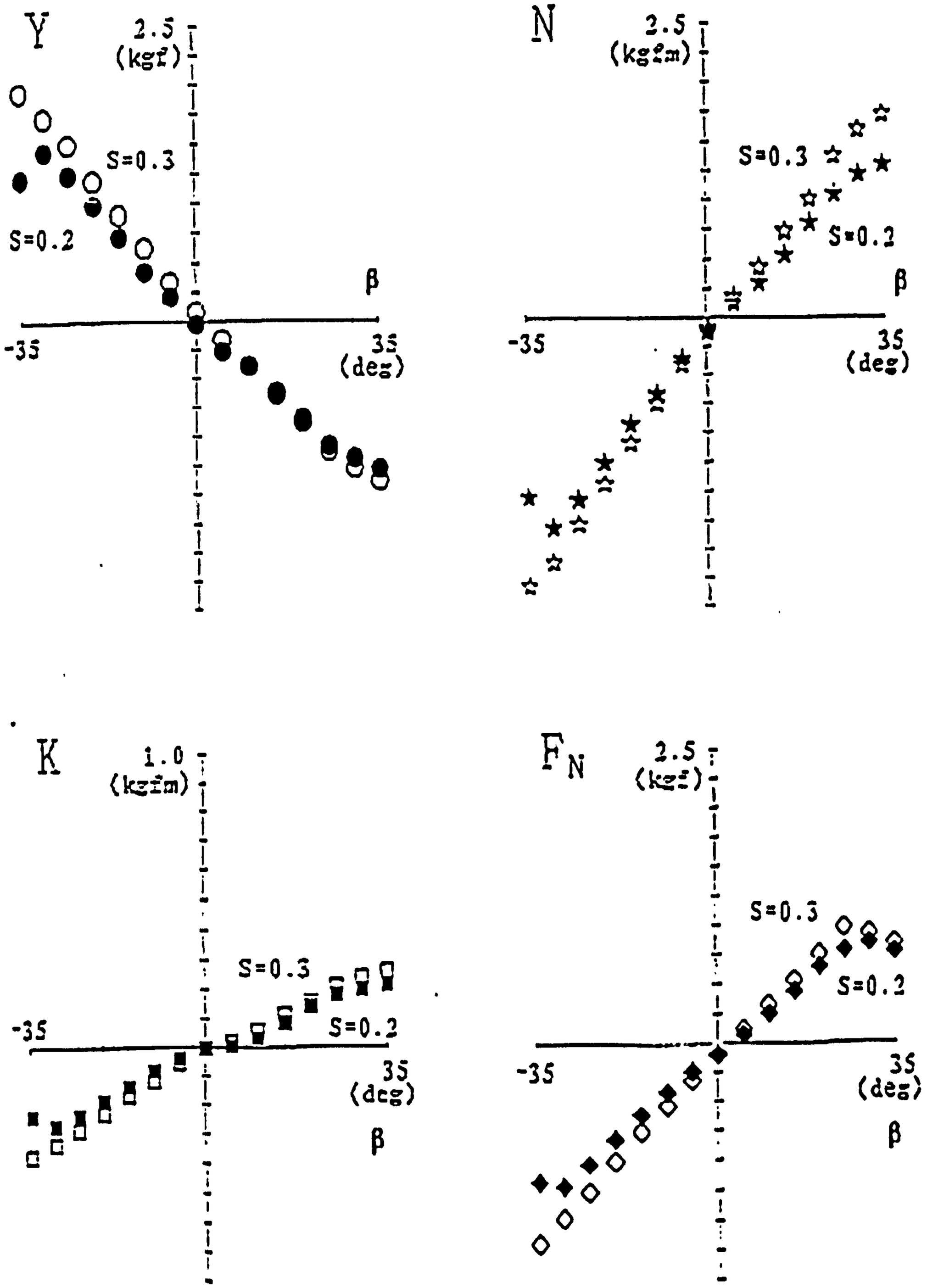

Figure E.4 Results of the rudder angle tests of the ship A-1 at Fn=0.242 in model scale where s is the propeller slip ratio

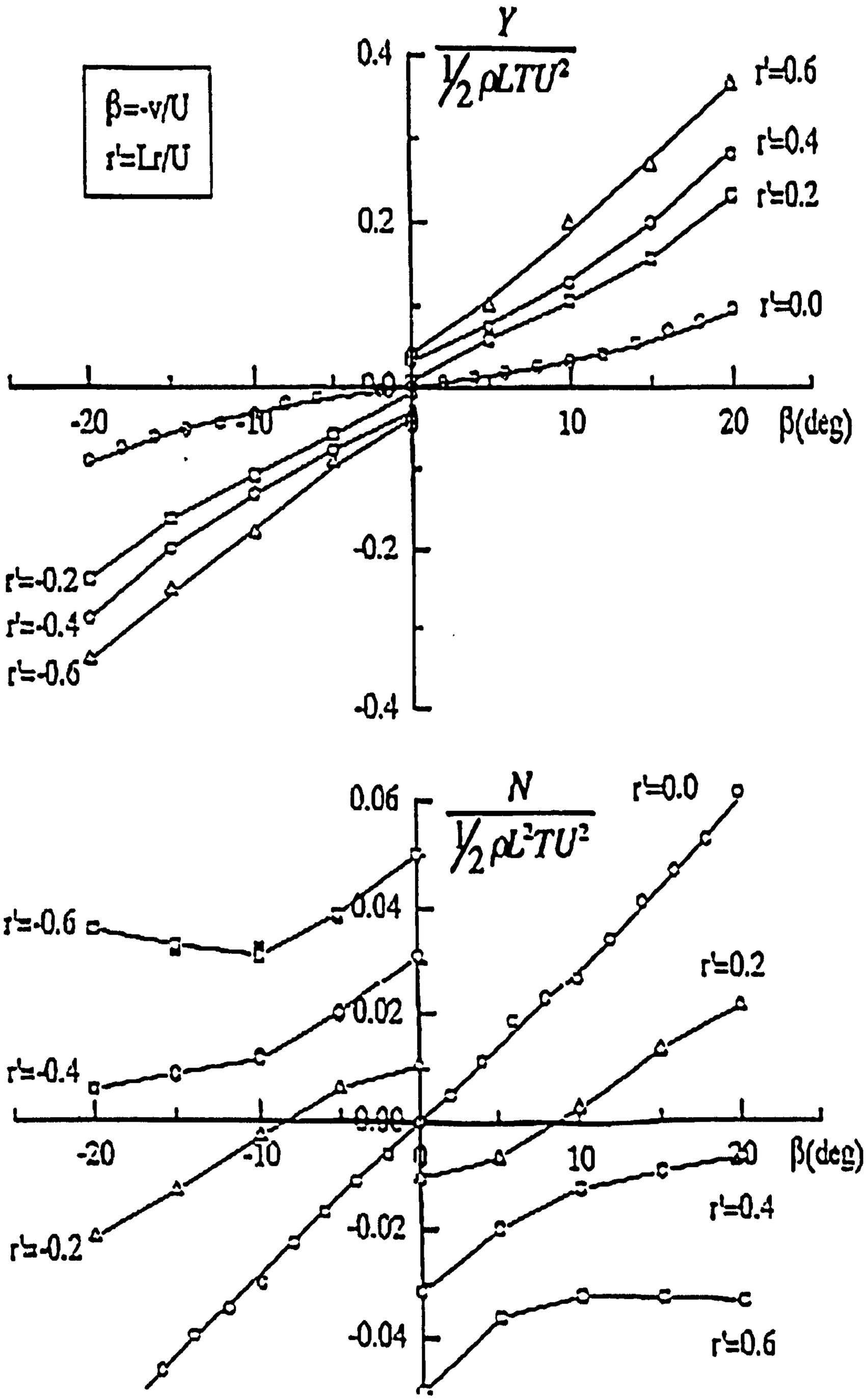

Figure E.5 Results of the circular motion tests of ship A-1 at Fn=0.242 where L is ship length between perpendiculars and v is ship lateral velocity.

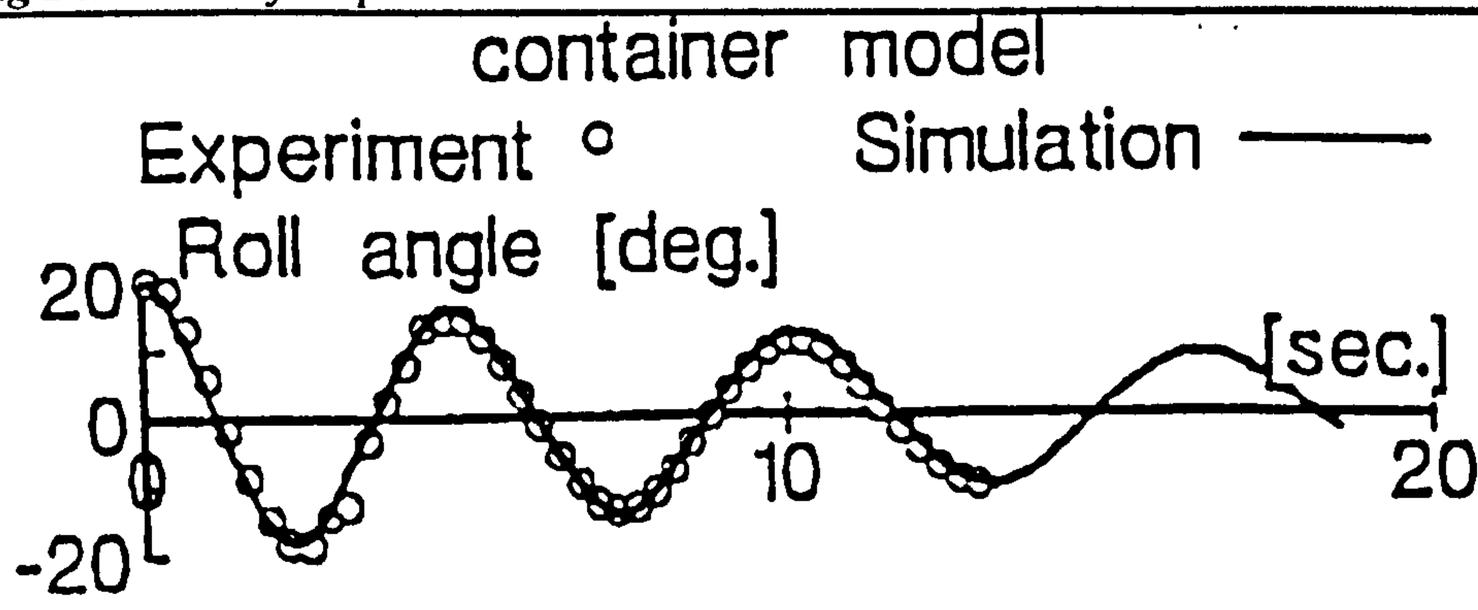

Figure E.6 Roll decay test of the ship A-1 in model scale without forward velocity.

Ship A-2 (Purse Seiner)

The GM parameter of ship is just on the limit of compliance with IMO intact stability code. The model is fitted with forecastle and bilge keels. Deckhouses were not modelled because stability criteria ignore them as non-watertight structures. In order to store experimental equipment, additional watertight hatches and their coamings were fitted on the upper deck. Body plan of the vessel and the details of the layout of upper deck are given in Figure E.7 and E.8.

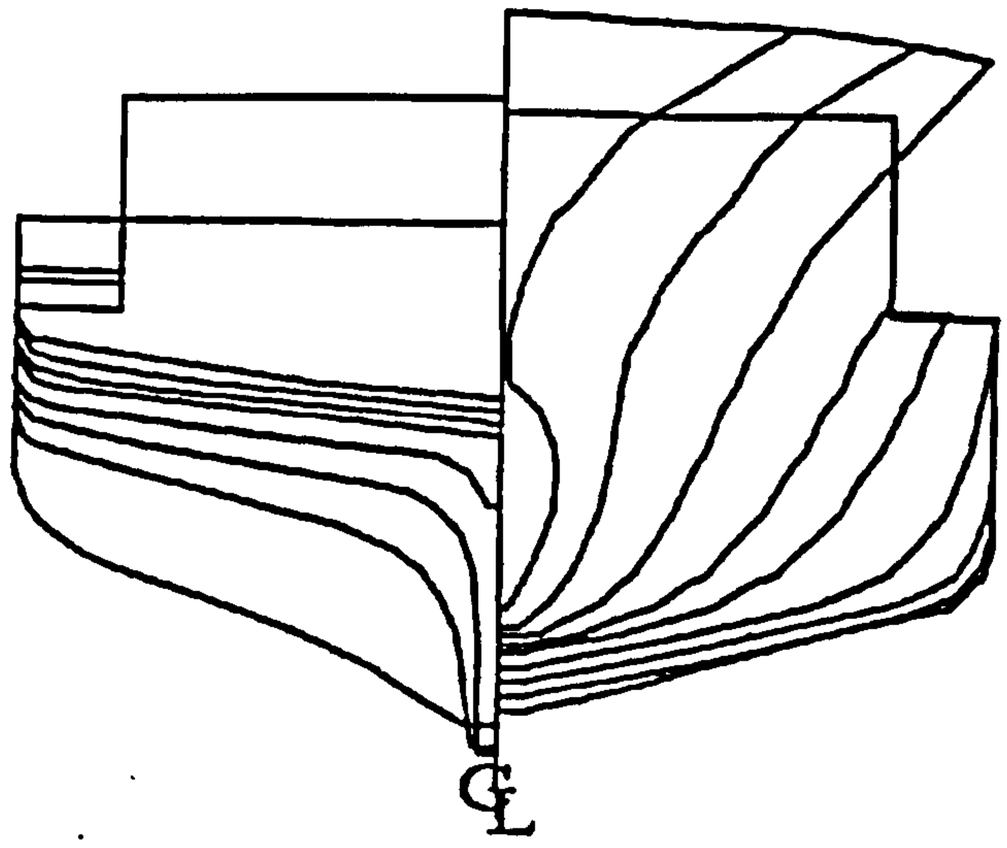

Figure E.7 Body plan of Ship A-2

Data of captive model tests: For estimating hydrodynamic coefficients, several captive model tests were carried out at the seakeeping and manoeuvring basin of National Research Institute of Fisheries Engineering (NRIFE). The results of the resistance tests and the heel angle tests are shown with several identified coefficients in Figures E.9 and E.10.

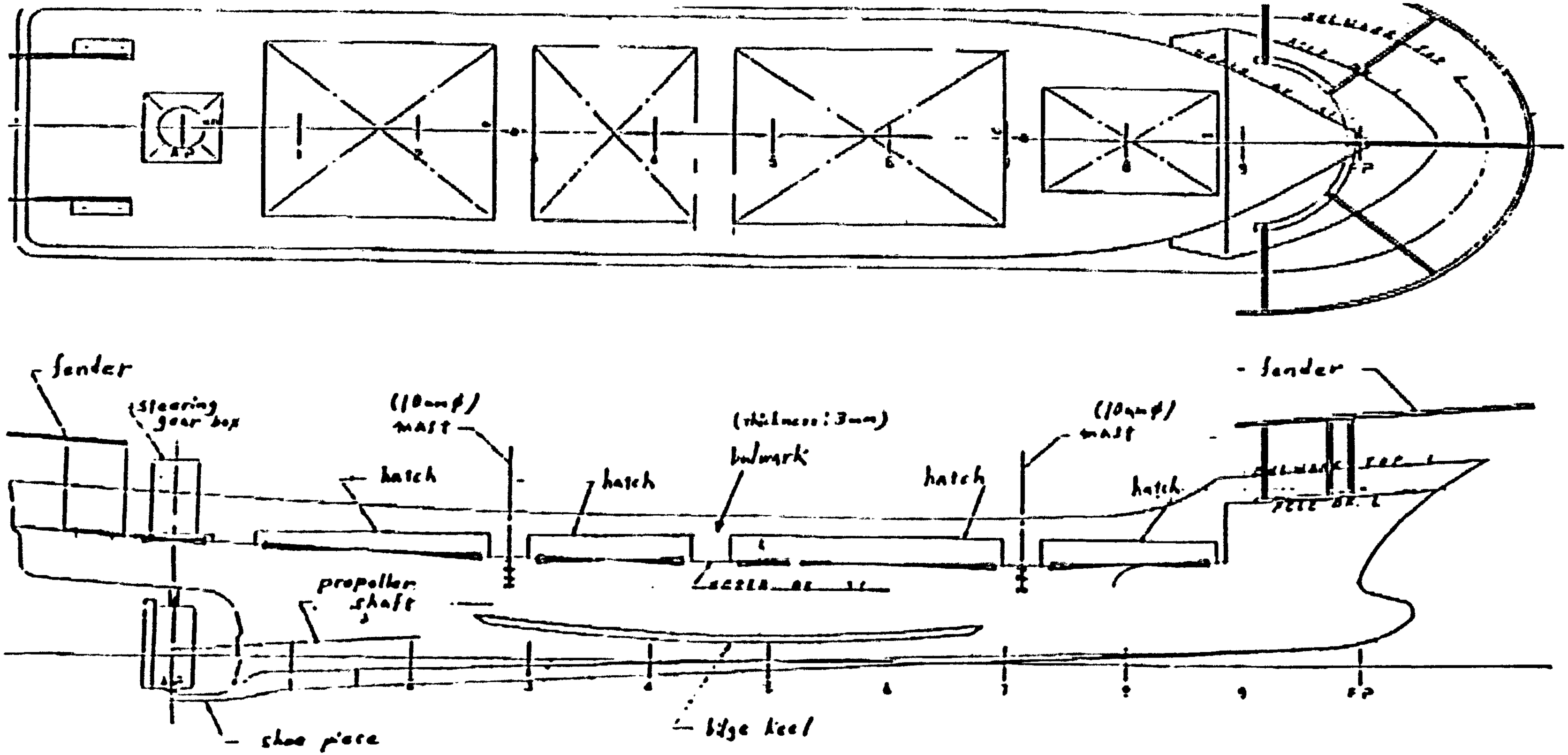

Figure E.8 Layout of the superstructure of the model of ship A-2 in model scale

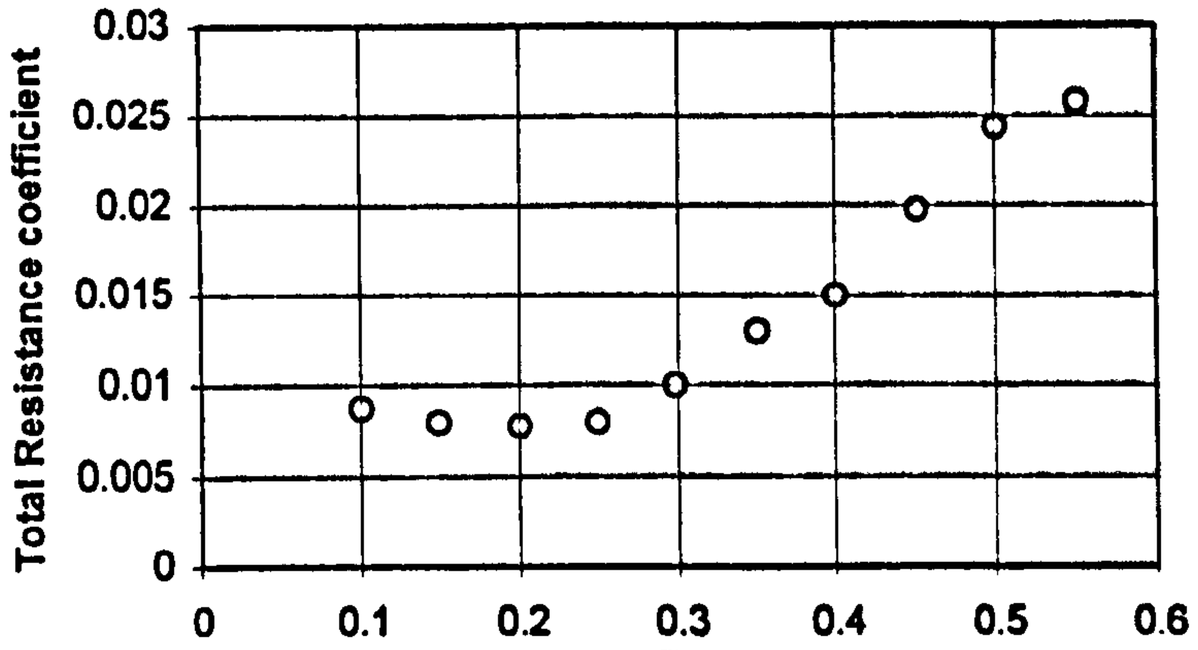

Figure E.9 Measured total resistance coefficient, C_T, as the function of the Froude number, Fn, obtained from the resistance test of the Ship A-2.

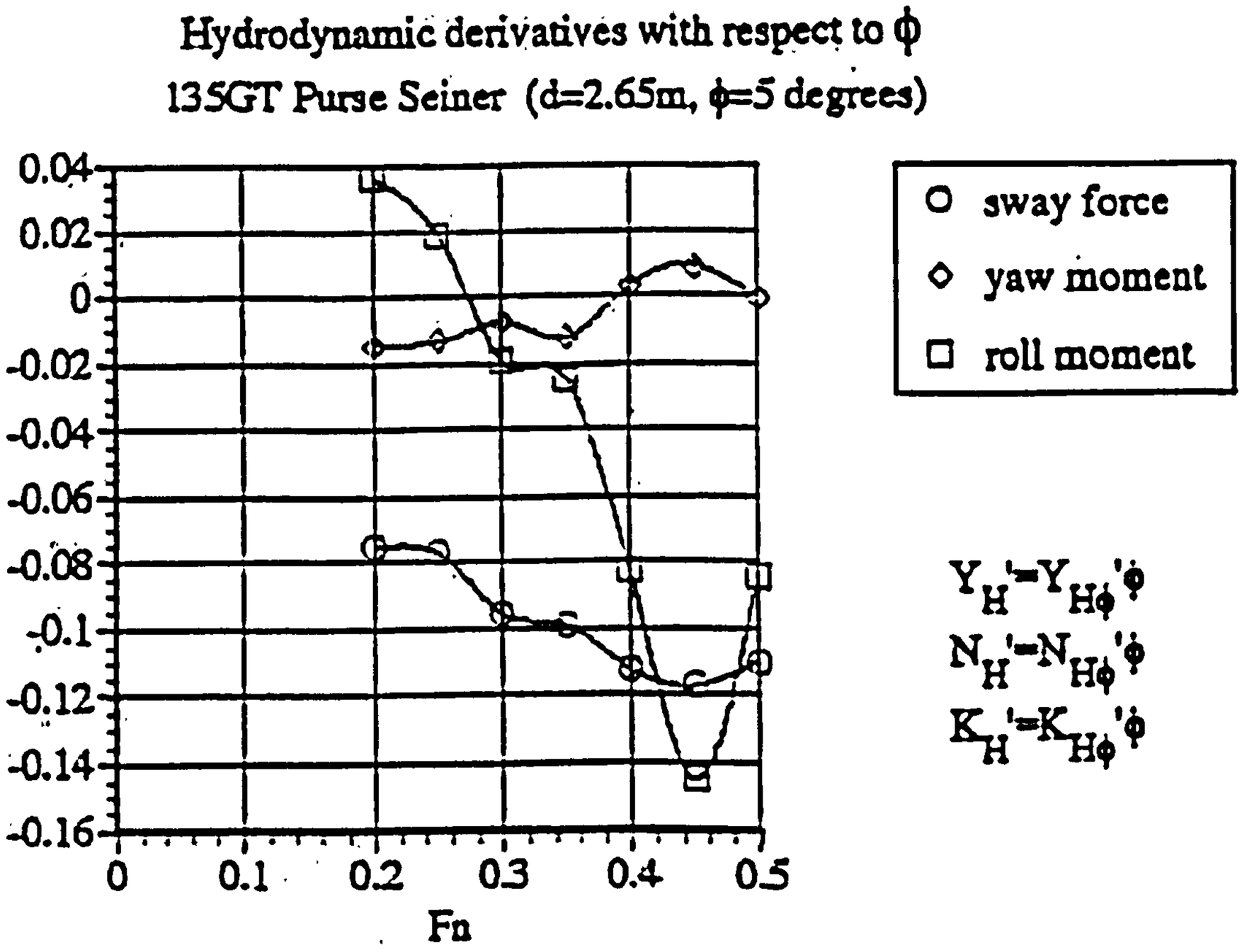

Figure E.10 Non-dimensional derivatives of hydrodynamic forces with respect of heel obtained from the heel angle tests for Ship A-2.

During the experiments, the ship model is self-propelled and is completely free. The propeller thrust coefficient, obtained from a propeller open water test, is given by Figure E.11. Damping force was obtained using the data from roll decay tests without forward speed (Figure E.12-13). The forward speed effect is included using Takahashi's empirical formula (Equation E.1).

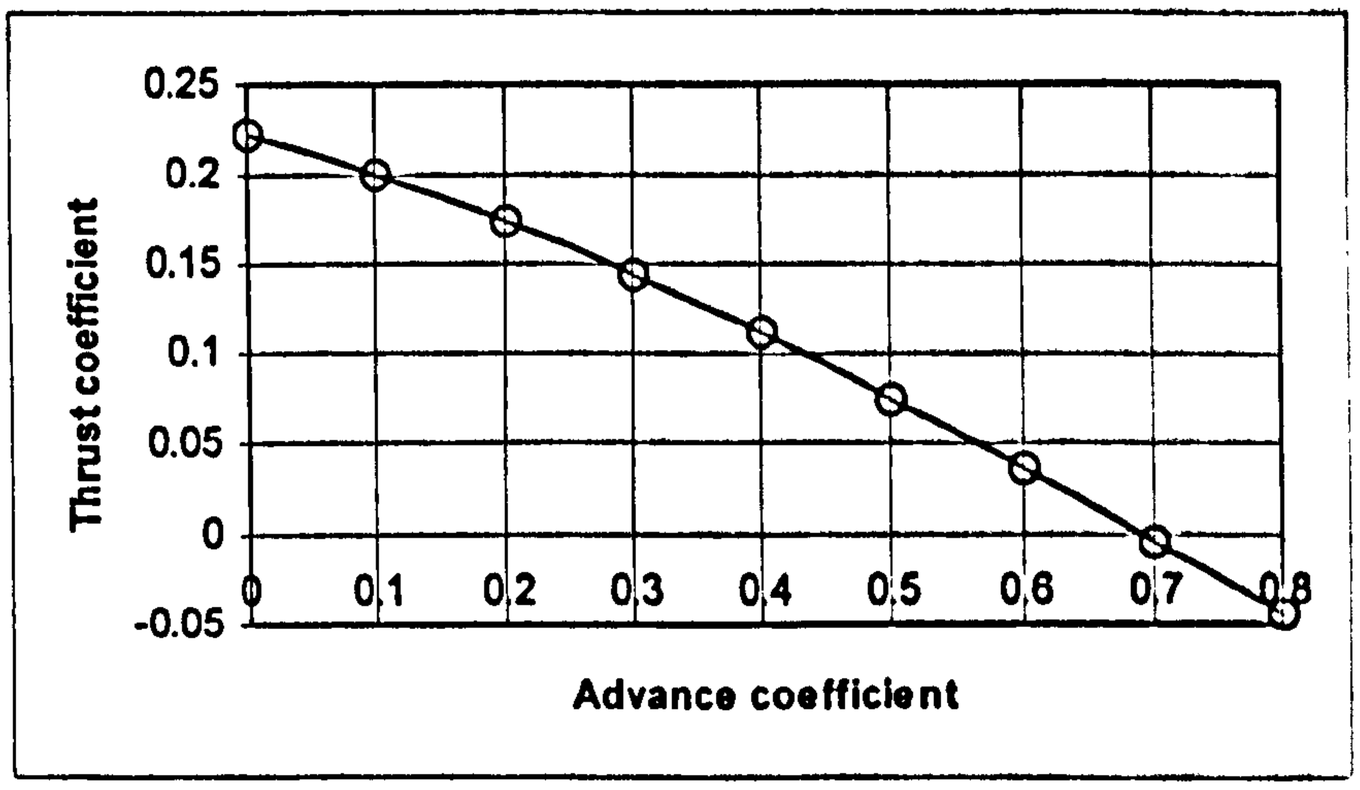

Figure E.11 Propeller thrust coefficient obtained from the propeller open test

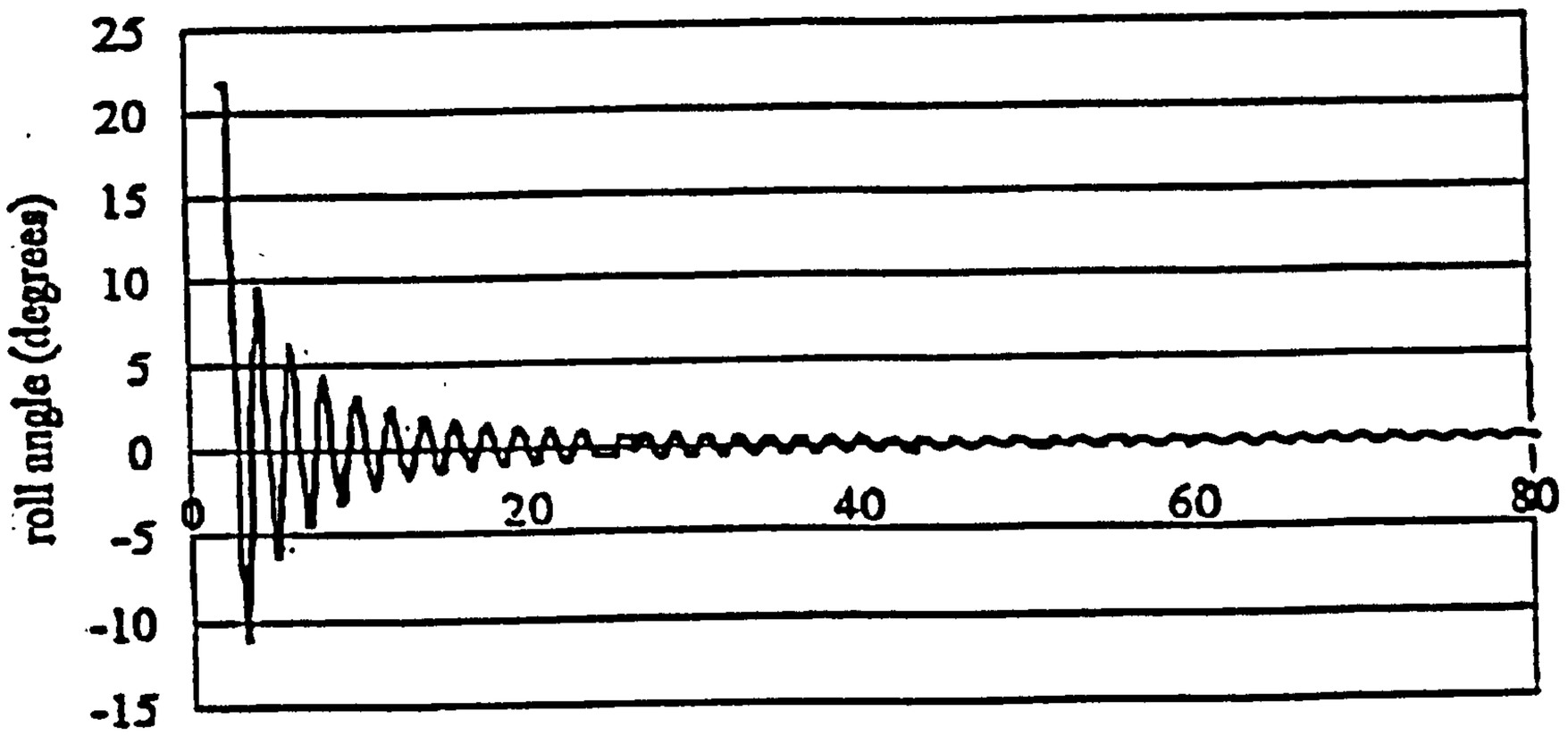

Figure E.12 Measured time history of the roll decay test of the ship A-2 without forward velocity in model scale

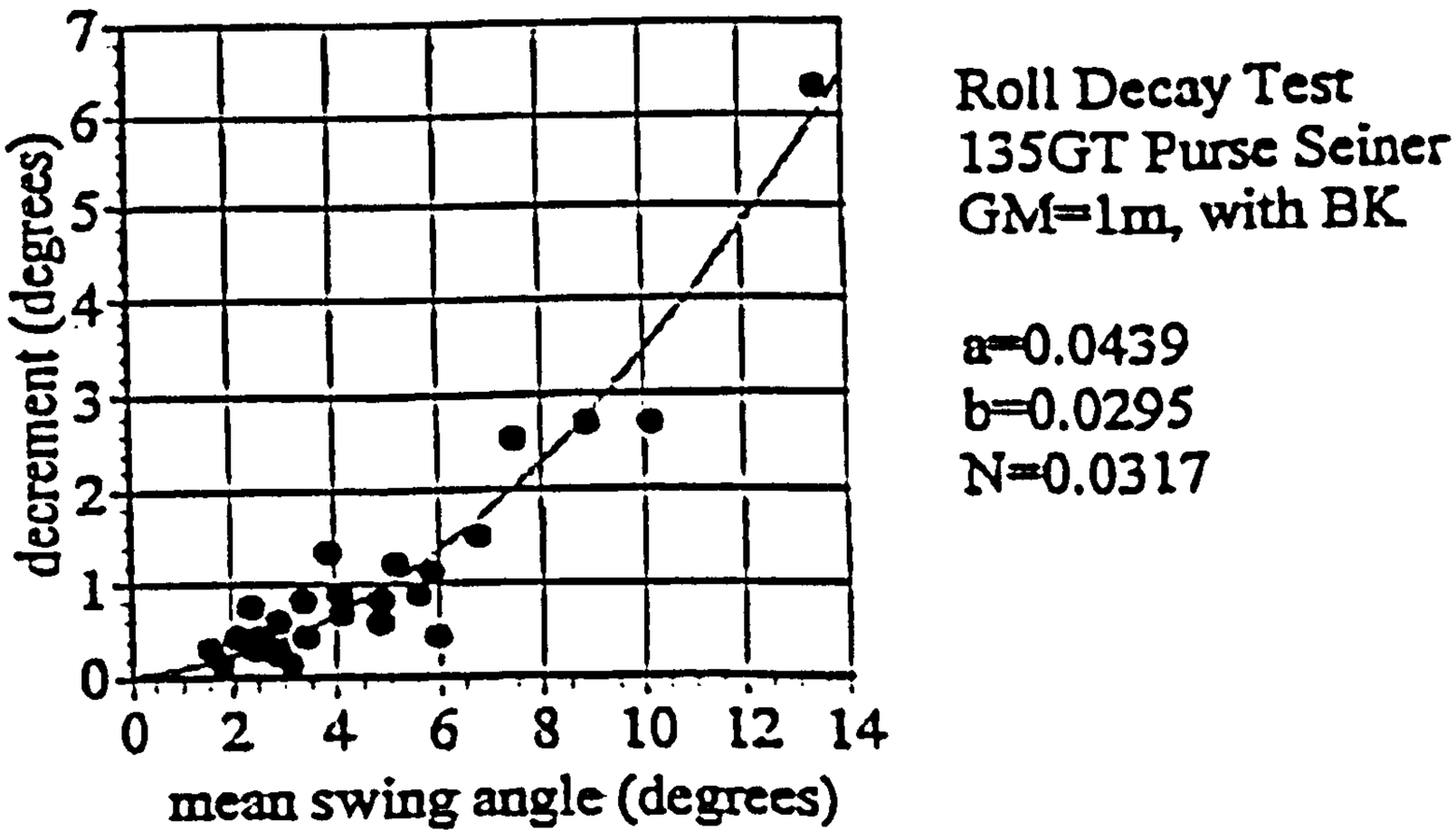

Figure E.13 Extinction curve from the roll decay test of Fig.E.12

The rudder angle test results are displayed with several identified coefficients in Figs. E.14-16.

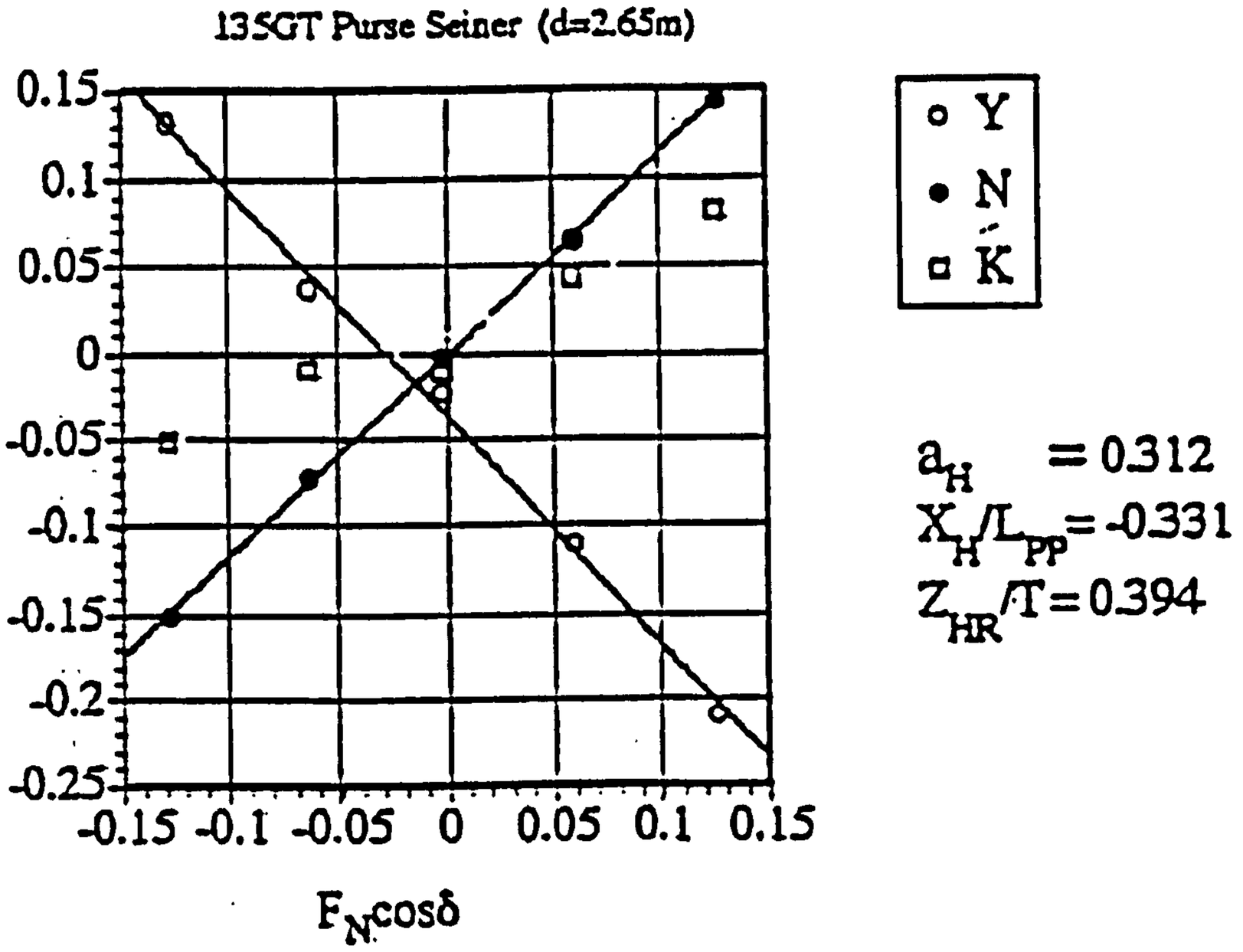

Figure E.14 Interaction between hull and rudder obtained from the rudder angle test results of Ship A-2 at Fn=0.2

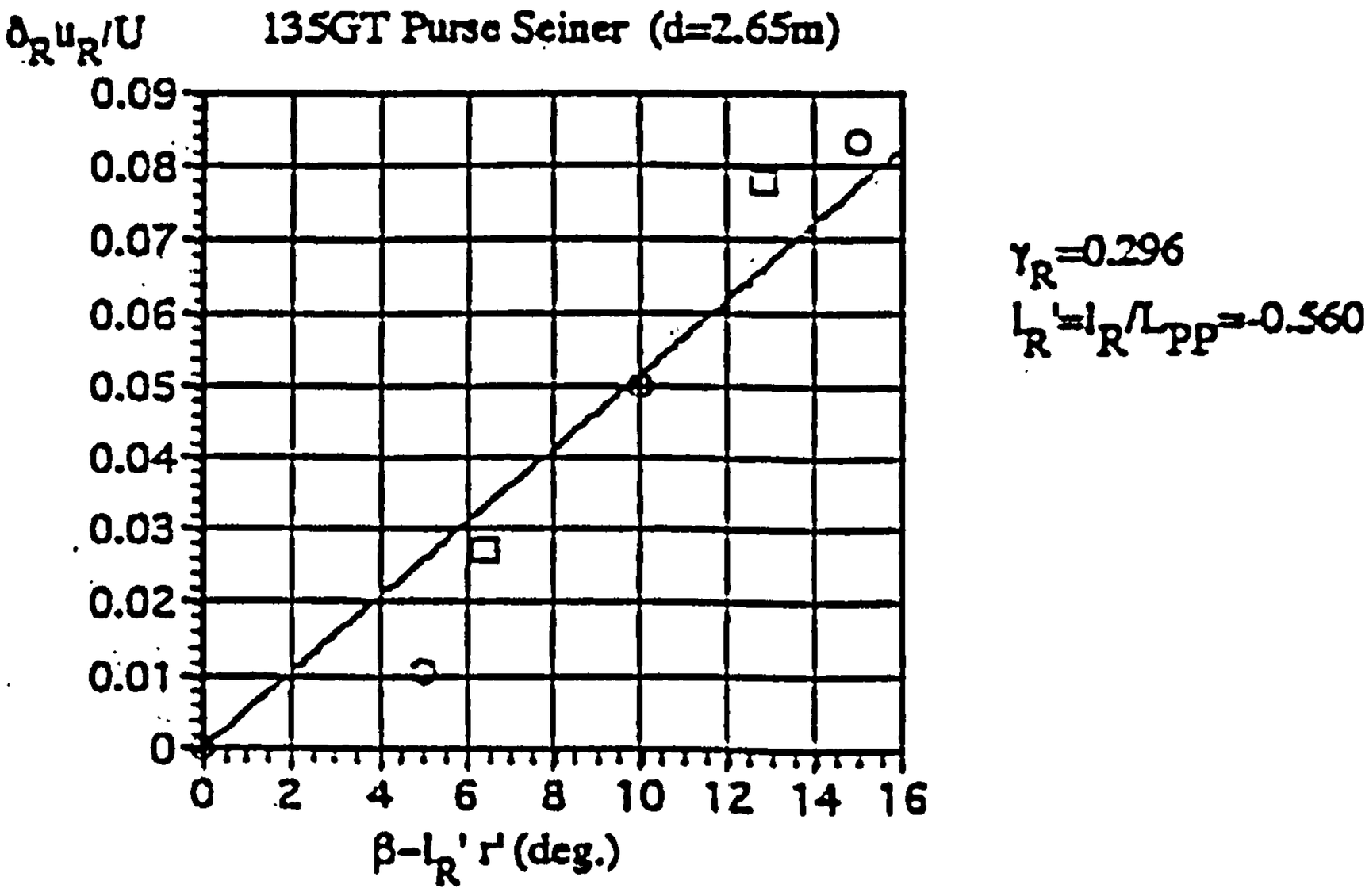

Figure E.15 Flow straightening effect obtained by the circular motion test with rudder angle for Ship A-2 at Fn=0.2

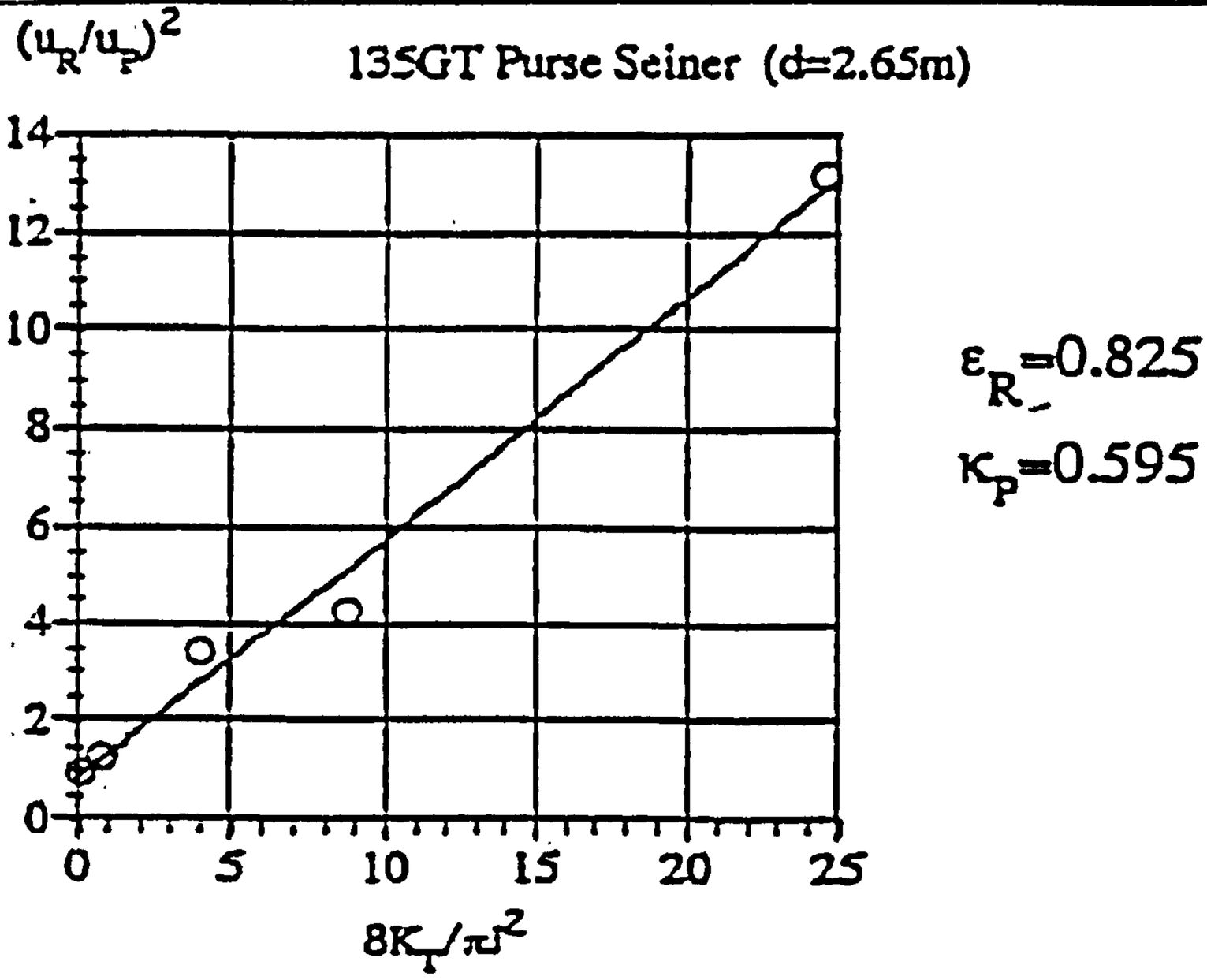

Figure E.16 Interaction between propeller and rudder obtained by the rudder angle tests for Ship A-2 at Fn=0.2

The results of circular motion tests (CMT) are shown in Figs E.17 and E.18. In the Figures E.17 and E.18, surge force X, sway force, Y and the yaw moment, N are plotted as functions the drift angle,β, and the non-dimensional yaw rate, r'.

Data of manoeuvring model test: The free running model test was also carried out at the seakeeping and manoeuvring basin of NRIFE. The control and measuring system is as same as that used for the capsizing model experiments but with different algorithm for manoeuvring tests. Fig. E.19 shows the time history of –35 degrees turning manoeuvre at the Froude number of 0.3. Those consist of the rudder, roll and yaw angles.

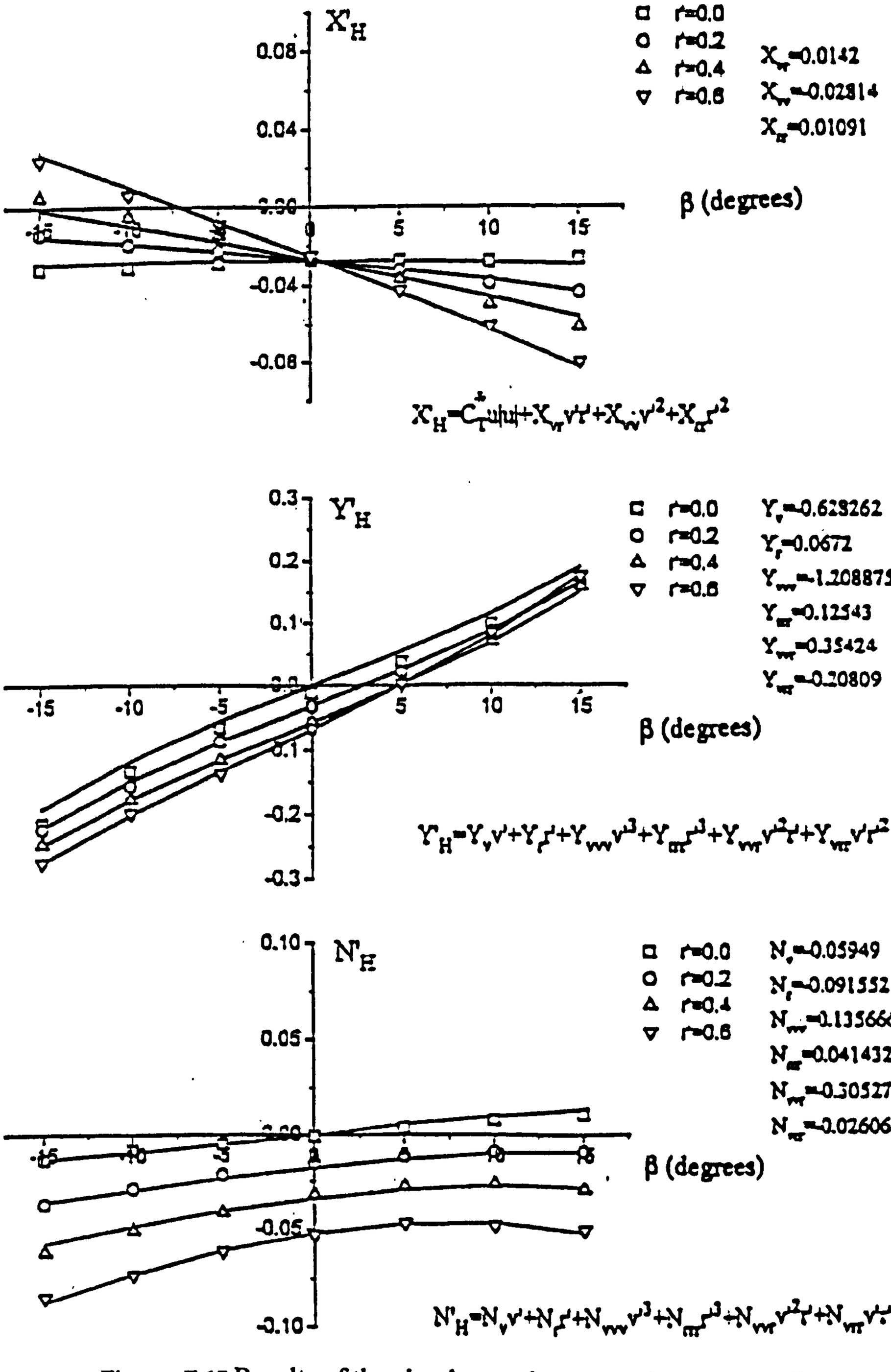

Figure E.17 Results of the circular motion tests of ship A-2 at Fn=0.2

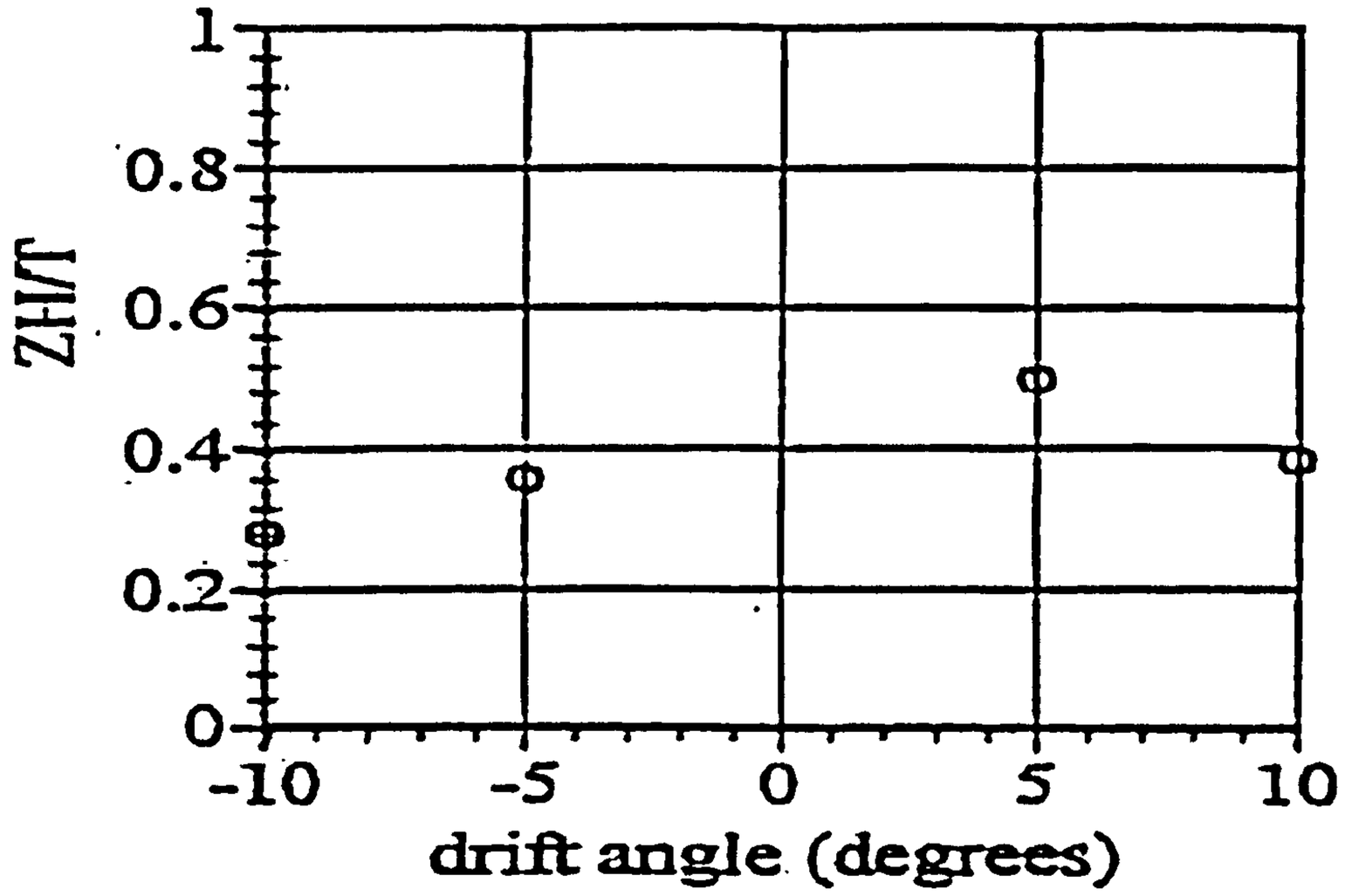

Figure E.18 Vertical distance of the centre of lateral force from the water surface obtained from the oblique towing tests for the ship A-2 at Fn=0.2.

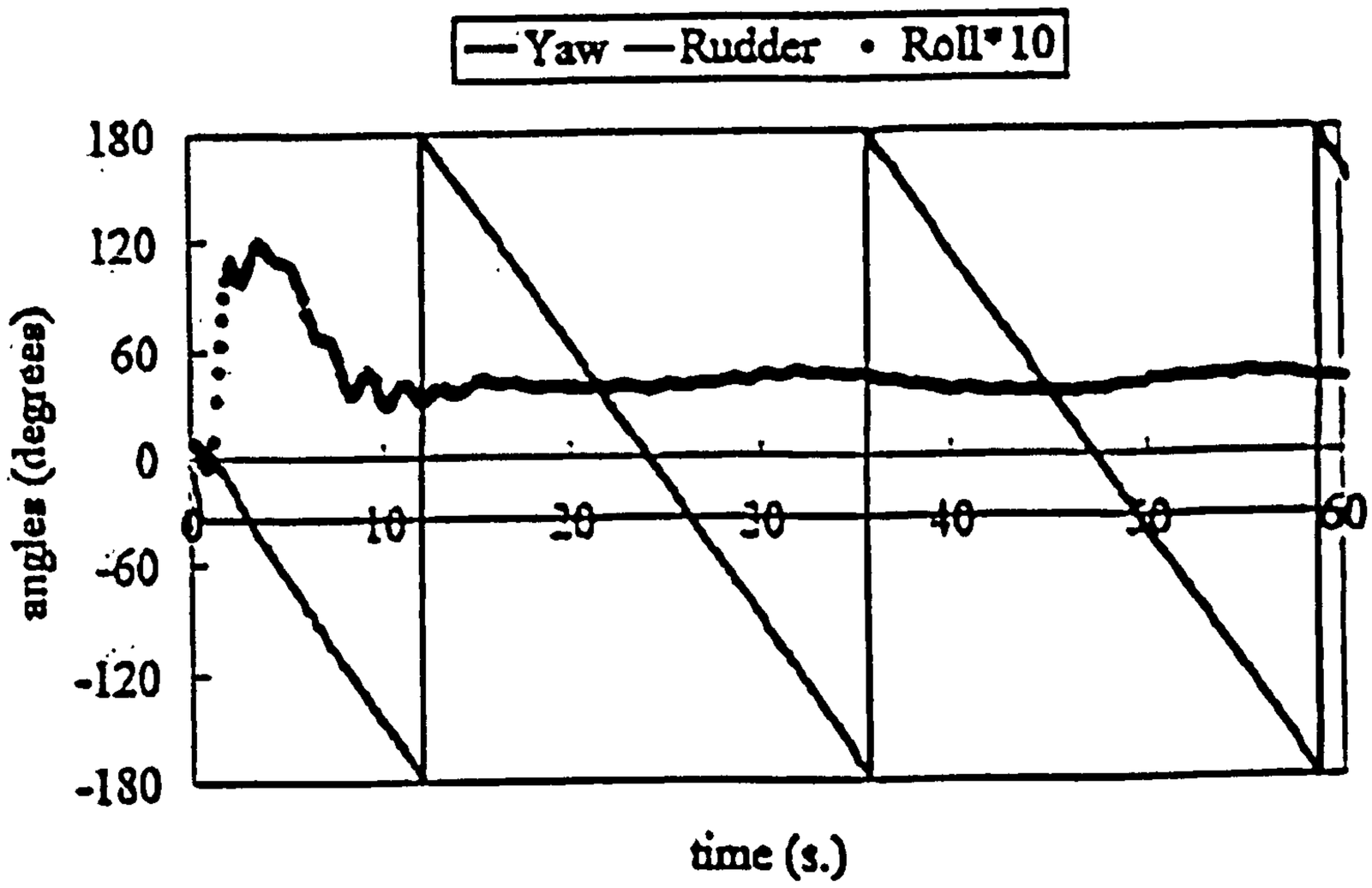

Figure E.19 Measured time histories of the –35 degrees turning test of Ship A-2 at Fn=0.30 in model scale.

F. NUMERICAL CODE

a. Solutions of equations of motions

In order to validate the developed numerical code and to carry out numerical simulations for manoeuvring behaviour of ships in astern seas, a time simulation numerical analysis program called "Simurg" has been developed in C++ code. The numerical calculations or programming for this sort of numerical codes are universal. Therefore instead of general procedure some important points regarding the numerical model will be emphasized here. Program follows the similar structure of Tsangaris [40], McCreight [49] and Elsimillawy et al. [64].

As it is described in Chapter 5, non-linear Equations 5.4 and 5.5 contain 12 variables and along with δ, rudder angle, and ξ_g and ζ_a, horizontal and vertical components of wave amplitude, those variables can be defined as follows:

X: State Vector $x \in |R''$

$$X:(\zeta_a,\xi_G,x,y,z,u,v,w,p,q,r,\varphi,\theta,\psi,\delta)^T$$

Equation F.1

where x, y, z are kinematics, u, v, w are linear and p, ,q, r are angular velocities, φ, θ, ψ are Eulerian angles of rotations, respectively. Equation F.1 can be generalized as follows;

$$(M+A)\ddot{X}+B(X)\dot{X}+C(X)X=F(\zeta_w,X,\dot{X},\ddot{X})$$

Equation F.2

where, M is inertia Matrix, A is added inertia matrix, B is damping coefficient matrix, C is restoring coefficient matrix, F is external force vector and ζ_w is wave amplitude. Aforementioned variables can be written in horizontal body axis system recalling Equations 10-11-12 in Chapter 5.

$$
\begin{aligned}
&1)\ x' \\
&2)\ y' \\
&3)\ z' \\
&4)\ \dot{U} = g_1(U, V, W,, P, Q, R, x', y', z', \varphi, 0, \psi, X', t) \\
&5)\ \dot{V} = g_2(U, V, W,, P, Q, R, x', y', z', \varphi, \theta, \psi, Y', t) \\
&6)\ \dot{W} = g_3(U, V, W,, P, Q, R, x', y', z', \varphi, \theta, \psi, Z', t) \\
&7)\ \dot{P} = g_1(U, V, W,, P, Q, R, x', y', z', \varphi, \theta, \psi, K', t) \\
&8)\ \dot{Q} = g_2(U, V, W,, P, Q, R, x', y', z', \varphi, \theta, \psi, M', t) \\
&9)\ \dot{R} = g_3(U, V, W,, P, Q, R, x', y', z', \varphi, \theta, \psi, N', t) \\
&10)\ \dot{\varphi} = \frac{P}{\cos\theta} \\
&11)\ \dot{\theta} = \dot{\Theta} \\
&12)\ \dot{\psi} = R + P\tan\theta
\end{aligned}
$$

Equation F.3

The system of equations is formed from the above six equations, six kinematics relations, autopilot and position on the wave as shown in above equations. From Equation F.3, it reduces to the solution of ordinary differential equations and in this numerical code, the calculations are performed using the equal time step, 4^{th} order Runge-Kutta method. The numerical code, thus, produces 14 output.

From Chapter 5 and 6, it is explained that two approaches were used for the simulations of ship motions in extreme astern seas. First one is the traditional approach of zero frequency added mass and damping terms, and the second approach is the introduction of frequency dependent added mass and damping terms for calculation of the radiation forces. For the first approach a standard zero frequency added mass and inertia matrix were calculated. The damping terms were added to right hand side of equations where all external forces (wave, hull (manoeuvring), rudder, propeller, resistance, wind) are calculated modularly and then they are added linearly as it is shown in Equation 5.9. While, for the second approach, since the calculation of frequency dependent coefficients in the numerical code for each second requires substantial amount of time in process, another approach was tried. The frequency dependent coefficients were calculated and restored for 10 degrees heading range in 360 degrees for zero speed, it is included by convolution integral in time domain for each required wave heading. If the required heading is in between stored range of heading angles, they are interpolated. Although, it could seen to be an unorthodox method accuracy of numerical simulations in Chapter 7 and 10 shows that it is good approach

and it significantly reduces processing time for the simulations especially considering the calculations of wave pressure up to instantaneous wave surface for each time as will explained below

Numerical calculation of incident wave forces:

It is described in Chapter 5 and Appendix B that two different approaches in 3-D panel method and 2-D strip theory are used to calculate he incident wave pressure on the hull, including hydrostatic terms based on instantaneous wave surface.

For the first approach, calculations are performed using the hull modelled by plane quadrilateral surface elements (Figure F.1).

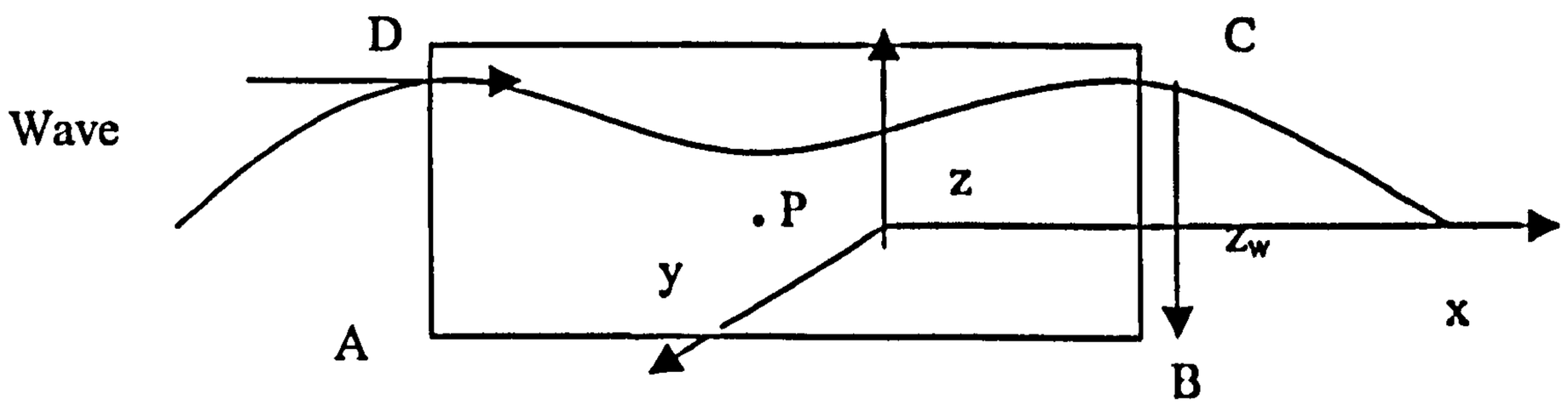

Figure F.1-Hull panel and intersection with wave

Here, the point where pressure is to be evaluated is chosen the mid-point of the quadrilateral element (P). For each panel the intersection points of the wave are calculated and the points defining the hull are interpolated. Hull panels and solid view of the vessels tested in this study are illustrated in Figures F.4-F.7.

For the second approach the pressure are calculated for each section as it is given in Appendix B and then integrated along the ship length. As for the 3-D panels, intersection points of the wave are identified and pressures are calculated up to that intersection point in each time step using the coordinate system shown in Figure A.1 in Appendix A.

Here, in Figures F.6, F.7 and F.8, the sequence of capsizing due to broaching, parametric rolling and harmonic rolling simulated by the numerical code for the purse seiner trawler and containership are illustrated.

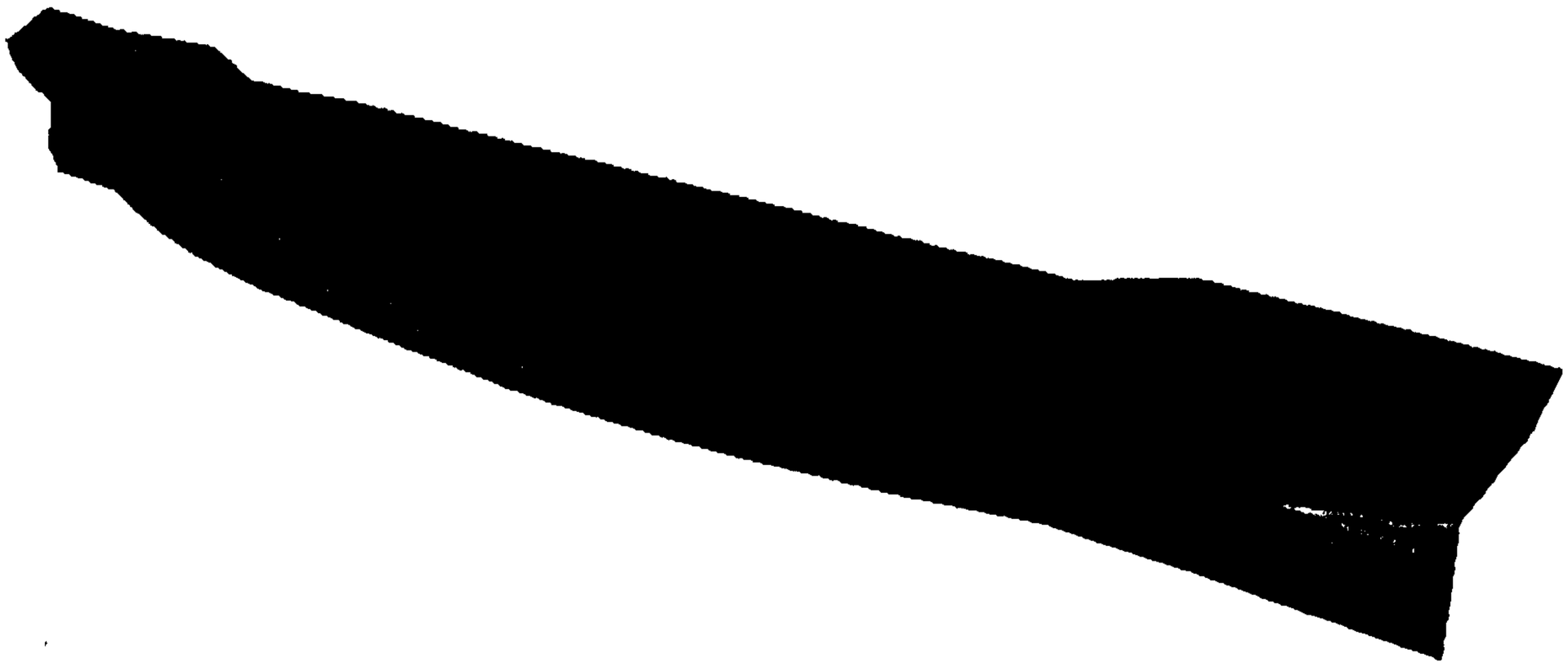

Figure F.2 Solid view of Ship A-1 with 240 panels

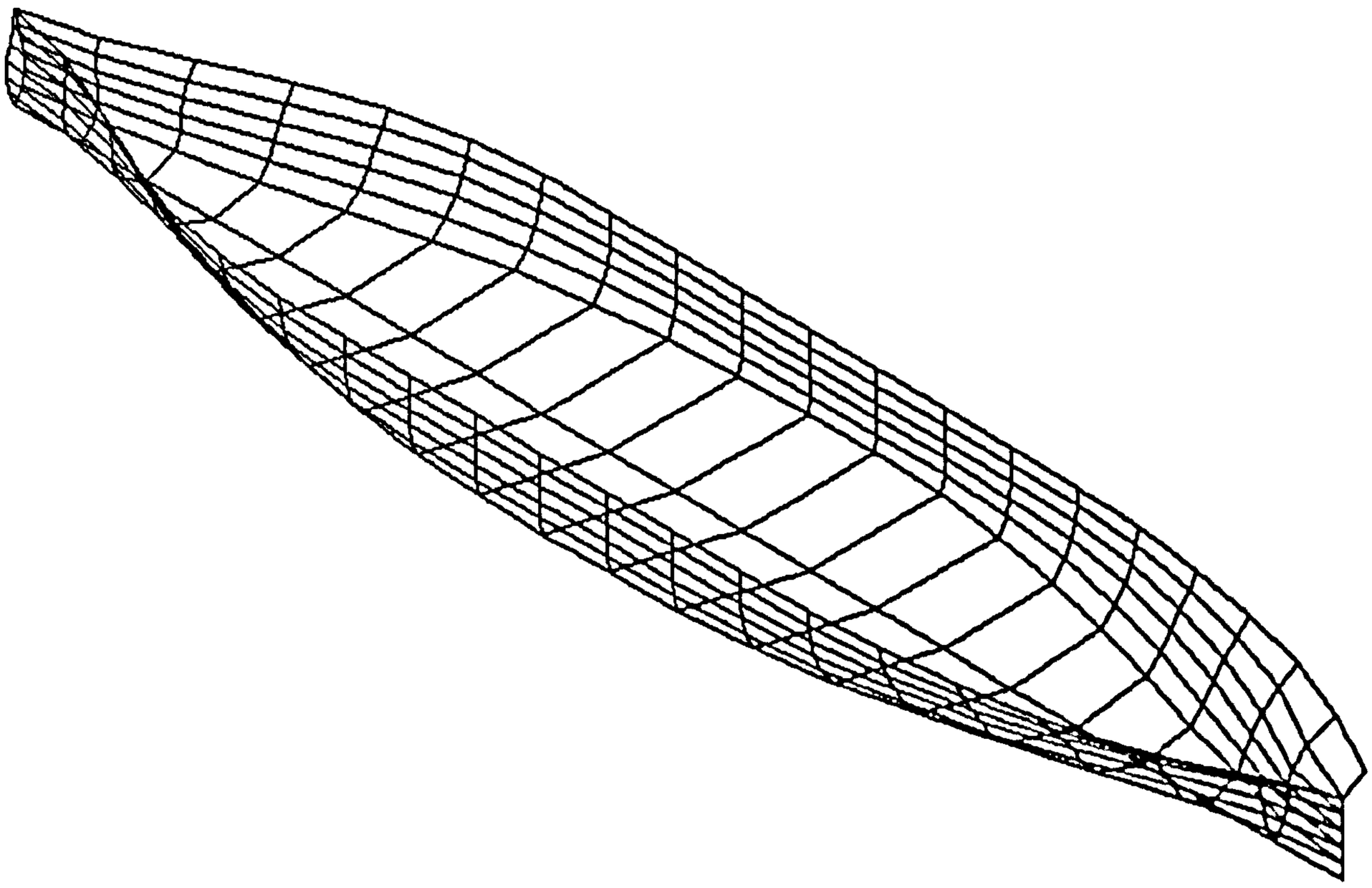

Figure F.3 Ship A-1 at waterline with 240 panels

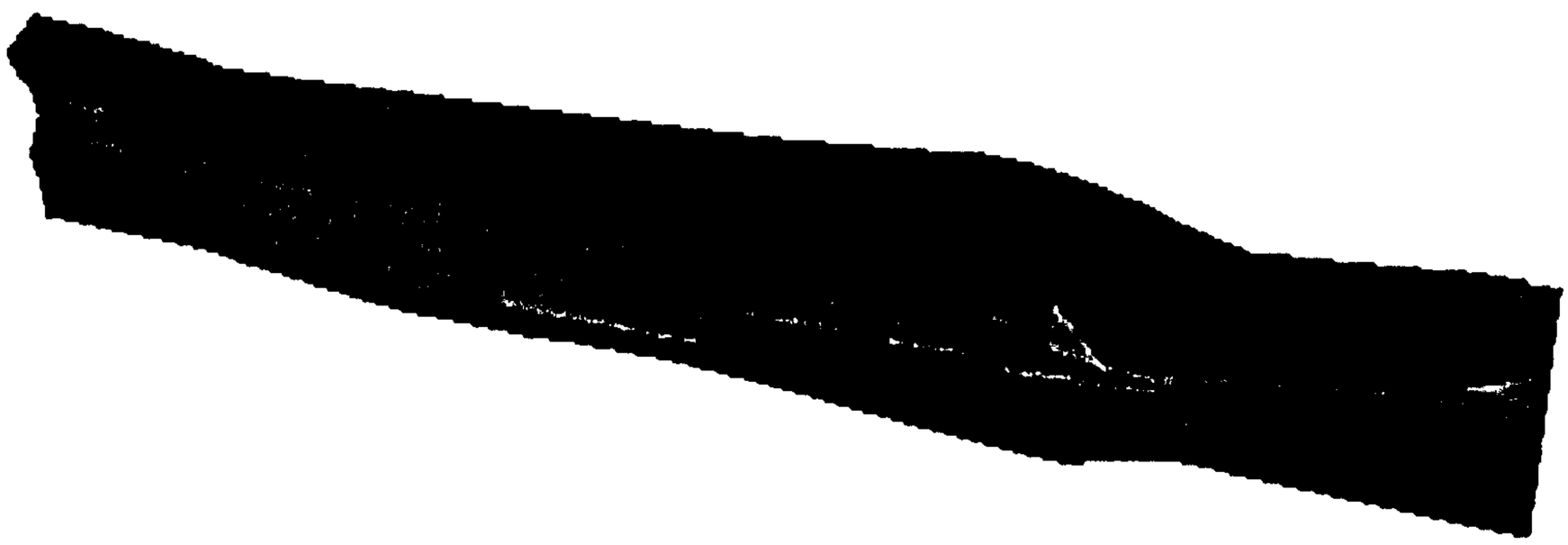

Figure F.4 Solid view of Ship A-2 with 480 panels

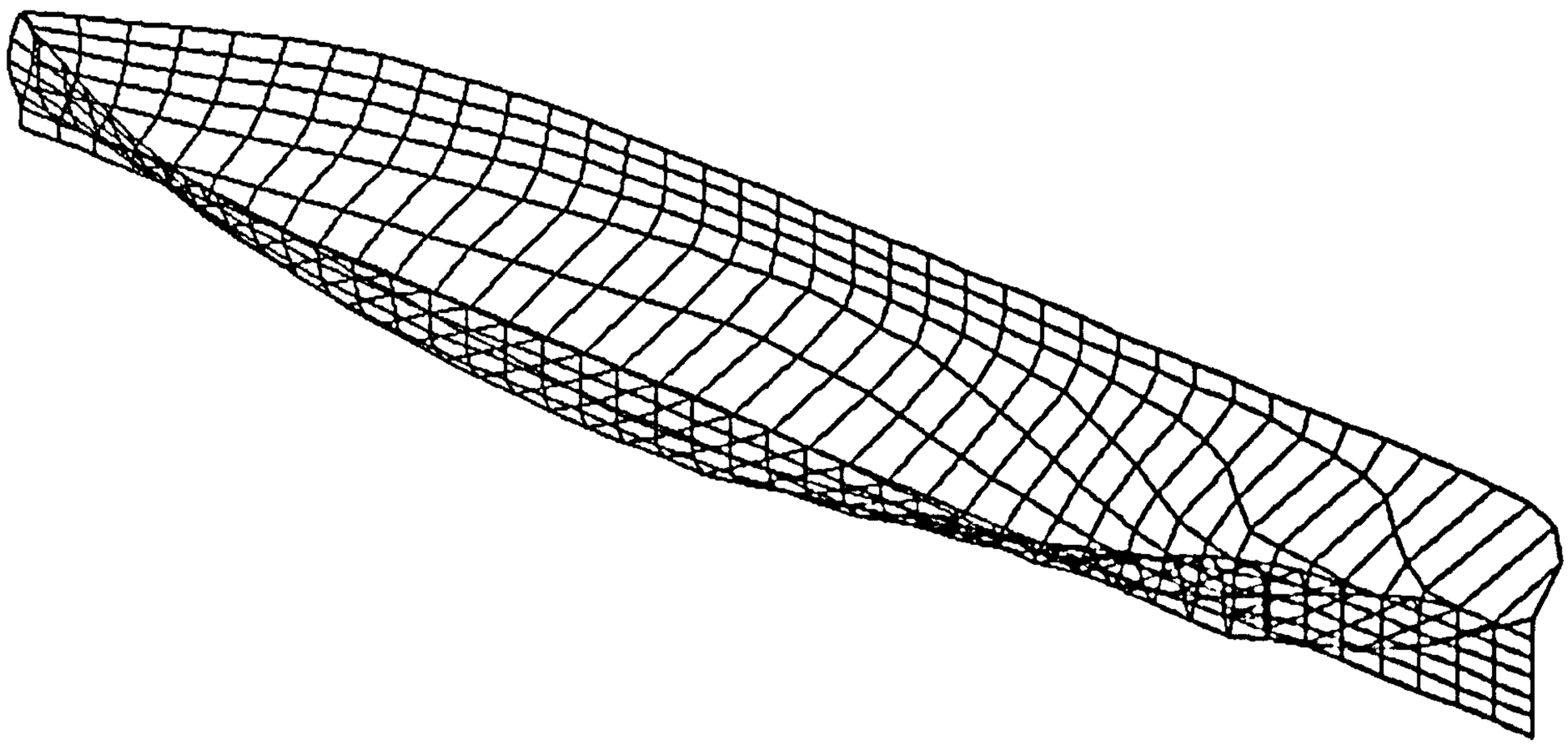

Figure F.5 Ship A-2 at waterline with 480 panels

Figure F.6 The sequence of capsize due to broaching for Ship A-2

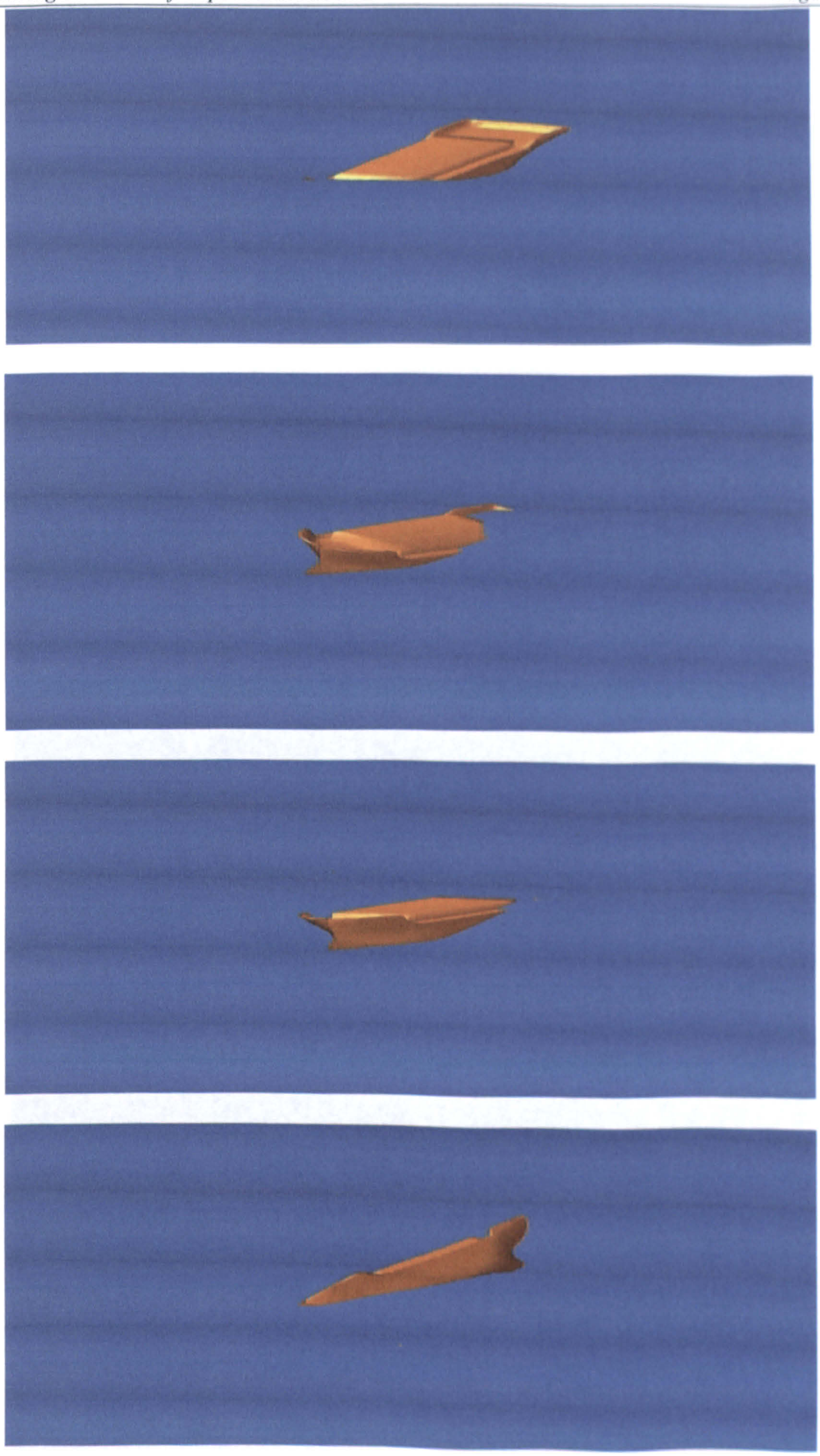

Figure F.7 The sequence of capsize due to parametric roll for Ship A-1

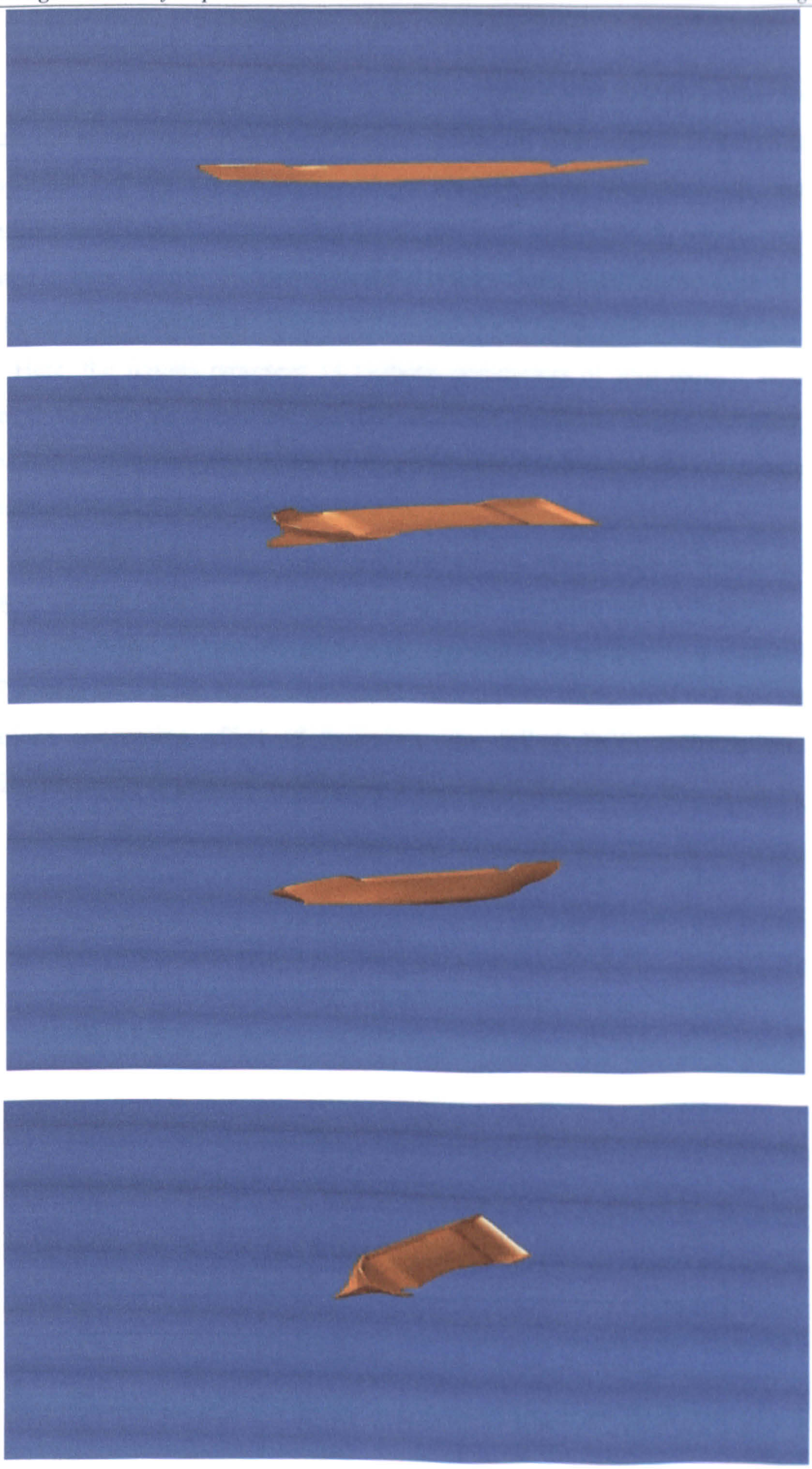

Figure F.8 The sequence of capsize due to harmonic rolling for Ship A-1

G. PARAMETRICAL STUDIES

As it mentioned in Chapter 8, the further numerical simulations were necessary to assess the environmental and performance effects on ship motions in astern seas and the capability of the numerical model to identify them Therefore the numerical simulations were conducted following the similar path to Chapter 8, and the results are presented in here. Further discussion on those results along with the outcome of Chapter 8 will be taken in Chapter 11.

Here, the figures represent 14 motions parameters of ship motion as given in Chapter 7: Kinematics, linear and angular velocities, rotational angles including rudder and position of ship on wave. As far as the parametrical investigations are concerned the important ones out of those 14 parameters are presented.

In a similar order, the effect of wave steepness, wave length to ship length ratio, loading conditions (GM), speed and heave angle and frequency are investigated.

For the effect of wave steepness a comparison with the new axis system and the 4 DOF system with static equilibrium on heave and pitch was carried out. Except in the simulations concerning effect of frequency, the full 6 DOF mathematical model including frequency dependent coefficients was used in all simulations.

FigureG.1 Numerical Simulation of Ship A-1 with 6 DOF mathematical model in $H/\lambda=1/25$, $\lambda/L_{pp}=1.5$, Fn=0.3,$\chi_c=0$ degrees

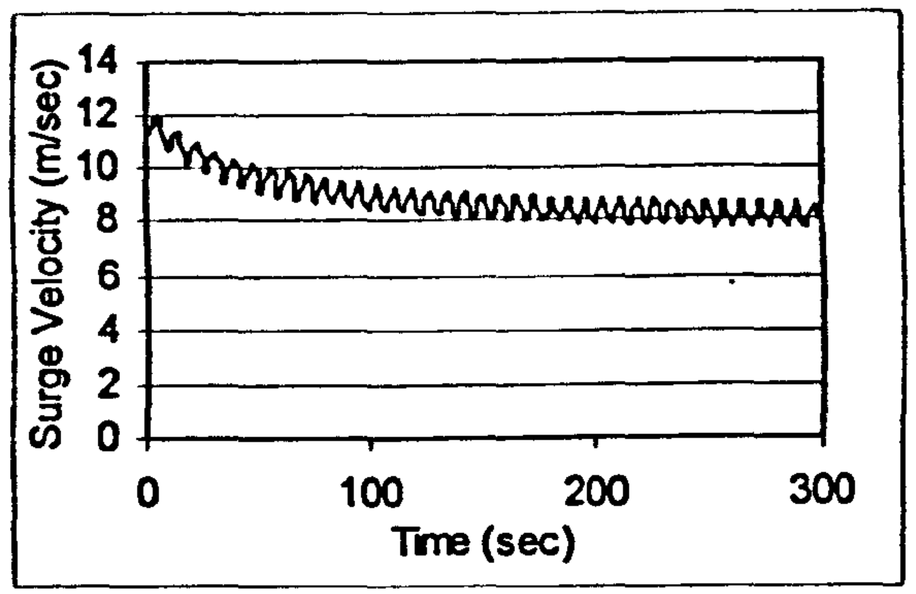

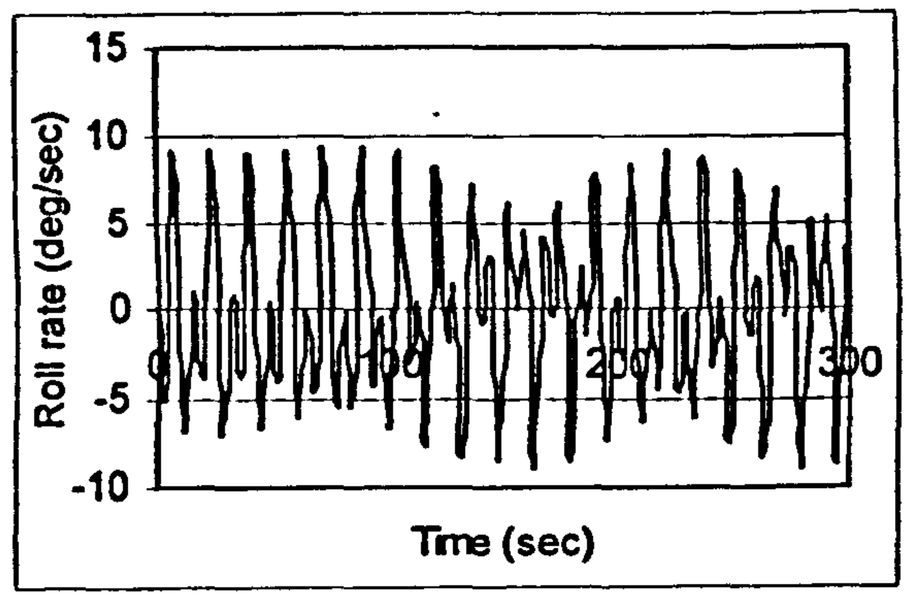

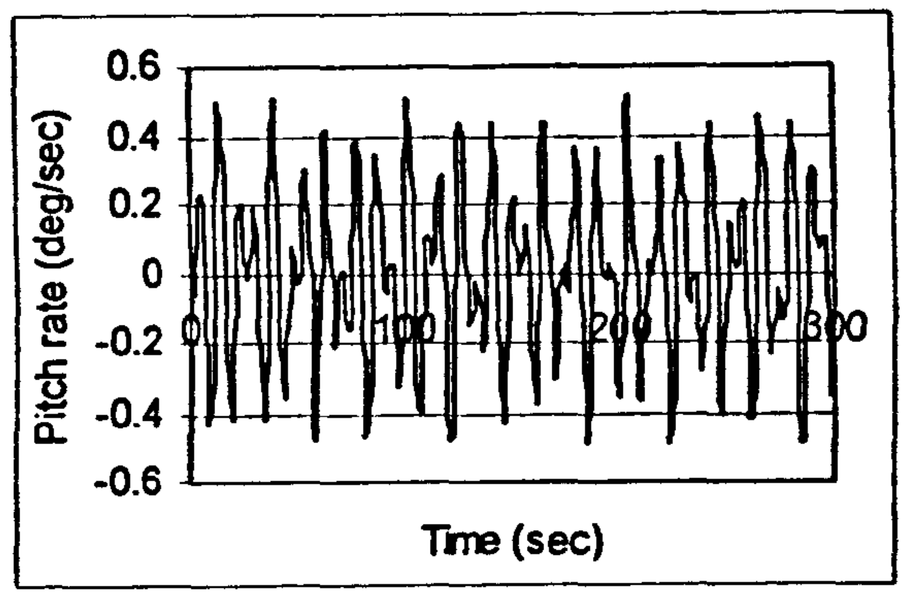

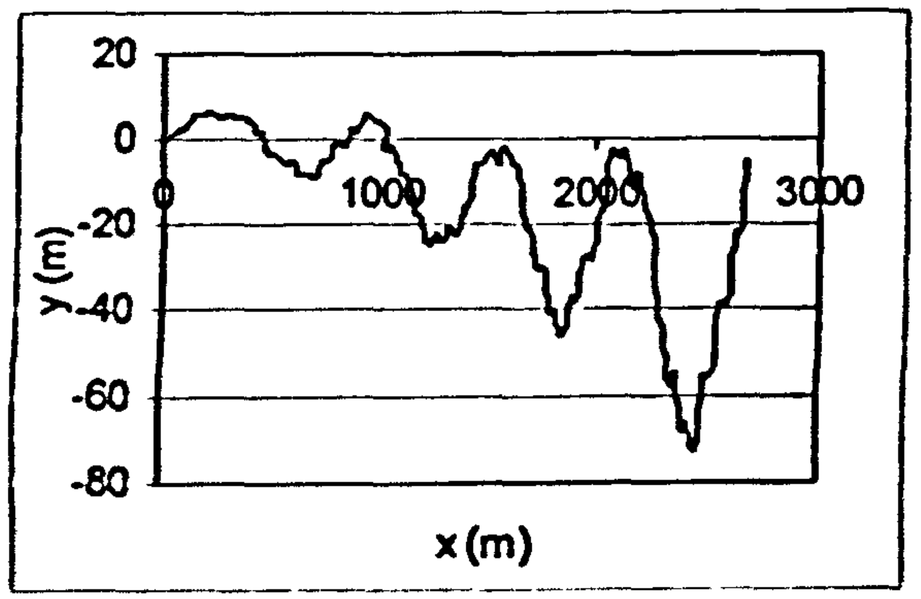

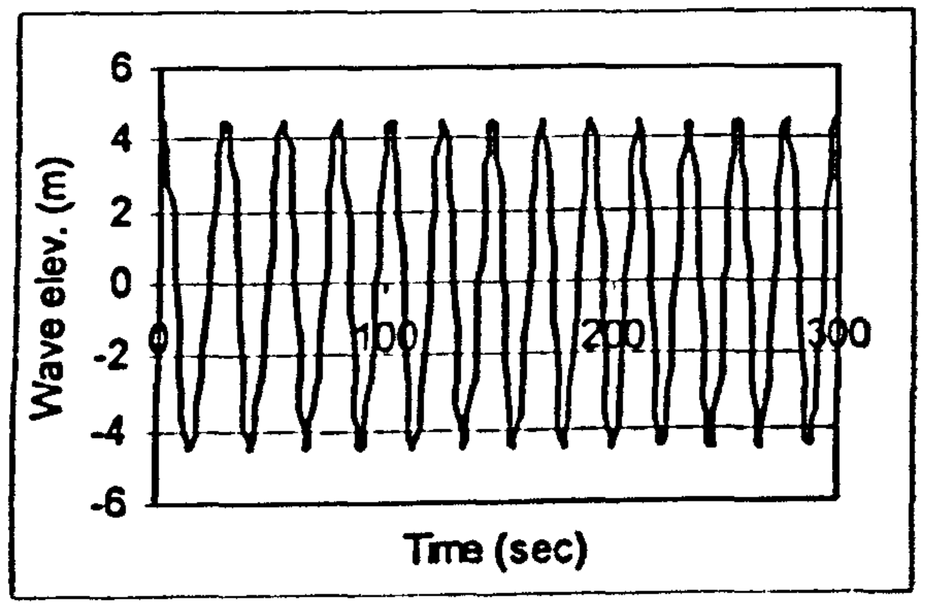

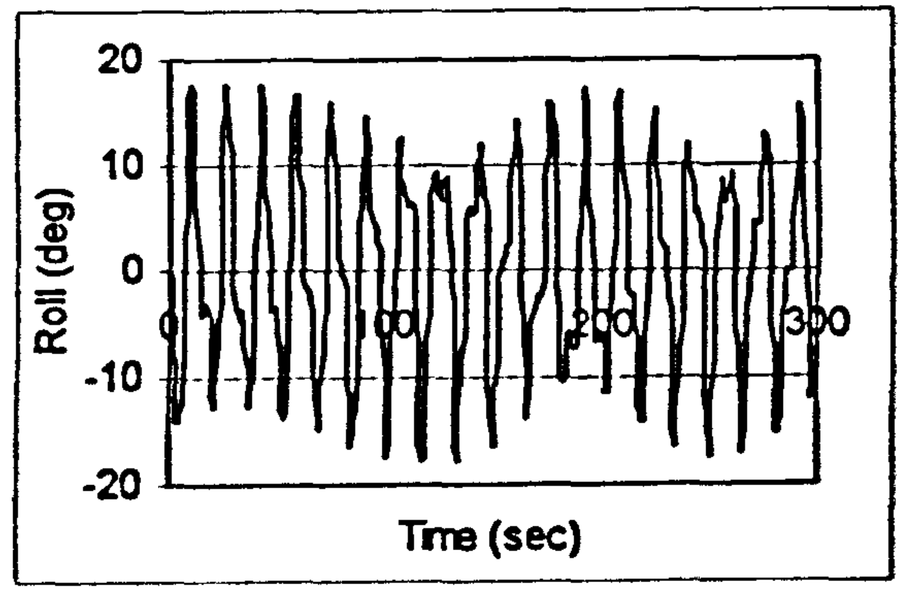

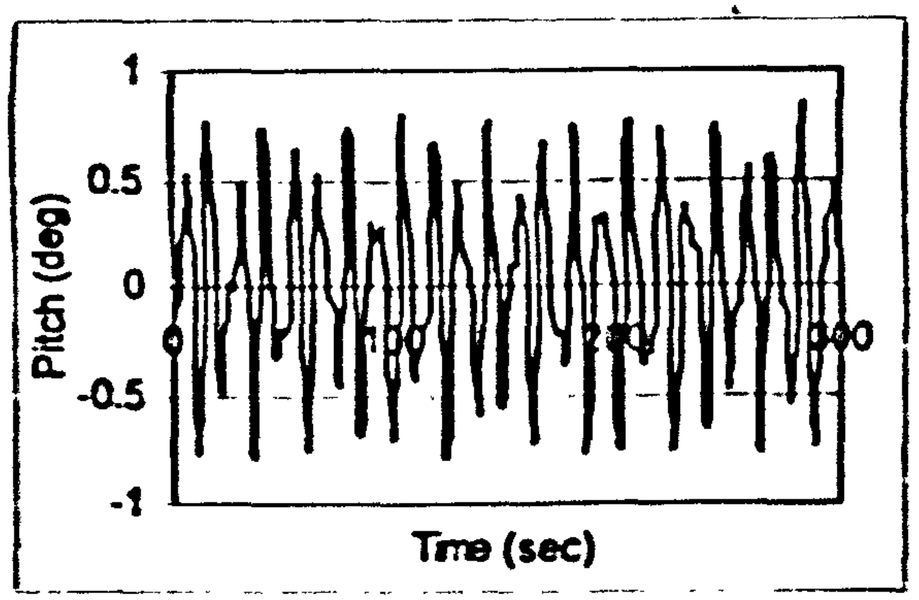

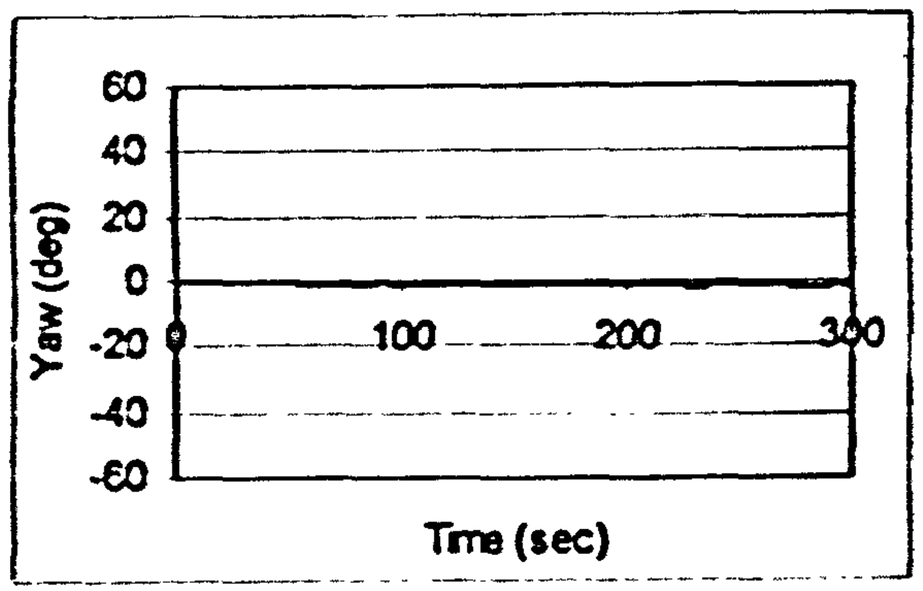

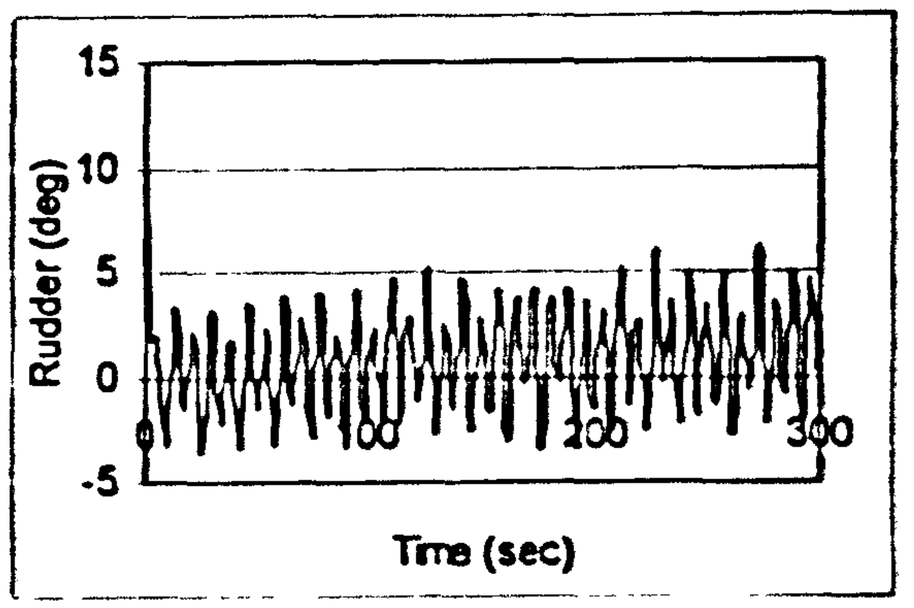

Figure G.2 Numerical Simulation of Ship A-1 with 4 DOF mathematical model in $H/\lambda=1/25$, $\lambda/L_{pp}=1.5$, Fn=0.3,$\chi_c=0$ degrees

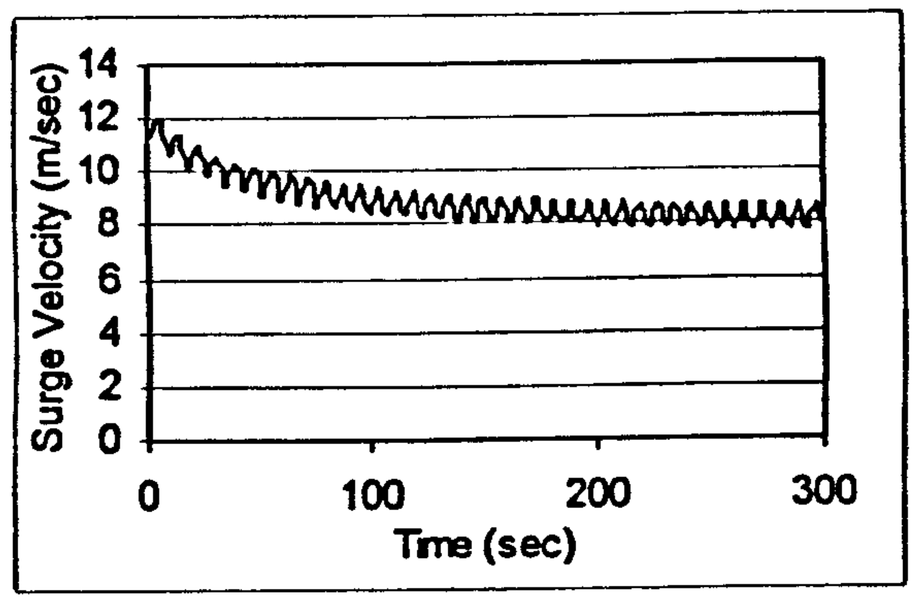

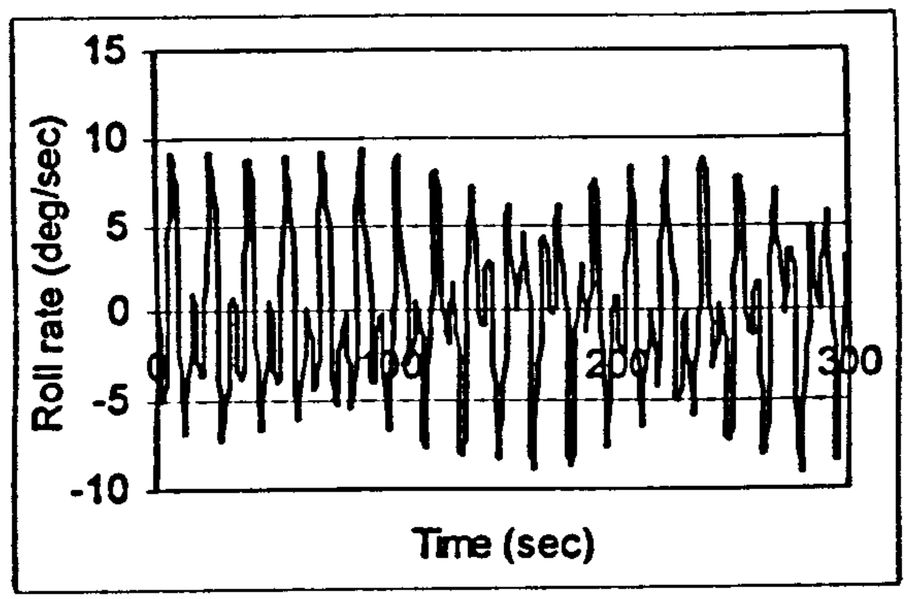

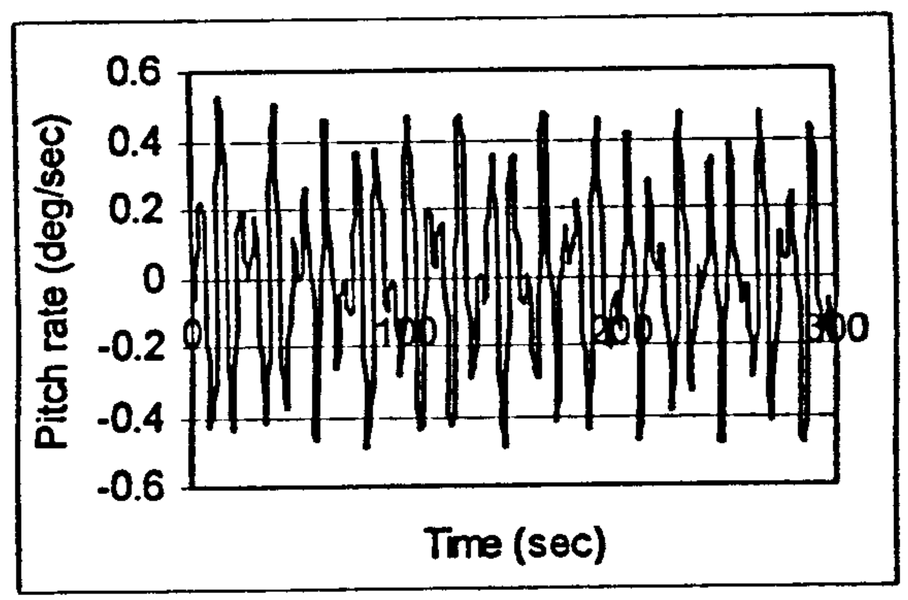

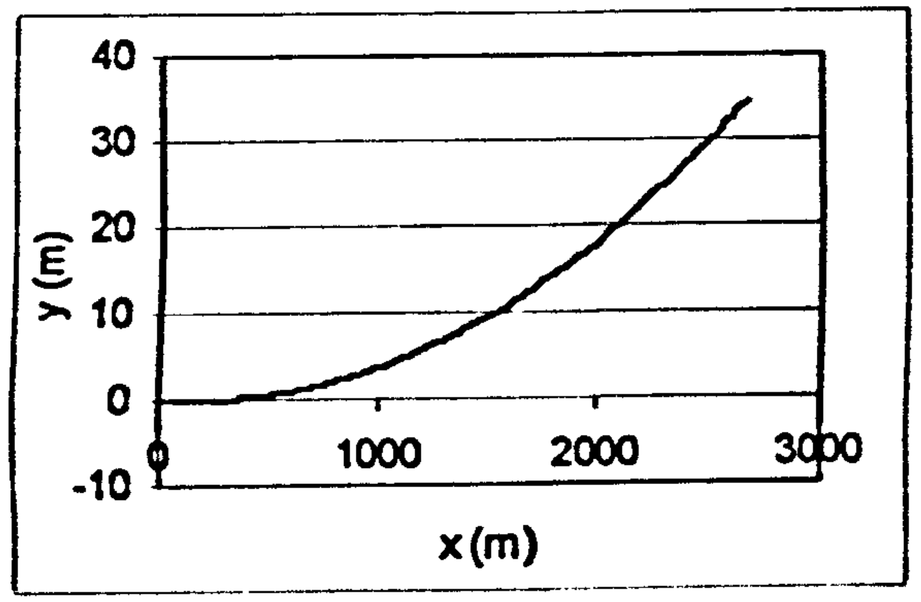

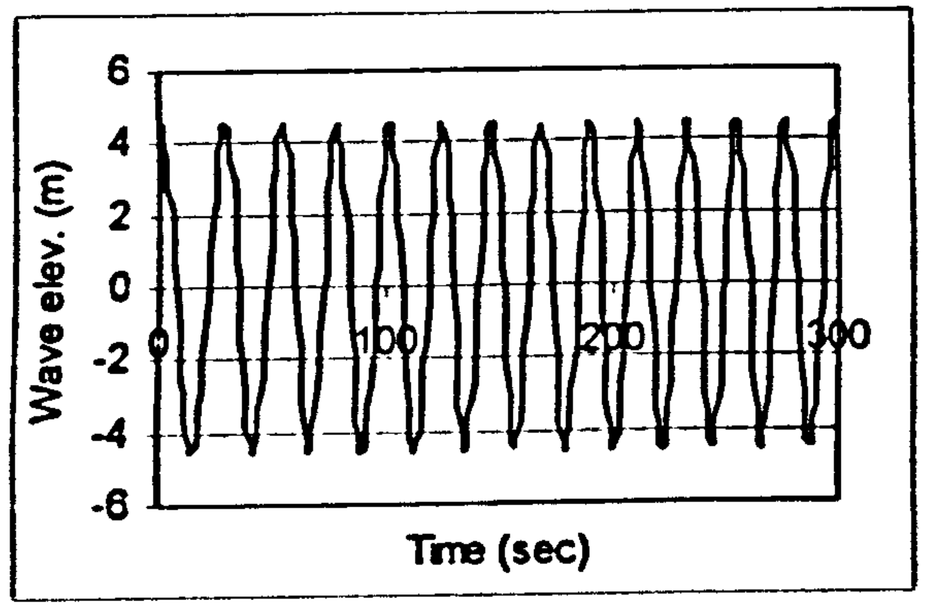

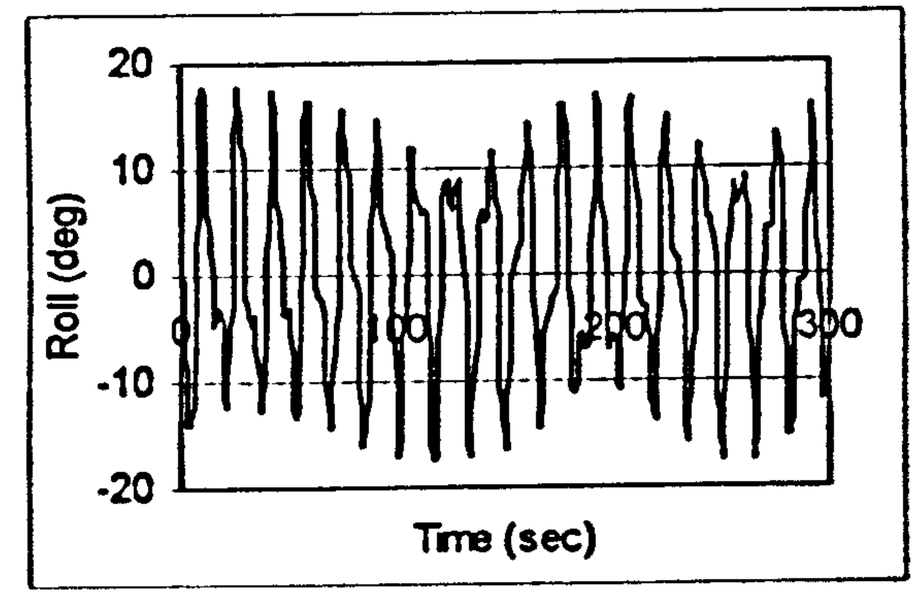

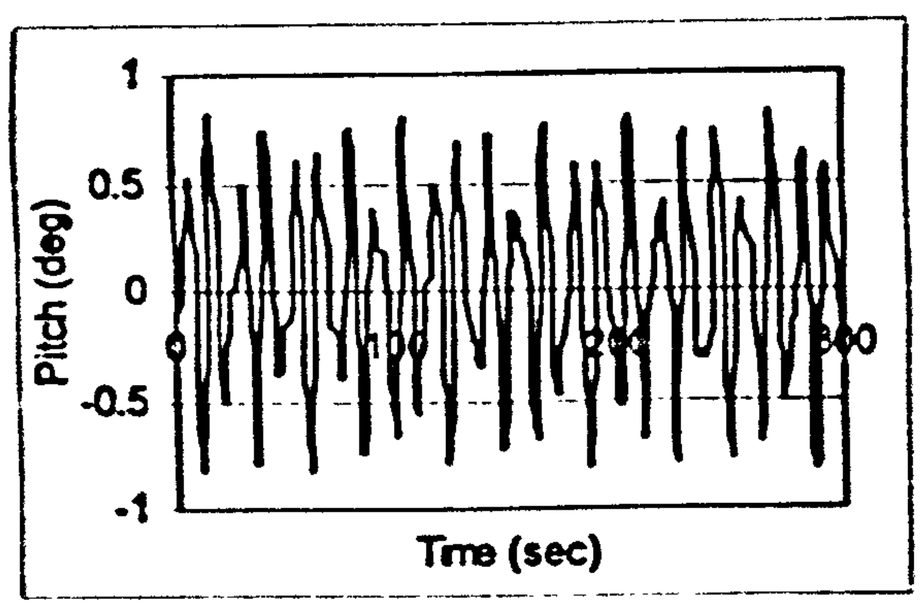

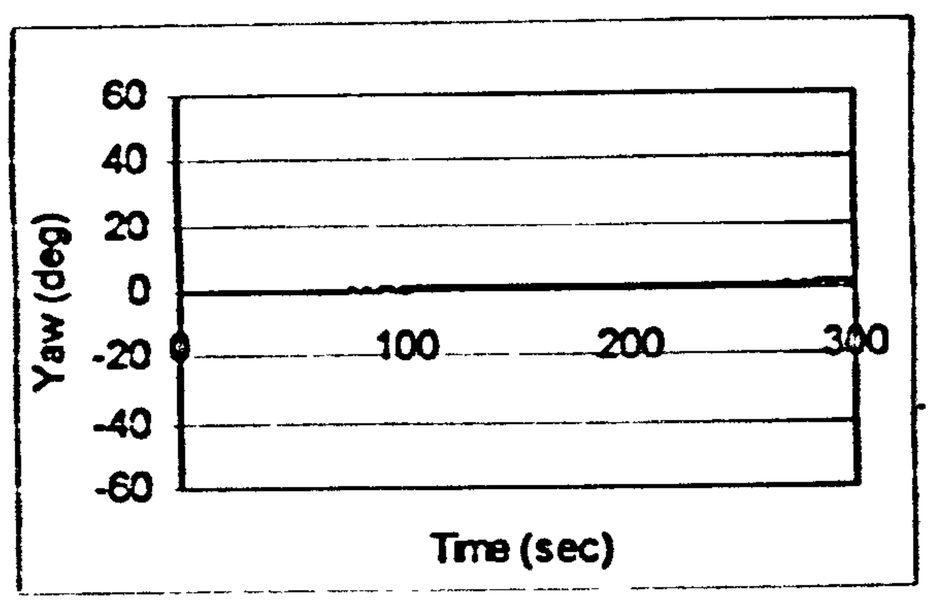

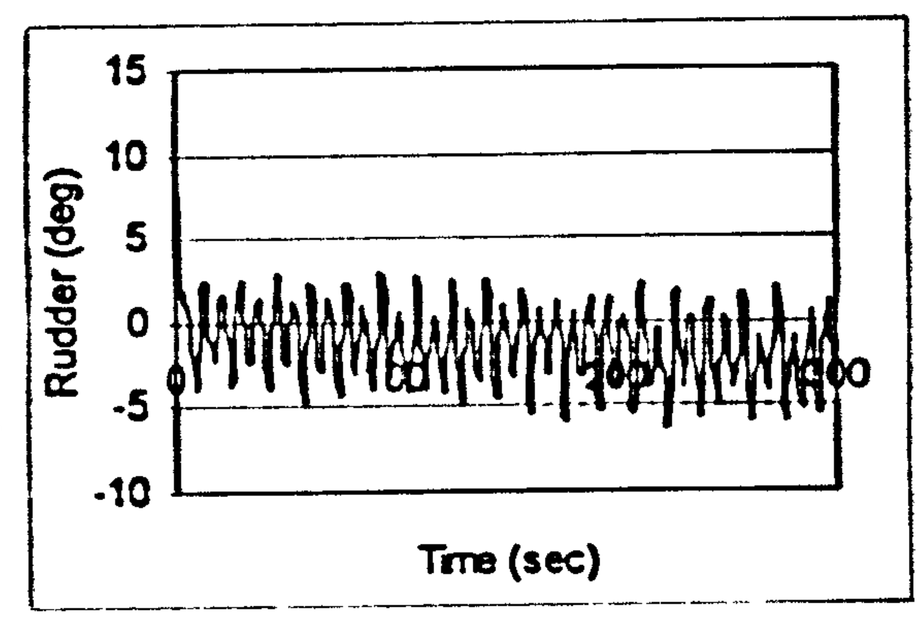

Figure G.3 Numerical Simulation of Ship A-1 with 6 DOF mathematical model in $H/\lambda=1/30$, $\lambda/L_{pp}=1.5$, $Fn=0.3$, $\chi_c=0$ degrees

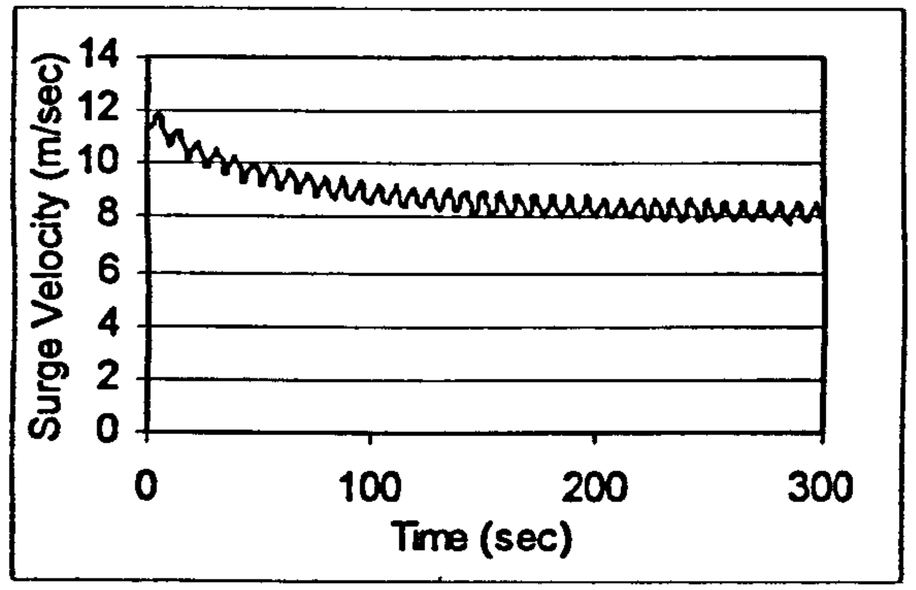

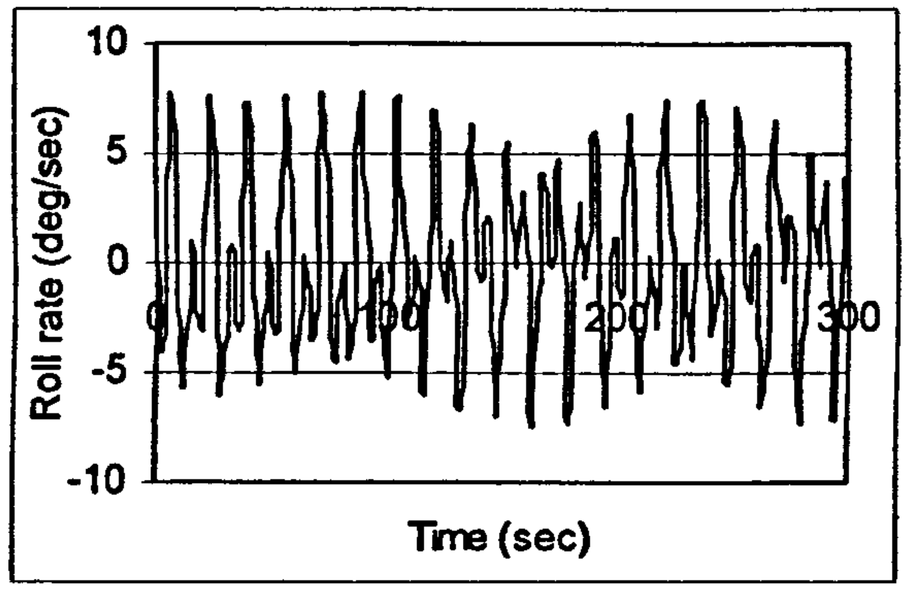

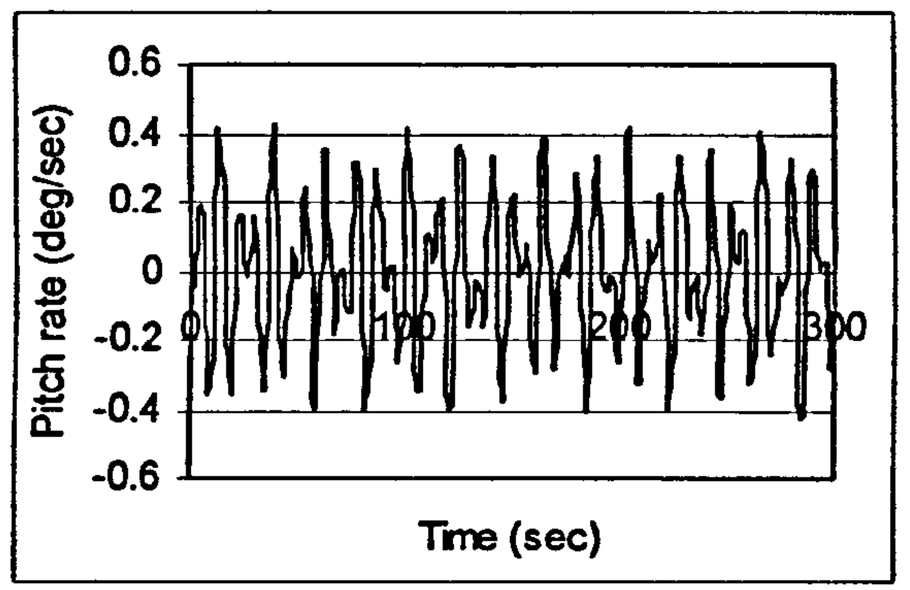

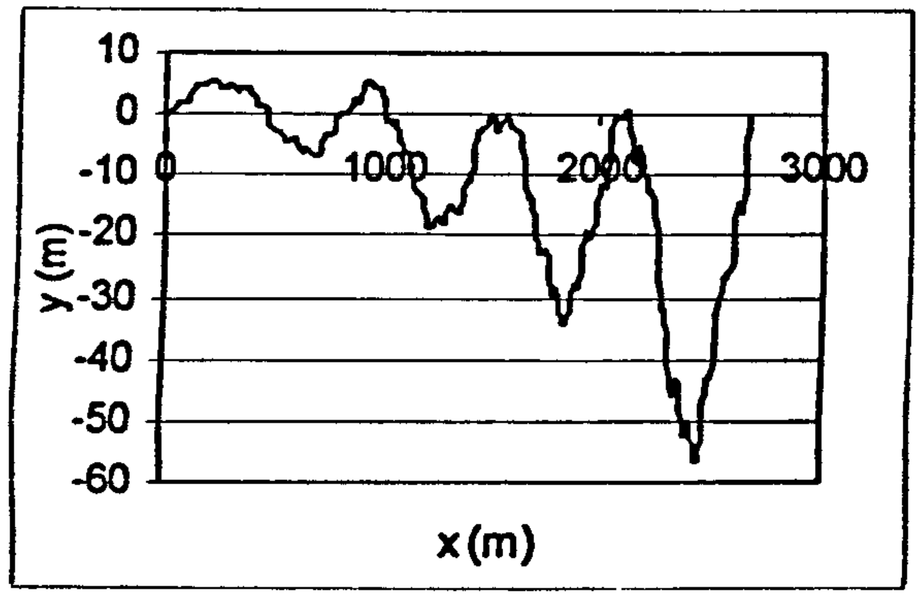

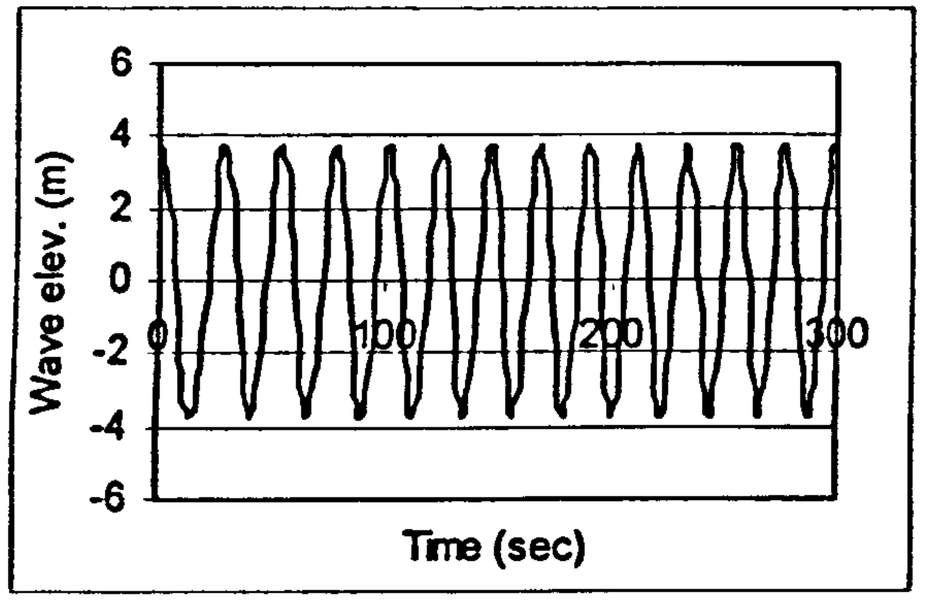

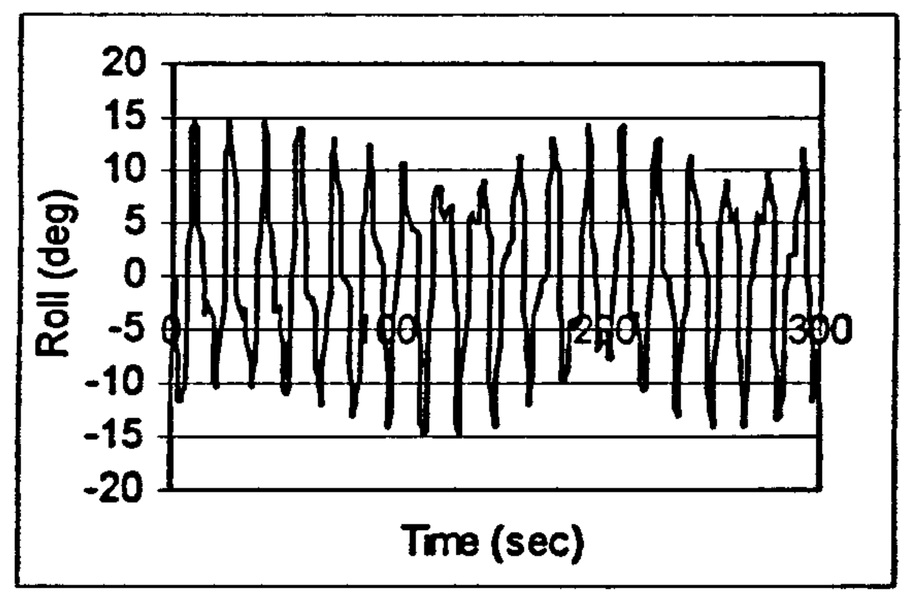

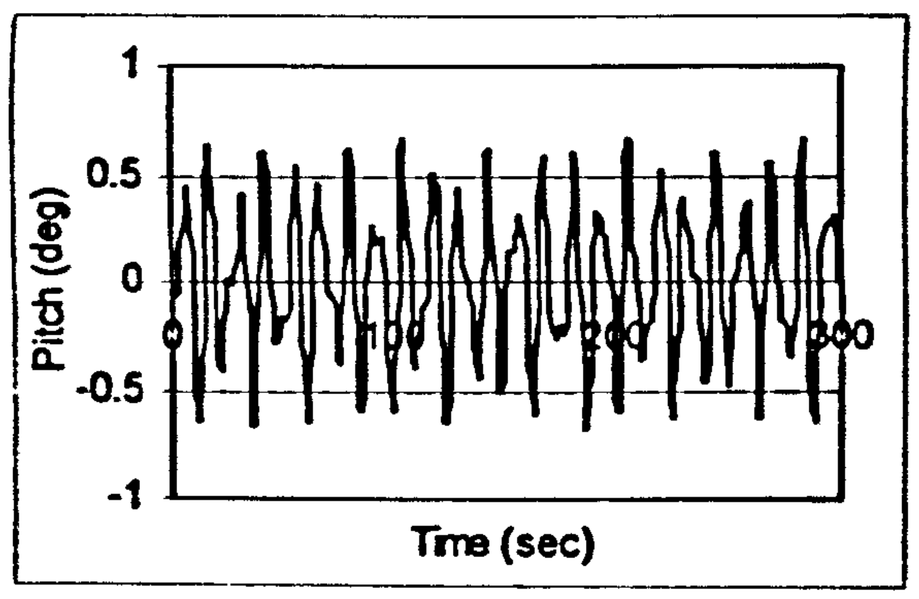

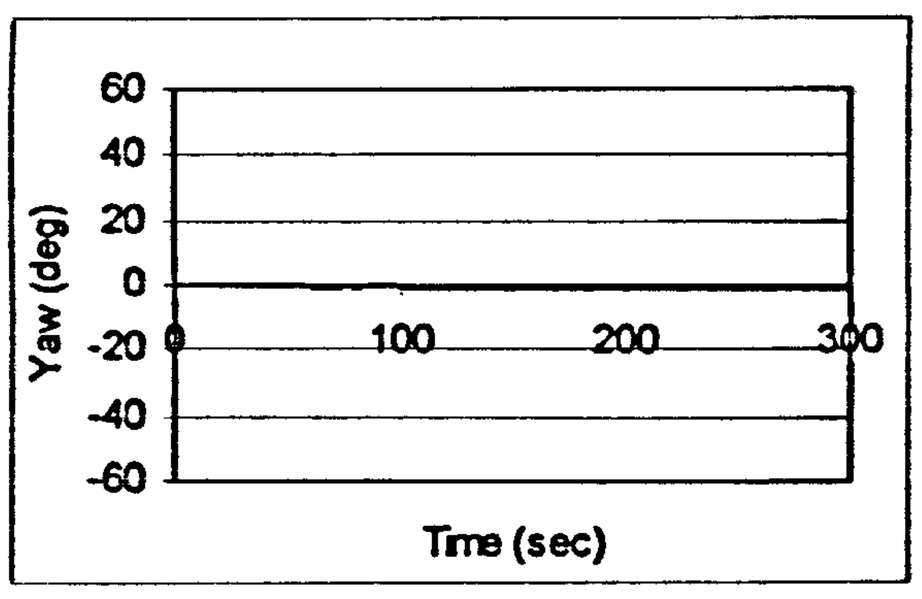

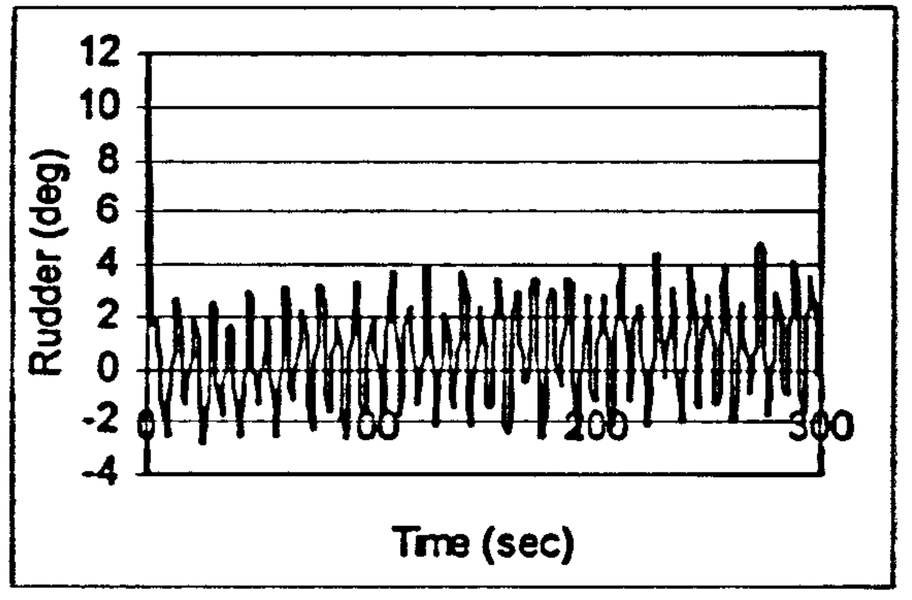

Figure G.4 Numerical Simulation of Ship A-1 with 4 DOF mathematical model in $H/\lambda=1/30$, $\lambda/L_{pp}=1.5$, Fn=0.3,$\chi_c=0$ degrees

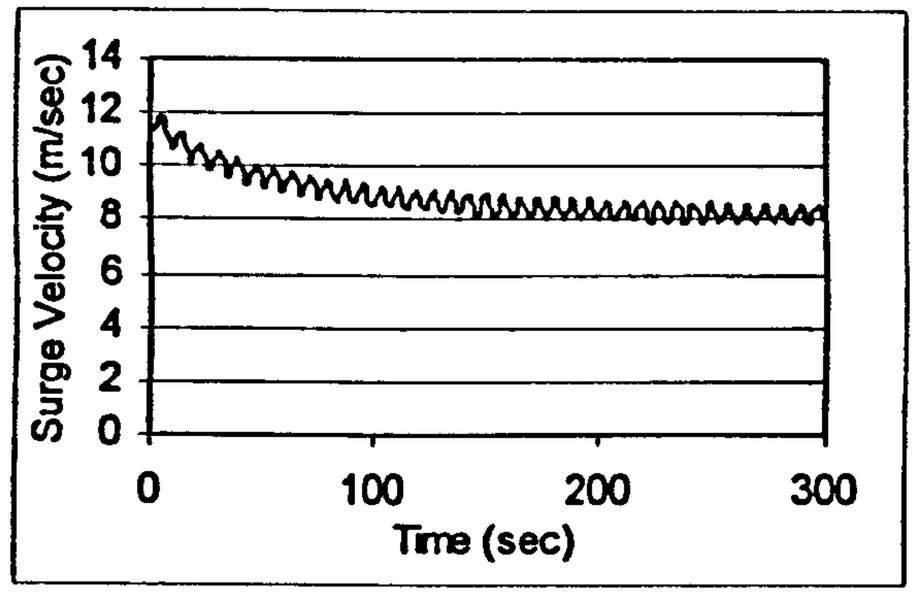

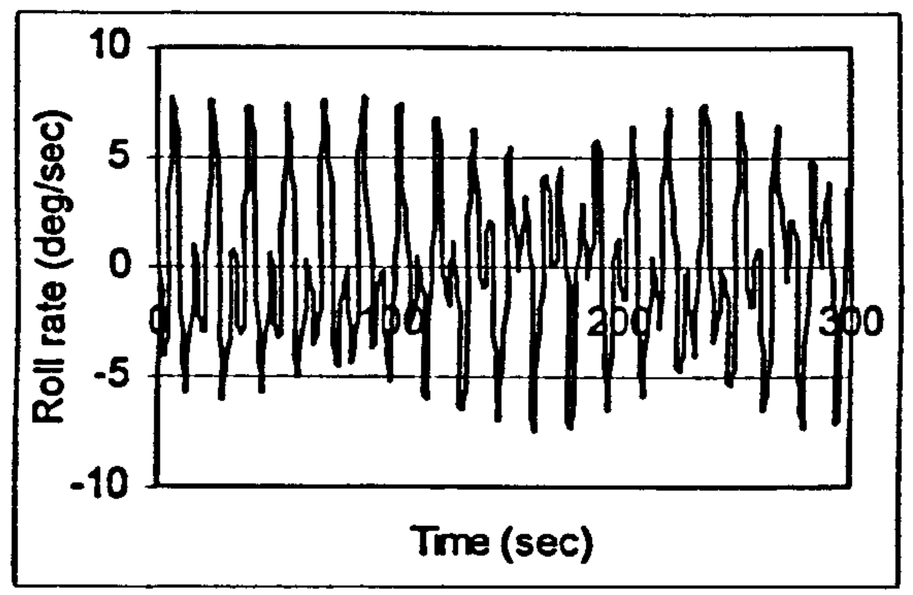

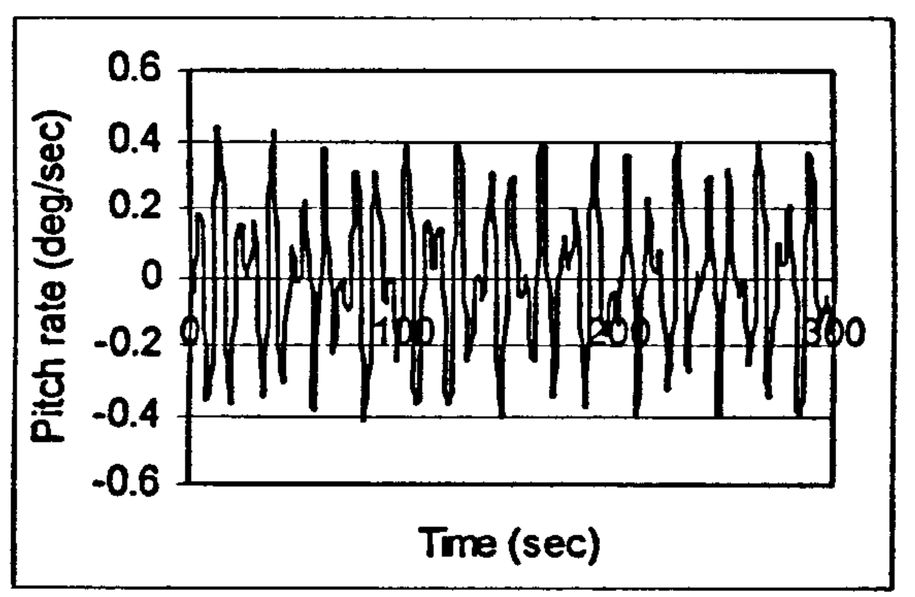

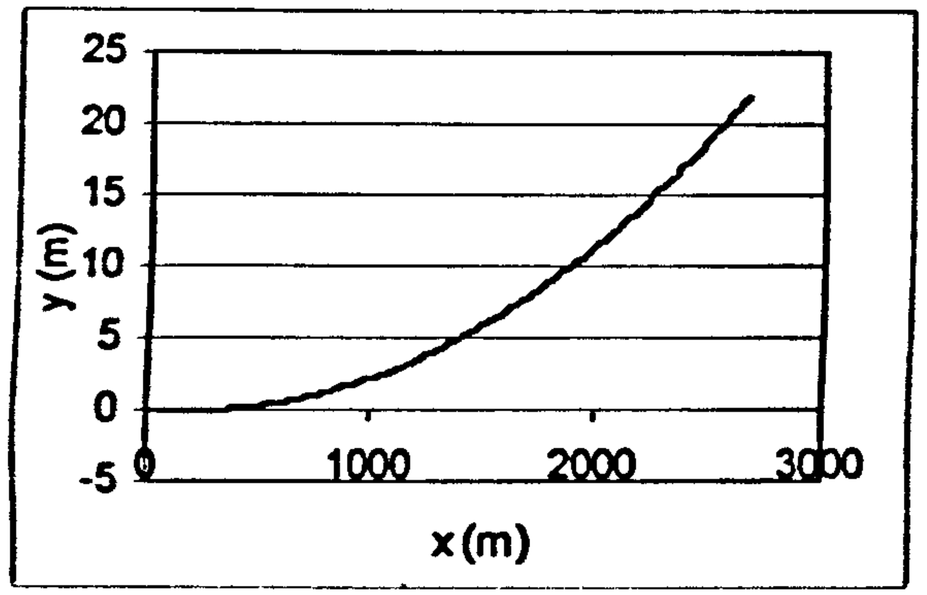

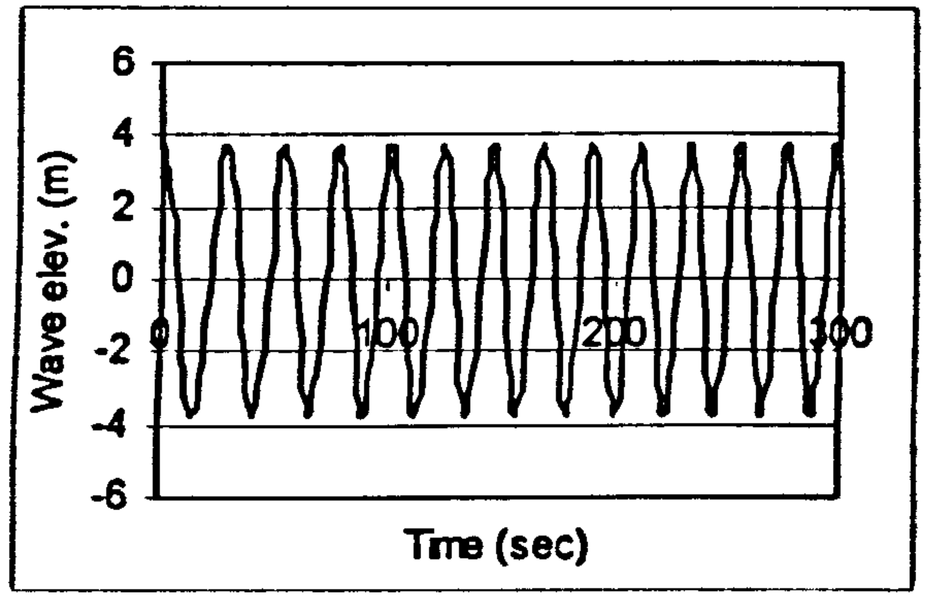

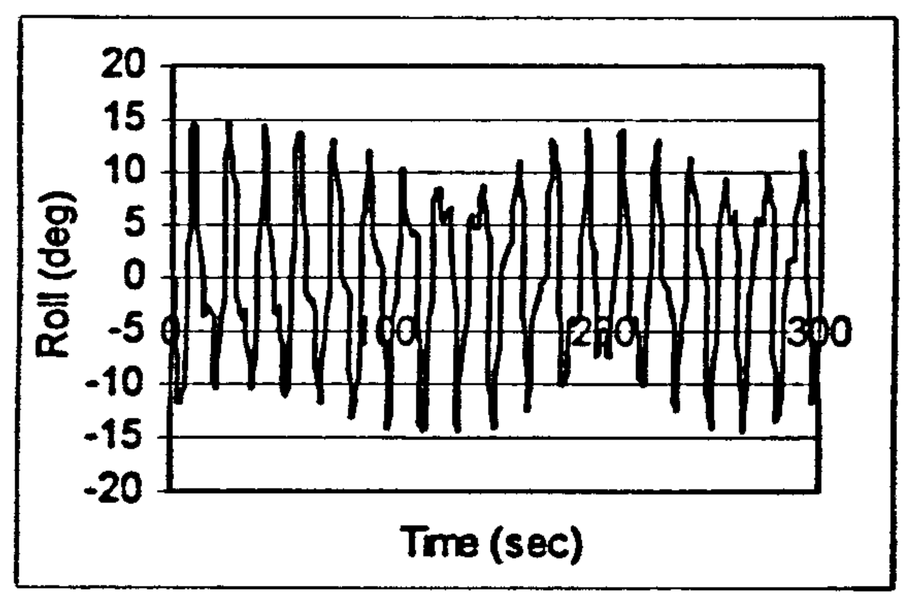

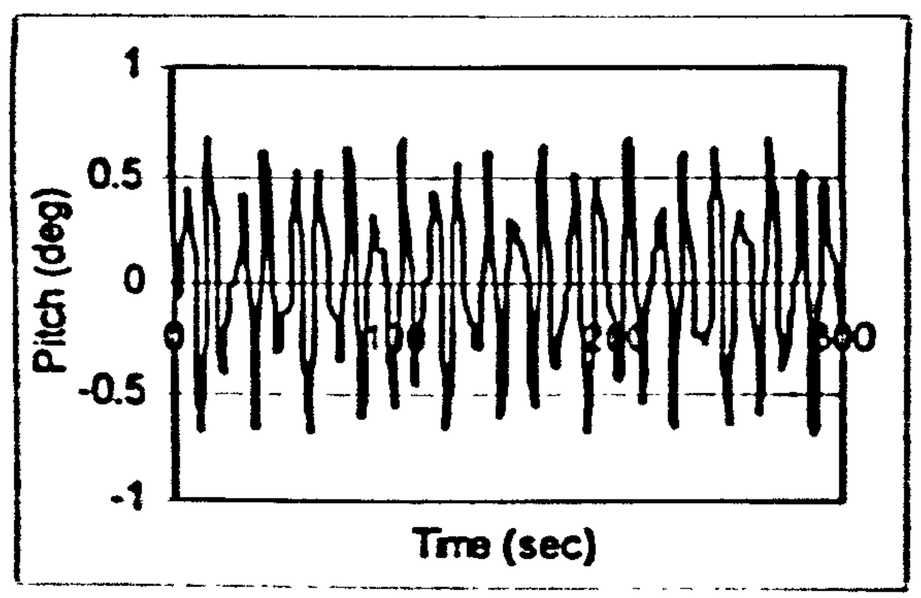

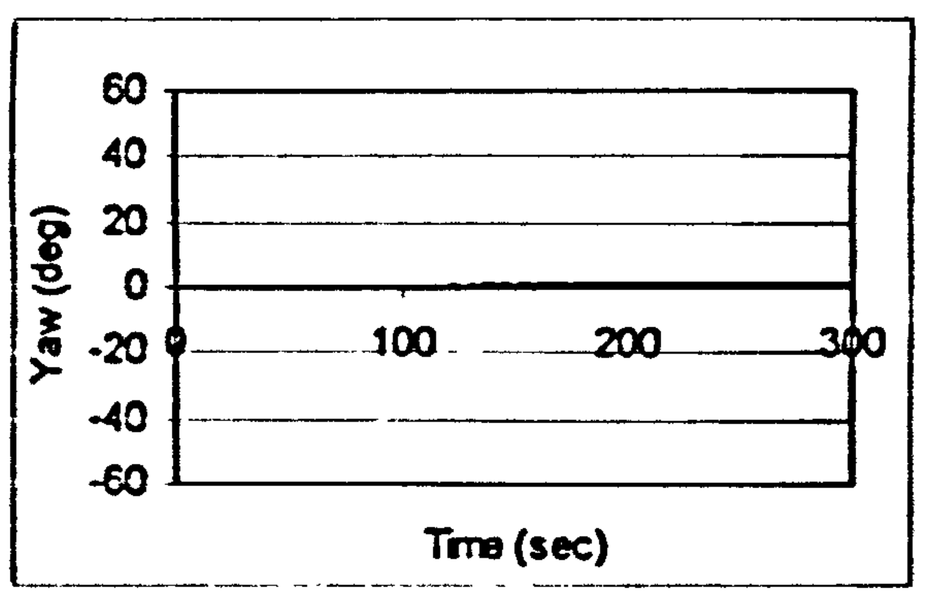

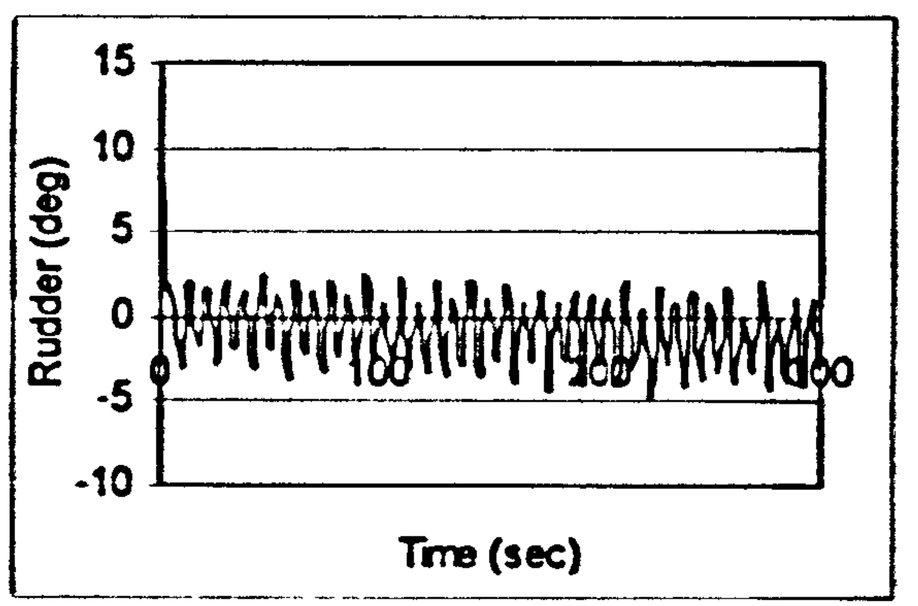

Figure G.5 Numerical Simulation of Ship A-1 with 6 DOF mathematical model in $H/\lambda=1/35$, $\lambda/L_{pp}=1.5$, Fn=0.3,$\chi_c=0$ degrees

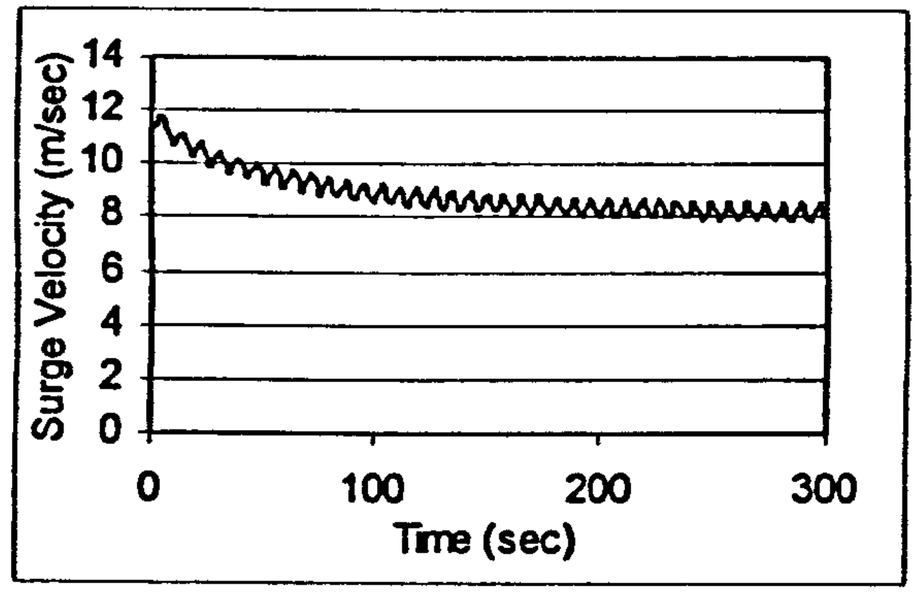

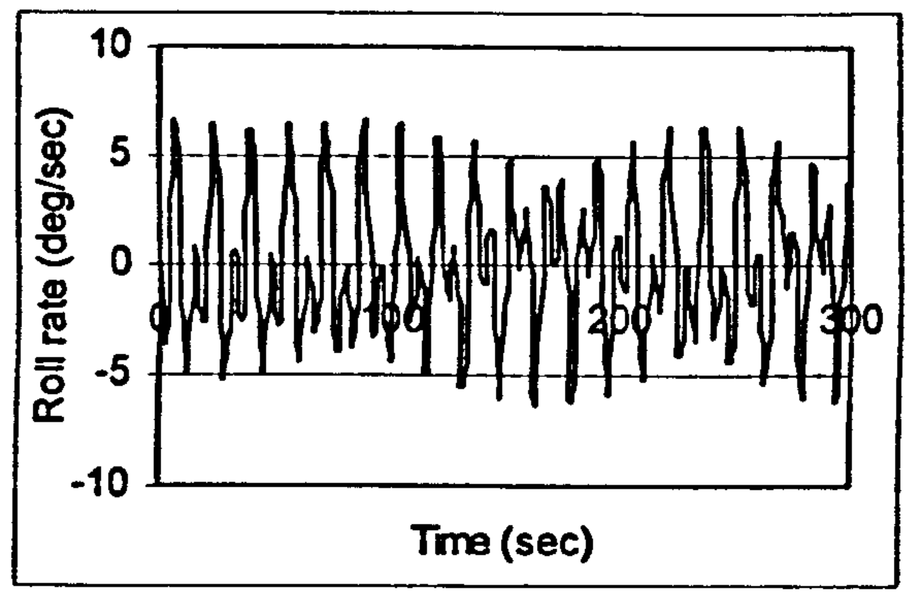

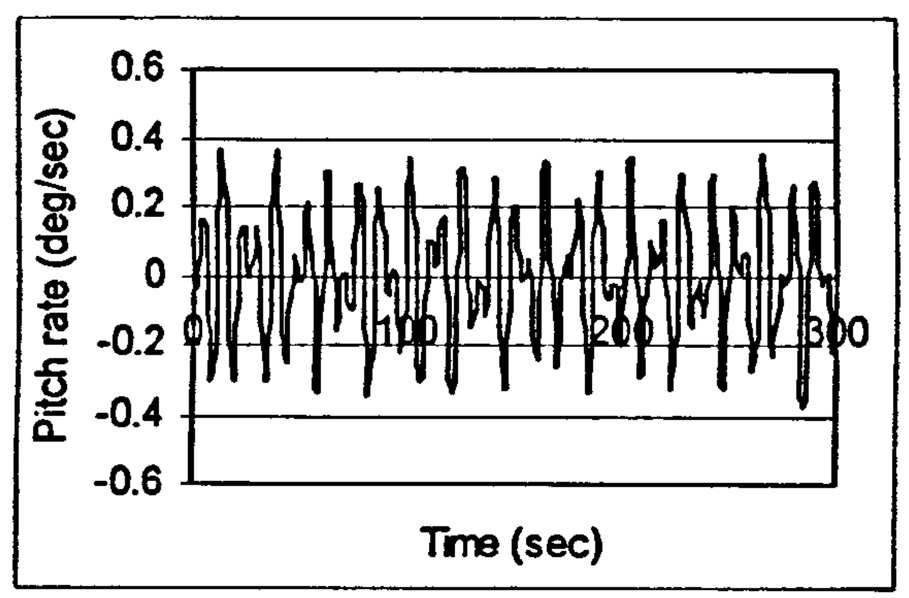

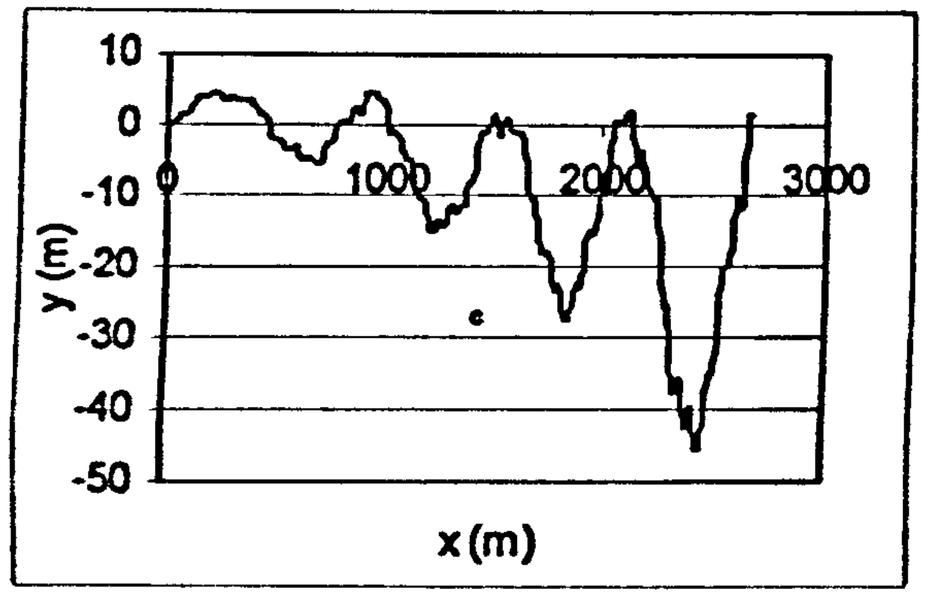

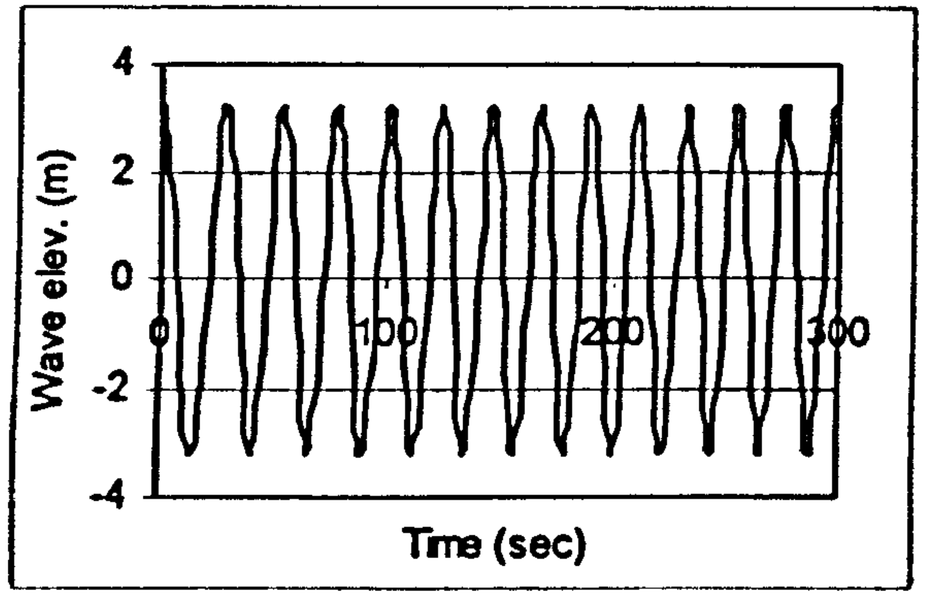

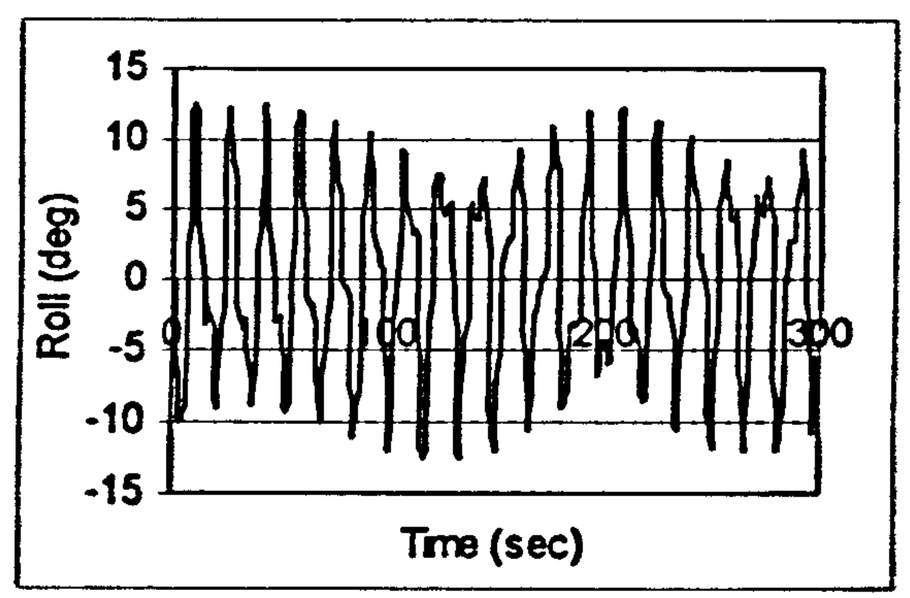

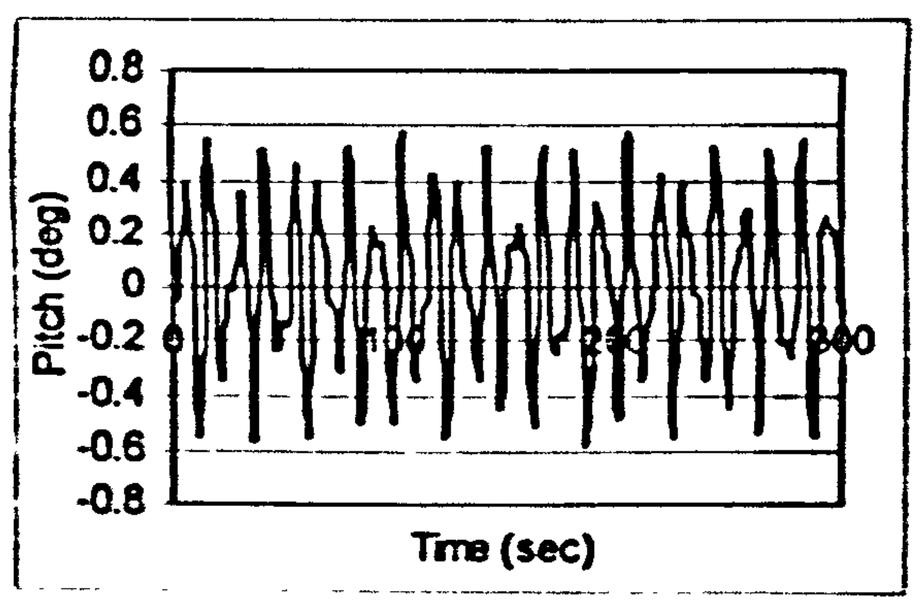

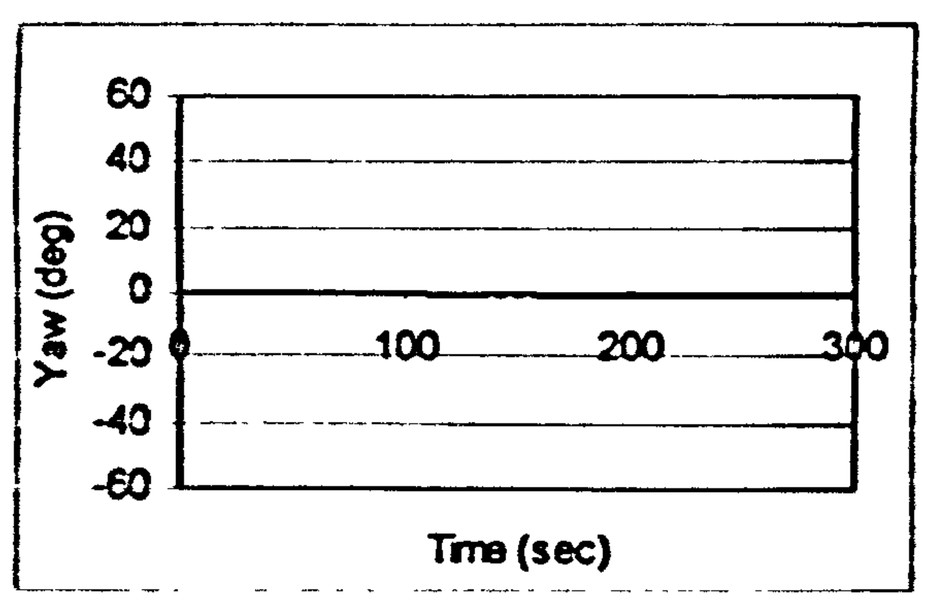

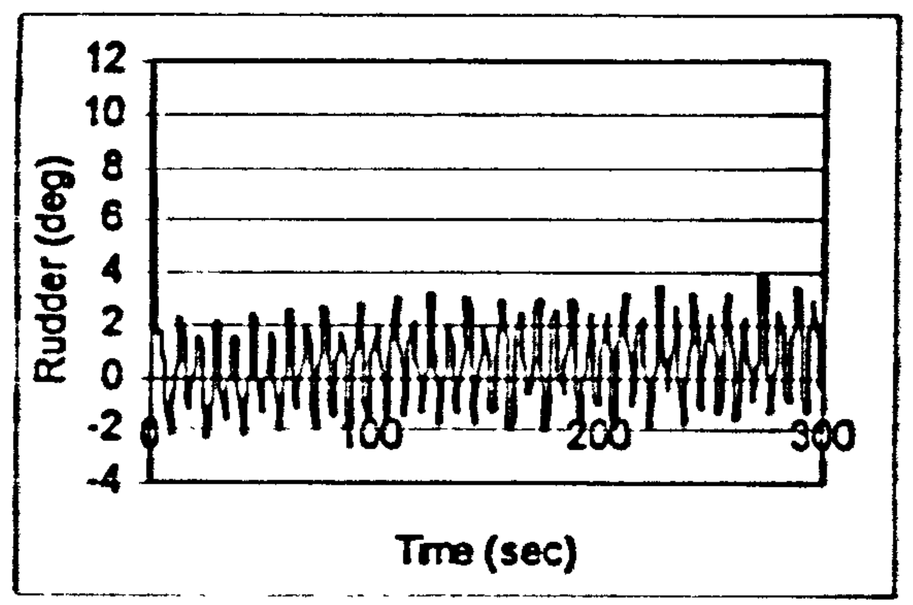

Figure G.6 Numerical Simulation of Ship A-1 with 4 DOF mathematical model in $H/\lambda=1/35$, $\lambda/L_{pp}=1.5$, $Fn=0.3$, $\chi_c=0$ degrees

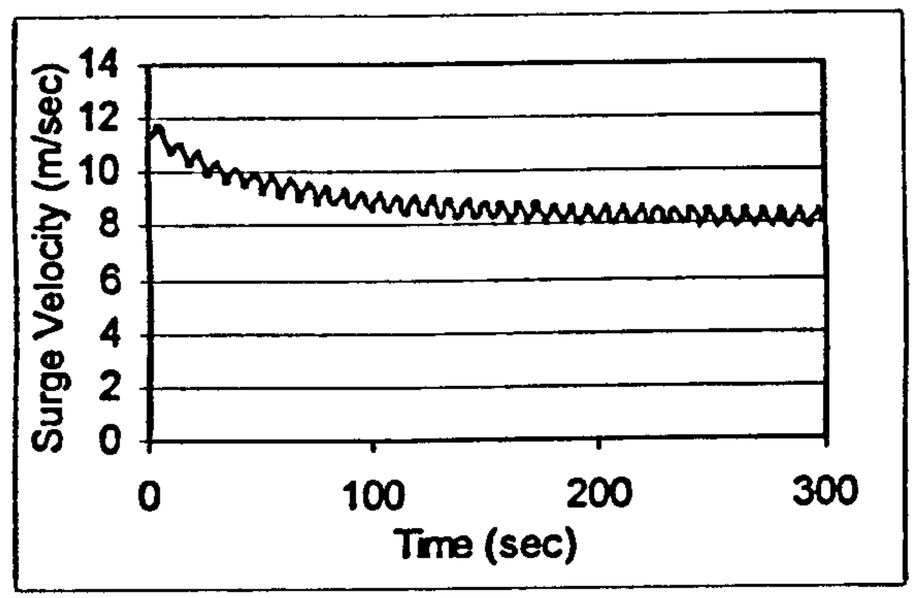

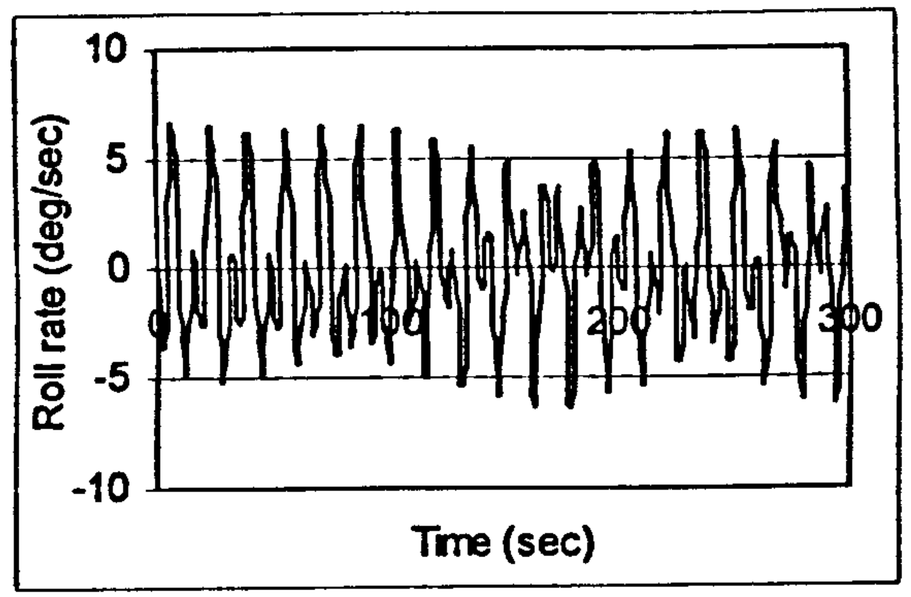

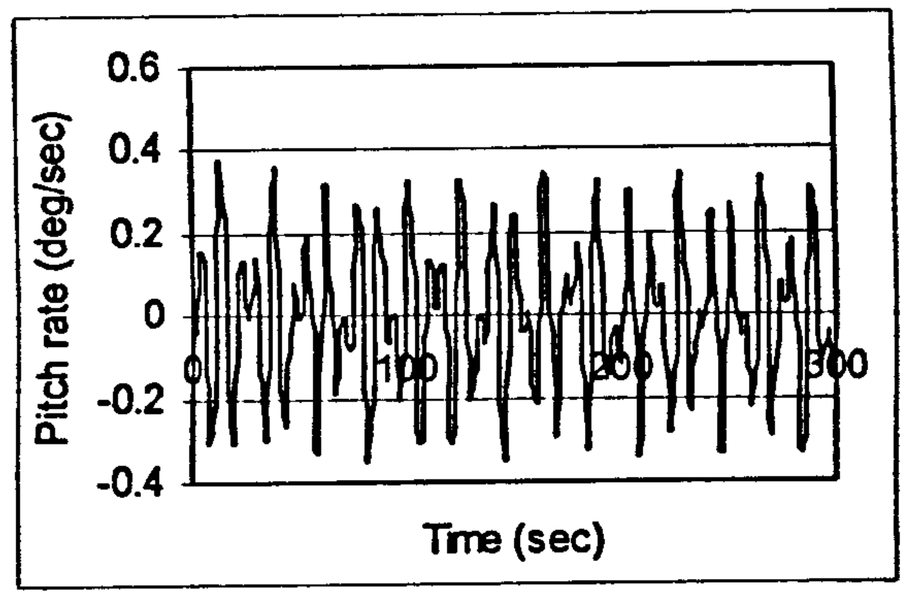

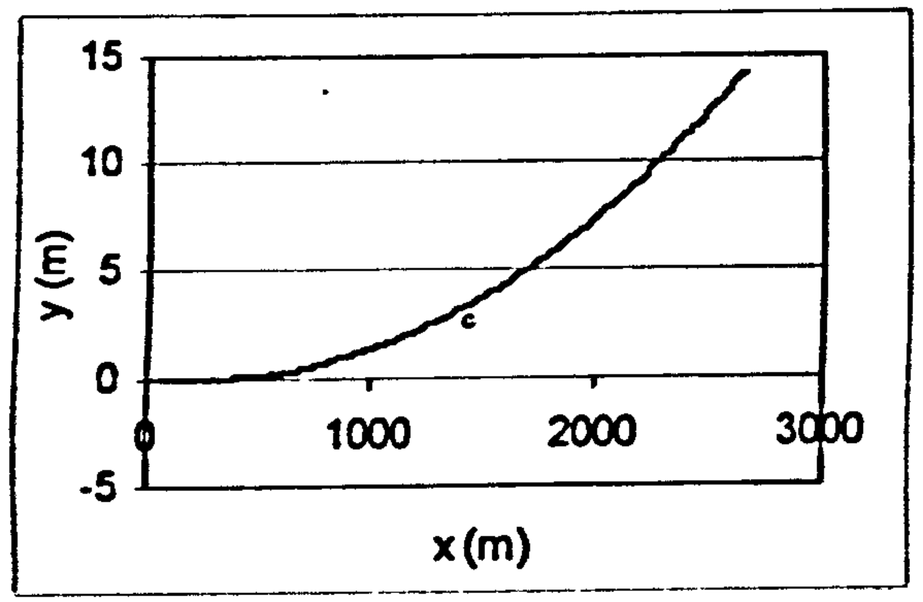

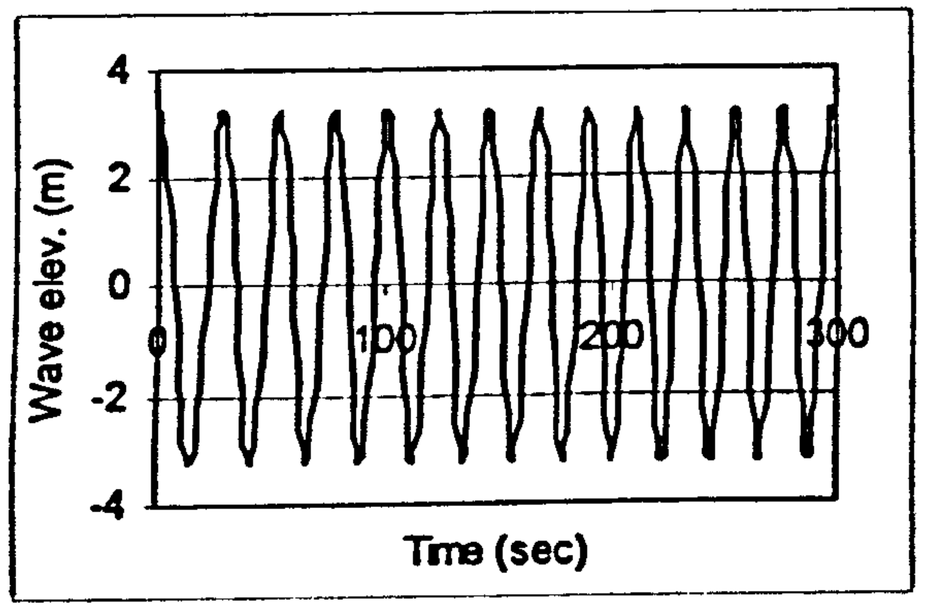

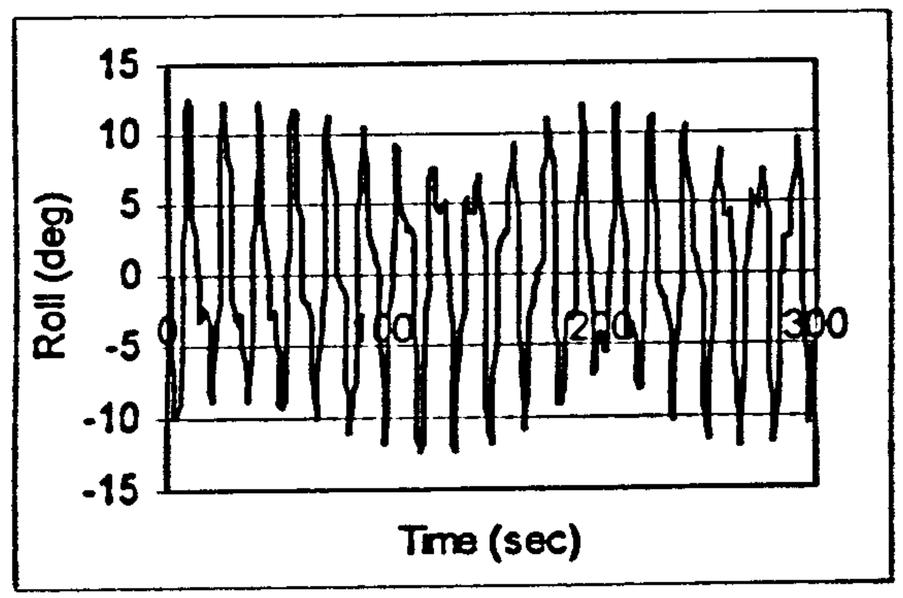

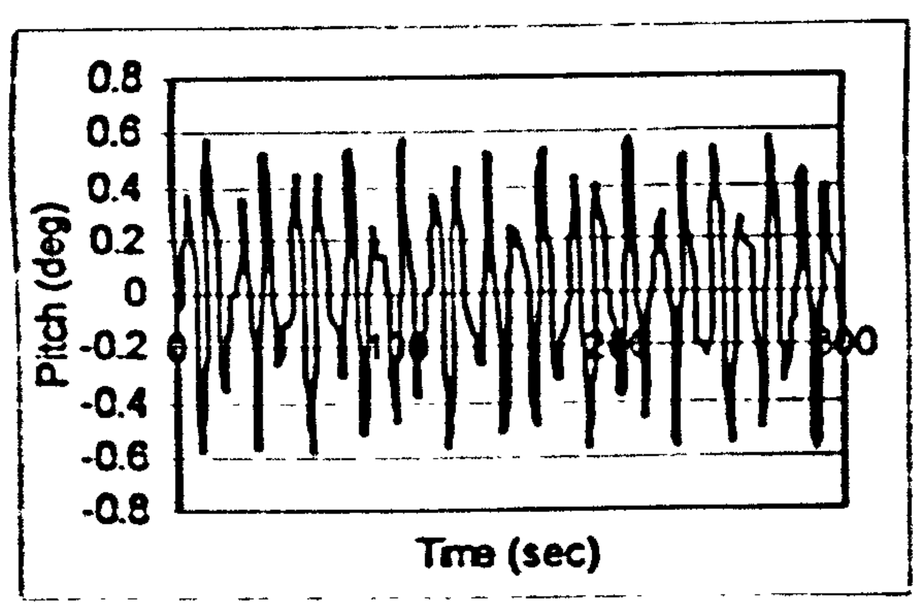

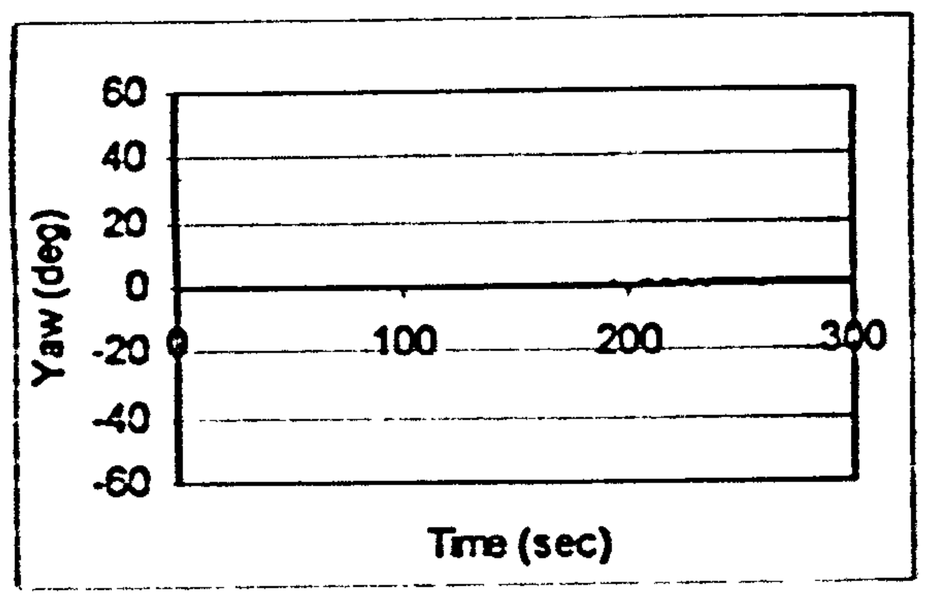

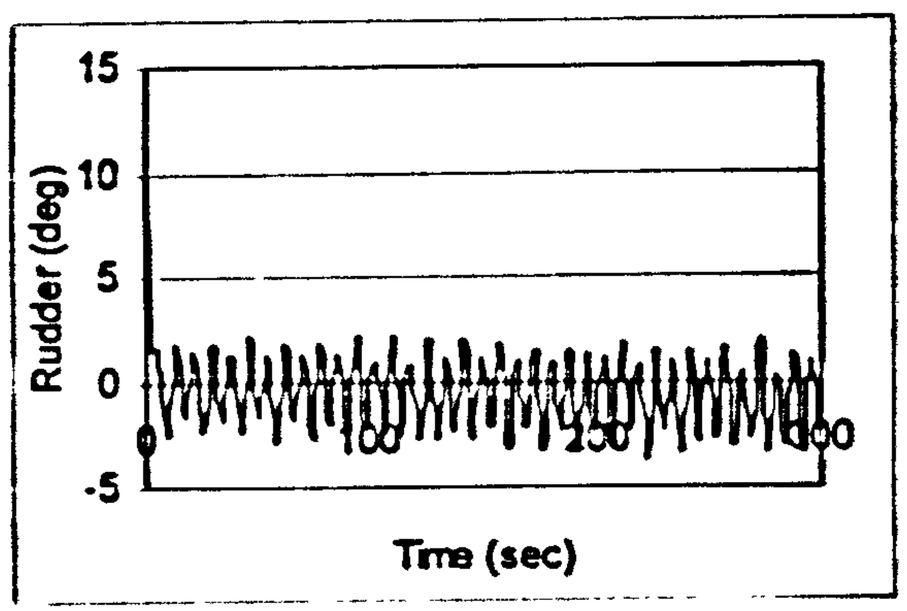

FigureG.7 Numerical Simulation of Ship A-1 with 6 DOF mathematical model in $H/\lambda=1/25$, $\lambda/L_{pp}=1.5$, Fn=0.3,χ_c=30 degrees

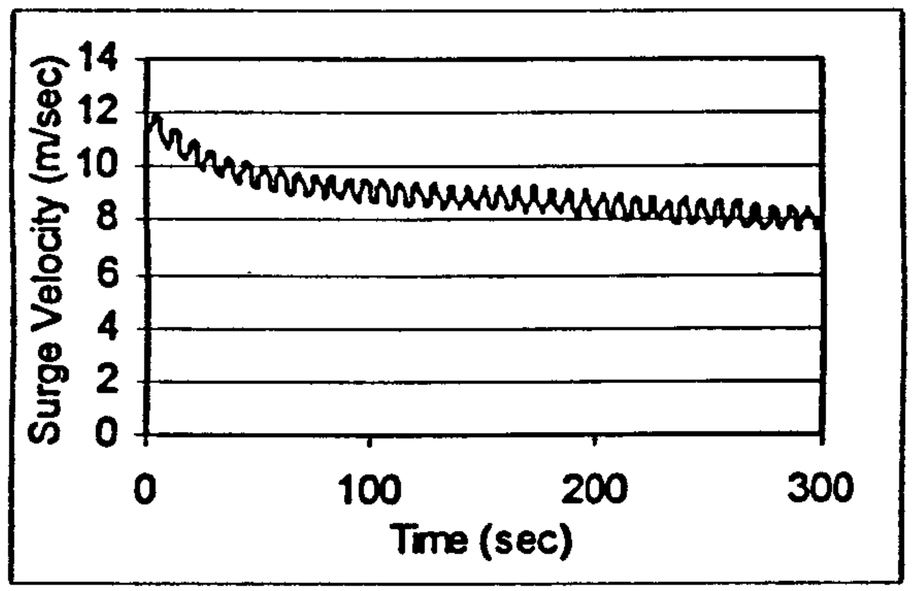

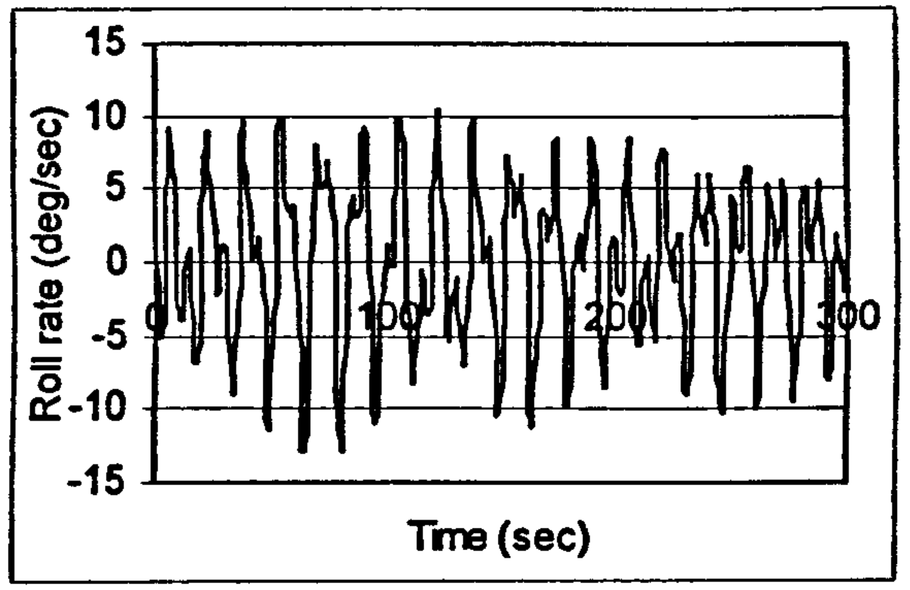

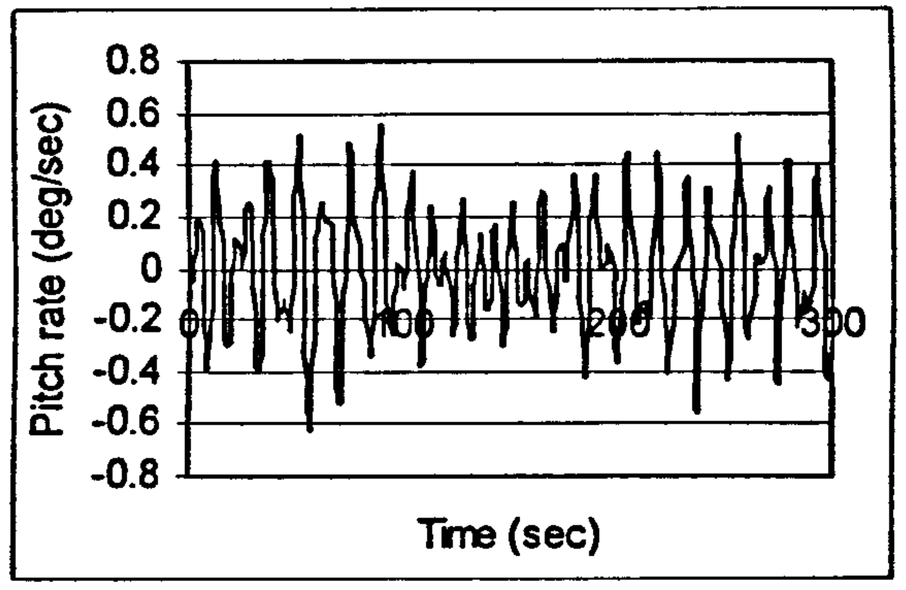

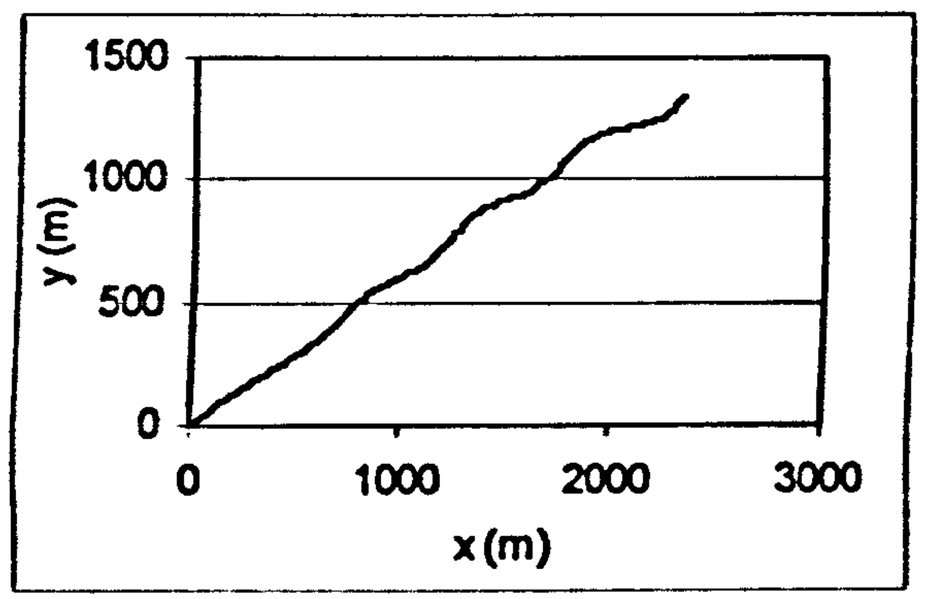

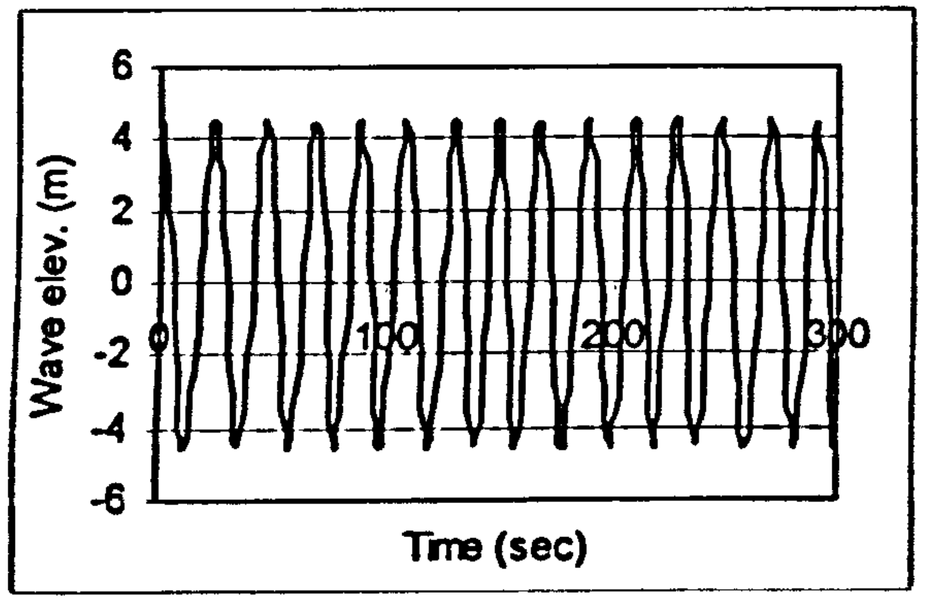

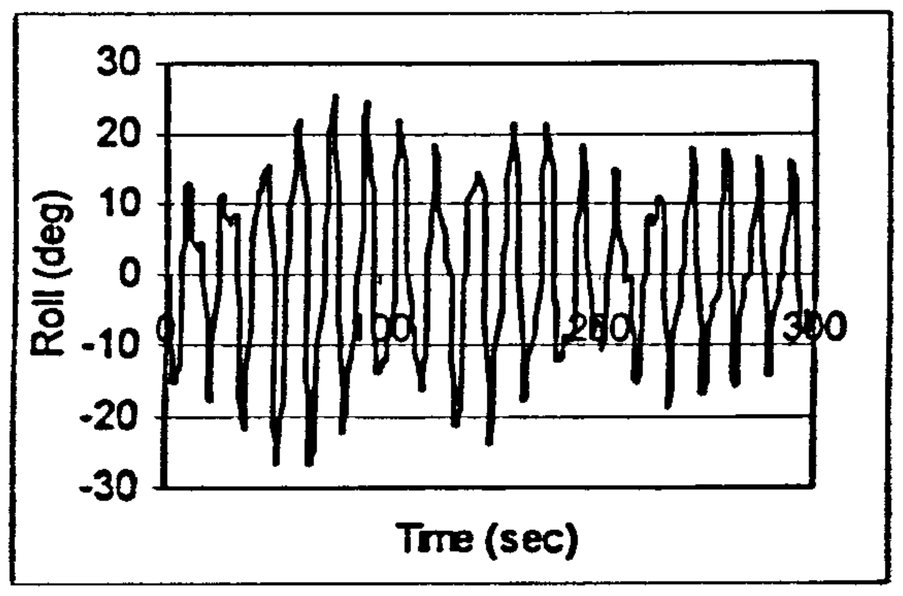

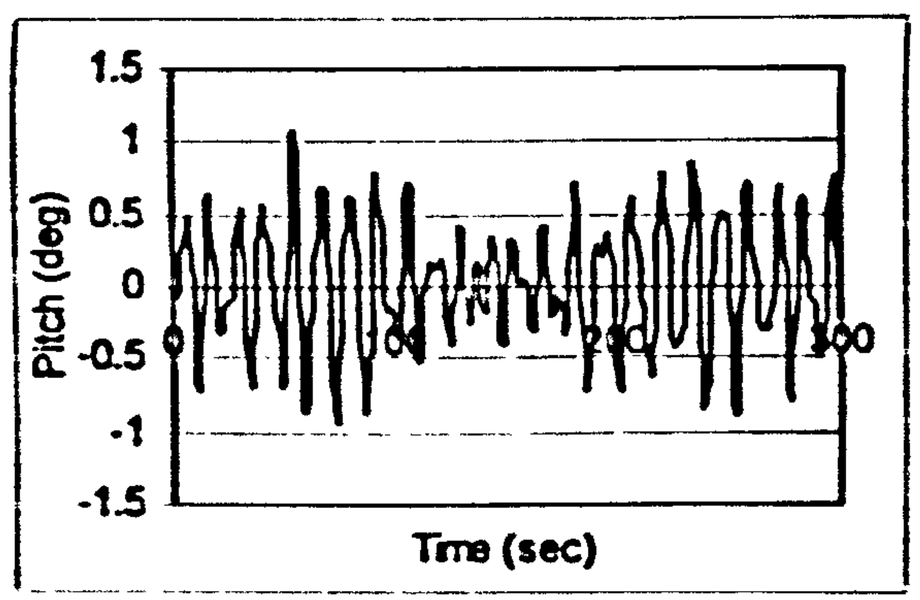

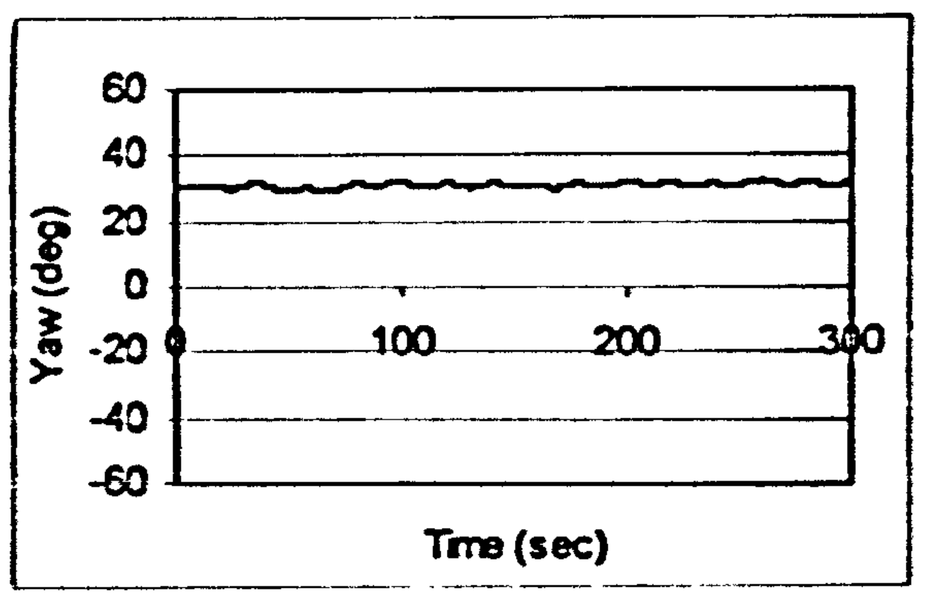

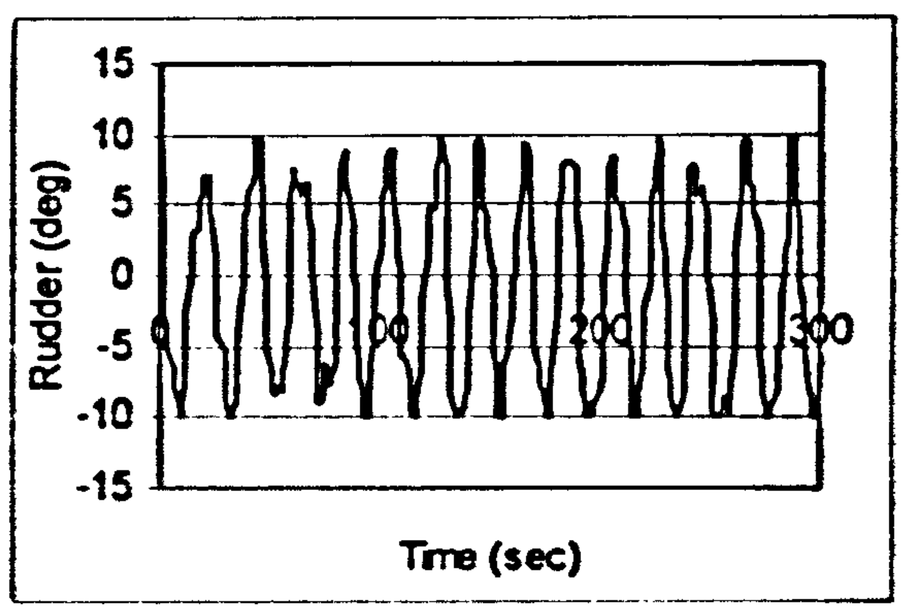

Figure G.8 Numerical Simulation of Ship A-1 with 4 DOF mathematical model in $H/\lambda=1/25$, $\lambda/L_{pp}=1.5$, Fn=0.3,$\chi_c=30$ degrees

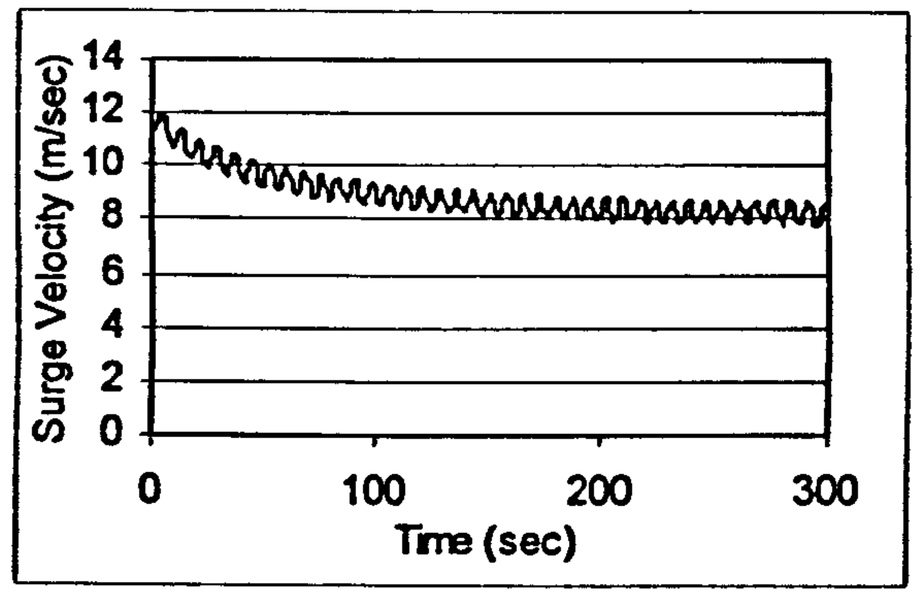

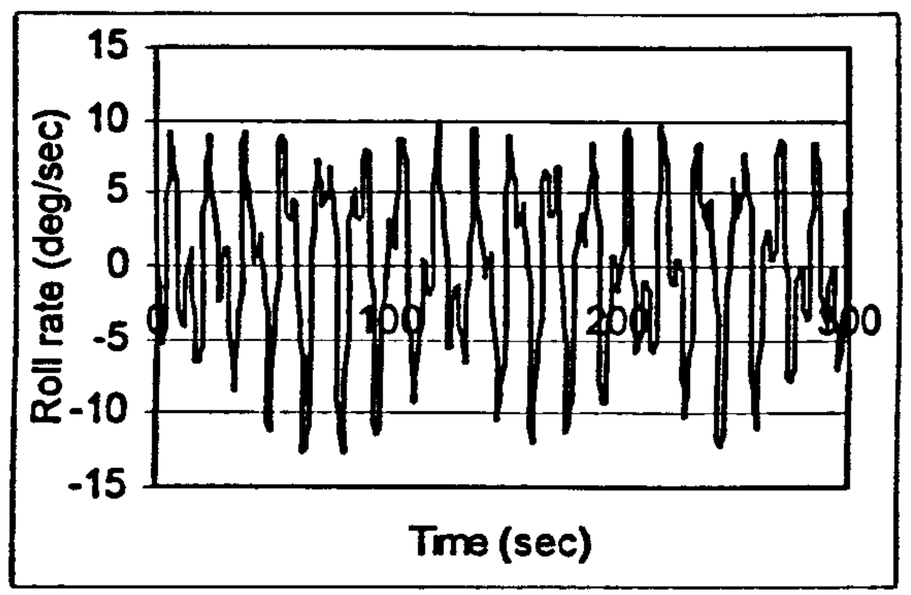

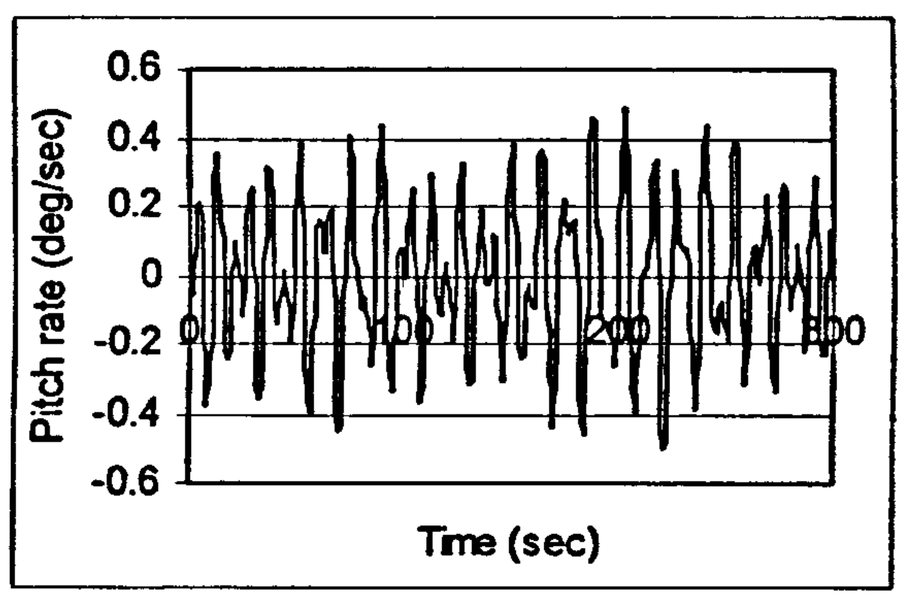

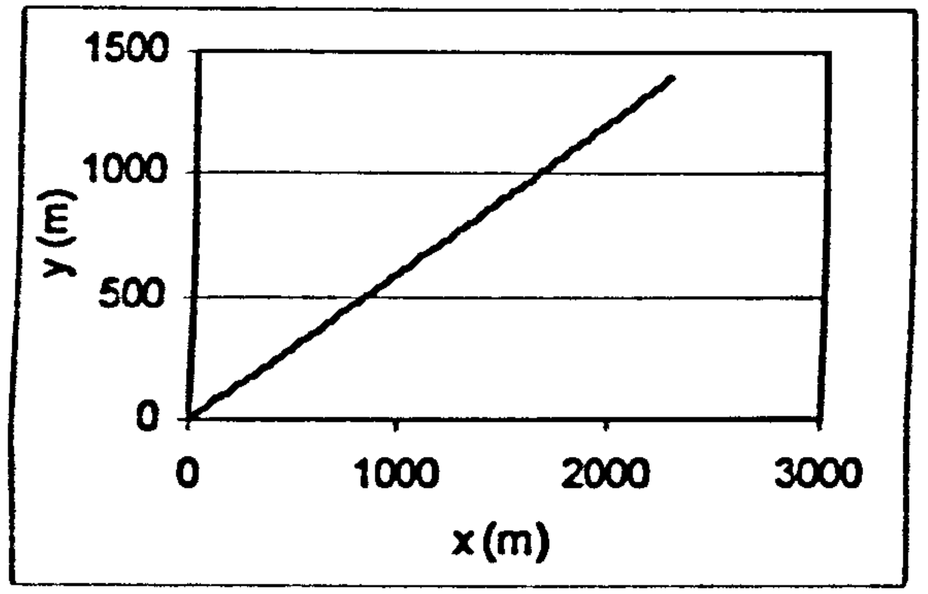

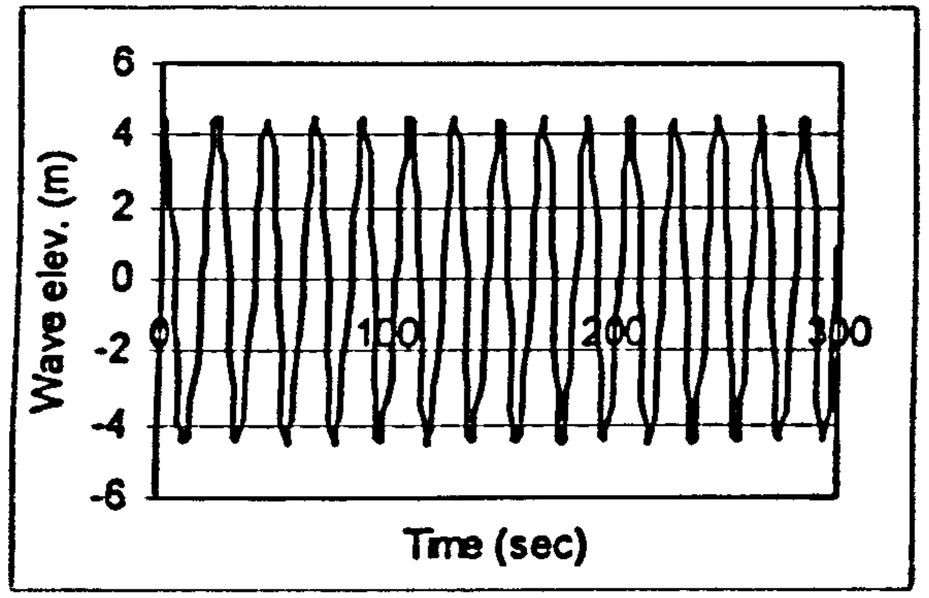

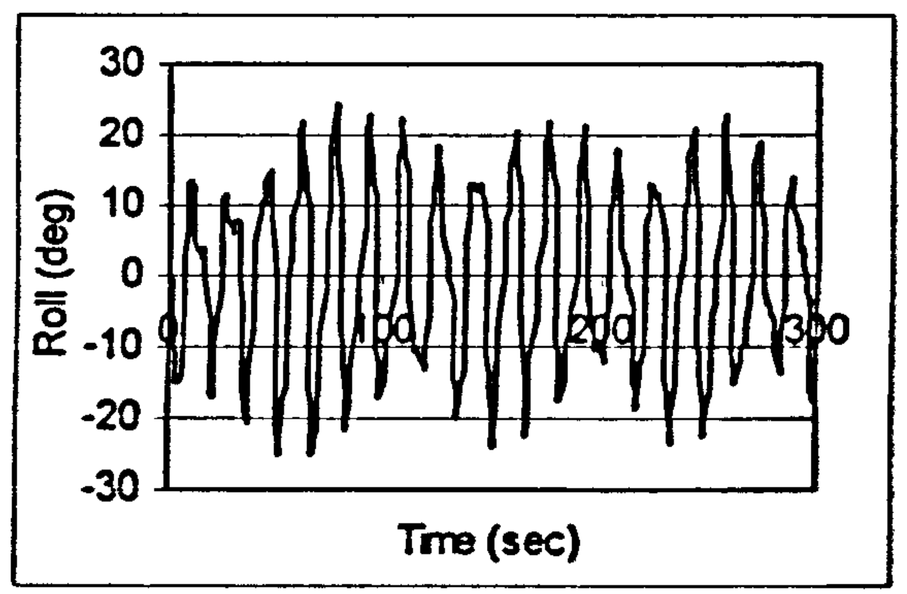

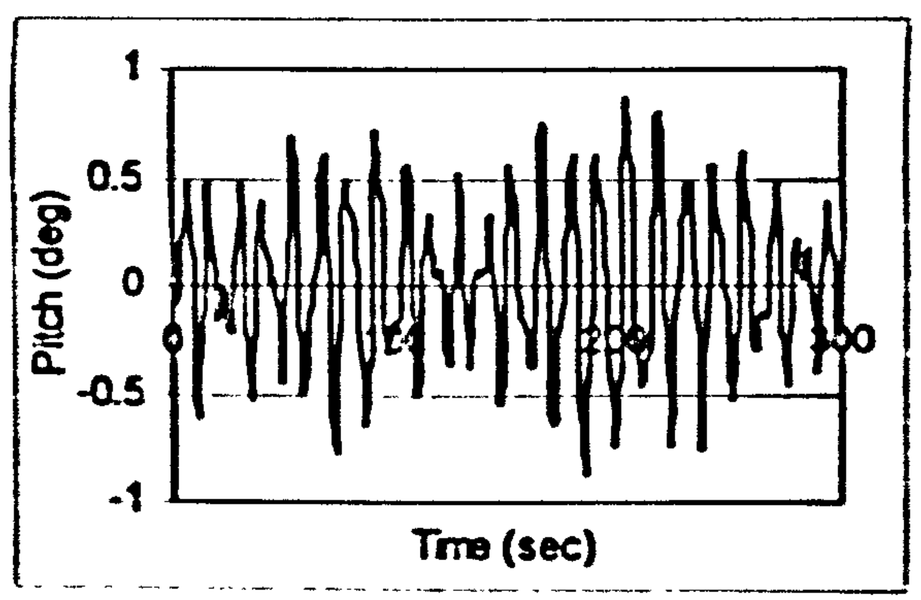

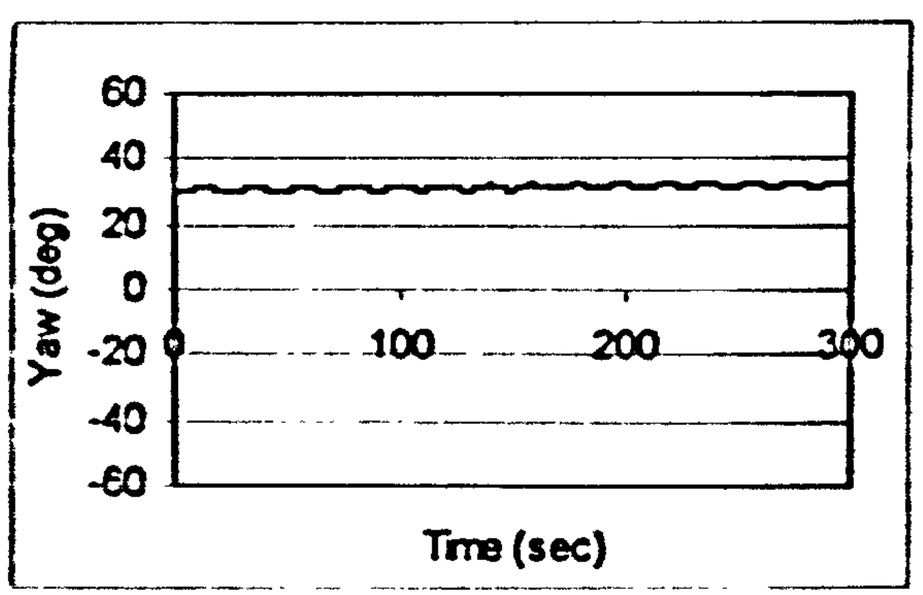

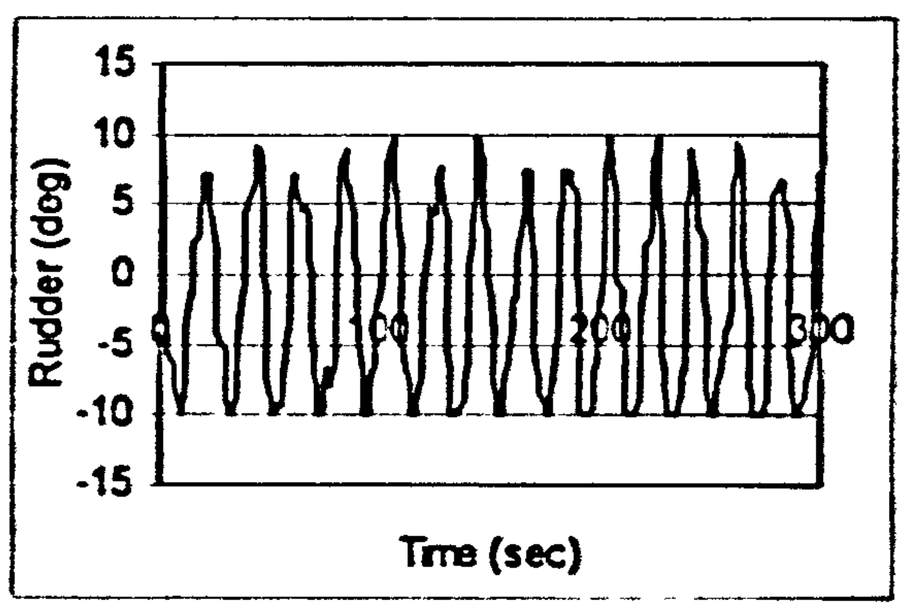

Figure G.9 Numerical Simulation of Ship A-1 with 6 DOF mathematical model in $H/\lambda=1/30$, $\lambda/L_{pp}=1.5$, Fn=0.3,χ_c=30 degrees

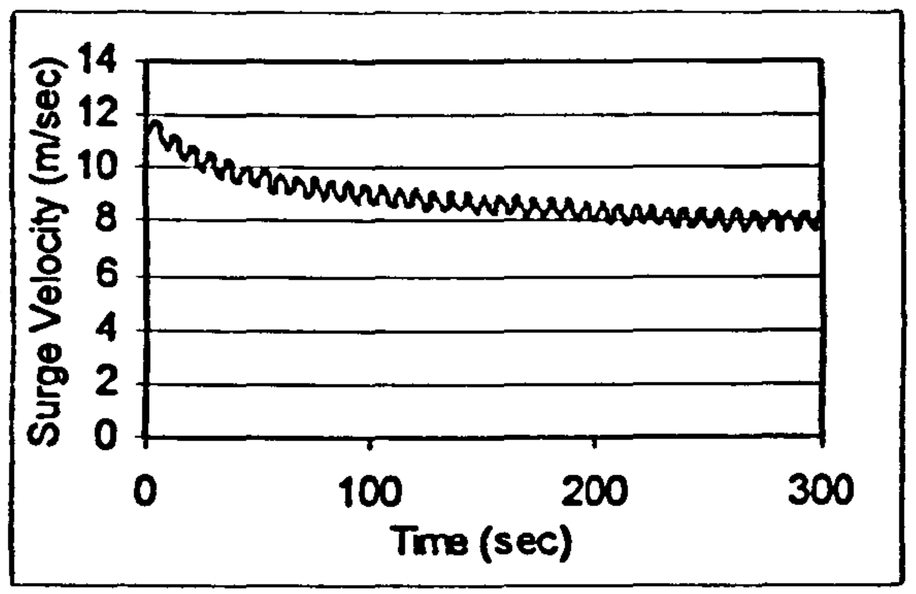

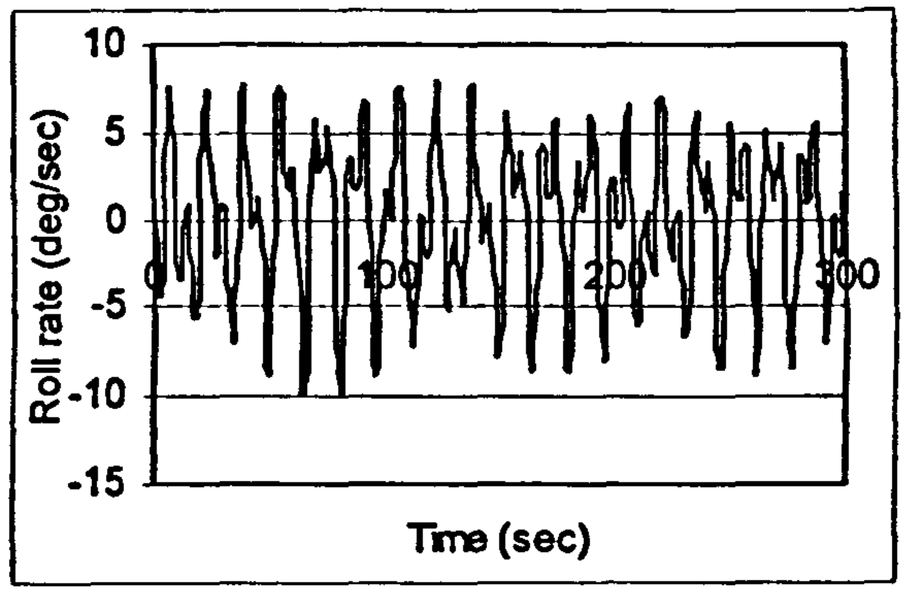

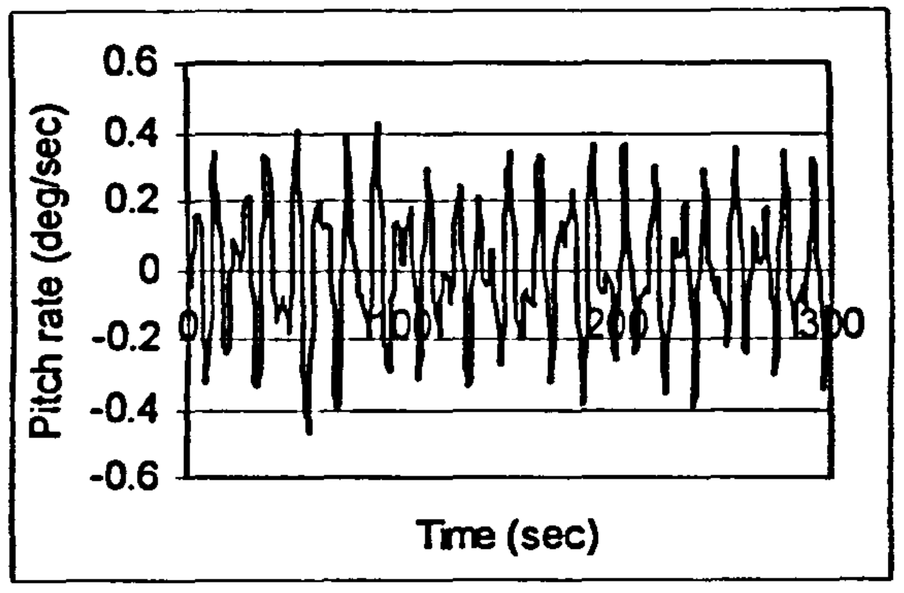

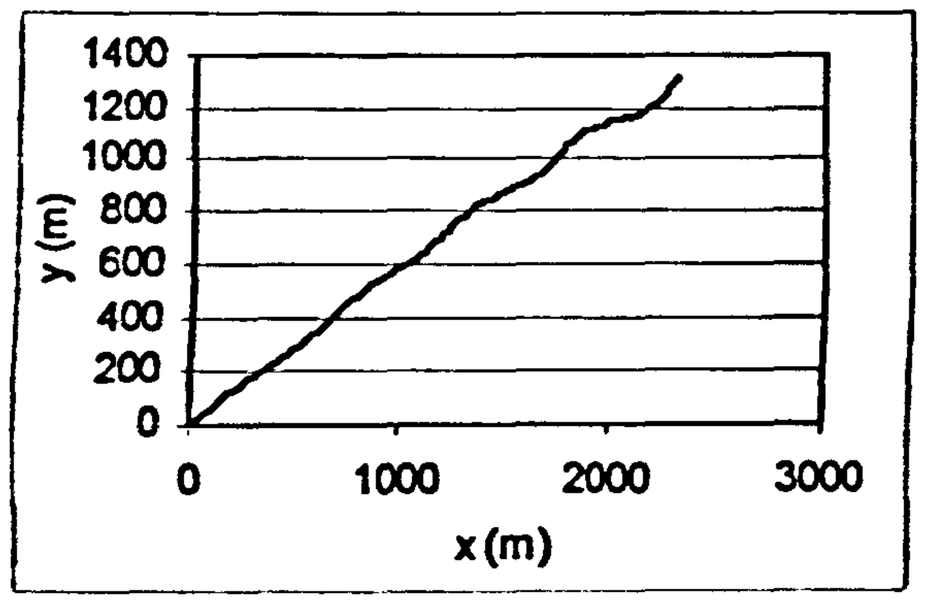

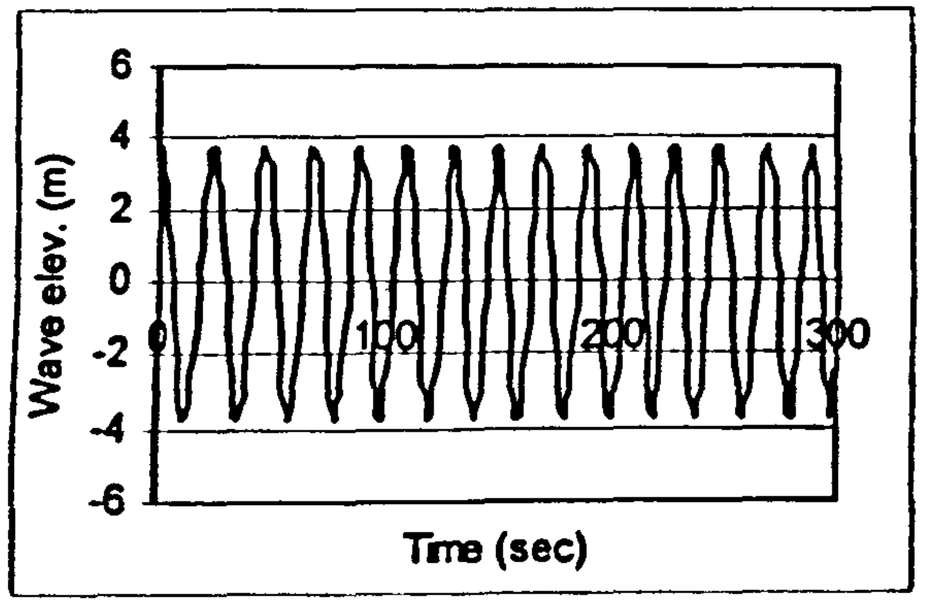

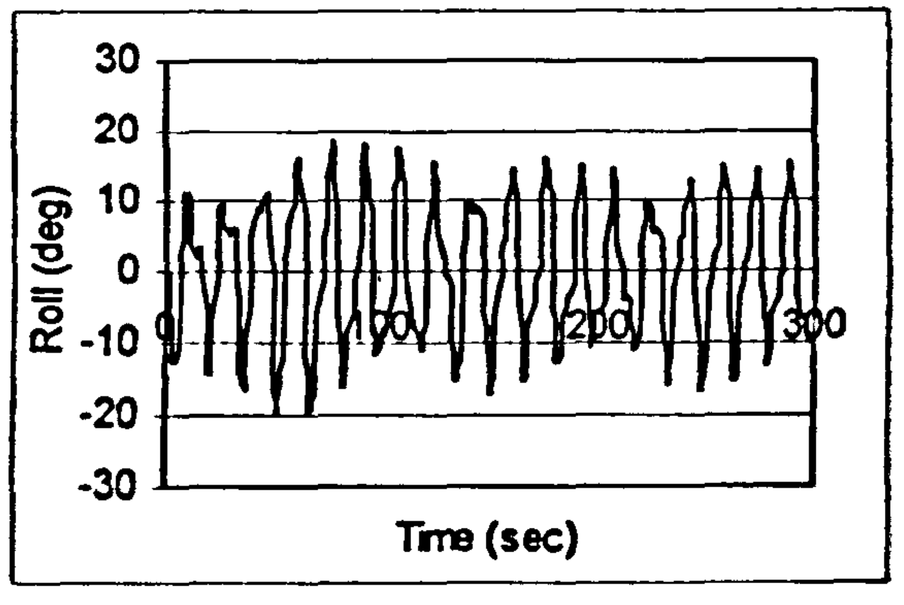

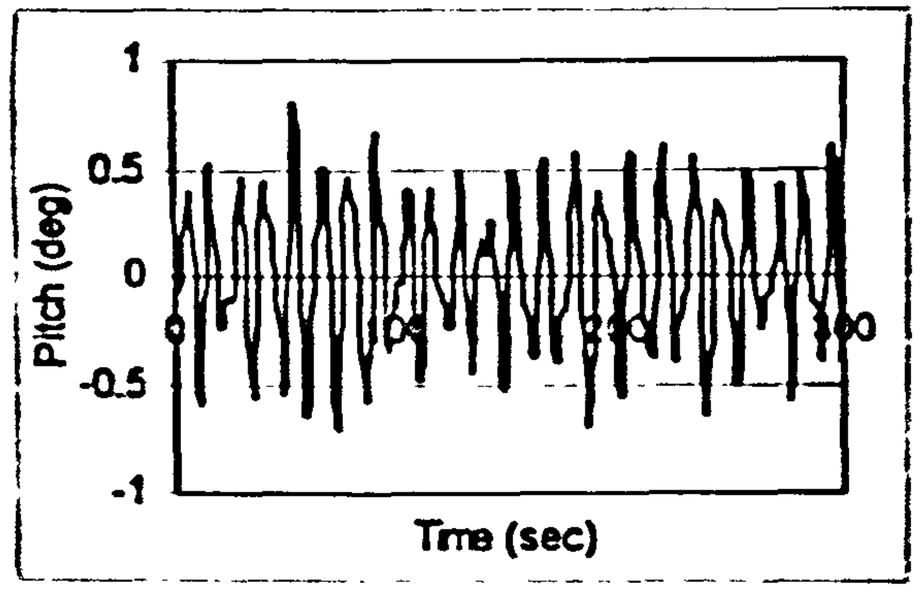

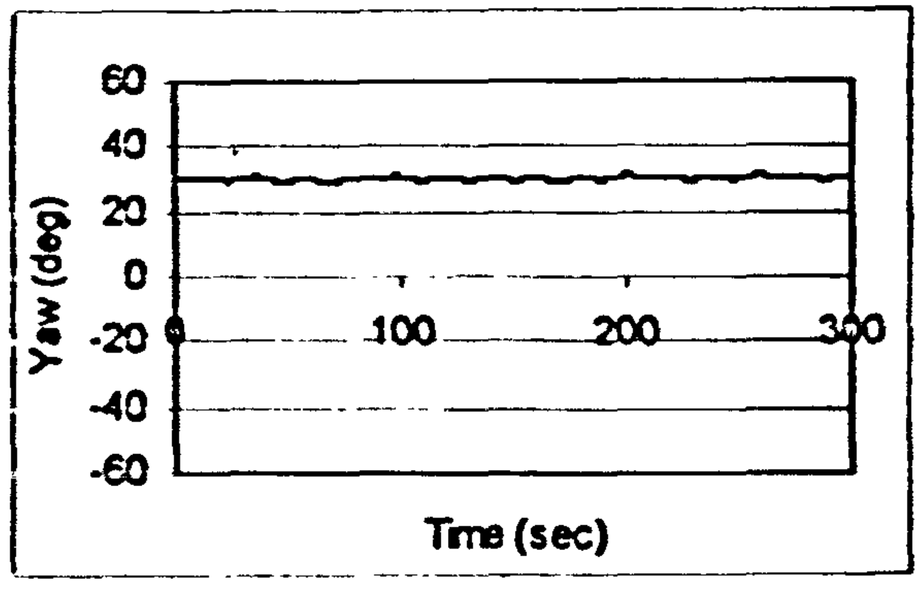

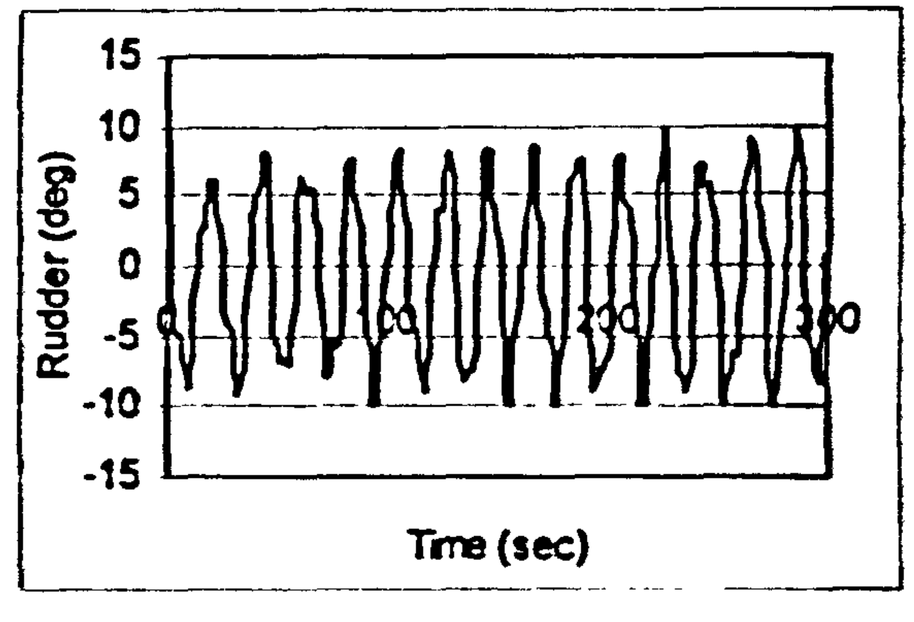

Figure G.10 Numerical Simulation of Ship A-1 with 4 DOF mathematical model in $H/\lambda=1/30$, $\lambda/L_{pp}=1.5$, Fn=0.3,$\chi_c=30$ degrees

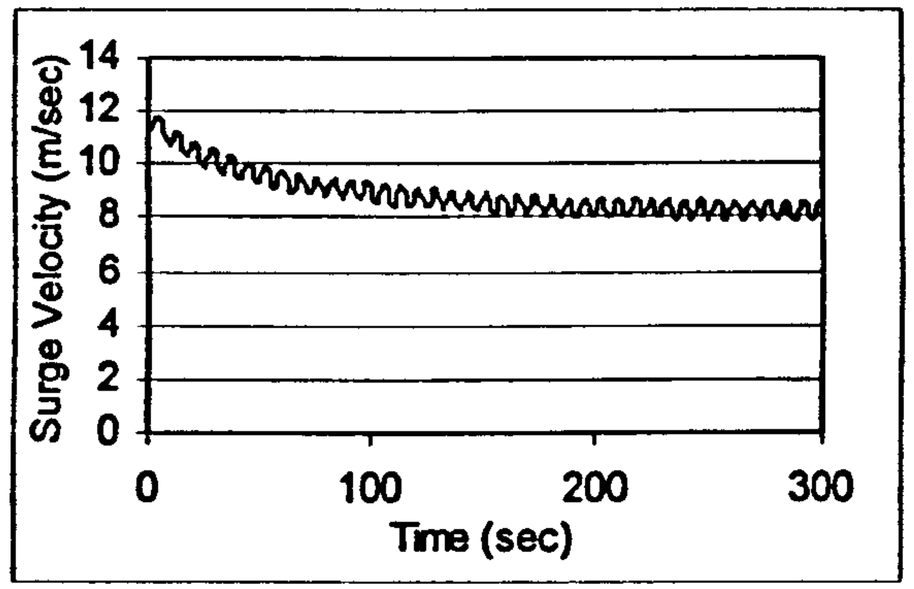

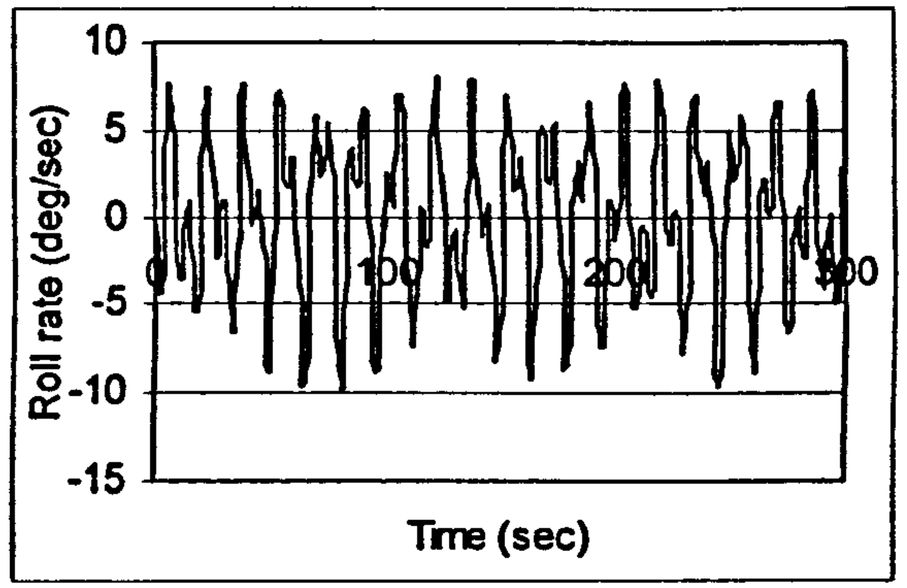

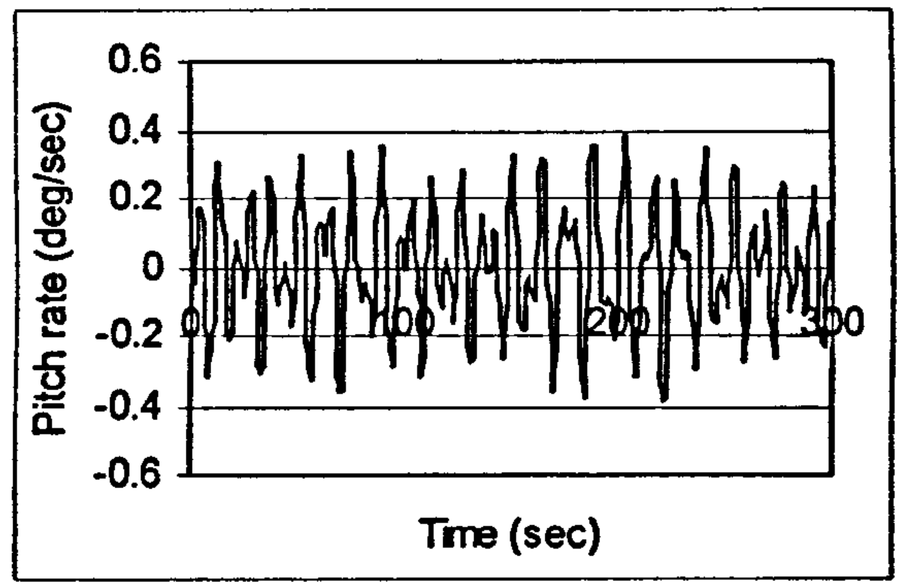

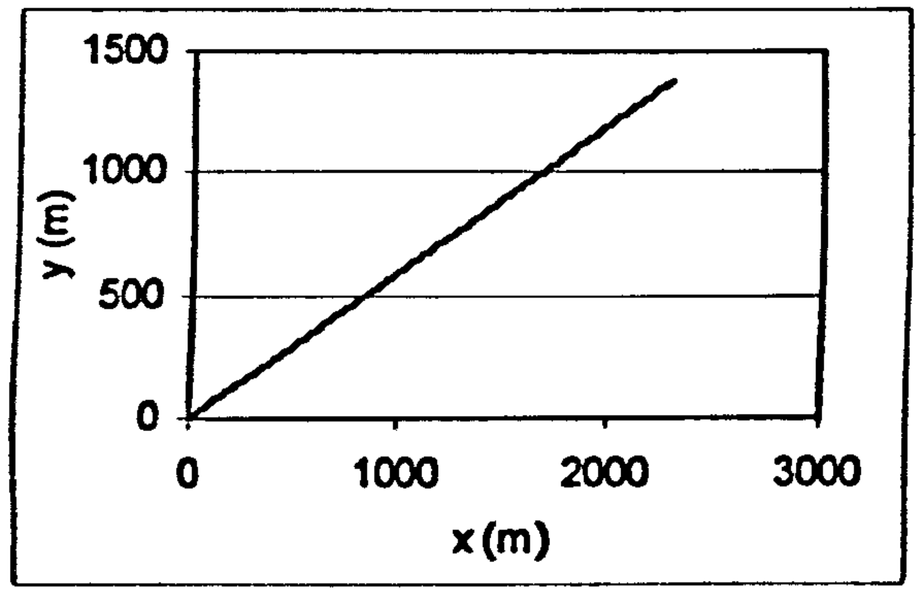

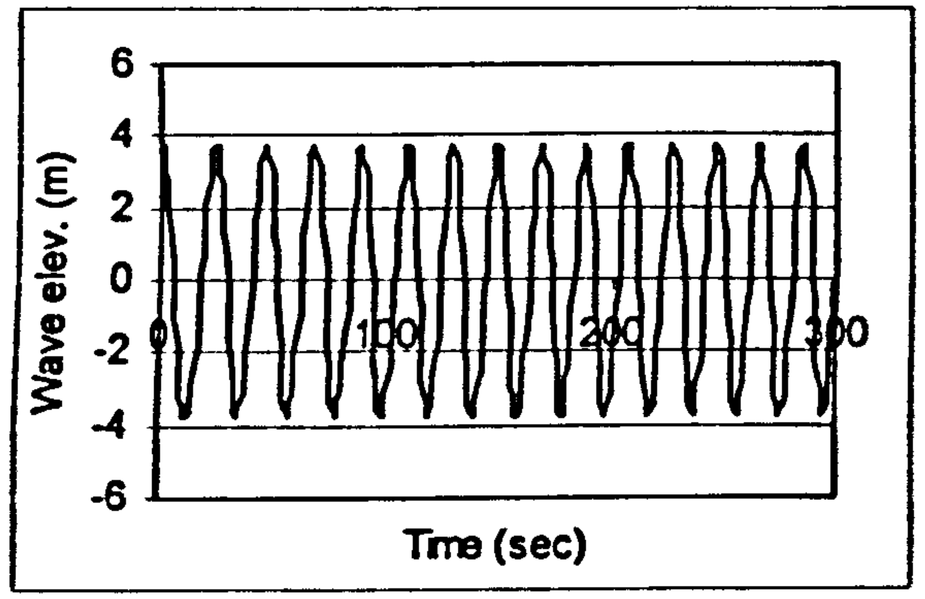

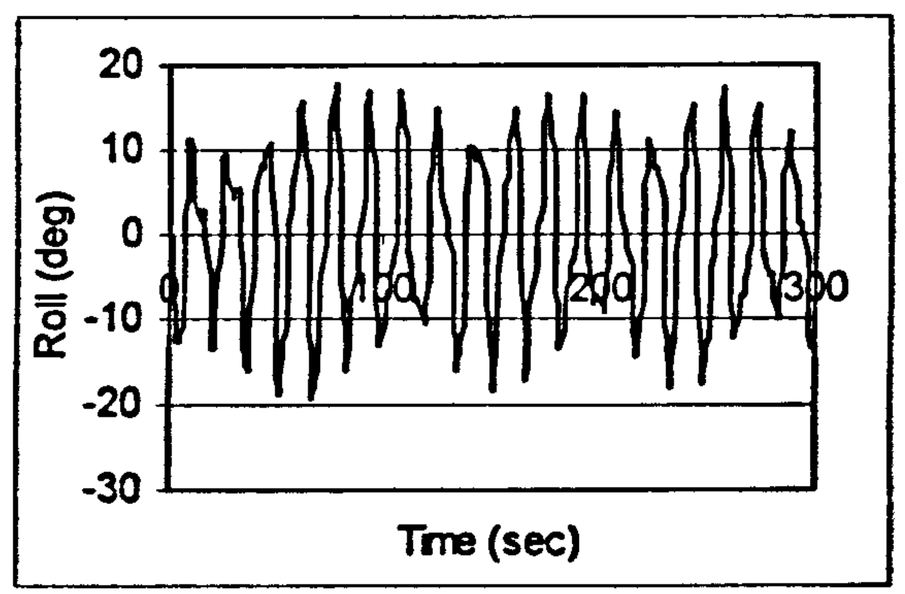

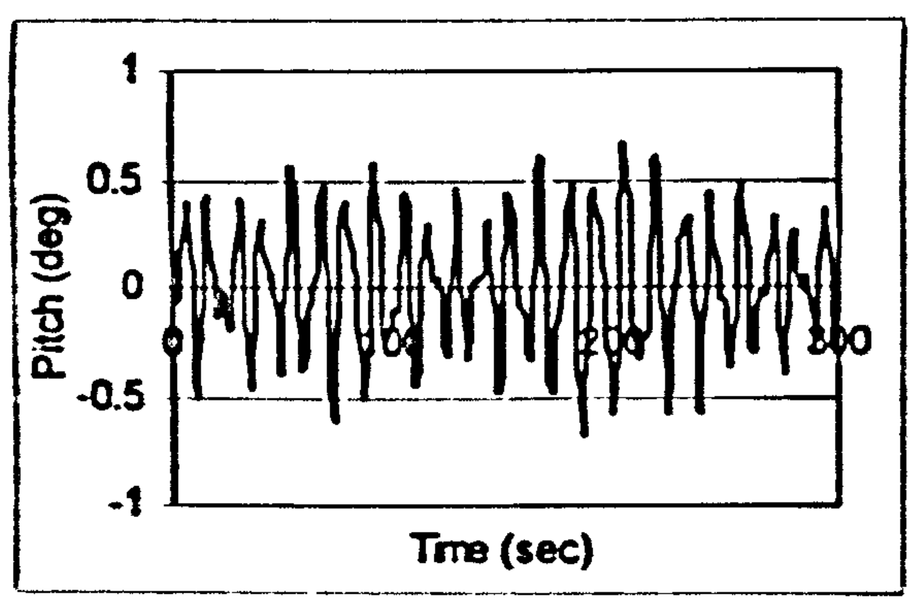

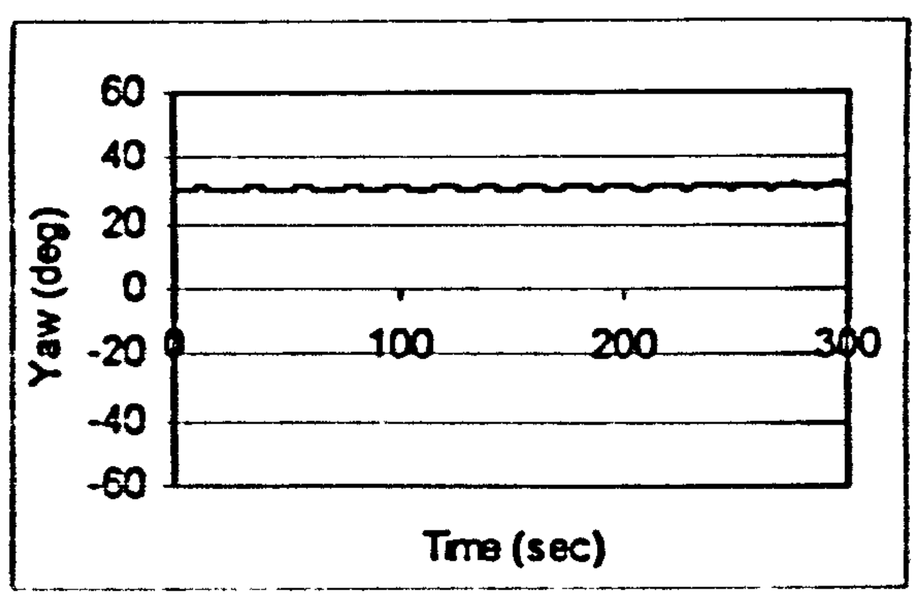

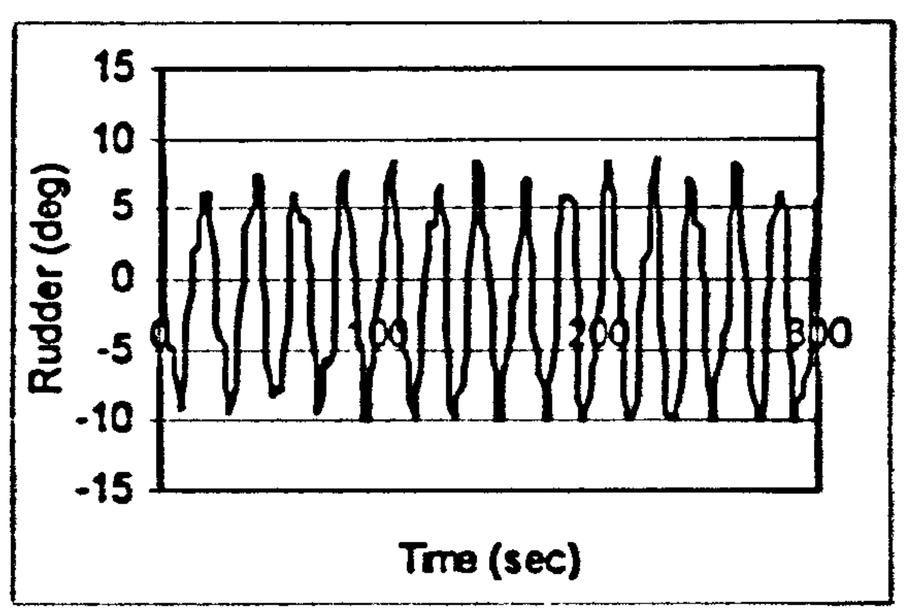

Figure G.11 Numerical Simulation of Ship A-1 with 6 DOF mathematical model in $H/\lambda=1/35$, $\lambda/L_{pp}=1.5$, $Fn=0.3$, $\chi_c=30$ degrees

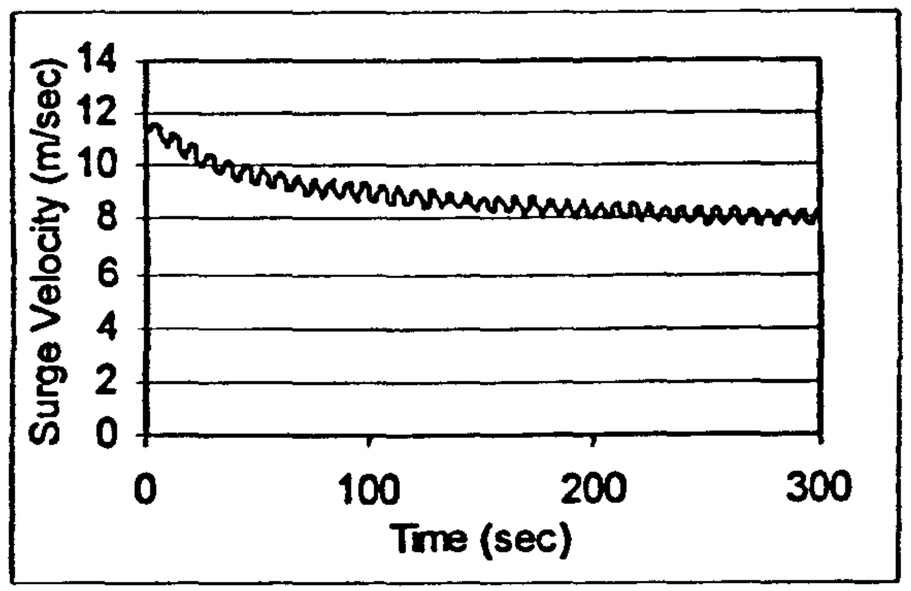

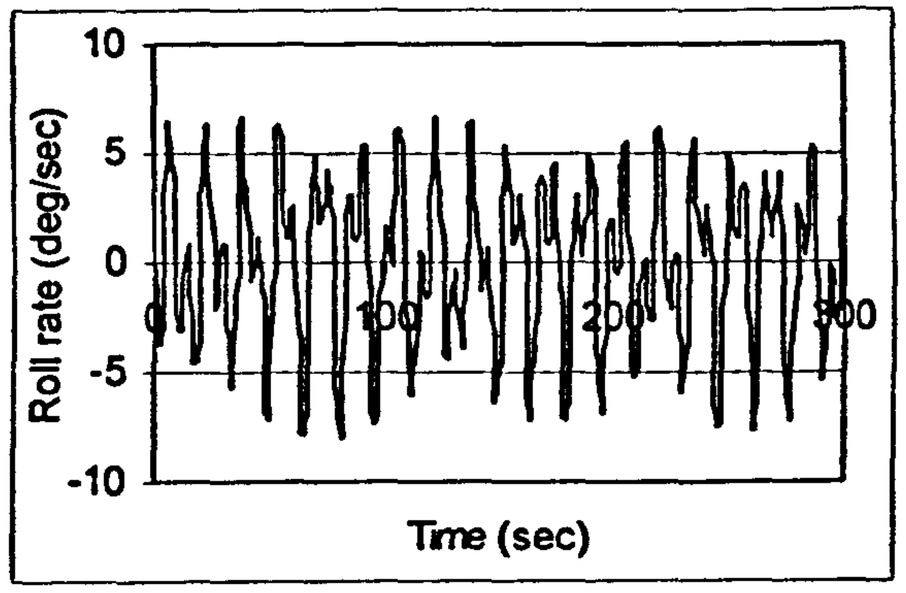

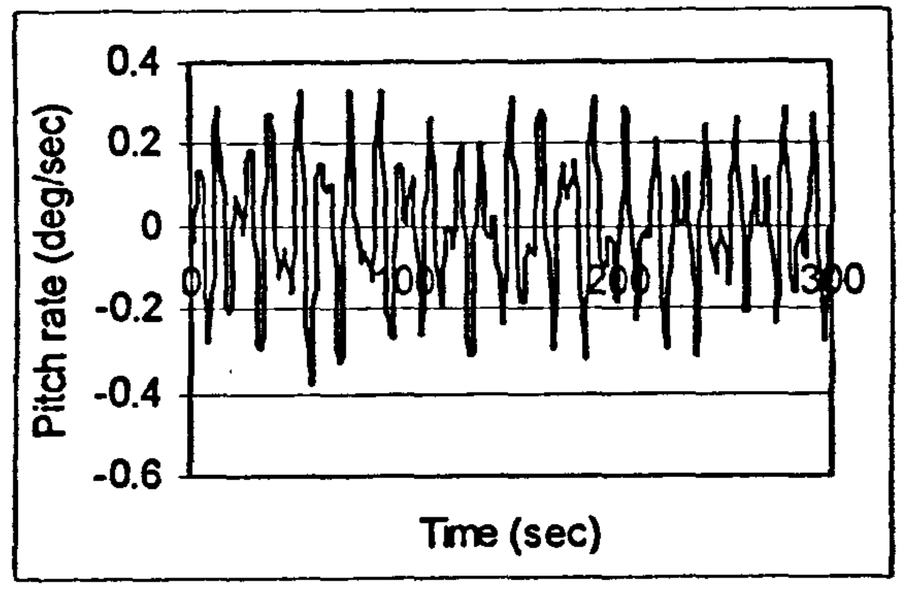

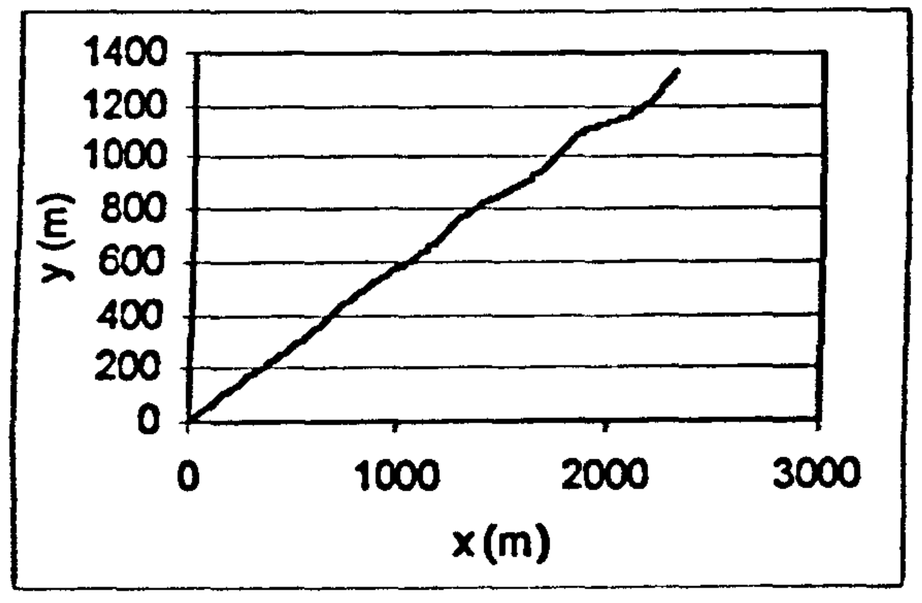

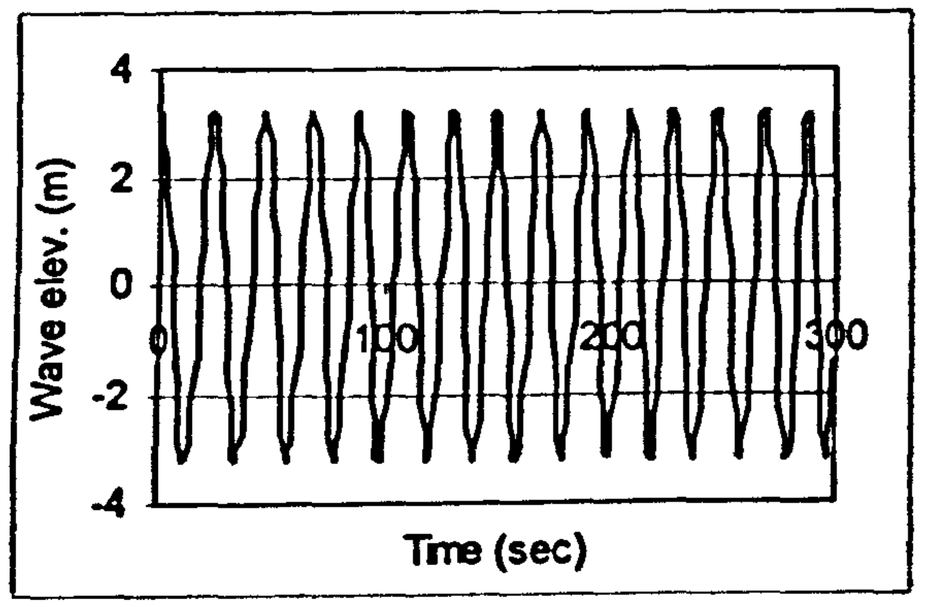

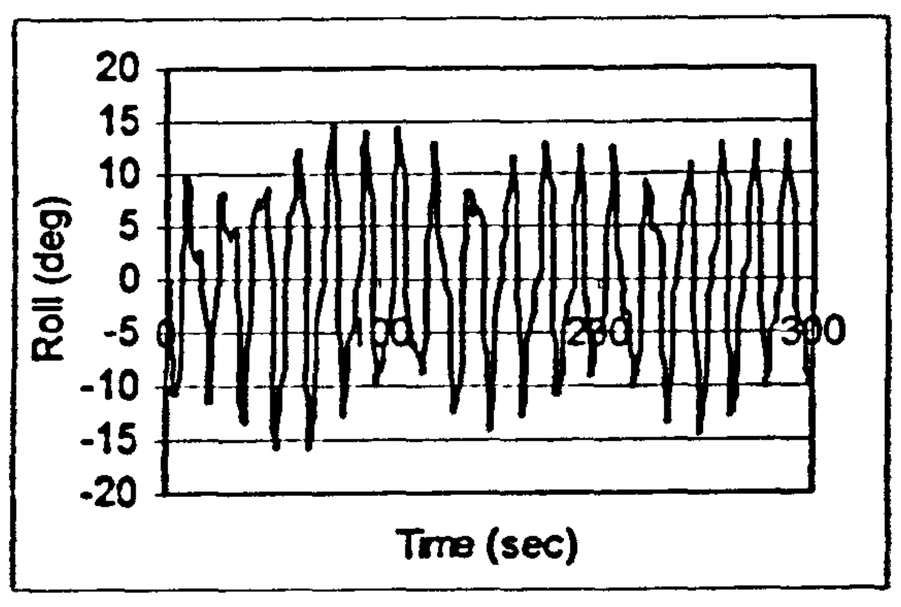

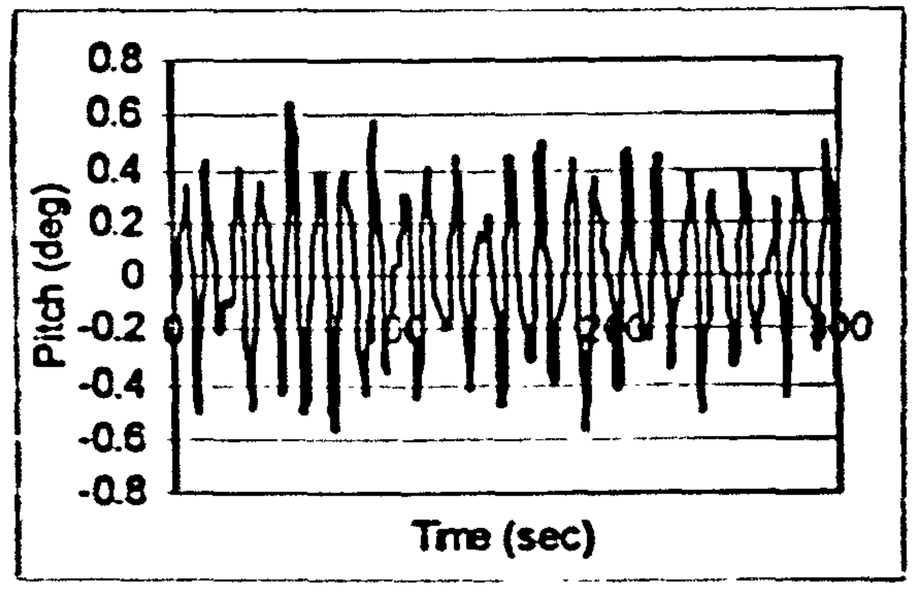

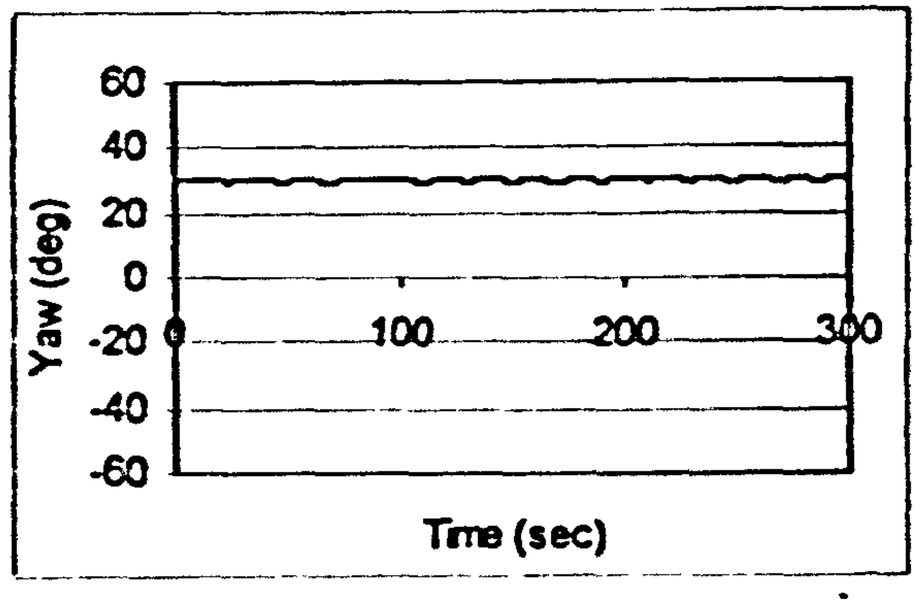

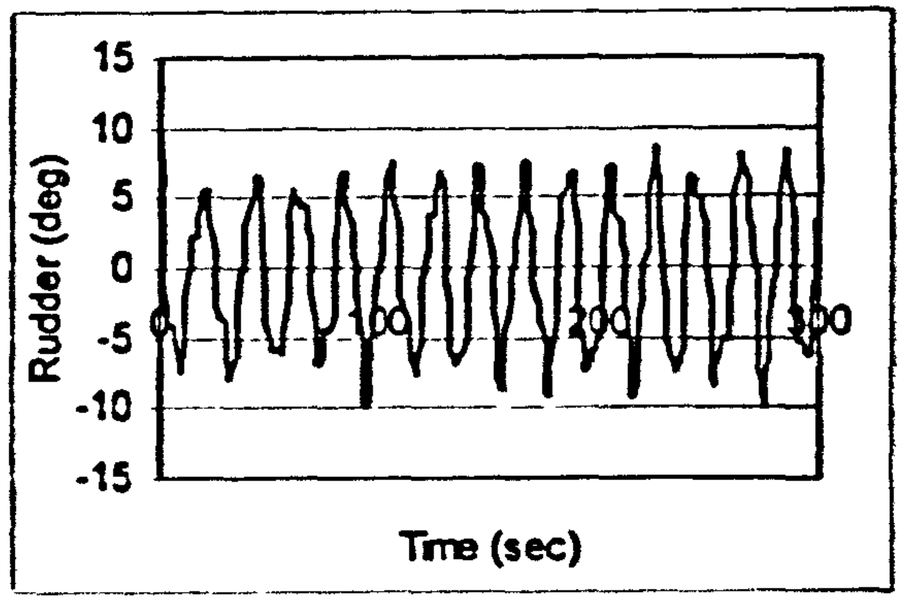

Figure G.12 Numerical Simulation of Ship A-1 with 4 DOF mathematical model in $H/\lambda=1/35$, $\lambda/L_{pp}=1.5$, Fn=0.3,$\chi_c=30$ degrees

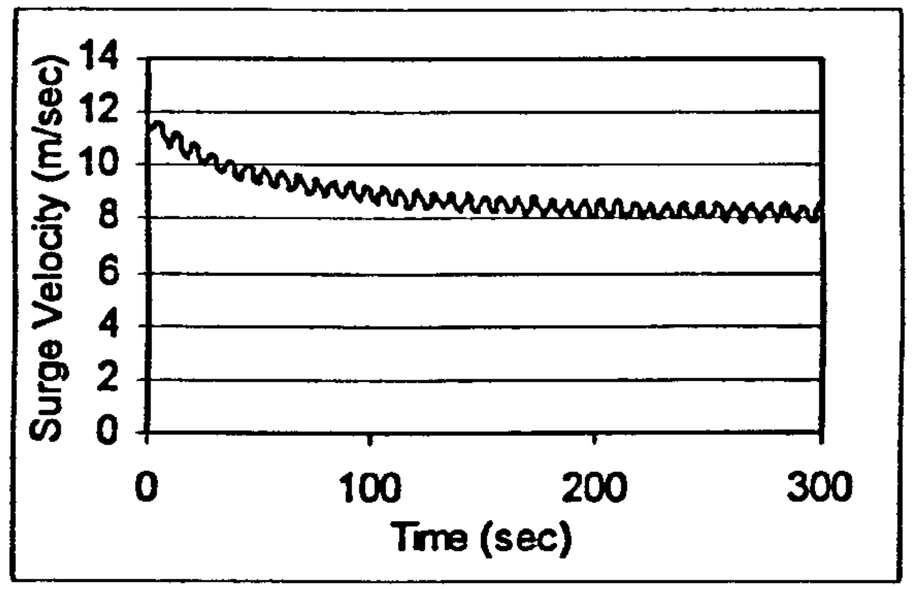

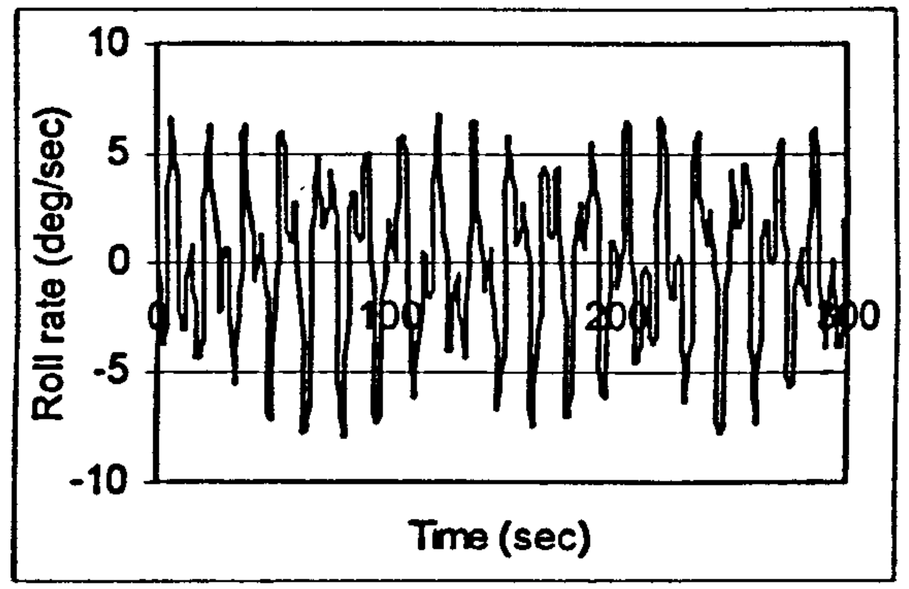

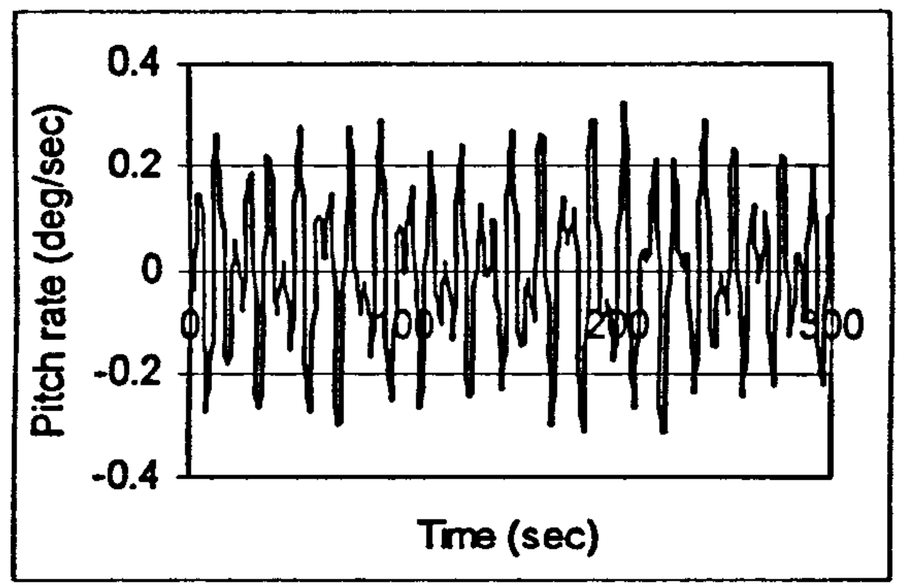

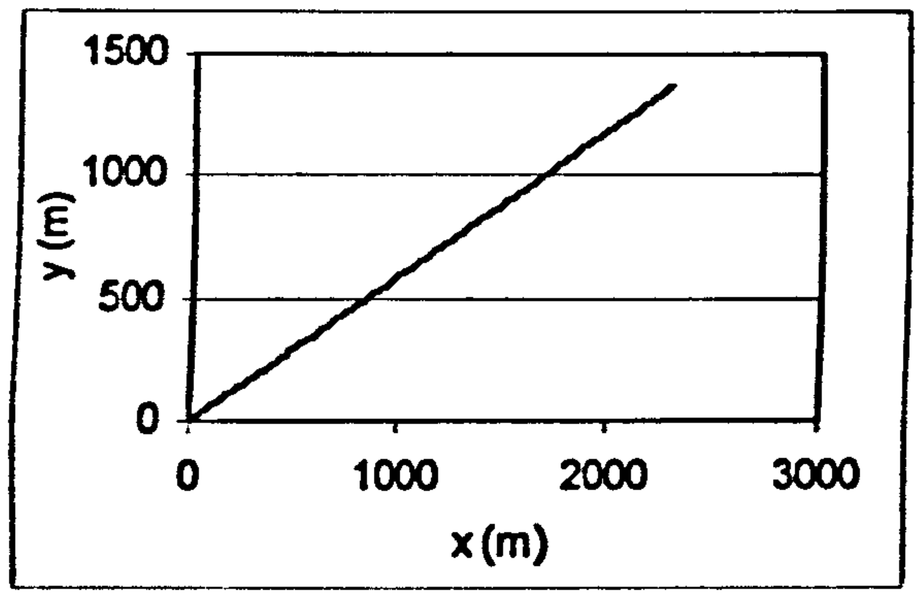

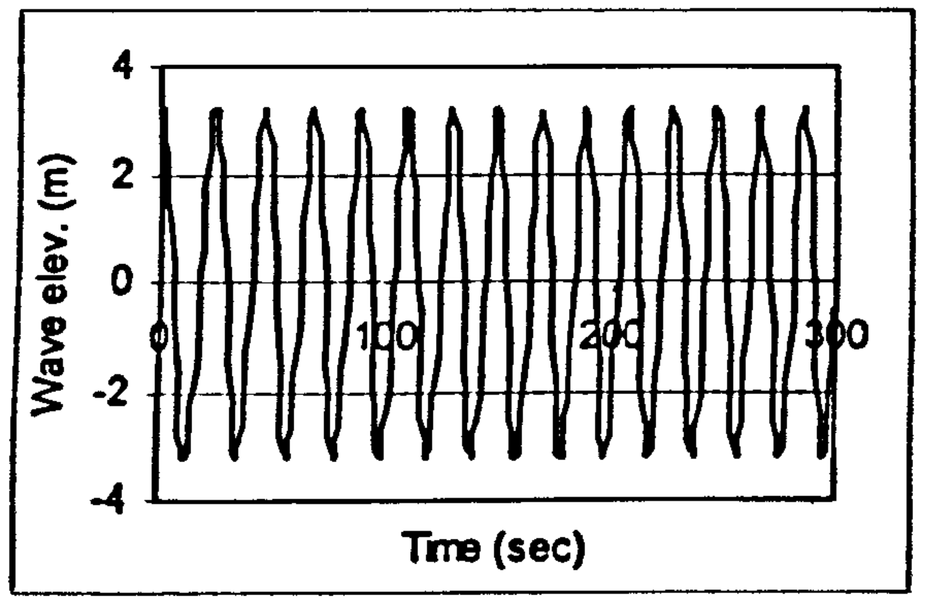

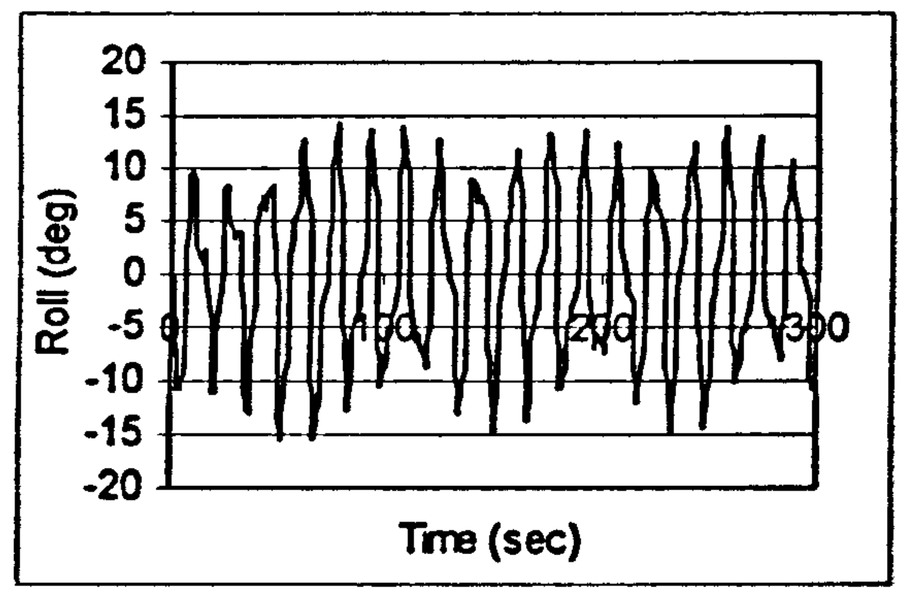

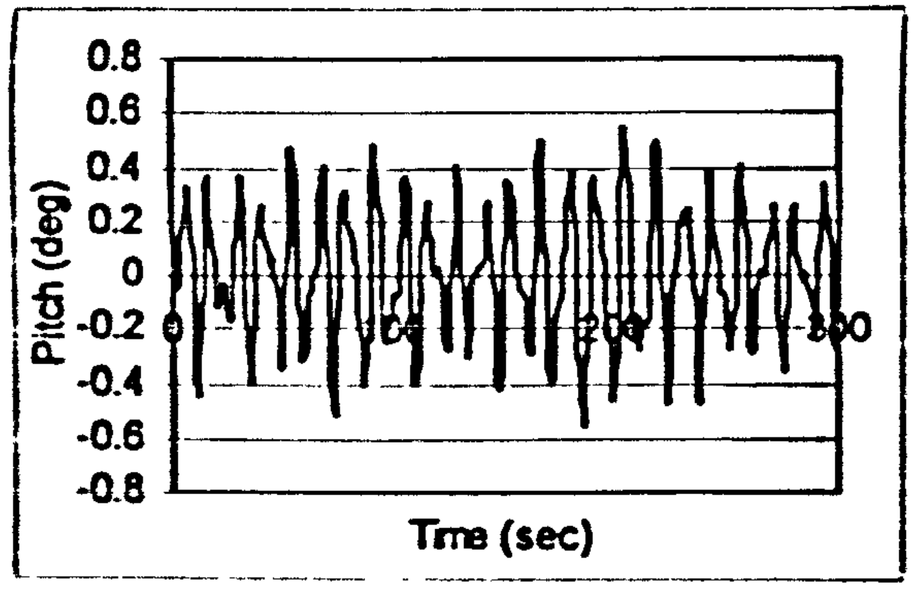

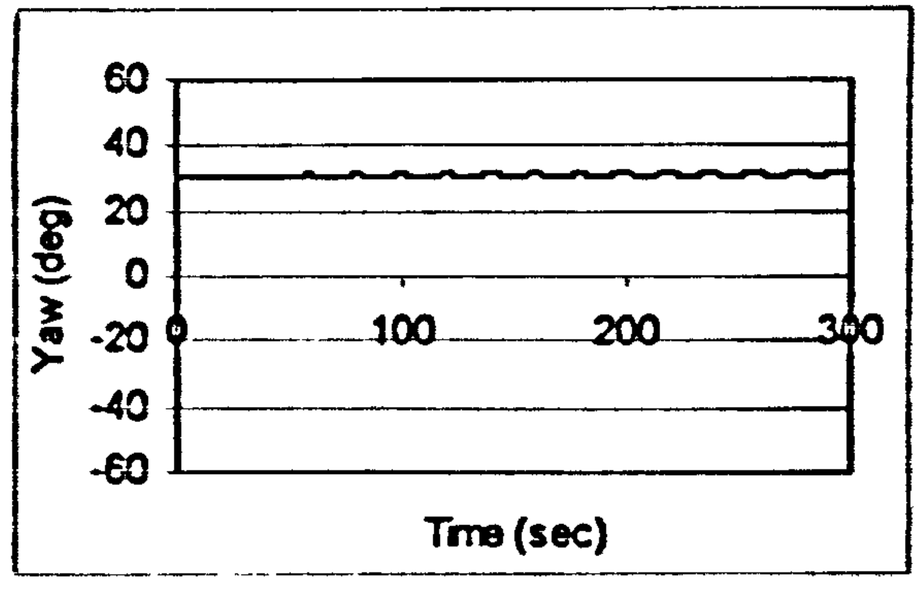

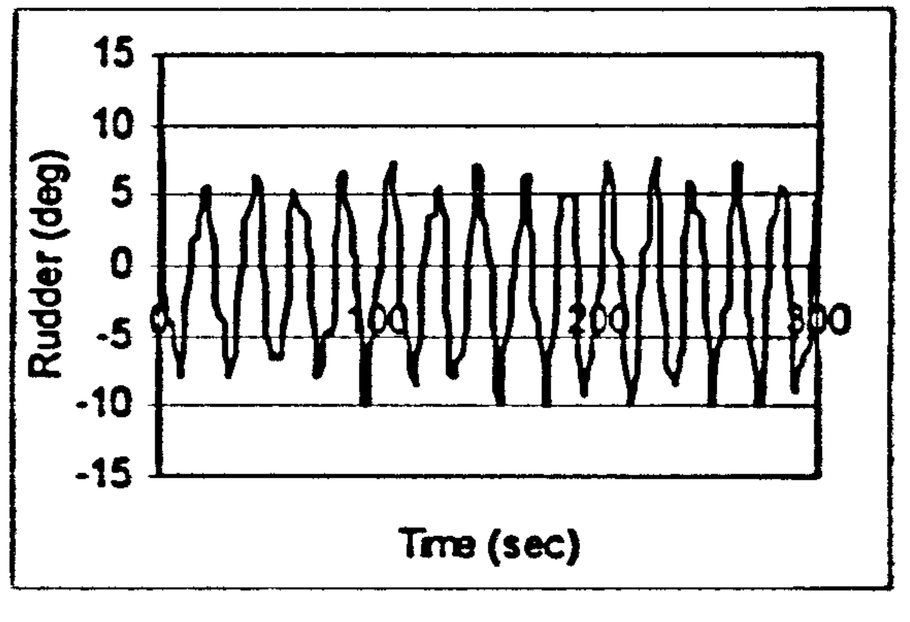

FigureG.13 Numerical Simulation of Ship A-1 with 6 DOF mathematical model in $H/\lambda=1/25$, $\lambda/L_{pp}=1.5$, $Fn=0.3$, $\chi_c=45$ degrees

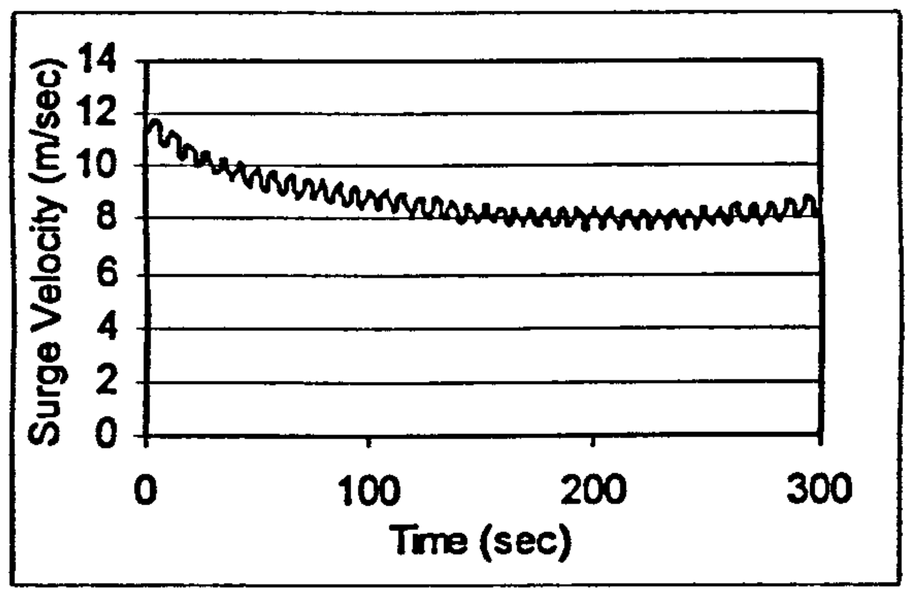

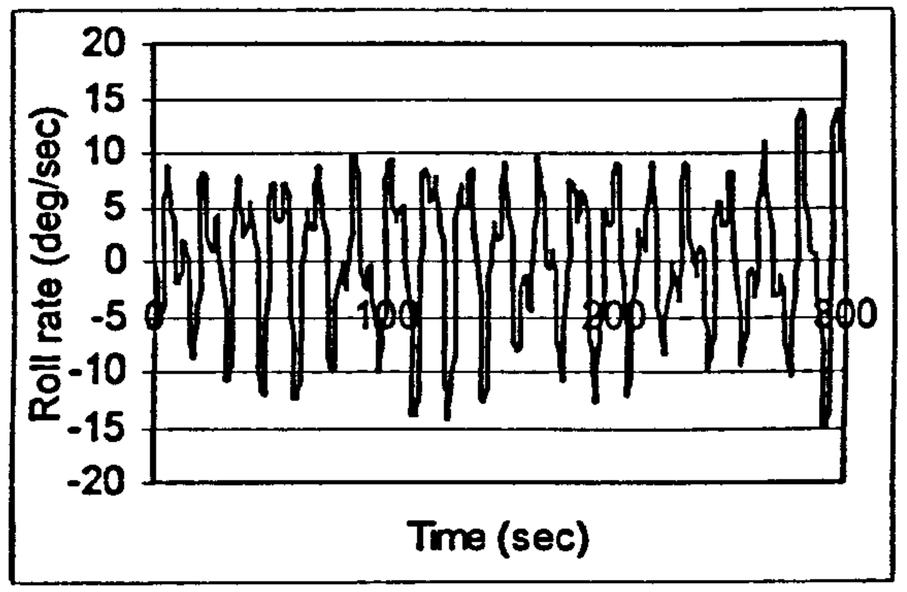

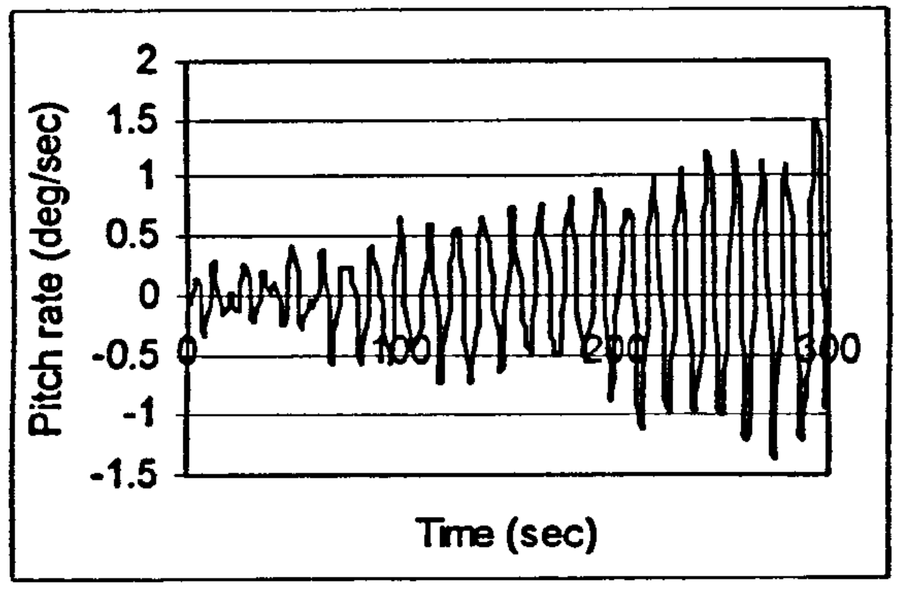

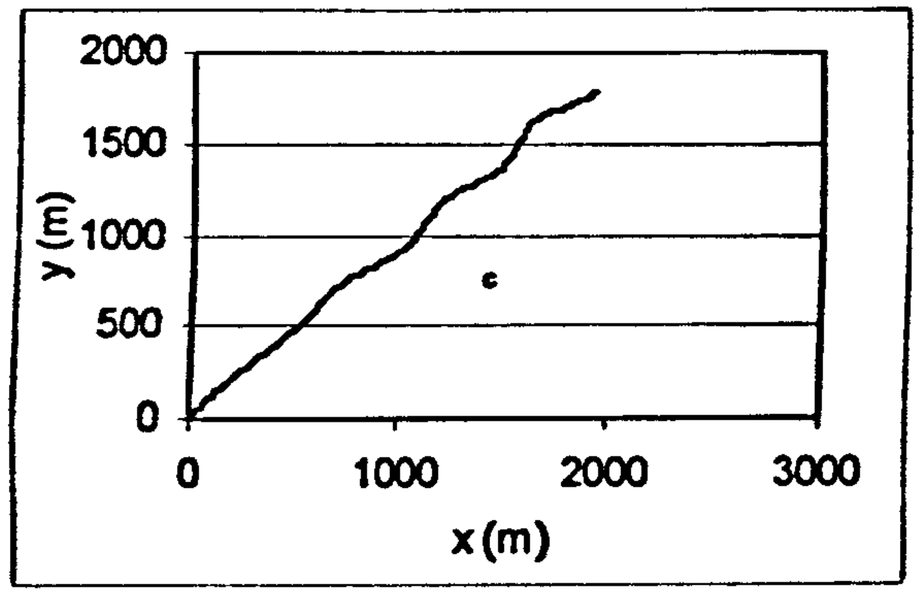

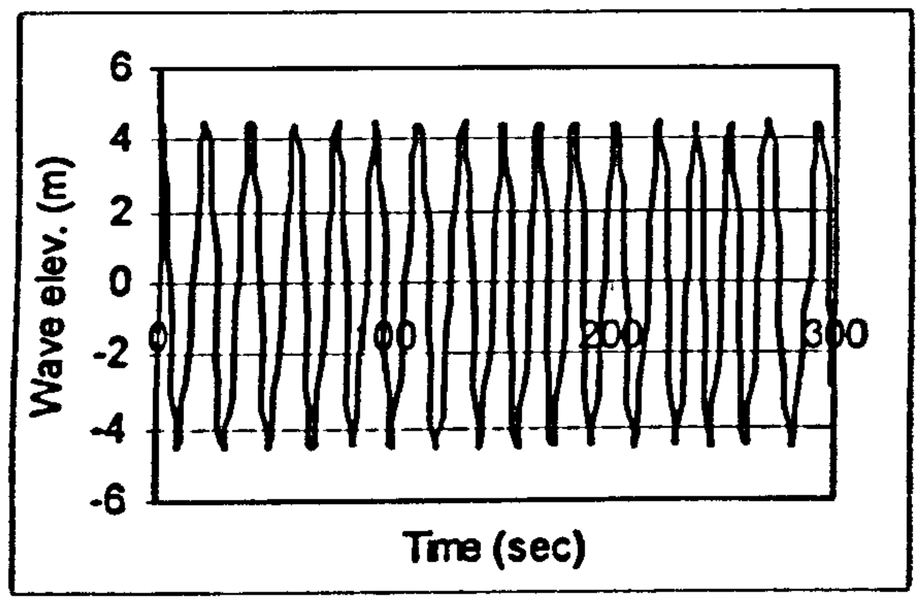

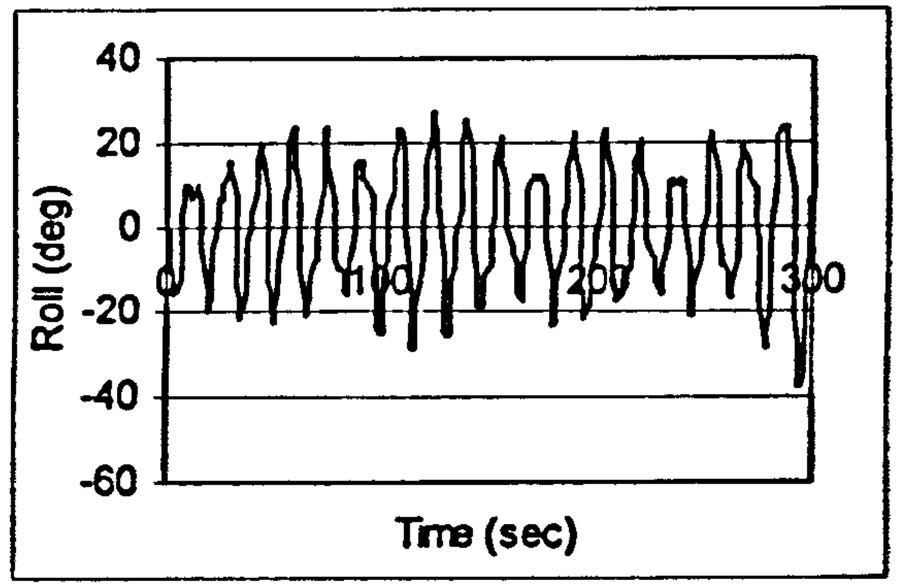

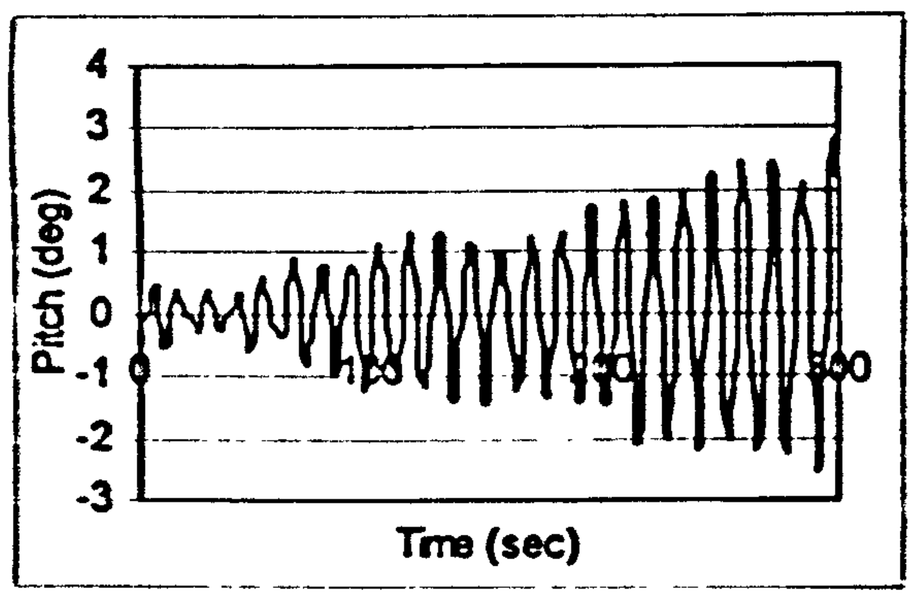

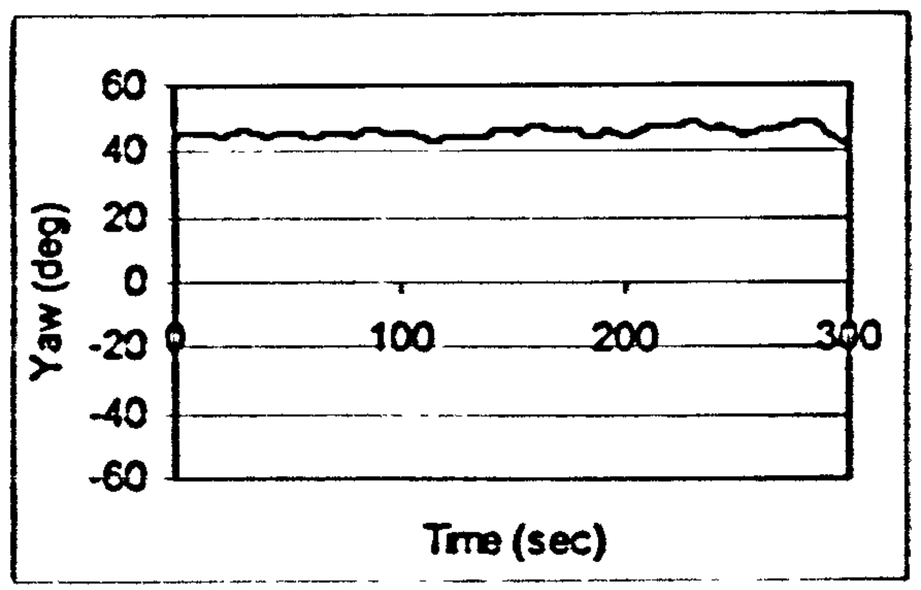

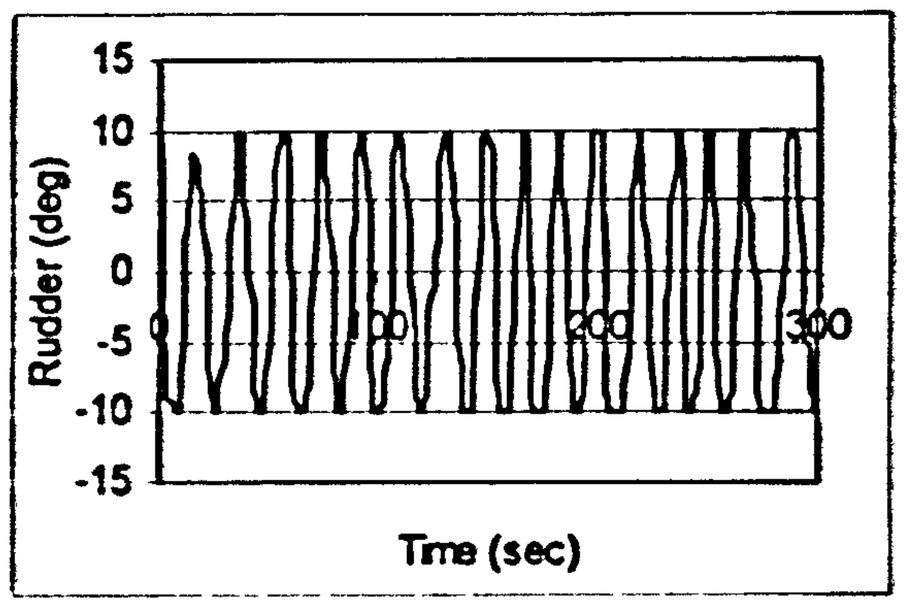

Figure G.14 Numerical Simulation of Ship A-1 with 4 DOF mathematical model in $H/\lambda=1/25$, $\lambda/L_{pp}=1.5$, Fn=0.3,$\chi_c=45$ degrees

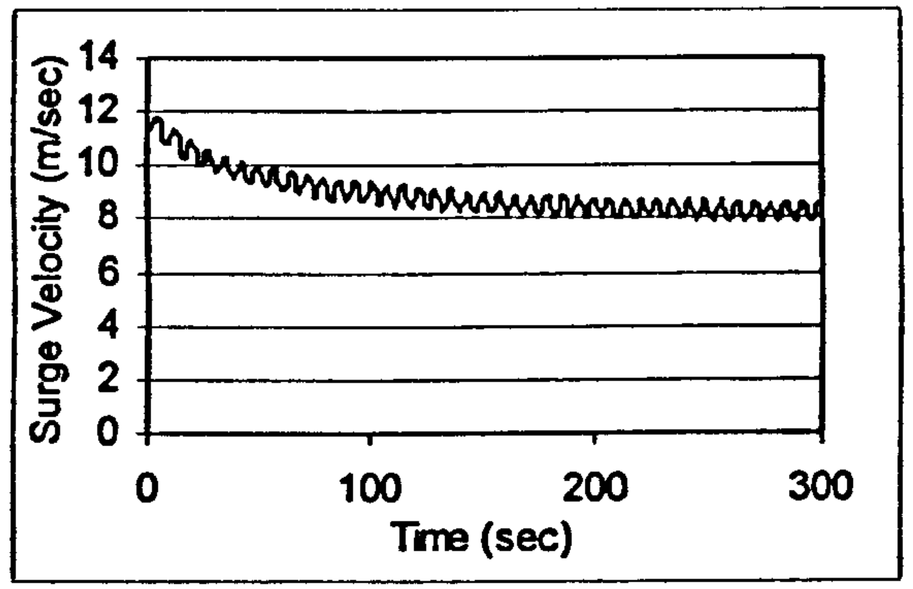

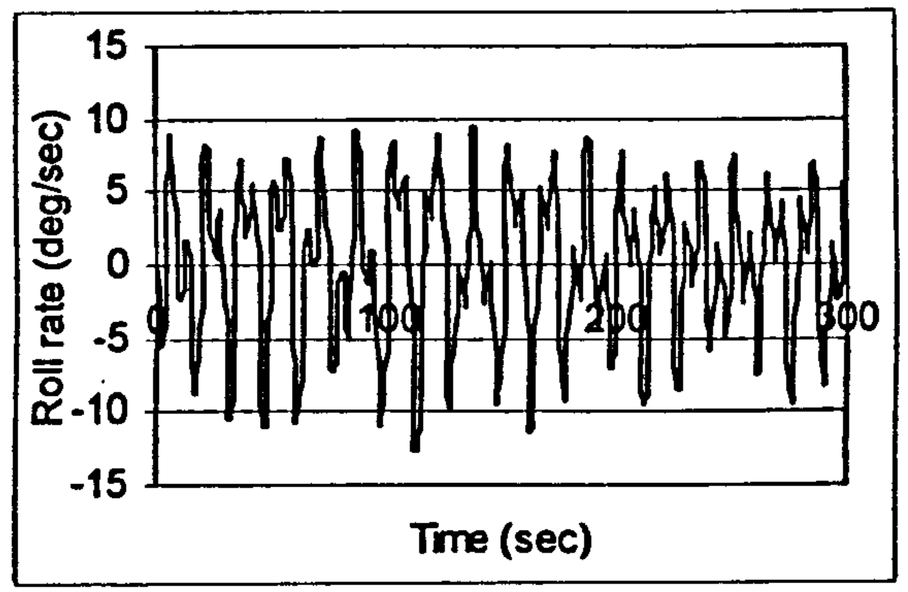

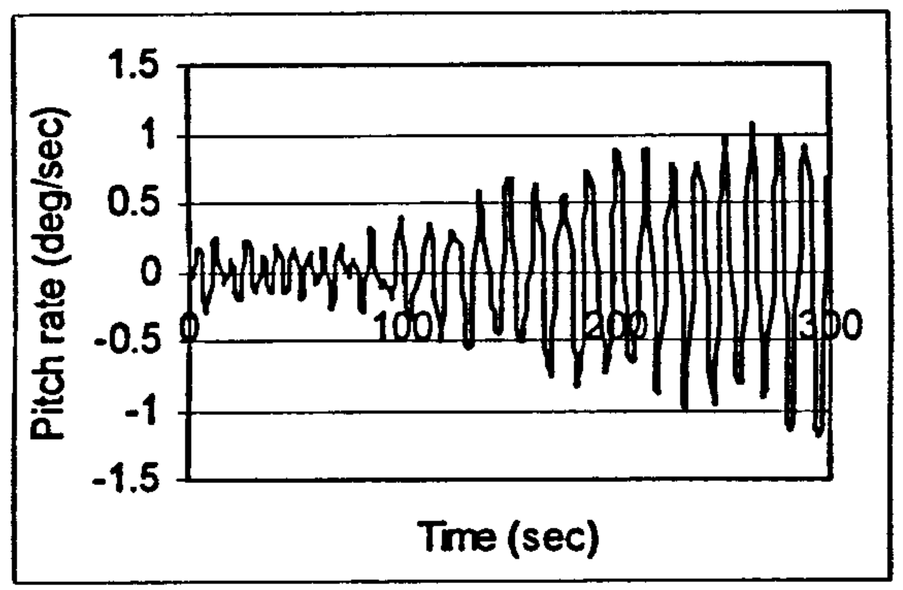

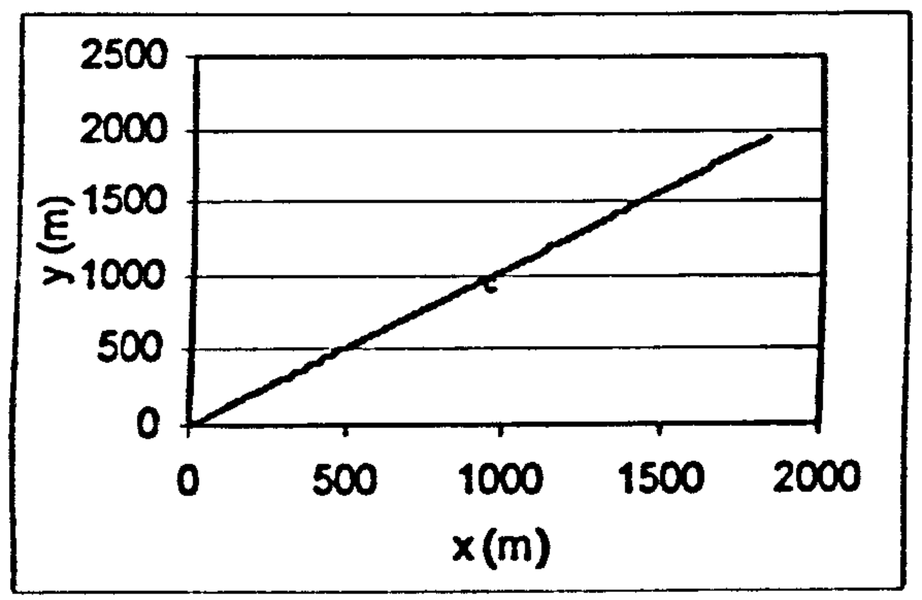

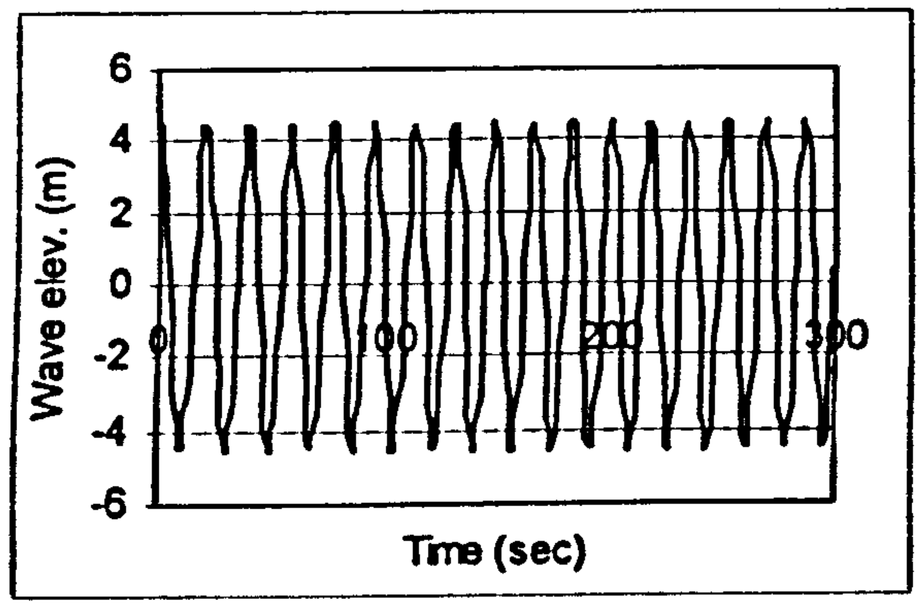

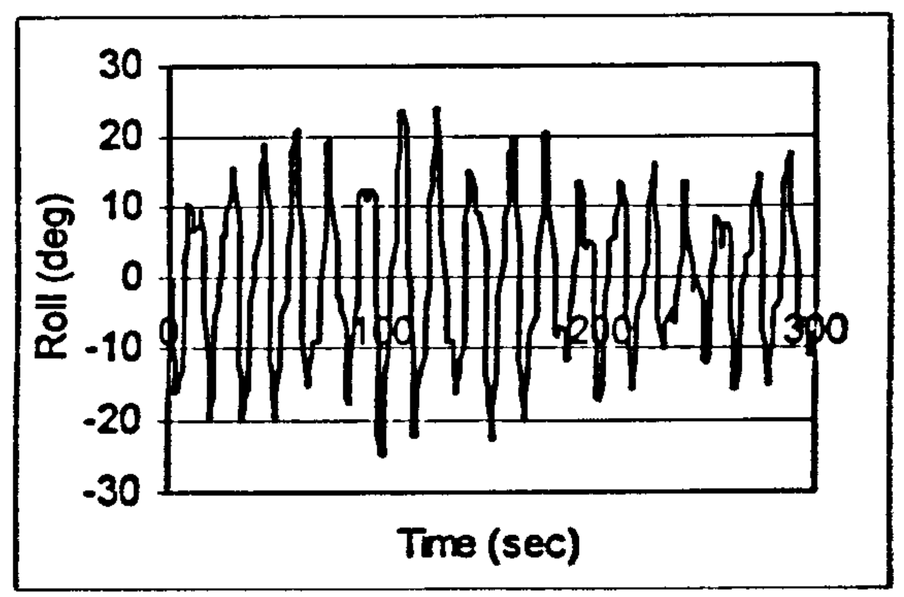

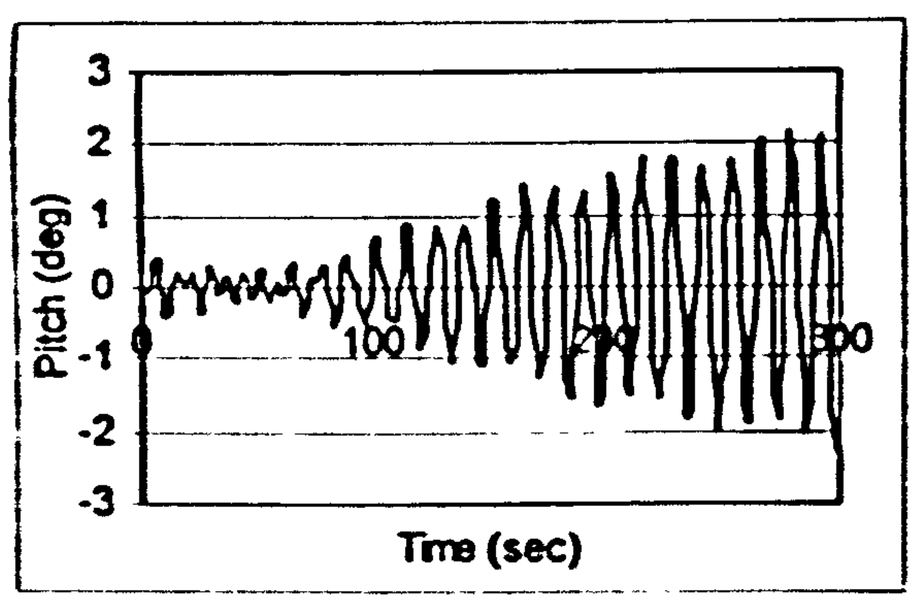

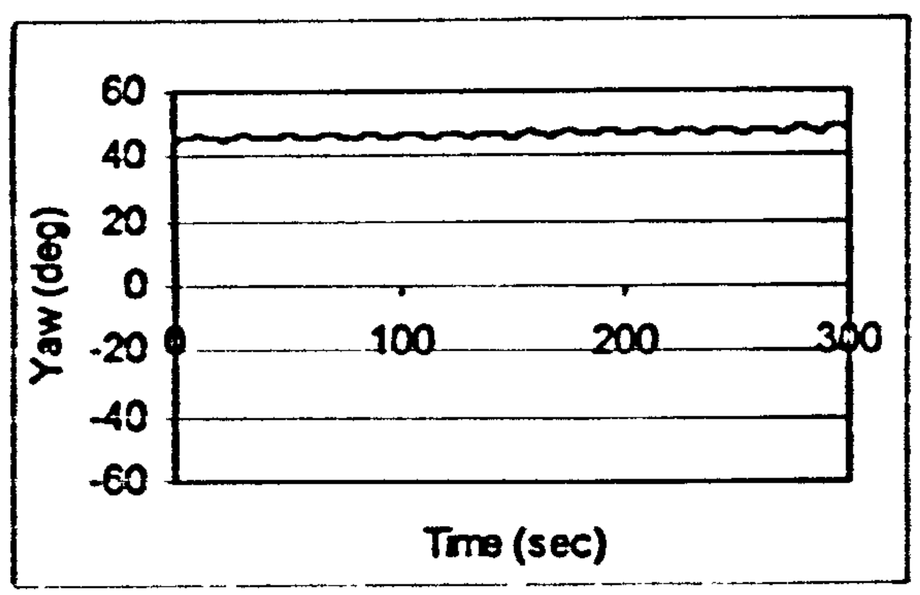

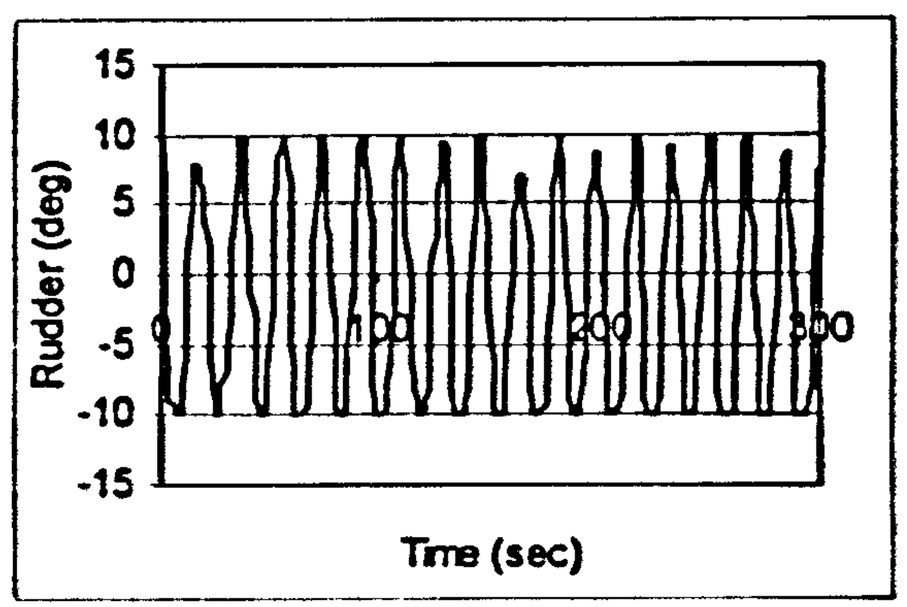

Figure G.15 Numerical Simulation of Ship A-1 with 6 DOF mathematical model in $H/\lambda=1/30$, $\lambda/L_{pp}=1.5$, $Fn=0.3$, $\chi_c=45$ degrees

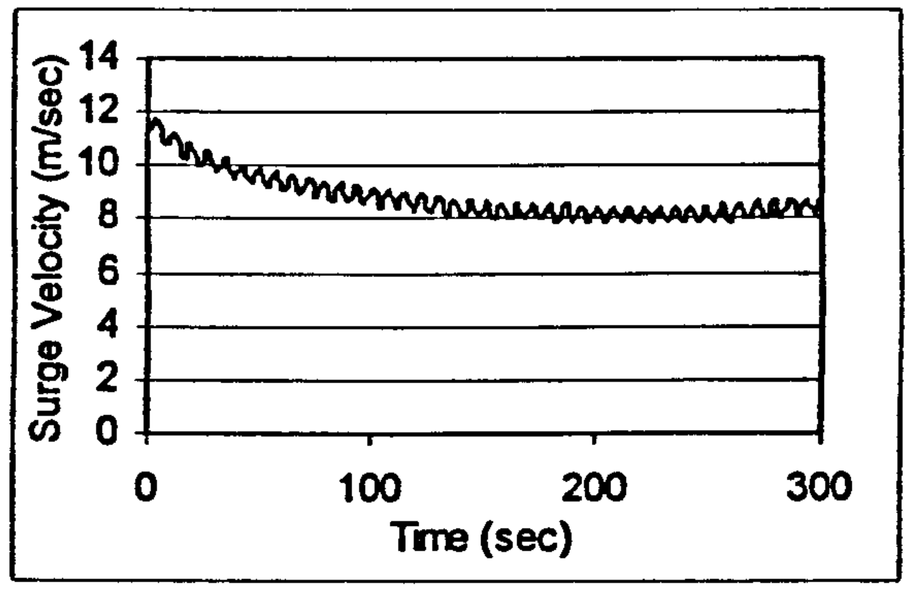

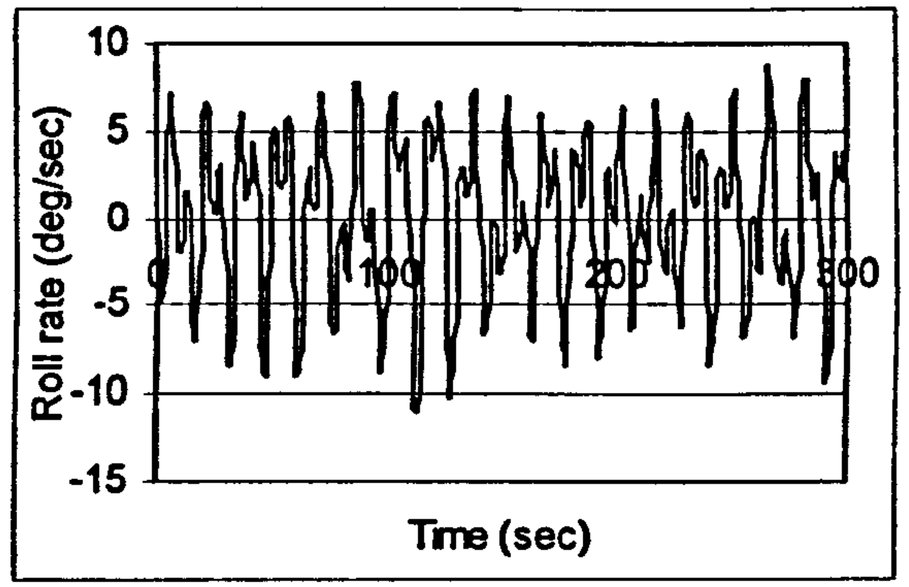

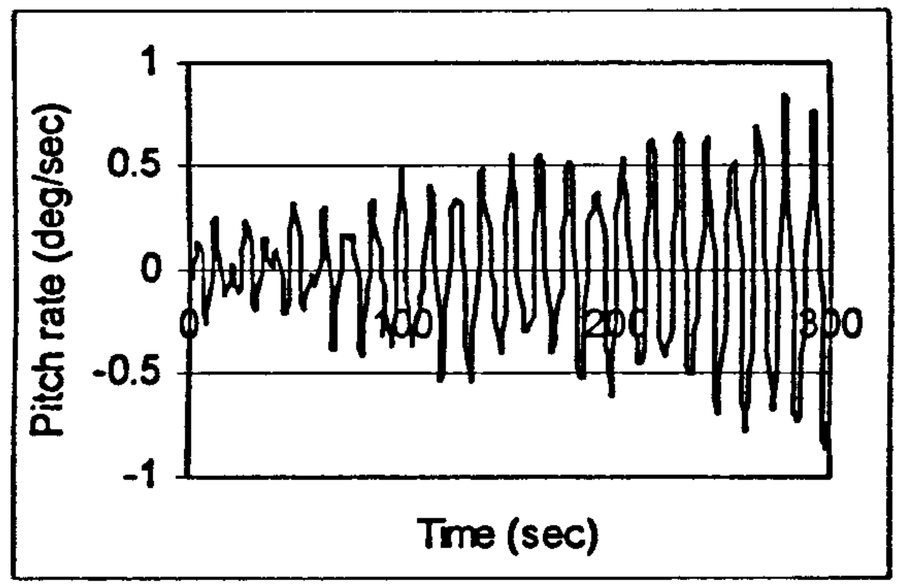

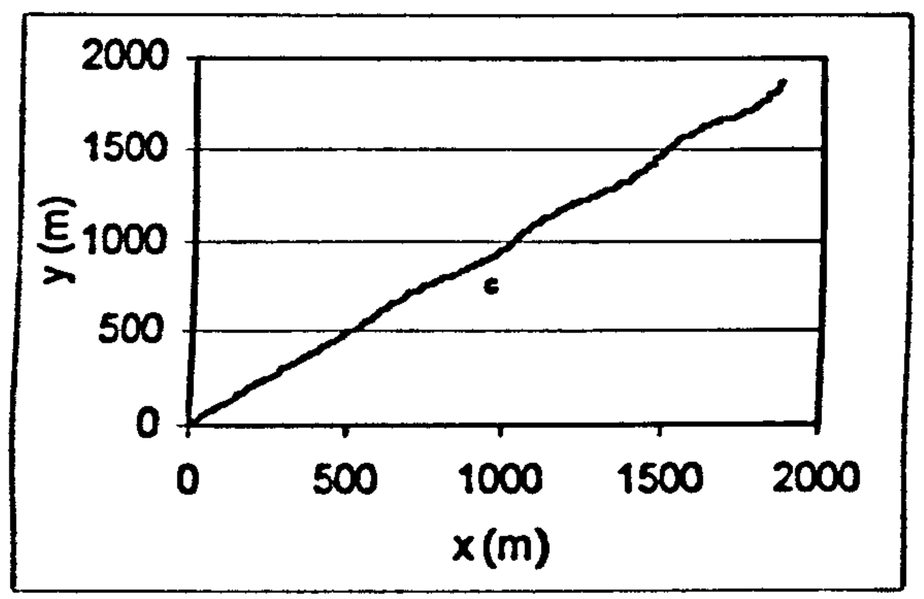

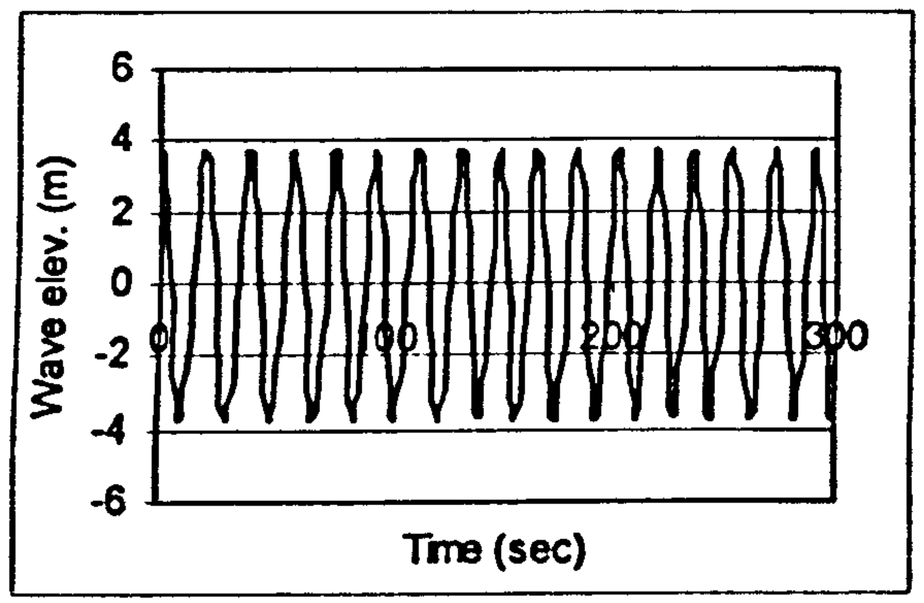

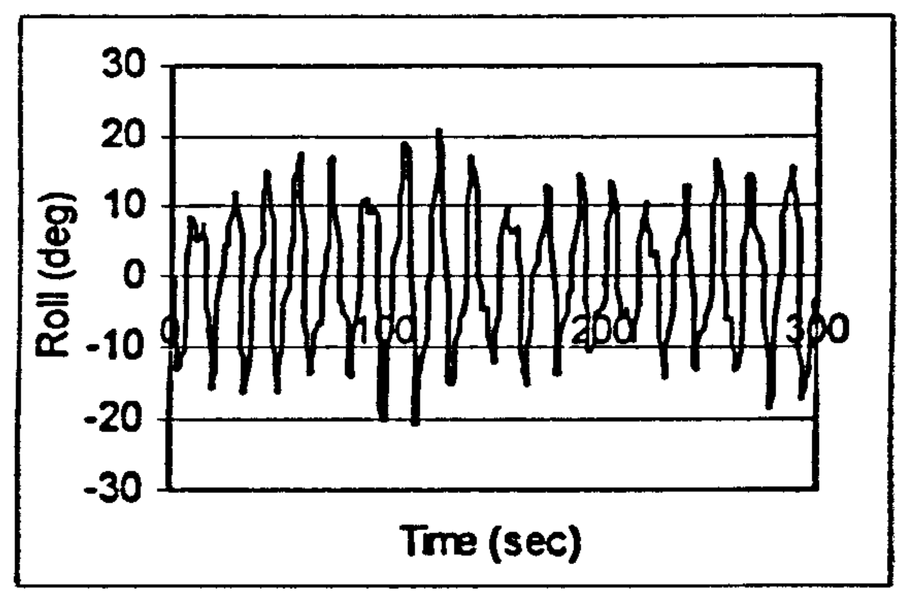

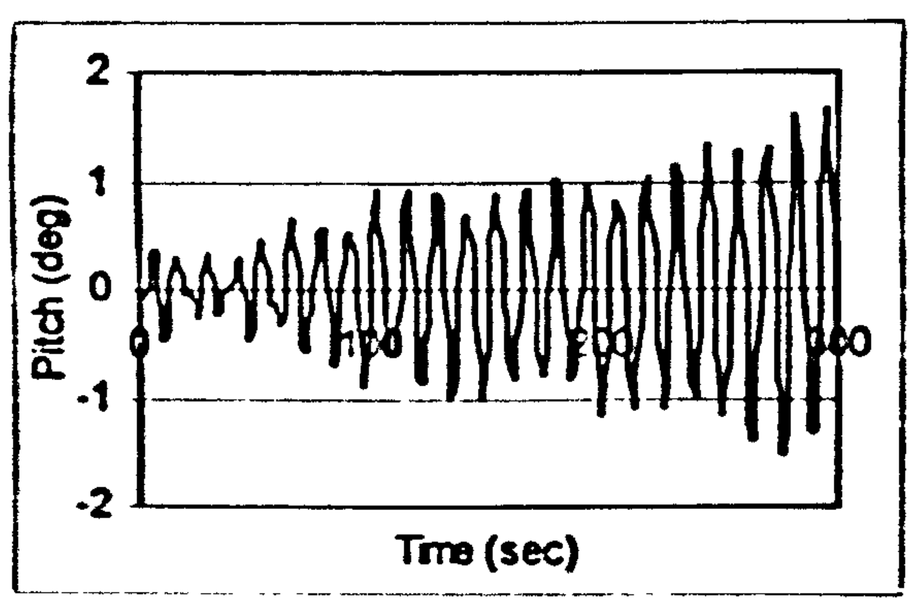

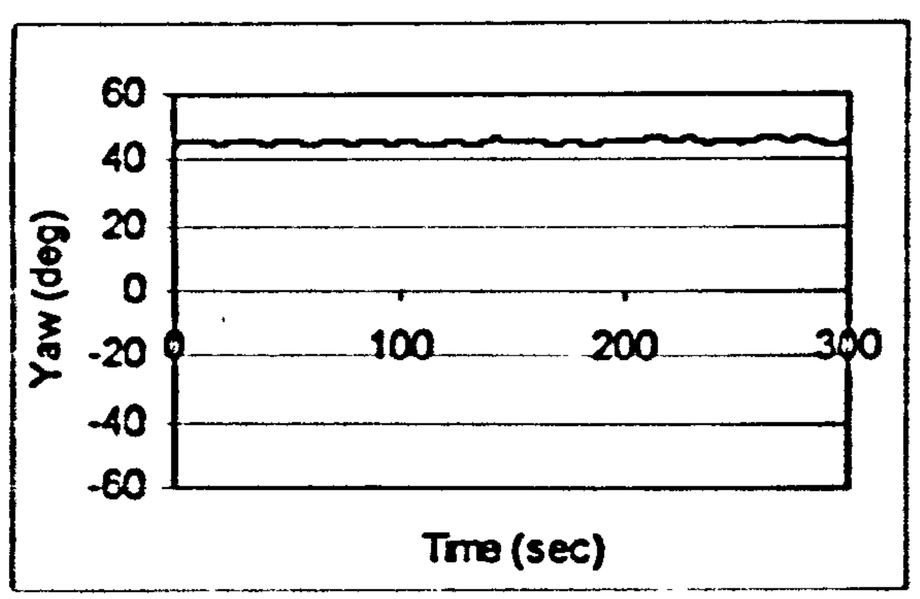

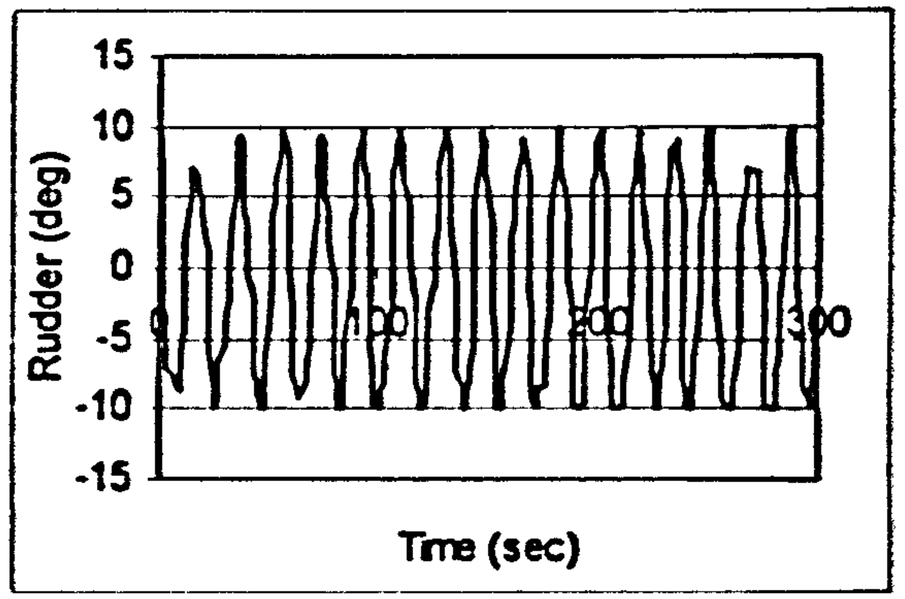

Figure G.16 Numerical Simulation of Ship A-1 with 4 DOF mathematical model in $H/\lambda=1/30$, $\lambda/L_{pp}=1.5$, Fn=0.3,χ_c=45 degrees

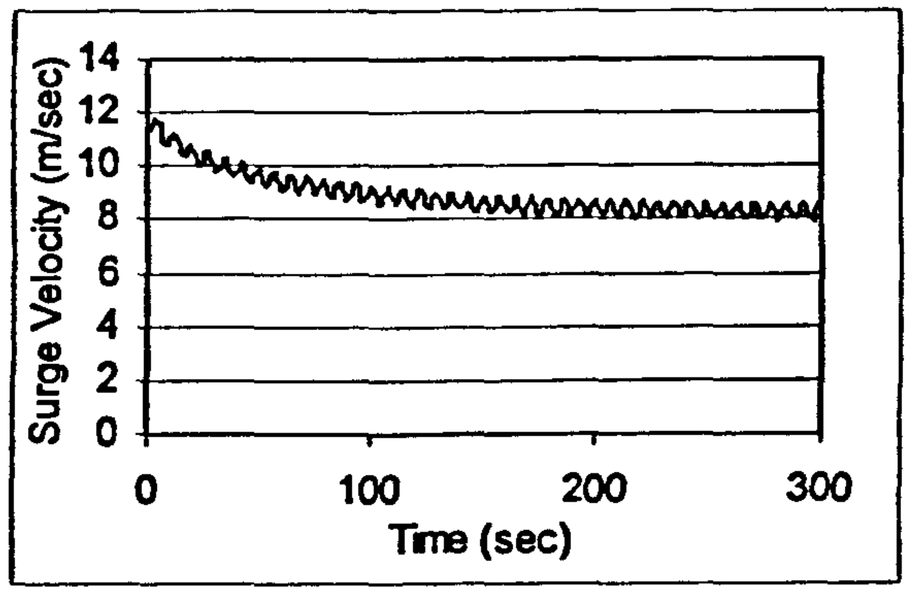

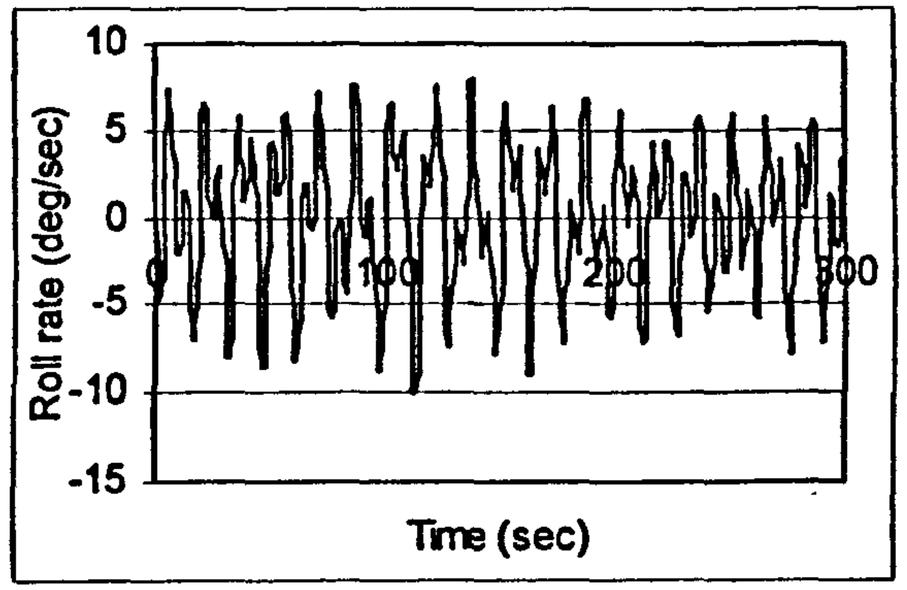

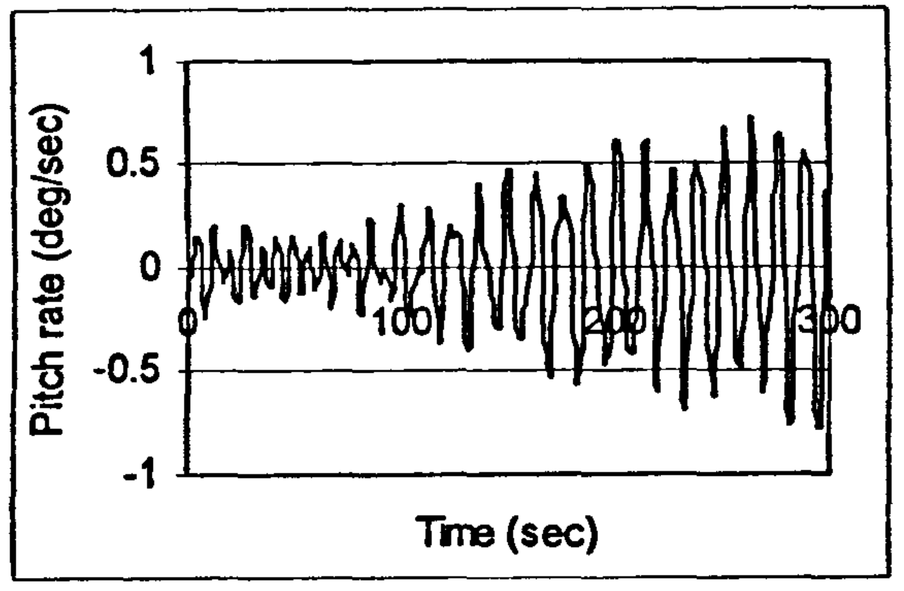

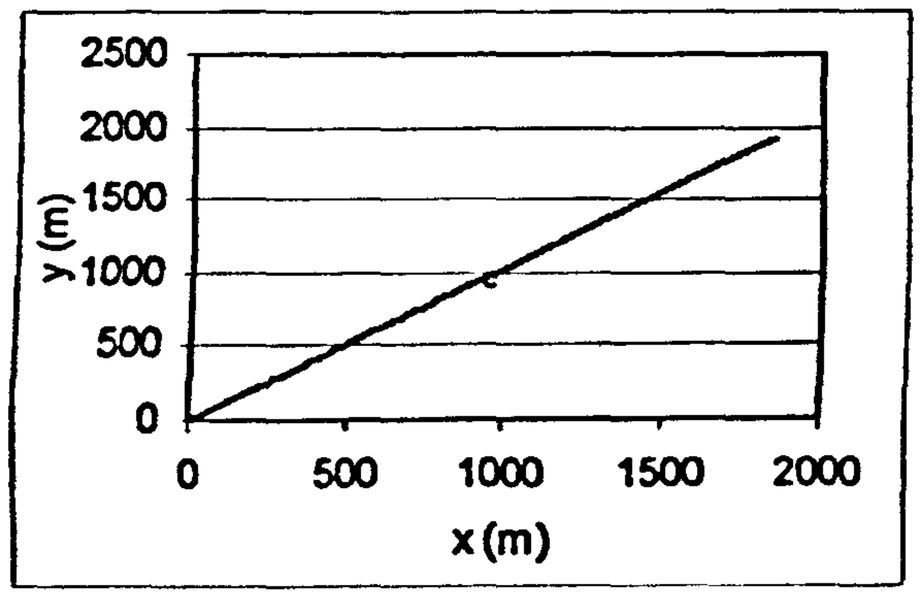

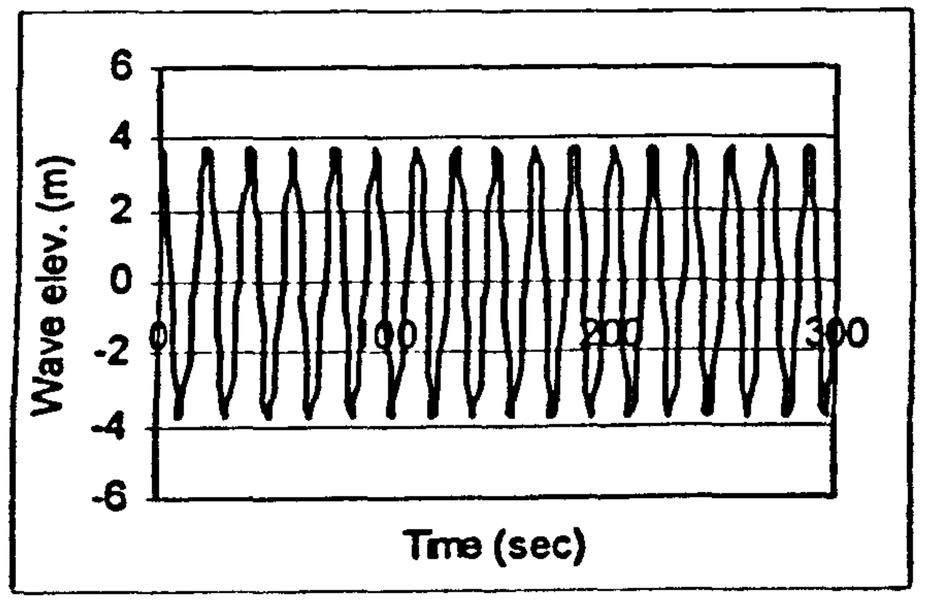

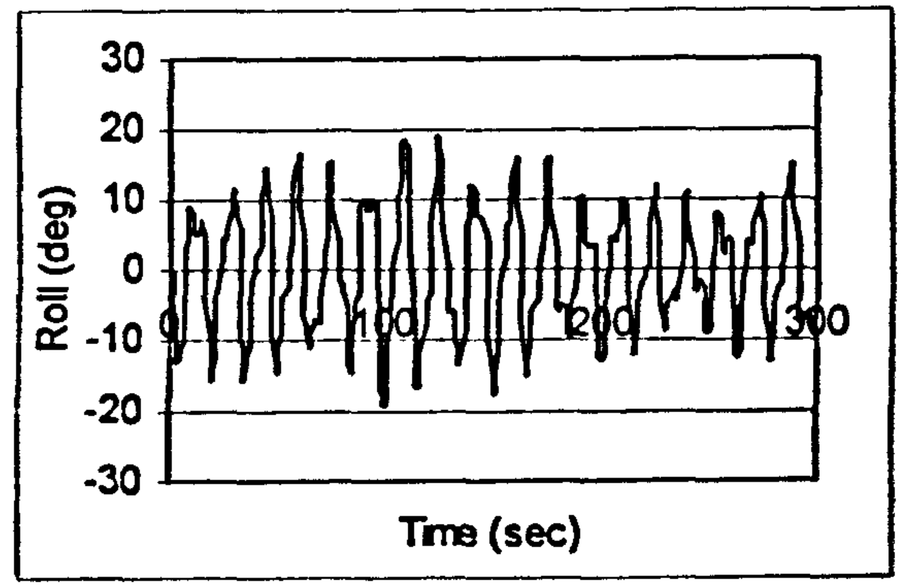

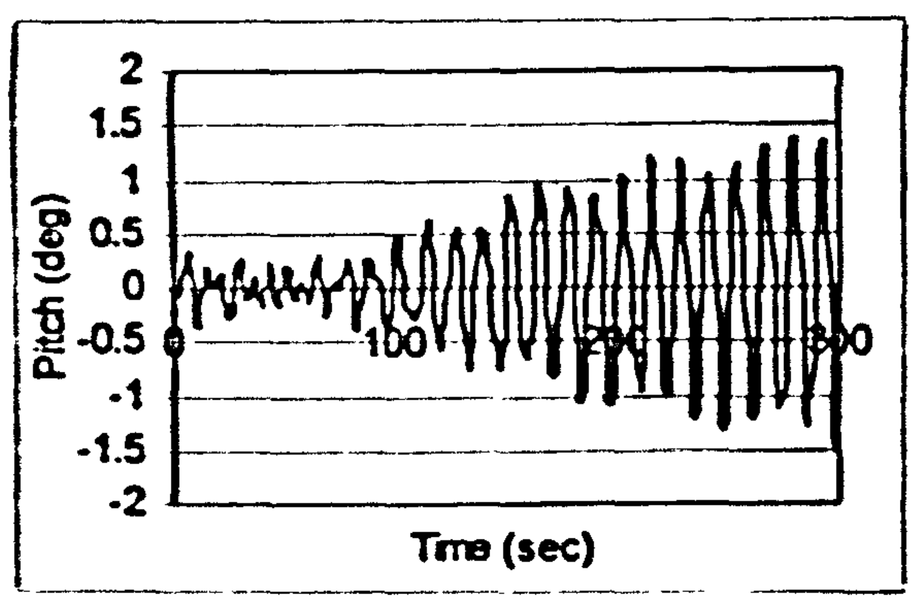

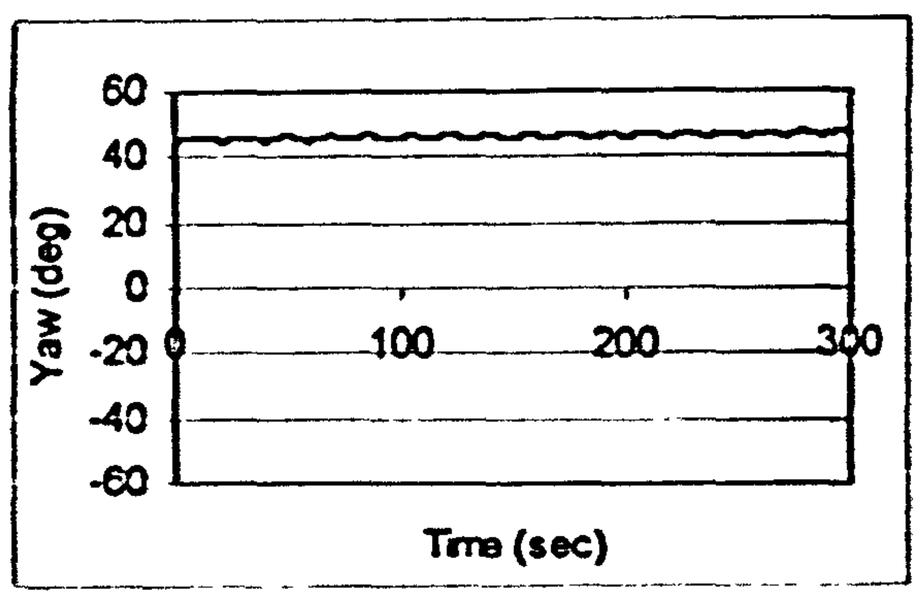

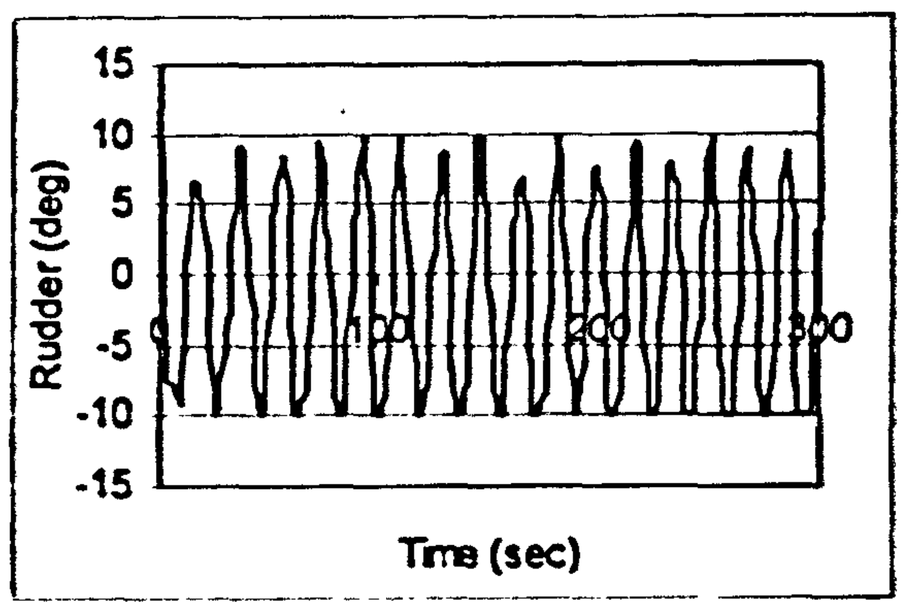

Figure G.17 Numerical Simulation of Ship A-1 with 6 DOF mathematical model in $H/\lambda=1/35$, $\lambda/L_{pp}=1.5$, $Fn=0.3$, $\chi_c=45$ degrees

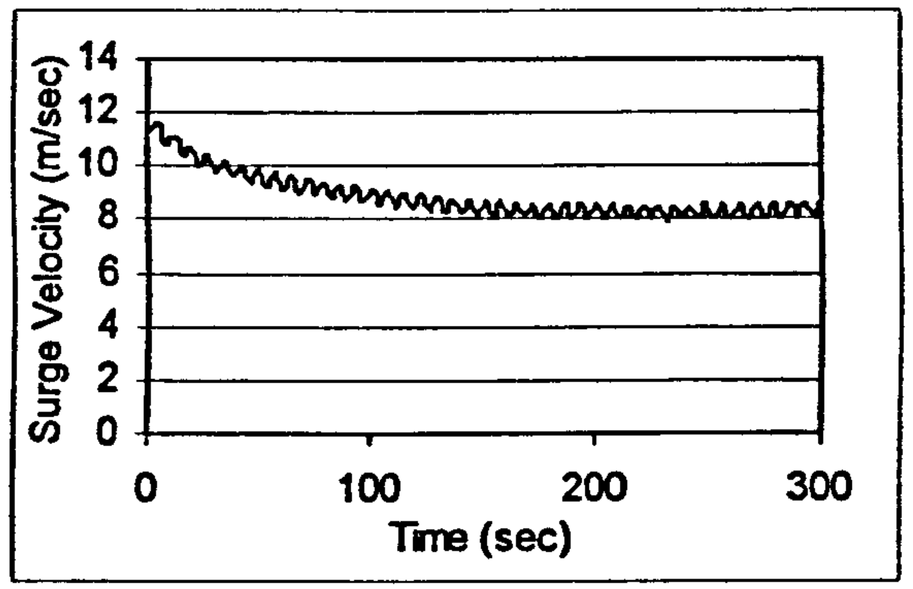

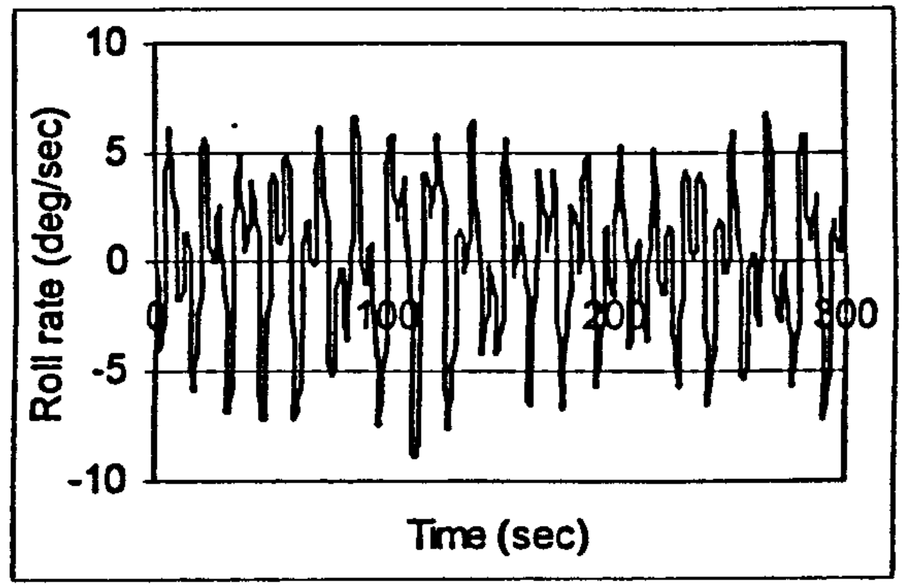

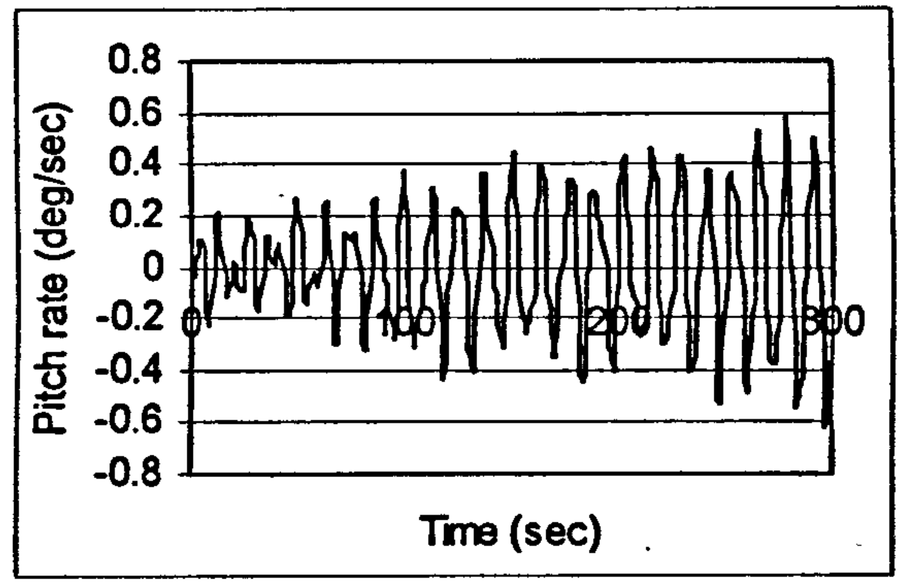

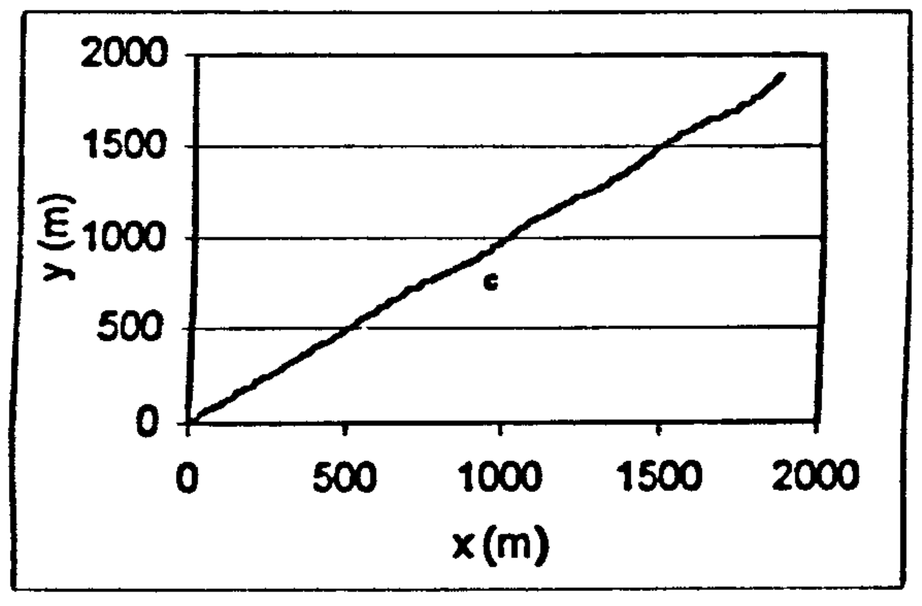

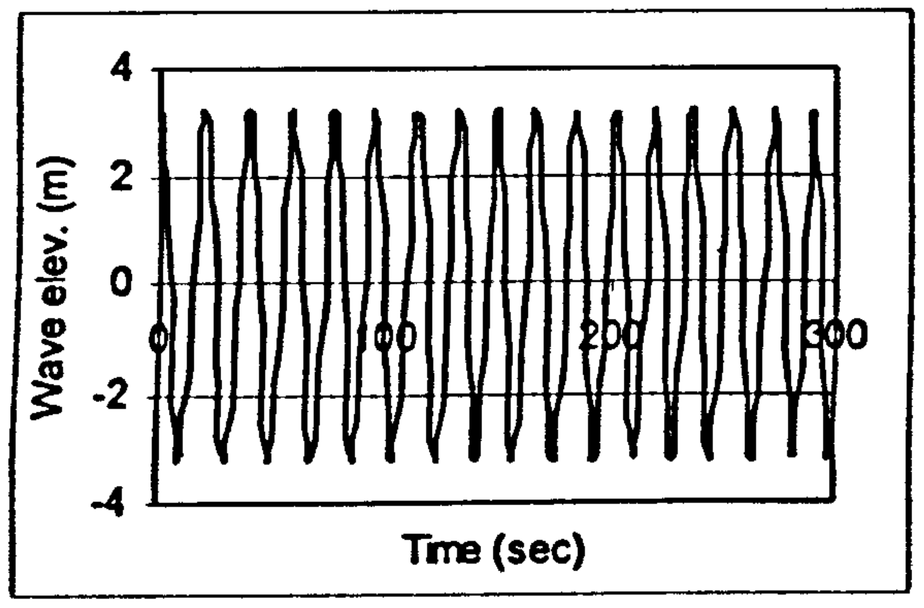

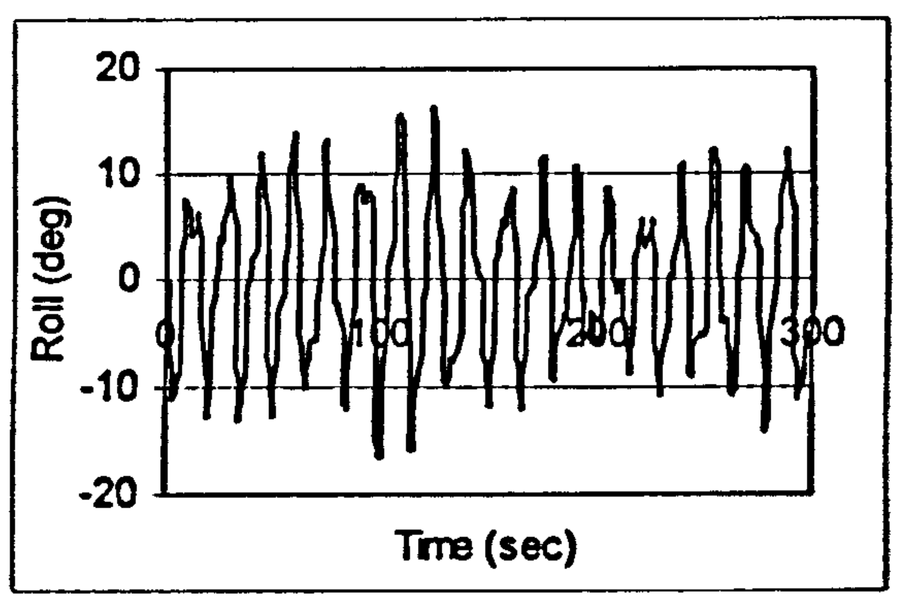

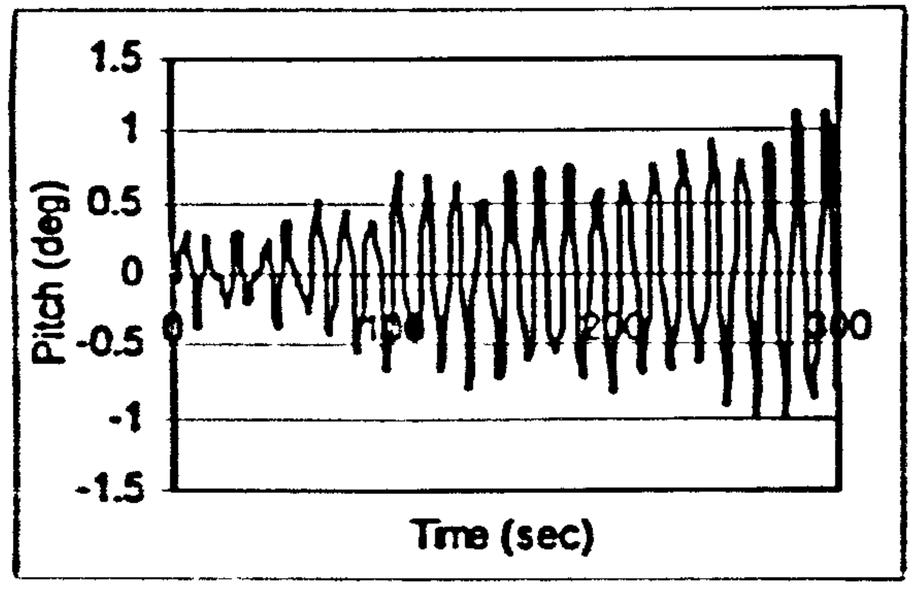

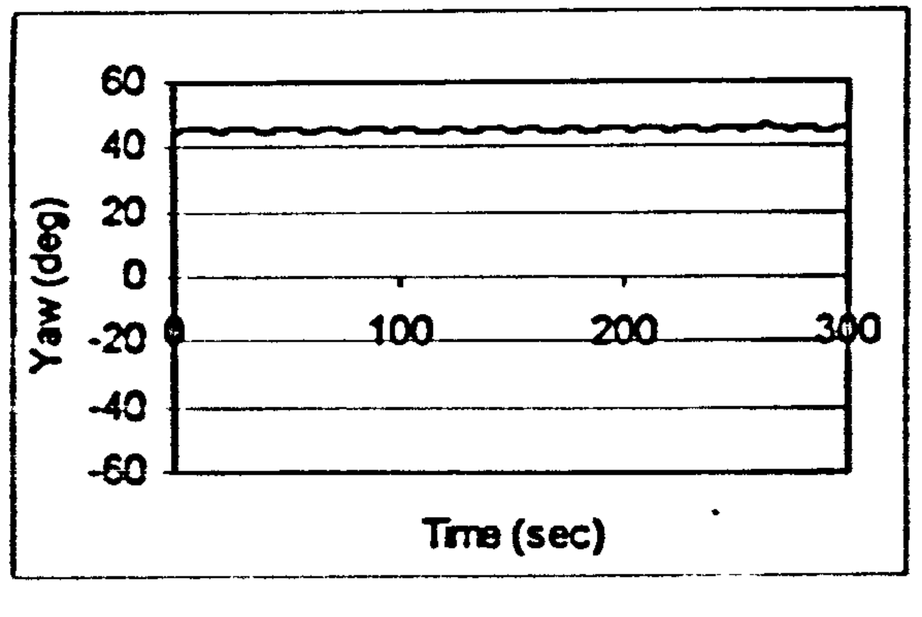

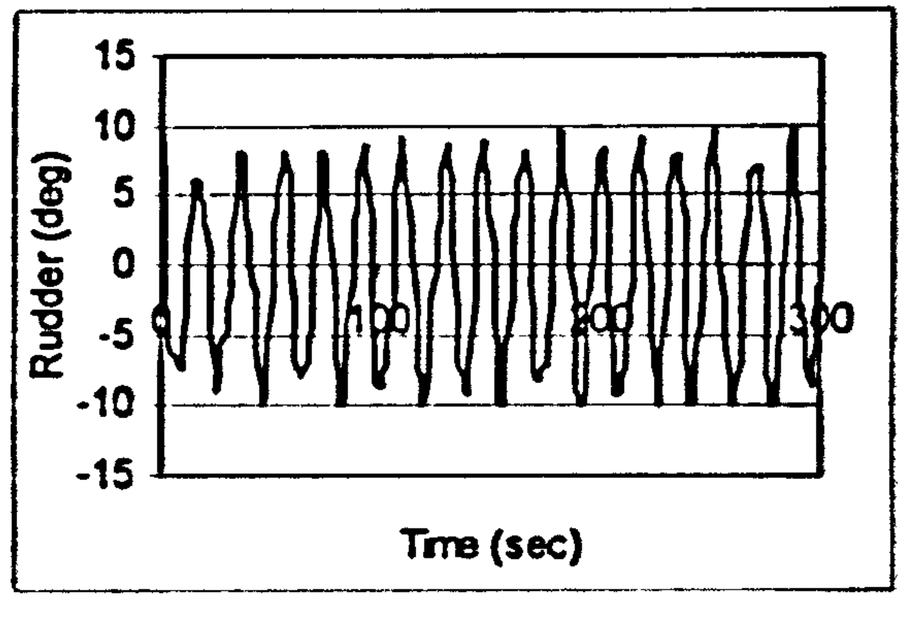

Figure G.18 Numerical Simulation of Ship A-1 with 4 DOF mathematical model in $H/\lambda=1/35$, $\lambda/L_{pp}=1.5$, Fn=0.3,χ_c =45 degrees

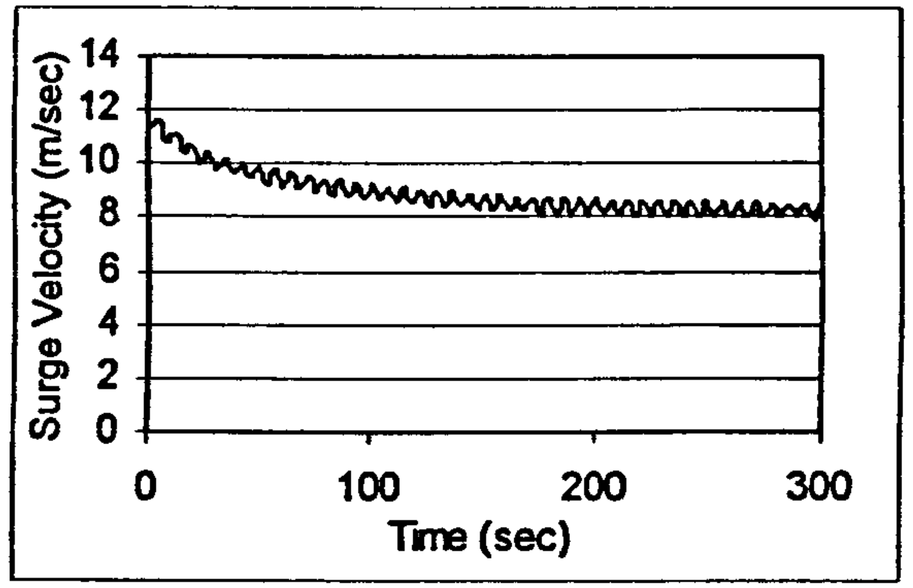

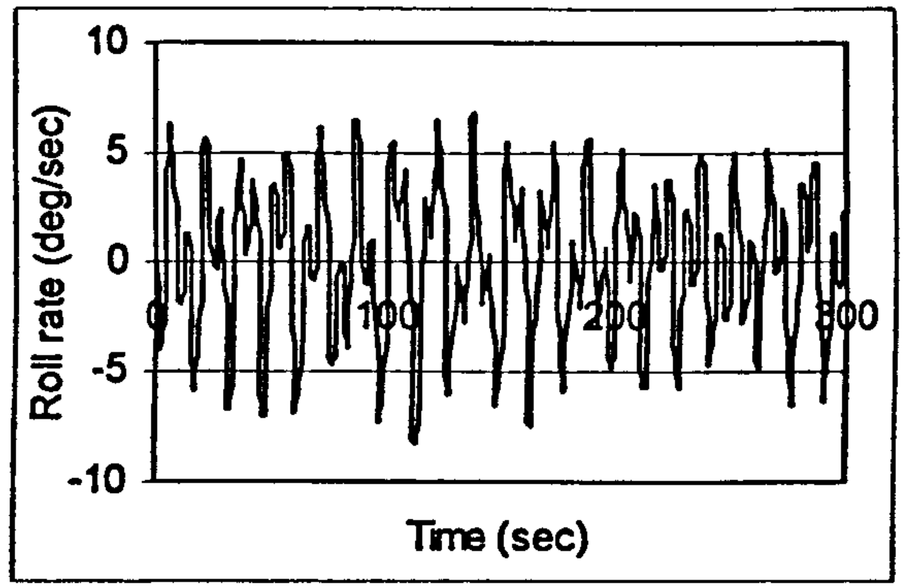

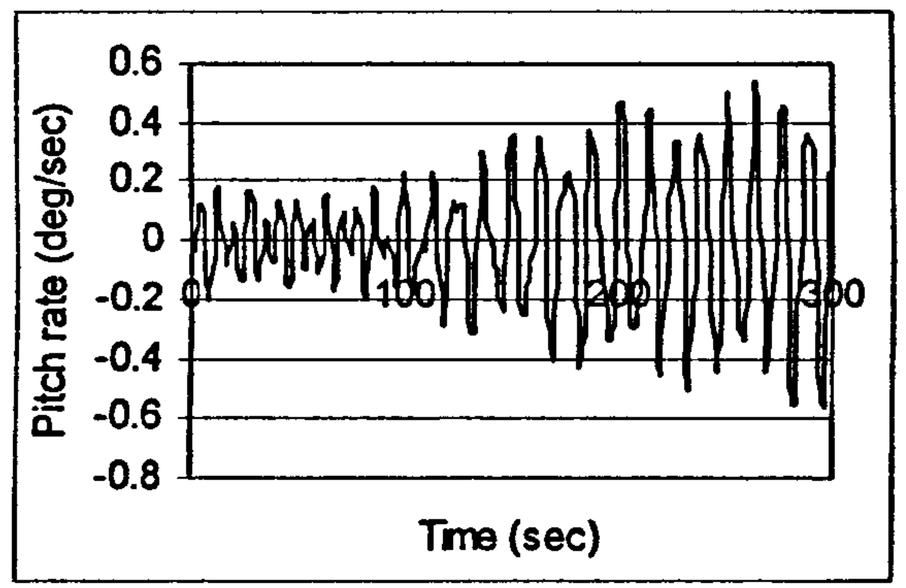

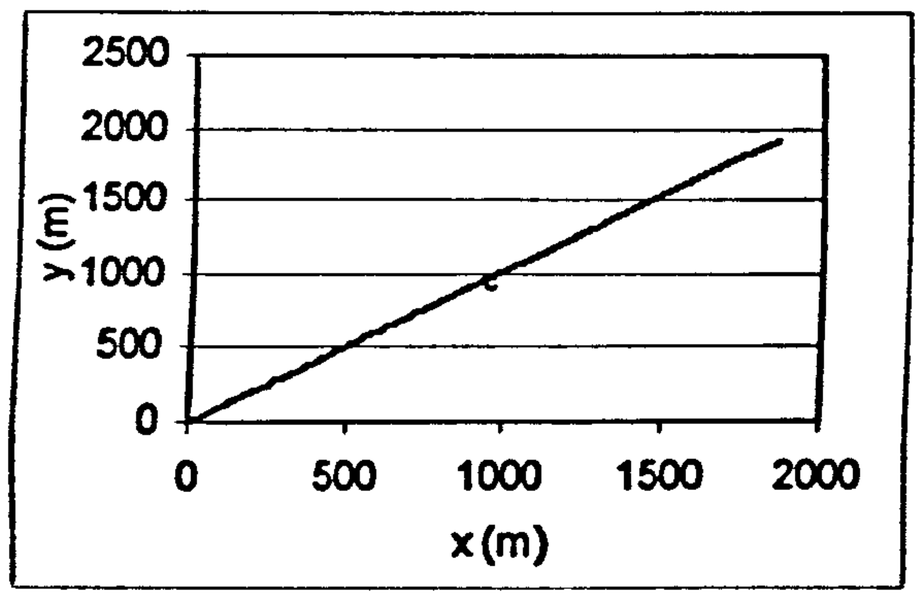

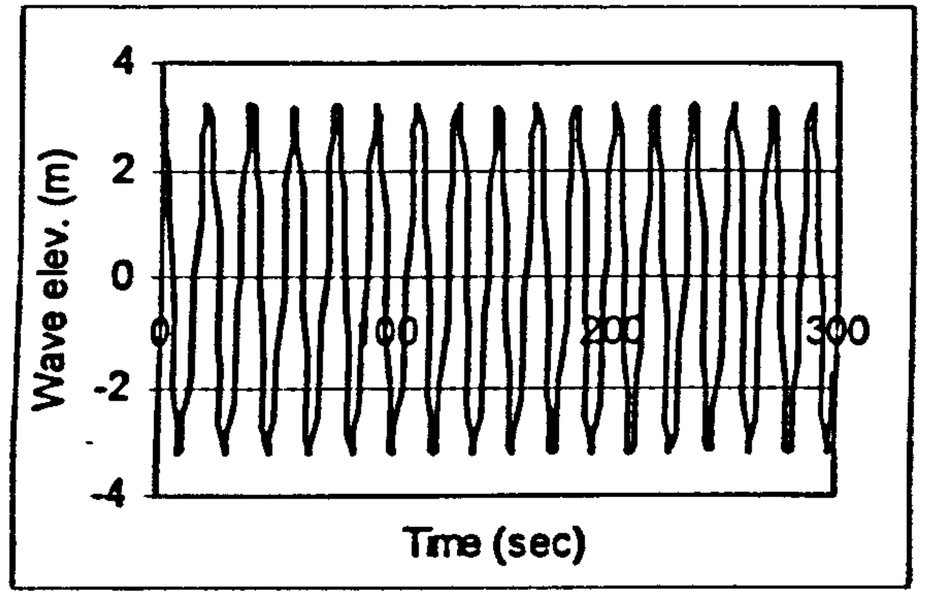

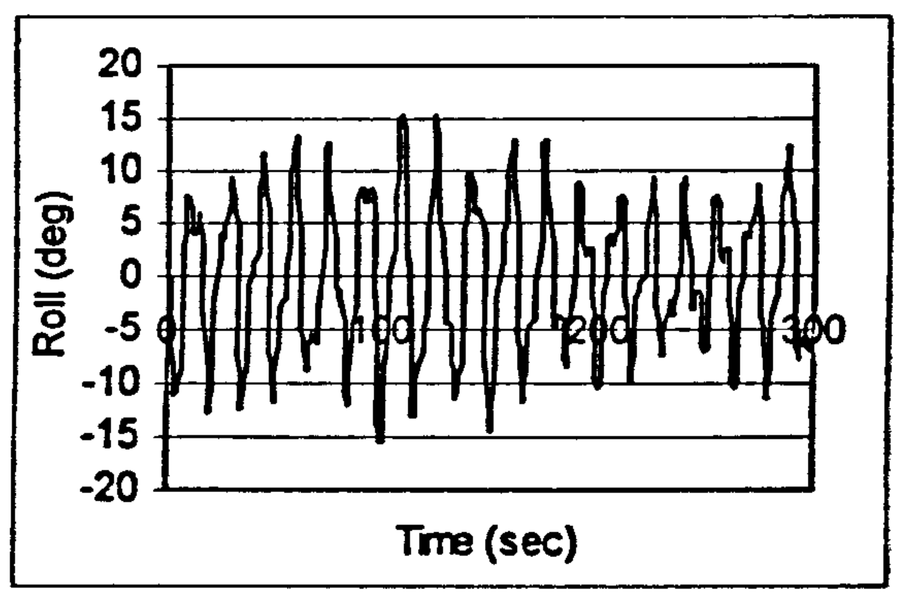

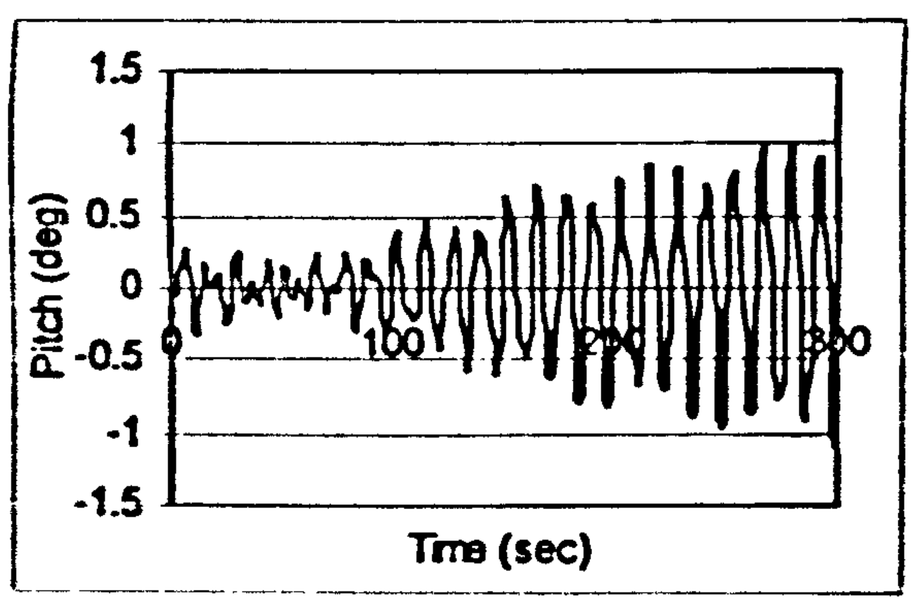

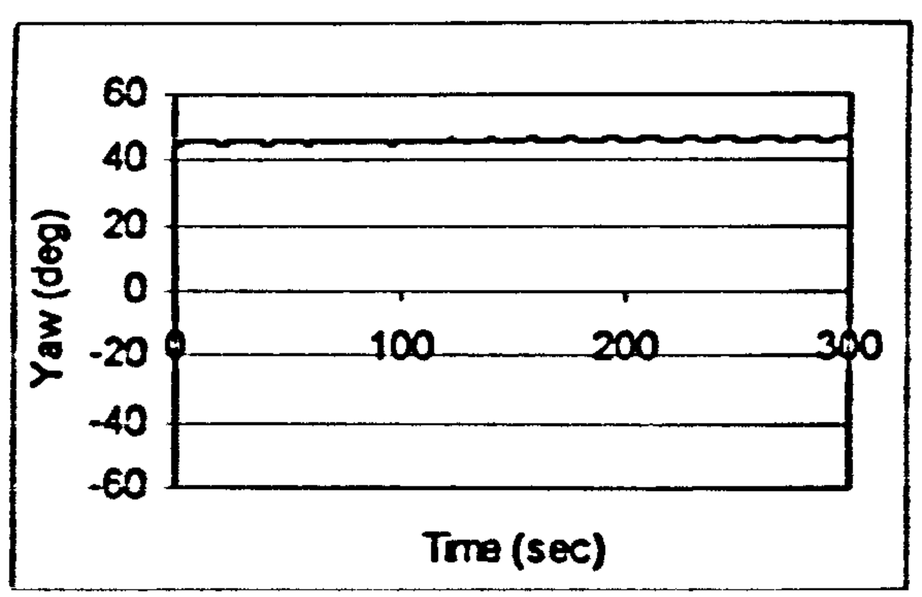

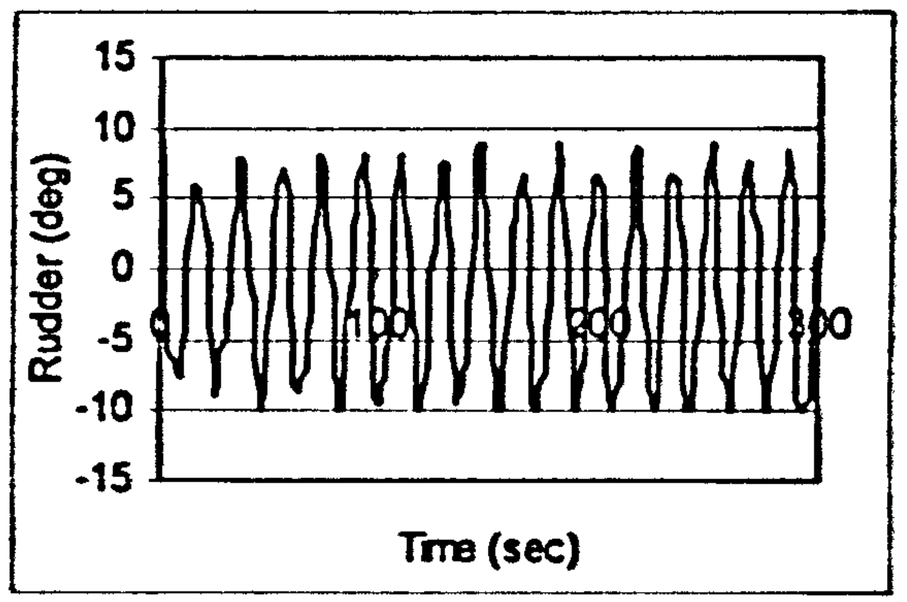

Figure G.19 Numerical Simulation of Ship A-1 with 6 DOF mathematical model in $H/\lambda=1/25$, $\lambda/L_{pp}=1.0$, $Fn=0.3$, $\chi_c=30$ degrees

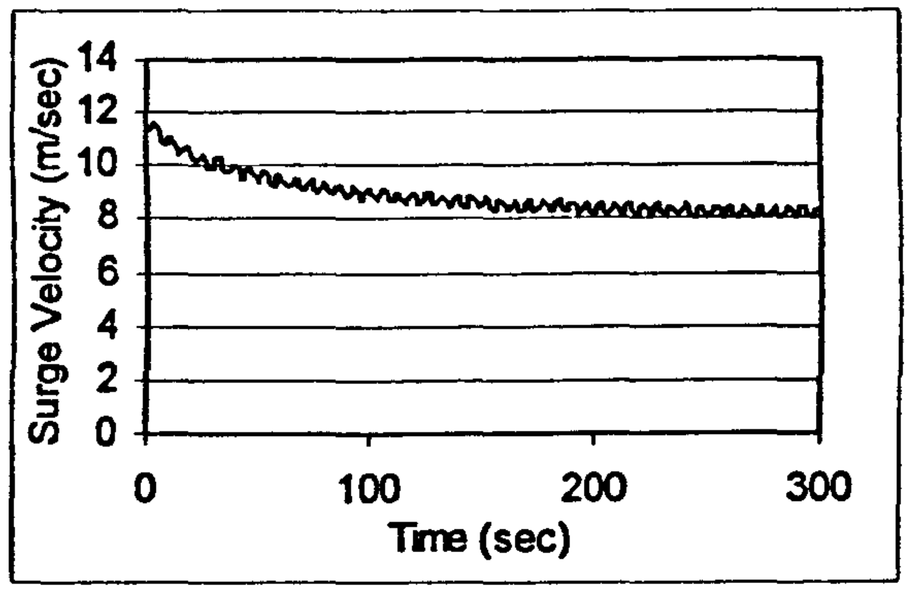

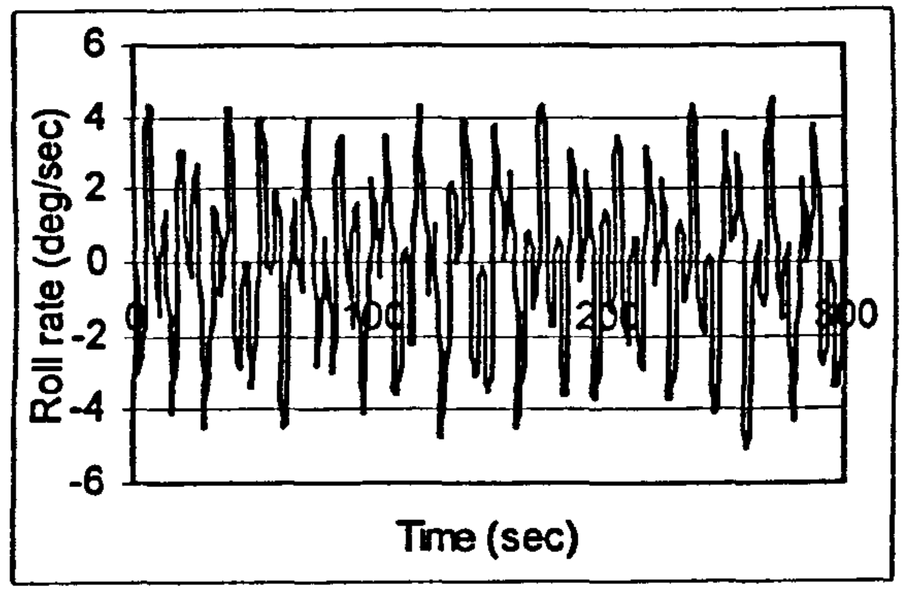

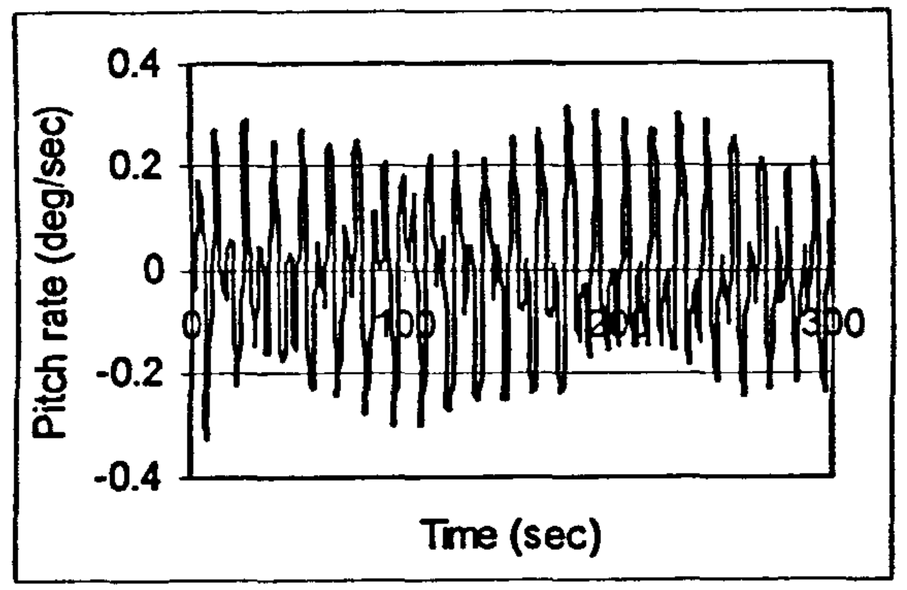

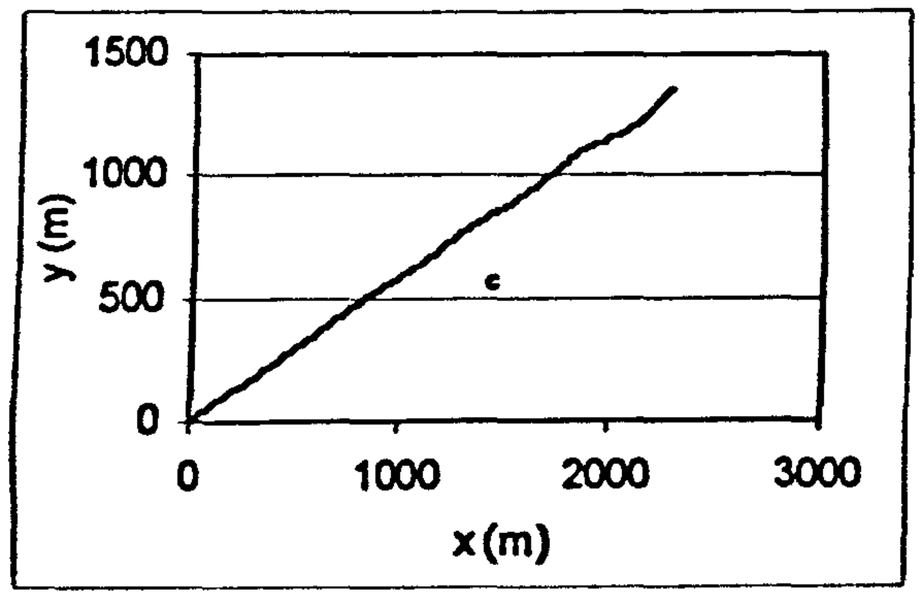

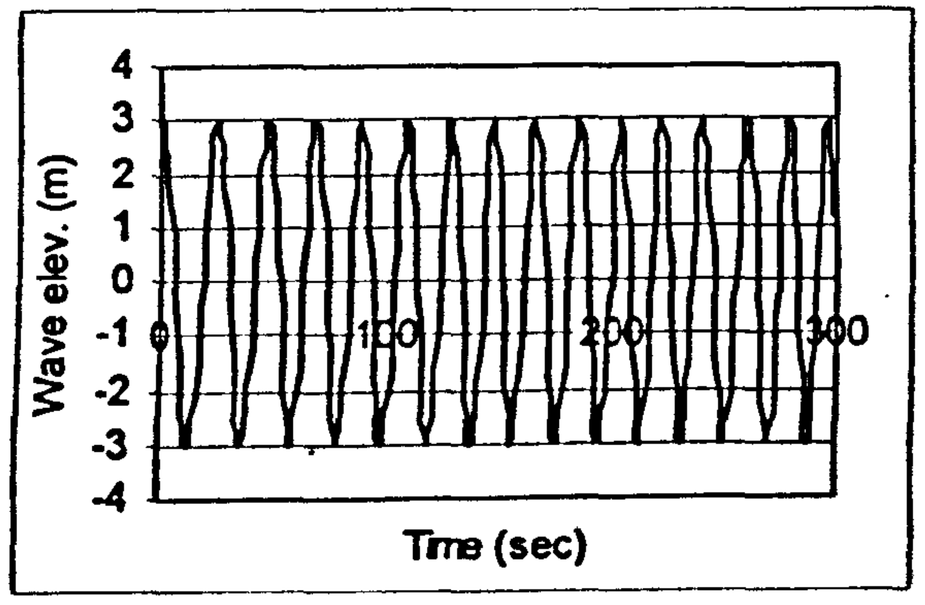

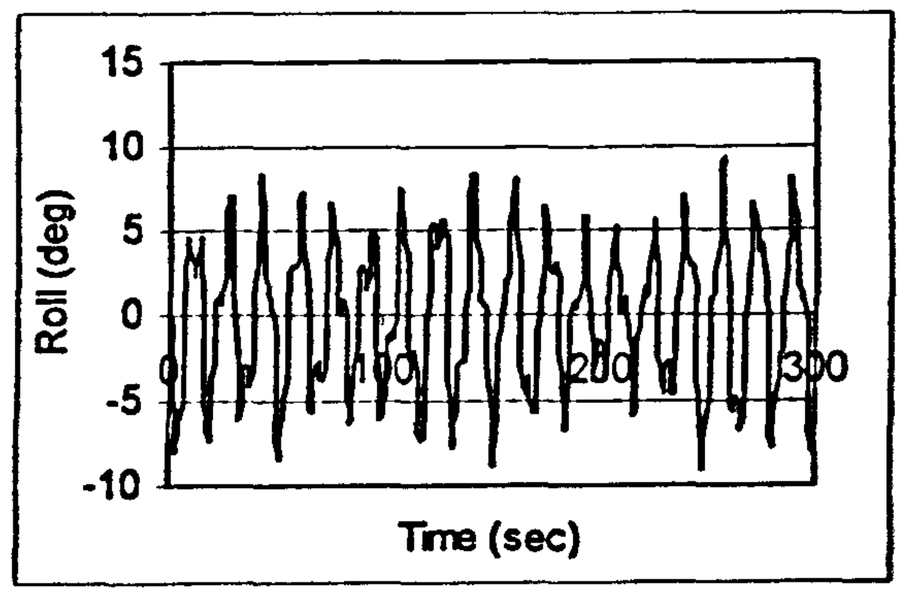

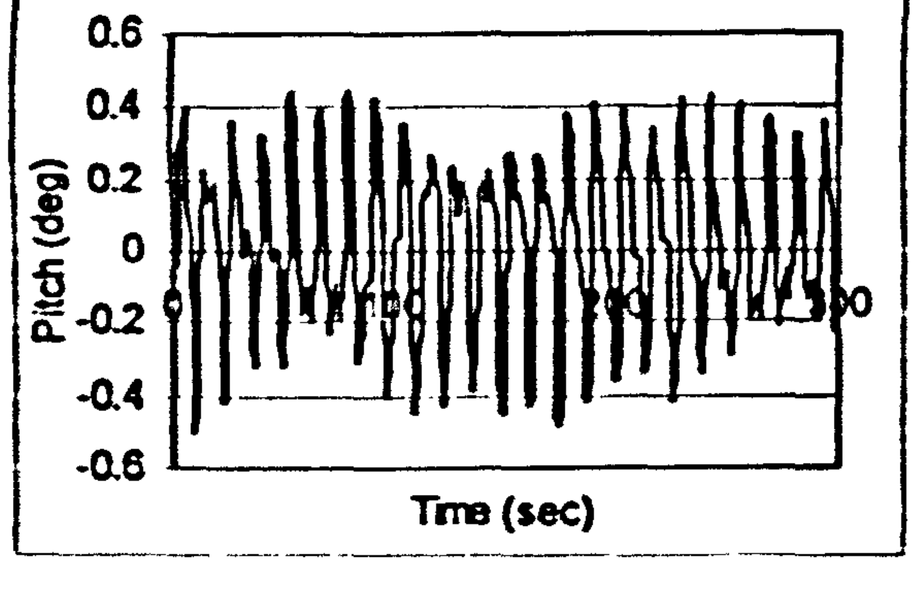

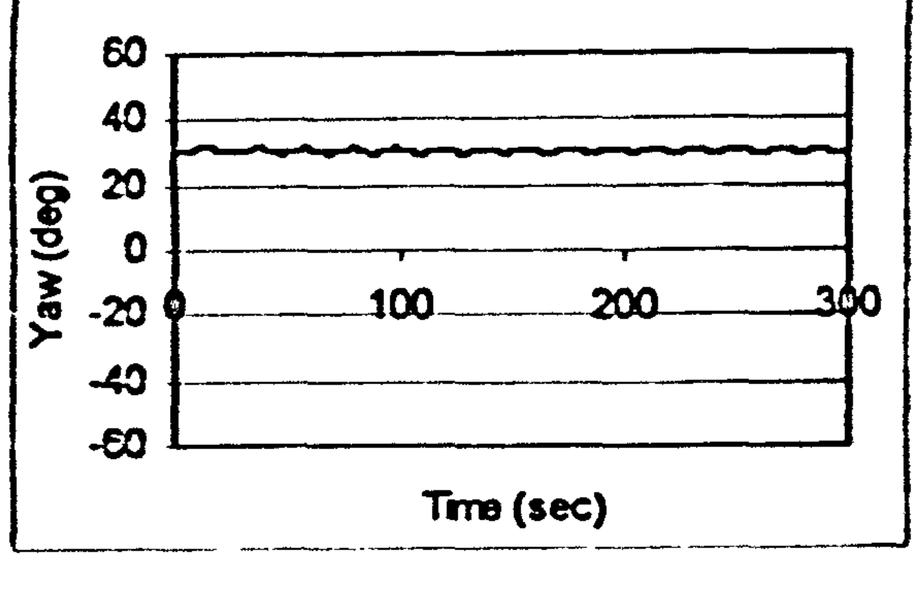

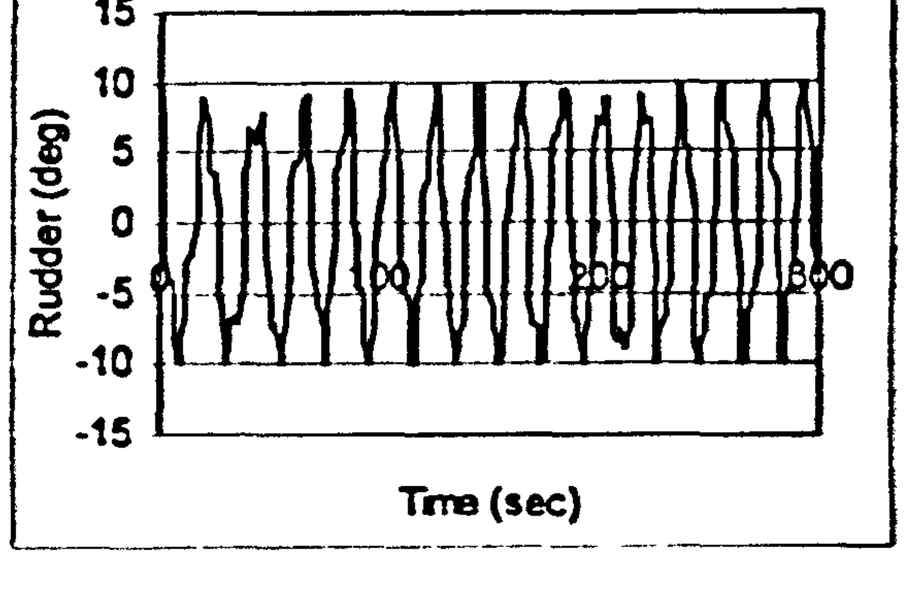

Figure G.20 Numerical Simulation of Ship A-1 with 4 DOF mathematical model in $H/\lambda=1/25$, $\lambda/L_{pp}=1.0$, Fn=0.3,χ_c =30 degrees

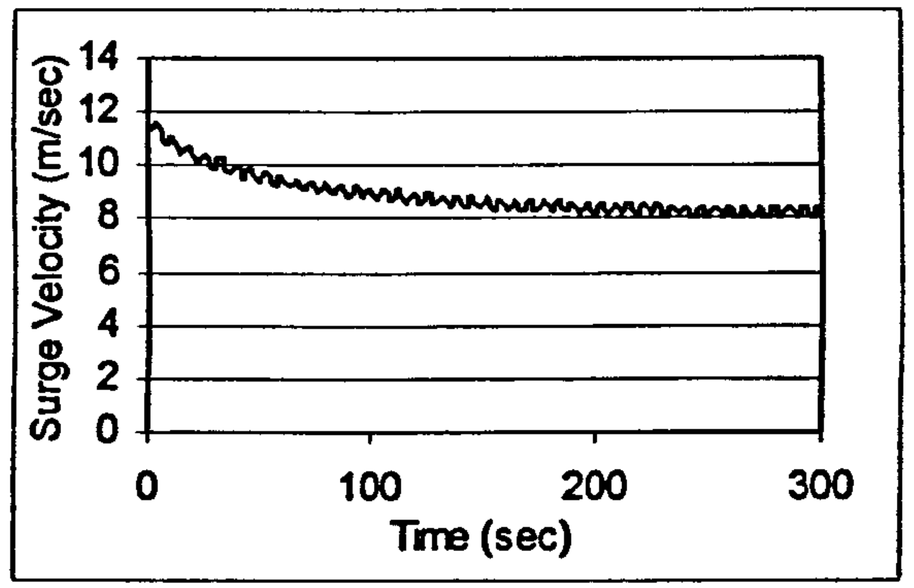

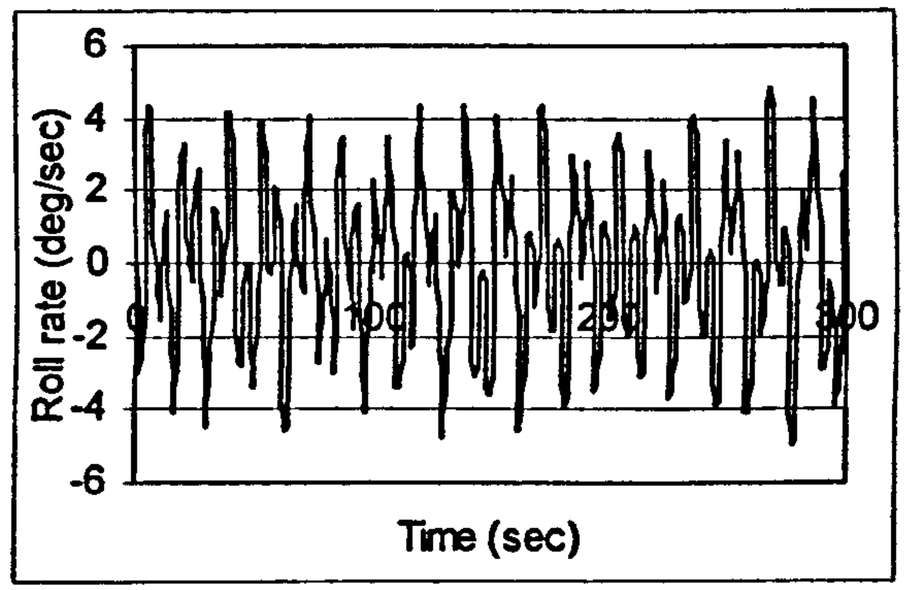

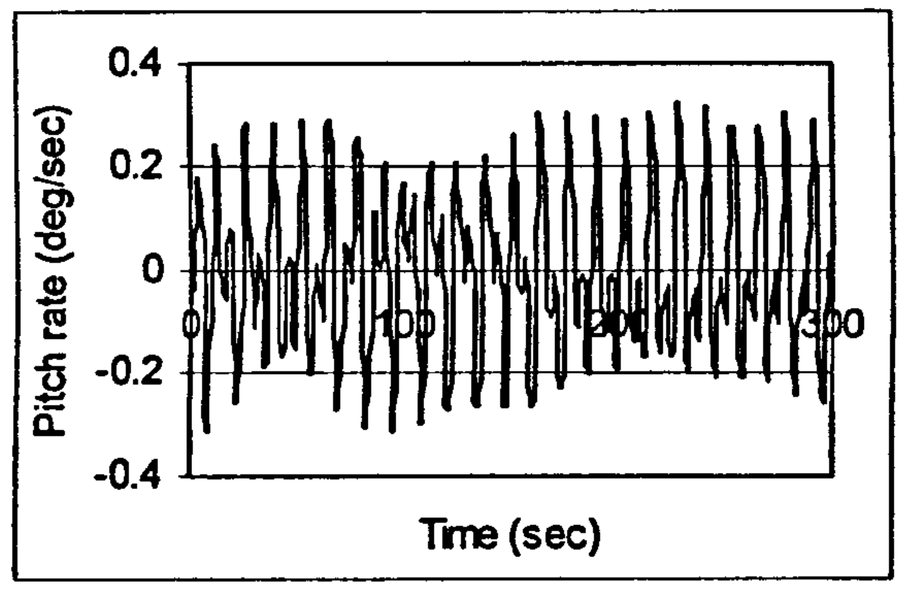

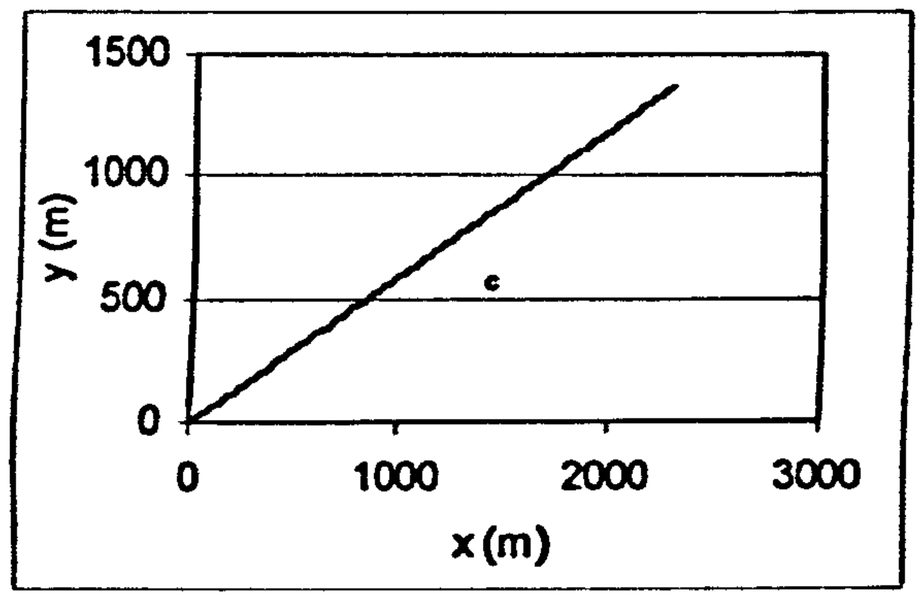

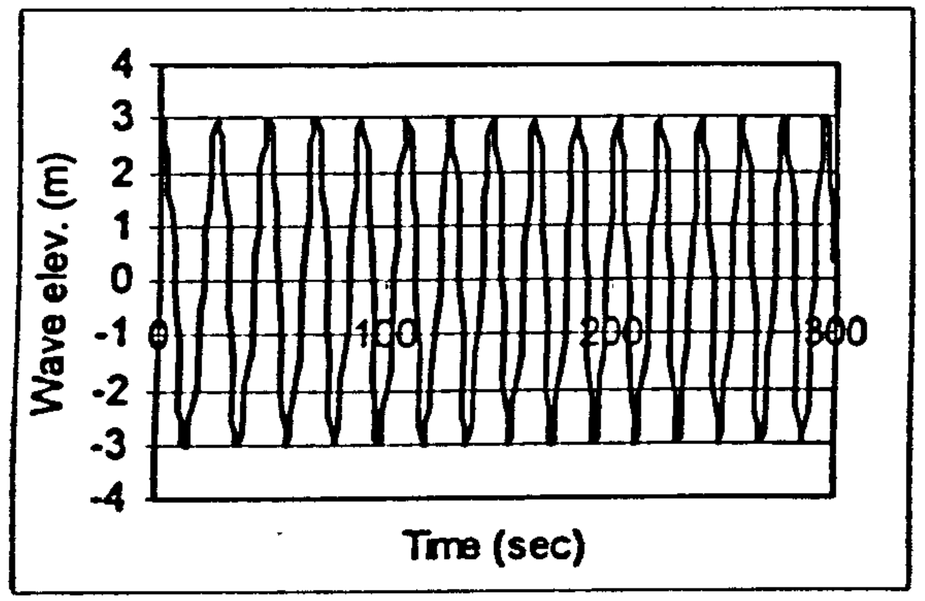

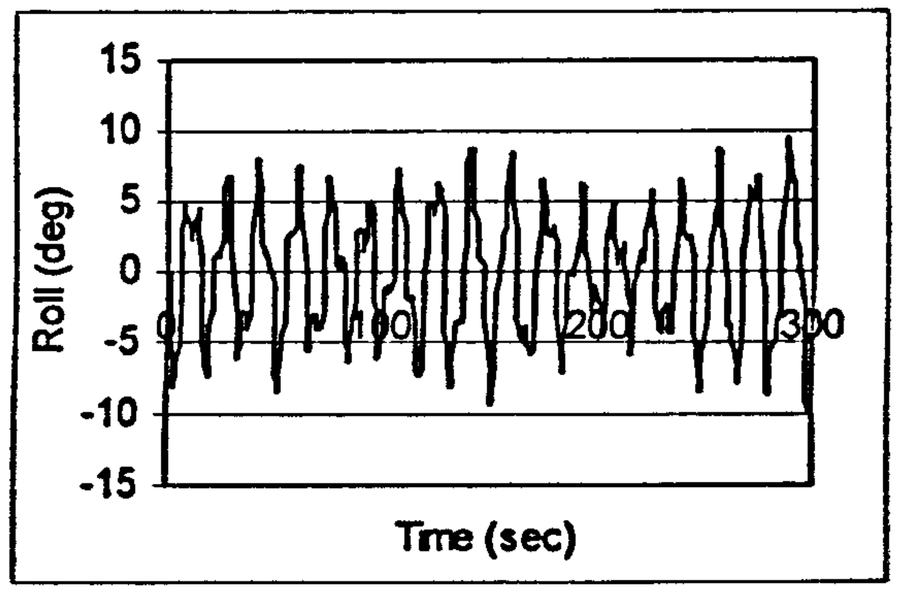

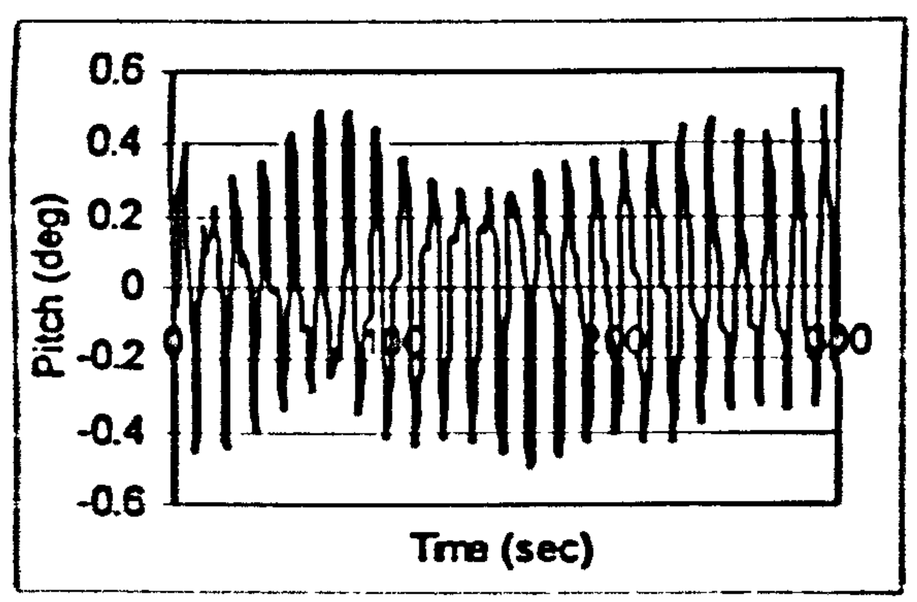

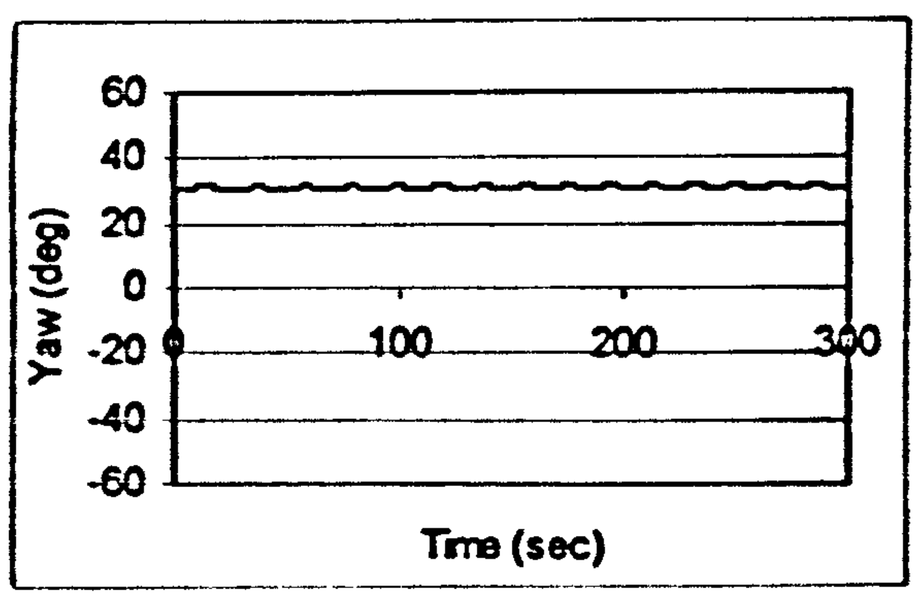

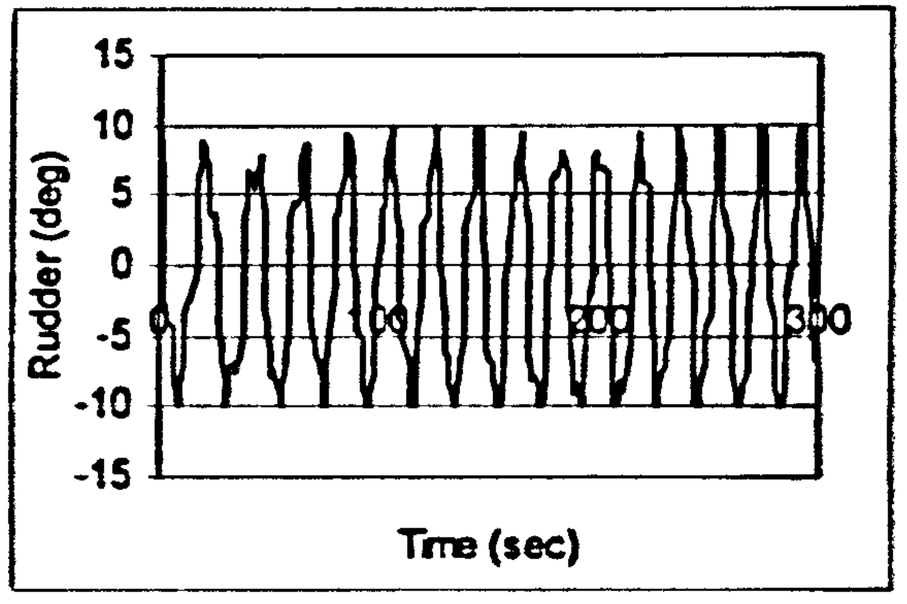

Figure G.21 Numerical Simulation of Ship A-1 with 6 DOF mathematical model in $H/\lambda=1/25$, $\lambda/L_{pp}=1.5$, Fn=0.3,χ_c=30 degrees

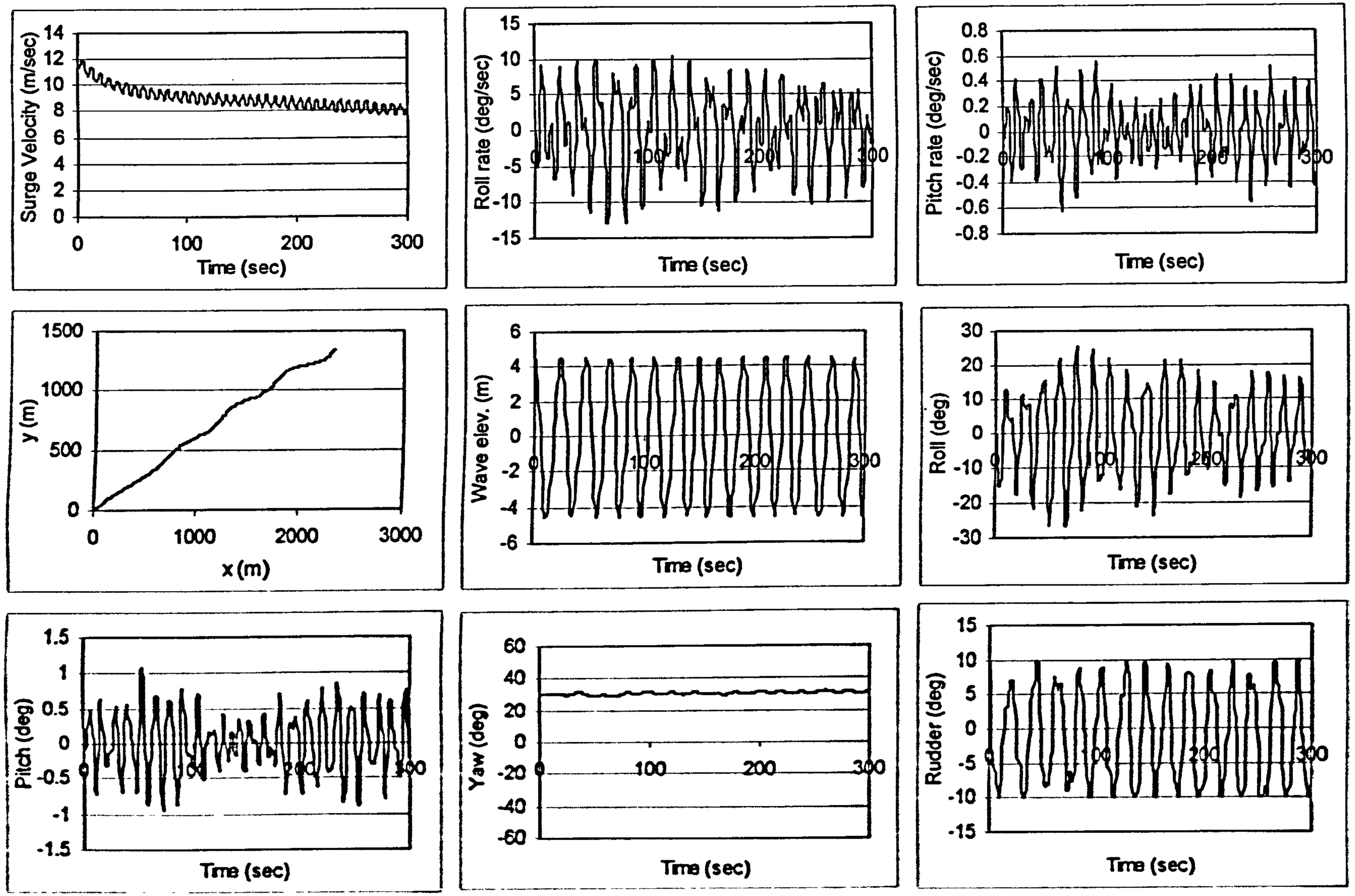

Figure G.22 Numerical Simulation of Ship A-1 with 4 DOF mathematical model in $H/\lambda=1/25$, $\lambda/L_{pp}=1.5$, Fn=0.3,$\chi_c=30$ degrees

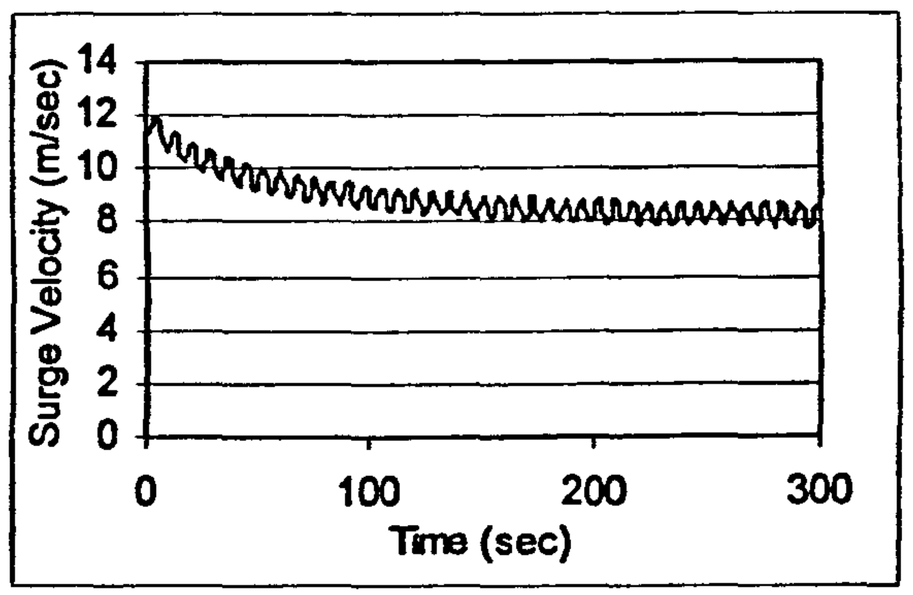

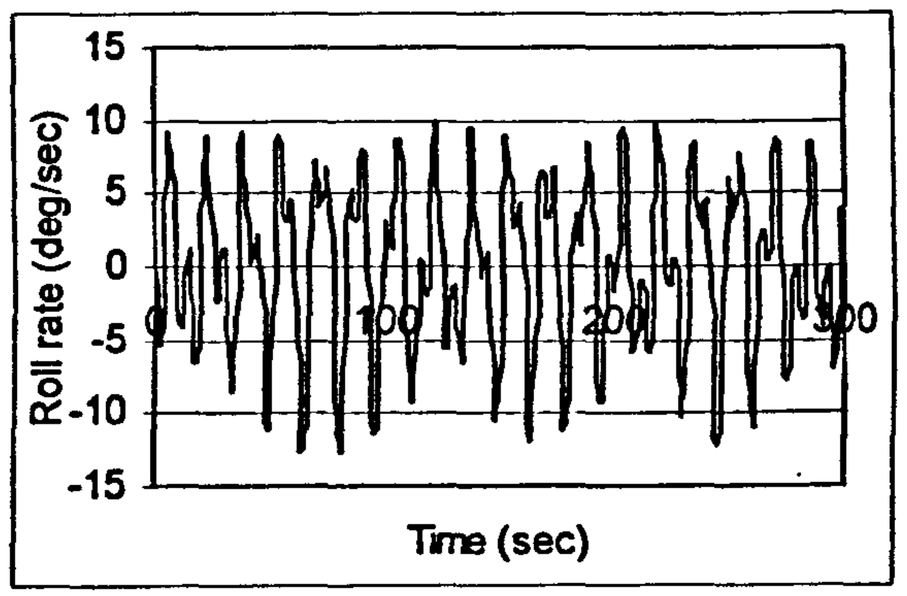

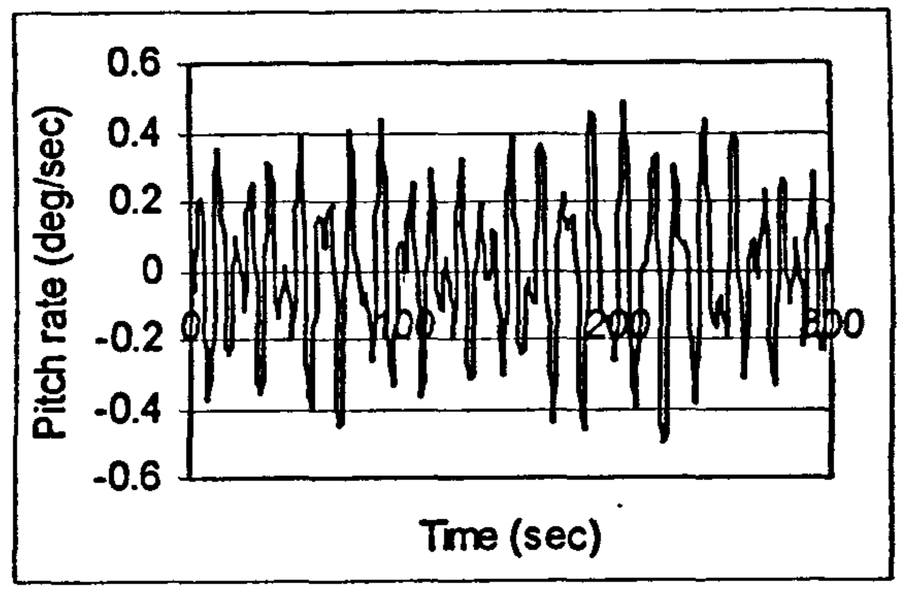

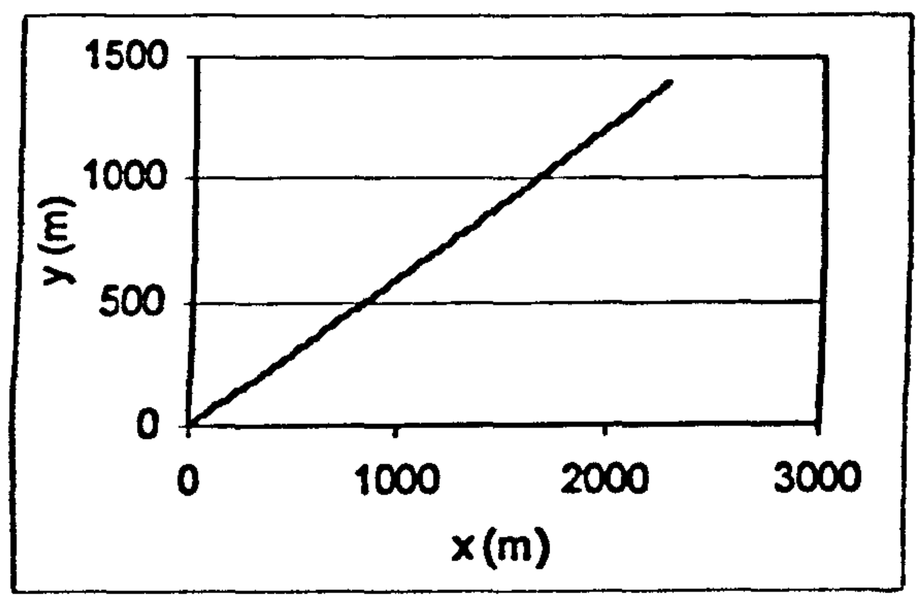

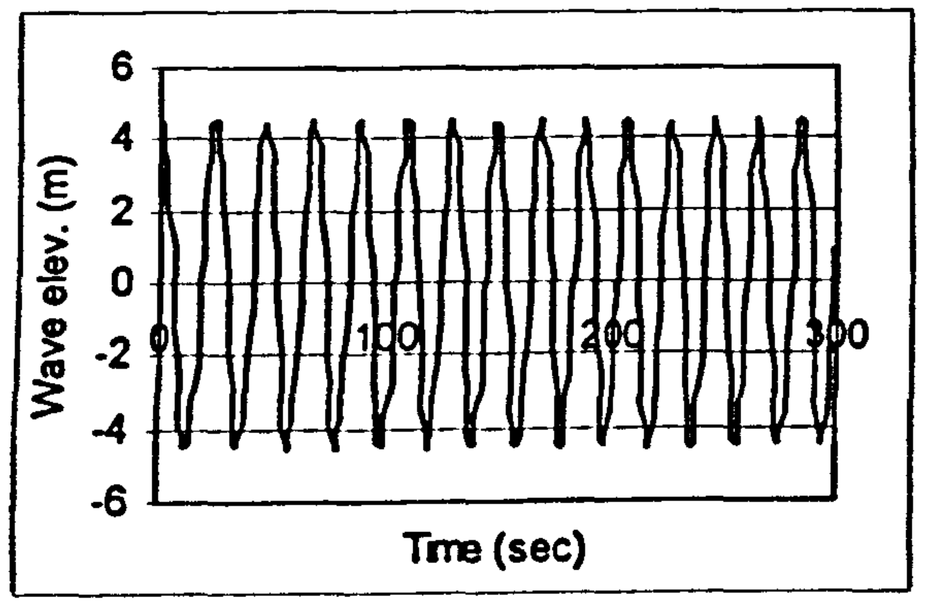

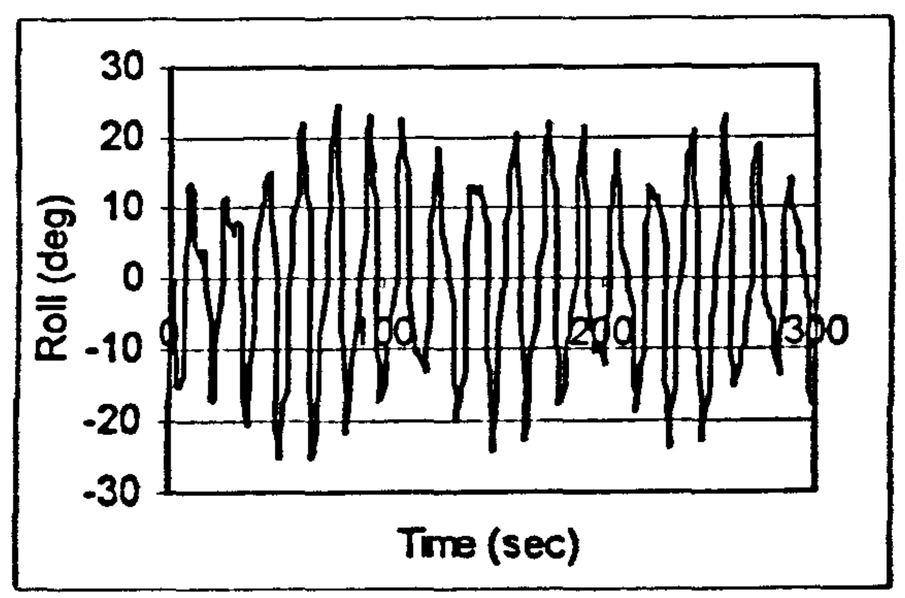

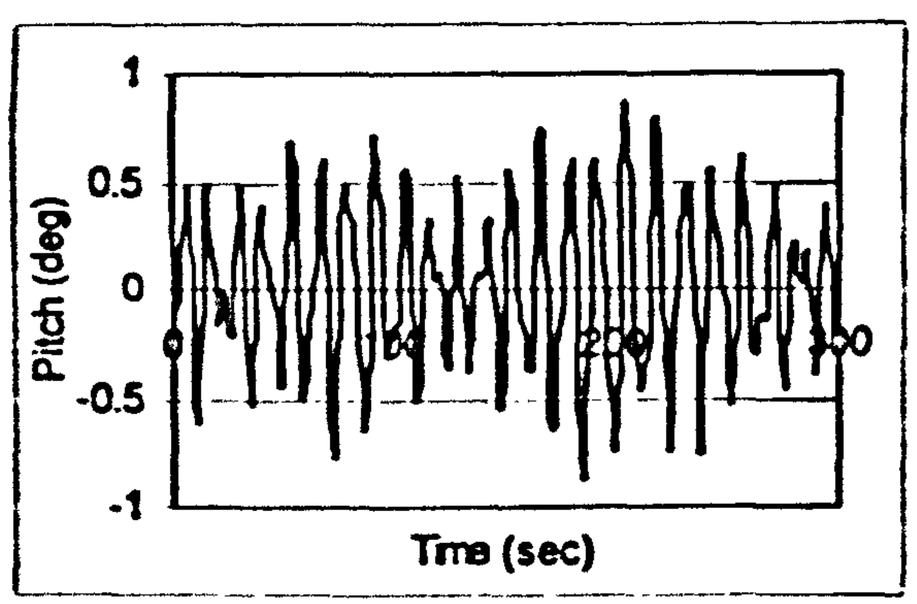

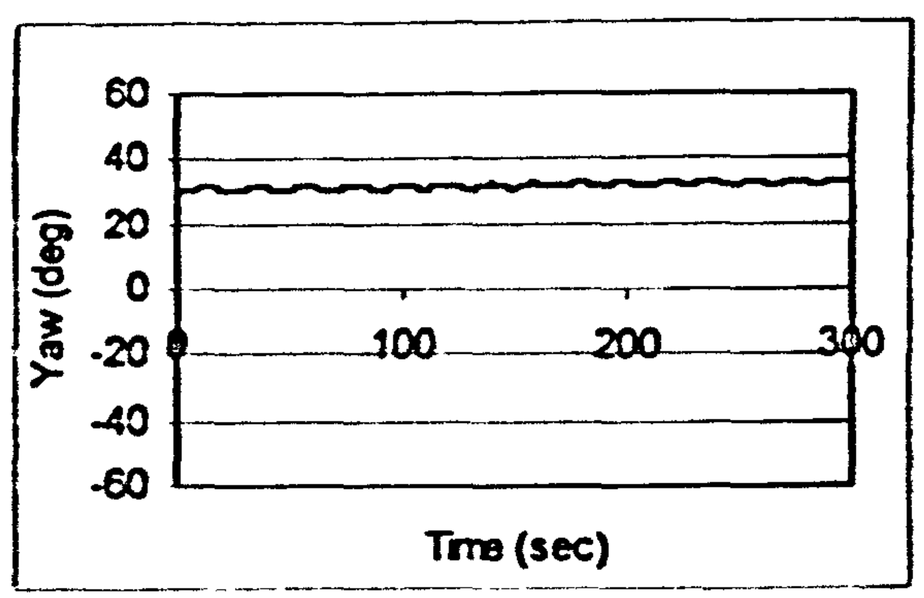

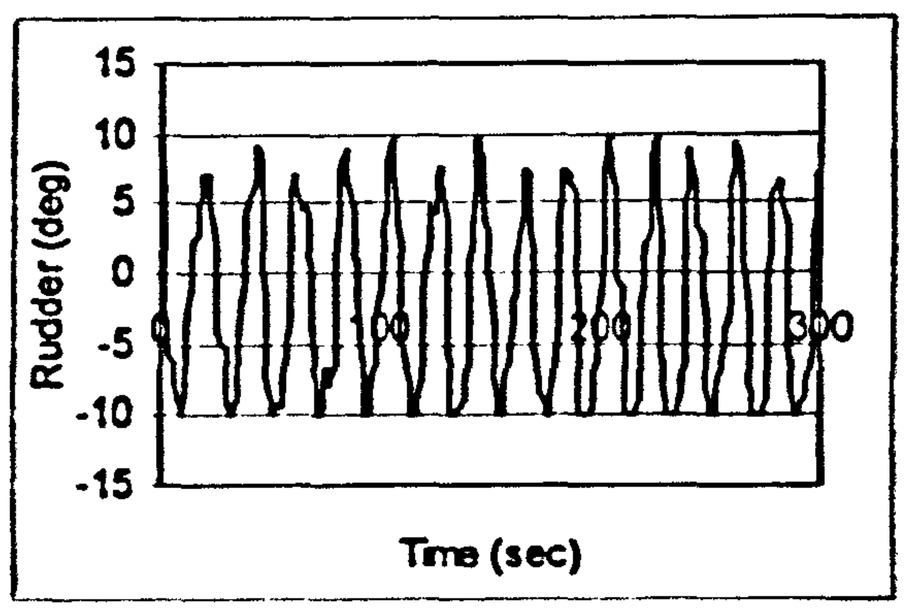

Figure G.23 Numerical Simulation of Ship A-1 with 6 DOF mathematical model in $H/\lambda=1/25$, $\lambda/L_{pp}=2.0$, $Fn=0.3$, $\chi_c=30$ degrees

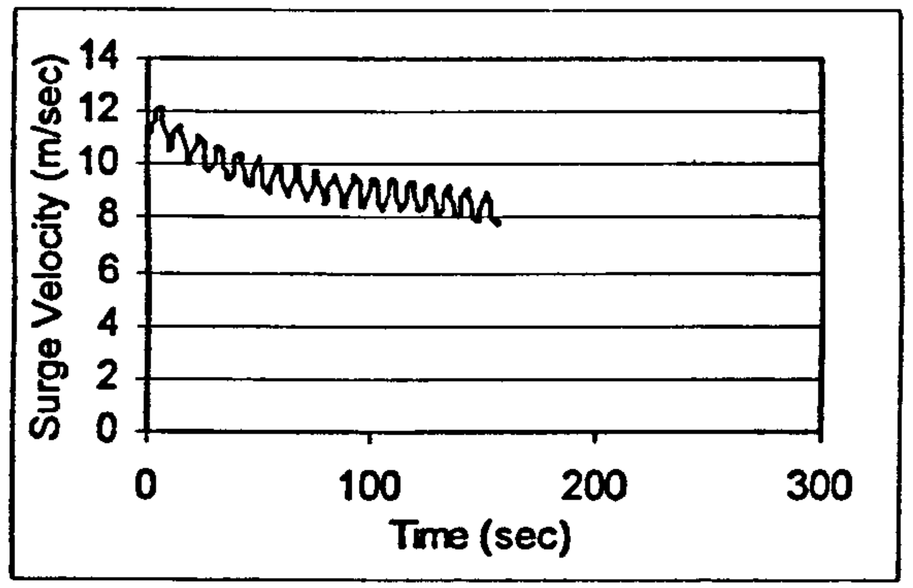

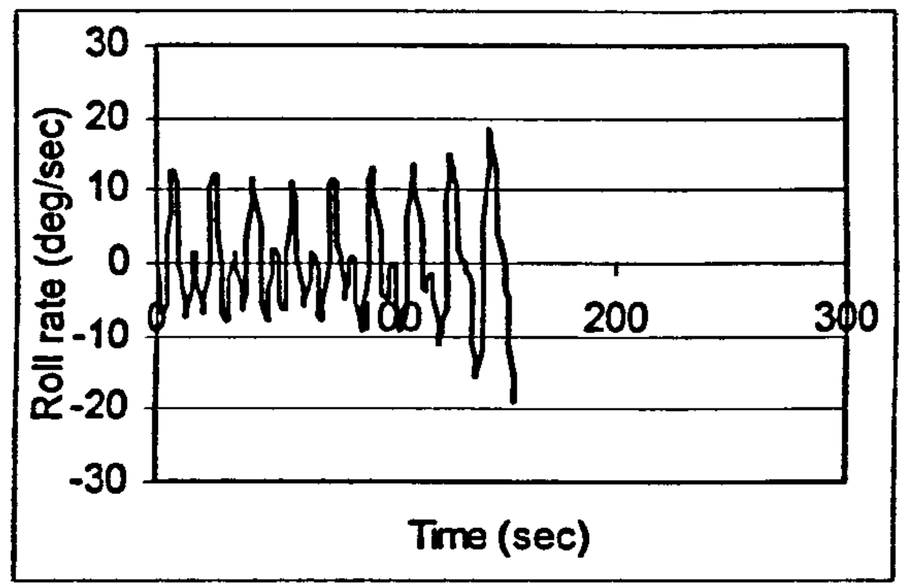

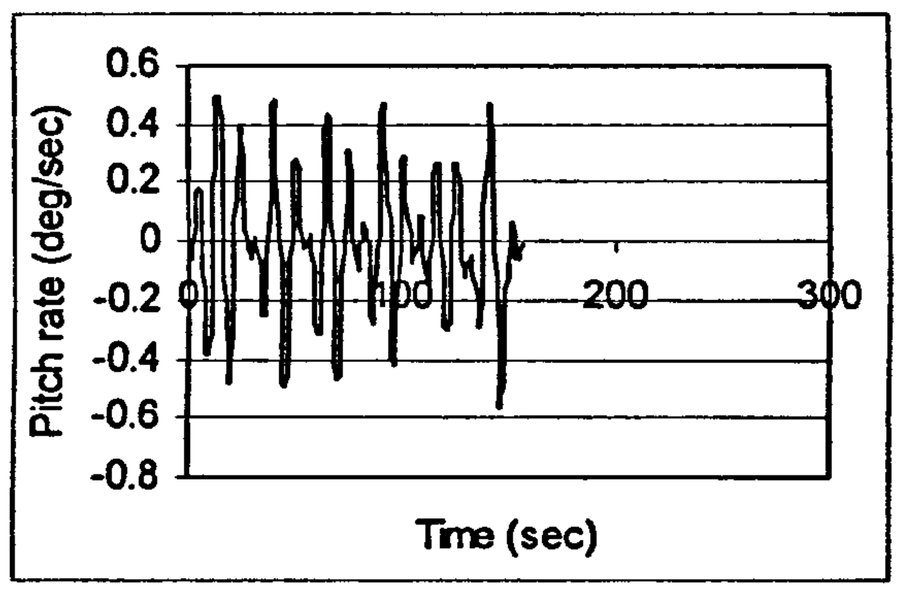

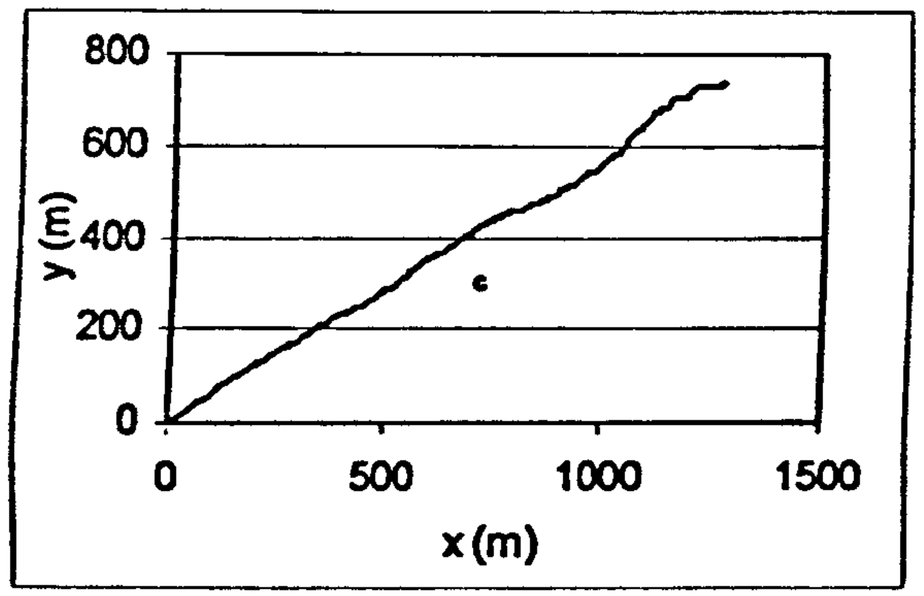

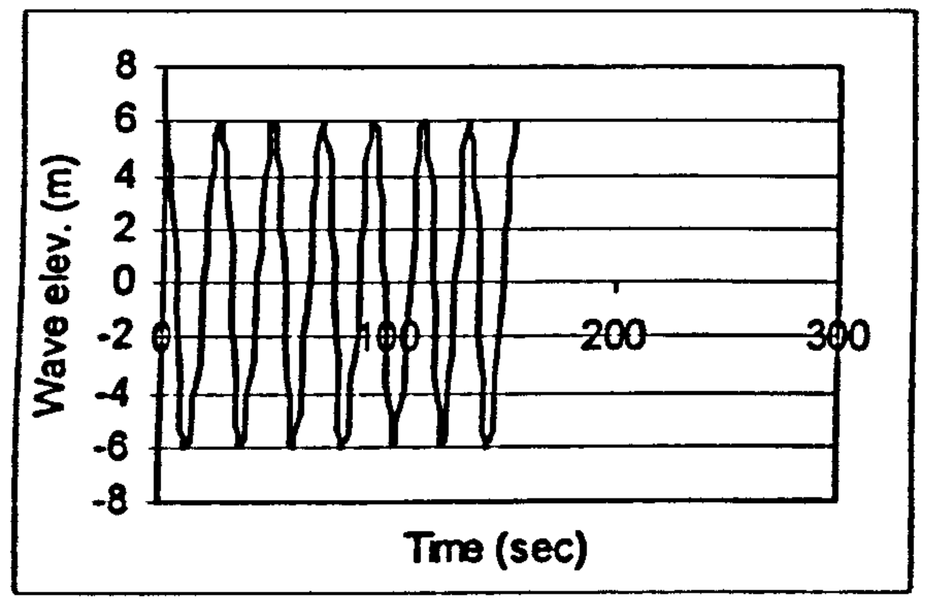

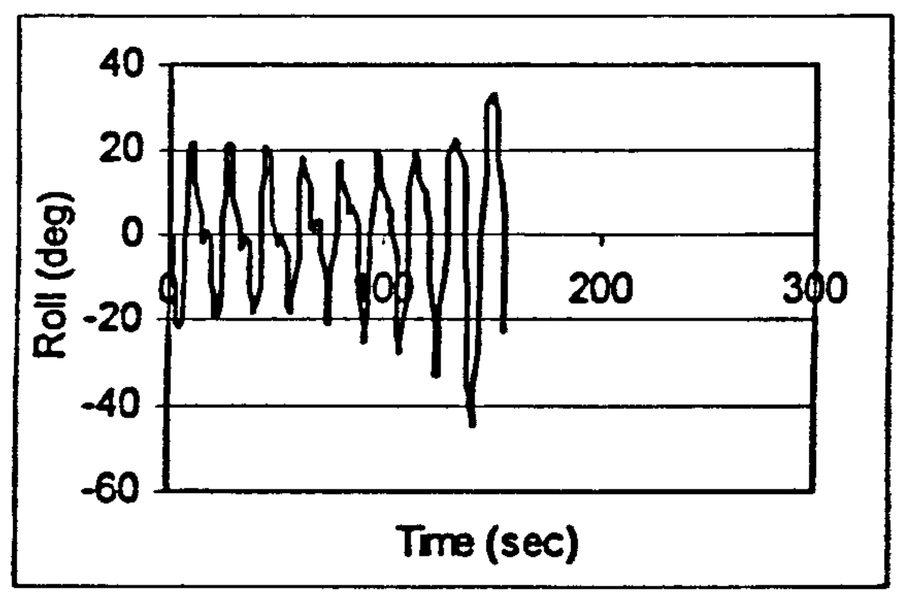

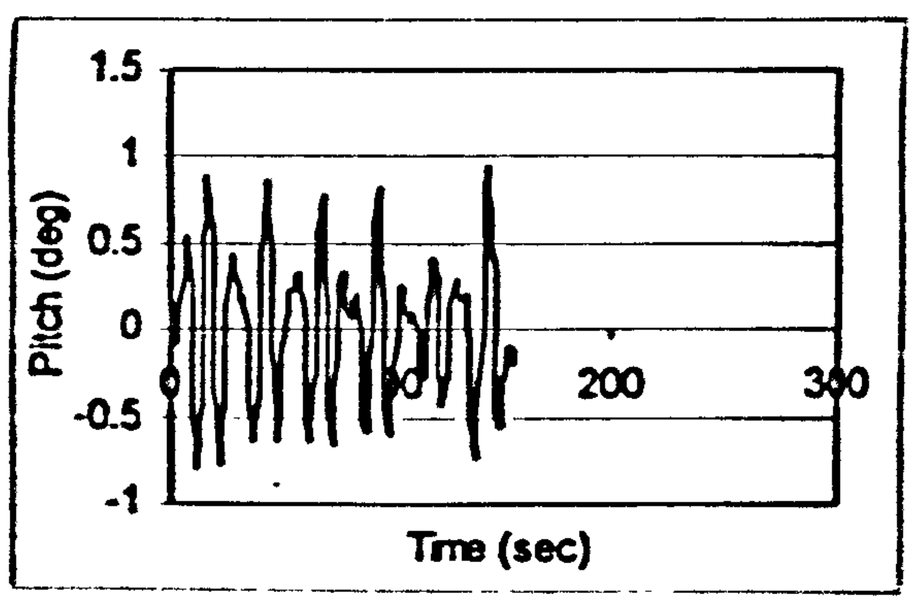

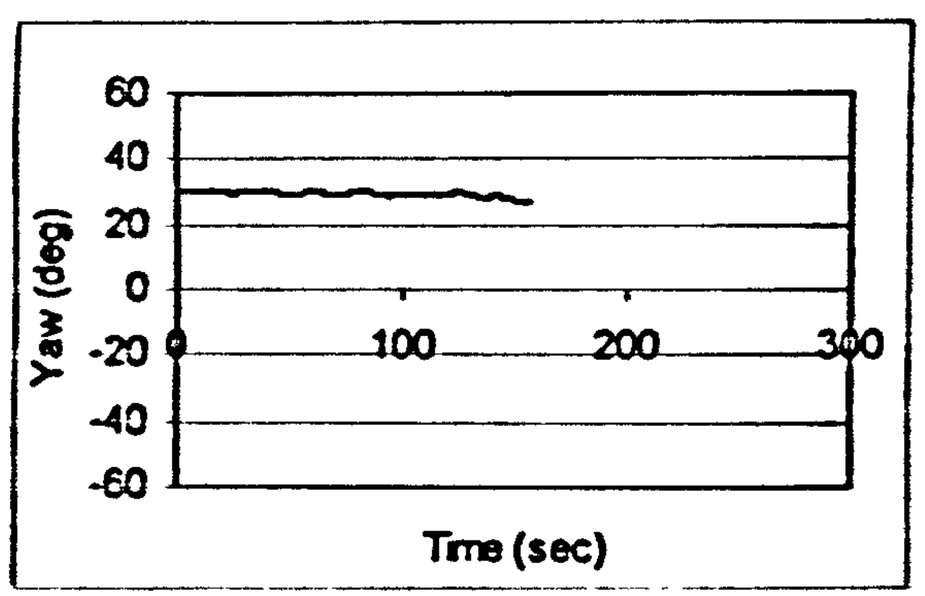

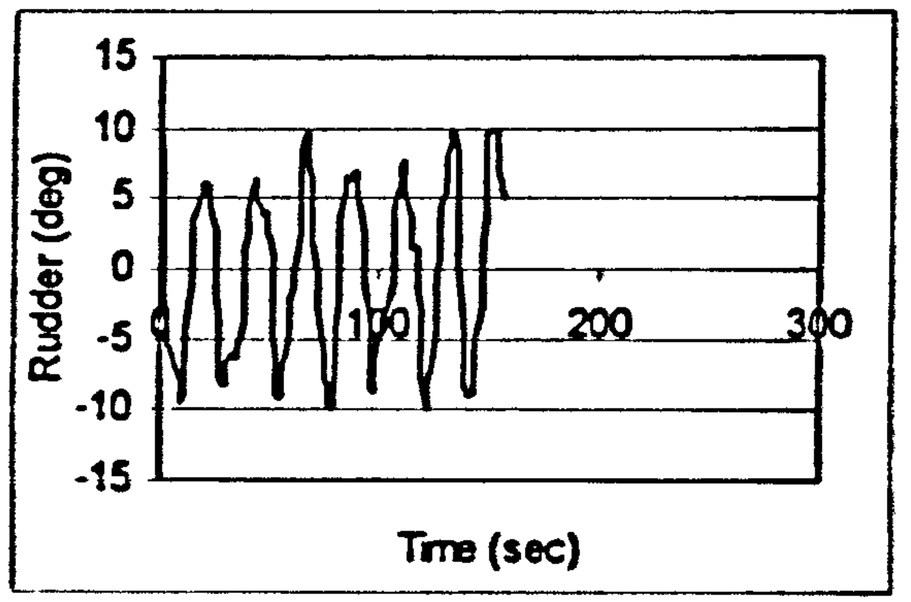

Figure G.24 Numerical Simulation of Ship A-1 with 4 DOF mathematical model in $H/\lambda=1/25$, $\lambda/L_{pp}=2.0$, $Fn=0.3$, $\chi_c=30$ degrees

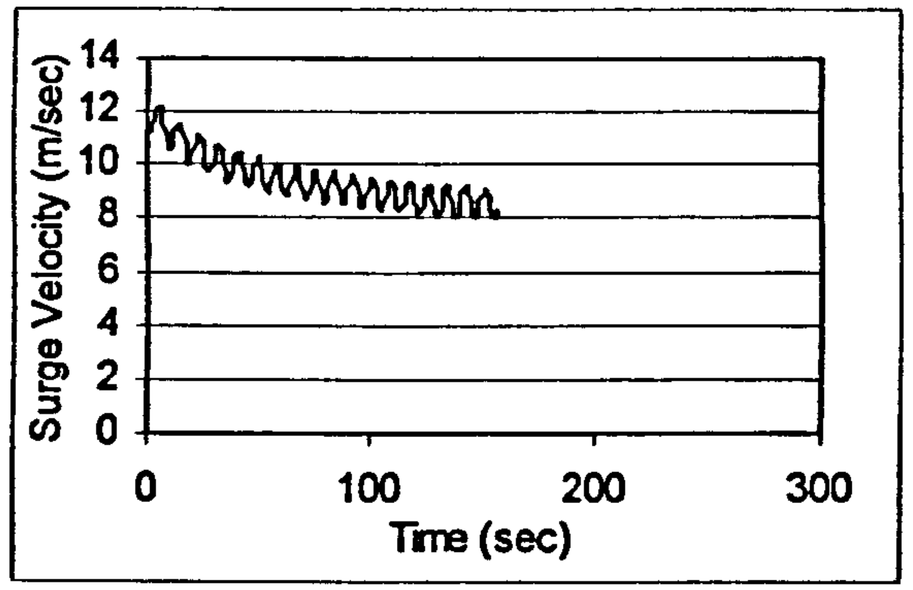

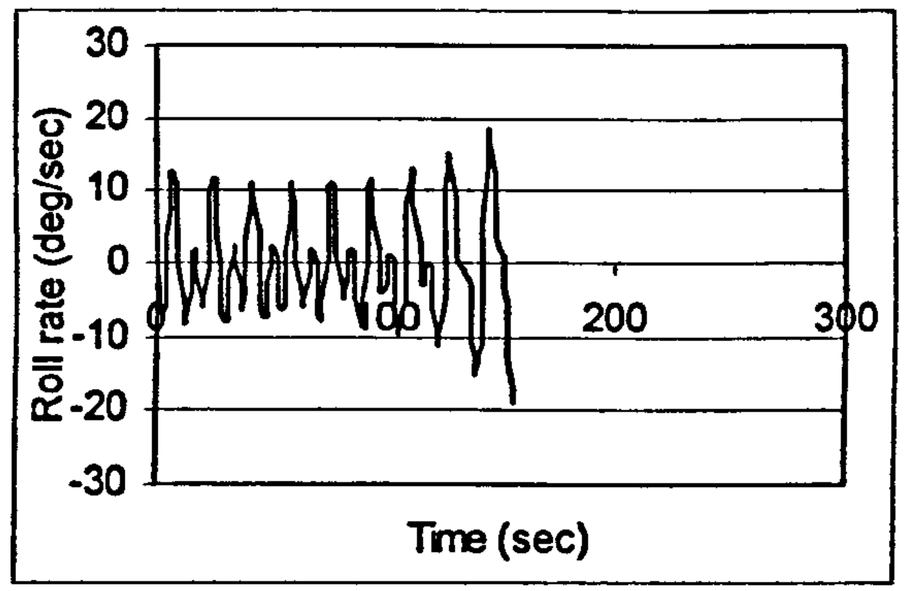

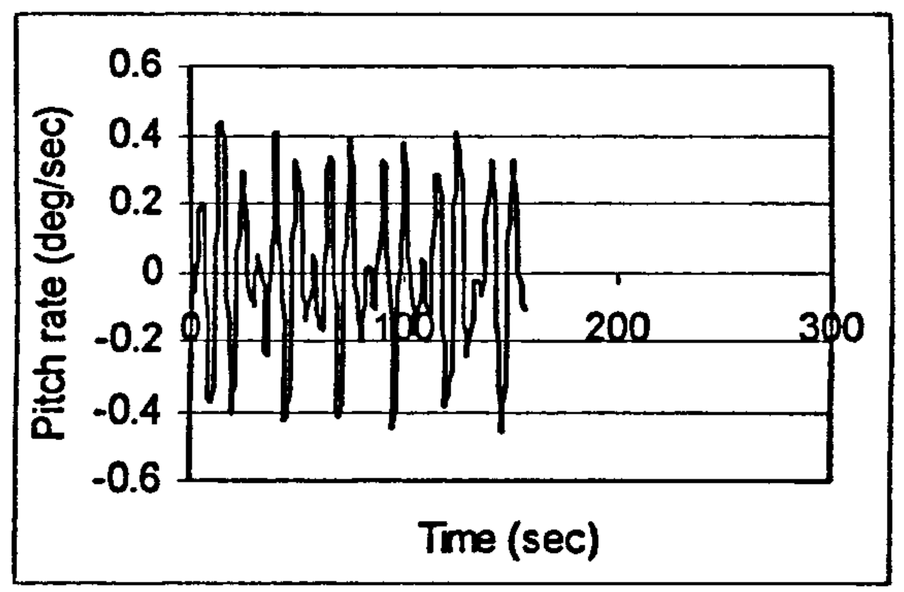

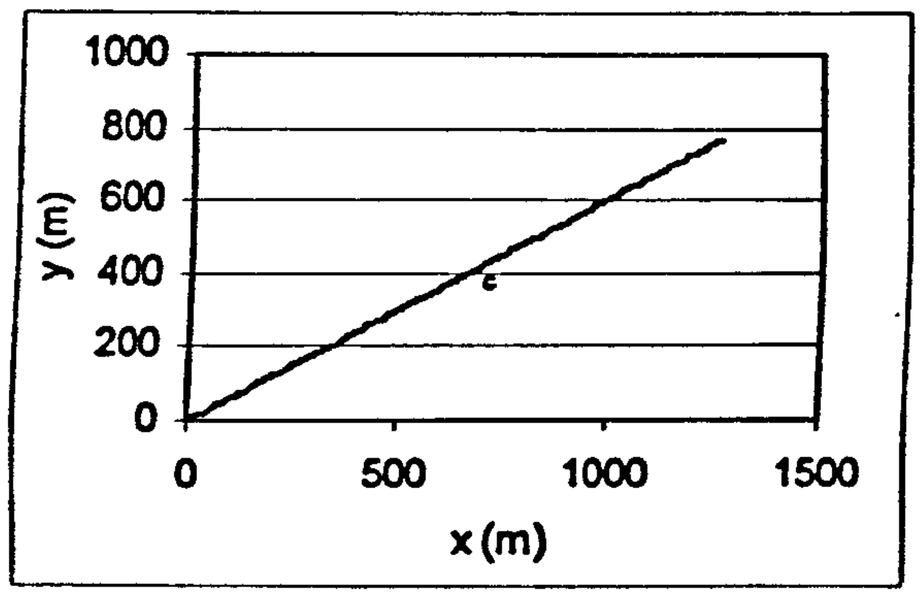

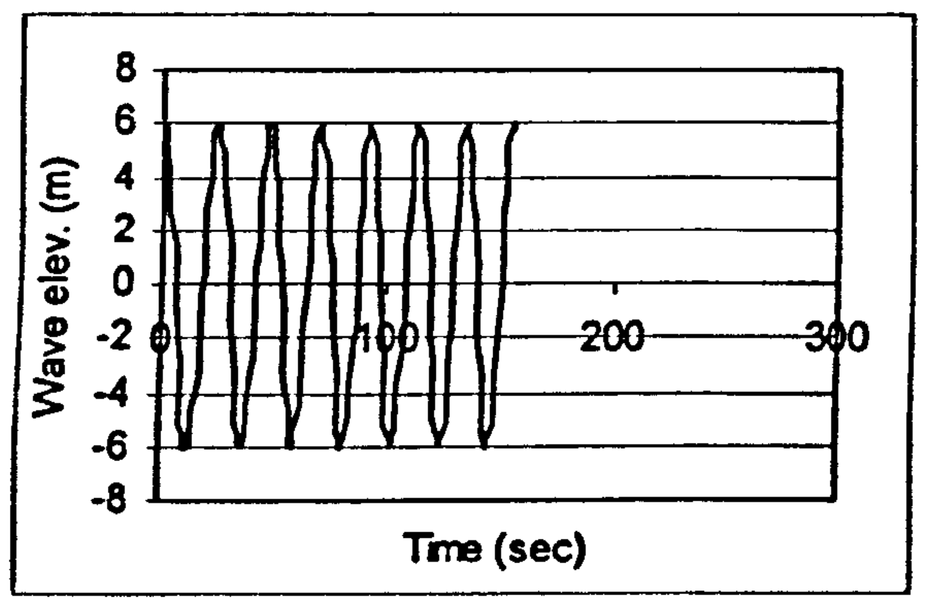

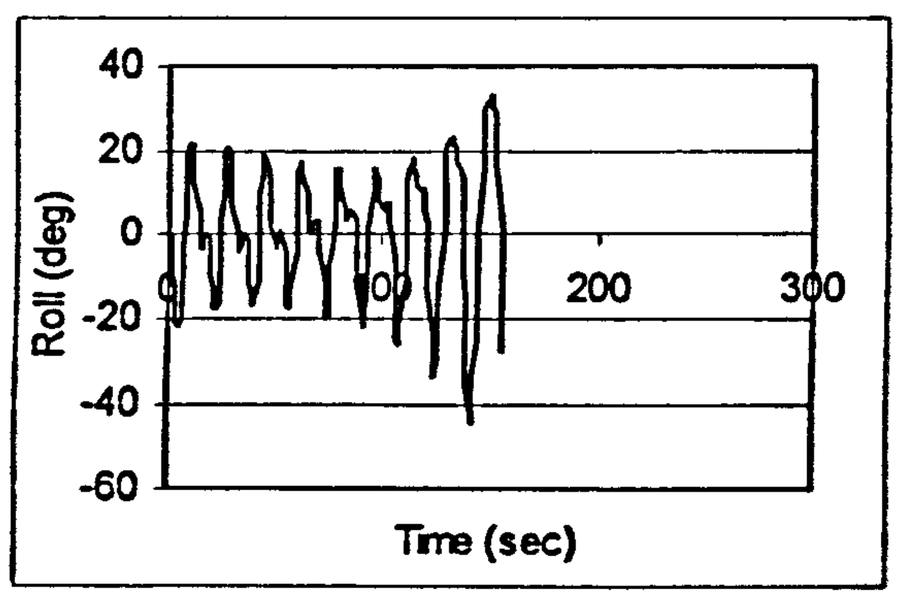

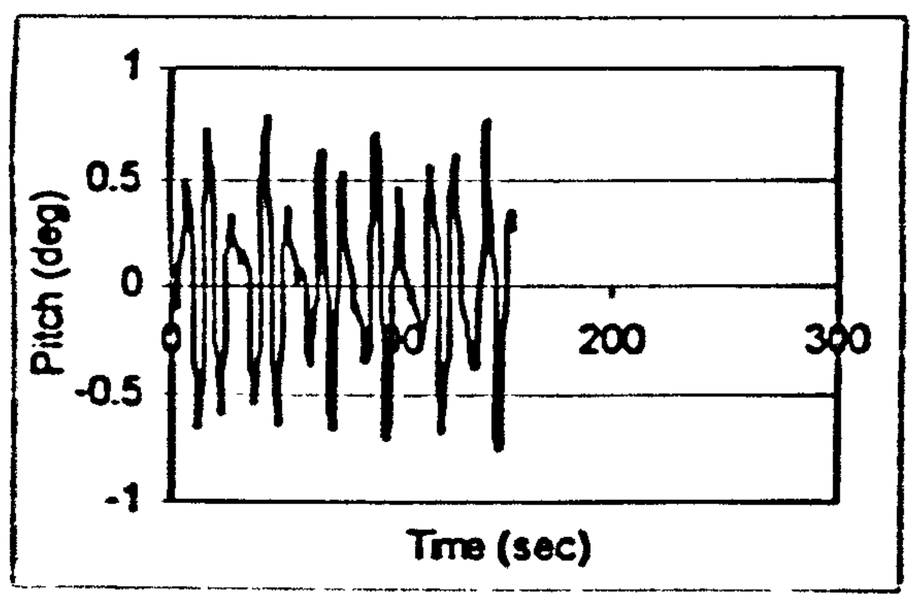

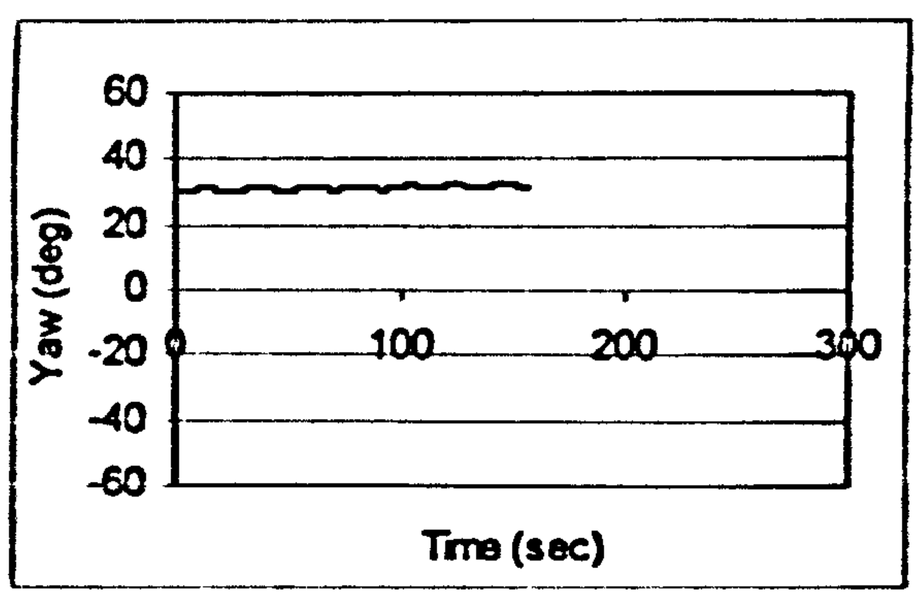

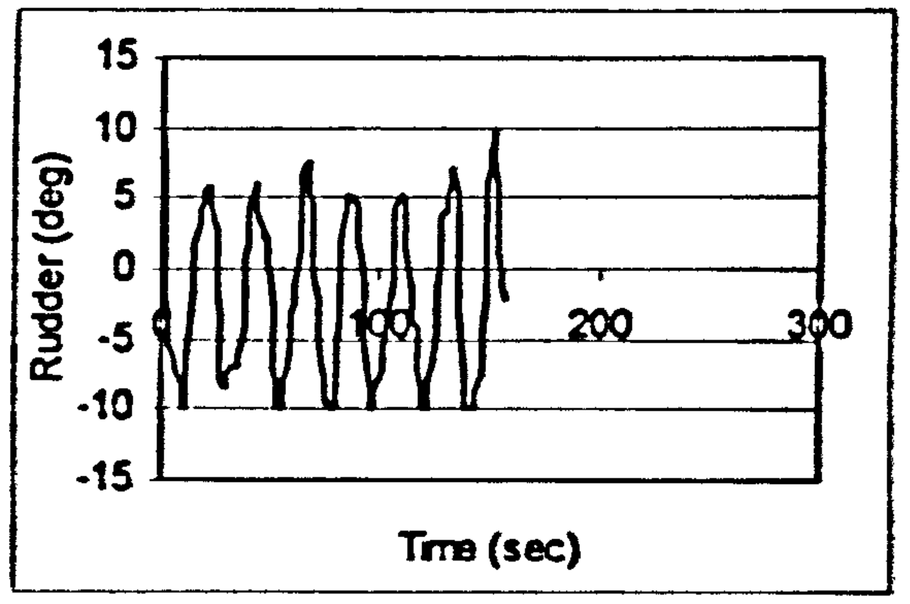

Figure G.25 Numerical Simulation of Ship A-1 in $H/\lambda=1/25$, $\lambda/L_{pp}=1.5$, Fn=0.4,χ_c =45 degrees, GM=0.15 m

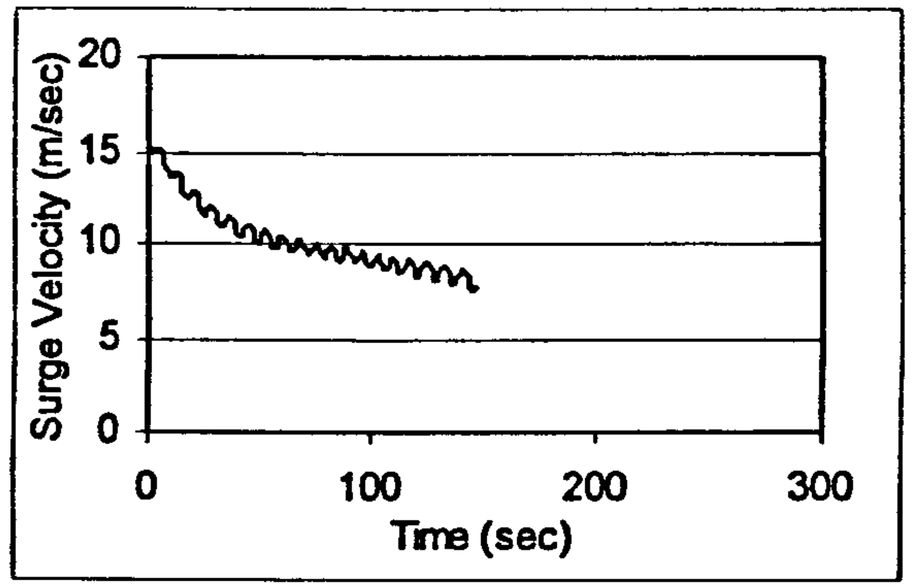

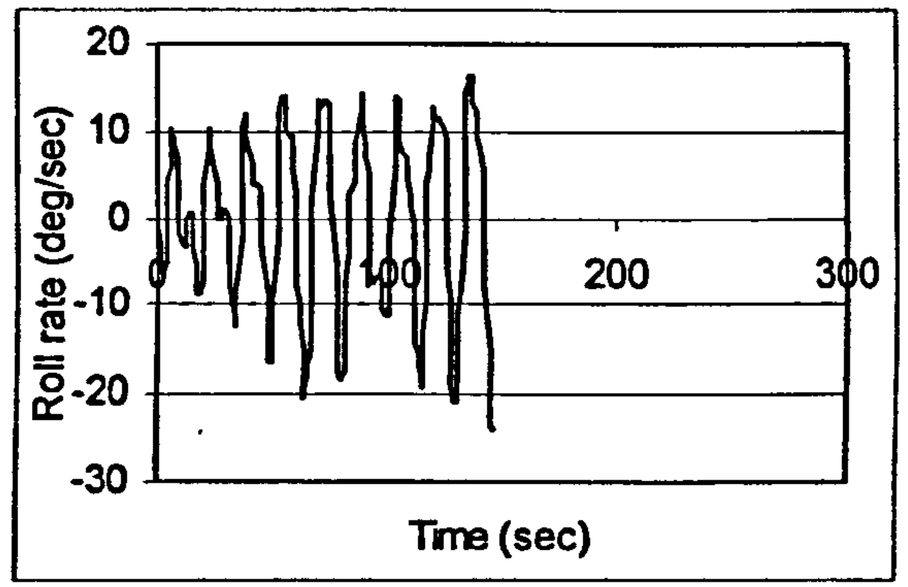

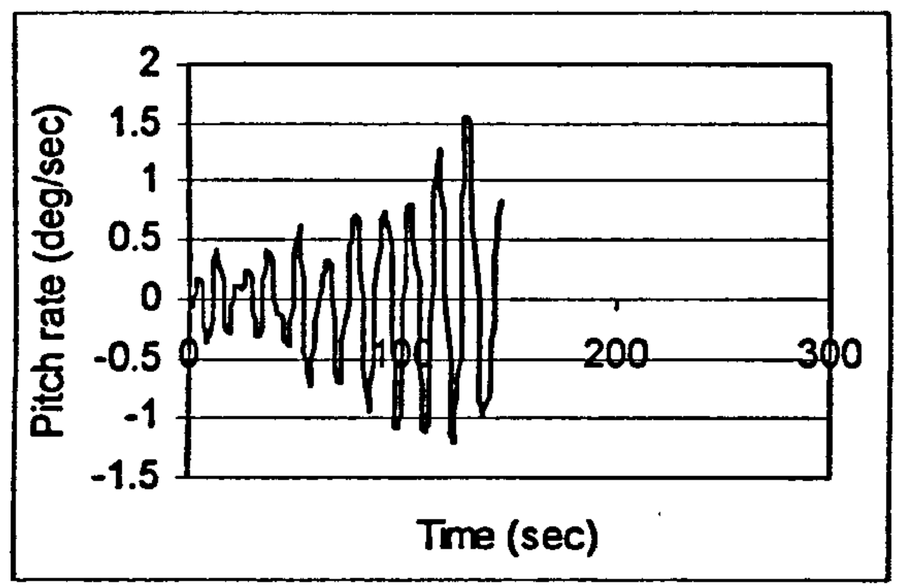

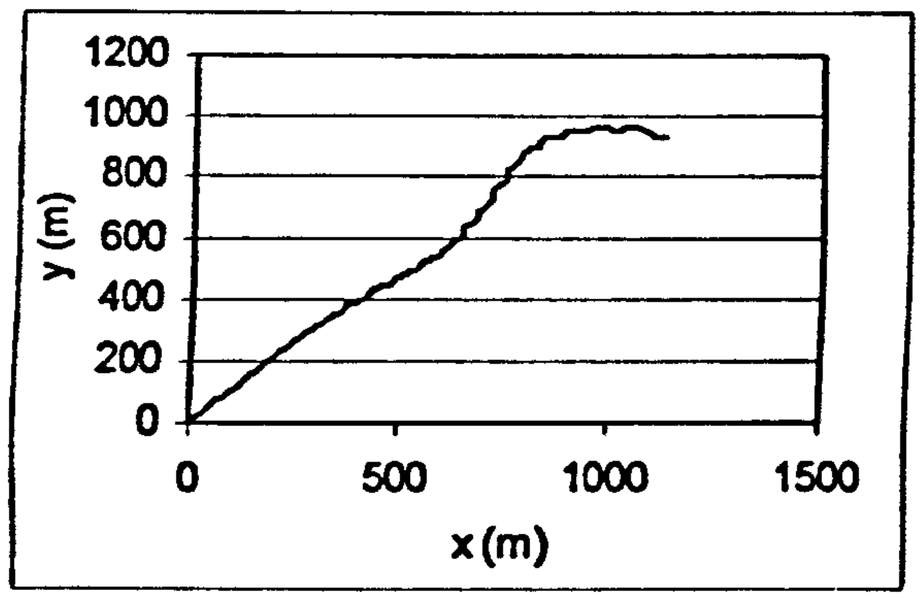

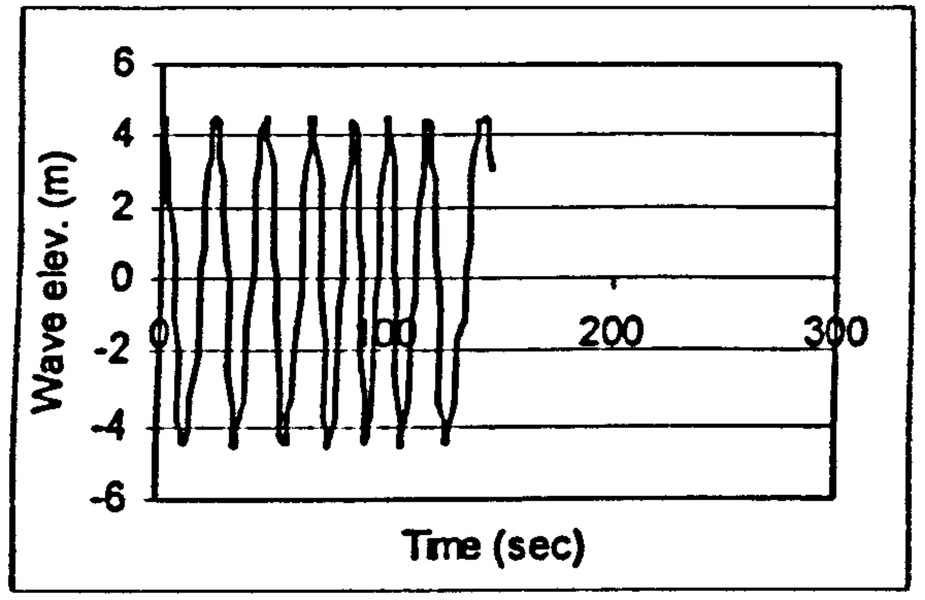

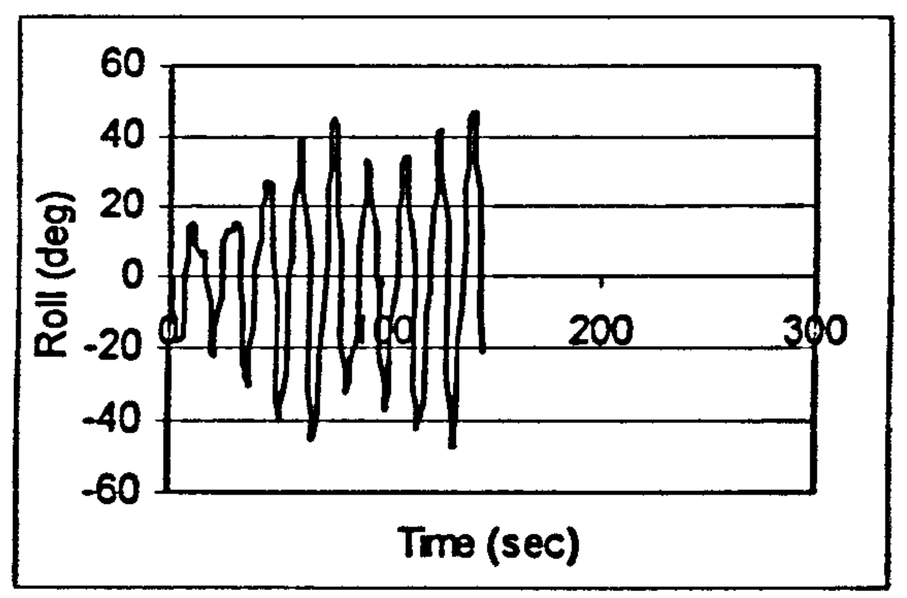

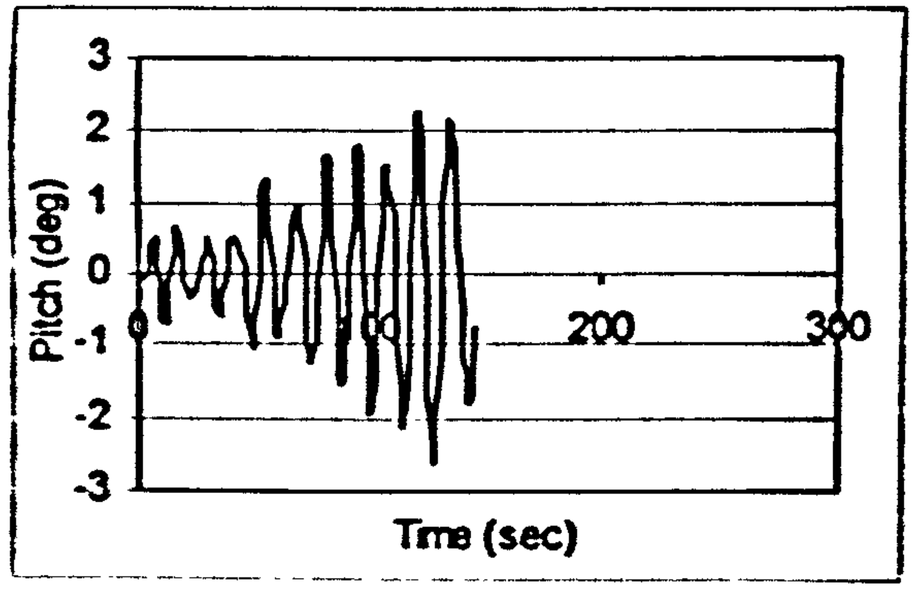

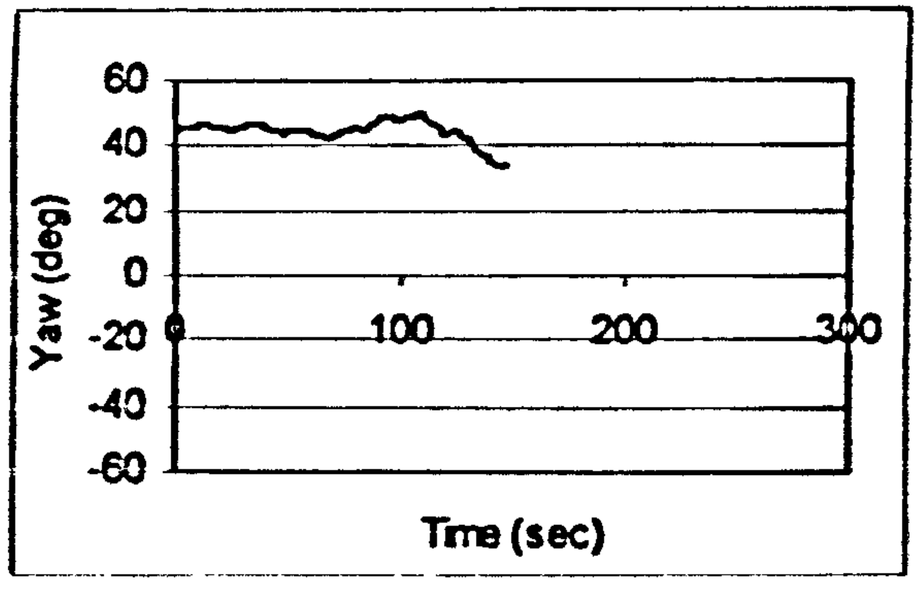

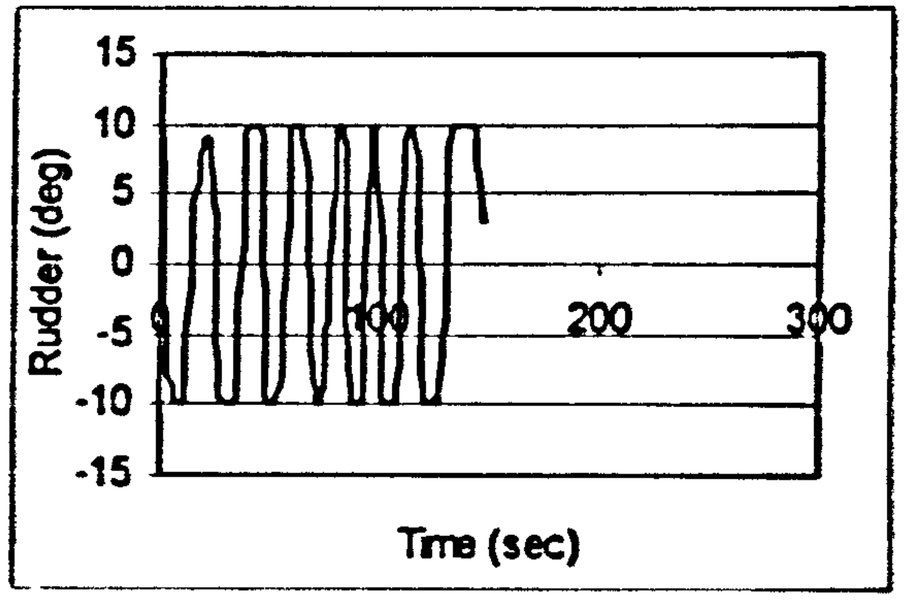

Figure G.26 Numerical Simulation of Ship A-1 in $H/\lambda=1/25$, $\lambda/L_{pp}=1.5$, Fn=0.4,χ_c =45 degrees, GM=0.30 m

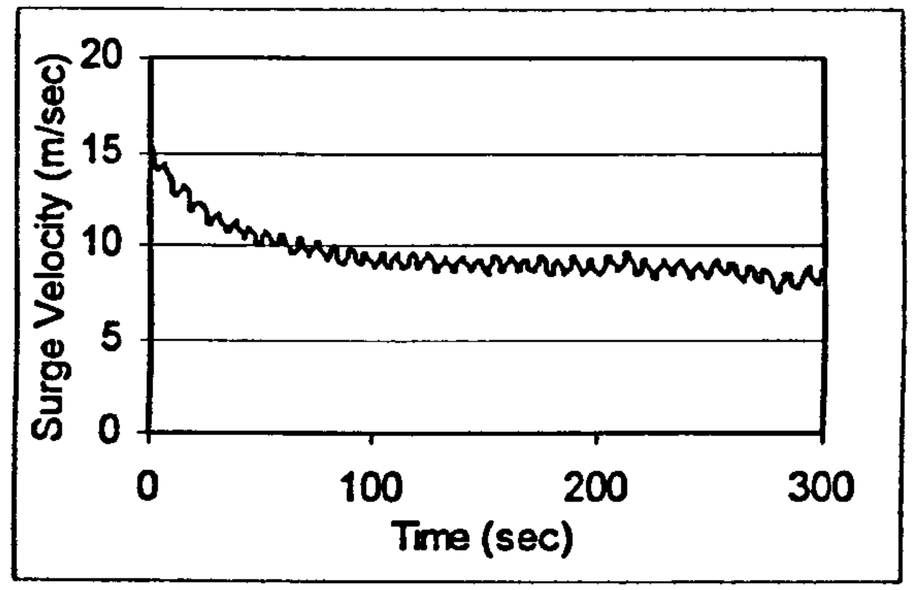

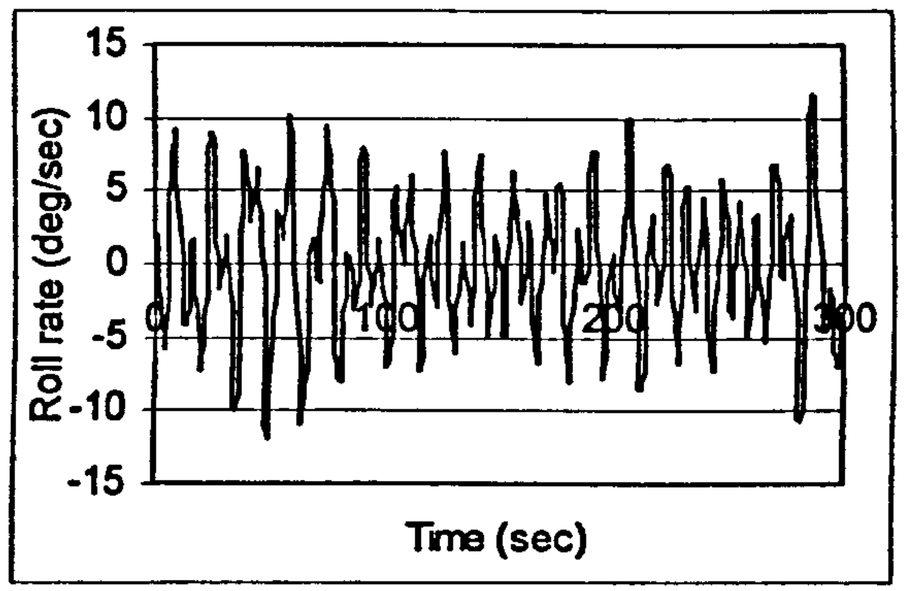

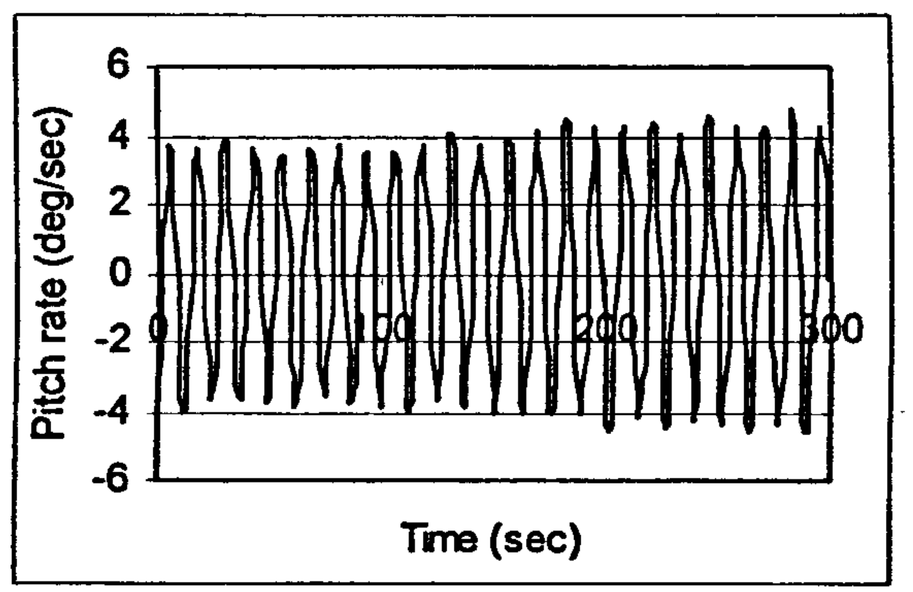

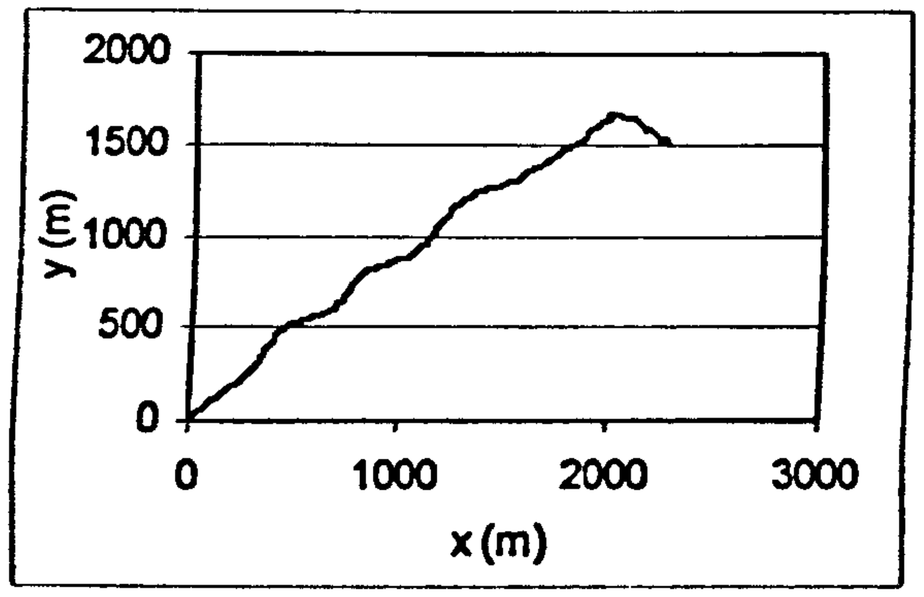

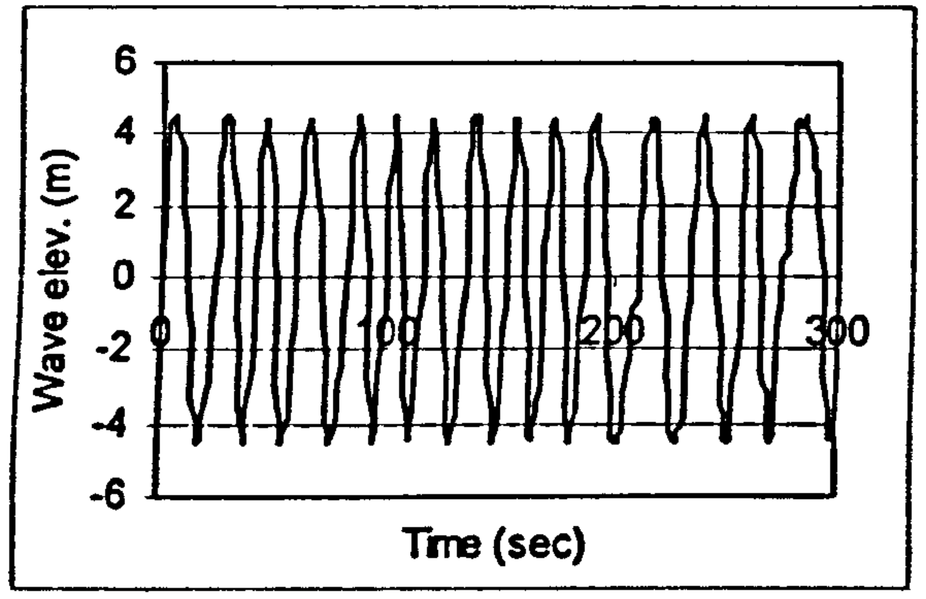

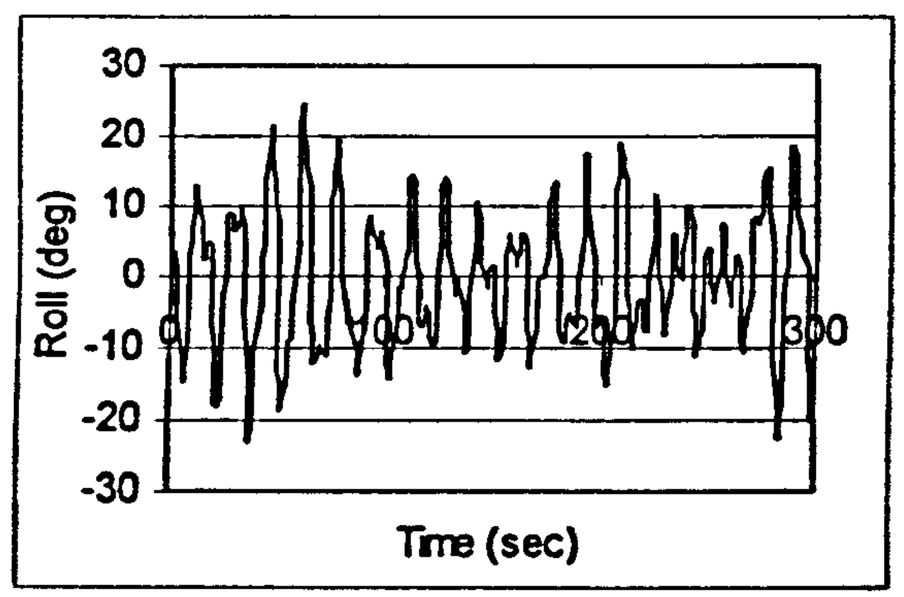

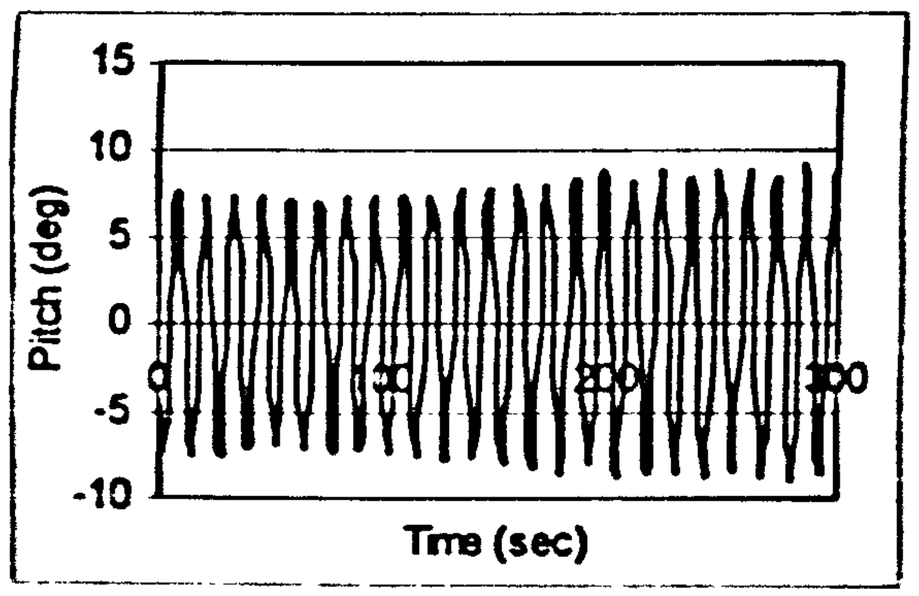

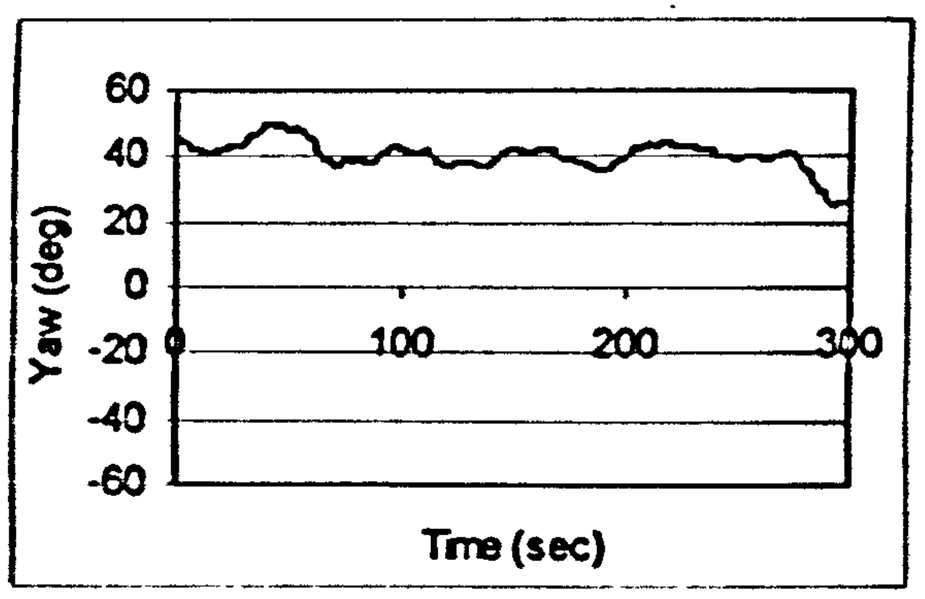

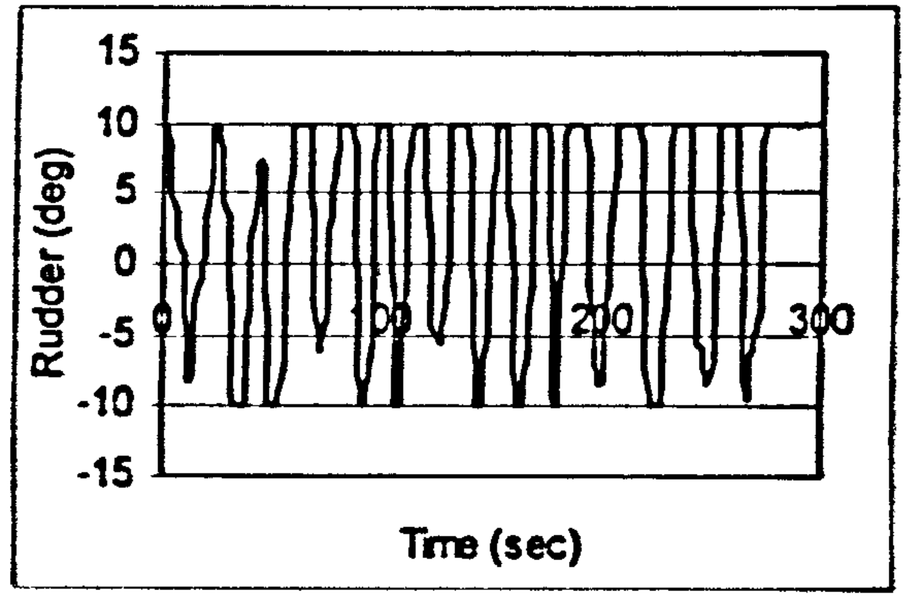

Figure G.27 Numerical Simulation of Ship A-1 in $H/\lambda=1/25$, $\lambda/L_{pp}=1.5$, Fn=0.2,χ_c =30 degrees (initial position at wave trough)

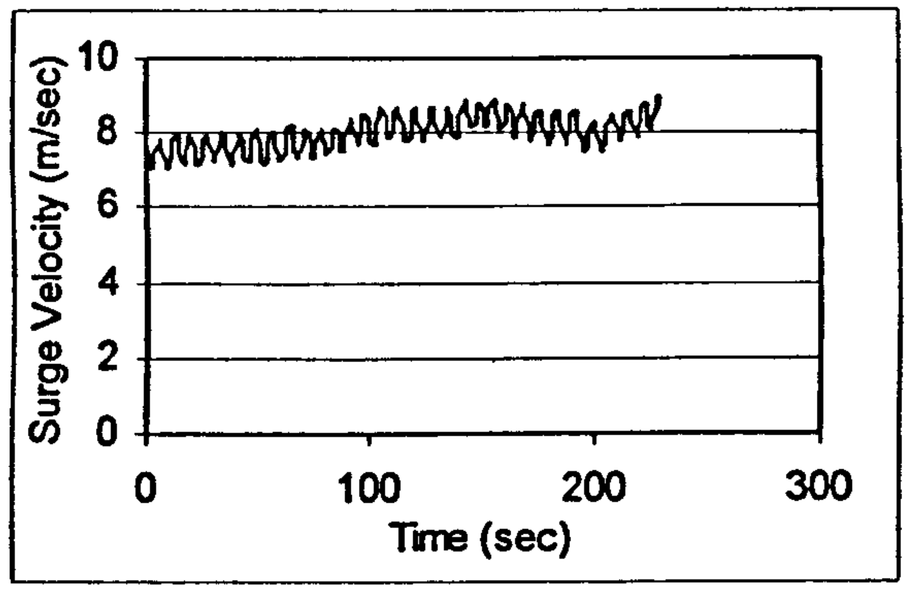

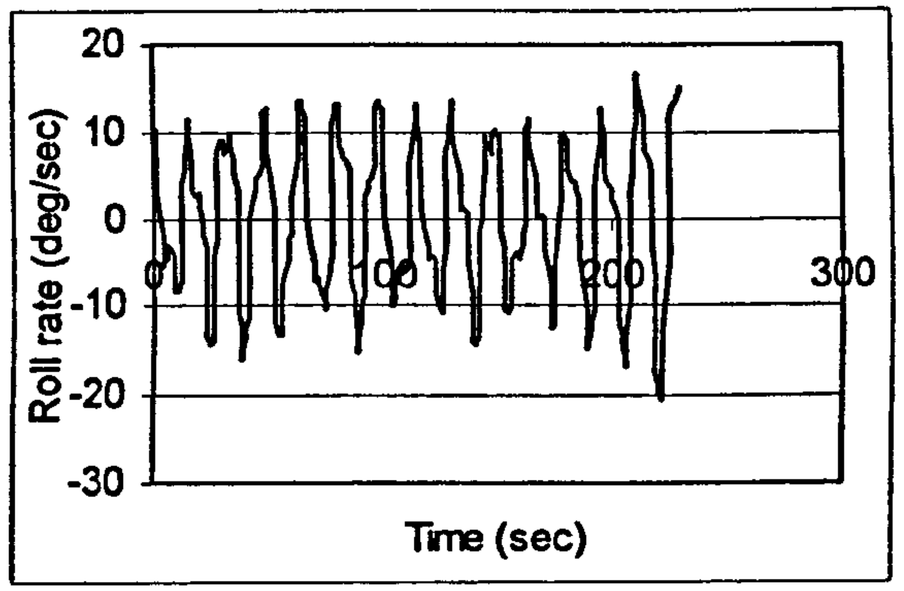

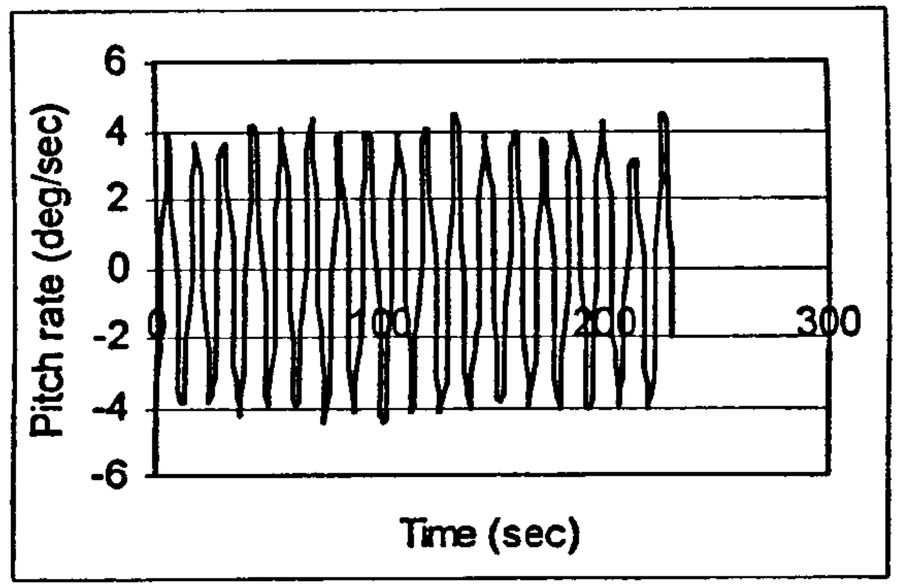

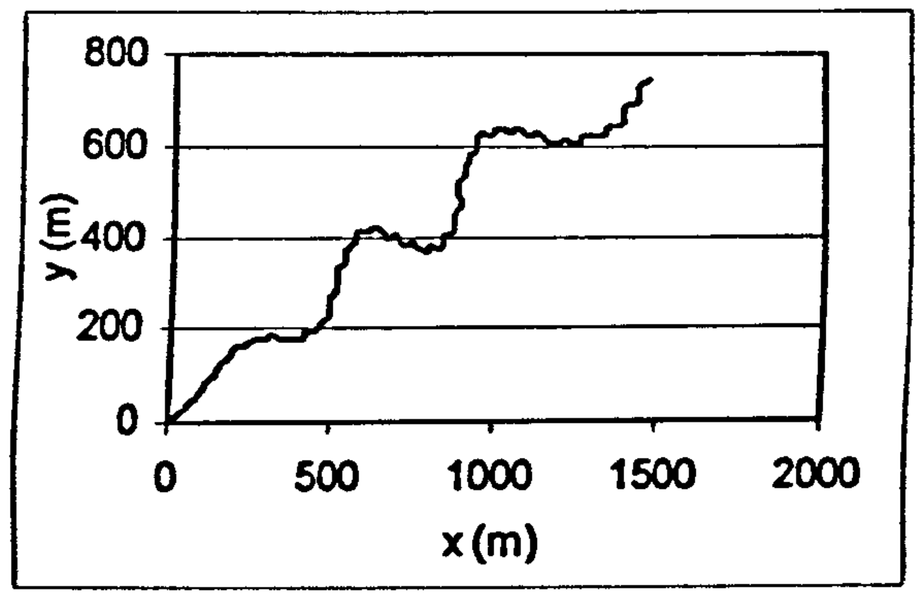

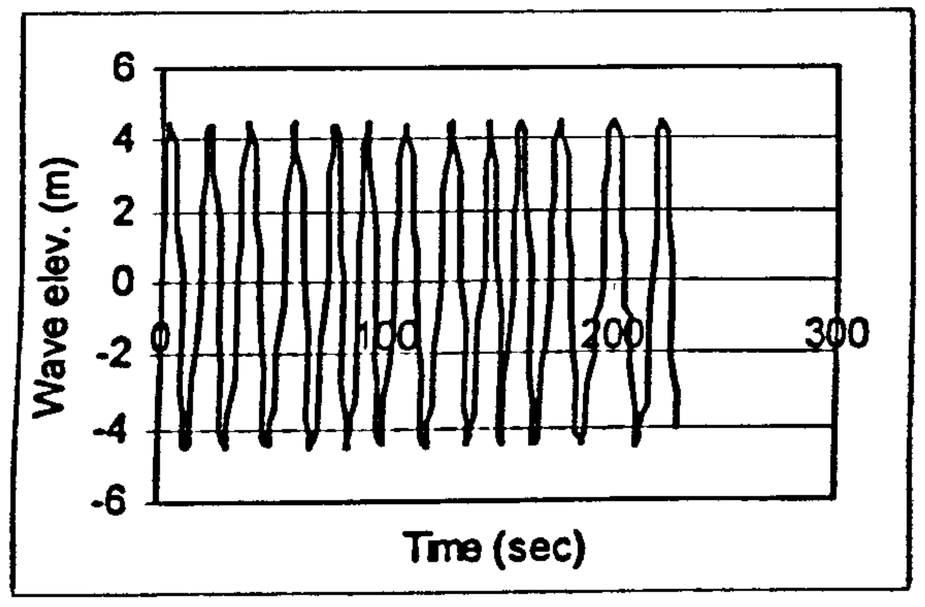

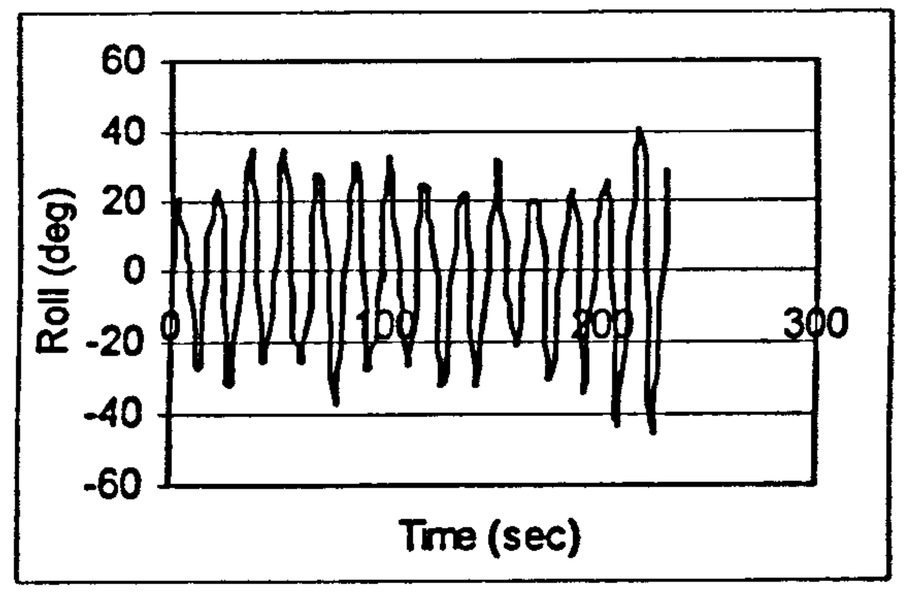

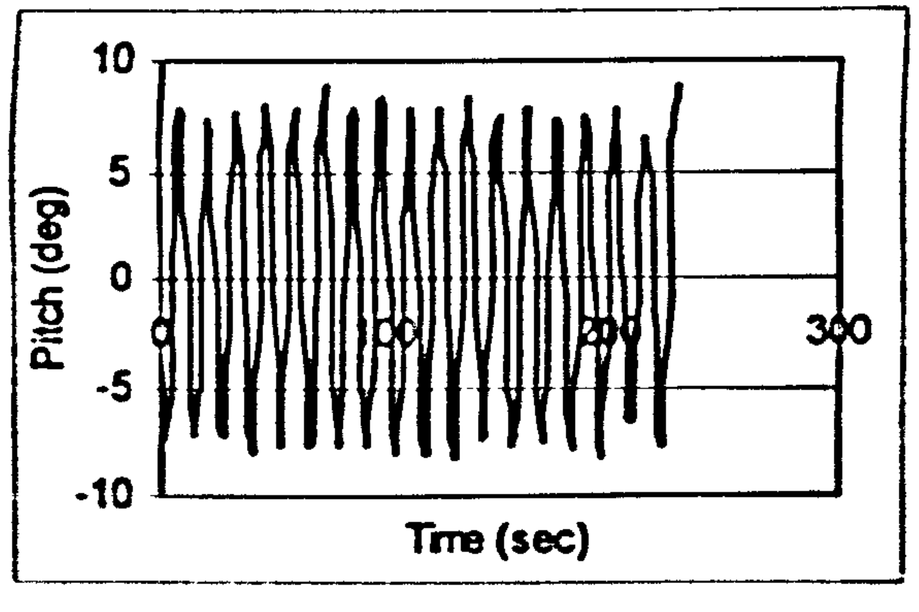

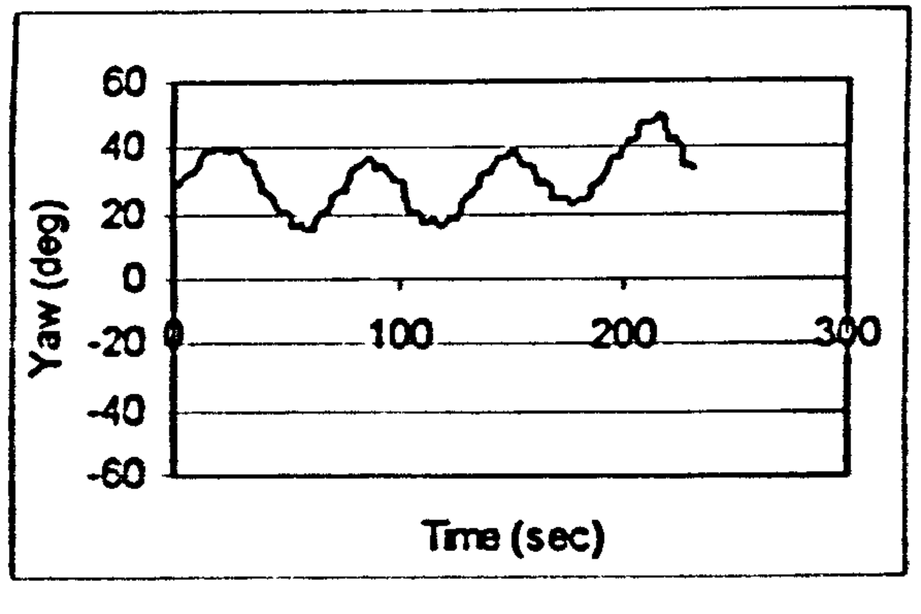

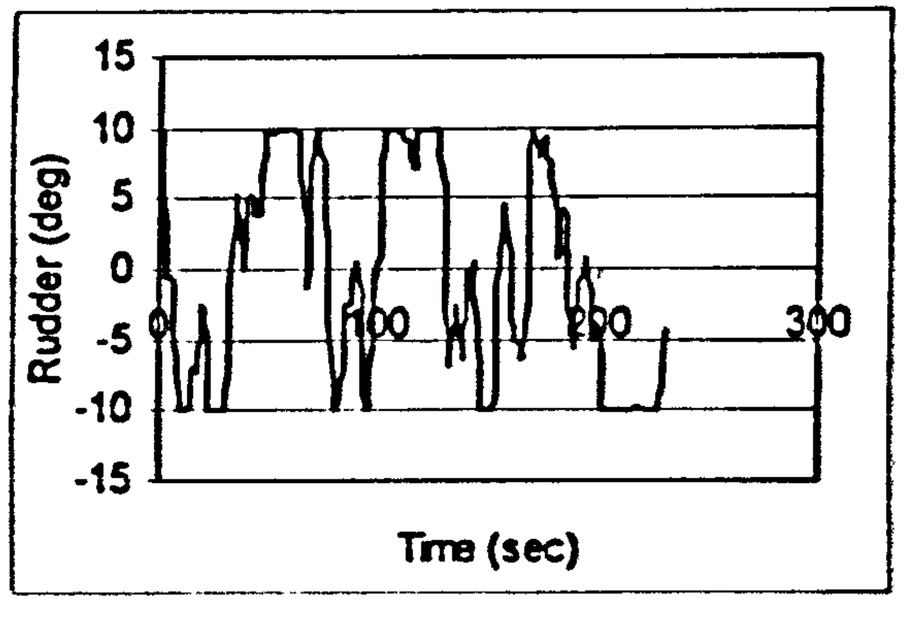

Figure G.28 Numerical Simulation of Ship A-1 in $H/\lambda=1/25$, $\lambda/L_{pp}=1.5$, $Fn=0.2$, $\chi_c=30$ degrees (initial position at wave crest)

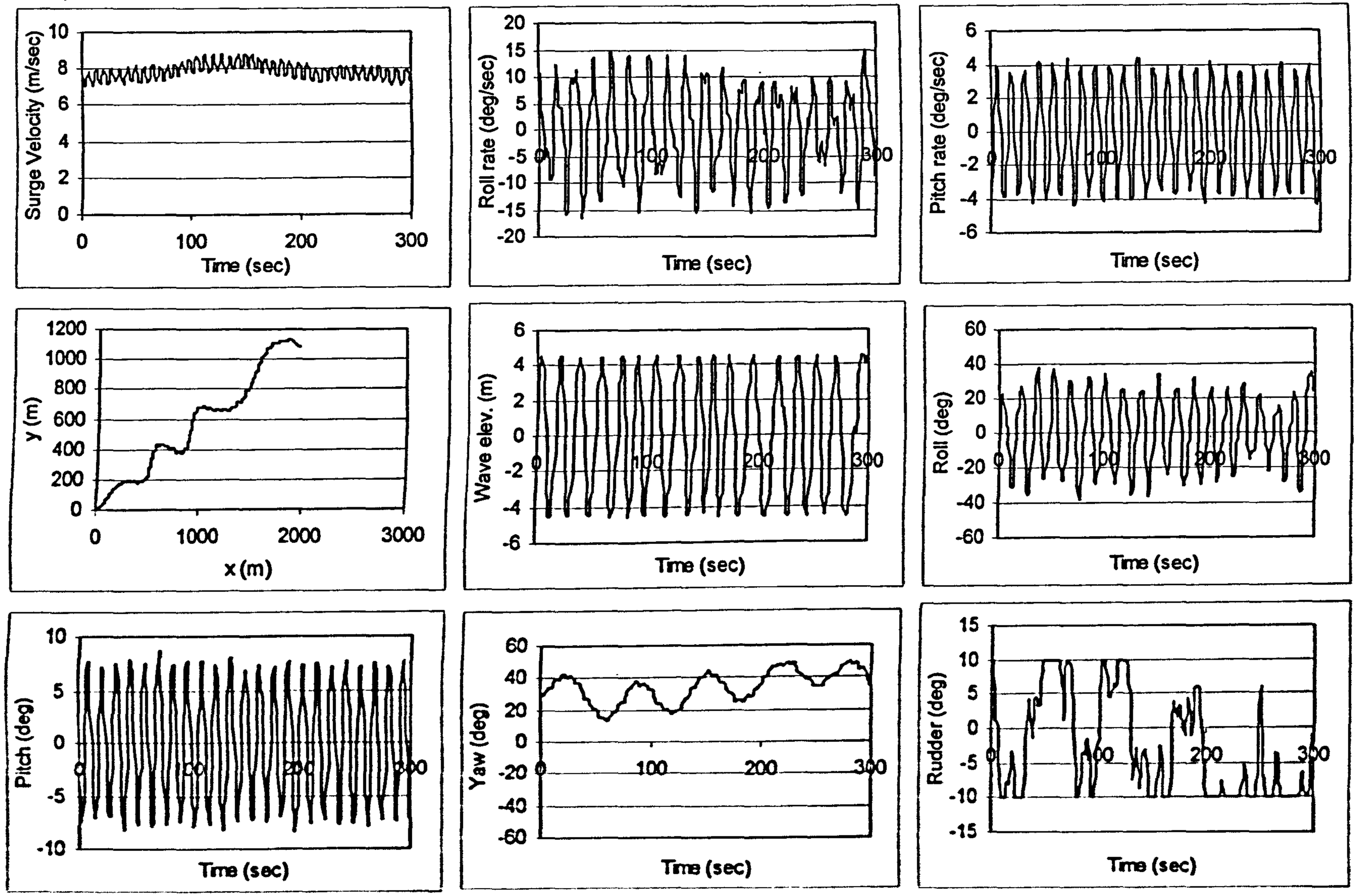

Figure G.29 Numerical Simulation of Ship A-1 in $H/\lambda=1/25$, $\lambda/L_{pp}=1.5$, Fn=0.2,χ_c =0 degrees

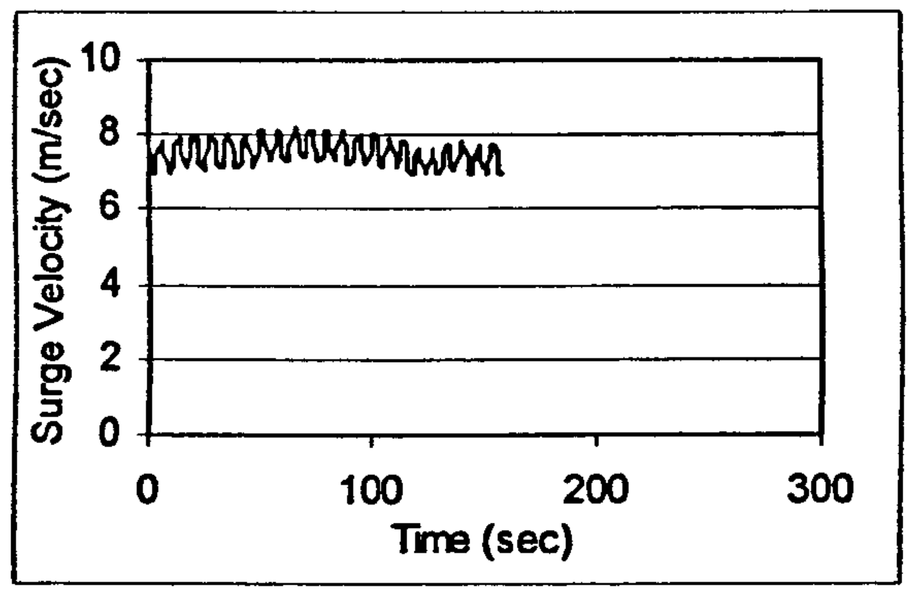

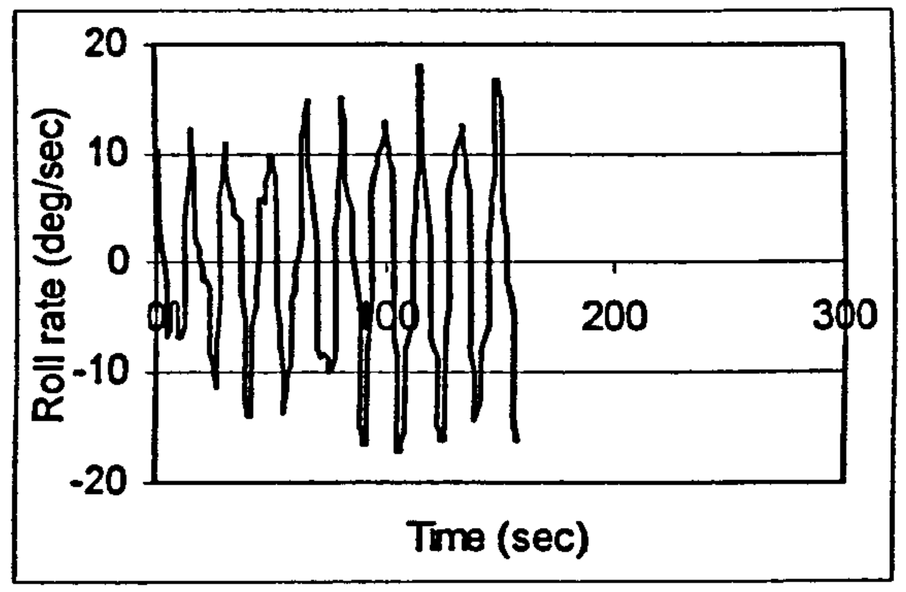

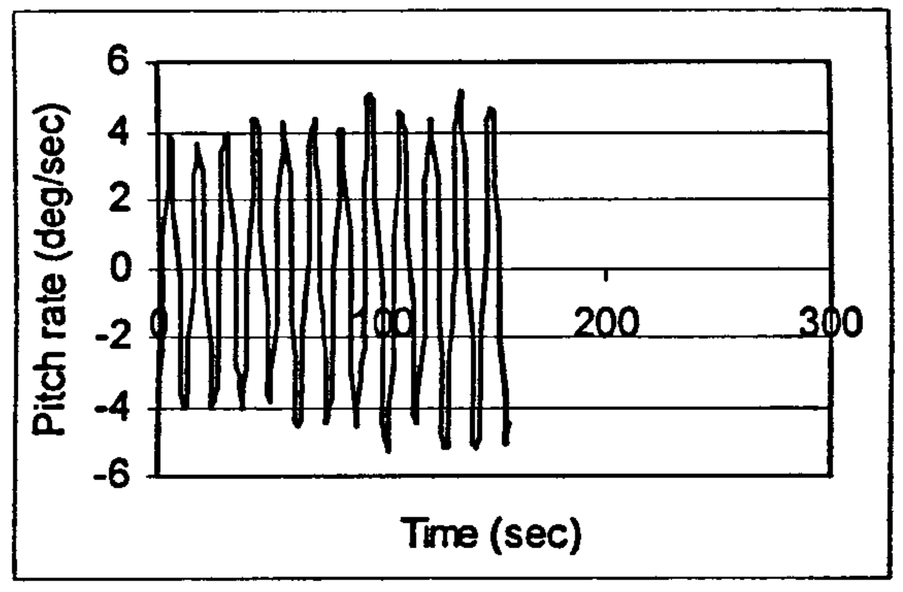

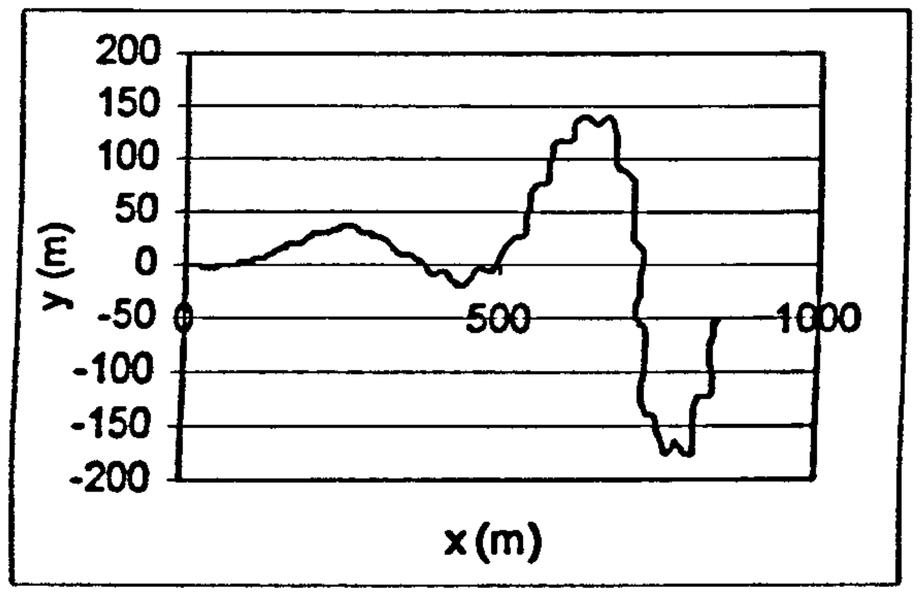

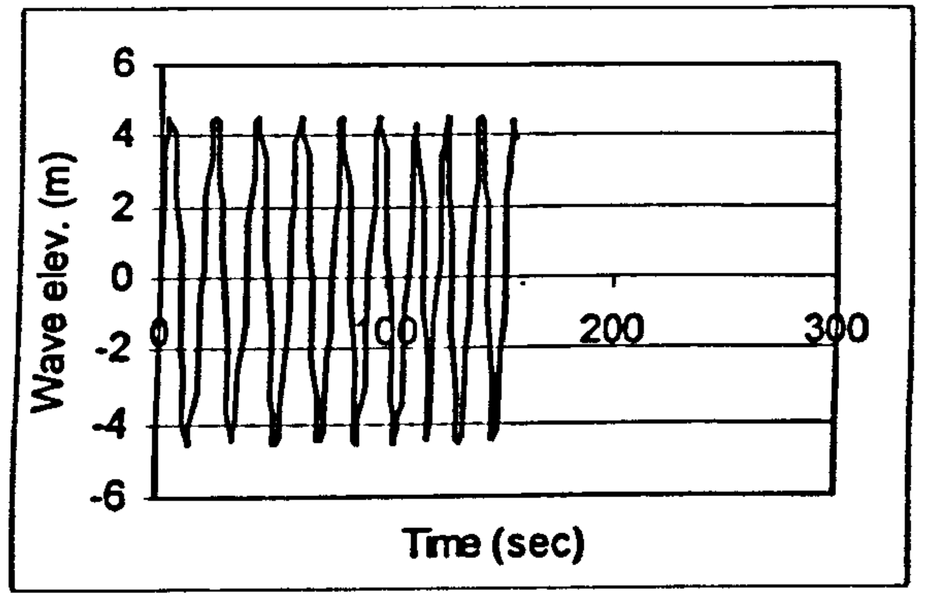

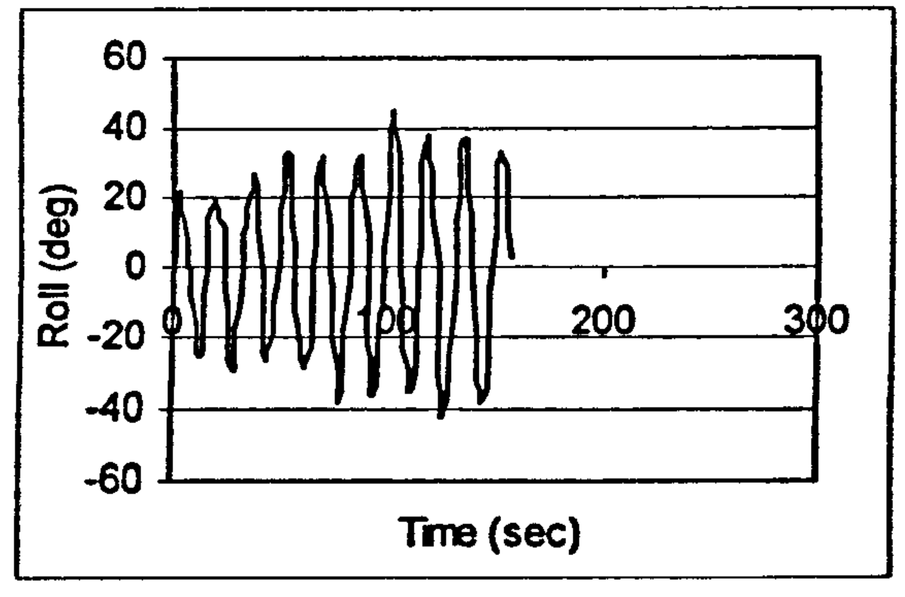

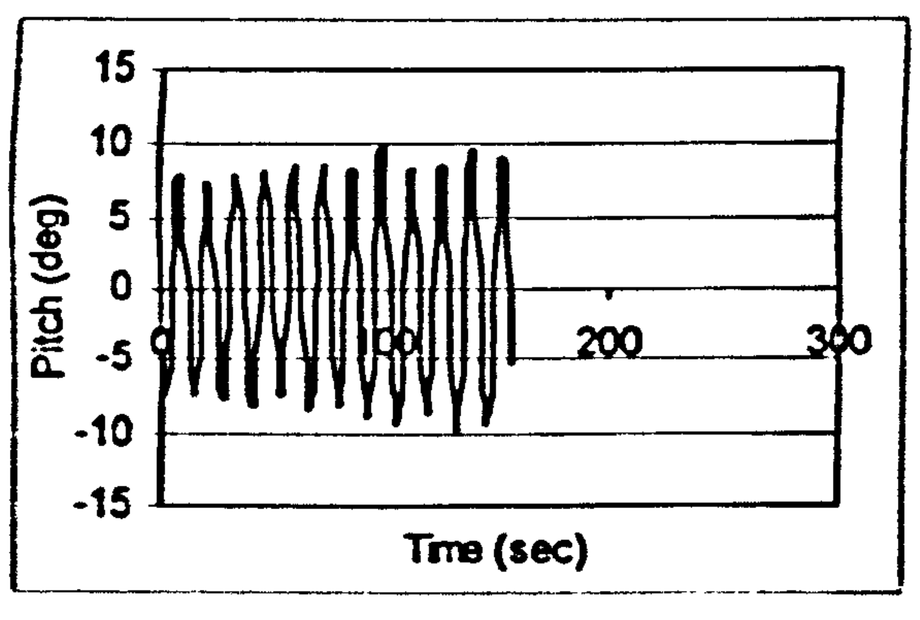

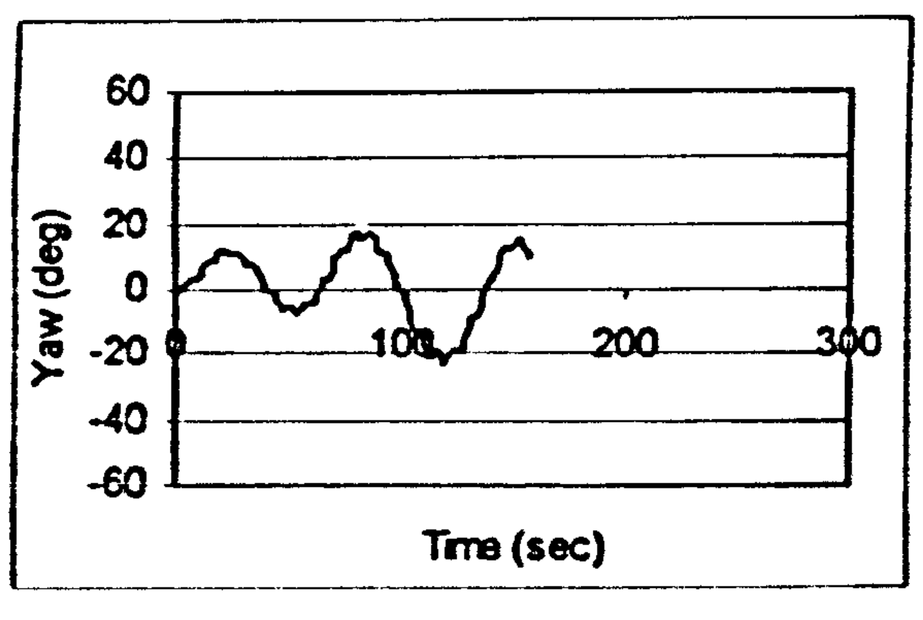

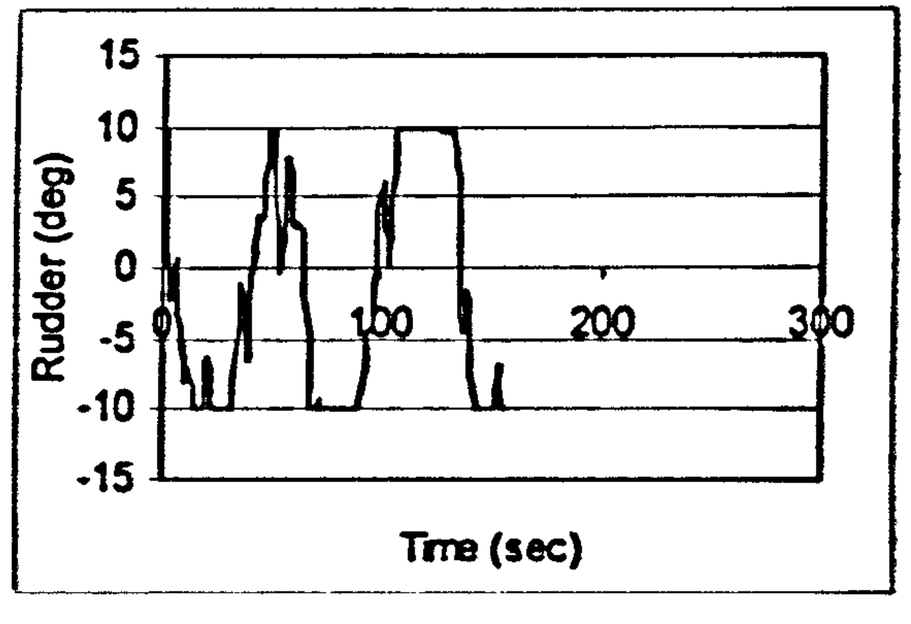

Figure G.30 Numerical Simulation of Ship A-1 in $H/\lambda=1/25$, $\lambda/L_{pp}=1.5$, Fn=0.2,χ_c =45 degrees

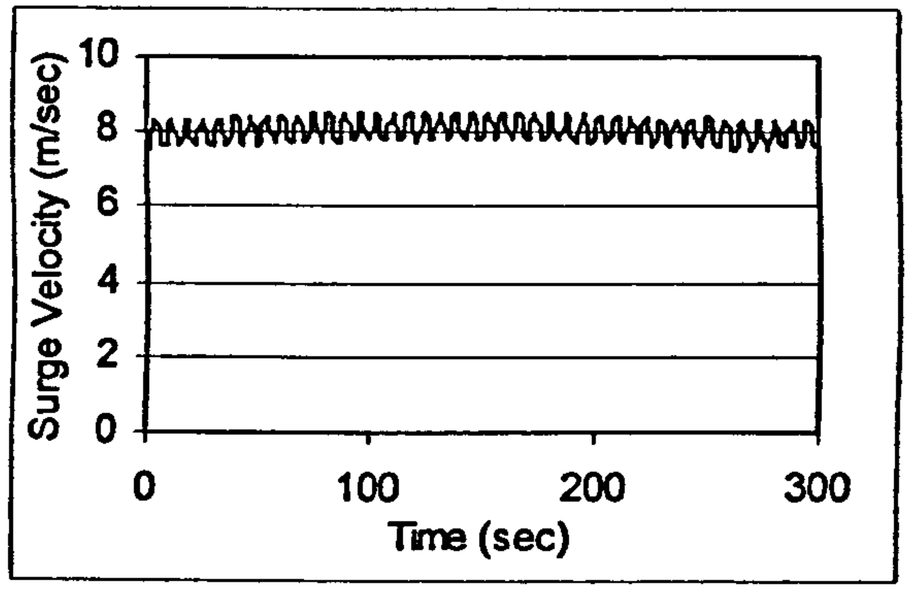

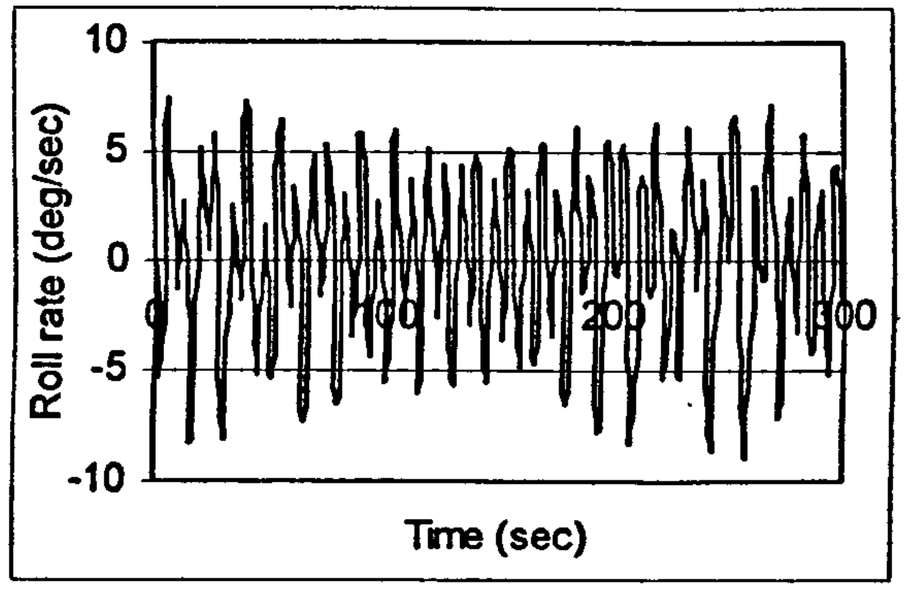

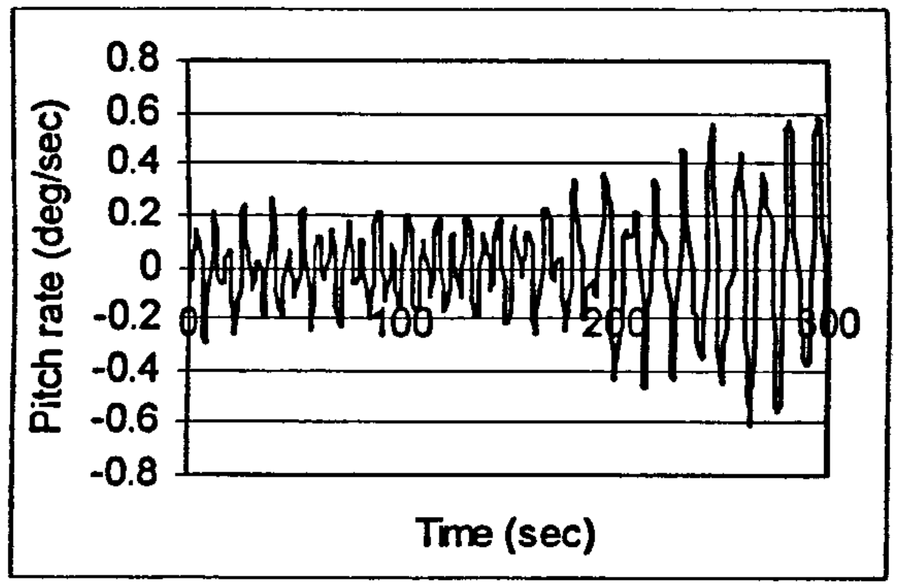

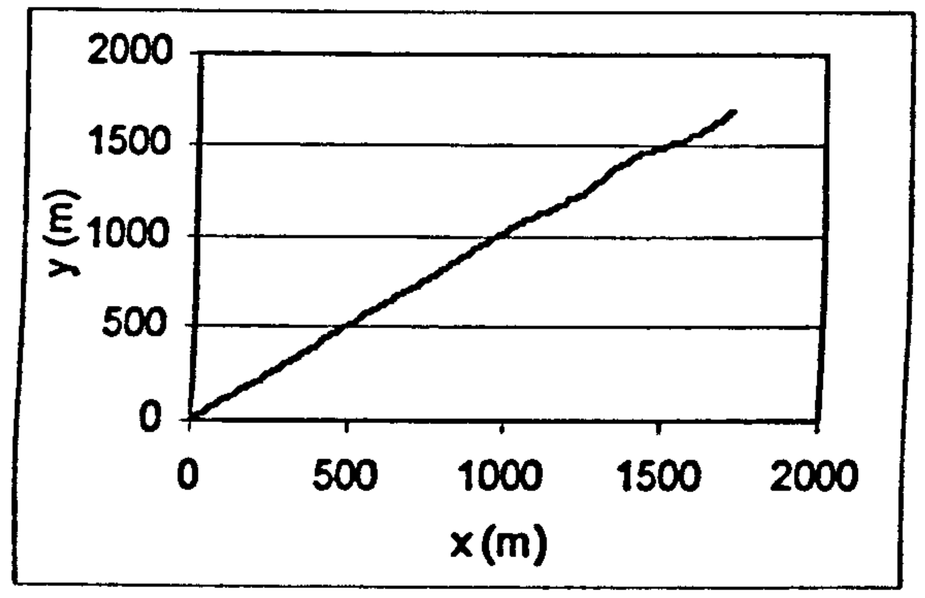

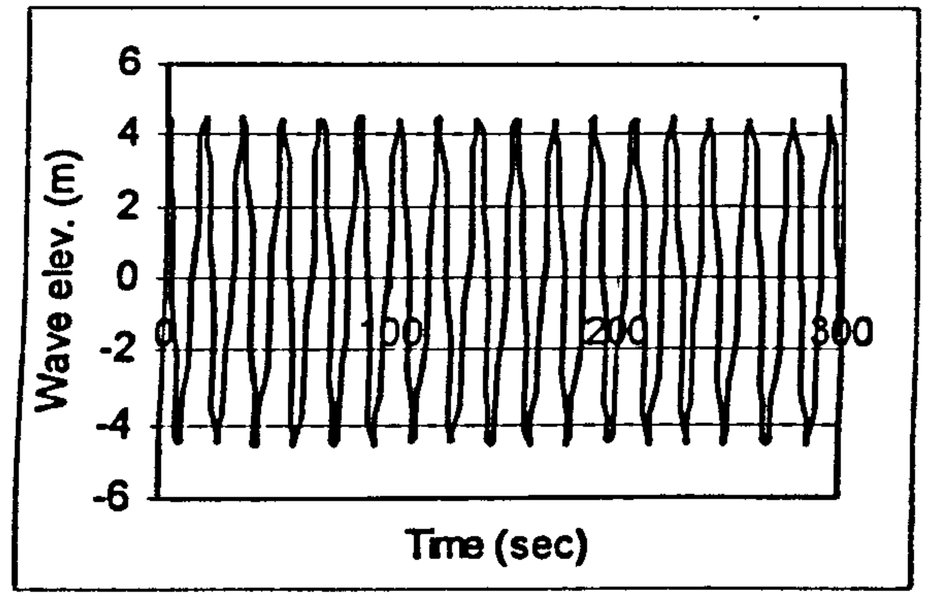

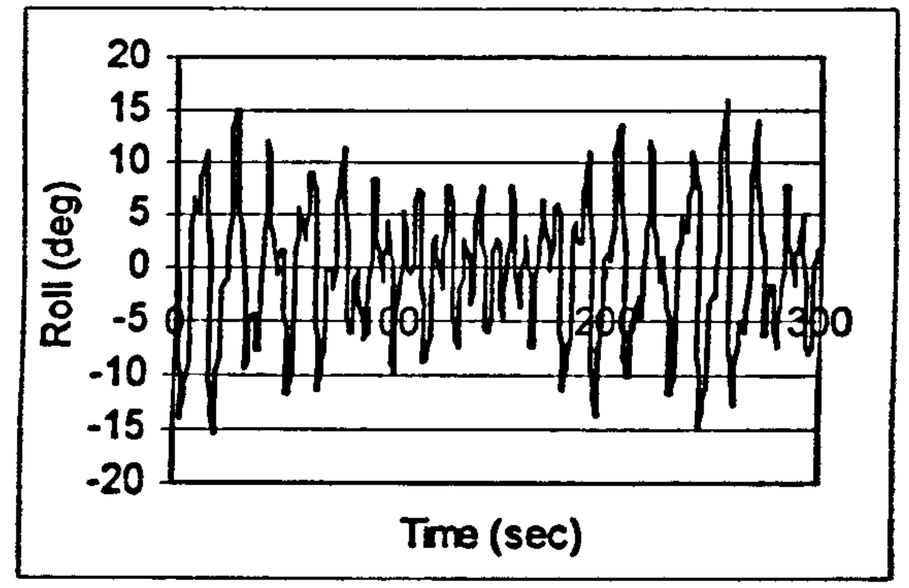

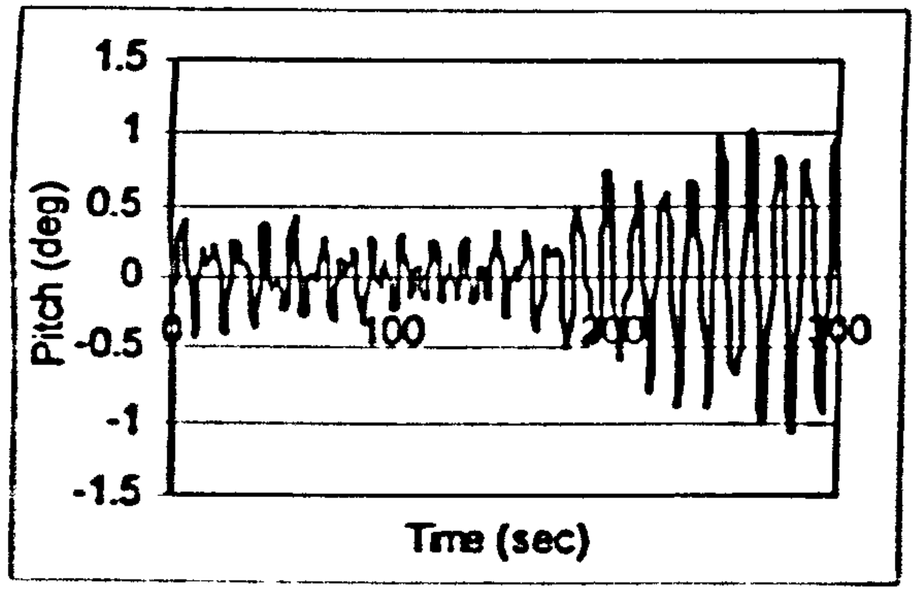

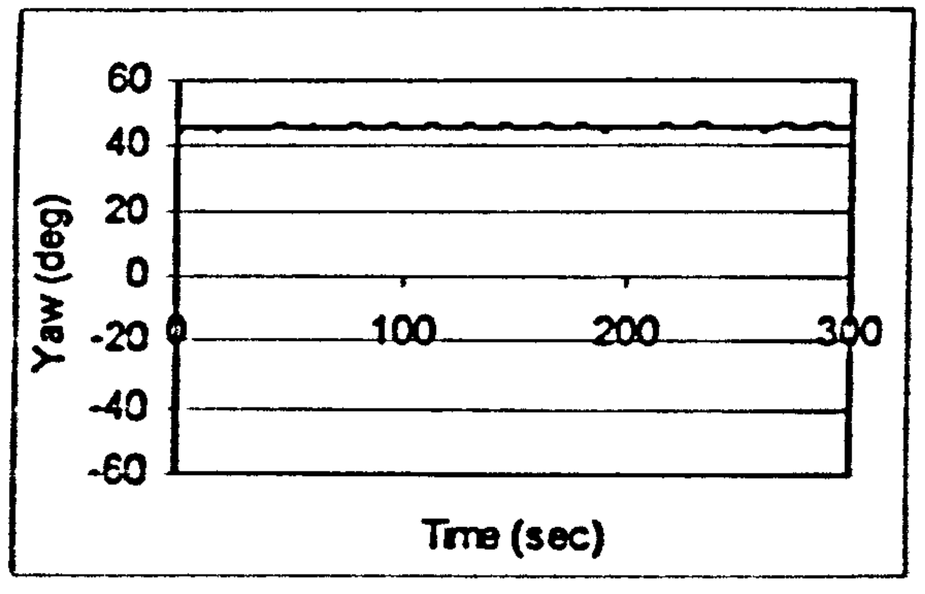

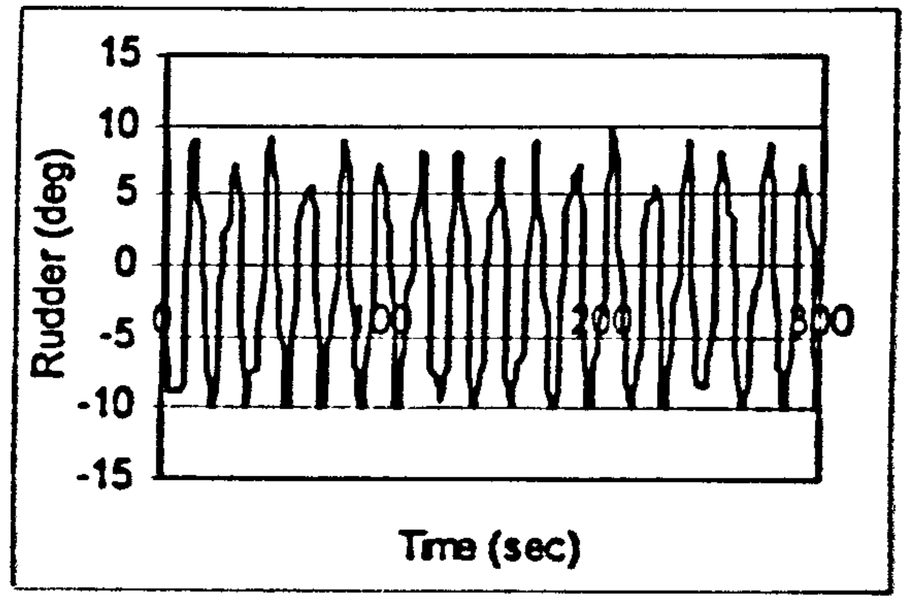

Figure G.31 Numerical Simulation of Ship A-1 in $H/\lambda=1/25$, $\lambda/L_{pp}=1.5$, Fn=0.3,χ_c =30 degrees

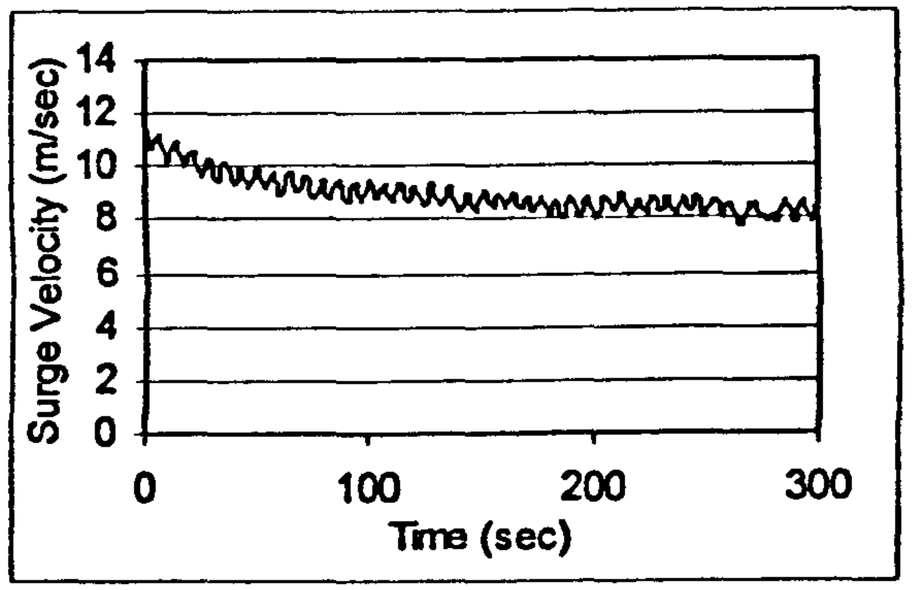

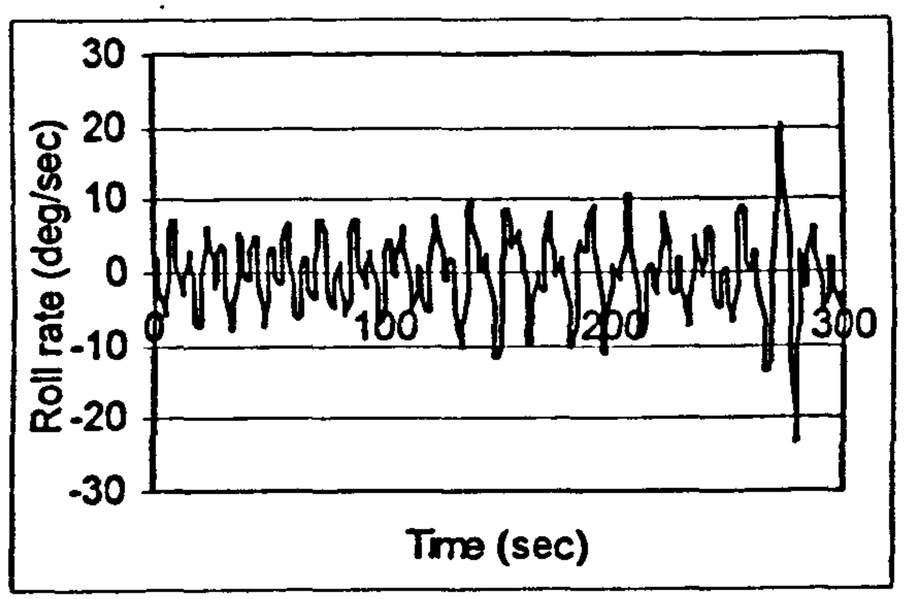

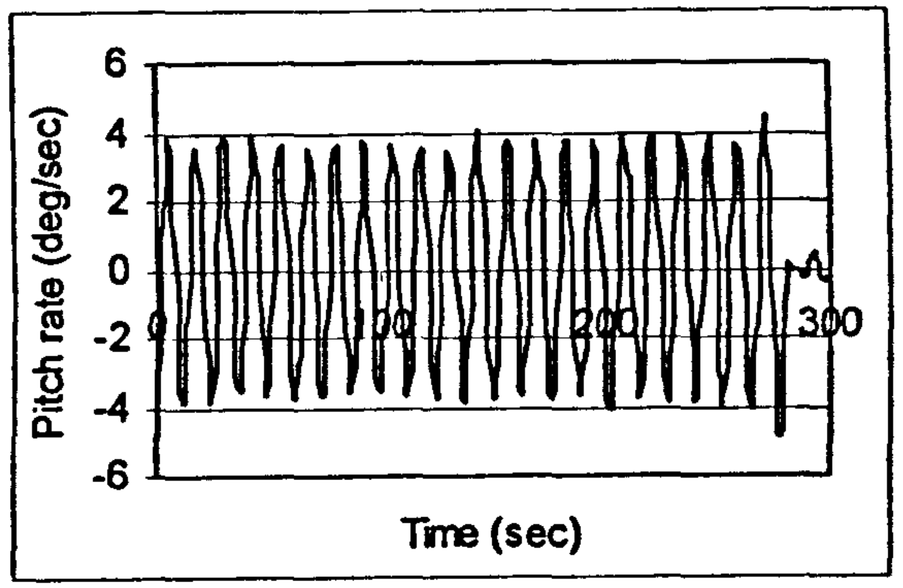

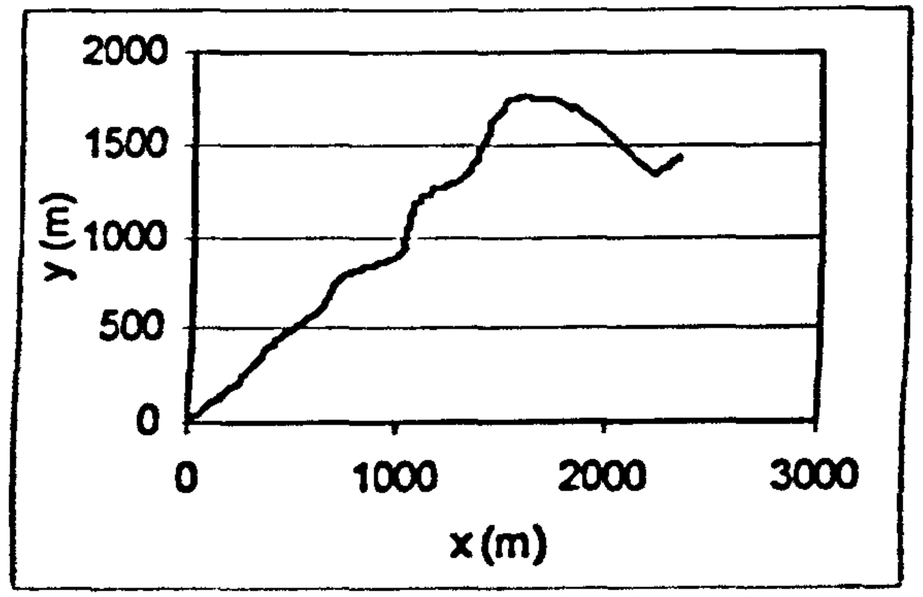

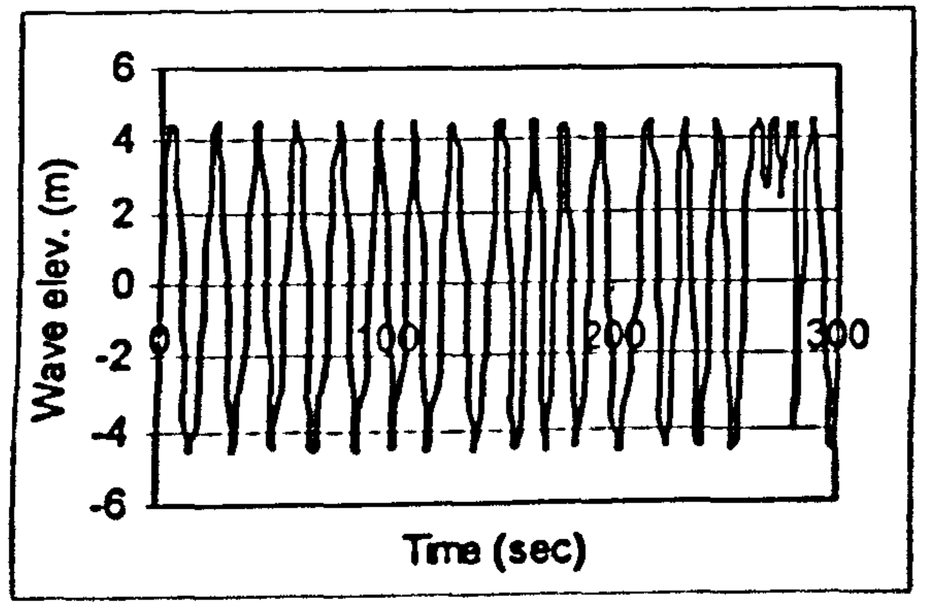

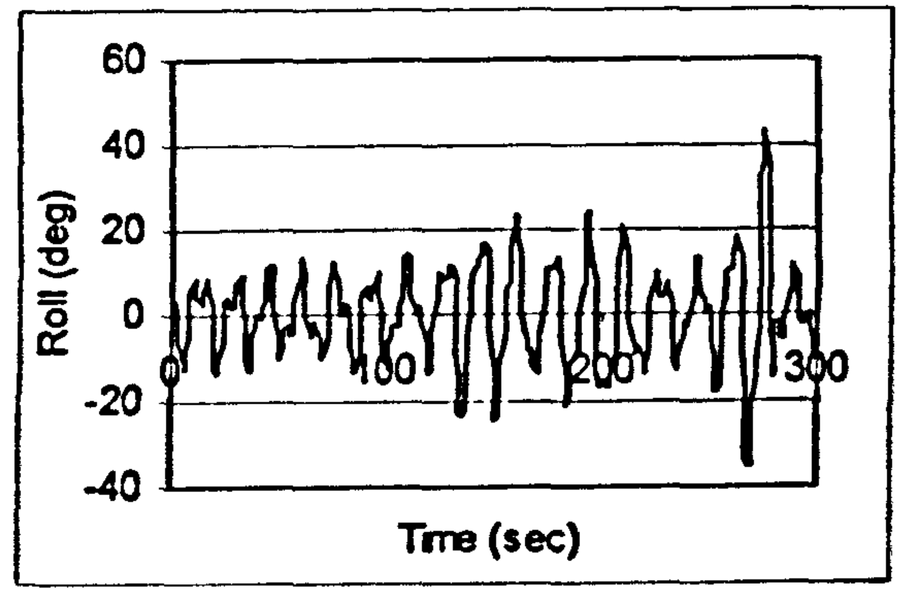

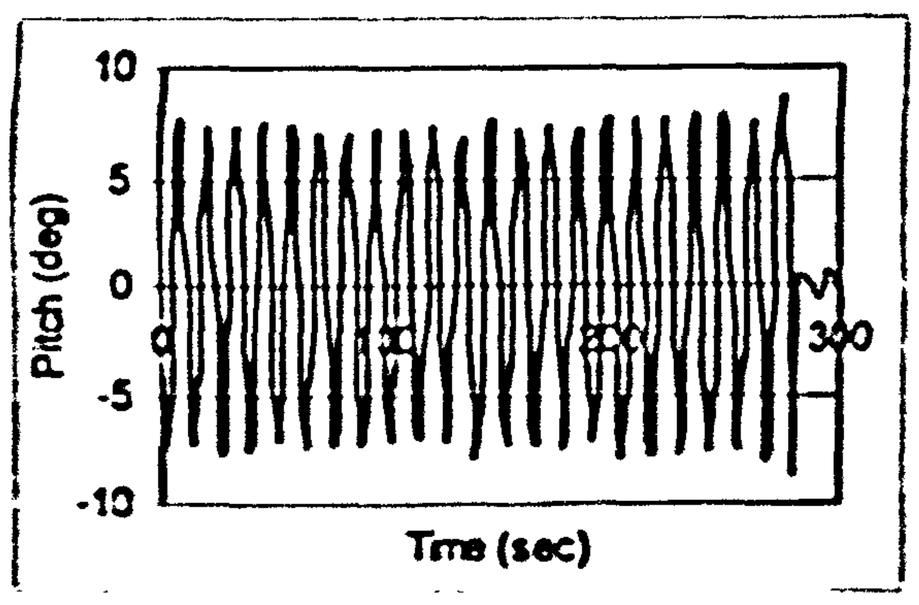

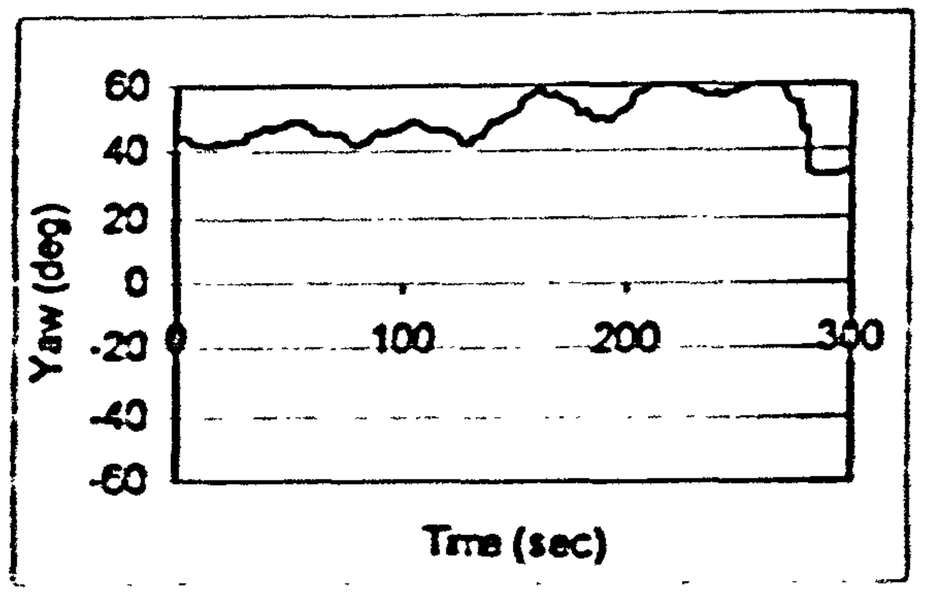

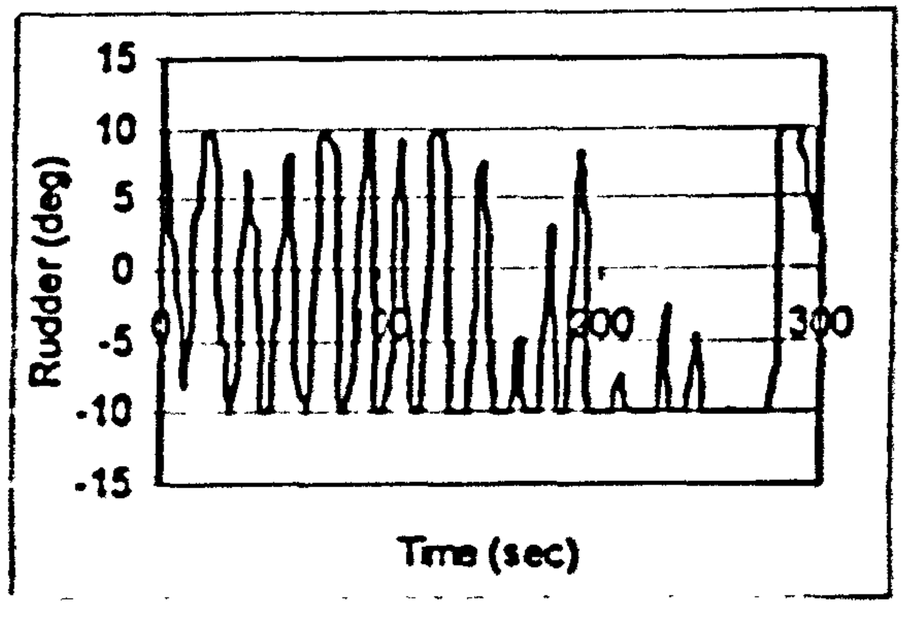

Figure G.32 Numerical Simulation of Ship A-1 in $H/\lambda=1/25$, $\lambda/L_{pp}=1.5$, Fn=0.2,$\chi_c=30$ degrees

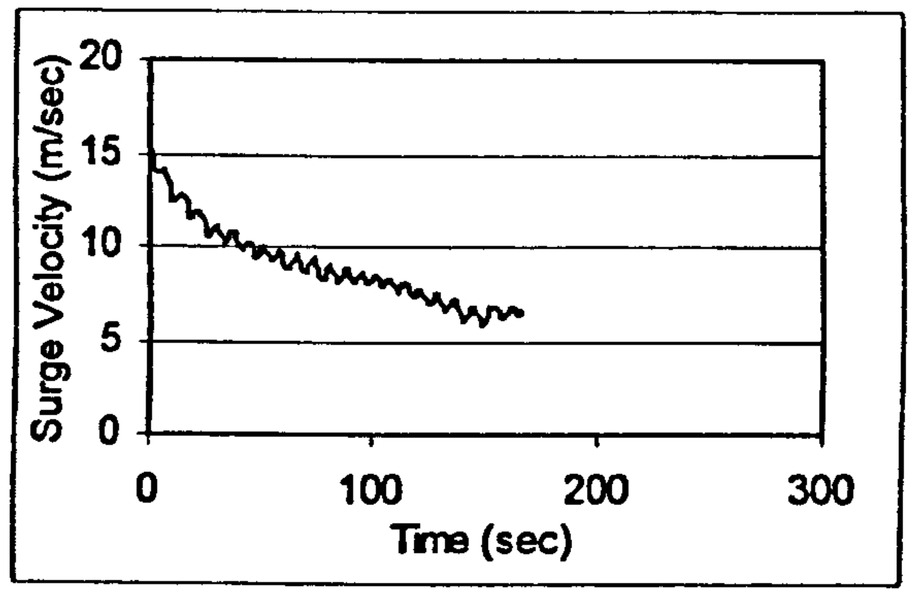

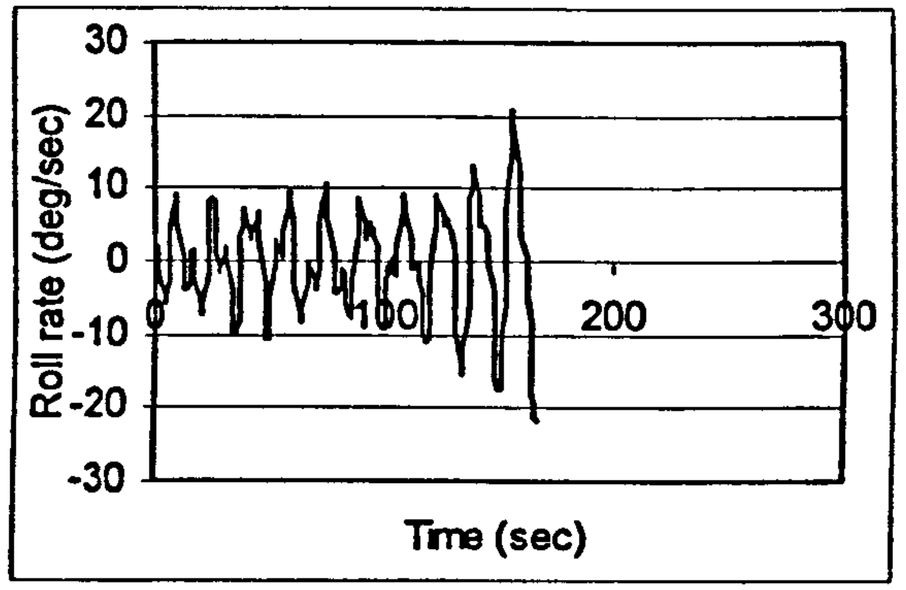

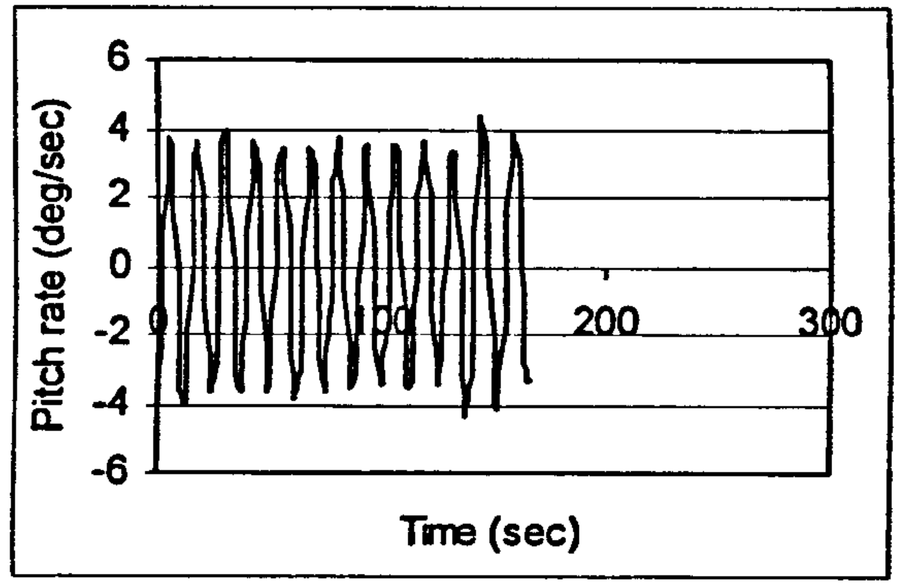

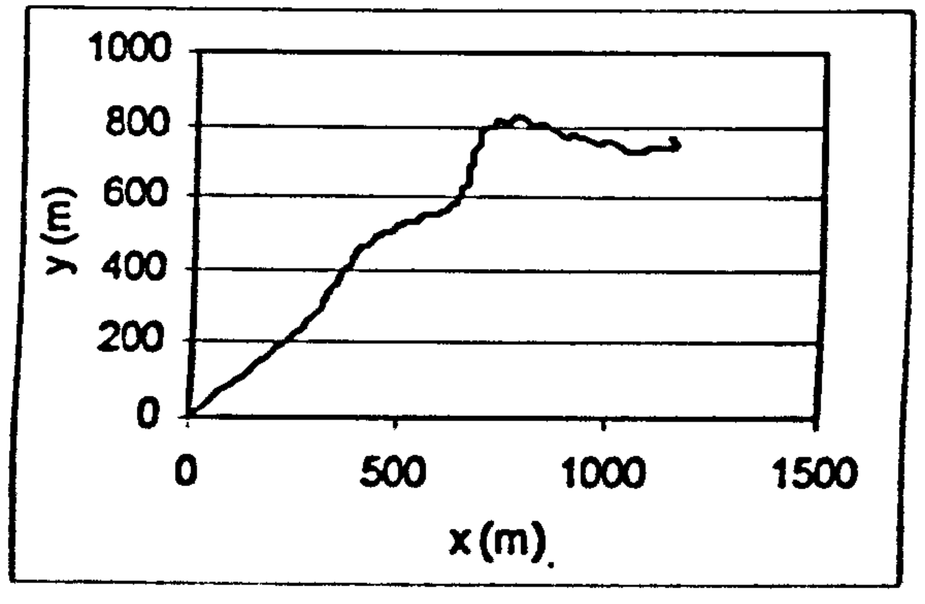

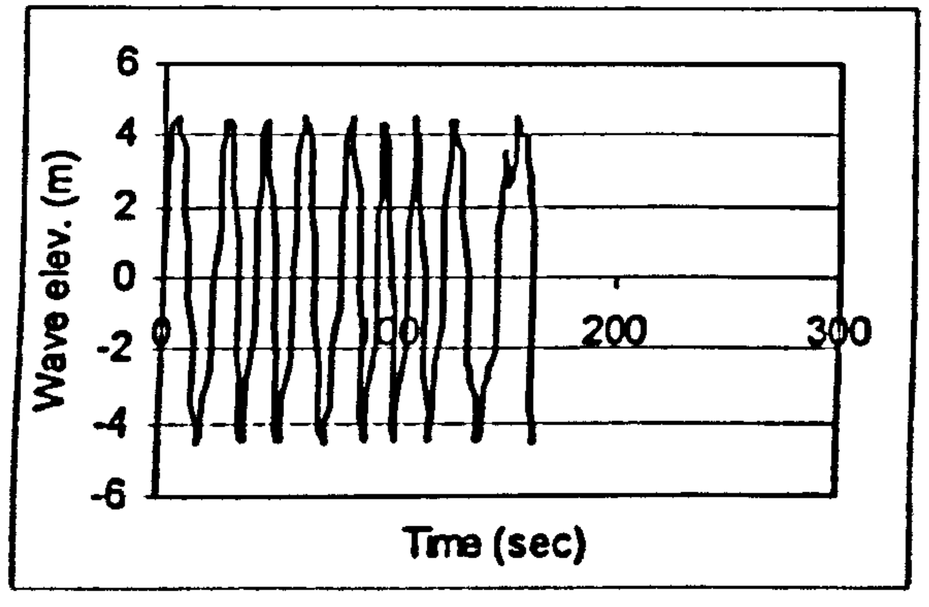

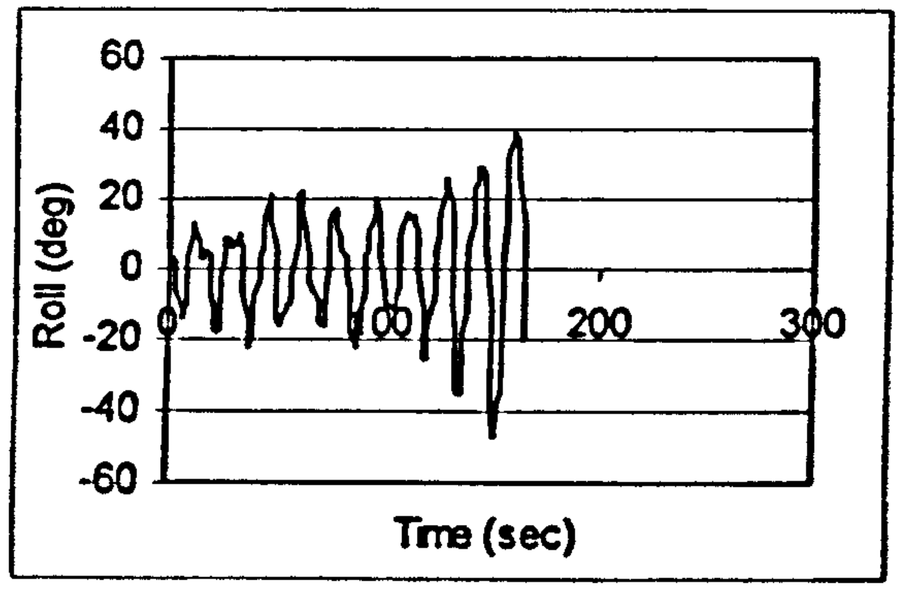

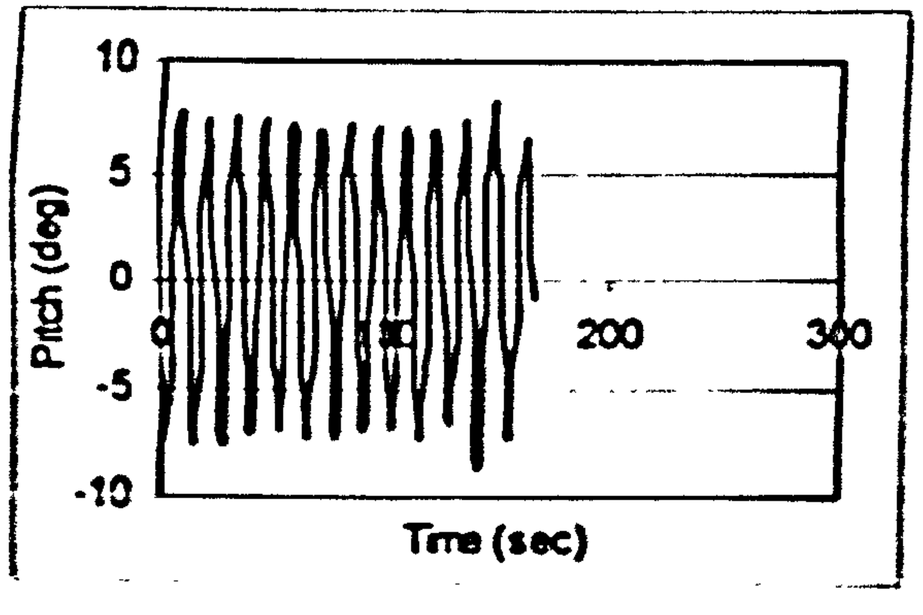

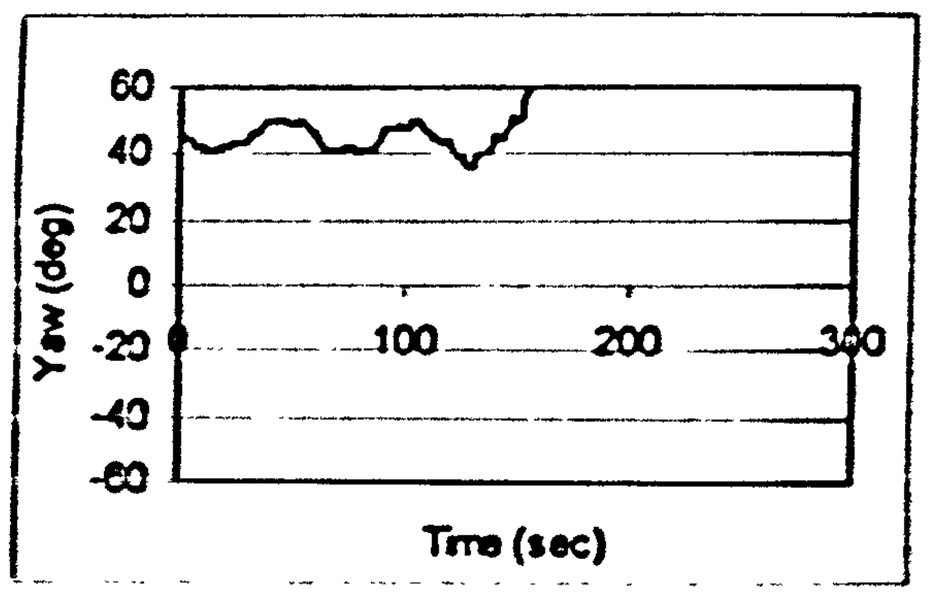

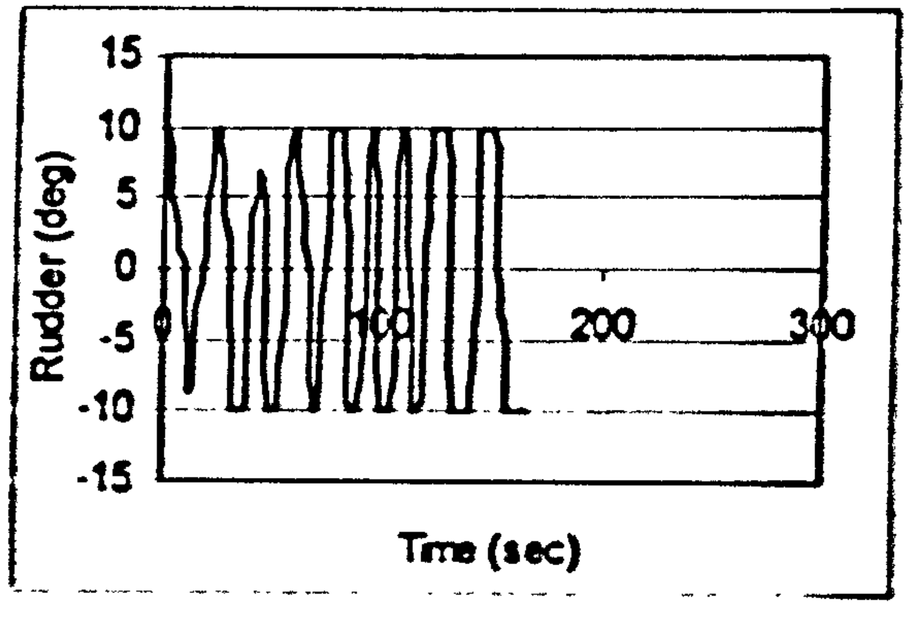

Figure G.33 Numerical Simulation of Ship A-1 in $H/\lambda=1/25$, $\lambda/L_{pp}=1.5$, Fn=0.2,$\chi_c=0$ degrees (with memory effect)

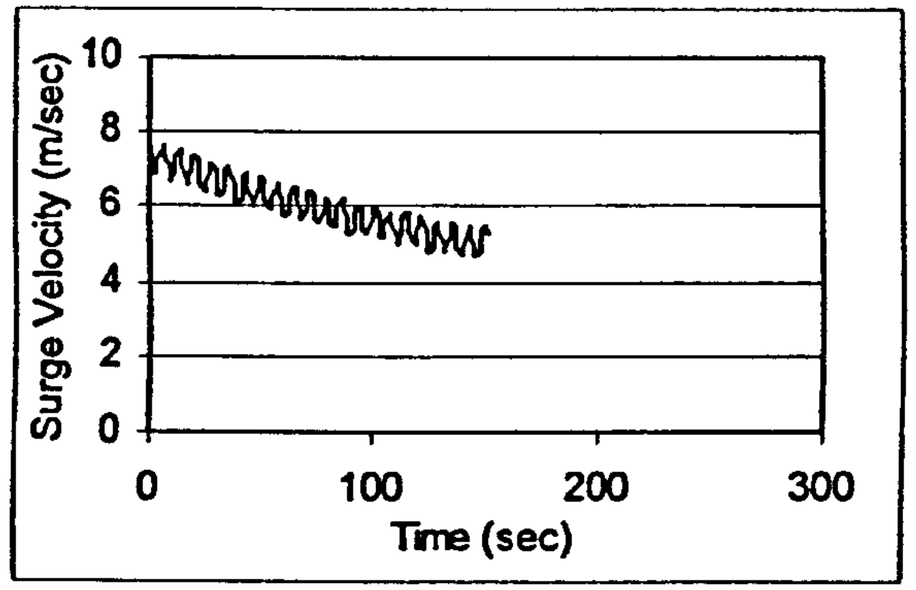

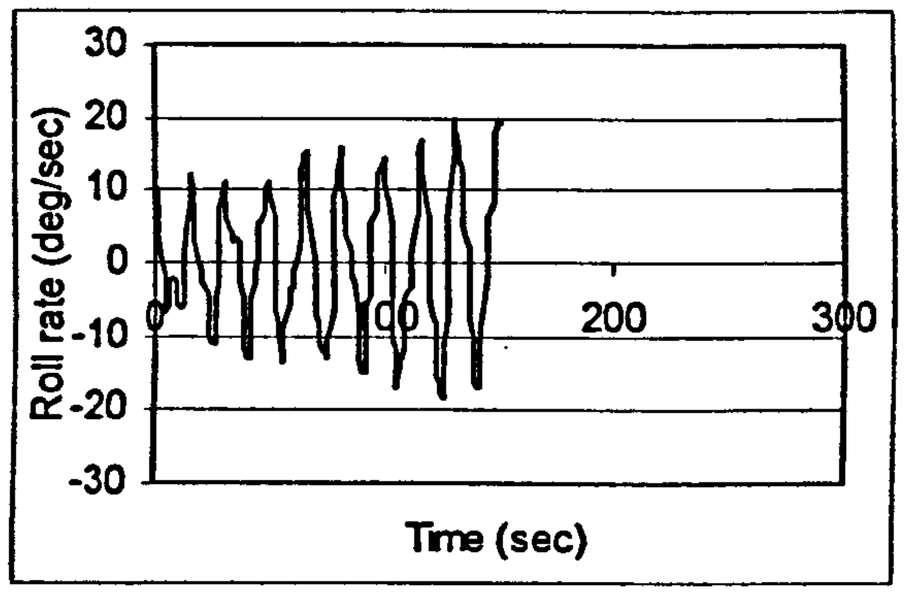

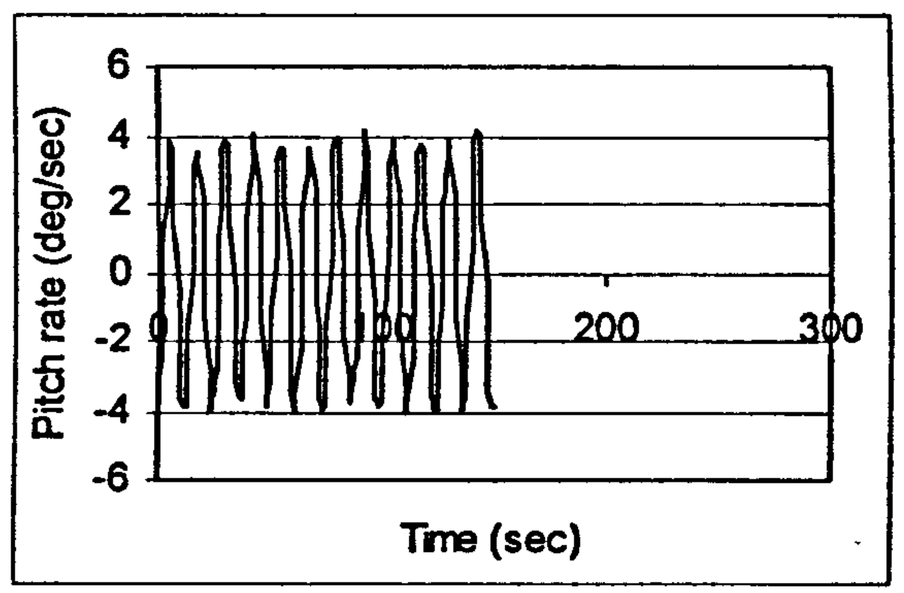

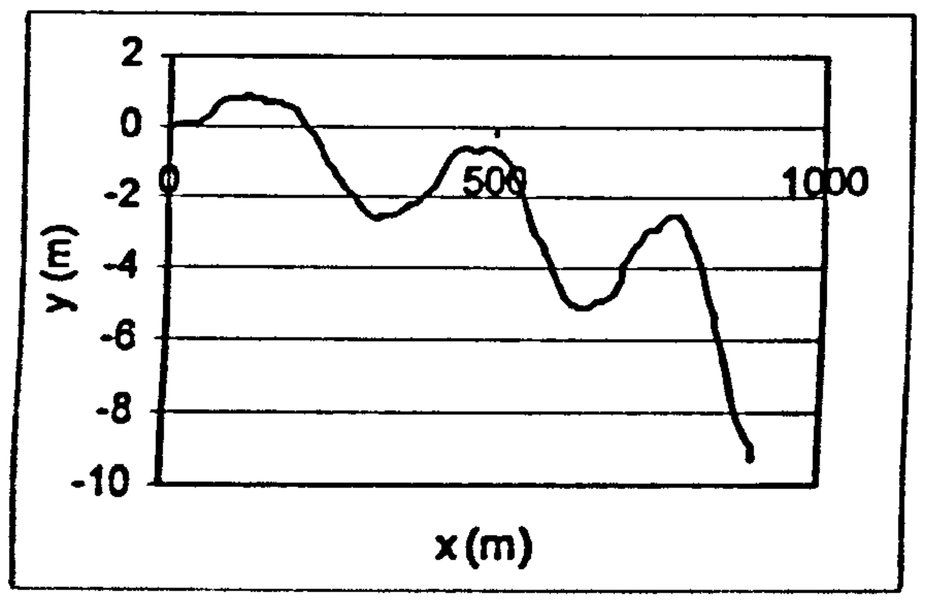

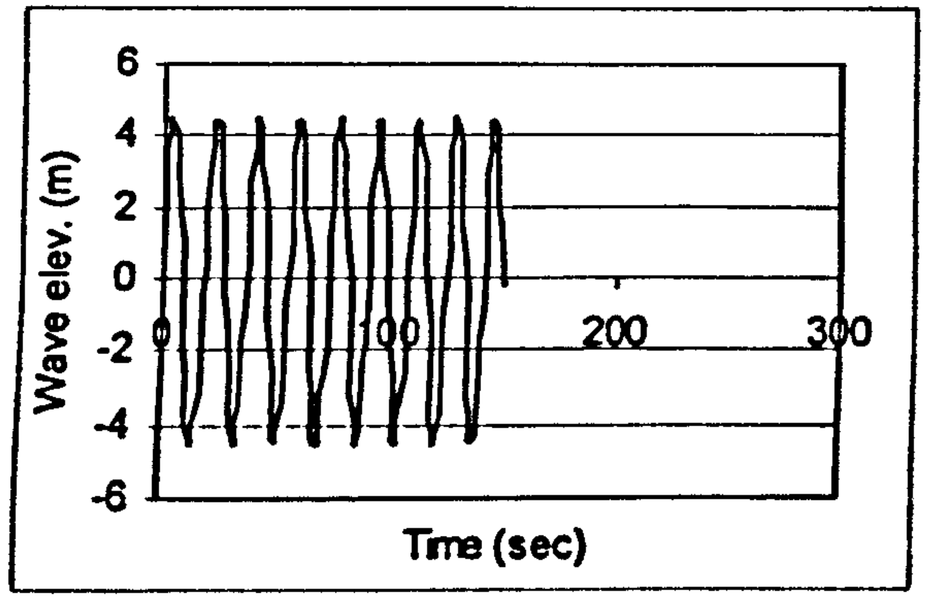

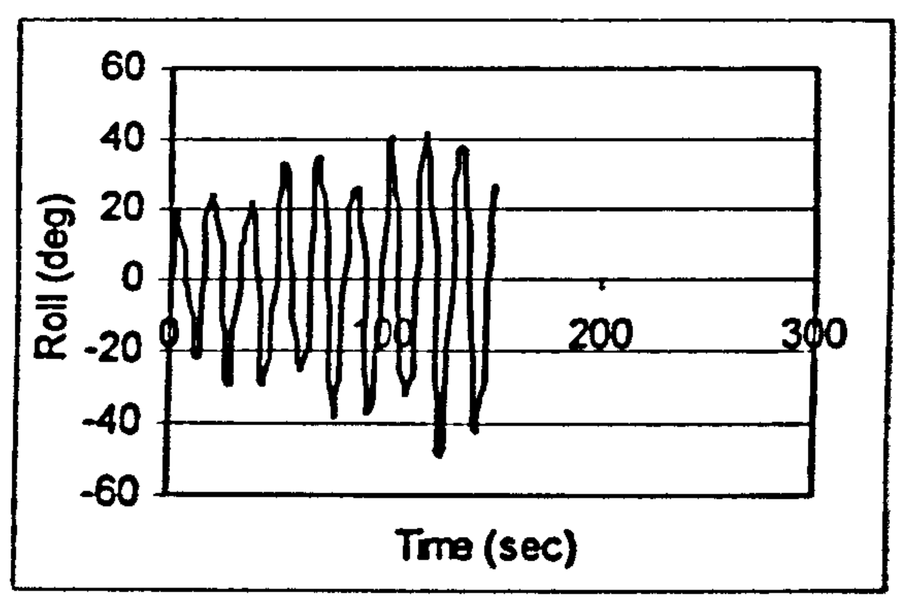

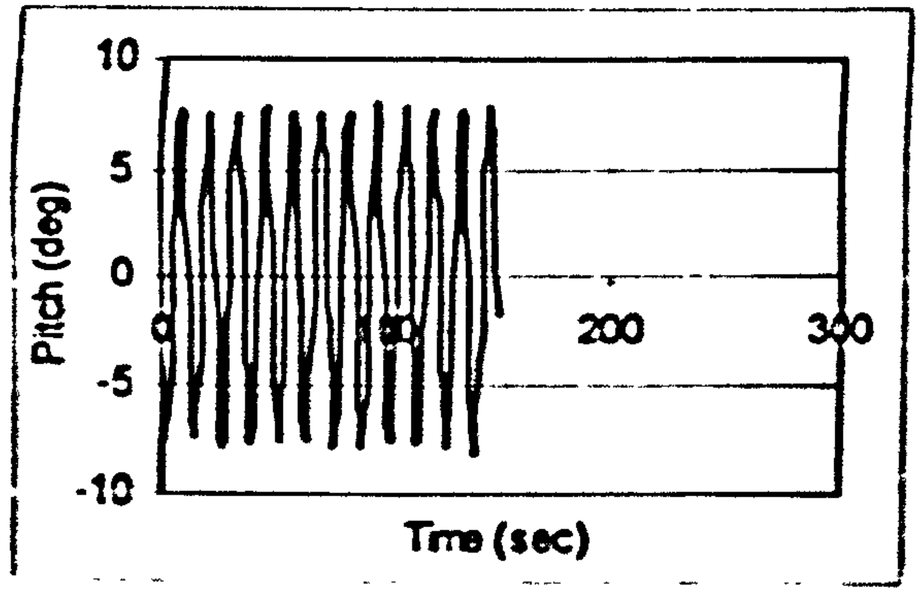

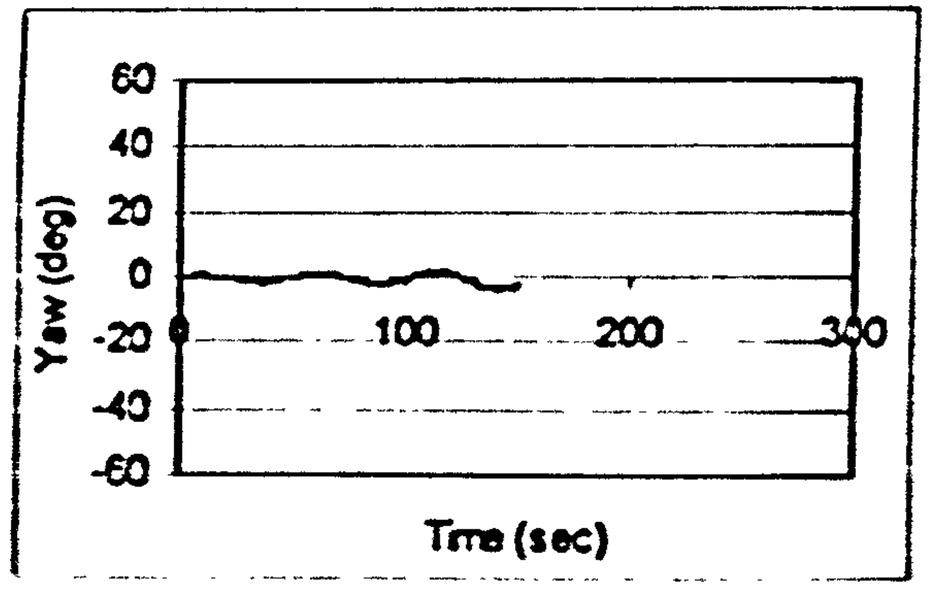

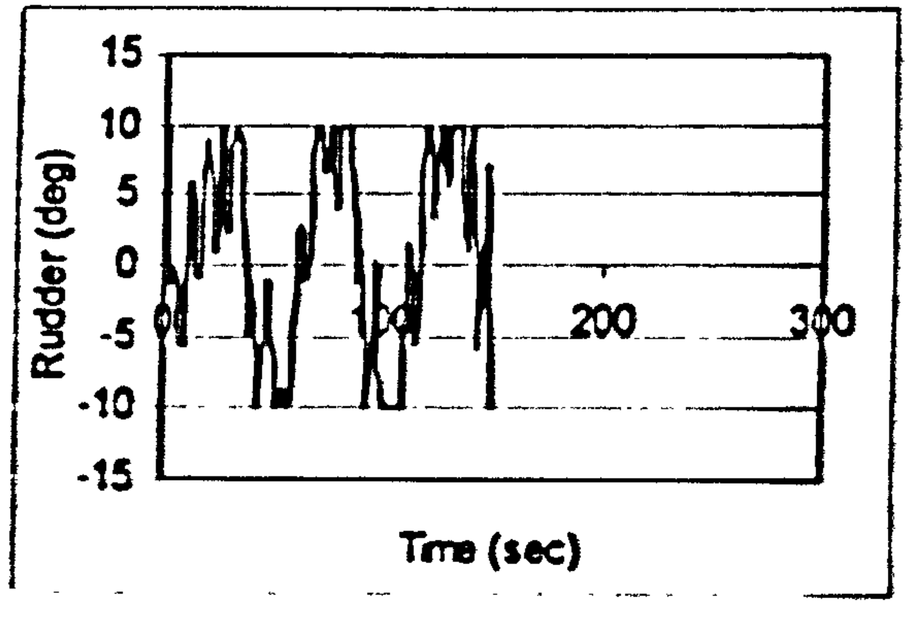

Figure G.34 Numerical Simulation of Ship A-1 in $H/\lambda=1/25$, $\lambda/L_{pp}=1.5$, Fn=0.2,$\chi_c=0$ degrees (without memory effect)

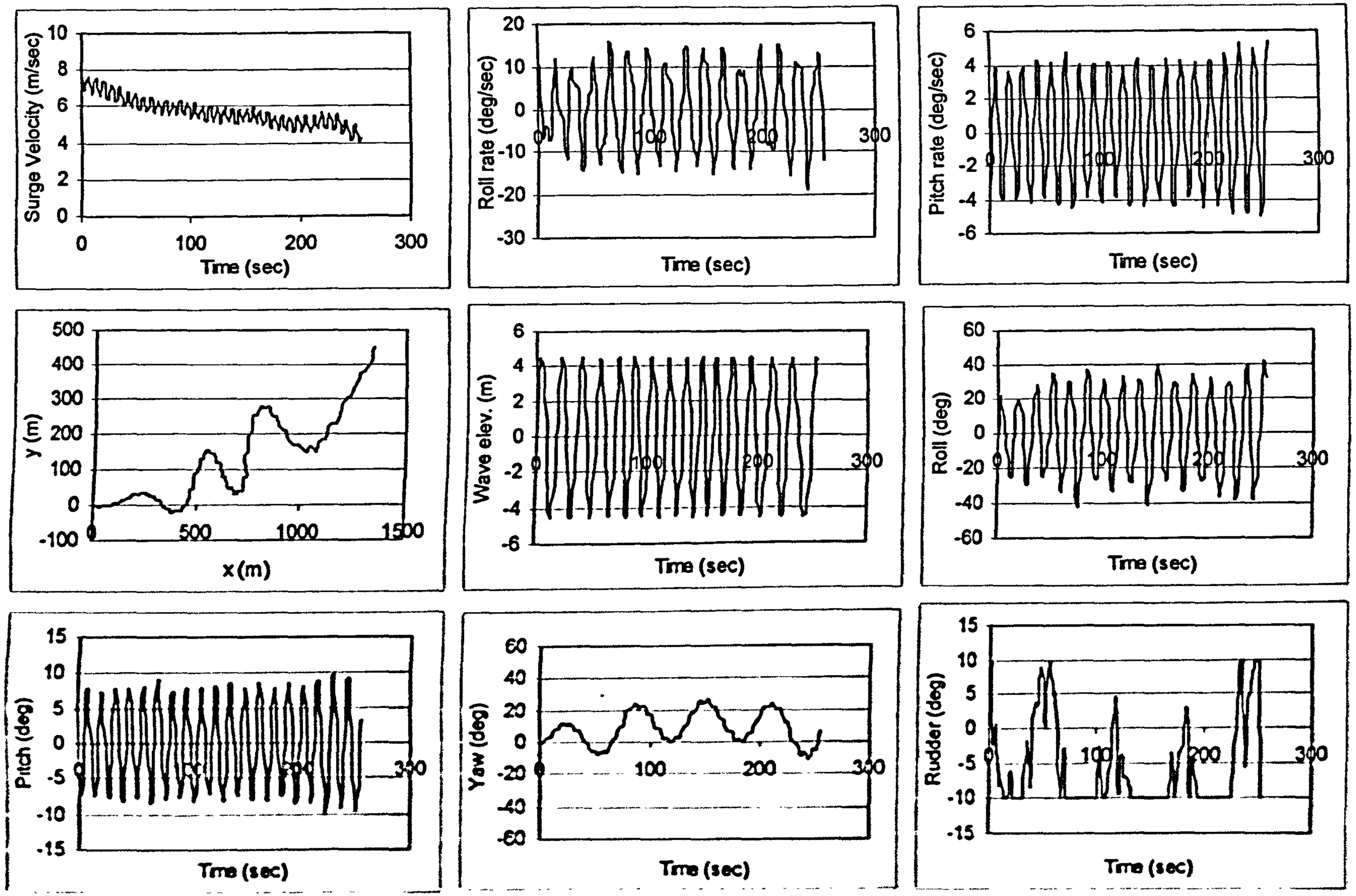

Figure G.35 Numerical Simulation of Ship A-1 in $H/\lambda=1/25$, $\lambda/L_{pp}=1.5$, Fn=0.2,χ_c=60 degrees (with memory effect)

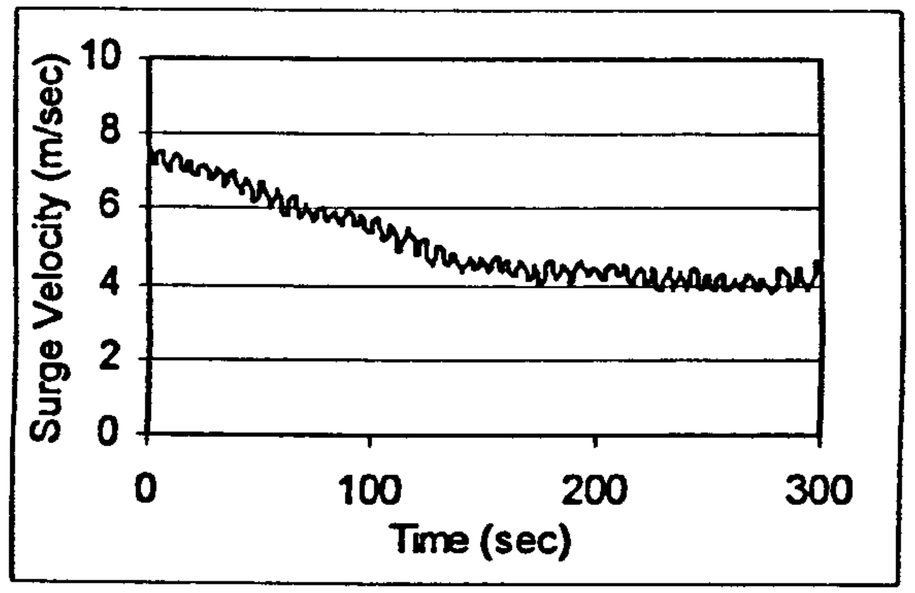

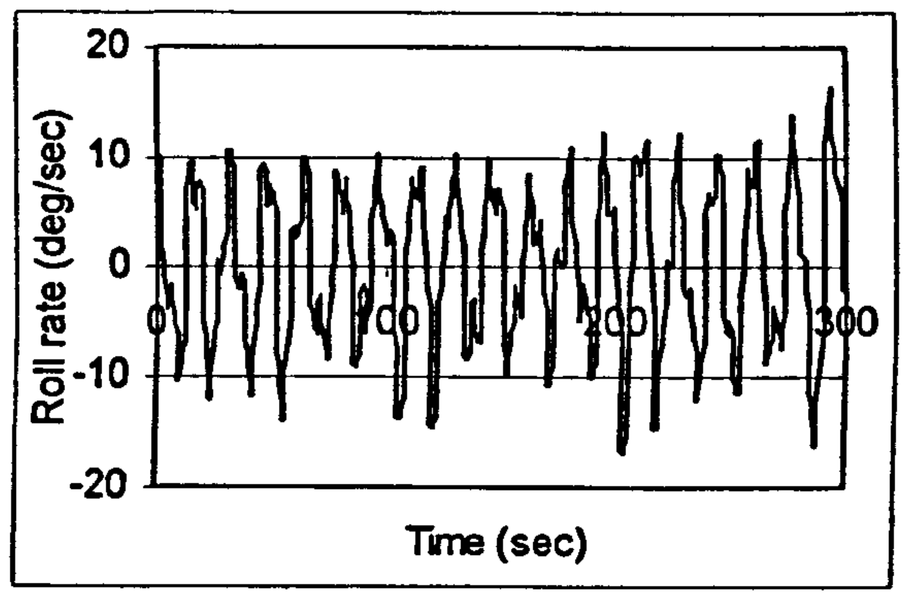

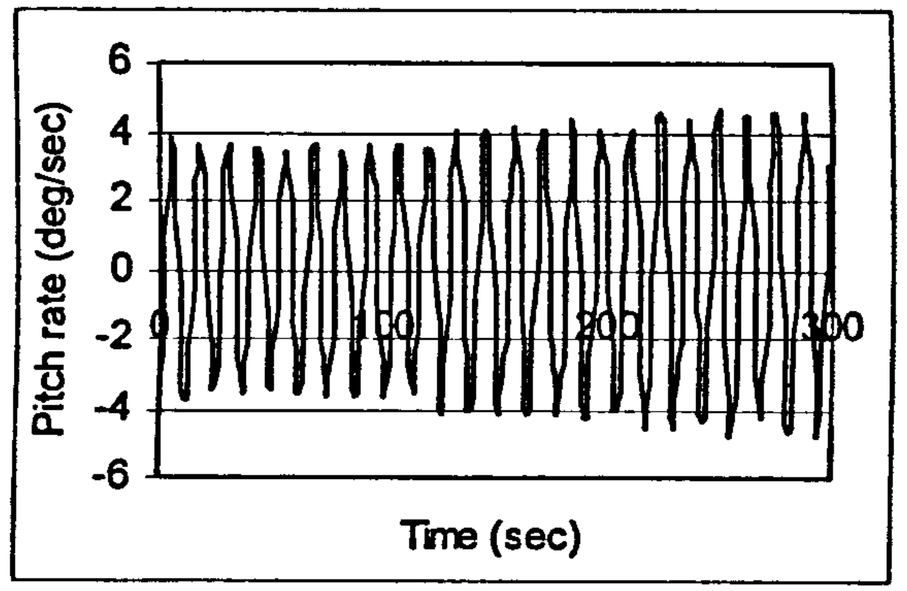

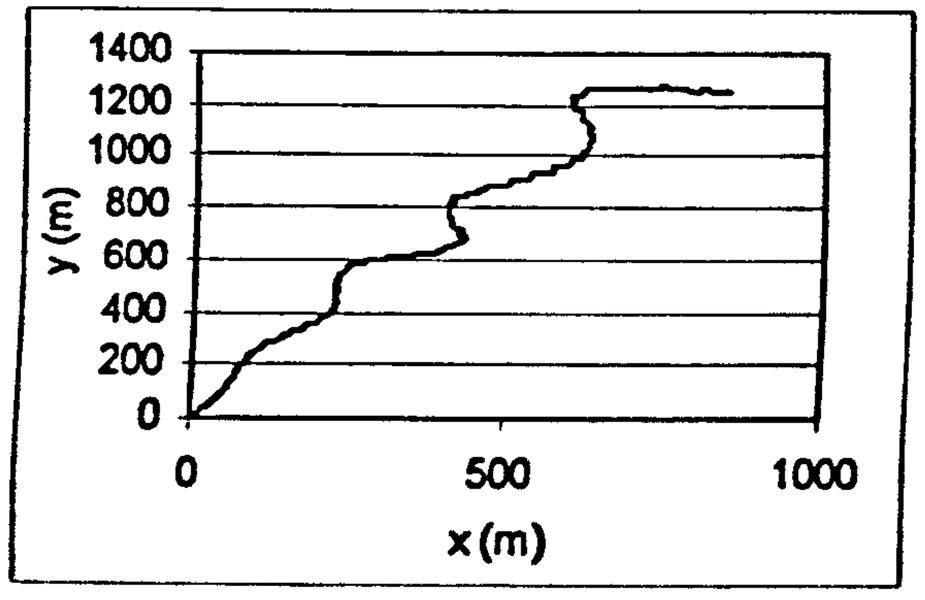

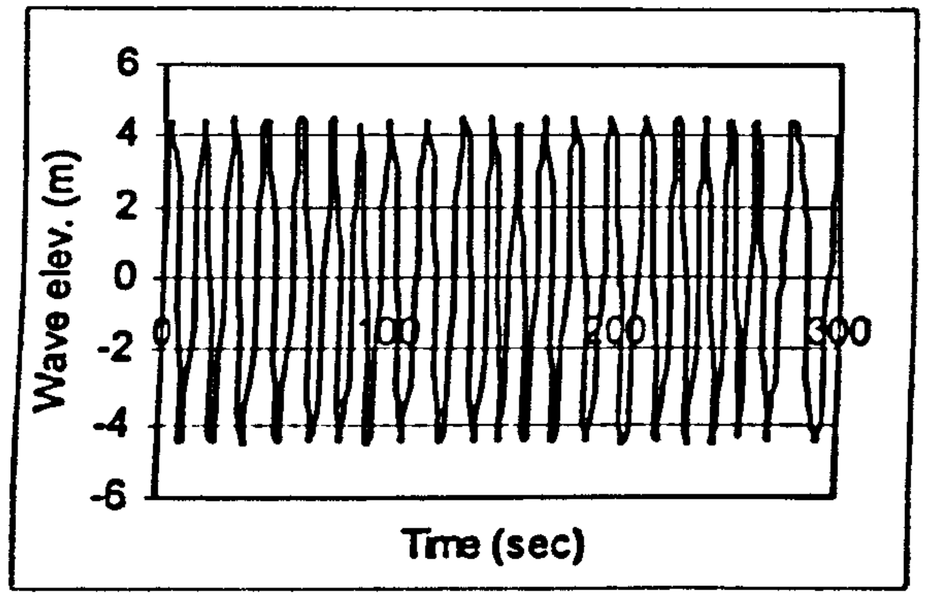

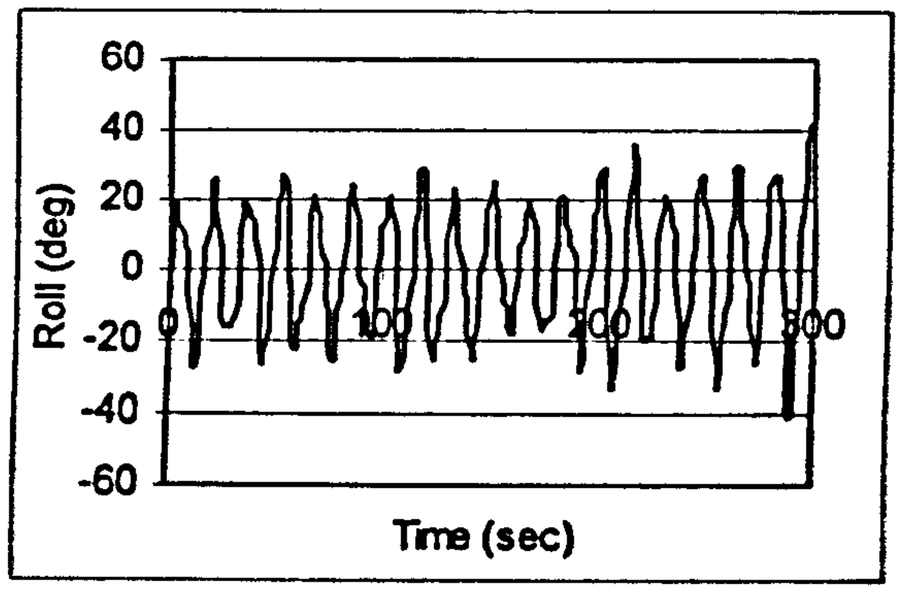

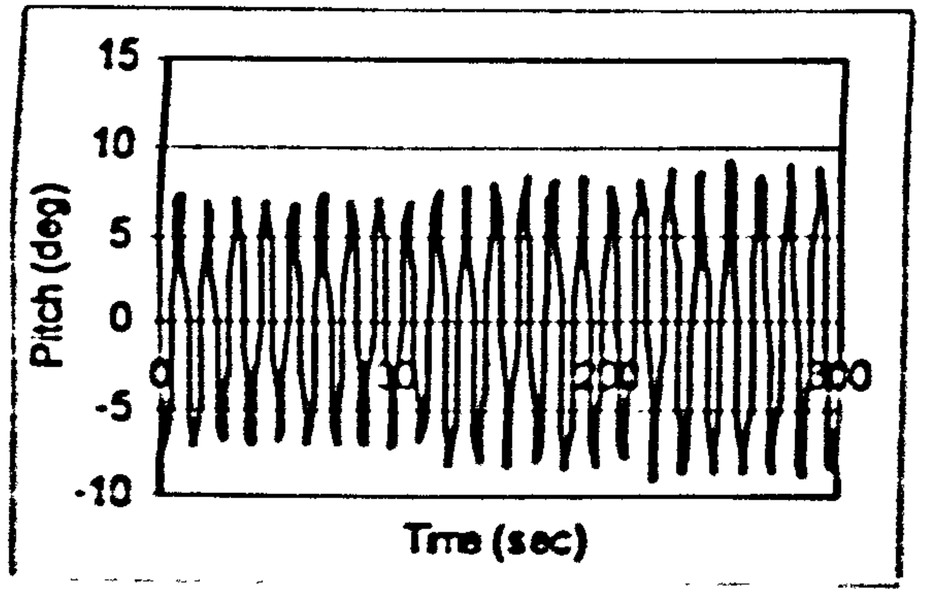

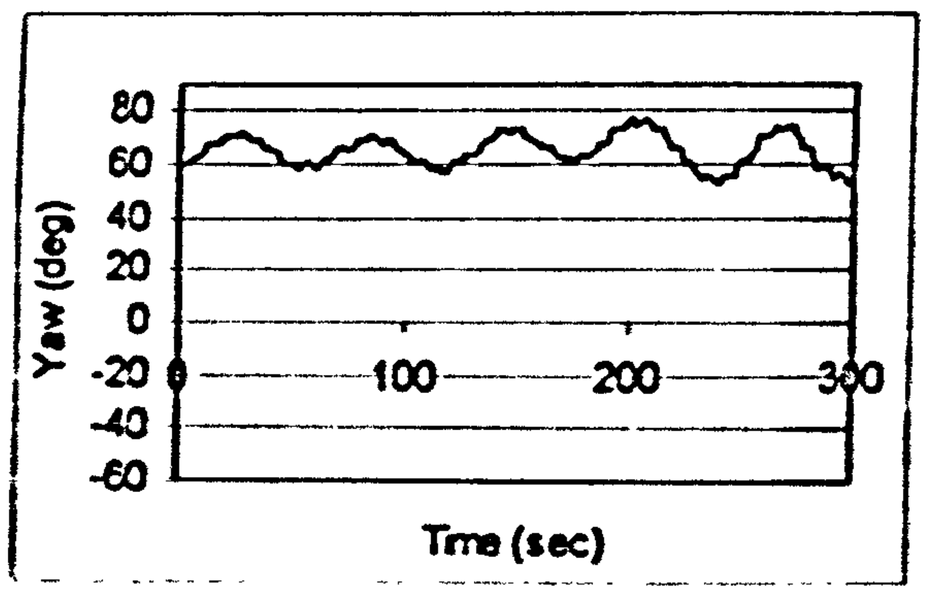

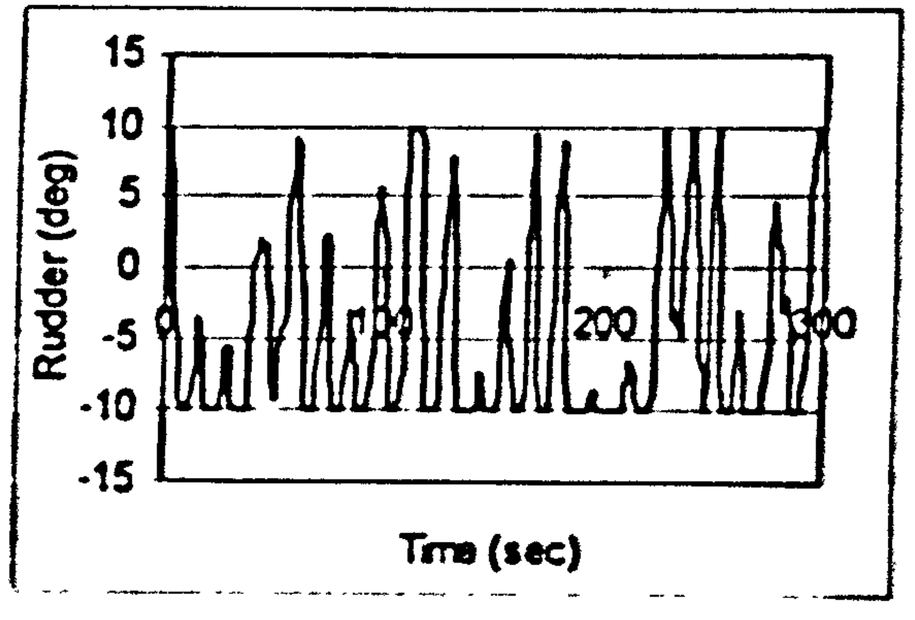

Figure G.36 Numerical Simulation of Ship A-1 in $H/\lambda=1/25$, $\lambda/L_{pp}=1.5$, Fn=0.2,χ_c=60 degrees (without memory effect)

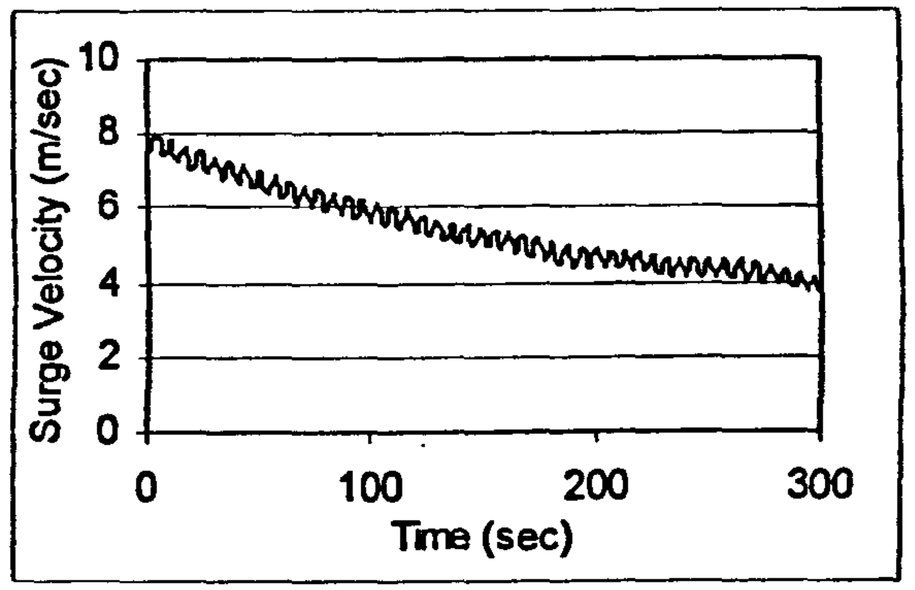

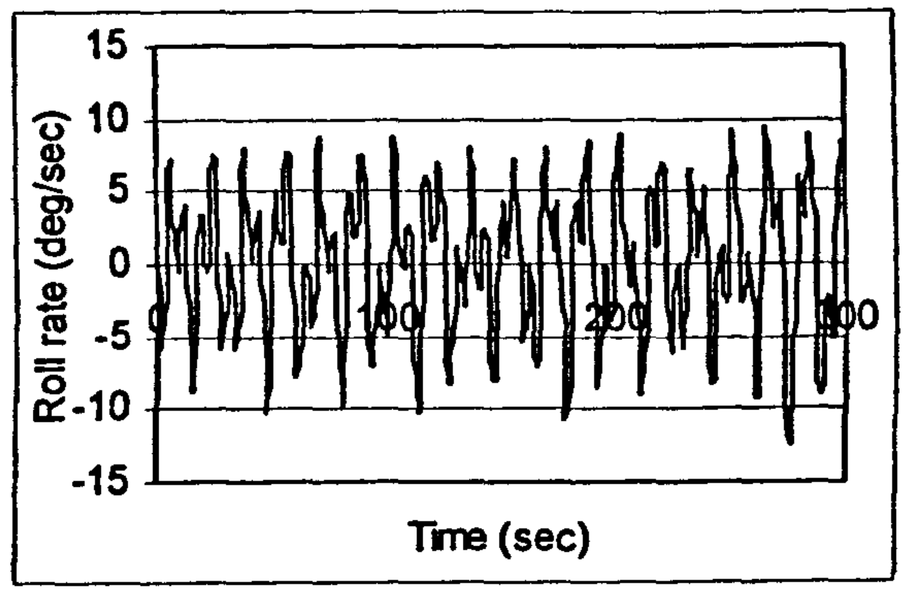

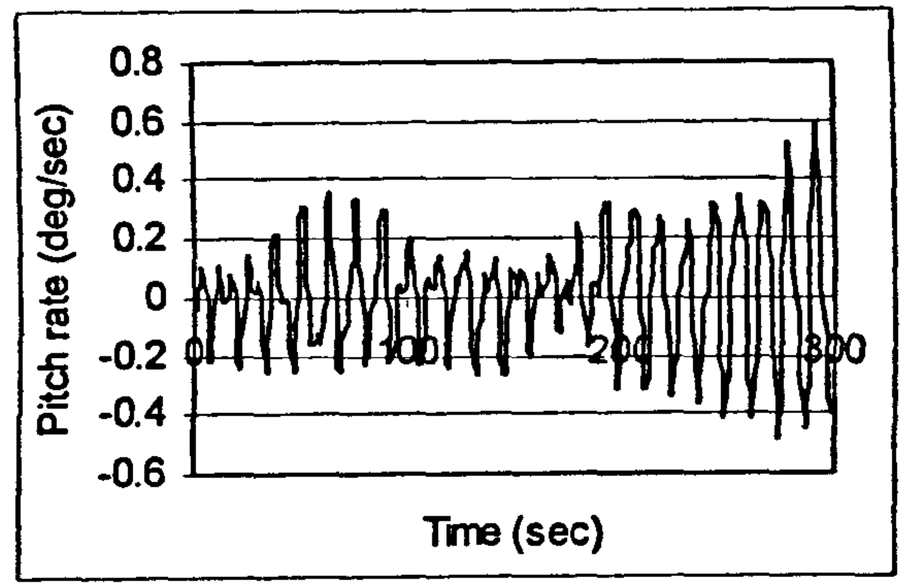

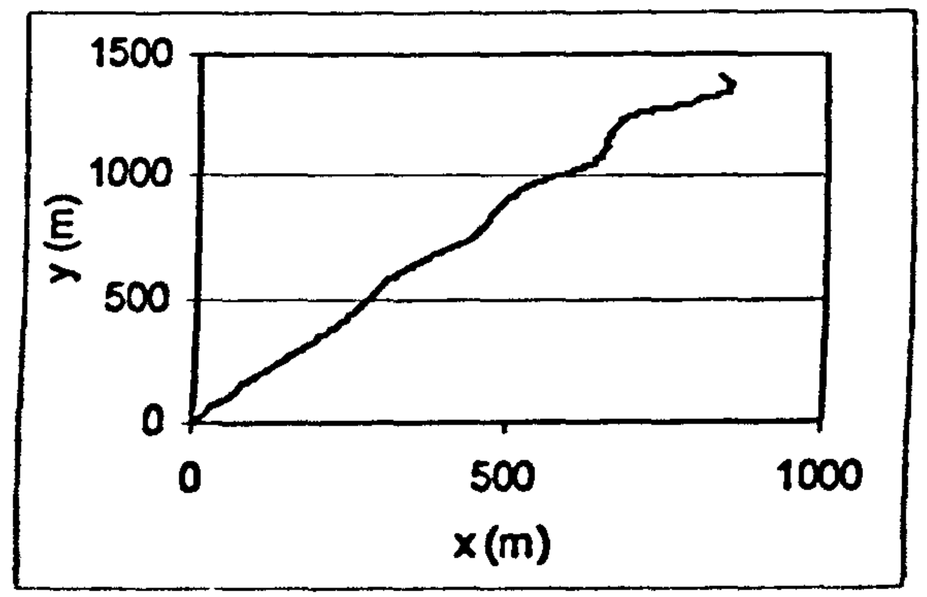

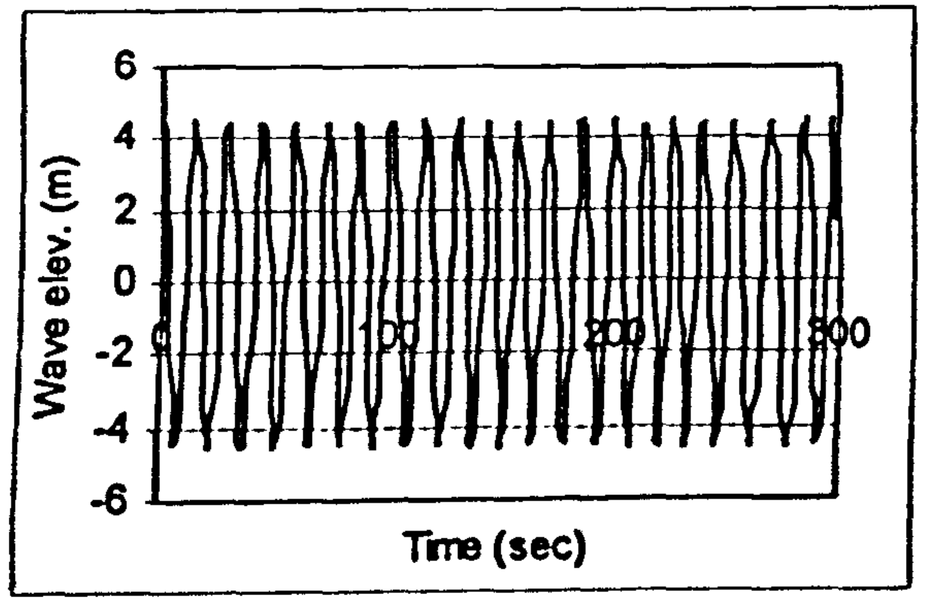

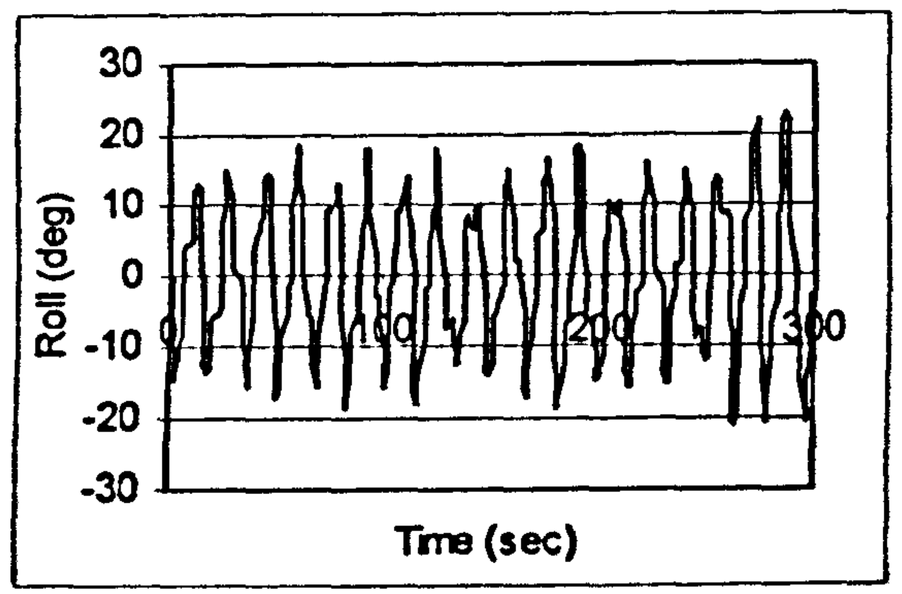

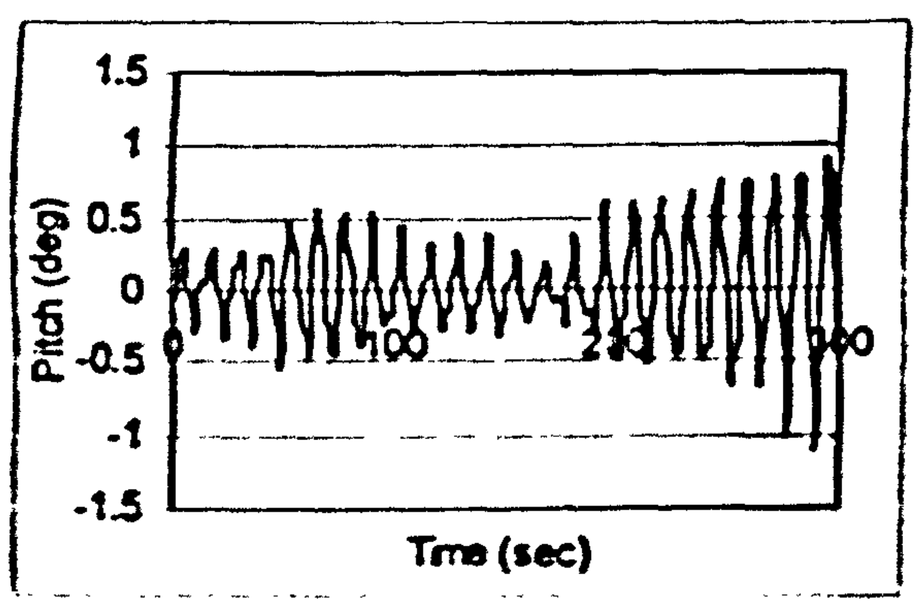

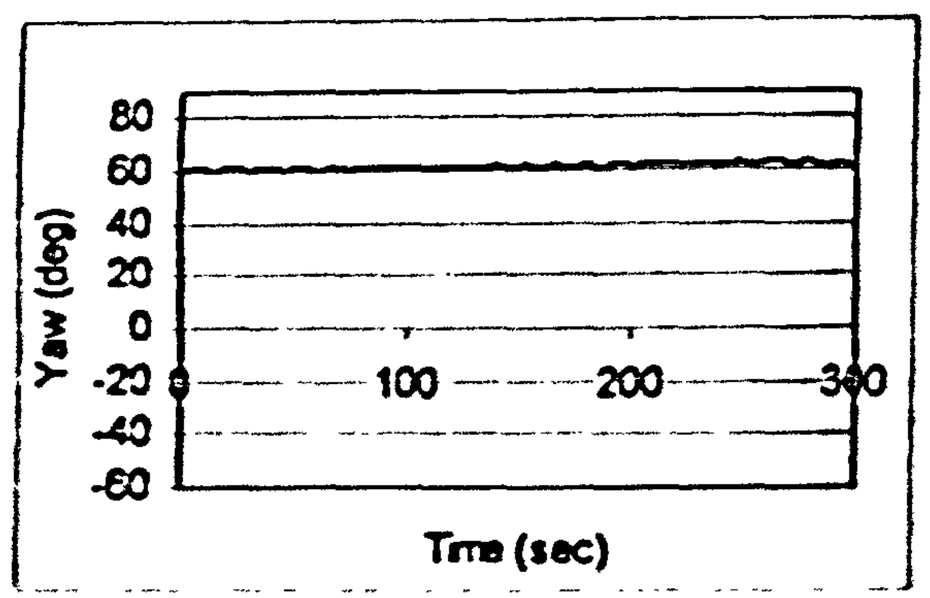

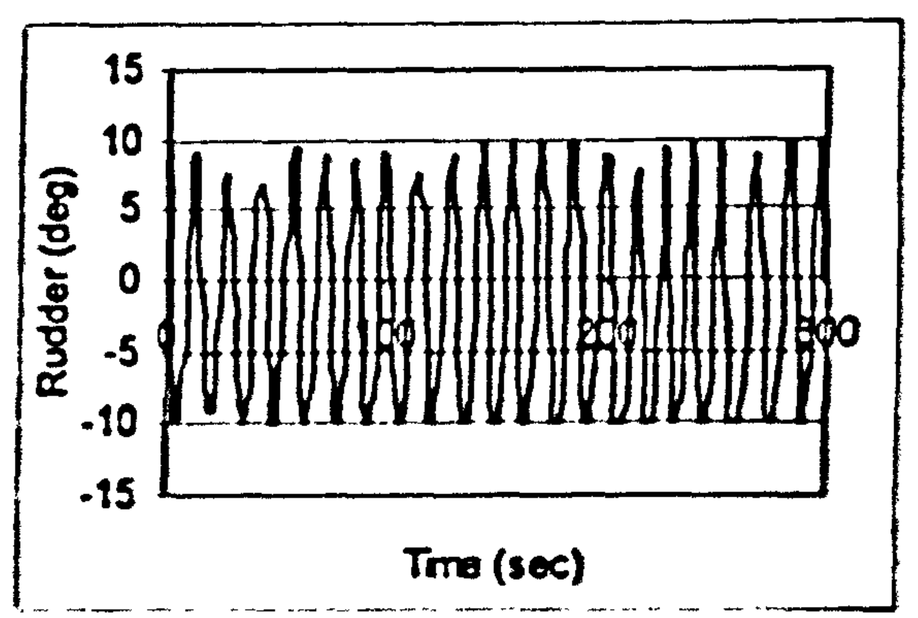

Figure G.37 Numerical Simulation of Ship A-1 in $H/\lambda=1/25$, $\lambda/L_{pp}=1.5$, Fn=0.4,$\chi_c=0$ degrees (with memory effect)

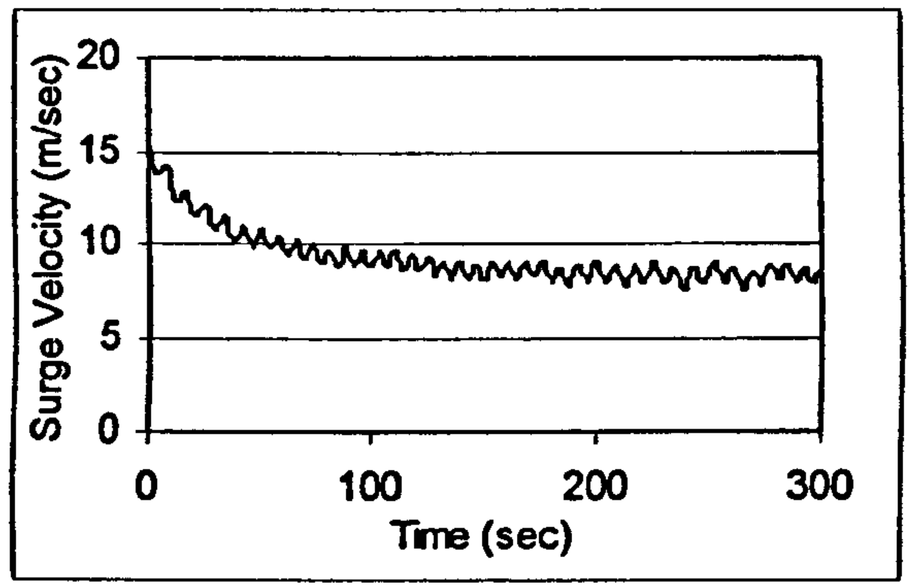

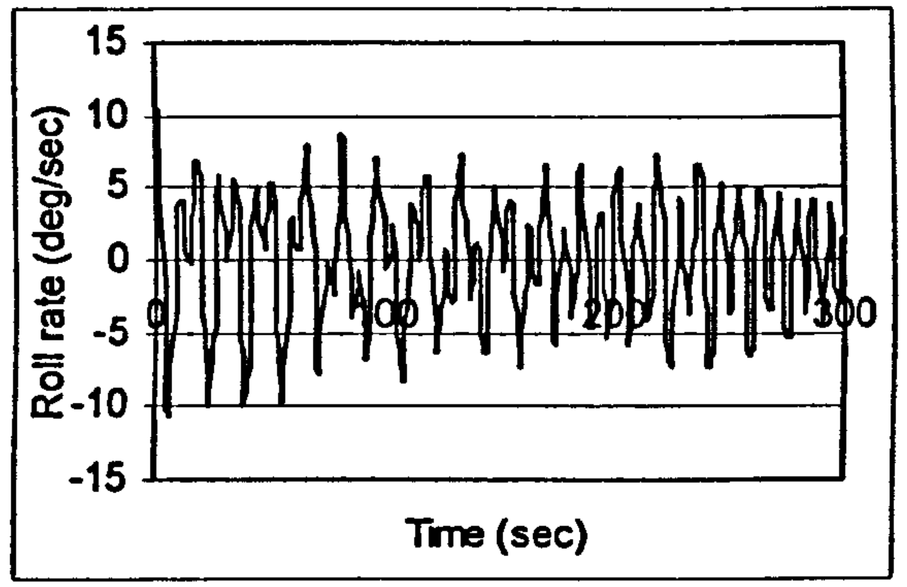

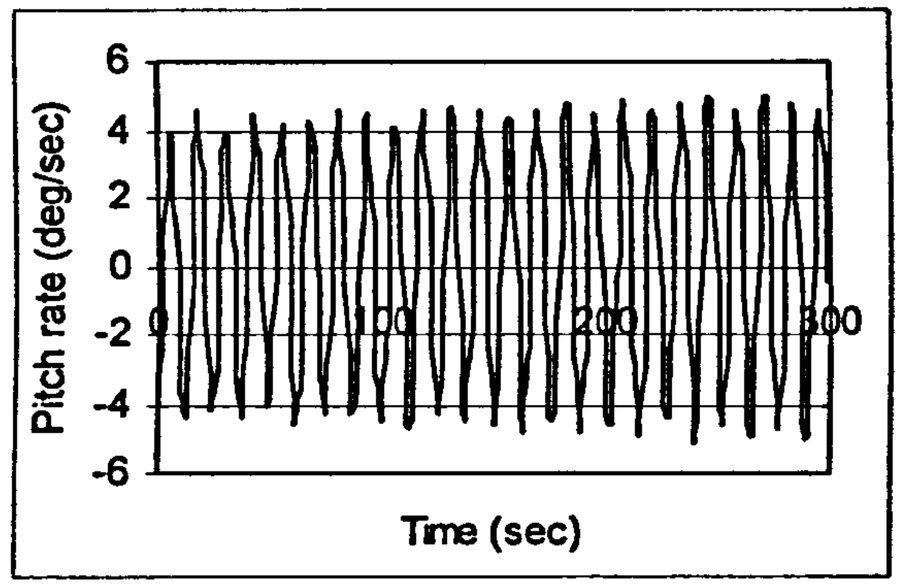

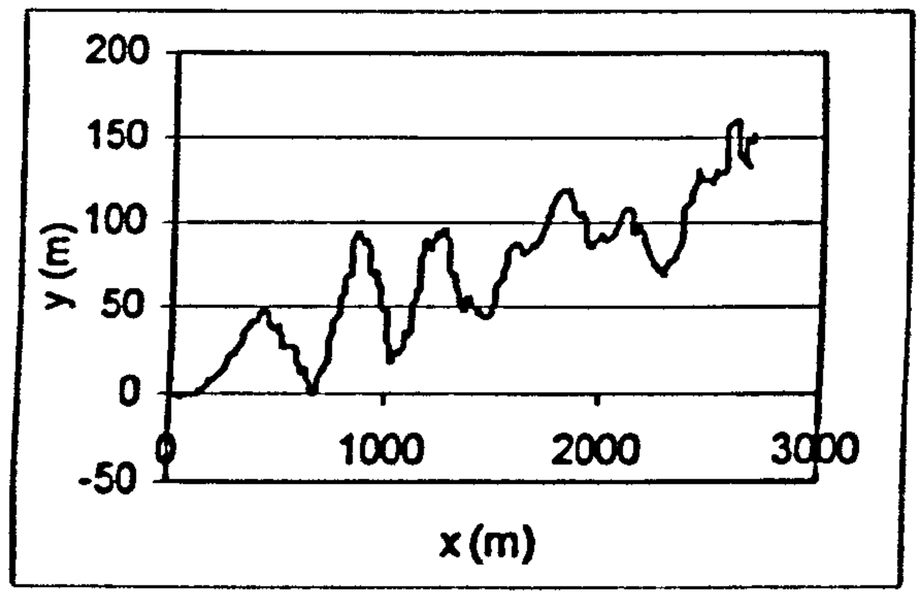

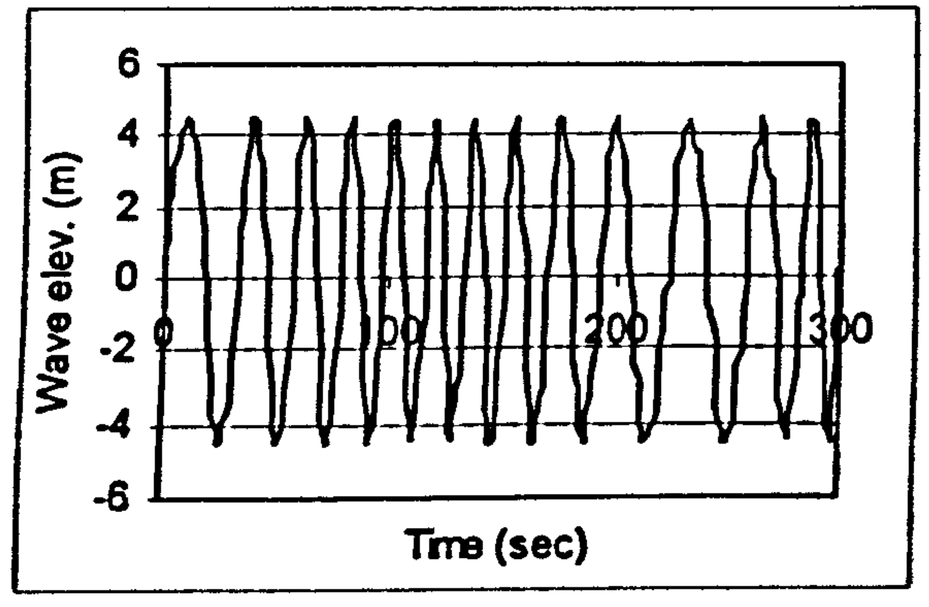

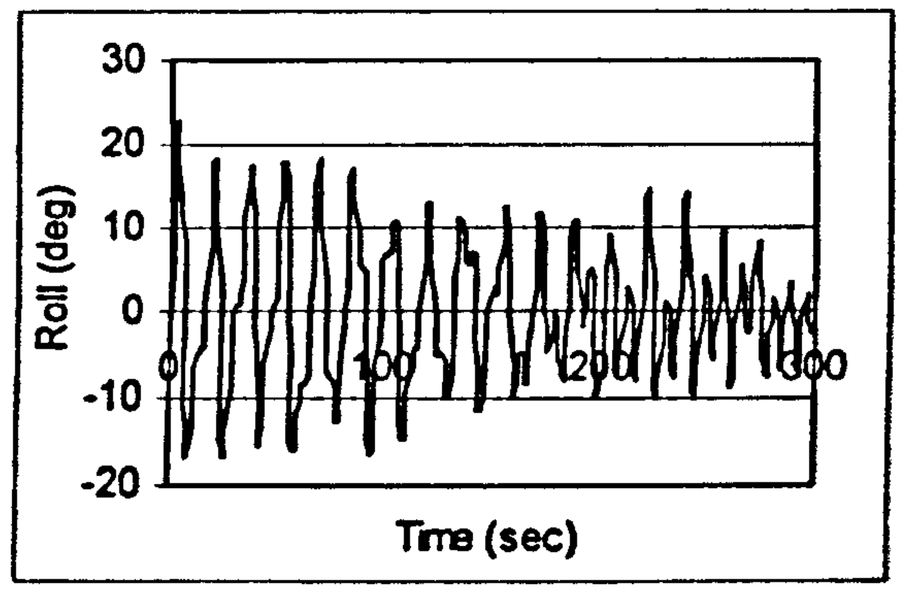

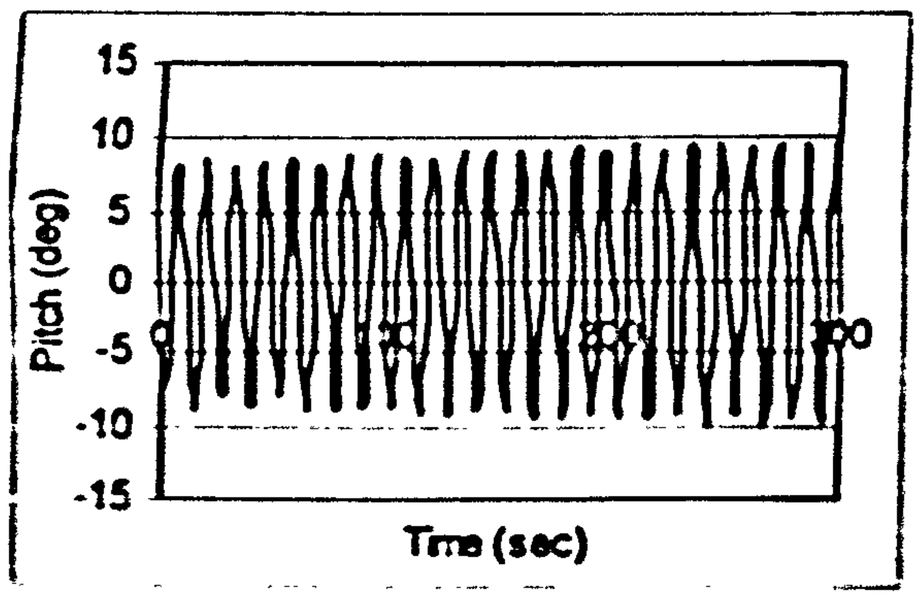

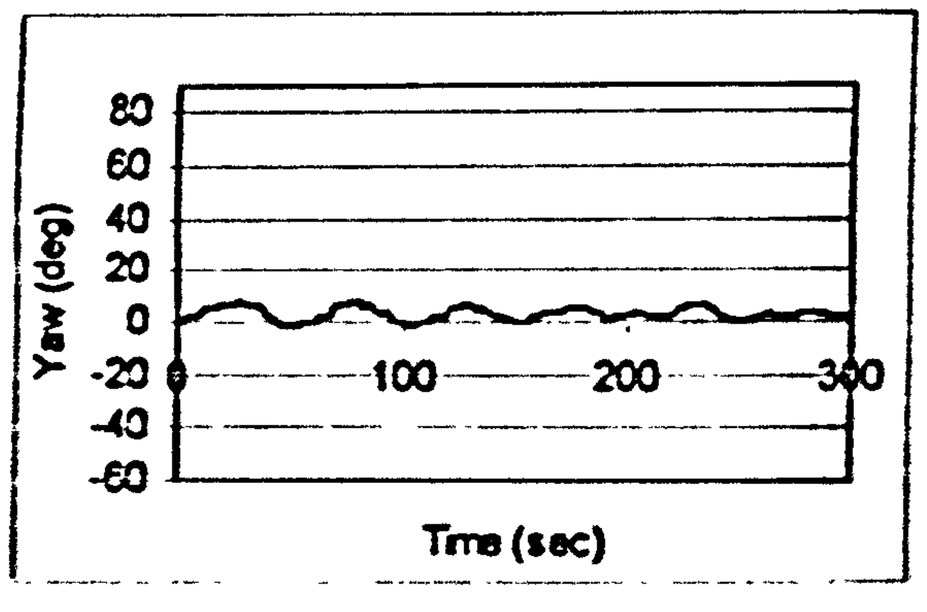

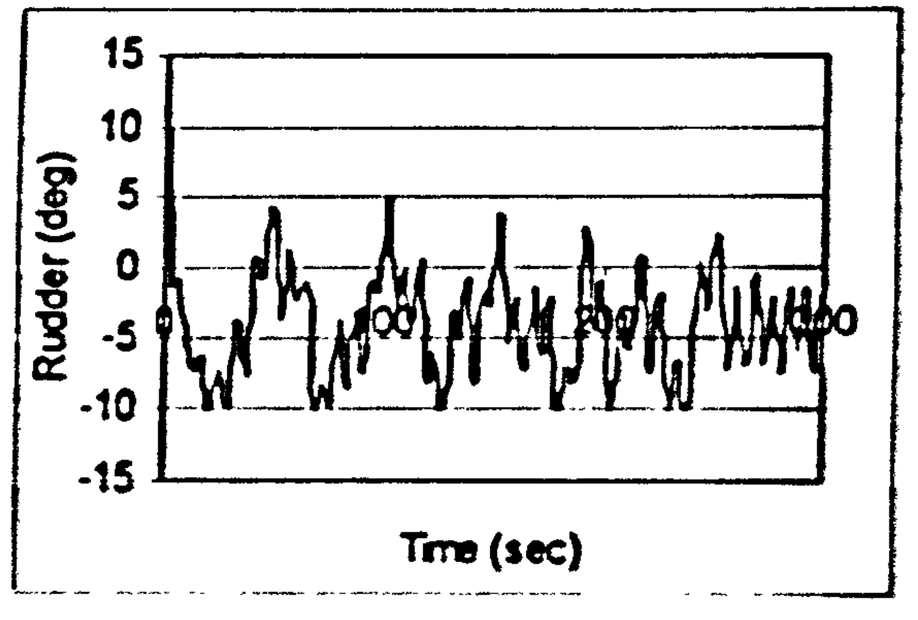

Figure G.38 Numerical Simulation of Ship A-1 in $H/\lambda=1/25$, $\lambda/L_{pp}=1.5$, Fn=0.4,$\chi_c=0$ degrees (without memory effect)

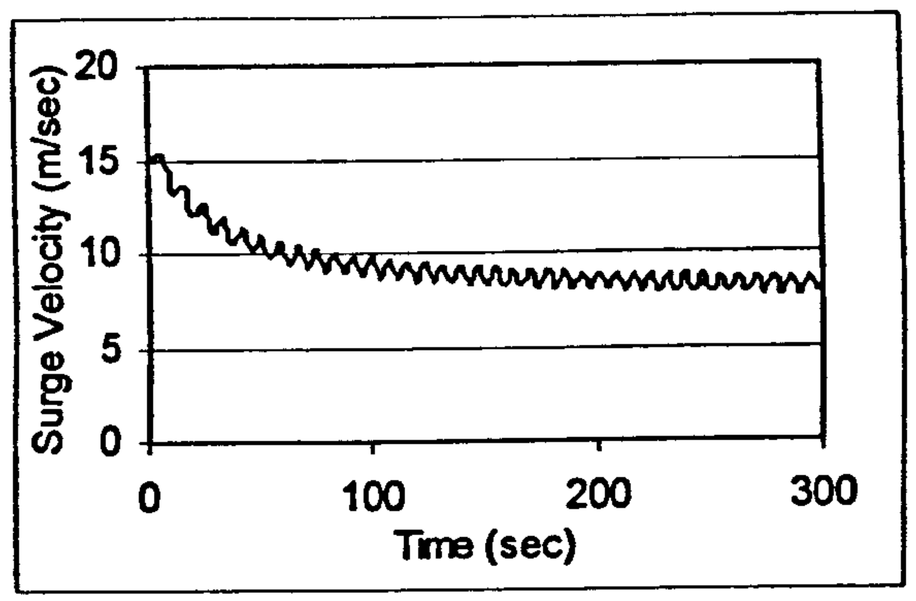

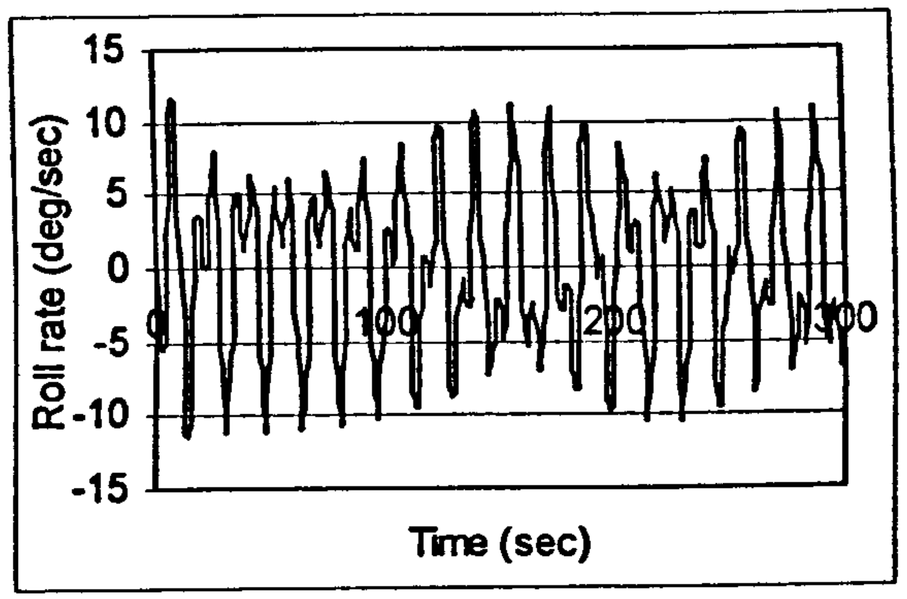

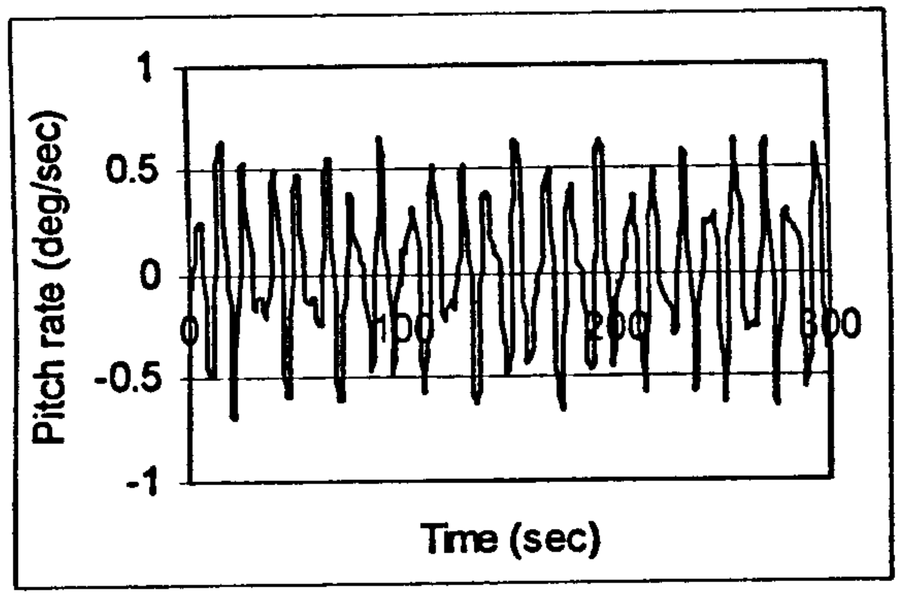

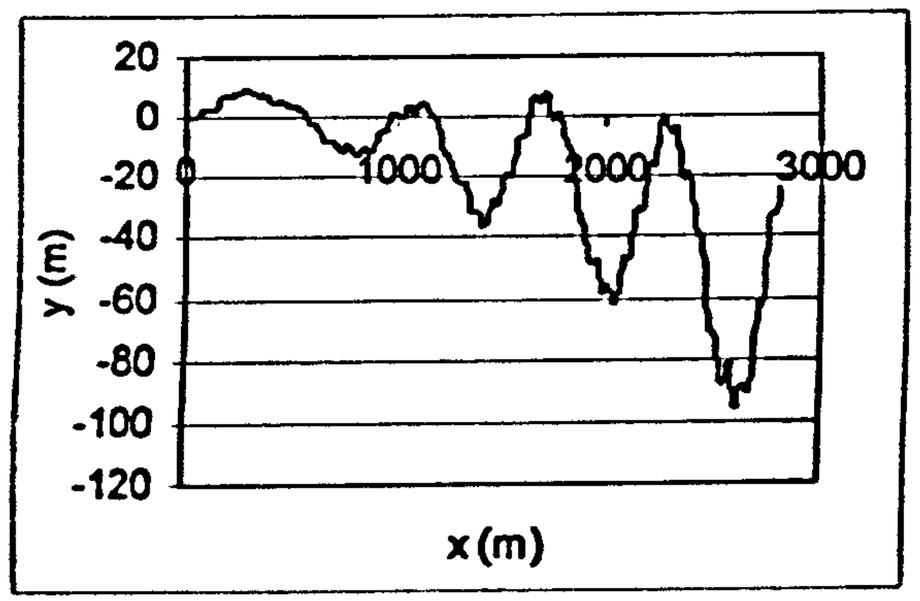

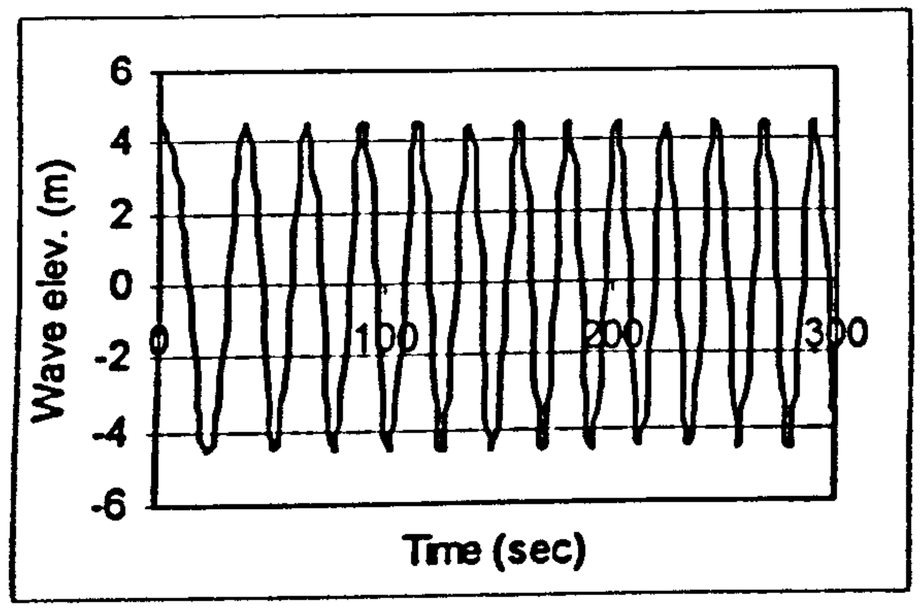

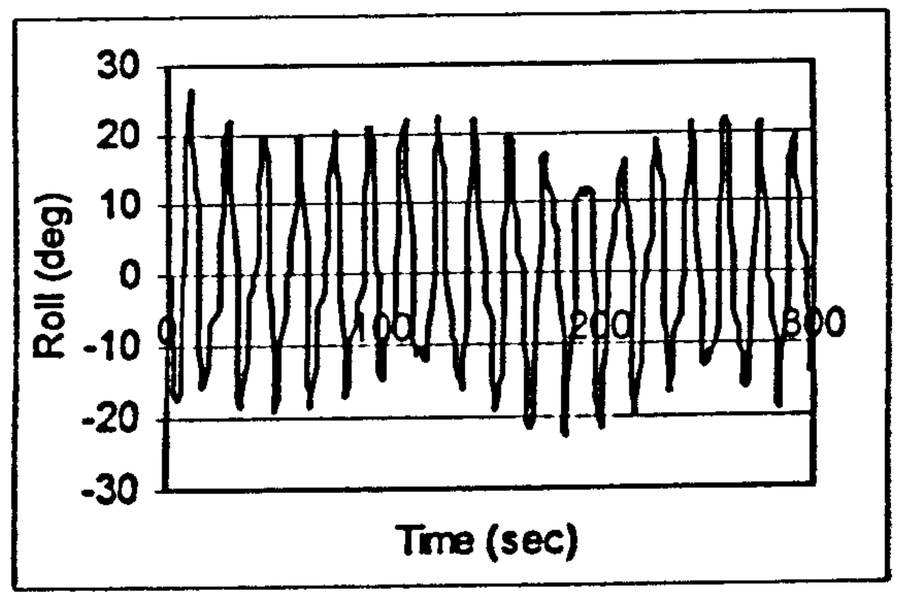

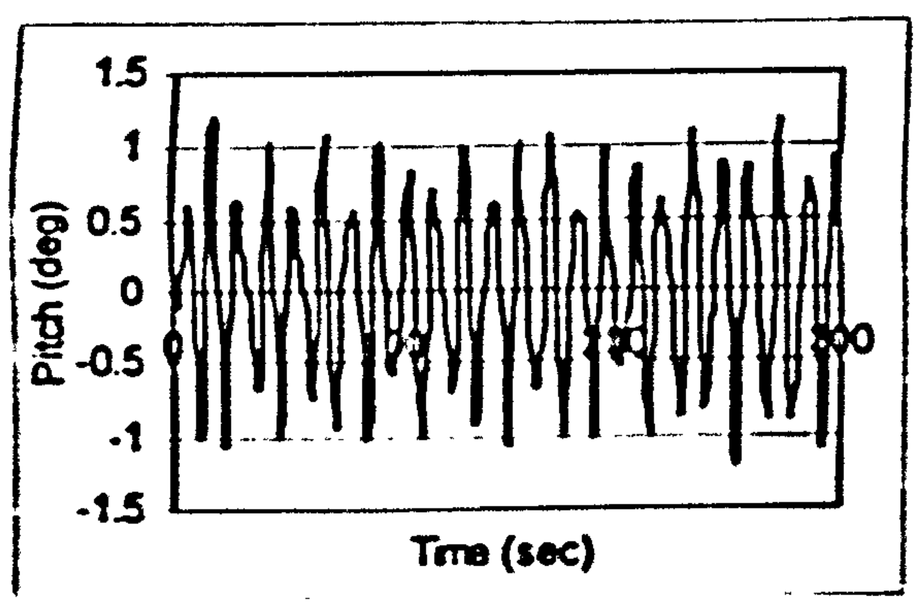

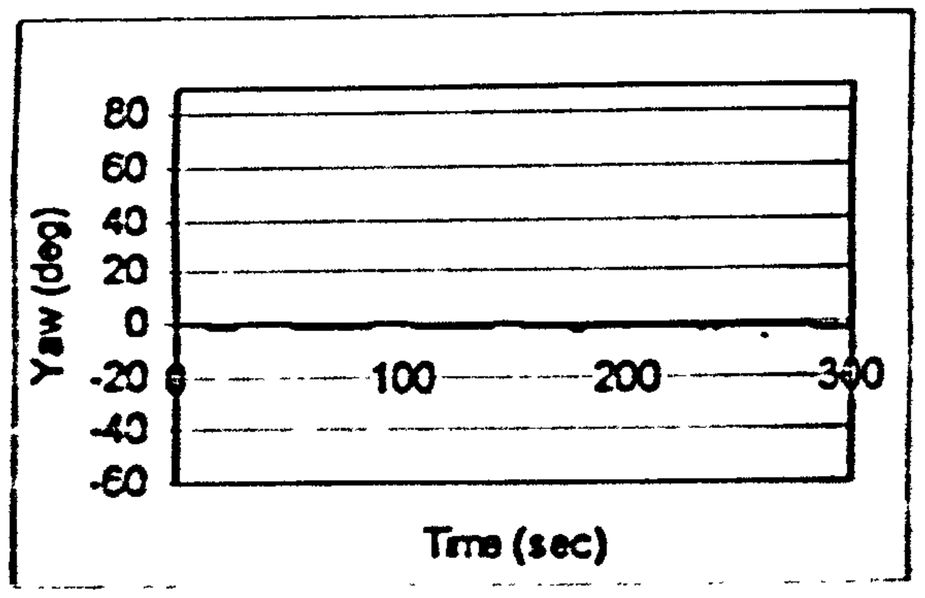

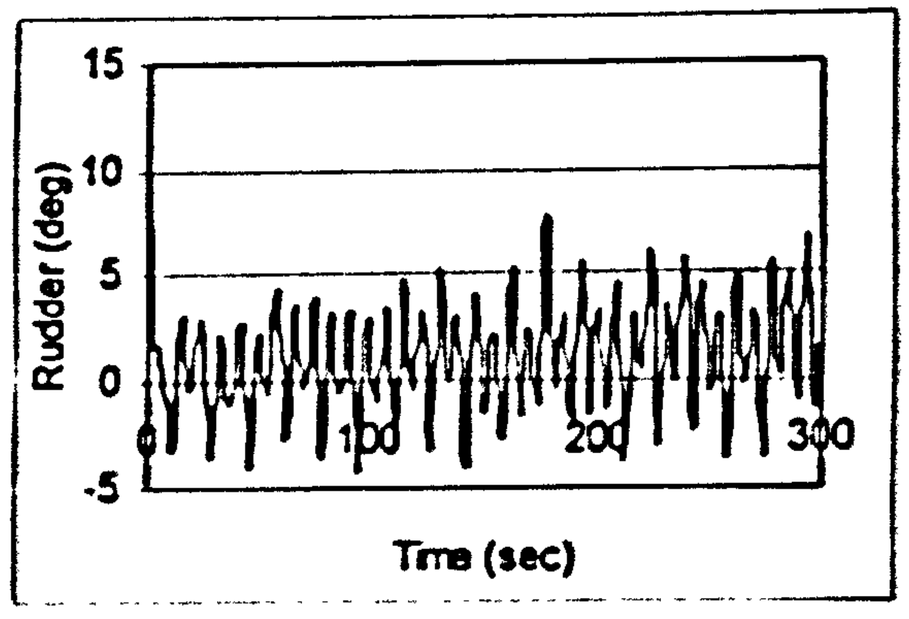

Figure G.39 Numerical Simulation of Ship A-1 in $H/\lambda=1/25$, $\lambda/L_{pp}=1.5$, Fn=0.4,$\chi_c=60$ degrees (with memory effect)

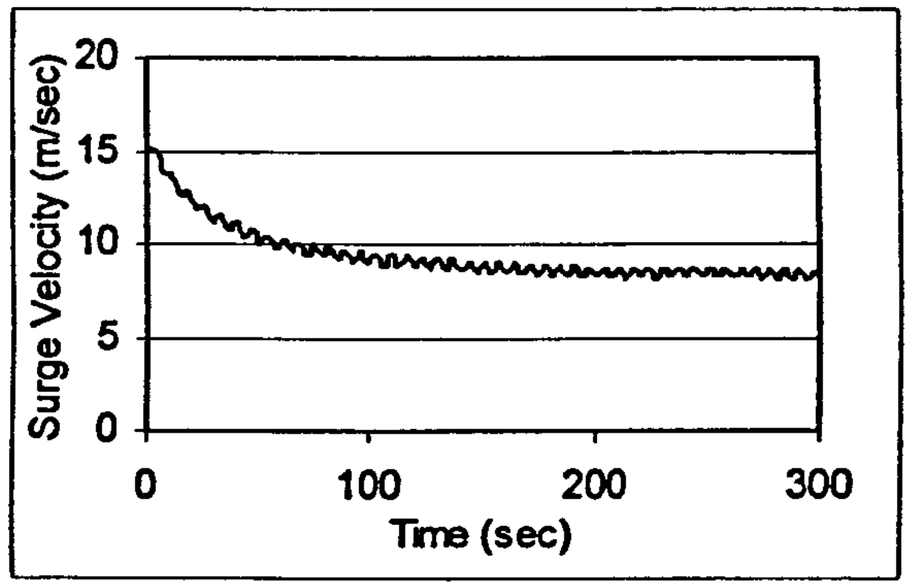

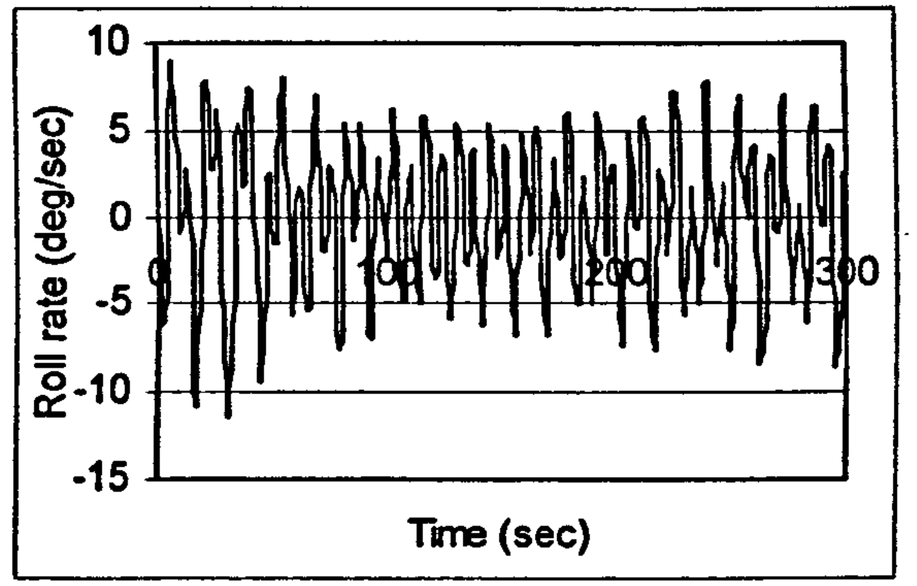

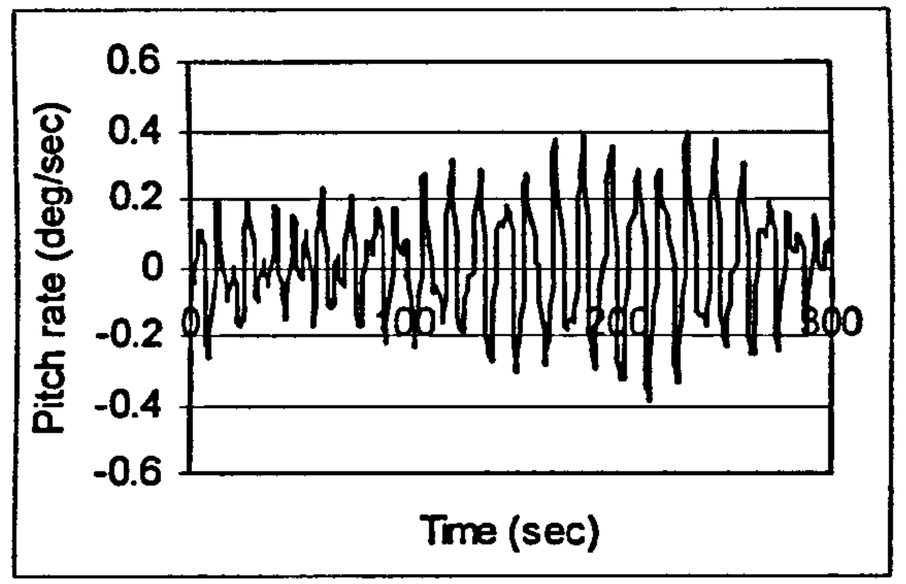

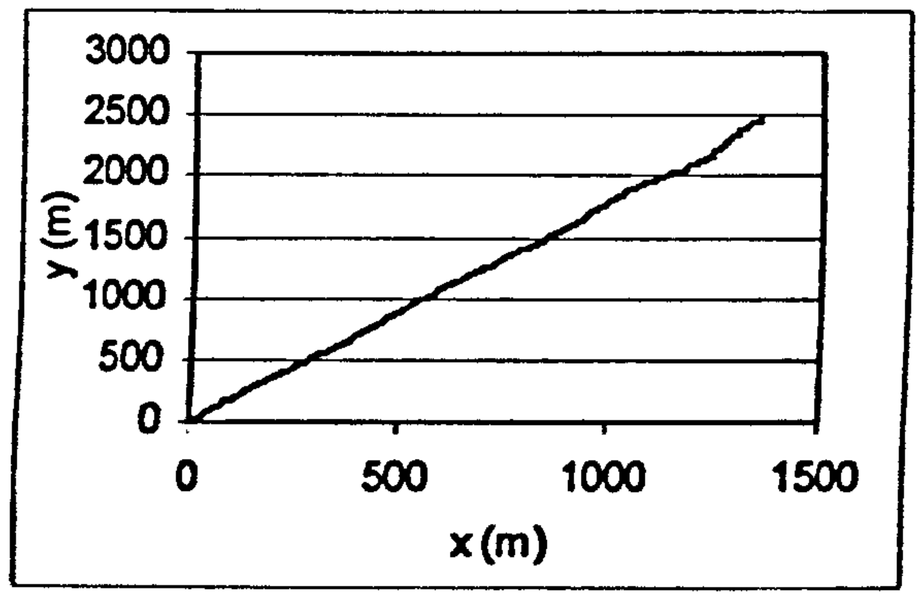

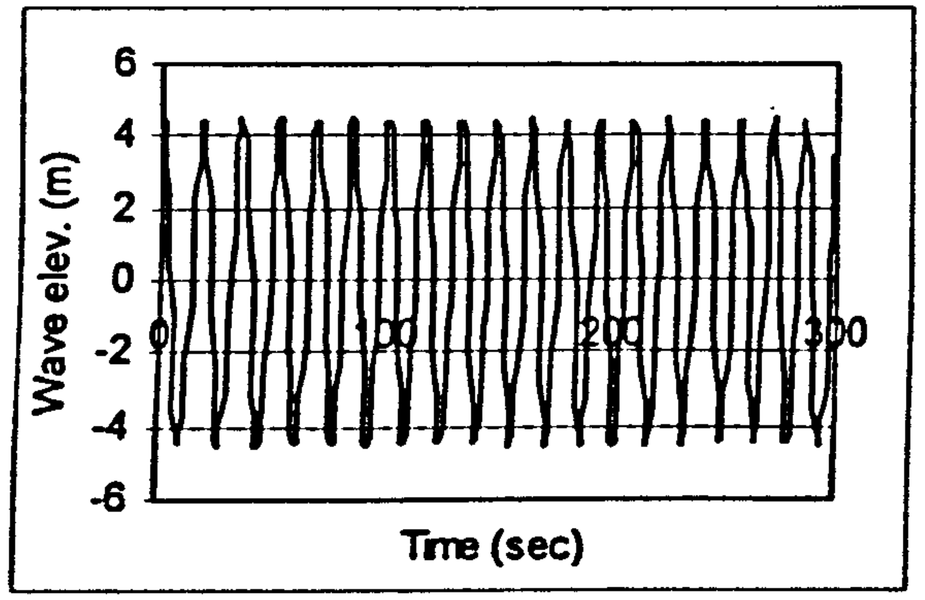

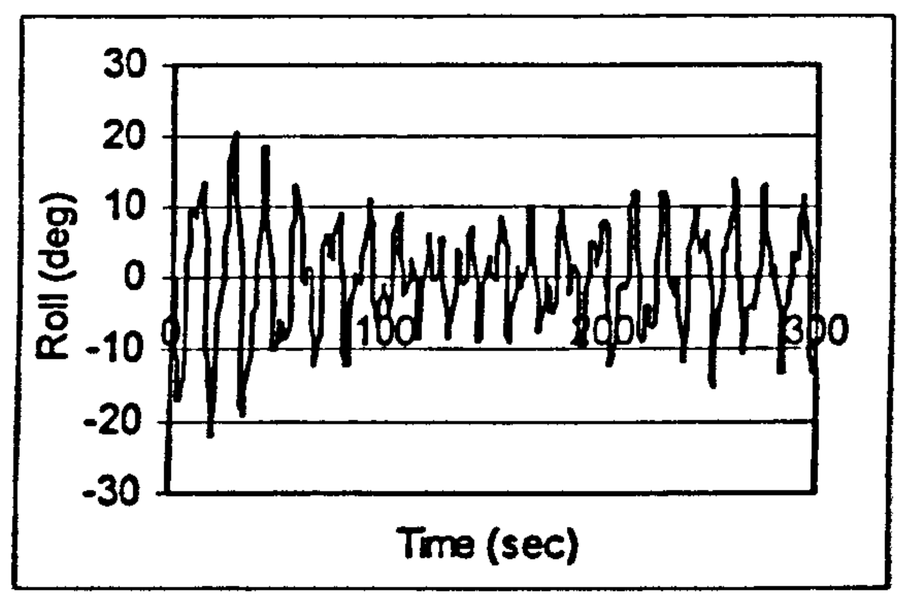

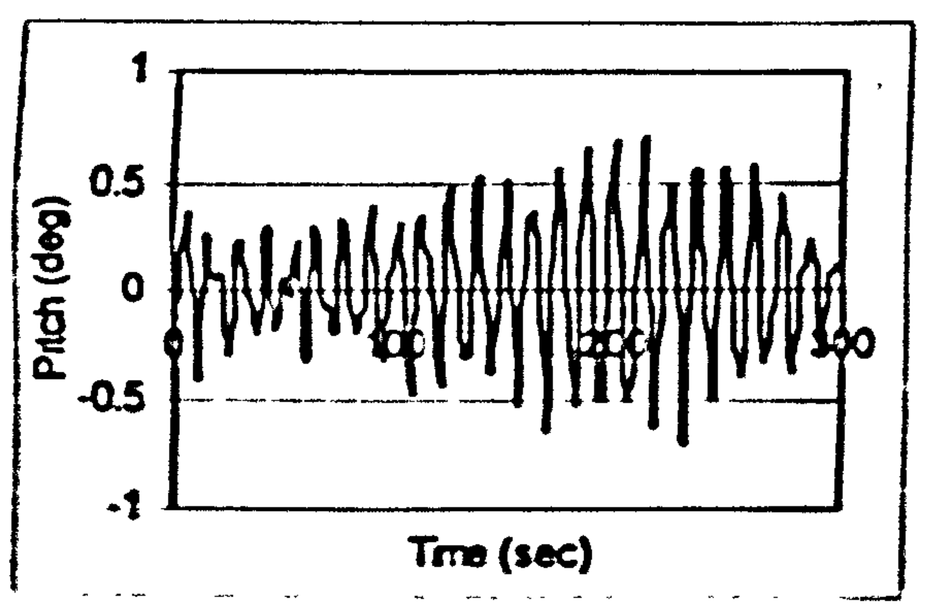

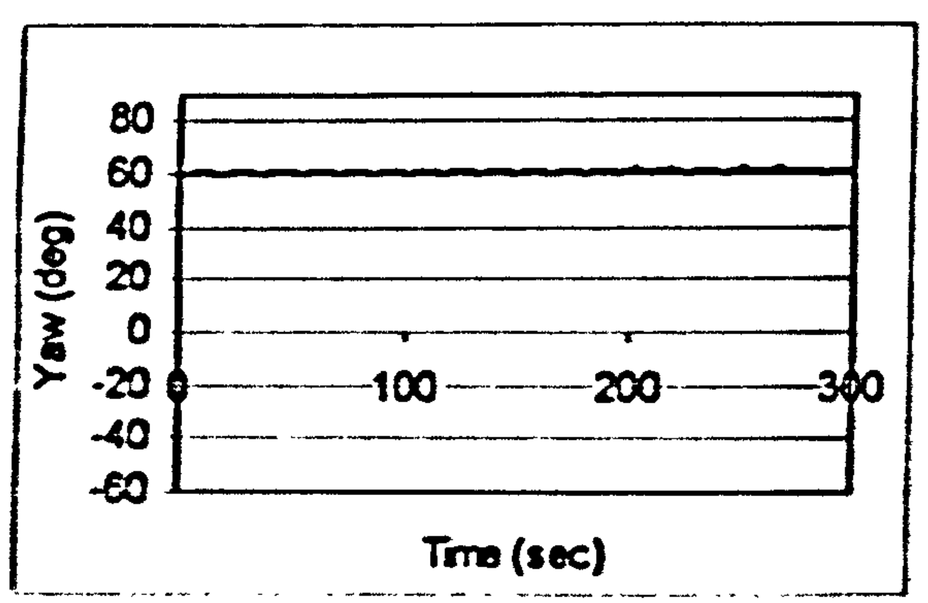

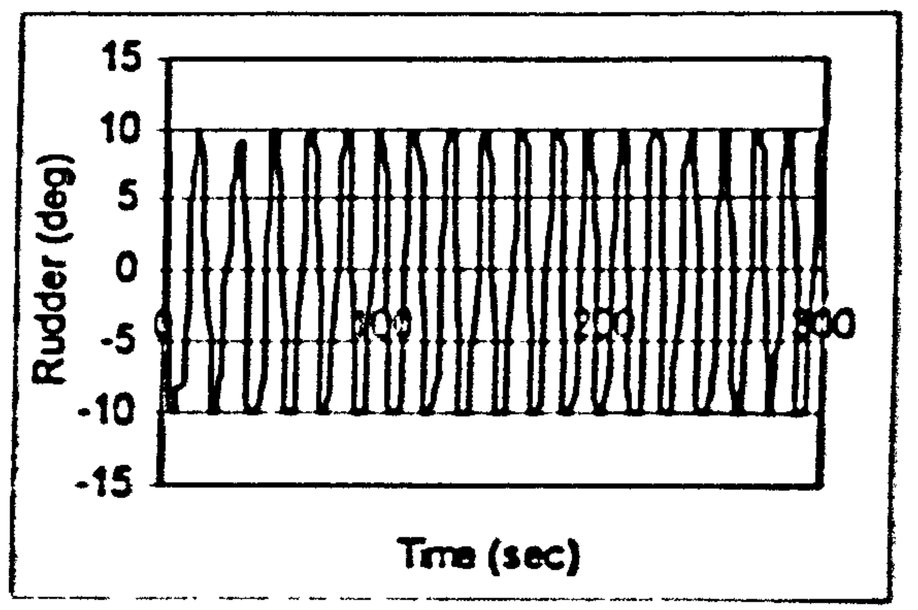

Figure G.40 Numerical Simulation of Ship A-1 in $H/\lambda=1/25$, $\lambda/L_{pp}=1.5$, Fn=0.4,χ_c=60 degrees (without memory effect)

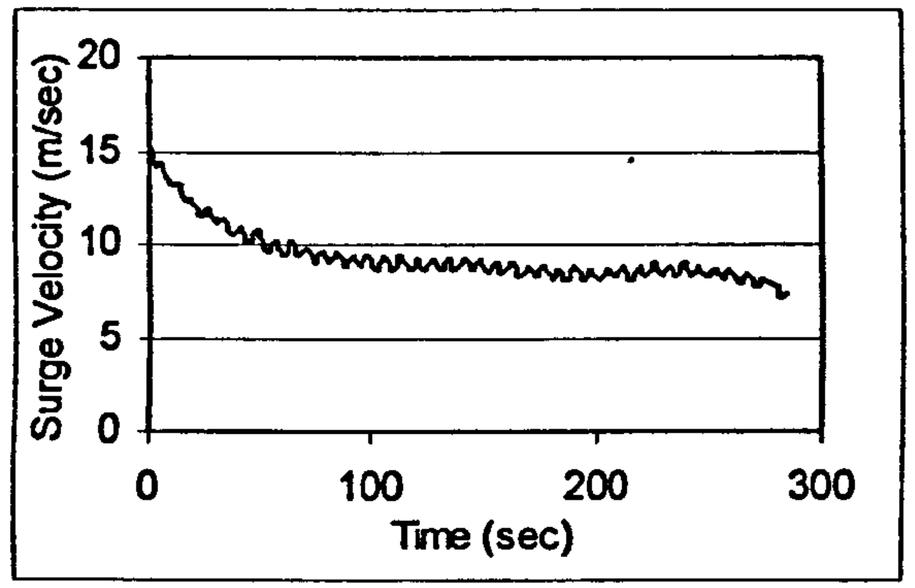

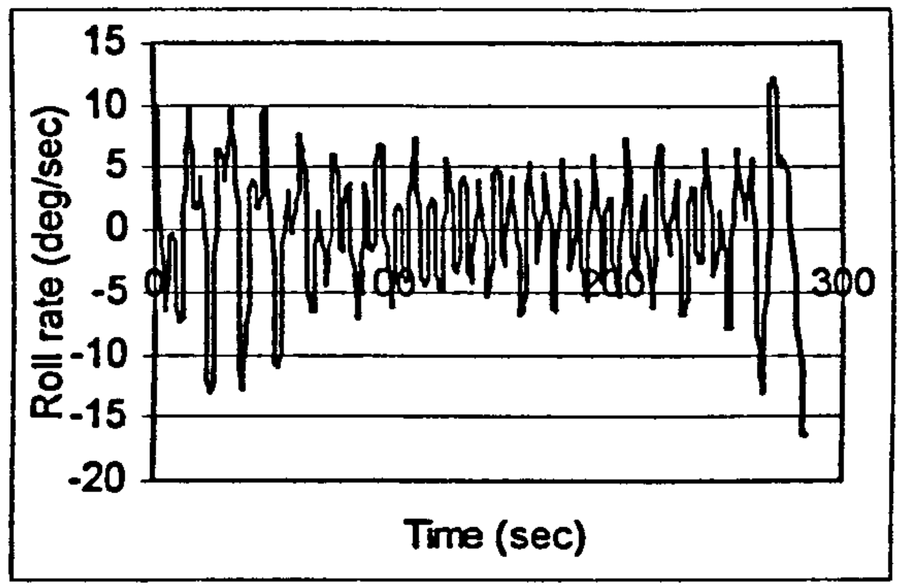

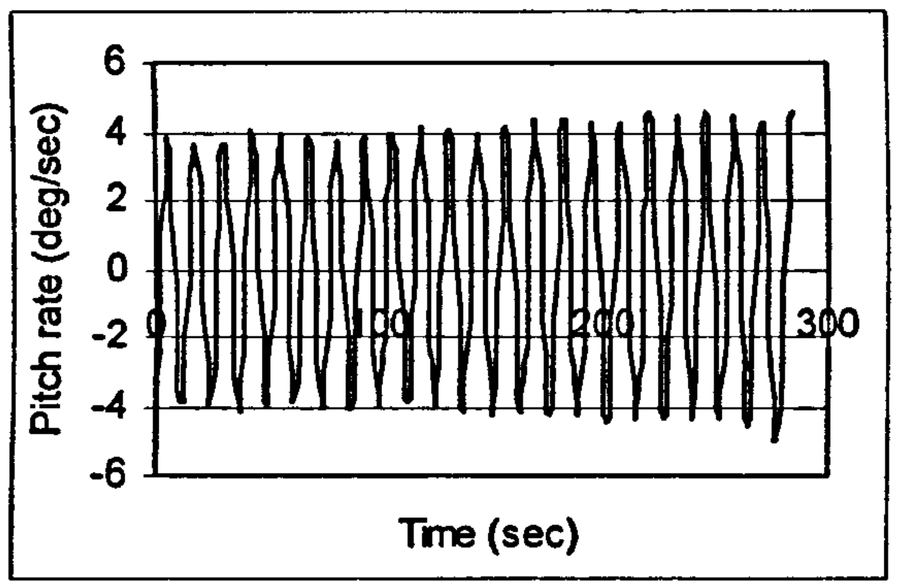

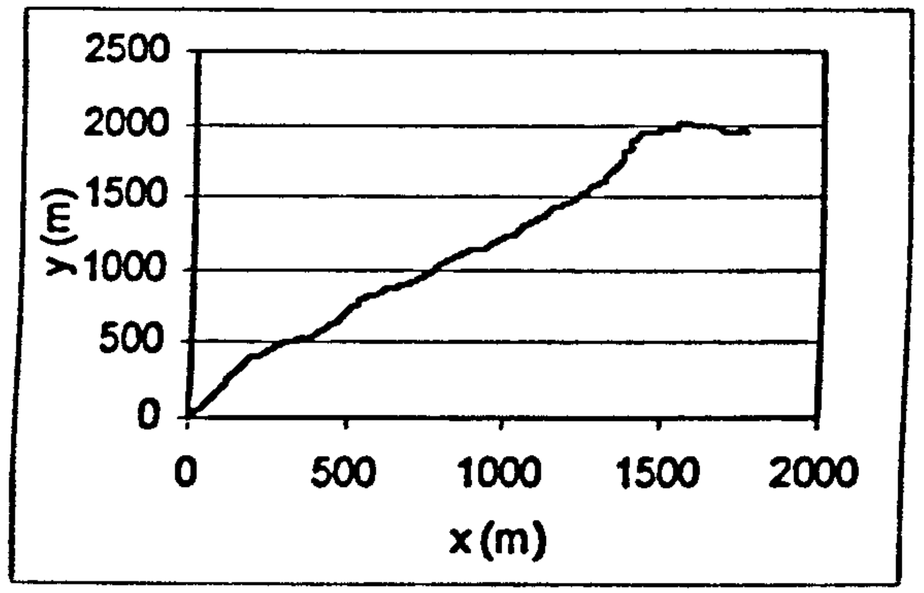

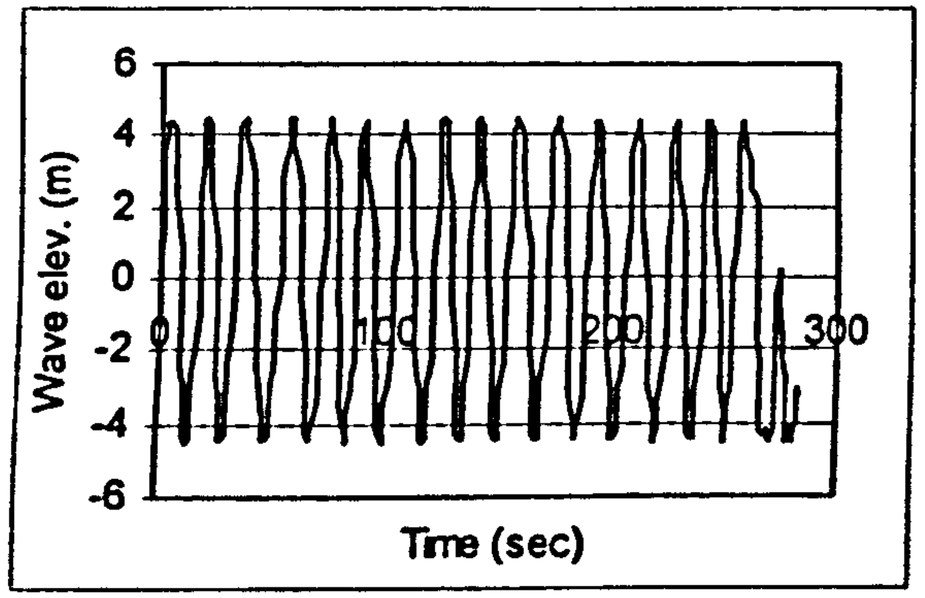

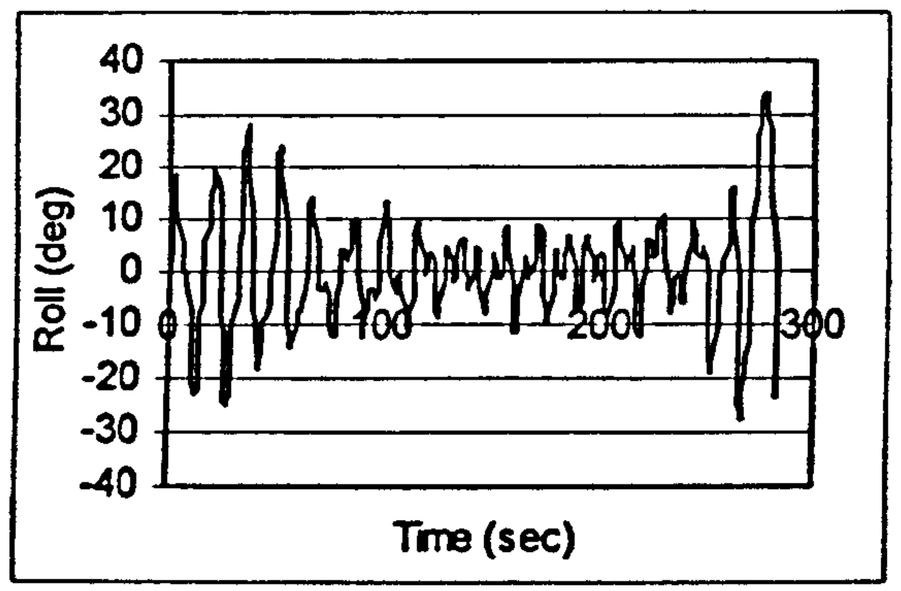

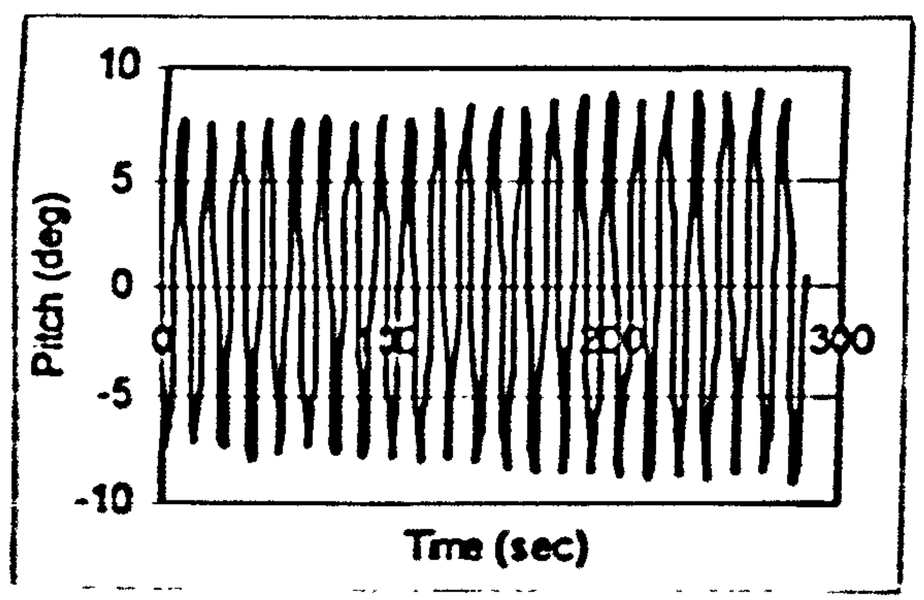

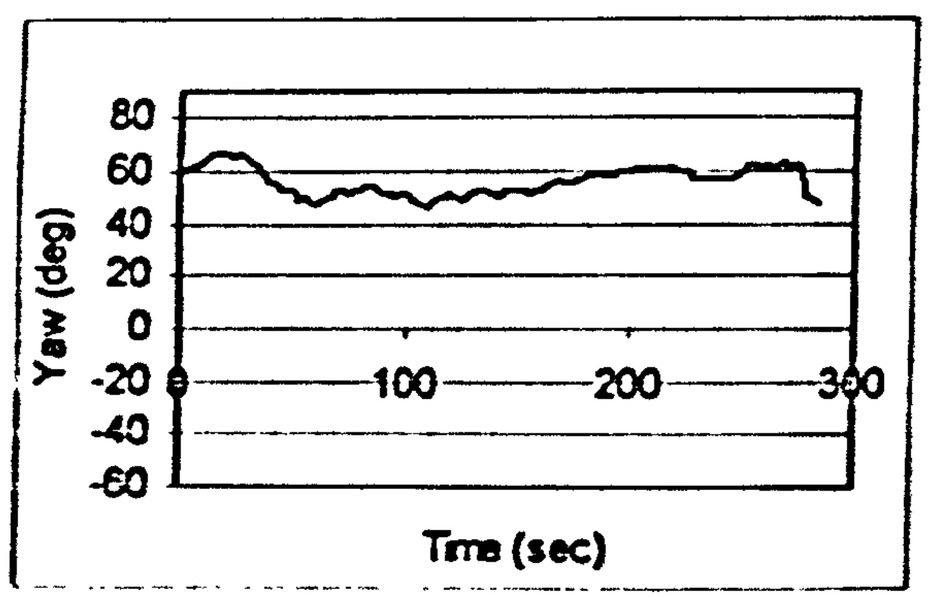

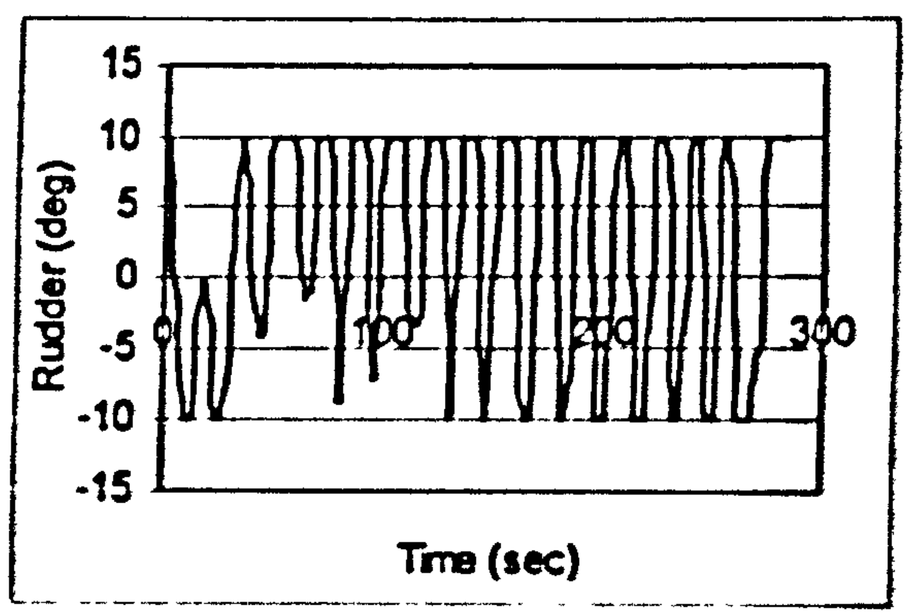

H. BENCHMARK STUDY OF ITTC VESSEL

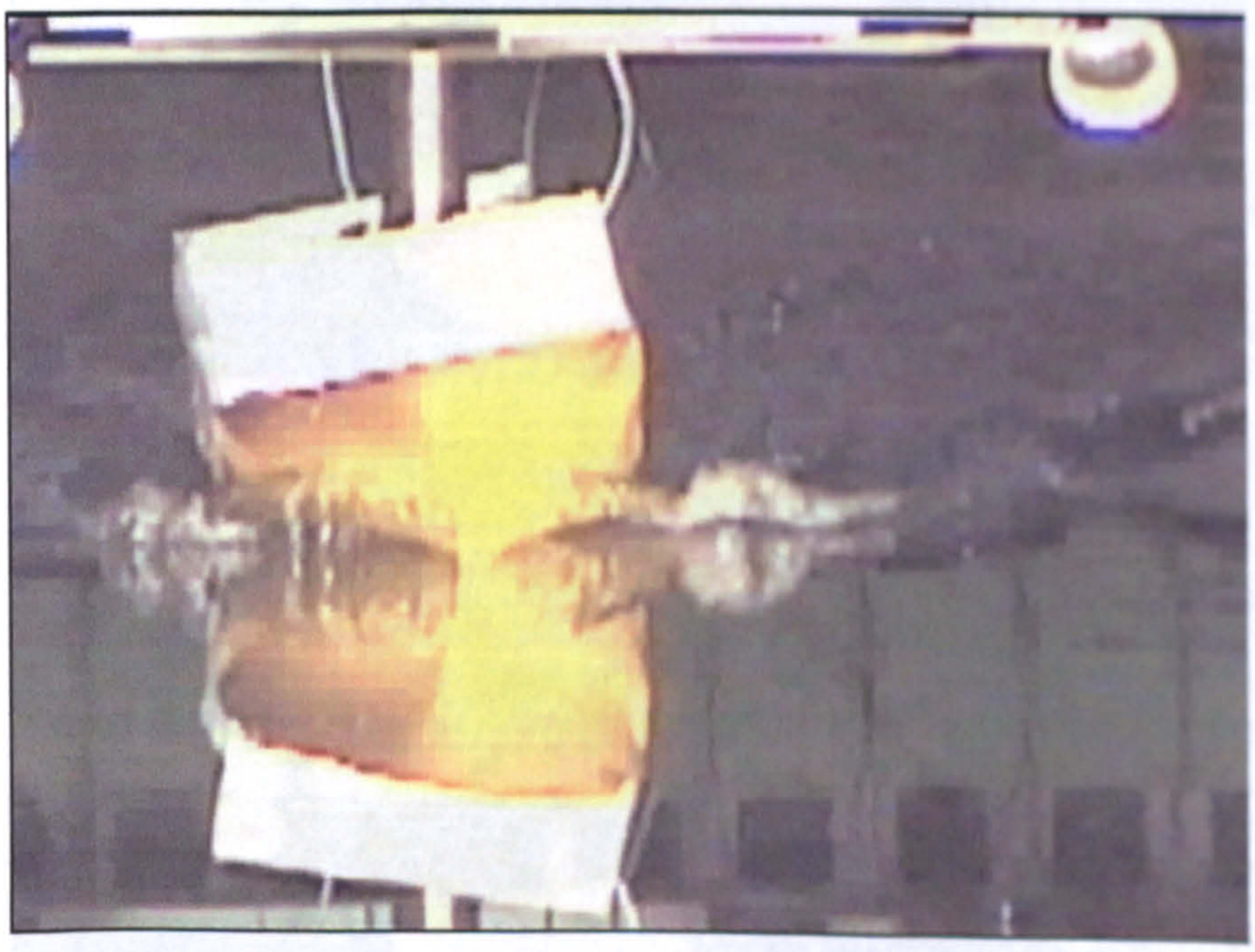

Figure H.1 Resistance test at Fn=0.3,ψ=0°, ϕ=10°, θ=0°,and sinkage=0

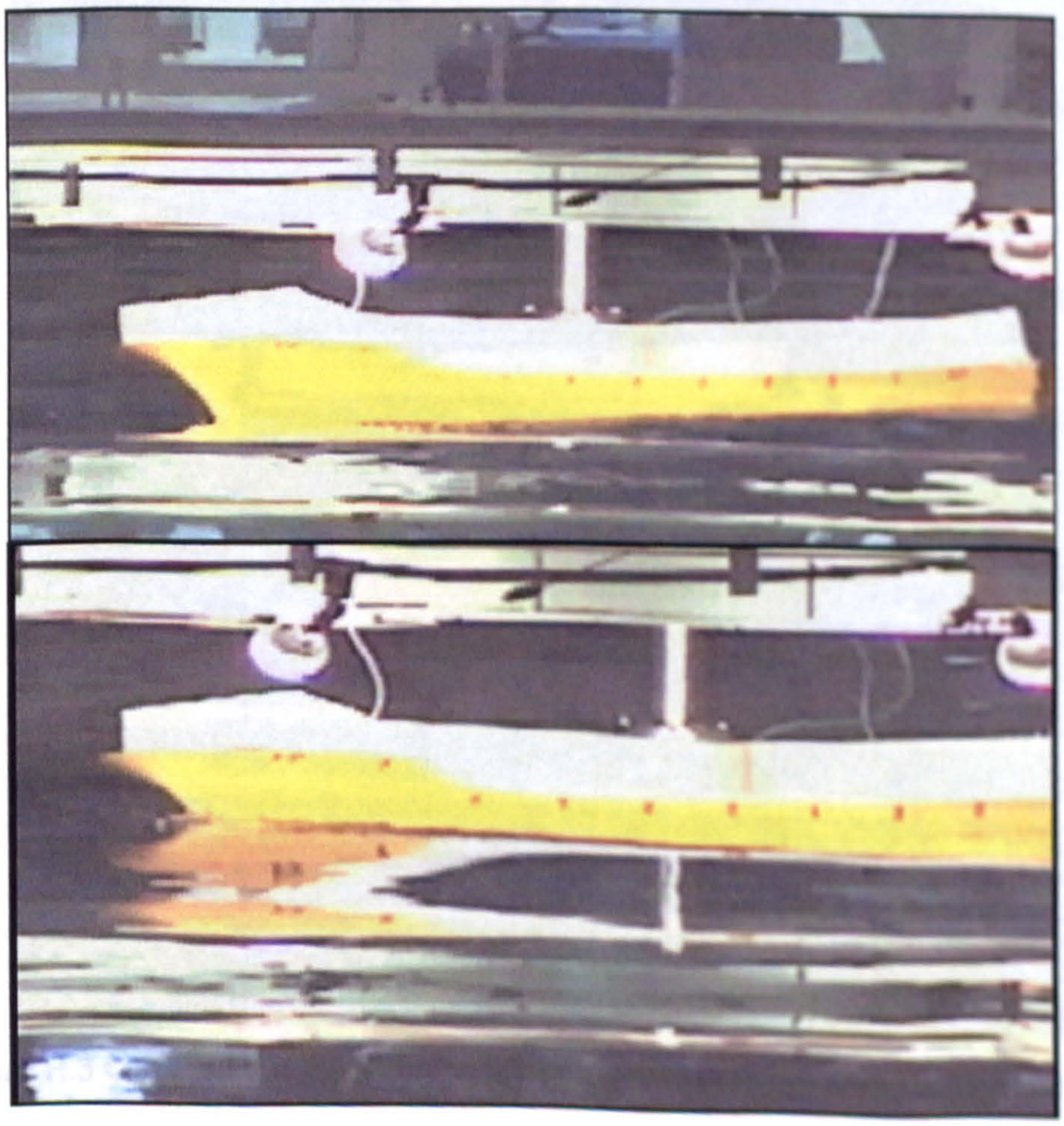

Figure H.2 Captive test at Fn=0.3,ψ=45°, ϕ=10°, θ=0°,and sinkage=0.2m

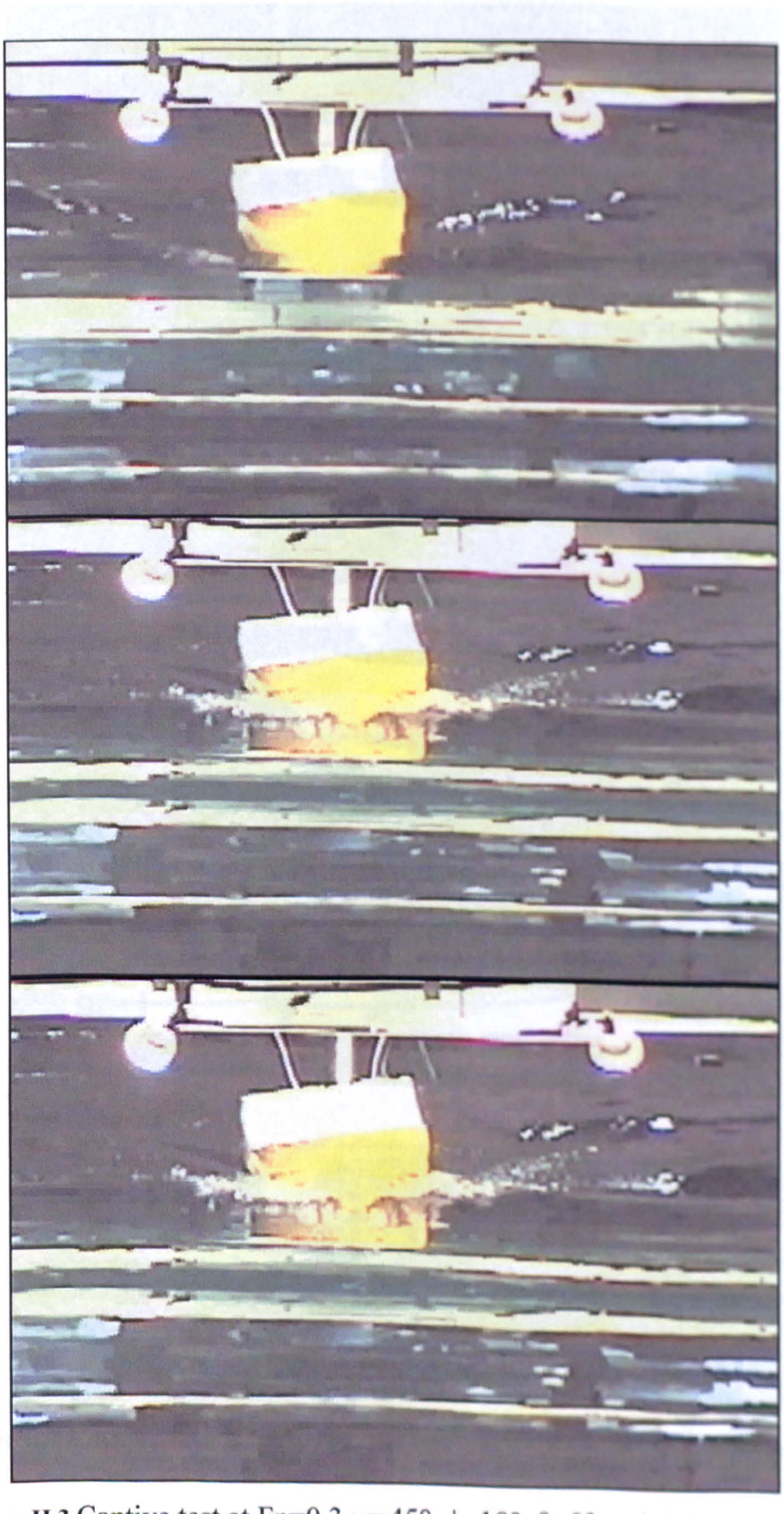

Figure H.3 Captive test at Fn=0.3,ψ=45°, ϕ=10°, θ=0°,and sinkage=-0.2m

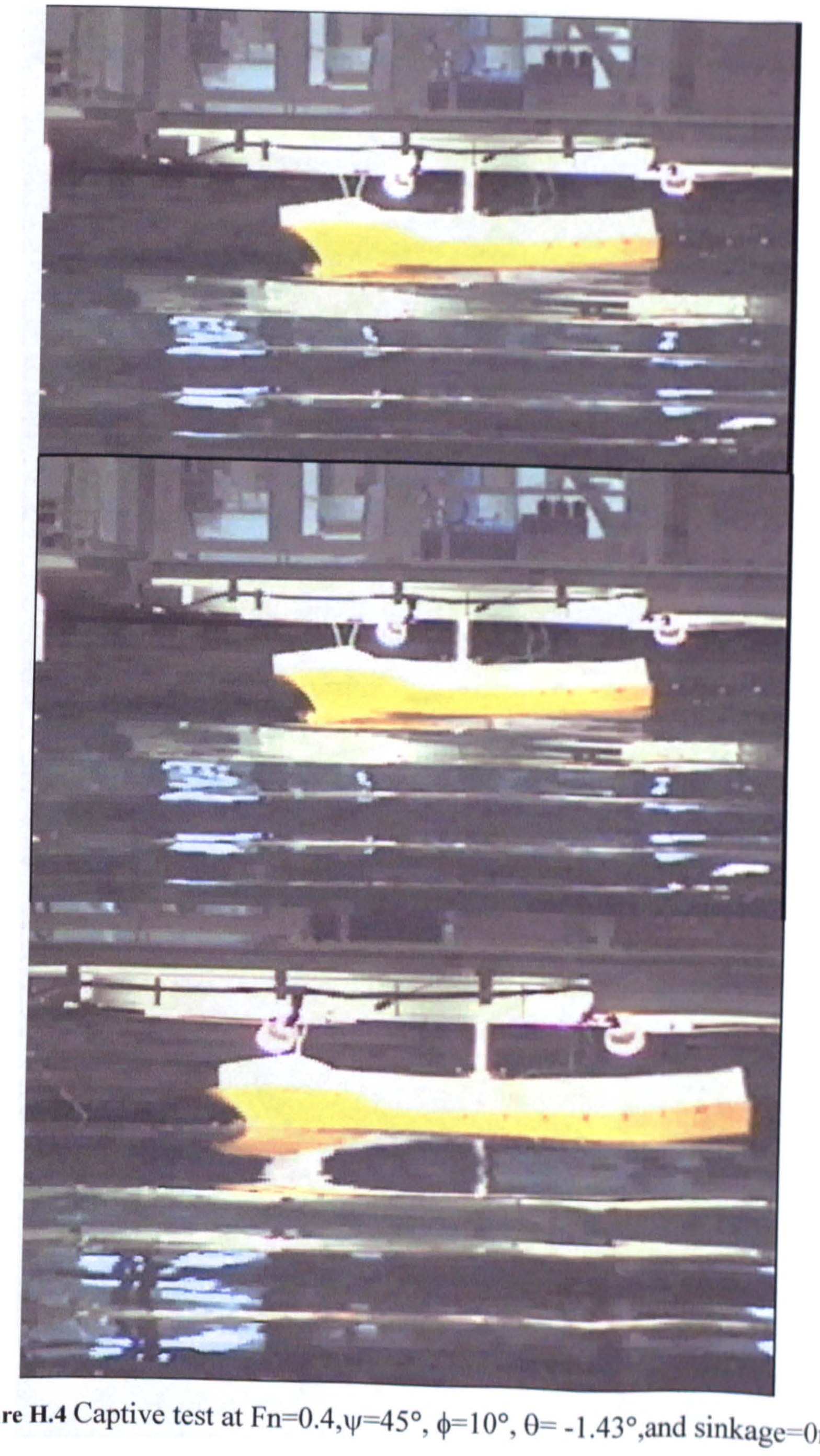

Figure H.4 Captive test at Fn=0.4,ψ=45°, ϕ=10°, θ= -1.43°,and sinkage=0m

Figure H.5 Free running test at Fn=0.4,ψ=0°,H_s=0.115, T_p=1.214 (ITTC)

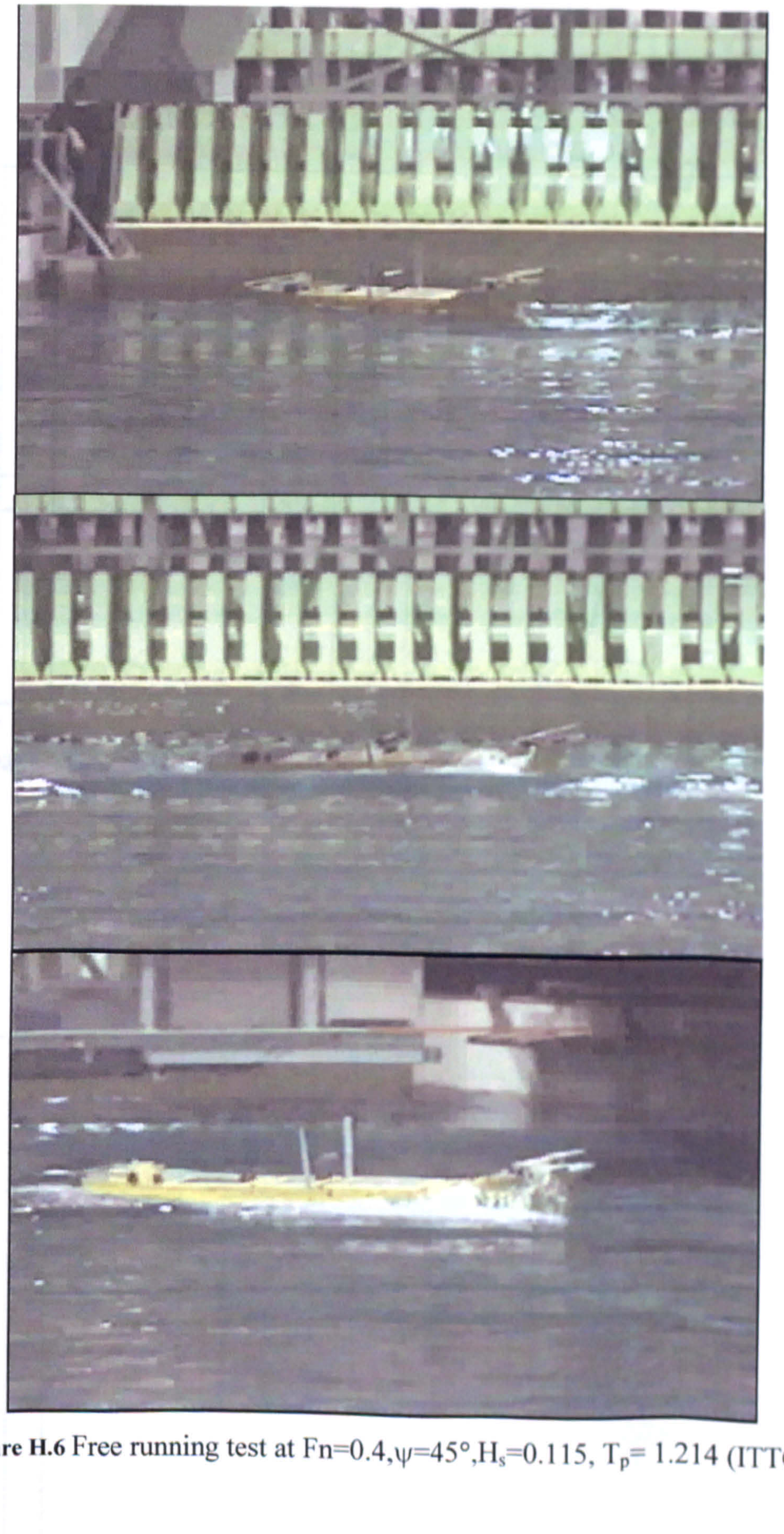

Figure H.6 Free running test at Fn=0.4,ψ=45°,H_s=0.115, T_p= 1.214 (ITTC)

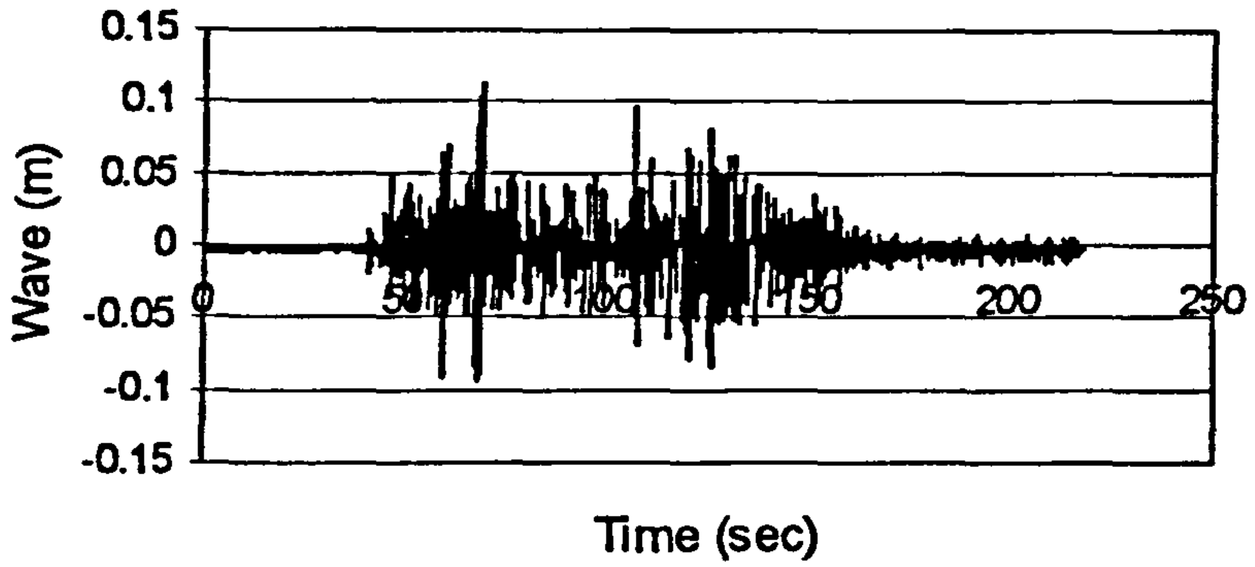

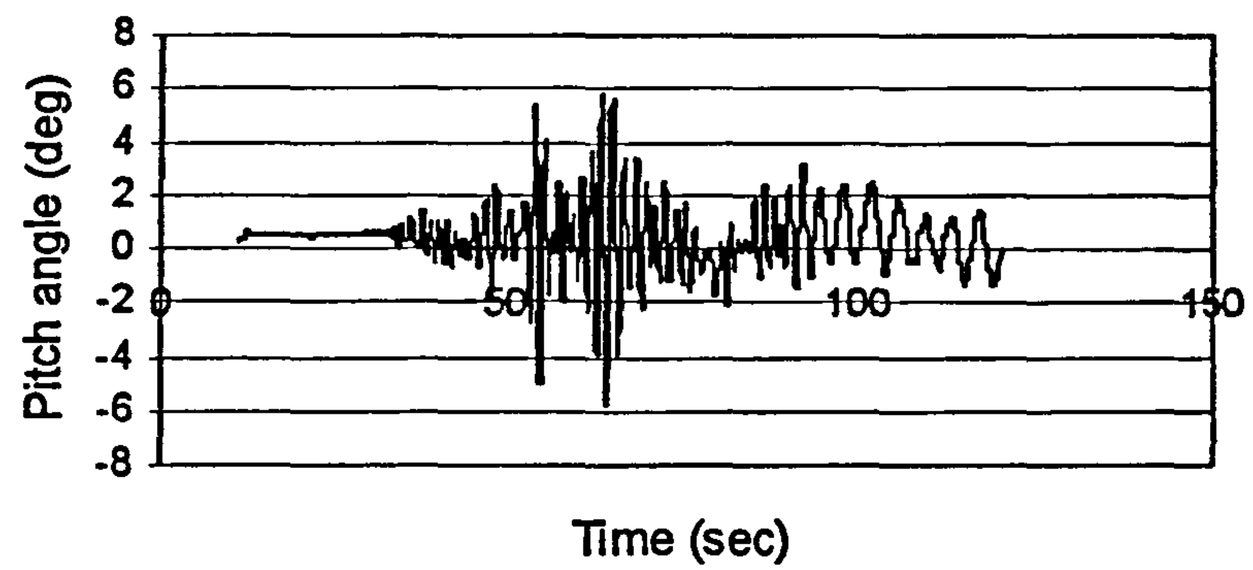

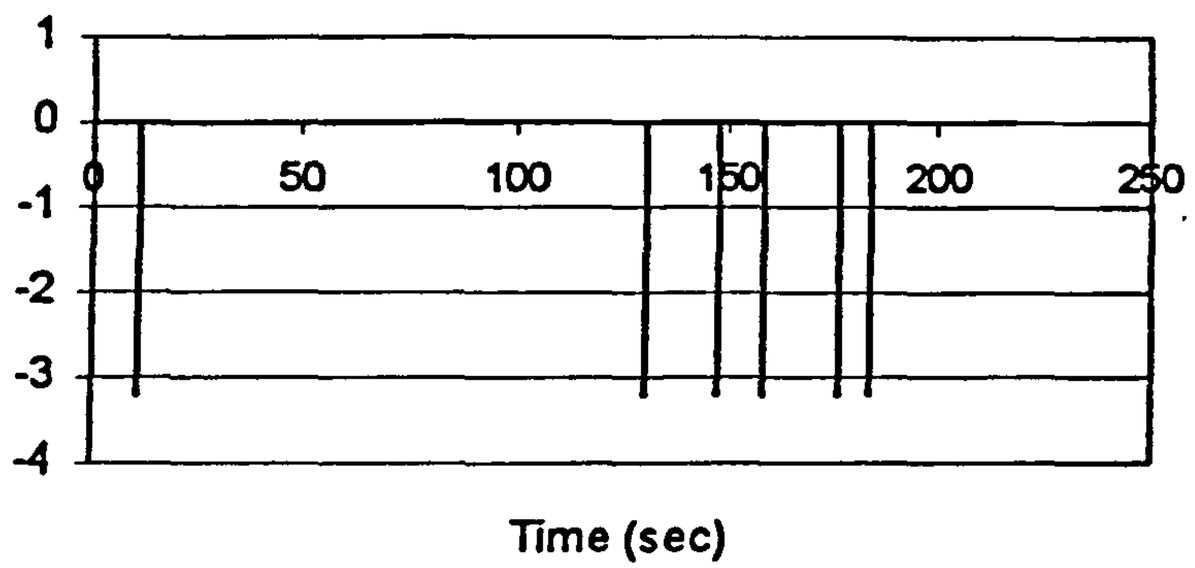

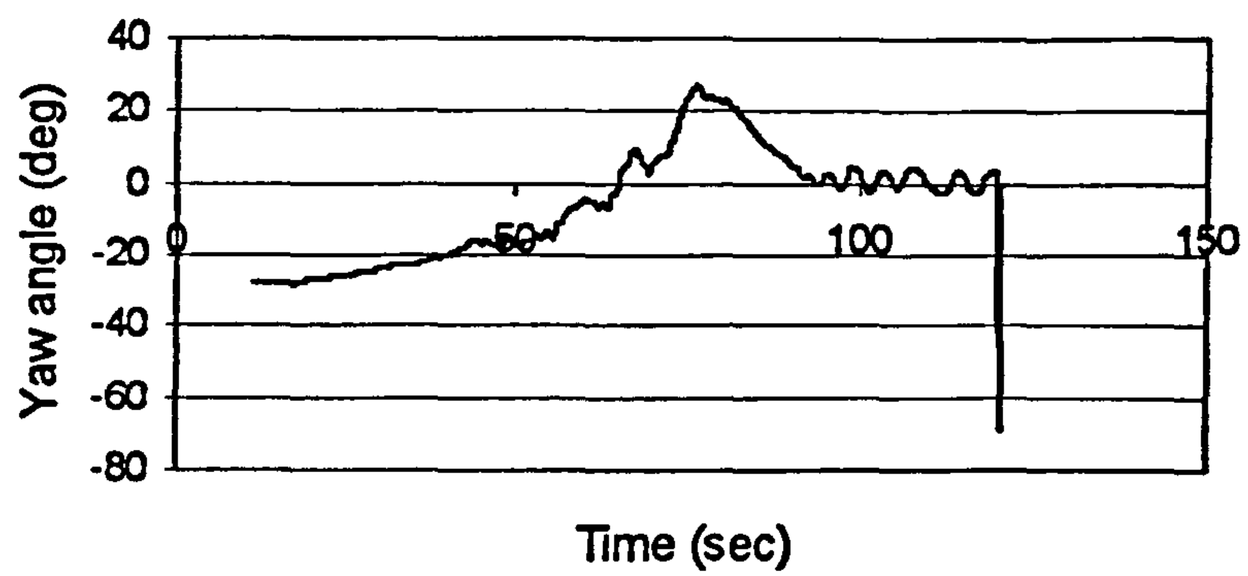

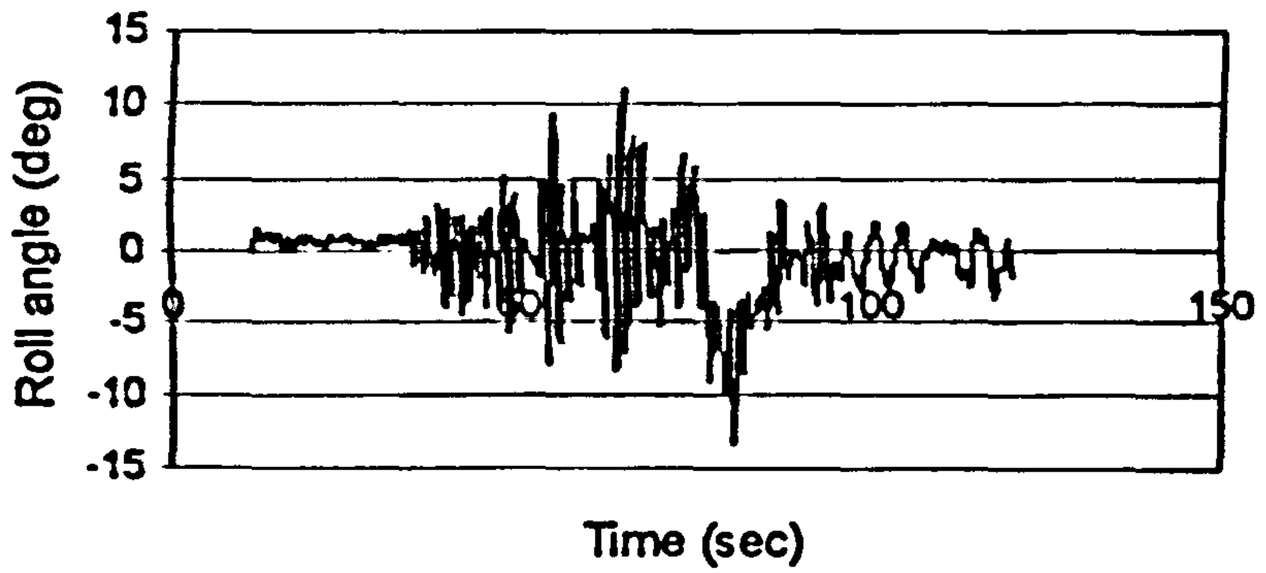

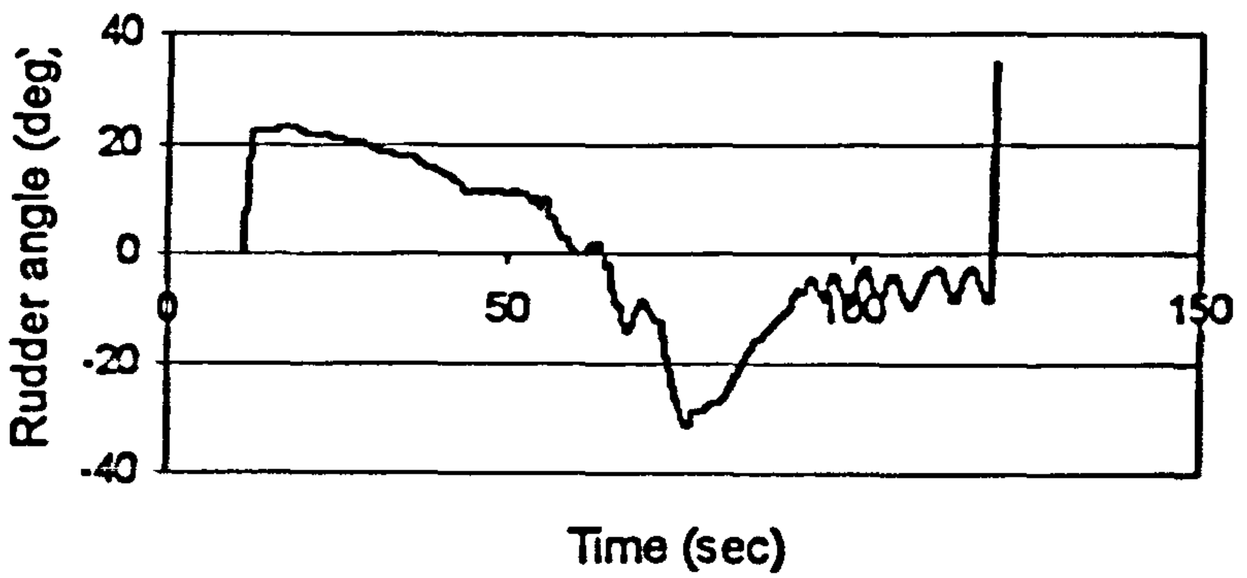

Figure H.7 ITTC, Fn=0.3, χ= -5°, H_s=0.115 m, T_p=1.214 sec.

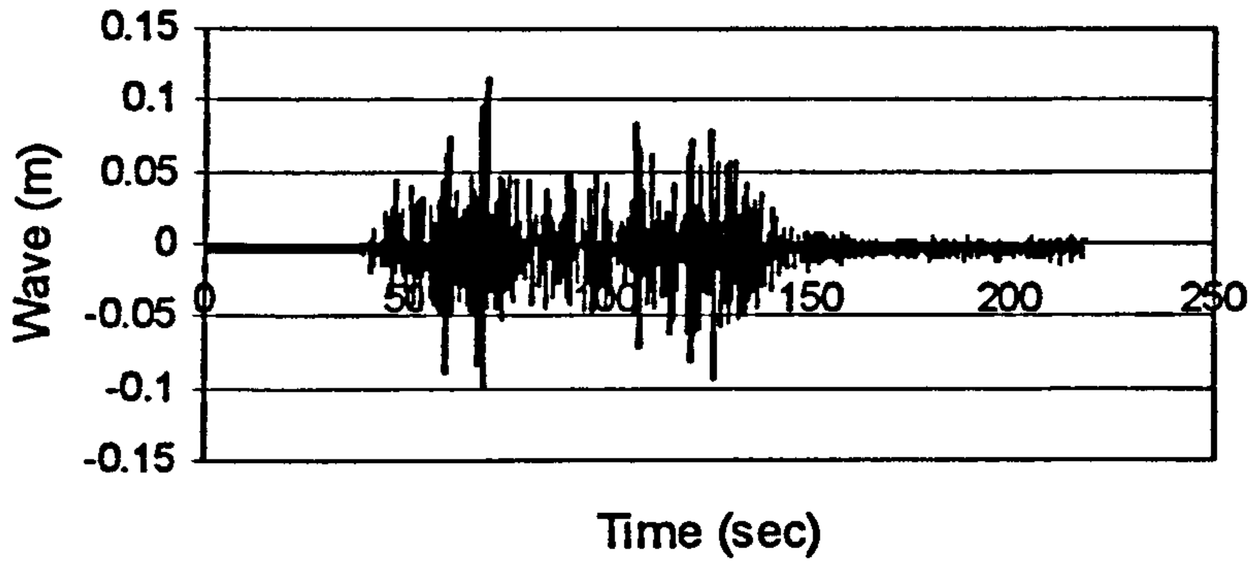

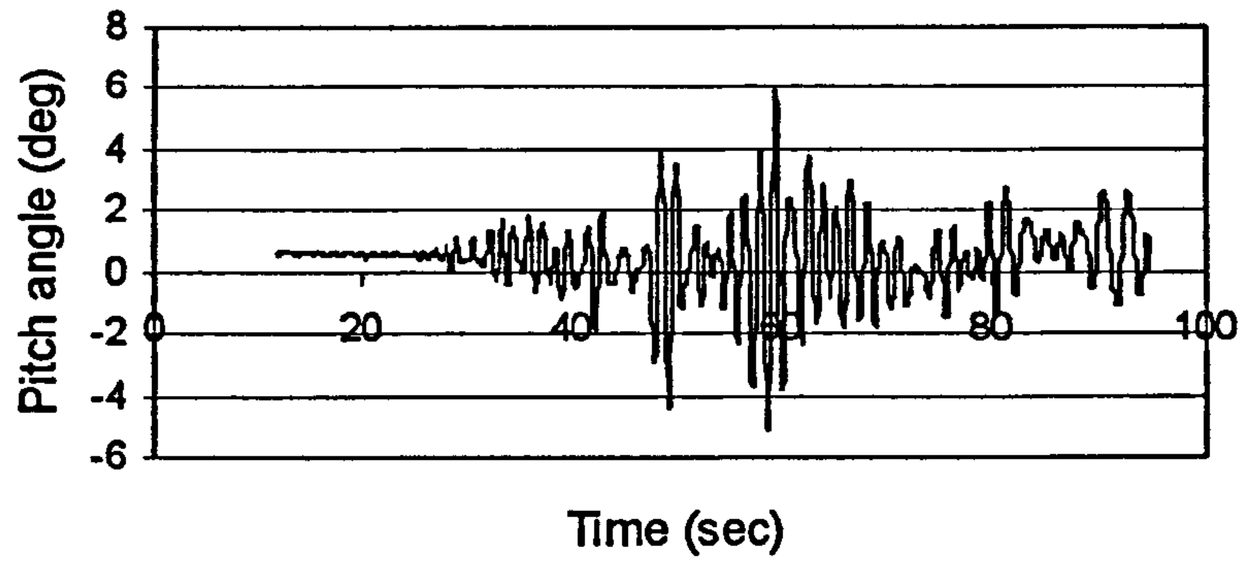

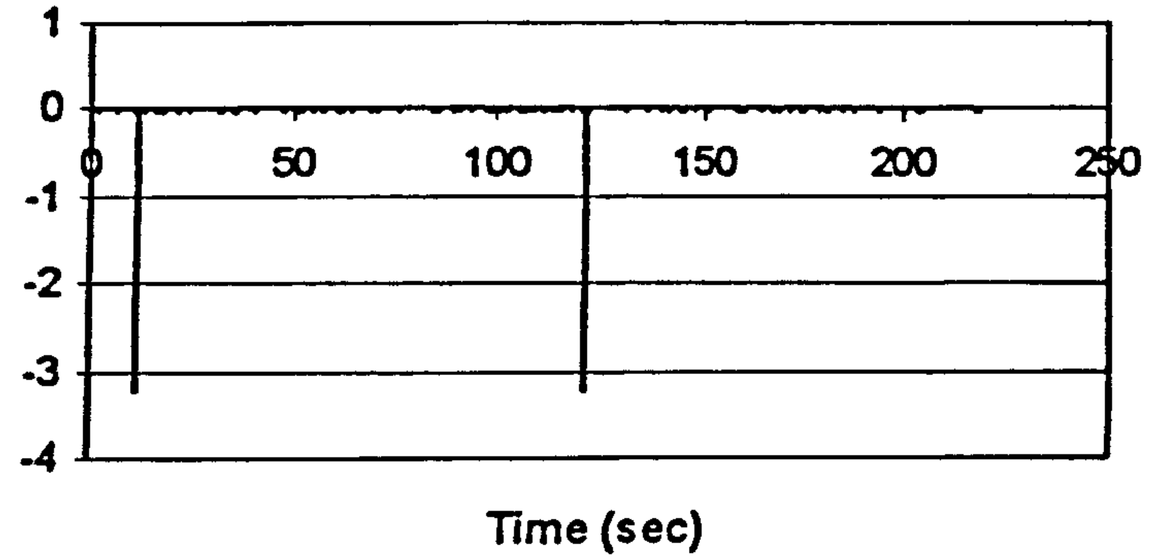

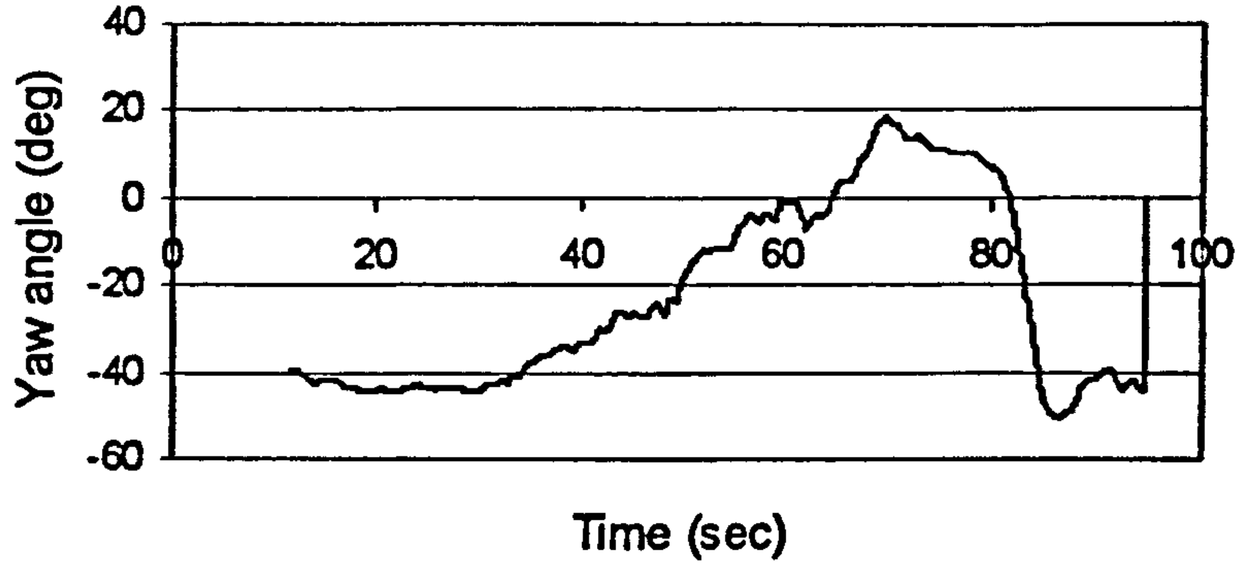

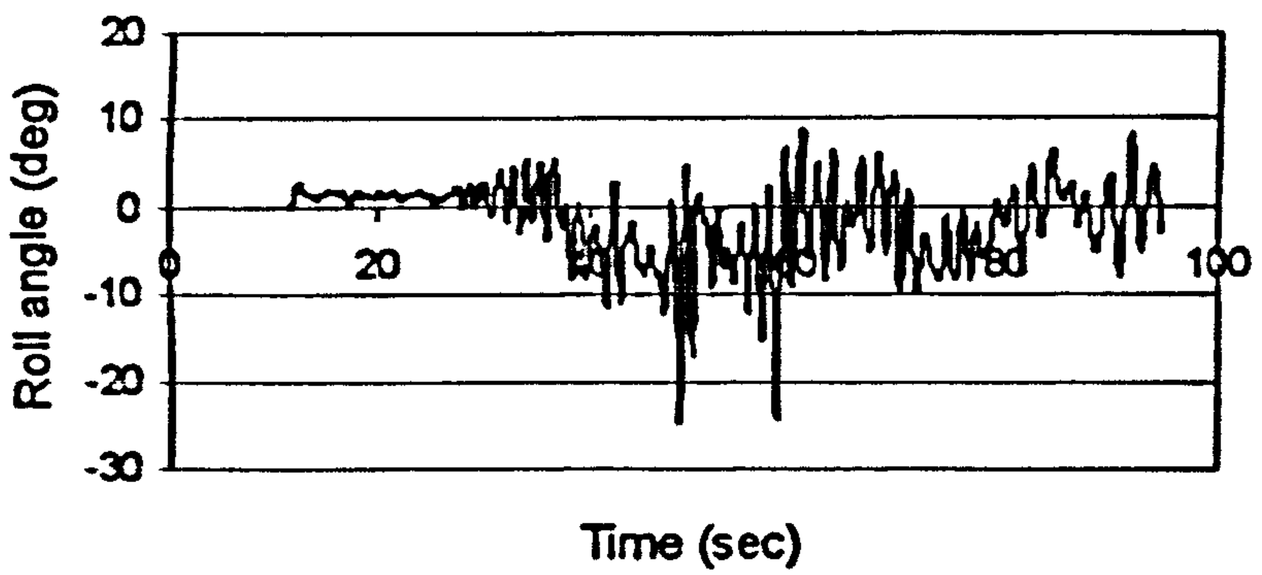

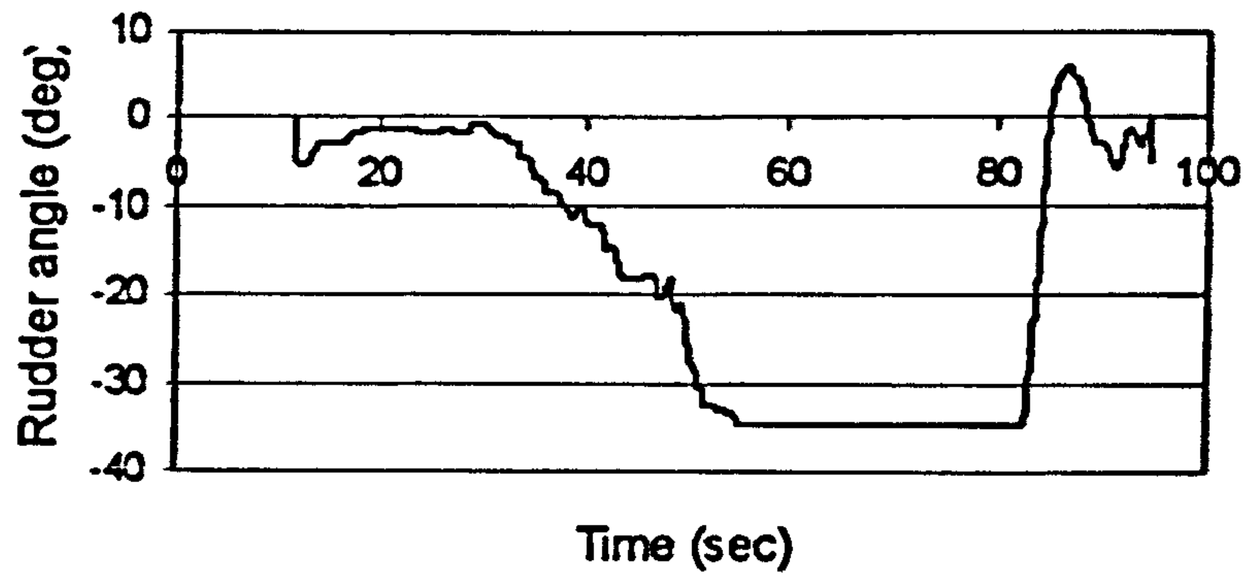

Figure H.8 ITTC, Fn=0.3, χ= -45°, H_s=0.115 m, T_p=1.214 sec.

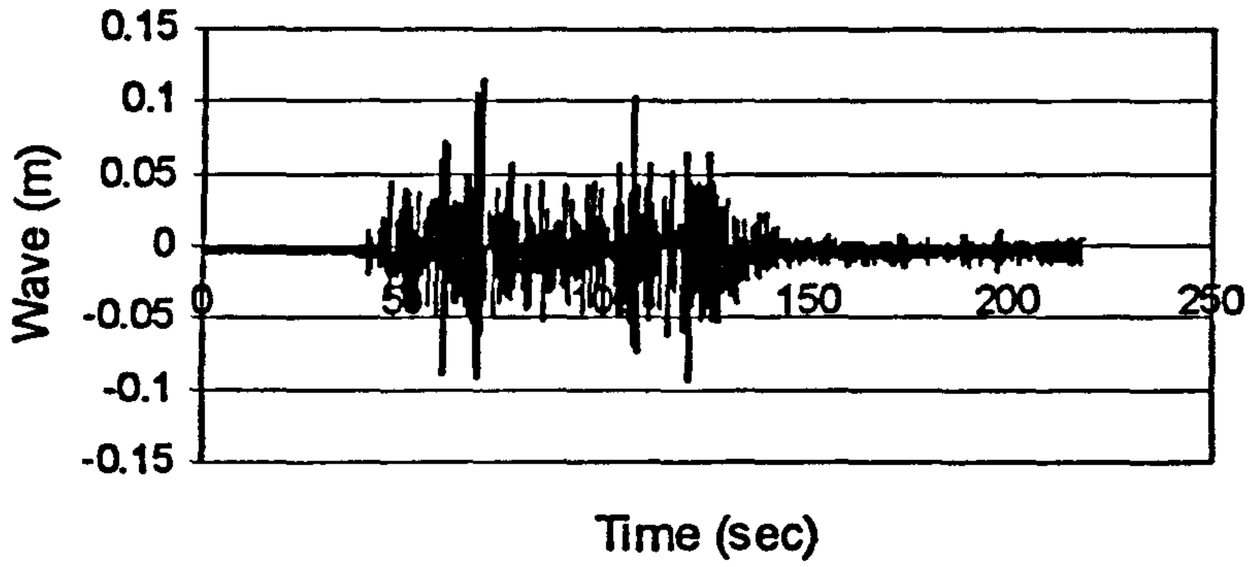

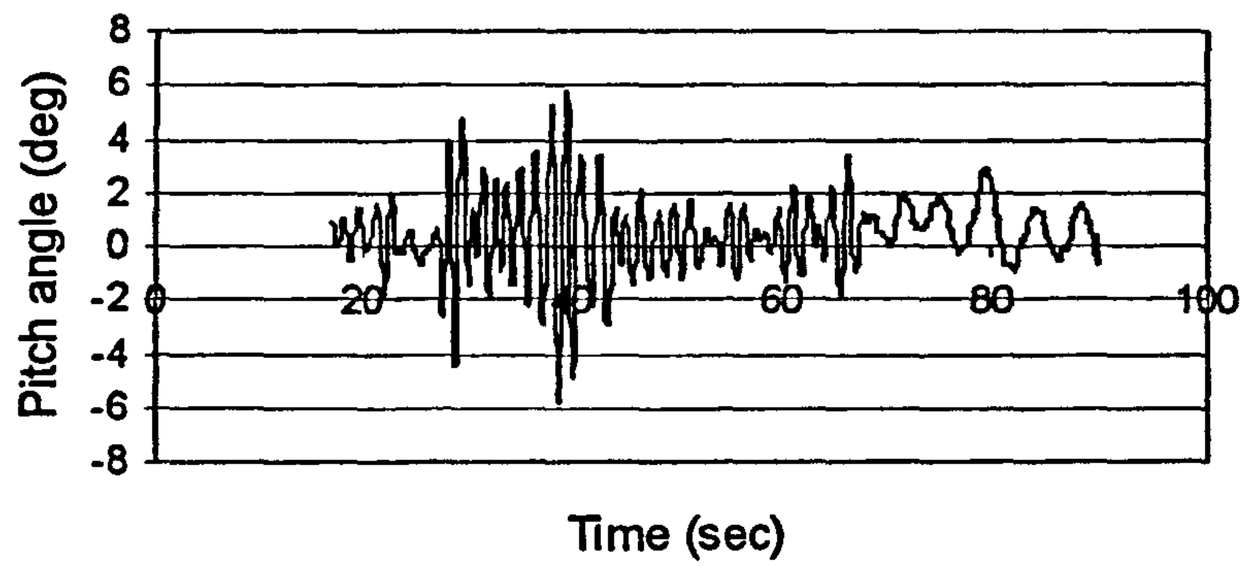

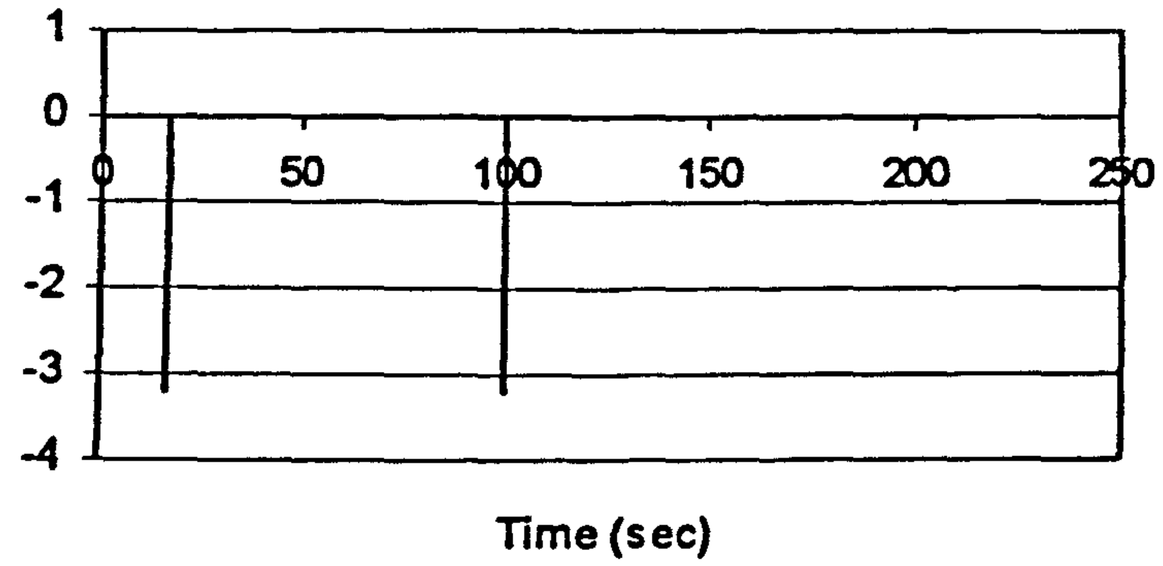

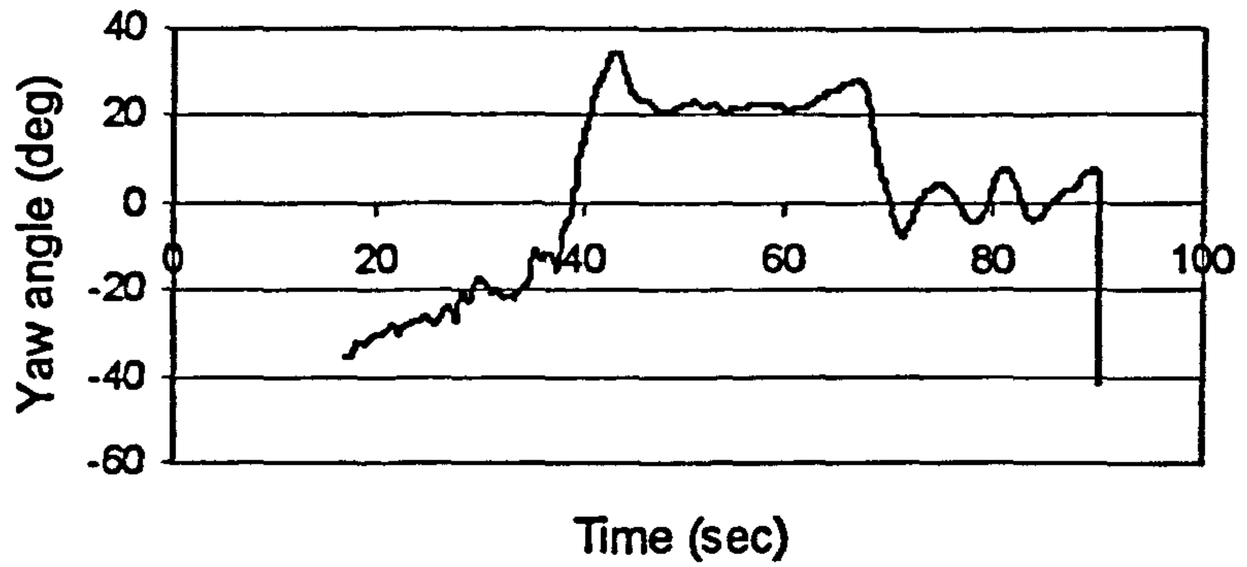

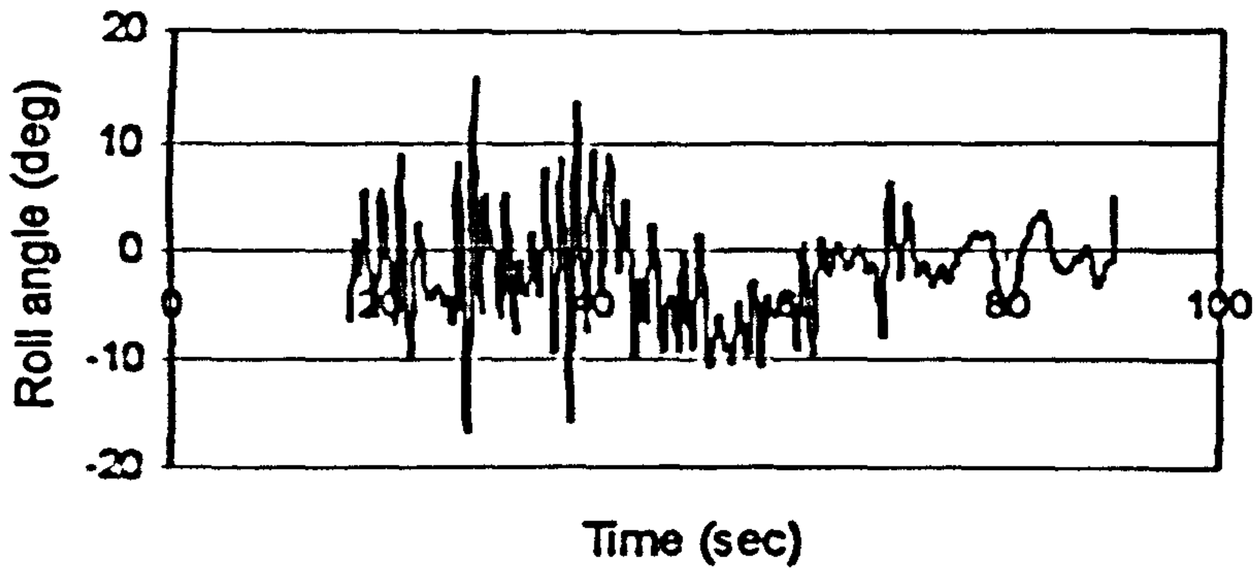

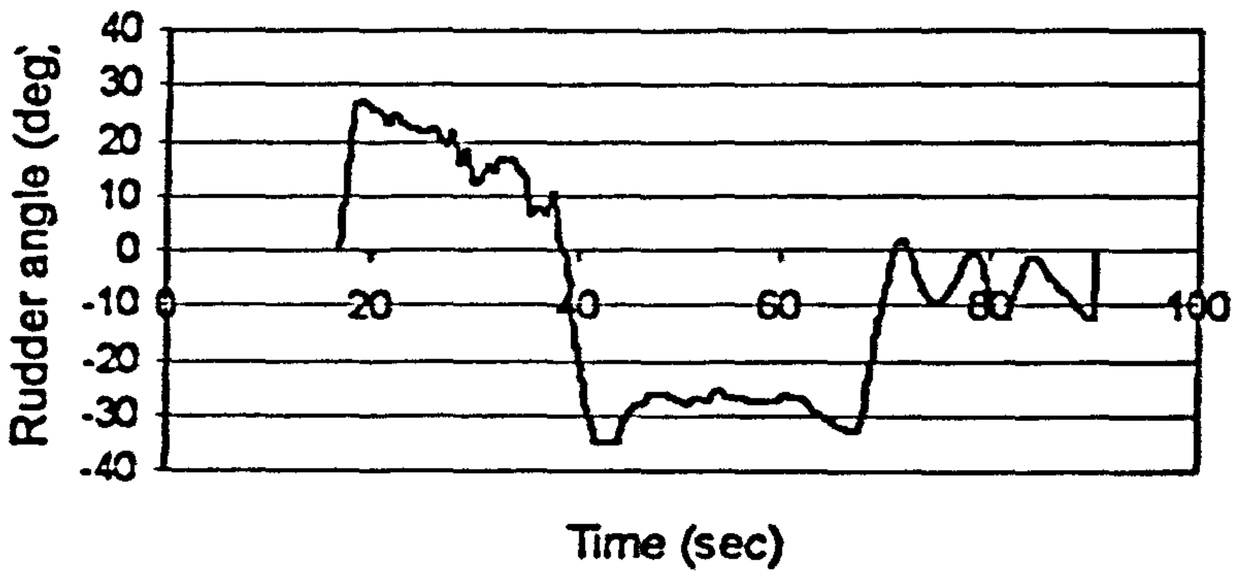

Figure H.9 ITTC, Fn=0.4, χ= -5°, H_s=0.115 m, T_p=1.214 sec.

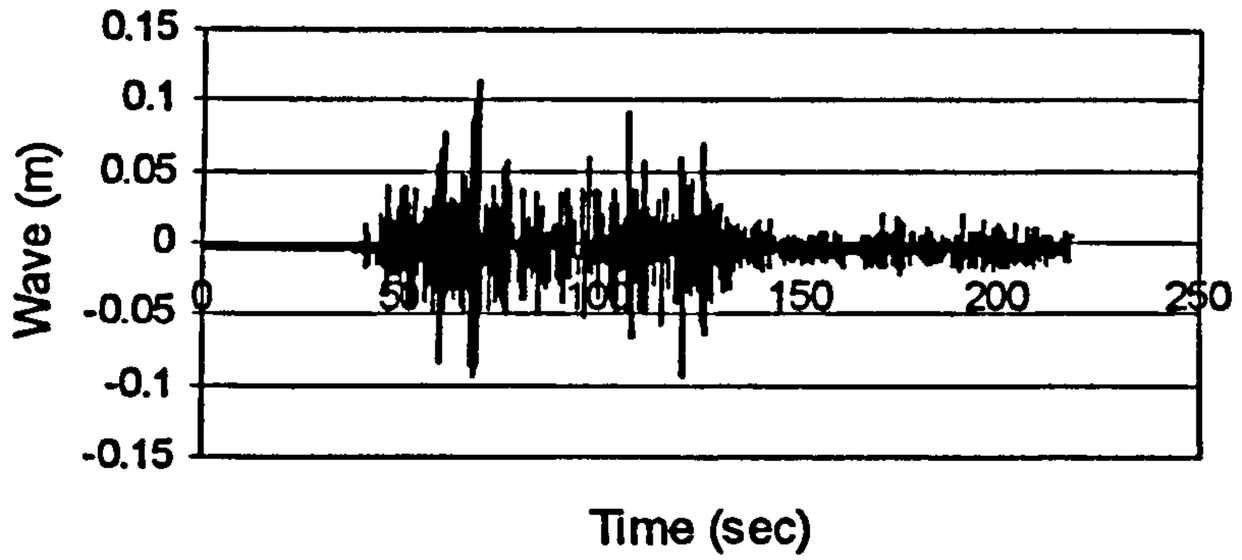

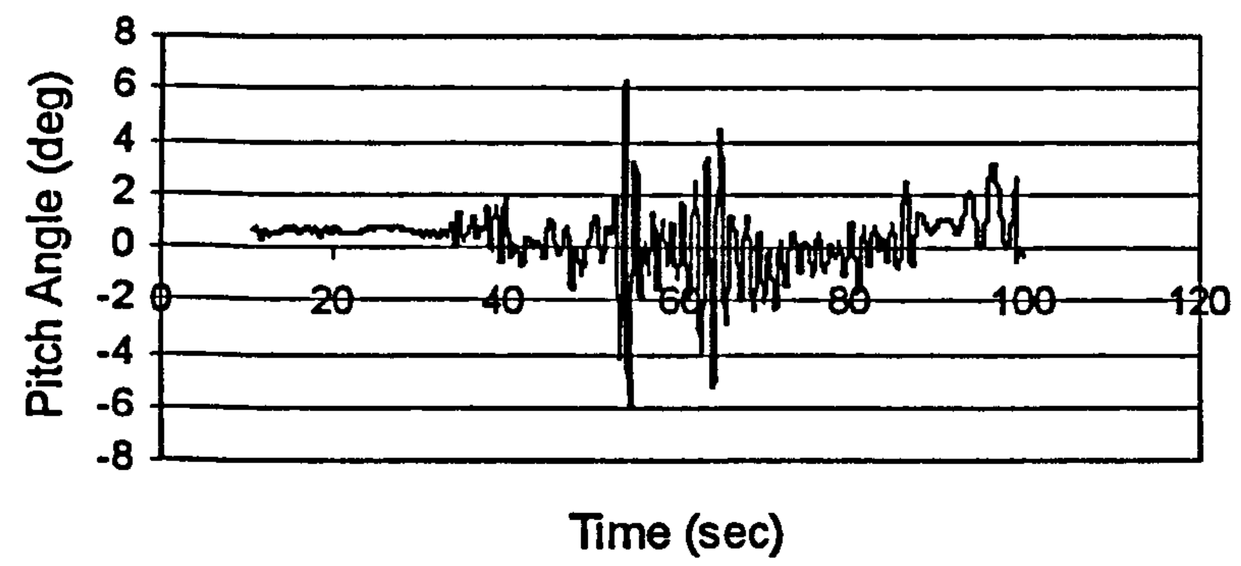

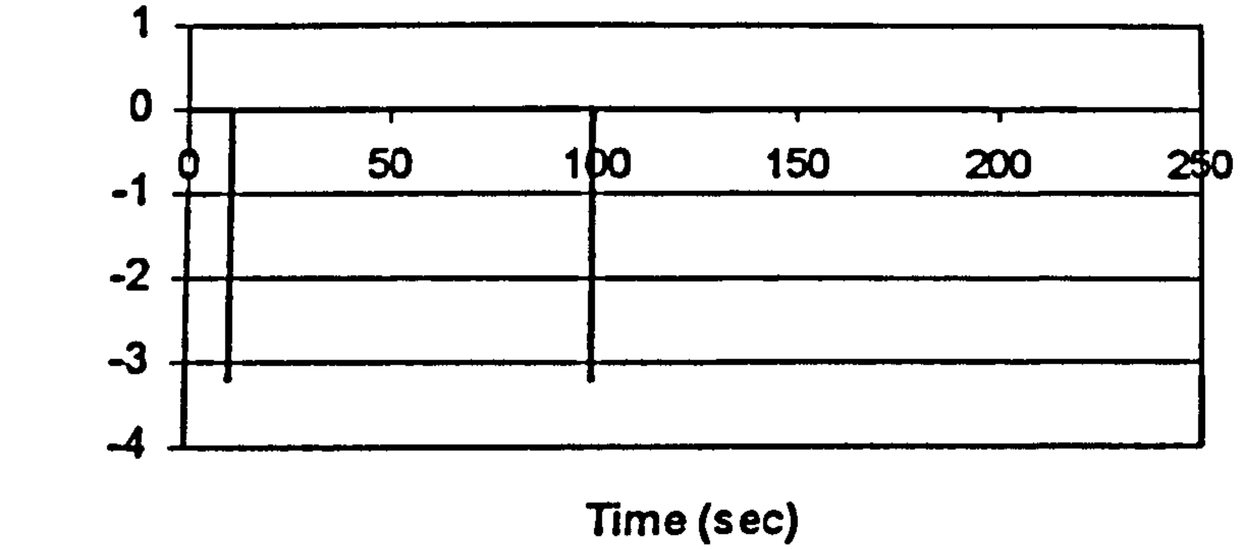

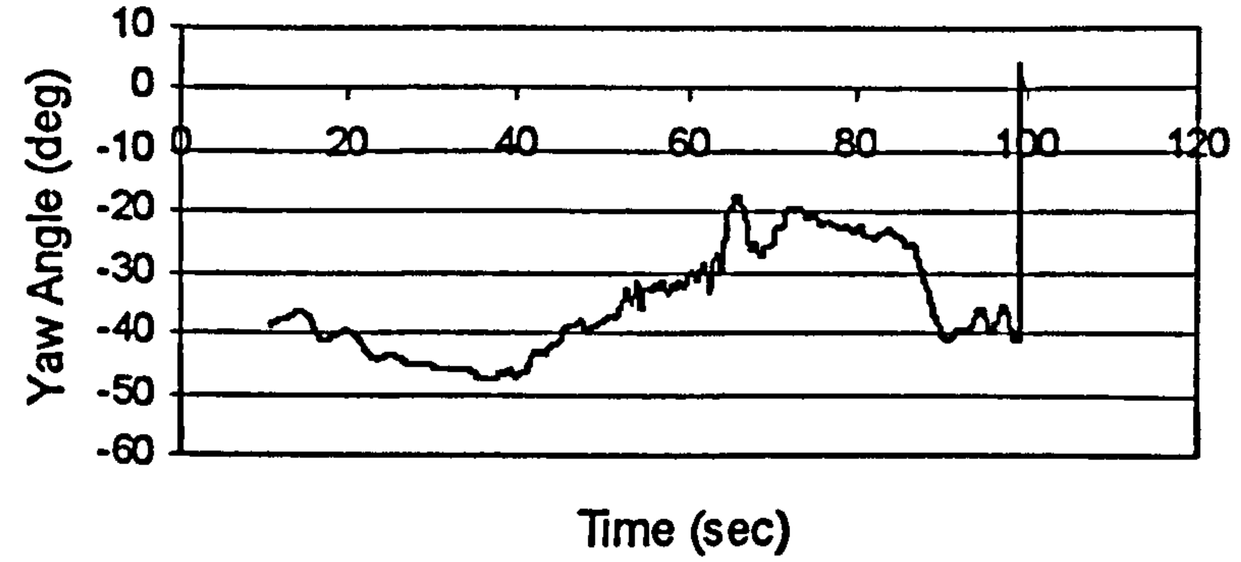

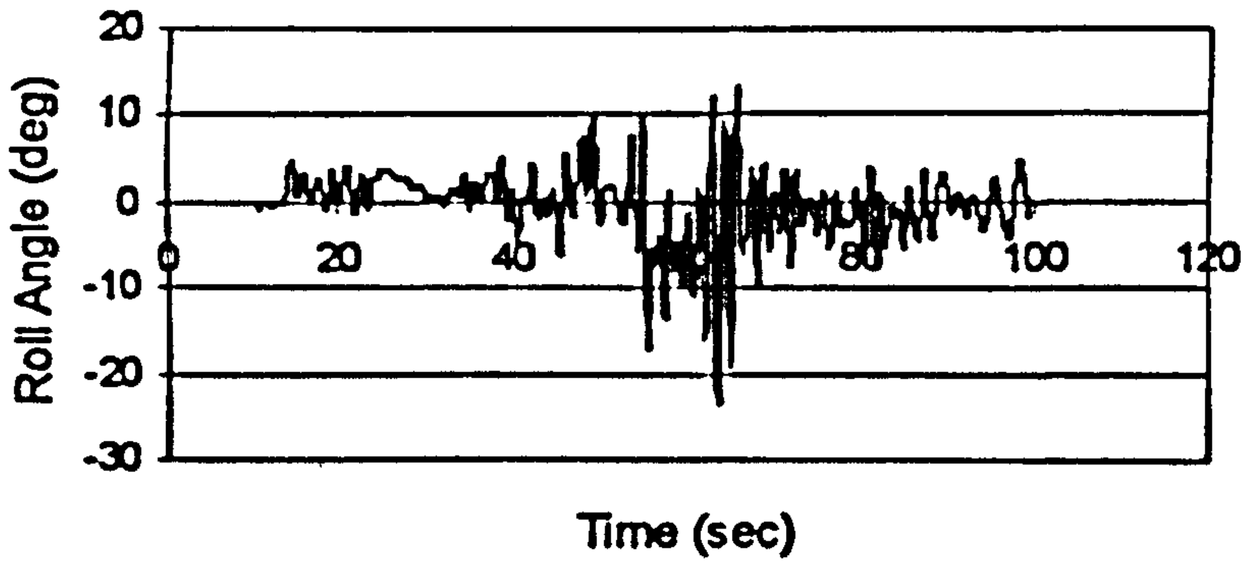

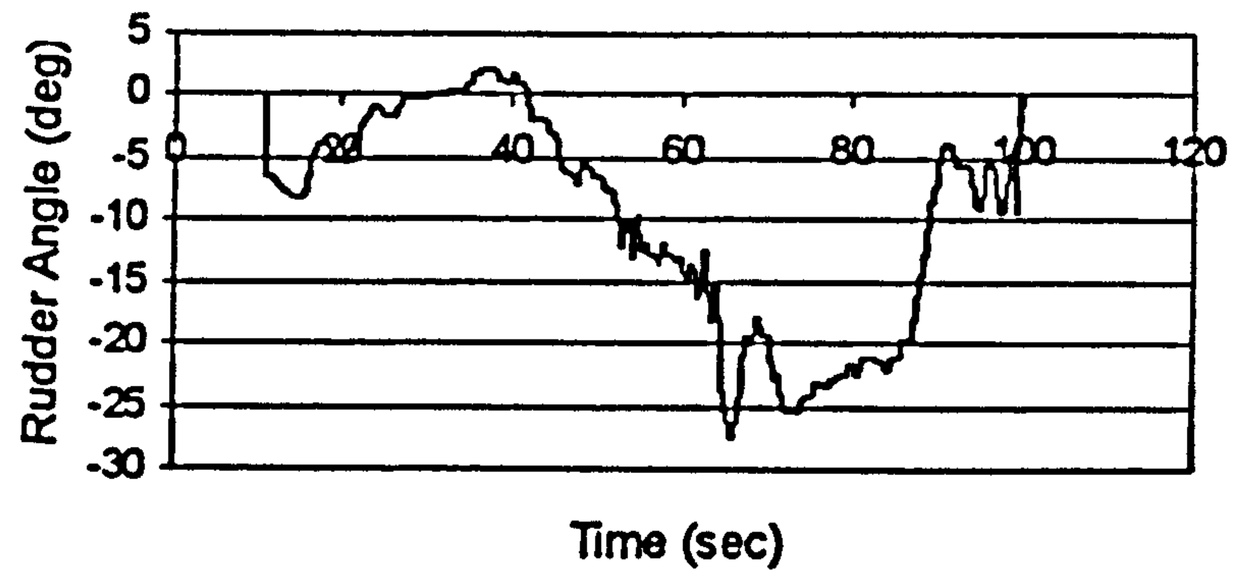

Figure H.10 ITTC, Fn=0.4, χ= -45°, H_s=0.115 m, T_p=1.214 sec.

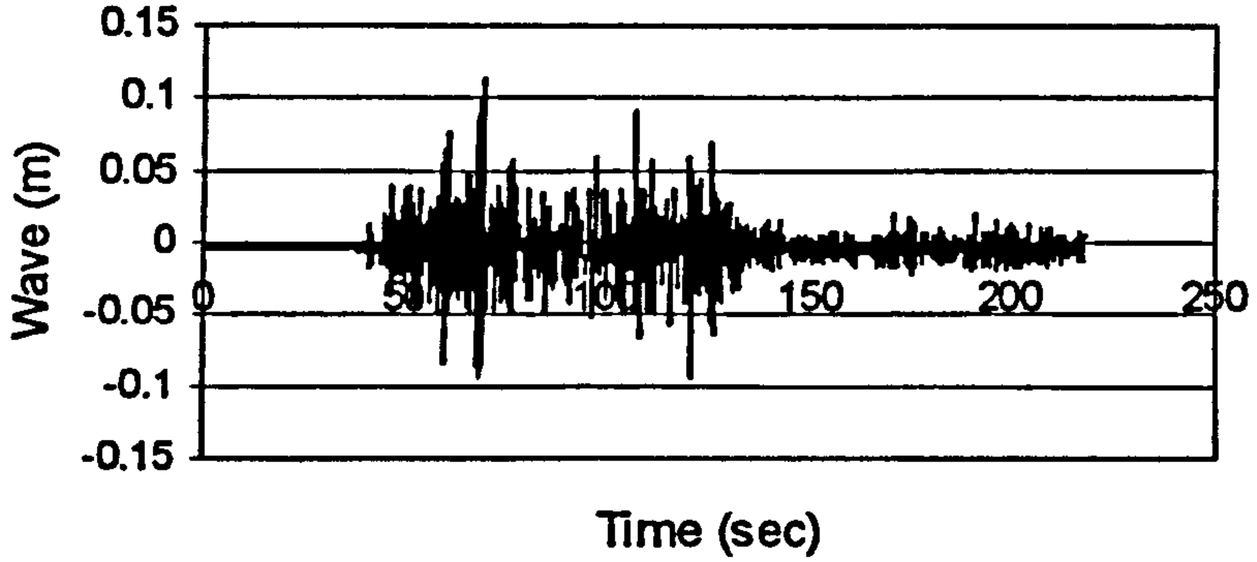

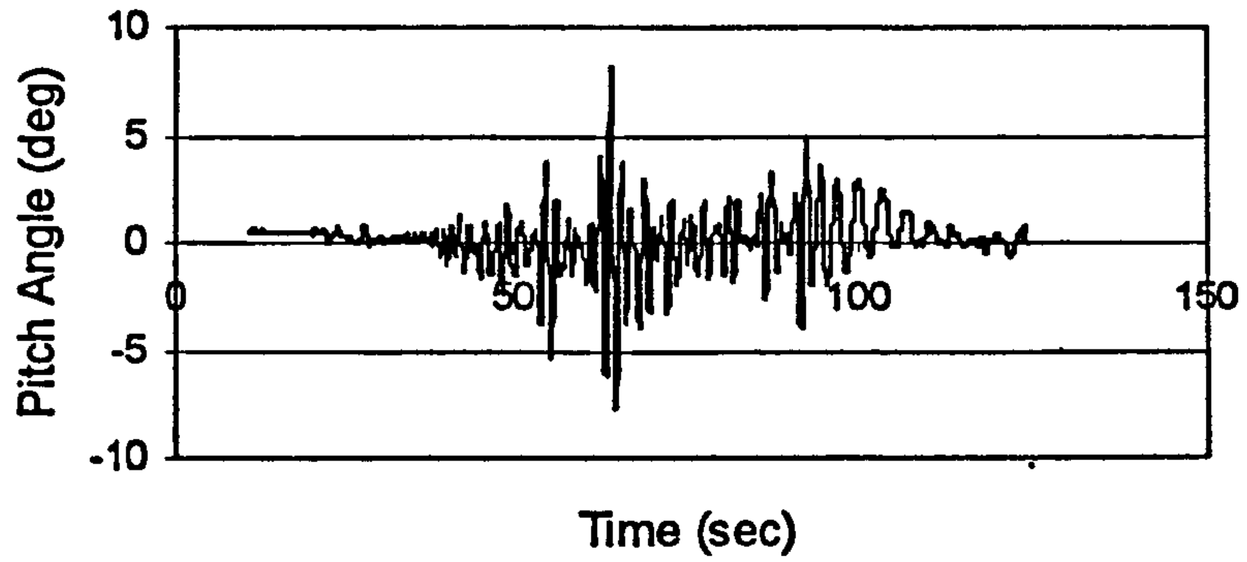

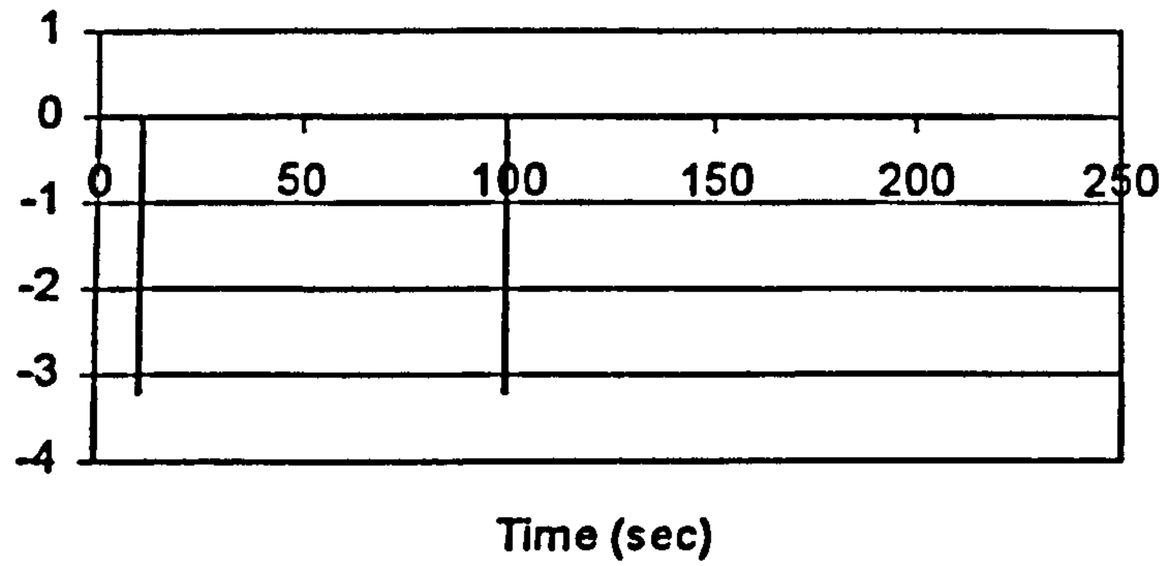

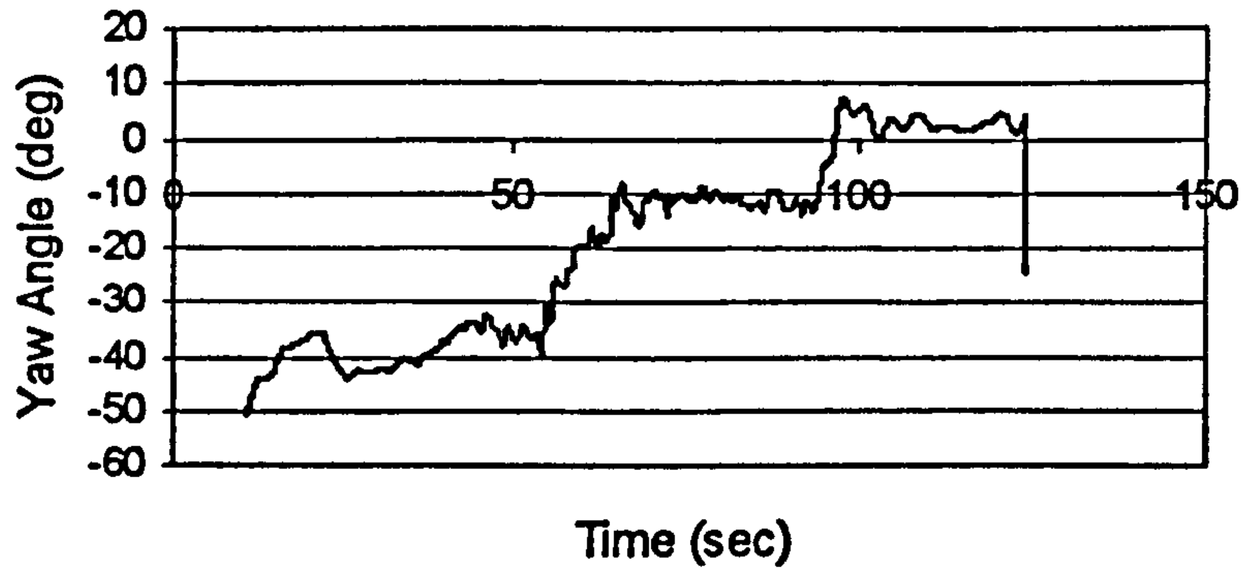

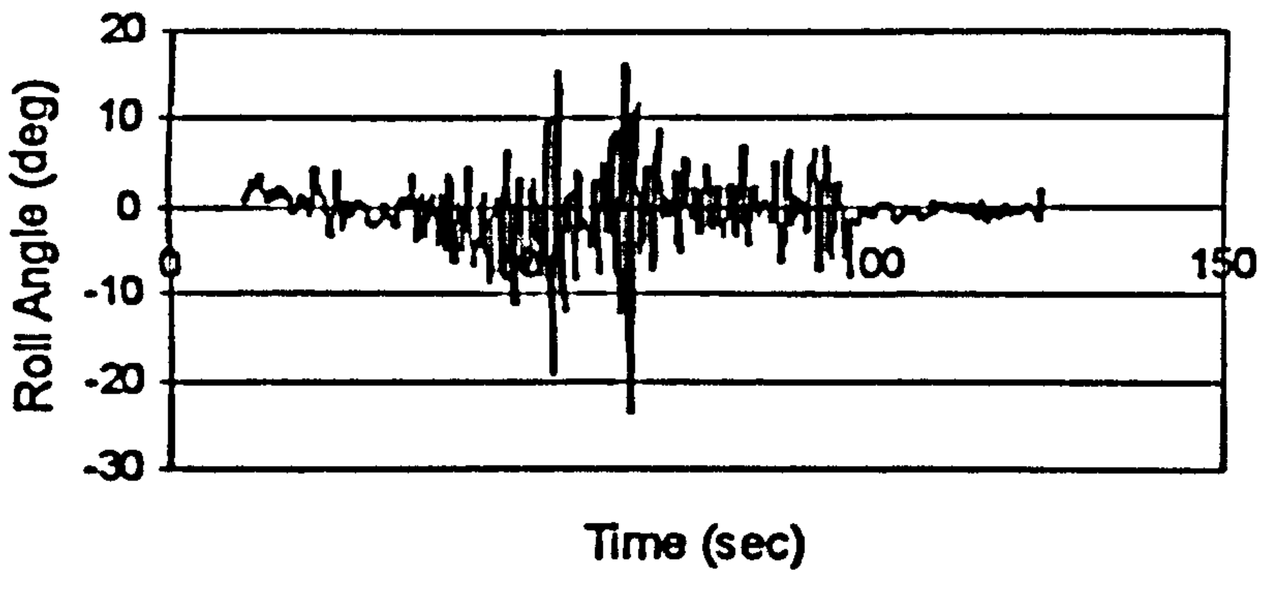

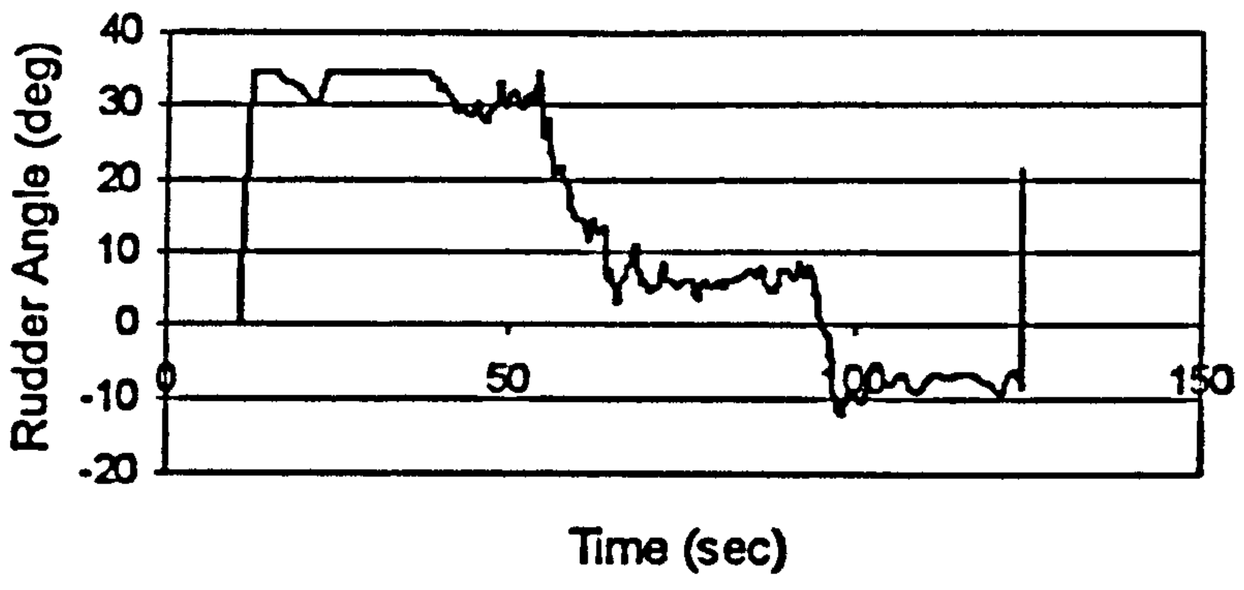

Figure H.11 ITTC, Fn=0.3, χ= -5°, H_s=0.1725 m, T_p=1.487 sec.

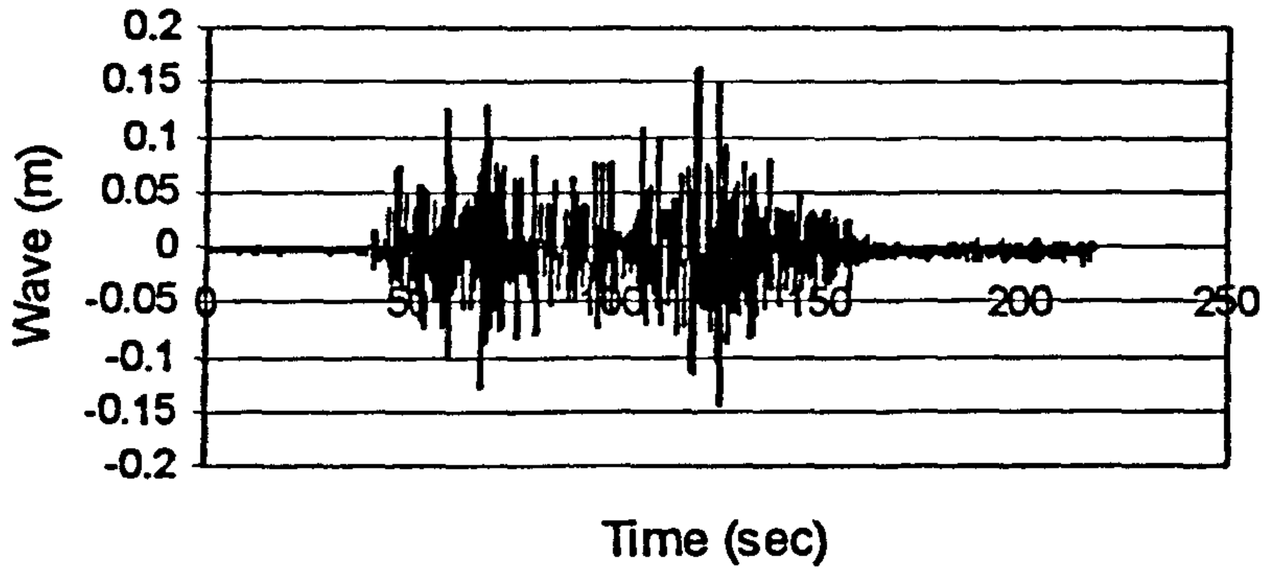

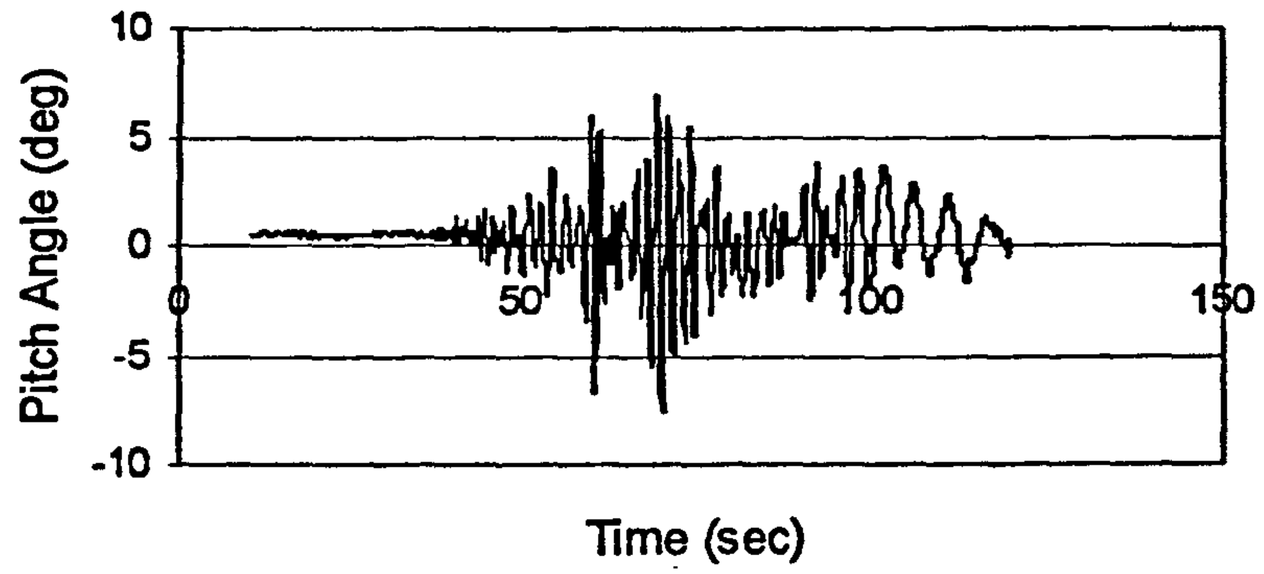

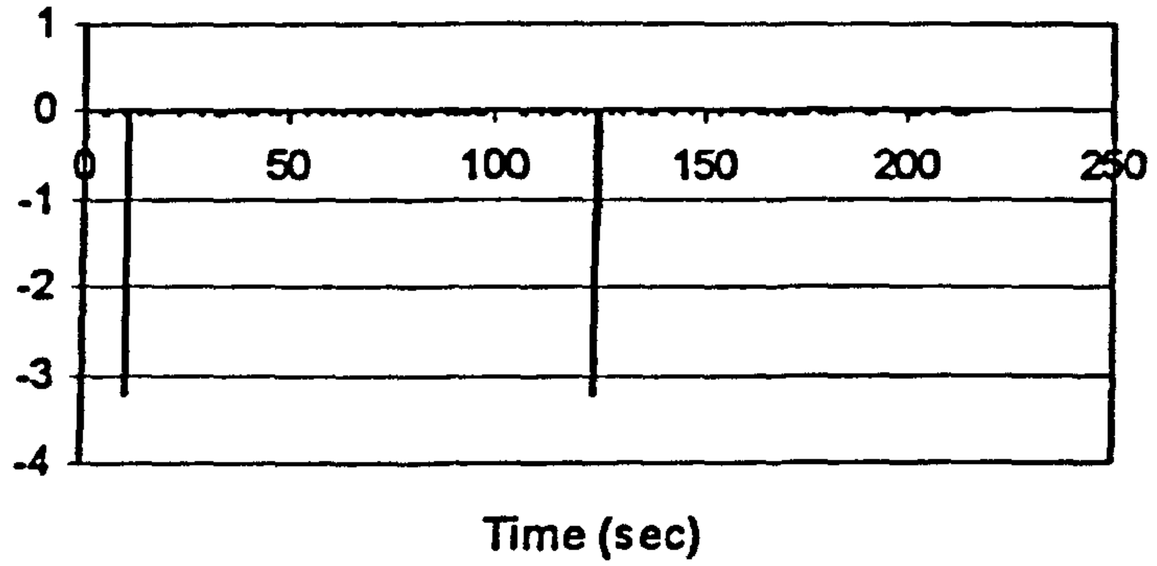

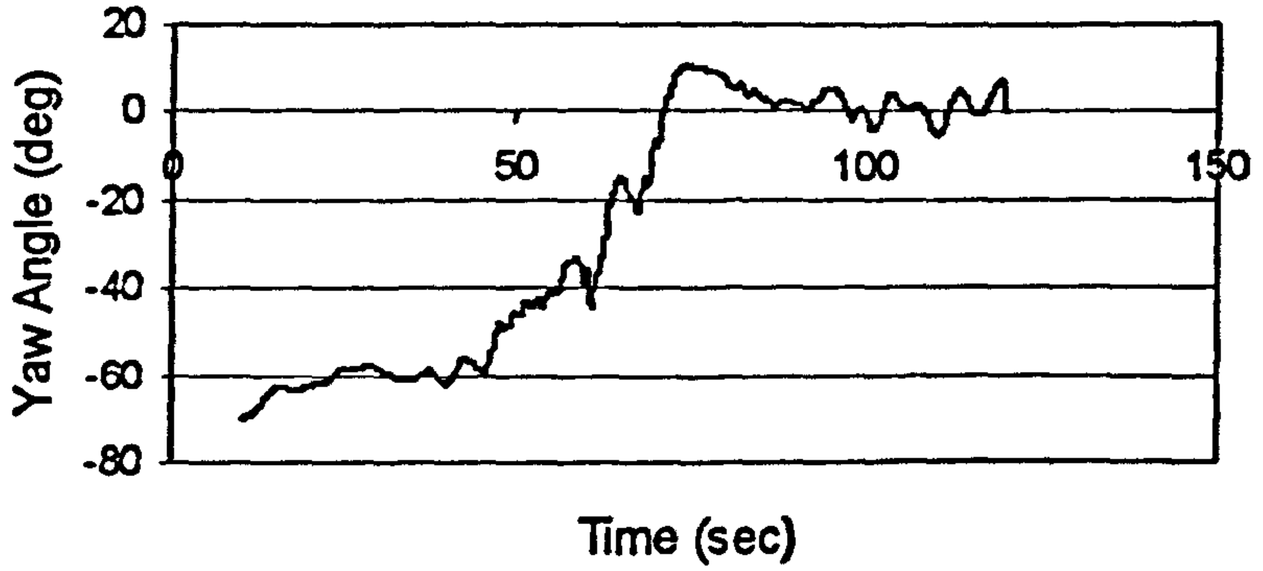

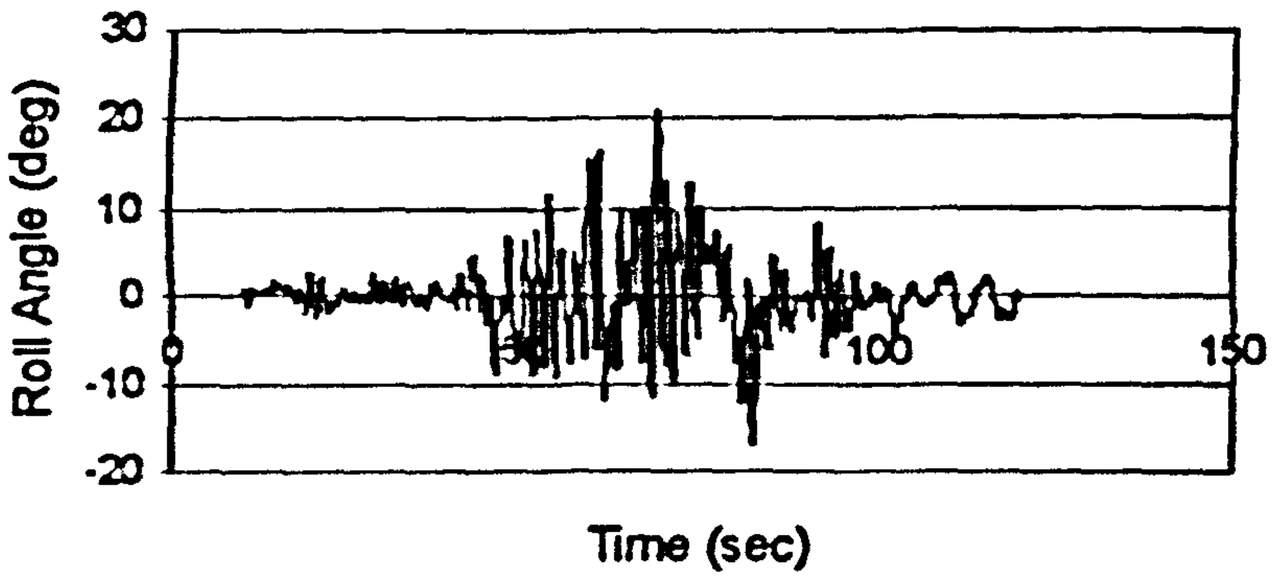

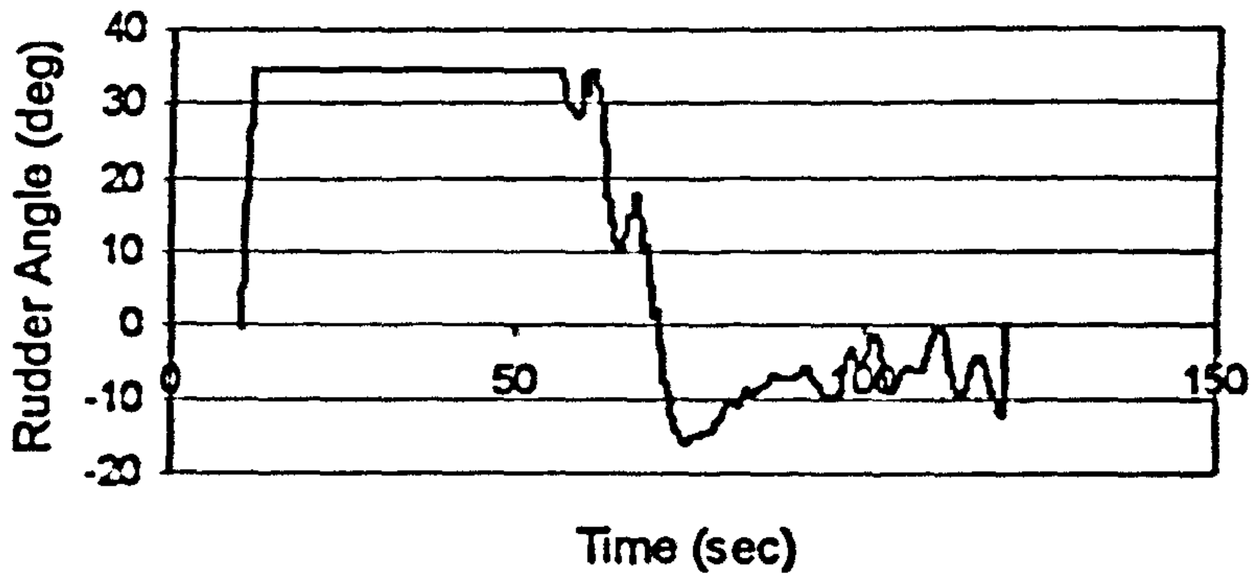

Figure H.12 ITTC, Fn=0.4, χ= -5°, H_s=0.1725 m, T_p=1.487 sec

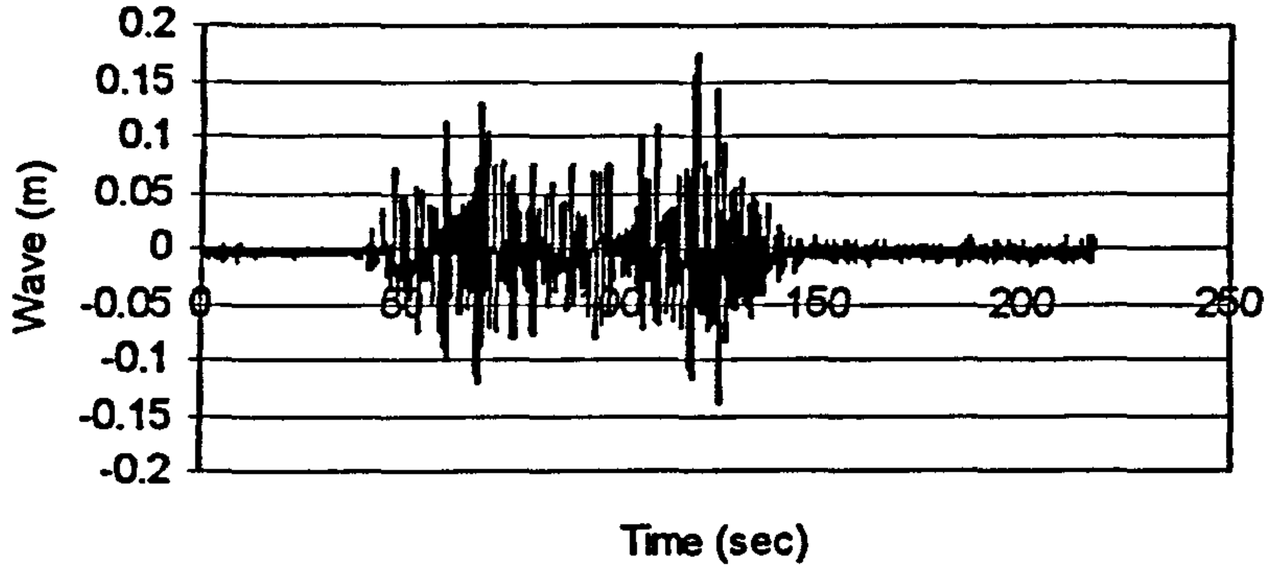

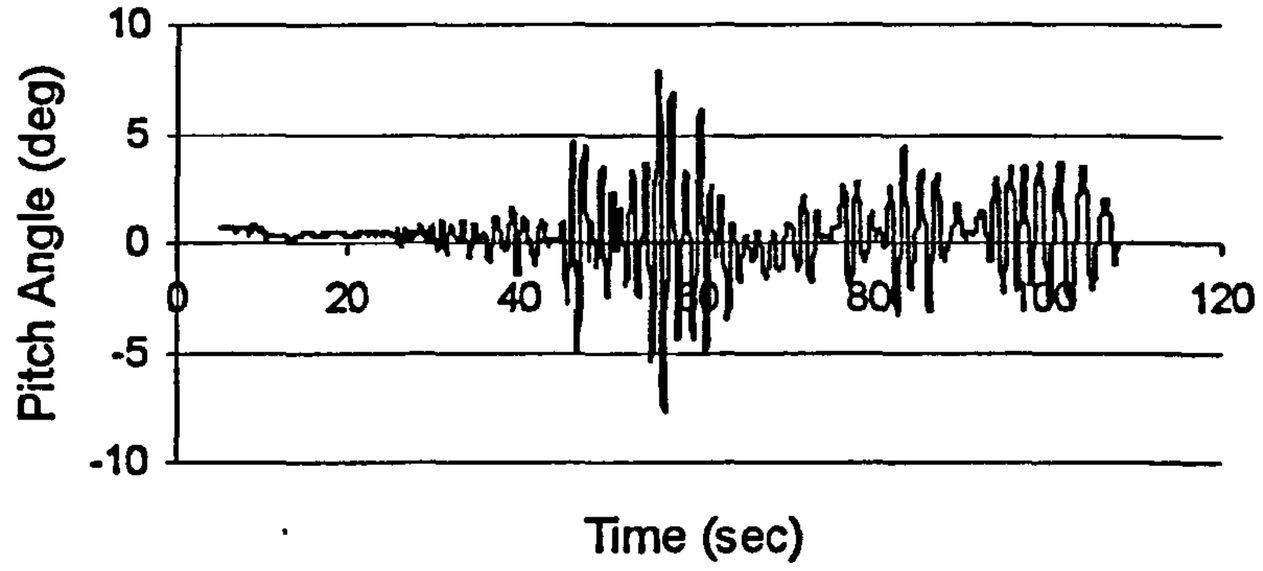

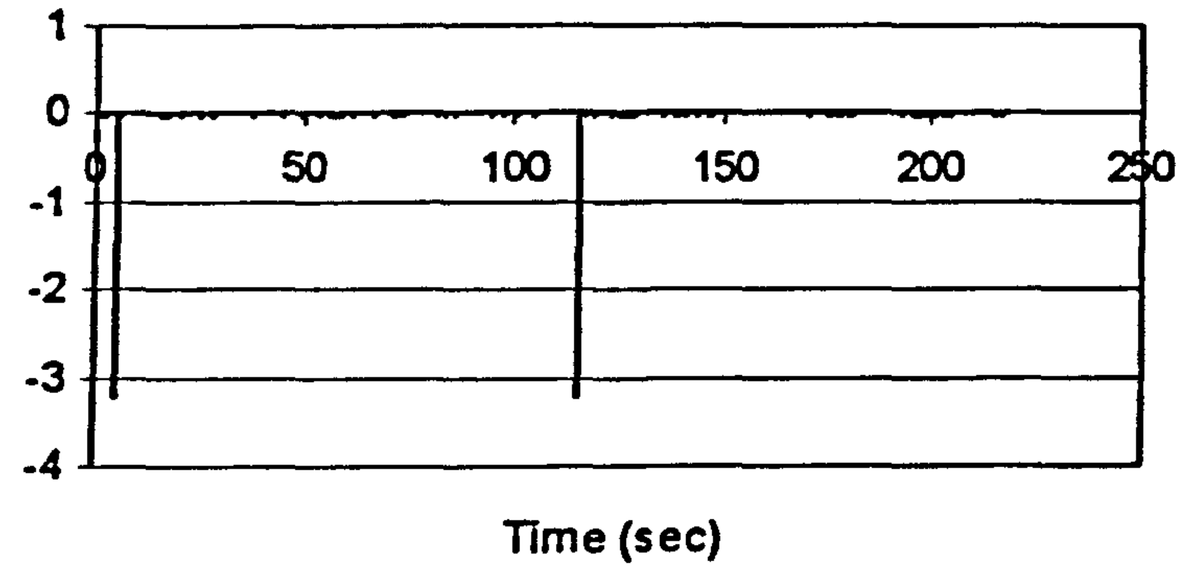

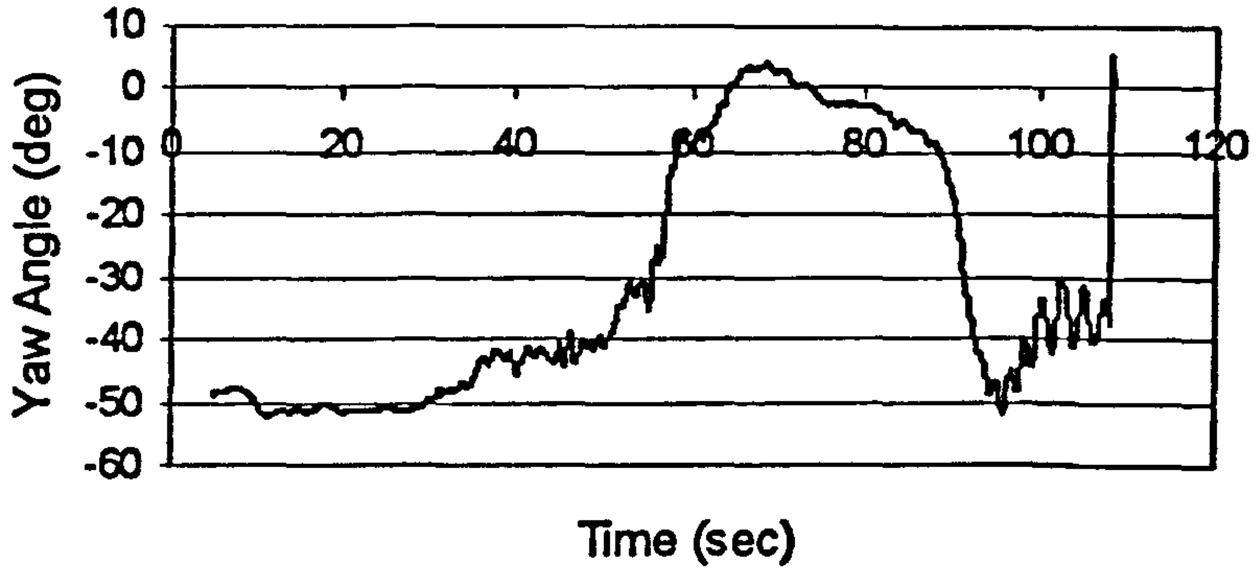

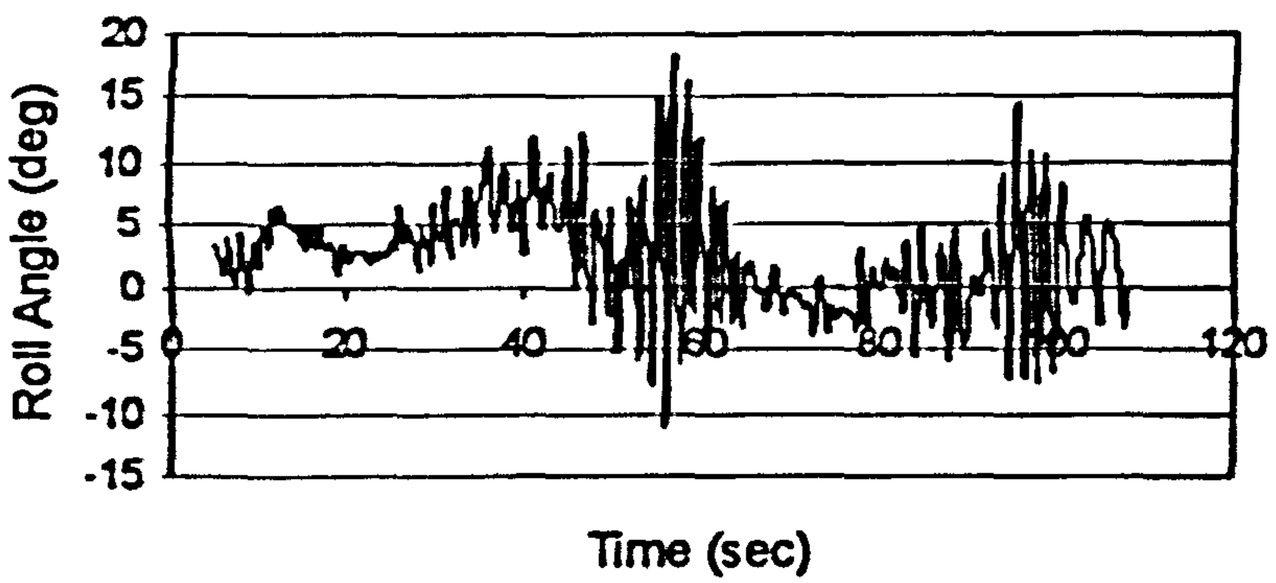

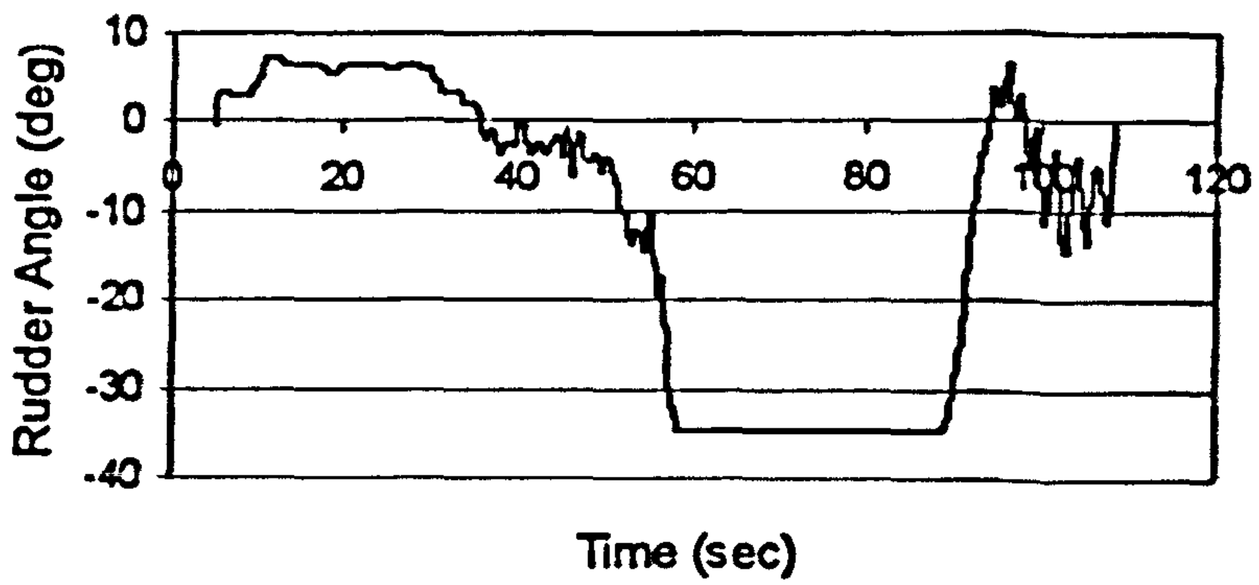

Figure H.13 ITTC, Fn=0.3, χ= -45°, H_s=0.1725 m, T_p=1.487 sec.

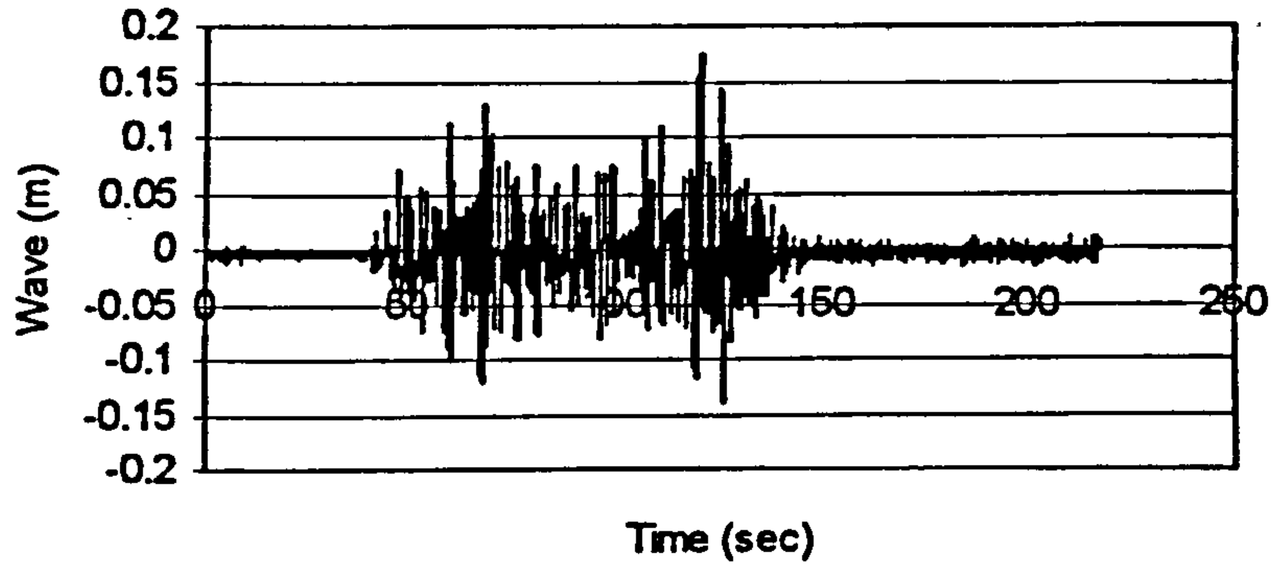

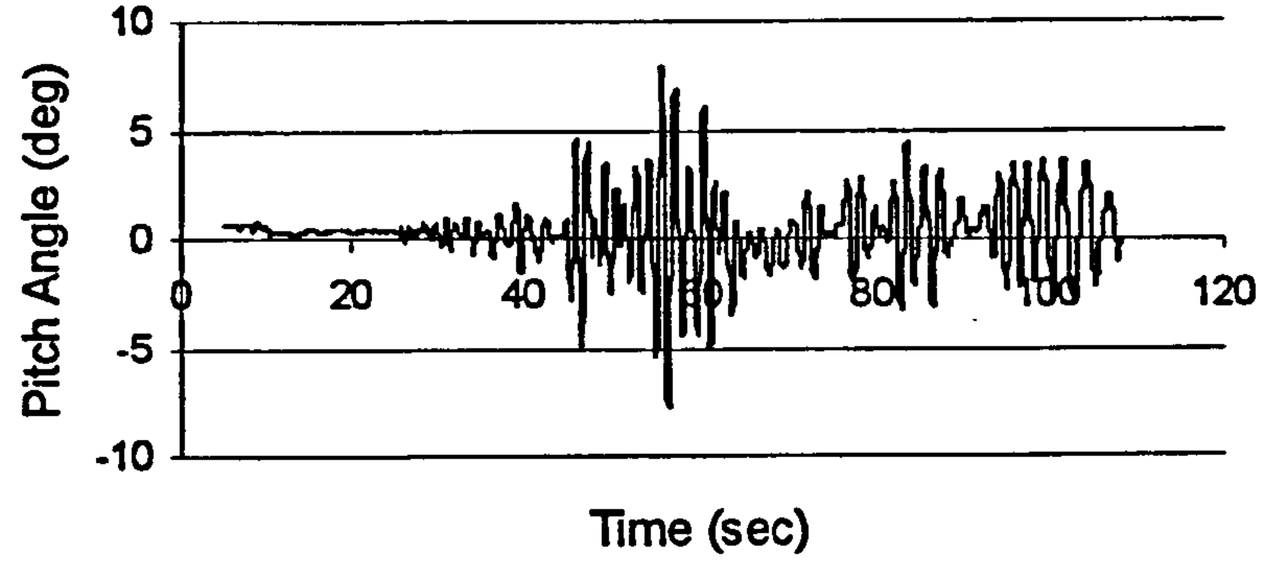

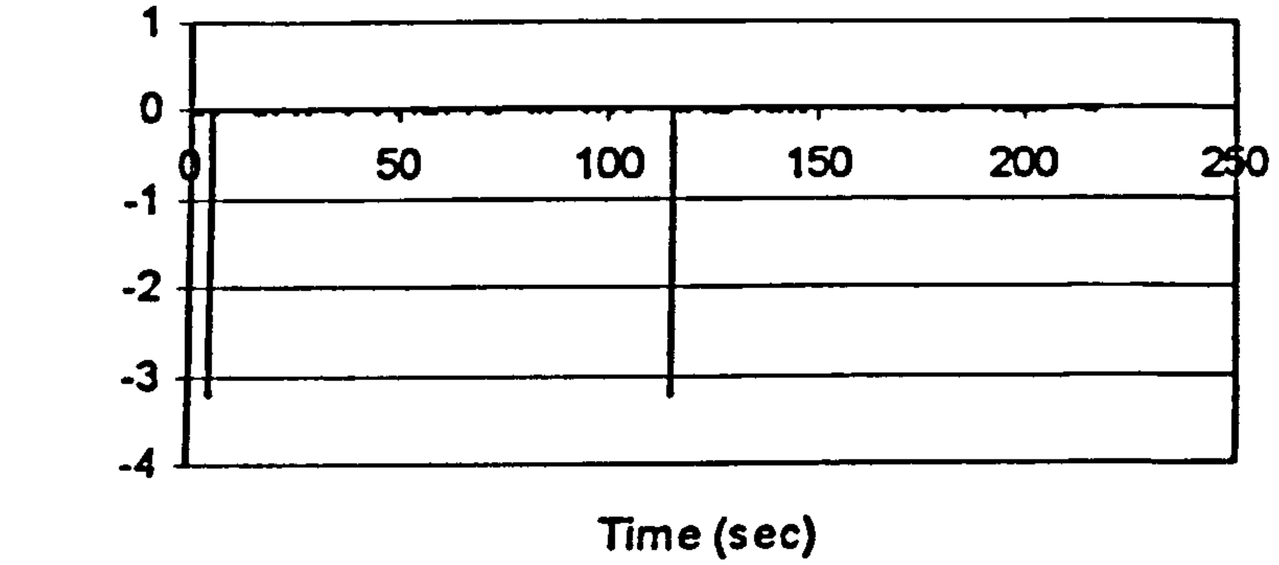

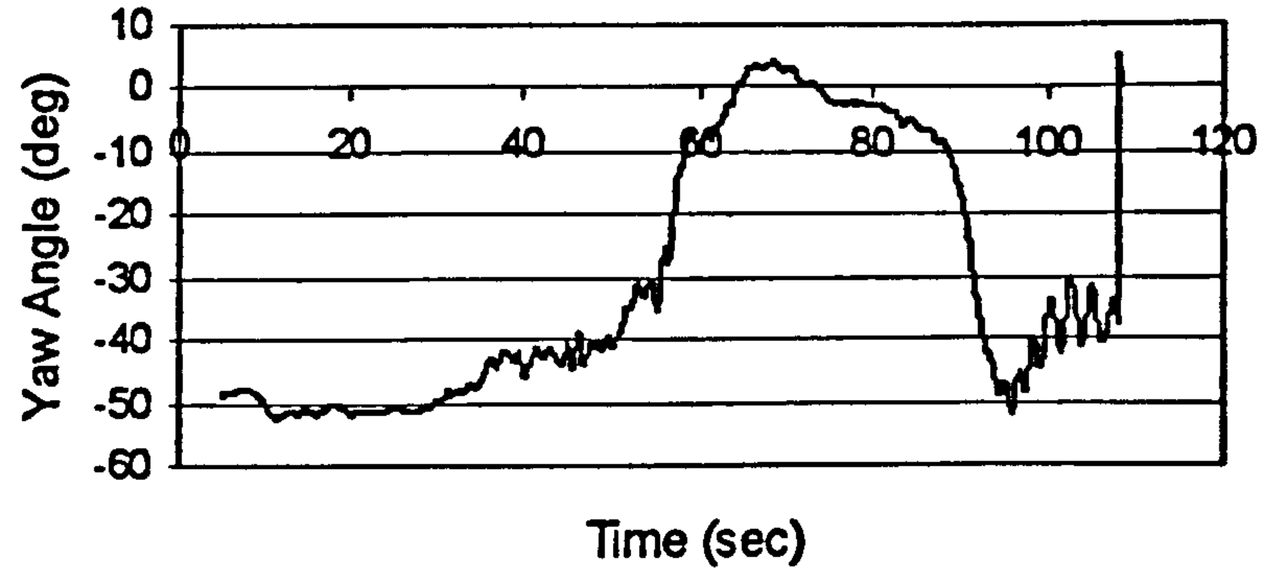

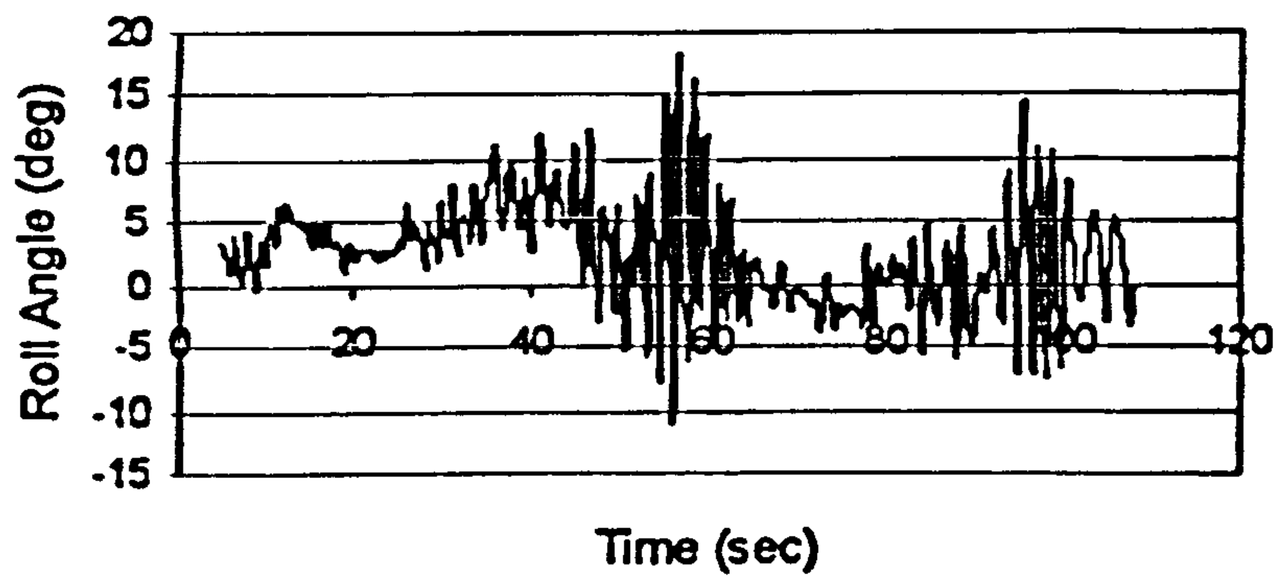

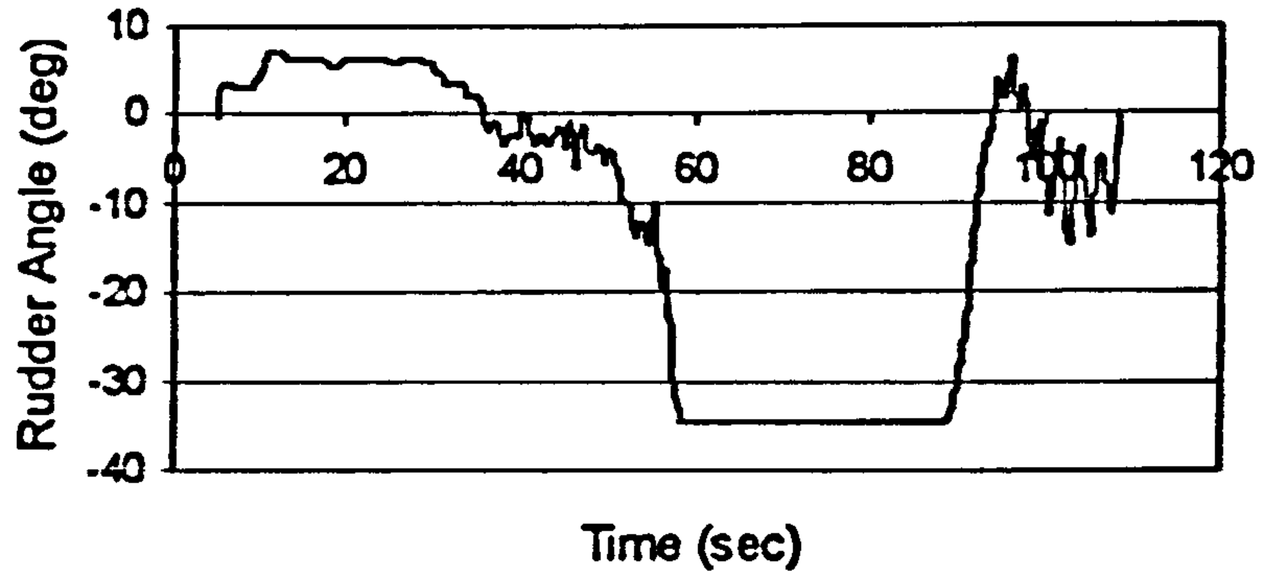

Figure H.14 ITTC, Fn=0.4, χ= -45°, H_s=0.1725 m, T_p=1.487 sec.

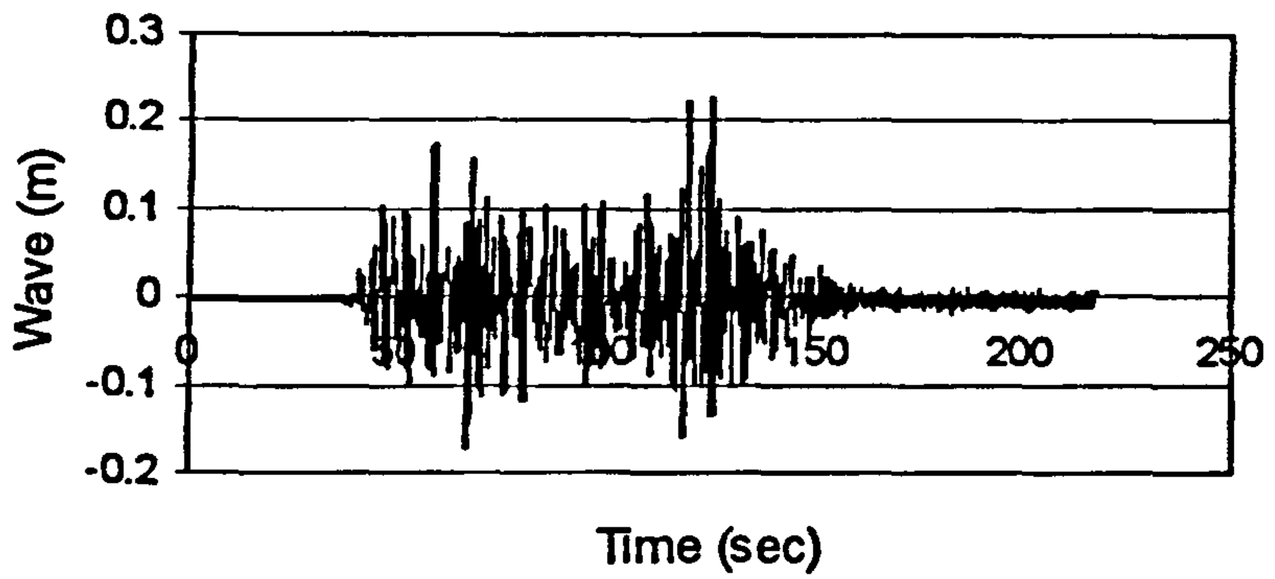

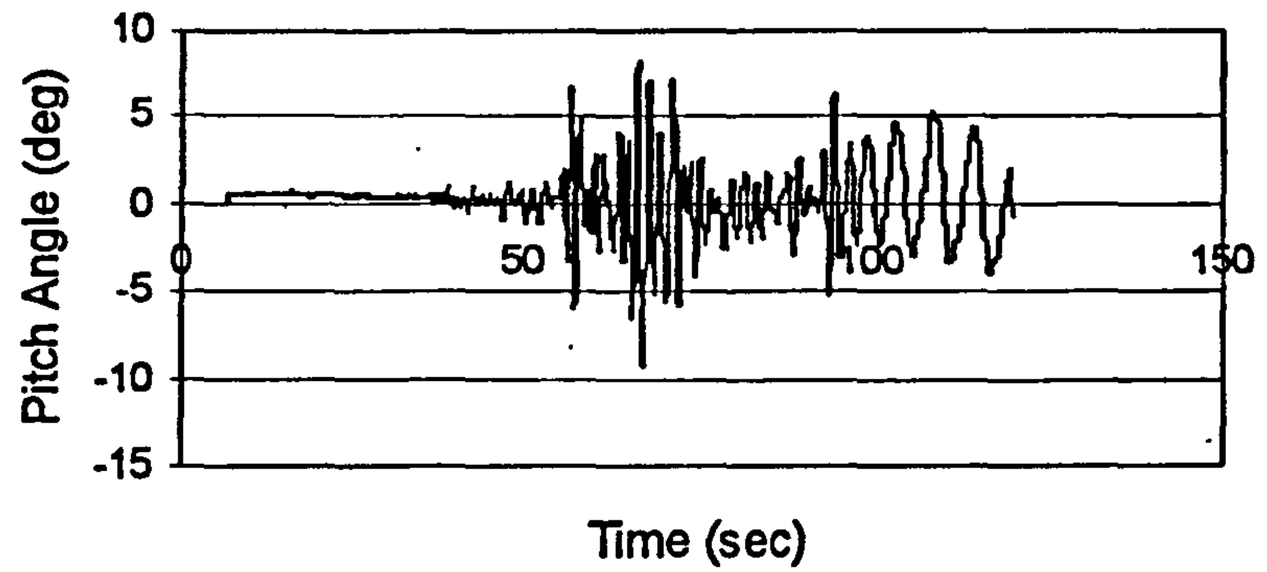

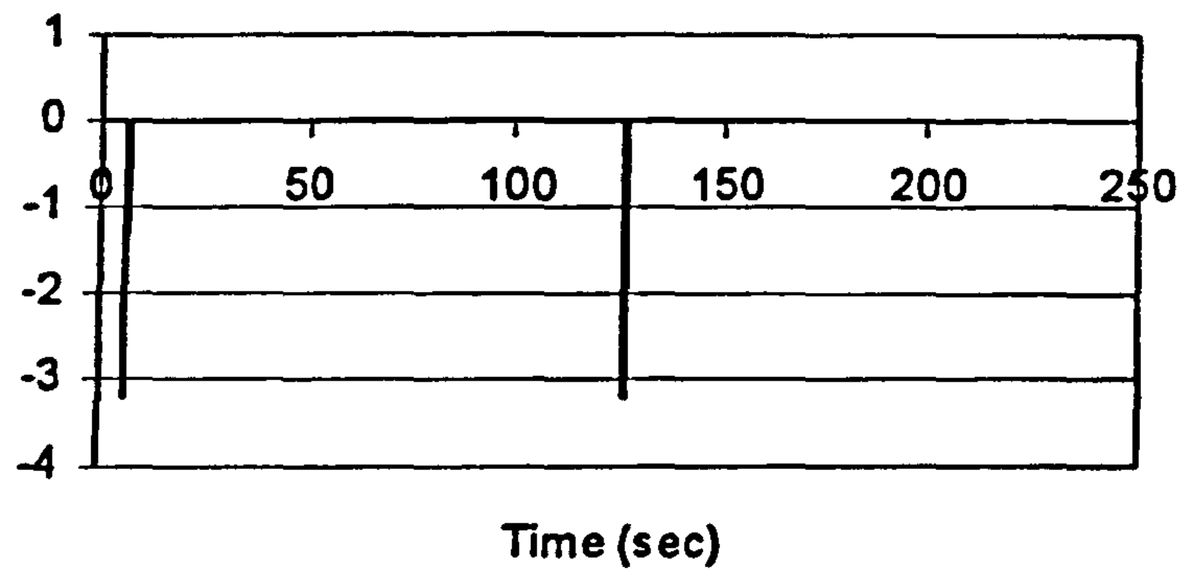

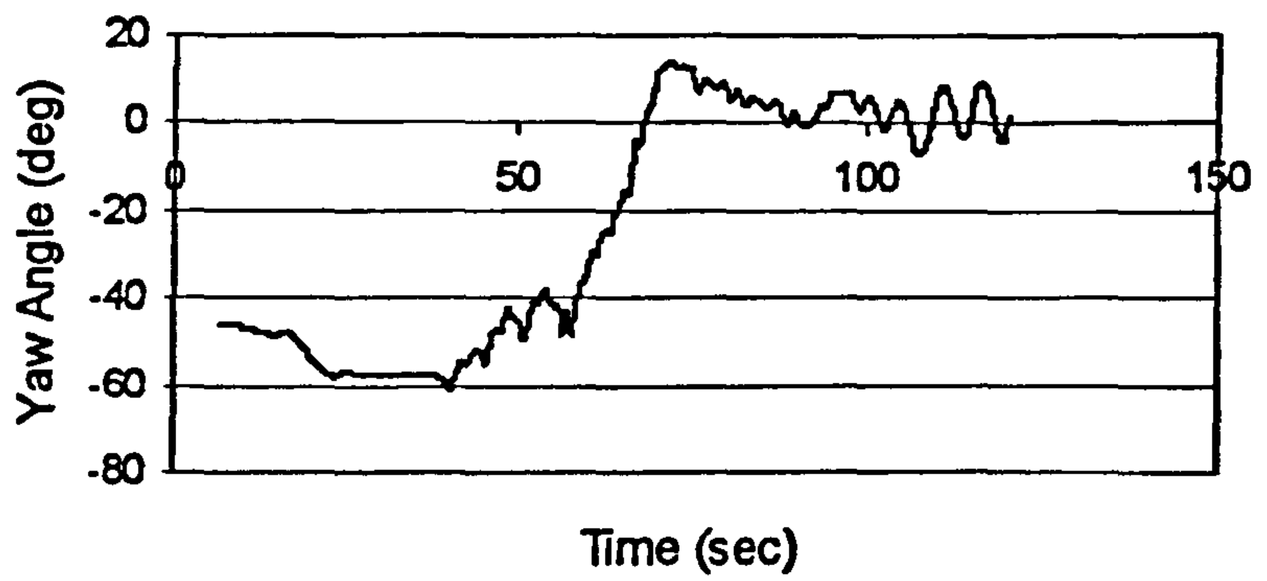

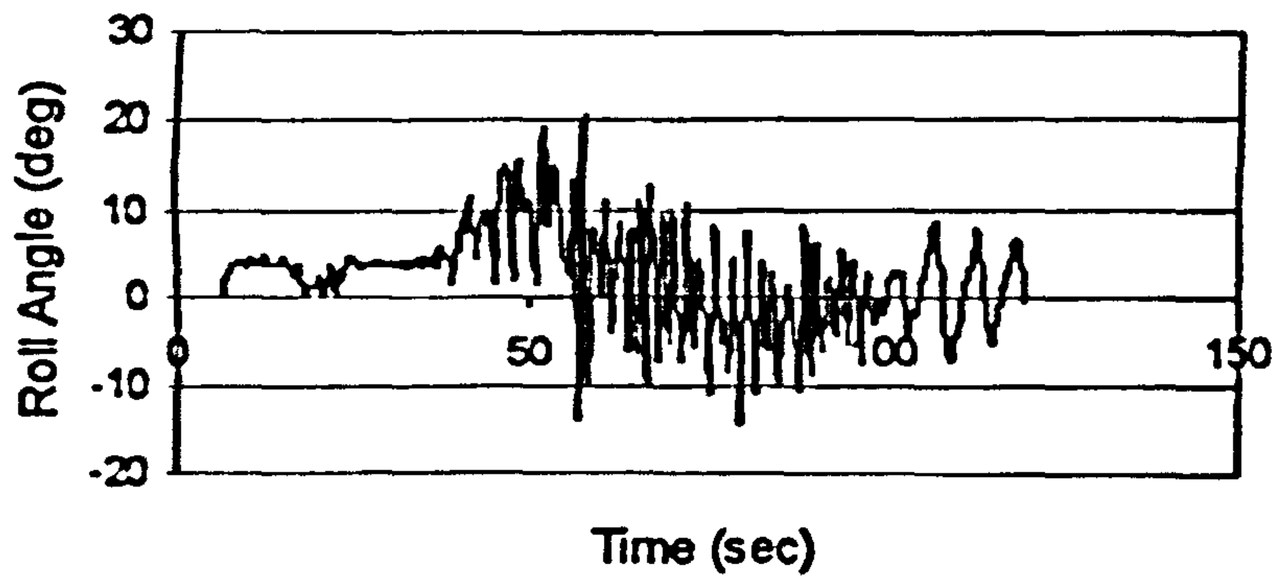

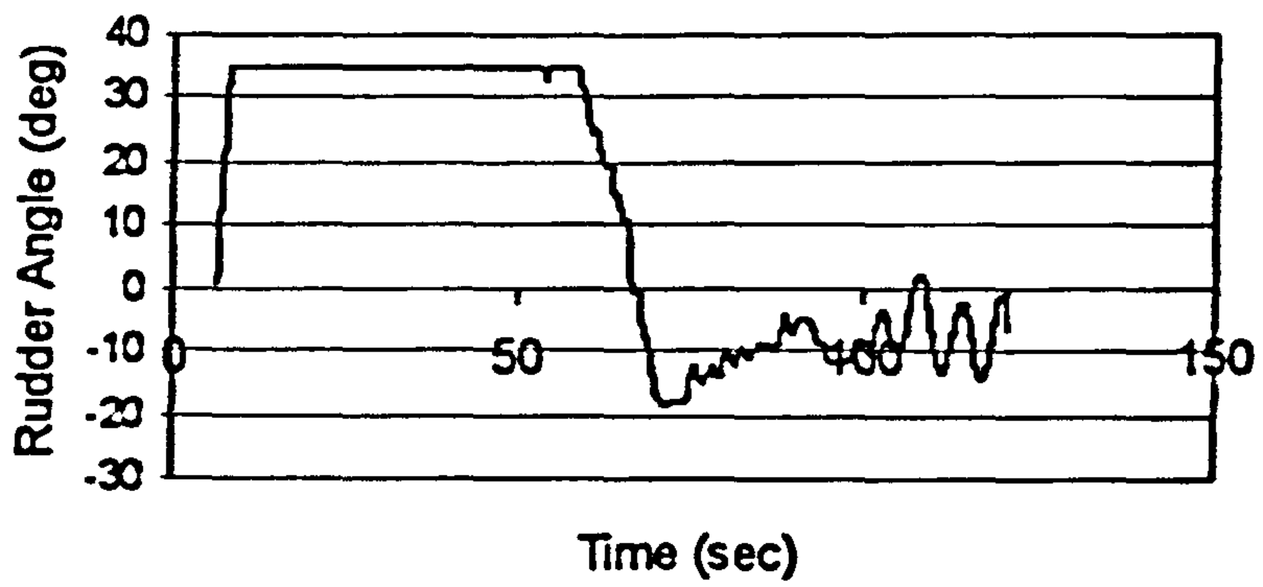

Figure H.15 ITTC, Fn=0.3, χ= -5°, H_s=0.23 m, T_p=1.717 sec.

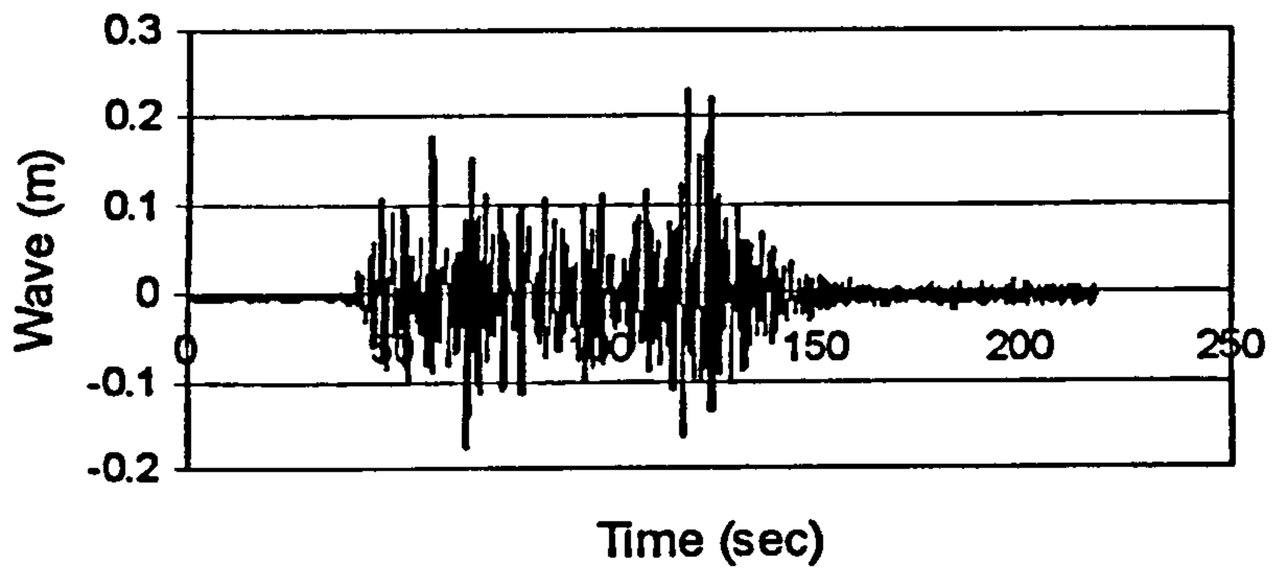

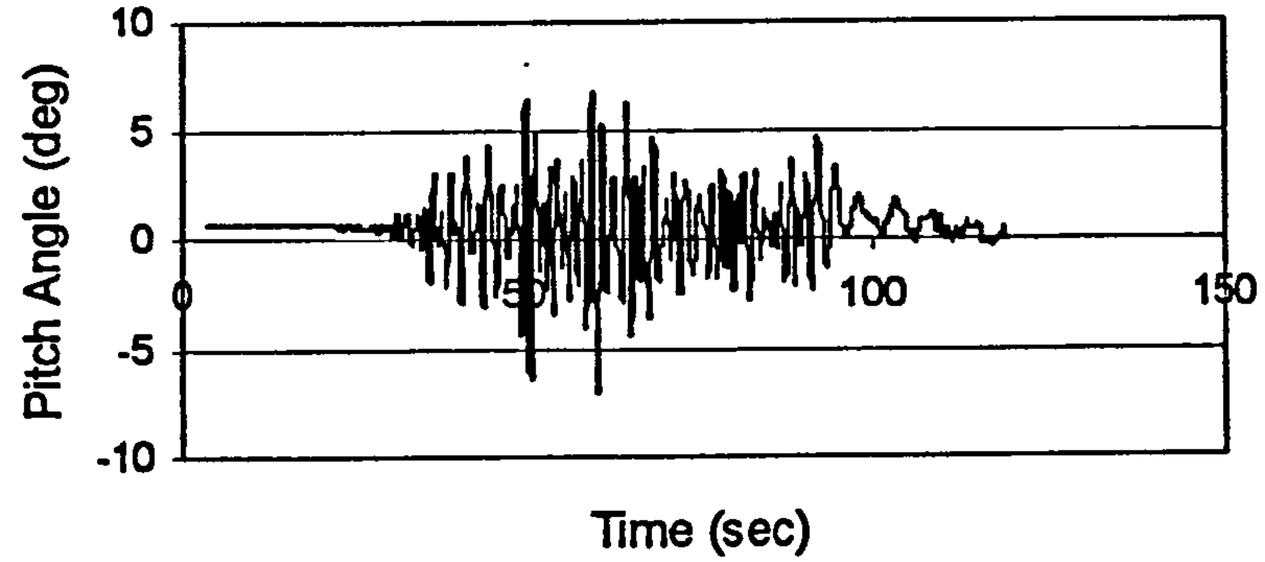

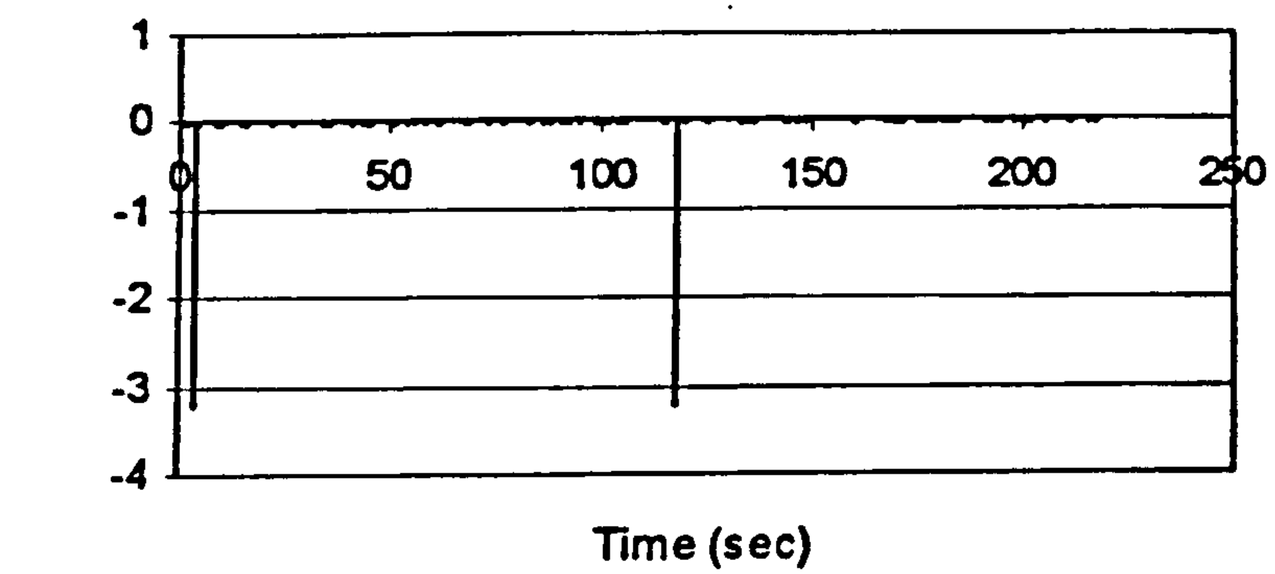

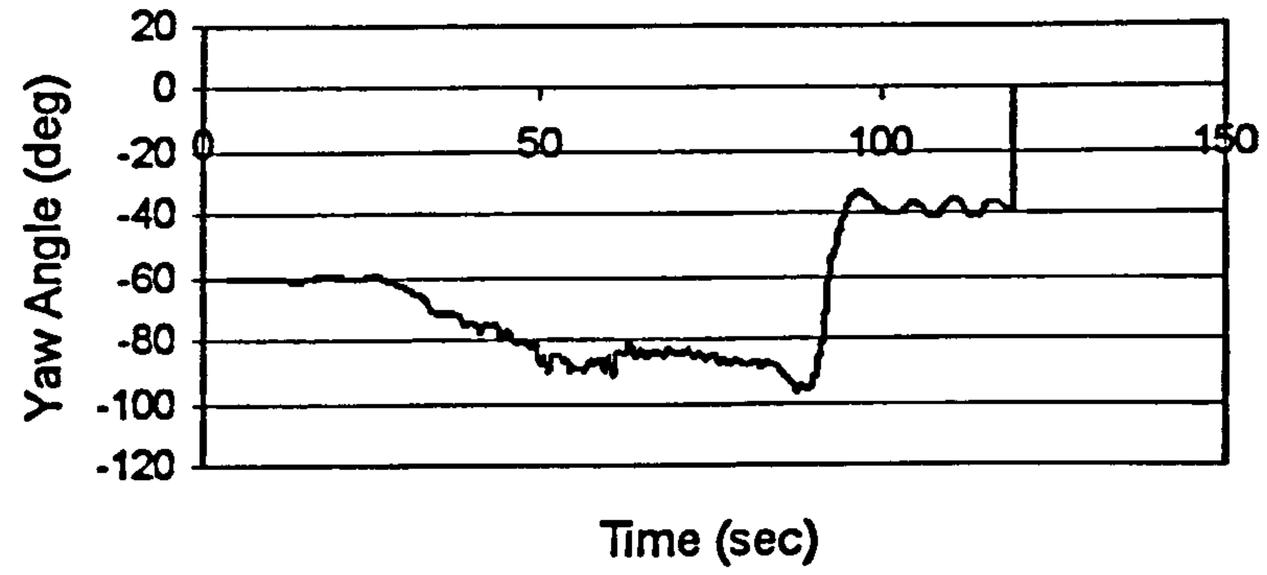

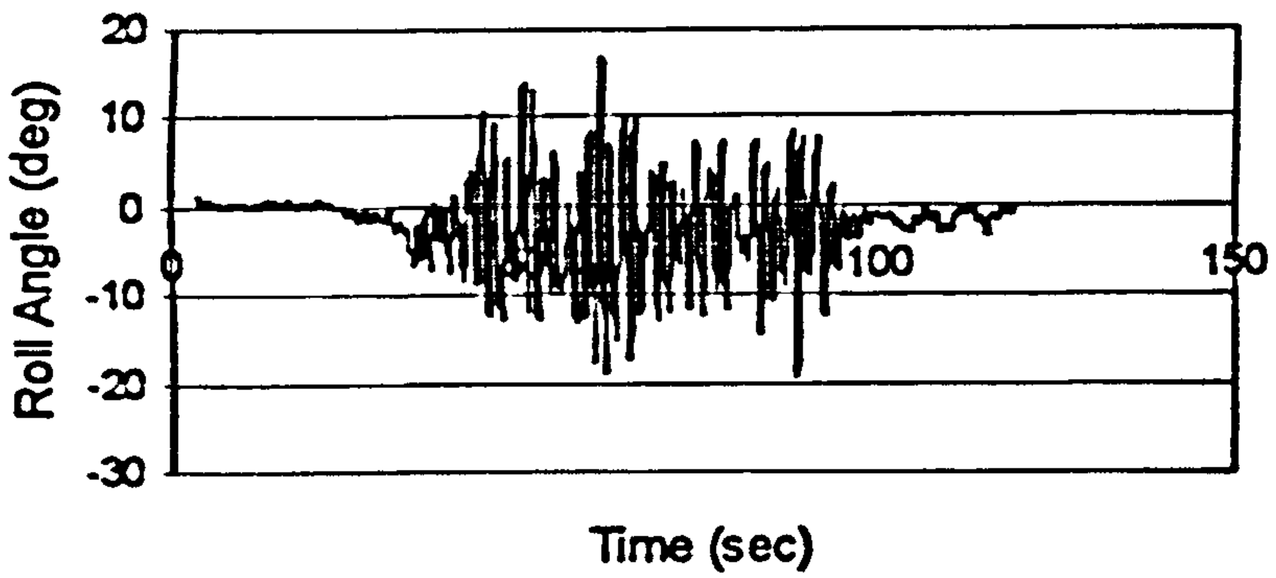

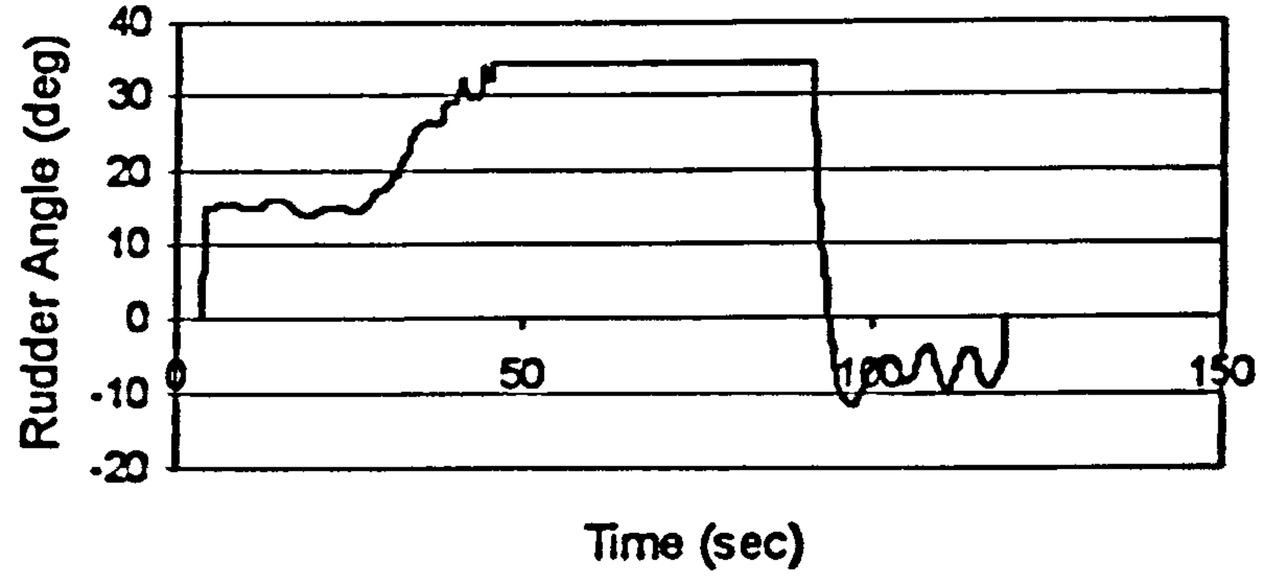

Figure H.16 ITTC, Fn=0.3, χ= -45°, H_s=0.23 m, T_p=1.717 sec.

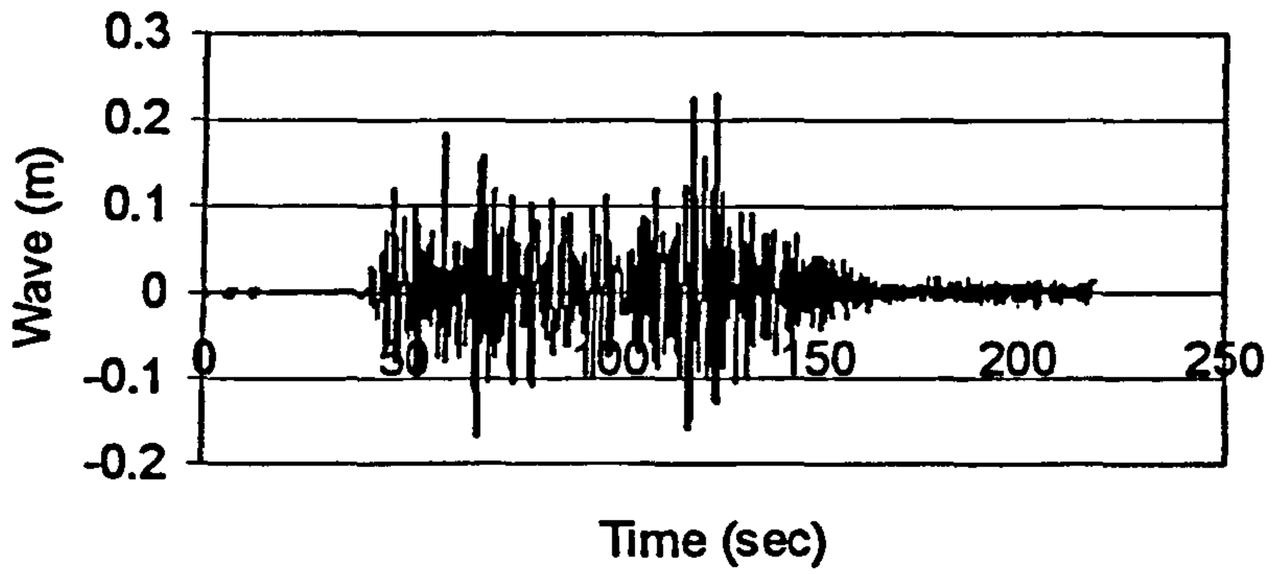

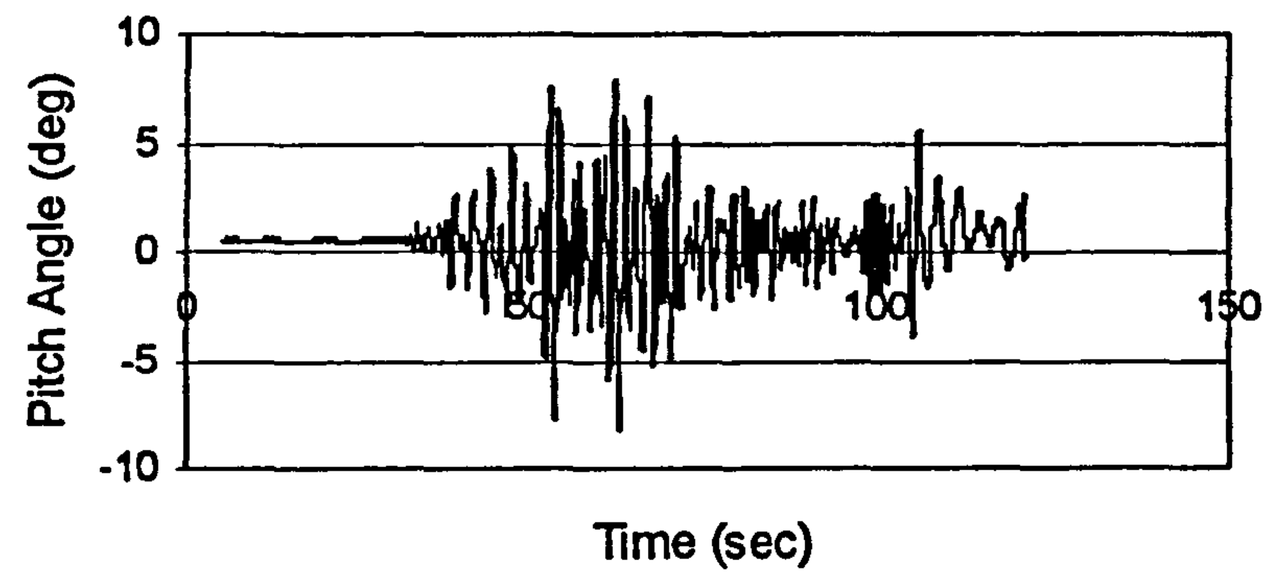

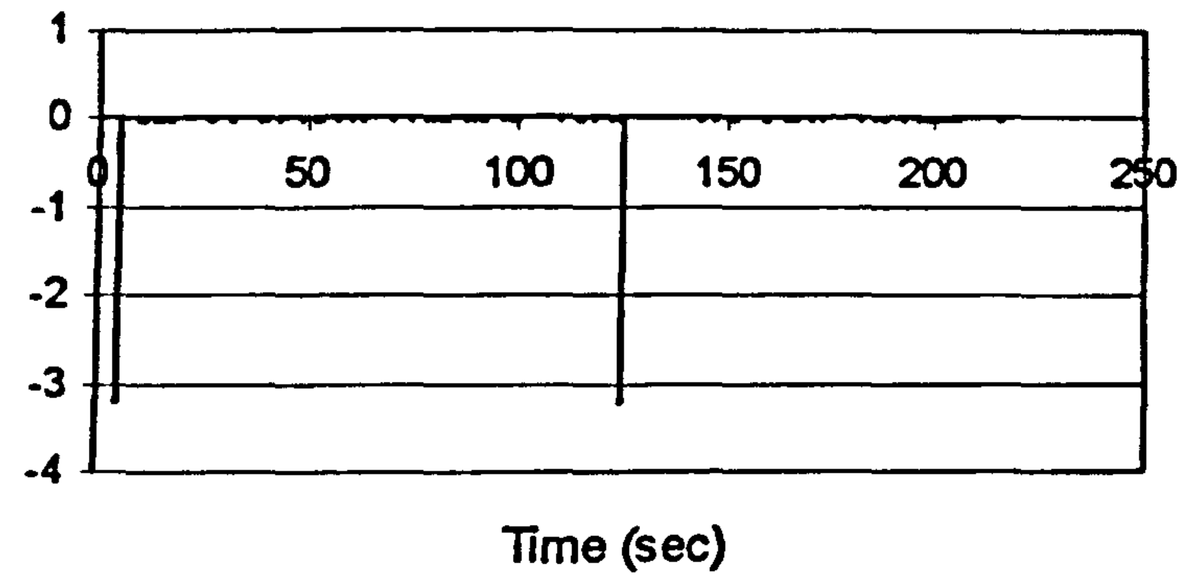

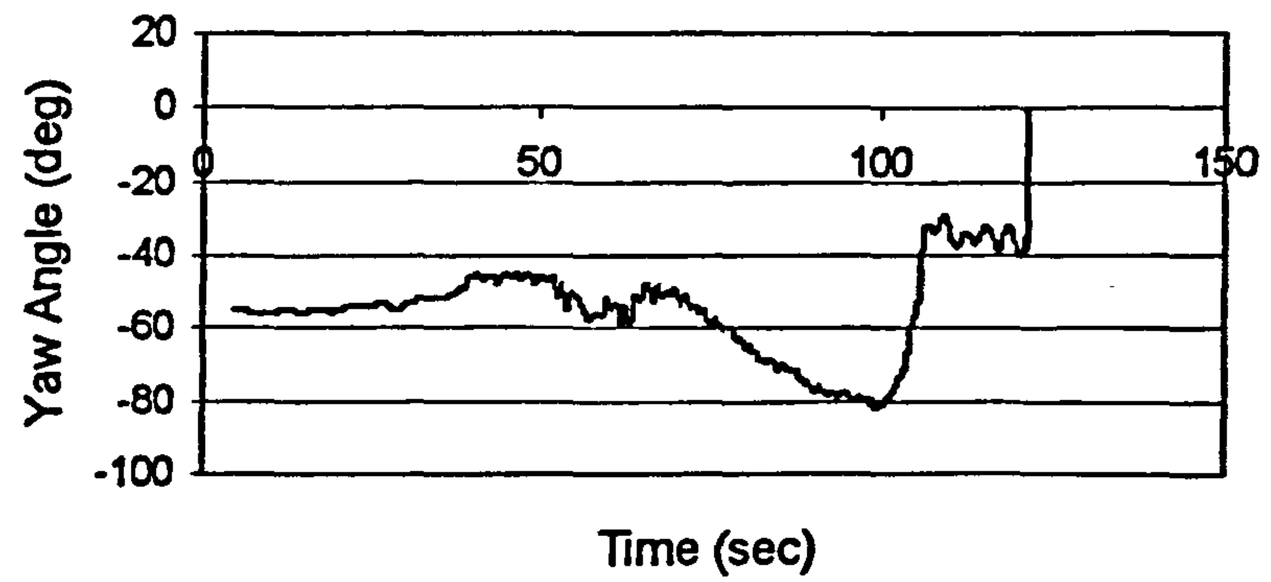

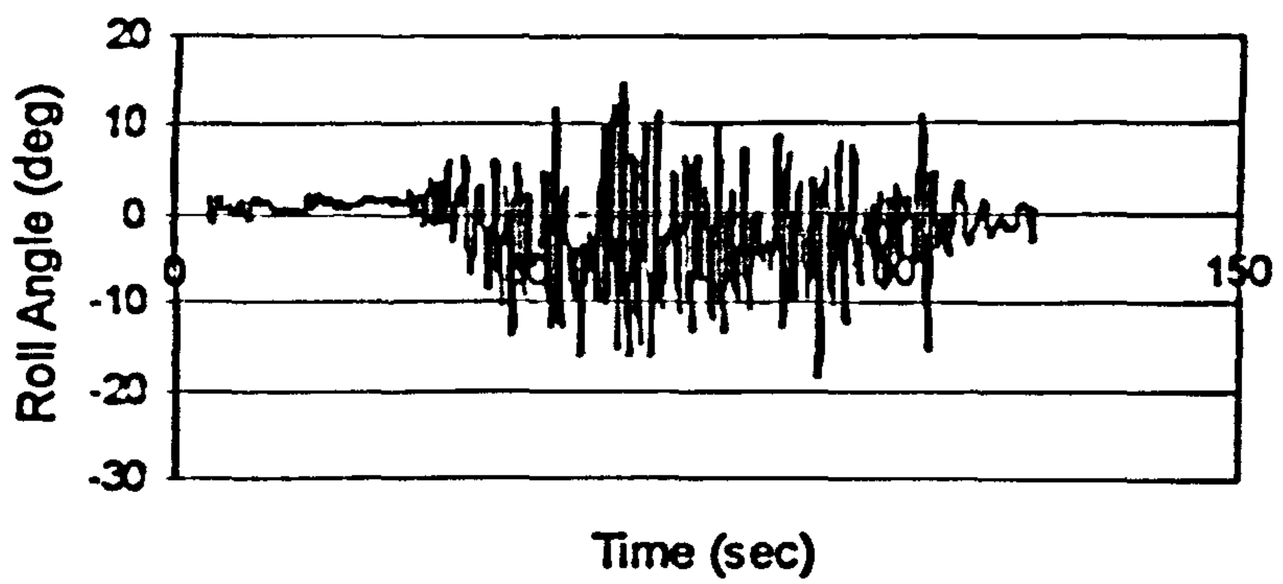

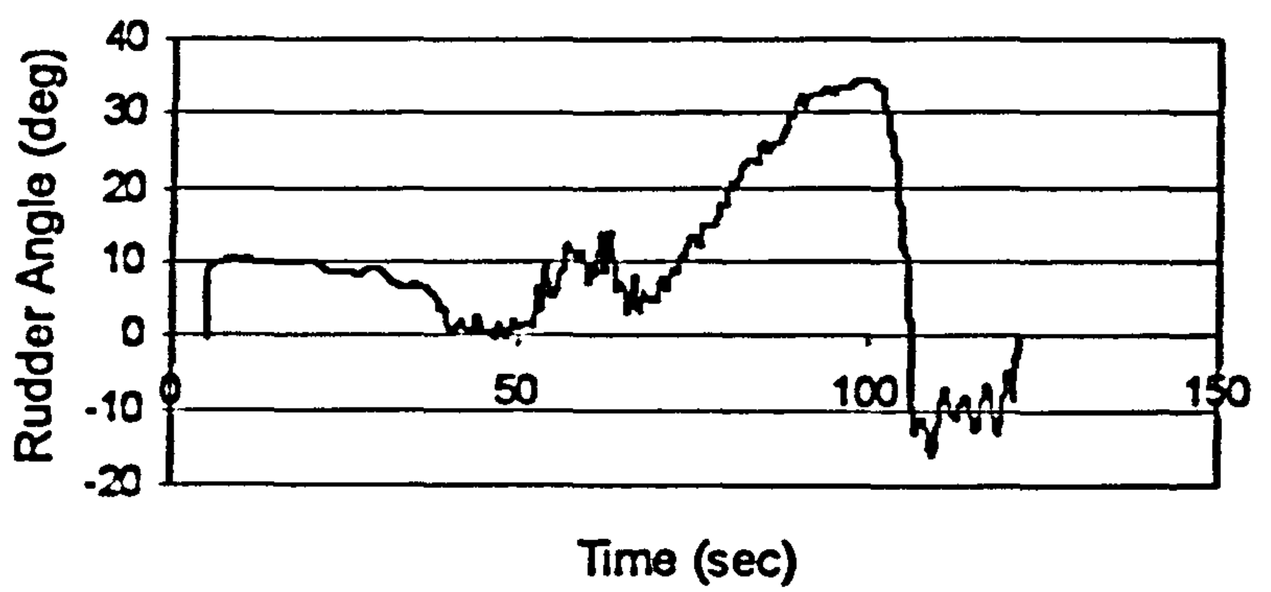

Figure H.17 ITTC, Fn=0.4, χ= -45°, H_s=0.23 m, T_p=1.717 sec.

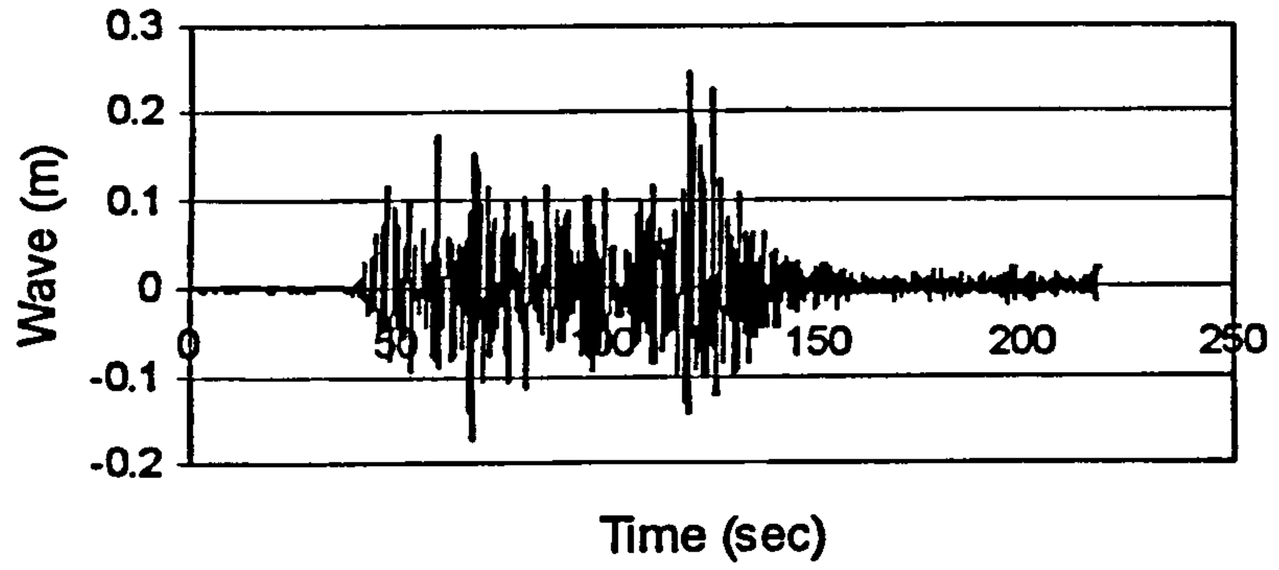

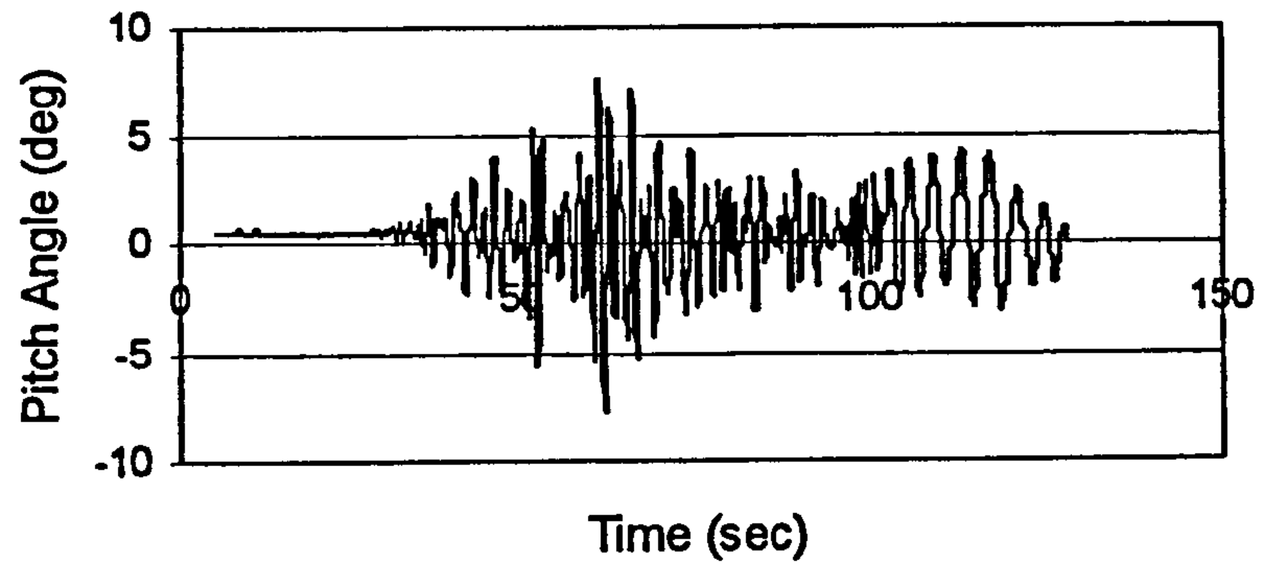

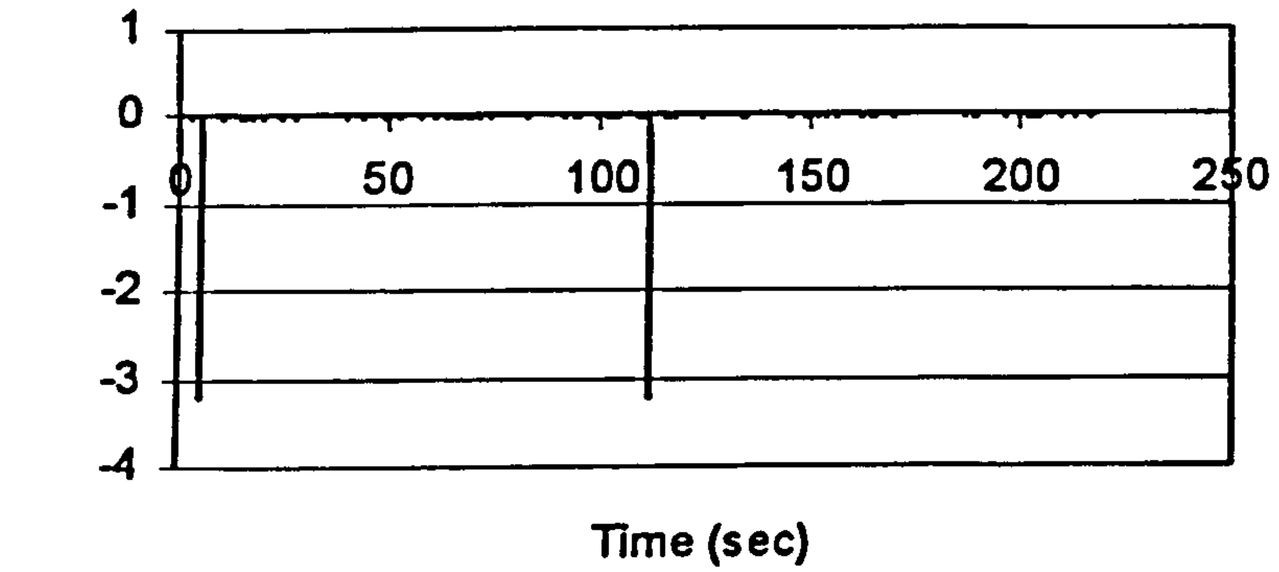

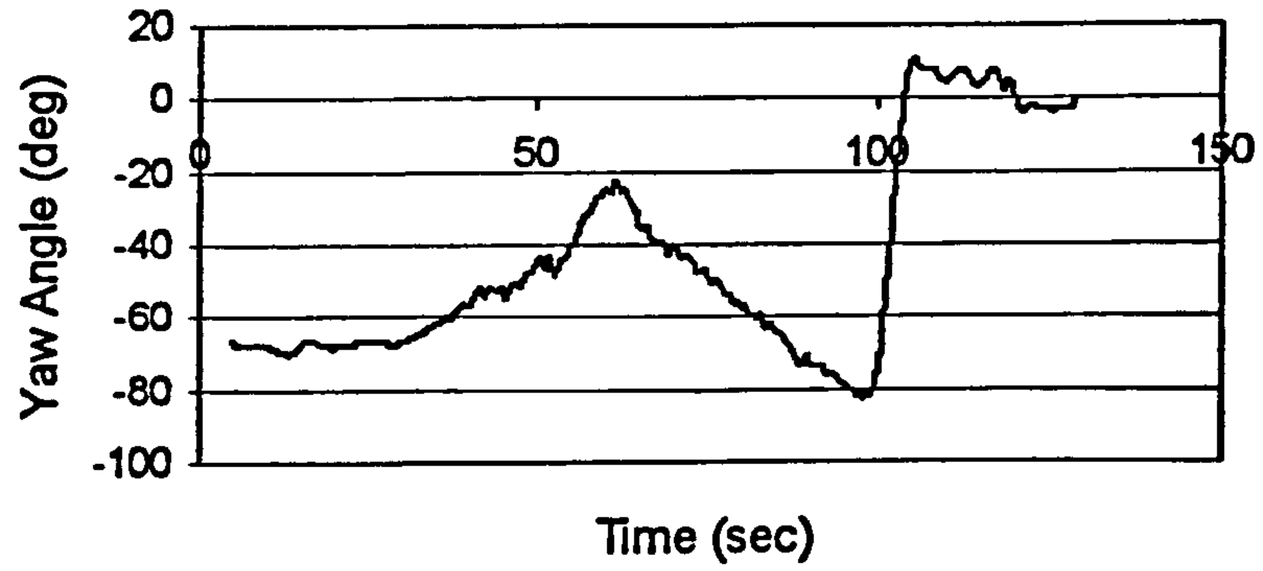

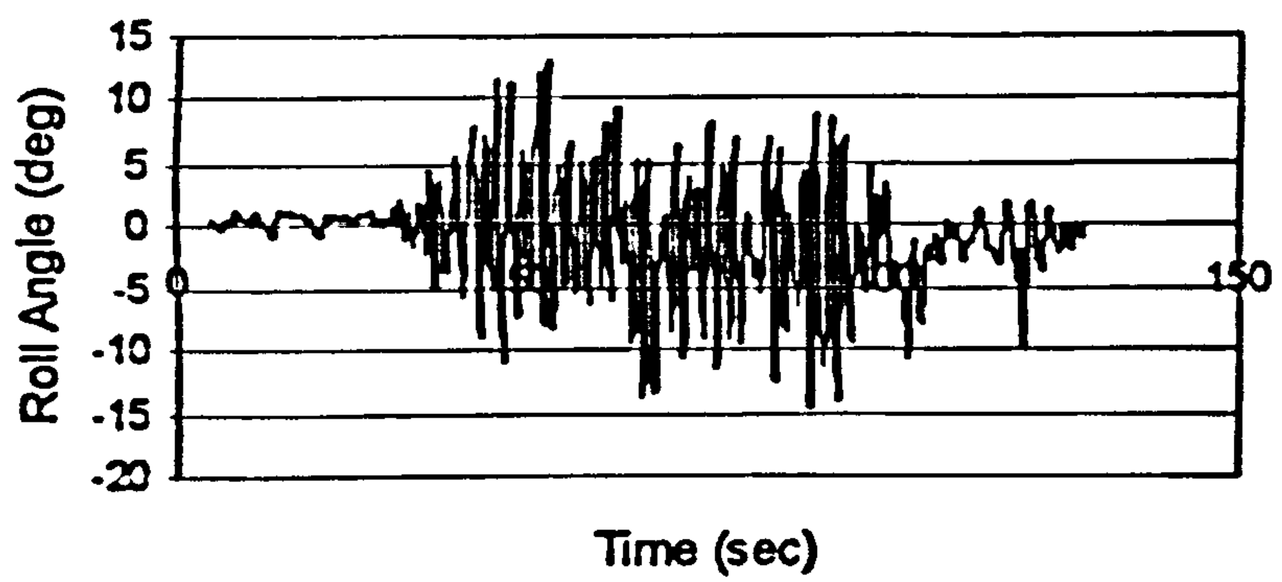

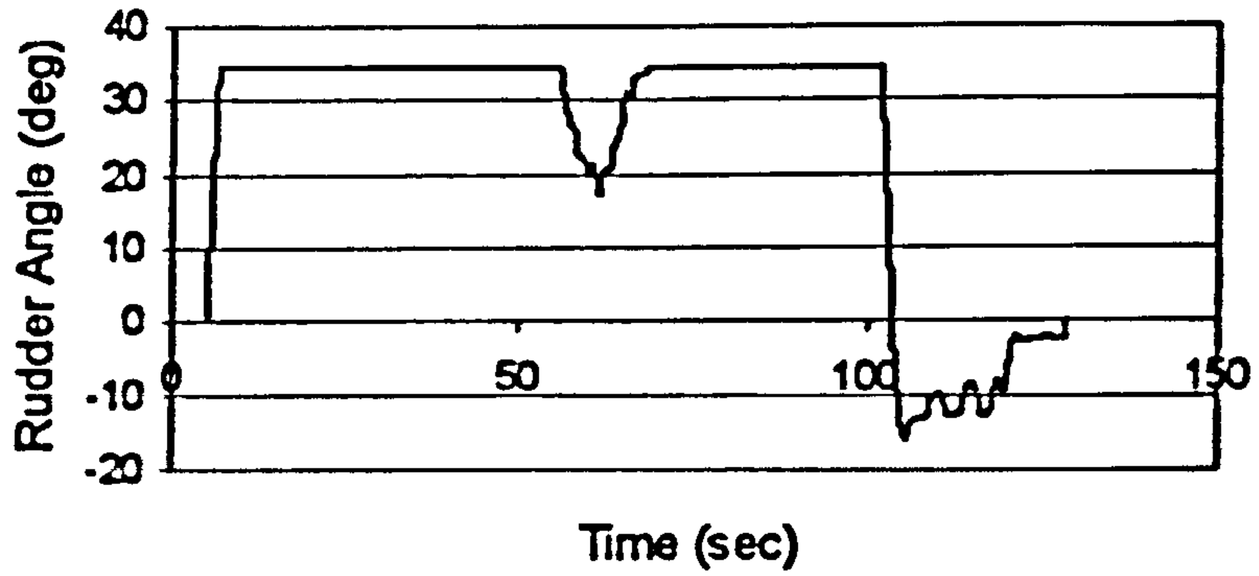

Figure H.18 JONSWAP, Fn=0.3, χ= -5°, H_s=0.115 m, T_p=1.214 sec.

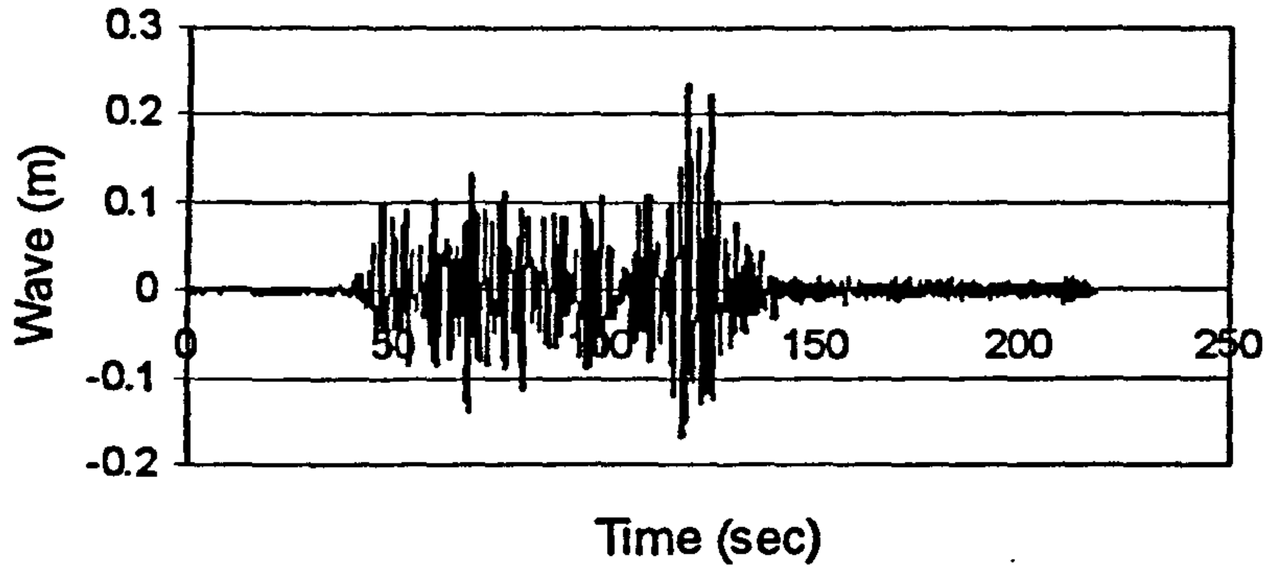

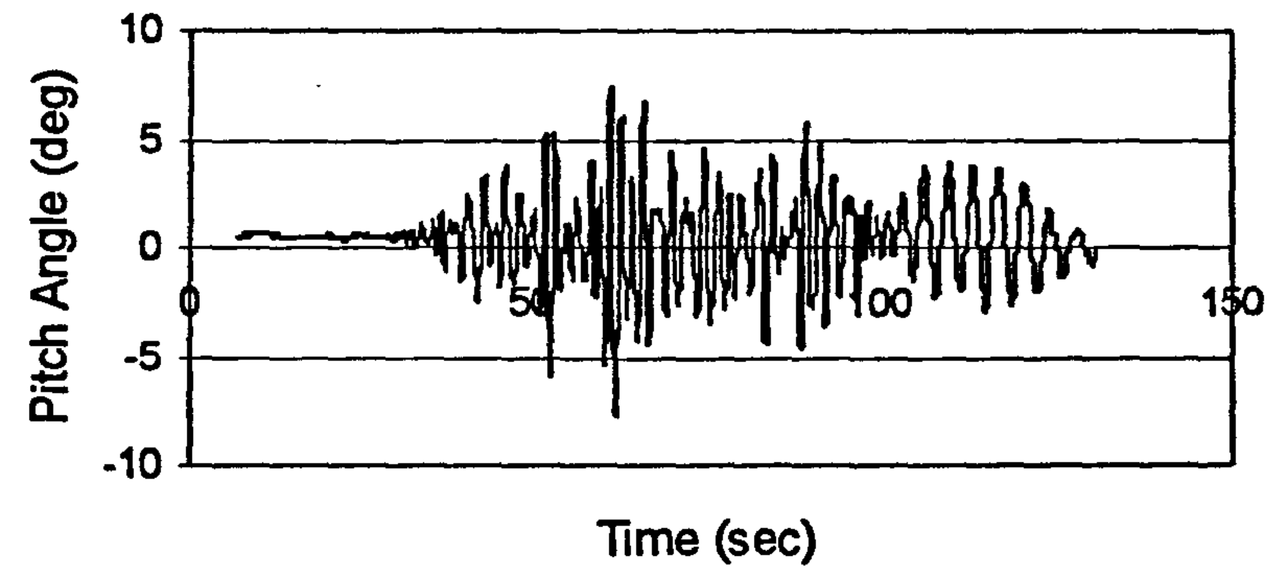

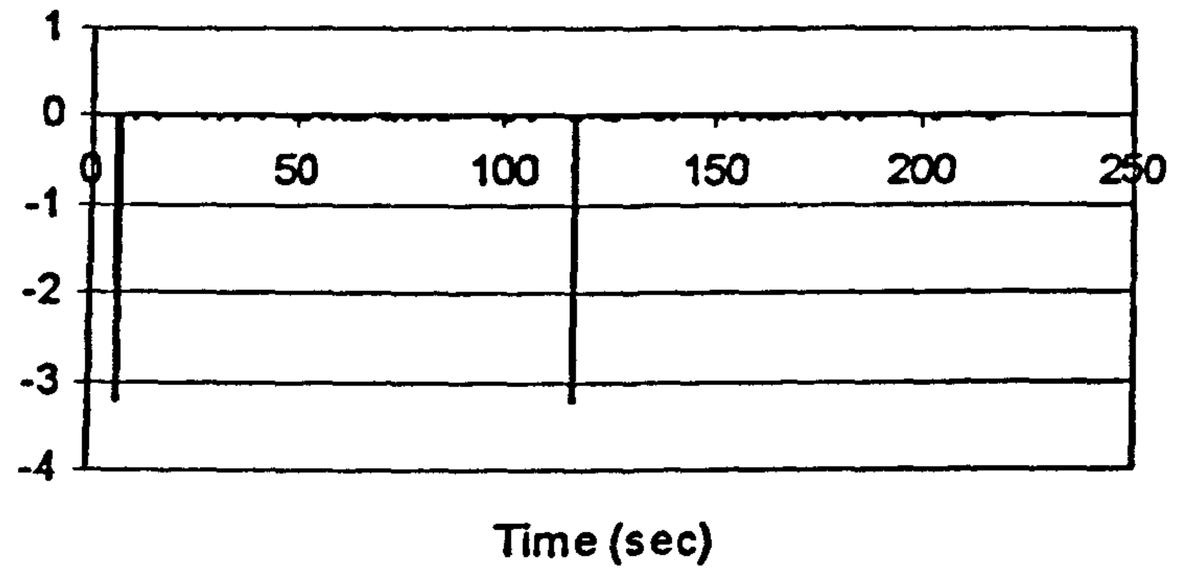

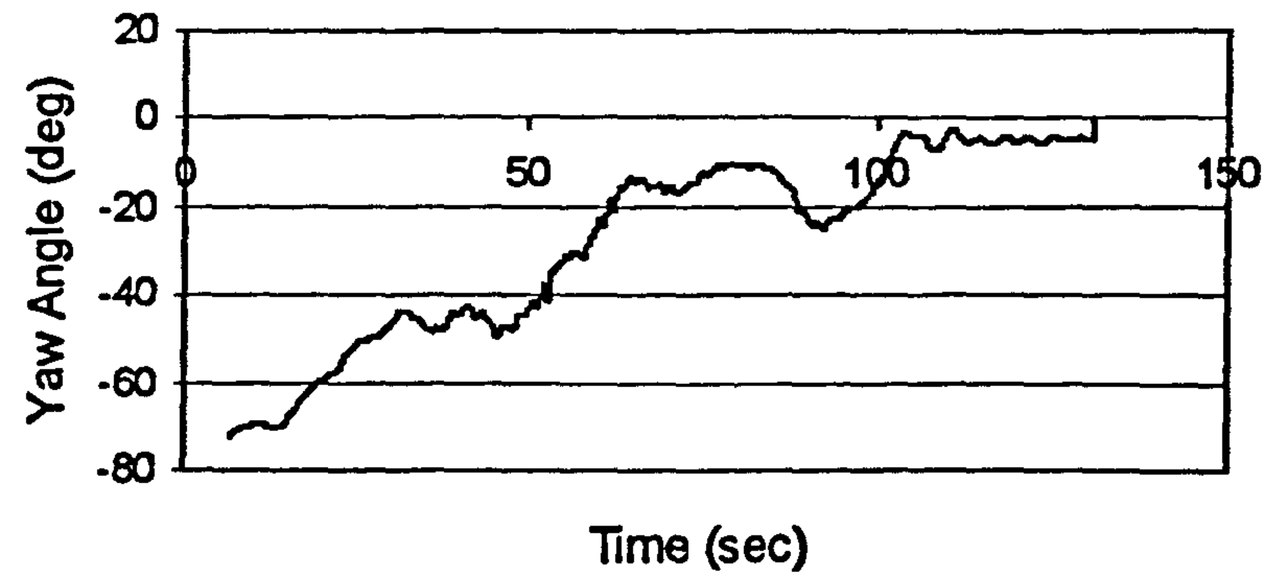

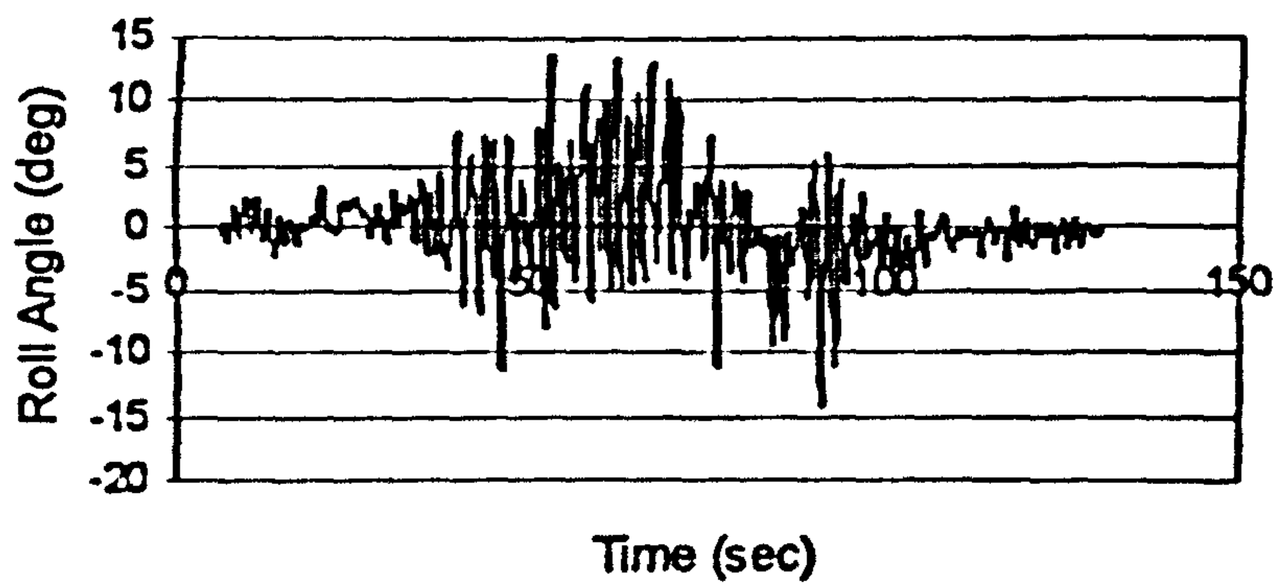

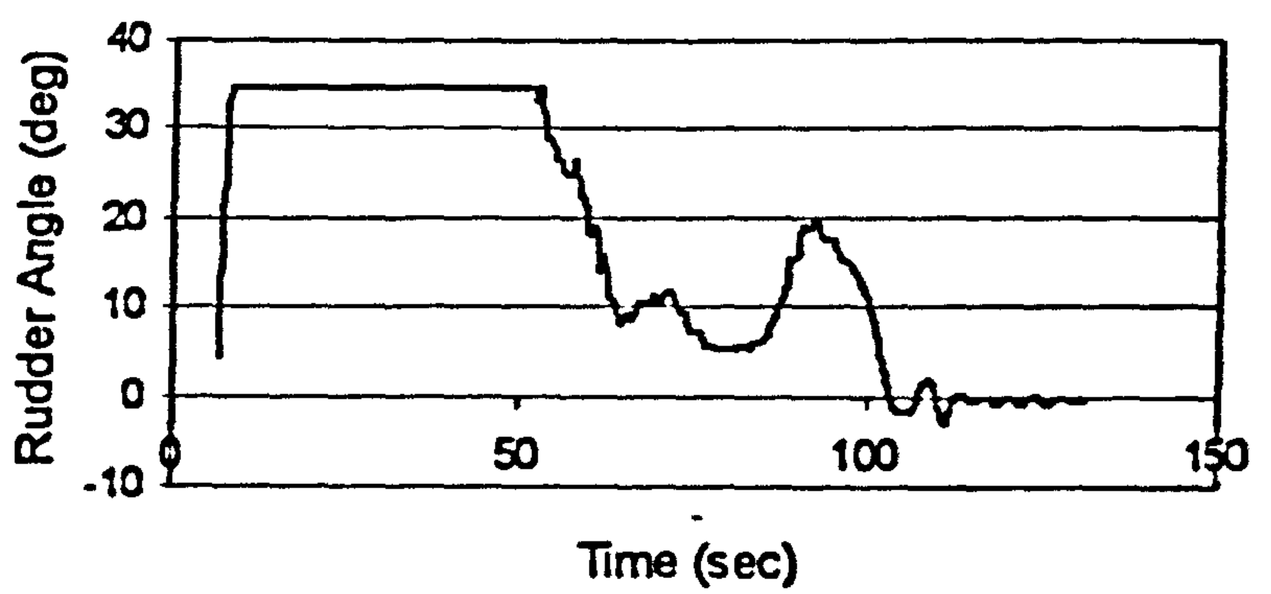

Figure H.19 JONSWAP, Fn=0.4, χ= -5°, H_s=0.115 m, T_p=1.214 sec.

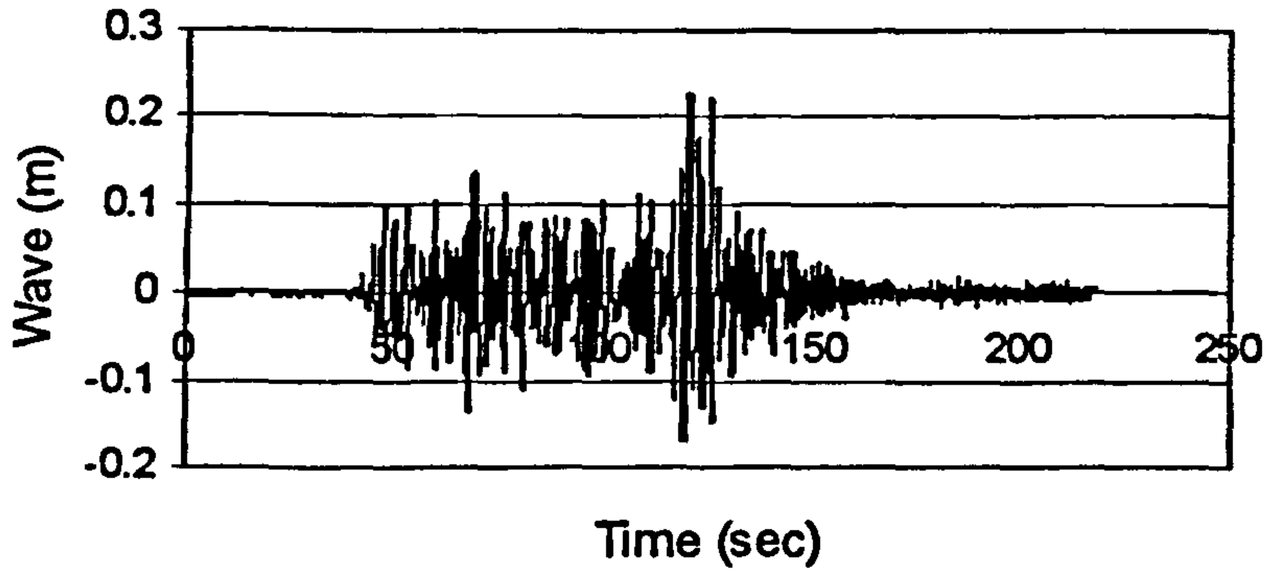

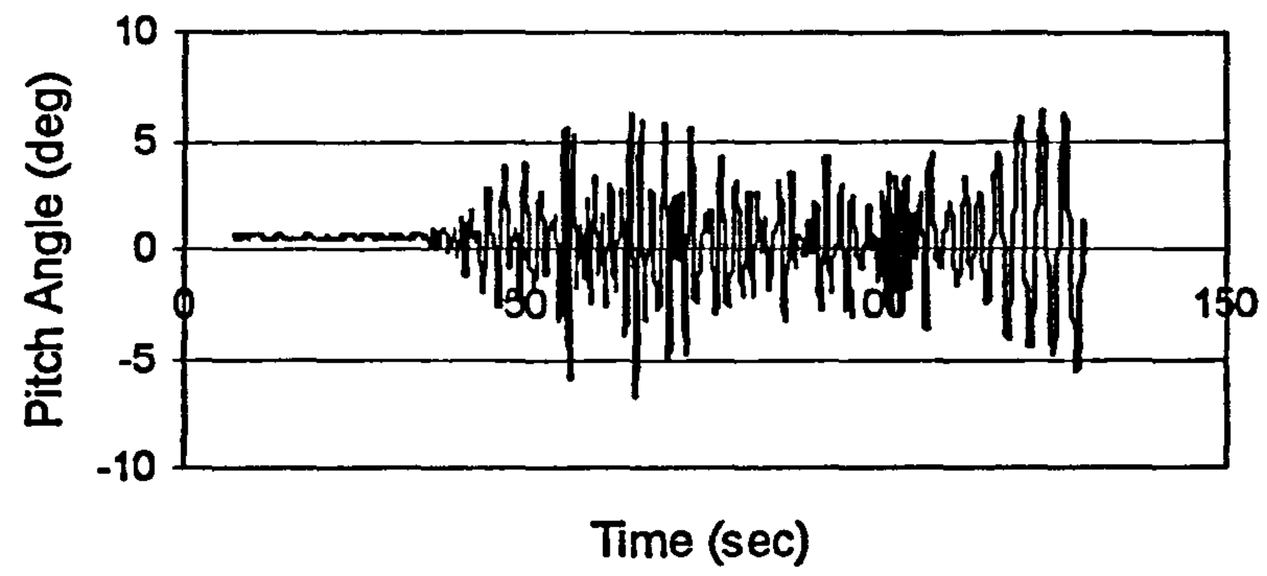

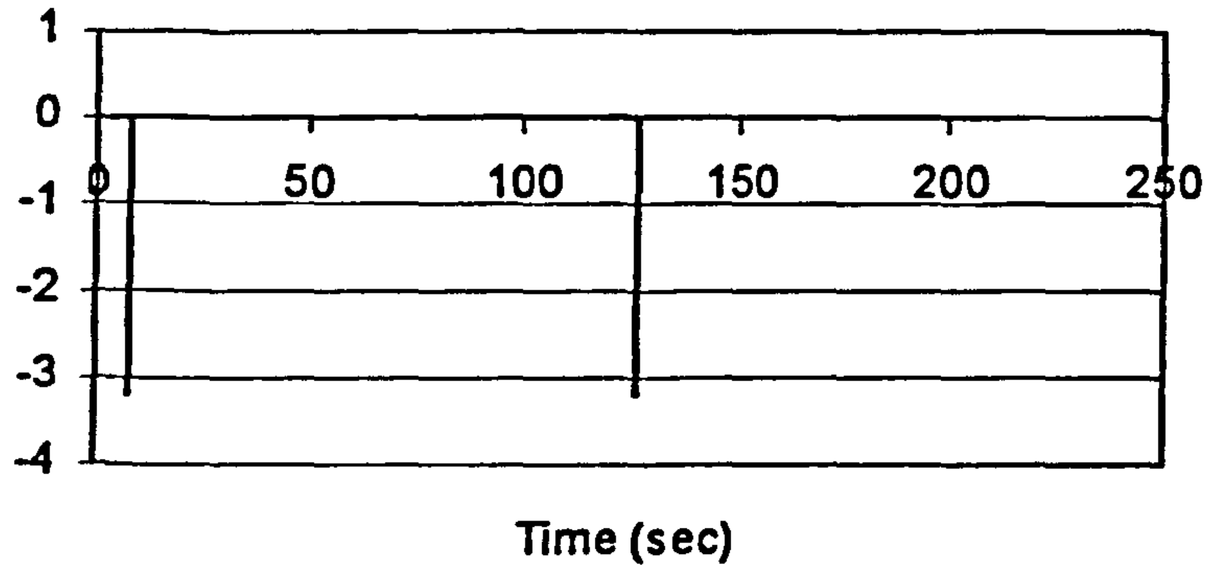

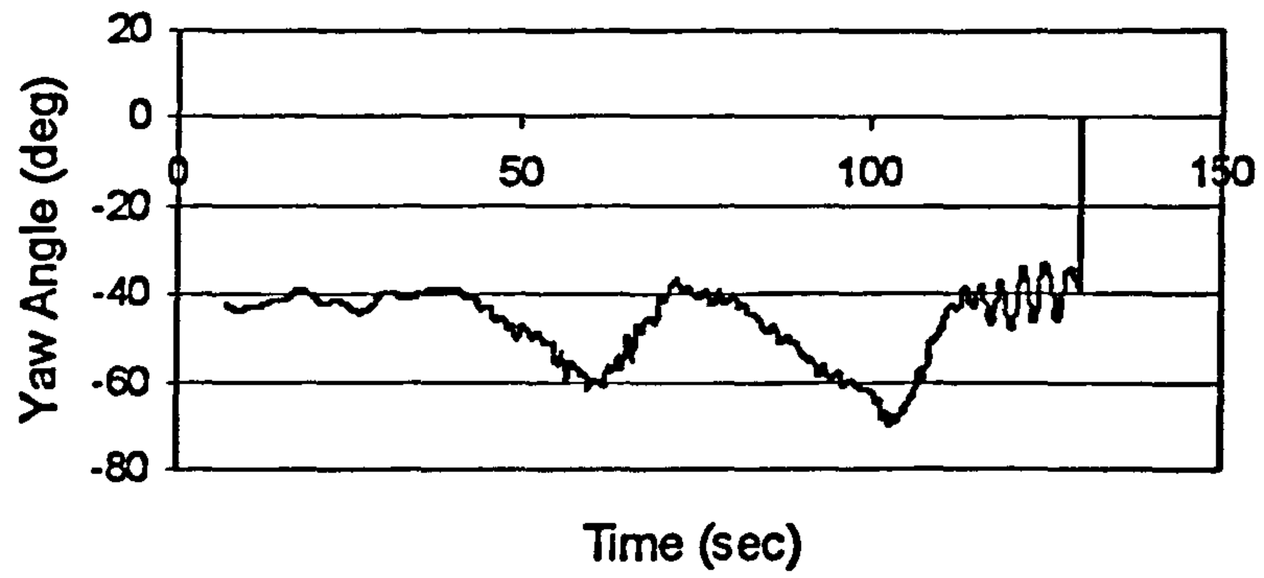

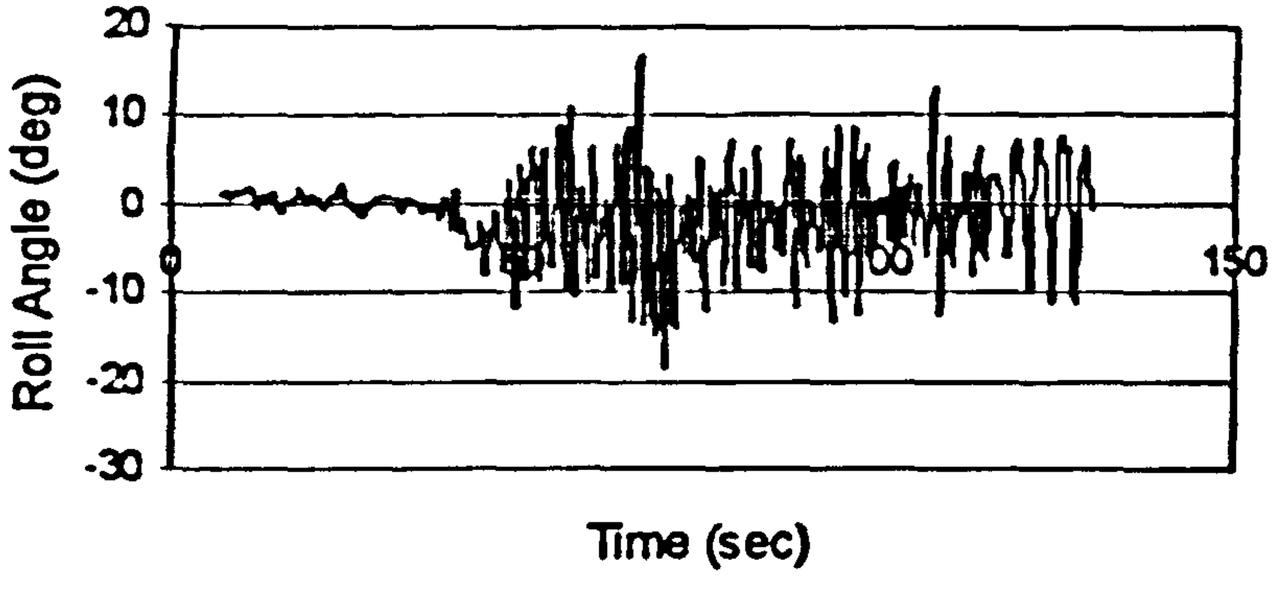

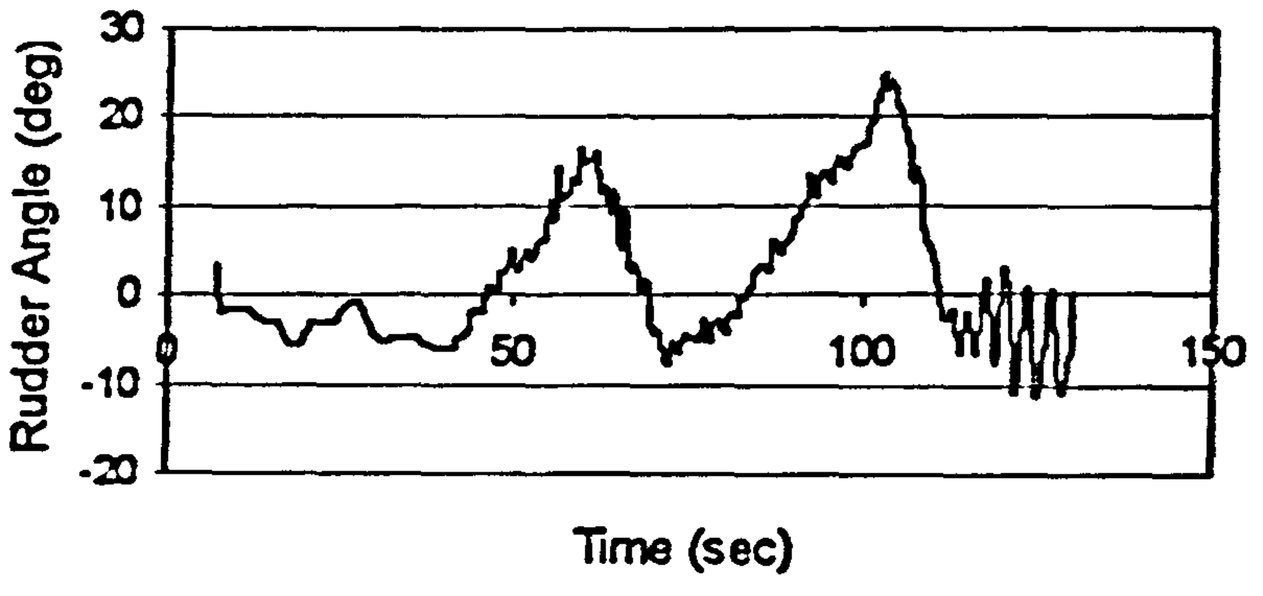

Figure H.20 JONSWAP, Fn=0.3, χ= -45°, H_s=0.115 m, T_p=1.214 sec.

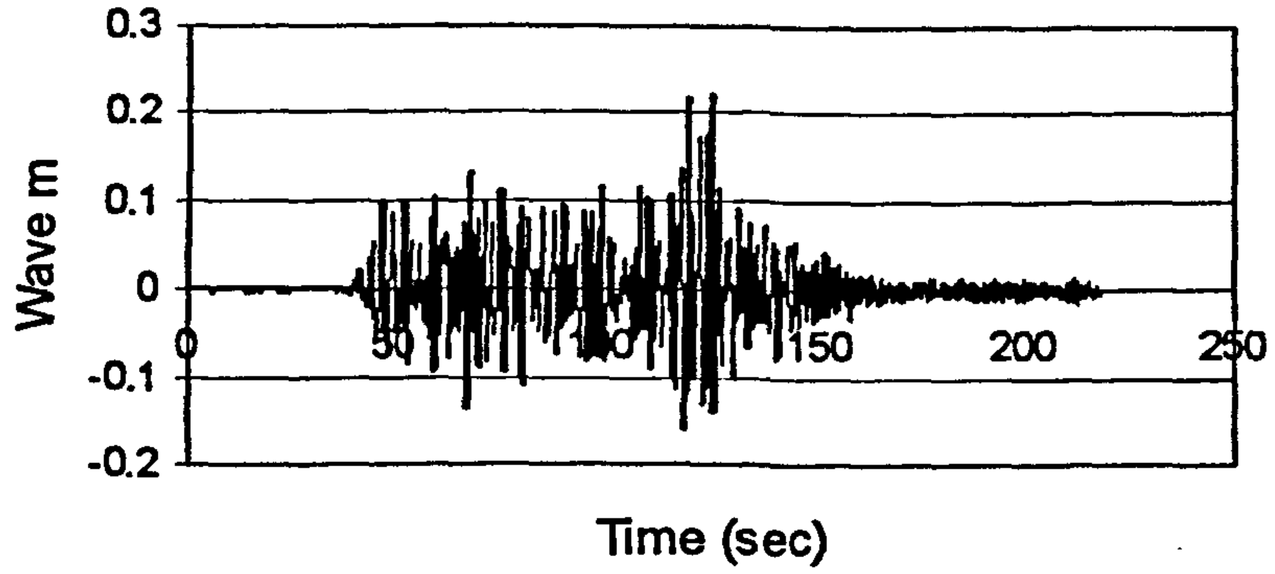

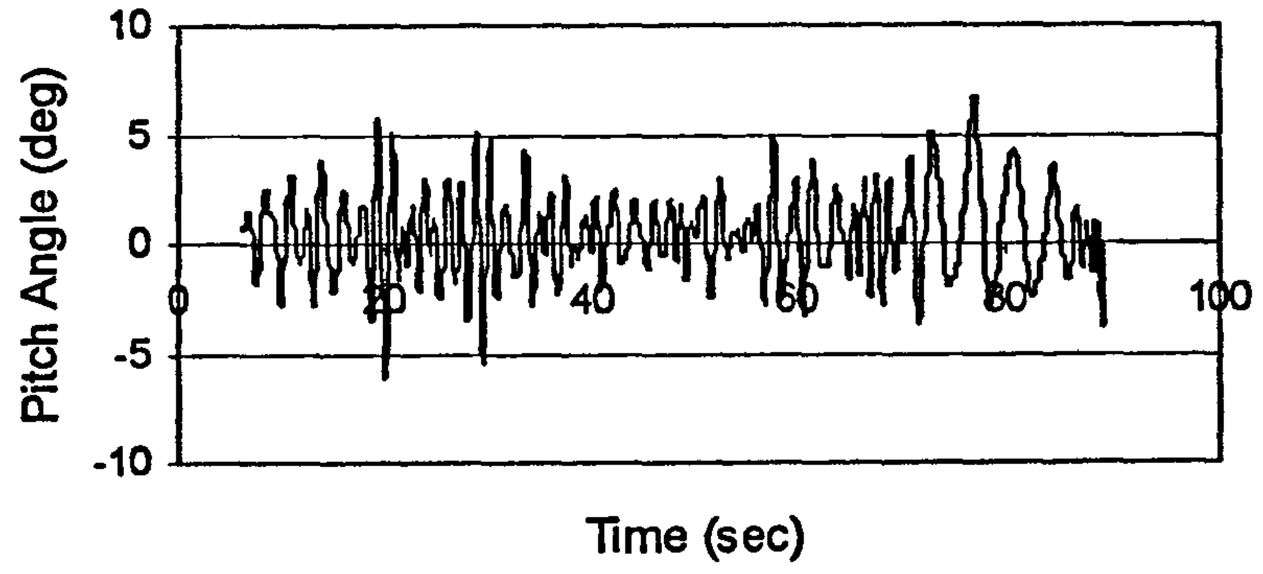

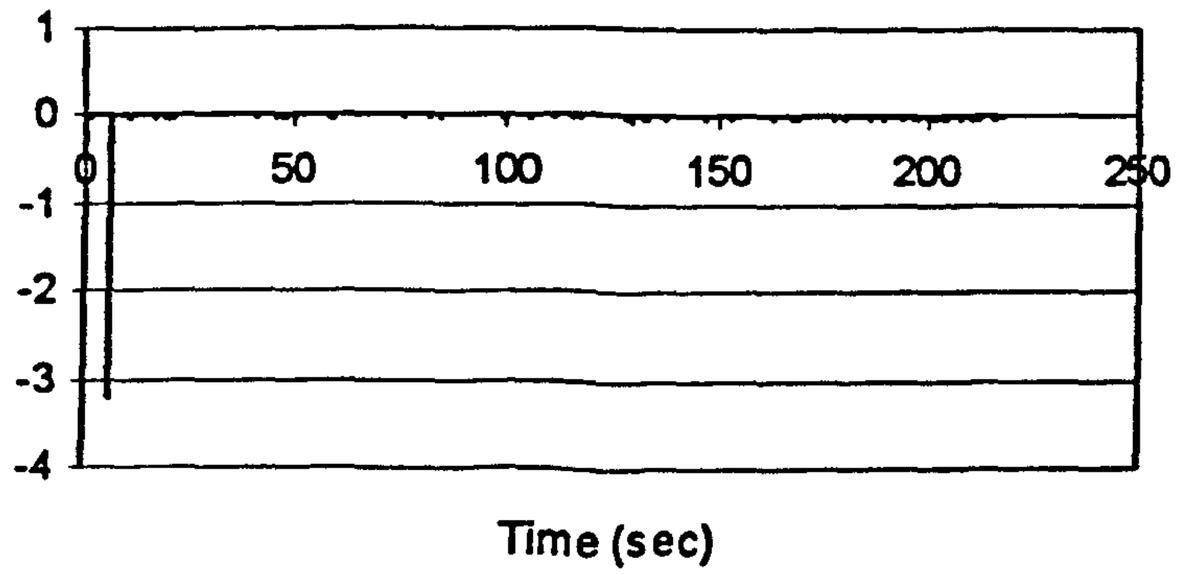

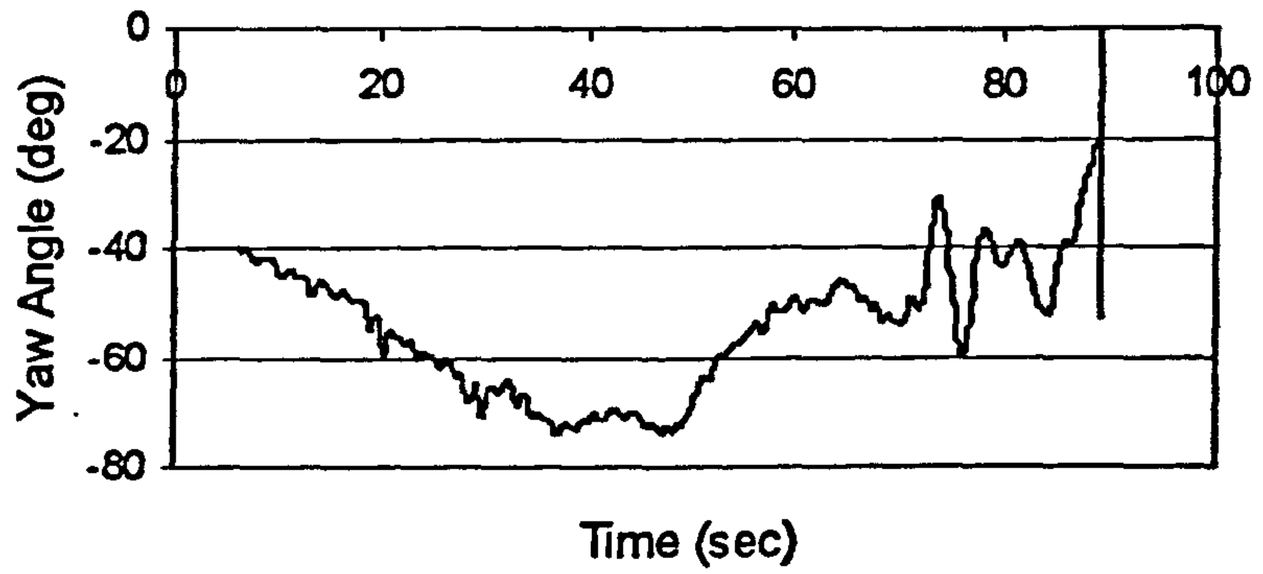

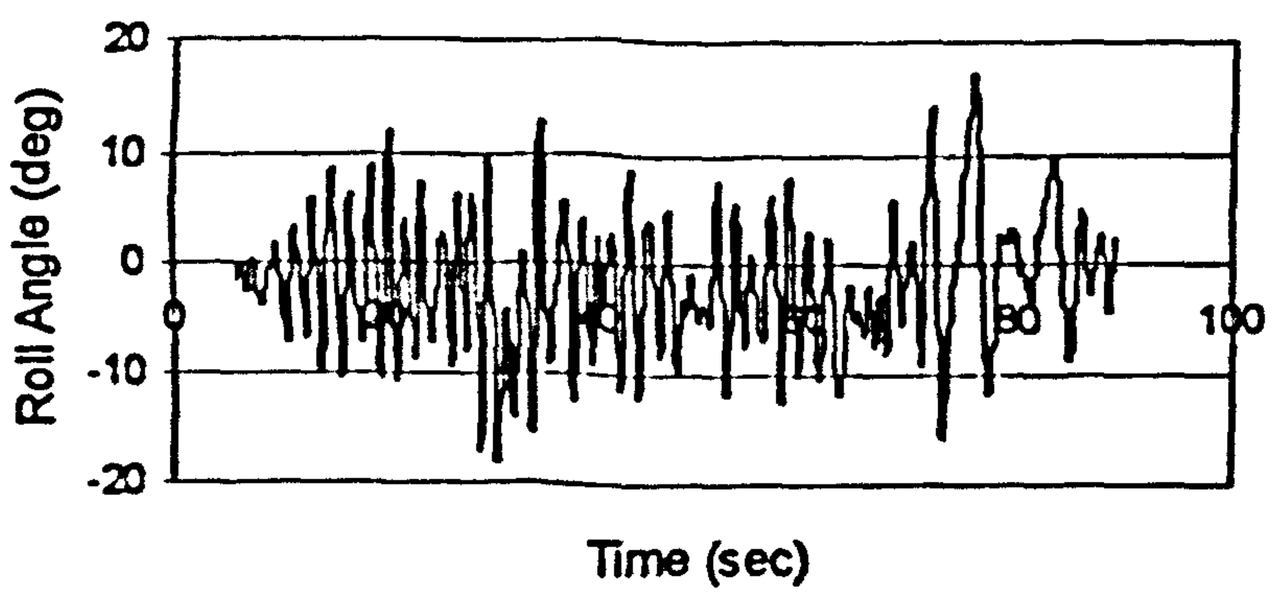

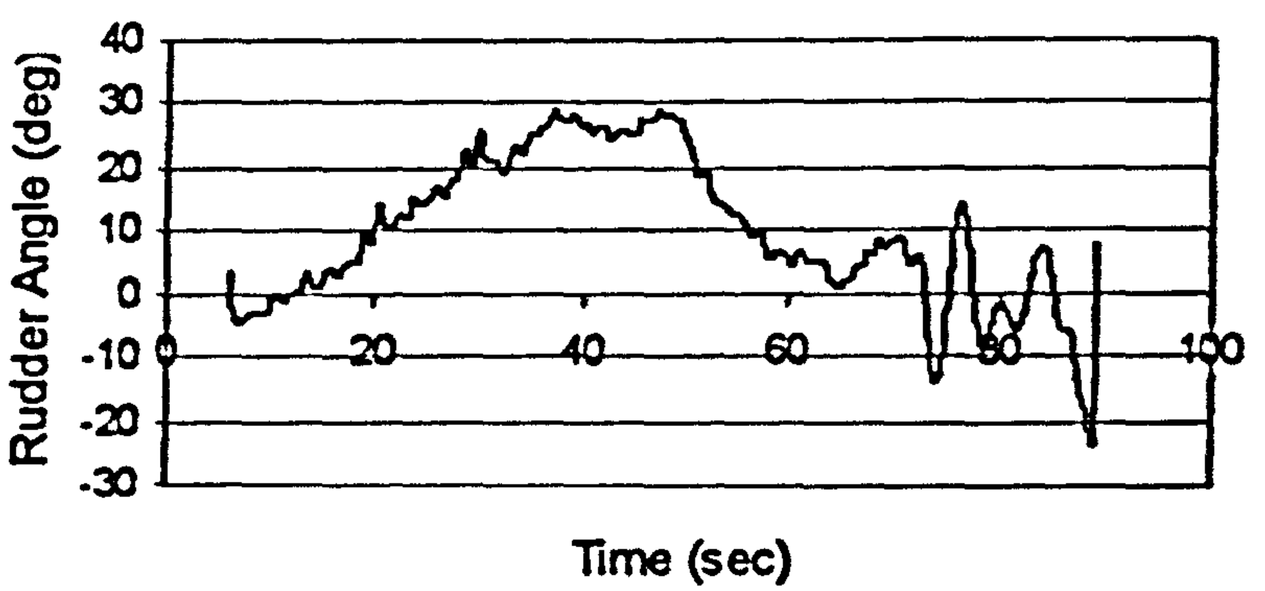

Figure H.21 JONSWAP, Fn=0.4, χ= -45°, H_s=0.115 m, T_p=1.214 sec.

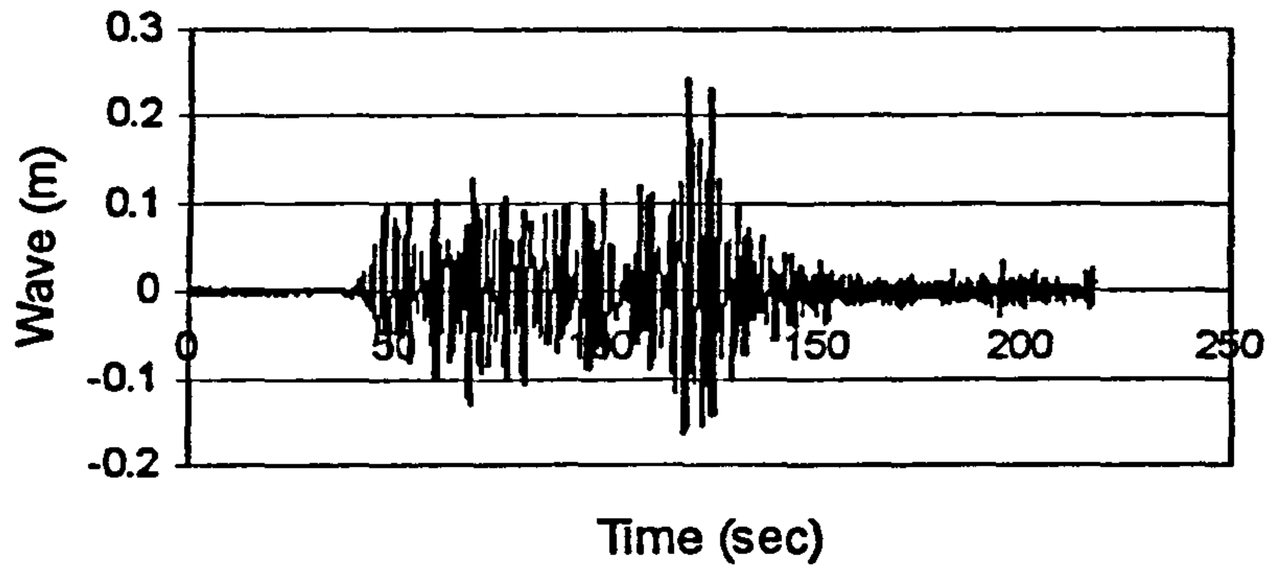

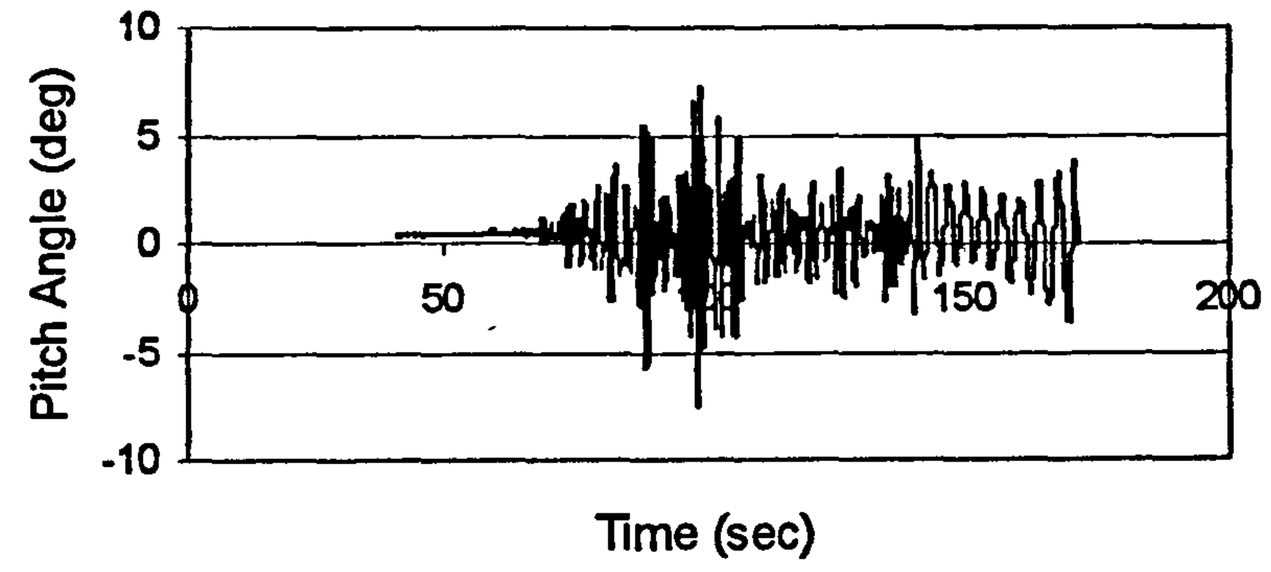

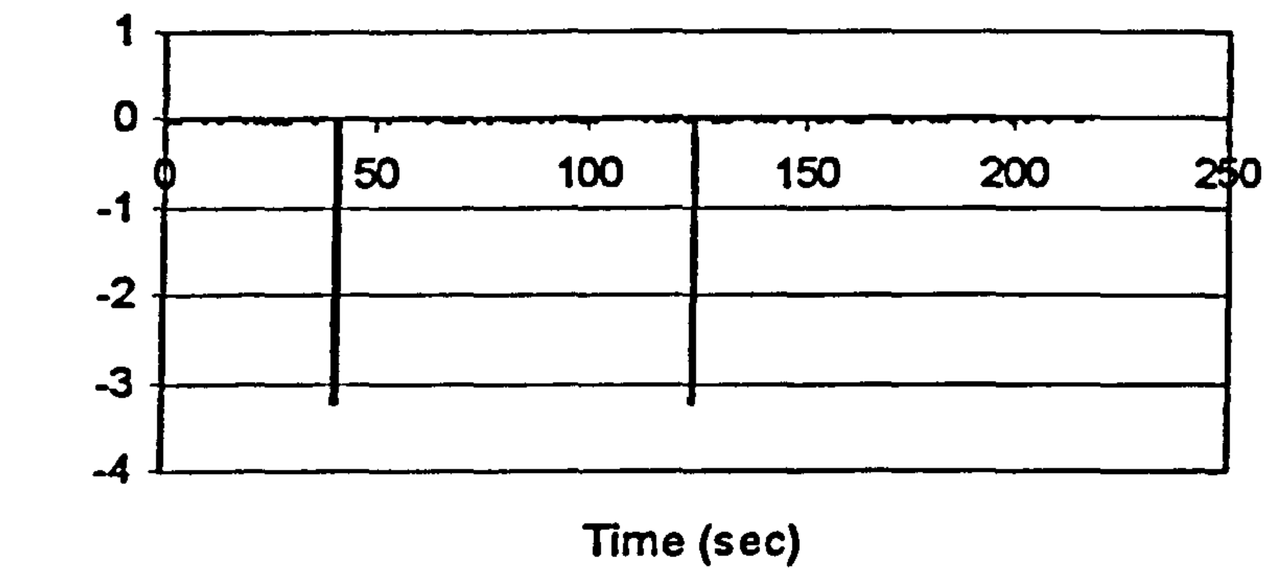

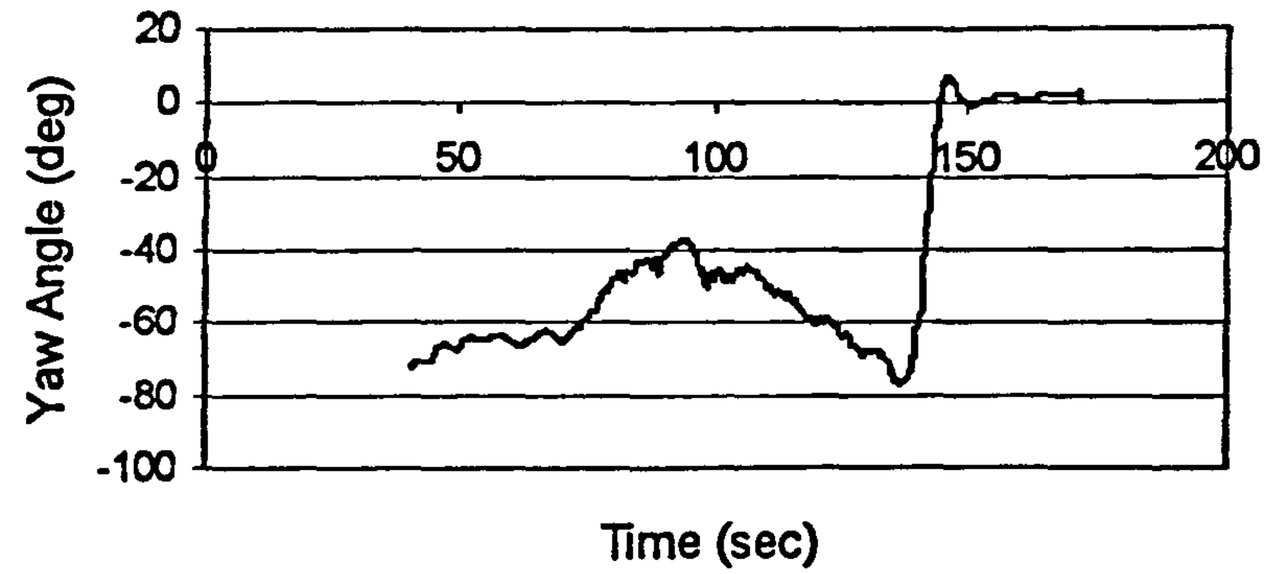

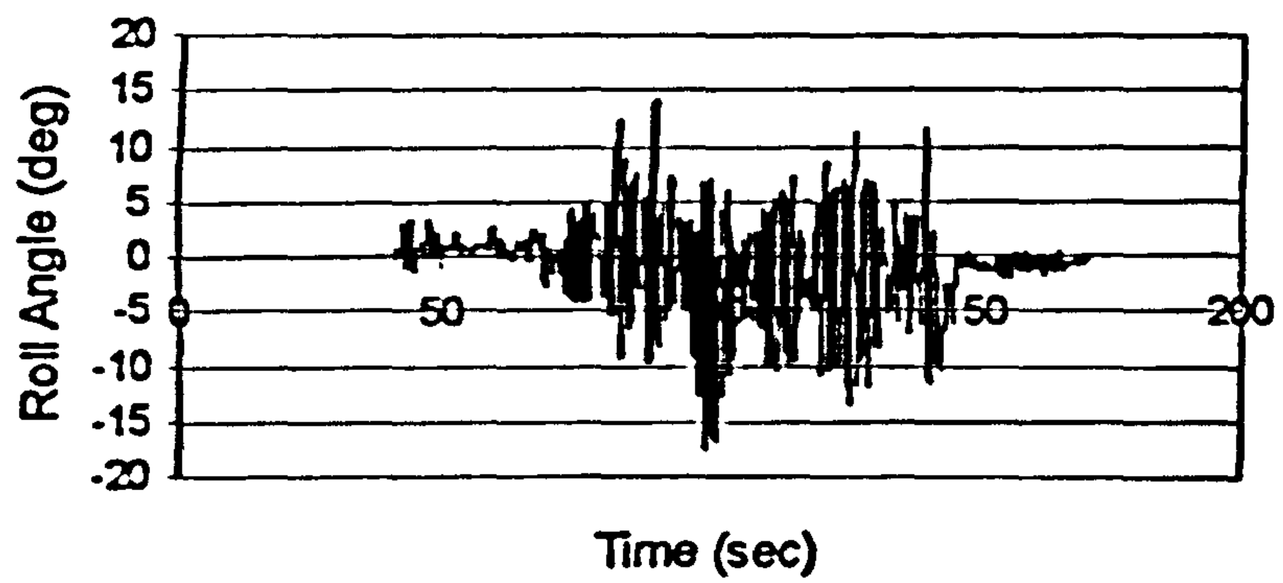

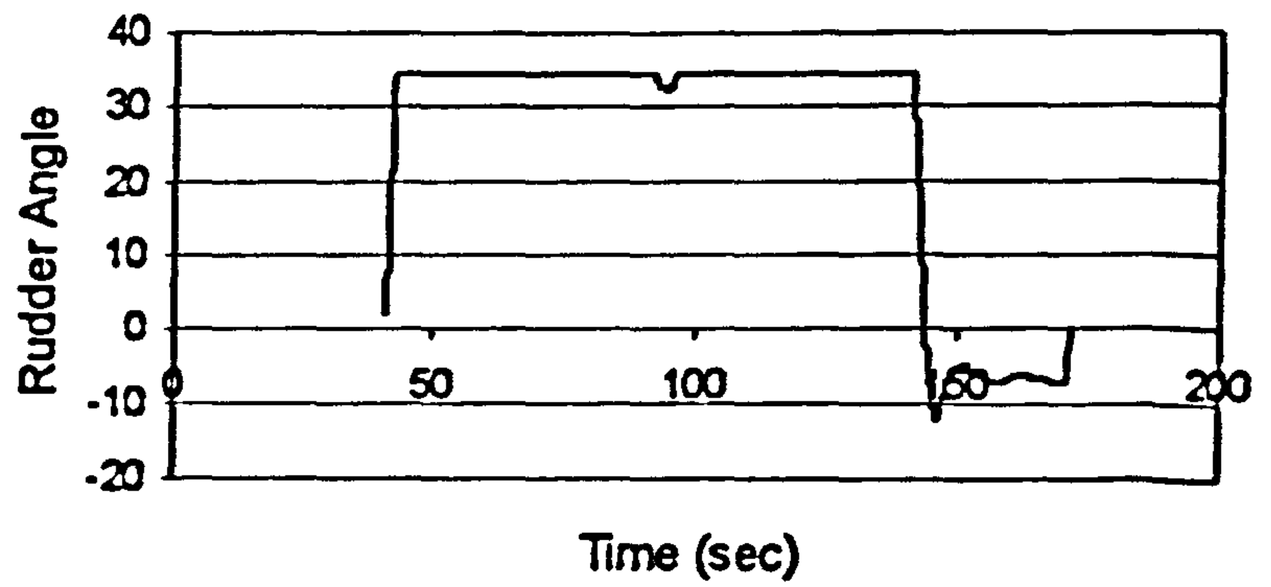

Figure H.22 JONSWAP, Fn=0.3, χ= -5°, H_s=0.1725 m, T_p=1.487 sec.

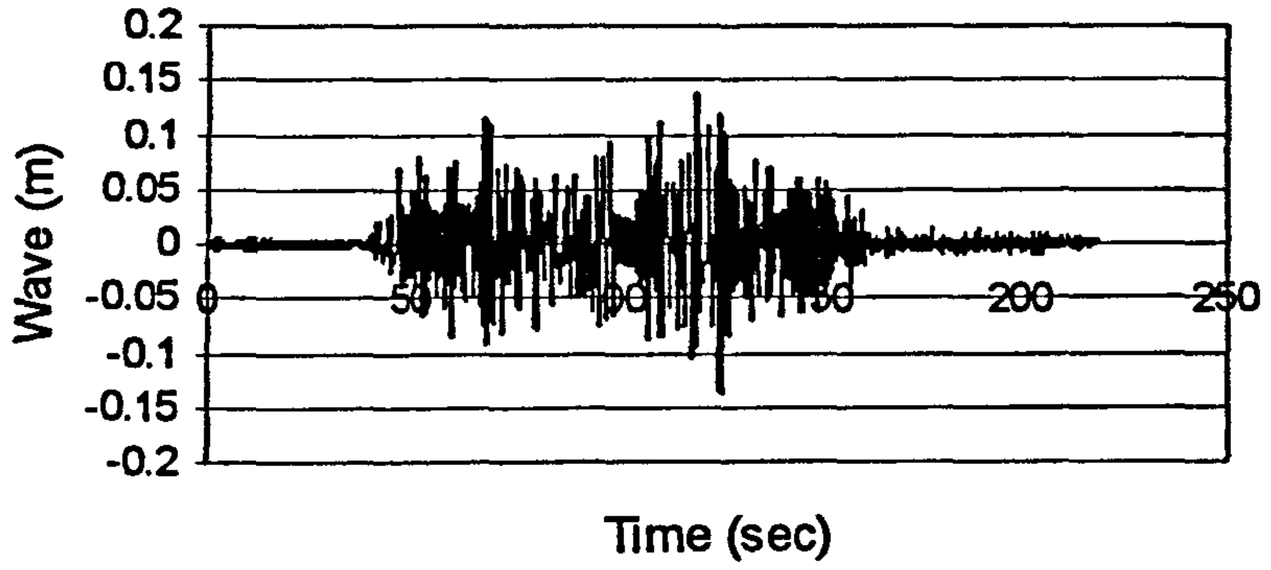

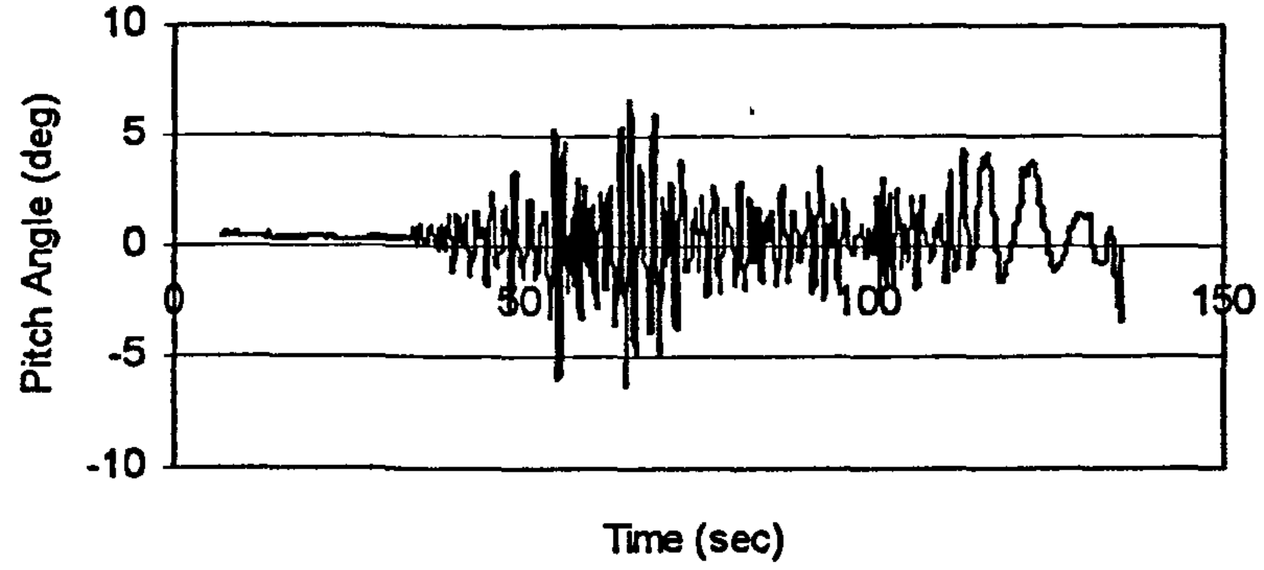

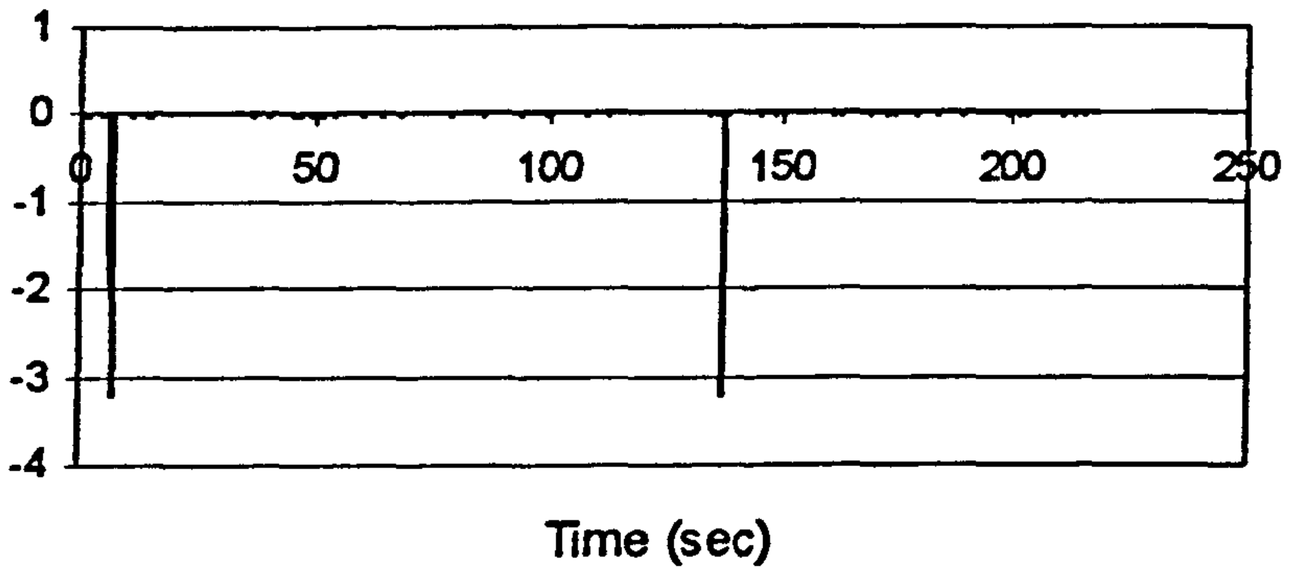

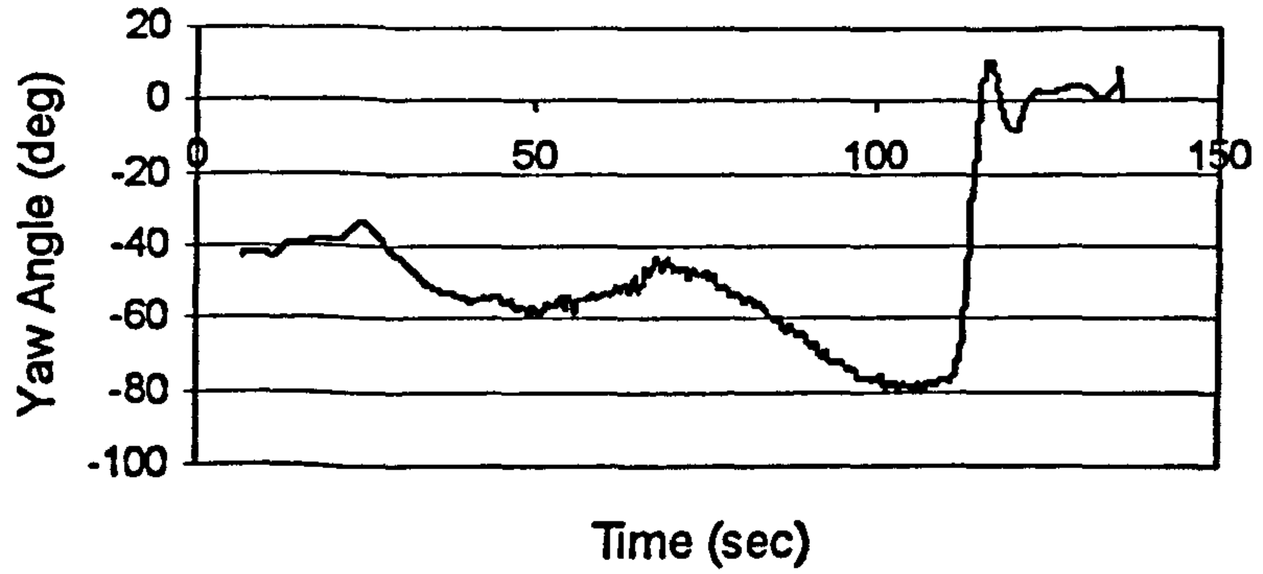

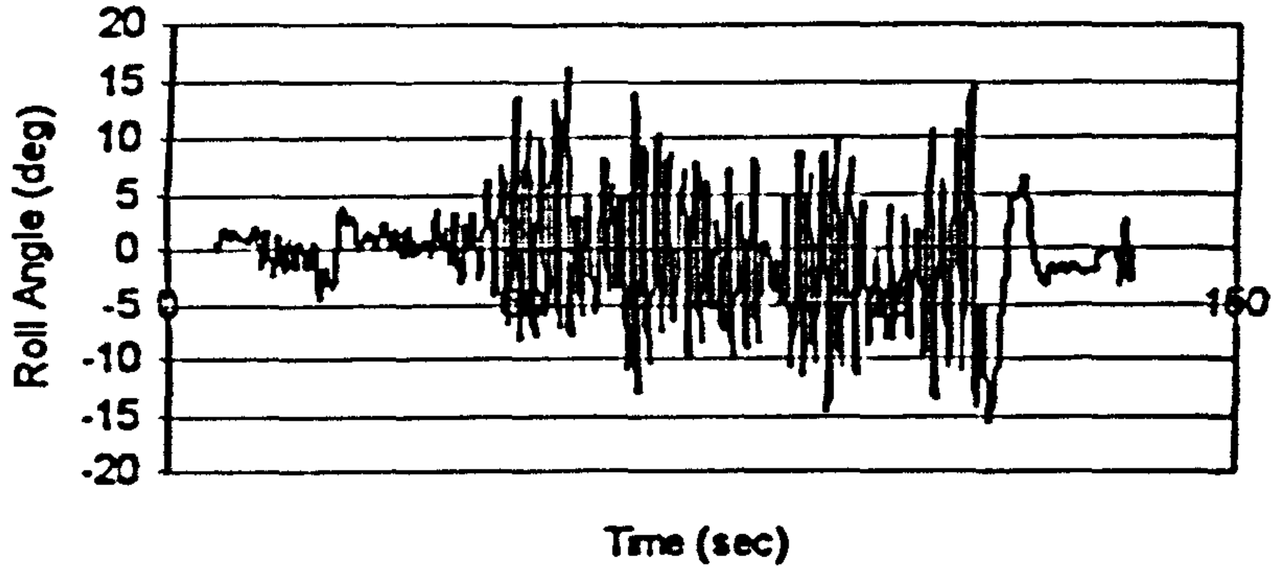

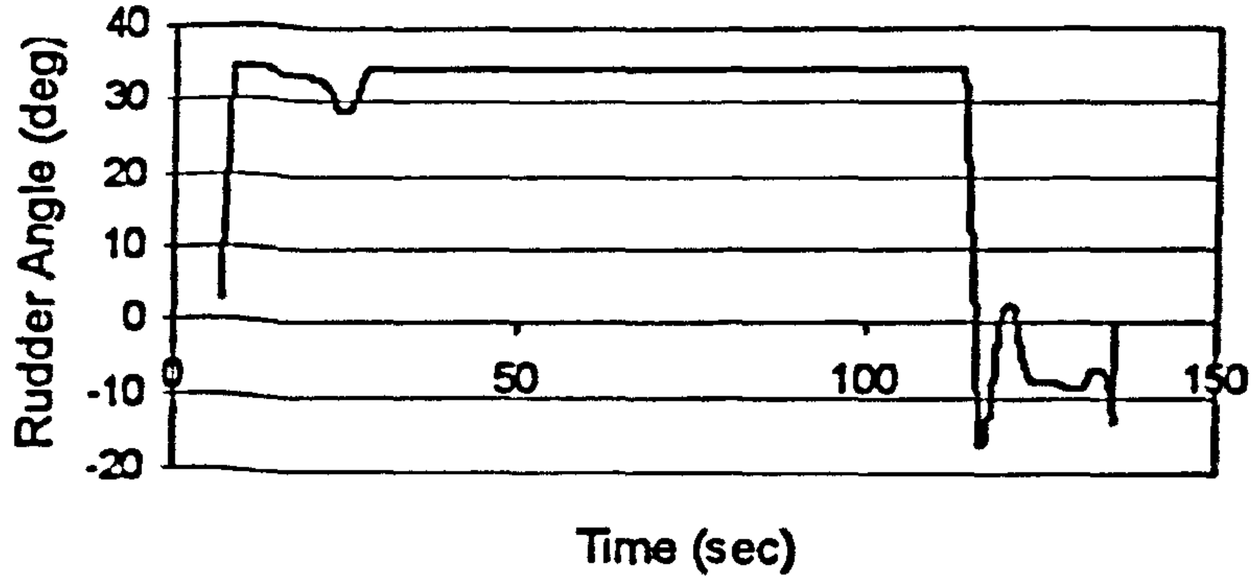

Figure H.23 JONSWAP, Fn=0.4, χ= -5°, H_s=0.1725 m, T_p=1.487 sec.

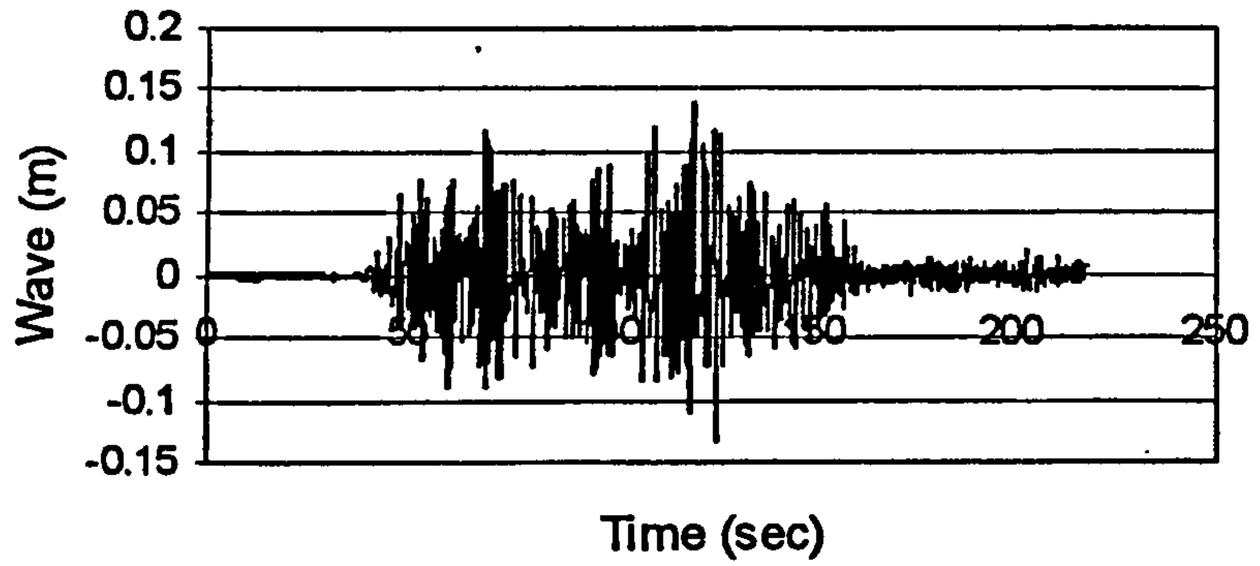

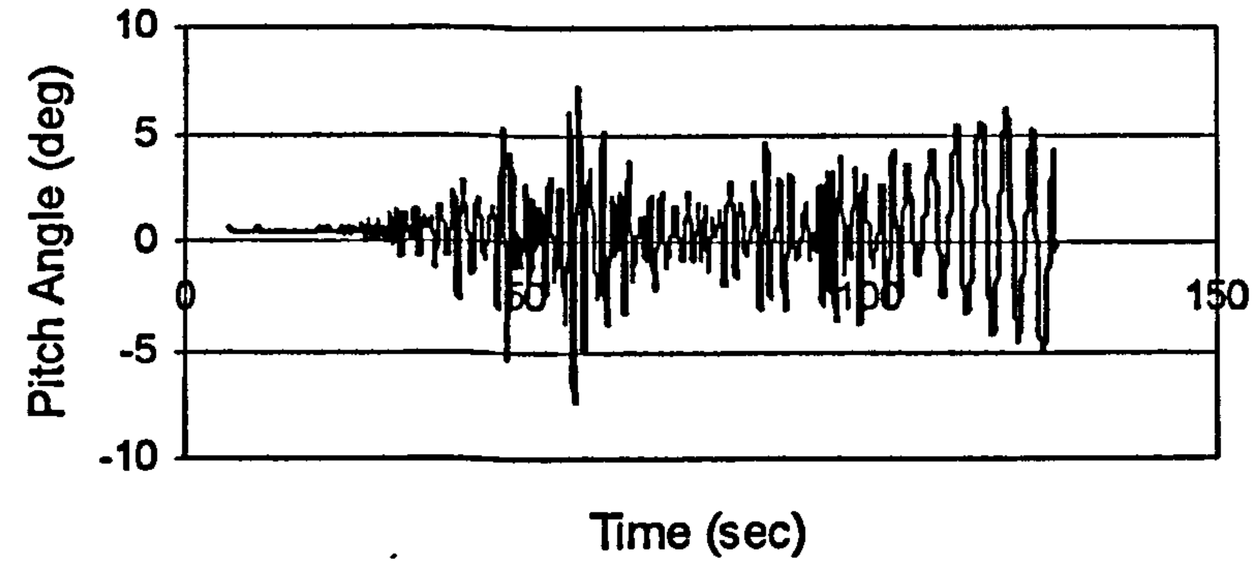

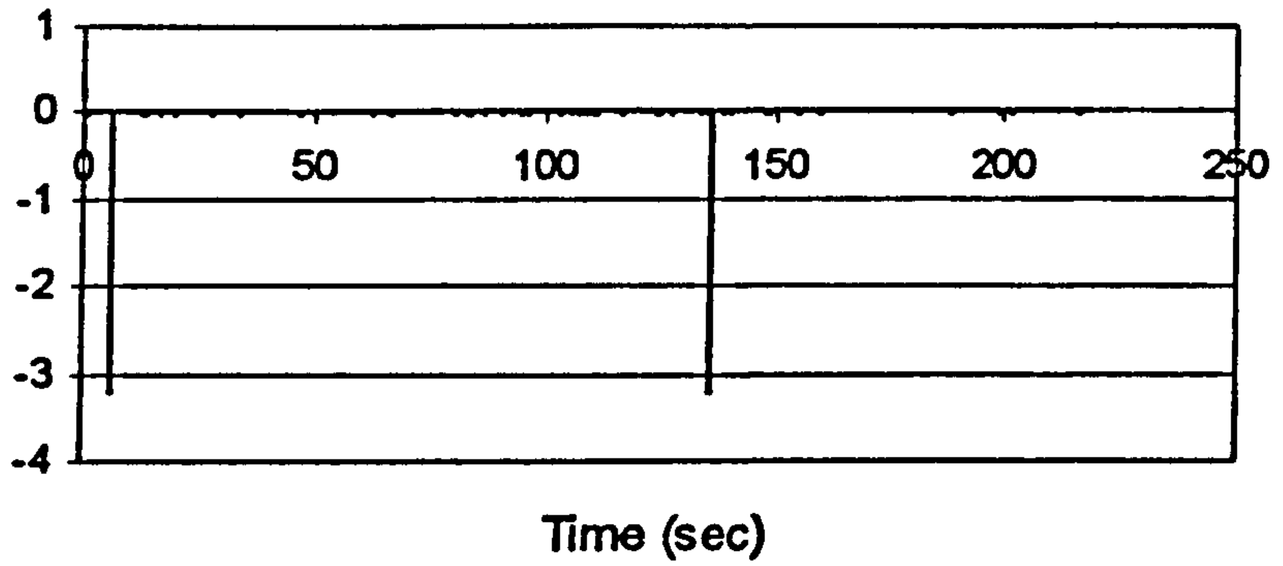

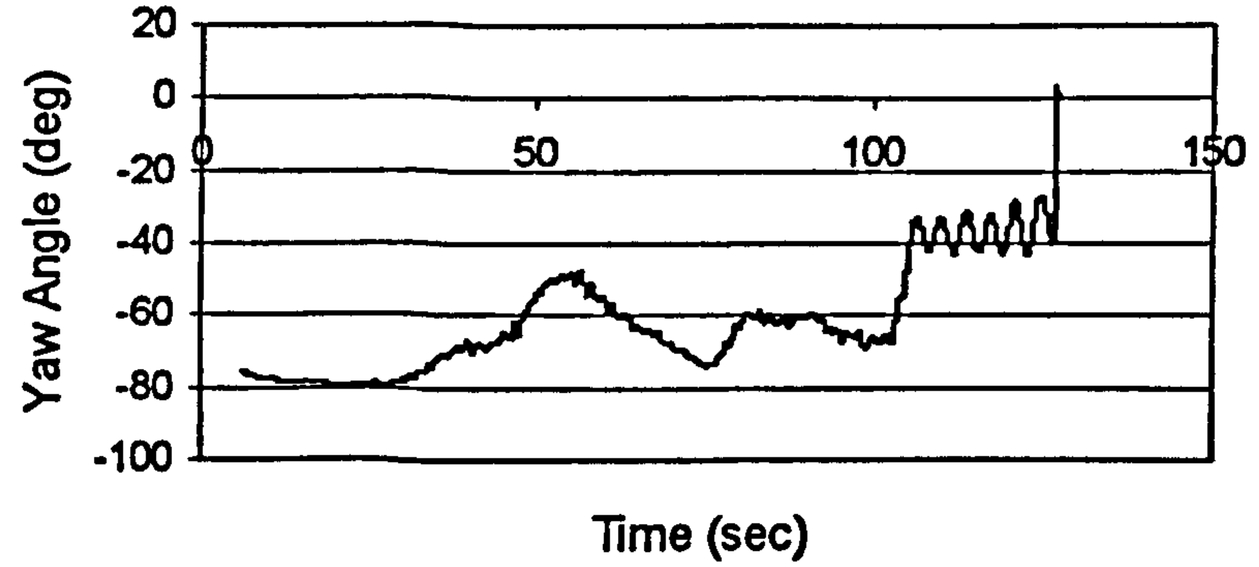

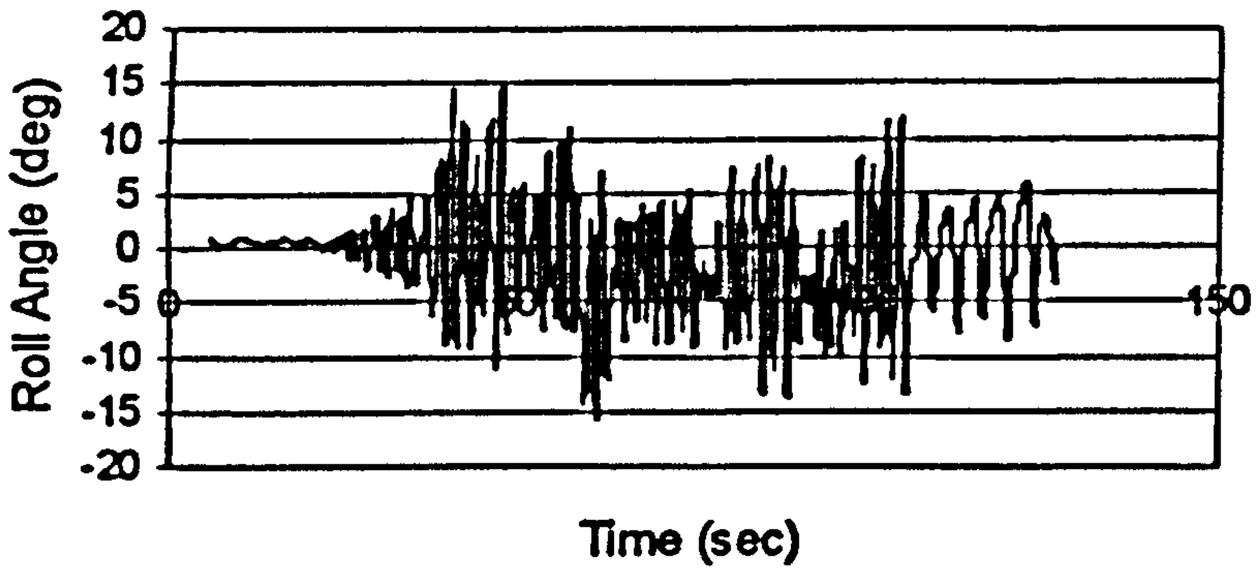

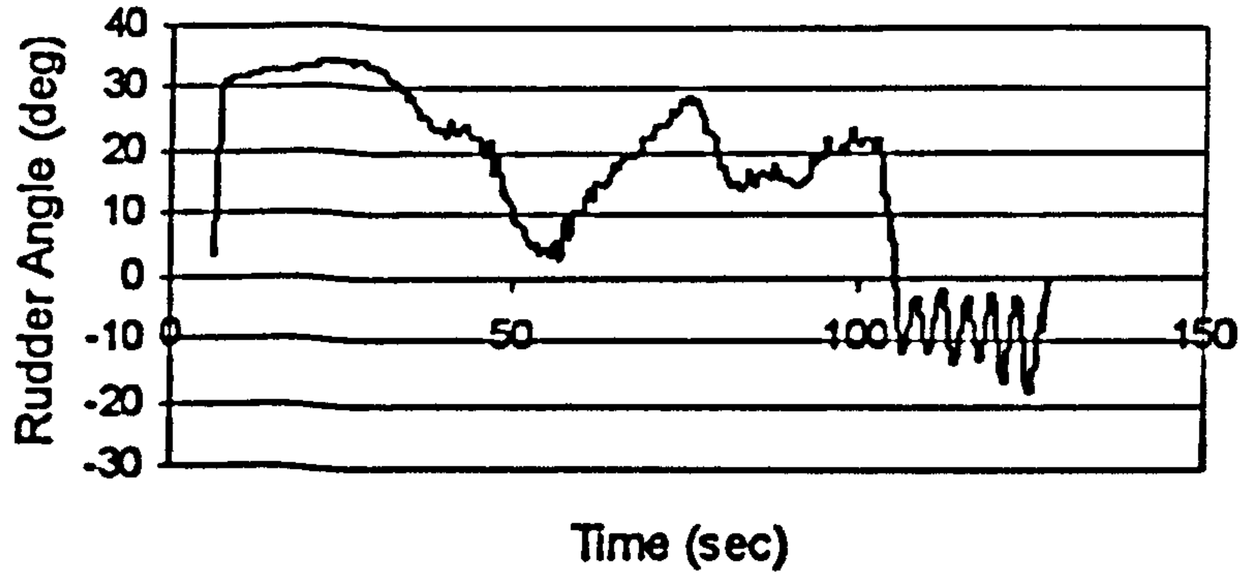

Figure H.24 JONSWAP, Fn=0.3, χ= -45°, H_s=0.1725 m, T_p=1.487 sec.

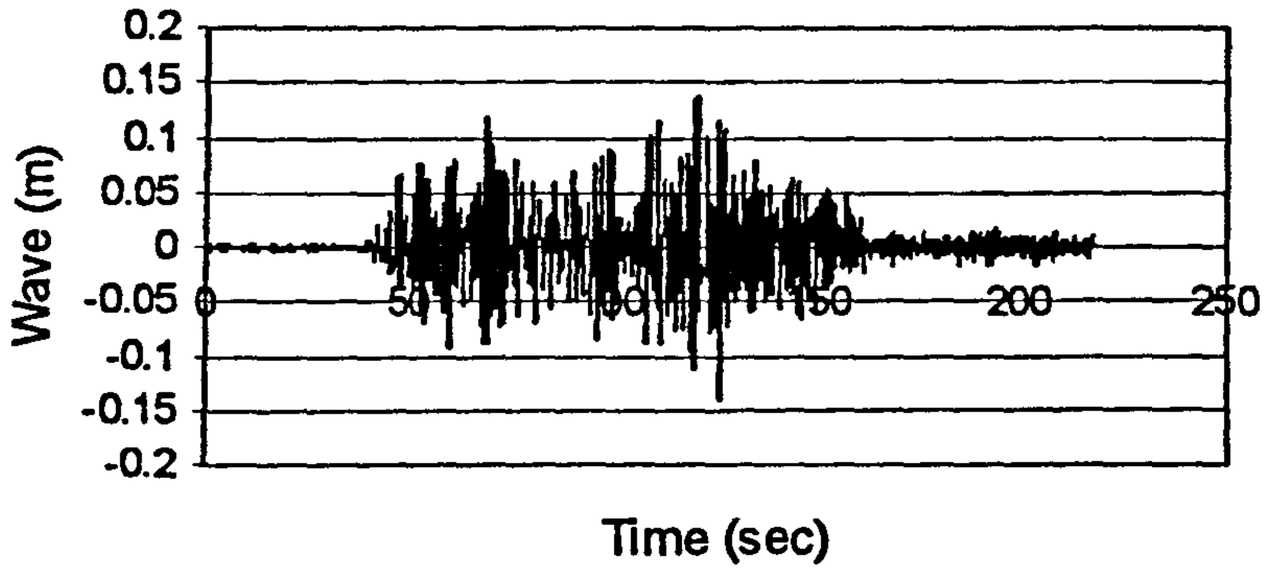

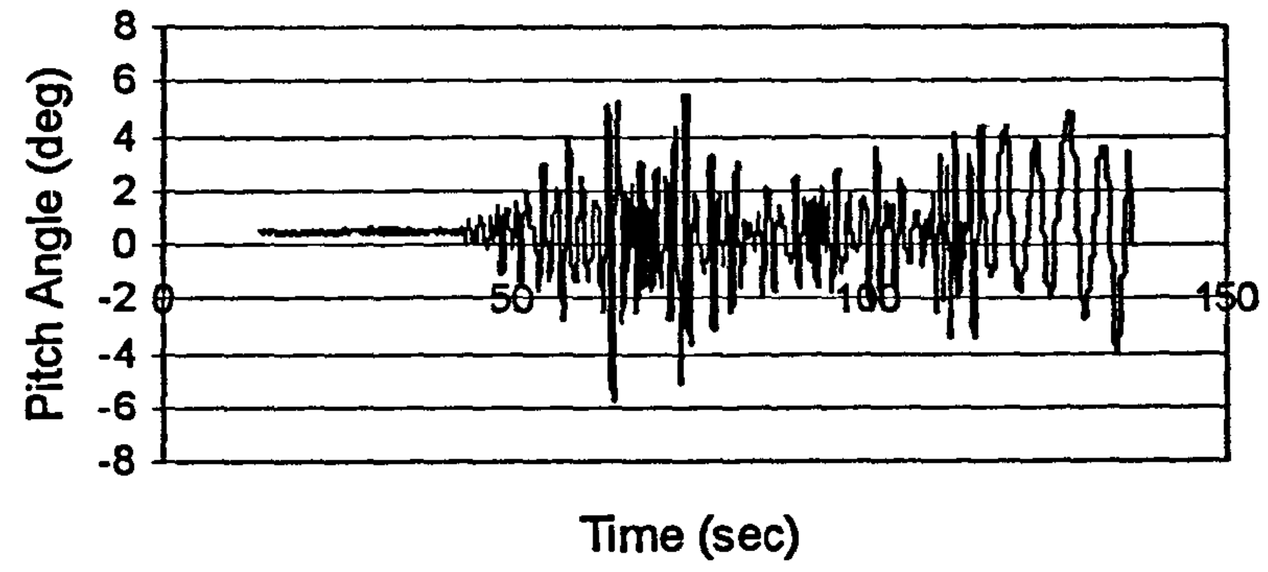

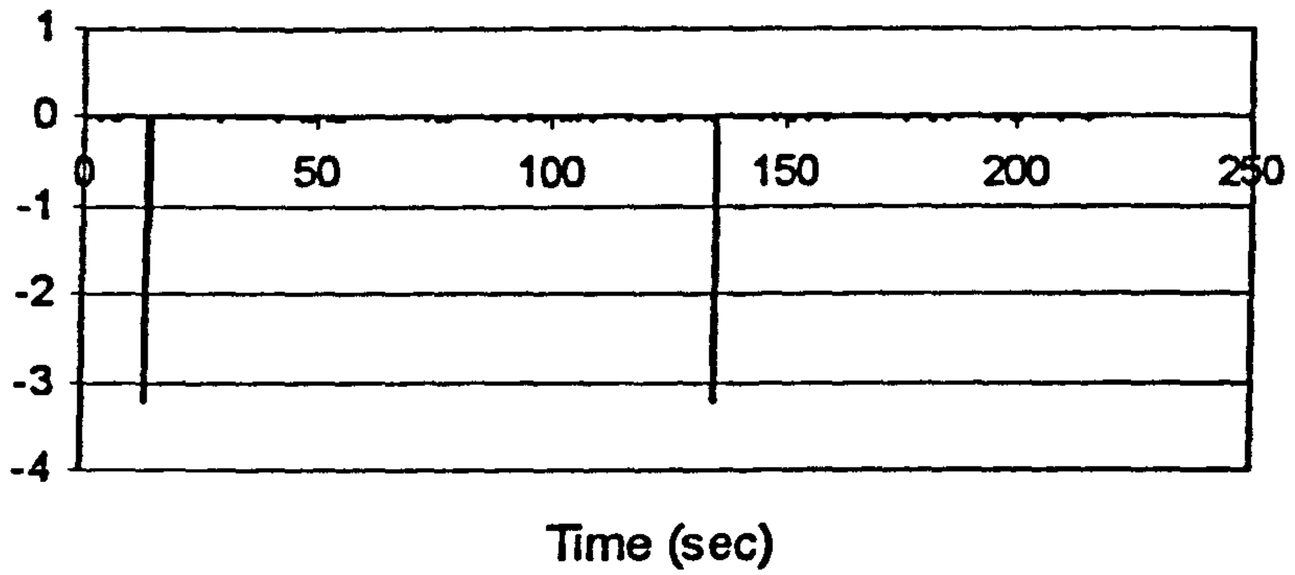

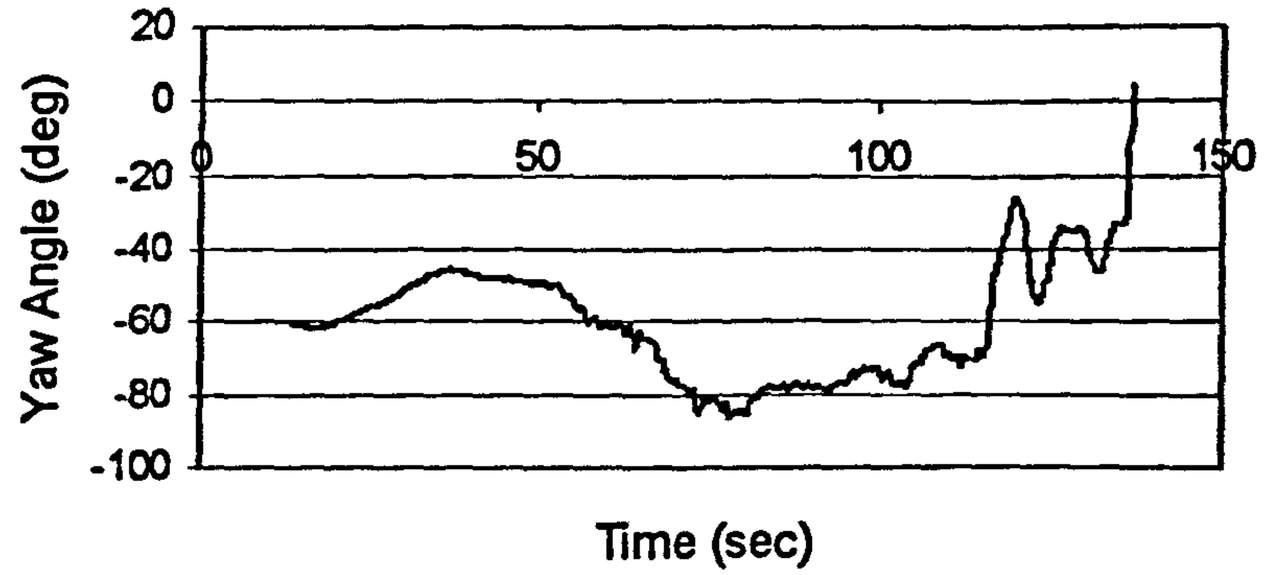

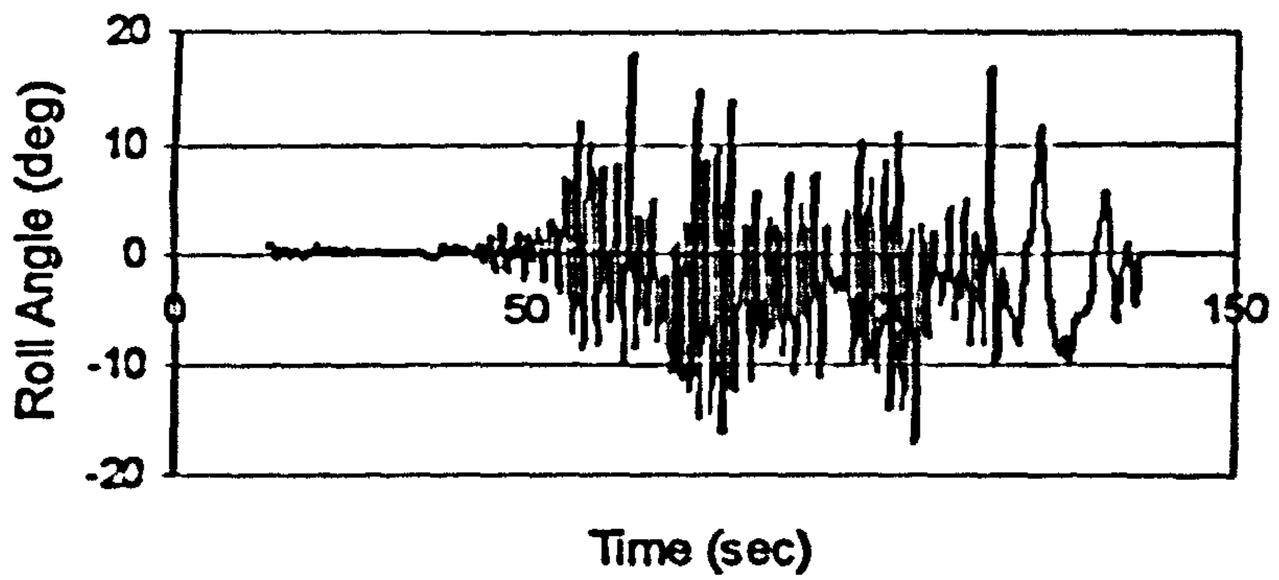

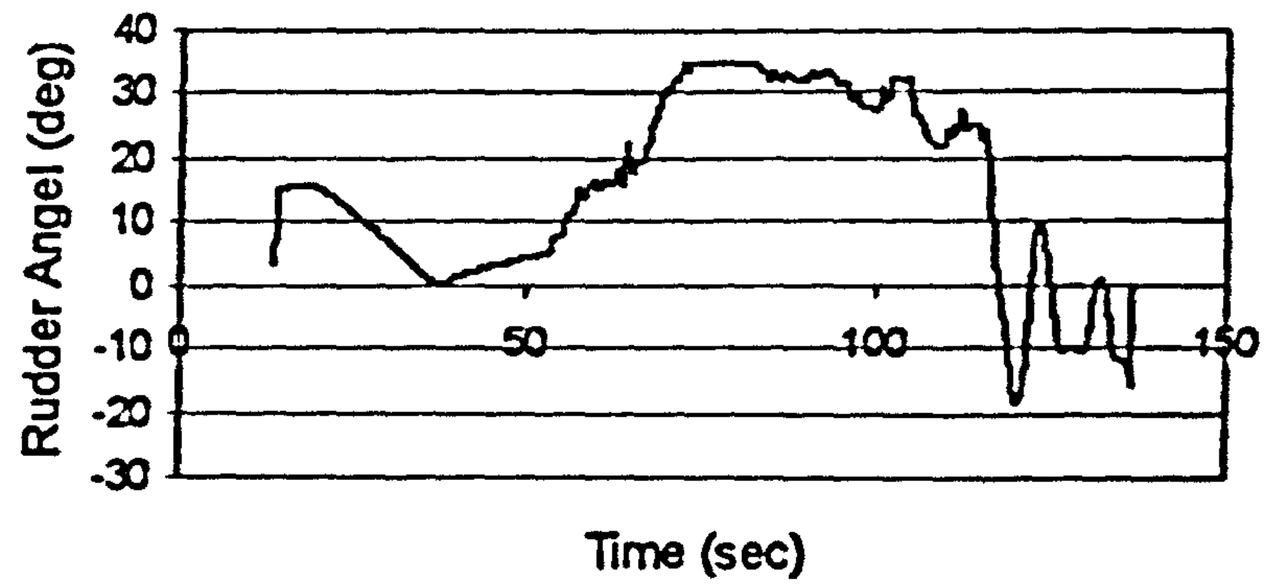

Figure H.25 JONSWAP, Fn=0.4, χ= -45°, H_s=0.1725 m, T_p=1.487 sec.

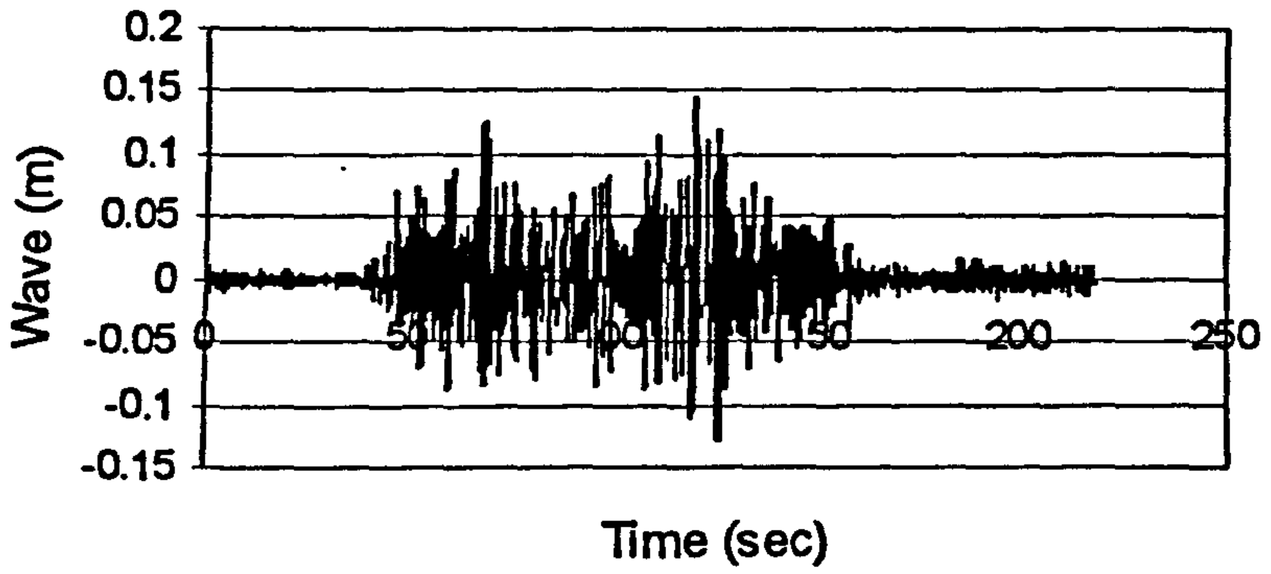

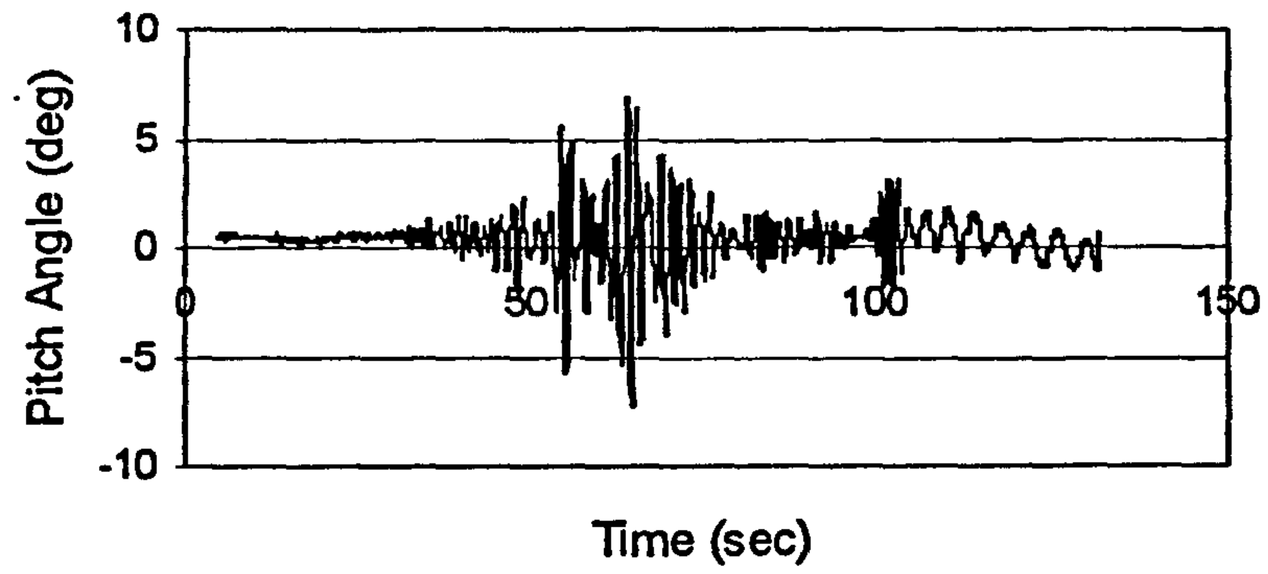

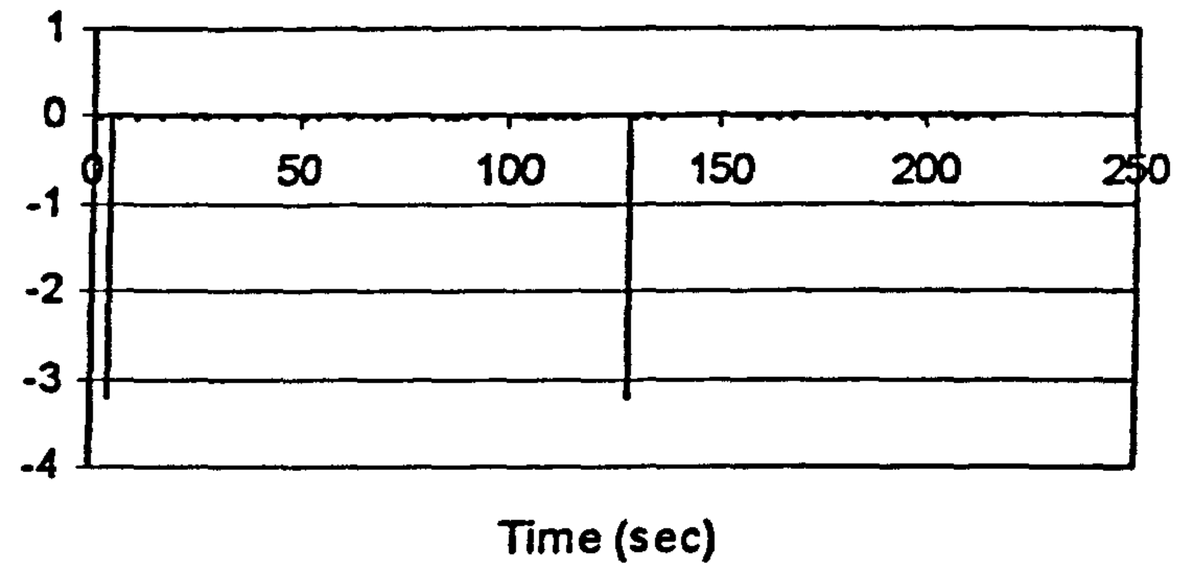

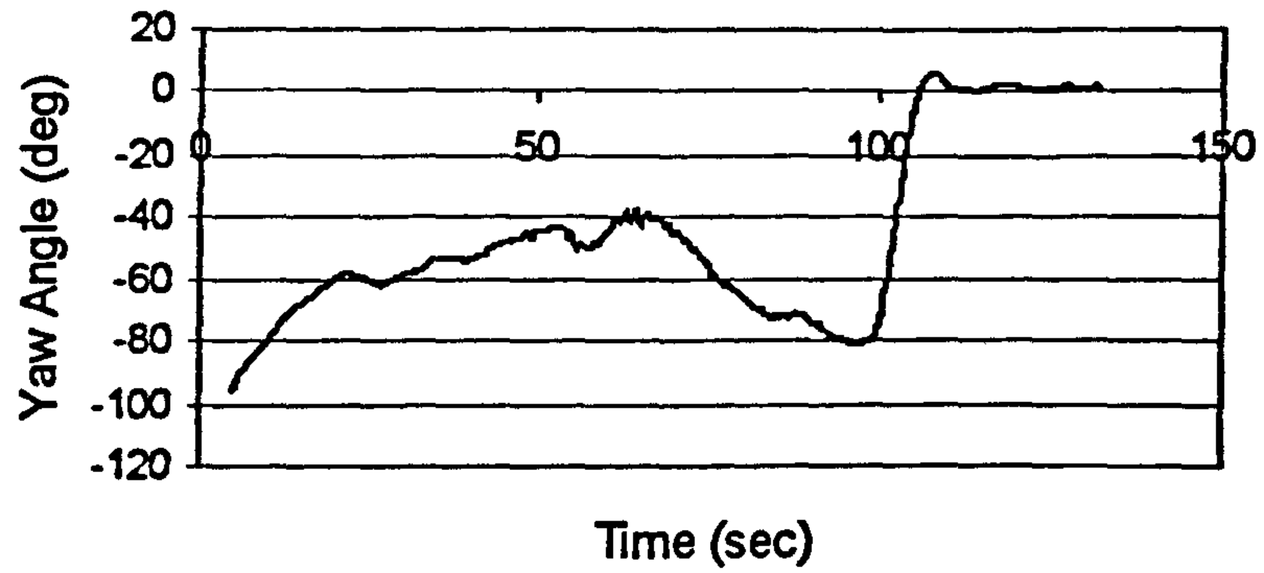

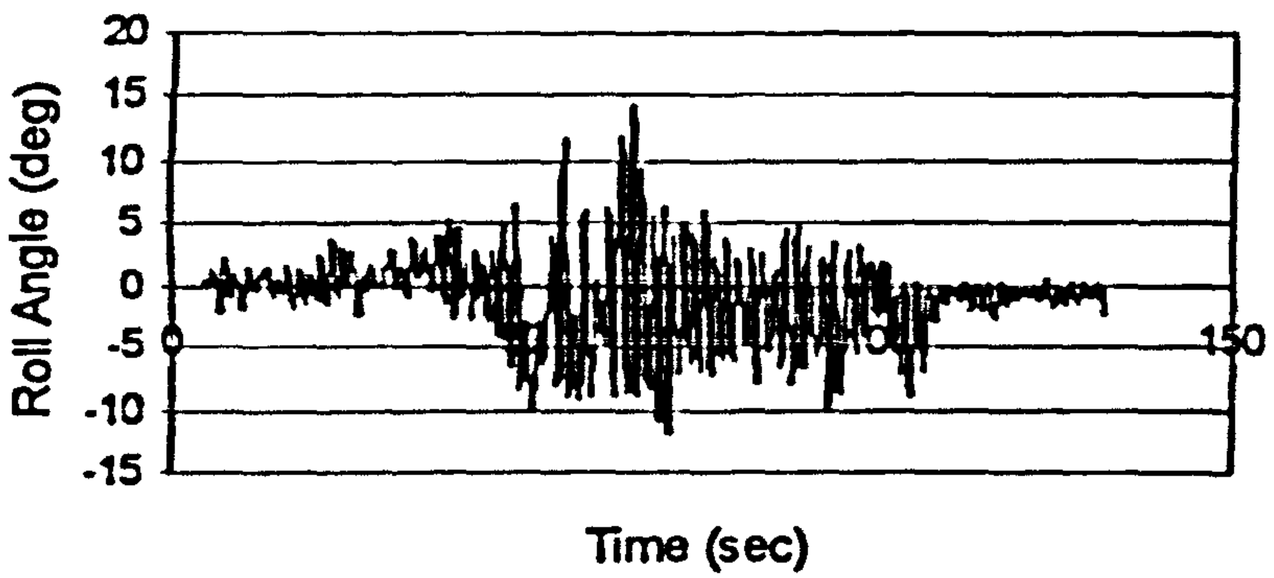

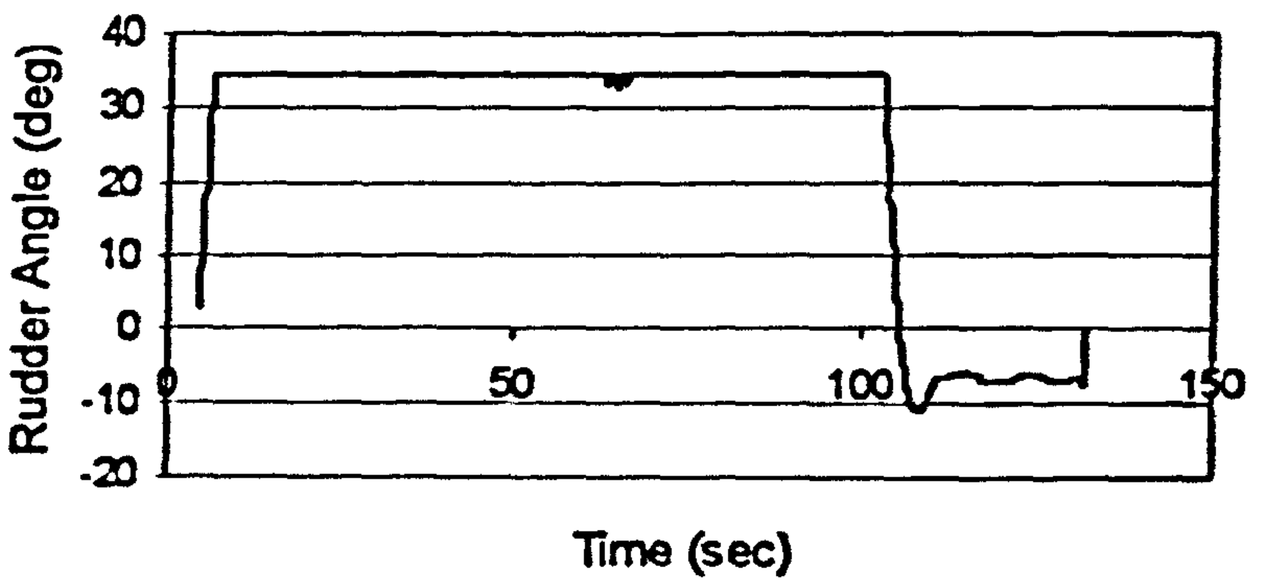

Figure H.26 JONSWAP, Fn=0.3, χ= -5°, H_s=0.23 m, T_p=1.717 sec.

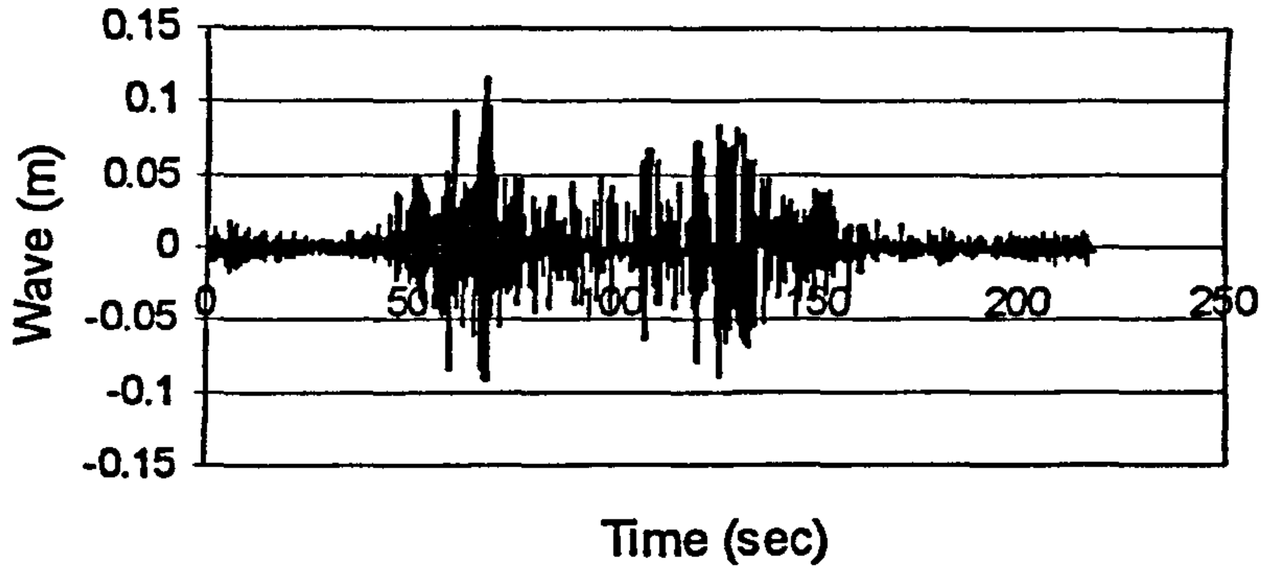

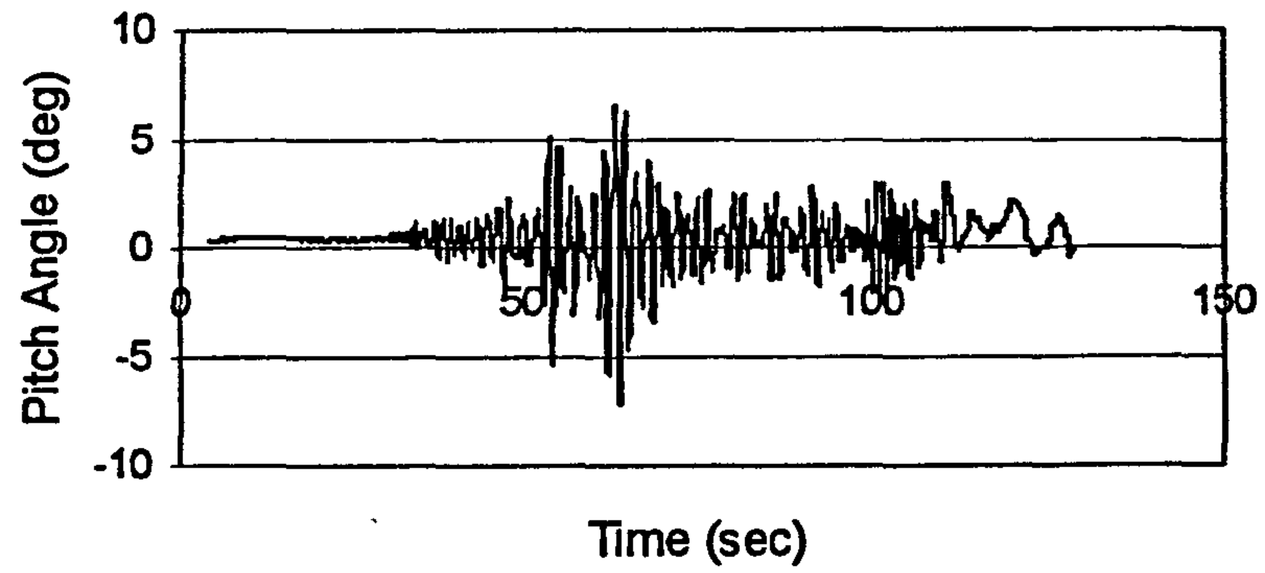

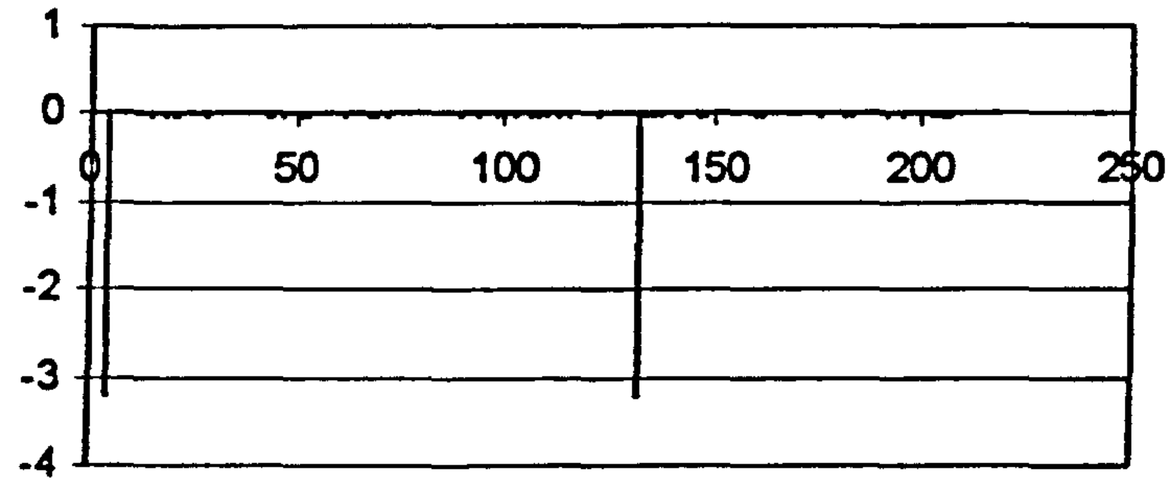

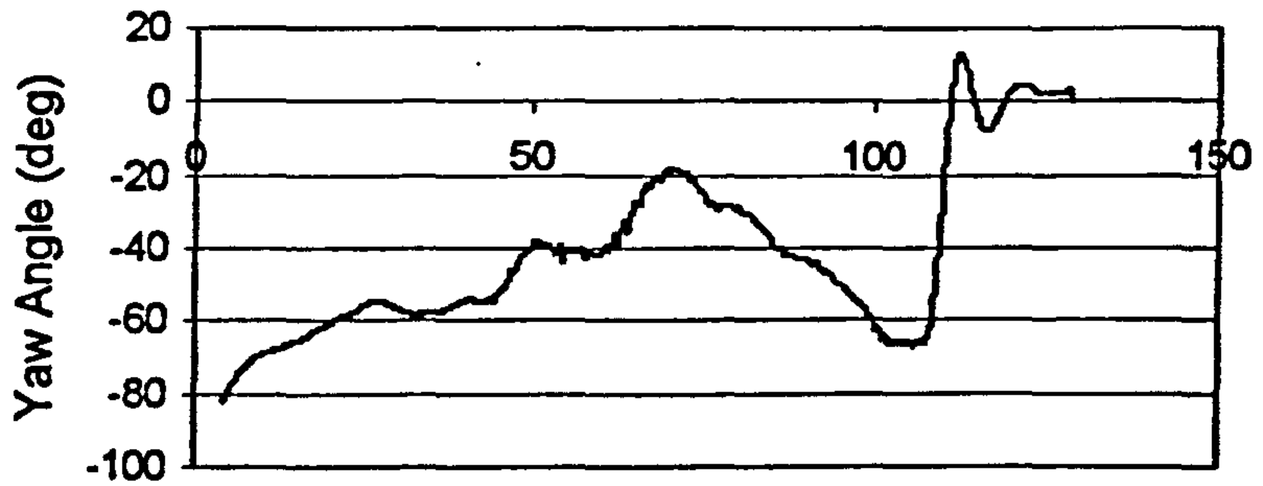

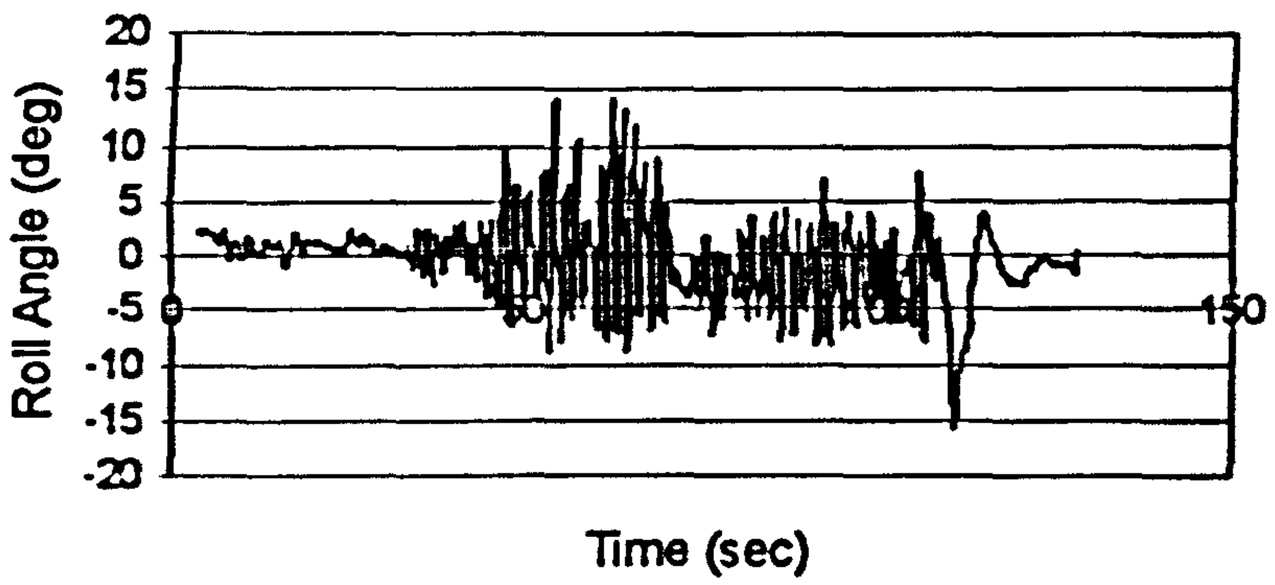

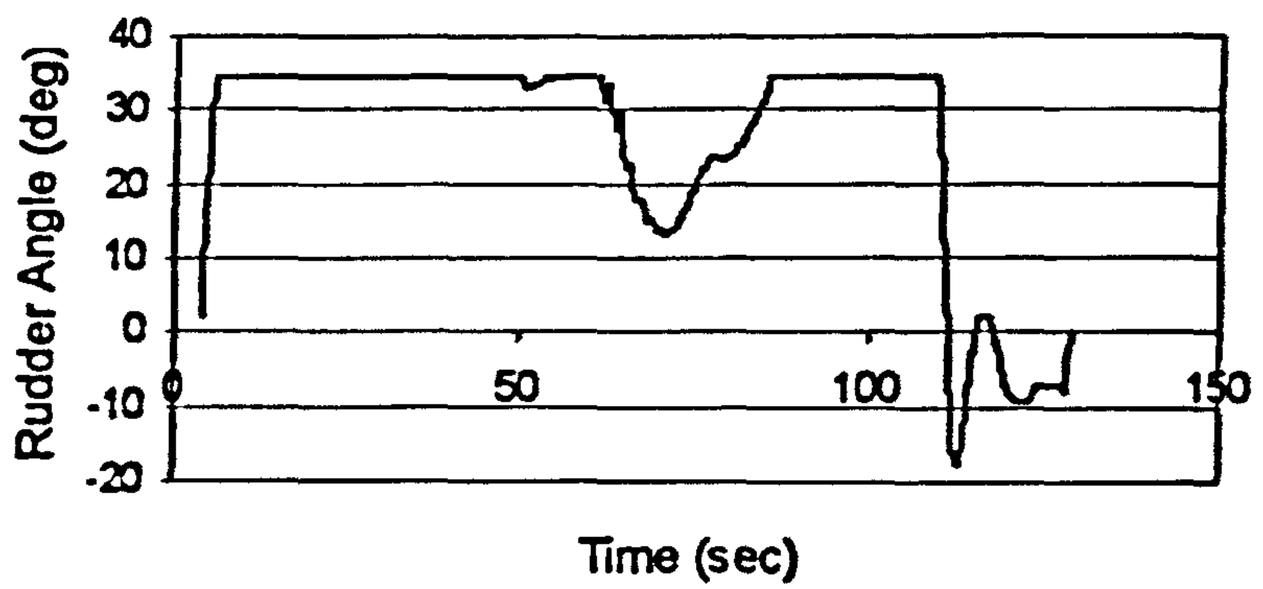

Figure H.27 JONSWAP, Fn=0.4, χ= -5°, H_s=0.23 m, T_p=1.717 sec.

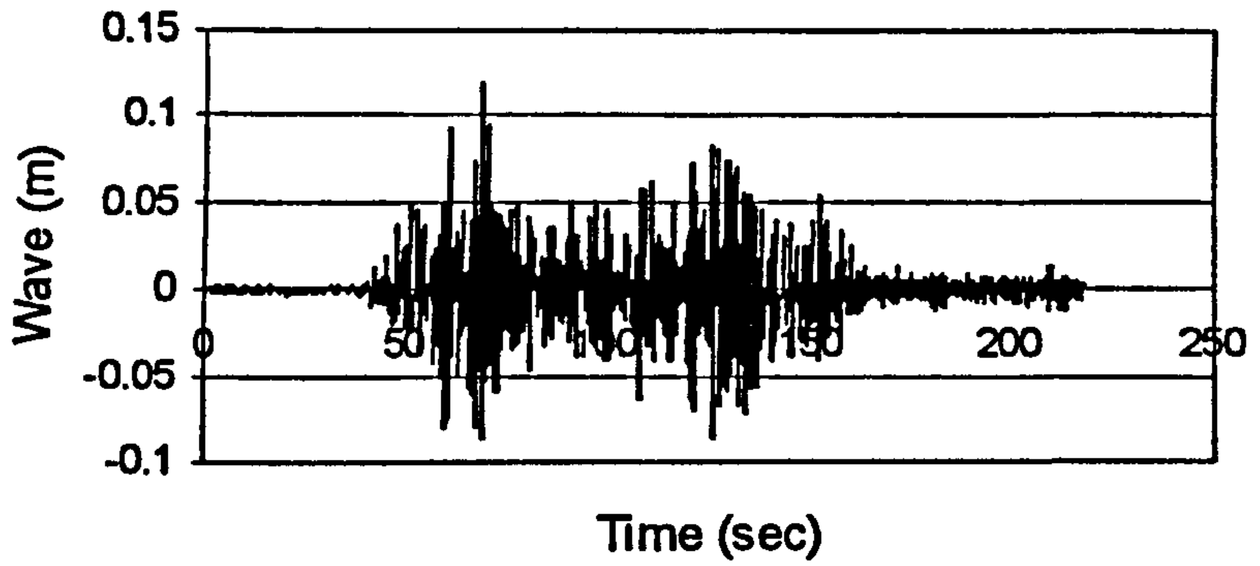

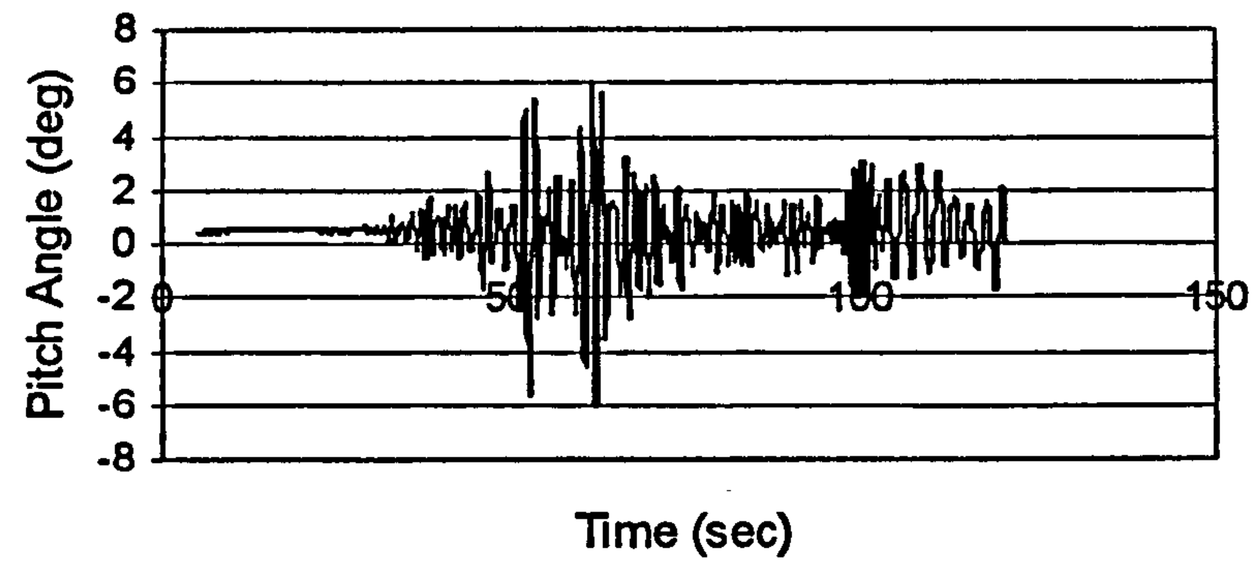

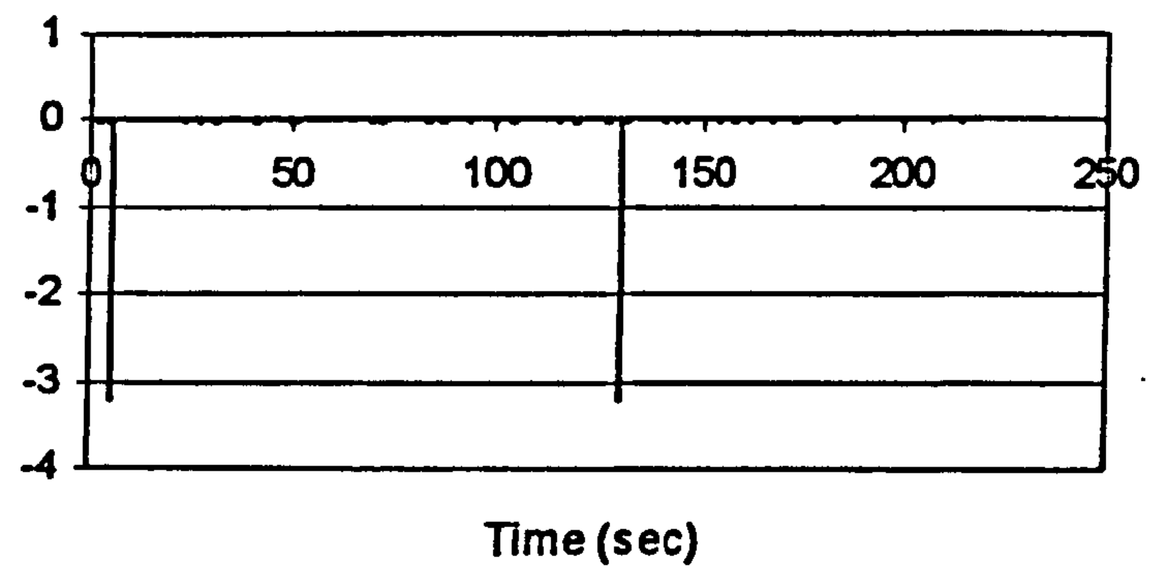

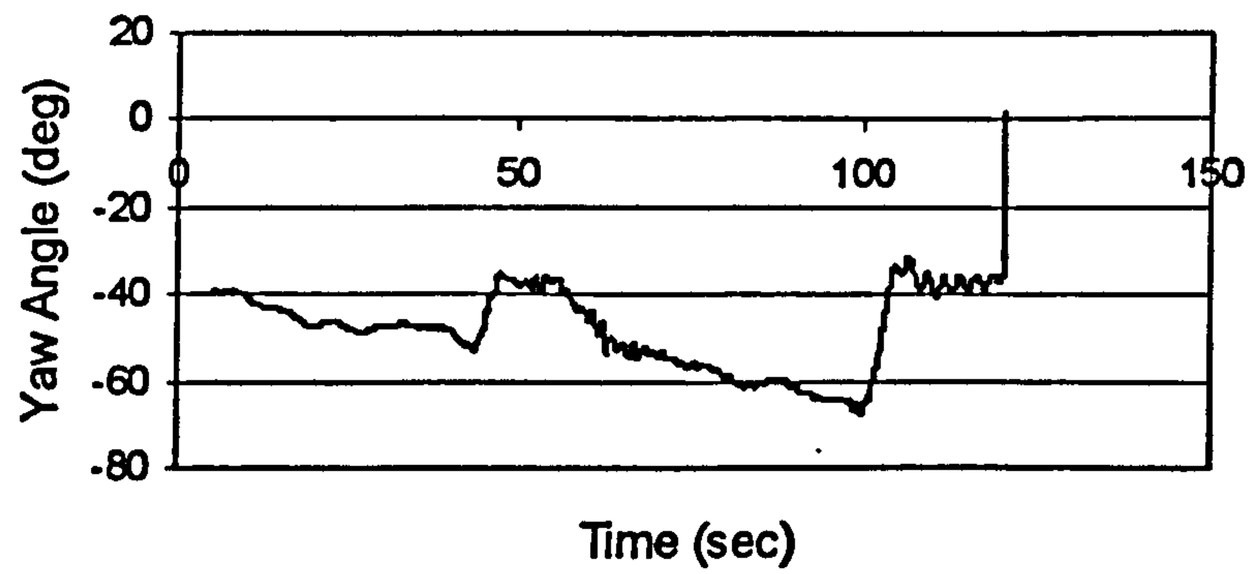

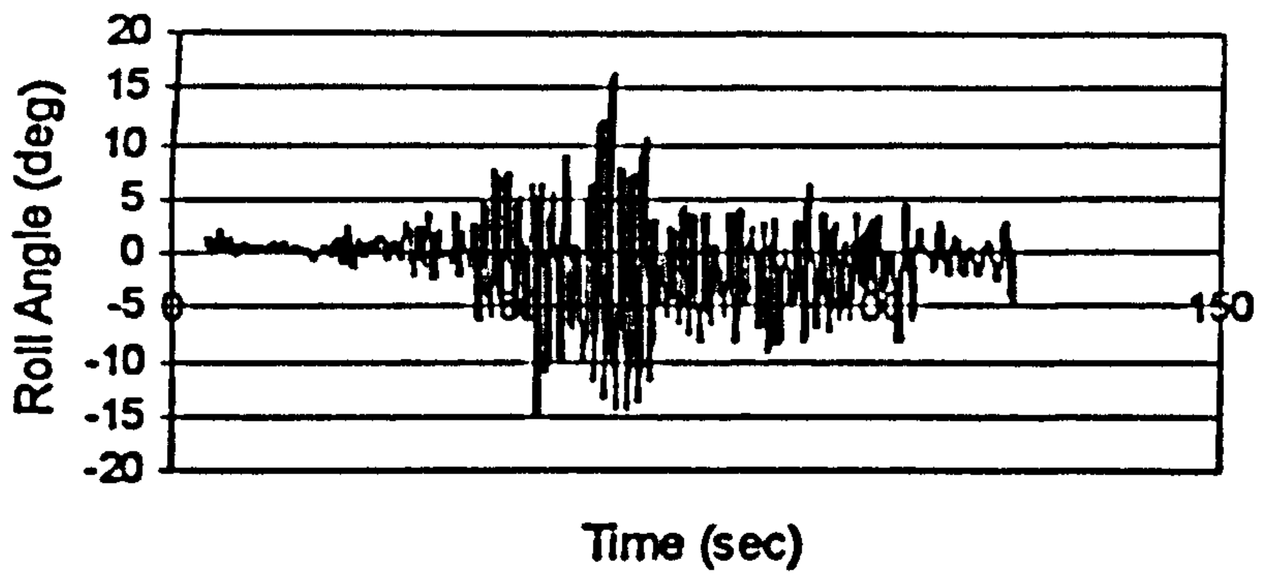

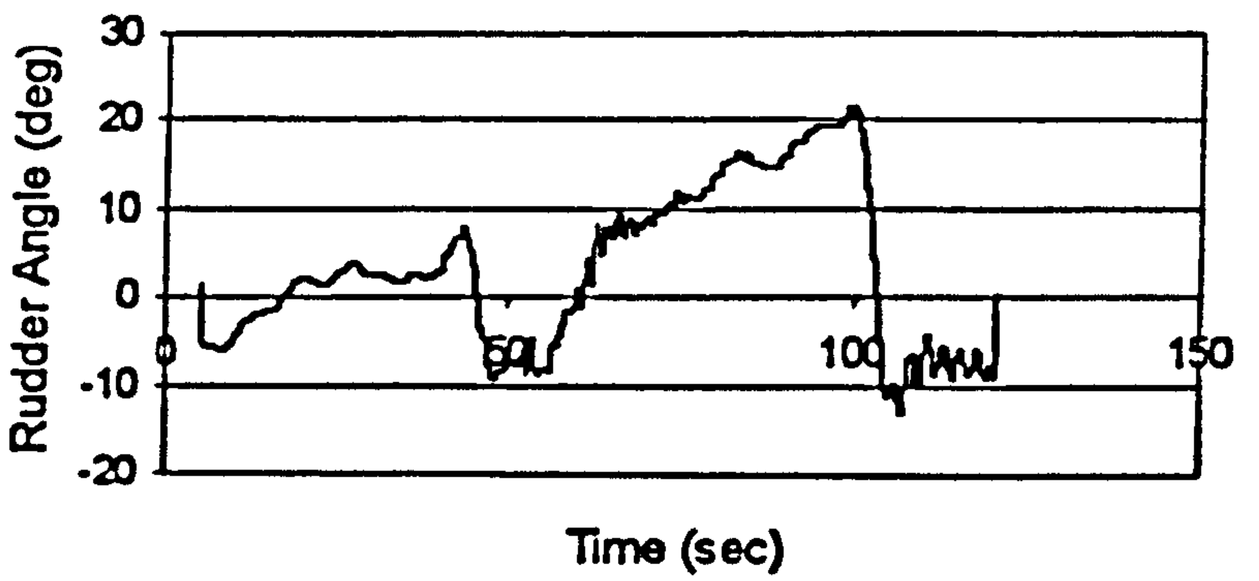

Figure H.28 JONSWAP, Fn=0.3, χ= -45°, H_s=0.23 m, T_p=1.717 sec.

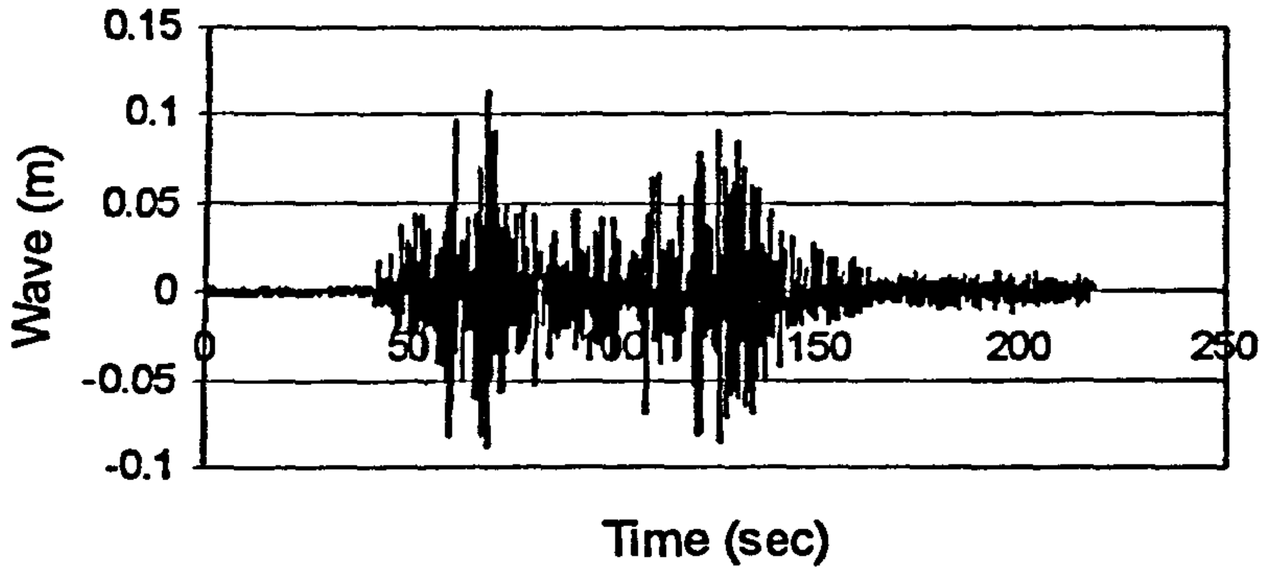

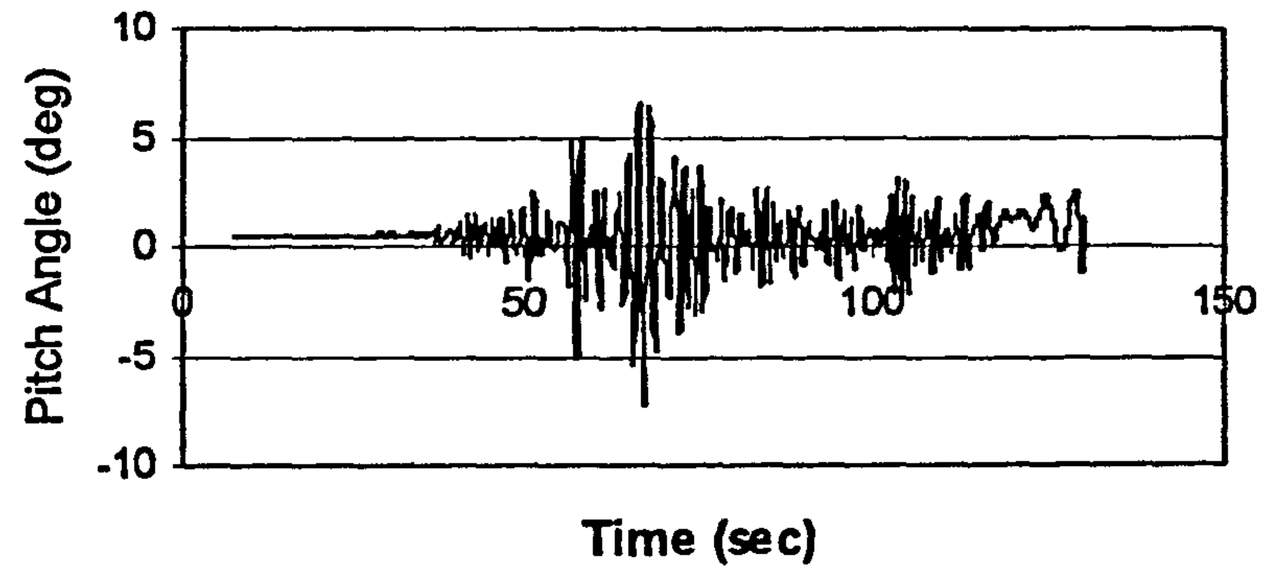

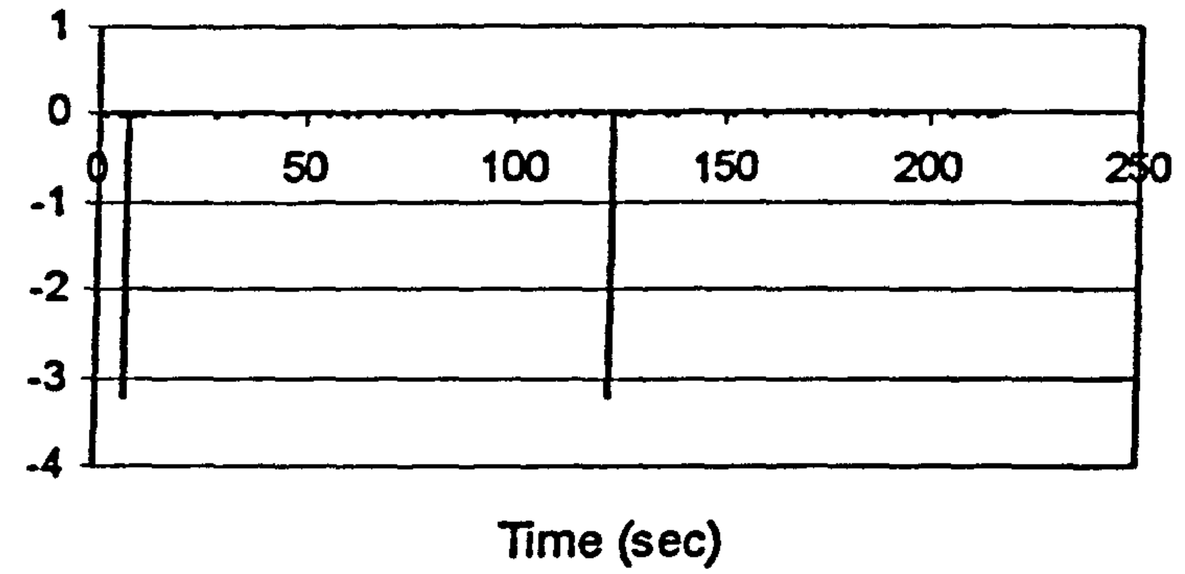

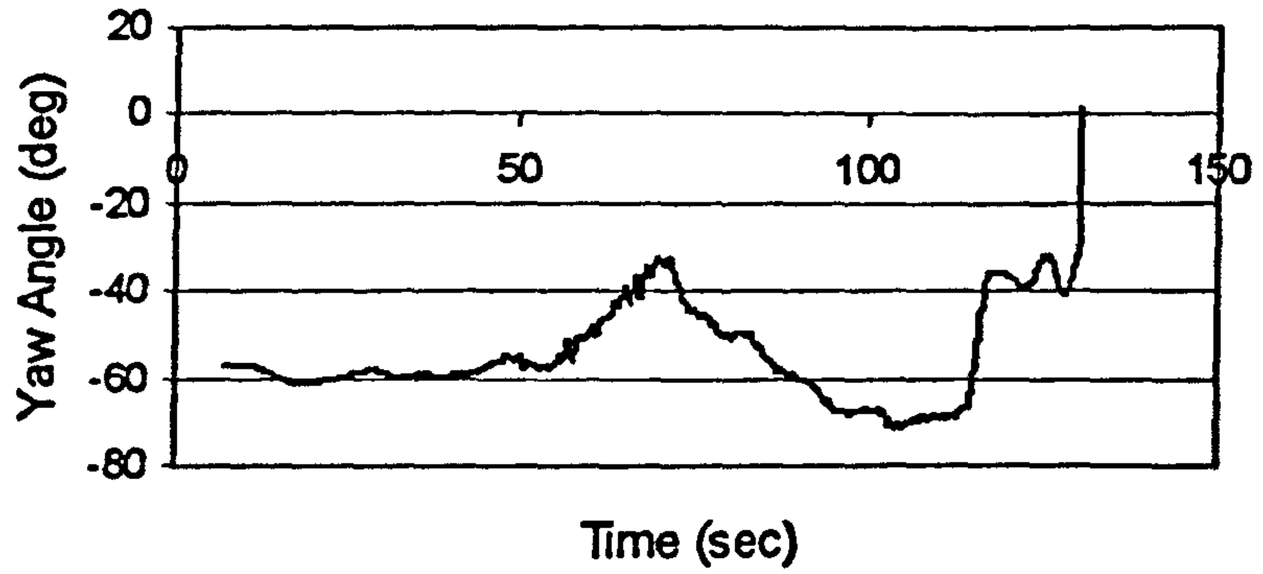

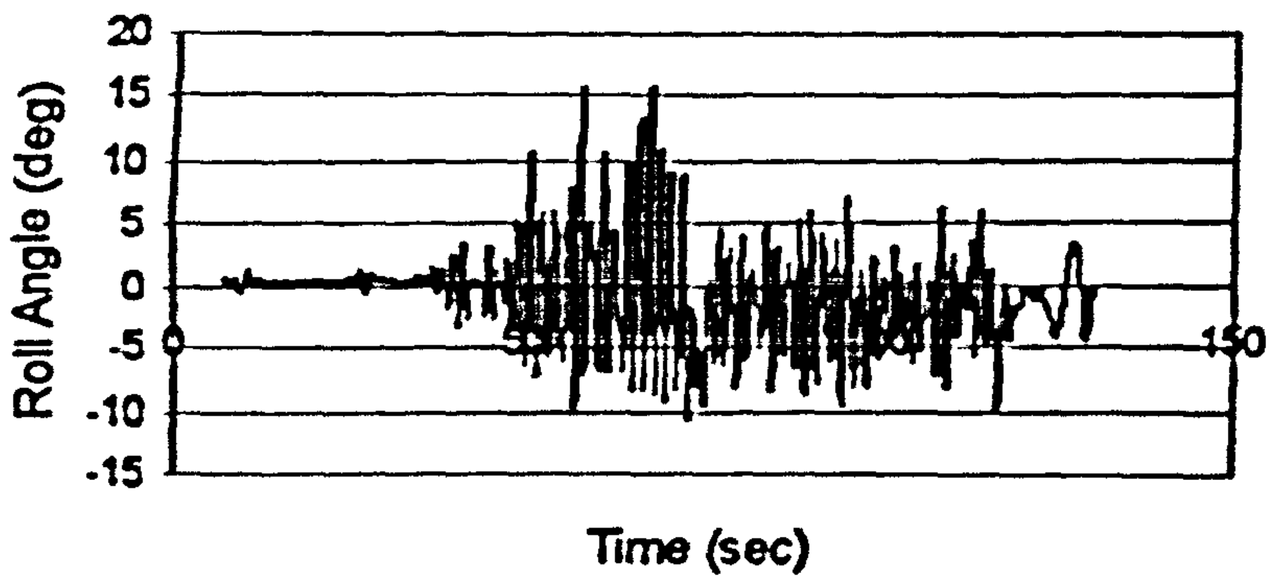

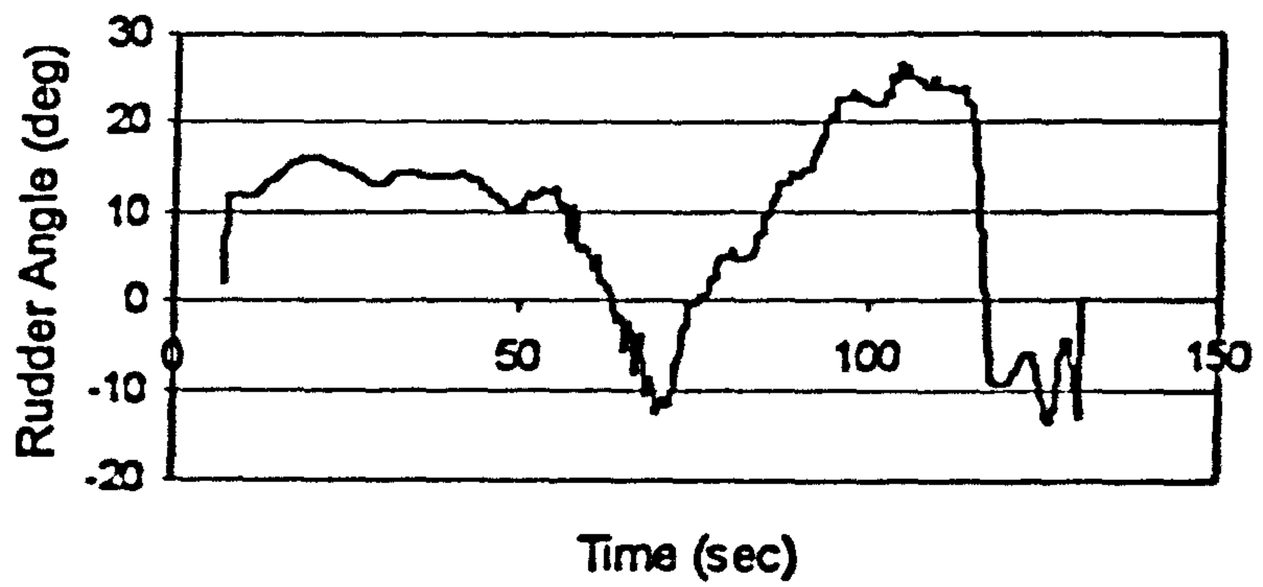

Figure H.29 JONSWAP, Fn=0.4, χ= -45°, H_s=0.23 m, T_p=1.717 sec.

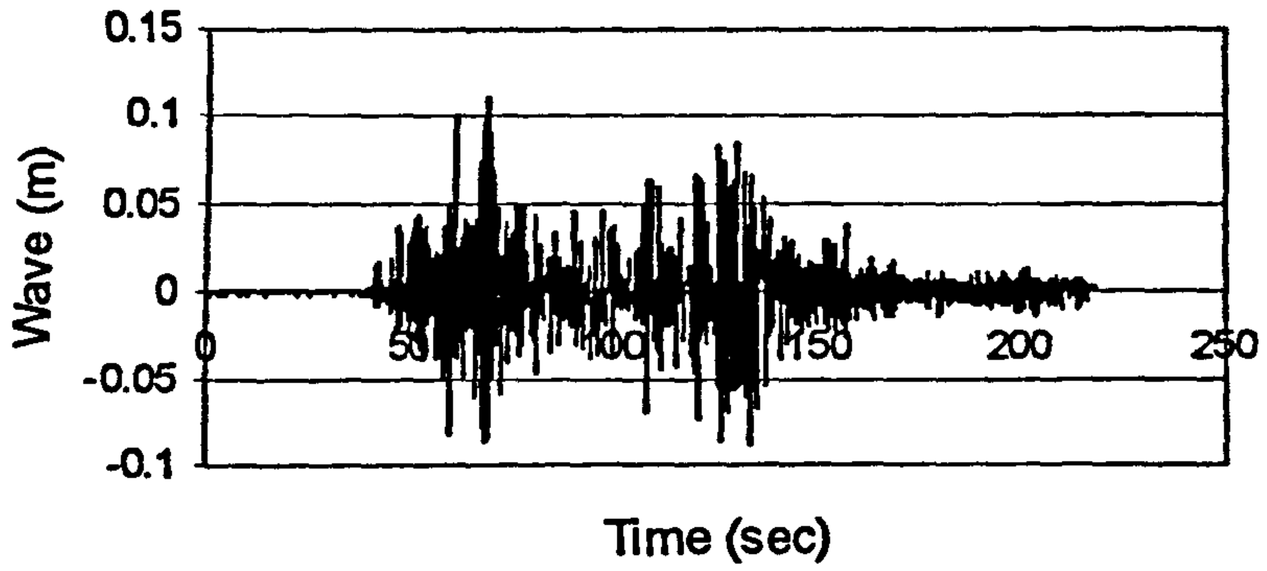

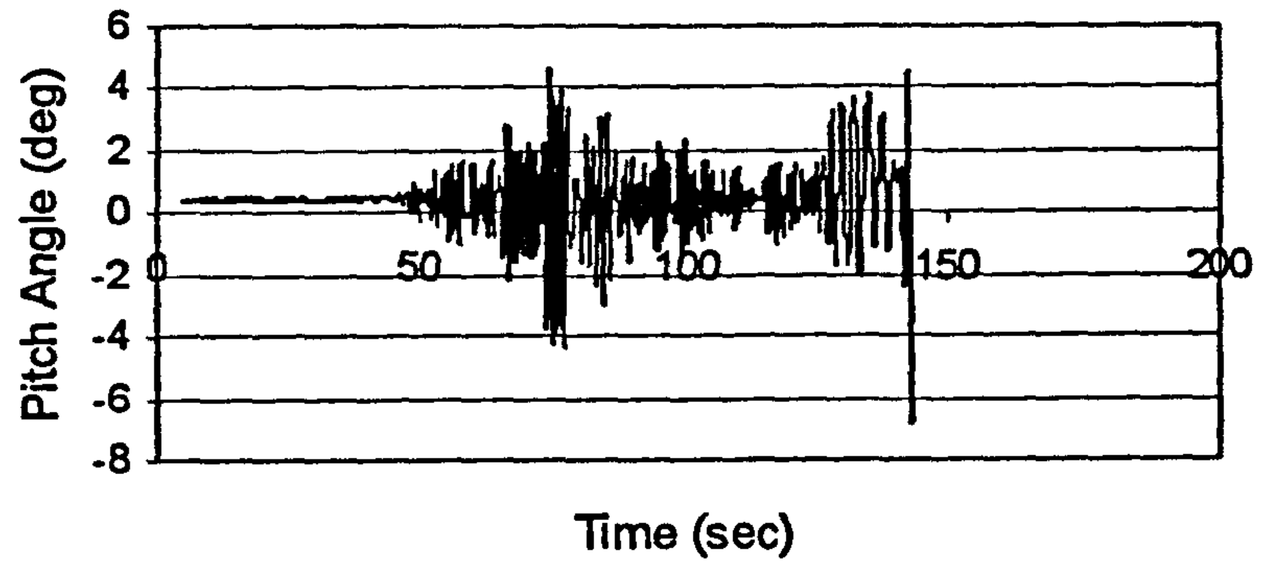

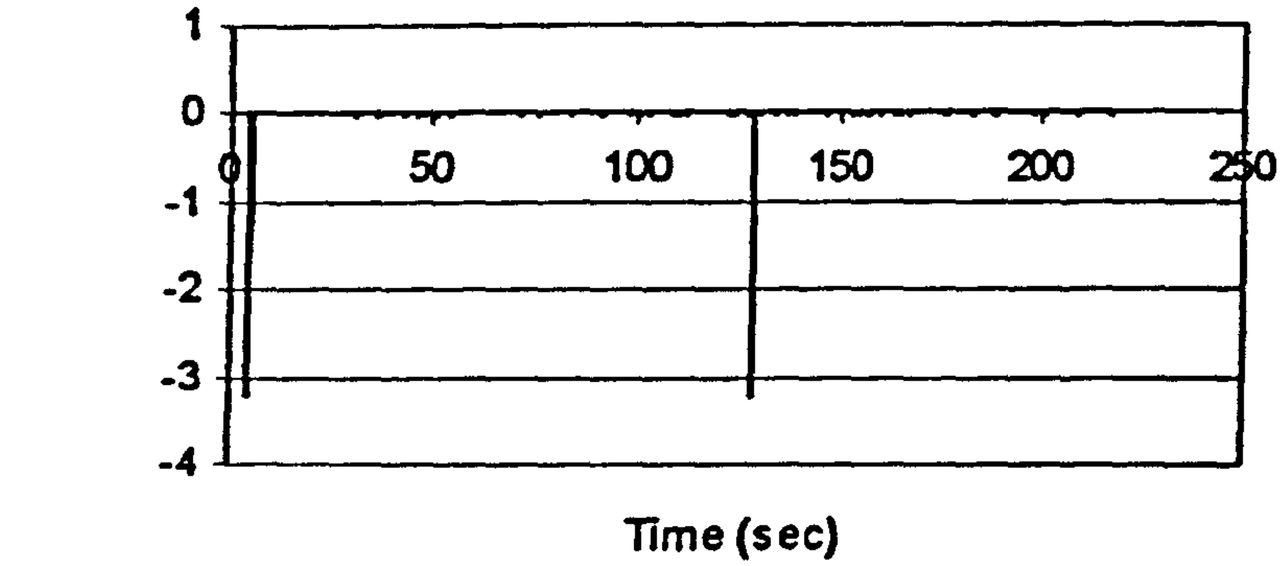

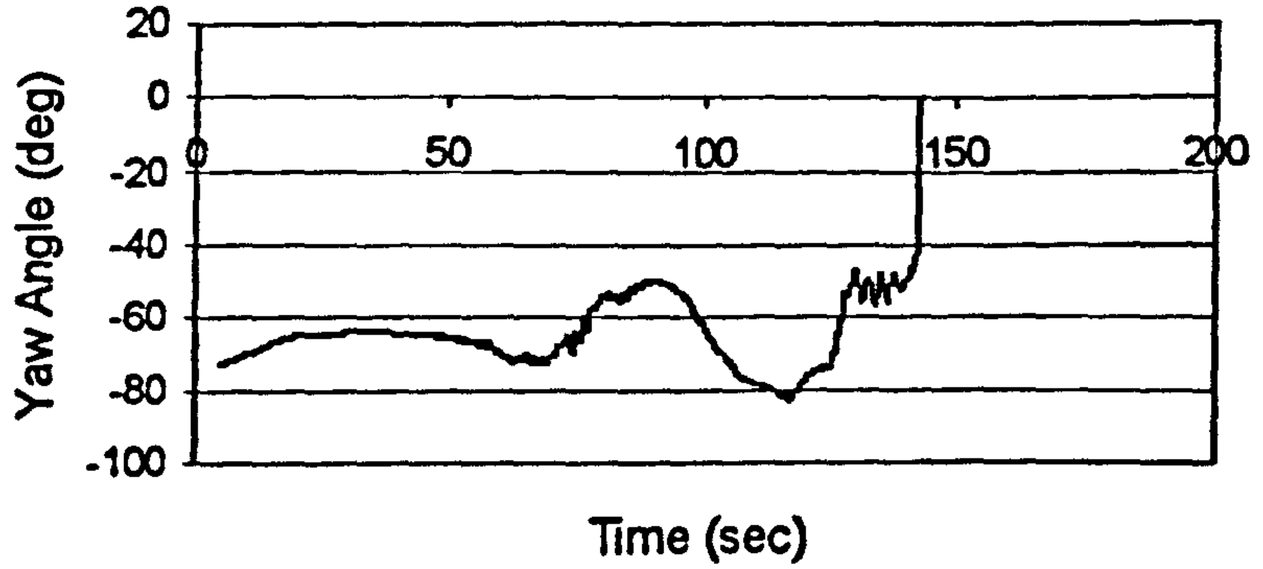

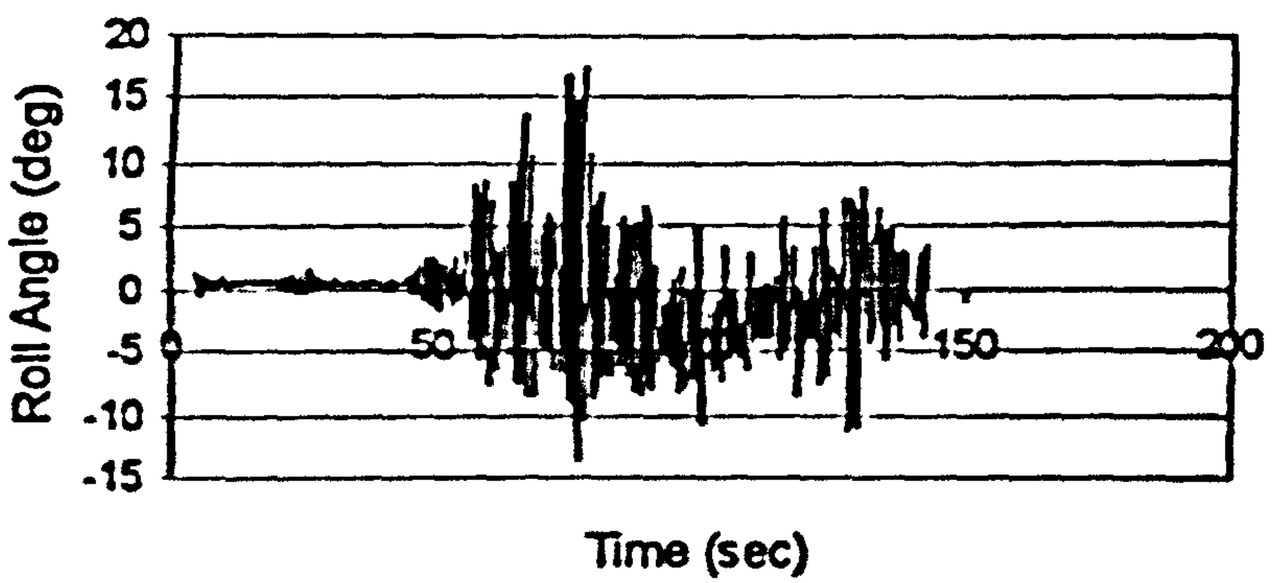

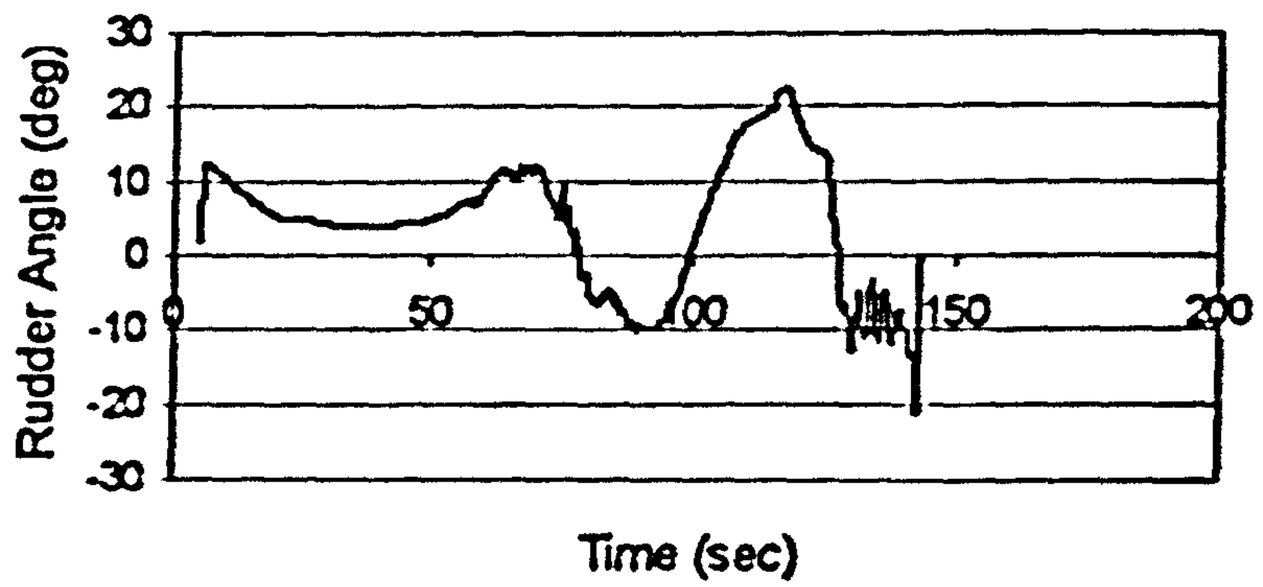

Figure H.30 JONSWAP, Fn=0.3, χ= -60°, H_s=0.23 m, T_p=1.717 sec.

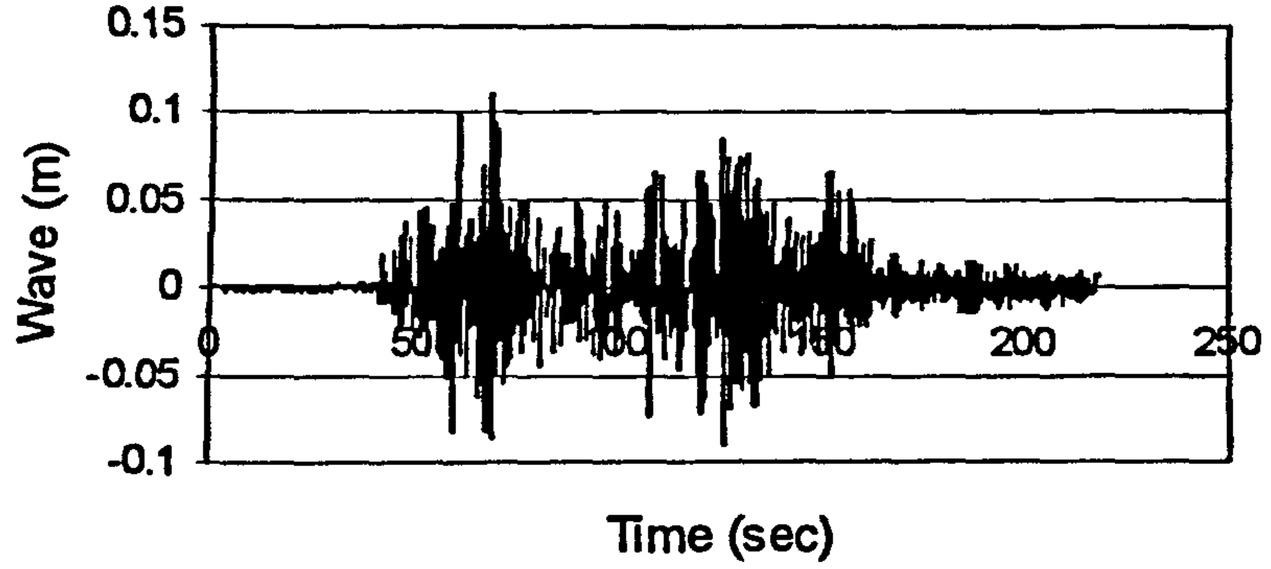

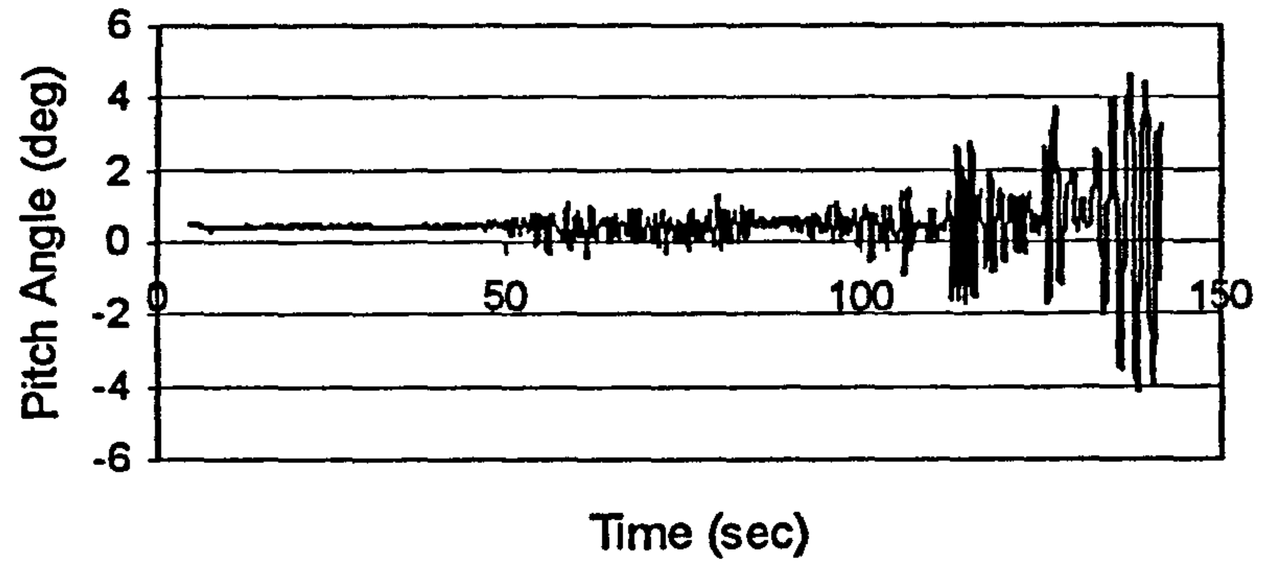

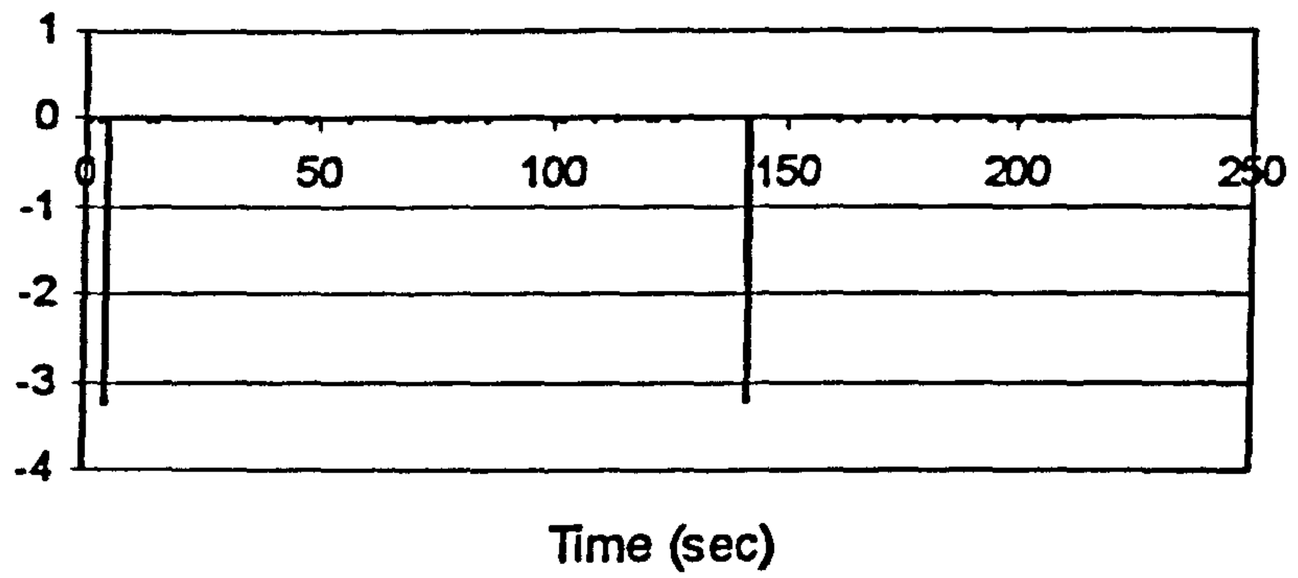

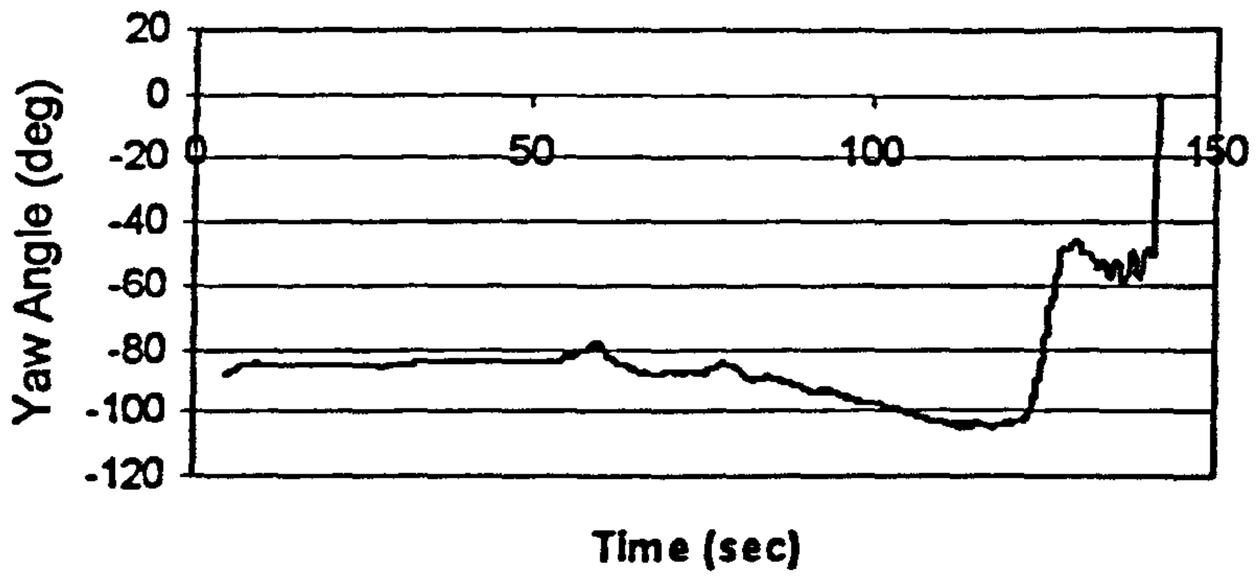

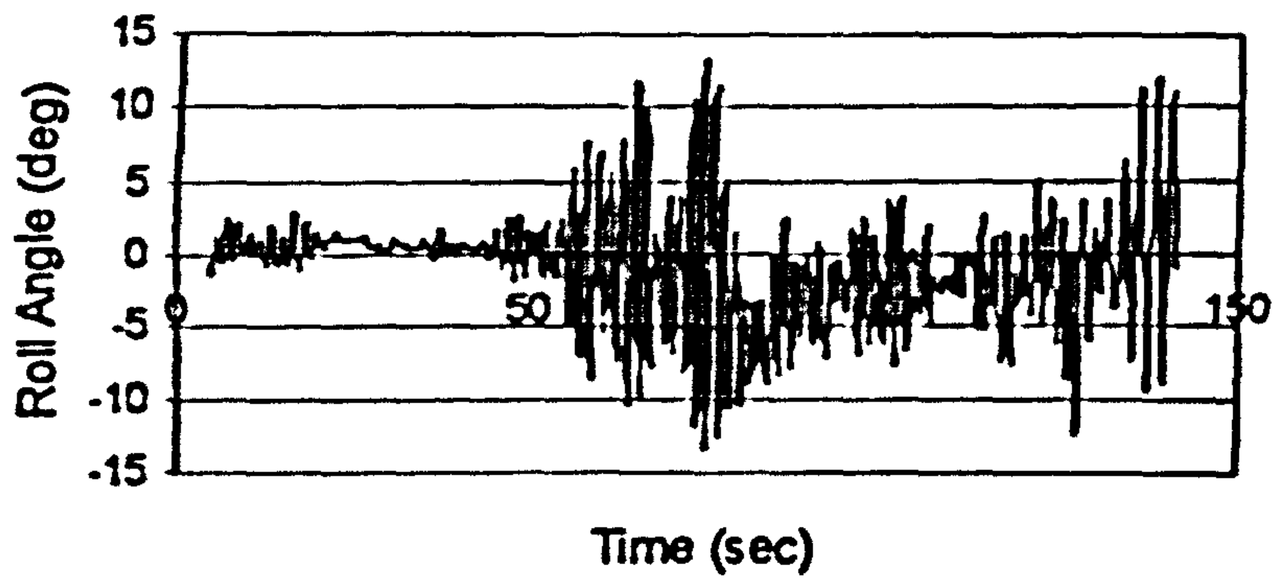

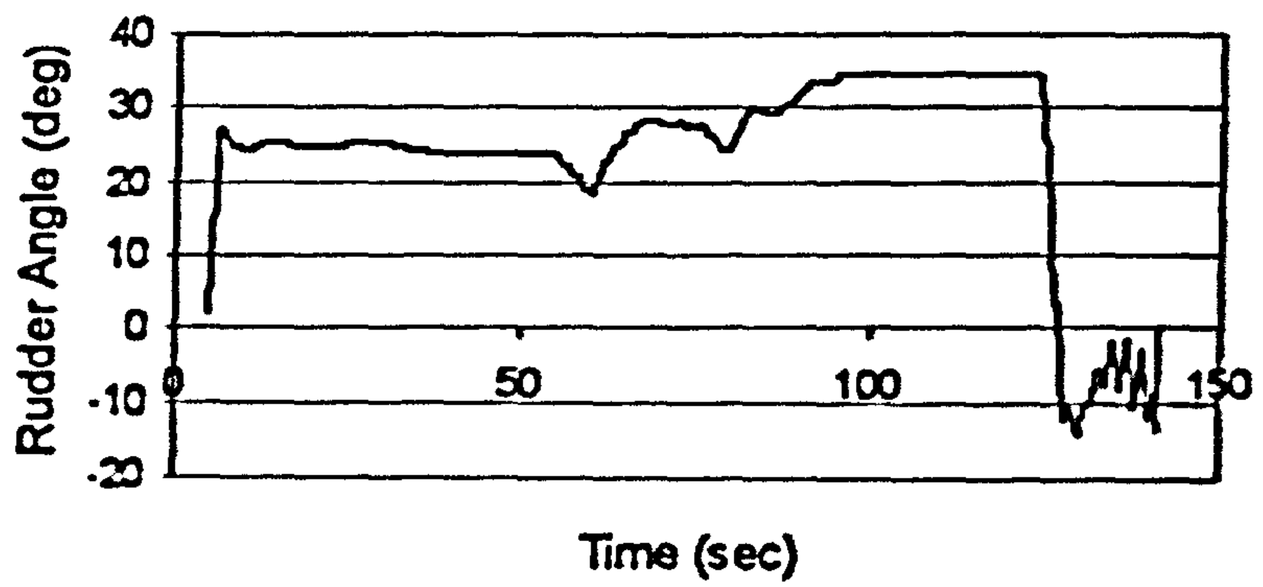

Figure H.31 JONSWAP, Fn=0.4, χ= -60°, H_s=0.23 m, T_p=1.717 sec.

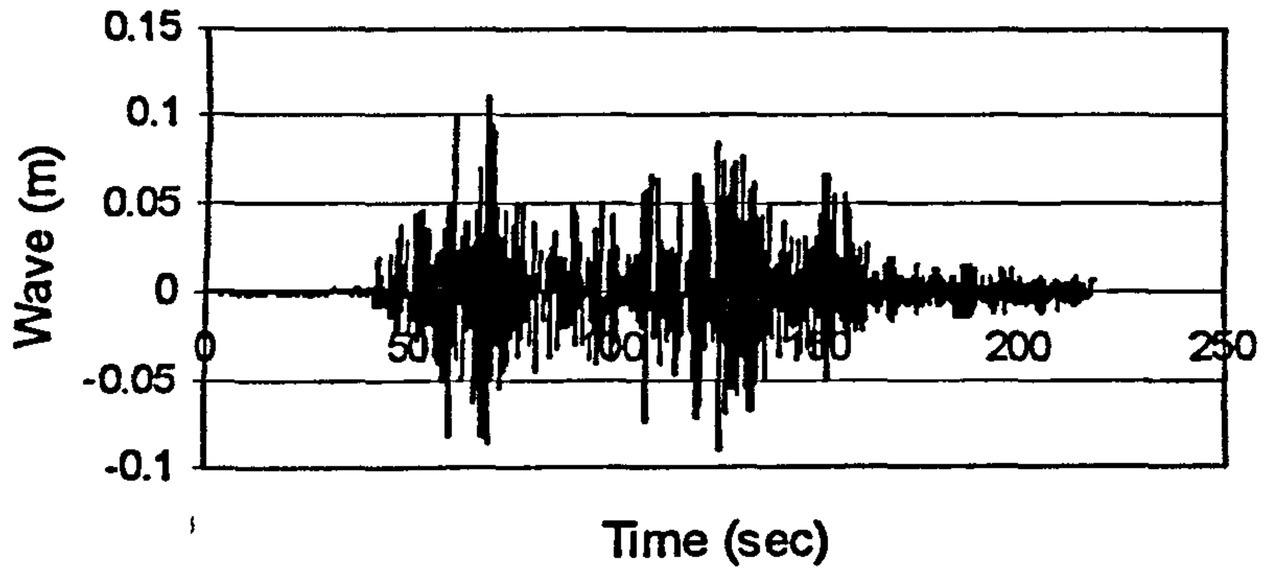

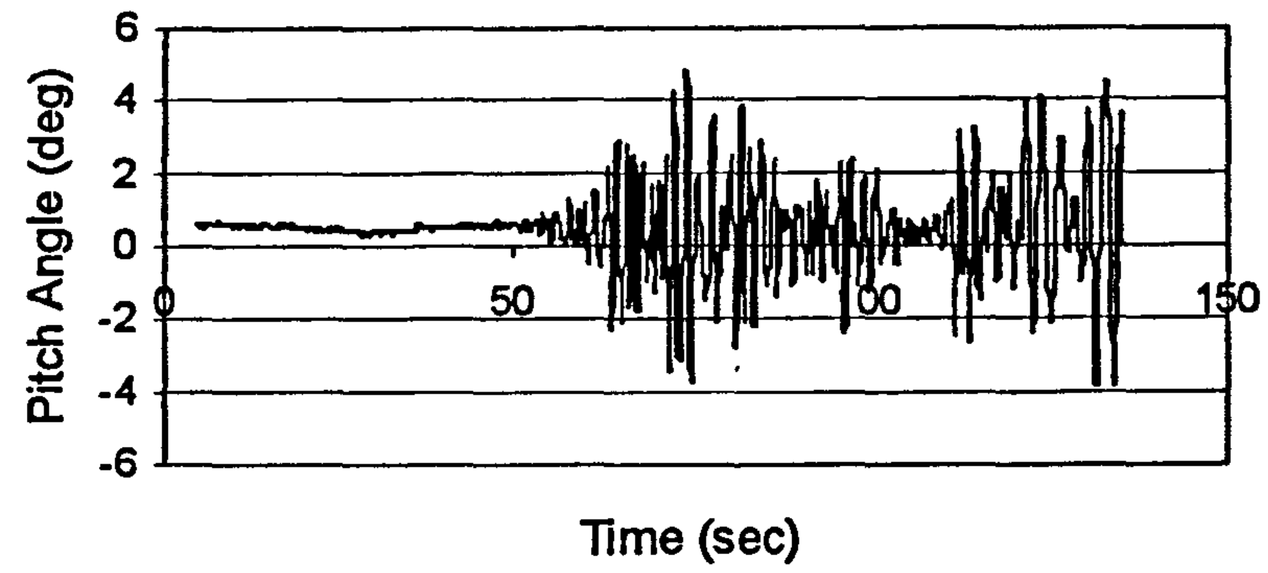

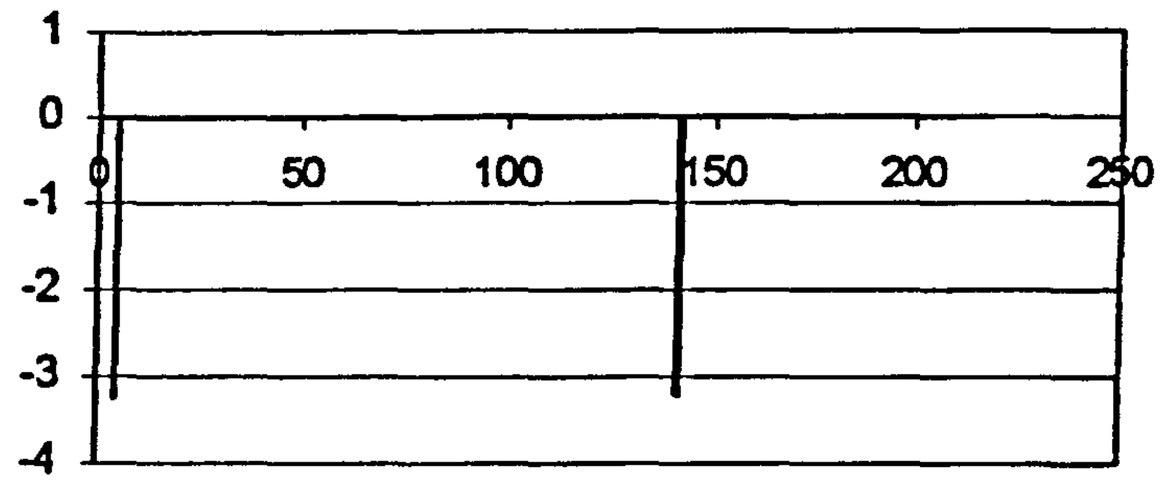

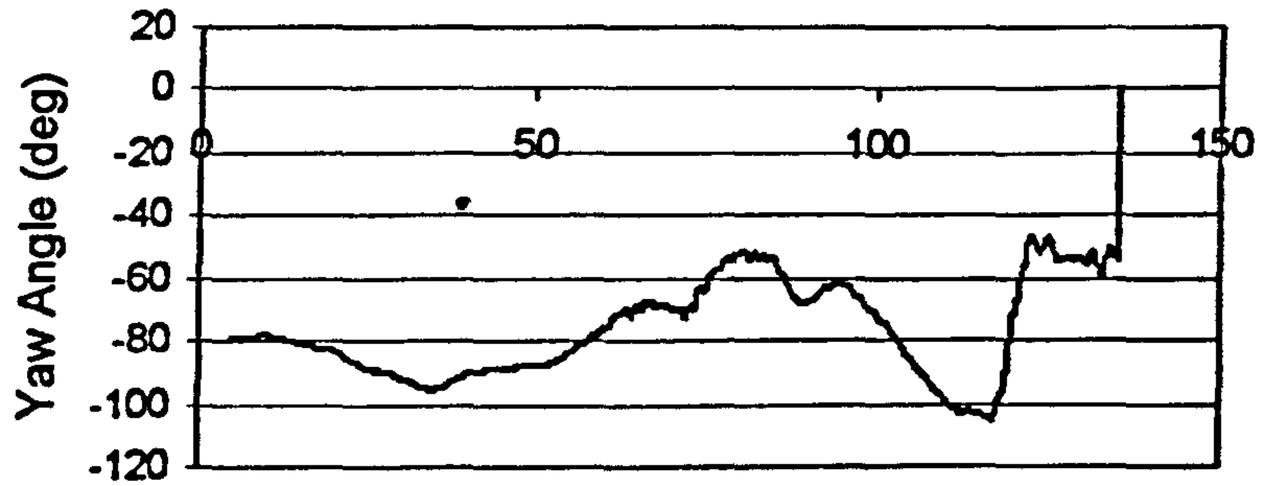

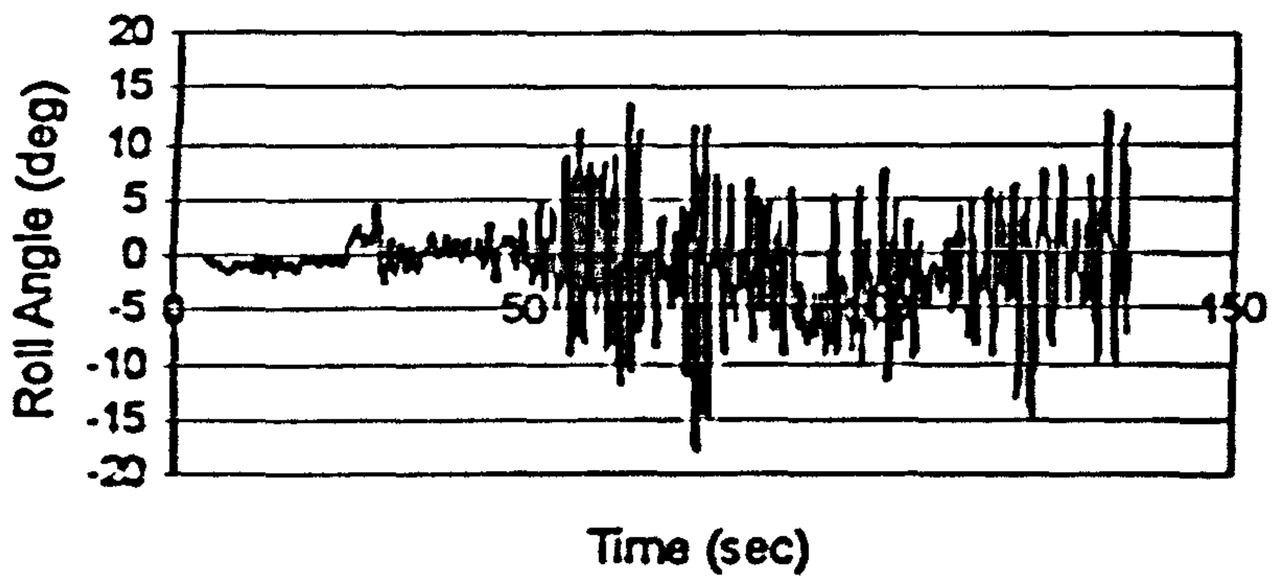

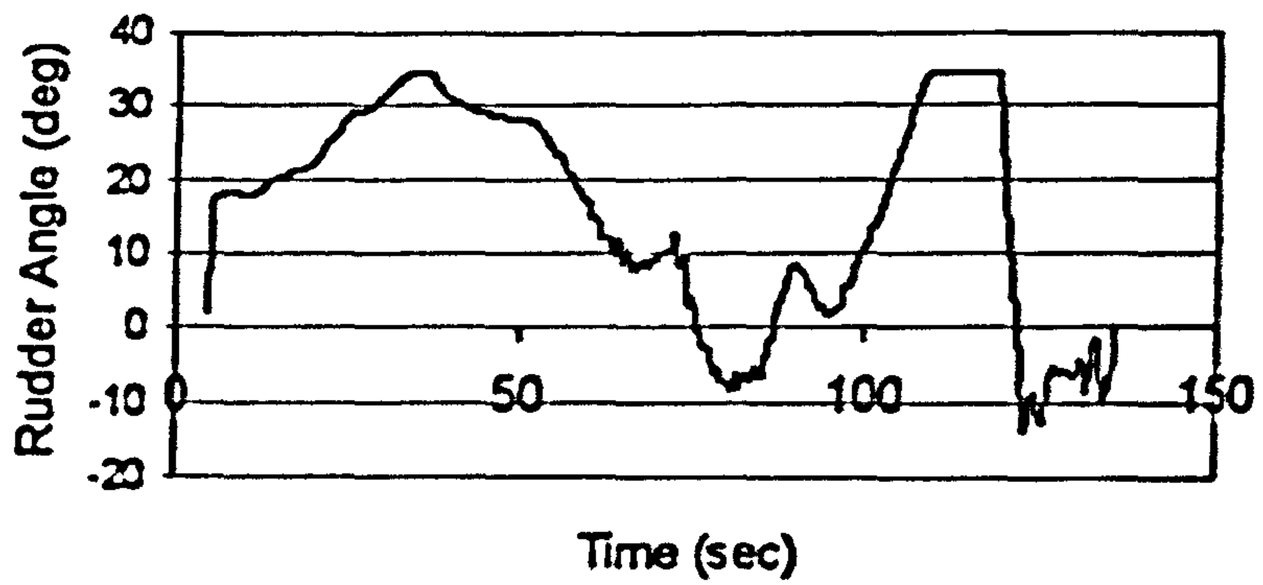

Figure H.32 JONSWAP, Fn=0.3, χ= -60°, H_s=0.1725 m, T_p=1.487 sec.

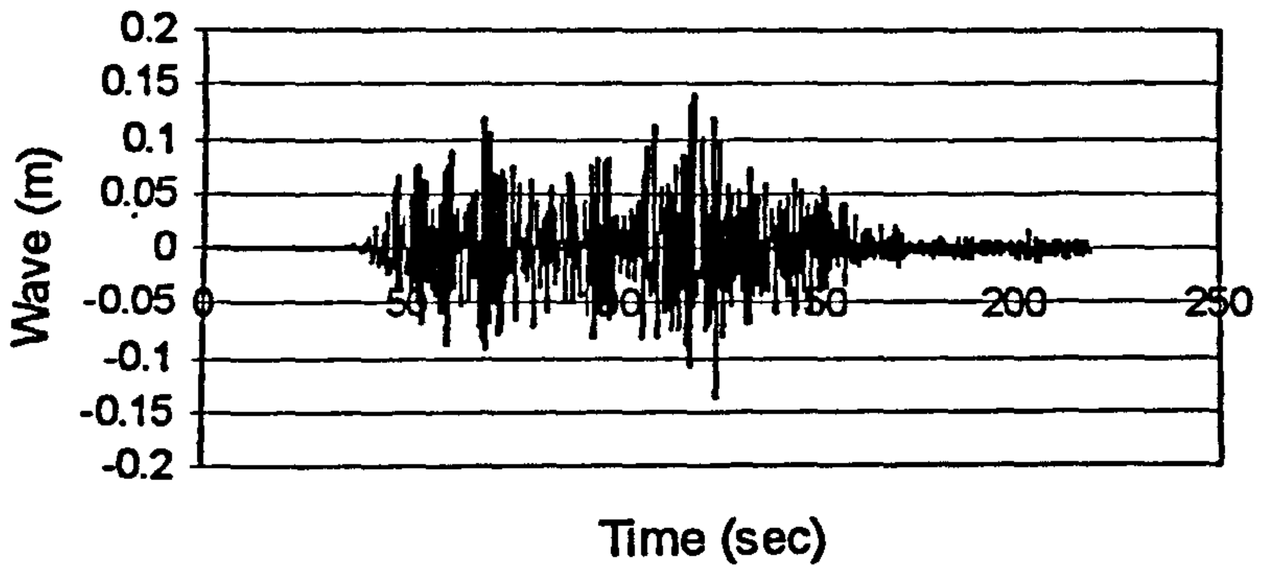

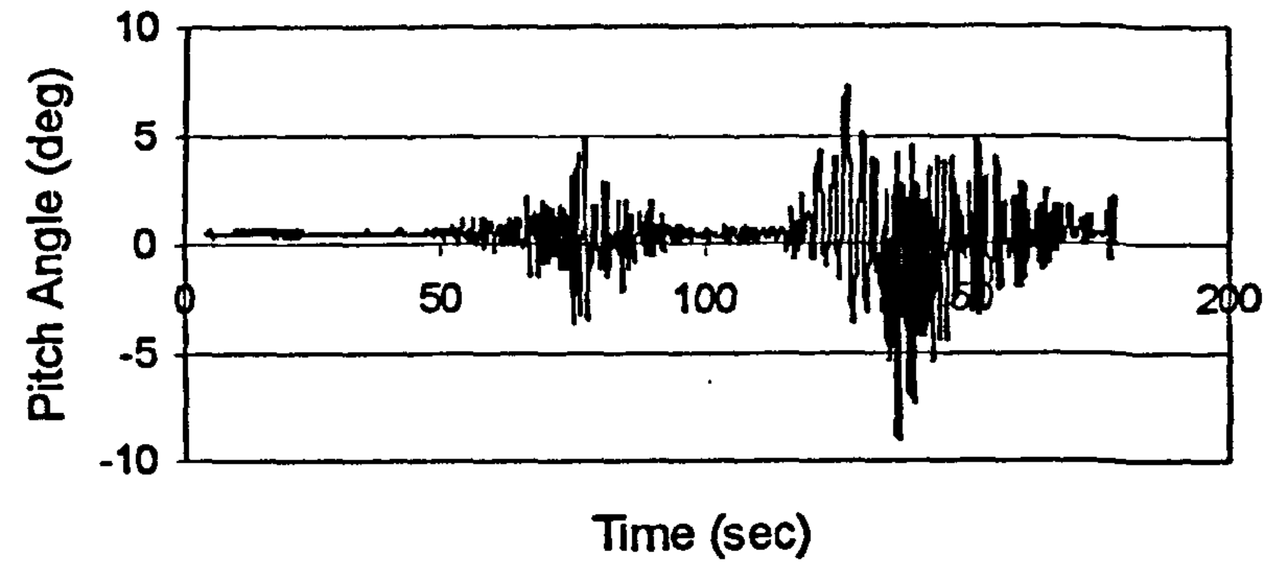

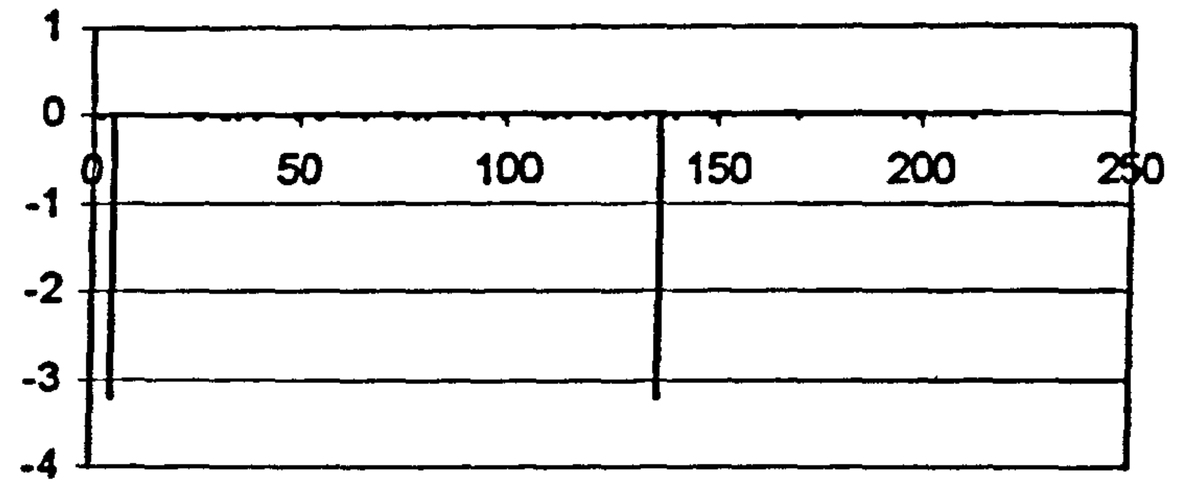

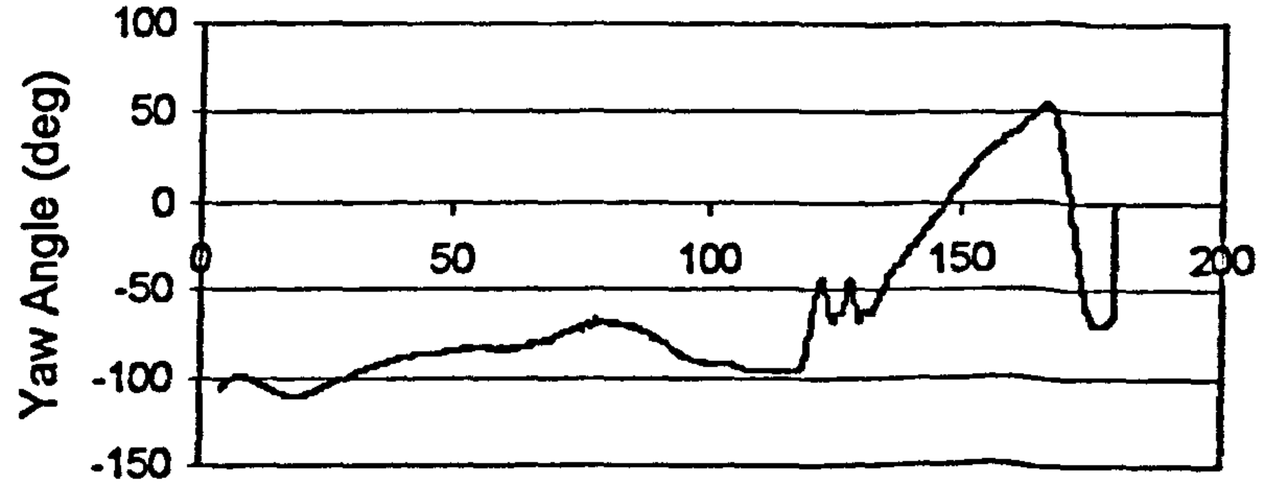

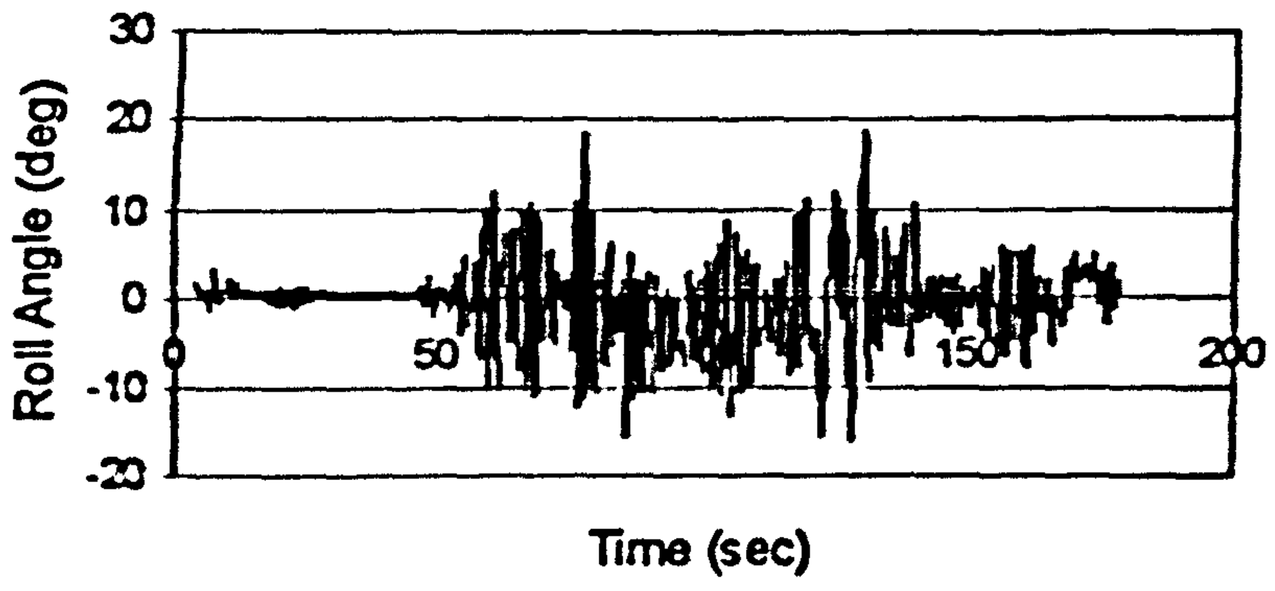

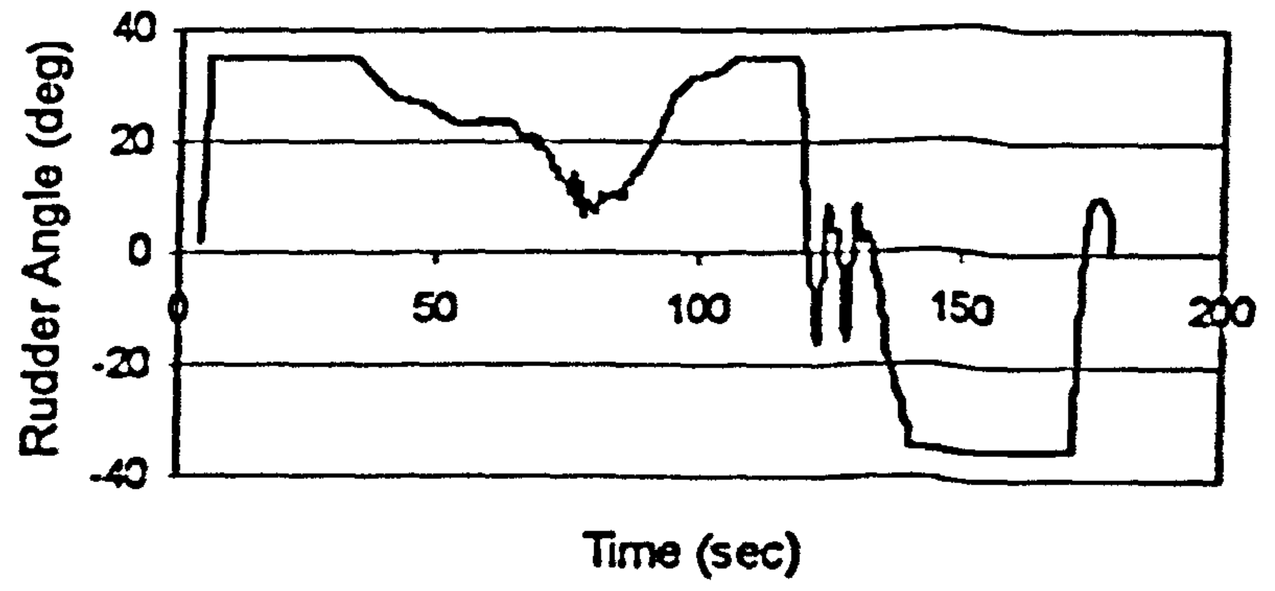

Figure H.33 JONSWAP, Fn=0.4, χ= -60°, H_s=0.1725 m, T_p=1.487 sec.

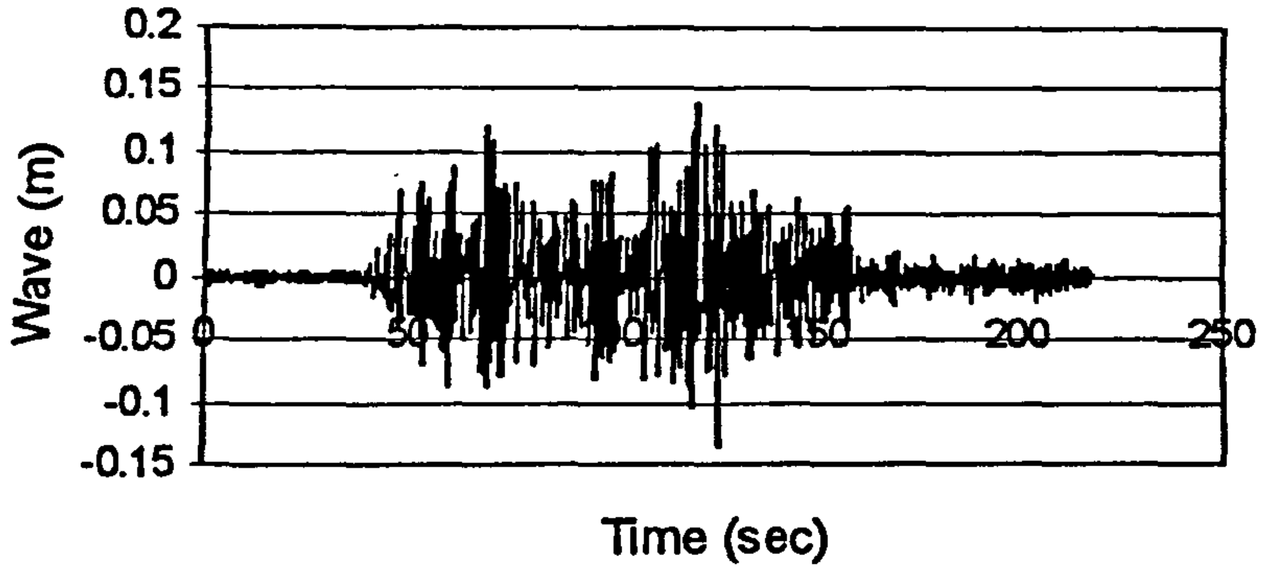

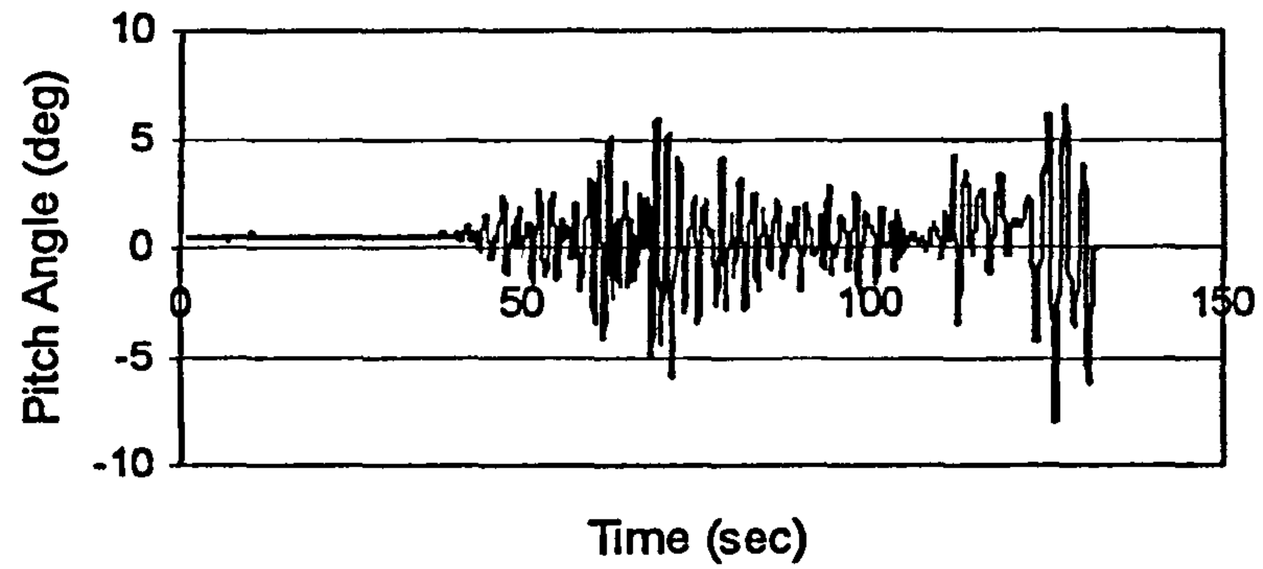

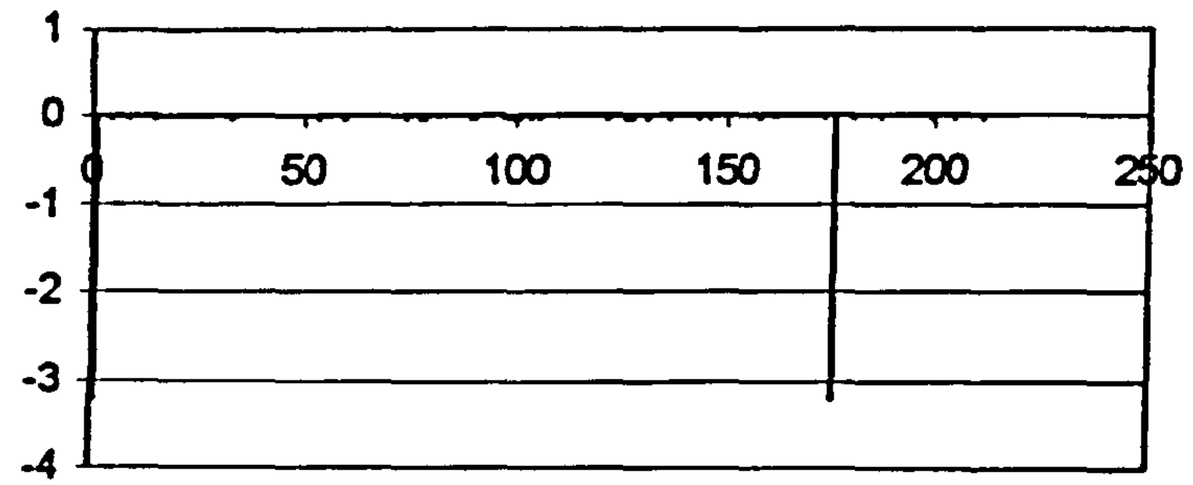

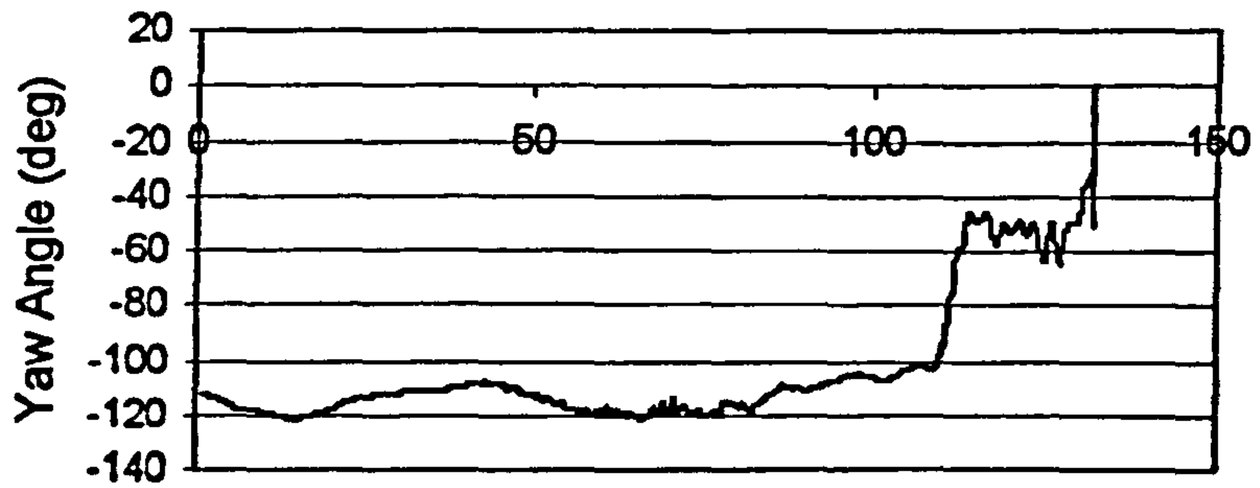

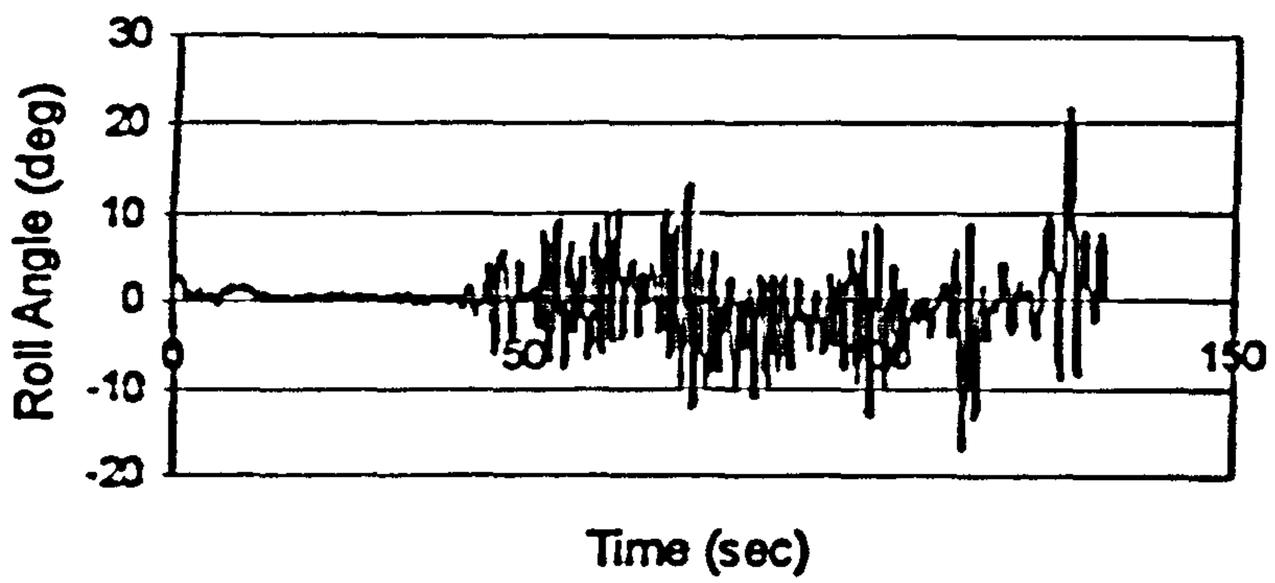

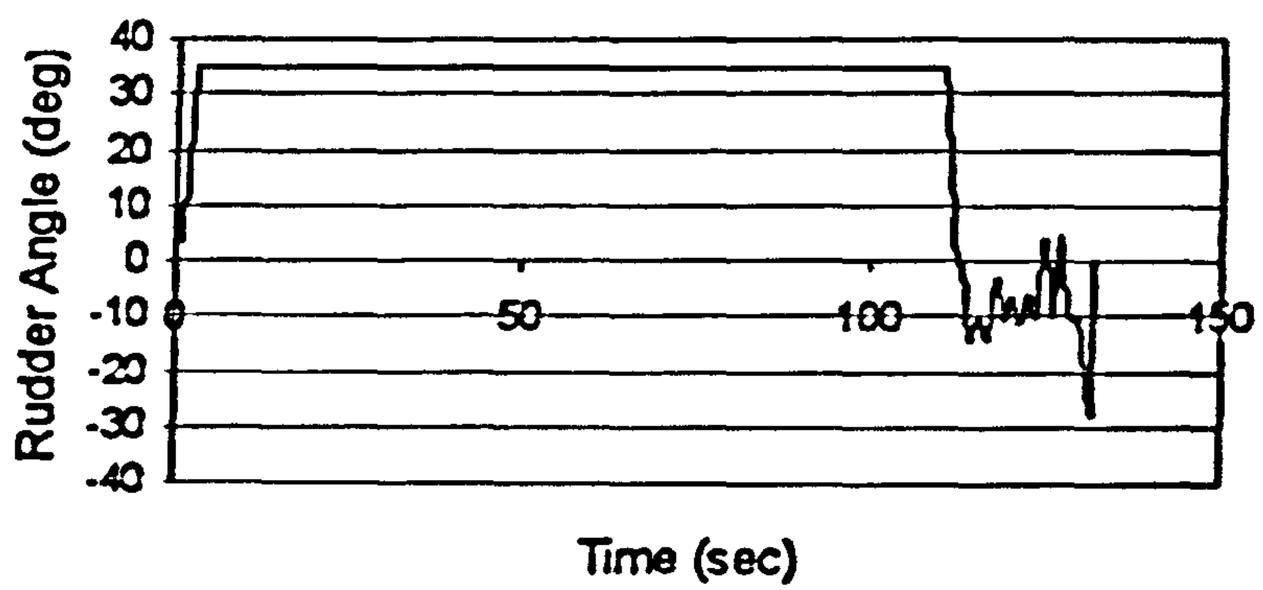

Figure II.34 JONSWAP, Fn=0.3, χ= -60°, H_s=0.115 m, T_p=1.214 sec.

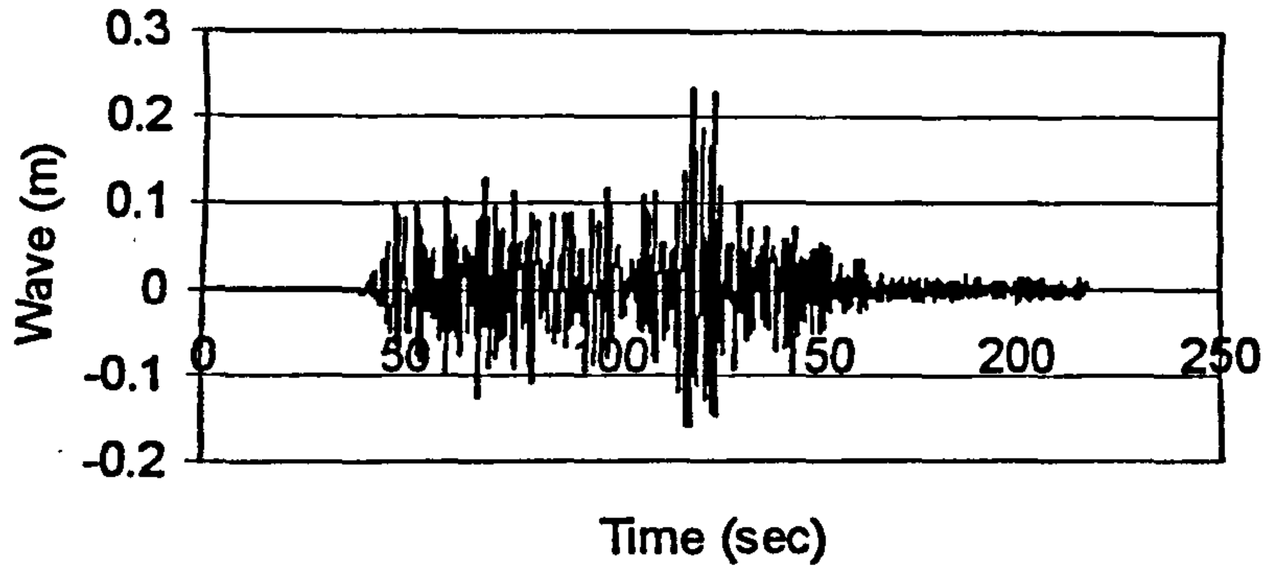

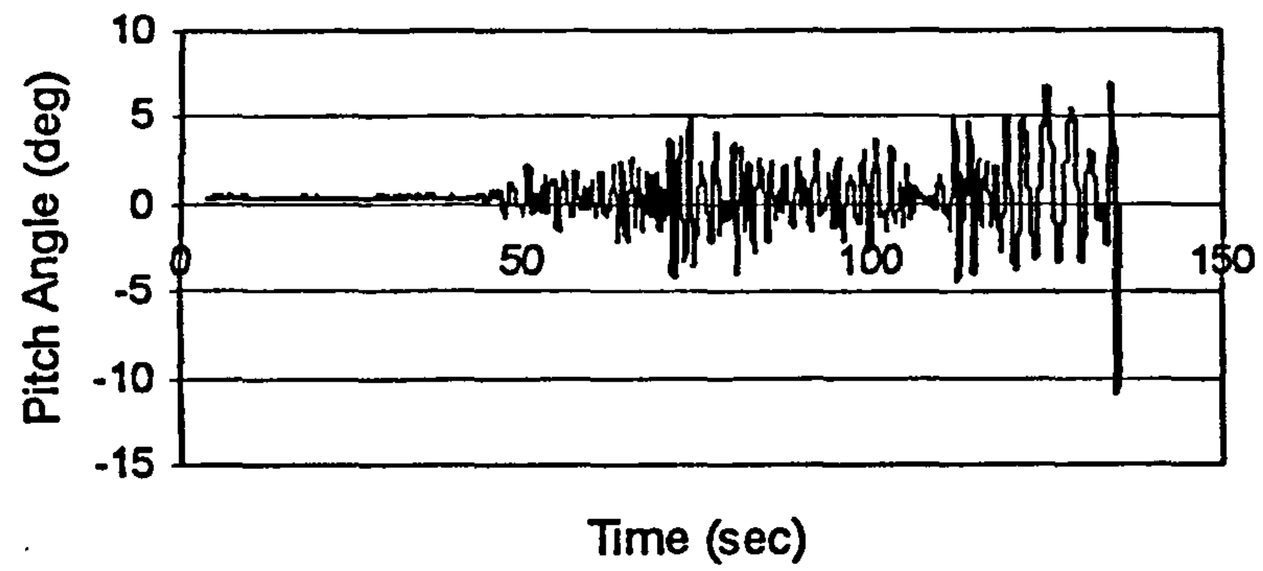

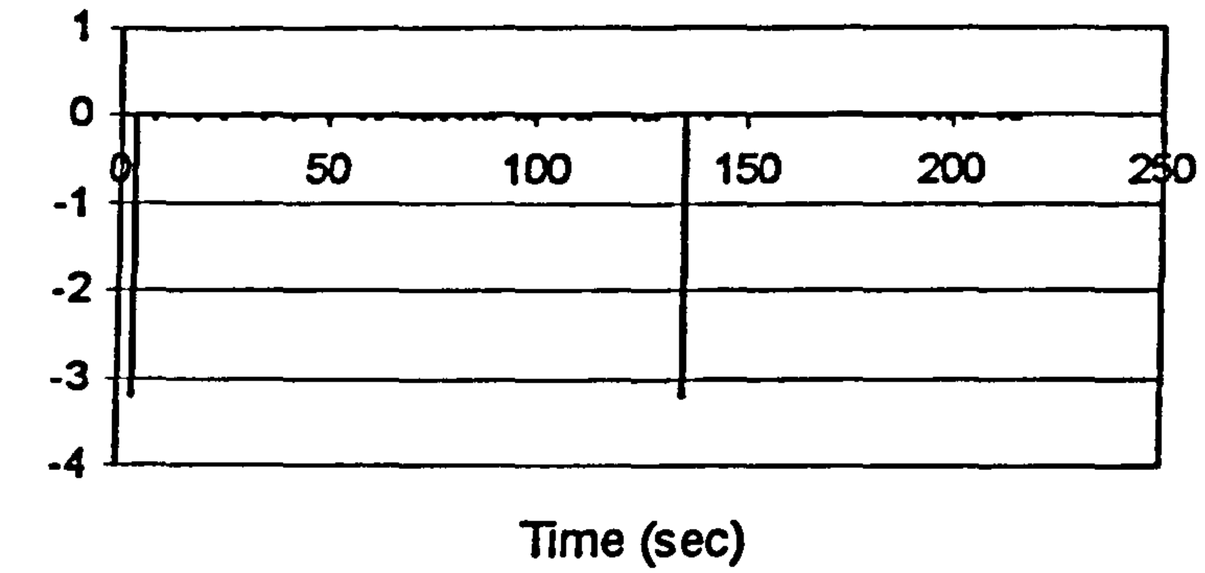

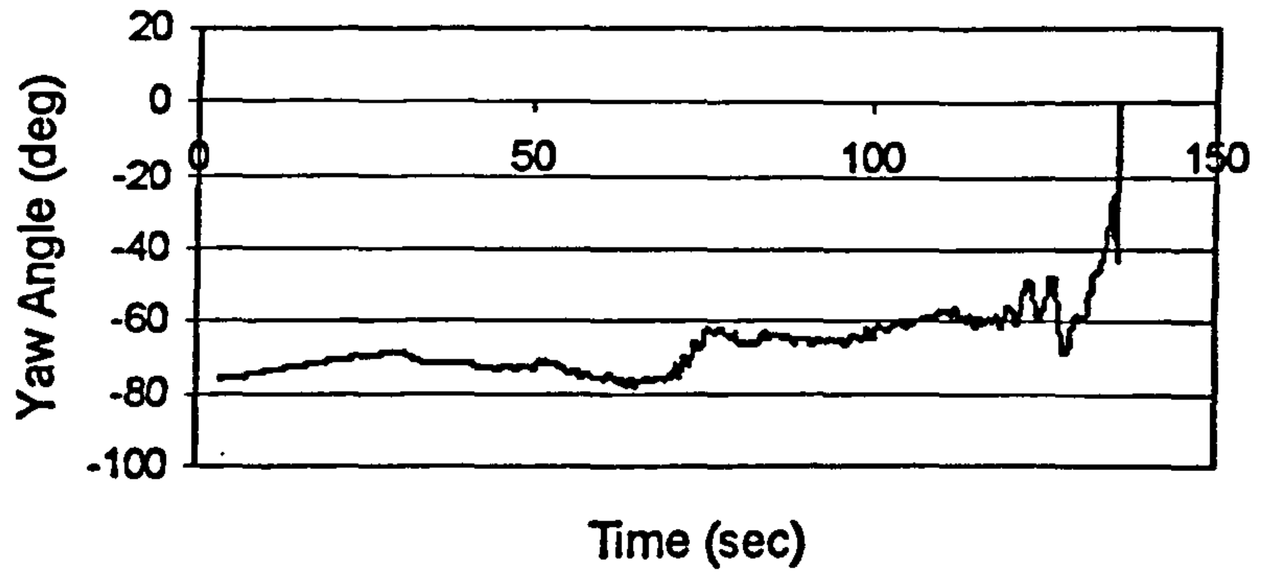

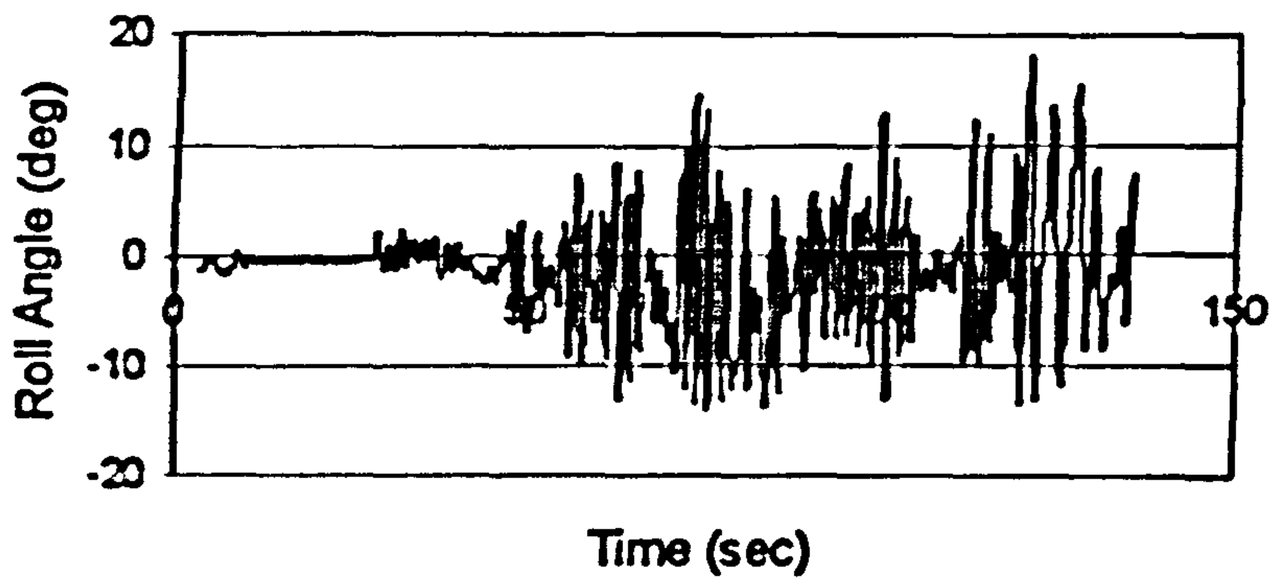

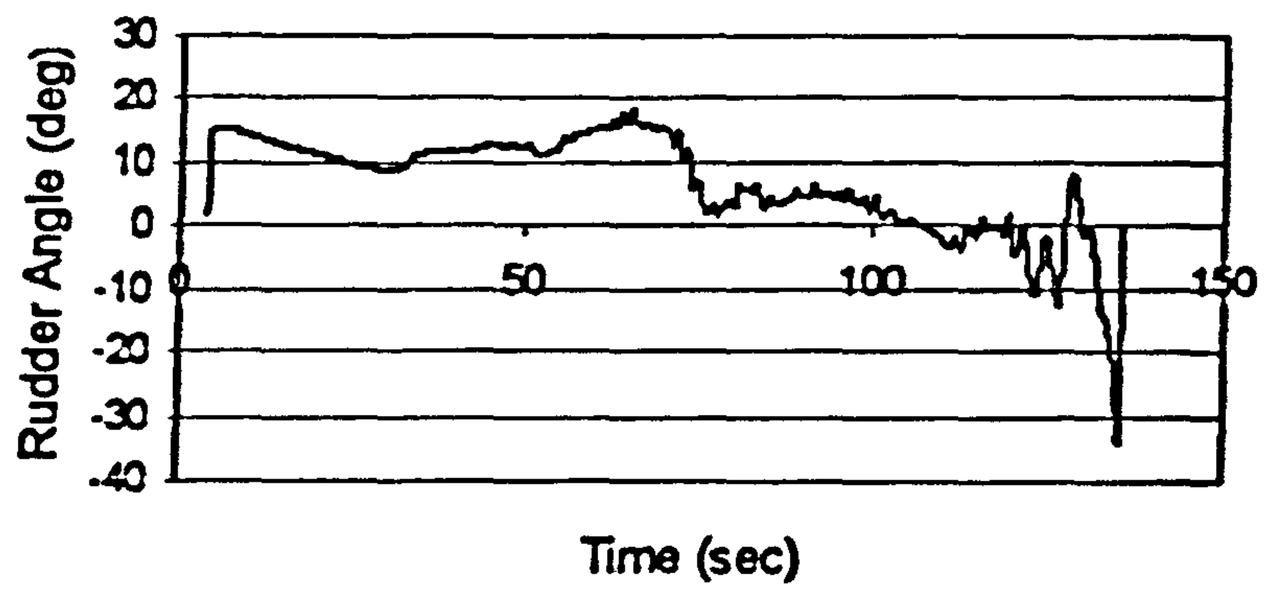

Figure H.35 JONSWAP, Fn=0.4, χ= -60°, H_s=0.115 m, T_p=1.214 sec.

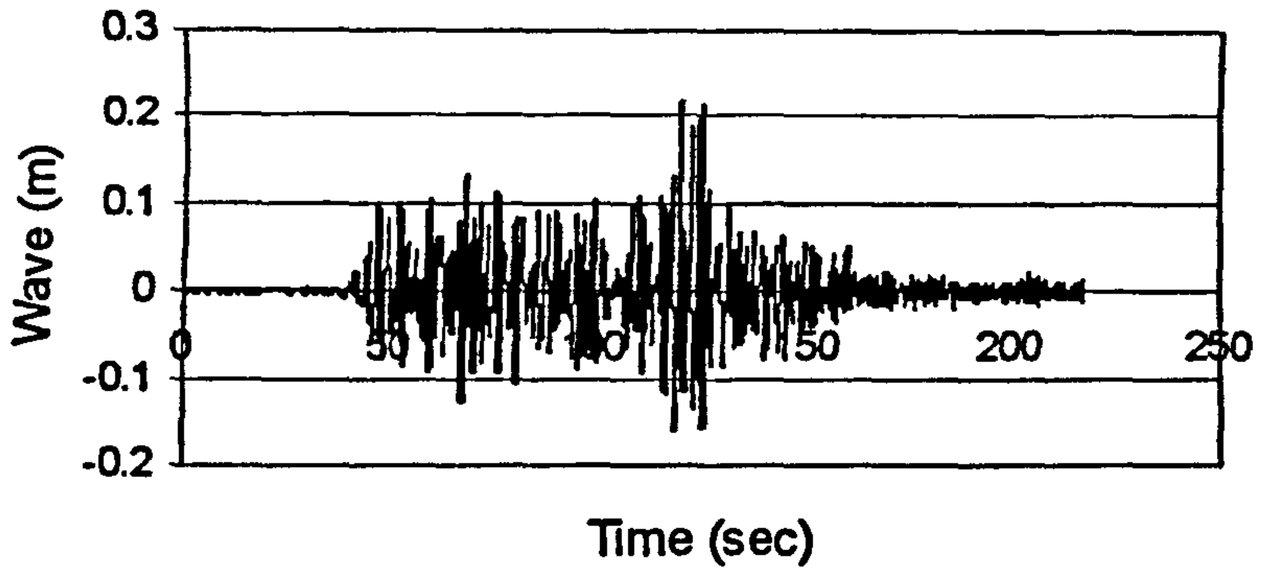

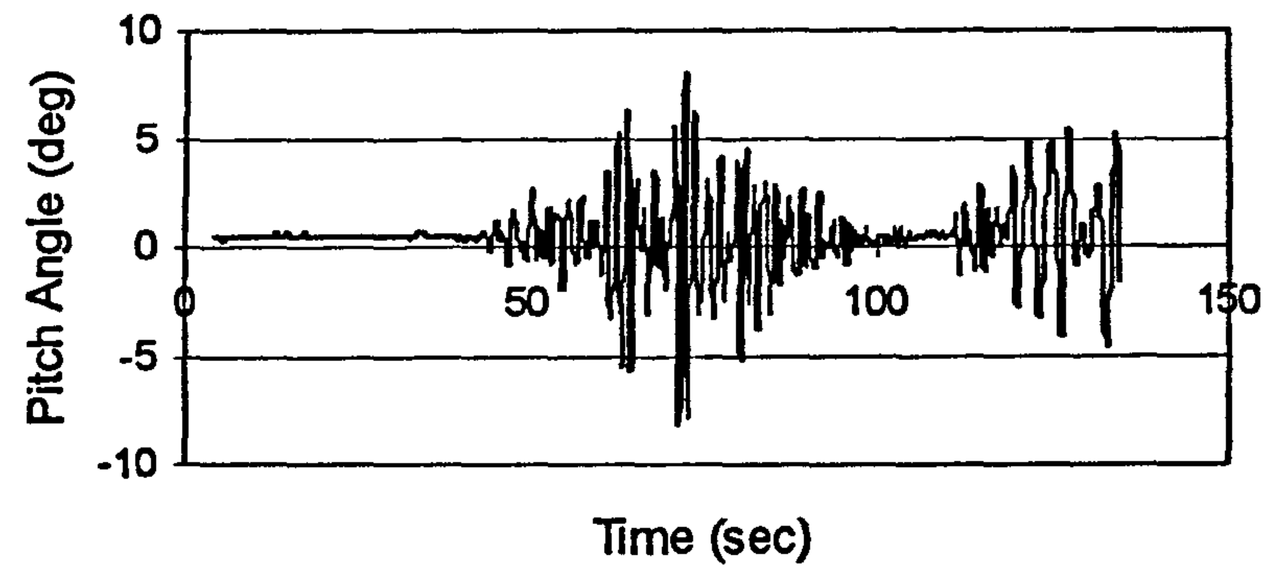

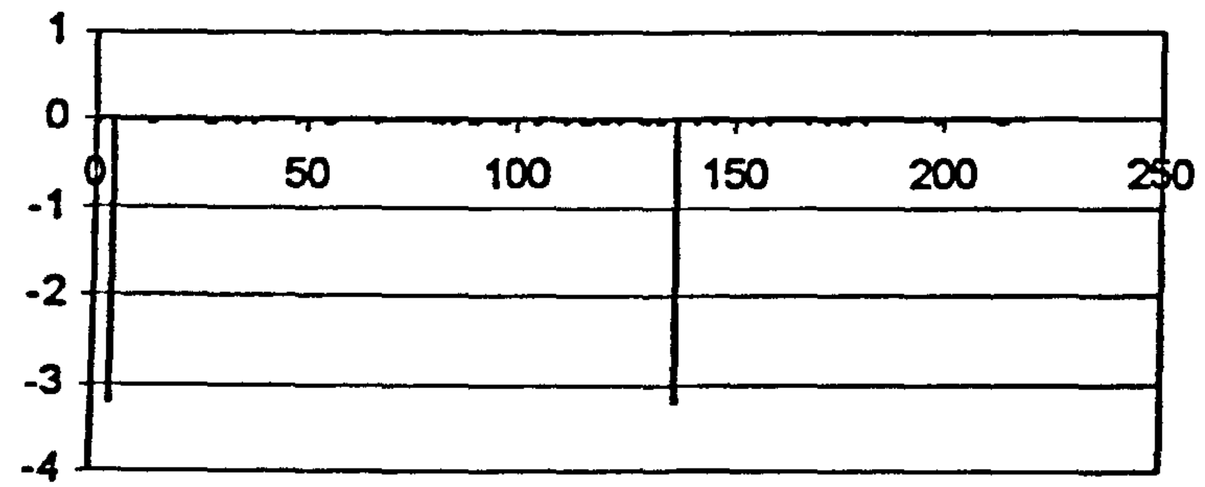

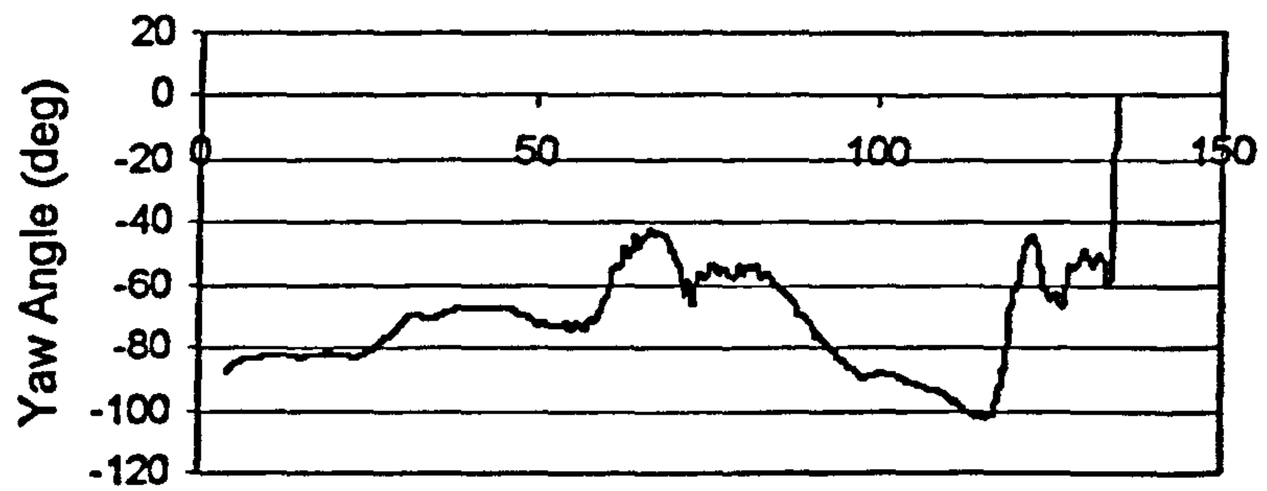

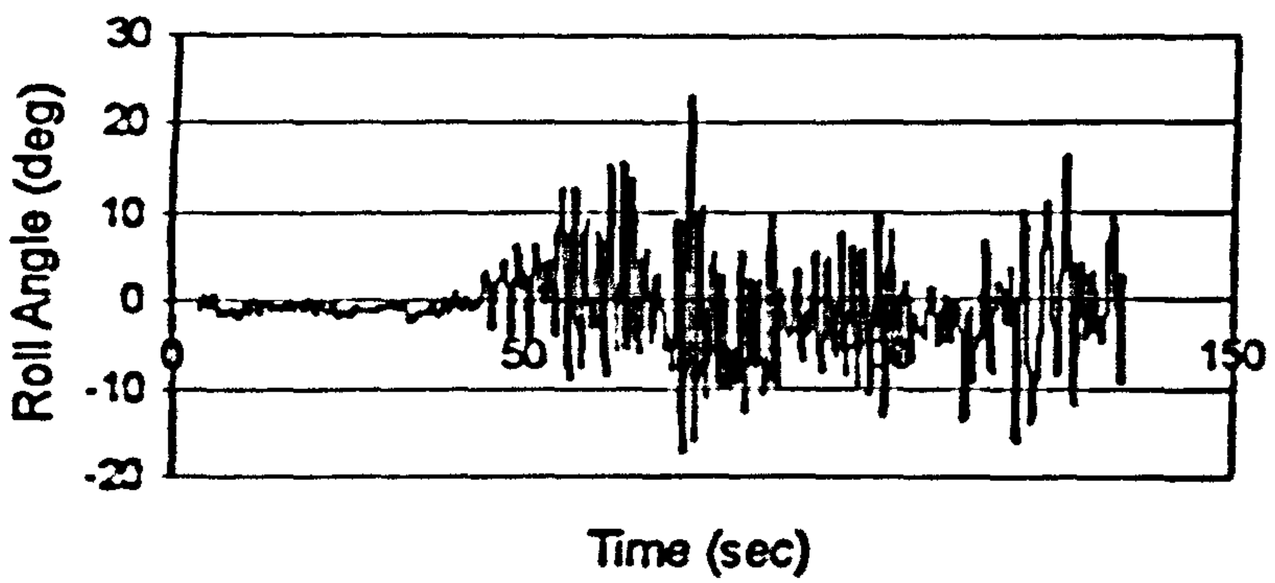

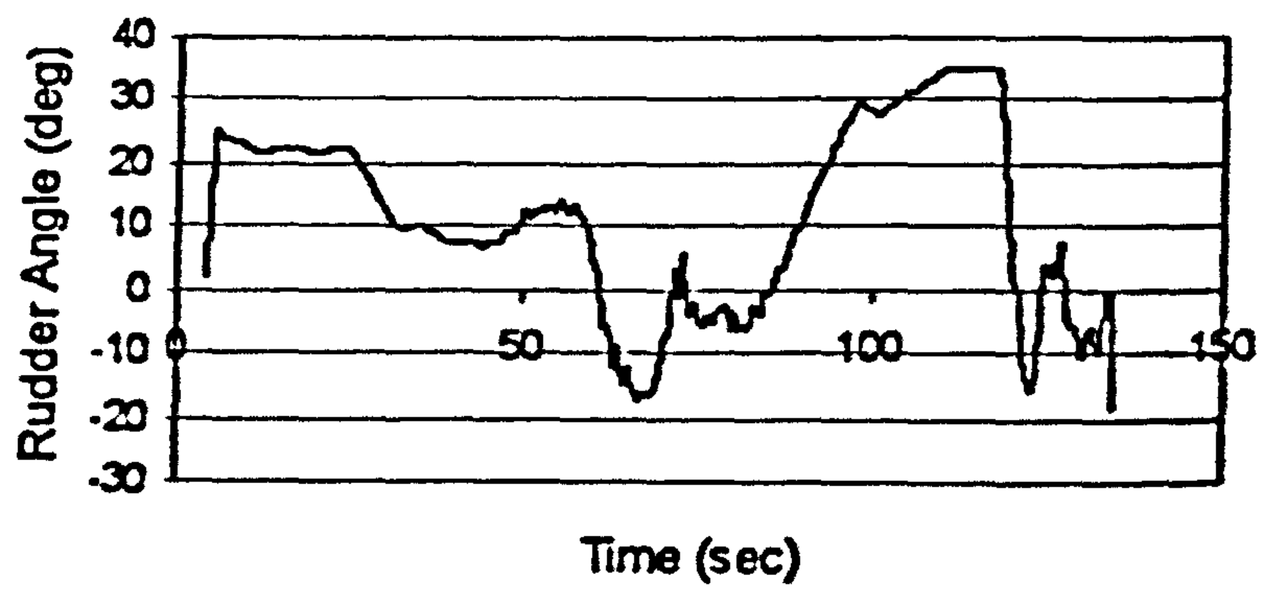

Figure H.36 ITTC, Fn=0.3, χ= -60°, H_s=0.115 m, T_p=1.214 sec.

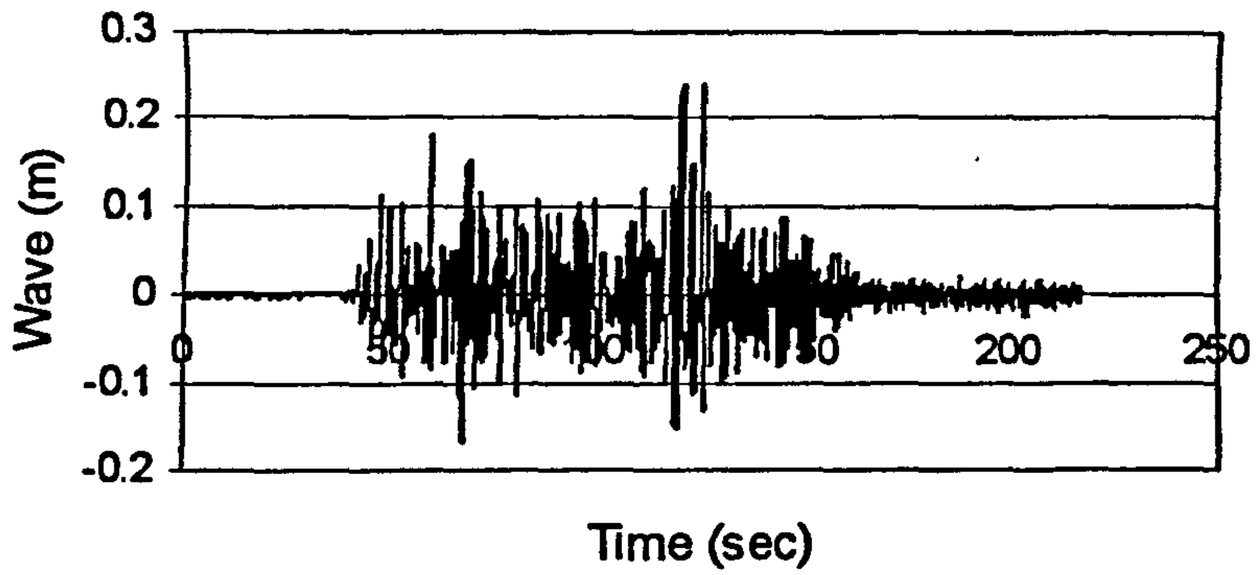

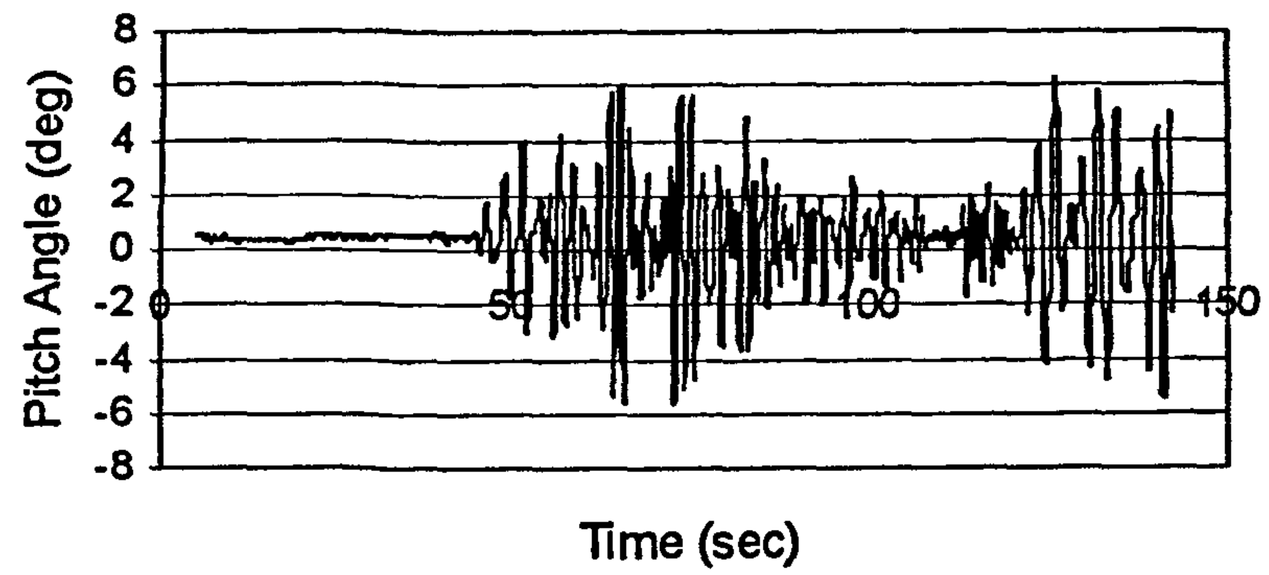

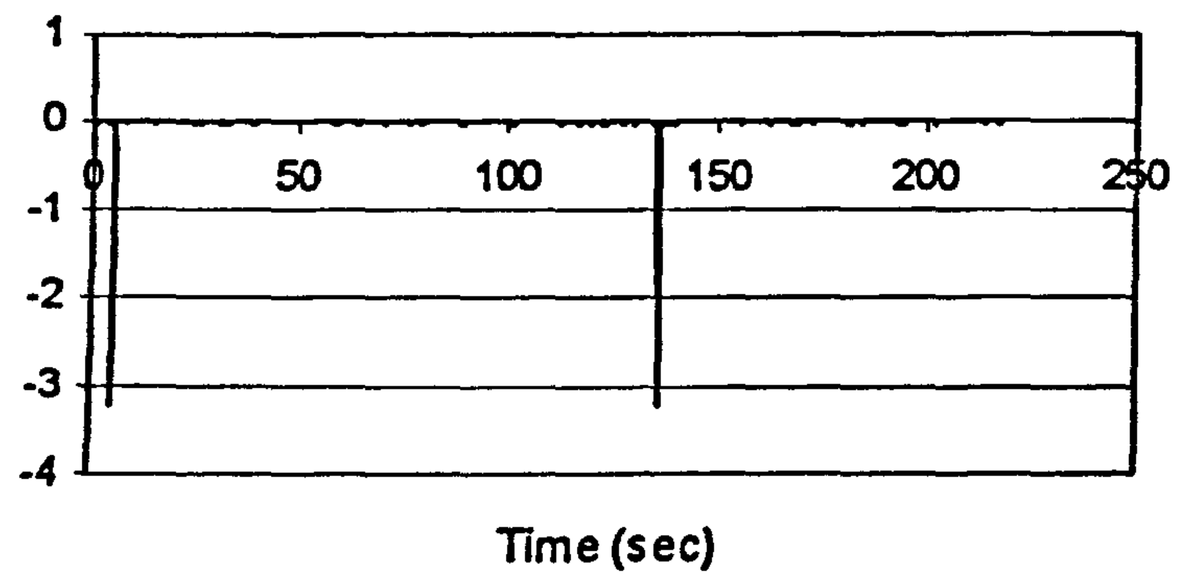

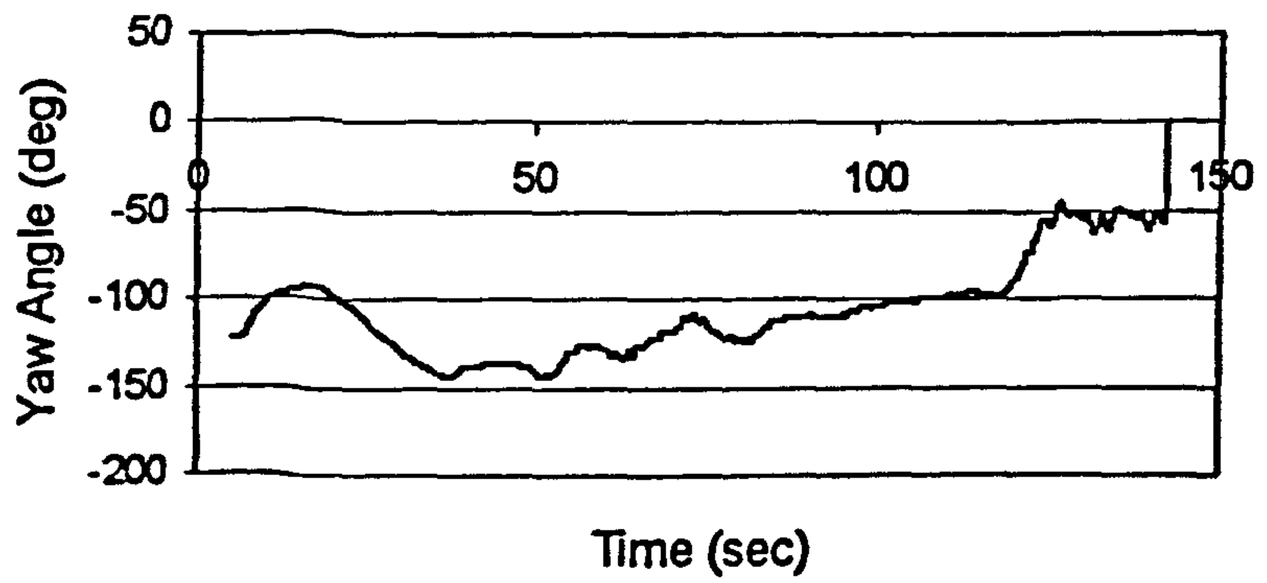

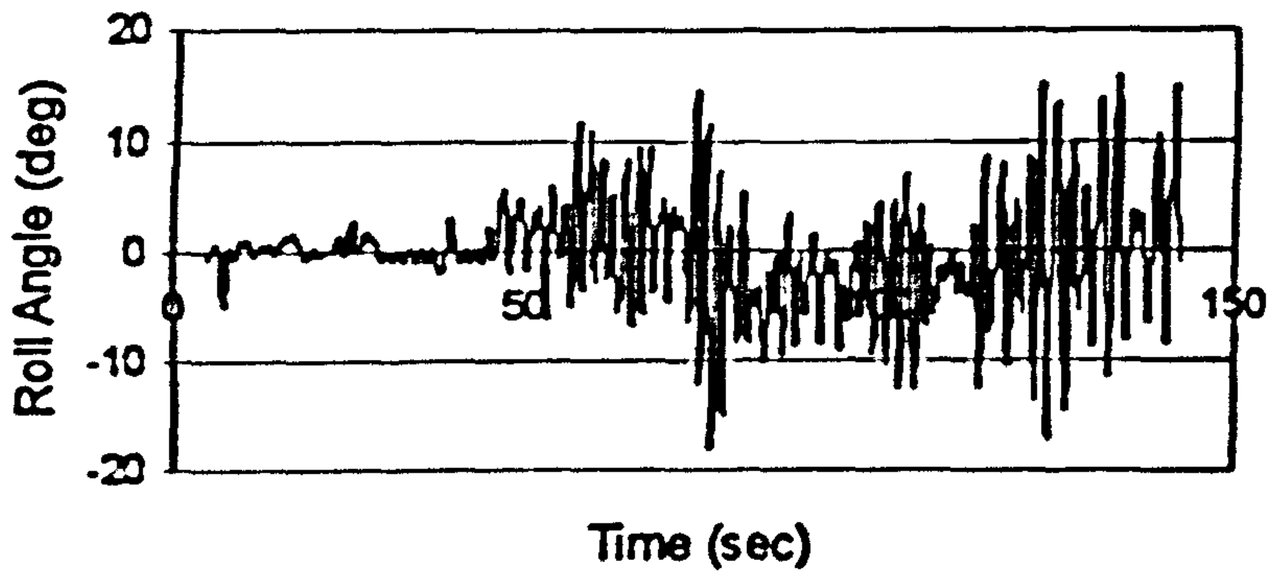

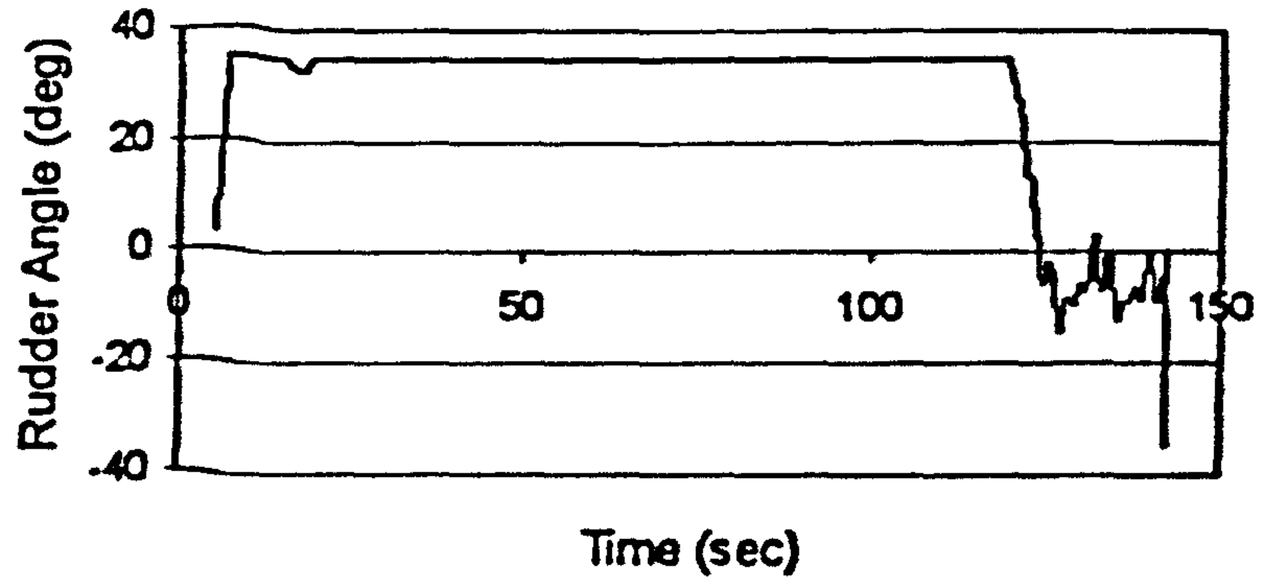

Figure H.37 ITTC, Fn=0.4, χ= -60°, H_s=0.115 m, T_p=1.214 sec.

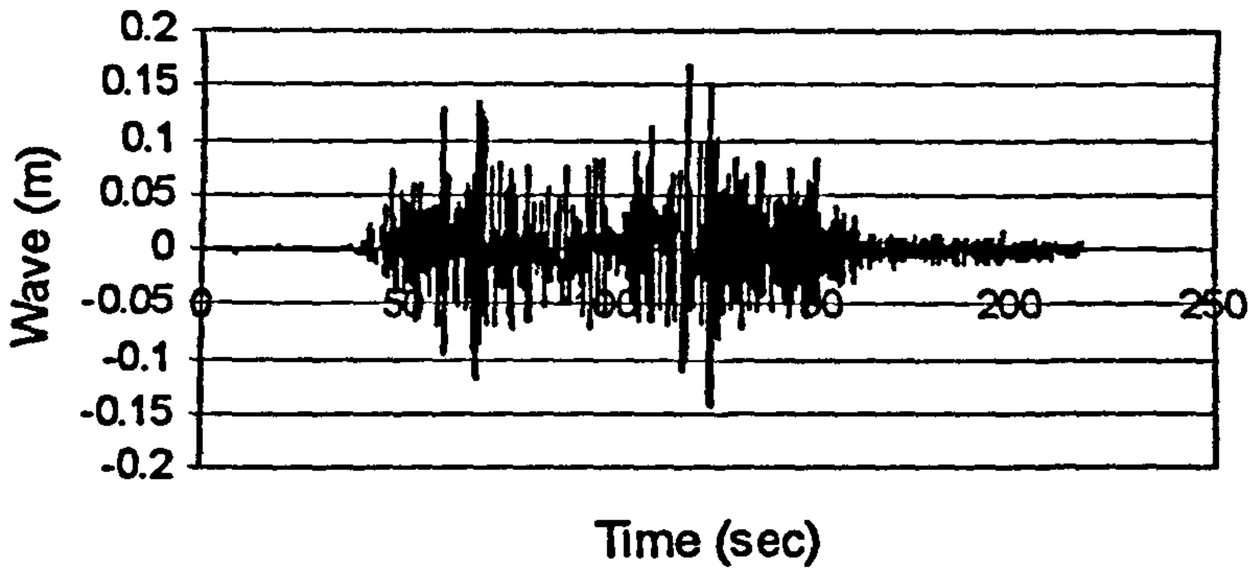

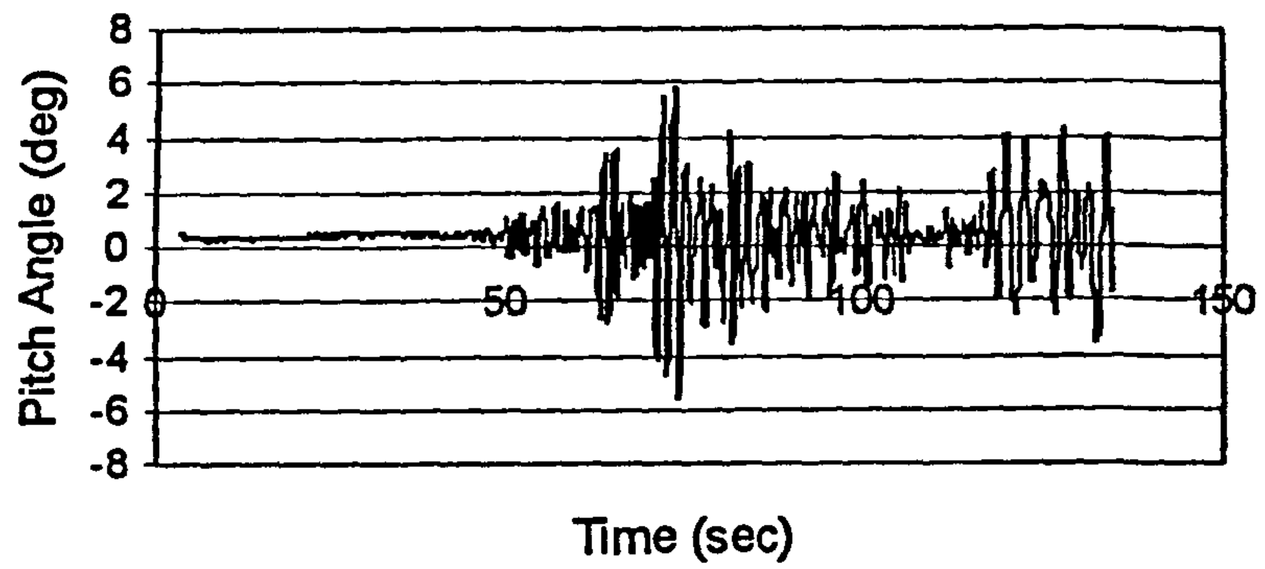

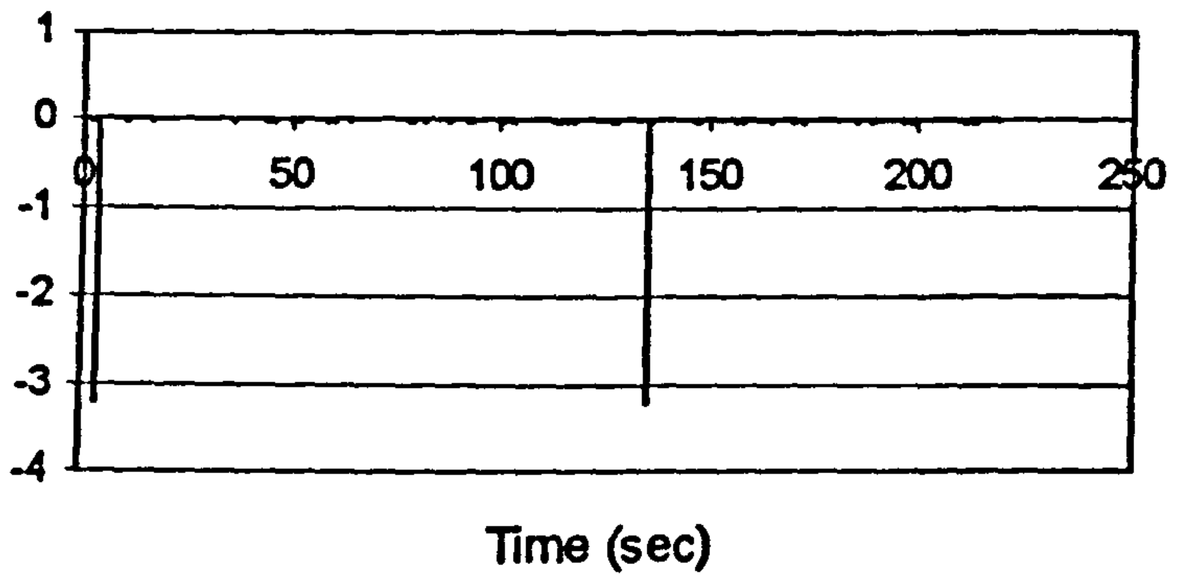

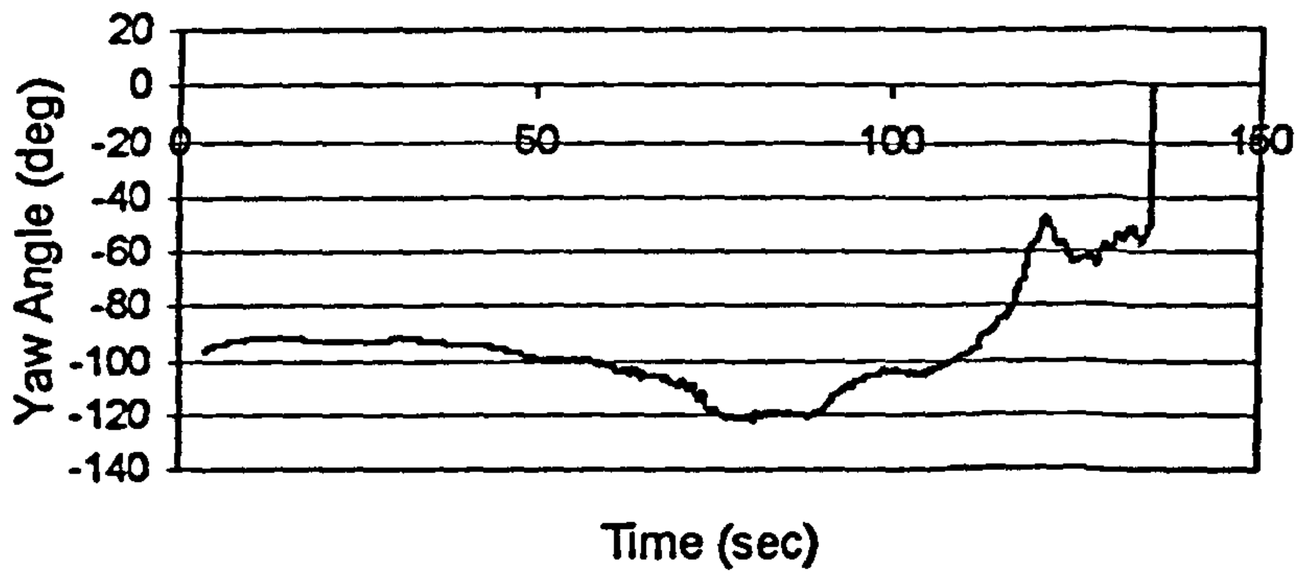

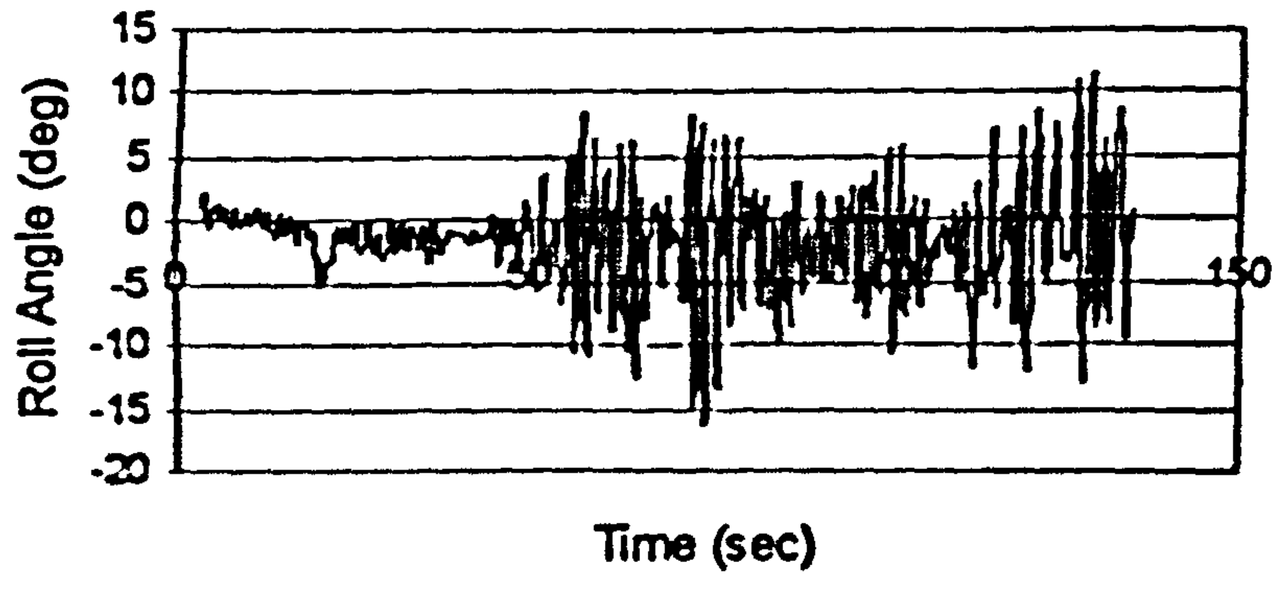

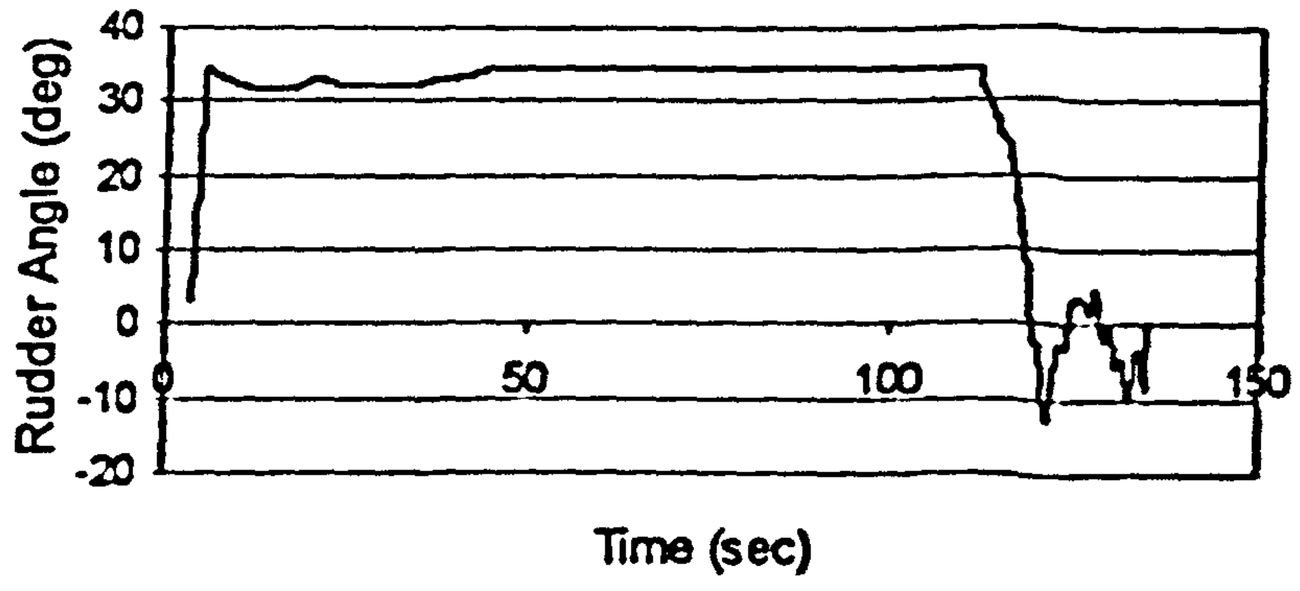

Figure H.38 ITTC, Fn=0.3, χ= -60°, H_s=0.1725 m, T_p=1.487 sec.

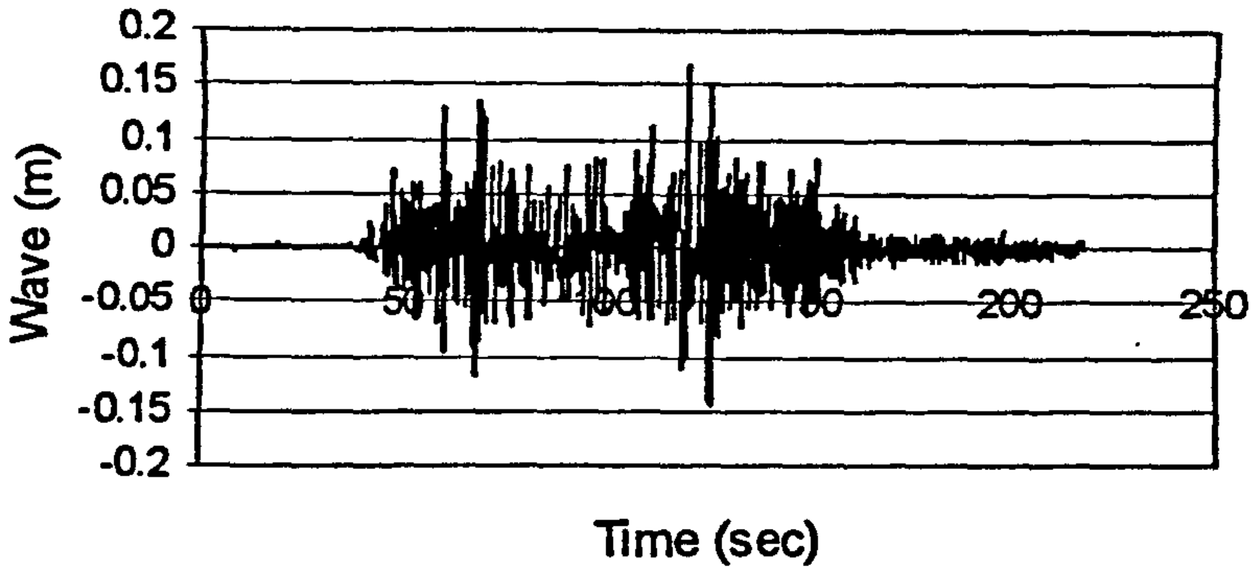

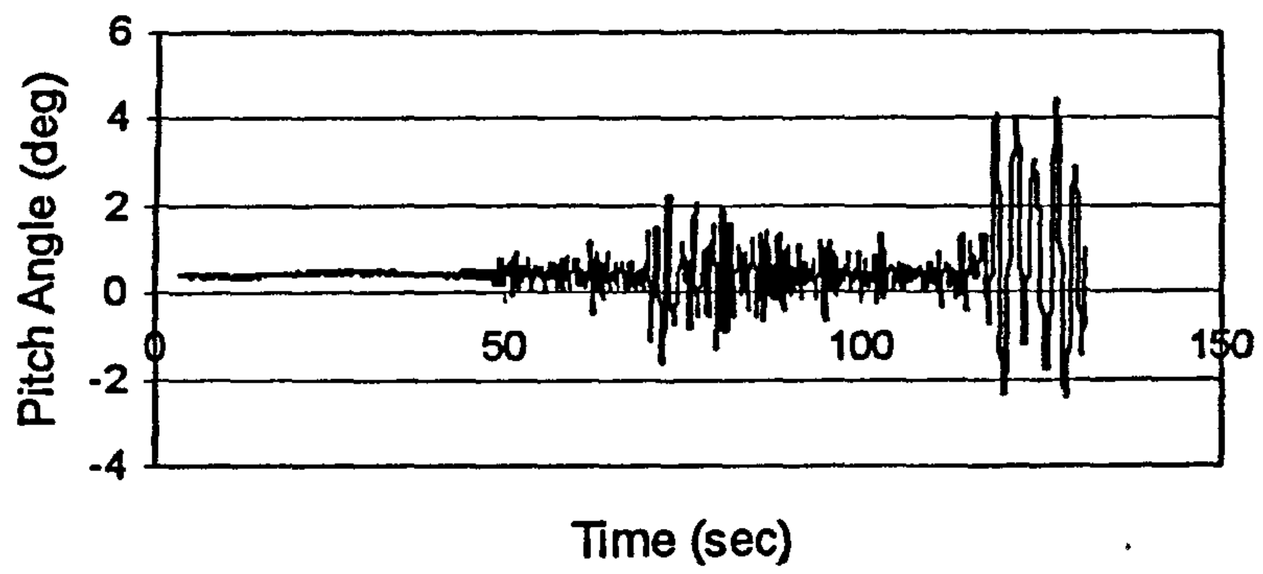

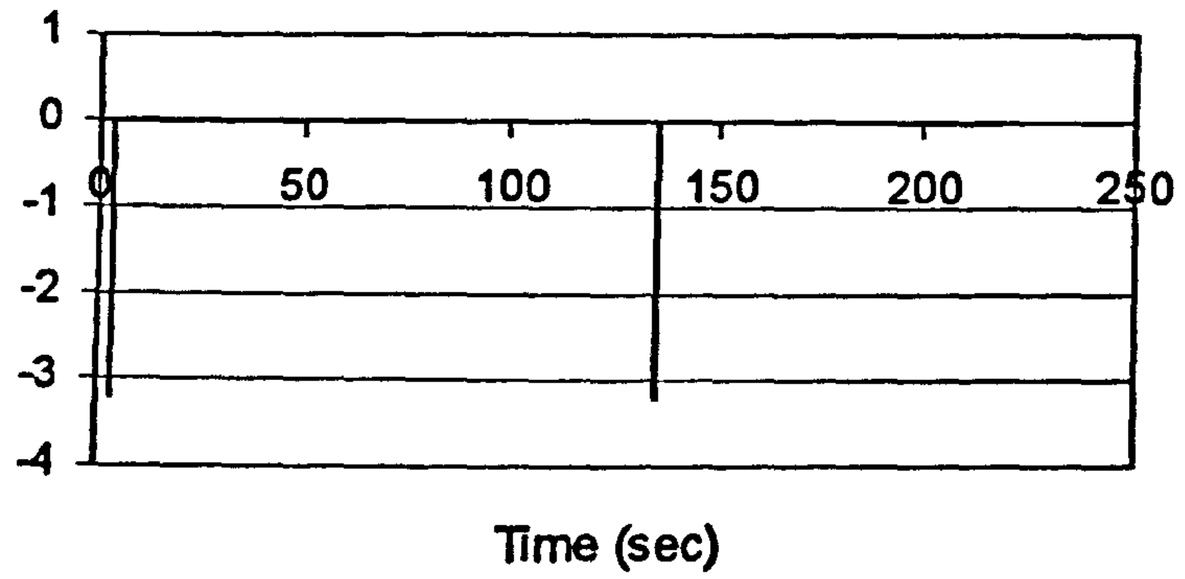

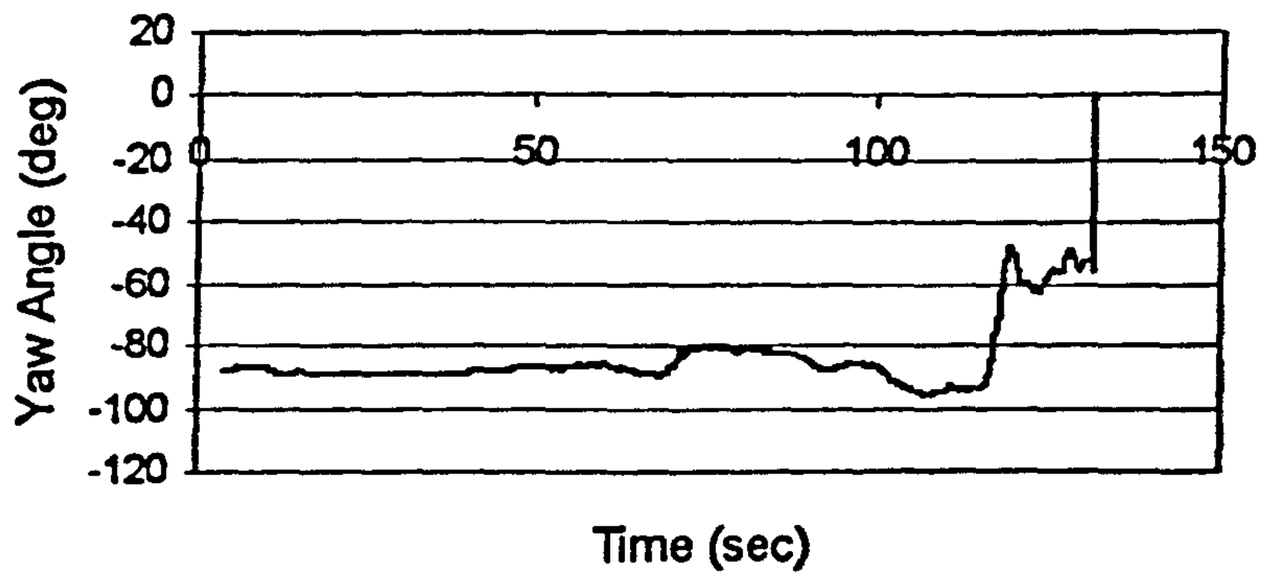

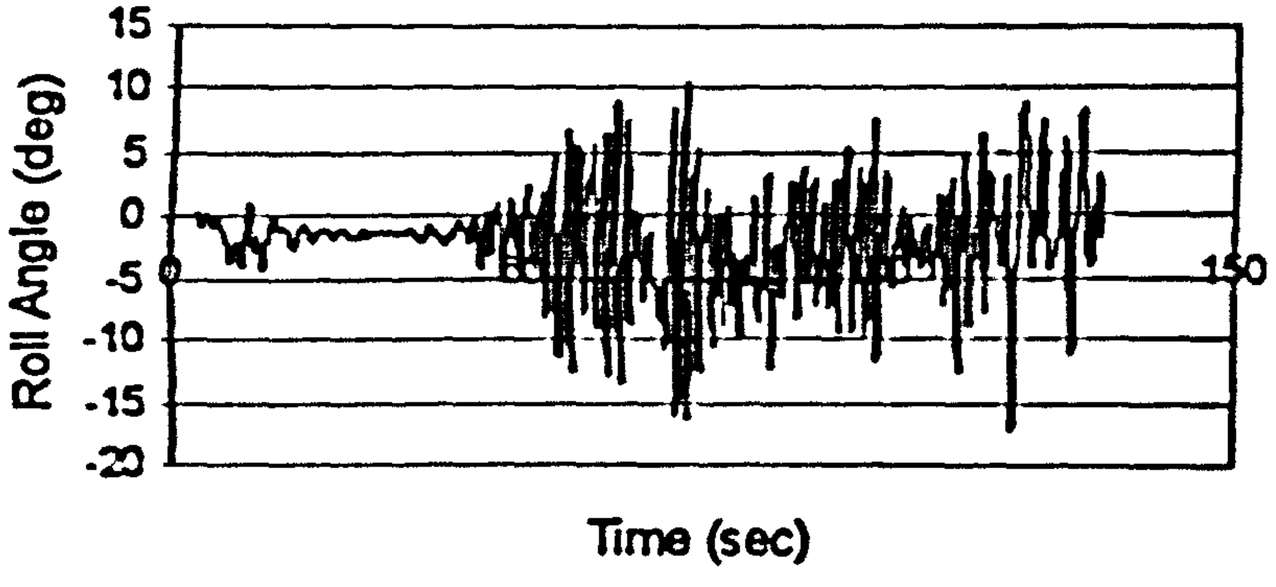

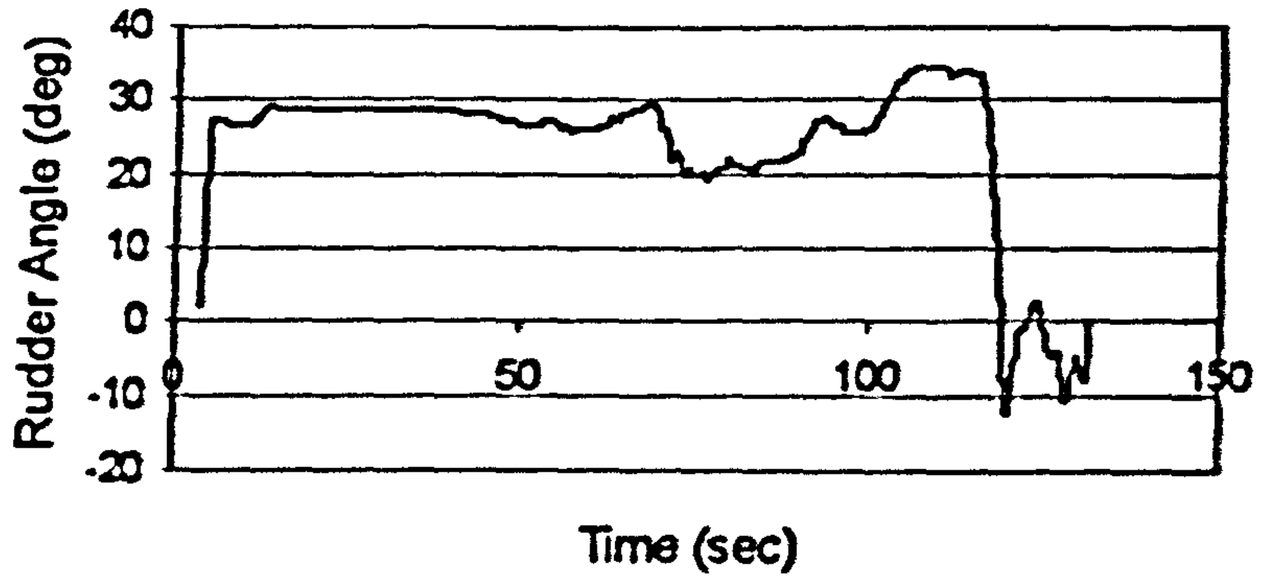

Figure H.39 ITTC, Fn=0.4, χ= -60°, H_s=0.1725 m, T_p=1.487 sec.

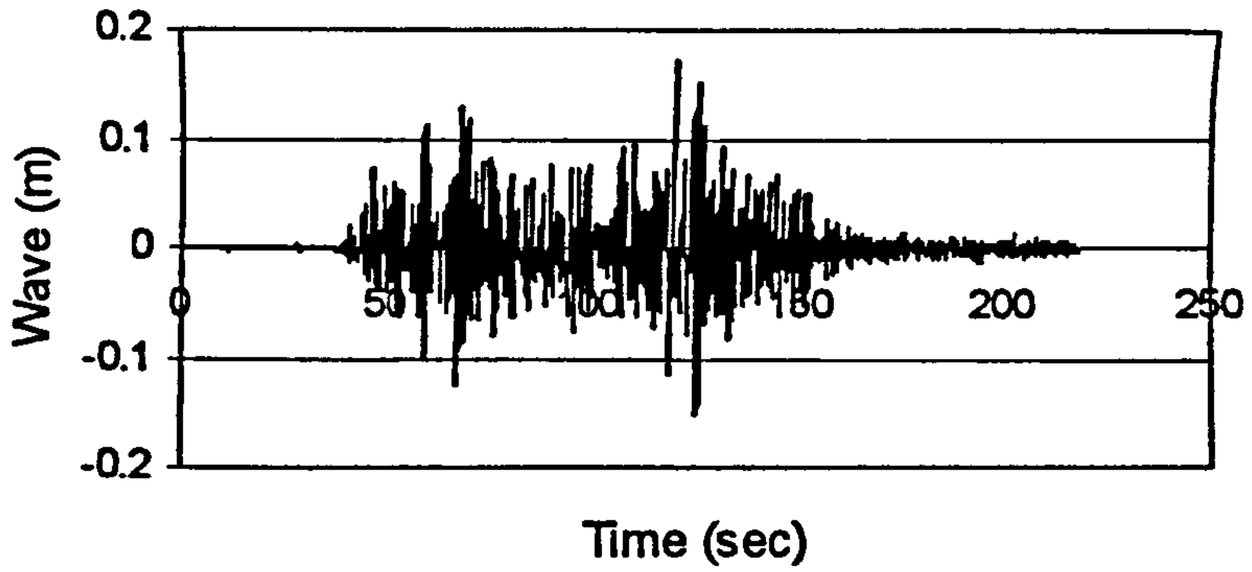

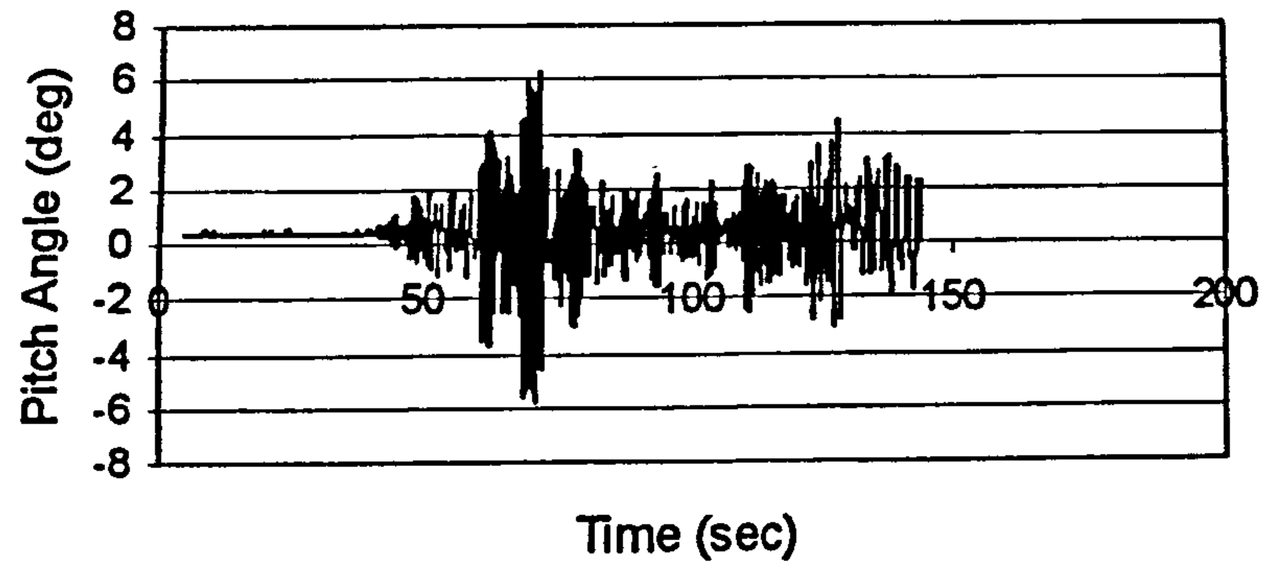

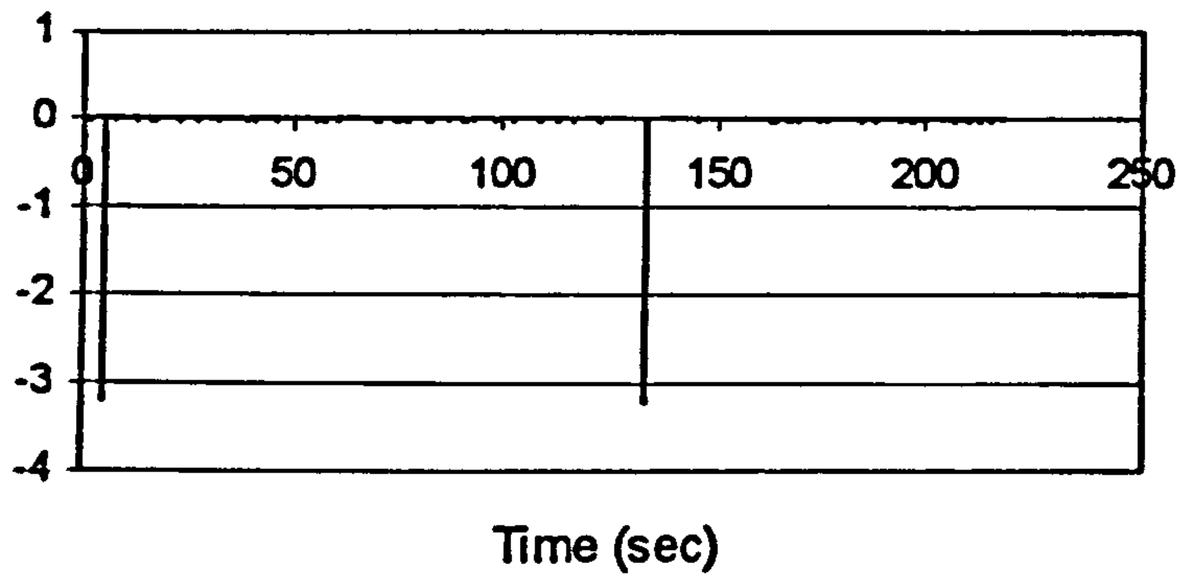

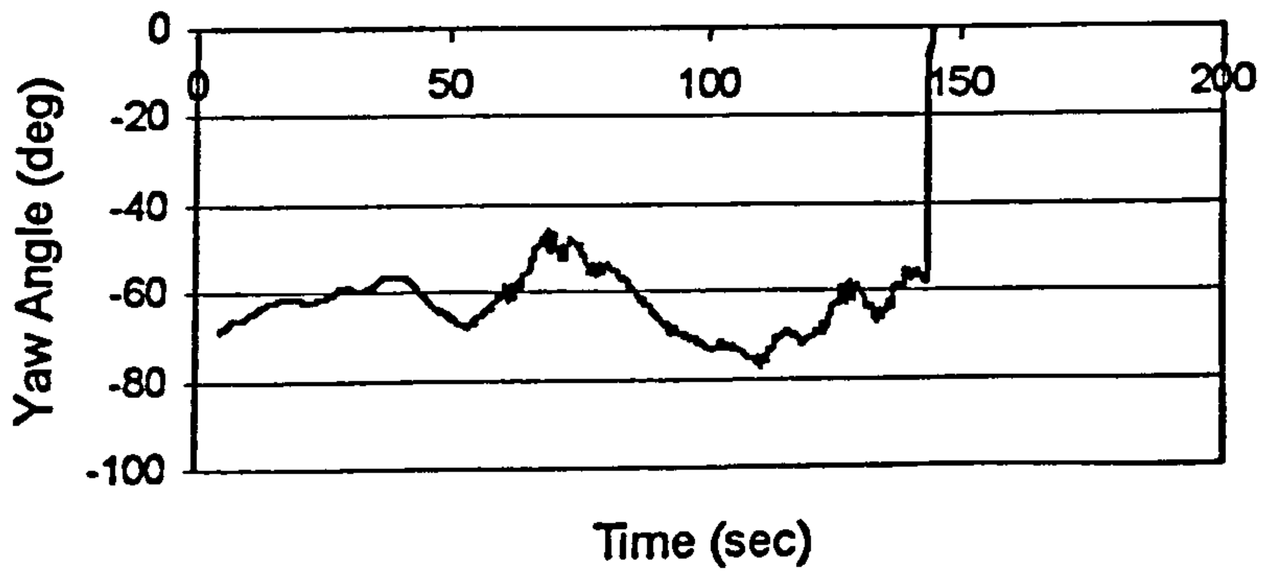

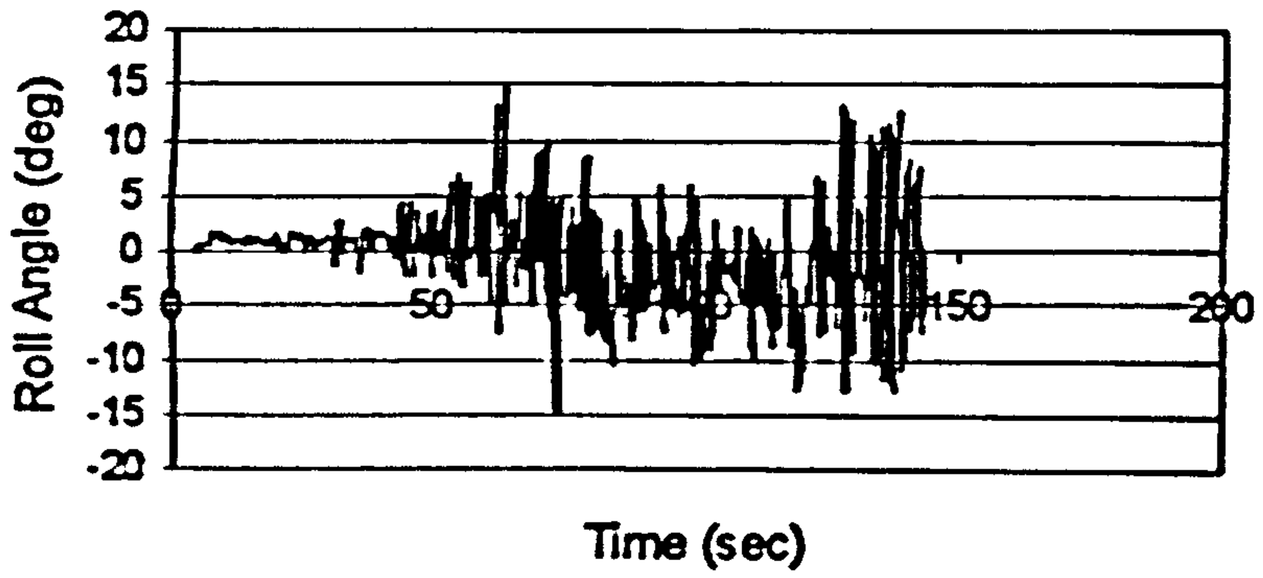

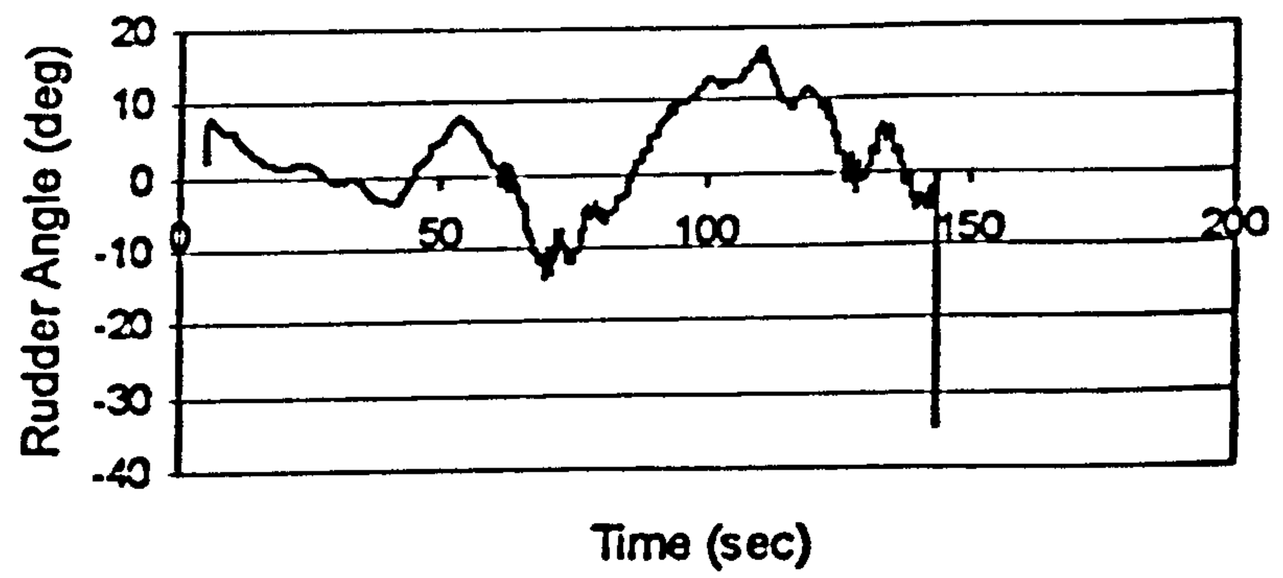

Figure H.40 ITTC, Fn=0.3, χ= -60°, H_s=0.23 m, T_p=1.717 sec.

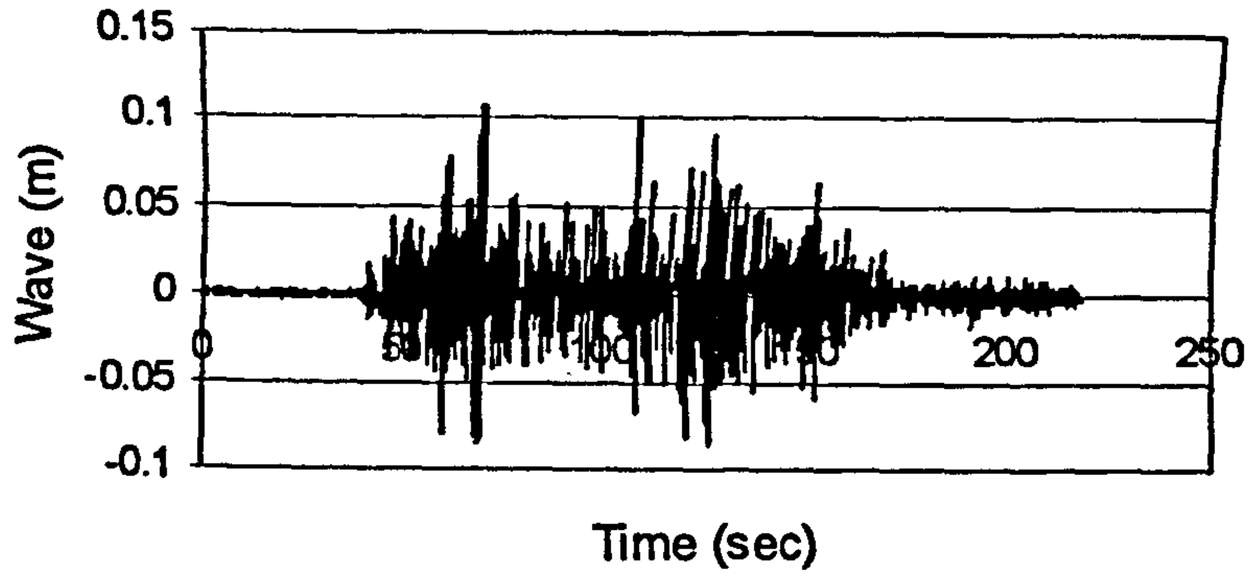

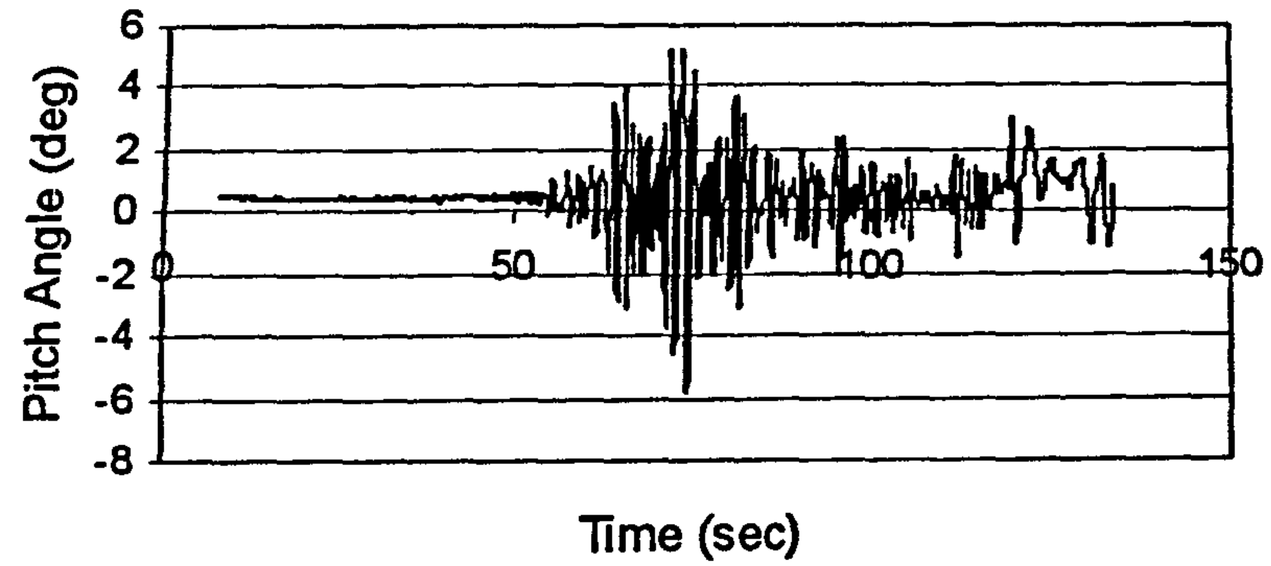

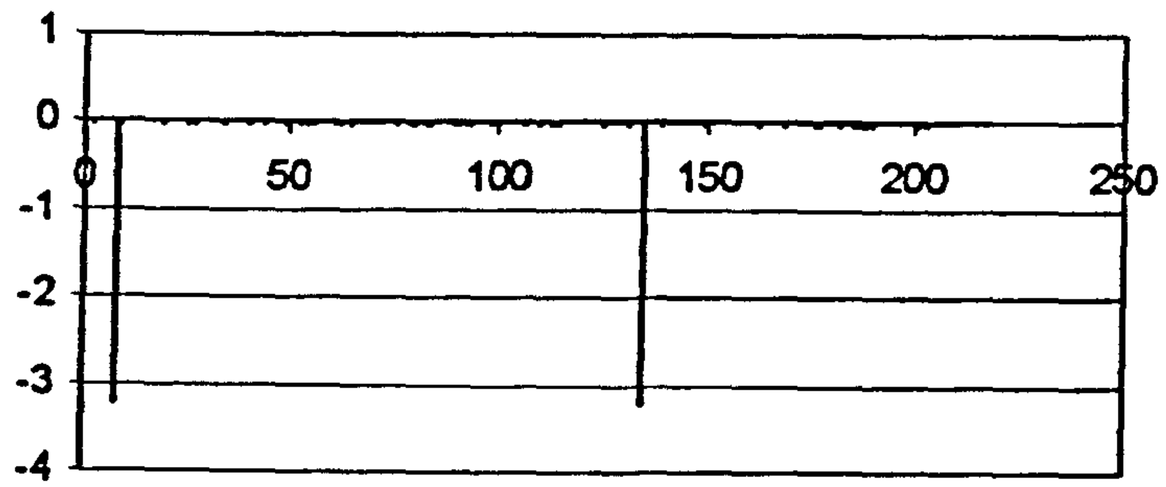

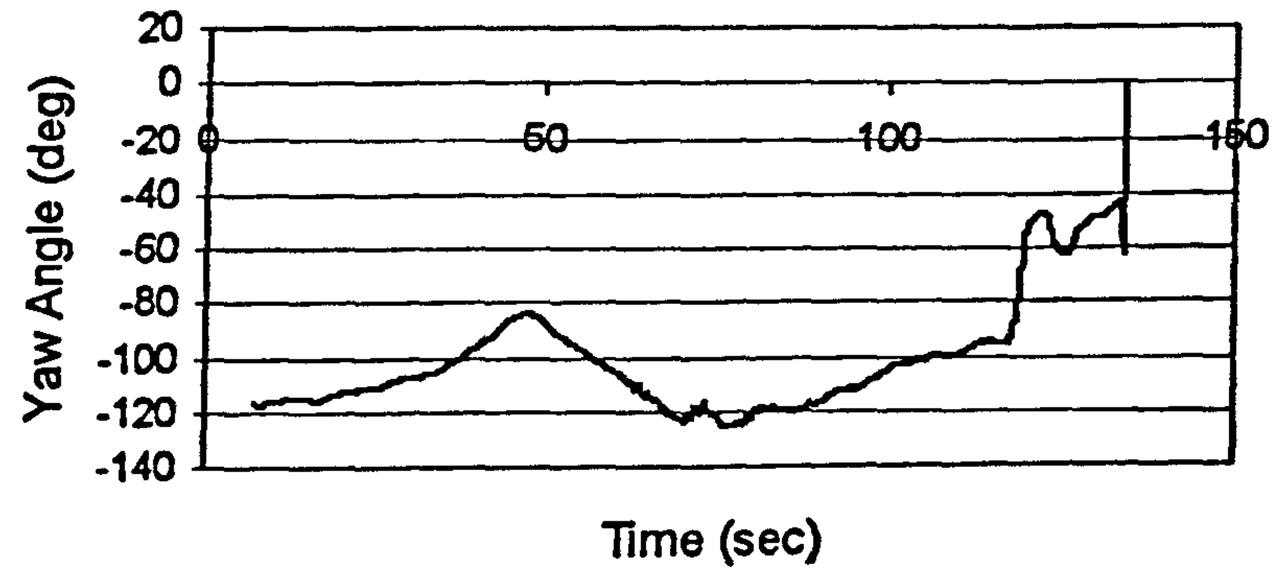

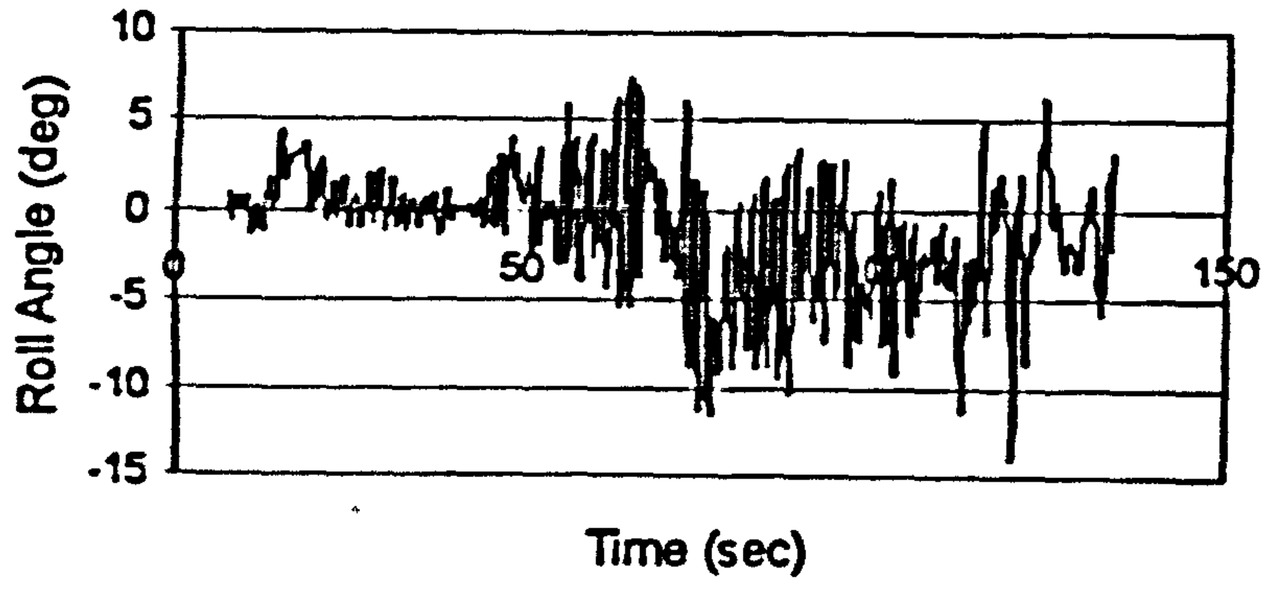

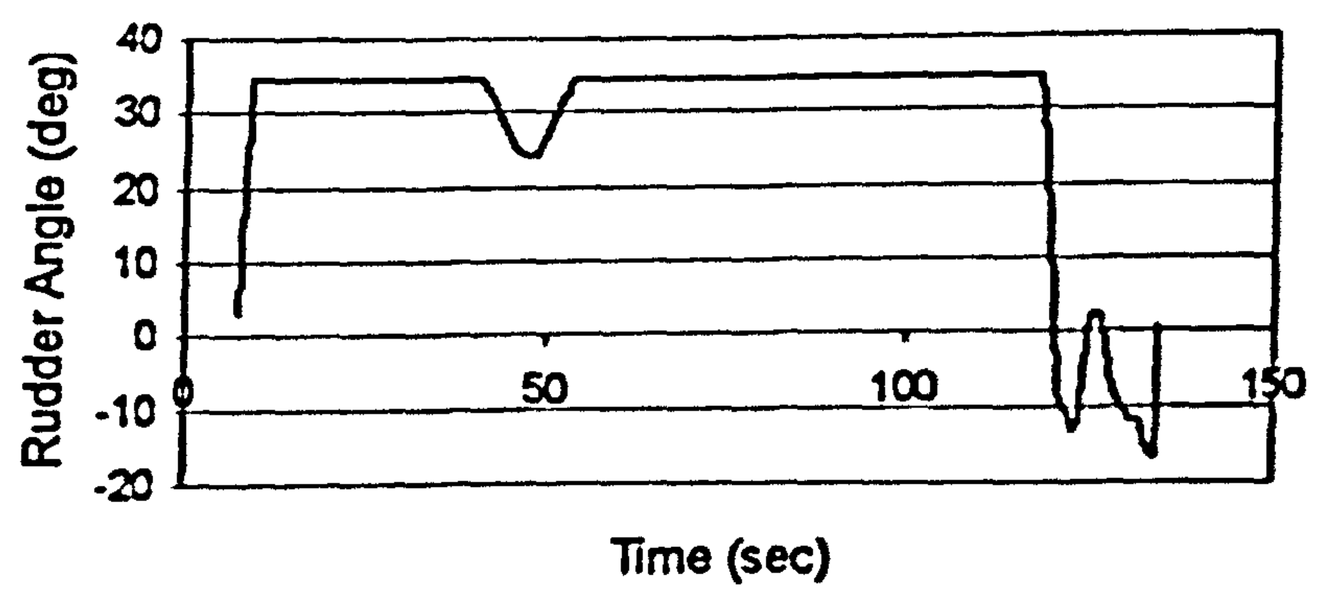

Figure H.41 ITTC, Fn=0.4, χ= -60°, H_s=0.23 m, T_p=1.717 sec.